

Proceedings of

SilviLaser 2008

8th international conference on LiDAR applications in forest
assessment and inventory



**September 17-19, 2008
Heriot-Watt University,
Edinburgh, UK**

Edited by:

**Ross Hill (Bournemouth University)
Jackie Rosette (Swansea University)
Juan Suárez (Forest Research, Edinburgh)**

ISBN 978-0-85538-774-7

Proceedings of *SilviLaser 2008: 8th international conference on LiDAR applications in forest assessment and inventory*. Hill R.A., Rosette, J. and Suárez, J. (Eds). September 2008. Edinburgh, UK.

ISBN 978-0-85538-774-7

Organised by:



Swansea University
Prifysgol Abertawe

Sponsored by:



PREFACE

SilviLaser 2008: September 17-19, 2008. Heriot-Watt University, Edinburgh, UK

SilviLaser 2008 will be the 8th international conference in a series focussing on applications of laser systems for forest assessment and inventory. Previous conferences have taken place in Canada, Australia, Sweden, Germany, USA, Japan and Finland. In 2006, the name SilviLaser was chosen by the Scientific Committee to create a recognisable identity for this highly successful series of international conferences. This year, we have chosen the James Watt II Centre at Heriot-Watt University, Edinburgh as the venue for this event. This is very modern and well equipped to suit our needs for such a prestigious event.

In recent years there has been rapid development and use of laser systems operating on a principal of Light Detection And Ranging (LiDAR) in the inventory, assessment, and monitoring of forests. Applications of laser technology have included the estimation of forest biophysical parameters (including carbon) at the individual tree or stand level as part of local, regional and even national forest inventory. In addition, laser data have been used to monitor forest change, model susceptibility to wind or fire damage, and map wildlife habitat. Laser systems can operate on ground-based, airborne and satellite platforms. They are typically categorised as profiling or scanning systems supplying range or waveform information per laser pulse. This distinction is, however, becoming increasingly blurred as laser systems evolve.

On September 17th we celebrated a pre-conference workshop focused on the use of Terrestrial Laser Scanning in forestry. There is now considerable interest in this non-disruptive technology, and the realisation of its full potential justified us organising this event. We limited attendance to 30 people and very quickly we had to turn down requests for attendance. Presentations demonstrated both state-of-the-art research and mature tools ready for operational use. This was complemented by the latest advances in scanning systems, all of which enabled practitioners to discover another useful tool for taking field measurements.

SilviLaser 2008 (September 18th and 19th) brings together research scientists and practitioners from around the world to share their experience in the development and application of LiDAR for forest assessment and inventory. Presentations cover all forms of laser system, from all possible platforms, and across a full range of forest applications. The conference has six session themes:

- forestry applications & inventory;
- data fusion;
- ecological applications & habitat mapping;
- waveform LiDAR;
- algorithm and techniques development;
- terrestrial laser scanning and laser cameras.

SilviLaser 2008 will discuss the state-of-the-art in laser systems and data processing techniques in order to meet a range of information needs. The conference aims to encourage new and stronger linkages between LiDAR practitioners, and in particular between researchers, data providers and end-users of derived products. All of the papers

in the proceedings have been double-blind peer reviewed by at least two experts in the field. This was performed mostly by the Scientific Committee but with additional assistance required due to the submission of 70 full manuscripts. The editorial board also read the papers. The standard of submission was extremely high, and competition for oral presentations was strong. We believe that through this rigorous reviewing process, we have improved the quality of the papers and selected a diverse range of high quality presentations. We are grateful for the efforts expended by the large team of reviewers.

The keynote speakers at SilviLaser 2008 are Professor Richard Lucas (Aberystwyth University), Dr Wesley Newton (U.S. Geological Survey) and Professor Ralph Dubayah (University of Maryland). The research interests of Prof. Lucas include the integration of airborne and spaceborne LiDAR, SAR and hyper-spectral data for assessing the structure and biomass of tropical and subtropical forests and woodlands. His current research sites include Brazil and Queensland, Australia. Dr Wesley Newton is the Supervisory Statistician in the USGS Northern Prairie Wildlife Research Center. His current projects include developing bird species-habitat models using LiDAR data in northern forests and developing management optimization algorithms. The research interests Prof. Dubayah include the estimation of Tropical Forest aboveground biomass using large-footprint LiDAR, and improving model carbon projections of the land surface using LiDAR remote sensing. He was principal investigator for the Vegetation Canopy Lidar (VCL) Mission.

We are particularly pleased to welcome five international post-graduate students to SilviLaser 2008 in Edinburgh, thanks to bursaries kindly supported by ESRI. In addition, we are also pleased to have a special session on ecological applications for forest habitat assessment, which is sponsored by the British Ecological Society.

We wish to thank all contributing authors, members of the Scientific Committee, all manuscript reviewers, our sponsors, and the local organising committee. Their support is highly appreciated and was essential for enabling this conference to take place. We hope you enjoy SilviLaser 2008 and that further develops your science and practice in the applications of laser systems for forest assessment and inventory.

SilviLaser 2008 Editorial Board:

Ross Hill (Bournemouth University)
Jackie Rosette (Swansea University)
Juan Suárez (Forest Research, Edinburgh)

SilviLaser 2008: Organising Committee

Conference Co-Chairs

Ross Hill (Bournemouth University)
Juan Suárez (Forest Research)

Conference Coordinators

Mark Lawrence (Forest Research)
Genevieve Patenaude (University of Edinburgh)
Jackie Rosette (Swansea University)

Conference Secretaries

Evelyn Hall (Forest Research)
Linda Legge (Forest Research)

Conference Web Coordinator

Shona Cameron (Forest Research)

SilviLaser 2008: Scientific Committee

Hans-Erik Andersen (USDA Forest Service, USA)
J. Bryan Blair (NASA, USA)
Nicholas Coops (University of British Columbia, Canada)
Terje Gobakken (Norwegian University of Life Sciences)
Ross Hill (Bournemouth University, UK)
Yasumasa Hirata (FFPRI, Japan)
Johan Holmgren (Swedish University of Agricultural Sciences)
Chris Hopkinson (Nova Scotia C.C., Canada)
Juha Hyyppä (Finnish Geodetic Institute, Finland)
Barbara Koch (University of Freiburg, Germany)
Mike Lefsky (Colorado State University, USA)
Matti Maltamo (University of Joensuu, Finland)
Felix Morsdorf (University of Edinburgh)
Erik Næsset (Norwegian University of Life Sciences)
Ross Nelson (NASA, USA)
Wesley Newton (United States Geological Survey, USA)
Håkan Olsson (Swedish University of Agricultural Sciences)
Norbert Pfeifer (Vienna University of Technology, Austria)
Sorin Popescu (Texas AandM, USA)
Petri Rönholm (Helsinki University of Technology, Finland)
Svein Solberg (Norwegian Forest and Landscape Institute, Norway)
Juan Suárez (Forest Research, UK)
Tatsuo Sweda (Ehime University, Japan)
Paul Treitz (Queen's University, Canada)
Pete Watt (Pöyry Forest Industry, New Zealand)
Mike Wulder (Canadian Forest Service, Canada)
Randy Wynne (Virginia Tech, USA)

SilviLaser 2008: Manuscript Reviewers

The SilviLaser 2008 Organising and Scientific Committees are grateful to the following people for providing reviews of submitted manuscripts:

Hans-Erik Andersen (USDA Forest Service, USA)
Christian Briese (Vienna University of Technology, Austria)
Nicholas Coops (University of British Columbia, Canada)
Wouter Dorigo (Vienna University of Technology, Austria)
Terje Gobakken (Norwegian University of Life Sciences)
Ross Hill (Bournemouth University, UK)
Yasumasa Hirata (FFPRI, Japan)
Bernhard Höfle (Vienna University of Technology, Austria)
Markus Hollaus (Vienna University of Technology, Austria)
Johan Holmgren (Swedish University of Agricultural Sciences)
Juha Hyypä (Finnish Geodetic Institute, Finland)
Barbara Koch (University of Freiburg, Germany)
Mike Lefsky (Colorado State University, USA)
Matti Maltamo (University of Joensuu, Finland)
Felix Morsdorf (University of Edinburgh)
Erik Næsset (Norwegian University of Life Sciences)
Ross Nelson (NASA, USA)
Wesley Newton (United States Geological Survey, USA)
Håkan Olsson (Swedish University of Agricultural Sciences)
Norbert Pfeifer (Vienna University of Technology, Austria)
Camillo Ressler (Vienna University of Technology, Austria)
Andreas Roncat (Vienna University of Technology, Austria)
Petri Rönholm (Helsinki University of Technology, Finland)
Jackie Rosette (Swansea University, UK)
Svein Solberg (Norwegian Forest and Landscape Institute, Norway)
Paul Treitz (Queen's University, Canada)
Mike Wulder (Canadian Forest Service, Canada)

Table of Contents

| | |
|---|-----------|
| Preface | III |
| SilviLaser 2008: Organising Committee | V |
| SilviLaser 2008: Scientific Committee | V |
| SilviLaser 2008: Manuscript Reviewers | VI |
| Keynote Presentation 1 | 1 |
| Advances in forest characterisation, mapping and monitoring through integration of LiDAR and other remote sensing datasets <i>Richard Lucas, Alex Lee, John Armston, Johanna Breyer, Peter Bunting and João Carreiras</i> | 2 |
| Session 1: Forestry applications & inventory | 13 |
| Assessing effects of sample plot positioning errors on biophysical stand properties derived from airborne laser scanner data <i>Terje Gobakken and Erik Næsset</i> | 14 |
| Comparison of individual tree detection and canopy height distribution approaches: a case study in Finland <i>Petteri Packalén, Juho Pitkänen and Matti Maltamo</i> | 22 |
| LiDAR forest inventory with single-tree, double- and single-phase procedures <i>Robert Parker and David Evans</i> | 30 |
| Variability of LiDAR volume prediction models for productivity assessment of radiata pine plantations in South Australia <i>Jan Rombouts, I.S. Ferguson and J.W. Leech</i> | 39 |
| Estimation of crown coverage using airborne laser scanning <i>Johan Holmgren, Fredrik Johansson, Kenneth Olofsson, Håkan Olsson and Anders Glimskär</i> | 50 |
| Airborne laser scanning for the identification of boreal forest site types <i>Mikko Vehmas, Kalle Eerikäinen, Jussi Peuhkurinen, Petteri Packalén and Matti Maltamo</i> | 58 |
| Session 2: Data fusion | 66 |
| Forest mensuration parameters derived from individual tree crown forest inventory method using airborne imagery and LiDAR <i>Baudouin Desclee, Alain Gingras, Valery Bemelmans and Emmanuel Patigny</i> | 67 |
| Full automatic detection of tree species based on delineated single tree crowns - a data fusion approach for airborne laser scanning data and aerial photographs <i>Johannes Nicolas Heinzl, Holger Weinacker and Barbara Koch</i> | 76 |

| | |
|---|-----|
| Estimation of stand volume by fusing low laser-sampling density LiDAR data with QuickBird panchromatic imagery in closed-canopy Japanese cedar (<i>Cryptomeria japonica</i>) plantations <i>Tomoaki Takahashi, Yoshio Awaya, Yasumasa Hirata, Naoyuki Furuya, Toru Sakai and Atsushi Sakai</i> | 86 |
| A method for linking field-surveyed and aerial-detected single trees using cross correlation of position images and the optimization of weighted tree list graphs <i>Kenneth Olofsson, Eva Lindberg and Johan Holmgren</i> | 95 |
| Performance of airborne laser scanning- and aerial photograph-based statistical and textural features in forest variable estimation <i>Markus Holopainen, Reija Haapanen, Sakari Tuominen and Risto Viitala</i> | 105 |
| Integration of LiDAR and QuickBird imagery for mapping riparian zones in Australian tropical savannas <i>Lara Arroyo, Kasper Johansen, John Armston, Stuart Phinn and Cristina Pascual...</i> | 113 |
| Keynote Presentation 2 | 123 |
| LiDAR and wildlife-habitat applications <i>Wesley E. Newton</i> | 124 |
| Session 3: Ecological applications & habitat mapping | 125 |
| Characterising the ecological structure of a dry Eucalypt forest landscape <i>Naoko Miura and Simon Jones</i> | 126 |
| Automatic detection of dominated vegetation under canopy using Airborne Laser Scanning data <i>Andrea Barilotti, Francesco Sepic and Elena Abramo</i> | 134 |
| Canopy and gap dynamics analysed using multi-temporal airborne laser scanner data in a temperate deciduous forest <i>Yasumasa Hirata, Hiroshi Tanaka and Naoyuki Furuya</i> | 144 |
| Forest microclimate modelling using gap and canopy properties derived from LiDAR and hyperspectral imagery <i>Zulkiflee Abd Latif and George Alan Blackburn</i> | 151 |
| Height growth of regeneration in boreal forest canopy gaps – does the type of gap matter, an assessment with lidar time series <i>Udayalakshmi Vepakomma, Benoit St-Onge and Daniel Kneeshaw</i> | 159 |
| Lidar remote sensing of bird canopy habitat use in the Northeastern United States <i>Scott Goetz, Daniel Steinberg, Matthew Betts, Richard Holmes, Patrick Doran, Ralph Dubayah and Michelle Hofton</i> | 168 |

| | |
|---|-----|
| Keynote Presentation 3 | 177 |
| The use of large footprint waveform lidar for landscape characterization: past experience and future prospects <i>Ralph Dubayah</i> | 178 |
| Session 4: Waveform LiDAR | 179 |
| Representation of vegetation and topography within satellite LiDAR waveforms for a mixed temperate forest <i>Jacqueline Rosette, Peter North, Juan Suárez and Sietse Los</i> | 180 |
| A Monte Carlo radiative transfer model of satellite waveform lidar <i>Peter North, Jacqueline Rosette, Juan Suárez and Sietse Los</i> | 189 |
| Assessing the accuracy of forest height estimation with long pulse waveform lidar through Monte-Carlo ray tracing <i>Steven Hancock, Philip Lewis, Mathias Disney, Mike Foster and Jan-Peter Muller</i> .. | 199 |
| Model Effects on GLAS-based regional estimates of forest biomass and carbon <i>Ross Nelson</i> | 207 |
| 3D segmentation and classification of single trees with full waveform LIDAR data <i>Josef Reitberger, Peter Krzystek and Uwe Stilla</i> | 216 |
| Area-based parameterization of forest structure using full-waveform airborne laser scanning data <i>Bernhard Höfle, Markus Hollaus, Hubert Lehner, Norbert Pfeifer and Wolfgang Wagner</i> | 227 |
| Session 5: Algorithm & techniques development | 236 |
| Estimation of effective plant area index using LiDAR data in forest of South Korea <i>Doo-Ahn Kwak, Woo-Kyun Lee and Hyun-Kook Cho</i> | 237 |
| Comparing discrete echoes counts and intensity sums from ALS for estimating forest LAI and gap fraction <i>Svein Solberg</i> | 247 |
| Modelling multi-spectral LIDAR vegetation backscatter – assessing structural and physiological information content <i>Felix Morsdorf, Caroline Nichol, Tim Malthus, Genevieve Patenaude and Iain Woodhouse</i> | 257 |
| Diameter distribution modelling using ALS <i>Johannes Breidenbach, Christian Gläser and Matthias Schmidt</i> | 266 |

| | |
|--|-----|
| A new automated approach for co-registration of national forest inventory and airborne laser scanning data <i>Wouter Dorigo, Markus Hollaus, Klemens Schadauer and Wolfgang Wagner</i> | 274 |
| Probability models for individually segmented tree crown images in a sampling context <i>James Flewelling</i> | 284 |
| Session 6: Terrestrial laser scanning & laser cameras | 294 |
| Single-scan TLS methods for forest parameter retrieval <i>Paula Litkey, Xinlian Liang, Juha Hyypä, Antero Kukko, Harri Kaartinen and Markus Holopainen</i> | 295 |
| Impact of the sampling design on the quality of ground-based LiDAR datasets <i>Dimitry Van der Zande, Inge Jonckheere, Jan Stuckens, Willem Verstraeten and Pol Coppin</i> | 305 |
| Accuracy and efficiency of the Laser-camera <i>Timo Melkas, Mikko Vastaranta and Markus Holopainen</i> | 315 |
| Spatial quantification of vegetation density from terrestrial laser scanner data for characterization of 3D forest structure at plot level <i>Sylvie Durrieu, Tristan Allouis, Richard Fournier, Cédric Véga and Laurent Albrech</i> | 325 |
| Terrestrial laser scanners to measure forest canopy gap fraction <i>F. Mark Danson, R.P. Armitage, V. Bandugula, F.A. Ramirez, N.J. Tate, K.J. Tansey and T. Tegzes</i> | 335 |
| Poster presentations | 342 |
| Extraction of vegetation for topographic mapping from full-waveform airborne laser scanning data <i>Cici Alexander, Kevin Tansey, Nicholas Tate, Sarah Smith-Voysey and Jörg Kaduk</i> ... | 343 |
| Use of airborne LIDAR in the estimation of individual tree heights in natural forest <i>Marcos Vinicius Giongo Alves, Ugo Chiavetta, Gherardo Chirici and Marco Marchetti</i> | 354 |
| LINHE Project: development of new protocols for the integration of digital cameras and LiDAR, NIR and Hyperspectral sensors <i>R. Antolín, C. Calzado-Martínez, A. Gómez, J.A. Manzanera, J.E. Meroño, D. Pedrazzani, H.H. Pérez, A. Roldán-Zamarrón, I. Santos and R. Valbuena</i> | 355 |
| A proposed approach incorporating lidar and aerial imagery for large area estimates of lodgepole pine (<i>Pinus contorta</i>) volume killed by mountain pine beetle (<i>Dendroctonus ponderosae</i>) <i>Christoher W. Bater, Nicholas C. Coops, Michael A. Wulder and Joanne C. White</i> ... | 365 |

| | |
|--|-----|
| Estimation of bivariate diameter and height distributions using ALS <i>Johannes Breidenbach, Christian Gläser and Matthias Schmidt</i> | 366 |
| Monitoring capercaillie habitat using ALS <i>Johannes Breidenbach and Veronika Braunsch</i> | 373 |
| Characterization of forest stands using full waveform laser scanner and airborne hyperspectral data <i>Henning Buddenbaum and Stephan Seeling</i> | 377 |
| Ticking all the boxes: the added value of heritage surveys of woodland by LiDAR <i>P. Crow, B.J. Devereux and G.S. Amable</i> | 384 |
| Small footprint, full waveform LiDAR modelling of canopy 3d structure in complex, semi-natural woodland communities <i>B.J. Devereux, G.S. Amable, J. Liadsky and P. Crow</i> | 386 |
| Estimating forest biomass in mixed broad-leaved forests of the Italian pre-Alps <i>Sara Fusco, Dirk Pflugmacher, Alan Kirschbaum, Warren Cohen, Donato Chiatante and Antonio Montagnoli</i> | 387 |
| A comparison of Gradient Nearest Neighbor and Most Similar Neighbor imputation methods to map forest cover types of Western Oregon <i>Donald Gagliasso and Hailemariam Temesgen</i> | 388 |
| Remote mining: from clustering to DTM <i>Jorge García-Gutiérrez, Francisco Martínez-Álvarez, Daniel Laguna-Ruiz and José Carlos Riquelme</i> | 389 |
| Planimetric offset adjustment of multitemporal laser scanner data <i>Mariano García, Elena Prado, David Riaño, Emilio Chuvieco and Mark Danson</i> | 398 |
| LiDAR mapping of canopy gaps in continuous cover forests; a comparison of canopy height model and point cloud based techniques <i>Rachel Gaulton and Tim J. Malthus</i> | 407 |
| Integration of intensity information and echo distribution in the filtering process of LIDAR data in vegetated areas <i>Jens Goepfert, Uwe Soergel, and Alexander Brzank</i> | 417 |
| Land cover classification of rural areas using LiDAR data: a comparative study in the context of fire risk <i>Gil Gonçalves, Luís Gonçalves-Seco, Fabian Reys and David Miranda</i> | 427 |
| Using LiDAR technology in forestry harvest planning <i>David González, Julio Becker, Eduardo Torres, José Albistur, Manuel Escudero, Rodrigo Fuentes, Helio Hinojosa and Felipe Donoso</i> | 437 |

| | |
|--|-----|
| Using LIDAR and Normalized Difference Vegetation Index to remotely determine LAI and percent canopy cover <i>Griffin Alicia, Popescu Sorin and Zhao Kaiguang</i> | 446 |
| Using airborne LiDAR and Landsat data to derive biomass at regional scale in the Canadian northern boreal forest <i>L. Guindon, Andre Beaudoin, Ross Nelson and J. Boudreau</i> | 456 |
| Utilization of tree species stratum data in forest planning simulations <i>Markus Holopainen, Antti Mäkinen, Mikko Vastaranta, Jussi Rasinmäki, Juha Hyypä, Hannu Hyypä and Petri Rönnholm</i> | 458 |
| Accuracy of automatic tree extraction using airborne laser scanner data <i>Harri Kaartinen, Juha Hyypä, Xinlian Liang, Paula Litkey, Antero Kukko, Xiaowei Yu, Hannu Hyypä and Markus Holopainen</i> | 467 |
| Distinguishing between live and dead tree biomass on North Rim of the Grand Canyon with lidar data <i>Yunsuk Kim, Zhiqiang Yang, Warren B Cohen, and Chris Lauver</i> | 477 |
| Detection of weak and overlapping pulses from waveform airborne laser scanning data <i>Yu-Ching Lin, Jon Mills and Sarah Smith-Voysey</i> | 478 |
| Estimation of tree lists from airborne laser scanning data using a combination of analysis on single tree and raster cell level <i>Eva Lindberg, Johan Holmgren, Kenneth Olofsson, Jörgen Wallerman and Håkan Olsson</i> | 488 |
| Observational evidence for links between increased drought severity and land-cover change <i>Sietse Los, Jacqueline Rosette and Peter North</i> | 497 |
| An analysis of the relationships between tree growth and crown information derived from airborne LiDAR data <i>Tohru Nakajima, Yasumasa hirata, Takuya Hiroshima, Naoyuki Furuya, and Satoshi Tatsuharas</i> | 498 |
| An improved method of individual tree detection using airborne LiDAR <i>Katsumasa Oono, Yoichi Numata and Atsushi Hirano</i> | 508 |
| Mean height and variability of height derived from lidar data and Landsat images relationship <i>Cristina Pascual, Warren Cohen, Antonio García-Abril, Lara Arroyo, Rubén Valbuena, Susana Martí-Fernández and José Antonio Manzanera</i> | 517 |
| The comparison of airborne laser scanning-based probability layers as auxiliary information for assessing coarse woody debris <i>Annikka Pesonen, Matti Maltamo, Petteri Packalén and Olli Leino</i> | 526 |

| | |
|--|-----|
| Regional applicability of forest height and aboveground biomass models for the Geoscience Laser Altimeter System <i>Dirk Pflugmacher, Warren B. Cohen, Robert E. Kennedy and Michael A. Lefsky</i> | 536 |
| Neural network and quad-tree approach to extract tree position and height from LiDAR data <i>Francesco Pirotti</i> | 537 |
| Tree filtering for high density airborne LiDAR data <i>M.Z.A. Rahman and B. Gorte</i> | 544 |
| Individual tree recognition using LIDAR and aerial images: preliminary results <i>Ramon Riera, Mario Lamfri and Cristina Vega-García</i> | 554 |
| Methods for improving the quality of a true orthomosaic of Vexcel UltraCam images created using a lidar digital surface model <i>Benoît St-Onge</i> | 555 |
| Quality assurance and quality control procedures of airborne scanning LiDAR for a nation-wide carbon inventory of planted forests <i>Peter Stephens, Robert McGaughey, Timothy Dougherty, Tim Farrier, Bridget Geard and David Loubse</i> | 563 |
| Combining airborne laser scanning and GIS data to estimate timber volume of forest stands based on yield models <i>Christoph Straub, Matthias Dees, Holger Weinacker and Barbara Koch</i> | 572 |
| A practical application of airborne LiDAR for forestry management in Scotland <i>Juan Suárez, Jacqueline Rosette, Bruce Nicoll and Barry Gardiner</i> | 581 |
| Red-cockaded Woodpecker (<i>Picoides borealis</i>) habitat analysis via remote sensing <i>Scott Tweddale, H. Alexis Londo, Joelle Carney, David Evans, Scott Roberts, Robert Parker and Stephen Grado</i> | 586 |
| Lidar and true-orthorectification of infrared aerial imagery of high <i>Pinus sylvestris</i> forest in mountainous relief Rubén Valbuena, Tomás Fernández De Sevilla, Francisco Mauro, Cristina Pascual, Antonio García-Abril, Susana Martín and José Antonio Manzanera | 596 |
| Comparison of different Laser-based methods to measure stem diameter <i>Mikko Vastaranta, Timo Melkas, Markus Holopainen, Harri Kaartinen, Juha Hyyppä and Hannu Hyyppä</i> | 606 |
| Estimating crown base height for Scots pine by means of the 3D geometry of airborne laser scanning data <i>Jari Vauhkonen</i> | 616 |

| | |
|---|-----|
| Potential and limits of extraction of forest attributes by fusion of medium point density LiDAR data with ADS40 and RC30 images <i>Lars Waser, Christian Ginzler, Meinrad Kuechler and Emmanuel Baltsavias</i> | 625 |
| Developing strategies for large scale forest inventories combining LiDAR data, satellite imagery and regional yield models <i>Markus Weidenbach, Roeland de Kok, Piotr Wezyk and Stanislaw Szombara</i> | 635 |
| Describing the selected canopy layer parameters of the Scots pine stands using ALS data <i>Wezyk Piotr, Tompalski Piotr, Marta Szostak, Marcin Pierzchalski and Mateusz Glista</i> | 636 |
| Author Index (first author only): | 646 |

Keynote Presentation 1

Advances in forest characterisation, mapping and monitoring through integration of LiDAR and other remote sensing datasets

Richard Lucas¹, Alex Lee², John Armston³, Johanna Breyer¹,
Peter Bunting¹ & João Carreiras⁴

¹Institute of Geography and Earth Sciences, Aberystwyth University, Aberystwyth,
Ceredigion, SY23 2EJ rml@aber.ac.uk

²Defence Imagery and Geospatial Organisation, Russell, Canberra, ACT 2600, Australia.
Alexander.Lee@defence.gov.au

³Joint Remote Sensing Research Program, Remote Sensing Centre, Department of
Natural Resources and Water, Climate Building, 80 Meiers Road, Indooroopilly,
Queensland, 4068, Australia john.armston@nrw.qld.gov.au

⁴Tropical Research Institute, Department of Natural Sciences, Rua João de Barros, 27,
Lisbon, Portugal. jmbcarreiras@gmail.com

Abstract

The diversity of scales and modes in which ground, airborne and spaceborne LiDAR operate has increased opportunities for quantitatively assessing forest structure, biomass and species composition and obtaining more general information on dynamics and ecological/commercial value. However, the level of information extracted can be increased even further by integrating data from other sensor types, including hyperspectral and Synthetic Aperture Radar (SAR). Examples include the generation of species-specific tree and stand level maps of biomass through inclusion of fine spatial resolution hyperspectral data and the use of LiDAR data and derived products for better interpreting the information content of SAR and optical data and parameterising models that simulate and assist understanding of the interaction of electromagnetic energy with forest components. Applications where synergistic use of LiDAR and other remote sensing data are advantageous include commercial forest inventory, quantifying carbon dynamics and biodiversity, and detecting change at scales from individual trees to landscapes. Recognition of the value of integrating other forms of remote sensing data with LiDAR is leading to the development of techniques for data fusion and also new synergistic sensors on platforms ranging from Unmanned Airborne Vehicles (UAVs) to satellites (e.g., DESDynI).

Keywords: LiDAR, hyperspectral, forests, biomass, structure, biodiversity, carbon

1. Introduction

For forest studies, ground-based, airborne and spaceborne LiDAR have been used primarily to retrieve basic structural attributes, including height, canopy cover and vertical profiles from which indirect measures (e.g., basal area, timber volume and biomass) have been derived (Lefsky *et al.*, 2005; Tickle *et al.*, 2006; Goodwin *et al.*, 2006; Brandtberg, 2007; Popescu and Zhao, 2008). Increasingly, however, studies are recognising or demonstrating that by integrating data from other sensors, including optical (e.g., hyperspectral) and Synthetic Aperture Radar (SAR), forests can be better characterised in terms of their structure, biomass and species composition (Hyde *et al.*, 2005; 2006; Chen *et al.*, 2007; Nelson *et al.*, 2007). Opportunities for detecting changes in these attributes over time and at various scales are also enhanced (Wulder *et al.*, 2007). Approaches to integration have varied but have typically involved combining data and derived products from other sensors to better quantify forest attributes (e.g., Hyde *et al.*, 2006; Nelson *et al.*, 2007; Lucas *et al.*, 2008) or using LiDAR-derived information to better

interpret data acquired by other sensors (e.g., Lucas *et al.*, 2006a; Simard *et al.*, 2008). Using our own case studies and based on a review of current literature, this paper provides an overview of such approaches and gives application examples relating to the inventory and conservation of forest resources. Future synergies of LiDAR and other forms of remote sensing data are noted, focusing particularly on integration techniques and the deployment of new platforms and sensors.

2. Measures derived using LiDAR data alone

Most early studies using LiDAR focused on retrieval of simple descriptors of forest structure (Table 1a), with the majority utilising height information in the form of canopy height surfaces/models interpolated from outer canopy point data. More recent studies have derived additional attributes (Table 1b), including diameter at breast height (DBH), basal area and density (Hudak *et al.*, 2008), timber volume and biomass (Naesset and Gobakken, 2008). In most cases, these attributes have been determined by establishing relationships with those directly measured (e.g., height or crown dimensions; Hyyppä *et al.*, 2001), summaries of the LiDAR data themselves (e.g., canopy geometric volume or profile area; Chen *et al.*, 2007; Wulder *et al.*, 2007), or LiDAR-based indices (e.g., the Height Scaled Crown Openness Index (HSCOI); Lee and Lucas, 2007).

Table 1: Examples of structural measures derived a) directly and b) indirectly from LiDAR data.

| a) | Attribute | b) | Attribute | Derived from: |
|----|-------------------------|-------------------------------------|-----------|---|
| | H ¹ | Diameter | | H or crown dimensions, HSCOI ² |
| | Crown/canopy cover | Basal area | | H or crown dimensions, CGV ³ |
| | Crown canopy depth | Volume | | CGV |
| | Crown/canopy profile | Biomass | | H, H-squared, HOME ⁴ |
| | Outer canopy ruggedness | | | canopy cover, depth volume, reflectance |
| | Gap fraction | Density | | HSCOI, counts of delineated crowns |
| | Forest type/species | LAI ⁵ , PAI ⁶ | | H or crown dimensions, profile area |
| | | FPC ⁷ | | Crown dimensions |

¹H, ²Height-Scaled Crown Openness Index, ³Canopy Geometric Volume,

⁴Height of median energy return, ⁵Leaf Area Index, ⁶Plant Area Index, ⁷Foliage Projected Cover.

A large number of studies have also identified and often adjusted for factors complicating retrieval including crown shape and leaf state (on/off; which vary within and between species), the location and spatial arrangement of trees within footprints of varying dimension, local slope, varying reflectivity of the ground and canopy, the LiDAR sampling intensity, atmospheric interference, and the reliability of ground measurement (e.g., Harding and Carabajal, 2005; Hyde *et al.*, 2005; 2006; Wulder *et al.*, 2007; Jang *et al.*, 2008; Reitberger *et al.*, 2008).

3. Terrestrial Laser Scanners and links with airborne LiDAR

Terrestrial Laser Scanners (TLS) provide detailed reconstructions of trunk, branch and leaf distributions from which tree locations, diameter and height (Maas *et al.*, 2008; Watt and Donoghue, 2005), timber volume by size class (Jupp *et al.*, 2005), and canopy gap fraction (Danson *et al.*, 2007; Henning and Radtke, 2006) can be quantified. Potential exists also for retrieving the woody biomass of individual trees, either by considering the sizes of the stems scanned or multiplying the volume of scanned branches and trunks by wood density. Although limited by survey times and occlusion as a function of stand density, TLS provide a permanent record of forest structure. A close correspondence between forest height (Breyer, 2008) and, to a

lesser extent, foliage profiles (Jupp *et al.*, 2005) retrieved separately using co-registered TLS and airborne LiDAR has also been reported. Linking TLS data with other remote sensing datasets (e.g., airborne LiDAR) does however require a high level of geolocational accuracy (Figure 1). Hence, establishment of a comprehensive and precise network of ground survey points and the use of high quality Inertial Navigation System (INS) for airborne systems is essential if all scan points are to be correctly located in three-dimensional space.



Figure 1: Airborne (full waveform) LiDAR point cloud (grey) with a sub-plot acquired by TLS (white) included, Lake Vyrnwy, mid-Wales.

4. Linking fine spatial resolution multi/hyperspectral data

Studies are increasingly incorporating data acquired by finer (typically < 1 m) spatial resolution multi/hyperspectral airborne (e.g., Compact Airborne Spectrographic Imager; CASI) and/or spaceborne sensors (e.g., Quickbird) to enhance descriptions of forests. The desire to simultaneously acquire complementary LiDAR and multi/hyperspectral datasets has also led to sensors being flown on the same platform (e.g., the Carnegie Airborne Observatory (CAO); Asner *et al.*, 2008). More commonly, however, data are acquired using different platforms and on a similar or proximal date and algorithms for automatic rather than manual co-registration of data are then desirable.

Accurate co-registration of datasets significantly increases the diversity of information that can be extracted. St-Onge *et al.* (2008), for example, used a LiDAR-derived digital terrain model (DTM) as a base for increasing the accuracy of tree height estimates generated from historical stereo aerial photography. Within co-registered datasets, stand density can be estimated by counting a) extracted high points in LiDAR or ‘bright points’ in multi/hyperspectral data (Wulder *et al.*, 2000) and/or b) tree crowns/clusters delineated using algorithms ranging from valley following to template matching (Bunting and Lucas, 2006). For open forests and orchard sites, retrieval accuracies have exceeded 70 % (Lee and Lucas, 2007) and 99 % (Jang *et al.*, 2008) respectively. The advantage of having co-registered datasets is that trees identified within one can be attributed with measures (e.g., height or species; Chen *et al.*, 2007) from the other, thereby leading to better descriptions of the forest. As an example, Bunting and Lucas (2006) applied an algorithm developed within Definiens Developer software and CASI data to delineate tree crowns of varying dimension. Once delineated, crowns were associated with a species type using spectra extracted from the sunlit portions as input to a linear discriminant function. A subsequent step then applied species-specific allometric equations relating LiDAR-derived height to the above ground and component (leaf, branch and trunk) biomass (Figure 2). Whilst performing well for isolated trees, the biomass was found to be over-estimated where trees with large expansive crowns occurred but was under-estimated where stem density was high (more than several per m^2). Whilst hyperspectral data provide superior classifications of tree species, several studies have discriminated species or broad forest types using LiDAR intensity data (Antonarakis *et al.*, 2008), relative height differences between

the first and last vegetation returns (Moffiet *et al.*, 2005) and directed graphs (Brandtberg, 2007). Holmgren *et al.* (2008) reported, however, best discrimination when using a combination of LiDAR and multi-spectral data.

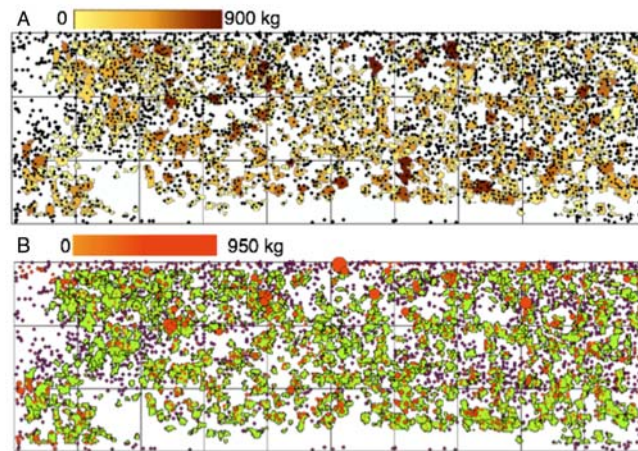


Figure 2: Estimates of A) branch and B) trunk biomass generated using a combination of LiDAR and CASI data. Dots/red circles indicate trunk locations (Lucas *et al.*, 2008a).

5. LiDAR for interpreting SAR data

5.1 Empirical relationships established between SAR and LiDAR-derived data

As with LiDAR, SAR is an active sensing technique and as emitted wavelengths at different frequencies and polarisations interact with components of the forest volume, the backscattered intensity relates partly to the overall structure and biomass of the forest. LiDAR-derived estimates of biomass and structural attributes can provide a basis for supporting the development of SAR-based retrieval algorithms, particularly as field-based measurements are often limited in amount and spatial distribution. As an example, and focusing on wooded savannas in Australia, Lucas *et al.* (2006a) established a relationship between LiDAR metrics and biomass ($r^2 = 0.92$). Relationships established subsequently between the LiDAR derived biomass and airborne SAR backscatter at different frequencies and polarisations (and for the equivalent of 4500 0.25 ha plots) then revealed differences in the saturation of backscatter above certain thresholds of biomass between SAR channels and suggested that L-band (~ 25 cm wavelength) cross polarised data acquired at incidence angles $> \sim 40^\circ$ provided the best option for biomass retrieval. The LiDAR-derived estimates of biomass also provided opportunities to evaluate existing biomass retrieval algorithms. For example, Le Toan (2008) proposed a Bayesian approach that utilised *a priori knowledge* of forest biomass to increase the accuracy of biomass retrieval and quantify uncertainties such that:

$$P(B | \gamma^0) \propto P(\gamma^0 | B).P(B) \quad \text{Equation 1.}$$

where $P(B|\gamma^0)$ is the probability of biomass given a value of backscatter (γ^0 ; γ^0) and $P(\gamma^0|B)$ is the probability of γ^0 given a value of biomass. In the case of woody savannas, the *a priori* information was obtained from the Gaussian probability distribution function for biomass ($P(B)$) derived from the LiDAR data. The algorithm of Saatchi *et al.* (2007) uses L and/or P-band (~ 68 cm wavelength) data to separately estimate the biomass of the trunk and crown, which are then summed to give total above ground biomass. This model was newly parameterised for wooded savannas by applying crown:trunk ratios to the LiDAR-derived biomass as a function of species type (e.g., conifer, eucalypt, acacia), as described using co-registered stereo aerial photography (Tickle *et al.*,

1996). The resulting model coefficients were then used to map biomass across the landscape, with best retrieval obtained using a combination of L-band (trunk biomass) and L- and P-band (crown biomass). By using these same biomass data, but adjusting for clearing since 2000 using time-series of Landsat sensor data, a modified version of the Saatchi *et al.* (2007) model was developed that used L-band dual polarimetric data acquired in 2007 from the Advanced Land Observing Satellite (ALOS) Phased Arrayed L-band SAR (PALSAR) as input. For regional application, further calibration and validation and consideration of a greater range of forest structural types is necessary. For this purpose, the Queensland Department of Natural Resources and Water (QDNRW) previously acquired discrete return LiDAR data for sites across Queensland ranging from sparse woodlands to dense tropical rainforests. Whilst biomass has yet to be estimated from these data, a close correspondence between LiDAR-derived attributes including height, foliage projected cover (FPC) and crown density and ALOS PALSAR data has been observed (Figure 3; Armston *et al.*, 2008) suggesting that characterisation and mapping across the wider landscape is achievable from regional coverages.

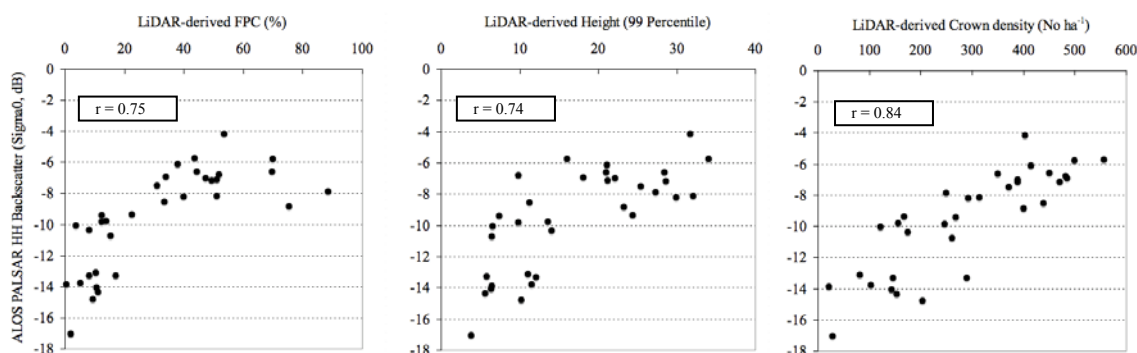


Figure 3: Correlations of PALSAR L-band HH σ^0 against LiDAR-derived overstorey structural attributes for 33 sites randomly sampled from the area of 19 LiDAR surveys covering open and closed forests.

5.2 Retrieval through integration of LiDAR and SAR

Whilst some success has been achieved in retrieving biomass and structural attributes from both SAR intensity data and LiDAR, the mechanism of retrieval differs because of the modes of observation. Within SAR data, the increase in backscatter with biomass, for example, is largely a consequence of the greater number, diversity and size of scatterers (leaves, branches, trunks) within the forest volume. Within LiDAR, biomass is retrieved because of an inherent relationship with height and also the canopy volume. As these sensors are responding to different elements of the forest volume, additional information might be retrieved through their combination. A useful example is that of high (e.g., > 15 m) mangroves dominated by *Rhizophora stylosa*. These mangroves exhibit a SAR backscatter (L- and P-band) that approaches that of non-forest because of microwave attenuation by the extensive root system (Lucas *et al.*, 2007). However, by integrating height information (e.g., from LiDAR), these mangroves can be identified as being of high biomass. Nelson *et al.* (2007) compared the retrieval of biomass using LiDAR and SAR (multi-angle BioSAR), concluding that whilst better retrieval was obtained when in combination, the small improvement over the use of LiDAR alone may not justify the increased resources required. Nevertheless, their combined use was considered to have greatest potential in retrieving the biomass of high biomass forests with excurrent growth forms.

5.3 Parameterisation of radar simulation models.

Radar simulation models are used primarily to understand the interaction of microwaves with different components of the forest volume and also the ground surface. These models are

typically two-dimensional and assume a random distribution of elements (e.g., disks or cylinders representing leaves and branches respectively). Comparisons between actual and simulated backscatter provided an indication of how well the SAR data are simulated and also permit then the signal to be decomposed such that the contributions from the different scattering mechanisms (e.g., trunk-ground) to the overall backscatter can be better quantified and understood. More recently, models that consider the distribution of elements in three-dimensional space have been established, but often the scattering elements are assumed to be distributed randomly within the volume space. However, LiDAR provides the opportunity to establish more precisely the location of scattering elements, which is particularly useful where the distribution is clumped rather than random. As an example, Lucas *et al.* (2006b) parameterised a coherent SAR image simulation model with structural attributes derived from discrete return LiDAR data. Key elements of the parameterisation involving LiDAR were a) the identification of stem locations based on low values within a Height Scaled Crown Openness Index (HSCOI) surface and estimation of biomass (based on allometric equations applied to diameter, as estimated from a relationship with the HSCOI, and/or height), b) the generation of voxels based on the three-dimensional distribution and frequency of LiDAR returns within 1 m³ integer intervals from ground level to the maximum height of the stand and assignment of an estimate of leaf and tertiary branch biomass (derived from allometrics and based on the number of voxels associated with each stem), and c) the approximation of primary and secondary branch locations based on position, distance and angle from the main stem and primary branches respectively and an association with volume based on logical rules. Ground surface parameters were also determined from the LiDAR digital terrain model (DTM). A close correspondence was observed between simulated and actual (AIRSAR) data, suggesting effective modelling of the SAR backscatter. The model is now available within the European Space Agency (ESA) software package POLSARPRO (<http://earth.esa.int/polsarpro/>). Whilst parameterisation is complex, the approach provides considerable insight into the interaction of microwaves with different components of the forest volume.

5.4 Evaluation of InSAR and polInSAR data based on LiDAR

As with LiDAR data, there is increasing demonstration of the potential of retrieving information on the distribution of scattering elements within the vertical profile of forests using SAR (repeat or single pass) interferometry (InSAR) and polarimetric SAR interference (PolInSAR). A particular advantage of such approaches is that the coverage of SAR is much greater compared to LiDAR (Hyde *et al.*, 2006; Baltzer *et al.*, 2007). Nevertheless, LiDAR data can play a key role in the verification of retrieved profiles (Slatton *et al.*, 2001), thereby leading to fine-tuning of algorithms. LiDAR can also provide a yardstick for assessing the retrieval of structural attributes from other sensors. For example, several studies have demonstrated differences of only a few metres in the errors associated with height retrieval from InSAR and LiDAR (e.g., Baltzer *et al.*, 2007, Breidenback *et al.*, 2008). Hyde *et al.* (2006) also suggested that InSAR was best suited for structurally homogeneous forests and that LiDAR provided better estimates of the height of larger trees.

6. Application examples

Relative to optical and SAR data sources, LiDAR technology is a new advance in the remote sensing of forests. As costs were high and the logistics of acquisition were complex, initial activities were concentrated largely in the research and government sectors, which were also in a better position to advance the development and evaluation of new sensor types (e.g., LVIS, SLICER). However, with the increased availability of commercial LiDAR (terrestrial and airborne) and freely accessible spaceborne LiDAR combined with an increasing capacity to integrate data from other sensors, significant expansions in both research and operational applications have occurred in recent years. The following sections give a brief overview of several applications.

6.1 Commercial forestry

The uptake of LiDAR for operational forestry applications has, until recently, been relatively low in many countries because of the perceived inability to retrieve the same level of information obtained through traditional forest survey techniques, the high costs involved, and also the lack of expertise within the intended user community (Suarez *et al.*, 2005). The uptake of LiDAR is, however, variable with Naesset *et al.* (2004) and Nelson *et al.* (2007) noting an increasing number of organisations using these data routinely for forest structural measurement and management planning, particularly in Scandinavia and North America. Furthermore, recognition of the wide range of information that can now be obtained from LiDAR (e.g., DTMs, forest structure and the identification of areas that cannot be logged such as habitat trees and riparian zones) and the potential of integrating with other remote sensing datasets has led to an increase in utilisation in many countries.

6.2 Carbon stocks and dynamics

The retrieval of biomass (carbon) from LiDAR metrics through empirical relationships with field measurements has been demonstrated in many studies (Culvenor *et al.*, 2005; Naesset and Gobakken, 2008; Lim and Treitz, 2004) and such estimates can potentially support carbon trading and national accounting (Patenaude *et al.*, 2004). As examples, Naesset and Gobakken (2008) used LiDAR-retrieved canopy height and density to estimate the biomass of boreal forests in Norway. Lefsky *et al.* (2005) integrated time-series of Landsat sensor data to age stands and, in conjunction with LiDAR-derived stem height and biomass, generated estimates of wood Net Primary Productivity (NPP). Using LiDAR combined with Landsat and SPOT sensor data in New Zealand (Ministry of the Environment, 2008), estimates of carbon stocks for extensive areas of forest have been generated as part of a national sampling program of greenhouse gas emissions monitoring. By contrast, the Australian National Carbon Accounting System (Brack *et al.*, 2006) has not integrated LiDAR data to the same extent because of the difficulty of calibration associated with the complexity of forests structures. Nevertheless, the potential benefits of using LiDAR for calibrating other forms of remote sensing data and supporting carbon accounting and reporting schemes in many countries have been recognised.

6.3 Biodiversity assessment

The high diversity of fauna and non-tree flora associated with forests is attributable to the diversity of habitats, which, in part, is reflected in the spatial distribution and arrangement of structural elements within the volume space that trees create and occupy. Several studies have noted that the distribution and richness of bird species in particular are closely linked to forest canopy structure (Hyde *et al.*, 2005) and heterogeneity (Goetz *et al.*, 2007), both of which can be quantified using airborne LiDAR. Hill *et al.* (2005) and Hinsley *et al.* (2006) also reported a link between habitat quality (defined by forest canopy structure and height) and the breeding success of Great Tits (*Parus major*). Such assessments might be improved by integrating information on tree species and the age and condition of stands, as obtained using, for example, multi/hyperspectral data (Hill and Thomson, 2005). Most studies focusing on biodiversity are confined to relatively small areas because of the limited coverage of airborne acquisitions. Extrapolation to regional areas requires the establishment of forest height and structural maps over larger areas, which can potentially be generated using SAR interferometry and/or IceSAT data. Such information would complement habitat maps generated at a commensurate scale using airborne/spaceborne optical datasets.

6.4 Environmental change

The detection of changes in forest cover (deforestation, degradation and regeneration/afforestation) using LiDAR is limited primarily by spatial coverage and the cost of

data acquisition. Nevertheless, the requirement for change mapping based on such data is compelling. Within Australia, trees of certain species identified in 2000 from a combination of LiDAR and hyperspectral data were noted to have died back in 2006, partly because of the intense drought (Lucas *et al.*, 2008b). This dieback has been observed previously over large areas and so repeat acquisition by both sensors and subsequent assessment of changes in structure, biomass and species can inform on the impacts of adverse change but also better understand how these might be detected using sensors with wider spatial coverage (e.g., ALOS PALSAR). Wulder *et al.* (2007) compared two profiling LiDAR transects 600 km in length across boreal forests in Canada in 1997 and 2002, indicating that global comparisons of structural attributes were less informative than spatially explicit comparisons undertaken for local areas (in this case, defined by segmenting Landsat ETM+ data). The local approach allowed LiDAR profiles to be treated as samples of a population, with the latter defined as a Landsat segment, thereby avoiding the issue of geolocation error. This study also raised the issue that long time-periods between comparisons are often required for monitoring certain processes such as vegetation growth and dieback in response to climate change. This has further implications for comparison of different LiDAR datasets as recent years have seen a rapid advancement of LiDAR technology from single discrete return profiling instruments to full waveform small-footprint scanning systems (e.g. Wagner *et al.*, 2004). Therefore, care needs to be taken when using different airborne LiDAR systems for monitoring because geolocation errors and different acquisitions specifications of the LiDAR surveys may cause differences in estimates of structural attributes that are not the result of real change (Goodwin *et al.*, 2006; Wulder *et al.*, 2007).

7. Overview and future opportunities

Through a series of case studies and with reference to the published literature, this review has highlighted the benefits of integrating LiDAR with other remote sensing datasets for furthering the characterisation, mapping and monitoring of forests at a range of scales. In particular, the integration of datasets can lead to a) an increase in the diversity and accuracy of information on forest structure, biomass and species composition and change, particularly at the individual tree and stand level, b) a greater capacity to establish empirical models with moderate to coarse spatial resolution (e.g., spaceborne optical and SAR) data, thereby facilitating retrieval across wider areas, c) unique opportunities for providing detailed parameterisation of simulation models that can be used to better understand the interaction of electromagnetic energy with forest components and/or be inverted to allow retrieval of a greater range of biophysical properties from remote sensing data (Koetz *et al.*, 2006), and d) greater provision of data or derived products for inclusion within multi-sensor biophysical retrieval algorithms.

Recognition of the benefits of data integration has led to the design of sensors that combine LiDAR with other optical or multi-angular (e.g., Carbon3D) or radar sensors (e.g., DESDynI) and also the development of systems (e.g., The Carnegie Airborne Observatory) and new platforms (e.g., Unmanned Airborne Vehicles) with capacity to support both LiDAR and multi/hyperspectral sensors. Such developments are anticipated to lead to a greater uptake of LiDAR for a range of applications. Advances in approaches to the integration of such data (e.g., automated registration) and algorithms for retrieving biophysical attributes of forests have also been ongoing and are anticipated to lead to their greater use within forest-related applications.

References

- Antonarakis, A.; Richards, K. & Brasington, J. 2008. Object-based land cover classification using airborne LiDAR, *Remote Sensing of the Environment* 112(6), 2988-2998.
- Armston, J., R. Lucas, J. Carreiras, P. Bunting, 2008. A first look at integrating ALOS PALSAR and Landsat data for assessing woody vegetation in Queensland. *Proceedings, 14th Remote*

- Sensing and Photogrammetry Conference*, Darwin (in press)
- Asner, G., Knapp, D. & Kennedy-Bowdoin, T., 2008. Invasive species detection in Hawaiian rainforests using airborne imaging spectroscopy and LiDAR. *Remote Sensing of the Environment* 112(5), 1942-1955.
- Balzter, H., Luckman, A., Skinner, L., Rowland, C. & Dawson, T., 2007. Observations of forest stand top height and mean height from interferometric SAR and LiDAR over a conifer plantation at Thetford Forest, UK, *International Journal of Remote Sensing* 28(6), 1173-1197.
- Brandtberg, T., 2007. Classifying individual tree species under leaf-off and leaf-on conditions using airborne lidar, *ISPRS Journal of Photogrammetry and Remote Sensing* 61(5), 325-340.
- Brack, C. L., Richards, G. & Waterworth, R., 2006. Integrated and comprehensive estimation of greenhouse gas emissions from land systems. *Sustainability Science* 1, 91-106.
- Breidenbach, J., Koch, B. & Kandler, G., 2008. Quantifying the influence of slope, aspect, crown shape and stem density on the estimation of tree height at plot level using lidar and InSAR data, *International Journal of Remote Sensing* 29(5), 1511-1536.
- Breyer, J., 2008, 3-D Biodiversity Networks, PhD thesis, Institute of Geography and Earth Sciences, Aberystwyth University.
- Bunting, P. & Lucas, R. M., 2006. The delineation of tree crowns in Australian mixed species forests using hyperspectral Compact Airborne Spectrographic Imager (CASI) data, *Remote Sensing of the Environment* 101, 230 - 248.
- Chen, Q., Gong, P., Baldocchi, D. & Tian, Y., 2007. Estimating basal area and stem volume for individual trees from lidar data, *Photogrammetric Engineering and Remote Sensing* 73(12), 1355-1365.
- Culvenor, D., Jupp, D. L. B., Lovell, J. & Newnham, G., 2005. Evaluation and validation of canopy laser radar systems for native and plantation forest inventory, Australian Government: Forest and Wood Products Research and Development Corporation.
- Danson, F., Hetherington, D., Morsdorf, F., Koetz, B. & Allgoewer, B., 2007. Forest Canopy Gap Fraction from Terrestrial Laser Scanning, *IEEE Geoscience and Remote Sensing Letters* 4(1), 157-160.
- Goetz, S., Steinberg, D., Dubayah, R. & Blair, B. J., 2007. Laser remote sensing of canopy habitat heterogeneity as a predictor of bird species richness in an eastern temperate forest, USA, *Remote Sensing of the Environment* 108, 254-263.
- Goodwin, N., Coops, N. & Culvenor, D., 2006. Assessment of forest structure with airborne LiDAR and the effects of platform altitude, *Remote Sensing of the Environment* 103(2), 140-152.
- Harding, D. J. & Carabjal, C. C., 2005. ICESat waveform measurements of within-footprint topographic relief and vegetation vertical structure, *Geophysical Research Letters* 32.
- Henning, J. & Radtke, P., 2006. Ground-based laser imaging for assessing three-dimensional forest canopy structure, *Photogrammetric Engineering and Remote Sensing* 72(12), 1349-1358.
- Hill, R. A., Hinsley, S. A., Gaveau, D. L. A. & Bellamy, P. E., 2004. Predicting habitat quality for Great Tits (*Parus major*) with airborne laser scanning data, *International Journal of Remote Sensing* 25(22), 4851-4855.
- Hill, R. A. & Thomson, A. G., 2005. Mapping woodland species composition and structure using airborne spectral and LiDAR data, *International Journal of Remote Sensing* 26(17), 3763--3779.
- Hinsley, S., Hill, R., Bellamy, P. & Balzter, H., 2006. The Application of Lidar in Woodland Bird Ecology: Climate, Canopy Structure, and Habitat Quality, *Photogrammetric Engineering and Remote Sensing* 72(12), 1399-1406.
- Holmgren, J., Persson, A. & Soederman, U., 2008. Species identification of individual trees by combining high resolution LiDAR data with multi-spectral images, *International Journal of Remote Sensing* 29(5), 1537-1552.
- Hudak, A., Crookston, N., Evans, J., Hall, D. & Falkowski, M., 2008. Nearest neighbor

- imputation of species-level, plot-scale forest structure attributes from LiDAR data, *Remote Sensing of the Environment* 112(5), 2232-2245.
- Hyde, P., Dubayah, R., Peterson, B., Blair, J. B., Hofton, M., Hunsaker, C., Knox, R. & Walker, W., 2005. Mapping forest structure for wildlife habitat analysis using waveform lidar: Validation of montane ecosystems, *Remote Sensing of Environment* 96(3-4), 427-437.
- Hyde, P., Dubayah, R., Walker, W., Blair, B. J., Michelle, H. & Hunsaker, C., 2006. Mapping forest structure for wildlife habitat analysis using multi-sensor (LiDAR, SAR/InSAR, ETM+, Quickbird) synergy, *Remote Sensing of the Environment* 102, 63-73.
- Hyypä, J., Kelle, O., Lehtikoinen, M. & Inkinen, M., 2001. A segmentation-based method to retrieve stem volume estimates from 3-D tree height models produced by laser scanners, *IEEE Transactions in Geoscience and Remote Sensing* 39(5), 969-975.
- Jang, J., Payan, V., Viau, A. & Devost, A., 2008. The use of airborne lidar for orchard tree inventory, *International Journal of Remote Sensing* 29(6), 1767-1780.
- Jupp, D. L. B., Culvenor, D., Lovell, J. & Newnham, G., 2005. 'Evaluation and validation of canopy laser radar systems for native and plantation forest inventory', Australian Government: Forest and Wood Products Research and Development Corporation.
- Koetz, B., Morsdorf, F., Sun, G., Ranson, K., Itten, K. & Allgoewer, B., 2006. Inversion of a Lidar Waveform Model for Forest Biophysical Parameter Estimation, *IEEE Geoscience and Remote Sensing Letters*, 3(1), 49-53.
- Lee, A. & Lucas, R. M., 2007. A LiDAR derived canopy density model for tree stem and crown mapping in Australian woodlands, *Remote Sensing of the Environment* 111, 493-518.
- Le Toan. 2007. Technical Notes to ESA on Intensity Inversion (unpublished)
- Lefsky, M. A., Hudak, A. T., Guzy, M. & Cohen, W. B., 2005. Combining LiDAR estimates of biomass and Landsat estimates of stand age for spatially extensive validation of modelled forest productivity, *Remote Sensing of the Environment* 95(4), 549-558
- Lefsky, M.A., Harding, D.J., Keller, M., Cohen, W.B., Carabajal, C.C., Espirito-Santo, F.D.B., Hunter, M.O., Oliveira Jr., R., 2005. Estimates of forest canopy height and aboveground biomass using ICESat. *Geophysical Research Letters*, 32, L22S02, doi:10.1029/2005GL023971.)
- Lucas, R. M., Lee, A. & Bunting, P., 2008. Retrieving Forest Biomass through intergration of CASI and LiDAR data, *International Journal of Remote Sensing* 29(5), 1553-1577.
- Lucas, R.M., Cronin, N., Lee, A., Moghaddam, M., Witte, C. & Tickle, P. 2006a. Empirical relationships between AIRSAR backscatter and LiDAR-derived forest biomass, Queensland, Australia. *Remote Sensing of Environment*, 100, 407-425.
- Lucas, R. M., Lee, A. & Williams, M., 2006b. The role of LiDAR data in understanding the relationship between forest structure and SAR imagery, *IEEE Transactions in Geoscience and Remote Sensing*, 44(10), 2736-2754.
- Lucas, R.M., Mitchell, A.L., Rosenqvist, A., Proisy, C., Melius, A. and Ticehurst, C., 2007. The potential of L-band SAR for quantifying mangrove characteristics and change. Case studies from the tropics and subtropics. *Aquatic conservation: marine and freshwater ecosystems - Special Issue: Radar Applications for Wetlands Management*. 17, 245-264.
- Lucas, R. M., Lee, A. C. & Bunting, P. J., 2008a. Retrieving forest biomass through integration of CASI and LiDAR data. *International Journal of Remote Sensing* (in press).
- Lucas, R. M., Accad, A., Randall, L. & Bunting, P., 2008b. Assessing human impacts on Australian forests through integration of airborne/spaceborne remote sensing data. In: *Patterns and Processes in Forest Landscapes: Multiple Uses and Sustainable Management*. Ed. R. Laforzezza, J. Chen, G. Sanesi and T.R. Crow (Springer, in press).
- Maas, H., Bienert, A., Scheller, S. & Keane, E., 2008. Automatic forest inventory parameter determination from terrestrial laser scanner data, *International Journal of Remote Sensing* 29(5), 1579-1593.
- Ministry of the Environment, 2008. Looking at New Zealand's Land Use and Carbon Analysis System (LUCAS). url: <http://www.mfe.govt.nz/publications/climate/looking-at-lucas/looking-at-lucas-issue2.html> (accessed July, 2008).
- Moffiet, T., Mengersen, K., Witte, C., King, R., and Denham, R., 2005. Airborne laser scanning:

- Exploratory data analysis indicates potential variables for classification of individual trees or forest stands according to species. *ISPRS Journal of Photogrammetry and Remote Sensing*, 59(5), 289-309.
- Nelson, R. F., Hyde, P., Johnson, P., Emessiene, B., Imhoff, M. L., Campbell, R. & Edwards, W., 2007. Investigating RaDAR-LiDAR synergy in a North Carolina pine forest, *Remote Sensing of Environment* 110(1), 98-108.
- Næsset, E. & Gobakken, T., 2008. Estimation of above- and below-ground biomass across regions of the boreal forest zone using airborne laser, *Remote Sensing of the Environment* 112(6), 3079-3090.
- Næsset, E., Gobakken, T., Holmgren, J., Hyypä, J., Maltamo, M., Nilsson, M., Olsson, H., Persson & Söderman, U., 2004. Laser scanning of forest resources: the nordic experience, *Scandinavian Journal of Forest Research* 19(6), 482-499.
- Patenaude, G., Hill, R., Milne, R., Gaveau, D., Briggs, B. & Dawson, T., 2004. Quantifying forest above ground carbon content using LiDAR remote sensing, *Remote Sensing of the Environment* 93, 368-380.
- Popescu, S. & Zhao, K., 2008. A voxel-based lidar method for estimating crown base height for deciduous and pine trees, *Remote Sensing of the Environment* 112(3), 767-781.
- Reitberger, J.; Krzystek, P. & Stilla, U., 2008. Analysis of full waveform LiDAR data for the classification of deciduous and coniferous trees, *International Journal of Remote Sensing* 29(5), 1407-1431.
- Saatchi, S., Halligan, K., Despain, D. G. & Crabtree, R. L., 2007. Estimation of Forest Fuel Load From Radar Remote Sensing, *IEEE Transactions on Geoscience and Remote Sensing* 45, 1726 - 1740.
- Simard, M., Rivera-Monroy, V., Mancera-Pineda, J., Castaneda-Moya, E. & Twilley, R., 2008. A systematic method for 3D mapping of mangrove forests based on Shuttle Radar Topography Mission elevation data, ICESat/GLAS waveforms and field data: Application to Ciénaga Grande de Santa Marta, Colombia, *Remote Sensing of the Environment* 112, 2131-2144.
- Slatton, K., Crawford, M. & Evans, B., 2001. Fusing Interferometric Radar and Laser Altimeter Data to Estimate Surface Topography and Vegetation Heights, *IEEE Transactions on Geoscience and Remote Sensing* 39(11), 2470-2482.
- Suarez, J. C., Ontiveros, C., Smith, S. & Snape, S., 2005. Use of airborne LiDAR and aerial photography in the estimation of individual tree heights in forestry, *Computers and Geosciences* 31, 253-262.
- St-Onge, B., Vega, C., Fournier, R. & Hu, Y., 2008. Mapping canopy height using a combination of digital stereophotogrammetry and lidar, *International Journal of Remote Sensing* 29(11), 3343-3364.
- Sun, G. & Ranson, K. J., 2000. Modeling Lidar returns from forest canopies, *IEEE Transactions in Geoscience and Remote Sensing* 38(6), 2617-2626.
- Tickle, P.K., Lee, A., Lucas, R.M., Austin, J. and Witte, C., 2006. Quantifying Australian forest and woodland structure and biomass using large scale photography and small footprint Lidar. *Forest Ecology and Management*, 223 (1-3), 379-394.
- Wagner, W., Ullrich, A., Melzer, T., Briese, C. & Kraus, K., 2004. From single-pulse to full-waveform airborne laser scanners: potential and practical challenges, *IAPRS* 35(Part B), 201-206.
- Watt, P. & Donoghue, D., 2005. Measuring forest structure with terrestrial laser scanning, *International Journal of Remote Sensing* 26(7), 1437-1446.
- Wulder, M., Han, T.; White, J., Sweda, T. & Tsuzuki, H., 2007. Integrating profiling LIDAR with Landsat data for regional boreal forest canopy attribute estimation and change characterization, *Remote Sensing of the Environment* 110(1), 123-137.
- Wulder, M., Niemann, K. O. & Goodenough, D. G., 2000. Local maximum filtering for the extraction of tree locations and basal area for high spatial resolution imagery., *Remote Sensing of Environment* 73, 103-114.

Session 1: Forestry applications & inventory

Assessing effects of sample plot positioning errors on biophysical stand properties derived from airborne laser scanner data

T. Gobakken¹, E. Næsset¹

¹ Norwegian University of Life Sciences, Dep. of Ecology and Natural Resource Management - (terje.gobakken, erik.naesset)@umb.no

Abstract

Canopy height distributions were created from small-footprint airborne laser scanner data with an average sampling density of 0.9 points m² collected over 100 georeferenced field sample plots and 57 stands. Height percentiles, mean and maximum height values, coefficients of variation of the heights, and canopy density at different height intervals above the ground were computed from the laser-derived canopy height distributions of the first return data. The plot positions were altered randomly by means of Monte Carlo techniques. The standard deviation (SD) of the differences for various metrics derived from the canopy height distributions between incorrect plot positions and ground-truth positions were compared. The SD increased with increasing plot position error.

The effects of sample plot position error on the accuracy of mean tree height (h_L), stand basal area (G), and stand volume (V) predicted at stand level using a two-stage procedure combining field training data and laser data were assessed. The standard deviation of the differences increased with increasing plot position errors. Except for h_L the largest increase in median SD was found for mature forest on poor sites. The effects of plot position error seem to be more pronounced for G and V compared to h_L .

Keywords: Airborne laser scanner, GPS, position error, sample plot

1. Introduction

The aim of forest inventories at a property/compartments level is to provide data for forest planning and management, and they are often carried out according to an area-based approach, which implies that the individual forest stands are the basic units of the inventories. During the last 15-20 years, several experiments have been carried out in order to determine various biophysical stand properties, such as mean tree height, basal area, and timber volume based on airborne laser scanning (ALS) measurements (Means *et al.* 2000; Næsset 1997, 2002). The operational area-based forest stand inventory method adopted in Scandinavia utilizes mainly ALS data in a two-stage procedure proposed by Næsset and Bjercknes (2001) and Næsset (2002). In a first stage, georeferenced field training plots with corresponding ALS data are used to develop empirical relationships between various metrics derived from the laser data and biophysical properties measured in field. These relationships provide, in the second stage, corresponding predicted values of each stand from the laser data.

Thus, accurate geographical co-registration of ALS data and field plots is essential for accurate predictions of biophysical stand properties. If the remotely sensed data and the field data are poorly co-registered, the basic laser-derived metrics will be subject to errors. If the basic laser-derived metrics are subjected to errors, it is likely that also the resulting stand predictions of the biophysical variables will be affected. However, since the biophysical properties are predicted from equations that are combinations of several laser variables, the effects of position errors can hardly be quantified by just assessing effects of one laser-derived metric at a time.

The Global Position System (GPS) technology is usually applied to obtain the geographical location of the field observations. GPS can provide timely and accurate spatial data under “clear sky” conditions. However, in forested landscapes, biological and topographic obstacles tend to degrade GPS position accuracy. Sophisticated GPS receivers are expensive to acquire and the logistics and data management in differential positioning is time-consuming in forest inventory applications, particularly in remote areas where it takes time to collect data and maintain base reference stations far from the field locations in the forest. In an operational context, there is a trade-off between costs and accuracy. One would often seek an accuracy that is “good enough” in order to save costs and simplify the work. In Norway, for example, the GPS accuracy for the National forest inventory (NFI) plots is expected to be within 10 m for 99% of the plots (Gjertsen 2007).

Gobakken and Næsset (2008b) assessed the effects of positioning errors and sample plot size on biophysical stand properties derived from ALS. They found significant effects of plot position errors and the effects were larger for poor sites with more scattered trees compared to productive sites with denser canopies and more evenly distributed of the trees. However, the study was limited to only one test site. The present study was carried out to verify the main findings based on data from another forest area. Thus, the objectives of this study were to assess the effects of field plot position errors (1) on selected laser-derived metrics and (2) on three important biophysical stand properties of interest in forest inventories predicted from the ALS data, i.e., mean tree height, stand basal area, and timber volume. Nine different levels of field plot position errors were assessed. The position errors were analysed using Monte Carlo techniques. The accuracy of the predicted biophysical properties was evaluated using an independent validation dataset.

2. Method

2.1 Study area

A forest area in the municipality of Krødsherad (60°10'N 9°35'E, 130-660 m a.s.l.), of about 6500 ha was selected for this study. The main tree species in the area were Norway spruce (*Picea abies* (L.) Karst.) and Scots pine (*Pinus sylvestris* L.). Further details can be found in Næsset (2004). This study was based on two different field data sets, i.e., (1) sample plots and (2) forest stands. The sample plots were used to assess the effects of different laser point densities on laser-derived metrics and to develop regression models for the three biophysical properties of interest. The forest stands were used to assess how sample plot position error affected the stand predictions of the three biophysical properties.

2.2 Sample plots

In total, 100 sample plots were distributed systematically throughout the entire 6500 ha study area according to a regular grid. The plots were divided into three strata according to age class and site quality of the stands in which they were located. The area of the sample plots was 232.9 m². The measurements were carried out during the summer 2001 (Næsset, 2004b). On each plot, all trees with $d_{bh} > 10$ cm were callipered. The d_{bh} was recorded in 2 cm classes. Basal area (G) was computed as the basal area per hectare of the callipered trees. The heights of sample trees were measured by a Vertex hypsometer. Mean height of each plot was computed as Lorey's mean height (h_L), i.e., mean height weighted by basal area. Volume of each tree was computed by means of volume equations of individual trees (Brantseg, 1967; Braastad, 1966; Vestjordet, 1967) with height and diameter as predictor variables. Total plot volume (V) was computed as the sum of the individual tree volumes.

Finally, to synchronize the h_L , G , and V values to the date the laser data were acquired the individual plot values were prorated by means of growth equations (Blingsmo, 1984; Braastad,

1975; Braastad, 1980; Delbeck, 1965). The prorated values were used as ground-truth. A summary of the ground-truth sample plots data is displayed in Table 1. Differential Global Positioning System (GPS) and Global Navigation Satellite System (GLONASS) were used to determine the position of the centre of each sample plot.

2.3 Stand inventory

In total, 57 large test plots distributed on the three pre-defined strata located in subjectively selected stands were selected. Ground reference data for the test plots were collected during summer 2001 following similar measurement and computational procedures as for the sample plots, see above. Each plot was a quadrature or had a shape close to a quadrature, and the size ranged from 2869 to 4219 m². The large test plots are hereafter denoted as stands. A summary of the ground-truth stand data is displayed in Table 1.

Table1: Summary of field inventory of sample plots and stands ^a.

| Characteristic | Small plots (233 m ²) | | Stands | |
|---|-----------------------------------|--------|---------------|--------|
| | Range | Mean | Range | Mean |
| <u>Young forest – stratum I</u> | | (n=30) | | (n=19) |
| h_L (m) | 8.1 - 19.5 | 13.4 | 10.5 - 19.7 | 15.4 |
| G (m ² ha ⁻¹) | 6.4 - 62.4 | 25.0 | 12.0 - 41.9 | 27.3 |
| V (m ³ ha ⁻¹) | 26.8 - 617.6 | 182.4 | 64.0 - 329.6 | 212.5 |
| <u>Mature forest, poor site quality – stratum II</u> | | (n=37) | | (n=19) |
| h_L (m) | 9.9 - 25.4 | 15.5 | 12.2 - 20.1 | 15.6 |
| G (m ² ha ⁻¹) | 5.6 - 42.7 | 22.6 | 12.0 - 31.5 | 21.1 |
| V (m ³ ha ⁻¹) | 29.6 - 446.3 | 173.7 | 83.0 - 292.7 | 162.3 |
| <u>Mature forest, good site quality – stratum III</u> | | (n=33) | | (n=19) |
| h_L (m) | 15.0 - 26.0 | 21.0 | 15.7 - 24.4 | 20.3 |
| G (m ² ha ⁻¹) | 15.5 - 57.0 | 34.2 | 21.9 - 37.7 | 29.8 |
| V (m ³ ha ⁻¹) | 116.8 - 674.8 | 338.0 | 186.0 - 378.9 | 286.6 |

^a h_L =Lorey's mean height, G =basal area, V =volume.

2.4 Laser scanner data

A fixed-wing aircraft carried the ALTM 1210 laser scanning system (Optech, Canada). The laser scanner data were acquired in the period between 23 July and 1 August 2001 (cf. Næsset 2004). The average sampling density was 0.9 m². A complete post-processing of the laser data was undertaken by the contractor (Blom Geomatics, Norway). A triangulated irregular network (TIN) was generated from the planimetric coordinates and corresponding height values of the individual terrain ground points. All the return observations (points) were spatially registered to the DTM according to their coordinates. Terrain surface height values were computed for each point by linear interpolation from the DTM. The relative height of each point was computed as the difference between the height of the return and the interpolated terrain surface height. Only the first returns were used for further analysis. The first return data were spatially registered to the field plots and stands.

2.5 Simulation of plot position error

To investigate the effects of position errors on metrics derived from the laser data for each field plot, the position errors were simulated. This was done by introducing a horizontal shift in the

field plot coordinates from the ground-truth positions prior to extracting laser points inside the plots. Horizontal shifts from true positions of 0.5, 1, 2, 3, 4, 5, 10, 15, and 20 m, respectively, were used. For each of these nine fixed levels of position errors, the error-contaminated positions were computed 500 times in a Monte Carlo simulation by using a randomly selected angle. 500 repetitions were used so that we could control the random effects in the simulations.

2.6 Computations of laser metrics

For each sample plot and stand inventoried in field, height distributions were created for those laser points that were considered to belong to the tree canopy, i.e., points with a height value of >2 m. Canopy height percentiles at 10% (h_{10}), 50% (h_{50}), and 90% (h_{90}) were computed. In addition, also the maximum (h_{\max}) and mean values (h_{mean}), and the coefficient of variation (h_{cv}) of the canopy height distributions were computed. Furthermore, several measures of canopy density were derived. Canopy density was computed as cumulative densities of 10 different vertical layers of equal height (Næsset 2004). The height of each layer was defined as one tenth of the distance between the 95% percentile and the lowest canopy height (>2 m) (Gobakken and Næsset 2008a). The cumulative canopy densities were then computed as the proportions of laser echoes above layer # 0 (>2 m), 1, . . . , 9 to total number of echoes. The cumulative densities for layer # 1 (d_1), # 5 (d_5), and # 9 (d_9) were selected for further studies.

To assess how sample plot position error influenced on the stability of laser-derived metrics, differences between corresponding metrics derived for the plots with error-contaminated positions and in true positions were computed for each sample plot. The standard deviations of the differences were then calculated for each of the 500 repetitions in the Monte Carlo simulation. Separate comparisons were carried out for the three strata. Further explorative data analysis of the Monte Carlo repetitions was performed using graphical methods, i.e., box-and-whisker plots (R Development Core Team 2006; Tukey 1977).

2.7 Predictions of biophysical stand properties

To assess the accuracy of laser-based predictions of mean tree height, basal area, and volume based on different field plot position errors, we followed the two-step procedure proposed by Næsset & Bjercknes (2001) and Næsset (2002) (1) by relating the three biophysical properties of interest to the laser data of the sample plots using regression analysis, and (2) by applying the estimated regression models to predict corresponding values of the test stands. As an additional step, (3) the differences between predicted values of the biophysical stand properties and ground-truth values were computed. The standard deviations of the differences were also calculated. The predicted values were restricted to predefined reasonable maximum values for the forest area in question.

As a preparation for the simulations, we wanted to determine a fixed set of explanatory variables to avoid effects of altering the variables in the regression models. Thus, variables to be included in the models were determined using the ground-truth field plot positions. The estimation of regression models was based on the height and density-related metrics derived from the first return height distributions as candidate explanatory variables. In the regression analysis, multiplicative models were estimated as linear regressions in the logarithmic variables.

The effects of field plot position error on the estimation and prediction of biophysical stand properties were assessed by means of Monte Carlo techniques as described above. The entire sequence in steps (1)–(3) above was repeated 500 times for each of the nine plot position errors. Thus, 500×9 estimates of the mean differences between predicted biophysical stand properties and ground-truth values and corresponding estimates of the standard deviations of the differences were derived. As a reference, the mean differences and the SD values when using ground-truth plot positions were calculated for the respective strata.

3. Result

3.1 Effects of plot position error on the stability of laser-derived metrics

Figure 1 shows the standard deviation (SD) of the differences between corresponding laser-derived metrics computed for the plots in error-contaminated positions and in true positions for different forest types (strata I-III) over the 500 repetitions of erroneous positions using the Monte Carlo procedure. The standard deviation of the differences for the height percentiles (h_{10} , h_{50} , and h_{90}), the three height-related metrics maximum laser canopy height (h_{\max}), arithmetic mean laser canopy height (h_{mean}), and coefficient of variation of laser canopy heights (h_{cv}), and for the density-related metrics (d_1 , d_5 , and d_9) increased with increasing plot position error. The amount of extreme observations increased with increasing plot position error.

3.2 Effects of plot position errors on predicted biophysical stand properties

The effects of using regression models estimated from plots with error-contaminated positions were assessed by using the estimated regressions and the two-step procedure to compute stand mean values of the three biophysical properties in 57 forest stands. As a reference, differences were computed assuming true plot positions. Using ground true plot positions the mean differences for h_L , G , and V were -1.4, 9.7, and 9.5% for stratum I, -1.9, 3.4, and 4.3% for stratum II, and -1.3, 8.8, and 6.9% for stratum III, respectively. The box plots illustrating the results of the simulations with error-contaminated plot locations show that the variation in mean difference between the 500 Monte Carlo repetitions in general increased with increasing plot location errors even if the median mean difference decreased for some of the comparisons (Fig. 2, Left).

Using ground-truth plot positions, the standard deviations (SD) of the differences for h_L were 6.6, 3.5, and 3.2% for strata I, II, and III, respectively (Fig. 2, Right). The SDs were 14.5, 9.3, and 12.4% for G and 19.1, 10.2, and 12.7% for V for strata I, II, and III, respectively, using ground-truth plot positions. The standard deviation of the differences increased with increasing plot position errors. Except for h_L , the largest increase in median SD was found for mature forest on poor sites (stratum II). The effects of plot position error seem to be larger for G and V compared to h_L .

4. Discussion

The results in this study are in line with Gobakken and Næsset (2008b). The main findings in the present study were that on poor sites where there normally are few stems it is important to have accurate plot positions to obtain accurate estimates of V and G . Improved GPS positioning by e.g. longer time periods of GPS data collection might be considered for more variable forests in order to reduce positional errors. However, there will often be fewer biological obstacles providing good conditions for GPS data collection in open forests and normally relatively precise GPS positions would be expected in such forests compared to dense forests.

Furthermore, cost-plus-loss analyses (cf. Eid *et al.* 2004) where the total costs of the inventory as well as the expected economic losses as a result of future incorrect decisions due to errors in measurements are considered, should be applied to evaluate the effects of plot position error. Cost-plus-loss comparisons between inventories with different positional accuracies might find that the requirements for positional accuracy is lower in variable and open forests compared to fully stocked and more even forests.

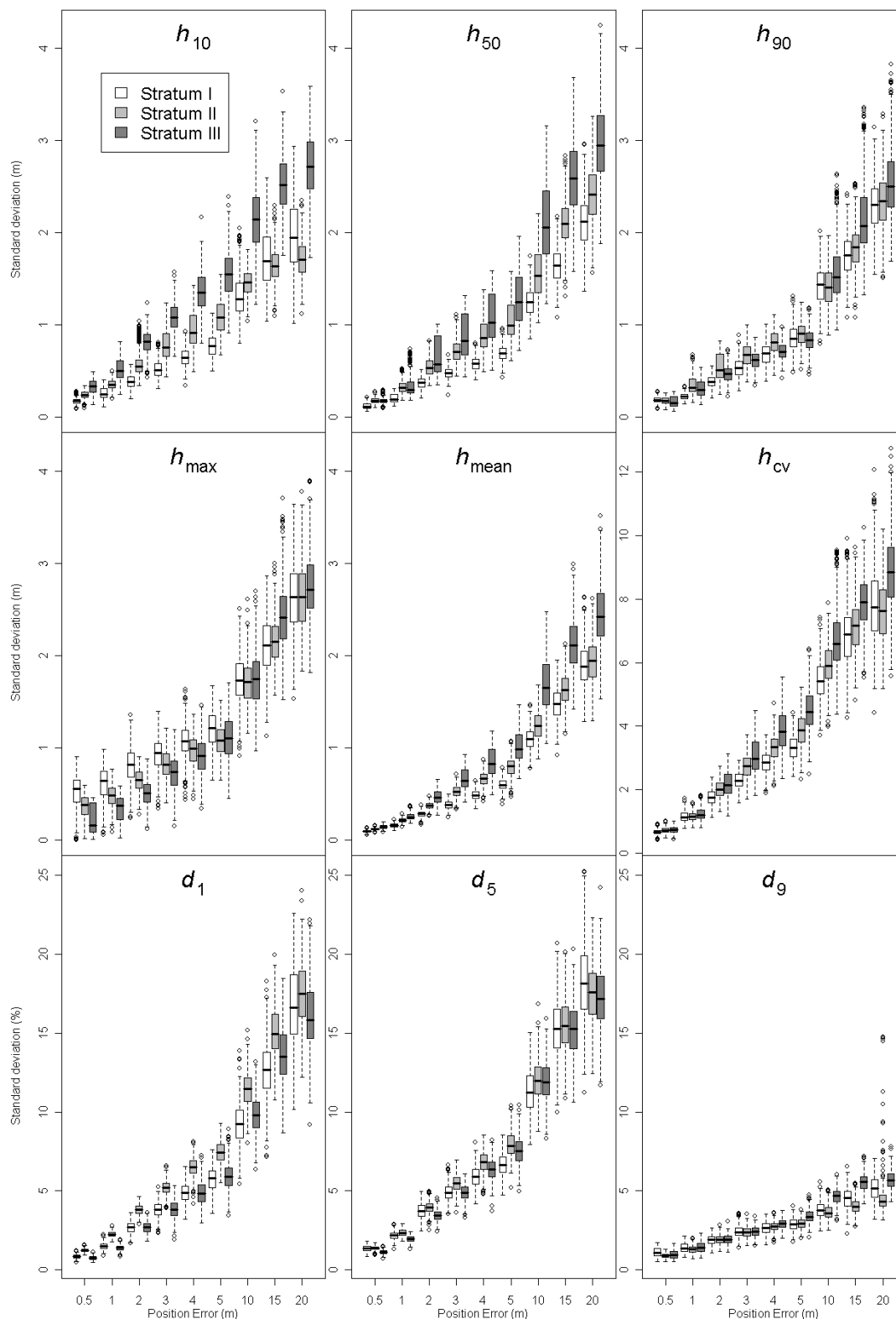


Figure 1: Standard deviation of the differences between laser-derived metrics (see text) of plots with error-contaminated positions generated with Monte Carlo simulation (500 repetitions) and true positions for different forest types (young forest=stratum I; mature forest with poor site quality= stratum II; mature forest with good site quality=stratum III)¹

¹ The box-and-whisker plots show first and third quartile as the box (“hinges”), the median as the horizontal line dividing the box and extreme values as points.

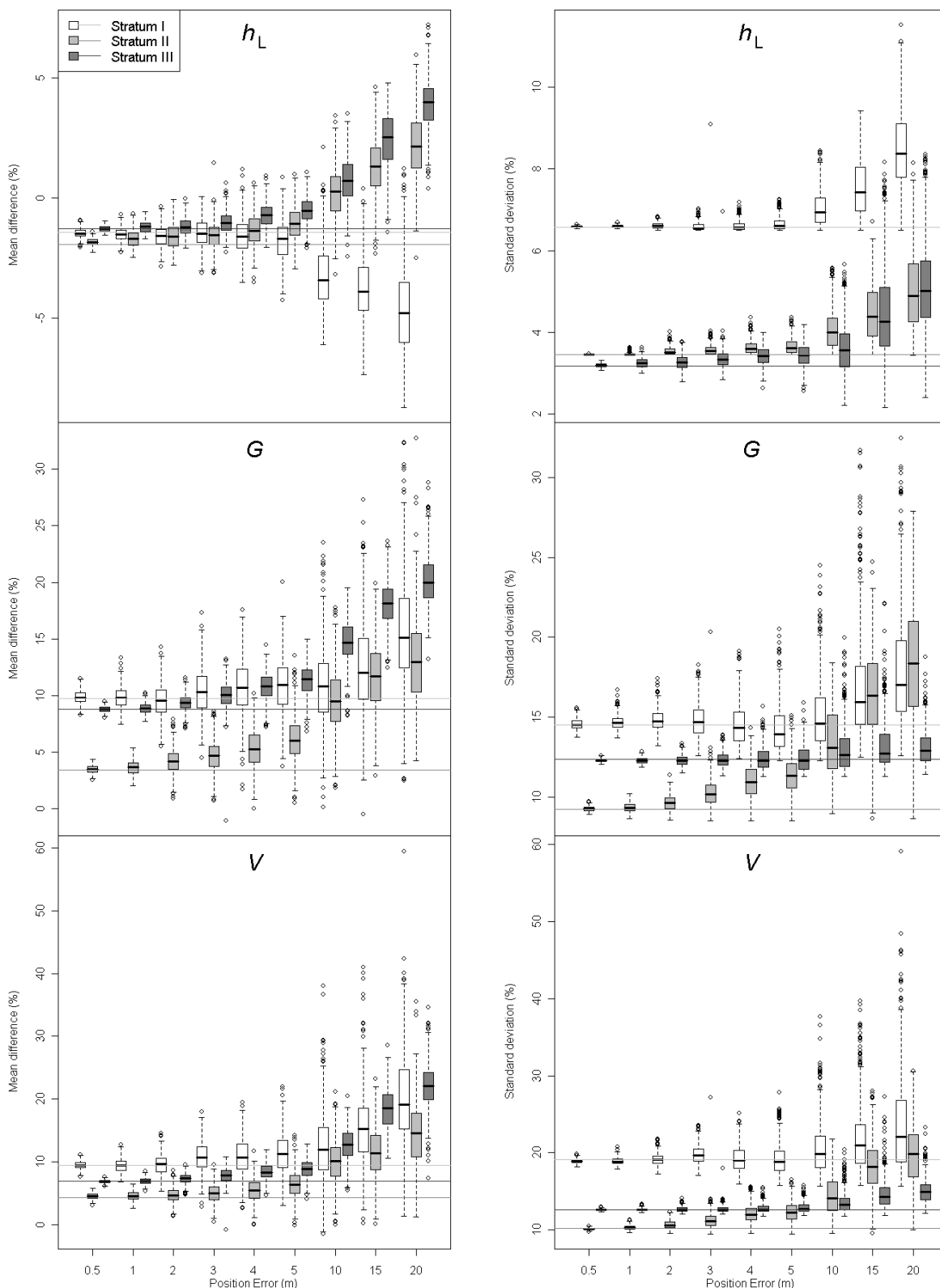


Figure 2: Mean difference (*left*) and standard deviation of the differences (*right*) between predicted and observed values of Lorey's mean height (h_L) (*top*), basal area (G) (*middle*), and volume (V) (*bottom*) in forest stands of different types (young forest=stratum I; mature forest with poor site quality= stratum II, mature forest with good site quality=stratum III) based on prediction models estimated with sample plots assuming different levels of position errors of the plot locations. Statistics for each level of position error is computed from the outcome of the 500 Monte Carlo repetitions¹. As a reference, the horizontal lines indicate the results when using ground-truth plot positions for stratum I, II, and III, respectively

The field-measured ground-truth plot positions were treated as if they were free from errors in this study. In fact, the computed ground-truth plot coordinates had an expected average accuracy of approximately 0.2 m (Næsset 2004), however, this miss-location should only have a marginal influence of the major findings.

Gobakken and Næsset (2008b) also found that larger plot sizes to a certain extent can compensate for sample plot position errors. Consequently more research is needed to find the optimal combination of field plot size and requirements for plot position accuracy.

To conclude, the results have shown that the accuracy of positions of the sample plots are an important factor affecting precision of forest inventory based on ALS data.

References

- Eid, T., Gobakken, T., & Næsset, E. 2004. Comparing stand inventories based on photo interpretation and laser scanning by means of cost-plus-loss analyses. *Scandinavian Journal of Forest Research*, 19, 512-523
- Gjertsen, A.K. 2007. Accuracy of forest mapping based on Landsat TM data and a kNN-based method. *Remote Sensing of Environment*, 110, 420-430
- Gobakken, T., & Næsset, E. 2008a. Assessing effects of laser point density, ground sampling intensity, and field sample plot size on biophysical stand properties derived from airborne laser scanner data. *Canadian Journal of Forest Research*, 38, 1095-1109
- Gobakken, T., & Næsset, E. 2008b. Assessing effects of positioning errors and sample plot size on biophysical stand properties derived from airborne Laser scanner data. *In submission*
- Means, J.E., Acker, S.A., Brandon J. F, Renslow, M., Emerson, L., & Hendrix, C. 2000. Predicting forest stand characteristics with airborne scanning lidar. *Photogrammetric Engineering and Remote Sensing*, 66, 1367-1371
- Næsset, E. 1997. Estimating timber volume of forest stands using airborne laser scanner data. *Remote Sensing of Environment*, 61, 246-253
- Næsset, E. 2002. Predicting forest stand characteristics with airborne scanning laser using a practical two-stage procedure and field data. *Remote Sensing of Environment*, 80, 88-99
- Næsset, E. 2004. Practical large-scale forest stand inventory using a small-footprint airborne scanning laser. *Scandinavian Journal of Forest Research*, 19, 164-179
- Næsset, E., & Bjerknes, K.-O. 2001. Estimating tree heights and number of stems in young forest stands using airborne laser scanner data. *Remote Sensing of Environment*, 78, 328-340
- R Development Core Team 2006. R: A language and environment for statistical computing. In. Vienna, Austria: R Foundation for Statistical Computing
- Tukey, J.W. 1977. Exploratory data analysis: Addison-Wesley Reading

Comparison of individual tree detection and canopy height distribution approaches: a case study in Finland

Petteri Packalén¹, Juho Pitkänen² & Matti Maltamo¹

¹ Faculty of Forest Sciences, University of Joensuu, P.O. Box 111, FIN-80101 Joensuu, Finland, Petteri.Packalen@joensuu.fi, Matti.Maltamo@joensuu.fi

² Finnish Forest Research Institute, Joensuu Research Unit, P.O. Box 68, FI-80101 Joensuu, Finland, Juho.Pitkanen@metla.fi

Abstract

The two main approaches in ALS based prediction of growing stock characteristics of forests have been individual tree detection (ITD) and canopy height distribution based modelling (CHD). There are numerous studies, in which either of these approaches have been used with a particular test area and dataset. However, the results obtained are not directly comparable between different datasets and areas. In this paper we present a comparison of ITD and CHD using the same validation dataset. The validation data consisted of 41 sample plots, located in a boreal managed forest. ITD and CHD produced equally accurate estimates with respect to stem volume and Lorey's height. The RMSE was about 22% for volume and about 8% for Lorey's height. The residuals were also similar with both methods. Stem number estimates were less accurate with both approaches; particularly ITD had a large RMSE and bias in the form of underestimation. This study indicated that, when considering total stem volume, both ITD and CHD are potential inventory approaches in managed boreal forests. CHD has a cost benefit in the acquisition of ALS data but, on the other hand, it requires more field work in the collection of modelling data.

Keywords: individual tree detection, canopy height distribution

1. Introduction

The two main approaches for predicting growing stock characteristics of forests using ALS data are the canopy height distribution approach (CHD), usually used with low-resolution data (e.g. Næsset 2002; Lim et al. 2003; van Aardt et al. 2006; Maltamo et al. 2006), and the individual tree detection approach (ITD), used with high-resolution data (e.g. Hyypä and Inkinen 1999; Persson et al. 2002; Popescu et al. 2003; Peuhkurinen et al. 2007). Low resolution means in this context that the pulse density at ground level is about one per square metre and high resolution means about 5-10 pulses per square metre. Most studies have concentrated on predicting characteristics of forest stands or trees as a whole, but characteristics by tree species have also been considered using both approaches (e.g. Holmgren and Persson 2004; Packalén and Maltamo 2007; Holmgren et al. 2008).

The major difference between the laser canopy height distribution and the individual tree based approach is that the latter relies on the detection of individual trees and allometric relationships at tree level, whereas the former uses height hits directly at the plot, microstand or stand level to estimate growing stock characteristics. A common method in individual tree delineation is to detect trees from an interpolated canopy height model by locating local maxima of the height values. After that trees are segmented around local maxima by some region growing algorithm, for instance. In the canopy height distribution approach regression modelling is the most often used estimation technique, although other techniques, such as non-parametric estimation, have also been utilized. Most actual forestry applications have so far been based on the canopy height distribution approach.

There are numerous studies regarding either of the two approaches in which the accuracy of some inventory attributes have been reported using a particular test area and dataset. This naturally raises the question which approach produces more accurate estimates for forest characteristics. However, obtained accuracies are not directly comparable between different datasets and areas. In this paper we present a comparison of ITD and CHD using the same validation dataset. Estimates are compared at the plot level and emphasis is given to the objectivity of the comparison. The aim is to compare the accuracy of ITD and CHD and to examine similarities and differences of the estimates.

2. Method

2.1 Study area and field data

The area concerned is a typical boreal managed forest area in eastern Finland, and hence it is dominated by coniferous tree species. A network of 472 circular sample plots with a radius of 9 metres was measured during the summer in 2004. Sample plots were distributed over 67 forest stands. Differential GPS was used to determine the position of the centre of each plot to an accuracy of approximately 1 m. The diameter at breast height (dbh), tree and storey class, and tree species were measured for each tree with a dbh greater than 5 cm. Height was measured for one sample tree of each species and storey class by plots. This data was required for calibration of the tree species-specific height models of Veltheim (1987), which were used to calculate the heights of the rest of the trees. The volumes of individual trees were calculated as a function of dbh and tree height using the models of Laasasenaho (1982) and summed at the plot level. Lorey's mean height was calculated for each plot by multiplying the tree height by its basal area and then dividing the sum of this calculation by the total basal area of a plot.

A subset of 41 of the sample plots described above were selected to be used as test data in this study (Table 1). These sample plots were the ones located in the area from which both high and low resolution ALS data were available and the dominant tree species in the selected plots was either Scots pine (*Pinus Sylvestris L.*) or Norway spruce (*Picea abies (L.) Karst.*). Another subset of 56 sample plots was used as modelling data in CHD (Table 1). First all the stands which contained test plots were excluded and then one sample plot was chosen randomly from each stand left to be included in the modelling data. Thus, the test data was not used in modelling.

Table 1: Main characteristics of the growing stock in the sample plots of the test and modelling datasets.

| | n | min | max | mean | std |
|---|----|------|-------|--------|-------|
| CHD Modelling data | 56 | | | | |
| Volume, m ³ ha ⁻¹ | | 51.4 | 447.1 | 204.1 | 101.6 |
| Lorey's height, m | | 7.8 | 25.4 | 15.9 | 4.4 |
| Stem number, ha ⁻¹ | | 550 | 3105 | 1529.8 | 101.6 |
| Test data | 41 | | | | |
| Volume, m ³ ha ⁻¹ | | 56.1 | 502.8 | 209.9 | 115.0 |
| Lorey's height, m | | 8.8 | 27.0 | 16.6 | 4.3 |
| Stem number, ha ⁻¹ | | 511 | 2790 | 1410.9 | 533.6 |

For ITD, a total of 32 height calibration trees were measured in the winter in 2008 to calibrate laser based tree heights to field measured ones. The dbh, height and tree species of 16 Scots pine and 16 Norway spruce within the high resolution ALS data area but outside the sample plots were registered. To predict tree height in 2004 from laser tree height, linear regression was used to get separate height calibration models for the two tree species. However, in order to get heights of trees in 2004, height increment of three growing seasons had to be first removed. Height increment was also modelled with regression by tree species. The modelling data were

obtained from the sample trees of 10th National Forest Inventory (Korhonen et al. 2007), measured in 2004-2006, that were within 50 km from the centre of the test area and that had a measurement for height increment of five years. Three fifths of the predicted five year height increment were then removed from the field measured tree heights to obtain tree heights in 2004.

2.2 ALS data

Two ALS data sets were used: high resolution data was used in ITD and low resolution data in CHD. The ALS data were collected on August 4th, 2004, using an Optech ALTM 2033 laser scanning system. Low resolution dataset covers all the sample plots in the area and its point density is about 0.7 measurements per square metre. Low resolution data was captured at an altitude of 1500 m above ground level (a.g.l.). Four overlapping flight lines were also captured at an altitude of 380 m a.g.l. These four flight lines together with the low resolution data from the same area comprise a high resolution dataset which covers the region of the 41 sample plots used as test data. The point density in high resolution data is about 7 measurements per square metre. The field of view of the laser scanner was 30 degrees in both altitudes.

The low resolution dataset was used to generate a digital terrain model (DTM) to a pixel size of one meter using the method explained in Axelsson (2000). The high resolution dataset was used to generate a canopy height model (CHM) for ITD. First the DTM height was subtracted from the orthometric laser scanning heights and this point dataset was rasterized to a CHM of 40 cm pixel size by taking the maximum point height value within a 28 cm radius from each centre of a pixel. To get a final CHM, the number of missing pixels and low, differing pixels was reduced with a median filtering in local windows of 3 by 3 pixels. First, each missing pixel that had at least n height values (parameter) within its eight-neighbours was replaced with the median of the height values. This was run three times with parameter n having the values 5, 3 and 3. After this, the remaining missing pixels were set to 0. Further, a pixel was considered to be a low, differing pixel, if at least seven of the eight-neighbours were more than five meters higher than the pixel itself. These pixels were replaced with the median of the neighbours that were more than five meters higher.

2.3 Individual Tree Detection

Laser based tree candidates were located and delineated in the CHM using watershed segmentation. Segmentation was done to remove some small tree crown segments, typically belonging to very small trees or caused by missing pixels at the tree crown boundaries. Other than that the method was similar to local maxima finding. Before segmentation, a CHM was low-pass filtered with height based selection of degree of filtering (Pitkänen et al. 2004). Three Gaussian filters were used so that the filter size increased along with the height of the pixel being filtered. The smallest and largest σ values were selected by verifying visually that the number of local maxima was reasonable at both ends of the tree height range. The height ranges and corresponding σ values used were 0-12 m and σ 0.4, 12-24 m and σ 0.6 and over 24 m and σ 0.8.

A negative image of the height filtered image was then created for the watershed segmentation that was used to separate tree crowns from each other. Watershed regions associated with the local minima in the negative image were identified using an algorithm which followed the drainage direction (Gauch 1999, see also Narendra and Goldberg 1980). To get boundaries between crowns and background, pixels lower than two meters in the height filtered image were masked out from the crown segments. Finally small segments, at most three pixels in size, were combined to one of the neighbour segments, be it a tree crown or background, based on the smallest average gradient on the common segment boundary.

Tree locations and heights were then obtained from the location of the pixel with the highest CHM value within each segment. These laser based heights were further calibrated to estimates of field measured tree height using height calibration models. Either the model of Scots pine or Norway spruce was used for all laser based trees within a plot, based on the dominant tree species of the plot, which was assumed to be known. A dbh was predicted for each laser based tree from the height estimate using the models by Kalliovirta and Tokola (2005); South boreal models for either Scots pine or Norway spruce were employed (see table 6, p. 236), again according to the dominant tree species of the plot. Within the plots, only trees with a dbh estimate greater than 5 cm were retained in stem number and other estimates. The volumes of individual trees were calculated from the dbh and tree height estimates using the same models (Laasasenaho 1982) as with the field data and summed at the plot level. Lorey's mean height was also calculated similarly as in the field data.

2.4 Canopy Height Distribution modelling

Orthometric laser scanning heights were transformed to above-ground heights by subtracting the DTM at the corresponding point. The ALS hits were then classified as ground and canopy hits, assuming that points with a canopy height value of less than 2 metres represented ground hits and the remaining points could be considered canopy hits. The first and last pulse height distributions were created from the canopy height hits and different height metrics were calculated for each sample plot. Percentiles for the canopy height were computed for 1, 5, 10, 20, ... , 90, 95 and 100 % (h_5, \dots, h_{100}) (see Næsset 2002), and proportional canopy densities were calculated for each of these quantiles (p_1, \dots, p_{100}). Furthermore, the proportion of canopy hits vs. ground hits (veg) was computed for each plot. All these characteristics were calculated separately for first and last pulse data, henceforth denoted by the prefix f or l.

Regression models were then constructed for the stand variables volume, Lorey's mean height and stem number, and ALS-based height characteristics were used as independent variables in these regression models. The candidate models, and all their different transformations, were compared to find as linear as possible a relationship between dependent and independent variables by using stepwise regression. The forms of the final models were then chosen on the basis of model accuracy. As it was assumed that the dominant tree species of the plots were known, the information about the dominant tree species was tested as a dummy variable while constructing regression equations.

2.5 Estimated stand characteristics and accuracy assessment

Accuracy assessment was performed with the test data (41 sample plots) that was not used in model creation either in the CHD or ITD. High resolution ALS data was used in ITD and low resolution ALS data in CHD. The stand characteristics mean volume, stem number and Lorey's mean height were estimated for the test plots. The results were validated in terms of relative RMSE and bias at the plot level:

$$RMSE - \% = \frac{\sqrt{\frac{\sum_{i=1}^n (y_i - \hat{y}_i)^2}{n}}}{y_{mean}} \times 100, \quad (1)$$

$$bias - \% = \frac{\frac{\sum_{i=1}^n (y_i - \hat{y}_i)}{n}}{y_{mean}} \times 100, \quad (2)$$

where n is the number of plots, y_i is the observed value for plot i , \hat{y}_i is the predicted value for plot i and y_{mean} is the observed mean of the variable in question.

3. Results

The variables used in the CHD models were $\ln(f_{h_1})$, $f_{h_{70}}$, $\ln(l_{veg})$ and l_{p_1} for square root of volume, f_{veg} and $l_{h_{20}}$ for square root of stem number and $f_{h_{10}}$ and $\ln(l_{h_{70}})$ for logarithmic mean height. Bias correction factors were also added to the model predictions. The dummy variable indicating the dominant tree species was not statistically significant in any of the constructed models.

The accuracies of volume, Lorey's mean height and stem number estimates at the plot level are presented in Table 2. ITD and CHD produced almost equally accurate estimates regarding stem volume and Lorey's height. The RMSEs for volume were 21.73% and 21.78% for CHD and ITD, respectively, and the corresponding figures for Lorey's height were 8.33% and 8.35%. The CHD slightly overestimated both volume and height, whereas the ITD slightly overestimated height and underestimated volume. However, bias was minor in both approaches for these two variables.

Stem number estimates were less accurate than the estimates of volume and height, as was expected. The CHD method was able to estimate stem number considerably more accurately than what was achieved with the ITD. The RMSEs of stem number were 27.29% for CHD and 49.12% for ITD. The ITD underestimated the stem number clearly, whereas the bias of the CHD was negligible. However, both methods had a trend in residuals: from sparse to dense plots, the ITD estimates changed from slight underestimates to clear underestimates whereas the CHD estimates changed from overestimates to underestimates.

Table 2: Accuracy of the estimated stand characteristics at the plot level for ITD and CHD.

| | | Volume | Lorey's height | Stem number |
|--------|-----|--------|----------------|-------------|
| RMSE-% | ITD | 21.78 | 8.35 | 49.12 |
| | CHD | 21.73 | 8.33 | 27.29 |
| BIAS-% | ITD | 3.00 | -2.75 | 36.55 |
| | CHD | -3.96 | -0.25 | 3.60 |

The study design enabled the comparison of residuals between the ITD and CHD because stand characteristics were estimated for the same plots. It was especially interesting to compare residuals as a function of stem number because ITD underestimated the stem number in most of the plots, the bias being 37%. Figure 1 depicts the relative error of volume as a function of stem number for the ITD and CHD. Stem volume was selected because it is often the most important outcome of a forest inventory. One could assume that the ITD was more biased in dense forests compared to the CHD. However, there is no observable trend of difference between the ITD and CHD in Figure 1. Thus, error in stem volume does not differ between the ITD and CHD as a function of stem number.

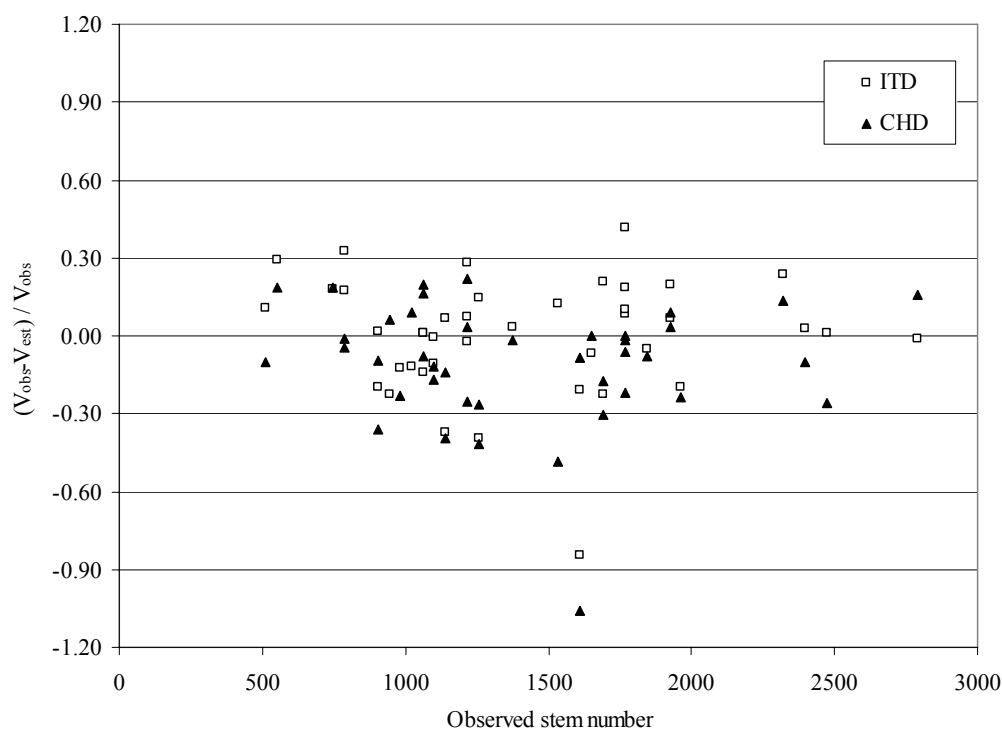


Figure 1: Relative error of volume at the plot level as a function of observed stem number for ITD and CHD. V_{obs} denotes observed and V_{est} estimated stem volume.

4. Discussion

ITD and CHD yielded almost equally accurate estimates for volume and Lorey's mean height. The bias was minor in these variables with both approaches, too. Regarding stem number, ITD was substantially less accurate than CHD and produced notable bias. The obtained accuracies are consistent with earlier studies carried out using CHD based methods in Finland (e.g. Havia 2006, Maltamo et al. 2006). Comparison to earlier works in the case of ITD is difficult since most of the studies done in Finland are carried out on unmanaged seminatural study areas (e.g. Hyypä and Inkinen 1999, Maltamo et al. 2004). The only exception is the work by Peuhkurinen et al. (2007), in which two mature stands of the current study material were used in pre-harvest inventory by means of ITD. It is also difficult to compare tree and plot level accuracies: in ITD studies, the accuracy assessment is often done at tree level.

This case study indicated that considering volume and mean height both ITD and CHD are potential inventory approaches in managed boreal forest. The results of stem number estimation were not so good, especially with ITD. With this method, the estimates of different variables are based on the same laser detected trees. Thus, there is some contradiction in the result that stem numbers were clearly underestimated but volume estimates were accurate. It is obvious that large, dominant trees, forming most of the stem volume, are more often detected by ITD than small or suppressed trees. Most of the difference is probably explained by this; the same tendency was observed by Persson et al. (2002), for instance. Other possibilities are overestimation of tree heights or dbh of the trees. Data for laser tree height to field tree height calibration was collected three growing seasons after the ALS data, which reduces the accuracy of height calibration. It is also possible that the models used to predict dbh from tree height gave overestimates in this area. However, this is left to be studied in a further work.

Another possibility than accuracy is to compare costs of the inventory methods. Of course the costs of the high pulse density data are higher than those of the low pulse density data. On the

other hand CHD methods require more field work. In our study only one field day was used to measure calibration data for ITD, whereas it will take about 1-2 weeks to measure about 50 plots used in CHD. However, we used considerably lower number of modelling plots than in many earlier CHD studies (e.g. Næsset 2002, Maltamo et al. 2006) but the accuracy was still correspondent. It is possible that the amount of reference data could still be reduced in CHD; the more important thing is to find the optimal placement of the sample plots. A cost factor which is very difficult to take into account is the time spent in the analysis. Especially those processing steps, which cannot be completely automated, increase costs. From this point of view CHD is maybe slightly more straightforward.

In Finland the prediction of species specific stand variables is of primary interest but here we only assumed that the main tree species of a stand is known. However, there exist also studies where Scandinavian tree species are taken into consideration. In the case of CHD based methods Packalén and Maltamo (2007) have shown that when ALS data and aerial photograph are combined tree species can also be successfully predicted. In the case of single tree detection there also exist some studies which have considered tree species information (e.g. Holmgren et al. 2008, Ørka et al. 2007, Vauhkonen 2007) but the calculation of tree volumes has not been taken into consideration. Diameter distributions are also of interest in many applications but they are not considered here. Thus, the deductions made in this paper do not take into account the ability of CHD or ITD to estimate species specific stand characteristics or diameter distributions.

The implemented study design enabled the comparison of estimates between ITD and CHD, when typical data sets for both methods were used. In addition to accuracy comparison it is interesting to examine whether they produce similar kind of residual structures or not. This might reveal if one or the other approach is more accurate in some type of forests, in mature or dense stands, for instance. One comparison of this kind was shown in Figure 1. It was also noted that especially in those plots where forest characteristics were estimated most inaccurately there is a clear correlation of residuals between ITD and CHD. This is an interesting observation that needs to be studied further in future.

References

- Axelsson, P. 2000. DEM Generation from Laser Scanner Data Using Adaptive TIN Models. *International Archives of the Photogrammetry and Remote Sensing* 33(B4): 110-117.
- Gauch, J.M. 1999. Image segmentation and analysis via multiscale gradient watershed hierarchies. *IEEE Transactions on Image Processing*, 8(1): 69-79.
- Havia, J. 2006. Puustotiedon sekä metsikkökuvioinnin tarkkuuden selvittäminen. M.Sc. thesis. University of Joensuu. (In Finnish).
- Holmgren, J. and Persson, Å. 2004. Identifying species of individual trees using airborne laser scanner. *Remote Sensing of Environment*, 90, 415-423.
- Holmgren, J., Persson, Å. and Söderman, U. 2008. Species identification of individual trees by combining high resolution LiDAR data with multi-spectral images. *International Journal of Remote Sensing*, 29, 1537-1552.
- Hyypä, J. and Inkinen, M. 1999. Detecting and estimating attributes for single trees using laser scanner. *The Photogrammetric Journal of Finland*, 16, 27-42.
- Kalliovirta, J. and Tokola, T. 2005. Functions for estimating stem diameter and tree age using tree height, crown width and existing stand database information. *Silva Fennica*, 39(2), 227-248.
- Korhonen, K.T., Ihalainen, A., Heikkinen, J., Henttonen, H. and Pitkänen, J. 2007. Suomen metsävarat metsäkeskuksittain 2004-2006 ja metsävarojen kehitys 1996-2006. *Metsätieteen aikakauskirja* 2B/2007, 149-213. (In Finnish).
- Laasasenaho, J. 1982. Taper curve and volume function for pine, spruce and birch.

- Communicationes Instituti Forestalis Fenniae*, 108, 1-74.
- Lim, K., Treitz, P., Baldwin, K., Morrison, I. and Green, J. 2003. Lidar remote sensing of biophysical properties of tolerant northern hardwood forests. *Canadian Journal of Remote Sensing*, 29, 648-678.
- Maltamo, M., Eerikäinen, K., Pitkänen J., Hyypä, J. and Vehmas, M. 2004. Estimation of timber volume and stem density based on scanning laser altimetry and expected tree size distribution functions. *Remote Sensing of Environment*, 90, 319-330.
- Maltamo, M., Malinen, J., Packalén, P., Suvanto, A. and Kangas, J. 2006. Nonparametric estimation of plot volume using laser scanning, aerial photography and stand register data. *Canadian Journal of Forest Research*, 36, 426-436.
- Narendra, P.M. and Goldberg, M. 1980. Image segmentation with directed trees. *IEEE Transactions on Pattern Analysis and Machine Intelligence*, 2(2):185-191.
- Næsset, E. 2002. Predicting forest stand characteristics with airborne scanning laser using a practical two-stage procedure and field data. *Remote Sensing of Environment*, 80, 88-99.
- Ørka, H.O., Næsset, E., Bollandsås, O.M., 2007. Utilizing airborne laser intensity for tree species classification. *International Archives of the Photogrammetry, Remote Sensing and Spatial Information Sciences*, Vol. XXXVI, Part 3/W52, 300-304.
- Packalén, P. and Maltamo, M. 2007. The k-MSN method for the prediction of species-specific stand attributes using airborne laser scanning and aerial photographs. *Remote Sensing of Environment*, 109, 328-341.
- Persson, Å., Holmgren, J. and Söderman, U. 2002. Detecting and measuring individual trees using an airborne laser scanner. *Photogrammetric engineering & Remote Sensing*, 68, 925-932.
- Peuhkurinen, J., Maltamo, M., Malinen, J., Pitkänen, J. and Packalén, P. 2007. Pre-harvest measurement of marked stand using airborne laser scanning. *Forest Science*, 63, 653-661.
- Pitkänen, J., Maltamo, M., Hyypä, J. and Yu, X. 2004. Adaptive methods for individual tree detection on airborne laser based canopy height model. *International Archives of Photogrammetry, Remote Sensing and Spatial Information Sciences*, Vol. XXXVI, Part 8/W2, 187-191.
- Popescu, S.C., Wynne, R.H. and Nelson, R.F. 2003. Measuring individual tree crown diameter with lidar and assessing its influence on estimating forest volume and biomass. *Canadian Journal of Remote Sensing*, 29, 564-577.
- van Aardt, J.A.N., Wynne, R.H. and Oberwald, R.G. 2006. Forest volume and biomass estimation using small-footprint lidar-distributional parameters on a per-segment basis. *Forest Science*, 52, 636-649.
- Vauhkonen, J. 2007. Identifying tree species of individual trees using airborne laser scanning data of different resolution. M.Sc. thesis. University of Joensuu. 63 p.
- Veltheim, T. 1987. Pituusmallit männylle, kuuselle ja koivulle. M.Sc. thesis, University of Helsinki, Department of Forest Mensuration and Management, Helsinki, Finland. 59 p. (In Finnish).

LiDAR forest inventory with single-tree, double- and single-phase procedures

Robert C. Parker and David L. Evans

Department of Forestry, Forest and Wildlife Research Center,
Mississippi State University, Mississippi State, MS 39762
rparker@cfr.msstate.edu, devans@cfr.msstate.edu

Abstract.

Light Detection and Ranging (LiDAR) data at 0.5- 2m postings were used with double-sample, stratified inventory procedures involving single-tree attribute relationships in mixed, natural, and planted species stands to yield sampling errors (one half the confidence interval expressed as a percentage of the mean) ranging from $\pm 2.1\%$ to $\pm 11.5\%$ at $\alpha=0.05$. LiDAR sample trees were selected with focal filter procedures and heights computed as the difference between interpolated canopy and DEM surfaces. Tree dbh and height data were obtained on LiDAR:ground samples ranging from a 5:1 ratio on 0.08 ha rectangular strips to a 10:1 ratio on 0.02 ha circular plots established with a real-time Differential Global Positioning System. Dbh-height and ground-LiDAR height models were used to predict dbh from adjusted LiDAR height and compute Phase 2 ground and LiDAR estimates of basal area and volume. Phase 1 LiDAR estimates were computed by randomly assigning heights to species classes using the probability distribution from ground plots in each inventory strata. Phase 2 LiDAR estimates were computed by randomly assigning heights to species-product groups using a Monte Carlo simulation for each ground plot. There was no statistical difference between double-sample, mean volume estimates from 0.5m and 1m LiDAR posting densities with and without height bias adjustment or on smoothed and unsmoothed LiDAR canopy surfaces. Volume estimates from single-phase LiDAR inventory procedures utilizing existing tree attribute and LiDAR-ground height bias relationships were obtained with sampling errors of 1.8% to 5.5% for full and minimized data sets to test minimum LiDAR inventory requirements.

1. Introduction

Light detection and ranging (LiDAR) is a relatively new remote sensing tool that has the potential for use in the acquisition of measurement data for inventories of standing timber. LiDAR systems have been used in a variety of forestry applications (Magnussen and Boudewyn 1998, Lefsky et al. 1999, Means et al. 2000) for the quantification of biomass (Nelson et al. 2003), basal area, and tree and stand height estimates. Stand level, LiDAR inventory procedures involving average values of tree attributes such as dominant height, mean diameter, basal area, and volume have been applied to obtain unbiased stand level predictions (Naeset 2002, Naeset 2004, Popescu et al. 2002). Since LiDAR has the capability to detect individual trees and measure tree height with predictable bias when correlated with ground measurements (Persson et al. 2002, Holmgren 2004), strata-level inventory estimates involving individual tree, double-sample inventory procedure have been used by researchers from Mississippi State University in conifer and mixed hardwood stands in the Northwest and Southeast (Collins 2003, Parker and Evans 2004, Parker and Glass 2004, Parker and Mitchel 2005, Parker and Evans 2006, Williams 2006). The individual tree approach to stand inventory when combined with double-sample, ground procedures permits relatively precise estimates of volume with a simple prediction function for ground-LiDAR height bias and ground-based attribute relationship functions for tree diameter and total height which can be used with any standard, standing tree volume function. Stand level approaches involving average tree attribute values for sampling

units require more sophisticated prediction models than an individual tree approach and procedures that differ radically from traditional ground-based inventory methods. The objective of this paper is to summarize and discuss the procedures, models, and advantages/disadvantages of the single-tree approach to using LiDAR data in double- and single-phase forest inventory methods.

2. Methods

2.1 Flight Planning for a LiDAR Inventory

Small-footprint, multi-return LiDAR data have been acquired with various sensors to attain nominal posting spacings of 0.5 -2.0 m, 0.25- 4 point/m², and footprint sizes of 0.122 - 0.330 m for two returns per pulse (Table 1). Aircraft altitudes of 600-1,000 m and swath widths of 189 - 609 m were used. The minimum required density of LiDAR hits is a function of the crown size, average height, and spatial density of the sample trees in the primary canopy. Acceptable sampling statistics were attained for sparse densities of large crown conifers in Idaho ($\pm 11.5\%$ sampling error at the 95% confidence level with a standard error of $\pm 5 \text{ m}^3$, Parker and Evans 2004) with 0.25 points/m²; however, 1 point/m² was required to achieve acceptable inventory results in natural pine and mixed pine-hardwood stands ($\pm 7.6\%$ sampling error, Parker and Glass 2004) and 2 points/m² in young (6+ years) pine plantations ($\pm 2.2\%$ sampling error, Parker and Evans 2006) in the Southeast. Increasing LiDAR density from 2 to 4 points/m² did not statistically improve the volume estimation precision and the increased “noise” in the high-density LiDAR data translated into additional sampling error about the volume estimate.

Table 1. LiDAR specifications for sample single-tree inventory projects in conifers and mixed hardwoods in Idaho and Coastal Plain (CP) and Flatwoods (FW) areas of Louisiana (LA).

| LiDAR specification | Example 1 (Idaho) | Example 2 (CP LA) | Example 3 (FW LA) | Example 3 (CP LA) |
|---------------------------|----------------------|----------------------|----------------------|----------------------|
| Points per m ² | 0.25 | 1 | 1.9 | 4 |
| Nominal spacing | 2.0 m | 1.0 m | 0.7 m | 0.5 m |
| Footprint size | 0.330 m | 0.213 m | 0.250 m | 0.122 m |
| Aircraft altitude | 1,000 m | 1,067 m | 1,000 m | 610 m |
| Swath width | 600+ m | 609 m | 243 m | 189 m |
| Tract size | 2,023 ha | 485 ha | 18,000 ha | 485 ha |
| Percent LiDAR Coverage | 1.43% | 100% | 10% | 100% |

Target aircraft altitude is a function of the desired swath width and scan angle for the LiDAR pulse generator and sensor and the technical ability of the sensor to achieve the desired posting density. The swath width diminishes as the desired posting density increases, but reasonable swath widths can be achieved with 2-4 points/m². An important factor influencing desired swath width was the size of the ground-based sample plots used in the inventory procedure. The swath should be sufficiently wide to encompass the sample ground and LiDAR plots within the center one-third of the swath so as to minimize the “edge effects” of the LiDAR data. Tree attribute measurements are severely compromised at the extremes edges of the swath and scan angle.

Percent LiDAR coverage is a function of economics and inventory design. LiDAR data is relatively expensive to obtain and complete area coverage is normally not required for most timber inventory designs. In some instances, the cost of complete LiDAR coverage to produce an accurate, up-to-date Digital Elevation Model (DEM) may be more justifiable than the expense for a timber inventory. The use of a current Geographical Information System (GIS) to

locate flight lines that cross the desired sampling strata can minimize the percent coverage of the LiDAR area. Most forested areas to be inventoried can be flown with ten percent or less LiDAR area coverage by orienting flight lines so as to cross the target inventory strata at desired flight line intervals.

2.2 Field and LiDAR Plot Design and Procedures

Inventory design for the single-tree LiDAR applications involved the use of circular (Parker and Evans 2006, Parker and Glass 2004) or rectangular plots (Parker and Evans 2004) with all plots being Phase 1 LiDAR plots and every r^{th} plot as a Phase 2 ground plot. Field designs varied from a 9:1 ratio of LiDAR to ground circular plots in a nested arrangement to a 10:1 ratio with rectangular or circular plots along a flight line (Figure 1). UTM coordinates were established at the center of each circular Phase 2 plot or at the endpoints of rectangular plots for navigation with a real-time Differential Global Positioning System (DGPS). Differential corrections from either the U.S. Government WAAS or private enterprise OmniStar geo-stationary satellite were obtained satisfactorily under tree canopies by using a large dome antenna. Based on informal field tests on surveyed bench marks, field locations were obtained with approximately 1 m accuracies with both systems.

2.3 LiDAR Surfacing for Tree Location and Height Determination

The LiDAR data were processed to produce a ground surface or digital terrain model (DTM) and a tree surface for determination of sample tree locations and tree heights within the sample field and LiDAR plot areas. LiDAR data sets were surfaced to produce 1st return canopy and last return DTM with 0.2 m cell sizes using a linear interpolation technique. Tree locations and heights were determined with algorithms and focal filter procedures developed by McCombs et al. (2003) that used a variable search window radius based on relative density. These procedures used moving 2.5, 4.0, or 5.5 ft radius search windows to identify each tree peak as the point that is higher than 85% of the surrounding maxima from one of the three search window, radius files. Tree height was interpreted as the difference between canopy and DTM z-values at each tree peak location. Tree heights were converted to point coverages and clipped to sample area boundaries using UTM coordinates to describe sample plot locations and sizes.

A spatial filtering technique derived from image analysis called smoothing was used to reduce commission errors by minimizing the abrupt elevation changes in the initial canopy surface. The Focal Analysis option in ERDAS' Imagine software performed smoothing based on user-defined inputs for window size and preferred statistical procedure. A 5-by-5 pixel window was used to create a 1 m² filter that would avoid removal of small peaks in the canopy surface (small trees), while maximizing the smoothing function. The filter moved across the LiDAR canopy surface, pixel by pixel, averaged the values within the window, and placed the result in the center pixel.

Smoothing heights on LiDAR surfaces improved the relationship between LiDAR and ground tree heights in terms of R^2 , reduced height biases for hardwoods, increased height biases for pines, and improved target recognition in terms of trees/ac estimates. There were however no statistical differences ($\alpha = 0.05$) between double-sample regression volume estimates with smoothed versus unsmoothed LiDAR surfaces from low- or high- density LiDAR. Standard errors and sampling errors of the regression estimates were lower for all unsmoothed LiDAR data models than with smoothed data models. Thus, smoothing heights on LiDAR surfaces did not produce a statistical gain for volume estimation using double-sample procedures.

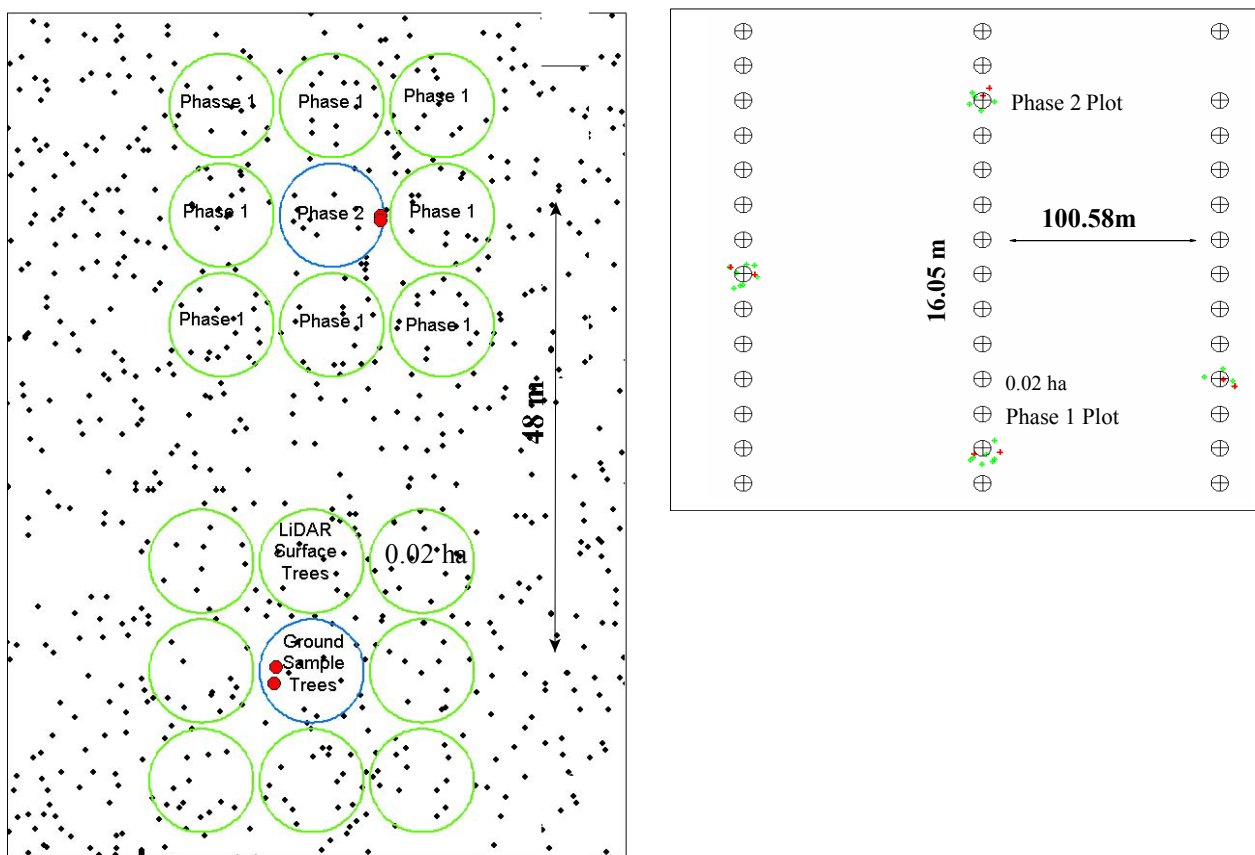


Figure 1. Sample designs for 0.02 ha plots with 9:1 and 10:1 ratios of LiDAR plots (Phase 1) to ground (Phase 2) circular plots in a nested arrangement and plots along a flight line.

3. Results

3.1 Double-Sample, Regression Estimator Procedures

The double-sample model widely used with ground-based point sampling (Avery and Burkhart 2002) and aerial photogrammetric inventories and adapted for these studies was:

$$\bar{Y}_{lr} = \bar{y}_2 + \beta(\bar{X}_1 - \bar{x}_2) \quad (1)$$

With traditional aerial photogrammetric inventories, the X_{1i} and x_{2i} variables are photographic volume/unit area and ground volume/unit area from Phase 1 and Phase 2 plots, respectively, and β is the regression slope coefficient for y_i (ground volume) over x_{2i} (photo volume) on ground plots. Thus, a Phase 1 (large sample) variable such as remotely sensed (i.e. photographic or LiDAR derived) volume has a strong, identifiable relationship with a Phase 2 (small sample) variable such as ground volume.

In applications of the double-sample model with single-tree LiDAR data, Phase 2 sample tree measures of dbh and height were used to derive height-dbh and dbh-height equations of the model type:

$$H_{gr} = b_0 + b_1[\ln(\text{dbh})]^{b_2}[\text{age}]^{b_3} + \varepsilon \quad (2)$$

$$\text{dbh} = b_0 + b_1[\ln(H_{\text{gr}})]^{b_2}[\text{age}]^{b_3} + \varepsilon \quad (3)$$

where H_{gr} was ground measured height, dbh was ground measured dbh, and age was average stand age (years) from GIS data. The age variable in Models (2) and (3) was removed when age did not contribute significantly to the relationship. Models (2) and (3) were derived from the ground-measured sample trees, but one is not a back transformation of the other. Model (2) was applied to ground-plot trees where dbh was measured on all trees and heights on a sub-sample. Model (3) was applied to LiDAR derived tree heights to obtain a dbh for single-tree volume computation.

Generally only 2 trees per ground plot were measured for height; dbh was measured on all trees. The height-dbh Model (2) was applied to trees on the ground plots for which height was not measured to obtain a height for single-tree volume computation. Sample tree heights from the Phase 2 ground plots were used to predict ground height of target trees identified on LiDAR surfaces. The dbh-height Model (3) was applied to the bias-adjusted, single-tree LiDAR height from the ground-LiDAR height bias Model:

$$H_{\text{gr}} = b_0 + b_1(H_{\text{Li}}) + \varepsilon \quad (4)$$

where H_{gr} was measured ground height of trees on Phase 2 plots and H_{Li} was interpolated height of the same trees from the LiDAR surface.

Derived dbh on LiDAR plots and derived height on ground plots permitted the use of a standard, standing-tree volume equation with dbh and height as variables to predict volume. Thus, the double-sample models used in this study involved LiDAR mean estimates of basal area (LiBA from Phase 1 and liba from Phase 2 with matching ground plot) and volume (LiVOL from Phase 1 and livol from Phase 2 with matching ground plot) for the x-variables as:

$$\bar{Y}_{lr} = \bar{y} + \beta(\text{LiBA} - \text{liba}) + \varepsilon \quad (5)$$

$$\bar{Y}_{lr} = \bar{y} + \beta(\text{LiVOL} - \text{livol}) + \varepsilon \quad (6)$$

with variance:

$$s_{y_{lr}}^2 = \frac{s_{yx}^2}{n_2} + \frac{s_y^2 - s_{yx}^2}{n_1} \quad (7)$$

where \bar{y} was Phase 2 mean ground volume, β was the regression slope coefficient for y_i (ground volume/unit area) over x_{2i} (LiDAR volume/unit area or basal area/unit area on ground plot) and x_{1i} was volume or basal area on the LiDAR plot. Data were fitted to Models (5) and (6) for all data combined (i.e. non-stratified), each ages-class strata, and combined strata. Combined strata, linear regression estimates of volume and associated standard error of each double-sample model were obtained by:

$$\bar{Y}_{lr,c} = \sum \frac{(n_{1i} + n_{2i})}{N} (\bar{Y}_{lr,i}) \quad (8)$$

$$S_{\bar{y}_{lr,c}} = \left[\sum \left(\frac{(n_{1i} + n_{2i})}{N} \right)^2 (S_{y_{lr,i}}^2) \right]^{0.5} \quad (9)$$

where n_{1i} and n_{2i} were Phase 1 and 2 sample sizes respectively for stratum i , $i=1$ to X strata.

All double-sample volume computations were performed with the Windows software program LIDARDS (LiDAR Double-Sample) developed by Parker (2005). The software allowed the user to specify dbh limits for species-product classes, regression coefficients for the dbh-height and ground height-LiDAR height models, stratum definitions of beginning and ending plot numbers and average age, and to enter comma delimited data files of Phase 1 LiDAR heights and Phase 2 ground-plot trees (species, product, dbh, and height of sample trees). LiDAR heights in the Phase 1 data were allocated in a Monte Carlo simulation to species-product classes on each matching Phase 2 ground plot on the basis of percent distribution by numbers on the ground plot. Since species and dbh of the LiDAR trees are unknown, the Monte Carlo simulation (50 iterations) would randomly allocate the LiDAR derived trees (dbh predicted from adjusted LiDAR-to-ground height) to species-product classes and obtain a mean basal area and volume estimate for the species-product class. Thus, basal area and volume estimates from Phase 1 LiDAR plots that had a matching Phase 2 ground plot became Phase 2 LiDAR plots. Phase 1 LiDAR heights that did not have a matching Phase 2 ground plot were randomly allocated to encountered species classes in each stratum in a single iteration and used to compute mean estimates of numbers of trees, basal area, and volume. Phase 2 tree measures of dbh and height were used to compute LiDAR estimates of mean basal area and volume by using field-derived dbh-height equations to predict dbh from LiDAR height and volume. Predicted dbh and height were used in a single-tree volume function to predict individual/single tree volume. Double-sample volume estimates and associated precision statistics were computed with Models (5) and (6) for each stratum and with Models (8) and (9) for combined strata.

3.2 Single-Phase Inventory Procedures

A recent study by Williams(2006) investigated the minimal data inputs for a LiDAR based timber inventory with single-phase procedures. Since the ground phase of a double-sample field procedure is both expensive and time consuming, Williams investigated the feasibility of using LiDAR data in single-tree approach to obtaining volume estimates by stratum with a single-phase inventory procedure. Previous studies have shown that LiDAR can provide precise, but biased estimates of tree numbers and heights. If the assumptions are made that (1) the LiDAR height bias is known and relatively constant for a given species-origin class (i.e. pine plantations) and (2) previously established tree attribute relationships are also known, inventory estimates of volume can be obtained with a single-tree approach and single-phase procedures from LiDAR data only.

The tree attribute relationship from Model (3) was developed from ground measurements of dbh and height within Continuous Forest Inventory (CFI) plots and from the Phase 2 ground plots in the double-sample approach by Parker and Evans (2006). Sample trees were randomly selected from the original data sets in groups of 75 and fitted to tree attribute Model (3) under the assumption that ground data were available from previous studies. The ground-LiDAR height bias equation obtained from Model (4) (Parker and Evans 2006) was assumed to be constant and known. LiDAR derived heights from Phase 1 plots were adjusted for bias with Model (4) then used with Model (3) to obtain single-tree dbh estimates for use with a single-tree volume function in a conventional, single-phase inventory processor. The stratum volume estimates and precision statistics were compared to estimates obtained from the Phase 2 ground plots by Parker and Evans (2006).

The single-tree, single-phase volume estimates from LiDAR data compared favorably with ground plot estimates (Table 2). At the tract level for 20 age class strata on 10,443 ha, there was no statistical difference between the single-phase LiDAR estimates and the ground plot estimate. Single-phase volume estimates were obtained for the full data set of Phase 1 LiDAR plots, the Phase 1 LiDAR plots that had a matching Phase 2 ground plot, and 5 iterations of reducing the LiDAR data set to a 5:1 ratio with ground plots within each stratum. The Williams (2006) study found no statistical difference ($\alpha=0.05$) between tract-level, single-phase volume estimates where the single-tree relationship model was developed with 1,539 sample trees from the Phase 2 ground plots by Parker and Evan (2006), 1,509 trees from the regional CFI plots, or 5 iterations of 75 randomly selected trees from the Phase 2 data set. The study concluded that precise single-phase LiDAR inventory estimates are feasible with minimal inputs of ground data for establishing tree attribute relationships. A potential application of the single-tree, single-phase inventory procedure would be the rapid post-thinning inventory of pine plantations and periodic inventories of forested holdings.

Table 2. Comparison of single-tree, single-phase, volume predictions from LiDAR data using 0.02 ha circular plots on 10, 443 ha of pine plantations with ground plot volume estimates where sampling error was half the $(1-\alpha)$ confidence interval expressed as a percentage of the mean.

| Data set description | No. of plots | Sampling error% | Tract volume vs. control |
|------------------------|------------------------|-----------------|---|
| Ground plots – Phase 2 | 842 | 2.8% | Control |
| LiDAR plots – Phase 1 | 7,562 | 1.8% | Not statistically different |
| LiDAR plots – Phase 2 | 842 | 5.2% | Not statistically different |
| LiDAR plots – Phase 1 | 5:1 ratio Phase 1:2 | 5.5% | Not statistically different in 3 of 5 iterations |

4. Discussion about Single-Tree LiDAR Inventory Procedures

LiDAR provides precise x, y, and z coordinate data that can be used to extract tree heights and locations; however, there are several sources of bias that can impact the accuracy of a per-unit area volume estimate. Height bias is primarily caused by the failure of the laser pulse to hit the terminal leader, but this bias can be predicted with acceptable success in conifers but not in hardwoods with broad rounded crowns. Height bias can also be introduced by the interpolation of tree heights with mixed linear and nonlinear procedures within the same data set. Tree count bias has at least two sources of origin; trees in the mid and lower canopy layers are hidden from the laser pulse by a dominant canopy and tree maxima locations may not be interpreted correctly during the LiDAR surfacing and height extraction process.

The precision of volume estimates with single-tree LiDAR procedures in a double-sample process is not affected by the height or tree count bias inherent in LiDAR data. These biases are effectively adjusted during the double-sample inventory procedures. The height bias can be adjusted prior to single-tree volume computations with LiDAR derived heights or afterwards during the double-sample volume adjustment process. Height bias correction prior to volume computation improves the accuracy of the resulting per-unit area volume estimate. The tree count bias caused by canopy coverage or LiDAR surfacing/processing is also effectively adjusted through the double-sample volume computations. Tree count bias however has a major impact on the accuracy of volume estimates in a single-tree procedure computed with single-phase inventory methods. Thus, if there is any doubt about the validity of the tree counts or height bias during LiDAR processing, a double-sample volume computation process should be used.

Ground sample tree measurements are needed to establish the ground-LiDAR height bias and the relationship between standing tree height and dbh. The number of sample trees is dependent upon the number of parameters in the regression models and variation in the data. A reasonable rule of thumb is 25 samples per parameter estimated in a regression model. Since the LiDAR height bias is relatively constant for a species in a local area and the dbh-height relationship for a give set of species-site conditions is also relatively stable, the sample trees can be obtained from either the LiDAR inventory or surrounding forested areas.

Establishing the LiDAR to ground tree height bias requires the matching of trees on the ground and on the LiDAR surface. Past experience has shown that the location of a plot center must be done with a real time, DGPS and the distance and direction to the sample trees from the plot center should be obtained with a laser so that the x, y coordinates of the sample trees can be located on the LiDAR surface.

Sample plot size and shape on the ground and on the LiDAR surface should be a function of tree density on the ground and the LiDAR processing procedures employed. Experience has shown that the ground plot size should be adjusted such that a minimum of 6 and a maximum of approximately 15 trees should be selected. The minimum number is associated with the within and between-plot variation and the maximum is a logistical consideration for minimizing omission/commission errors in tallying trees. Rectangular plots are easier to handle during the LiDAR processing, but more difficult to establish in the field and to use in establishing distance and direction to sample trees from a DGPS location. The cost of a LiDAR inventory can be minimized by flying only a portion of the desired inventory area. As long as the LiDAR swaths cover the desired strata, ground plots could be located randomly or systematically within strata within swaths. DGPS permits the location of sample plots and trees with relative ease and precision.

References

- Avery, T.E; Burkhardt,H.E.. 2002. *Forest Measurements* 5th Edition. McGraw-Hill, New York, NY. 456p.
- Collins, C.A. 2003. Comparing integrated LiDAR and multi-spectral data with field measurements in hardwood stands. MS Thesis. Mississippi State Univ., Starkville, MS, 158 p.
- Holmgren J. 2004. Prediction of tree height, basal area and stem volume in forest stands using airborne laser scanning. *Scandinavian Jour. of For. Res.* 19(6);543-553.
- Lefsky, M.A; Cohen,W.B.; Acker,S.A.; Parker,G T.; Spies, A.; Harding, D..1999. LIDAR remote sensing of the canopy structure and biophysical properties of Douglas-fir western hemlock forests. *Remote Sensing of Environ.* 70(3):339-361.
- Magnussen, S.; Boudewyn; P. . 1998. Derivations of stand heights from airborne laser scanner data with canopy-based quantile estimators. *Can. J. For. Res.* 8:1016-1031.
- Means, J.E.; Acker, S.A.; Fitt, J.B; Renslow, M.; Emerson, L.; Hendrix, C.J. 2000. Predicting forest stand characteristics with airborne scanning lidar. *Photo. Eng. and Remote Sensing* 66(11):1367-1371.
- McCombs, J.W.; Roberts, S.D.; Evans;D.L. 2003. Influence of fusing LiDAR and multispectral imagery on remotely sensed estimates of stand density and mean tree height in a managed loblolly pine plantation. *For. Sci.* 49(3):457-466.
- Naesset, E. 2004. Accuracy of forest inventory using airborne laser scanning: evaluating the first nordic full-scale operational project. *Scandinavian Jour. of For. Res.* 19(6);554-557.
- Naesset, E. 2002. Predicting forest stand characteristics with airborne scanning laser using a practical two-stage procedure and field data. *Remote Sensing of Environment* 80(1):88-99.

- Nelson, R.; Valenti, M.A.; Short, A.; Keller, C.. 2003. A multiple resource inventory of Delaware using airborne laser data. *BioScience* 53(10):981-992.
- Parker, R.C. 2005. Computer automation of a LiDAR double-sample forest inventory. Forest and Wildlife Research Center Publication No. FO275, Mississippi State University, Starkville, MS.
- Parker, R.C.; Evans, D.L. 2006. Industrial application of a LiDAR double-sample forest inventory. Forest and Wildlife Research Center Publication No. FO317, Mississippi State University, Starkville, MS.
- Parker, R.C.; Evans, D.L. 2004. An application of LiDAR in a double-sample forest inventory. *West. Jour. of Appl. For.* 19(2):95-101.
- Parker, R.C.; Glass, P.A. 2004. High versus low-density LiDAR in a double-sample forest inventory. *South. Jour. of Appl. For.* 28(4):205-210.
- Parker, R.C.; Mitchel, A.L. 2005. Smoothed versus unsmoothed LiDAR in a double-sample forest inventory. *South. Jour. of Appl. For.* 29(1):40-47.
- Persson, A.; Holmgren, J.; Soderman, U. 2002. Detecting and measuring individual trees using an airborne laser scanner. *Photogrammetric Engineering and Remote Sensing* 68(9):925-932.
- Popescu, S.; Wynne, W. H.; Nelson, R.F. 2002. Estimating plot-level tree heights with lidar: local filtering with a canopy-height based variable window size. *Computers and electronics in agriculture* 37:71-95.
- Williams, E.C. 2006. Minimum data input for a LiDAR based timber inventory. MS Thesis. Mississippi State Univ., Starkville, MS, 38 p.

Variability of LiDAR volume prediction models for productivity assessment of radiata pine plantations in South Australia

J. Rombouts¹, I.S. Ferguson² & J.W. Leech³

¹School of Forest and Ecosystem Science, University of Melbourne & Resource Planning Section, ForestrySA, rombouts.jan@forestrysa.sa.gov.au

²School of Forest and Ecosystem Science, University of Melbourne, iansf@unimelb.edu.au

³Forestry Systems, jleech@ozemail.com.au

Abstract

Site Quality (site productivity) information underpins many aspects of radiata pine plantation management in South Australia. The criterion of Site Quality is volume production at age 10 and is directly assessed by means of plot based and ocular assessments. Trials examining the use of LiDAR for Site Quality assessment were commenced in 2002. LiDAR data was captured using three different LiDAR systems in 2002, 2006, 2007 and 169 field plots were measured across 9 sites. A study was carried out to investigate the effect of LiDAR data capture parameters Campaign and Site on the regression relationships between forest and LiDAR variables. The study found that the factor Campaign had a significant effect on volume prediction models while a possible Site effect was detected for one Site. Predominant height prediction models were unaffected. Introducing Campaign and Site parameters in volume prediction models reduced Root Mean Square Error by up to 25.5%. Predominant height and volume prediction models explained 95.3% and 95.2% of the variance respectively. Campaign effects were not due to scanning angle, flying altitude or point density effects but appear to reflect differences in LiDAR systems and drought effects. Calibration protocols and modelling strategies are therefore needed for general application.

Key words: site productivity, LiDAR, modelling, stand volume, radiata pine

1. Introduction

Site Quality (site productivity) information underpins many aspects of radiata pine plantation management in South Australia. The productivity criterion used is total volume production to small end diameter underbark 10 cm, at or near age 10 y (Lewis *et al.*, 1976). The Site Quality assessment method, in use since 1949, relies on objective (plot based) and subjective (ocular) assessments before any commercial thinning takes place. It results in a map showing seven Site Quality classes at a resolution of 0.1 ha (Figure 5).

The literature describes many examples of LiDAR estimation of stand volume (Maclean and Krabill, 1986; Nelson *et al.*, 1988 and many others). Recognising that Site Quality assessment is a problem of assessing spatial variation in stand volume, studies were commenced in 2002 to test the feasibility of LiDAR based Site Quality assessment. The methodological framework adopted was the area based or height distribution method (Næsset, 2002). At the core of this method is the development of regression relationships between forest and LiDAR variables at the plot level.

Field data collection for calibration of prediction models constitutes a necessary and costly step in the method. The site and forest-type dependency of forest-LiDAR relationships has been the subject of several studies (Næsset *et al.*, 2005; Lefsky *et al.*, 2005; and others). These studies found that many forest-LiDAR relationships held across a broad range of sites and forest types when identical LiDAR instruments and comparable data collection parameters were applied. Changes in LiDAR

systems and flight parameters may change the relationships between forest and LiDAR variables (Holmgren *et al.*, 2003, Lovell *et al.*, 2005; Chasmer *et al.*, 2006 and others).

The data for this study were collected in 2002, 2006 and 2007. Each trial contributed new sites and soil types. Each trial made use of a different LiDAR system. The objective of this study was to detect, describe and incorporate any “Site” and “Campaign” effects in the regression relationships between forest and LiDAR variables. The structurally homogenous, even aged, plantations of radiata pine comprising the study sites were particularly suited to the pursuit of this objective. As used in this text “Site” refers to the complex of soil, genetics, climate, silviculture and “Campaign” to the complex of LiDAR system and data capture parameters including seasonal effects.

2. Data and materials

2.1 Study sites

Figure 1 shows the location and rainfall at the nine study sites in the South East of South Australia. Because preferred assessment age would be between 8 and 10 plantations were selected in age range 7-11 (see Table 1). Sites were also selected so as to represent the main soil groups. In total 1756.2 ha of plantations were included in the study. All plantations were unthinned at time of data capture except for 100 metre wide Fuel Management Zones (FMZ) at the edges of some compartments in sites SP, MH, HO and DR.

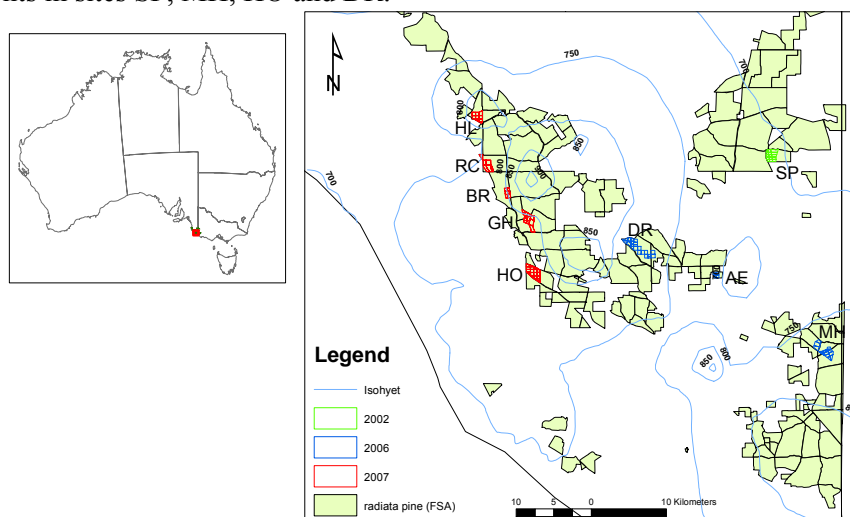


Figure 1: Study sites established in 2002, 2006 and 2007 in the South East of South Australia

2.2 Calibration plots

A total of 169 rectangular (20x25m) calibration plots were measured in 2002, 2006 and 2007. Plot locations were purposively selected so as to sample the full range of the Site Qualities and soil groups found on site. The grouping of soils followed Leech (1978) who identified 7 soil groups, each producing different growth patterns (Table 1 list soil groups in order of importance). At Site DR seven plots were located in the thinned FMZ. Plot corners were located by surveying along compartment boundaries and tree rows using measurement tape. Plantation boundaries had been surveyed by theodolite or differential GPS, with sub metre precision.

Table 1: Site specifics and measurement dates

| Site | SP | DR | AE | MH | BR | RC | HL | HO | GH |
|----------------|---------|---------|---------|----------|---------|---------|---------|---------|---------|
| Area (ha) | 210.9 | 377.4 | 51.5 | 239.0 | 83.6 | 170.6 | 151.4 | 250.5 | 221.3 |
| Soil Groups(*) | C, B | C, E, B | C, E | B | D, E | E, C | C, E | C, D, E | C, E |
| Measured | 04/2002 | 04/2006 | 05/2006 | 05/2006 | 08/2007 | 07/2007 | 08/2007 | 05/2007 | 07/2007 |
| Plantation age | 10 | 9, 10 | 10 | 7, 9, 11 | 10 | 10 | 10 | 9,10 | 9 |

* B: Caroline sand; C: Other sand; D: Tantanoola flinty sand; E: Loamy sand and Terra Rossa

Table 2 shows that the number of plots measured per Site was poorly balanced with no replication of Sites across Campaigns.

Table 2: Number of plots measured by Campaign and Site

| Campaign | Site | | | | | | | | | |
|----------|------|----|----|----|----|----|----|----|----|-------|
| | SP | DR | AE | MH | BR | RC | HL | HO | GH | Total |
| 2002 | 28 | 0 | 0 | 0 | 0 | 0 | 0 | 0 | 0 | 28 |
| 2006 | 0 | 47 | 7 | 25 | 0 | 0 | 0 | 0 | 0 | 79 |
| 2007 | 0 | 0 | 0 | 0 | 9 | 13 | 8 | 17 | 15 | 62 |

Diameter at breast height and predominant height (PDH) were measured in the plots. In South Australia PDH is defined as average height of the 75 tallest trees per ha, restricted so that trees are evenly spaced in each quadrant of the plot. PDH was estimated as the average height of the 4 trees with largest diameter in each plot quadrant, increased by a constant of 0.45m to convert from largest to tallest (based on unpublished analysis).

Stand volume was predicted using a model fitted to stand volume data collected from Permanent Sample Plots (PSP) across the State. Some 372 measurements in stands aged 4-20 years old were used to calibrate a form-factor model predicting under-bark volume to small-end diameter 10cm underbark (V_{10}) with basal area, stocking, PDH and age as predictor variables. Figure 2 shows the range of PDH and V_{10} by Site.

2.3 LiDAR data and pre-processing

A different LiDAR system was used in each of the campaigns, as summarised in Table 3.

Table 3: LiDAR system details and flight parameters of three campaigns

| | 2002 | 2006 | 2007 |
|-----------------------------------|---------------------------|----------------------------|----------------------------|
| System | Optech ALTM 3025 | Leica ALS 50 | Optech ALTM 3100 |
| Date | 7 th July 2002 | 9 th April 2006 | 20 th July 2007 |
| Flying altitude (m) | 1,100 | 1,040 | 1,100 |
| Pulse repetition rate (Hz) | 25,000 | 73,200 | 33,000 |
| Max scanning angle (dgrs) | 15.0 | 13.5 | 12.5 |
| Pulse density (m ⁻²) | 0.5-2.1 | 1.2-9.5 | 2.3-3.2 |
| Returns per pulse | First and last echo | Up to four echoes | Up to four echoes |

Data were captured at comparable flying heights and scanning angles. Point densities varied due to pulse repetition rates, number of fly-overs by the aircraft, scanner properties and data processing by the supplier. During Campaign 2006 higher point densities of up to 9.5 m⁻² were recorded in narrow bands at the edges of flight strips, due to overlapping of strips as well as scanning mirror deceleration effects. Several calibration plots were located in those bands.

LiDAR returns were classified as ground or non-ground points by the supplier. The ground points provided the basis for the construction of a Digital Terrain Model (DTM) using an ESRI ArcGIS implementation of Delaunay triangulation. The height of LiDAR points above ground level was calculated as the difference between a point's z value and the z value of its projection on the DTM.

3. Methods

Ordinary Least Squares regression (OLS) is commonly used to calibrate prediction models in LiDAR applications. One of the base assumptions in OLS is that prediction errors are independent and normally distributed. In the presence of grouping structures in the data set, each with slightly different relationships between response and predictor variables, this assumption may be violated leading to biased estimates of the significance of predictor variables. Grouped data sets are a common occurrence in forest mensuration (for example multiple measurements on a single tree, remeasures of a permanent plot). Several strategies have been proposed to address the problem: data culling to minimise data grouping (Vanclay, 1994), stratifying data and fitting separate models to different strata (Næsset, 2002), introducing new explanatory variables including the use of dummy variables (Næsset *et al.*, 2005), 2-stage modelling coupled with Generalised Least Squares techniques (Ferguson and Leech, 1978) and Mixed Effect Modelling (Gregoire *et al.*, 1995; Breidenbach *et al.*, 2007). Mixed-effects models are primarily used to describe relationships between a response variable and some covariates in data that are grouped according to one or more classification factors. The term mixed effects refers to the distinction between fixed effects (effects associated with an entire population or with certain repeatable levels of an explanatory variable) and random effects (localised effects associated with individual experimental units drawn at random from a population and regarded as additional terms, to account for correlation among observations within the same group), (Pinheiro and Bates, 2000).

Fixed and random effect variables have different roles: fixed effect variables explain variation while random effect variables help organise unexplained variation (Robinson, 2008).

Models were developed in two stages. In the first stage single predictor variable models were fitted for PDH and V_{10} , using OLS. Model residuals were analysed by Campaign and Site to reveal any structures indicative of grouping of the data. In the second stage one, two and three-predictor variable models were fitted, with incorporation of Campaign and Site effects, either as dummy variables in OLS models or as fixed or random effects in linear mixed effect (LME) models.

A range of LiDAR predictor variables were considered, describing different aspects of the distribution of laser heights in the calibration plots. To minimise the impact of differences in LiDAR system capabilities only the first return (i.e. first recorded echo) data were used. *All* first return data were used regardless of classification (ground or vegetation points) or pulse type (single or multiple return pulses). Variables included:

- mean height (mh), mean quadratic height (mqh), standard deviation of heights (sdh)
- maximum height ($hmax$), average of the maximum height in each plot quadrant ($hmax4$)
- percentile heights of the ordered cumulative height distribution ($h0, h10, \dots, h90$)
- proportion of ground returns ($propg$), proportion of returns in height frequency distribution classes ($d0, d10, \dots, d90$).

Most of these variables have been proposed in other studies. Additional predictor variables considered in the models were age, LiDAR point density and scanning angle.

To identify the most effective predictor variables a combinatorial screening approach was adopted whereby models were fitted to all possible combinations of the predictor variables mentioned above. Logarithmic transformations or quadratic forms of the variables were considered. The criterion for selecting the preferred one, two and three-variable models was the Akaike Information Criterion (AIC) – following Gregoire *et al.* (1995) - with the added constraint that each explanatory variable had to be significant at $p < 0.05$. Root Mean Square Error (RMSE) was used as a measure of the precision of model predictions.

In OLS regression the dummy variables were used to distinguish Campaign and Site subgroups in the data set. Hypotheses of difference in slope and/or intercept dummy variables were compared.

In LME models Campaign was introduced as a fixed effect because of the low number of levels of the variable and its specific nature. Site was introduced as a random effect for reasons explained later. Several possible assumptions regarding the random effects were tested: (1) variable intercept but constant slope, (2) variable slope but constant intercept or (3) variable intercept *and* slope. Models with the same fixed effects but different random effect assumptions were compared using likelihood-ratio tests.

Analysis was performed using R statistical software (R-Development-Core-team, 2007).

Volume prediction models were used to generate volume surfaces which were then converted to Site Quality maps using volume to Site Quality conversion tables. LiDAR Site Quality maps were compared with conventional Site Quality maps using an error matrix approach. Because of space constraints the results of this analysis could not be reported here. However an example of a LiDAR and conventional Site Quality map was presented for illustrative purposes.

4. Results

4.1 Models without Site and Campaign effects

Single variable OLS models for PDH and V_{10} were fitted to the whole data set and residuals were

examined. The best predictor for PDH (lowest AIC) was *hmax4* (the mean of the highest returns in each of the four plot quadrants). This was interesting because *hmax4* was the variable that most closely matched the way PDH was measured in the field. There was no evidence of curvature in the relationship. The best single predictor variable for V_{10} was *mgh* (mean quadratic height of first returns, including ground returns). This is a somewhat similar result to that obtained by Nelson *et al.* (2007) in loblolly pine plantations in the south eastern United States. The PDH and V_{10} models explained 95.3% and 91.1% of the variance in the data. Figure 2 shows the fitted models.

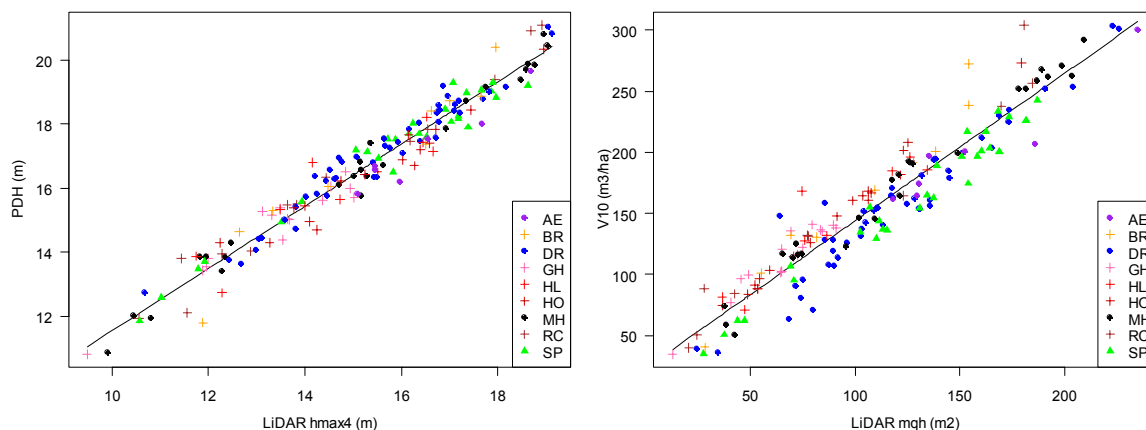


Figure 2: Single variable OLS models for PDH and V_{10}

The PDH model residuals were indifferent to the factor Campaign and evidence of Site effects was weak. The V_{10} model residuals however were strongly correlated with the factor Campaign. There were also significant differences at the Site level but those mostly mirrored Campaign trends, with the notable exception of Site MH (see Figure 3, left). Further analysis showed that the residuals of the models were not significantly correlated with scanning angle or LiDAR point density. Furthermore, plots located in the thinned FMZ of Site DR did not produce different residual patterns compared to unthinned plots and were therefore left in the data set (in fact this confirms the efficiency of the variable *mgh* as a predictor of volume).

It was concluded that Campaign, and possibly Site effects, were affecting volume-LiDAR relationships, suggesting that models in Figure 2 could be improved.

4.2 Models incorporating Site and Campaign effects

Comparison of AIC and likelihood ratio tests showed that Site and Campaign effects were not significant in PDH models and no further analysis was carried out of those models.

Dummy variables for Campaign and Site were introduced into a single variable OLS volume model. Table 4 shows 3 variants of this model. Models with Campaign dependent slope or Campaign dependent intercept *and* slope had a lower AIC indicating that a model structure consisting of parallel lines best fit the data. *C_2006*, *C_2007* and *S_MH* are dummy variables that take the value of 1 when Campaign is equal to 2006 or 2007, or Site is equal to “MH”. Otherwise they have a value of zero.

Table 4: Ordinary Least Squares volume prediction models incorporating Campaign and/or Site effects

| Model | Parameters (standard error) | RMSE | AIC |
|-------|--|------|------|
| 1 | $V_{10} = 22.91 + 1.209\ mqh$ (3.50) (0.029) | 18.4 | 1472 |
| 2 | $V_{10} = -2.36 + 1.300\ mqh + 8.49\ C_2006 + 30.77\ C_2007$ (4.14) (0.025) (3.22) (3.46) | 14.4 | 1388 |
| 3 | $V_{10} = 0.10 + 1.301\ mqh + 28.25\ C_2007 + 15.89\ S_MH$ (3.32) (0.024) (2.51) (3.18) | 13.7 | 1372 |

Model 2 showed significant differences between all three Campaigns at p=95%. Model 3 expressed that without the data for Site “MH”, the difference between Campaign 2002 and 2006 was no longer significant. While the variable S_MH indicated a possible Site effect, its significance had to be questioned given the limitations of the data set (such as no replication of Sites across Campaigns). There was no evidence of Site effects in Campaign 2007 despite the important soil differences between Sites (See Table 1). Analysis showed that the distribution of the Campaign 2007 model residuals was not correlated with Soil Groups.

Campaign and mqh were introduced into LME models as fixed effects. Site was introduced as a random effect because the OLS result for Site “MH” is difficult to rationalise against a range of anticipated effects from other Sites and the ill-balanced distribution of the data (see Table 2). Analysis of model fit parameters and log likelihood parameters showed that random effects were most effectively modelled as random intercepts (parallel lines). Table 5 shows three variants of the model. RMSE are provided both for global and localised (Best Linear Unbiased Predictors - BLUP) predictions.

Figure 3 shows the marked improvement of the distribution of residuals of models including Campaign and Site effects (OLS Model 3 and LME Model 2) compared to the model without these effects.

Table 5: Linear Mixed Effect volume prediction models incorporating Campaign and/or Site effects.

| Model | Effects | | RMSE | | AIC |
|-------|--|-------------|--------|-------|------|
| | fixed (standard error) | random | global | local | |
| 1 | $V_{10} = 18.10 + 1.293\ mqh$ (5.27) (0.024) | <i>Site</i> | 19.3 | 13.7 | 1405 |
| 2 | $V_{10} = -2.26 + 1.299\ mqh + 8.78\ C_2006 + 30.90\ C_2007$ (6.18) (6.20) (0.024) (6.37) | <i>Site</i> | 14.5 | 13.7 | 1382 |
| 3 | $V_{10} = 4.01 + 1.300\ mqh + 24.59\ C_2007$ (4.36) (0.024) (4.39) | <i>Site</i> | 14.8 | 13.7 | 1388 |

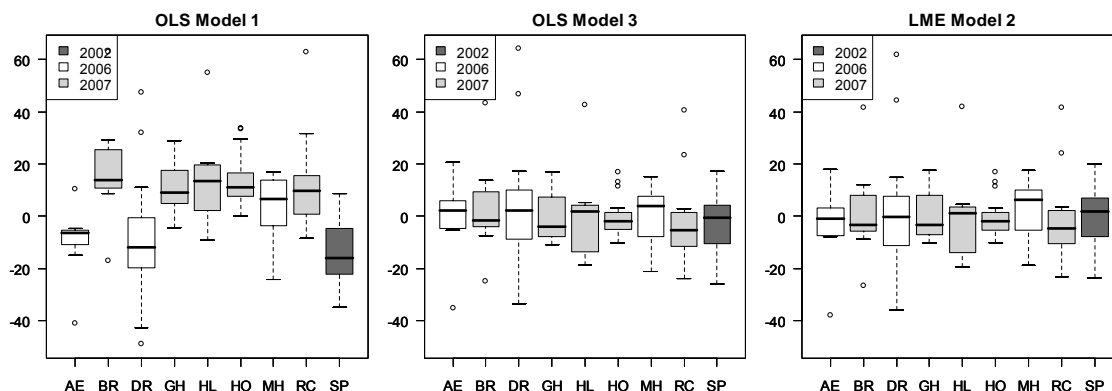


Figure 3: Residuals of OLS and LME volume prediction models grouped by Campaign and Site

Likelihood ratio tests comparing the LME models with their corresponding OLS form were all significant at the 95% probability level. Model 2 was the model with the lowest AIC, and interestingly the variable C_{2006} was not significant at 95%. According to this model therefore the difference between the Campaign 2002 and 2006 effects was not as important as indicated by corresponding OLS model 2. Given the data and the Campaign circumstances (rainfall in preceding year, see Discussion) the LME inference seems the more plausible one.

Incorporating Campaign and Site effects in prediction models reduced RMSE by up to 25.5%. Analysis not reported here showed that the inclusion of additional LiDAR variables failed to improve model fit and that Campaign and Site effects remained significant. OLS model 3 explained 95.2% of the variance, LME model 1 (BLUP) explained 95.1%.

Site Quality maps were compiled using LME, Model 1 and were compared with conventional Site Quality maps. An example is shown in Figure 4 and clearly demonstrates the potential of LiDAR as an alternative basis for Site Quality assessment.

5. Discussion

Significant Campaign effects were observed in the relationship between mqh and plot V_{10} . No such effects were observed in the relationship between $hmax4$ and plot PDH. This indicated that Campaign effects affected the shape but not the range (minimum, maximum) of the distribution of LiDAR first returns heights observed in a plot. Differences in flying height, scanning angle and point density were rejected as possible explanations of these effects. There simply were no significant differences in flying height between Campaigns and there was no correlation whatsoever between scanning angle or point density and the model residuals of OLS, Model 1. The observations in this study were mostly consistent with the findings of Chasmer *et al.* (2006) who reported greater canopy penetration rates as laser pulse energy increased. However, that study considered *all* pulse echoes (up to four) rather than just the first echoes used in this study. A more plausible hypothesis perhaps was that the severe drought in the year leading up to Campaign 2007 reduced plantation leaf area and hence the relationship between mqh and plot V_{10} . Linder *et al.* (1987) found that in a period of drought radiata pine responds by producing shorter needles, as well as shedding significantly more older needles earlier in the summer. The rainfall in the 12 months preceding Campaign 2007 data capture was 554 mm while it was 762 and 707 mm in the year leading up to Campaign 2002 and 2006 respectively. Nelson *et al.* (2000) offered a similar explanation in a study in Costa Rica.

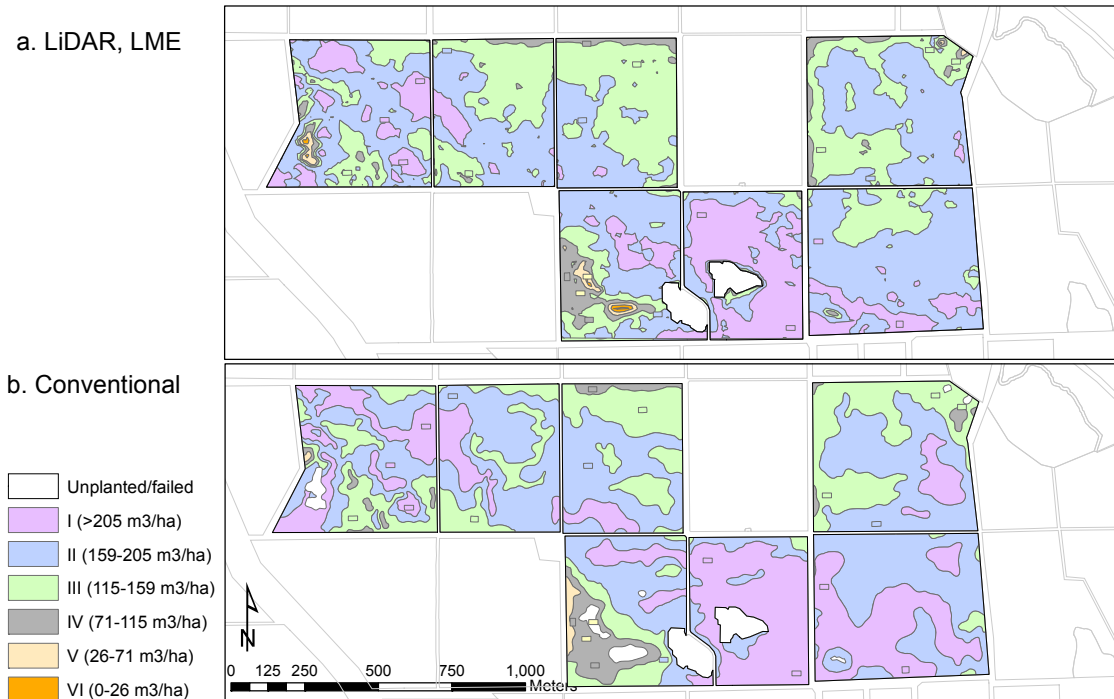


Figure 4: LiDAR and conventional Site Quality maps for Site DR, 9 year old plantation. Calibration plots are shown in a colour indicating field measured Site Quality.

The only evidence of a possible Site effect was observed in Site MH. It has been well documented that soil and climate differences may lead to site specific relationships between stand height and stand volume (Lewis *et al.*, 1976; Skovsgaard and Vanclay, 2007). However, given the isolated occurrence of a Site effect in this study, given that there was no replication of comparable Site conditions in the study and given the ill-balanced distribution of data, treating Site as a random effect in a mixed effect model seemed a more prudent path for prediction.

Mixed effect modelling may also provide advantages where a model needs to be applied outside the model's domain (where Site is unknown) or when the number of dummy variables becomes unmanageable. The inclusion of LiDAR variables additional to *mgh* into the prediction models did not significantly improve the models. This is consistent with the findings of Nelson *et al.* (2007).

The objective of Site Quality assessment is to make site-specific, spatially explicit estimates of forest productivity. The Campaign and Site effects detected in this study can therefore not be ignored. Calibration data collection protocols need to be developed that produce the field data necessary to detect and quantify these effects. Alternative sampling strategies such as random, systematic and purposive sampling need to be compared to identify the strategy that best fits the purpose of the data, which is to fit a calibration model of known structure. Modelling techniques need to be adopted that allow for Campaign and Site effects to be expressed and make efficient use of calibration data collected in the past. Planned research aims to address these questions.

6. Conclusion

The study has produced evidence that Campaign and possibly Site effects influence the relationships between stand and LiDAR variables in young age radiata pine plantations. Of the two effects Campaign is by far the more important one; volume relationships were significantly affected while predominant height relationships were not. These effects were successfully incorporated in volume prediction models using Ordinary Least Squares and Mixed Effect

modelling techniques resulting in reductions of RMSE by up to 25.5%. Hypotheses as to the cause of the effects were presented. The evidence indicates that Site and Campaign effects cannot be ignored in the calibration of LiDAR prediction models for Site Quality assessment and should be considered in field data collection protocols and modelling techniques. Research needs were highlighted.

Acknowledgements

The considerable support of ForestrySA in conducting this study is gratefully acknowledged. Many thanks to ForestrySA technical staff for their professionalism in the field.

References

- Breidenbach, J., McGaughey, R.J., Andersen, H.-E., Kandler, G. and Reutebuch, S., 2007. A mixed-effect model to estimate stand volume by means of small footprint airborne LiDAR data for an American and a German study site. *Proceedings ISPRS Workshop on Laser Scanning 2007 and SilviLaser 2007*, Espoo, September 12-14, 2007, Finland.
- Chasmer, L., Hopkinson, C., Smith, B. and Treitz, P.M., 2006. Examining the influence of Changing Laser Pulse Repetition Frequencies on Conifer Forest Canopy Returns. *Photogrammetric Engineering & Remote Sensing*, 72(12) pp. 1359-1367.
- Ferguson, I.S. and Leech, J.W., 1978. Generalised least squares estimation of yield functions. *Forest Science*, 24 (1) pp. 247-262.
- Gregoire, T.G., Schabenberger, O. and Barrett, J.P., 1995. Linear modelling of irregularly spaced, unbalanced, longitudinal data from permanent-plot measurements. *Canadian Journal Forest Research*, Vol. 25 pp. 137-156.
- Holmgren, J., Nilsson, M., & Olsson, H. (2003) Simulating the effects of lidar scanning angle for estimation of mean tree height and canopy closure. *Canadian Journal Of Remote Sensing*, Vol. 29, No. 5 pp. 623-632.
- Leech, J.W., 1978. Radiata pine yield models. Ph.D. Thesis, 262 pp. Australian National University.
- Lefsky, M.A., Hudak, A.T., Cohen, W.B. and Acker, S.A., 2005. Geographic variability in LiDAR predictions of forest stand structure in the Pacific Northwest. *Remote-Sensing-of-Environment*, 95(4) pp. 532-548.
- Lewis, N.B., Keeves, A. and Leech, J.W., 1976. Yield Regulation in South Australian Pinus radiata plantations. *Bulletin No 23, Woods and Forests Department, South Australia*.
- Linder, S., Benson, M.L., Myers, B.J. and Raison, R.J., 1987. Canopy dynamics and growth of Pinus radiata. I Effects of irrigation and fertilization during a drought. *Canadian Journal Forest Research*, Vol. 17 pp. 1157-1165.
- Lovell, J.L., Jupp, D.L.B., Newnham, G.J., Coops, N.C. and Culvenor, D.S., 2005. Simulation study for finding optimal lidar acquisition parameters for forest height retrieval. *Forest Ecology and Management*, 214 pp. 398-412.
- Maclean, G.A. and Krabill, W.B., 1986. Gross-merchantable timber volume estimation using an airborne LiDAR system. *Canadian Journal of Remote Sensing*, Vol. 12(5) pp. 7-18.
- Næsset, E., 2002. Predicting forest stand characteristics with airborne scanning laser using a practical two-stage procedure and field data. *Remote Sensing of Environment*, 80(1) pp. 88-99.
- Næsset, E., Bollandsås, O.M. and Gobakken, T., 2005. Comparing regression methods in estimation of biophysical properties of forest stands from two different inventories using laser scanner data. *Remote Sensing of Environment*, 94(4) pp. 541-553.
- Nelson, R. *et al.*, 2007. Investigating RaDAR-LiDAR synergy in a North Carolina pine forest. *Remote Sensing of Environment*, 110 pp. 98-108.
- Nelson, R. *et al.*, 2000. Canopy height models and airborne lasers to estimate forest biomass: two problems. *International Journal of Remote Sensing*, 21(11) pp. 2153-2162.
- Nelson, R., Krabill, W. and Tonelli, J., 1988. Estimating forest biomass and volume using airborne laser data. *Remote-Sensing-of-Environment*, 24(2) pp. 247-267.
- Pinheiro, J.C. and Bates, D.M., 2000. Mixed-effects models in S and S-plus. *Springer-Verlag* 528 pp.

- R-Development-Core-team, 2007. R: A language and environment for statistical computing. *Technical report, R Foundation for Statistical Computing.*
- Robinson, A., 2008. icebreakeR. <http://www.ms.unimelb.edu.au/~andrewpr/r-users/icebreakeR.pdf> /last accessed 15 May 2008.
- Skovsgaard, J.P. and Vanclay, J.K., 2007. Forest site productivity: a review of the evolution of dendrometric concepts for even-aged stands. *Forestry*, 81(1) pp. 13-32.
- Vanclay, J.K., 1994. Modelling Forest Growth and Yield. *Originally published CAB International, Wallingford UK ISBN 085 198 913 6*, 312 pp.

Estimation of crown coverage using airborne laser scanning

J. Holmgren¹, F. Johansson¹, K. Olofsson¹, H. Olsson¹ & A. Glimskär²

¹Swedish University of Agricultural Sciences, Department of Forest Resource Management, johan.holmgren@srh.slu.se; w03frjo1@stud.slu.se; kenneth.olofsson@srh.slu.se; hakan.olsson@srh.slu.se

²Swedish University of Agricultural Sciences, Department of Ecology, anders.glimskar@ekol.slu.se

Abstract

Vegetation mapping for environmental monitoring is today conducted by manual photo-interpretation combined with field surveys. This study is the first attempt in Sweden to investigate the potential of using Airborne Laser Scanning (ALS) for the estimation of crown coverage of tree crowns and shrubs. Thirty field plots were randomly allocated within a 1×1 km² area in southern Sweden. All plants with any part inside the 10 m radius and with a height greater than 0.3 m were measured. The field data were used to derive crown coverage for each plot. Proportions of laser returns within height intervals were derived from ALS data and used as explanatory variables in simple linear regression models for estimation of crown coverage of trees and shrubs. For estimation of tree crown coverage (> 3.0 m height) the root-mean-square-error (RMSE) was 4.9%. For estimation of total (trees and shrubs) crown coverage (> 0.3 m height) the RMSE was 6.3%. These RMSE values were achieved despite a mixture of tree species on the field plots. However, the analysis was not sufficient for high accuracy estimations of the amount crown coverage from shrubs (0.3-3.0 m height interval) below a tree canopy.

Keywords: crown coverage, shrubs, vegetation mapping, LiDAR

1. Introduction

Detailed vegetation mapping for selected areas is, in Sweden, conducted by using field surveys in combination with manual photo interpretation. The manual photo interpretation technique is however costly and the results are dependent on the interpreter. It is therefore difficult to obtain objective quantitative measurements that are suitable for comparisons over time. In addition, aerial photo interpretation will only provide information about the uppermost layers of a vegetation canopy.

Use of aerial photo interpretation for vegetation assessment in Sweden includes: (1) the general vegetation map that is created on a regional basis, (2) the sample based National Inventory of Landscapes in Sweden (NILS) program (<http://nils.slu.se/>), and (3) the mapping and monitoring of Natura 2000 sites. For both the NILS program and for the Natura 2000 monitoring there is a need to develop objective and cost efficient methods for following changes in different layers of the vegetation canopy. A study of the early specifications for monitoring of Natura 2000 sites in Sweden (Naturvårdsverket 2005) revealed that vegetation cover and height are of high relevance for monitoring of more than 40 Natura 2000 nature types.

In Scandinavia, Airborne Laser Scanning (ALS) is now an operational technique for producing maps of forest timber and pulp resources. ALS data based methods for estimation of variables of relevance for the forest industry, such as tree heights, stem volume, and stem diameter, have already been successfully developed. These methods have also been introduced as commercial services that are provided by forest inventory companies (Næsset *et al.* 2004). However, there are so far only limited developments of laser remote sensing for vegetation mapping in the

context of habitat monitoring. For example, canopy height derived from ALS was found to be a strong predictor of bird species richness in the temperate forests of Maryland, USA (Goetz *et al.* 2006). Some of the variables that are important for vegetation mapping have been estimated in several studies, for example above ground biomass (*e.g.*, Nelson *et al.* 1988; Means *et al.* 1999; Lefsky *et al.* 2002a; Lim and Treitz 2004). The height and cover of the canopy surface are usually estimated but it is also possible to estimate canopy gaps and canopy height profiles (Lefsky *et al.* 2002b). Some studies reports estimates of Leaf Area Index (LAI) (*e.g.*, Parker *et al.* 2001; Hagiwara *et al.* 2004; Morsdorf *et al.* 2006, Solberg *et al.* 2006), as well as the canopy fraction (*e.g.*, Hopkinson and Chasmer 2007).

The current pilot study is the first Swedish attempt to asses ALS based vegetation mapping for environmental monitoring. The study was limited to investigating the ability to estimate crown coverage of tree crowns and shrubs using ALS data. The objective was to build regression models based on ALS data for estimation of crown coverage on field plots, and validate these models.

2. Material and Methods

2.1 Study area

The study area is located in southern Sweden (Lat. 56° 41' N., Long. 13° 9' E.). The area is the inner 1×1 km² of a NILS-survey-unit (Essen *et al.* 2007).

2.2 ALS data

The study area was laser scanned the 28th of October 2006 by using a LiteMapper 5600 ALS system operated from a fixed winged aircraft, Partinavia P68B, with an altitude of 180 m above ground level and a flight speed of 75 ms⁻¹. The strip side overlap was 80% and the field of view was 45 degrees, but by not using overlapping data the maximum used field of view could be reduced to 35 degrees. The pulse repetition rate was 100 kHz. The pulse density was approximately 20 returns per square meter. Each emitted laser pulse could result in three different return pulses: single return pulse (P0), first return pulse of a double return (P1), or second return pulse of a double return (P2). ALS data were processed in order to provide measures of vegetation height above ground level by first classifying each laser return as either ground or vegetation using the TerraScan software (Soininen 2005). Interpolation was then performed, by using the laser return classified as ground hits in order to create a Digital Elevation Model (DEM). Laser canopy height, *i.e.* the vertical distance to ground (DEM-value), was derived for each laser return.

2.3 Field data

A total of 30 circular field plots with 10 m radius located within the laser scanned area were field surveyed from June to August 2007. The aim of the field survey was to describe the three dimensional structure of trees and shrubs with high accuracy. Prior to the field survey, homogenous polygons (forest stands) had been delineated and for each polygon tree crown coverage had been estimated by photo-interpretation. For the allocation of field plots, the polygons were classified according to tree crown coverage and field plots were randomly placed within each class. The position of the field plot centre was measured using Global Navigation Satellite System (GNSS). The GNSS data were post processed by using data from a reference station. After post processing sub-meter accuracy was expected for open areas, *i.e.* areas with no tree cover. However, position data could be less accurate due to poor satellite configuration and a dense tree cover. All plants with a height greater than 3.0 m were classified as trees, and all plants with a height of 0.3 to 3.0 m were classified as shrubs. A tree or shrub was measured if it

had at least some part that could be projected on the ground within the circular field plot. There was a mixture of several species on each field plot (Table 1).

2.3.1 Tree crown coverage

For all trees on a field plot, stem diameter was measured and species registered. The azimuth and distance from the plot centre to the centre of the tree stem was measured by using a compass and an ultrasonic distance measuring device, respectively. Tree height was measured for a sample of five trees from each of the tree species groups: Scots Pine (*Pinus silvestris*), Norway spruce (*Picea abies*), and deciduous trees, on each field plot, or less if there not were enough of trees of a particular tree species group. For each tree, major and minor axes were measured for an ellipse describing the extent of the living part of the crown. One axis of the ellipse was in the direction to the plot centre in order to make it possible to calculate the proportion of the ellipse that was within the field plot. For each tree individual, the ellipse coverage, a value between 0 and 1, was estimated as the projected area on ground of all leaves and branches inside the ellipse that were alive divided by the total area of the ellipse.

2.3.2 Shrub crown coverage

All shrubs were measured that were totally or partially situated within the field plot. For all individuals, species were registered and height was measured. The distance and azimuth from the plot centre to the centre of a shrub was measured in the same way as for the trees. For each shrub, major and minor axes were measured of an ellipse that describes the extent. One of the axes of the ellipse was in the direction to the plot centre. For each shrub individual, the ellipse coverage, a value between 0 and 1, was estimated as the projected area on ground of all leaves and branches inside the ellipse that were alive divided by the total area of the ellipse.

2.3.3 Calculation of crown coverage

For each field plot, a raster image with 0.1 m raster cell size was created and all cell values were first set to zero. For a specific raster cell, estimates of crown coverage were accumulated by using the crown coverage value of all ellipses that covered the raster cell. If the accumulated value of a raster cell was greater than one, the raster cell value was set to one. This procedure resulted in 30 field-survey data generated images of crown coverage (see Figure 1), one for each field plot. The crown coverage area C for height interval h and for plot i was calculates as

$$C_i = \sum_{k=1}^m \sum_{l=1}^n A_{kl} \times L_{kl} \times P_{kl} \quad (1)$$

where A_{kl} is the raster cell area, L_{kl} is the accumulated ellipse coverage values from trees or shrubs with height within height interval h and with ellipses covering the raster cell of column k and row l for the $m \times n$ raster. The value of P_{kl} was set to one if the raster cell was inside the 10 m radius plot, otherwise zero. Field measured tree crown coverage (C_c) was derived for plot i by using $h \geq 3$ m and dividing C_i with the total plot area. Field measured total crown coverage (C_v) was derived for plot i by using $h \geq 0.3$ m and dividing C_i with the total plot area.

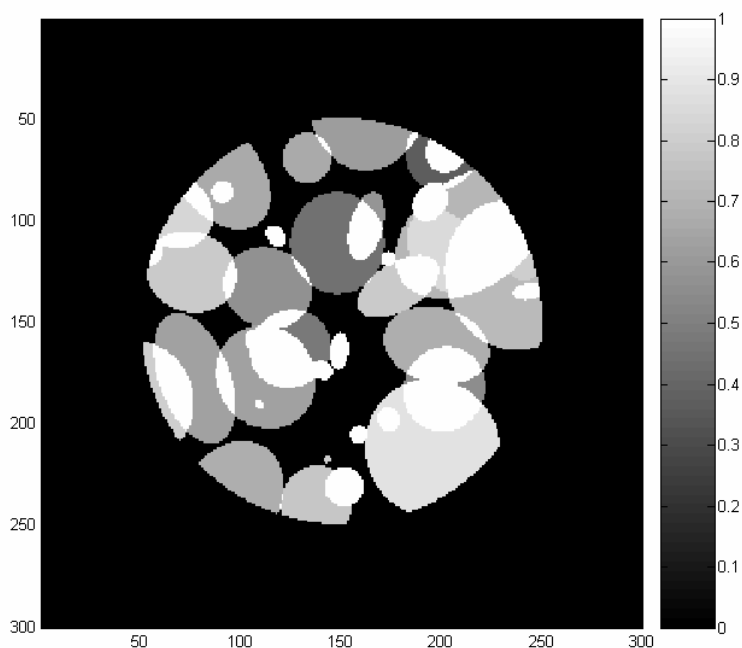


Figure 1: Raster image (1 dm resolution) for one of 30 field plots with measured ellipses that describe extent and proportion of projected area of leaves and branches (crown coverage).

Table 1: Number of shrubs and trees grouped into Norway spruce, Scots pine, and deciduous trees for 30 field plots, and mean height and mean stem diameter (range within brackets) for shrubs and trees, respectively

| Plot | Shrubs (0.3-3.0 m height) | | | Height (cm) | Trees (> 3.0 m height) | | | Diameter (mm) |
|------|---------------------------|--------|-----------|---------------|------------------------|--------|-----------|---------------|
| | Pine | Spruce | Deciduous | | Pine | Spruce | Deciduous | |
| 1 | 0 | 3 | 1 | 137 (59-230) | 16 | 1 | 4 | 244 (40-488) |
| 2 | 1 | 1 | 2 | 51 (32-67) | 0 | 25 | 0 | 126 (50-312) |
| 3 | 0 | 22 | 2 | 154 (42-300) | 8 | 14 | 0 | 197 (36-600) |
| 4 | 0 | 14 | 1 | 144 (60-271) | 18 | 4 | 3 | 241 (30-520) |
| 5 | 0 | 0 | 6 | 69 (46-97) | 9 | 0 | 8 | 285 (41-457) |
| 6 | 0 | 32 | 0 | 117 (34-270) | 4 | 18 | 3 | 247 (41-545) |
| 7 | 0 | 5 | 3 | 113 (34-265) | 9 | 6 | 2 | 307 (74-620) |
| 8 | 0 | 3 | 2 | 130 (43-250) | 13 | 4 | 11 | 235 (61-429) |
| 9 | 0 | 21 | 15 | 144 (47-299) | 18 | 5 | 12 | 245 (69-436) |
| 10 | 0 | 1 | 31 | 111(34-246) | 10 | 2 | 26 | 202 (19-417) |
| 11 | 0 | 4 | 15 | 52 (36-89) | 15 | 11 | 1 | 261 (29-520) |
| 12 | 0 | 41 | 0 | 114 (37-300) | 11 | 11 | 5 | 285 (30-585) |
| 13 | 0 | 8 | 3 | 195 (112-297) | 3 | 9 | 29 | 184 (40-603) |
| 14 | 0 | 12 | 11 | 134 (59-264) | 17 | 16 | 9 | 232 (36-456) |
| 15 | 0 | 2 | 11 | 191 (48-290) | 0 | 49 | 0 | 162 (98-248) |
| 16 | 20 | 4 | 31 | 90 (33-243) | 0 | 0 | 1 | 46 (46-46) |
| 17 | 88 | 21 | 86 | 92 (32-280) | 3 | 0 | 0 | 70 (66-74) |
| 18 | 30 | 3 | 19 | 70 (32-162) | 0 | 0 | 0 | 0 |
| 19 | 189 | 6 | 65 | 70 (27-208) | 0 | 0 | 0 | 0 |
| 20 | 114 | 6 | 34 | 69 (31-193) | 0 | 0 | 0 | 0 |
| 21 | 14 | 5 | 63 | 101 (31-291) | 12 | 1 | 13 | 147 (18-330) |
| 22 | 14 | 4 | 102 | 124 (33-298) | 46 | 1 | 22 | 106 (19-363) |
| 23 | 72 | 16 | 116 | 105 (38-269) | 3 | 0 | 13 | 65 (30-147) |
| 24 | 133 | 19 | 127 | 78 (30-298) | 7 | 0 | 1 | 121 (61-149) |
| 25 | 155 | 35 | 55 | 71 (30-271) | 9 | 0 | 1 | 143 (73-224) |
| 26 | 5 | 16 | 63 | 129 (36-286) | 7 | 1 | 39 | 86 (20-267) |
| 27 | 21 | 16 | 73 | 105 (31-281) | 11 | 16 | 5 | 142 (39-355) |
| 28 | 127 | 15 | 113 | 109 (31-297) | 17 | 4 | 21 | 80 (21-282) |
| 29 | 84 | 13 | 124 | 81 (31-287) | 11 | 1 | 8 | 111 (26-227) |
| 30 | 19 | 6 | 49 | 87 (34-297) | 16 | 1 | 19 | 131 (35-351) |

2.4 Correction of field plot positions

Tree crowns of an area of $50 \times 50 \text{ m}^2$ around each plot were automatically delineated by using an earlier developed algorithm (Holmgren and Wallerman 2006). The delineation of tree crowns from laser data was based on template matching. First, from a Digital Canopy Model (DCM) that was derived from laser elevation data, a binary crown area image was derived with value one for crown area, and closing (dilation followed by erosion) was performed on this image. A new height value was then interpolated for the DCM at cells with zero height value, but crown area according to the crown area image. Templates were tested at each raster cell of the DCM by setting the height of the template to the value of the DCM value. There were some restrictions when calculating the correlation between templates and laser elevation data: only realistic width-height ratios of the templates were allowed, and no template was tested with less than 25 laser returns. For a correlation image, the value of a raster cell was set to the highest found correlation at that location. The correlation image was then smoothed and used for segmentation: A seed was placed at each raster cell, with a DCM value greater than a height threshold and with a positive correlation value, and was allowed to climb to the neighbour raster cell with the highest correlation value. The raster cells with seeds climbing to the same local maximum defined a tree crown segment.

The result was crown segments; each included an individual tree or a group of trees. The tree position was estimated by taking the x, y-position of the maximum canopy height value within the segment, and a measure of tree height was achieved from the value of the maximum. A crown area of an individual tree was derived by counting the number of raster cells of the crown segment but was not used in this study for further analysis.

The three dimensional spatial pattern of the laser detected trees were matched with the spatial pattern of field measured positions of individual trees on a plot. A matching algorithm was used for this task (Olofsson *et al.* 2008). The plots were both translated and rotated until the best match, *i.e.* maximum correlation value, between the spatial tree-patterns were found. In this way the position of field plots with poor GNSS data could be corrected.

2.5 Statistical analysis

Different combinations of laser return types (first return, second return, or only return) were grouped. The corrected locations of the field plots were used to extract ALS data within the 10 m radius field plots. The proportions of laser returns on a plot that were located 3.0 or 0.3 m above ground level were derived, and used for estimation of tree crown coverage (C_c) and total vegetation coverage (C_v) (trees and shrubs), respectively. The field estimated crown coverage values versus proportions of laser returns within the different height intervals were plotted. Simple linear regression models with and without an intercept were tested for estimation of crown coverage.

3. Result

The proportion of laser returns from the tree canopy was highly correlated with the field measured tree ($h > 3.0 \text{ m}$) crown coverage C_c . The best tested explanatory variable D_c was the proportion of first and only returns (P0+P1) above the height threshold 3.0 m. The best model found was simple linear regression without intercept (Equation 2). The root-mean-square-error (RMSE) was 4.9%. The sizes of residuals (ε) were about the same for the full range of tree crown coverage (Figure 2A). The correlation coefficient was 0.98 between estimated and field measured tree crown coverage.

$$\hat{C}_c = 0.77 \times D_c + \varepsilon \quad (2)$$

There was a low correlation with the crown coverage of only shrubs and the proportion of laser returns within the corresponding height interval, *i.e.* between 0.3 and 3.0 m distance from the ground. No attempts were therefore made to estimate this fraction separately

The proportion of laser returns from the vegetation was highly correlated with the field measured total crown ($h > 0.3$ m) coverage C_v . The best tested explanatory variable D_v was the proportion of first and only returns (P0+P1) above the height threshold 0.3 m. The best model found was a simple linear regression with an intercept (Equation 3). The RMSE was 6.3%. The sizes of residuals (ε) were about the same for the full range of total crown coverage (Figure 2B). The correlation coefficient was 0.96 between estimated and field measured total crown coverage.

$$\hat{C}_v = 0.079 + 0.68 \times D_v + \varepsilon \quad (3)$$

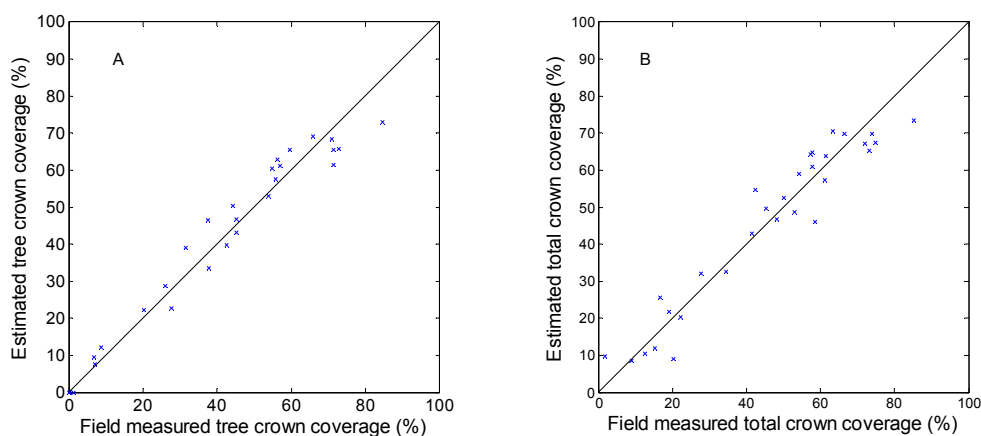


Figure 2: (A) Estimated tree crown coverage versus field measured tree crown coverage (trees with a height above 3.0 m); (B) Estimated total crown coverage versus field measured tree crown coverage (trees and shrubs with a height above 0.3 m).

4. Discussion

The results of this study indicate that it is possible to use airborne laser scanning to obtain objective measurements of vegetation crown coverage. Despite a diverse composition of tree species on the plots, simple regression models could be used to estimate crown coverage with high accuracy.

Morsdorf *et al.* (2006) used the proportion of pulses above a height threshold to estimate fractional cover, *i.e.* crown coverage, but used hemispherical photographs as ground truth data. They derived laser variables, first and last returns separately, and found the highest explanation power for the first return data. They argued that one source of error could be the difference of view angles between the hemispherical camera and the laser scanner sensor. For the simple field method of the present study, different view angles were not a problem because crown coverage was estimated separately for each plant. However, different view angles of the ALS data could be an error source that needs to be accounted for if the method is used operationally.

There might be several reasons for the low correlation of the present study between laser derived variables (proportions within height intervals) and the crown coverage of shrubs (plants within 0.3 and 3.0 m). There are problems in distinguishing small plants and other low objects, *e.g.*, stones, grass, blueberry shrubs. The classification algorithm only uses the position of

reflection locations. It would probably be possible to improve the classification if also full waveform laser data would have been used.

In the present study, only a first attempt was done to estimate crown coverage. It might be possible to improve estimates by extracting more information from ALS data. For instance, Hopkinson and Chasmer (2007) found that intensity based power distribution has higher correlation with the canopy gap fraction than just the laser pulse return distribution for the subclasses single, first, intermediate and last laser returns.

Full waveform data have earlier been used to estimate the vegetation structure at different height levels. For instance, Parker *et al.* (2001) studied the correlation between the power (*i.e.* the waveform) of the accumulated laser pulse return at different heights and the irradiance at the same heights. The use of full waveform data should therefore also be suitable to use in estimating of the amount of shrubs below a tree canopy.

The possibility of using ALS data for estimation of crown coverage should be studied further in order to develop tools for the monitoring of vegetation. It would for instance be of interest to study in more detail how well a layer of bushes might be detected, given different types of over storey. Since the proportion of laser returns also will be dependent on factors such as sensor settings, flight altitudes, *etc.*, there will during the foreseeable future also be a need to use a limited set of field data for the calibrations of the measurements and a suitable design for this field sample should also be studied. It would also be important to carry out real tests of change assessments, where experiments with both increased and decreased canopy coverage between several time points of laser scanning is evaluated.

Acknowledgements

The research in this study was funded by the Swedish Environmental Board. Scancort A/S in Denmark provided the laser scanner data at a reduced price for research and development purposes.

References

- Essen, P.A., Glimskär, A., Ståhl, G., Sundquist, S., 2007. Field instruction for the national inventory of the landscape in Sweden – NILS. Department of Forest Resource Management, Swedish University of Agricultural Sciences, Umeå, Sweden. (available at <http://nils.slu.se/>).
- Goetz, S., Steinberg, D., Dubayah, R. and Blair, B., 2007. Laser remote sensing of canopy habitat heterogeneity as a predictor of bird species richness in an eastern temperate forest, USA. *Remote Sensing of Environment*, 108, 254-263.
- Hagiwara, A., Imanishi, J., Hashimoto, H. and Morimoto, Y., 2004. Estimating leaf area index in mixed forest using an airborne laser scanner. *International Archives of Photogrammetry, Remote Sensing and Spatial Information Sciences*, Vol. XXXVI – 8/W2, pp. 298-300.
- Holmgren, J. and Wallerman, J., 2006. Estimation of tree size distribution by combining vertical and horizontal distribution of LIDAR measurements with extraction of individual trees. In: T. Koukal and W. Schneider (Eds.). *Proceedings from Workshop on 3D Remote Sensing in Forestry*, Vienna, Austria, 14-15 February 2006, pp. 168-173. University of Natural Resources and Applied Life Science, Vienna, Austria.
- Hopkinson, C. and Chasmer, L., 2007. Modelling canopy gap fraction from lidar intensity. In P. Rönnholm, H. Hyypä, and J. Hyypä (Eds.). *Proceedings of the ISPRS Workshop Laser Scanning 2007 and SilviLaser 2007*, Espoo, Finland, 12-14 Sep 2007, pp. 190-194. Helsinki University of Technology, Finland.

- Lefsky, M.A., Cohen, W.B., Harding, D.J., Parker, G.G., Acker, S.A. and Gower, S.T., 2002a. Lidar remote sensing of above-ground biomass in three biomes. *Global Ecology and Biogeography*, 11, 393-399.
- Lefsky, M.A., Cohen, W.B., Parker, G.G. and Harding D.J., 2002b. Lidar remote sensing for ecosystem studies. *BioScience*, 52, 19-30.
- Lim, K.S. and Treitz, P.M., 2004. Estimation of above ground forest biomass from airborne discrete return laser scanner data using canopy-based quantile estimators. *Scandinavian Journal Forest Research*, 19, 558-570.
- Means, J.E., Acker, S.A., Harding, D.J., Blair, J.B., Lefsky, M.A., Cohen, W.B., Harmon, M.E. and McKee, W.A., 1999. Use of Large-Footprint Scanning Airborne Lidar To Estimate Forest Stand Characteristics in the Western Cascades of Oregon. *Remote Sensing of Environment*, 67, 298-308.
- Morsdorf, F., Kötz, B., Meier, E., Irren, K.I. and Allgöwer, B., 2006. Estimation of LAI and fractional cover from small footprint airborne laser scanning data based on gap fraction. *Remote Sensing Environment*, 104, 50-61.
- Næsset, E., Gobakken, T., Holmgren, J., Hyypä, H., Hyypä, J., Maltamo, M., Nilsson, M., Olsson, H., Persson, Å. and Söderman, U., 2004. Laser scanning of forest resources: the nordic experience. *Scandinavian Journal of Forest Research*, 19, 482-499.
- Naturvårdsverket, 2005. Uppföljning av Natura 2000 i Sverige. Rapport 5334, Januari 2005 [In Swedish].
- Nelson, R., Krabill, W. and Tonelli, J., 1988. Estimating Forest Biomass and Volume Using Airborne Laser Data. *Remote Sensing of Environment*, 24, 247-267.
- Olofsson, K., Lindberg, E. and Holmgren, J., 2008. A method for linking field-surveyed and aerial-detected single trees using cross correlation of position images and the optimization of weighted tree list graphs. In *Proceedings of SilviLaser 2008, September 17-19, Edinburg, UK*.
- Parker, G.G., Lefsky, M.A. and Hardin, D.J., 2001. Light transmittance in forest canopies determined using airborne laser altimetry and in-canopy quantum measurements. *Remote Sensing of Environment*, 76, 298-309.
- Soininen, A., 2005. TerraScan for Microstation, Users Guide. Terrasolid Ltd., Helsinki, Finland. (available at www.terrasolid.fi).
- Solberg, S., Næsset E., Hanssen K.H. and Christiansen, E., 2006. Mapping defoliation during a severe insect attack on Scots pine using airborne laser scanning. *Remote Sensing of Environment*, 102, 364-376.

Airborne laser scanning for the identification of boreal forest site types

Mikko Vehmas¹, Kalle Eerikäinen², Jussi Peuhkurinen¹, Petteri Packalén¹ & Matti Maltamo¹

¹Faculty of Forest Sciences, University of Joensuu, P.O.Box 111, FI-80101 Joensuu, Finland. mikko.vehmas@joensuu.fi, jussi.peuhkurinen@joensuu.fi, petteri.packalen@joensuu.fi, matti.maltamo@joensuu.fi

²Finnish Forest Research Institute, Joensuu Research Unit, P.O.Box 68, FI-80101 Joensuu, Finland. kalle.eerikainen@metla.fi

Abstract

Boreal forests site types are used to assess the growth potential of the forests and therefore provide important inventory information. A new approach is proposed here for the site quality assessment of mature forests using airborne laser scanner (ALS) data and the k-NN classifier. Both the echo z-value and the intensity value percentiles of different echo types of ALS data were used in the analysis. The data comprised 274 forest stands of varying sizes belonging to five forest site types varying from very fertile to poor forests in the Koli National Park, Finland. The best overall classification accuracy of all the forest site types achieved was 58.0 %, and for a single class 73%. It is concluded that this ALS-based data analysis technique is applicable to the detection of boreal forests site types in large-scale forest inventories.

Keywords: K-NN Classification; Vegetation.

1. Introduction

In Finland forests are classified into fertility site types according to their underground vegetation (Cajander 1926). The current forest site types of Finland have been located and mapped in conventional stand-based forest inventories (Poso 1983). Aerial photographs have also been used to find different forest habitats, but the results have not been accurate or useful enough for large-scale forest inventories (see Uuttera and Hyppänen 1998). However, Airborne Laser Scanning (ALS), which provides spatially accurate 3D information on forests and is already being applied in practical forestry, could potentially replace conventional field inventory methods for determining tree stocking quantities (see Næsset 2004). ALS data are derived from the measured travel times of pulses between a sensor and a target, and since ALS echoes from targets form three-dimensional point clouds (Lim et al. 2003), they provide accurate information on landscapes and forests (see Ritchie et al. 1992; Næsset 1997; Magnussen and Boudewyn 1998; Maltamo et al. 2006).

Multiple ALS echoes with precise x , y and z coordinates can be identified by processing the backscatter energy of a simple pulse. The data yielded by this technology include various echo types (e.g. first, last, intermediate and only echoes), z -values and intensity values, where the z -value is the height of the echo and the intensity value describes the amount of backscattering from it. Height of the above-ground vegetation is usually of greatest interest in forestry applications (see Hyyppä et al. 2001; Lim et al. 2003; Maltamo et al. 2006; Hopkinson et al. 2006). Intensity values have been studied by Brennan and Webster (2006), for example, who found them to be suitable for distinguishing between different surfaces, but it is only very recently that their applicability to the determination of forest characteristics has been investigated (e.g. Hopkinson and Chasmer 2007; Ørka et al. 2007). This is mainly due to difficulties in scaling and normalizing these values or in their interpretation (Ahokas et al. 2006).

The ALS technique has already been applied to the determination of site quality indicators based on the height distribution characteristics of stands containing certain tree species, which is logical since the height characteristics can be obtained accurately from laser data (see Rombouts 2006; Gatzliolis 2007). This can, in fact, be seen as a remote sensing-based modification of traditional growth and yield studies in which the classification of sites was based on dominant height-age dependences. The site type classification used in Finnish forest inventories, however, is based on Cajander's (1926) system of fertility classes, which operates on assessable stand characteristics, i.e. ground vegetation characteristics and indicator species, rather than explicitly measurable tree variables.

ALS technology should be capable of distinguishing the forest site types because of differences in crown structures and vertical profiles that differ between different forest site types. We present here an ALS data-based k-nearest neighbour method for doing this employing two alternative uses of data, 1) the use of whole data and leave-one-out cross-validation, and 2) use of separate model and test data, which will be compared in terms of classification accuracy.

2. Method

2.1. Study area and forest inventory data

The forest area concerned here is located in the Koli National Park (29°50'E, 63°05'N) in eastern Finland, on the borderline between the southern and middle boreal forest vegetation zones after Kalela (1970, in Kalliola 1973). The total area of the Koli National Park is about 3000 hectares. Extensive areas in its northern part have been left unmanaged for decades; whereas forest management operations were carried out in the southern part until the early 1990s. The area is characterized by a highly variable landscape and tree species structure, with altitudes varying between 95–347 metres above sea level (Lyytikäinen 1991). Following the classification of Cajander (1926), the forest site types identified in the Koli National Park were: 1) very rich (e.g., *Oxalis-Maianthemum* type, OMaT), 2) rich (*Oxalis-Myrtillus*, OMT, herb-rich heath forest), 3) medium (*Myrtillus* type, MT, mesic heath forest), 4) rather poor (*Vaccinum* type, VT/EMT, subxeric heath forest) and 5) poor (*Calluna* type, CT/MCCIT, xeric heath forest).

Table 1. Descriptive statistics for stand areas in hectares by forest site type in the whole data.

| Forest site type | Whole data 336.7 ha (N=274) | | | | | | |
|------------------|-----------------------------|----|------|-------|-------|------|------|
| | N | % | Min | Max | Sum | Mean | S.D. |
| Herb-rich (1) | 61 | 22 | 0.03 | 5.8 | 44.36 | 0.73 | 0.91 |
| OMT (2) | 60 | 22 | 0.13 | 12.13 | 89.04 | 1.48 | 2.12 |
| MT (3) | 60 | 22 | 0.16 | 7.77 | 82.95 | 1.38 | 1.37 |
| VT (4) | 60 | 22 | 0.12 | 6.46 | 77.7 | 1.29 | 1.14 |
| CT (5) | 33 | 12 | 0.04 | 7.02 | 42.92 | 1.3 | 1.58 |

N is the number of stands; % is the proportion of site types; Min is the minimum, Max is the maximum,

Mean is the average area of the forest site types in hectares and S.D. the standard deviation. Herb-rich denotes very rich (1), OMT rich (2), MT medium (3), VT rather poor (4) and CT poor (5) forest site types (Cajander 1926).

The data were randomly assigned into the modelling data and test data, both of which included stands from the northern and southern parts of the National Park. In terms of development classes, the stands used in the analyses were either advanced thinning or mature stands, as these closed boreal forest stands represented advanced successional stages with an advanced ground vegetation and were therefore ideal for site type classification by the method of Cajander (1926). The data comprised 274 forest stands covering an area of 337 ha. The modelling data consisted of 184 forest stands and comprised an area of 241 ha, while the test data consisted of 90 forest stands and covered a total area of 96 ha. The data is presented by forest site types in Table 1.

2.2. Airborne laser scanner data

The scanning was performed on 13th July, 2005, using an Optech ALTM 3100 laser scanner. Two Global Positioning System (GPS) ground stations were used and a total of nine transects were flown at an altitude of 900 metres and a flight speed of 75 m/s. The area covered was approximately 2200 hectares. The laser pulse repetition rate was 100 KHz and the scanning frequency of a swath was 70 Hz, at an angle of ± 11 degrees. The pulse density of the data was 3.9/m², but because of nominal side overlap (35%) and variation in the terrain the actual ground hits varied from approximately 3.2/m² to 7.8/m². The data echoes collected included EUREF-FIN coordinates (x , y and z), flight line numbers, intensity values and echo types in four classes: 1 = only echo, 2 = first echo, 3 = intermediate echo and 4 = last echo. The DTM was produced by the Finnish Geodetic Institute from the last and only echo data using a pixel size of one metre, employing the TerraScan software, which uses the method proposed by Axelsson (2000). In order to analyse the ALS data, the first step was to convert the orthometric heights to an above-ground scale by subtracting the DTM from the corresponding ALS heights (Hyypä et al., 2005). The laser hits are presented by forest site types in Table 2.

Table 2. Numbers of laser echoes/m² by forest site types and proportions (%) of the different types of echoes including the z value and intensity value in the whole data. The letters f, o, l and i indicate the first, only, last and intermediate echoes, respectively, whereas fo is the sum of first and only echoes.

| Forest site type | all | fo | f/fo, % | o/fo % | l/fo % | i/fo % | all/fo % |
|------------------|-----|-----|---------|--------|--------|--------|----------|
| Herb-rich (1) | 7.3 | 5.0 | 37.3 | 62.7 | 38.0 | 6.2 | 144.2 |
| OMT (2) | 7.0 | 5.0 | 35.7 | 64.3 | 36.3 | 5.6 | 141.9 |
| MT (3) | 6.8 | 4.8 | 34.9 | 65.1 | 35.7 | 5.1 | 140.8 |
| VT (4) | 6.4 | 4.7 | 32.1 | 67.9 | 32.8 | 4.0 | 136.8 |
| CT (5) | 6.2 | 5.0 | 22.5 | 77.5 | 22.9 | 1.7 | 124.6 |

2.3. k -NN classification

Classification of forest site types was obtained by using the non-parametric k -NN classifier. Consequently, nearest neighbour methods have been widely used for estimating continuous forest variables (e.g. by Moeur and Stage 1995; Holmström et al. 2001; Maltamo et al. 2006), although they have not been extensively studied in connection with estimating discrete forest variables.

We applied two different ways to use our data. The whole data was divided into reference (modelling) and target (test) data; method described below is the same in both approaches, i.e. whole data approach and model/test data approach. Then a suitable distance metric is chosen to find the nearest neighbour(s). After that the distances between the target units and the reference units are calculated and nearest neighbour(s) are assigned to the target units. Finally estimates for the target units are calculated based on the attributes of the chosen neighbours. At least three issues need to be considered when using the k -NN method: 1) a suitable distance metric, 2) the number of neighbours to be used, and 3) the weighting of the neighbours (LeMay and Temesgen 2005).

A Minkowski distance of order one between the distributions was taken as the distance metric. In the case of discrete distributions it can be defined with the equation (Eqn 1):

$$D_{pq} = \sum_{i=1}^n |p_i - q_i| \quad , \quad (1)$$

where D_{pq} is the distance between the laser echo distributions to be compared, p_i is the proportion of observations of target units in class i , q_i is the proportion of observations of

reference units in class i , and n is the number of classes in the distributions. The value of D_{pq} ranges between 0 (the distributions compared are the same) and 2 (the distributions compared have no observations in the same classes). The chosen distance metric is based on the absolute differences between the laser echo distributions of the target and reference stands and is suitable in situations in which the predictor variables are distributions with unknown characteristics (in this case laser echo height and intensity distributions) and it is assumed that the form of the distribution contains most of the information on the variables of interest (in this case forest site type classes). The distance value can be used in weighting the neighbours by subtracting it from the maximum value, which is 2. When using more than one predictor (i.e. distributions of laser echoes of different types), the distances are calculated separately for the various distributions and then summed using subsequently determined optimal weights.

The classification rule needed for applying the k-NN based classifier was adjusted for the case of several neighbours (n) as follows:

1. $n = 1$: the value of the predicted variable is the value of the nearest neighbour
2. $n > 1$: the weights of the neighbours are summed by class and the estimated class for the target unit is the one with the highest sum of weights.

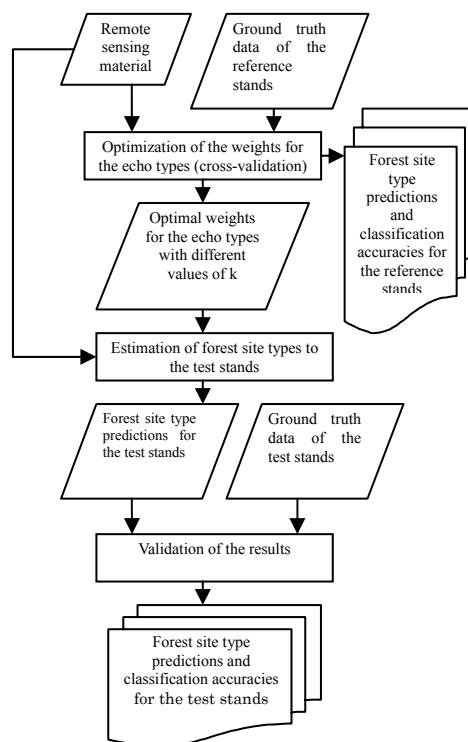


Figure 1: The k-NN estimation procedure.

For the k-NN classification procedure the laser echo heights were classified into 10 cm classes, with the negative echo heights assigned to a class 0 (note that some ALS hits always occur below the DTM level). This classification provided enough observations for all the approximately 300 classes. The laser echo intensities were thereafter classified with a class width that resulted in a corresponding number of classes. The optimal weights for the different types of echoes were searched for by optimizing the overall classification accuracy. The optimization algorithm weighted the combinations systematically so that every echo type was given a weight from 0 to 1 at intervals of 0.1. In addition, all the combinations of weights, which summed to 1, were examined. The optimization was performed on the whole data and modelling data only and used a leave-one-out cross-validation technique in which the target unit

was left out of the reference data. The test stands were classified using the optimal weights found from modelling data and the nearest neighbours were searched for only from the modelling (reference) data. In the case of several neighbours ($n > 1$), the procedure provides not only class estimates but also an idea of the closeness of the target unit to the other classes. However, it should be remembered that the forest site type classes may express the fertility levels on an ordinal scale, but the tree cover of those types should be handled as they are in a nominal scale. The k-NN estimation procedure applied for in the case of using separate modelling and test data is presented in the form of a flowchart in Figure 1.

3. Results

The classification results were calculated with one, three and five nearest neighbours, and optimal weights were determined for the accuracy of classification of the stands into all forest site types. All the neighbourhood combinations were computed for the stands in the whole data as well as to the test data and both z and intensity values were used with different weights (Table 3) to optimize the classification results. The z -values have the highest weights with one neighbour, whereas the weight of the intensity increases with three and five neighbours.

Table 3: Weights of variable distributions used in the k-NN method with 1, 3 and 5 neighbours in two approaches: 1) whole data (N=274) 2) test data (N=90)

| Classification method | Z-values (z) | | | | | | Intensity values (i) | | | | | |
|-----------------------|------------------|-----|-----|---|-----|-----|--------------------------|-----|-----|-----|-----|-----|
| | sum z | F | l | i | fo | lo | sum i | f | l | i | fo | lo |
| 1NN – 1) | 0.8 | | 0.2 | | 0.1 | 0.5 | 0.2 | 0.1 | | | | 0.1 |
| 1NN – 2) | 0.9 | 0.1 | 0.2 | | 0.3 | 0.3 | 0.1 | | | | | 0.1 |
| 3NN – 1) | 0.4 | 0.1 | 0.1 | | | 0.2 | 0.6 | 0.1 | 0.1 | | 0.4 | |
| 3NN – 2) | 0.2 | | 0.2 | | | | 0.8 | 0.1 | 0.1 | 0.4 | 0.2 | |
| 5NN – 1) | 0.5 | | 0.2 | | 0.1 | 0.2 | 0.5 | 0.3 | | 0.1 | 0.1 | |
| 5NN – 2) | 0.4 | 0.1 | | | | 0.3 | 0.6 | 0.2 | 0.2 | 0.1 | | 0.1 |

f denotes the first pulse, l the last pulse, i the intermediate pulse, fo the first and only pulses together and lo the last and only pulses together.

A forest classification percentage matrix for all of the five forest types is presented in Table 4, where the diagonal shows the correct classifications. The best overall classification result (58.0%) was achieved with the whole data with 5 nearest neighbour and the best single class classification (poor, CT 72.7%) with 1 nearest neighbour. In the case of the whole data, the decreased numbers of neighbours (1 or 3) altered the classification of some stands and decreased the overall classification accuracy (Table 4). The success rates obtained for the classification of herb-rich forests, for example, were 52.5% and 62.3% with one and five neighbours, respectively. The classification done by the test data gave only slightly worse overall classification percentages than with the whole data. In addition, some single class classifications were even better when using the test dataset.

With one nearest neighbour the classification percentage was highest (34.4%) in class 3 (medium, MT) and decreased to classes 1 (17.8%) (very rich, OMaT) and 5 (11.1%) (poor, CT). With five nearest neighbours the classification percentage varied more evenly over the five classes (Table 4).

Table 4: Classification success rates (%) matrix obtained by the k-NN method with 1, 3 and 5 nearest neighbours for all forest site types in two approaches: 1) whole data (N=274) 2) test data (N=90)

| 1NN – 1) 56.6 % | | | | | | 3NN – 1) 56.9 % | | | | | | 5NN – 1) 58.0 % | | | | | |
|-----------------|----|----|----|----|----|-----------------|----|----|----|----|----|-----------------|----|----|----|----|----|
| | 1* | 2 | 3 | 4 | 5 | | 1 | 2 | 3 | 4 | 5 | | 1 | 2 | 3 | 4 | 5 |
| 1* | 52 | 23 | 18 | 2 | 5 | 1 | 59 | 21 | 15 | 2 | 3 | 1 | 62 | 20 | 13 | 0 | 5 |
| 2 | 15 | 45 | 32 | 8 | 0 | 2 | 18 | 47 | 27 | 8 | 0 | 2 | 20 | 43 | 28 | 8 | 0 |
| 3 | 7 | 15 | 63 | 13 | 2 | 3 | 10 | 18 | 60 | 10 | 2 | 3 | 10 | 20 | 58 | 10 | 2 |
| 4 | 2 | 3 | 23 | 57 | 15 | 4 | 0 | 8 | 17 | 65 | 10 | 4 | 0 | 8 | 12 | 68 | 12 |
| 5 | 0 | 0 | 3 | 24 | 73 | 5 | 0 | 0 | 6 | 42 | 52 | 5 | 0 | 0 | 0 | 42 | 58 |
| | 17 | 19 | 30 | 20 | 14 | | 19 | 21 | 27 | 24 | 9 | | 20 | 20 | 24 | 24 | 11 |

| 1NN – 2) 55.6 % | | | | | | 3NN – 2) 55.6 % | | | | | | 5NN – 2) 54.4 % | | | | | |
|-----------------|----|----|----|----|----|-----------------|----|----|----|----|----|-----------------|----|----|----|----|----|
| | 1 | 2 | 3 | 4 | 5 | | 1 | 2 | 3 | 4 | 5 | | 1 | 2 | 3 | 4 | 5 |
| 1 | 60 | 20 | 20 | 0 | 0 | 1 | 60 | 10 | 30 | 0 | 0 | 1 | 65 | 25 | 10 | 0 | 0 |
| 2 | 10 | 50 | 40 | 0 | 0 | 2 | 25 | 45 | 20 | 5 | 5 | 2 | 20 | 40 | 35 | 5 | 0 |
| 3 | 10 | 15 | 60 | 15 | 0 | 3 | 15 | 15 | 65 | 5 | 0 | 3 | 5 | 30 | 55 | 10 | 0 |
| 4 | 0 | 5 | 35 | 45 | 15 | 4 | 10 | 10 | 20 | 50 | 10 | 4 | 10 | 15 | 15 | 50 | 10 |
| 5 | 0 | 0 | 0 | 30 | 70 | 5 | 0 | 0 | 0 | 40 | 60 | 5 | 0 | 0 | 0 | 30 | 70 |
| | 18 | 20 | 34 | 17 | 11 | | 24 | 18 | 30 | 18 | 10 | | 22 | 24 | 26 | 18 | 10 |

* 1 denotes very rich herb-rich forests (e.g. OMaT), 2 rich (OMT), 3 medium (MT), 4 rather poor (VT) and 5 poor (e.g. CT), including all poor forest sites (Cajander 1926).

4. Discussion

The aim of this work was to employ ALS data in an automated search for different forest site types using the k-NN method to classify forest stands. The method yielded promising results for separating forest site types. We used two data approaches and found that the difference between the analyses based on the whole data approach and the modelling and test data approach were negligible. With the whole data k-NN provided slightly better results in classification with more neighbours, whereas if we used separate modelling and test data the best results were achieved with only one neighbour. However, there is no major difference depending on which approach is used; the larger data provides with more options to choose the “right” site type.

One interesting result was that more fertile site types appeared to have higher proportion of first, last and intermediate laser echoes as well as the total amount of echoes. In addition, higher proportions of only echoes were observed in stands belonging to the poor forest site types (Table 2).

The forests of the southern part of the National Park were subject to forest management practices until the mid-1990's and the proportion of forests at early stages in their development was higher there than in the northern part. In addition, the variation in altitude was smaller. It was not possible, however, to make any division between the northern and southern parts of the area when distributing the stands into the modelling and test data, because the number of forest stands applicable to the analysis was somewhat limited. It is therefore not completely certain how the ALS data-based automated search for forest site types would perform on an independent test dataset. However, the whole data approach did not separate different data sets and provided only results how the method works if there were larger reference data available. We used leave one out method, and in this case every stand had 273 possibilities to the nearest neighbours. We found that with larger reference data and appropriate delineation of the forest stand the results would be improved.

The method is based on vertical changes in echo clouds in different forest site types. One explanation for the significance of vertical indicator characteristics may be that the proportion

of deciduous trees, which differ from spruce in the shape of their crowns, for instance, is often higher in more fertile forests. It was also observed that the intensity value correlated positively with the number of deciduous trees. One explanation for this could be that the laser pulse is in the near-infrared part of the spectrum and therefore reflects more strongly from deciduous canopies.

One advantageous property of the k-NN estimator is its ability to utilise a high number of explanatory variables, so that it uses data efficiently. In most of the cases when classification failed the resulting class was, however, in the “nearby” classes with a most similar tree species structure and silvicultural recommendations corresponding to the correct forest type class. This result is worthwhile because it shows that ALS data and the k-NN non-parametric classifier are suitable for forest site type classification in general. Mistakes in the determination of forest site type classes are also possible in a forest inventory by stands, especially in borderline cases. In general, nearest neighbour methods are sensitive to the reference data, and biased estimates are often obtained for a forest stand with counterparts that are missing from the reference data. More emphasis should therefore be placed on the process of choosing the reference data.

The k-NN method was applicable to the selection of mature forests site types, and the results show that the success rates were moderate, varying from 54 to 58%. In many cases the characteristics used in the forest site type classification were so diverse that at this point it was not possible to say whether the subjective stand-wise inventory technique or the objective ALS data-based method provides more reliable results. One issue to be also considered is the variation within forest stands. It would be possible in future work to divide the stands into more homogeneous “micro-stands” or grids, and apply them as the basic units for forest site type classification. An overall forest site type map could then be produced by combining adjacent grids or micro-stands. In addition, digital aerial images and digital terrain models could give valuable additional information for classification purposes. Moreover, our method based on the vertical distribution of vegetation and can therefore be used in other vegetation zones where the ALS is applicable (e.g., no echoes originate from the ground in dense rain forests). However, further studies are needed to ensure the applicability of the method to different local conditions.

Acknowledgements

This research was conducted in the Faculty of Forestry, University of Joensuu, and the Joensuu Research Unit of the Finnish Forest Research Institute. It was partly funded by the Maj & Tor Nessling foundation and Finnish Ministry of the Environment through the project “A monitoring system based on modern remote sensing imagery for natural forests and restored forests in conservation areas” (decision no. YM89/5512/2004). This conference expenses was mainly funded by Metsämiestensäätiö. We are grateful to these institutions for resources and funding.

References

- Ahokas, E., Kaasalainen, S., Hyypä, J., Suomalainen, J., 2006. Calibration of the Optech ALTM 3100 laser scanner intensity data using brightness targets. In: *The International Archives of the Photogrammetry, Remote Sensing and Spatial Information Sciences*, Marne-la-Vallée, France, Vol. 36, Part A1, CD-ROM.
- Axelsson, P., 2000. DEM generation from laser scanner data using TIN models. *The International Archives of the Photogrammetry and Remote Sensing*, Amsterdam, The Netherlands, Vol. XXXIII, Part B4/1, 110-117.
- Brennan, R., Webster, T.L., 2006. Object-oriented land cover classification of lidar-derived surfaces. *Canadian Journal of Remote Sensing*, 32, 162-172.
- Cajander, A.K., 1926. The Theory of Forests Types. *Acta Forestalia Fennica*, 29, 1-108.

- Gatziolis, D., 2007. Lidar-derived site index in the U.S. Pacific Northwest – challenges and opportunities. *The International Archives of the Photogrammetry, Remote Sensing and Spatial Information Sciences*, Espoo, Finland. Vol. XXXVI, Part 3/W52, 136-143.
- Holmström, H., Nilsson, M., Ståhl, G., 2001. Simultaneous estimations of forest parameters using aerial photograph interpreted data and the k nearest neighbour method. *Scandinavian Journal of Forest Research*. 16, 67-78.
- Hopkinson, C., Chasmer, L., Lim, K., Treitz, P., Creed, I., 2006. Towards a universal lidar canopy height indicator. *Canadian Journal of Remote Sensing*, 32, 139–152.
- Hopkinson, C., Chasmer, L., 2007. Modelling canopy gap fraction from lidar intensity. *The International Archives of the Photogrammetry, Remote Sensing and Spatial Information Sciences*, Espoo, Finland. Vol. XXXVI, Part 3/W52, 190-194.
- Hyypä, J., Kelle, O., Lehikoinen, M., Inkinen, M., 2001. A segmentation-based method to retrieve stem volume estimates from 3-dimensional tree height models produced by laser scanner. *IEEE Transactions on Geoscience and Remote Sensing*, 39, 969–975.
- Hyypä, H., Yu, X., Hyypä, J., Kaartinen, H., Kaasalainen, S., Honkavaara, E., Rönholm, P., 2005. Factors affecting the quality of DTM generation in forested areas. *The International Archives of the Photogrammetry, Laser scanning 2005*, Enschede, Netherlands. Vol. XXXVI, Part 3/W19, 85-90.
- Kalliola, R., 1973. *Suomen kasvimaantiede*. Werner Söderström Osakeyhtiö, Porvoo. (in Finnish)
- LeMay, V., Temesgen, H., 2005. Comparison of Nearest Neighbor Methods for Estimating Basal Area and Stems per Hectare Using Aerial Auxiliary Variables. *Forest Science*, 51, 109-119.
- Lim, K., Treitz P., Wulder, M., St-Onge, B., Flood, M., 2003. ALS remote sensing of forest structure. *Progress in Physical Geography*, 27, 88-106.
- Lyytikäinen, A., 1991. Kolin luonto, maisema ja kulttuurihistoria. Kolin luonnonsuojelututkimukset. *Vesi- ja ympäristöhallituksen monistesarja* 308. (in Finnish)
- Magnussen, S., Boudewyn, P., 1998. Derivations of stand heights from airborne laser scanner data with canopy-based quantile estimators. *Canadian Journal of Forest Research*, 28, 1016-1031.
- Maltamo, M., Malinen, J., Packalén, P., Suvanto, A., Kangas, J., 2006. Nonparametric estimation of stem volume using airborne laser scanning, aerial photography, and stand-register data. *Canadian Journal of Forest Research*, 36, 426–436.
- Moeur, M., Stage, A.R., 1995. Most Similar Neighbor: An improved sampling inference procedure for natural resource planning. *Forest Science*, 41, 337-359.
- Næsset, E., 1997. Determination of mean tree height of forest stands using airborne laser scanner data. *ISPRS Journal of Photogrammetry & Remote Sensing*, 52, 49-56.
- Næsset, E., 2004. Practical large-scale forest stand inventory using small-footprint airborne scanning laser. *Scandinavian Journal of Forest Research*, 19, 164–179.
- Ørka, H.O., Næsset, E., Bollandsås, O.M., 2007. Utilizing airborne laser intensity for tree species classification. *The International Archives of the Photogrammetry, Remote Sensing and Spatial Information Sciences*, Espoo, Finland. Vol. XXXVI, Part 3/W52, 300-304.
- Poso, S., 1983. Kuvioittaisen arviomismenetelmien perusteita. Basic features of forest inventory by compartments. *Silva Fennica*, 17, 313-349. (in Finnish, with English summary)
- Ritchie, J.C., Jackson, T.J., Everitt, J.H., Escobar, D.E., Murphey, J.B., 1992. Airborne Laser: A Tool to Study Landscape Surface Features. *Journal of Soil and Water Conservation JSWCA3*, 47, 104-107.
- Rombouts, J.H., 2006. Exploring the potential of airborne LiDAR for site quality assessment of radiata pine plantations in South Australia: initial results. *Research Working Group 2, Forest Measurement and Information Systems*, Biennial meeting, 21-24 November 2006, Woodend.
- Uuttera, J., Hyypänen, H., 1998. Determination of potential key-biotope areas in managed forests of Finland using existing inventory data and digital aerial photographs. *Forest & Landscape Research*, 1, 415-429.

Session 2: Data fusion

Forest mensuration parameters derived from individual tree crown forest inventory method using airborne imagery and LiDAR

Desclée B.¹, Gingras A.², Bemelmans V.³ & Patigny, E.⁴

¹Sodiplan SA, Rue Phocas Lejeune, 8 -5032 Gembloux, Belgium – bd@sodiplan.be

²ICTrees, 885 de la Carrière, Gattineau, QC – Canada J8Y 6S6 -

alain.gingras@ictrees.biz

³SPRL Daniel Bemelmans, Les Villettes, 32, 4990 Lierneux, Belgium –

valery@bemelmans.eu

⁴Unisylva SCA, 44 Avenue de la Libération, 87000 Limoges, France -

emmanuel.patigny@unisylva.com

Abstract

Precise forest inventory and mapping are needed for supervising the different functions of the forest (management, planning, biodiversity and carbon stock). The recent improvements in remote sensing tools in terms of precision allow the achievement of forest inventory at single tree level close to total field inventory. Based on an individual tree crown (ITC) forest inventory method using airborne images, the approach has been extended for deriving tree mensuration parameters (height and stem volume) thanks to LiDAR data. This methodology has been tested in south-eastern Belgium over 1500 hectares of forest combining airborne image, LiDAR and field measurements. Forest map and inventory have been produced with information on species, density, height, basal area and stem volume. Based on a stratified random sample, the overall accuracy of the tree crown discrimination of eight tree species have been assessed to 85 %. Forest mensuration parameters have been compared to field measurements over coniferous and deciduous stands with high precision in coniferous. Height estimations from LiDAR have been compared with ground-based laser-scanning over two stands, proving the robustness of LiDAR data over field measurements. These results will still be improved by the development of tree mensuration models dedicated to remote sensing approach and better exploitation of LiDAR in tree crown delineation processes.

Keywords: Forest mapping, Remote sensing, Image classification, Terrestrial laser-scanning, Forest management, Digital orthophotos, Stem volume, Basal area

1. Introduction

Forestry requires more and more precise inventory associated with forest map in order to guide forest management (wood selling, expertises, appraisal and monitoring), for forest planning (assessment of stem volume and its distribution) and specific applications including environmental monitoring (natural habitat description for specific management), wood energy and carbon stock. Classical forest inventory methods based only on field measurements are either (1) statistical inventory based on sample plots or (2) total field inventory. The first approach is generally adopted for large regions. However, spatial distribution of volume and tree species is lacking and the precision of estimated forest parameters is generally not sufficient for precision forestry. The second forest inventory method produces detailed information on forest stocks but is time-consuming and thus limited to very limited areas.

Thanks to recent improvements in remote sensing technologies, tree crowns can now be distinguished thanks to the very high spatial resolution of airborne or satellite images. The

semi-automatic Individual Tree Crown (ITC) forest inventory developed by Gougeon (1995) has already proved its efficiency for forest inventory in North America. But, until now, this approach has not been assessed over European forests for operational forest management.

The real interest of single tree forest inventory is the estimation of forest mensuration parameters including height, basal area and stem volume. The measurement of these parameters on the field is quite hard and expensive over large areas. Light Detection And Ranging (LiDAR) instruments provides Digital Surface Model (DSM) and Digital Terrain Model (DTM) with high precision (below 15 cm). This is an interesting alternative for deriving tree measurements, often difficult to measure on the field. Several researches have been done for assessing LiDAR data (e.g. Maltamo *et al.* 2004; St Onge *et al.* 2004). Leckie *et al.* (2003a) have combined high-density LiDAR (2 points by m²) and multispectral imagery using individual tree crown analysis over small Douglas-fir plots. They found that heights derived from LiDAR were underestimated versus ground reference with an average error of 1.3 m. The estimation of other forest mensuration parameters such stem volume and basal area is quite more complex and can be done by at different level, (1) stand level or (2) tree level. A new approach for estimating basal area and stem volume based on canopy geometric model is proposed by Chen *et al.* (2007). However, this efficient approach has been evaluated with only one tree species at plot level. Dedicated relations between tree crown and stem volume to such applications have been investigated but they are generally region-specific (Kalliovirta and Tokola 2005). At single-tree level, regional allometric equations (Dagnelie *et al.* 1999) have been produced but they have not been assessed yet with remote sensing data.

The objective of this study is to develop an operational method for estimating forest mensuration parameters based on an individual tree crown forest inventory method using remote sensing. This approach should combine mapping and inventory at single tree level over large areas using remote sensing technologies including airborne images, multi spectral analysis and LiDAR surveys, coupled with optimized field data collection by local teams. The performance of this methodology will be assessed over Belgian forests using data from airborne data acquisition and field survey.

2. Materials and method

2.1. Study area

The study area is located in south-eastern Belgium (50° 12'N; 5° 41' E). Forest covers about 1500 ha which accounts for 85% of the region area. The altitude of the study area ranges from 400 to 600 meters. The study region includes around 650 forest stands with average stand area of 2 hectares. The forest consists of mixed deciduous trees (*Fagus sylvatica* and *Quercus spp.* as dominant tree species) and coniferous trees (*Picea abies* and *Pseudotsuga menziesii* as dominant tree species). This region has been selected given its accessibility and stand diversity (coniferous and deciduous, small and large stands).

2.2 Data acquisition

2.2.1 Airborne survey and pre-processing

One airborne survey was performed for both image and LiDAR acquisition with Falcon II system. This combined acquisition limits aerial flight costs and increase the data consistency having the same flight configuration. However, an offset should be found for defining appropriate acquisition period, between leaves on (for reliable trees species discrimination) and leaves off (for producing reliable DTM). The most appropriate period was selected at the start of vegetation period for having leaves of deciduous trees but not too dense for acquiring sufficient

LiDAR points from the ground. Over the study region, the flight survey was performed in May 2006 with average flight altitude around 1200 meters.

The airborne image, acquired from line-scanner camera, includes four spectral bands (Blue, Green, Red and Near-InfraRed (NIR)) with 50 cm spatial resolution. High quality airborne image is crucial for tree crown forest inventory as this image is the key element for tree crown delineation and tree species classification. The airborne survey should be done in clear sky weather conditions and limited time period. These two conditions are crucial in order to obtain aerial image with homogenous radiometry. After data collection, two pre-processings steps are required to produce digital orthophotos. First, the orthorectification is based on the DSM produced by the LiDAR and some reference points from the field. The precision of planimetric accuracy relies on these points. Over the study area, the absolute accuracy of the digital orthophotos was below 0.5 m. Secondly, relative radiometric corrections have been performed between flight bands in order to obtain homogenous radiometry over the whole region of interest.

LiDAR data were acquired with average point density of 4 points by m² and height accuracy below 15 cm. The sensor is a discrete return LiDAR system with laser pulse rate of 83 000 Hz. Based on point clouds, both DSM and DTM have been produced at 1 m spatial resolution. The grid used for processing stages has a higher resolution than the final grid. The elevation assigned to the final grid shall be the most relevant, namely the highest value for DSM and the lowest value for DTM (Löffler 2003). Due to acquisition in “leaves on” conditions, the raw DTM has been interpolated using bilinear interpolation over zones without ground altitude information. The Canopy Height Model (CHM) has been derived from the subtraction between DSM and interpolated DTM.

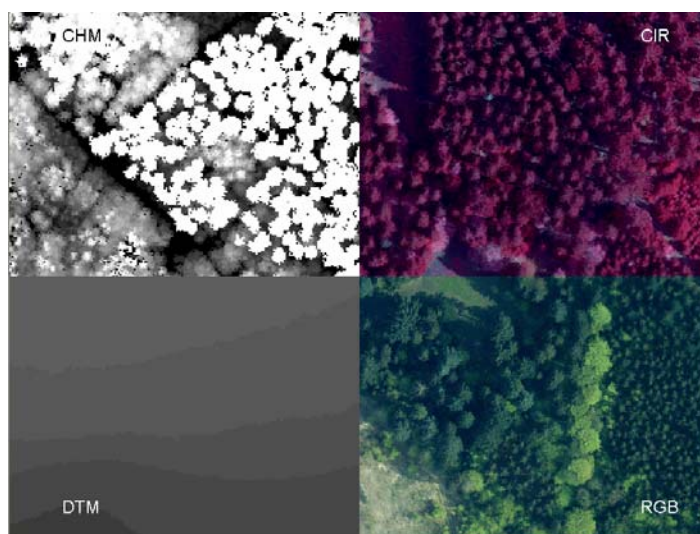


Figure 1: Extract of the airborne data acquisition including LiDAR and imagery

2.2.2 Field survey

Field measurements are required for calibrating the forest inventory method to the region of interest. However, the number of sample plots is considerably reduced compared to a classical systematic sampling thanks to preliminary photo-interpretation of the aerial image. Plots are visually selected in order to cover all species and age classes of interest and to be dispersed over the study area. The main purpose of this field survey is to define training sites for the image classification. These plots also provide information for forest mensuration estimation using LiDAR. Sample plots are circular with average diameter of 40 m (0.12 ha) where its center is

localised using GPS. Over the study area, the field campaign has been done in October 2007 over 42 plots.

2.3 Image processing

The methodology of image processing for identifying tree crowns and their species has been adapted from Gougeon (1995, 2000). This method called Individual Tree crown (ITC) analysis is based on the delineation of each tree crown prior to tree-species classification. This semi-automatic approach is divided in three separate steps: tree crown delineation, classification and estimation of some forest inventory parameters.

The tree crown isolation is based on a valley approach which separates shaded areas from sunlit areas and then isolates tree crowns based on intensity gradient (Leckie *et al.* 2003b). This algorithm starts with low value areas and follows any valleys in image brightness. Large shaded areas without trees are also removed based on specific masks in order to avoid false tree tops. Valleys are also created between tree crowns, thus producing segments of valley and crown material. Finally, the boundaries of each segment of crown material are refined to produce segments or isolations (isols), which generally represent tree crowns and sometimes clusters of crowns.

Supervised classification is performed for identifying tree crown species and producing the ITC forest map based on tree crown delineation. Spectral signatures are defined using information from field survey. The multispectral information of each isol is summarized and compare with spectral signatures. The algorithm is based on maximum likelihood classifier using minimum and maximum thresholds. The purity of these spectral signatures is crucial because it affects the accuracy of the classification. In order to reduce inter-classes confusion, the study region can be segmented in sub-regions based on stand composition, topography or radiometry differences. Spectral signatures for five coniferous classes (Spruce, Douglas-fir, Larch, Fir and Pine) and four deciduous classes (Beech, Oak, Birch and other deciduous trees) were computed in study area for producing the ITC forest map.

Several stand-based forest inventory parameters can be derived directly from this ITC forest map without LiDAR information. The forest stand can be delineated from the aerial image or provide by other GIS data. The estimated parameters include density (number of trees by hectares), canopy closure (in percent), species distribution (in cover percentage), and average tree crown diameter (in meters). This information is provided both globally at stand level or by tree species included in the stand.

2.4 Forest mensuration estimation

LiDAR gives information about forest canopy structure which are used for estimating forest mensuration parameters including dominant height, basal area and stem volume. These parameters are derived thanks to relations between remote sensing data and field measurements. Two types of approach have been assessed using the CHM produced from LiDAR data. Relations can be computed at (1) stand level or (2) tree level defined by the ITC tree crown delineation.

2.4.1 Stand level approach

The stand level approach consists in global estimation of forest mensuration parameters for each forest stand. Dominant height is estimated on the field by the height of the 100 higher trees by hectares. In order to derive height of the dominant tree over each 100 m², a new CHM, called *maxCHM*, is computed on 10 meters raster cells and deriving the maximum height value. Based on stand delineation, dominant height is derived from the mean value of all *maxCHM* cells included in the stand polygon.

Basal area and stem volume are estimated using a new metric called canopy geometric volume defined by Chen *et al.* (2007). This metric is computed by the geometric volume for a polygon under the CHM. The regression model is calibrated with field inventory based on local tree mensuration method compared on canopy geometric volume based on LiDAR over sample stands. Over the study area, two different regressions (one for coniferous and one for deciduous) have been derived.

2.4.2 Tree level approach

Starting from the tree crown delineation produced by the ITC classification, tree mensuration parameters can be estimated at single tree level using LiDAR information. The estimation of tree height can be done by intersecting tree crown delineations over the CHM and deriving the highest height value under tree crown shape. Allometric equations are required to derive basal area and stem volume from the tree crown diameter. Several relations are provided by Dagnelie *et al.* (2007) for estimating DBH from tree crown diameter and stem volume from DBH and height. It is important to note that these allometric equations have been derived from on-the-field measurements which were not dedicated to remote sensing applications. The species information required for these species-specific relations is provided by the ITC classification. Thanks to these relations, basal area and stem volume are computed for each tree and summarized by stand.

2.5 Field validation

In order to assess the performance of this methodology, a field survey has been performed in November 2007 over several sample plots and some entire stands. The ITC classification has been first assessed by visual interpretation using random stratified sampling of 265 sites. A subset of 37 validation sites, different from training sites, focused on sites hard to qualify by photo-interpretation, has been described on the field. For assessing the accuracy of tree mensuration parameters, total inventories have been performed on entire stands, both coniferous and deciduous. Total inventories were preferred to plot inventory in order to avoid errors due to extrapolation of plot information.

The assessment of tree height estimations is complex and three methods of height estimation have been compared. First, height can be estimated thanks to LiDAR data extracted at tree top. Second, a classical and rapid method for height measurement on the field is performed with a laser instrument called vertex. Finally, height can be measured thanks to terrestrial laser scanner survey providing 3d information from the ground.

This last technique of height estimation can be considered as the reference as it provides very high precision measures. The equipment included Leica HDS 300 laser-scanner, theodolite and RTK-GPS. The measurements have been performed over two different stands, coniferous and deciduous. The laser-scanner point density is about 400 points by m² at a distance of 30 meters from the laser source. The theodolite measurements provide information of the tree location at breast height. The laser-scanner information has been analysed for deriving tree heights which have also been estimated by vertex instrument on the field.

4. Results

4.1 Individual tree crown forest inventory

A detailed forest inventory has been produced over an operational study case in eastern Belgium (Figure 2). This individual tree crown inventory is georeferenced, identifies tree location and species and provides tree mensuration estimations. Information is summarized at stand level for forest management and stored in database linked to cartographic data. Among numerous forest parameters provided by the inventory, tree species distribution, stem density, dominant height, stem volume and basal area are the main parameters. The estimation accuracy of these parameters has been assessed based on field validation survey.

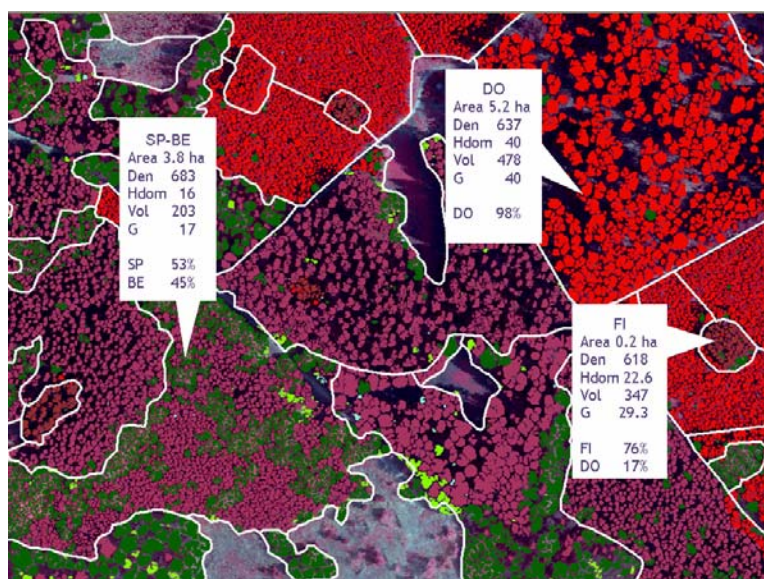


Figure 2: Forest map extract showing tree crown with color linked to species and stand-based forest mensuration parameters (Area in hectares (ha); Density (Den) in trees by ha; Dominant height (Hdom) in m; Volume (Vol) in m³ by ha and basal area (G) in m² by ha)

4.2 Tree species classification

The performance of the ITC classification has been assessed by comparing its tree crown species with trees analysed on sample field plots. Eight tree species, 5 in coniferous and 3 in deciduous, have been distinguished. High classification overall accuracy (85 %) has been obtained by the ITC classification assessed on more than 2000 tree crowns (Table 1). The accuracy is better for coniferous which have lower omission and commission errors than deciduous trees.

Table 1: Confusion matrix from the accuracy assessment of the ITC classification using field reference on sample plots (based on tree crown number; C.E. = Commission errors)

| ITC Classification | Field reference | | | | | | | | | Total | C.E. (%) |
|---------------------|-----------------|------------|-----------|------------|------------|-----------|-----------|------------|-----------|-------------|----------|
| | SP | DO | LA | FI | PI | BE | OA | BI | OD | | |
| Spruce - SP | 729 | 51 | | 8 | | 11 | 1 | | | 800 | 8.9 |
| Douglas-Fir -DO | | 448 | | 14 | | 1 | | | | 463 | 3.2 |
| Larch - LA | | | 86 | | | | | | | 86 | 0.0 |
| Fir - FI | | | | 167 | | | | | | 167 | 0.0 |
| Pine - PI | 8 | | | | 136 | | 11 | | | 155 | 18.6 |
| Beech - BE | 139 | 2 | 7 | 8 | | 21 | 2 | 4 | 7 | 190 | 88.9 |
| Oak - OA | 5 | 3 | 1 | | | 2 | 25 | 12 | 14 | 62 | 59.7 |
| Birch - BI | | | | | | | | | 230 | 230 | 0.0 |
| Other Decid. - OD | | 12 | | | | | | | | 12 | 100.0 |
| Total | 881 | 516 | 94 | 197 | 136 | 35 | 39 | 246 | 21 | 2165 | |
| Omission Errors (%) | 17.3 | 13.2 | 8.5 | 15.2 | 0.0 | 40.0 | 35.9 | 6.5 | 100.0 | | 85.1 |

4.3 Tree mensuration estimation

Estimations of forest parameters using stand level and tree level approaches based on remote sensing data have been compared to total field inventory over two representative stands, one coniferous and one deciduous (Table 2). The assessed parameters included stem density, dominant height, stem volume and basal area. The deciduous stand has been evaluated using only the stand level approach given the lack of tree mensuration models for some species which are required for the tree level approach.

For both stands, tree density measured on the field was very close to measurements by the ITC approach. Dominant height was also correctly estimated by the ITC approach and was even better using tree level approach than the stand level. The analysis of the other tree mensuration parameters, namely basal area and stem volume, revealed large differences between each forest inventory techniques. Stem volume of coniferous stand estimated from ITC-Stand was very close from field estimations. These differences are larger for the deciduous stand than for the coniferous one.

Table 2: Comparison of forest mensuration parameters estimated by the stand-level (ITC-Stand) and tree level (ITC-Tree) approach with total field inventory data from two validation stands.

| Stand | Coniferous (8.6 ha) | | | Deciduous (2.5 ha) | |
|----------------------------------|---------------------|----------|-------|--------------------|-------|
| | ITC-Stand | ITC-Tree | Field | ITC-Stand | Field |
| Density (nb trees/ha) | 519 | 519 | 512 | 120 | 119 |
| Dominant height (m) | 25.1 | 25.6 | 25.8 | 28.5 | 28.2 |
| Basal area (m ² /ha) | 28.5 | 24.4 | 31.4 | 34.1 | 22.3 |
| Stem volume (m ³ /ha) | 343 | 244 | 340 | 171 | 136 |

The tree level approach has been evaluated by comparing ITC-Tree estimations with field measurements. Large differences were found for basal area and stem volume estimations. The Diameter Breast Height (DBH) classes distributions have been analysed for both ITC-Tree and field inventories (Figure 3). The shift of DBH classes distribution of ITC-Tree to lower values can be explained by underestimation of the crown diameter having a direct impact on the estimations of basal area and stem volume.

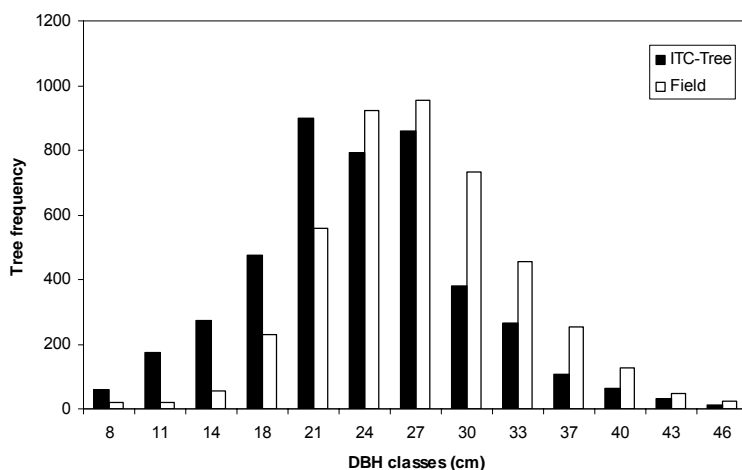


Figure 3: Comparison of stand distributions of Diameter Breast Height (DBH) derived from the ITC-Tree inventory and the field inventory over the coniferous validation stand.

4.4 Tree height comparison with terrestrial laser-scanner

The comparison of tree height estimations from LiDAR and field measurement based on vertex instrument have been compared with information extracted from high precision terrestrial laser scanner survey (Table 3). This comparison shows discrepancies in height estimations. These differences and RMSE are lower using LiDAR (mean height difference below the meter) than using vertex on the field. This proved the interest of using LiDAR for more robust height estimation required for reliable forest mensuration. Finally, these differences are smaller for coniferous than for deciduous.

Table 3: Comparison of tree height estimations based on (1) airborne laser scanner (LiDAR), (2) Vertex with terrestrial laser scanner measurements (RMSE: Root Mean Square Errors).

| | Coniferous (0.14 ha, n=14) | | Deciduous (0.44 ha, n=44) | |
|---|----------------------------|------|----------------------------|------|
| | Mean height difference (m) | RMSE | Mean height difference (m) | RMSE |
| 1) Airborne - Terrestrial laser scanner | 0.31 | 1.45 | -0.71 | 3.95 |
| 2) Vertex - Terrestrial laser scanner | -1.18 | 2.09 | -1.61 | 5.24 |

5. Discussion and conclusion

The originality of the present study is the integration of several new technologies in an operational tool for producing georeferenced forest inventory. The developed methodology includes individual tree crown forest inventory, optimized field survey with GPS and LiDAR. This first assessment of ITC technique over European forests is promising given its high

classification overall accuracy (85%) for eight tree species. This study also has evaluated the potential of LiDAR data for deriving forest mensuration parameters based on relations between remote sensing and field information. Several parameters including stem density, dominant height, stem volume and basal area have been estimated with good accuracy at stand level by comparison with ground truth measurements.

This forest inventory methodology could still be improved at tree level for reaching higher precision thanks to new technologies or dedicated relations. Classification could use new hyperspectral sensors in order to cover larger range of tree species. The integration of LiDAR data together with the aerial image in tree crown isolation could also improve tree crown delineation and thus related forest mensuration estimation. Finally, specific field measurements are needed for developing tree mensuration models dedicated to remote sensing technologies. The proposed methodology is not focused only on forest management but also provides valuable information for several applications as the assessment of biodiversity reduction or the integration of the global warming impacts in adaptable forest management system.

Acknowledgements

The authors gratefully acknowledge the Regional Government of Wallonia (DGTRE, Belgium) for supporting this research project.

References

- Chen, Q., Gong, P., Baldocchi, D. and Tian, Y., 2007. Estimating Basal Area and Stem Volume for Individual Trees from Lidar Data. *Photogrammetric Engineering & Remote Sensing*, 73, 1355-1365.
- Dagnelie, P., Palm, P., Rondeux, P. and Thill, A., 1999. Tables de cubage des arbres et des peuplements forestiers. *Les Presses Agronomiques de Gembloux*, 128 p.
- Gougeon, F., 1995. A crown-following approach to the automatic delineation of individual tree crowns in high spatial resolution aerial images. *Canadian Journal of Remote Sensing* 21: 274-284.
- Gougeon, F., 2000. Towards semi-automated forest inventories using individual tree crown (ITC) recognition. *Technology Transfer Note No. 22*. Victoria, BC: Canadian Forest Service, Natural Resources Canada, Pacific Forestry Centre, 6 pp.
- Leckie, D., Gougeon, F., Hill, D., Quinn, R., Armstrong, L. and Shreenan, R., 2003a. Combined high-density lidar and multispectral imagery for individual tree crown analysis. *Canadian Journal of Remote Sensing*, 29, 633-649.
- Leckie, D., Gougeon, F., Walsworth, N. and Paradine, D., 2003b. Stand delineation and composition estimation using semi-automated individual tree crown analysis. *Remote Sensing of Environment*, 85, 355-369.
- Löffler, G., 2003. Aspects of raster DEM data derived from laser measurements. *ISPRS workshop "3-D reconstruction from airborne laserscanner and InSAR data"*, Dresden, Germany.
- Maltamo, M., Mustonen, K., Hyypä, J., Pitkänen, J. and Yu, X., 2004. The accuracy of estimating individual tree variables with airborne laser scanning in a boreal nature reserve. *Can. J. For. Res./Rev. Can. Rech. For.*, 34, 1791-1801.
- St-Onge, B., Jumelet, J., Cobello, M. and Vega, C., 2004. Measuring individual tree height using a combination of stereophotogrammetry and lidar. *Canadian Journal of Forest Research*, 34, 2122-2130.

Full automatic detection of tree species based on delineated single tree crowns - a data fusion approach for airborne laser scanning data and aerial photographs

Johannes N. Heinzl¹, Holger Weinacker¹ & Barbara Koch¹

¹Department for Remote Sensing and Landscape Information Systems,
Albert-Ludwigs-University Freiburg, Germany
johannes.heinzl@felis.uni-freiburg.de, holger.weinacker@felis.uni-freiburg.de,
barbara.koch@felis.uni-freiburg.de

Abstract

A full automated classification of tree species was tested on single tree level. This approach intends to classify without any parameter input or predefined knowledge. In the forerun it was therefore necessary to build algorithms which combine the LiDAR data based 2D single tree delineation with the spectral information from colour infrared (CIR) images. During the tree species classification the LiDAR based classification is improved by means of spectral information. The overall accuracy of the classification is more than 83 % for the tree types beech, oak and conifer and more than 90 % for deciduous trees and conifers. Splitting LiDAR based single tree polygons by spectral features improves the results by 7.42 %.

Keywords: tree species, single tree delineation, laser scanning, aerial photographs, data fusion

1. Introduction

Single tree based parameter extraction from airborne laser scanner (ALS) data is of increasing importance for forestry applications. Under special circumstances and for certain questions single trees are the only reliable units to work on. Where several tree species with a different growing behaviour occur within one stand, like in temperate forest, a stand-wise approach is often very difficult and needs a lot of a-priori knowledge (Koch *et al.* 2006). The tree species itself is highly correlated to a large number of other forestry parameters. It is a pre-requisite necessary to derive information like biomass and tree damage.

Tree delineation provides the system with objects that can be further classified. Numerous approaches have been undertaken, which make use of different data types and techniques. First techniques were based on multispectral data and are still being developed (Wang *et al.* 2004, Leckie *et al.* 2005, Wang *et al.* 2006). LiDAR predicated methods can be subcategorized by the usage of first and last pulse data, which mainly find use in 2D delineations (Koch *et al.* 2006, Tiede *et al.* 2006), and full waveform data, which allows to gain more exact 3D models of the crowns (Rossmann *et al.* 2007, Wang *et al.* 2007). In comparison there are only few attempts, as done by Leckie *et al.* (2003) and Wolf *et al.* (2007), to combine multispectral and LiDAR data.

Comparable data types have been used for the classification of tree species on single tree level. Multispectral based methods mostly build on thresholds of the spectral data or derived information (Koch *et al.* 2002, Leckie *et al.* 2005). Bohlin *et al.* (2006) work with crown templates which are matched to the trees on the image. Most of these operations use training samples and are therefore semiautomatic. Liang *et al.* (2007) and Reitberger *et al.* (2006) achieve good results in distinguishing coniferous and deciduous trees with LiDAR based attempts. Ørka *et al.* (2007) test the significance of intensity from multiple return data for classifying tree species. One of the few authors who tested a combination of laser data and multi-spectral images were Persson *et al.* (2006). They achieved an improved accuracy due the

combination. Most procedures have in common that they work well for a number of about three species. The average accuracy ranges from 50 to 80 % of correctly classified objects from which the best results are achieved in distinguishing coniferous and deciduous trees.

The method developed in this study is structured in three main steps. (1) First the LiDAR based delineation of single trees is conducted with an algorithm developed by Koch *et al.* (2006). (2) Second the full automated tree species classification is done with spectral data and (3) third the LiDAR based delineation is corrected.

2. Method

2.1 Study areas

The first study area is located in the forest district ‘Milicz’ in Poland. The method was developed on a test site with a side length of 500 m which covers an area with the most variety and best mixture of tree types (see Figure 1). The algorithm was later tested on a second site with same dimensions. It contains four sample plots with field measured trees, but is characterised by more difficulties like large shadowed areas and more tree height levels.

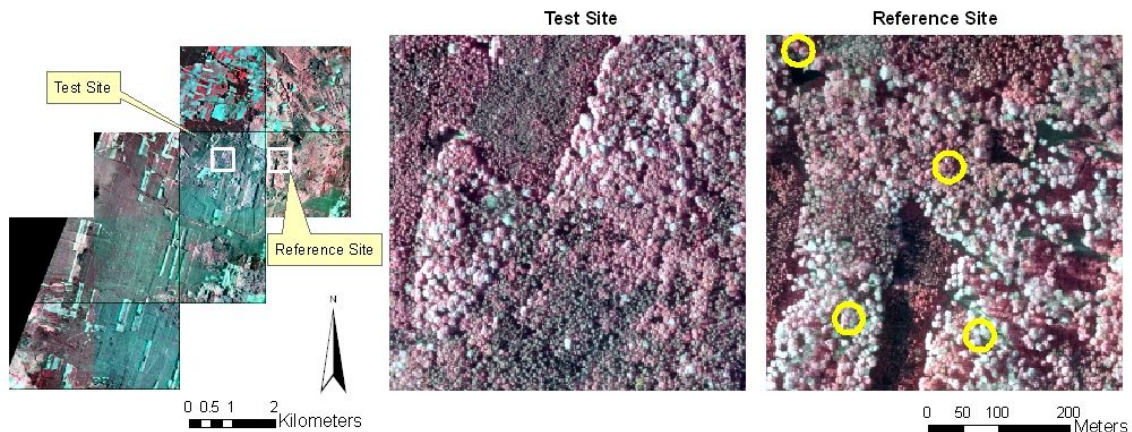


Figure 1: Left: location of the work sites in the ‘Milicz’ forest district, middle: CIR aerial photograph of the test site, right: CIR aerial photograph of the reference site with sample plots.

A second study area with a side length of 500 m was selected in the black forest in southern Germany close to the city of Freiburg. The developed method was severely tested under very different conditions and with good single tree reference data. In comparison to the Polish area it is characterised by high relief energy of 242 m in a low mountain range, a different time of the year and a lower resolution of the CIR images. Both are mixed forests.

2.2 Data

On the Polish sites LiDAR data and multispectral images have been captured simultaneously with a Falcon II system from TopoSys in 2-3 May 2007 while trees being in a full on-leaf state. The LiDAR raw data consists of first- and last pulse reflections with an average point density of 7 points/m². Due to the structure of the sensor, the points are irregularly spaced in a line pattern. CIR true ortho images with 25 cm pixel resolution were used as spectral information source. Further within 25 sample plots reference data on single tree level was forthcoming. Every circular plot has a radius ranging from 7.98 m to 12.62 m depending on the stand’s age and was measured in the field in 2006. The contour of each tree crown was obtained from the ground by orthogonal surveying eight vertices of its borderline. Other parameters are the crown’s layer in

the vertical structure, the tree species and tree height. Because only crowns were used that are visible from above, the hidden border polygons were deleted manually. We chose different sites for algorithm development and referencing due to the irregular distribution of the sample plots. From the LiDAR raw data three different surface models with 0.5 m and 1 m resolution were calculated. These are the digital terrain model (DTM), the digital surface model (DSM) and the vegetation height model (nDSM). Filtering and interpolation of the raw data was performed with the “active Contour Algorithm” implemented in the software package TreesVis (Weinacker *et al.* 2004).

The data for the German study area was captured with a Falcon I system from TopoSys in 2002. Last pulse LiDAR reflections were acquired on 4 March and first pulse together with spectral data on 22 July. Average point density is 10 points/m² and CIR true orthophotos have a pixel resolution of 50 cm. A DTM, DSM and nDSM with 1m resolution were calculated from the LiDAR raw data. As reference data tree crowns were manually digitised within a 200*200 m field from stereo images taken in June 2001. The digitisation was transferred into 2D with higher trees covering lower trees and showing the tree outlines like seen from above. A visual classification of the tree types broad-leaved and conifers was carried out. Further subdivision of the species was not possible, but due to the dry conditions of midsummer damaged deciduous trees could be spectrally separated. From the forest management plan the following species composition on the test site is given: Broad-leaved trees 57.84 % with beech 48 %, oak 8 %, sycamore 2 % and conifers 42 % with fir 27 %, spruce 4 %, douglas fir 10 %.

2.3 LiDAR based single tree delineation

The 2D single tree delineation was conducted with a parameter reduced program executing the algorithm developed by Koch *et al.* (2006). The input data given to this program are the DSM and the DTM. Setting program internal height class thresholds for trees was abdicated and substituted by a new method to improve the results. Therefore a supplemental program module was developed in C++ with use of the Halcon 8.0 image processing library (MVTec 2007).

From the nDSM a histogram of the gray values was calculated and its local minima were used as thresholds for the height classes. In the case of the Polish test site, two classes could be separated at a height of 2114 cm (see Figure 2 and Figure 3).

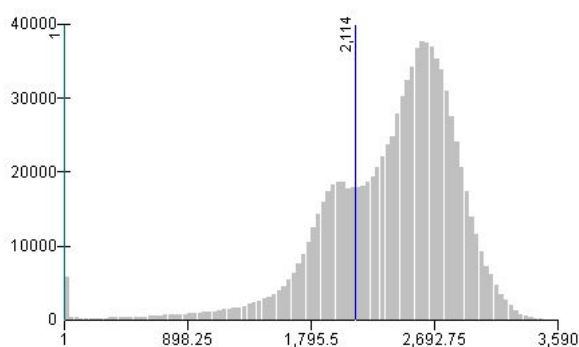


Figure 2: Local minimum separating height classes in the gray value histogram of the nDSM. The abscissa indicates the gray values (heights in cm), the ordinate indicates the number of occurrence for every value interval.

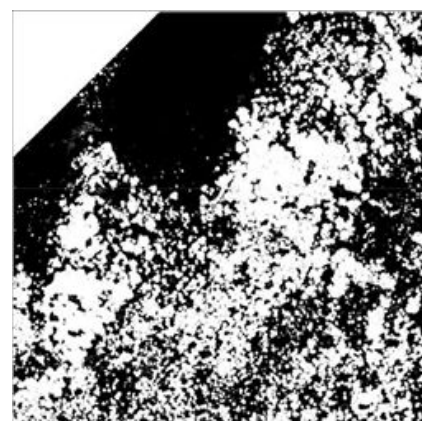


Figure 3: nDSM classified in two height classes. High regions are white low regions black colored (the top left corner is out of the valid area and defined as no data).

The 2D delineation program is then run with a 0.5 m and a 1 m resolution DSM. The more generalized lower resolution DSM achieves better results for the high trees and the higher

resolution DSM for the low trees. Larger crowns are represented by more pixels and are therefore more structured. A DSM with a lower resolution works similar like a higher smoothing of the crowns. The delineation algorithm (Koch *et al.* 2006) itself works by finding local maxima on a Gaussian smoothed image, from which regions are extended until neighbouring pixels with a lower or the same height value are met. From this first approximation of the tree shape several morphological corrections are conducted. Finally the actual crown-edge is determined by separating the tree from neighbouring canopy gaps. A vector starts from the tree top to each border point and stops at the inflexion point or at a local minimum.

As result one delineation for each DSM resolution is achieved. Together with the determined height threshold these are used as input images for the new algorithm. Each tree is defined as a region with a certain height value. Referring to this, the tree regions are taken from the concerning delineation (see Figure 4 and Figure 5) and copied into a new image (see Figure 6). The result allows single lower trees to be placed between higher trees which is not the case when large connected height level regions are used instead. After combining the tree regions several small regions, derived from intersections, occur at the borderlines. They are iteratively reallocated to neighbouring larger polygons corresponding to spectral, height concerning and morphological conditions. If these requirements are fulfilled the small region is allocated to that neighboured region with the least spectral difference, which is defined as the mean value of all spectral bands.

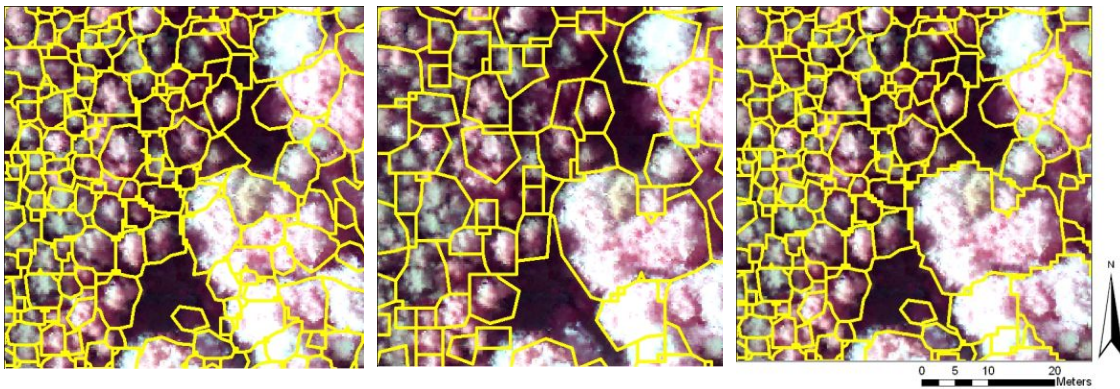


Figure 4: Delineation with 0.5 m DSM

Figure 5: Delineation with 1 m DSM

Figure 6: Combined delineation for both height classes

On the German study area only one main height level occurs and all the delineation is done with a 1 m resolution DSM.

2.4 Tree species classification

The LiDAR data derived single tree polygons are classified by species according to their spectral features. In advance some pre-processing has to be done. To enhance the contrast of the CIR image its histogram is linearised after equation (1) (Gonzales *et al.* 2002, p 115).

$$s_k = T(r_k) = \sum_{j=0}^k p_r(r_j) = \sum_{j=0}^k \frac{n_j}{n} \quad k = 0,1,2,\dots,L-1 \quad (1)$$

r_k = pixel in the input image, s_k = pixel in the output image, k = discrete pixel value, L = total number of possible gray levels in the image, p_r = probability density function of variable r , n = total number of pixels in the image, n_k = number of pixel that have gray level r_k

Then the spectral bands are separated into near infrared (NIR), red and green and further transformed into the channels hue (H), saturation (S) and intensity (I). The HSI colour model is used due to its ideal applicability to describe colours intuitively to human perception. Hue describes the pure colour, like yellow or red, saturation indicates to which degree the pure colour is diluted by white light and intensity is an achromatic measure of what the human interpreter calls brightness (Gonzales *et al.* 2002, p 317). Prior to classification the tree polygons are fitted to the usable spectral data and too shaded areas are removed. This is done by subtracting pixels with an intensity value between 0 and 100 from the tree polygons. Colors within that intensity interval are defined to be too dark for any interpretation. The contour of the resulting regions is smoothed with a morphological opening operation.

The classification itself is divided into two steps (see Figure 7). Within both, classes are separated relative to histogram features and the according tree species is assigned later due to the reference data.

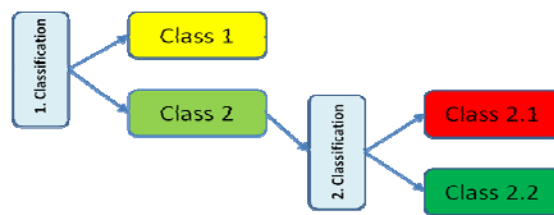


Figure 7: Hierarchy of the tree species classification

During the first cycle two classes can be separated at the local minima from the hue-channel's histogram (see Figure 8). The thresholds are determined automatically by smoothing the histogram with a Gaussian function as long until the number of local minima is appropriate.

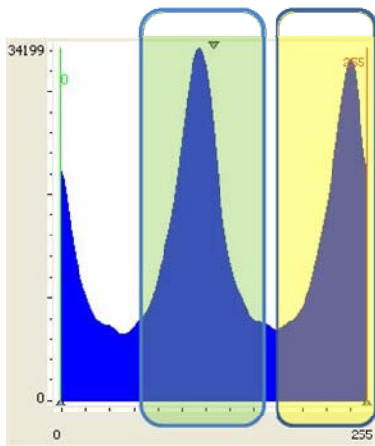


Figure 8: First classification threshold. Smoothed histogram of the hue-channel with gray values on the abscissa and frequency on the ordinate. Class 1 and class 2 are separated at the local minima and indicated by color.

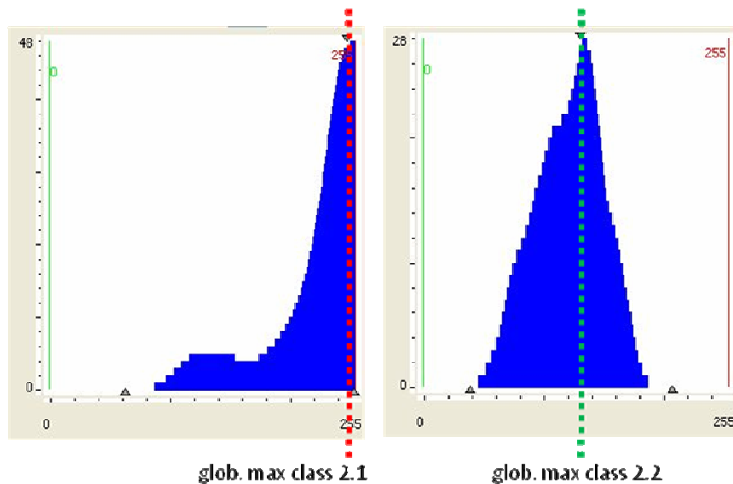


Figure 9: Second classification threshold. Global maxima from single polygons. The position in the left diagram belongs to class 2.1, the position in the right to class 2.2. Abscissa and ordinate same as in Figure.

The second classification cycle subdivides class two as shown in Figure 9. It is carried out by calculating the global maximum position of the NIR band within each tree polygon (see Figure 9). From these values a function is derived that describes the frequency of the maximum distribution for all trees. The discrimination threshold is gained from the local minimum of the

automatically smoothed function.

On a first approach the classification results were visually compared to the reference sample plots located on the reference site for the Polish dataset and visually interpreted based on the known species composition for the German dataset. From this comparison it was possible to allocate all classes to certain tree species or compositions of them. The resulting classes from the first classification match with the following species:

| | | | | | |
|---------|----------|----------------|----------|----------|------------------------|
| Poland: | Class 1: | oak/hornbeam | Germany: | Class 1: | deciduous healthy |
| | Class 2: | beech/conifers | | Class 2: | conifers/ dec. damaged |

The subdivision of class 2 refers to the following species:

| | | | | | |
|---------|------------|----------|----------|------------|-------------------|
| Poland: | Class 2.1: | beech | Germany: | Class 2.1: | deciduous damaged |
| | Class 2.2: | conifers | | Class 2.2: | conifers |

Finally a total of 3 classes could be separated (see Figure 10).

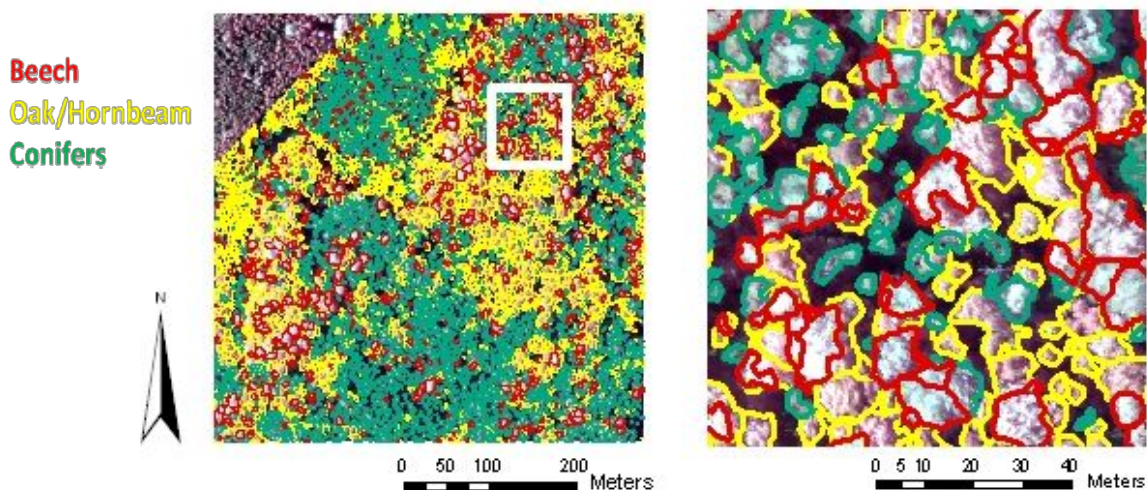


Figure 10: Final tree species classification (Poland). Left figure shows the complete test site, right figure shows a subset.

2.5 Multispectral correction of the single tree delineation

The original LiDAR-based 2D delineation was improved and corrected by multispectral data. These corrections are calculated simultaneously with the spectral adaption of the polygons and the species classification.

While fitting the LiDAR derived polygons to the spectral information certain polygons are divided into two and more crowns. This happens when a polygon contains two or more crowns which are divided from their neighbors by a gap in spectral intensity. Small residual connections between the new splitted polygons are broken by a morphological opening operation in advance.

The crowns of mature deciduous trees are often interlocked and not always possible to delineate with geometrical information. On the Polish test site this was the case with the crowns from oaks and beeches. Due to the spectral domain of each species, which is detected automatically in the hue channel, it is possible to separate beeches from oaks as well as conifers from oaks within one polygon (see Figure 11). On the German study area it was the same for the corresponding classes. For separation further conditions must be fulfilled and a minimum relative area of at least 20 % from the original polygon is required. A series of morphological opening and closing operations smoothes the borders and fills gaps within the new polygons.

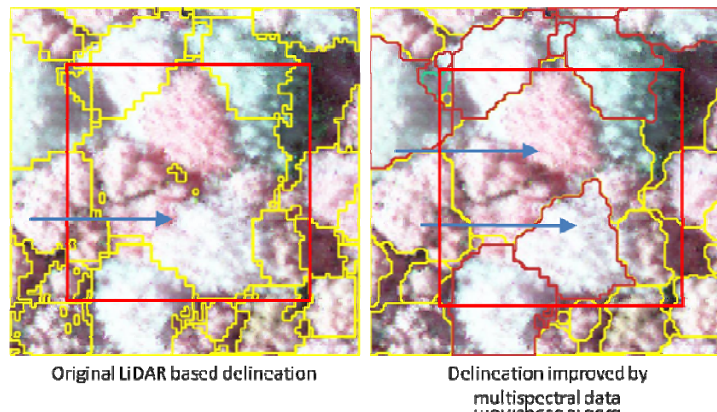


Figure 11: Separation of tree crowns by information of the hue channel (Poland). Here the beech crown is delineated from the neighbored oaks. The blue arrows point to the LiDAR derived polygon on the left and the separated polygons on the right.

On the German study area the problem occurred that different spectral regions can be within a single tree crown. This is due to partly damaged tree crowns or differences in illumination. If the algorithm would be run without an adaption to this situation, single LiDAR based polygons could be divided though they only contain one crown. Because the differences within one crown are in most cases significantly smaller than between two crowns of different classes a sensitivity factor was implemented. This factor refers to a minimum distance of the mean spectral values from divided subparts of a polygon. It ranges from 0 (no reduced sensitivity) to 1 (completely reduced sensitivity) where polygon splitting is not possible anymore. If it is undercut the two neighbored subparts are merged again (see Figure 12).

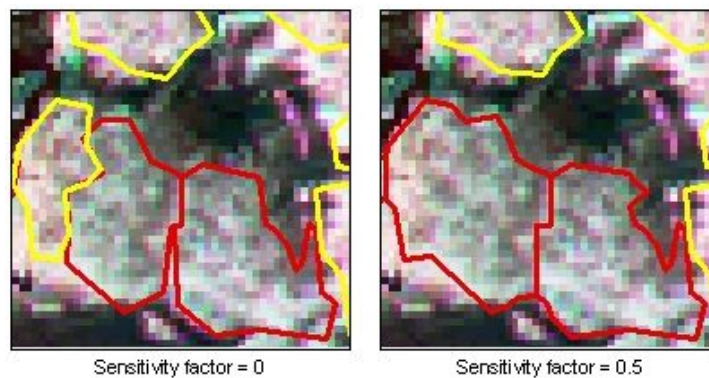


Figure 12: Left figure shows a split crown when not using a reduced sensitivity. Right figure shows the same crown with half sensitivity (Germany).

2.6 Assessment of the classification

The tree type classes are determined automatically by features of the image histograms. An allocation to certain species and an accuracy assessment is done with help of the reference sample plots in the case of the Polish study area and for the German area by the visual interpreted stereo delineation. Therefore the developed algorithm was executed on the reference sites and the classified crowns are compared to the species or damage degree of the reference crowns. Because the automatic delineation doesn't fit completely to the reference delineation in all cases, it is visually determined to which reference polygon they accord. If a polygon is not possible to assign this is recorded in the statistics and it is not further considered.

On the German test site additionally the single tree delineation was verified. According to Leckie et al. (2003) six grades of matching with the corresponding reference crowns (refs) were

defined for the automatic isolated crowns (isols): perfect match (one-to-one correspondence), good match (one-to-one, but overlap less than 50 %), grouped (isols with more than one ref), split (more than one isol per ref), commission error (isol without ref) and not detected (ref without isol).

3. Result and discussion

The main aim of this study was to use LiDAR data based single tree delineation for a fully automated multispectral tree species classification. Due to the adaption of the LiDAR polygons to the spectral data and the following classification procedure it was also possible to improve the delineation results. For the Polish site the delineation improvement was only evaluated visually as stated above and occurs in every polygon where the described conditions are fulfilled. For the German site verification was conducted with 579 reference crowns on an area of 200*200 m.

The accuracy assessment of the tree species classification showed an overall accuracy of 83.87 % of correctly classified polygons for the Polish and 90.79 % for the German site. The total number of delineated trees is 31 with 26 correctly classified and 467 with 424 respectively. Two reference polygons on the Polish and 31 on the German site were not assignable. The confusion matrices in Table 1 and Table 2 additionally show the wrong classified crowns and their classes.

Table 1: Total statistics for accuracy assessment (Poland)

| | | Automatic classification | | | |
|----------------|--------------|--------------------------|--------------|-------|---------|
| | | Class | Oak/hornbeam | Beech | Conifer |
| Reference data | Oak/hornbeam | 16 | 0 | 1 | 17 |
| | Beech | 1 | 8 | 3 | 12 |
| | Conifer | 0 | 0 | 2 | 2 |
| | Σ | 17 | 8 | 6 | 31 |

Table 2: Total statistics for accuracy assessment (Germany)

| | | Automatic classification | | | |
|----------------|-------------------|--------------------------|-------------------|-------------------|---------|
| | | Class | Deciduous healthy | Deciduous damaged | Conifer |
| Reference data | Deciduous healthy | 221 | 7 | 5 | 233 |
| | Deciduous damaged | 4 | 68 | 18 | 90 |
| | Conifer | 4 | 5 | 135 | 144 |
| | Σ | 229 | 80 | 158 | 467 |

In both matrices most frequent failures happen in classifying class 2.1 (beech/deciduous damaged) as class 2.2 (conifer). This shows that the threshold for distinguishing classes in the NIR band seems to be some weaker than the first classification with the hue band. The current state of algorithm development needs a forest composition with all three tree types being present and a minimum contingent of about 20 % for each species. This value is empirical and not fixed. It depends on the overall gray value distribution of the used images.

Two definite and stable spectral features have been determined which allow a classification of mixed forest even under different conditions. The content of the derived classes must be referenced on the used dataset whereas the base classes “conifer” and “deciduous” seem to be constant. Since full automation was the aim of this study no standard classification methods like

nearest neighbor were used. Most of them need interaction by setting training samples.

The LiDAR based single tree delineation shows an overall accuracy of 43.87 % when comparing perfect and good matches of isols to the total number of refs and 56.95 % compared to the total number of isols. After spectral correction of certain polygons the overall accuracy is 51.29 % (isols from refs) and 60.37 % (isols from isols) (see Table 3).

Table 3: Statistics for the single tree delineation (Germany)

| | Perfect match | Good match | Grouped | Split | Comission error | Not detected | Total number of isols | Total number of refs |
|----------------------------|----------------------|-------------------|----------------|--------------|------------------------|---------------------|------------------------------|-----------------------------|
| LiDAR delineation | 165 | 89 | 95 | 95 | 2 | 16 | 446 | 579 |
| After spectral enhancement | 213 | 84 | 79 | 90 | 6 | 31 | 492 | 579 |

From the statistics an improvement of 7.42 % can be calculated when comparing the number of matches with the number of reference trees. Considering the low accuracy of the LiDAR polygons and the fact that only certain polygons are corrected this is a remarkable number. The low accuracy of LiDAR delineation reflects the study of Heurich (2006) who describes an average accuracy of 40 % with similar delineation algorithms in the Bavarian forest. Difficulties are made by dense forest stands and interlocking tree crowns as they occur in temperate mixed forest. Since the spectral improvement is applied to the LiDAR delineation it cannot completely change the result but it is a good tool for corrections.

Further development should be invested in finding new approaches for the LiDAR based delineation algorithm. Spectral correction could be improved by finding more stable features for class separation. Maybe the spectral and the LiDAR data can be directly combined in one process.

Acknowledgements

The authors would like to express their gratitude to the Warsaw University of Life Science for commissioning this study and providing the data.

References

- Bohlin, J., Olsson, H., Olofsson, K. and Wallerman, J., 2006. Tree species discrimination by aid of template matching applied to digital air photos. In: *Workshop on 3D Remote Sensing in Forestry – Session 6a*. Vienna: 199-203.
- Gonzales, R. C. and Woods, R. E., 2002. Digital image processing, Second Edition. Upper Saddle River, New Jersey.
- Heurich, M., 2006. Evaluierung und Entwicklung von Methoden zur automatisierten Erfassung von Waldstrukturen aus Daten flugzeuggetragener Fernerkundungssensoren. *Forstliche Forschungsberichte München*, No. 202.
- Koch, B., Svoboda, J., Adler, P. and Dees, M., 2002. Automatische Baumartenerkennung auf der Grundlage digitalisierter CIR-Luftbilder. *Allgemeine Forst- u. Jagdzeitung*, 173, JG, 07-08, 131-140.
- Koch B., Heyder U. and Weinacker, H. (2006). Detection of individual tree crowns in airborne lidar data. *Photogrammetric Engineering & Remote Sensing*, Vol. 72, No. 4, 357-363.
- Leckie, D., Gougeon, F., Hill, D., Quinn, R., Armstrong, L. and Shreenan, R., 2003. Combined

- high-density lidar and multispectral imagery for individual tree crown analysis. *Can. J. Remote Sensing*, Vol. 29, No. 5, 633-649.
- Leckie, D.G., Tinis, S., Nelson, T., Burnett, C., Gaugeon, F.A., Cloney, E. and Paradine, D., 2005. Issues in species classification of trees in old growth conifer stands. *Can. J. Remote Sensing*, Vol. 31, No. 2, 175-190.
- Liang, X., Hyyppä, J. and Matikainen, L., 2007. Deciduous-coniferous tree classification using difference between first and last pulse laser signatures. In: *ISPRS Workshop on Laser Scanning 2007 and SilviLaser 2007, Volume XXXVI, Part 3/W52*, Espoo: 253-257.
- MVTec Software GmbH, 2007. HALCON, <http://www.mvtec.com/halcon> (last date accessed: 24.April 2008).
- Ørka, H. O., Næsset, E. And Bollandsås, O. M., 2007. Utilizing airborne laser intensity for tree species classification. In: *ISPRS Workshop on Laser Scanning 2007 and SilviLaser 2007, Volume XXXVI, Part 3/W52*, Espoo: 300-304.
- Persson, Å., Holmgren, J. and Söderman, U., 2006. Identification of tree species of individual trees by combining very high resolution laser data with multi-spectral images. In: *Workshop on 3D Remote Sensing in Forestry – Session 6a*. Vienna: 91-96.
- Reitberger, J., Krzystek, P. and Stilla, U., 2006. Analysis of full waveform data for tree species classification. In: *Symposium of ISPRS Commission III Photogrammetric Computer Vision PCV' 06*, Bonn: 228-233.
- Rossmann, J., Schluse, M., Bücken, A. And Krahwinkler, P., 2007. Using airborne laser scanner data in forestry management: A novel approach to single tree delineation. In: *ISPRS Workshop on Laser Scanning 2007 and SilviLaser 2007, Volume XXXVI, Part 3/W52*, Espoo: 350-354.
- Tiede, D. and Hoffman C., 2006. Process oriented object based algorithms for single tree detection using laser scanning. In: *Workshop on 3D Remote Sensing in Forestry – Session 6a*. Vienna: 151-156.
- Wang, L., Gong, P. and Biging, G. S., 2004. Individual tree-crown delineation and treetop detection in high-spatial-resolution aerial imagery. *Photogrammetric Engineering & Remote Sensing* Vol. 70, No. 3, 351-357.
- Wang, Y., Soh, Y. S. and Schultz, H., 2006. Individual tree crown segmentation in aerial forestry images by mean shift clustering and graph-based cluster merging. *International Journal of Computer Science and Network Security*, Vol. 6, No. 11, 40-45.
- Wang, Y., Weinacker, H. and Koch, B., 2007. Development of a procedure for vertical structure analysis and 3D single tree extraction within forest based on LiDAR point cloud. In: *ISPRS Workshop on Laser Scanning 2007 and SilviLaser 2007, Volume XXXVI, Part 3/W52*, Espoo: 419-423.
- Wolf, B.-M. and Heipke, C., 2007. Automatic extraction and delineation of single trees from remote sensing data. *Machine Vision and Applications*, 18, 317-330.

Estimation of stand volume by fusing low laser-sampling density LiDAR data with QuickBird panchromatic imagery in closed-canopy Japanese cedar (*Cryptomeria japonica*) plantations

Tomoaki Takahashi¹, Yoshio Awaya², Yasumasa Hirata³, Naoyuki Furuya⁴, Toru Sakai⁵
& Atsushi Sakai⁶

¹Forestry and Forest Products Research Institute, 1, Matsunosato, Tsukuba, Ibaraki, 305-0044, Japan, tomokun@ffpri.affrc.go.jp

²Forestry and Forest Products Research Institute, 1, Matsunosato, Tsukuba, Ibaraki, 305-0044, Japan, awaya@ffpri.affrc.go.jp

³Forestry and Forest Products Research Institute, 1, Matsunosato, Tsukuba, Ibaraki, 305-0044, Japan, hirat09@ffpri.affrc.go.jp

⁴Japan International Research Center for Agricultural Sciences, 1-1, Ohwashi, Tsukuba, Ibaraki 305-8686, Japan, nfuruya@affrc.go.jp

⁵Forestry and Forest Products Research Institute, 1, Matsunosato, Tsukuba, Ibaraki, 305-0044, Japan, torus@ffpri.affrc.go.jp

⁶Japan International Research Center for Agricultural Sciences, 1-1, Ohwashi, Tsukuba, Ibaraki 305-8686, Japan, golgo@affrc.go.jp

Abstract

This study investigated the potential of fusing low laser-sampling density LiDAR data with QuickBird panchromatic imagery for estimating stand volumes. The study area was in closed-canopy, mountainous Japanese cedar (*Cryptomeria japonica*) plantations in Japan. Stand volume in the area ranged from 250.5 to 913.1 m³/ha and terrain was undulating with an elevation ranging from 135 to 391 m above sea level. A total of 13 circular sample plots (0.04 ha) were established and stand volume within the plots was measured as validation data for evaluating stand volume estimates derived from the fused data through a regression model. The independent variables of the empirical model were individual tree height and crown projection area and the dependent variable was individual stem volume of Japanese cedar. To estimate stand volume with the fused data, LiDAR-derived tree heights and panchromatic imagery-derived crown projection areas were computed for individual tree crowns delineated by the Voronoi tessellation. All results of this study revealed that fusing low laser-sampling density LiDAR data (e.g. 1 point/4 m²) with QuickBird panchromatic imagery (0.6-m resolution) would have great potential to estimate stand volume precisely in Japanese cedar plantations regardless of different footprint sizes (e.g. 0.16–0.47 m).

Keywords: LiDAR, QuickBird, panchromatic, data fusion, Voronoi tessellation

1. Introduction

Many previous studies have revealed that small-footprint airborne scanning LiDAR (Light Detection and Ranging) can estimate or measure tree and canopy heights accurately in a variety of forest types (e.g. Hyypä *et al.* 2001; Næsset 2002; Persson *et al.* 2002; Popescu *et al.* 2002; Holmgren *et al.* 2003; Yu *et al.* 2004; Takahashi *et al.* 2005a, 2008a). Although acquisition of high laser-sampling density LiDAR data (e.g. over 10 points/m²) in vast forests is expensive, such data can provide accurate information on individual tree numbers and crown properties such as diameter and projection area of upper-storey trees. Some research has shown the feasibility of estimating stem or stand volumes accurately from LiDAR-derived tree heights and

crown properties in some coniferous forests (Hyypä *et al.* 2001; Persson *et al.* 2002; Holmgren *et al.* 2003; Takahashi *et al.* 2005b). Although the number of detected trees and the measurement accuracy of the properties apparently deteriorate with decreasing laser-sampling density, the estimates of tree heights with varying laser-sampling density data (i.e. laser shot spacing ranging from less than a meter to a few meters) reported in much of the previous research seem to be comparable with field-measured tree heights. In contrast, high spatial resolution satellite imagery with less than 1-m resolution, such as IKONOS and QuickBird panchromatic images, can cover local/regional scale forests with fine spatial resolution. As QuickBird panchromatic imagery has approximately 0.6-m resolution at nadir, there is a possibility of extracting by image processing individual tree crown properties for upper-storey trees with crown diameters exceeding approximately 1.8 m. Therefore, laser shots of at least approximately 1 point/4 m² could hit each crown that can be identified in the panchromatic imagery and so provide approximate estimates of individual tree heights. Assuming that fusion of such low laser-sampling density data with the panchromatic imagery has potential to estimate stem and stand volumes adequately, we therefore attempted to estimate by data fusion stand volumes of Japanese cedar (*Cryptomeria japonica*) plantations in a variety of stand conditions.

In this study, we investigated (1) the potential of high-laser sampling density LiDAR data alone for stand volume estimation and (2) the potential of fusing low laser-sampling density LiDAR data with a QuickBird panchromatic imagery for stand volume estimation. Because laser footprint sizes might affect the tree height estimation (Yu *et al.* 2004; Andersen *et al.* 2006; Takahashi *et al.* 2008b), LiDAR data with different footprint sizes were used for the investigation of (2). A previously constructed regression model whose independent variables were individual tree height and crown projection area and whose dependent variable was individual stem volume of Japanese cedar (Takahashi *et al.* 2005b) was used to estimate stand volumes.

2. Method

2.1 Study area

The study area of approximately 75.2 ha was located in a national forest in Ibaraki Prefecture in central Japan (lat. 36° 10' N, long. 140° 10' E). More than 80% of the area is dominated by plantations of evergreen coniferous Japanese cedar and hinoki cypress (*Chamaecyparis obtusa*) trees, with the remainder dominated by several broadleaved deciduous tree species. Stand age in the coniferous forests ranged from 20 to 100 years. Terrain is undulating with an elevation ranging from 135 to 391 m above sea level. During the fall and winter of 2006, we established 13 circular sample plots (0.04 ha) within the closed-canopy Japanese cedar plantations. All plots consisted purely of planted Japanese cedar and dense understorey vegetation consisting of *Aucuba japonica* and *Eurya japonica*, which are evergreen shrubs with a height of less than approximately 3–5 m.

To locate the center of each sample plot, global positioning system (GPS) surveys were conducted under the static survey performance using a single-frequency ProMark2 receiver (Magellan, Santa Clara, CA, U.S.A.). Details of the GPS surveys are shown in Takahashi *et al.* (2008b). Within each sample plot, all trees with a diameter at breast height (DBH) > 4 cm were callipered. Tree heights were measured for sample trees within plots in young and middle-aged forests using a Häglof Vertex hypsometer (Häglof, Langsele, Sweden). For the young and middle-aged forests, the sample trees (> 50% of the trees within each plot) were selected with equal probability. Next, height-diameter curves were produced for each plot and unmeasured tree heights were estimated from each model. In mature forests, tree heights of all standing trees within each plot were measured using the hypsometer. Trees with heights exceeding the arithmetic mean tree height within each plot were regarded as dominant trees in the present

study. Individual stem volumes were calculated from tree height and DBH using standard two-way volume equations for Japanese cedar (Forestry Agency, Japan, 1970). Finally, stand volume (m^3/ha) in each plot was calculated by summing stem volumes of all standing trees within each plot. Summary statistics for 13 field sample plots are shown in Table 1.

Table 1: Summary of field plot data

| Plot | A | B | C | D | E | F | G | H | I | J | K | L | M |
|---|-------|-------|-------|-------|-------|-------|-------|-------|-------|-------|-------|-------|-------|
| Stand age | 20 | 20 | 23 | 25 | 25 | 29 | 40 | 41 | 43 | 59 | 59 | 100 | 100 |
| Stand density (trees/ha) | 2000 | 1725 | 2800 | 2675 | 2725 | 1375 | 1200 | 2125 | 475 | 925 | 875 | 1075 | 1050 |
| No. of trees | 80 | 69 | 112 | 107 | 109 | 55 | 48 | 85 | 19 | 37 | 35 | 43 | 42 |
| No. of dominant trees | 49 | 36 | 57 | 53 | 58 | 24 | 29 | 49 | 9 | 16 | 19 | 21 | 22 |
| Mean DBH (cm) | 17.9 | 16.3 | 13.9 | 16.6 | 17.0 | 22.1 | 25.2 | 16.4 | 37.1 | 29.5 | 31.0 | 28.9 | 26.6 |
| Basal area (m^2/ha) | 52.8 | 37.6 | 44.0 | 61.2 | 65.1 | 55.3 | 62.9 | 47.1 | 54.1 | 65.3 | 71.3 | 76.8 | 62.8 |
| Mean tree height (m) | 13.9 | 13.5 | 10.8 | 14.3 | 14.5 | 19.3 | 20.8 | 12.6 | 24.8 | 22.6 | 23.6 | 24.6 | 22.6 |
| Dominant tree height (m) | 14.9 | 14.7 | 11.5 | 15.4 | 15.4 | 20.7 | 22.4 | 13.4 | 26.4 | 24.4 | 25.1 | 26.8 | 24.5 |
| Stand volume (m^3/ha) | 387.1 | 270.3 | 250.5 | 461.5 | 490.6 | 539.0 | 653.8 | 310.8 | 605.3 | 725.3 | 794.8 | 913.1 | 700.0 |

2.2 LiDAR data

The LiDAR data used in the analysis were those of Takahashi *et al.* (2008b), acquired on 31 August 2006 by Aero Asahi Co., Ltd., Japan. A helicopter-borne laser scanner (Optech ALTM 3100), which is a multi-return system that also collects intensity data, was used. The study site was sampled at three different flight altitudes; 500 m, 1000 m and 1500 m above ground level (a.g.l.). The beam divergence of 0.31 mrad produced footprint diameters of 0.16 m, 0.31 m and 0.47 m, respectively. At each flight altitude, several parallel flight paths were recorded to cover the entire area with average overlapping of 64% between adjacent flight paths. Transmitted laser pulses with scan angles exceeding 8° were excluded from the final analysis to avoid the inclusion of inferior quality data at the edge of strips. Although the laser-sampling densities were approximately 57, 25 and 9 points/ m^2 , respectively, at each flight altitude, the densities of all datasets were thinned out and finally converted into approximately 1 point/ 4 m^2 . The 57 points/ m^2 dataset at 500-m flight altitude was defined as the high-density LiDAR dataset and the 1 point/ 4 m^2 datasets at three flight altitudes were defined as the low-density LiDAR datasets.

2.3 Processing high-density LiDAR data for delineating individual tree crowns and estimating stand volumes

The high-density (57 points/ m^2) LiDAR dataset was used to create a canopy height model (CHM) with a pixel size of 0.25 m (see Figure 1). The CHM was generated by subtracting a digital terrain model (DTM) from a digital surface model (DSM) produced by assigning the height value of the highest laser reflection point within each pixel using only first pulse data.

The DTM was generated by a conventional human-assisted method in which an operator visually inspected the elevations of the DTM after an initial automated filtering (Takahashi *et al.* 2008b). Hereafter, the DTM is defined as DTM_{ref} . Through refining by the maximum filter with variable window sizes (3 x 3 window for $CHM \leq 20$ m; 5 x 5 window for $CHM > 20$ m) and smoothing with a 3 x 3 low-pass filter (Hyypä *et al.* 2001) for the CHM, the watershed method (e.g. Wang *et al.* 2004) was then applied to delineate individual tree crowns. Next, individual tree stem volume was estimated using the regression model presented in Takahashi *et al.* (2005b). The empirical model consisted of LiDAR-derived tree height and crown projection area as follows:

$$\ln V = \ln \beta_0 + \beta_1 \ln H + \beta_2 \ln CA \quad (1)$$

where V (m^3) is estimates of individual stem volume, H (m) is LiDAR-derived tree height, and CA (m^2) is LiDAR-derived crown projection area. The values of $\ln \beta_0$, β_1 and β_2 were -8.312 , 2.282 and 0.389 , respectively. Adjusted coefficient of determination of the model was 0.734 . The value of H was assigned to the highest value of the CHM within each segmented crown and the value of CA was the segmented crown area. Finally, stand volume estimates (m^3/ha) in each plot were calculated by summing the individual stem volume estimates of all segmented trees within each plot.

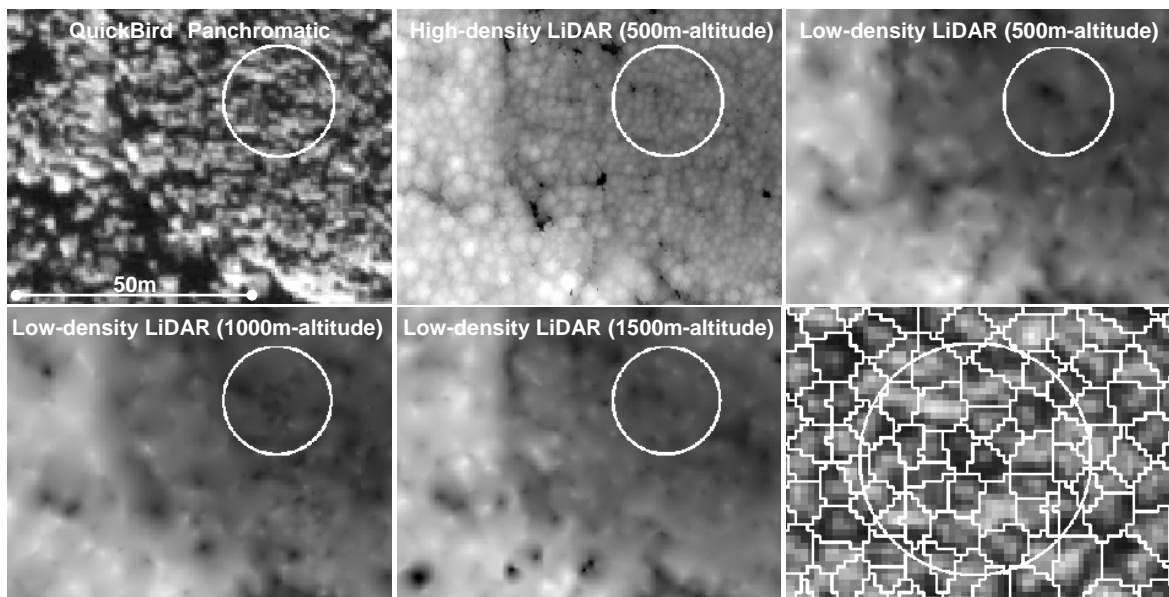


Figure 1: The images of QuickBird panchromatic (0.6-m resolution) and canopy height models (0.25-m resolution) derived from different flight altitude LiDAR data. High and low-densities are approximately 57 points/ m^2 and 1 point/ 4 m^2 , respectively. The circle denotes plot C (0.04 ha; 11.28 m radius) and the segmented individual tree crowns were produced by the Voronoi tessellation on the panchromatic imagery.

2.4 Processing low-density LiDAR data and panchromatic imagery for delineating individual tree crowns and estimating stand volumes

The low-density (1 point/ 4 m^2) LiDAR datasets at three flight altitudes were used to create CHMs with a pixel size of 0.25 m (see Figure 1). To create the CHMs, DSMs were created through interpolation by the natural neighbour method (Bater and Coops 2006). Because the number of ground return laser data was poor at all flight altitudes in the study area, as shown in Takahashi *et al.* (2008b), it was difficult to distinguish ground return laser data from overstorey and understorey vegetation return laser data. Therefore, in the present study, if the difference between the elevation of a given laser data in each altitude dataset and the elevation of the

DTM_{ref} at the same horizontal location did not exceed 1 m (absolute value), then such laser data were regarded as ground return data. DTMs at all flight altitudes were then created through interpolation by the natural neighbour method.

The panchromatic imagery (11-bit data) used in the analysis was acquired on 4 February 2006. The imagery was orthorectified using both the CHM derived from the high-density LiDAR dataset as ground control points (GCP) and a digital elevation model (DEM). The resampling method used in the orthorectification was the cubic convolution method and the resolution of the orthorectified imagery was 0.6 m. Through refining by a 3 x 3 median filter and 3 x 3 local maximum filtering (Wulder *et al.* 2000) to detect local maximum pixel, which can be regarded as individual tree apex or near apex pixel, the Voronoi tessellation (e.g. Worboys and Duckham 2004) was then applied to delineate individual tree crowns (see Figure 1). Next, individual tree stem volumes were estimated by using equation (1). The value of H was assigned to the highest value of the CHMs within each segmented crown on the panchromatic imagery and the value of CA was the segmented crown area. Finally, stand volume estimates (m³/ha) in each plot were calculated by summing the individual stem volume estimates of all segmented trees within each plot. In addition to fusing these low-density LiDAR datasets with the panchromatic imagery, the high-density LiDAR dataset were also fused with the panchromatic imagery to investigate the effects on the volume estimation of height difference between the low- and high-density LiDAR datasets.

2.5 Validation of stand volume estimates

Before evaluating stand volume estimates, we first investigated the number of detected tree crowns derived from the high-density LiDAR dataset and the panchromatic imagery. The biases and root mean square errors (RMSE) of the dominant mean tree height estimates were computed. Next, to evaluate the accuracy and precision of the stand volume estimates, the systematic errors (i.e. bias), random errors and RMSEs were computed. The relationships between field-measured and estimated stand volumes were investigated by regression analysis, in which models were fitted to the data using the least-squares method.

3. Result

Table 2: Number of detected tree crowns derived from high-density LiDAR data and QuickBird panchromatic imagery

| Plot | A | B | C | D | E | F | G | H | I | J | K | L | M |
|----------------|----|----|----|----|----|----|----|----|----|----|----|----|----|
| LiDAR-detected | 61 | 59 | 66 | 63 | 65 | 39 | 31 | 56 | 20 | 25 | 27 | 20 | 24 |
| QB-detected | 27 | 30 | 32 | 29 | 34 | 23 | 21 | 27 | 21 | 21 | 25 | 20 | 24 |

High density means 57 points/m². QB denotes QuickBird imagery. The watershed and Voronoi tessellation methods were applied for the high-density LiDAR data (0.25-m resolution) and the panchromatic imagery (0.6-m resolution), respectively.

The number of detected tree crowns derived from the high-density LiDAR dataset and the panchromatic imagery is shown in Table 2. The differences in the number of detected crowns between the two sets of data are large in dense forests (more than 1200 trees/ha) and small in non-dense forests (less than 1200 trees/ha). The errors in dominant tree height estimates are shown in Table 3. Both the high- and low-density LiDAR datasets underestimated dominant mean tree heights. The tree height estimates with each low-density LiDAR dataset were approximately 1 m less than those derived from the high-density LiDAR dataset.

The errors of stand volume estimates are shown in Table 4. The systematic errors of the estimates were negative values for all datasets. As seen in Figures 2 and 3 and Table 4, the random errors were small for all datasets and there was a strong liner relationship between

field-measured and estimated stand volumes for all datasets. According to the regression analysis, the slopes for all regression equations could be regarded statistically as one ($p < 0.05$).

Table 3: Errors of dominant tree height estimates (m)

| | | Bias | RMSE |
|--------------------|-----------------|-------|------|
| High-density LiDAR | (500 m a.g.l.) | -0.69 | 1.19 |
| Low-density LiDAR | (500 m a.g.l.) | -1.47 | 2.09 |
| Low-density LiDAR | (1000 m a.g.l.) | -1.85 | 2.61 |
| Low-density LiDAR | (1500 m a.g.l.) | -1.60 | 2.27 |

High and low-densities mean 57 points/m² and 1 point/4 m², respectively. QB denotes QuickBird imagery and the parenthetic values denote flight altitudes.

Table 4: Errors of stand volume estimates (m³/ha) and the results of regression analysis

| | | Systematic error | Random error | RMSE | RMSEr | Slope | Intercept | Ajusted R ² |
|-------------------------|-----------------|------------------|--------------|-------|--------|---------|---------------------|------------------------|
| High-density LiDAR | (500 m a.g.l.) | -47.2 | 46.9 | 66.6 | 12.2 % | 0.880** | 18.52 ^{NS} | 0.946 |
| QB + high-density LiDAR | (500 m a.g.l.) | -124.5 | 57.5 | 137.2 | 25.1 % | 0.989** | -118.64* | 0.915 |
| QB + low-density LiDAR | (500 m a.g.l.) | -182.3 | 44.1 | 187.5 | 34.3 % | 0.899** | -126.88** | 0.951 |
| QB + low-density LiDAR | (1000 m a.g.l.) | -200.1 | 44.8 | 205.1 | 37.5 % | 0.861** | -123.98** | 0.957 |
| QB + low-density LiDAR | (1500 m a.g.l.) | -188.8 | 42.0 | 193.4 | 35.4 % | 0.878** | -122.17** | 0.960 |

High and low-densities mean 57 points/m² and 1 point/4 m², respectively. QB denotes QuickBird imagery and the parenthetic values denote flight altitudes. RMSEr means a relative RMSE divided by average field-measured stand volume. ** ($p < 0.01$); * ($p < 0.05$); NS ($p > 0.05$)

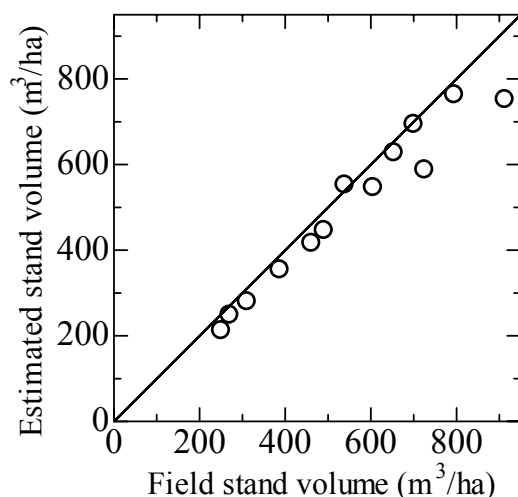


Figure 2: The relationship between field-measured and estimated stand volumes from high-density LiDAR data

4. Discussion

Figure 2 and Table 4 indicate that the high-density LiDAR dataset could estimate stand volumes accurately. Although the number of LiDAR-detected tree crowns was less than the number of field-measured tree crowns, the sum of individual stem volumes estimated by the regression model could explain most of the total volumes within each plot, except for two plots (plots J and L). This

result indicates that a large portion of the LiDAR-detected trees had larger individual stem volumes than the undetected trees in each plot. Moreover, these results indicate that the empirical model (Eq. 1) is very useful for estimating stand volumes of Japanese cedar stands with a variety of stand conditions in Japan, despite the model having been constructed within a restricted forest area (stand density; 800–1227 trees/ha, stand volume; 504.8–602.9 m³/ha). One weakness in the present study is that only 13 field plots were used although the 13 plots cover a good range (250.5–913.1 m³/ha). We should have increased the number of field sample plots to examine the variability of volume estimates among plots with nearly the same volume.

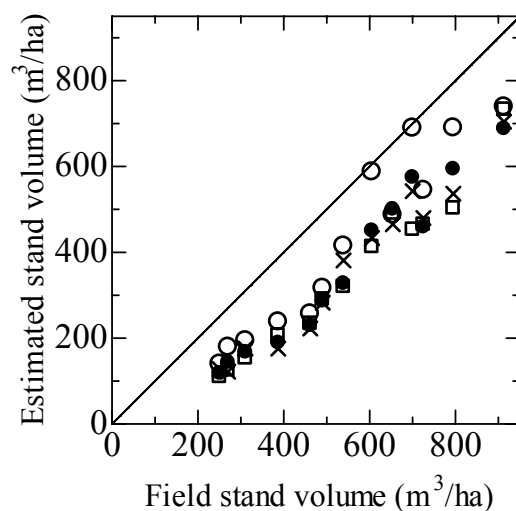


Figure 3: The relationship between field-measured and estimated stand volumes from fused data. Solid circles, 500-m low-density data; square, 1000-m low-density data; cross, 1500-m low-density data; open circles, 500-m high-density data

By contrast, all the fused datasets produced large negative systematic errors in the estimates of stand volumes, although the random errors were as small as those of the non-fused LiDAR datasets. As seen from Figure 3, the dataset (open circles) made by fusing the high-density LiDAR dataset with the panchromatic imagery hardly improved estimates of stand volumes in plots A, B, C, D, E and H (stand volume < 500 m³/ha: dominant mean tree height < 16 m), whose crown numbers detected by the panchromatic imagery were almost half those detected by LiDAR; however, the fused dataset improved the estimates of stand volumes in some plots (stand volume > 500 m³/ha: dominant mean tree height > 20 m) whose crown numbers detected by the panchromatic imagery were similar to those detected by LiDAR. This result indicates that the cause of the negative systematic errors in the three fused datasets would be based on an interaction of the omission errors of panchromatic imagery-detected crown numbers (Table 2), the underestimations of LiDAR-derived tree heights (Table 3), and the characteristic/behavior of the logarithmic regression model. Although the reason why the slopes of all regression equations of the fused datasets were regarded statistically as one remains unknown, the three fused datasets could provide almost the same accuracy of stand volume estimates in this study area. These results demonstrate that high-density LiDAR is not needed for all applications, such as estimation of stand volume, especially when fused with other optical remote sensing technologies and over large areas. Also, there seems to be a misconception that one needs near perfect one-to-one correspondence between field data and those predicted empirically from LiDAR.

All results of this study revealed that data fusion of low laser-sampling density LiDAR data (e.g. 1 point/4 m²) with QuickBird panchromatic imagery would have a great potential for estimating stand volume precisely in Japanese cedar plantations regardless of different footprint sizes (e.g. 0.16–0.47 m). Moreover, if the systematic errors in the estimates were revealed as

site-independent values, we would be able to estimate stand volume accurately and precisely with LiDAR data acquisition at a lower cost in vast Japanese cedar forests by using methods presented in this study.

Acknowledgements

We thank Kenichi Shibuya and Kouji Oomori from Aero Asahi Co., Japan for planning the flight and acquiring the LiDAR data. Many thanks to two anonymous reviewers for providing valuable comments on the original manuscript.

References

- Andersen, H.E., Reutebuch, S.E. and McGaughey, R.J., 2006. A rigorous assessment of tree height measurements obtained using airborne lidar and conventional field methods. *Canadian Journal of Remote Sensing*, 32, 355-366.
- Bater, C.W. and Coops, N.C., 2006. Comparing interpolation algorithms for deriving digital elevation models from unevenly distributed LiDAR ground returns. *Proceedings of the international conference Silvilaser2006*, 43-48.
- Forestry Agency, 1970. Timber volume table (Western Japan) (in Japanese). Nihon Ringyo Chosakai, Tokyo, Japan, 13.
- Holmgren, J., Nilsson M. and Olsson, H., 2003a. Estimation of tree height and stem volume on plots using airborne laser scanning. *Forest Science*, 49, 419-428.
- Hyypä, J., Kelle, O., Lehikoinen, M. and Inkinen, M., 2001. A segmentation-based method to retrieve stem volume estimates from 3-D tree height models produced by laser scanners. *IEEE Transactions on Geoscience and Remote Sensing*, 39, 969-975.
- Næsset, E. and Økland, T., 2002. Estimating tree height and tree crown properties using airborne scanning laser in a boreal nature reserve. *Remote Sensing of Environment*, 79, 105-115.
- Persson, A., Holmgren, J. and Soderman, U., 2002. Detecting and measuring individual-trees using an airborne laser scanner. *Photogrammetric Engineering and Remote Sensing*, 68, 925-932.
- Popescu, S.C., Wynne, R.H. and Nelson, R.F., 2002. Estimating plot-level tree heights with lidar: local filtering with a canopy-height based variable window size. *Computers and Electronics Agriculture*, 37, 71-95.
- Takahashi, T., Yamamoto, K., Senda, Y. and Tsuzuku, M., 2005a. Estimating individual-tree heights of sugi (*Cryptomeria japonica* D. Don) plantations in mountainous areas using small-footprint airborne LiDAR. *Journal of Forest Research*, 10, 135-142.
- Takahashi, T., Yamamoto, K., Senda, Y. and Tsuzuku, M., 2005b. Predicting individual stem volumes of sugi (*Cryptomeria japonica* D. Don) plantations in mountainous areas using small-footprint airborne LiDAR. *Journal of Forest Research*, 10, 305-312.
- Takahashi, T., Yamamoto, K. and Senda, Y., 2008a. Comparison of different sampling density data for detecting and measuring individual trees in a mountainous coniferous forest using small-footprint airborne LiDAR. *Journal of Forest Planning*, 13, 249-258.
- Takahashi, T., Awaya, Y., Hirata, Y., Furuya, N., Sakai, T. and Sakai, A., 2008b. Effects of flight altitude on LiDAR-derived tree heights in mountainous forests with poor laser penetration rates. *The Photogrammetric Journal of Finland*, 21, 86-96.
- Wang, L., Gong, P. and Biging, S., 2004. Individual tree-crown delineation and treetop detection in high-resolution aerial imagery. *Photogrammetric Engineering and Remote Sensing*, 70, 351-357.
- Worboys, M. and Duckham, M., 2004. GIS A computing perspective. *CRC PRESS*, Florida, USA, 190-192.
- Wulder, M., Niemann, K.O. and Goodenough, D.G., 2000. Local maximum filtering for the extraction of tree locations and basal area from high spatial resolution imagery. *Remote Sensing of Environment*, 73, 103-114.

Yu, X., Hyypä, J., Hyypä, H. and Maltamo, M. 2004. Effects of flight altitude on tree height estimation using airborne laser scanning. *International Archives Photogrammetric, Remote Sensing and Spatial Information Science*, 36, part8/w2

A method for linking field-surveyed and aerial-detected single trees using cross correlation of position images and the optimization of weighted tree list graphs

Kenneth Olofsson¹, Eva Lindberg¹ & Johan Holmgren¹

¹Remote Sensing Laboratory, Department of Forest Resource Management, Swedish University of Agricultural Sciences, kenneth.olofsson@srh.slu.se, eva.lindberg@srh.slu.se, johan.holmgren@srh.slu.se

Abstract

With the present number of forestry remote sensing and field plot survey methods several data sources can be combined to potentially achieve a higher accuracy than with a single data source. Some of these datasets contain single tree information and it would be of great value when designing survey techniques if one could automatically link data from different sources belonging to the same tree. In this paper such a method for linking field-surveyed and aerial detected trees is described and evaluated. A simulation study and experimental data show the accuracy of the algorithm at different settings. The method correctly links >90 % of the trees if the corresponding datasets have a position error standard deviation of 1 [m] and 10 % omission and commission errors.

Keywords: LiDAR, digital aerial images, data fusion, field plots, single tree detection and linking.

1. Introduction

New remote sensing technology allows for high precision measurements of vegetation. Low resolution airborne laser scanner (ALS) data can be used to establish statistical models for the prediction of biophysical properties, *e.g.* stem volume and mean tree height, on a raster cell level (*e.g.* Means *et al.* 2000; Næsset 2002). In high resolution ALS data, individual trees are identified which makes it possible to establish statistical models on the tree level (*e.g.*, Hyypä *et al.* 2001; Persson *et al.* 2002; Solberg *et al.* 2006). The size of the random errors for statistical models will become a problem if there is a poor co-registration of field surveyed data and remote sensing data and this will affect the quality of remote sensing based forest inventories. High precision position measurements can be achieved with advanced GPS equipment but only below a clear sky where no canopy obscures the satellite signal. The GPS errors will be large within a forest stand with a high basal area (Næsset and Jonmeister 2002). Thus there is a need for an automatic tree linking algorithm that rectifies poorly registered coordinates in raw data. This paper presents a method for the automatic co-registration of field surveyed and remotely sensed data. The performance of the method was tested by using simulations. The algorithm was tested empirically in a forest in west Sweden.

2. Method

Linking field surveyed and aerial detected trees requires input data from a remote sensing single tree detection method (*e.g.*, Gougeon, 1995; Holmgren and Wallerman 2006; Hyypä *et al.* 2001; Korpela 2004; Persson *et al.* 2002; Pinz, A., 1989; Pollock 1996; Solberg *et al.* 2006). In the empirical study in this paper the ALS single tree detection method developed by Holmgren and Wallerman (2006) has been used. Single tree data collected from a field plot is also necessary.

The method for linking field surveyed and aerial detected single trees is a two stage process: first, the field plot coordinate-system is rectified to the aerial data coordinate-system, and second, the field surveyed trees within the plot are linked to the most probable candidates of the aerial detected trees positioned nearby.

2.1 Field data

The study area is located in the west of Sweden (lat. $60^{\circ} 43'$ N, long. $15^{\circ} 10'$ E). The dominating tree species are Norway spruce (*Picea Abies*), birch (*Betula spp*) and Scots pine (*Pinus Silvestris*). Field reference data was collected in 155 field plots with 10 m radius each. The position of the field plots were measured using a Global Navigation Satellite System (GNSS). Within the plots, all trees with a stem diameter larger than 50 mm were callipered and tree species was recorded. The positions of the trees were registered relative to the centre of each plot by measuring azimuth and distance.

2.2 ALS data

The laser data was acquired using an Optech scanner with a scan density of approximately 10 points/m². The flying height was 900 m, the pulse repetition rate 100 kHz and the field of view 34° . The ALS single tree detection method used is developed by (Holmgren and Wallerman 2006).

2.3 Rectifying the field plot coordinate system

Usually field plot measured tree positions have good precision but lower accuracy. The data is biased. Therefore, the two coordinate systems need to be rectified before the field plot trees can be linked to the aerial detected trees. The algorithm in this study uses an estimated position of the field plot centre to start the search, and a search area that contains the real field plot centre. The search area is set depending on the expected bias error in the experimental setup. From the start position, aerial single tree data from within the search area is collected as a list. This list must contain the tree position coordinates, x and y , and a variable that represents the tree size, e.g. the tree height, H , or the crown diameter, D . In this study the tree height was used. For the field plots a similar list is required with the positions of the trees and a size variable. In this study the stem diameter at breast height, DBH , was chosen to represent the size of the tree.

The tree lists are used to create two single tree position images, figure 1. Within the image, each tree is displayed as a Gaussian surface where the x and y coordinates determine the position within the image, the tree size variable determines the amplitude of the Gaussian function, and the standard deviation is set to the expected tree position precision, figures 1 and 2. Since large trees often are detected from above whereas small trees often are hidden, the maximum surface is used; from all of the Gaussian functions that cover the same area, the highest value is chosen, figure 2.

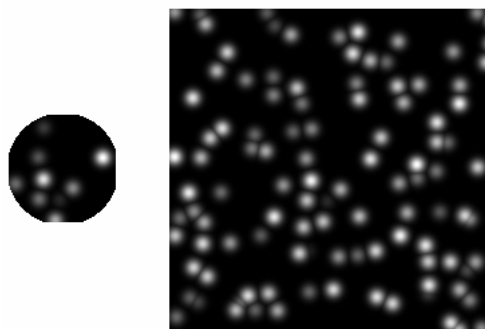


Figure 1: Two single tree position images where each tree is modelled as a Gaussian surface with the amplitude proportional to the tree size and the standard deviation equal to the radial position error. LEFT: The position image of a circular field plot where the stem diameter at breast height is used as amplitude. RIGHT: The position image of an area with aerial detected trees, with the tree height as amplitude.

The two single tree position images are then cross correlated to find the closest match between the patterns in the two images. The field plot image can be rotated a few degrees between each correlation run, in order to compensate for possible compass errors. The normalized correlation coefficient, cc (Gonzalez and Wintz, 1987) is defined as:

$$cc(m, n) = \frac{\sum_x \sum_y [g(x, y) - \bar{g}(x, y)][k(x - m, y - n) - \bar{k}]}{\sqrt{\sum_x \sum_y [g(x, y) - \bar{g}(x, y)]^2 \sum_x \sum_y [k(x - m, y - n) - \bar{k}]^2}} \quad (1)$$

where g is the aerial position image, k is the field plot position image, \bar{k} is the average intensity of k and $\bar{g}(x, y)$ is the average intensity of g of the region coincident with $k(x, y)$. The position and rotation with the highest correlation coefficient, equation 1, is assumed to be the place where the real field plot center is located. The greater the position image resolution results in the higher accuracy of the field plot matching achieved.

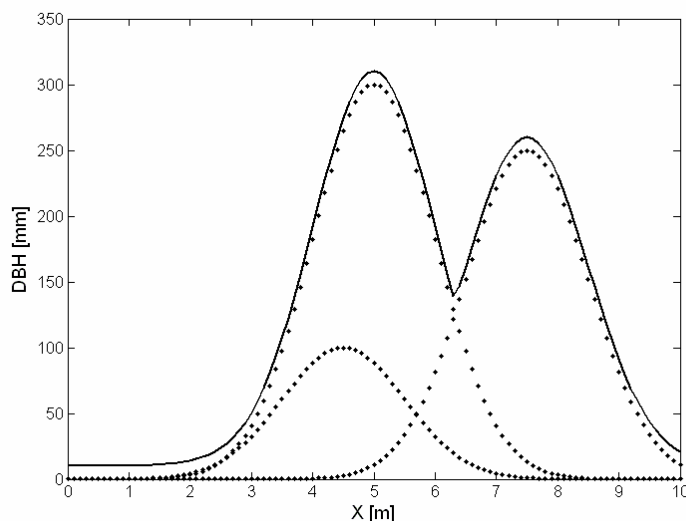


Figure 2: [DOTTED CURVES]: Three field plot trees with a stem diameter at breast height (DBH) of 100, 300, and 250 [mm] and positions in the x-direction of 4.5, 5 and 7.5 [m], displayed as Gaussian functions with the DBH as amplitude and the position error (1 [m]) as standard deviation. [SOLID CURVE]: The maximum surface of all trees in the plot.

2.4 Linking field surveyed and aerial detected trees

The algorithm uses the tree heights for both the aerial detected trees and the field surveyed trees. If the tree height is not sampled by the single tree detection method or the field survey – if for instance the crown diameter and the *DBH* is used instead – the tree heights must be estimated from the size parameters used. In order to get an estimate of the tree height, when the information is missing, a regression function from an area with similar climate and similar forest types is necessary. These size parameters to tree height functions can be pre-calculated in a database or curve fitted prior to a large scale experiment. In this study the single tree detection method samples the tree height directly but the field survey only samples the *DBH*. The field tree heights were estimated by a hyperbolic tangent function:

$$H = C * \tanh(p * DBH) \quad (2)$$

where *C* is the tree height amplitude parameter and *p* is the tree height phase parameter. *C* and *p* were estimated by a non linear regression of data from forest areas similar to the one used in the experiment.

For every field surveyed tree the algorithm calculates the radial ground distance, *r*, and the normalized Euclidian distance of the tree tops, *d'*:

$$d' = \sqrt{\left(\frac{r}{\sigma_r}\right)^2 + \left(\frac{H_{aerial} - H_{field}}{\sigma_h}\right)^2} \quad (3)$$

where *H_{aerial}* is the height of the aerial detected tree, *H_{field}* is the height of the field surveyed tree, *σ_r* is the estimated radial error and *σ_h* is the estimated height error, figure 3. To limit the size of the calculation only aerial detected trees close to field trees are used. The largest distance to accept an aerial tree is defined as:

$$r_{Accept} = b + f * DBH \quad (4)$$

where the parameters *b* and *f* should be set to include a reasonable number of trees. All aerial trees inside this radius are added to a list of tree links. To get an indication of how good a link is, a weight based on the normalized Euclidian distance of the tree tops is set to every tree link:

$$w = \frac{1}{(d' + 1)^2} \quad (5)$$

The weight is higher the closer the linked trees are; a zero tree top distance gives a weight of one.

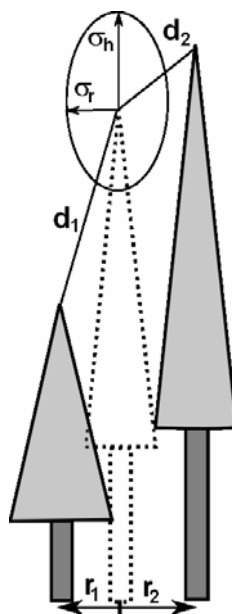


Figure 3: Two field plot trees (gray) with possible links to an aerial detected tree (dotted lines) with position and height errors. The tree top distances d_1 and d_2 , the radial distances r_1 and r_2 , the height error standard deviation σ_h and the radial error standard deviation σ_r , are used by the linking algorithm to determine which tree to choose.

In the tree link list the algorithm then searches for connected tree clusters, *i.e.* a group of field surveyed and aerial detected trees that are linked together. Each link only contains one field surveyed tree and one aerial detected tree, but since each field tree can be linked to several aerial trees and each aerial detected tree can be linked to several field trees, a network of connections can become a cluster of trees – a tree list graph.

Since every field surveyed tree should only be connected to one aerial detected tree, multiple links must be removed from the list. The algorithm solves this by trying every possible combination of links in a tree cluster. Combinations with multiple links are discarded. The link combination with the highest sum of weights is the solution that is chosen for each tree cluster. All other links are removed from the list. This brute force method can be time consuming if the tree clusters are large and therefore the problem was minimized by only trying aerial detected trees standing close to a field surveyed tree.

2.5 Simulations

To get an estimate of how well the method works, the matching and linking algorithm were applied to 1125 simulated field plots.

2.5.1 Generating simulated trees

In order to have a realistic virtual tree lists, distribution generating functions were curve fitted from the field data. The relative frequency distributions of the *DBH* were modelled by two-parameter Weibull functions, $f(DBH; k, \lambda)$, for the three dominating species: pine, spruce and birch; equation 6.

$$f(DBH; k, \lambda) = \frac{k}{\lambda} \left(\frac{DBH}{\lambda} \right)^{k-1} e^{-(DBH/\lambda)^k} \quad (6)$$

The simulated field tree *DBH* to height curves were modelled as hyperbolic tangent functions, equation 2, with added residuals calculated from a Gaussian distribution with standard deviations also modelled as hyperbolic tangent functions, equation 7,

$$\sigma_H = C_{residual} \cdot \tanh(p_{Residual} \cdot DBH) \quad (7)$$

where σ_H is the simulated field tree height standard deviation, *DBH* is the field surveyed stem diameter at breast height, $C_{residual}$ is the tree height residual amplitude parameter and $p_{Residual}$ is the tree height residual phase parameter. The settings for the distribution generating functions are shown in table 1.

Table 1: Simulation settings for the different tree species: the scale and shape parameter for equations 6, the C and p parameters for equation 2 and the $C_{residual}$ and $p_{Residual}$ parameters for equation 7.

| | Pine | Spruce | Birch |
|-------------------|--------|--------|--------|
| k, scale | 286.0 | 252.0 | 206.0 |
| λ , shape | 2.69 | 2.46 | 2.77 |
| C | 24.0 | 28.0 | 22.0 |
| P | 0.0042 | 0.0035 | 0.0075 |
| $C_{Residual}$ | 3 | 2.7 | 1.8 |
| $p_{Residual}$ | 0.01 | 0.01 | 0.01 |

Since the field surveyed data had an approximate ratio of 45 % pine, 45 % spruce and 10 % birch this setting was chosen for the simulation. When generating a tree, the function first chooses a species. Then a *DBH* is generated from equation 6 with parameters corresponding to the chosen species. Finally the tree height is calculated from equation 2; with a residual calculated from equation 7.

2.5.2 Simulation of field plot and aerial single tree data

To create a field plot, the algorithm was used to add trees, until the correct number of trees per hectare (*SPH*) was achieved. The stem diameter at breast height was saved as field data and the tree height was saved as aerial data. The position was saved in both the aerial and the field data. To simulate position errors the coordinates of the aerial data was translated in a random direction in the ground plane, with a radial magnitude generated by a Gaussian distribution. If the tree crowns (modelled as ellipsoids of revolution) of two specimens were intertwined (had a cross section radius overlap of more than 30 % of the distance between the trees) the algorithm discarded the solution and tried a new tree. If the tree had a *DBH* < 50 mm it was discarded since the field plot sampling had 50 mm as a lower size limit. To get the correct number of omissions, some of the trees were not saved in the aerial data, and to get the correct number of commissions some trees were added only to the aerial data. To get a larger search area, trees outside of the field plot were added to the aerial data. Each tree in the field data and aerial data had a label to make it possible to identify a correct link. The simulation was run with three different numbers of stems per hectare (*SPH*), 300, 600 and 900; with five different position error standard deviations, 0, 0.5, 1, 1.5 and 2.0; and with three combinations of commission and omission errors, 0/0, 10/10 and 20/20 %. For each setting 25 plots were tested giving a total of 1125 plots in the simulation. The field plot radius was set to 10 m for all plots.

2.5.3 Configuration of the software

In order not to use the same field plot data for both the simulation and for the *DBH*-height estimate in the field plot matching software, forest data from other areas in the same climate zone was used to calibrate the algorithm. The parameters *C* and *p* in table 2 was estimated this

way. The other parameters were set to values estimated to be feasible in an inventory of a real forest.

Table 2: The settings of the configuration file for the software. A = size of search area, $\Delta\theta$ = field plot rotation angle increment, min/max θ = field plot rotation end values, b = tree position search bias, eq 4, f = tree position search factor, eq 4. C = tree height estimation amplitude parameter eq 2, p = tree height estimation phase parameter, eq 2. σ_h = height residual error, σ_r = ground distance radial error. mpp = correlation image resolution.

| A | $\Delta\theta$ | min / max θ | b | f | C | p | σ_r | σ_h | mpp |
|-------------------|----------------|-----------------------|-----|----------|------|--------|------------|------------|-----------|
| [m ²] | [°] | [°] | [m] | [m]/[mm] | [m] | 1/[mm] | [m] | [m] | [m]/pixel |
| 3600 | 2 | ±16 | 1.5 | 0.002 | 25.5 | 0.0036 | 1.0 | 3.0 | 0.5 |

2.6 Empirical tests

To support the simulation study a small empirical test was performed. In this test the trees did not have labels as in the simulation study so the number of correct links were not possible to achieve but it was possible to see if the method had a high connection rate. That is, if it managed to connect all the trees in the plot. This would be difficult if the tree position patterns differed too much between the field plot and the aerial data. It was also possible to see if the rectified field plot coordinate systems had a large bias and a large compass error. Since the field plot centres were measured using a Global Navigation Satellite System (GNSS) the expected bias and compass error was small. However if the found plot is not the correct one, any compass direction and bias within the search space is equally possible. Therefore small bias and compass errors indicate that the true field plots have been located.

The field plot matching algorithm was applied to the material both for original field data coordinates and for data where the coordinates of each tree had been deliberately displaced 60 m, in order to have two datasets: one set containing field plots and one set not containing any field plots. The proportion of connected trees for each aerial detected tree within the plot and the average bias of the field plots were calculated for different search area sizes and field plot rotation.

3. Results

3.1 Simulation results

Results from the simulation show that the method has a high connection rate if the position radial error standard deviations are 1 [m] or smaller, figure 6. Even with as high omission and commission errors as 20 % the method still links more than 70 % of the trees correctly. When the position errors increase, the connection rate decreases, especially for dense forests and a single tree detection method with large omission and commission errors.

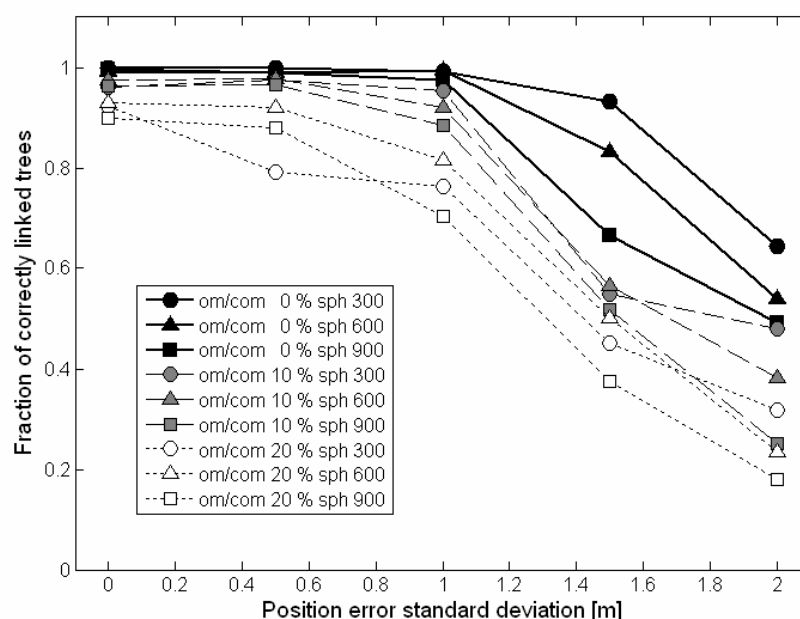


Figure 4: Simulation of the expected amount of correct links between field trees and aerial detected single trees for 300, 600 and 900 stems per hectare, 0, 10 and 20 % omission and commission errors, and 0.0, 0.5, 1.0, 1.5 and 2.0 [m] radial position error standard deviations.

3.2 Results empirical test

Table 3 shows the results of the empirical tests for different search area sizes and field plot rotation, both for search areas containing field plots and for search areas without field plots.

Table 3: The results for the empirical test of the automatic tree linking algorithm

| | Search areas with field plots | Search areas without field plots | Search areas with field plots | Search areas without field plots | Search areas with field plots | Search areas without field plots |
|--|-------------------------------|----------------------------------|-------------------------------|----------------------------------|-------------------------------|----------------------------------|
| Search area [m ²] | 1600 | 1600 | 3600 | 3600 | 10000 | 10000 |
| Min/max compass search angles [deg] | ±8 | ±8 | ±16 | ±16 | ±16 | ±16 |
| Proportion of connected aerial trees | 92.9% | 76.9% | 93.1% | 79.5% | 93.5% | 84.5% |
| Average field plot radial bias displacement [m] | 1.68 | 7.94 | 3.06 | 15.81 | 5.42 | 31.83 |
| Average compass angular displacement [deg] (absolute values) | 2.23 | 5.56 | 2.95 | 9.14 | 3.24 | 7.96 |

Table 3 shows that the search areas with field plots have a higher connection rate than the search areas without field plots. That is they connect more trees even though they are not necessarily the correct ones as indicated in the simulation study. In the case with the search areas without

field plots of course none of the tree links are correct. The radial displacements and the compass shifts are also fairly small and constant for the search areas containing field plots whereas for the search areas without field plots the displacements increase with increasing search area, indicating that the algorithm manages to find a field plot if it is present in the search space.

4. Discussion and conclusions

A new method for automatically linking of field-surveyed and aerial-detected individual trees was implemented and tested by using simulations and an empirical field data set with high accuracy GPS measurements. The method could be used for any remote sensing method that produces a map with tree positions and relative tree sizes. The simulation results show that a high proportion of correctly linked trees can be obtained if the chosen single tree detection method has a small tree position random error (≤ 1 m standard deviation) and less than 20 % commission and omission errors. With a higher random error of the tree positions the performance of the method will become more affected by a greater omission and commission error. The empirical results also indicate that the algorithm manages to find and connect trees in a field plot if it is present in the search space.

Acknowledgements

The research of this study was founded by Formas (www.formas.se). The field data and airborne laser scanner data was financed by the Swedish Forest Agency.

References

- Gonzalez, R. C. and Wintz, P., 1987. Digital Image Processing. Second edition. Addison-Wesley Publishing Company. ISBN 0-201-11026-1. correlation coefficient: equation (8.4-4), pp. 426.
- Gougeon, F. A. 1995. A crown-following approach to the automatic delineation of individual tree crowns in high spatial resolution aerial images. *Canadian Journal of Forest Research*, 21, 274-284.
- Holmgren, J. and Wallerman, J., 2006. Estimation of tree size distribution by combining vertical and horizontal distribution of LIDAR measurements with extraction of individual trees. In: T. Koukal and W. Schneider (Eds.). Proceedings from Workshop on 3D Remote Sensing in Forestry, Vienna, Austria, 14-15 February 2006, pp. 168-173. University of Natural Resources and Applied Life Science, Vienna, Austria.
- Hyypä, J., Kelle, O., Lehikoinen, M. and Inkinen, M., 2001. A segmentation-based method to retrieve stem volume estimates from 3-D tree height models produced by laser scanners. *IEEE Transactions on Geoscience and Remote Sensing*, 39, 969-975.
- Korpela, I. 2004. Individual Tree Measurements by Means of Digital Aerial Photogrammetry. (Doctoral dissertation. The Finnish Society of Forest Science, The Finnish Forest Research Institute). SILVA FENNICA Monographs 3-2004.
- Means, J. E., Acker, S. A., Brandon, J. F., Renslow, M., Emerson, L. and Hendrix, C. J., 2000. Predicting forest stand characteristics with airborne scanning lidar. *Photogram. Eng. Remote Sensing*, 66, 1367-1371.
- Næsset, E., 2002. Predicting forest stand characteristics with airborne scanning laser using a practical two-stage procedure and field data. *Remote Sens. Environ.*, 80, 88-99.
- Næsset, E. and Jonmeister, T., 2002. Assessing point accuracy of DGPS under forest canopy before data acquisition, in the field, and after processing. *Scandinavian Journal of Forest Research*, 17:4, 351-358.
- Persson, Å., Holmgren, J. and Söderman, U., 2002. Detecting and measuring individual trees using an airborne laser scanner. *Photogram. Eng. Remote Sensing*, 68, 925-932.

- Pinz, A., 1989. Final results of the vision expert system VES: finding trees in aerial photographs, in *Wissensbasierte Masterkennung. (Knowledge-based pattern recognition.) OCG - Schriftenreihe* 49, pp 90-111. Oldensbourg Verlag.
- Pollock, R. J. 1996. The automatic recognition of individual trees in aerial images of forests based on a synthetic tree crown image model. Unpublished doctoral dissertation. The University of British Columbia, Vancouver, B. C.
- Solberg, S., Næsset, E. and Bollandsås, O. M., 2006. Single tree segmentation using airborne laser scanner data in a heterogeneous spruce forest. *Photogram. Eng. Remote Sensing*, 72, 1369-1378.

Performance of airborne laser scanning- and aerial photograph-based statistical and textural features in forest variable estimation

Markus Holopainen¹, Reija Haapanen², Sakari Tuominen³ & Risto Viitala⁴

¹University of Helsinki, Department of Forest Resource Management,
markus.holopainen@helsinki.fi

²Haapanen Forest Consulting reija.haapanen@haapanenforestconsulting.fi

³Finnish Forest Research Institute sakari.tuominen@metla.fi

⁴HAMK University of Applied Sciences risto.viitala@hamk.fi

Abstract

In the present study we tested the performance of different combinations of airborne laser scanning (ALS) and aerial photograph-based features in the estimation of forest variables. The combinations were subsets of a total of 172 features extracted from the remotely sensed material. The subsets were based on expert judgment or a genetic algorithm (GA). The non-parametric k -nearest neighbour (k -NN) algorithm was applied to derive the estimates. The best performing feature set was obtained after four consecutive steps of GA, each starting with the best features found in the previous step. The best set contained 11 features, 8 of them originating from the ALS data. This set was further weighted with a downhill simplex algorithm, and a relative mean volume RMSE of 27.1% was obtained. The results were slightly worse than in other Finnish ALS studies, most probably due to a larger amount of deciduous trees and greater variation of forests in the study area.

Keywords: k-NN, feature selection, genetic algorithm, species-specific estimates

1. Introduction

The main approaches to deriving forest information from small-footprint airborne laser scanning (ALS) data are plot-level estimation based on features derived from height information (e.g., Næsset 1997, Suvanto *et al.* 2005) and individual tree detection (e.g., Hyypä and Inkinen 1999, Maltamo *et al.* 2004). The latter method is computationally heavier and requires greater pulse density; thus in large-area inventories the plot-level approach can, at least currently be considered more cost-efficient.

Estimation accuracies can typically be improved with a combination of data sources with complementary properties. Examples are datasets comprising of Landsat-type satellite images with good spectral resolution, and colour-infrared aerial photographs (Haapanen and Tuominen 2008) or even black-and-white photographs, with good spatial resolution (Tuominen and Haakana 2005).

High spatial resolution, a property of e.g., aerial photographs and ALS data, allows the use of two-dimensional (2D) textural features - even three-dimensional (3D) in the latter case. Generally, adding more features in the estimation process improves the output accuracy, but with increasing dimensionality the distinctive capacity of the data may weaken, with increasing noise. Therefore, the dimensionality of large datasets must be reduced. The usefulness of any input variable can be studied by measuring the correlation between the image features and forest attributes. In cases of large feature sets this is extremely tedious. Furthermore, the image features are often highly correlated, and adding additional variables having high correlation with the other variables does not generally improve the estimation accuracy (although it is still

possible). Guyon and Elisseef (2003) showed that even a useless variable may be useful when taken with others, and two useless variables can be useful together. Thus, filters that rank features based on correlation coefficients are not sufficient and subset selection algorithms or feature transformation is needed. Principal component analysis is one example of feature transformation, while e.g., stepwise regression (backward or forward selection) or genetic algorithms (GAs) can be used to construct subsets of features. GAs are search algorithms that mimic natural selection and natural genetics (Goldberg 1989). Kudo and Sklansky (2000) compared several feature selection algorithms and concluded that sequential floating search methods worked best for small- and medium-scale problems, whereas for problems with a large number of dimensions (>50), the GAs worked best.

In model construction, it is important to base the feature selection on the researcher's knowledge of the phenomenon and the variables affecting it; thus the use of stepwise selection methods is generally discouraged. However, there are situations in which the superiority of variables A and B over C and D is not clear. In remote sensing (RS), the relationships of recorded radiation or returned laser pulses and forest variables are not too straightforward (the exception being the canopy surface generated from laser height readings) and there are numerous potentially useful statistical/textural variables that can be extracted from the data. Therefore, the use of automated selection methods is justified to a certain extent.

In the present study, we examined the predictive capacity of several feature sets extracted from aerial photographs and low-pulse ALS data. While it is known, that the laser-based features perform far better than the aerial photograph-based features when estimating mean height, mean volume, etc., a combination is better when detecting tree species (Maltamo *et al.* 2006; Packalén and Maltamo 2006, 2007). One of the tested feature sets was based on automatic selection with GAs, others on expert knowledge. The estimation was carried out with the nonparametric *k*-nearest neighbour (*k*-NN) algorithm and we operated at the field plot level. The forest variables estimated included the mean volume of growing stock (m³/ha), basal area (m²/ha), height (m), diameter at breast height (DBH; cm), and the volumes of Scots pine (*Pinus sylvestris* L.), Norway spruce (*Picea abies* H. Karst.), and deciduous trees (m³/ha).

2. Material and methods

2.1 Study area and field measurements

The study area is located in Evo, Finland (61.19°N, 25.11°E) and it consists of approximately 2000 ha of managed boreal forest. The average stand size in the area was slightly less than 1 ha. Field measurement data from 282 fixed-radius (9.77 m) field plots were collected from the study area in summer 2007. The sampling of the field plots was based on prestratification of existing stand inventory data. There was a 1-year gap between the acquisition of RS data (see section 2.2) and field data measurements; only plots that had remained untreated during the year were measured and the latest growth in height was subtracted. The plots were located with Trimble's GEOXM 2005 Global Positioning System (GPS) device (Trimble Navigation Ltd., Sunnyvale, CA, USA), and the locations were postprocessed with local base station data, resulting in an average error of app. 0.6 m. The following variables were measured of trees having a DBH of over 5 cm: location, tree species, crown class, DBH, height, lower limit of living crown and crown width. The volumes were calculated with standard Finnish models. Plot-level data were obtained by summing the tree data. The values of forest attributes of plots located in clear-cut areas or treeless mires were set at zero. The basic characteristics of the field data are presented in Table 1. Of the mean volume, 40% was Scots pine, 35% Norway spruce and 24% deciduous trees, mainly birch (*Betula* L.).

Table 1. Characteristics of the field plots.

| | Mean | Min | Max | Std |
|---|-------|-----|-------|-------|
| Basal area-weighted mean height, m | 17.0 | 0 | 30.5 | 6.7 |
| Basal area-weighted mean DBH, cm | 21.1 | 0 | 50.3 | 9.4 |
| Basal area, m ² /ha | 19.9 | 0 | 45.5 | 10.3 |
| Mean volume of growing stock, m ³ /ha | 179.0 | 0 | 575.4 | 115.4 |
| Mean volume of pine, m ³ /ha | 69.9 | 0 | 560.6 | 89.8 |
| Mean volume of spruce, m ³ /ha | 63.5 | 0 | 575.4 | 94.8 |
| Mean volume of deciduous trees, m ³ /ha | 42.9 | 0 | 302.2 | 51.2 |
| Mean volume of other tree species, m ³ /ha | 2.7 | 0 | 210.1 | 19.0 |

2.2 Remote sensing material

The ALS data were acquired in midsummer 2006. The flying altitude was 1900 m. The density of the returned pulses within the field plots was 1.8/m² (only, first, intermediate or last; 1.3/m² if only or first pulses were considered). A digital elevation model (DEM) and consequently, heights above ground level, were computed by the data provider. Same-date aerial photographs were obtained with a digital camera, as well. The photographs were orthorectified, resampled to a pixel size of 0.5 m and mosaiced to a single image covering the entire area. Only near-infrared (NIR), red (R) and green (G) bands were available.

Several statistical and textural features were extracted from the RS material. The extraction window was generally 20 x 20 m, which was proved suitable in earlier studies (e.g. Holopainen and Wang 1998). The features included means and standard deviations of spectral values and ALS height and intensity, Haralick textural features (Haralick *et al.* 1973; Haralick 1979) derived from spectral values, ALS height and intensity, and 'standard texture' referring to a set of averages and standard deviations of spectral values, ALS height and intensity calculated within a 32 x 32 pixel window. In the case of ALS, these were derived from the first pulse data only. The Haralick textural features were computed from 4 directions: 0, 45, 90 and 135°. Additionally, the height statistics for the first and last pulses (F, L) were calculated as in Suvanto *et al.* (2005): mean and maximum height (hmea, hmax), standard deviation and coefficient of variation of height (hstd, hcv), heights where certain relative amounts of laser points had accumulated (p05-p95), as well as percentages of laser points accumulated at various relative heights (r05-r95). Only pulses exceeding a 2 m height limit were included in order to remove hits to ground vegetation and bushes. Finally, percentages of points under 2 m in height were added (Fvege, Lvege; in Suvanto *et al.* 2005 the opposite, percentages of points over 2 m in height, was used). Means and standard deviations of ALS height were included only once in the final dataset, where the total number of features was 172. All features were standardized to a mean of 0 and std of 1.

2.3 Methods

2.3.1 Estimation algorithm

The estimation method was *k*-NN, which has long been used in Finnish RS-aided forest inventory applications (e.g. Kilkki and Päivinen 1987; Muinonen and Tokola 1990; Tomppo 1991). The nearest neighbours were determined by calculating the Euclidean distances between the observations in the *n*-dimensional feature space. The nearest plots were weighted with inverse squared distances. The number of nearest neighbours was set at 5. Leave-one-out cross-validation

was applied to calculate the results within the field dataset. The accuracy of the estimates was assessed by calculating the root-mean squared error (RMSE) of the studied variables.

2.3.2 Feature selection

Nine feature sets were created for tests:

- A: all aerial photograph features (72)
- B: all laser features (100)
- A + B (172)
- C: aerial photograph spectral features from three bands + their std's (6)
- D: ALS hmea, hmax, hstd, hcv, and vege of first and last pulse separately (10)
- C + D (16)
- E: D + local homogeneity of ALS height of first pulse (four directions) (14)
- F: D + ALS intensity and its std of first pulse (12)
- GA1-GA4: features selected by a genetic algorithm, starting from set A+B (all 172 features). From each step, the best features were fed to next step, e.g., from GA1 to GA2.

Feature sets A, B and A+B were created for benchmarking the results. Sets C, D and C+D were small feature sets containing simple statistics such as averages and variations. Set E was constructed of central laser height features and one height-based Haralick texture, local homogeneity, which performed well in an earlier study by Tuominen and Pekkarinen (2005), when derived from aerial photograph features. At this point in our project, the intensity values were not calibrated in any way, and thus little was expected from them. However, we created a subset containing two ALS intensity-based features, as well (F).

Automatic feature selection was carried out using a simple GA presented by Goldberg (1989), implemented in the GAlib C++ library (Wall 1996). It performed well in an earlier feature selection study by Haapanen and Tuominen (2008). The GA process starts by generating an initial population of strings (chromosomes or genomes), which consist of separate features (genes). The strings evolve during a user-defined number of iterations (generations). The evolution includes the following operations: selecting strings for mating using a user-defined objective criterion (the better the more copies in the mating pool), letting the strings in the mating pool to swap parts (crossing over), causing random noise (mutations) in the offspring (children), and passing the resulting strings into the next generation.

In the present study, the starting population consisted of 300 random feature combinations (genomes). The length of the genomes corresponded to the total number of features in each step, and the genomes contained a 0 or 1 at position i , denoting the absence or presence of image feature i . The number of generations was 30. The objective variable was a weighted combination of relative RMSEs of total volume, volume of pine, volume of spruce, volume of deciduous trees, diameter and height, with total volume having a weight of 50%, and the remaining variables 10% each. Genomes that were selected for mating swapped parts with each other with a probability of 60%, producing children. Occasional mutations (flipping 0 to 1 or vice versa) were added to the children (probability 1%). The strings were then passed to the next generation. The overall best genome of the current iteration was always passed to the next generation, as well. Four successive steps (all including 30 generations) were taken to reduce the number of features to a reasonable minimum (GA1-GA4). Only features belonging to the best genome in each step were included in the next step. The parameters used were selected via some explorative tests.

Even after careful selection, the features are not equally important in describing the forest attributes and should be weighted. Here we searched for optimal weights for the best subset of features by a downhill simplex method (Nelder and Mead 1965). In the search, the objective was to minimize the RMSE of the mean volume estimates.

3. Results

Estimation errors (RMSE%) obtained using the studied datasets are presented in Table 2 for mean total volume, mean height, basal area, mean DBH and species-specific mean volumes. The results are as follows:

- The ALS-based features (sets B, D, E, F) performed far better than aerial photograph-based features (sets A and C).
- Simply adding aerial photograph features into laser feature sets (A+B, C+D) gave worse results than the laser sets in question (B, D), except in the case of species-specific volumes.
- No expert judgment-based selection was able to surpass the set of all extracted laser features (B), when all variables were considered.
- However, even the first round of the GA produced lower RMSEs for most of the variables compared with full laser feature set B, by combining ALS- and aerial photograph-based features in a successful way.
- When all variables were considered, the most usable results were already obtained in step 3 of the GA process (GA3) with 19 features. Therefore, both GA3 and GA4 were weighted.
- After feature weighting, GA4 produced the lowest RMSEs and the weighted set of 11 features represents our final result. Both ALS and aerial photograph-based features were included. A test was also run without the aerial photograph features, but the accuracies then again lowered.

The 11 features selected into the final set were Fvege, Hvege, Fp30, Lp30, Fp90, mean height in the 32 x 32 pixel window, angular second moment 45° of intensity, local homogeneity 90° of height, average NIR, std of NIR of 64 blocks within the 32 x 32 pixel window, and std of G of 1024 blocks within the 32 x 32 pixel window.

Table 2: *K*-NN estimation results obtained with tested datasets. The feature set giving the best results (GA4 weighted) is in bold face.

| Dataset | Bands | RMSE, % | | | | | | |
|---------------------|-----------|-------------|-------------|-------------|-------------|-------------|---------------|------------------|
| | | Mean height | BA | Mean DBH | Mean volume | Pine volume | Spruce volume | Deciduous volume |
| A | 72 | 30.9 | 44.4 | 35.5 | 57.2 | 111.2 | 120.8 | 104.0 |
| B | 100 | 17.9 | 28.1 | 23.6 | 32.2 | 88.5 | 106.9 | 89.2 |
| A+B | 172 | 20.0 | 30.5 | 26.1 | 34.7 | 87.4 | 93.2 | 83.0 |
| C | 6 | 33.6 | 44.2 | 39.1 | 57.1 | 106.7 | 124.3 | 95.3 |
| D | 10 | 19.1 | 26.7 | 25.2 | 32.7 | 96.0 | 97.9 | 92.7 |
| C+D | 16 | 19.5 | 30.1 | 25.2 | 35.1 | 89.3 | 91.5 | 80.8 |
| E | 14 | 18.7 | 26.1 | 24.4 | 31.6 | 92.2 | 97.0 | 90.2 |
| F | 12 | 19.6 | 26.8 | 25.4 | 32.4 | 95.0 | 98.2 | 94.0 |
| GA1 | 85 | 19.6 | 27.6 | 25.8 | 31.6 | 82.9 | 90.0 | 78.5 |
| GA2 | 41 | 18.3 | 26.1 | 24.8 | 29.0 | 85.5 | 89.1 | 79.6 |
| GA3 | 19 | 17.2 | 23.9 | 23.0 | 27.9 | 81.8 | 86.5 | 81.0 |
| GA3 weighted | 19 | 17.2 | 23.3 | 23.2 | 27.1 | 82.1 | 84.2 | 83.2 |
| GA4 | 11 | 17.5 | 24.2 | 24.5 | 28.4 | 82.1 | 84.4 | 79.2 |
| GA4 weighted | 11 | 16.9 | 23.2 | 23.8 | 27.1 | 81.4 | 84.6 | 79.6 |

4. Discussion

In the present study, we tested the estimation of the most important forest attributes with a combination of ALS and aerial photograph data, using feature selection and the nonparametric k -NN algorithm. Based on our results, the lowest RMSEs, all variables considered, were obtained with a relatively small subset of the original features, comprising of both ALS and aerial photograph-based features. It was found via a GA-based feature selection process. Further weighting of the features was able to slightly lower the RMSEs of most of the variables. Our final RMSE for the mean volume was 27.1% of the mean. In comparison to results obtained using purely aerial photograph-based features, the drop in RMSE% was app. 30 percentage points and in comparison to other ALS-based results, 5-6 percentage points. The poor performance of aerial photograph-based features was in line with earlier studies (e.g. Haapanen and Tuominen 2008). The low spectral and radiometric resolution of these optical area data cannot distinguish forest characteristics: the grey values saturate at relatively low forest volumes (approx. 250 m³/ha in this study). Even when complemented with textural features, the RMSEs tend to be only slightly lower than with Landsat-type satellite images, which in turn produce field plot level RMSEs of 60% or greater (Haapanen and Tuominen 2008). Naturally, this applies only to large-scale forest inventories based on two-phase sampling, and the situation in applications based on single tree detection is different.

Aerial photograph-based features lowered the estimation accuracies of general forest variables in sets A+B and C+D, which were constructed in a straightforward way. However, the species-specific accuracies were improved, compared with laser-based (or aerial photograph-based features). After the feature selection and weighting, all variables were more accurately estimated with a combination of laser and aerial photograph-based features, than with solely laser-based features. This implies that some aerial photograph-based features can improve the estimation of general forest parameters, as well.

Our results were poorer than the plot-level ALS results in a study area in eastern Finland presented by Suvanto *et al.* (2005), obtained by regression functions, or by Packalén and Maltamo (2007), obtained with a k -most similar neighbour (k -MSN) method using ALS features and aerial photographs. Our study area had greater variation in forest parameters and a larger proportion of deciduous trees, both being properties that reduce the estimation accuracy (Næsset 2004a; Maltamo *et al.* 2004). In comparison to the results in a study area in southern Finland (Maltamo *et al.* 2004), where the amount of deciduous trees is larger and understories denser than in eastern Finland, the relative mean volume RMSEs were similar (25% vs. our 27%). However, Maltamo *et al.* (2004) were able to reduce the relative mean volume RMSE to 16% by predicting the small trees separately.

To improve the estimation in forest areas with deciduous stands, stratification by cover types (Næsset 2004a) was suggested and later implemented based on aerial photograph-aided prestratification (Næsset 2004b). Aerial photographs were also integrated into the estimation process (Maltamo *et al.* 2006; Packalén and Maltamo 2006, 2007). Our approach resembled those of the latter studies: we fed the aerial photograph features together with the ALS features into a feature selection process. The feature selection criterion was tailored to take the tree species-specific volumes into account.

The large amount of deciduous trees is again seen in the estimation accuracies of the tree-species specific volumes: our accuracies for pine and spruce were lower, but for deciduous trees higher than in the studies by Packalén and Maltamo (2006, 2007). Packalén and Maltamo (2007) obtained RMSEs of 20.5%, 51.2%, 55.7% and 102.8% for mean total volume and mean volumes of pine, spruce and deciduous trees, respectively. Clear-cut areas or small seedling stands were excluded (minimum volume was 54 m³/ha). When we removed volumes under 50 m³/ha, our corresponding results were 25.6%, 75.7%, 77.9% and 74.7%, respectively. Weighting

had no effect on these results.

Regression, in which each variable is separately modelled, produces more accurate variable-specific results than k -NN. However, k -NN and its special case k -MSN (based on canonical correlations and Mahalanobis distance; Moeur and Stage 1995) have the property of predicting all required variables simultaneously, preserving the concordance between variables. The k -MSN method is probably able to perform better than the k -NN method.

We did not perform extensive sets of GA runs with varying parameters and repetitions in this study. Since the k -NN is sensitive to a large number of features, which is the case at the upper levels of GA runs, our next step will be to test the feature selection separately within both datasets. Better feature sets can probably be found by continuing these efforts. However, our results were promising, and the features selected are a logical mixture of ALS and aerial photograph-based features. Of these features, Fvege and Lvege appeared in all but one of the regression models by Suvanto *et al.* (2005), as well: mean volume, basal area, stem number and mean diameter (it was not needed in the height model). Various height statistic features were selected in both studies. Three aerial photograph features were selected for our final set: mean of NIR values and two standard texture features based on NIR and G. The presence of NIR is logical, since it helps to separate deciduous trees from conifers. The mean of R could also have entered into the final dataset, but the proportion of ALS hits of under 2 m in height (Fvege, Lvege) apparently described the amount of vegetation biomass better than the R band.

Our study provides ALS data-based accuracy estimates from a relatively heterogeneous area in southern Finland. In conclusion, we can say that the accuracies were in line with other Finnish studies operating on low pulse density data (Suvanto *et al.* 2004; Maltamo *et al.* 2006; Packalén and Maltamo 2007), but slightly poorer. In our data, the proportion of deciduous trees was considerable, and forests of all development classes were included, as well as both mineral soil and mire sites. This method is suitable for large area forest inventories, since it works with low pulse density and is simple. The feature selection algorithm tested (GA) worked well, outperforming the selections made by the researchers. However, stepwise regression could have performed as well (Haapanen and Tuominen 2008). The ALS data were superior to aerial photograph data (which in turn are slightly better than Landsat-type satellite image data; Haapanen and Tuominen 2008). However, some aerial photograph features were selected to the best performing feature set. More elaborate processing of intensity data (calibration) or higher pulse density of ALS data may eliminate the need for aerial photographs. Bearing in mind the further use of the resulting estimates, the species-specific estimates are a disappointment. If the estimates are to be used as input data in decision-making, or when simulating forest development, far more accurate estimates are needed. However, these figures concern the plot level only, and stand level estimates have typically been better, and similar or even more accurate than those obtained by field inventory of forest stands (Packalén and Maltamo 2007).

Acknowledgements

This study was made possible by financial aid from the Finnish Academy. HAMK University of Applied Sciences provided the ALS and field measurement data.

References

- Goldberg, D.E., 1989. Genetic algorithms in search, optimization, and machine learning. Addison-Wesley Publishing Company, Reading, Massachusetts, 412 p.
- Guyon, I., and Elisseeff, A., 2003. An introduction to variable and feature selection. *Journal of Machine Learning Research*, 3, 1157-1182.

- Haapanen, R. and Tuominen, S., 2008. Data combination and feature selection for multi source forest inventory. *PE&RS* 74(7), 869-880.
- Haralick, R. M., Shanmugan, K., and Dinstein, I., 1973. Textural features for image classification. *IEEE Transactions on Systems, Man and Cybernetics*, 3(6), 610-621.
- Haralick, R., 1979. Statistical and structural approaches to texture. *Proceedings of the IEEE*, 67(5), 786-804.
- Holopainen, M. and Wang, G., 1998. The calibration of digitized aerial photographs for forest stratification. *International Journal of Remote Sensing*, 19, 677-696.
- Kilkki, P., and Päivinen, R. 1987. Reference sample plots to combine field measurements and satellite data in forest inventory. *Department of Forest Mensuration and Management, University of Helsinki. Research notes*, 19, 210-215.
- Kudo, M. and Sklansky, J., 2000. Comparison of algorithms that select features for pattern classifiers. *Pattern Recognition*, 33, 25-41.
- Muinen, E., and Tokola, T., 1990: An application of remote sensing for communal forest inventory. *Proceedings from SNS/IUFRO workshop: The usability of remote sensing for forest inventory and planning, 26-28 February 1990, Umeå, Sweden. Remote Sensing Laboratory, Swedish University of Agricultural Sciences, Report 4*, 35-42.
- Maltamo, M., Eerikäinen, K., Pitkänen, J., Hyyppä, J. and Vehmas, M., 2004. Estimation of timber volume and stem density based on scanning laser altimetry and expected tree size distribution functions. *Remote Sensing of Environment*, 90, 319–330.
- Maltamo, M., Malinen, J., Packalén, P., Suvanto, A. and Kangas, J., 2006. Non-parametric estimation of stem volume using laser scanning, aerial photography and stand register data. *Canadian Journal of Forest Research*, 36, 426-436.
- Moeur, M., and Stage, A.R., 1995. Most similar neighbor: an improved sampling inference procedure for natural resource planning. *Forest Science*, 41, 337–359.
- Næsset, E., 1997. Estimating timber volume of forest stands using airborne laser scanner data. *Remote Sensing of Environment*, 51, 246-253.
- Næsset, E., 2004a. Practical large-scale forest stand inventory using a small footprint airborne scanning laser. *Scandinavian Journal of Forest Research*, 19, 164-179.
- Næsset, E., 2004b. Accuracy of forest inventory using airborne laser-scanning: Evaluating the first Nordic full-scale operational project. *Scandinavian Journal of Forest Research*, 19, 554-557.
- Nelder, J.A., and Mead, R., 1965. A simplex method for function minimization. *Computer Journal*, 7, 391-98.
- Packalén, P. and Maltamo, M., 2006. Predicting the plot volume by tree species using airborne laser scanning and aerial photographs. *Forest Science*, 56, 611-622.
- Packalén, P. and Maltamo, M., 2007. The k-MSN method in the prediction of species specific stand attributes using airborne laser scanning and aerial photographs. *Remote Sensing of Environment*, 109, 328-341.
- Suvanto, A., Maltamo, M., Packalén, P. and Kangas, J., 2005. Kuviokohtaisten puustotunnusten ennustaminen laserkeilauksella. *Metsätieteen aikakauskirja*, 4/2005, 413-428.
- Tomppo, E., 1991. Satellite image-based national forest inventory of Finland. *International Archives of Photogrammetry and Remote Sensing*, 28, pp. 419-424.
- Tuominen, S., and Haakana, M., 2005. Landsat TM imagery and high altitude aerial photographs in estimation of forest characteristics. *Silva Fennica*, 39(4), 573-584.
- Tuominen, S., and Pekkarinen, A. 2005. Performance of different spectral and textural aerial photograph features in multi-source forest inventory. *Remote Sensing of Environment*, 94, 256-268.
- Wall, M., 1996. GALib: A C++ Library of Genetic Algorithm Components Version 2.4 Documentation, revision B. Massachusetts Institute of Technology. 101 p.

Integration of LiDAR and QuickBird imagery for mapping riparian zones in Australian tropical savannas

Lara A Arroyo^{1,2}, Kasper Johansen^{1,2}, John Armston^{1,3} Stuart Phinn^{1,2} and Cristina Pascual⁴

¹Joint Remote Sensing Research Program

²Centre for Remote Sensing and Spatial Information Science, School of Geography, Planning and Architecture, University of Queensland, Brisbane, QLD 4072, Australia.

l.arroyomendez@uq.edu.au

³Remote Sensing Centre, Queensland Department of Natural Resources and Water, Climate Building, 80 Meiers Road, Indooroopilly, QLD 4068, Australia.

⁴E.T.S.I. Montes, Universidad Politécnica de Madrid, Ciudad Universitaria s.n., 28040 Madrid, Spain

Abstract

Riparian zones are exposed to increasing pressures because of disturbance from agricultural and urban expansion and overgrazing. Accurate and cost-effective mapping of riparian environments is important for managing their functions associated with water quality, biodiversity, and wildlife habitats. The objective of this research was to integrate Light Detection and Ranging (LiDAR) and high spatial resolution QuickBird-2 imagery to estimate riparian zone attributes. A digital terrain model (DTM), a tree canopy model (TCM) and a plant projective cover (PPC) map were first obtained from the LiDAR data. The LiDAR-derived products and the QuickBird bands were then combined in an object-oriented approach to map riparian vegetation, streambed, vegetation overhang, bare ground, woodlands and rangelands. These products were also used to assess the riparian zone width. The overall result was a combined method, taking advantage of both optical and airborne laser systems, for mapping riparian forest structural parameters and riparian zone dimensions. This work shows the accuracy able to be obtained by integrating LiDAR data with high spatial resolution optical imagery to provide more detailed information for riparian zone management.

Keywords: LiDAR, QuickBird, Riparian zone, Object-oriented image analysis

1. Introduction

Riparian zones are defined as the interface of terrestrial and aquatic ecosystems and constitute a rich ecosystem both in terms of biomass and biodiversity. Several riparian health indicators can be employed when assessing the riparian zone condition. The most commonly used are compositional and structural parameters, such as dominant vegetation community, PPC, riparian zone width, presence of vegetation overhang, tree crown size, large trees and bank stability.

Optical remotely sensed data have been used to map these parameters (Congalton *et al.*, 2002; Johansen and Phinn, 2006; Johansen *et al.*, 2007a; Johansen *et al.*, 2007b). These studies have been hampered by a missing third dimension in terms of structural information on the forest height and vertical distribution of foliage. Optical sensors often have difficulties distinguishing between canopy cover and ground cover (e.g. grass *versus* trees). Moreover, they cannot detect features underneath area of dense canopy cover.

LiDAR introduces the possibility of three-dimensional analysis of vegetation and terrain features. The validity of airborne laser scanning to retrieve forest parameters has been widely tested (Lefsky *et al.*, 2001; Persson *et al.*, 2002; Zimble *et al.*, 2003; Clark *et al.*, 2004; Suarez

et al., 2005; Popescu and Zhao, 2008). LiDAR techniques provide useful information on forest structural attributes, encouraging the incorporation of LiDAR data to the riparian zone analysis.

The aim of this paper was to integrate LiDAR and QuickBird data to estimate structural parameters of the riparian zone and its component vegetation. Object-oriented classification was used for the analysis, given its ability to integrate and process data with very different properties. Both data sets were employed in order to accurately map: PPC; the river's streambed; the riparian zone width; a land-cover map; a DTM and a TCM. As a result, a combined methodology, taking advantage of the benefits of both optical and airborne laser systems, was developed.

2. Data and Methodology

2.1 Study area

The study area was located within the Fitzroy catchment in Queensland, Australia (Figure 1). It covered a 5 km stretch of Mimosa Creek and associated riparian vegetation situated upstream of the junction with the Dawson River (24°31'S; 149°46'E). The riparian vegetation was mainly surrounded by rangelands used for cattle and some agriculture, but also showed some remnant patches of woodland vegetation.

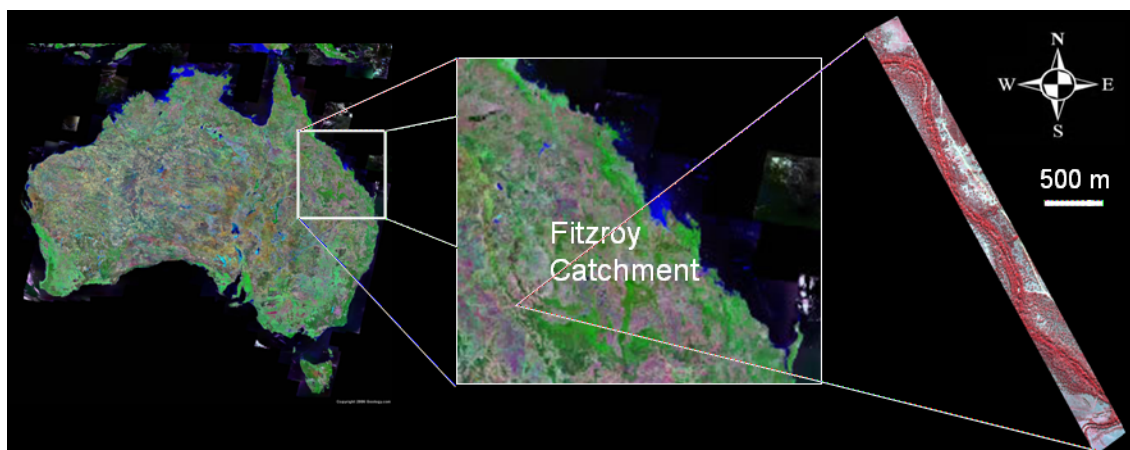


Figure 1: Location of the riparian zone study area in the Fitzroy catchment, central Queensland, Australia.

2.2. Data acquisition and processing

A QuickBird image was captured of the study area on 11 August 2007 with an off-nadir angle of 14.6°. The image was first radiometrically corrected to at sensor spectral radiance using the pre-launch calibration coefficients provided by DigitalGlobe Inc. The FLAASH module in ENVI 4.3 was then used to atmospherically correct the image to at-surface spectral reflectance. A total of 18 ground control points derived in the field were used to geometrically correct the image (root mean square error (RMSE) = 0.59 pixels for the multi-spectral bands).

Data acquired by the Leica ALS50-II LiDAR sensor on 15 July 2007 were provided in American society for Photogrammetry and Remote Sensing (ASPRS) Lidar Exchange Format (LAS), specification 1.1. LiDAR returns were classified as ground or non-ground by the data provider using proprietary software. Four products were derived from this dataset according to the methods described below: DTM, TCM, PPC and a streambed map.

A 0.5 m DTM was produced from the Leica ALS50-II data by inverse distance weighted interpolation of returns classified as ground with an exponent of two. Elevation of the ground at

the position of non-ground returns was also estimated using the same interpolation technique. The DTM and a slope image obtained from the DTM were employed for the location of the streambed within the study area.

The height of all first returns above the ground was calculated by subtracting the ground elevation from the first return elevation. These estimates of first returns were then aggregated into 2.4 m x 2.4 m data bins to match the QuickBird multi-spectral spatial resolution and employed for the derivation of the TCM and the PPC. The TCM is a representation of the top of the canopy (Suarez *et al.*, 2005) and it was calculated as the maximum height of first returns in each bin. PPC was estimated from the LiDAR cover fraction, defined as one minus the gap fraction probability, P_{gap} , at a zenith of zero. This was calculated from the proportion of counts in each data bin by

$$1 - P_{gap}(z) = \frac{C_V(z)}{C_V(0) + C_G}, \quad (1)$$

where $C_V(z)$ is the number of first return counts above z metres, $C_V(0)$ is the number of first returns above the ground and C_G is the number of first return counts from the ground (Lovell *et al.*, 2003). z was set to 2 m. The fraction of LiDAR pulses intercepted by the canopy above a height of z is determined by the PPC, but calibration is required to account for the sampling properties of the sensor (Goodwin *et al.*, 2006). The calibration of LiDAR cover fraction to PPC was developed using independent LiDAR survey data from an Optech ALTM3025 with the same flying altitude and beam divergence settings used in this study. The minimum intensity required to register a return at the sensor was assumed to be the same. A total of 47 field measurements of PPC were acquired coincident with these LiDAR data. These LiDAR and field surveys were used to develop a calibration curve from LiDAR fractional cover to PPC and are described in detail by Armston *et al.* (2008). Using the same procedures as Armston *et al.* (2008) and Johansen *et al.* (2008), a simple power function was found to fit the scatter well (RMSE 3.33) and had the property of being bounded 0–100 %,

$$PPC = 1 - P_{gap}^{0.6447}, \quad (2)$$

Since there was excellent agreement between the field estimates of PPC and LiDAR derived fractional cover and the residuals were consistent with a binomial sampling distribution, the LiDAR cover fraction estimates were calibrated to estimates of PPC using equation (2).

2.3. Land cover classification

All the above information (four multi-spectral bands, DTM, PPC, TCM and streambed map) was incorporated into a Definiens project for object-oriented image processing. Two processing steps were applied. One is the segmentation of the data into homogenous segments (image objects); and the other is the assignment of these objects to discrete classes.

Segmentation is controlled by scale, colour, and shape. A stepwise approach was chosen here due to the very different information content of the different data sets. An initial segmentation was carried out on the basis of the LiDAR-derived information (using PPC and TCM products). Those objects that showed low and similar TCM values (areas with no vegetation or low vegetation) were merged into bigger segments. Then, a second segmentation was performed using the optical information. The location of the streambed was also incorporated into the segmentation, to make sure that there were no objects covering areas from both the streambed and the riparian zone.

After segmentation, objects can be classified on the basis of spectral values, spectral variability, size, shape or in relation to neighbouring objects. In this case, both multi-spectral and

LiDAR-derived information were used to define the following six classes: riparian vegetation, woodlands, rangelands, bare ground, streambed without vegetation overhang and streambed with vegetation overhang. Four types of features were used for the classification: mean, standard deviation, context information and the normalised difference vegetation index (NDVI). Mean refers to the mean value of all pixels within an object, e.g. mean RED is the mean spectral value of the red band of all pixels within an object. The standard deviation features were employed as an estimation of the level of variability within each object. For instance, rangeland areas, which characteristically showed smooth surfaces, displayed low values of standard deviation in the near infrared (NIR) band. Context information refers to features such as “existence of streambed”, used in the description of overhanging vegetation, or “distance to riparian vegetation”, used to discard isolated forested areas misclassified as riparian vegetation. The NDVI values were calculated for each object as a new arithmetical feature, using the mean spectral values of the red and NIR bands. Each class was described by one or more of these features. Table 1 shows an overview of the features used for each class. The classification was performed in a hierarchical manner, with objects of one level informing the classification of other-level objects.

Table 1: Object and class related features used for the object-oriented classification.

| Class | Features used |
|------------------------|---|
| Bare ground | Mean RED; Mean TCM |
| Riparian vegetation | NDVI; Number of neighbour "Riparian vegetation" objects; Enclosed by class "Riparian vegetation"; Distance to "Streambed" |
| Rangelands | NDVI; Standard deviation NIR; Mean TCM |
| Woodlands | NDVI; Relative border to "Riparian vegetation" |
| Streambed without veg. | Mean RED; Presence of "Streambed" |
| Vegetation overhang | NDVI; Presence of "Streambed" |

2.4. Riparian zone and streambed widths estimation

The riparian zone width was estimated as the perpendicular length from the toe of the stream bank to the external perimeter of the riparian vegetation zone, where abrupt change in vegetation height and density occurred (Johansen and Phinn, 2006). The land-cover classification was employed to establish this distance. All the riparian vegetation objects were first subdivided into objects consisting of one pixel and only those ones corresponding to the edge of the riparian vegetation were considered for the analysis. The riparian zone width was then extracted from the value of the feature “Distance to class”. Definiens’ “Distance to class” feature measures the distance from the centre of each object to the closest object of the specified class. In this case, the distance of every pixel from the edge of the riparian vegetation to the streambed was extracted. The same approach was employed for the streambed width.

2.5 Validation

Field sampling was conducted between 28 May and 5 June 2007. Coincident field measurements of vegetation structural properties for image calibration and validation were derived along 25 m wide and 70 – 100m long transects located perpendicular to the stream at each of five field sites. Each site had six transect lines each separated by 5 m starting at the edge of the streambed, going through the riparian zone and finishing 10-20 m beyond the external perimeter of the riparian zone. Quantitative field measurements of PPC were derived along each of the six transect lines from upward looking photos taken at 5 m intervals (figure 2). The photos were subsequently classified into canopy photosynthetic and non-photosynthetic elements and sky to calculate the plant projective cover within the field of view using the approach by van Gardingen *et al.* (1999). Riparian zone width and streambed width were directly measured to the nearest meter using a measuring tape.



Figure 2: Example of the quantitative field measurements of PPC from upward looking photos. Photos (left) were classified (right) into canopy elements (black) and sky (white). PPC corresponds to the relative area of canopy elements in the classified photo (0.49 in this example)

The LiDAR-derived PPC estimations were validated using the actual field PPC measurements. To allow this validation, each field site was subdivided into smaller plots of 225 m². This plot size (15 x 15 m) is equivalent to the area covered by nine photos (3 x 3 photos) and represents a feasible compromise to allow geographic correspondence between both data sets. The average of the LiDAR-derived PPC values for each plot was then compared to the average of the corresponding nine field PPC measurements. A total number of 48 plots were used.

An error matrix was constructed to estimate the land cover classification accuracy. Sixty randomly selected objects were visually classified using both the multi-spectral and the panchromatic bands from the QuickBird image and employed as reference sites. The overall accuracy of the classification and the Kappa statistic were calculated.

Field measurements of streambed width were compared to those automatically obtained from the land cover classification. Since the streambed was frequently hidden underneath the canopy cover of the riparian vegetation, visual assessment of the streambed width from optical information was unreliable. Hence, only field measurements were employed for streambed validation. In the case of the riparian zone width measurements, a set of 34 visually assessed measurements of the riparian zone width was also produced from the multi-spectral and the panchromatic QuickBird bands. They corresponded to 17 sites located along the river where the riparian zone width was measured from both edges of the streambed (right and left hand side of the river) to the external perimeter of the riparian zone. Both in-situ and image-based riparian zone width measurements were compared to the automatically obtained riparian zone widths.

3. Results and Discussion

The 0.5 m DTM extracted from the LiDAR data revealed a fairly flat area, with a total height difference of only 25 m (Figure 3a). This information was employed for mapping the streambed of the river according to its geomorphology (Figure 3b). The high precision of this LiDAR-derived streambed map allowed very accurate estimation of the streambed width. Thus, the streambed width measurements obtained from the LiDAR-derived streambed map and the ones measured in the field showed a very high correlation, with a correlation coefficient (r) of 0.98 (RMSE = 1.53).

The PPC product showed the percentage of land covered by green foliage and non-photosynthetic vegetation (branches, trunks, dead leaves) (Figure 3c). This is an important riparian zone health indicator that is difficult to estimate by means of optical information. The comparison between the estimated PPC and the field measurements of PPC also showed a

strong correlation (Figure 4; $r = 0.86$). Previous studies based on optical information (QuickBird imagery) had revealed that the presence of dense grass cover heavily affects the accuracy of the optical-based PPC estimates (Johansen and Phinn, 2006). In this sense, the use of LiDAR data represents a benefit for the riparian zone analysis.

A TCM estimating the heights of the top of the canopy was also derived from the LiDAR data (Figure 3d). The canopy height ranged from 0 to 41.35 m. This layer of information facilitated the image segmentation and land cover classification. The TCM was useful for tree crown identification and tree height estimation.

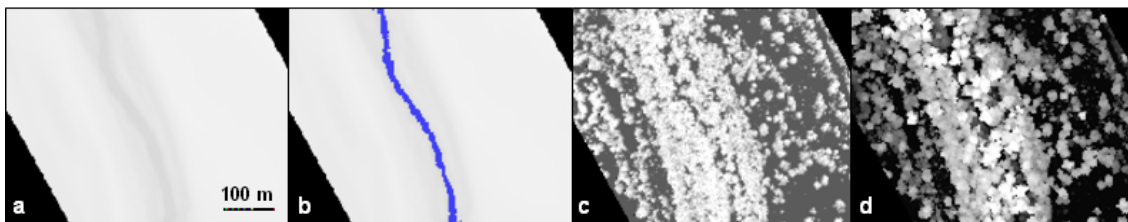


Figure 3: LiDAR-derived products: (a) DTM; (b) streambed map (in blue); (c) PPC and (d) TCM. Bright areas correspond to high values for the terrain elevation (a, b), PPC (c) and tree heights (d).

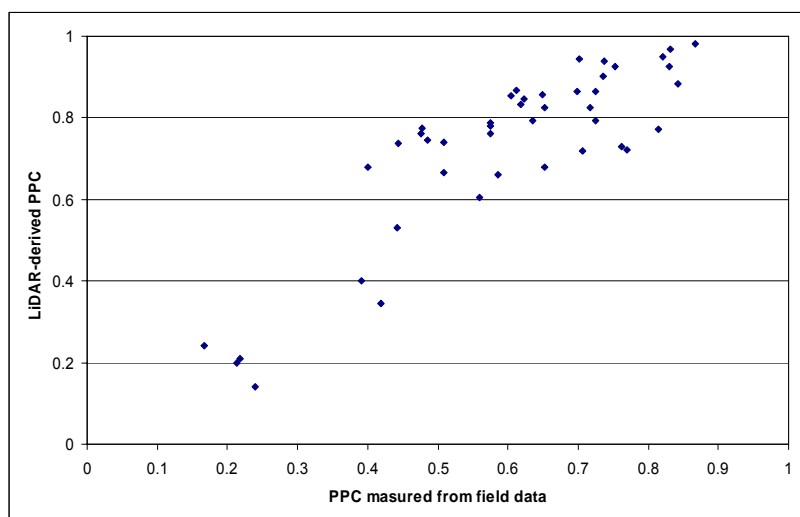


Figure 4: Scatter plot of the PPC estimations from the LiDAR data vs the PPC measurements extracted from upward looking photos.

Image segmentation was carried out using the LiDAR-derived information first (Figure 5a). This information on its own was useful for the tree identification, but it was insufficient for segmenting cover types with similar heights (such as bare ground and grasslands). The second level was created by incorporating the multi-spectral information (Figure 5b), and the result was a more suitable separation of tree crowns and other features. Here, the multi-spectral information allowed identification of features such as bare ground and grasslands. Finally, the incorporation of the streambed boundaries assisted the land cover classification and allowed the estimation of the riparian zone width.

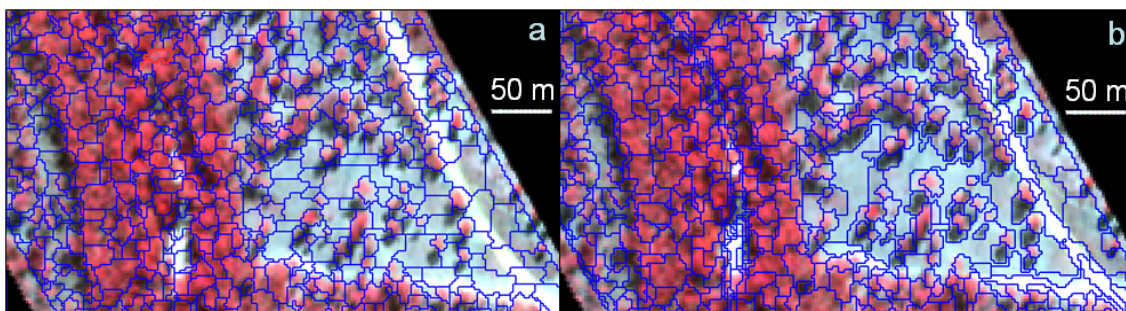


Figure 5: Segmentation levels: (a) LiDAR-derived segmentation and (b) incorporating optical information.

Classification was performed on the final segmentation level using the parameters defined in Table 1. The combined use of LiDAR, spectral and context information allowed accurate identification of the six land cover classes (Figure 6). Fifty-two out of sixty objects were correctly identified as one of the six land cover types, which provided an overall classification accuracy of 88% (Table 2). The Kappa value for the land cover classification was 85%. Riparian vegetation and woodland classes were predicted with the lowest accuracy (63 and 69% respectively), due to the high level of spectral and positional similarity between them in the transitional area between riparian and woodland vegetation.

The LiDAR-derived streambed map was essential for correct identification of vegetation overhang and riparian zone width. A total area of 4.1 hectares of streambed (83.5% of the total streambed mapped for this study area) were located underneath vegetation overhang and would have been impossible to map by means of optical sensors alone. Accurate location of the streambed was also necessary for the riparian zone width estimation. At the same time, the spectral information improved the LiDAR-derived streambed map, which was underestimated in some areas. The original streambed map, derived only from LiDAR data, was missing 4.5% of the final streambed area, mapped after including the QuickBird multi-spectral bands. This confirms the feasibility of combining both sensors for the riparian zone analysis, rather than selecting one over the other.

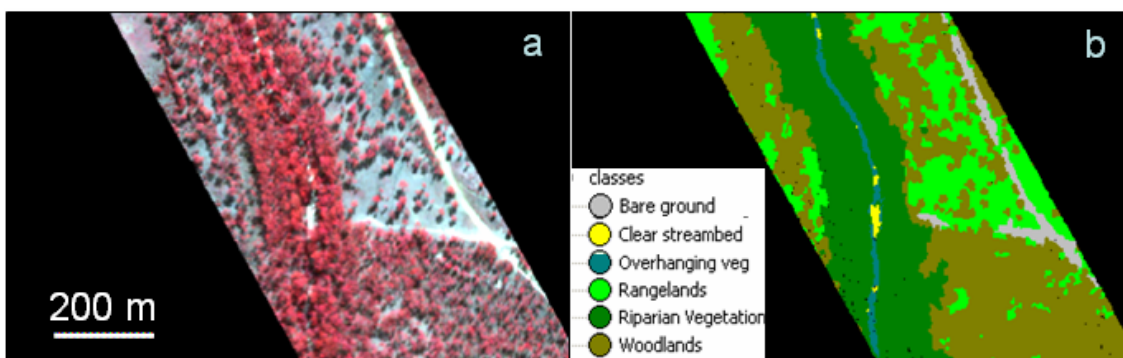


Figure 6: Land cover classification: (a) Subset of the study area (bands green, red and NIR) and (b) classification result for the same subset.

Measurements of the riparian zone width and the streambed width were derived from the land cover classification map (Figure 7). By reducing the size of the objects to one single pixel, we ensured a reliable measurement of both the riparian zone width and the streambed width. The distance in Definiens is estimated from the centre of each object, being influenced by its shape and orientation. This bias was eliminated by working with individual pixels. The average riparian zone width and streambed width for the study area were 57.11 m and 13.23 m respectively.

Table 2: Error matrix of the land cover classification for bare ground (BG), riparian vegetation (RV), woodlands (WL), rangelands (RL), streambed without vegetation overhang (SC) and streambed with vegetation overhang (VO).

| | | Reference Data | | | | | | | User's Accuracy |
|-----------------------------------|-----|----------------|------|-------|------|-------|-------|-----|-----------------|
| | | BG | RV | WL | RL | SC | VO | Sum | |
| Classified Data | BG | 6 | 0 | 0 | 0 | 0 | 0 | 6 | 100% |
| | RV | 0 | 12 | 4 | 0 | 2 | 1 | 19 | 63.2% |
| | WL | 0 | 0 | 9 | 0 | 0 | 0 | 9 | 100% |
| | RL | 0 | 0 | 0 | 7 | 0 | 0 | 7 | 100% |
| | SC | 0 | 0 | 0 | 0 | 9 | 0 | 9 | 100% |
| | VO | 0 | 0 | 0 | 0 | 0 | 10 | 10 | 100% |
| | Sum | 6 | 12 | 13 | 7 | 11 | 11 | 60 | |
| Producer's Acc. | | 100% | 100% | 69.2% | 100% | 81.8% | 90.9% | | |
| Overall Classification Accuracy = | | 88.3% | | | | | | | |

Forty nine measurements of the riparian zone width (five measured in the field and 34 visually assessed from the optical information) were employed for the validation of the riparian zone width assessment. Comparison between the reference and estimated riparian zone widths showed a strong correlation ($r = 0.82$; $RMSE = 13.9$), with an overestimation of the automatic assessment in some areas (Figure 8). This overestimation was linked to the presence of woodland areas close to the riparian zone, which were in some cases misclassified as riparian vegetation, and therefore included in the riparian zone width estimation. Because the riparian zone width estimation was based on the land cover classification map, the results relied heavily on the image classification accuracy. Even though establishing the boundary between riparian vegetation and woodlands is challenging (even when it is performed in the field), the overall accuracy of the automatic estimation was high, with an average error of 3.9 m, equivalent to less than 2 pixels in the image.

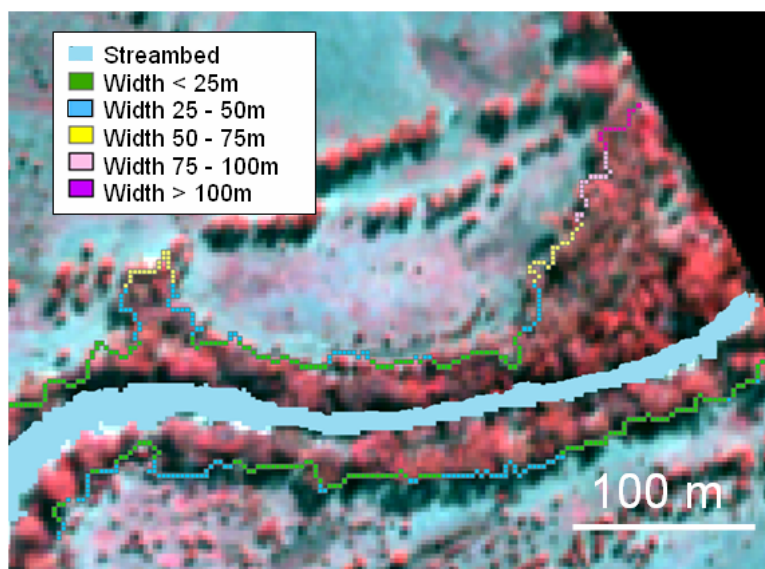


Figure 7: Riparian zone width estimation. Pixels representing the edge of the riparian zone are presented in different colours according to their distance to the streambed.

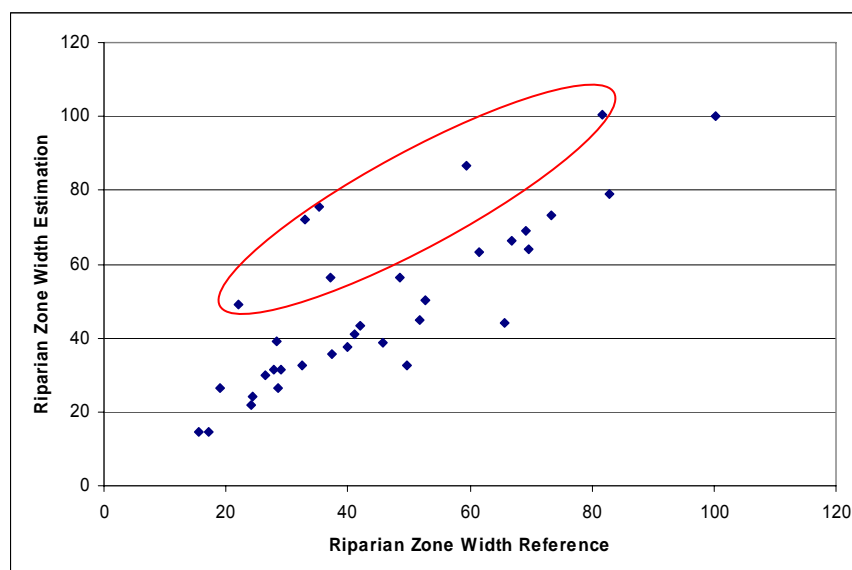


Figure 8: Scatter plot of the riparian zone width estimations vs the reference values (i.e. measured in the field and visually assessed from the optical information). The red ellipse shows examples of overestimation of the riparian zone width.

Conclusions

Several parameters of the riparian zone have been accurately mapped by combining LiDAR and high spatial resolution optical data. These include PPC, streambed with vegetation overhang, streambed without vegetation overhang, the riparian zone width, the streambed width and a land cover map.

Combining LiDAR and high spatial resolution satellite imagery can significantly improve the mapping and assessment of vegetation structure and condition of the riparian zones in Australian tropical savannas. The integration of both sources of information produced an accurate land cover map, despite the high heterogeneity of the riparian landscape. This allowed accurate identification of riparian vegetation, vegetation overhang and the streambed, all of which are commonly used indicators of the riparian zone condition. Moreover, the analysis developed allowed an accurate estimation of the riparian zone width and improvement of the streambed map.

The object-oriented image analysis was appropriate for this type of data integration. This approach also assisted the classification by allowing the incorporation of context information to the classes' definition. Our results have implications for riparian management in tropical savannas as a tool for monitoring vegetation structure and composition remotely. Further research in this direction should be focused on the estimation and incorporation of other remotely-derived riparian health indicators, such as bank stability and weed mapping.

Acknowledgements

Help with the fieldwork and analysis was provided by Santosh Bhandari and Andrew Clark. L.A. Arroyo is funded by the Fundacion Alonso Martin Escudero (Spain). K. Johansen is supported by an Australian Research Council Linkage Grant to K. Mengersen, S. Phinn, and C. Witte.

References

- Armston, J.D., Denham, R.J., Danaher, T.J., Scarth, P.F. and Moffiet, T., 2008. Prediction and validation of foliage projective cover from Landsat-5 TM and Landsat-7 ETM+ imagery for Queensland, Australia. *Journal of Applied Remote Sensing*, in review.
- Clark, M.L., Clark, D.B. and Roberts, D.A., 2004. Small-footprint lidar estimation of sub-canopy elevation and tree height in a tropical rain forest landscape. *Remote Sensing of Environment*, 91, 68 - 89.
- Congalton, R.G., Birch, K., Jones, R. and Schriever, J., 2002. Evaluating remote sensed techniques for mapping riparian vegetation. *Computers and Electronics in Agriculture*, 37, 113 - 126.
- van Gardingen, P.R., Jackson, G.E., Hernandez-Daumas, S., Russel, G. and Sharp, L., 1999. Leaf area index estimates obtained for clumped canopies using hemispherical photography. *Agricultural and Forest Meteorology*, 94, 243 - 257.
- Goodwin, N.R., Coops, N.C. and Culvenor, D.S., 2006. Assessment of forest structure with airborne LiDAR and the effects of platform altitude. *Remote Sensing of Environment*, 103, 140-152.
- Johansen, K. and Phinn, S., 2006. Mapping structural parameters and species composition of riparian vegetation using IKONOS and Landsat ETM+ data in Australian tropical savannahs. *Photogrammetric Engineering and Remote Sensing*, 72, 71 - 80.
- Johansen, K., Coops, N.C., Gergel, S.E. and Stange, Y., 2007a. Application of high spatial resolution satellite imagery for riparian and forest ecosystem classification. *Remote Sensing of Environment*, 110, 24 - 44.
- Johansen, K., Phinn, S., Dixon, I., Douglas, M. and Lowry, J., 2007b. Comparison of image and rapid field assessments of riparian zone condition in Australian tropical savannahs. *Forest Ecology and Management*, 240, 42 - 60.
- Johansen, K., Clark, A., Denham, R., Armston, J., Phinn, S. and Witte, C., 2008. Mapping plant projective cover in riparian zones: integration of field and high spatial resolution QuickBird, Spot-5 and LiDAR data. In Australasian Remote Sensing & Photogrammetry Conference, pp. 12, Darwin (Australia).
- Lefsky, M.A., B., C.W. and Spies, T.A., 2001. An evaluation of alternate remote sensing products for forest inventory, monitoring and mapping of Douglas fir forests in western Oregon. *Canadian Journal of Forestry Research*, 31, 78 – 87.
- Lovell, J.L., Jupp, D.L.B., Culvenor, D. and Coops, N.C., 2003. Using airborne and ground-based ranging lidar to measure canopy structure in Australian forests. *Canadian Journal of Remote Sensing*, 29, 607 - 622.
- Persson, A., Holmgren, J. and Soderman, U., 2002. Detecting and measuring individual trees using an airborne laser scanner. *Photogrammetric Engineering and Remote Sensing*, 28, 1 – 8.
- Popescu, S.C. and Zhao, K., 2008. A voxel-based lidar method for estimating crown base height for deciduous and pine trees. *Remote Sensing of Environment*, 112, 767 - 781.
- Suarez, J.C., Ontiveros, C., Smith, S. and Snape, S., 2005. Use of airborne LiDAR and aerial photography in the estimation of individual tree heights in forestry. *Computers & Geosciences*, 31, 253 - 262.
- Zimble, D.A., Evans, D.L., Carlson, G.C., Parker, R.C., Grado, S.C. and Gerard, P.D., 2003. Characterizing vertical forest structure using small-footprint airborne LiDAR. *Remote Sensing of Environment*, 87, 171 - 182.

Keynote Presentation 2

LiDAR and wildlife-habitat applications

Wesley E. Newton

USGS Northern Prairie Wildlife Research Center, 8711 37th Street Southeast,
Jamestown, North Dakota, 58401, USA. wnewton@usgs.gov

Abstract

Vegetative composition (e.g., conifer and deciduous trees) and structure (e.g., over- and under-story tree densities and heights) are among the most important factors affecting habitat selection by wildlife, particularly breeding birds in forest ecosystems. Estimating the composition of vegetation can be done using high resolution digital imagery for each mapping unit (e.g., forest stands) across the entire landscape. However, current imaging systems do not provide a mechanism for estimating vegetation structure for each mapping unit. Such information has to be collected by intensive and extensive ground surveys, which are impractical for large landscapes, especially where a complete census is required. Therefore, the challenge is to estimate vegetation structure in a spatially explicit manner at every mapping unit across the entire landscape that can then be used to assess and predict habitat for wildlife. LiDAR offers an opportunity to capture and model vegetation structure across entire landscapes. These estimated structural metrics, which are typically the same metrics of interest to foresters, can then be used as explanatory variables in various empirical models for predicting wildlife species occurrences, or other demographic metrics (e.g., densities, nest survival). Here we describe the utility of LiDAR, combined with imagery, in predicting wildlife demographics and discuss many applications, not in only forest ecosystems but also in riparian, shrubland, and urban (i.e., urban forestry) ecosystems.

Session 3: Ecological applications & habitat mapping

Characterising the ecological structure of a dry Eucalypt forest landscape

N. Miura¹, S.D. Jones¹

¹School of Mathematical and Geospatial Sciences, RMIT University, GPO Box 2476V,
Melbourne VIC 3001 Australia
naoko.miura@student.rmit.edu.au, simon.jones@rmit.edu.au

Abstract

Characterising forest structure is an essential part of any comprehensive biodiversity assessment. In this study, the utility of LiDAR for characterising the ecological structure of a dry Eucalypt forest landscape was examined. An eight class scheme derived from LiDAR point density is proposed. This was validated using a network of field sites that recorded commonly used metrics of biodiversity. The proposed categories allow for the mapping of gaps (both above bare ground and low vegetation), canopy cover and its density as well as the presence of various canopy strata (low, medium and high). Regression analysis showed a high correlation between LiDAR derived variables and field recorded variables reporting the highest R-square 0.82 between LiDAR derived presence of low vegetation and field derived LAI for low vegetation. Although some refinement is necessary, the proposed scheme clearly shows the potential of LiDAR to provide information on the complexity of habitat structure.

Keywords: LiDAR, point density, canopy cover, ecological structure

1. Introduction

Characterising forest structure is an essential part of any comprehensive biodiversity assessment. There is often a good correlation between biodiversity and measures of the variety and / or complexity of arrangement of structural components within an ecosystem (Mac Nally et al., 2001). Furthermore, the habitat complexity of a forest can be used to predict the occurrence of some species, since such information provides locally specific descriptions of faunal habitat (Catling and Burt, 1995; Jorgensen, 2002).

In order to characterise the ecological structure of forests, a series of generally applicable, robust, reliable measurements are required. LiDAR (Light Detection and Ranging) has been recognized as a powerful tool for forest structure characterisation. Numerous papers have documented the utility of LiDAR for the estimation of forest attributes. Næsset (1997) showed the potential of LiDAR to estimate fractional cover. Næsset derived fractional cover from LiDAR as the ratio of canopy returns to the total number of returns per unit area. Similar methods utilising the point density of LiDAR returns to estimate fractional cover were presented in other studies (e.g. Coops et al., 2007; Hopkinson and Chasmer, 2007; Morsdorf et al., 2006; Riaño et al., 2004; Solberg et al., 2006) and showed promising results. Hopkinson and Chasmer (2007) also incorporated the intensity of LiDAR returns into this algorithm. These authors estimated gap fraction calculating the ratio of the sum of all ground level return intensities to the sum of total return intensity, and achieved a high correlation with gap fraction recovered from ground-based digital hemispherical photography. Vertical forest structure is also an important component. Zimble et al. (2003) used LiDAR derived tree height variance to differentiate single-storey and multi-storey vertical structural classes with a 97% accuracy. Riaño et al. (2003) used a cluster analysis of LiDAR height information to discriminate between overstorey and understorey canopies. Maltamo et al. (2005) tested the existence and the number of understorey trees by analysing the height distribution of LiDAR returns. These authors found

that multi-layered stand structures can be recognised and quantified, however, the accuracy of the results depends on the density of the dominant tree layer. The main focus of many previous studies has been on forest resource measurement rather than ecological applications. The later requires an assessment of complexity of habitat structure at a landscape scale.

The purpose of this paper is to present a draft methodology for characterising the ecological structure of a dry Eucalypt forest landscape using LiDAR data alone. An eight class scheme is proposed and validated using a network of field sites that recorded commonly used metric of biodiversity.

2. Method

2.1 Study area

The study area (Upper left S 41.12°, E 146.45°; Lower right S 41.32°, E 146.58°) covers the Rubicon catchment in the Cradle Coast Region of Tasmania, Australia and is approximately 20,000 ha. The area is classified as *Eucalyptus amygdalina* coastal forest and woodland. The forests are dry sclerophyll communities dominated by *E. amygdalina* and have heathy, sedgy and shrubby understorey variants (Harris and Kitchener, 2005). In this area, the human population is growing in coastal towns such as Devonport which is one of the two major centres in this region. Most people are employed in primary industries (agriculture, forestry and fishing), mining, manufacturing, retail and tourism. As the population grows, change in land use such as land clearing for grazing, and conversion of native forest to plantation is causing terrestrial habitat loss or modification. Subdivision for urban or industrial development in areas of high vegetation conservation values has also become an issue. This is the major threat to biodiversity in this area (The Cradle Coast Natural Resource Management Committee, 2005). Assessment of the present state of ecological structure in forests is useful to make conservation strategy.

2.2 LiDAR data

LiDAR data was acquired over the study area using a RIEGL LMS-Q560 sensor in February 2007. This is a waveform system and was configured to record up to six returns for this study. The scan angle for this mission was set to $\pm 22.5^\circ$. The flying height was 500m above the ground, yielding a footprint of approximately 20cm in diameter. For this study, the pulse repetition frequency was 100 kHz and the wavelength of interaction was 1500 nm. The overall survey was coordinated using static and rapid static GPS methods. This was undertaken to establish a small accurate network of points.

2.3 Field data

Fieldwork was conducted in February 2007 and 2008. Initial ground data collection assessed native vegetation condition using the 'Biometric' tool – a generic plot-based ecological survey method designed to guide natural resource managers (Gibbons et al., 2004). Subsequently, an additional ground survey was developed and implemented specifically to collect ecological structural information. In this paper, the later information is used to validate the LiDAR data.

Fourteen plots were surveyed within remnant dry Eucalypt forests across the study area. A 25m radius circular plot was established by defining a centre point and taking a hand-held GPS (eTrex of GARMIN Corporation) measurement. This includes resident positional error ± 5.5 m of x y on average. Five transects running from East to West, parallel to each other were deployed in each plot (Figure 1). Assessment points were located every 7m along each transect, comprising twenty seven assessment points in a plot. Canopy Cover (CC) as a percentage was recorded in two ways. The first method (CC₁) assessed only photosynthetic elements and was

conducted in situ with the aide of reference photographs. The second method (*CC₂*) assessed both photosynthetic and non-photosynthetic facets by acquiring vertical images from a 1.7m vantage point and calculating *CC* later in the laboratory. Bare ground cover, grass cover, litter cover and low vegetation (*Low veg*; 0-1m from the ground) cover were also recorded as a percentage within a 3.5m radius of each assessment point. Coarse woody debris on the ground (defined as woody components $\geq 10\text{cm}$ in diameter) was recorded noting the diameter and length of logs on each transect. The Leaf Area Index (LAI) for low vegetation was measured using LAI2000 Plant Canopy Analyzer of LI-COR, INC for each plot. It should be noted that the LAI values recorded using this instrument include non-leaf elements such as stems and branches. Tree top and the height to the first branch were measured using a Total Station, TCR705 of Leica Geosystems. All tree height information was then classified into two classes. First, the height information was divided into two categories (vegetation upto 5m and vegetation greater than 5m). Next the relative proportion of each of these categories was calculated by comparing them to the total number of height records. It is noted that the height to the first branch was not recorded for all trees due to the field of view being obscured at times. In this case, only tree top height information was used for the classification.

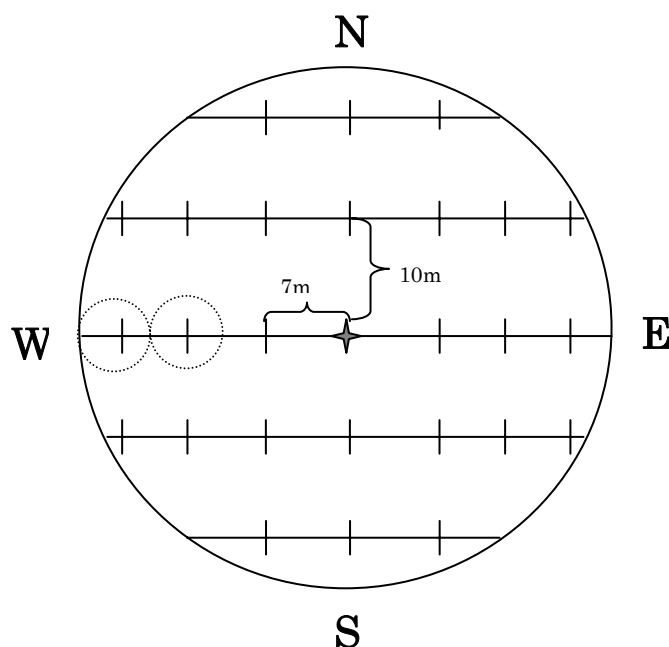


Figure 1: Each field plot comprises five transects running from East to West, parallel to each other, with assessment points located every 7m. In total this yields twenty seven assessment points for each plot. Small circles (only two shows for clarity) indicate the 3.5m radius assessment areas for understory cover measurement (these were recorded for each assessment point).

3. Proposed forest characterisation

In order to create a scheme to characterise the ecological structure of a dry Eucalypt forest landscape, LiDAR data was first classified into four groups; *Ground*, Low vegetation (*Low veg*, 0-1m from the ground), Medium vegetation (*Medium veg*, 1-5m from the ground) and High vegetation (*High veg*, $5\text{m} <$) using TerraScan software of Terrasolid, Ltd. The number of singular (Type 1), first of many (Type 2), intermediate (Type 3) and last of many returns (Type 4) was calculated for each of the four groups and divided by the total number of returns in each plot. Type 1 and Type 2 returns are the result of the first interaction with objects, which suggests that there is opening above this pulse interaction (i.e. no interaction above these points). The number of returns in *Low veg*, *Medium veg* and *High veg* groups suggests presence of vegetation in each

of these strata. Of particular importance is the presence of Type 3 and Type 4 returns in *High veg* strata, since these indicate a dense canopy. Using calculated ratios, we propose the following scheme (Table 1). Where, 1) *Ground* Type 1; opening above the ground. 2) *Low veg* Type 1 & 2; opening above low vegetation. 3) *Low veg* total (Type 1, 2, 3 & 4); presence of understorey vegetation. 4) Canopy cover (*CC*) is defined as the following equation;

$$CC = \frac{\sum \text{MediumVegType1 \& 2} + \text{HighVegType1 \& 2}}{\sum \text{GroundType1} + \text{LowVegType1 \& 2} + \text{MediumVegType1 \& 2} + \text{HighVegType1 \& 2}} \quad (1)$$

5) *Medium veg* Type 1 & 2; opening above medium vegetation. 6) *Medium veg* total (Type 1, 2, 3 & 4); presence of mid-storey vegetation. 7) *High veg* Type 3 & 4; dense canopy of high trees. 8) *High veg* total (Type 1, 2, 3 & 4); presence of high trees. This scheme was subsequently compared to the field data to validate its utility in characterising ecological structure.

Table 1: Forest characterization scheme

| | LiDAR return ratio | Description |
|---|--|------------------------------------|
| 1 | <i>Ground</i> Type 1 | opening above the ground |
| 2 | <i>Low veg</i> Type 1 & 2 | opening above low vegetation |
| 3 | <i>Low veg</i> total (Type 1, 2, 3 & 4) | presence of understorey vegetation |
| 4 | See equation (1) | canopy cover |
| 5 | <i>Medium veg</i> Type 1 & 2 | opening above medium vegetation |
| 6 | <i>Medium veg</i> total (Type 1, 2, 3 & 4) | presence of mid-storey vegetation |
| 7 | <i>High veg</i> Type 3 & 4 | dense canopy of high trees |
| 8 | <i>High veg</i> total (Type 1, 2, 3 & 4) | presence of high trees |

4. Result

The comparison between the LiDAR derived structural characterisation scheme and the field data is shown in Figure 2. In this paper, we will focus on four variables only; canopy cover, low vegetation, medium vegetation and high vegetation.

4.1 Canopy cover

Figure 2(a) and (b) show LiDAR derived *CC* (scheme 4) was strongly correlated with the two ground-based measures of *CC* (photosynthetic / photosynthetic and non-photosynthetic), with an R-square value of 0.78 and 0.77 respectively. As displayed in Figure 2(a) and (b), LiDAR *CC* and Field *CC* were highly correlated across a broad range of *CC* values. It was noted that the ground-based measures consistently reported a lower *CC* than LiDAR derived measures. This will be discussed in section 5. Both *CC_1* and *CC_2* report an anomaly whereby the canopy cover for plot 4a was higher in LiDAR *CC*. This can be explained by the difference in canopy cover estimation between LiDAR and field methods. LiDAR *CC* assessed vegetation cover

higher than 1m from the ground, while field *CC* was recorded at the height of 1.7m from the ground. If there are dense vegetation components between 1m and 1.7m, field measured *CC* estimation would miss this strata and therefore underestimate *CC*. Our field data confirms that plot 4a has extremely dense mid-storey vegetation; 553 trees (mostly shrubs, *Melaleuca squarrosa* and *Leptospermum scoparium*, approximately 98% of the trees in the plot) are less than 5m in height and with less than 30 cm DBH.

4.2 Low vegetation

LiDAR derived *Low veg* presence (scheme 3) showed strong correlation with field recorded LAI for *Low veg* (R-square value 0.82), and moderate correlation with field recorded mean *Low veg* cover (R-square value 0.58) (Figure 2(c) & (d)). As can be seen in Figure 2(c), LiDAR derived *Low veg presence* and Field LAI for *Low veg* were significantly correlated across a range of LAI values. Comparison between LiDAR derived *Low veg* presence and field recorded mean *Low veg* cover reveal that plot 13a was underestimated in the LiDAR. Plot 13a has grass and blackberry as understorey vegetation. It was noted in the field that the southern half of the plot was covered with very short grass. This could lead to misclassification of LiDAR returns. The grass is too short to be classified as *Low veg* and the LAI2000 is not designed to measure such low vegetation. This explains the good correlation between LiDAR derived *Low veg* presence and Field LAI for *Low veg*.

4.3 Medium vegetation

LiDAR derived *Medium veg* presence (scheme 6) displayed a good correlation with field recorded *Medium veg* class with R-square value 0.66 (Figure 2(e)). Again, this association was observed across a range of *Medium veg* class ratios. Plot 6a was underestimated by LiDAR. In this plot, significant recruitment of small trees and annual growth was noted in the field for all 52 trees (average height 2.27m with less than 10cm DBH) in *Medium veg*. Since there is a one year difference between the LiDAR acquisition date and tree height measurement, these trees would have been much smaller and classified as *Low veg* when the LiDAR data was acquired.

4.4 High vegetation

LiDAR derived *High veg* presence (scheme 8) showed moderate correlation with field recorded *High veg* class with R-square value 0.46 (Figure 2(f)). Comparison between the field derived height measurements and LiDAR derived *High veg* presence scheme proved problematic. This could be due to a number of issues.

- Problems with field measurement, in particular siting true tree top height
- Problems in categorising the field data into height classes (canopy strata)

Further work is being undertaken to resolve these issues.

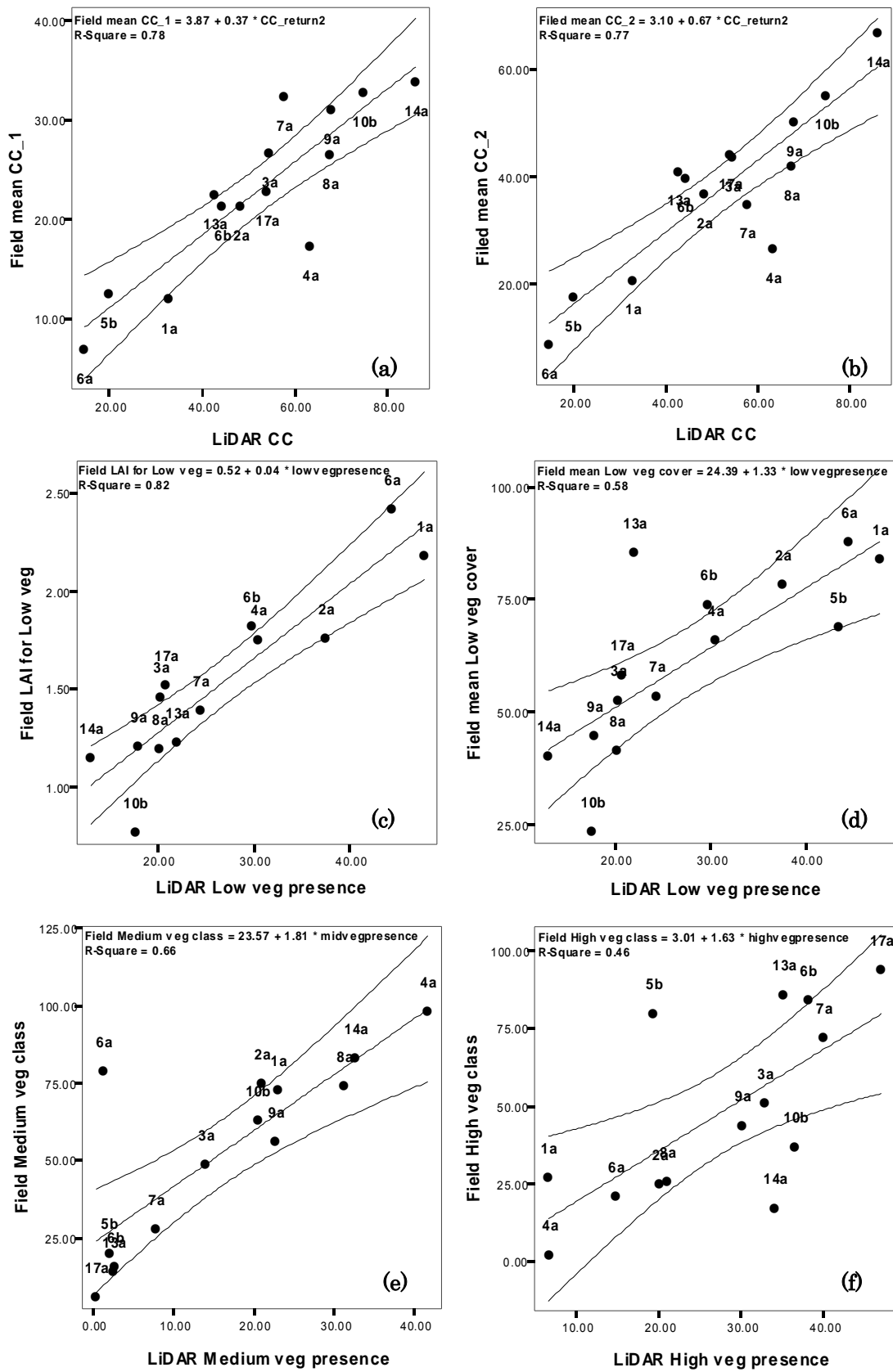


Figure 2: Linear regression between LiDAR derived structural characterization scheme and field data with 95% mean prediction interval. The labels are surveyed plot names.

5. Discussion

In the comparison between LiDAR derived *CC* and the two field measured *CC* assessments, strong correlation was observed. Interestingly, the two different assessment methods of canopy cover described in section 2.3 showed the similar results (R-square 0.77 and 0.78). One would expect higher correlation between LiDAR *CC* and Field *CC*₂, since both variables measure all perturbing canopy objects from laser pulse or sun light, while Field *CC*₁ measures only some portion of these objects. In our study site, the vegetation community of the canopy strata is all evergreen and dominated by Eucalypt species. The ratio of leaf area to non-photosynthetic elements (stems and branches) should be consistent unless there is defoliation caused by disease. In fact, *CC*₁ and *CC*₂ were significantly correlated with each other presenting Pearson Correlation Coefficient value 0.903 ($P \leq 0.01$) in our companion study. In terms of *CC* values, Field *CC* reports a consistently lower value than LiDAR *CC*. We assume that ground based measurements underestimate “true” *CC*. Since field derived measures are based on twenty seven independent observations over an approximately 0.2ha plot area, while LiDAR derived measures are based on more than seven thousand returns in average over the 0.2ha plot. LiDAR would be more capable of assessing *CC* at a landscape scale.

The result of regression analysis between LiDAR *High veg* presence and Field *Hig veg* class provided relatively lower R-square value (0.46). The method to classify field tree height information (see section 2.3) may not represent vertical structure of the plots sufficiently. Further improvement would be required to validate LiDAR scheme.

In conclusion, the proposed method to characterise the ecological structure of a dry Eucalypt forest landscape was promising. Regression analysis reported high correlation between LiDAR derived variables and field recorded variables across a different range of forest structural types. Although some refinement is necessary, particularly in the high vegetation class, the proposed scheme clearly showed the potential of LiDAR to provide information on the complexity of habitat structure. Future work will concentrate on examining the applicability of this scheme to develop habitat suitability models.

Acknowledgements

We would like to thank the Royal Melbourne Institute of Technology, Melbourne –Australia, for support via its RUIS scholarship scheme. We also acknowledge the Australian Commonwealth Environment Research Fund “Landscape Logic” Project for its support.

References

- Catling, P.C. and Burt, R.J., 1995. Studies of the Ground-Dwelling Mammals of Eucalypt Forests in South-Eastern New South Wales: the Effect of Habitat Variables on Distribution and Abundance. *Wildlife Research*, 22(3): 271-288.
- Coops, N. et al., 2007. Estimating canopy structure of Douglas-fir forest stands from discrete-return LiDAR. *Trees - Structure and Function*, 21(3): 295-310.
- Gibbons, I., Ayers, D., Seddon, J., Doyle, S. and Briggs, S., 2004. BioMetric Decision Support Tool Version 1.4. Biodiversity Assessment Tool To Support the NSW Property Vegetation Plan Developer, NSW Department of Environment and Conservation, Canberra.
- Harris, S. and Kitchener, A., 2005. From Forest to Fjaeldmark: Descriptions of Tasmania's Vegetation. Department of Primary Industries, Water and Environment, Printing Authority of Tasmania, Hobart.

- Hopkinson, C. and Chasmer, L.E., 2007. Modeling canopy gap fraction from Lidar intensity. In: P. Rönholm, H. Hyypää and J. Hyypää (Editors), ISPRS Workshop on Laser Scanning 2007 and SilviLaser 2007, Espoo, Finland.
- Jorgensen, E.E., 2002. Small mammals: consequences of stochastic data variation for modeling indicators of habitat suitability for a well-studied resource. *Ecological Indicators*, 1(4): 313-321.
- Mac Nally, R., Parkinson, A., Horrocks, G., Conole, L. and Tzaros, C., 2001. Relationships between terrestrial vertebrate diversity, abundance and availability of coarse woody debris on south-eastern Australian floodplains. *Biological Conservation*, 99(2): 191-205.
- Maltamo, M. et al., 2005. Identifying and quantifying structural characteristics of heterogeneous boreal forests using laser scanner data. *Forest Ecology and Management*, 216(1-3): 41-50.
- Morsdorf, F., Kötz, B., Meier, E., Itten, K.I. and Allgöwer, B., 2006. Estimation of LAI and fractional cover from small footprint airborne laser scanning data based on gap fraction. *Remote Sensing of Environment*, 104(1): 50-61.
- Næsset, E., 1997. Estimating timber volume of forest stands using airborne laser scanner data. *Remote Sensing of Environment*, 61(2): 246-253.
- Riano, D., Meier, E., Allgower, B., Chuvieco, E. and Ustin, S.L., 2003. Modeling airborne laser scanning data for the spatial generation of critical forest parameters in fire behavior modeling. *Remote Sensing of Environment*, 86(2): 177-186.
- Riaño, D., Valladares, F., Condés, S. and Chuvieco, E., 2004. Estimation of leaf area index and covered ground from airborne laser scanner (Lidar) in two contrasting forests. *Agricultural and Forest Meteorology*, 124(3-4): 269-275.
- Solberg, S., Næsset, E., Hanssen, K.H. and Christiansen, E., 2006. Mapping defoliation during a severe insect attack on Scots pine using airborne laser scanning. *Remote Sensing of Environment*, 102(3-4): 364-376.
- The Cradle Coast Natural Resource Management Committee, 2005. Cradle Coast natural Resource Management Strategy, Burnie.
- Zimble, D.A. et al., 2003. Characterizing vertical forest structure using small-footprint airborne LiDAR. *Remote Sensing of Environment*, 87(2-3): 171-182.

Automatic detection of dominated vegetation under canopy using Airborne Laser Scanning data

Andrea Barilotti¹, Francesco Sepic² & Elena Abramo²

¹Department of Georesources and Territory, University of Udine, Via del Cottonificio
114, 33100, Udine (Italy), e-mail: andrea.barilotti@uniud.it

²e-laser srl, Via Jacopo Linussio, 51 –33100 Udine (Italy), e-mail:
francesco.sepic@e-laser.it, elena.abramo@e-laser.it

Abstract

In this paper we explore the potential of Airborne Laser Scanning to measure the understorey vegetation in variously composed Alpine forests, proposing an innovative method of laser scanning data processing to automatically determine the spatial distribution of the dominated layer. To this aim, a complete processing chain was developed, starting with the point cloud as input data and ending with derived three dimensional parameters for each single tree. First, the dominant trees are detected by means of a mathematical morphology approach. Afterwards, the laser points belonging to the single crowns are clustered and crown shapes are delineated. To enhance the quality of the calculated crown parameters (area, base height, volume), a statistical analysis of the height frequency distribution is performed which allows the re-filtration of the low vegetation (border or under-canopy vegetation). The extracted data, integrated in a GIS environment in order to create a database for the forestry sector, integrate the information on the vertical structure of the forest. A field survey campaign in some mountainous geo-referenced plots was performed in coniferous and mixed forests characterized by mono-storey and multistorey canopies. The results highlighted interesting performances of the re-filtering method as far as the automatic detection of the dominated vegetation in both forest typologies are concerned.

Keywords: LiDAR, Forestry, Tree extraction, Cluster analysis, Vertical structure, Understorey

1. Introduction

Monitoring of the forestry ecosystem is a current topic in the wooded resources sustainability debate. To characterize the vegetation from an ecological state and biomass content point of view, a detailed knowledge of the vertical structure is needed. In actual fact, the vertical structure of forest plays an important role in determining microclimatic conditions, the availability of niche space, habitat quality, the distribution of fuels and subsequent fire risk (Hill, 2007). Moreover, even if the majority of the above ground biomass is stocked in the dominant layer, information on the understorey layer can be essential to determine the carbon content of an ecosystem and is very important for forestry inventories (Patenaude et al., 2005). There are numerous case studies involving airborne laser scanning for the extraction of forest parameters at tree level (Andersen et al., 2001; Pyysalo and Hyyppä, H., 2002; Morsdorf et al., 2003; Hyyppä et al, 2004; Pitkänen et al, 2004; Weinacker et al., 2004, Tiede et al., 2005; Barilotti et al., 2007a). In these studies, the attention has been focused on assessing the dominant vegetation layer while, recently, a trend toward the undercover has been noticed (Zimble et al., 2003; Hyde et al., 2005; Maltamo, 2005; Barilotti et al., 2007b; Hill, 2007; Wang et al., 2007). Forests belonging to the alpine and boreal latitudes can have simple mono-storey structures or more complicated bi-storey or multistorey structures. In forests characterized by a heterogeneous vertical structure, photogrammetry and, in general, remote sensing techniques can have some limits concerning their capacity to furnish information on single trees. This is particularly true when understorey vegetation has no direct access to light and grow underneath a relatively close canopy (bi-storey forests). The structure in which the dominated vegetation

can have free access to light, even if it does not occupy the upper canopy (co-dominant layer) is relatively simpler. In this case, the laser scanning technique can be useful in order to distinguish single trees and, consequently, classify the stand structure.

In Maier et al. (2006) for instance, the authors developed an automatic approach for assessing and quantifying forest structure using landscape metrics on height class patches of the normalized crown model (nCM). Previously, Zimble demonstrated that differences between mono-storey and multistorey vertical structural classes could be detected with 97% of accuracy by analysing LiDAR-derived tree height variance. However, a common limit highlighted in these studies is that where the dominant trees form a dense and closed canopy it is not possible to distinguish the smaller trees and, consequently, the different forest structures. This is probably due to the fact that these approaches are essentially based on the LiDAR-extracted Crown Height Models. Consequently, the morphology of the canopy is the main source of information used. Maltamo et al. (2005) developed a histogram threshold method to calculate the distribution of LiDAR canopy height returns. The method (HistMod) was applied to the height distribution of laser points in order to classify them as uni or bi-modal distribution. In such a way they separated different forestry storeys. The results showed that multi-layered stand can be recognised and quantified using quantiles of laser scanner height distribution data. In this work, the analysis is carried out by using a plot-level approach.

It is clear that the method used and the plot compositions are not the only factors affecting the accuracy of the forestry parameters to be estimated. Goodwin et al. (2006) for instance investigated the effect of a number of intrinsic LiDAR survey specification by comparing the results from three different platform altitudes (up to 3000 meters), two different scan angles at flight altitude of 1000 m, and three footprint sizes (0.2, 0.4, and 0.6 m). The authors found that higher platform altitudes record a lower proportion of first/last return combinations, with the direct effect of reducing the number of laser points available for Digital Elevation Models and, subsequently, for forestry structure assessment.

The work reported in this paper makes use of multipulse LiDAR data acquired in leaf-on conditions in two different study sites. The method implemented for the understorey detection is based on firstly identifying the single trees and crowns belonging to the dominant storey. A subsequent algorithm makes it possible to automatically determine a local threshold value for filtering the clustered crowns and, at the same time, classifying the understorey point cloud. Field data is surveyed and used ad hoc for this study, both in mono-storey and in bi-storey forestry plots, enabling the method setting and the verification of the results obtained.

2.1 Study area

Two different study areas located in some mountainous sectors of the Friuli Venezia Giulia Region (N-E Italy) were investigated in this paper. The first area (MB) is essentially characterized by spruce, and spruce-fir, with a sparse presence of beech (Figure 1). As far as the vertical structure is concerned, the area is a managed mono-storey forest (zone marked as A2 in the image), without the presence of vegetation under the canopy. Significant for the aim of this study is the extensive presence of growing vegetation along the border line between forest and adjacent open stand (zone A1 in the image).

The second area (BA) is a bi-storey forest in which the higher level is dominated by black pine with a population density of about 530 trees/hectar (Figure 2). The dominant layer has a homogeneous stand structure and the canopy is relatively closed. The lower level is characterized by a natural regeneration of different species: hop hornbeam, pubescent oak, flowering ash. In this area different population densities are to be found with the result that two different sub-zones can be distinguished within this forest: one with dense homogeneous low vegetation (B1) and the other with more sparse vegetation (B2).



Figure 1: MB area, characterized by a mono-storey spruce forest. The average of crown base height is about 7-8 meters inside the forest (A2). The area shows the presence of border vegetation (A1).



Figure 2: BA area, characterized by bi-storey black pine forest with different low vegetation population density. In the B1 part the understorey vegetation has a regular pattern while in B2 it is irregular (patched).

Within these areas some sub-zones of interest have been located and geo-referenced using topographic total station and GPS. This has allowed the precise and accurate determination of the coordinates of 6 circular plots (transects), with radius ranging between 12 and 25 meters. The general forestry characteristics of these plots are reported in Table 1.

Table 1 – Summary of the geo-referenced forestry plot characteristics in the MB forestry area.

| Plot ID | trees /ha | Area (m ²) | Management type | Age | Composition | Structure |
|---------|-----------|------------------------|-----------------|----------|-------------|-------------|
| MBA | 619 | 450 | stand | mature | mixed | mono-storey |
| MBB | 1525 | 450 | stand | juvenile | spruce | mono-storey |
| MBC | 575 | 450 | stand | juvenile | spruce | mono-storey |
| MBD | 463 | 2000 | stand | mature | spruce | mono-storey |
| BAA | 536 | 2000 | stand | mature | black pine | bi-storey |
| BAB | 510 | 450 | stand | mature | black pine | bi-storey |

As far as the BA forestry area is concerned, the low vegetation was detected at area-level using GPS, enabling the detection of the small broad-leaved clumps of trees. In particular, two types of undercover were surveyed: regular pattern and patched.

The principal characteristics of the LiDAR datasets are reported in Table 2. As shown in the table, the datasets were surveyed in leaf-on condition. This must be taken into consideration, especially in the cases of beech forests because the presence of foliage decreases the capacity of the laser beam to penetrate the canopy and detect the intermediate strata (Barilotti et al. 2006).

Table 2 – Summary of the laser data characteristics for each forestry transect.

| Plot_ID | Period of survey | N° of echoes | Local point density |
|----------------|-------------------------|---------------------|----------------------------|
| MBA | June | Multiple | 6 pt/m ² |
| MBB | June | Multiple | 7 pt/m ² |
| MBC | June | Multiple | 8 pt/m ² |
| MBD | June | Multiple | 10 pt/m ² |
| BAA | June | Multiple | 5 pt/m ² |
| BAA | June | Multiple | 6 pt/m ² |

The datasets were detected using a multiple pulse laser scanner (Optech ALTM 3100) that increases the capacity to sample the intermediate layers of the vegetation if compared to the First & Last instrument. The flight altitude was about 1000 m above ground and the laser beam divergence was 0.2 mrad for both campaigns.

3. Method

A complete processing chain was developed, starting with raw laser points as input data and ending with derived tree parameters for each single tree of the dominant layer. The procedure is composed of a series of elaborations and transformations that can be schematically related to the following methodological aspects:

- Application of mathematical morphology algorithms, following a dynamic approach, to extract the canopy apexes (Barilotti et al, 2007a);
- Identification of the laser points belonging to the single crowns by means of a cluster analysis algorithm (Barilotti et al, 2007b).

Resuming this last point, the single crowns are identified by means of a region growing algorithm. Starting from the apexes previously extracted, the algorithm classifies the vegetation points according to the criteria defined below:

- If the points located in the proximity of the starting apex are lower (height difference) than a fixed threshold, these are marked as belonging to the same cluster;
- When the same laser point is marked as belonging to different apexes (this is particularly true when the forest is characterized by close vegetation), the algorithm associates the point to the nearest apex.

An example of clustered data resulting from this method is given in Figure 3.

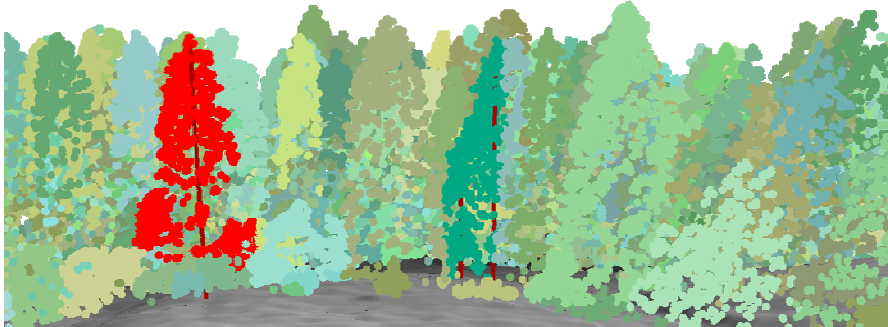


Figure 3: Example of clustered laser data in the ecotone of MB area. The red colored cluster emphasizes the cases in which the same cluster contains both dominant tree and dominated vegetation undercover.

As can be noticed, the cluster shape is not predefined but is closely related to the vertical distribution of the LiDAR point cloud. For this reason, if points reflected by low vegetation are recorded, they are located within the dominant clustered tree. A method for cluster filtering was implemented to isolate these low points. First, the histogram of the height frequency distribution of points is calculated cluster by cluster. Afterwards, a polynomial regression function is used to interpolate frequency histograms, obtaining a curve of frequency distribution for each one. Finally, the curves are explored by means of a study function looking for the presence or absence of a local frequency minimum. If this value is present, this is used as a threshold to perform a local filtering of the cluster, making it possible to eliminate those points that have less height than the class corresponding to the function minimum. An example of this process is given in Figure 4. The figure shows some different clusters of the MB area reported with their relative height frequency distribution (blue histograms) which was calculated using a height class of 1 meter. The first cluster is located within a mono-storey forested area (see figure 1-A2) while the other two clusters are located in the ecotone (see fig. 1-A1 and fig. 3). In the histogram images, the respective interpolating curves (in black) are reported as well.

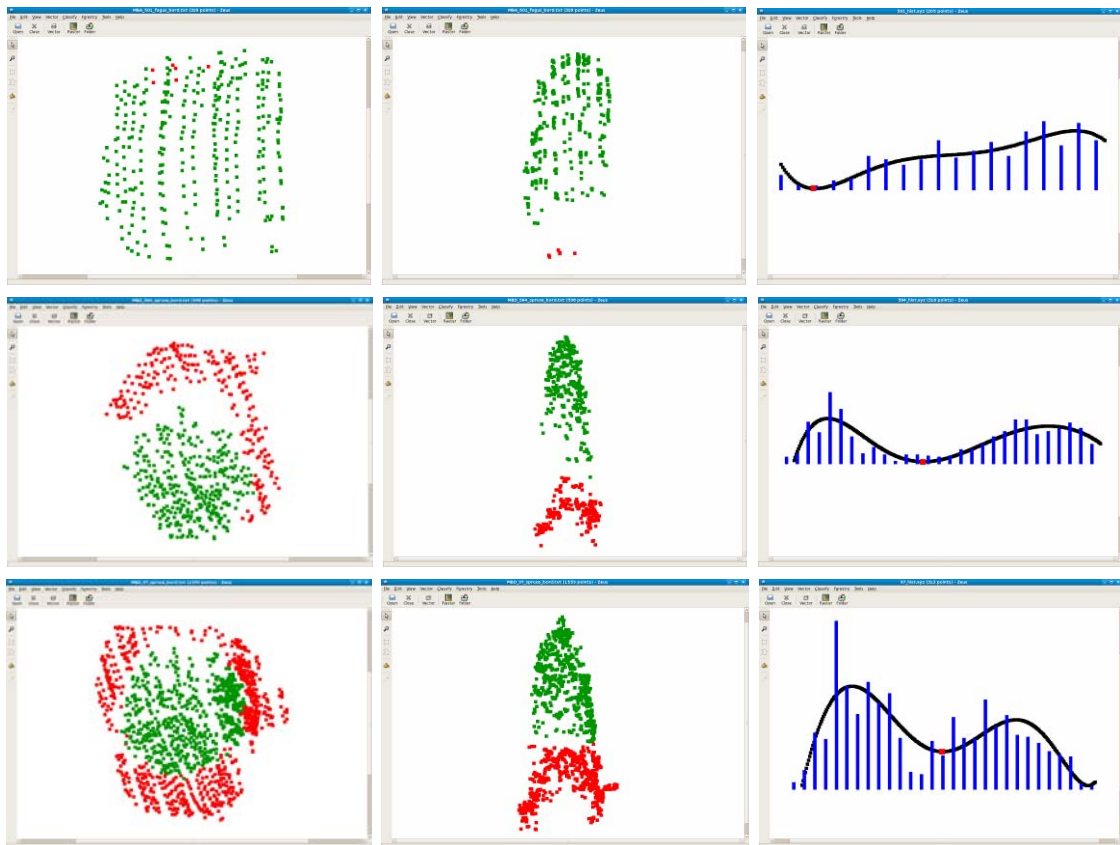


Figure 4: Cases of clustered trees located in different positions in the forest. From the top to the bottom respectively: tree within close vegetation and two trees dominating low vegetation. On the right the relative height frequency distribution of clusters is reported (blue line). For each frequency diagram, the polynomial regression is calculated (black line) and then it is used to re-filter the sub-clusters after its minimum (in red) is calculated by means of a study function.

In the three examples, the minimum of interpolated curves is reported in red. In the first cluster the minimum is found in the lower height classes and the curve shows an increasing trend. In this case, the tree seems to be well clustered and just a few low points are filtered. On the contrary, the other two examples (cases 2 and 3), showing a bi-modal trend, indicate the presence of anomalies in the height frequency distribution (higher point density in the lower classes of points). Such anomalies are evidently caused by the presence of vegetation under the dominant tree. Those points can be re-filtered and classified as low vegetation by using the curve minimums as local threshold value.

3. Results

Starting from this re-filtering approach on single clustered crowns, it is possible to obtain a zonal distribution of laser points belonging to the undercover vegetation. Two examples of the elaboration process are given in Figure 5 and 6. The left side shows in a green ramp color the clustered dominant layer while the re-filtered points, classified as belonging to the undercover vegetation, are shown in red. Those points are highlighted on the right side in the image sequence. The right side of the two figures also highlights the peculiar parts of the study areas:

1. the ecotone (A1) and the georeferenced transect (A2) in the mono-storey forest;
2. the dense undercover vegetation (B1) and the sparse one (B2) in the bi-storied forest.

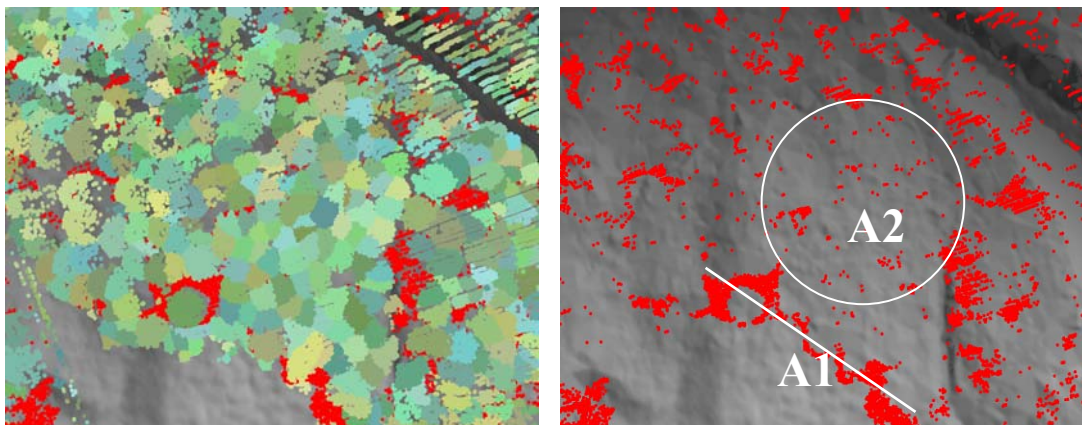


Figure 5: Example of cluster re-filtering method to locally isolate the low vegetation (red colored points) under dominant trees (green colored cluster) in the MB area. The ecotone (A1) and the mono-storey MBD transect (A2) are shown in white in the image on the right.

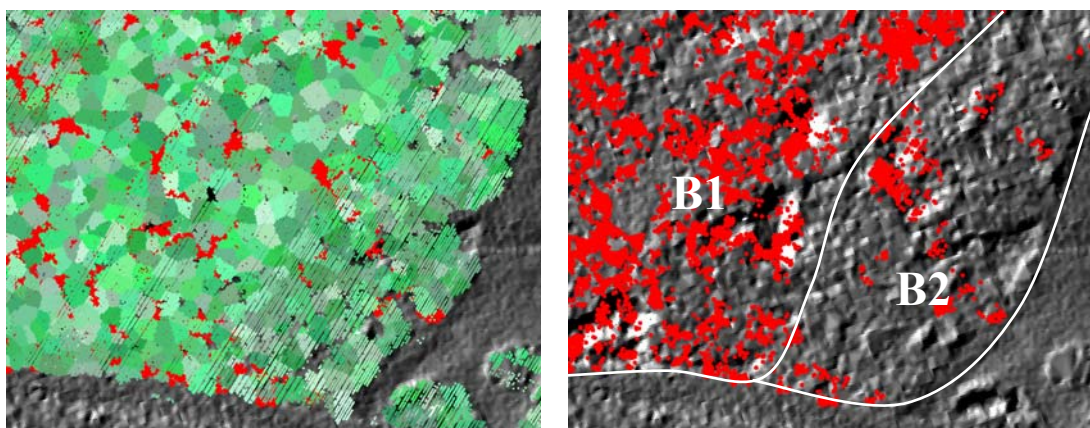


Figure 6: Example of cluster re-filtering method to locally isolate the low vegetation (red colored points) under dominant trees (green colored cluster) in the BA area. A dense understory zone (B1) and a sparse one (A2) are shown in white in the image on the right.

Some qualitative considerations are possible by comparing the LiDAR-extracted forestry layers and the corresponding field evidences. In the MB area, the first part of the ecotone is directly individuated by the tree extraction process, as a matter of fact that here the vegetation has a direct access to the light. The second part, composed by co-dominant trees (red points in the fig.5), was correctly individuated by means of the re-filtering process. As expected, in the mono-storey transects (e.g. A2) just few isolated points were removed from the clusters of the dominant storey. The elimination of these points does not seem to reduce the quality of dominant crown shape. On the contrary, those points can be considered as outliers because resulting from some random reflections on the lower part of the dominant layer (e.g. trunks or branches).

As far as the BA area is concerned, the re-filtering method enables the localization of the second storey. Differences between the two different composed areas (B1 and B2 in Fig. 6) are also mapped in terms of consistency: in B1 the low re-filtered points assume a homogeneous distribution, corresponding to the rather spread density of the understory vegetation. Differently, in B2 just few clusters of points are filtered given that in this area the second storey assumes a patched distribution. In this cases, confronting the field surveyed area of the dominated vegetation with the correspondent area resulting from the filtered points, an underestimation of about 15% was observed. This is probably due to the poor density of the LiDAR point clouds used in this work.

4. Discussion and conclusions

In this paper we explored the potential of Airborne Laser Scanning to measure the understorey vegetation in variously composed Alpine forests. A complete processing chain was developed, starting with the point cloud as input data and ending with derived three dimensional parameters for each single tree of the dominant layer as well as the automatic individuation of the understorey cover. As far as the dominant storey is concerned, the accuracy level of the extracted parameters is generally high as reported in the previously cited works.

Concerning the understorey, a statistical analysis of the height (z) frequency distribution was performed allowing the local (single tree level) re-filtration of the low laser points that belong to the forestry ecotone or to the under-canopy vegetation. The method enables the automatic determination of the spatial distribution of the dominated layer, without a-priori knowledge of the forestry structure.

Comparing the approach shown in this paper with the one presented in Maltamo et al. (2005), follows that both are based on the analysis of histogram of height frequency distribution of laser point cloud. However, in this paper a tree level analysis is used whereas a plot level analysis was performed in the paper by Maltamo et al. (2005). This could give significant differences when the study site is composed by heterogeneous bi-storey structure, particularly when the dominated level is characterized by different population heights. In these cases, the analysis carried out by the single tree approach should increase the capacity of the histogram method to find gaps between the two structural storeys.

A field survey campaign in some mountainous geo-referenced plots was performed in coniferous and mixed forests characterized by mono-storey and bi-storey structures. The analysis of the extracted data highlighted that the method is able to correctly individuate the areas characterized by the presence of dominate forestry layers. Moreover, the method does not introduce false positive vegetation layer in the mono-storey transects, as expected.

However, some problems in finding bi-modal frequency distribution has been noticed when the branches of under-storey are very close to the crowns of dominant layer. Moreover, the reduced penetration capacity of the laser beam in correspondence of very dense dominant storey contributes to affect the results in terms of understorey discrimination. Further studies will concern the application of the re-filtration method to the full waveform data that increases the capacity of LiDAR technique to collect data on lower vegetation strata.

The approach presented in this paper gives information on the existence and the area covered by the dominated tree layer. These information are of primary interest for forestry assessment and planning, due to high naturalistic value of bi-storied areas as peculiar habitats and also because of their relatively higher fire risk, compared to the mono-storey areas.

Starting from here, further works will be also devoted to investigate the possibility to obtain quantitative information on the number, size and composition of suppressed trees, which could be of interest in the determination of carbon content of the above ground biomass.

Acknowledgements

This work was carried out as a part of the research activities supported by the extension of the INTERREG IIIA Italy-Slovenia 2003-2007 project "Cadastral map updating and regional technical map integration for the Geographical Information Systems of the regional agencies by testing advanced and innovative survey techniques". We thank the Civil Protection Agency of the

Friuli Venezia Giulia Region that has kindly furnished some of the laser scanning data used in this work.

References

- Andersen, H.E., Reutebuch, S.E., Schreuder, G.F., 2001. Automated Individual Tree Measurement through Morphological Analysis of a LIDAR-based Canopy Surface Model. *Proceedings of the first International Precision Forestry Cooperative Symposium*, Seattle, Washington, 2001.
- Barilotti, A., Turco, S., Alberti, G., 2006. LAI determination in forestry ecosystem by LiDAR data analysis. *Proceedings of the International Workshop 3D Remote Sensing in Forestry*, pp. 248-252, Wien, 14-15 Feb. 2006.
- Barilotti, A., Sepic, F., Abramo, E., Crosilla, F., 2007(a). Improving the morphological analysis for tree extraction: a dynamic approach to lidar data. *Int. Archives of Photogrammetry, Remote Sensing and Spatial Information Sciences*, Vol. XXXVI, Part 3/W52.
- Barilotti, A., Sepic, F., Abramo, E., Crosilla, F., 2007(b). Assessing the 3D structure of the single crowns in mixed alpine forests. *International Archives of Photogrammetry, Remote Sensing and Spatial Information Sciences*, Vol. XXXVI, 3/W49A.
- Goodwin, N., Coops, N.C., Culvenor, D.S., 2006. Assessment of forest structure with airborne LiDAR and the effects of platform altitude. *Remote Sensing of Environment*, 103, 140-152.
- Hill, R.A., 2007. Going undercover: mapping woodland understorey from leaf-on and leaf-off lidar data. *International Archives of Photogrammetry, Remote Sensing and Spatial Information Sciences*, Vol. XXXVI, Part 3/W52.
- Hyde, P., Dubayah, R., Peterson, B., Blair, J.B., Hofton, M., Hunsaker, C., Knox, R., Walker, W., 2005. Mapping forest structure for wildlife habitat analysis using waveform lidar: Validation of montane ecosystems. *Remote Sensing of Environment*, 96, 427 – 437.
- Hyypä, J., Hyypä, H., Litkey, P., Yu, X., Hagrré, H., Rönnholm, P., Pyysalo, U., Pitkänen, J., and Maltamo, M., 2004. Algorithms and methods of airborne laser scanning for forest measurements. *International Archives of Photogrammetry, Remote Sensing and Spatial Information Sciences*, Vol. XXXVI - 8/W2.
- Hyypä, J., Mielonen, T., Hyypä, H., Maltamo, M., Yu, X., Honkavaara, E., Kaartinen, H., 2005. Using individual tree crown approach for forest volume extraction with aerial images and laser point clouds. *ISPRS WG IIIA, V/3 Workshop "Laser scanning 2005"*, Enschede, Sept. 12-14.
- Maier, B., Tiede, D., Dorren, L., 2006. Assessing mountain forest structure using airborne laser Scanning and landscape metrics. *Proceedings of the International Conference on Object-Based Image Analysis*, Salzburg, Austria, July, 4-5, 2006.
- Maltamo, M., Packalén, P., Yu, X., Eerikäinen, K., Hyypä, J. and Pitkänen, J. 2005. Identifying and quantifying structural characteristics of heterogeneous boreal forests using laser scanner data. *Forest Ecology and Management*, 216, 41-50.
- Morsdorf, F., Meier, E., Koetz, B., Nüesch, D., Itten, K., Allgöwer, B., 2003. The potential of high resolution airborne laser scanning for deriving geometric properties of single trees. In *EGS - AGU - EUG Joint Assembly*, Nice, France. 2003.
- Patenaude, G., Milne, R., Dawson, T.P., 2005. Synthesis of remote sensing approaches for forest carbon estimation: reporting to the Kyoto Protocol. *Environmental Science & Policy*, 8, 161-178.
- Pitkänen, J., Maltamo, M., Hyypä, J., 2004. Adaptive methods for individual tree detection on airborne laser based canopy height model. *International Archives of Photogrammetry, Remote Sensing and Spatial Information Sciences*, Vol. XXXVI - 8/W2.
- Pyysalo, U. and Hyypä, H., 2002. Reconstructing Tree Crowns from Laser Scanner Data for Feature Extraction. *ISPRS Commission III Symposium*, Graz, Austria, 2002.
- Tiede, D., Hochleitner, G., Blaschke, T., 2005. A full GIS-based workflow for tree identification and tree crown delineation using laser scanning. *IAPRS, Vol XXXVI, Part 3/W24*, Vienna, 29-30 Aug. 2005.

- Weinacker, H., Kock, B., Heyder, U., Weinacker, R., 2004. Development of filtering, segmentation and modelling modules for LiDAR and multispectral data as a fundament of an automatic forest inventory system. *International Archives of Photogrammetry, Remote Sensing and Spatial Information Sciences*, Vol. XXXVI – Part 8/W2, 2004.
- Wang, Y., Weinacke, H., Koch, B., 2007. Development of a procedure for vertical structure analysis and 3d-single tree extraction within forests based on lidar point Cloud. *International Archives of Photogrammetry, Remote Sensing and Spatial Information Sciences*, Vol XXXVI, Part 3/W52, 2007.
- Zimble, D. A., Evans, D. L., Carlson, G. C., Parker, R. C., Grado, S. C., Gerard, P. D., 2003. Characterizing vertical forest structure using small-footprint airborne LiDAR. *Remote Sensing of Environment*, 87, 171-182.

Canopy and gap dynamics analysed using multi-temporal airborne laser scanner data in a temperate deciduous forest

Yasumasa Hiarta¹, Hiroshi Tanaka² & Naoyuki Furuya³

¹Forestry and Forest Products Research Institute (FFPRI), Tsukuba, Japan,

[e-mail: hirat09@affrc.go.jp](mailto:hirat09@affrc.go.jp)

²Kyusyu Research Center, FFPRI, Kumamoto, Japan

³Japan International Research Center for Agricultural Sciences, Tsukuba, Japan

Abstract

Forest measurement using airborne laser scanner makes it possible to obtain detailed information of canopy surface including its roughness and its applicability for the studies of gap dynamics in natural forest is considerably high. This study aims to compare multi-temporal canopy surface conditions using multi-temporal airborne laser scanner data and to extract gaps in a canopy for the clarification of gap dynamics in a temperate deciduous forest. The study was conducted in the 6-ha (300m*200m) permanent plot in the Ogawa Forest Reserve. The laser scanner data were acquired on 24 August 2001, 14 April 2002 and 9 August 2005. Digital canopy models (DCM) were created from the data in 2001 and in 2005. Gaps were extracted from each DCM using the threshold, which was decided from the vertical distribution of heights above the ground where lasers reach. Gap dynamics are classified into four patterns, i.e., appearance, enlargement, reduction, and disappearance, and the number of gaps for each pattern was strongly affected by the gap size. For the gaps that were classified into the reduction and the disappearance, their annual decreased areas (S_{diff}) could be described using their gap sizes (S_{gap}) as $S_{diff} = 1.03S_{gap}^{0.64}$ ($R^2=0.75$).

Keywords: airborne laser scanner data, canopy, digital canopy model, gap dynamics

1. Introduction

Natural disturbance is one of most important factors for the structure and succession of forest communities (White, 1979; Pickett and White, 1985). Gaps in a canopy that occur after natural disturbance alter light condition in a forest stand. Crown growth of trees that consist of canopy layer in the edge of gaps and height growth of trees consist of second layer are promoted by the appearance of gaps. Nevertheless the importance of gaps to understand forest dynamics, it is difficult to evaluate them quantitatively from the ground observation. In previous studies, the methods to detect gaps from multi-temporal DSM derived from stereo-pair aerial photographs (Nakashizuka *et al.*, 1995; Tanaka and Nakashizuka, 1997; Itaya *et al.*, 2004; Ticehurst *et al.*, 2007) and from the difference between a past aerial photograph and a late high-resolution satellite image (Clark *et al.*, 2004) were proposed. In these methods, however, there is a likelihood that the difference of shade between aerial photographs or images in different seasons leads to mis-interpretation of gaps particularly in steep slopes. Measurement of forest using airborne laser scanner makes it possible to obtain detailed information of canopy surface including its roughness and its applicability for the studies of gap dynamics is considerably high. This study aims to compare multi-temporal canopy surface conditions using multi-temporal airborne laser scanner data and to clarify gap dynamics in a temperate deciduous forest.

2. Methods

2.1 Study area

This study area was located in the Ogawa Forest Reserve at the southern end of Abukuma Mountains, central Japan (36°56' N, 140°35' E, 610 - 650 m above sea level). The mean annual temperature is 9.0 °C, with the highest monthly mean of 20.5 °C in August and the lowest one of -1.6 °C in February. Annual precipitation is about 1750 mm, concentrated in August and September, and there is little rainfall in December and January. Maximum snow depth is occasionally 50 cm in winter, but it usually melts away in a few days. The forest has been protected from human impact for 80 years or more. There are more than 50 woody species in it, dominated by *Quercus serrata* Murray, *Fagus japonica* Maxim., and *Fagus crenata* Blume.

2.2 Plot description and field data

The study was conducted in the 6-ha (300m*200m) permanent plot in the Reserve. This permanent plot has been established since 1987 for the long-term ecological research (Nakashizuka *et al.*, 1992). All trees with 5cm of the diameter at breast height (DBH) in the plot were identified, tagged and measured. The plot was divided into 10m*10m quadrats and a pole has been put at each corner of quadrat. All trees were remeasured every four years. Detailed delineations of the stand structure and dynamics of the community are available in Masaki *et al.* (1992), Nakashizuka *et al.* (1992), and Abe *et al.* (1995).

Geographic coordinates at pole positions established at four corners of the plot and those of every 100 m-interval were positioned using a differential GPS (Ashtech Solution, USA) and they were calculated as the UTM coordinates (datum: WGS84) with the measurement data and the data of electric ground control point, which were offered by the Agency of Geographic Survey, in post-processing. Other poles were measured using a laser range finder (LaserAce 300, Measurement Devices, UK) and their geographic coordinates were calculated with the results. The data concerning individual trees in 2001 were used for the study. Positions of trees, which formed canopy layer, were measured from a nearest pole using the laser range finder.

2.3 Airborne laser scanner data

The ALMAPS (Asahi Laser Mapping System), which consists of the ALTM 1225 or ALTM 3100 laser scanning system produced by the Optech, Canada, the GPS airborne and ground receivers, and the inertial measurement unit (IMU) reporting the helicopter's roll, pitch and heading, was used to acquire the laser scanner data. The laser scanner system transmits the laser pulse at 1064 nm (near-infrared) and receives the first and last echoes of each pulse. The elapsed time between transmittance and receipt is measured to calculate the distance between the system and the object.

The laser scanner data were acquired on 24 August 2001 and 14 April 2002 using ALTM 1225, and 9 August 2005 using ALTM 3100. For the measurement in 2001, the flight altitude of the helicopter above the ground was about 250 meters and the average of the flight speed was approximately 13.9 m/sec. The pulse repetition frequency was 25 kHz and the scan frequency was 25 Hz. Maximum scan angle (off nadir) was 12°. The beam divergence was 1.0 mrad. Measurement density was 25.0 points/m². Therefore, the footprint diameter was approximately 25 cm and the distance between neighbouring footprints was about 20 cm. For the measurement in 2002, the flight altitude of the helicopter above the ground was about 300 meters and the average of the flight speed was approximately 13.9 m/sec. The pulse repetition frequency was 25 kHz and the scan frequency was 30 Hz. Maximum scan angle (off nadir) was 10°. The beam divergence was 1.0 mrad. Measurement density was 31.9 points/m². Therefore, the footprint diameter was approximately 30 cm and the distance between neighbouring footprints was about

18 cm. For the measurement in 2005, the flight altitude of the helicopter above the ground was about 500 meters and the average of the flight speed was approximately 19.4 m/sec. The pulse repetition frequency was 70 kHz and the scan frequency was 27 Hz. Maximum scan angle (off nadir) was 18°. The beam divergence was 1.2 mrad. Measurement density was 50.2 points/m². Therefore, the footprint diameter was approximately 60 cm and the distance between neighbouring footprints was about 14 cm. Both first pulse and last pulse were acquired to extract forest canopy and topography in rugged terrain.

Digital elevation model (DEM) and digital surface model (DSM) for the plot were prepared from the airborne laser scanner data with 25cm cell size (Figure 1). DEM was generated from the last pulse data acquired in the leafless season in 2002. Digital surface model (DSM) was generated as assigning highest value of first pulse data of each full-leaved season in 2001 and 2005 involving in each cell to the cell value.

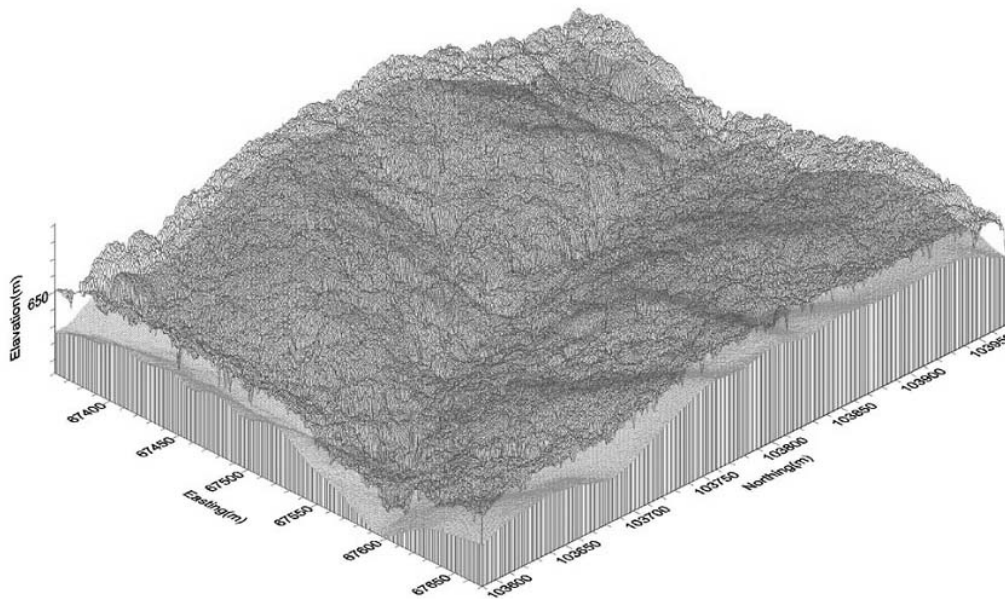


Figure 1: DSM and DEM of the study area derived from airborne laser data.

2.4 Data Analysis

Clarification of gap dynamics requires understanding of multi-temporal canopy surface condition. Digital canopy model (DCM), which delineates canopy height from the ground, was created by subtracting the DEM from each DSM of full-leaved season. The canopy heights using DCM in 2001 and 2005 were compared and change of canopy heights for 4 years from the difference between them was investigated.

Gap is defined as “open hole in canopy which occurs due to loss of crowns that consist of canopy”. While gaps appear owing to the death, uprooting, stem breakage and so on, definitions such as the size and the height are not clear (Nakasizuka *et al.*, 1995). In this study, we defined the gap as the area where canopy height is lower than a certain height above the ground. Here, we assumed three thresholds to extract gaps from DCM, that is, 15 m, 10 m and 5 m. Gap size was defined as more than 1 m² for noise reduction. An area, which was extracted as a gap, was converted to a polygon of vector format. The area of gap of each polygon was calculated and the number of gaps and the total area in 2001 and in 2005 were investigated.

The gap dynamics are classified into four patterns, that is, appearance (Figure 2 (a)), enlargement (Figure 2(b)), reduction (Figure 2(c)) and disappearance (Figure 2(d)) in comparison with gaps of two periods. Gaps, which occur newly, come from death, uprooting, stem breakage and so on. Enlargement of an existing gap is caused by death, uprooting, stem breakage of trees around the gap and isolated tree in the gap. Reduction of a gap results from both the height growth of trees in second layer in the gap and the enlargement of crown of trees around the gap. Finally, this reduction leads to the close of gap, that is, disappearance. We investigated the gap dynamics of the study area from these patterns and the speed of gap closing against gap size.

3. Results and discussion

Mean heights of canopy derived from the DCM and their standard deviations in 2001 and 2005 were shown in Table 1. The difference of mean canopy heights was 0.48m and its slight growth was identified. While the increase of canopy height arises from height growth of individual trees as well as closing process of gaps due to enlargement of crowns that are located around gaps, the decrease of canopy height results from occurrence of new gaps. The growth of canopy height comes from the balance of them.

The number and total area of extracted gaps by threshold was shown in Table 2. The number of extracted gaps by area class using the threshold below 15 m was shown in Table 3. The number of gaps, which area was less than 5 m², is more than half of the total number, and the area class of 10 to 50 m² was next to that.

The summary of gap dynamics by area class was shown in Table 4. We selected larger area of a gap in 2001 and the same in 2005 as “area of a gap” in Table 4. We found from Table 4 that a large gap with the area of more than 100 m² appeared during the period. We confirmed that this gap was caused by the uprooting of *F. Japonica* M. and some stem breakages of surroundings, which resulted from the uprooting from field survey. In general, the appearances of gap, which are caused by uprooting or stem breakage near the ground trend to become large in comparison with ones from death of standing trees. Enlargement of gap could be found in all area classes, and the ratio of the number against the total number of gaps in area class was smaller in small area class. Reduction in gap dynamics patterns could be found in all area classes of gap except the smallest area class. The ratio of disappearance in the smallest area class was largest instead of the pattern of reduction. There were few gaps which area was constant during the period.

Relationship between gap area in 2001 (S_{gap}) and annual decreased area of the gap (S_{diff}) was shown in Figure 3. This relationship could be expressed as follow;

$$S_{\text{diff}} = 1.03 S_{\text{gap}}^{0.64} \quad (R^2=0.75) \quad (1)$$

When crown enlargement of trees around a gap is found in the process of gap closing, a gap, which has large area, are surrounded by many trees and, as a result, closing area of gap becomes large.

In this analysis, the period between two forest measurements of airborne laser scanner was only 4 years; therefore, contribution of trees in second layer or understory to gap closing process was not found. However, gap closing requires much time when gap size is large and it is considered that annual decreased area of a gap is composed of both enlargement of crowns that are located around the gap and intrusion of trees in second layer to canopy layer. Continuous monitoring of canopy condition using airborne laser scanner is required to clarify the dynamics in natural forest.

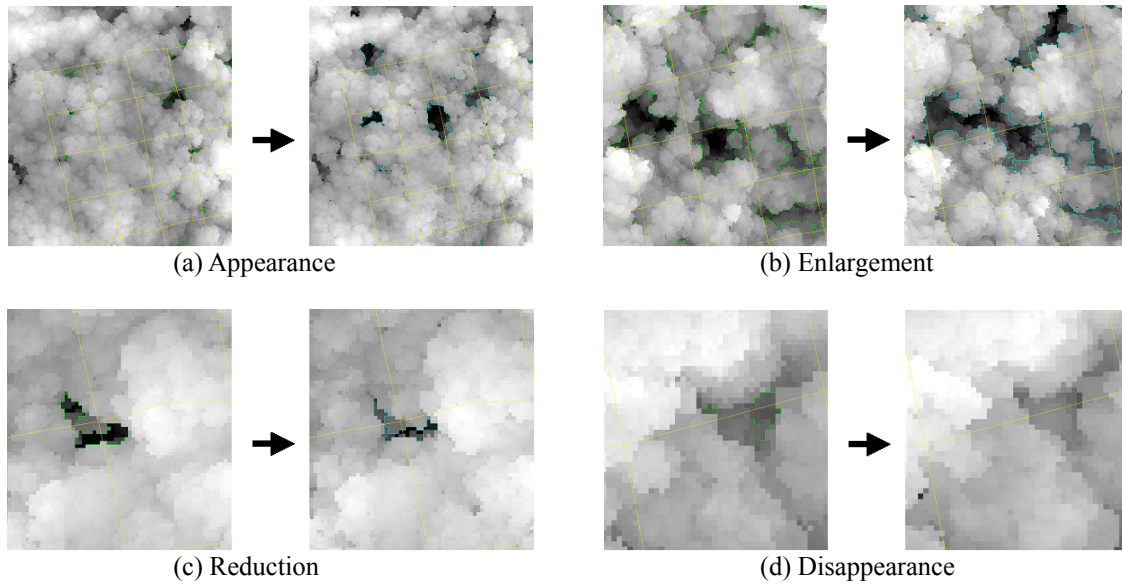


Figure 2: Patterns of gap dynamics.

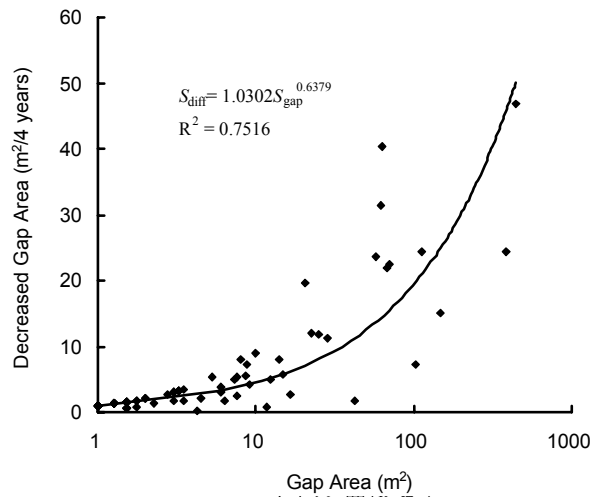


Figure 3: Relationship between gap area and annual decreased area of the gap.

Table 1: Mean heights of canopy and their standard deviation in 2001 and 2005.

| Year | Mean height (m) | Standard deviation (m) |
|------|-----------------|------------------------|
| 2001 | 22.03 | 3.88 |
| 2005 | 22.51 | 4.07 |

Table 2: The number and total area of extracted gaps by thresholds.

| Threshold (m) | The number of gaps | | Total area (m ²) | |
|------------------|--------------------|---------|------------------------------|---------|
| | 2001 yr | 2005 yr | 2001 yr | 2005 yr |
| 5 | 18 | 26 | 170 | 171 |
| 10 | 55 | 52 | 930 | 972 |
| 15 | 113 | 116 | 3048 | 3234 |

Table 3: The number of extracted gaps by area class using the threshold below 15 m.

| Area of a gap (m ²) | 2001 yr | 2005 yr |
|---------------------------------|---------|---------|
| >100 | 8 | 8 |
| 50-100 | 7 | 5 |
| 10-50 | 20 | 24 |
| 5-10 | 17 | 13 |
| 1-5 | 61 | 56 |
| Total number | 113 | 116 |

Table 4: The summary of gap dynamics by area class.

| Area of a gap (m ²) | Appearance | Enlargement | Reduction | Disappearance | No change |
|---------------------------------|------------|-------------|-----------|---------------|-----------|
| >100 | 1 | 3 | 6 | 0 | 0 |
| 50-100 | 0 | 3 | 5 | 0 | 0 |
| 10-50 | 4 | 8 | 11 | 0 | 0 |
| 5-10 | 1 | 7 | 9 | 2 | 1 |
| 1-5 | 18 | 3 | 8 | 37 | 4 |
| Total number | 24 | 23 | 40 | 39 | 5 |

4. Conclusions

In this study, we examined to apply airborne laser scanner data to the clarification of gap dynamics in a temperate deciduous forest. The patterns of gap dynamic were classified four categories, that is, occurrence, enlargement, reduction and disappearance, and the trend of dynamics was clarified. Monitoring of canopy condition using airborne laser scanner makes it possible to evaluate gap dynamics quantitatively, and further acquisitions of airborne laser scanner data a expected to contribute to ecological studies of natural forest dynamics.

Acknowledgements

This work was supported by the program of the Ministry of Education, Culture, Sports, Science and Technology. We thank Yukihide Akiyama and Kazunori Iwamura at Aero-Asahi Co. for their supports of data pre-processing. We also thank to Kaoru Niiyama, Mitsue Shibata, Asako Miyamoto and Hidesato Kanomata for the field survey and their useful comments about dynamics of the temperate deciduous forest.

References

- Abe, S., Masaki, T. and Nakashizuka, T., 1995. Factors influencing sapling composition in canopy gaps of a temperate deciduous forest. *Vegetatio*, 120, 21-32.
- Clark, D.B., Read, J.M., Clark, M.L., Cruz, A.M., Dotti, M.F., and Clark, D.A., 2004. Application of 1-m and 4-m resolution satellite data to ecological studies of tropical rain forests. *Ecological Application*, 14, 61-74.
- Itaya, A., Miura, M., and Yamamoto, S., 2004. Canopy height changes of an old growth evergreen broad-leaved forest analyzed with digital elevation models. *Forest Ecology and Management*, 194, 403-411.
- Masaki, T., Suzuki, W., Niiyama, K., Iida, S., Tanaka, H. and Nakashizuka, T., 1992. Community structure of a species rich temperate forest, Ogawa Forest Reserve, central Japan. *Vegetatio*, 98, 97-111.
- Nakashizuka, T., Iida, S., Tanaka, H., Shibata, M., Abe, S., Masaki, T. & Niiyama, K., 1992. Community dynamics of Ogawa Forest Reserve, a species rich deciduous forest, central Japan. *Vegetatio* 103, 105-112.
- Nakashizuka, T., Katsuki, T. and Tanaka, H., 1995. Forest canopy structure analyzed by using aerial photographs. *Ecological Research* 10, 13–18.
- Pickett, S.T.A. and Ehite, P.S., 1985. The ecology of natural disturbance and patch dynamics. Academic Press, New York.
- Tanaka, H. and Nakashizuka, T., 1997. Fifteen years of canopy dynamics analyzed by aerial photographs in a temperate deciduous forest, Japan. *Ecology*, 78, 612-620.
- Tichehurst, C., Phinn, S., and Held, A., 2007. Using multitemporal digital elevation model data for detecting canopy gaps in tropical forests due to cyclone damage: An initial assessment. *Austral Ecology*, 32, 59-69.
- White, P.S., 1979. Pattern, process, and natural disturbance in vegetation. *Botanical Review*, 45, 229-299.

Forest microclimate modelling using gap and canopy properties derived from LiDAR and hyperspectral imagery

Z. Abd Latif, G.A. Blackburn

Division of Geography, Lancaster Environment Centre,
Lancaster University, Lancaster LA1 4YQ, United Kingdom.
z.abdlatif@lancs.ac.uk, alan.blackburn@lancs.ac.uk

Abstract

The creation of gaps in forest canopies can dramatically change the microclimate and soil water balance which strongly influences the process of regeneration and biodiversity within forest ecosystems. Hence, understanding the microclimatic conditions in canopy gaps is a prerequisite in developing and improving techniques for forest management and conservation practices. However, information is scarce on how the size and shape of gaps and their spatial distribution affects the microclimate and soil water balance across forest stands. In the present study we investigated the potential for retrieving forest gap and canopy attributes from LiDAR and hyperspectral sensors in order to provide new opportunities for modelling forest microclimates. A spatially explicit microclimate model (FORGAP-3D) was developed which could be driven using inputs from remote sensing. The model was implemented for a study site in the New Forest, UK in order to quantify the spatio-temporal dynamics of microclimates over an entire forest stand. Further work will focus on improving the methods for deriving gap and canopy properties from LiDAR and hyperspectral data and evaluating the impact of these techniques on the accuracy of microclimate model outputs.

Key words: Hyperspectral, LiDAR, Meteorology, Spatial, Three-dimensional

1. Introduction

Forests are crucial to the well being of humanity; they provide foundations for life on Earth through ecological functions, by regulating the climate and water resources, and by serving as habitats for plants and animals. In temperate forests wind throw often creates canopy gaps which can dramatically change the microclimate and soil water balance (Spice *et al.*, 1990, Yamamoto, 1995). Hence, understanding the microclimate conditions in canopy gaps is a prerequisite in developing and improving techniques for forest management and conservation practices. Figure 1 demonstrates the nature of these changes, in general terms. However, information is scarce on how precisely gap size and shape affects the microclimates within canopy gaps and beneath surrounding tree canopies and how the spatial distribution of gaps influences microclimates across entire forest stands.

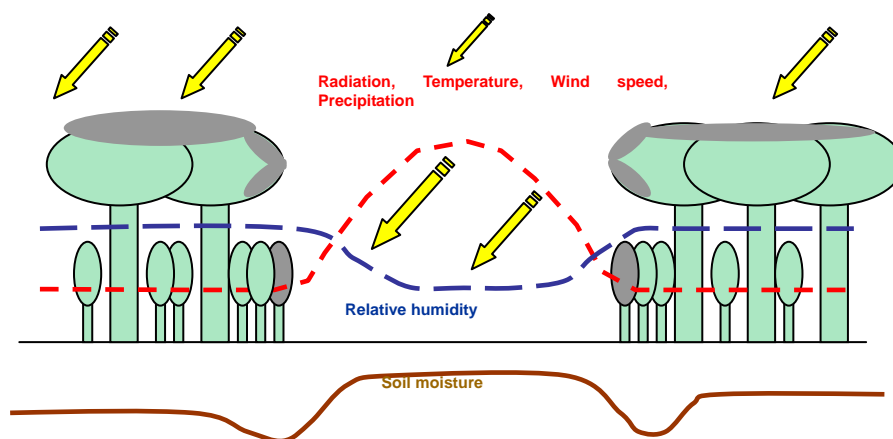


Figure 1. Gradients of microclimate conditions and soil moisture in forest canopy gaps. The grey areas on the vegetation represent the parts of the crowns that can receive direct solar radiation.

Remote sensing is increasingly seen as an important tool for providing information for the achievement of sustainable and efficient forest management. The past decade has seen growing interest in the use of remote sensing technologies in forest studies. Devices such as Light Detection and Ranging (LiDAR) and hyperspectral sensors together with new analytical techniques allow increasingly detailed information to be extracted from such imagery. LiDAR technology is becoming capable of providing 3-dimensional information at high spatial resolutions and vertical accuracies (Lee and Lucas, 2007). Hyperspectral data provides much finer spectral resolution than conventional multispectral data. Forest attributes such as crown heights and individual canopy gap delineations can be directly retrieved from LiDAR data (Koukoulas and Blackburn, 2005) while tree species classifications may be derived from hyperspectral imagery (Lucieer *et al.*, 2005). LiDAR is a relatively new technology that offers an alternative to *in situ* field surveys and photogrammetric techniques for the collection of elevation data. LiDAR provides accurate, timely data, is capable of operating in difficult terrain and is increasingly affordable (Flood and Gutelius, 1997). With high spatial resolution remotely sensed imagery, the spatial properties and composition of tree canopies and gaps can be obtained over large areas. With the capabilities of direct retrieval of forest attributes offered by remote sensing, this provides new opportunities to model forest gap microclimates. Modelling the spatial patterns of microclimates in a gap and its surroundings using traditional methods would require a large volume of ground-based measurements and many model runs in order to cover a large spatial extent. By developing an inherently spatial microclimate model and driving this with inputs from remote sensing we have the potential to quantify forest gap microclimates over entire forest stands. This study aims to examine the feasibility of such an approach using a case study of a broadleaved deciduous forest in the UK.

2. Data collection

2.1 Study site

The LiDAR and hyperspectral imagery used for this research were collected at Frame Wood, New Forest (1°30'W, 50°50'N), southern England, an area recognized as being of international importance to nature conservation. There are 4049 ha. of unenclosed primary woodland where the dominant tree species are *Quercus (pendula and pubescens)* and *Fagus sylvatica*. *Betula (pendula and pubescens)* can be found mainly in canopy gaps and in association with *Quercus* spp.. The specific study site, Frame Wood presents a wide range in all of the gap and canopy

variables of interest, being described by Flower (1977) as primary woodland dominated by *Quercus robur*. Previously, this area has been the focus of a number of ecological remote sensing studies (e.g. Koukoulas and Blackburn, 2004, 2005).



Figure 2: Location of the New Forest, U.K.

2.2 Airborne data

The LiDAR data used in this research were acquired by the UK Environment Agency (EA) using an Optech Airborne Laser Terrain Mapping (ALTM) 1020. The altitude of the aircraft was 730 m (2400 ft) above the ground level and a swath width of approximately 600 m was surveyed along each flight line. The laser scans across the aircraft flight line at 5000 light pulses per second (at 1047 nm wavelength), sweeping left and right in a zig-zag movement over the ground. Individual measurements were made at approximately 1 return per square metre. The travel times of the laser pulses, from the aircraft to the ground and vice versa, were measured with a precise timer. This instrument recorded the time of the first returned pulse. The time intervals are then converted into range measurements using the velocity of light. In this way, the surface height is calculated to accuracy of within 15 cm. The LiDAR data provided contained single return.

Imagery of the study site was also acquired using an Itres Compact Airborne Spectrographic Imager (CASI) onboard the Natural Environment Research Council (NERC) Airborne Research and Survey Facility. The aircraft altitude was 670 m (2200 ft) which generated imagery with a spatial resolution of 1 m. The CASI instrument acquired imagery in 12 narrow wavebands across the visible and near-infrared.

3. Methodology

3.1 Derivation of a Canopy Height Model and gap delineation

Gap identification from LiDAR imagery was performed using Erdas Imagine (v.9.1) and ArcGIS (v.9.2) software (Environmental Systems Research Institute, Inc.). Canopy heights were

derived from LiDAR data; however an estimate of the ground elevation is needed. Because the LiDAR sensor recorded only the first return, a digital terrain model (DTM) was constructed from elevation data provided by the U.K. Ordnance Survey (OS). A canopy height model (CHM) was calculated as the difference between elevation values in the LiDAR data and ground elevation at corresponding locations. Figure 3 shows the CHM model where tree heights are classified into five classes for display purposes. Based on the field visits of previous work by Koukoulas and Blackburn (2005), it was determined that the height below which areas would be identified as gaps should be between 3 and 5 m. Thus, the height of 4 m was therefore selected as the threshold for distinguishing canopy from gap areas. From the CHM all grid cells with a height less than or equal to 4 m were assigned as gap areas.

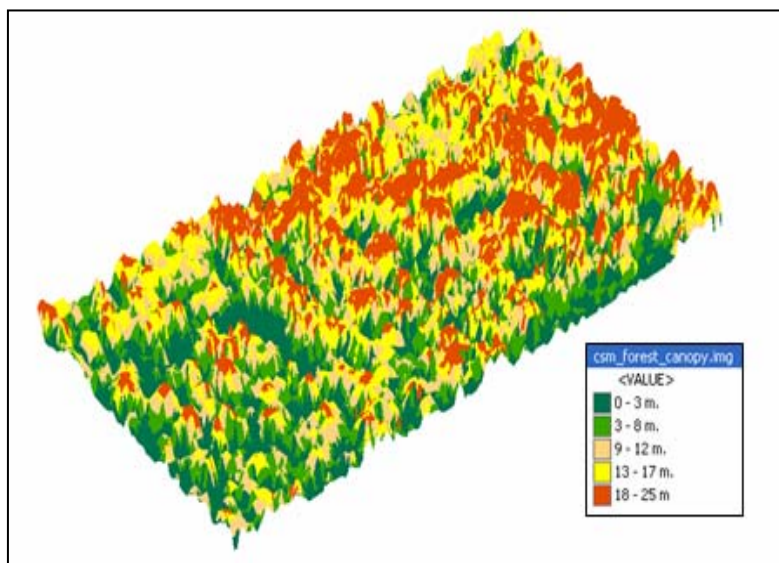


Figure 3. Canopy Height Model (CHM) extracted from LiDAR data.

3.2 Derivation of LAI

Leaf area index (LAI) is a major parameter in understanding forest microclimate and a key input to forest microclimate models in order to quantify the interception of light by the canopy. The following relationship, derived from a previous work at the study site (Blackburn, 2002) between a simple ratio (SR) of CASI bands 12/3 and LAI ($R^2 = 0.71$) was used:

$$LAI = 0.6348 (SR) - 1.3985 \quad (3)$$

where Simple Ratio (SR) = $NIR_{CASI} / Green_{CASI} = 865 \text{ nm} / 553 \text{ nm}$

3.3. Forest gap microclimate modelling

A spatially explicit model of forest gap microclimates and soil water balance was developed based on previous reviewed literatures and field measurements of microclimates and soil water balance (Van Dam, 2001). FORGAP-3D is written in the dynamic script modelling language PcRaster (PcRaster, 1995) and comprises two sub-modules, radiation and soil water balance. The radiation module calculates the potential radiation on the vegetation, the potential radiation on the saplings in the gap and area surrounding the gap and the potential radiation on the soil. The second sub module calculates the soil moisture content at 5cm depth both within gaps and

beneath the forest canopy. FORGAP-3D was developed to be driven by a set of spatial inputs derived from remote sensing (canopy height, gap map and LAI) together with a DEM and meteorological data from a nearby weather station (Figure 4). In order to refine the model, future work will concentrate on validation using ground-based micrometeorological measurements.

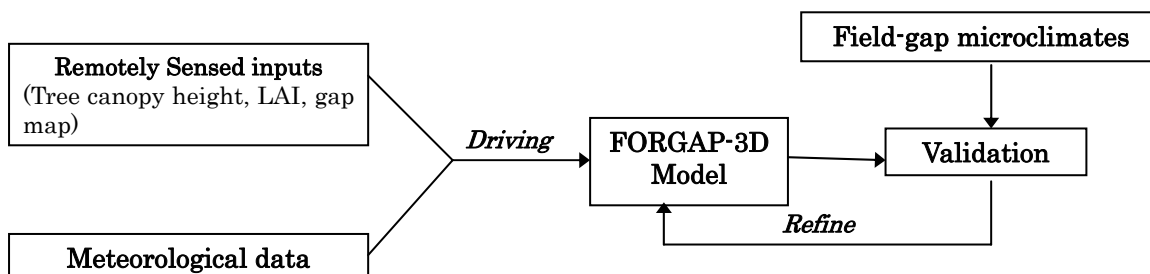


Figure 4. Methodological framework of the integration of remotely sensed and meteorological data into the FORGAP-3D model.

4. Results and Discussion

Gap areas extracted from the LiDAR data in Frame wood are shown in Figure 5 while the map of LAI derived from CASI is shown in Figure 6.

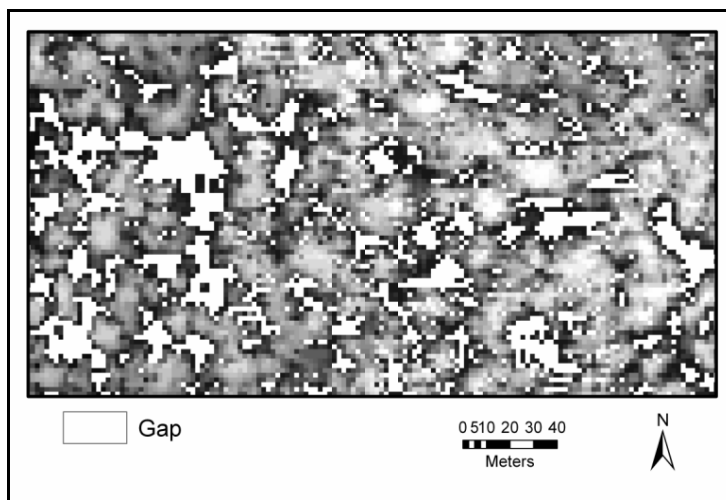


Figure 5. Canopy gaps in Frame Wood as estimated from the CHM. Gaps are shown as white areas outlined in black.

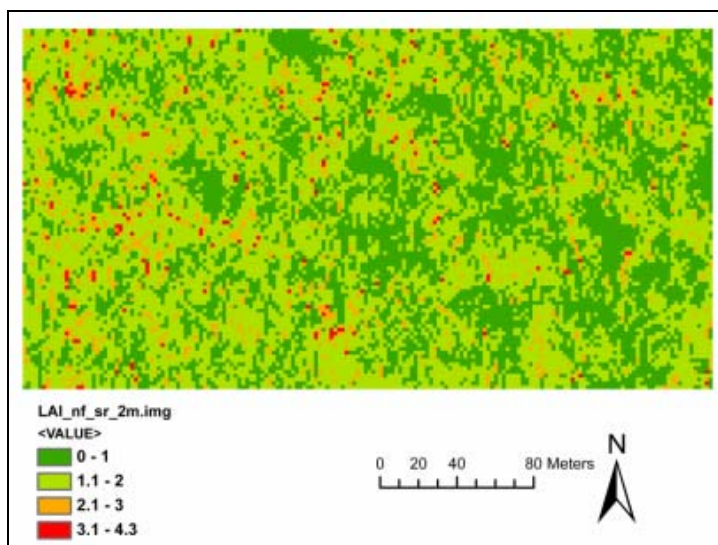


Figure 6. LAI map of study area derived from CASI.

The spatial data above were used to drive the FORGAP-3D model in order to generate both spatial and temporal simulations of forest microclimates. In order to demonstrate the output from the FORGAP-3D model, Figure 7 shows diurnal time series of microclimate conditions (total radiation, air temperature, relative humidity and wind speed) for a specific location at the centre of a gap as well as a location beneath the adjacent forest canopy. At solar noon total solar radiation in the gap was higher than that beneath the adjacent forest canopy by 192 W.m^{-2} . Likewise air temperature and wind speed was higher at the gap centre than beneath the forest. However, relative humidity values were lower than in the forest at noon. Figure 8 shows examples of the spatial output from FORGAP-3D for a specific time point (solar noon), which illustrates the detailed spatial information concerning microclimate that the model is able to generate.

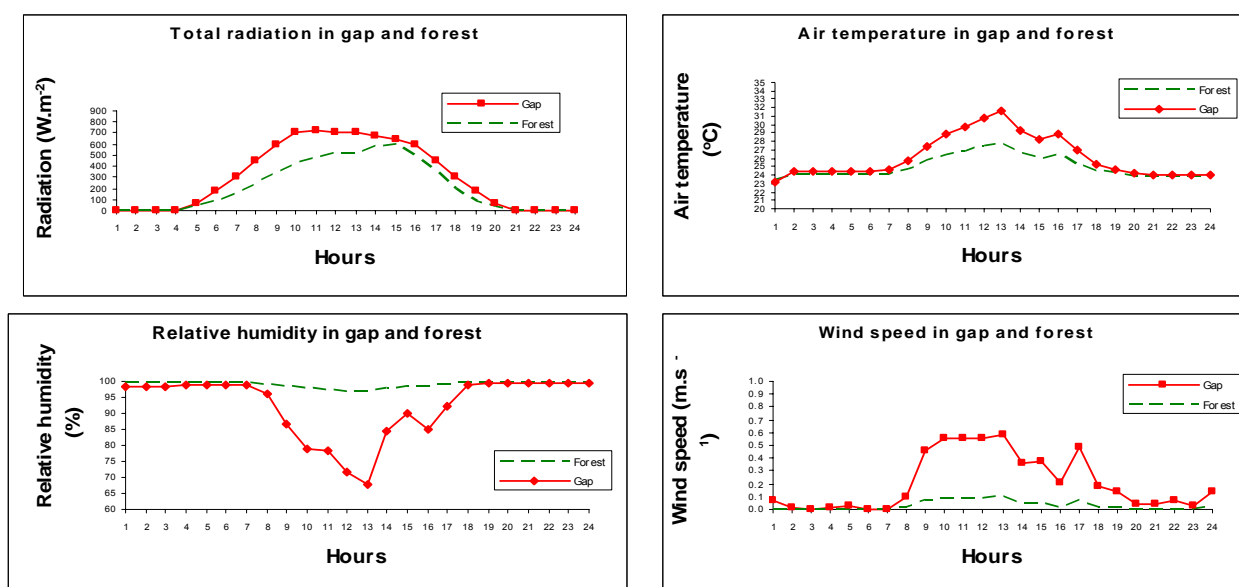


Figure 7. FORGAP-3D diurnal pattern outputs of total solar radiation, air temperature, wind speed and relative humidity at a gap centre and beneath the adjacent forest canopy.

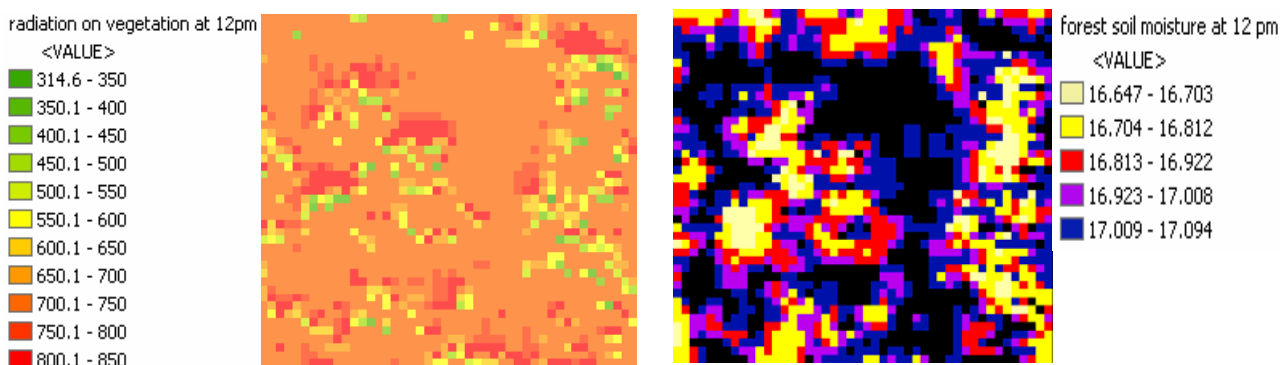


Figure 8. Examples of the spatial output from FORGAP-3D for a sample area within Frame Wood at a specific point in time (solar noon). Area covered by each image is 50 x 50m.

5. Conclusion

This preliminary study has demonstrated that remote sensing is a promising tool for forest microclimate modelling, in particular when combining LiDAR and hyperspectral data sources. The use of remote sensing technology greatly reduces the time and fieldwork effort required and can provide a comprehensive set of spatial information that is difficult to obtain using traditional methods. Forest gap microclimate modelling can be a valuable tool for understanding the spatio-temporal characteristics of microclimates within gaps and across the entire forest landscape. Remote sensing provides an increasing variety of spatial data layers that are potentially useable as model input. This study has demonstrated that it is possible to drive a simulation model using gap and canopy data derived from remote sensing in order to generate spatial and temporal estimates of microclimate. Further work will focus on improving the methods for delineating gaps and extracting canopy properties from LiDAR and hyperspectral data, driving the model using a seasonal time series of gap and canopy variables and evaluating the impact of these techniques on the accuracy of microclimate model outputs.

Acknowledgements

We are grateful to Research Committee, Lancaster University for providing research and equipment grants, the UK NERC ARSF for the provision of CASI imagery and the UK Environmental Agency for the LiDAR data.

References

- Brokaw, N.V.L.,1982. The definition of treefall gap and its effect on measures of forests dynamics. *Biotropica*, 14, 158-160.
- Chason, J.W., Baldocchi, D.D., Huston, M.A., 1991. A comparison of direct and indirect methods for estimating forest canopy leaf area. *Agricultural and Forest Meteorology*, 57, 107–128.
- Flood, M. and Gutelius, B., 1997. Commercial applications of Topographic Terrain Mapping Using Scanning Airborne Laser Radar. *Photogrammetric Engineering and Remote Sensing*, 63, 327 pp.
- Flower, N., 1977. An historical and ecological study of enclosed and unenclosed woods in the New Forest, Hampshire. *Ph.D. Thesis, Department of Geography, King's College*,

University of London, London, U.K.

- George, C., Rowland, C., Gerard, F. and Baltzer, H., 2006. Retrospective mapping of burnt areas in Central Siberia using a modification of the normalized difference water index. *Remote Sensing of Environment*, 104, 346-359.
- Koukoulas, S. and Blackburn, G.A., 2004. Quantifying the spatial properties of forest canopy gaps using LiDAR imagery and GIS, *International Journal of Remote Sensing*, 25 (15), 3049-3071.
- Koukoulas, S. and Blackburn, G.A., 2005. Spatial relationships between tree species and gap characteristics in broad-leaved deciduous woodland. *Journal of Vegetation Science*, 16, 587-596.
- Lee, A.C and Lucas, R.M., 2007. A LiDAR-derived canopy density model for tree stem mapping in Australian forests. *Remote Sensing of Environment*, 111, 493-518.
- Lucieer, A. Stein, A. and Fisher, P., 2005. Multivariate texture-based segmentation of remotely sensed imagery for extraction of objects and their uncertainty. *International Journal of Remote Sensing*, 26(14), 2917-2936.
- Nemani, R. and Running, S.W., 1996. Implementation of a Hierarchical Global Vegetation Classification in Ecosystem Function Models. *Journal of Vegetation Science*, 7(3), 337-346.
- PCRaster, 1995. PCRaster manual. *Department of Physical Geography Utrecht University, Netherlands.*
- Pontailleur, J.Y, Hymus, G.J. and Drake, B.G., 2003. Estimation of leaf area index using ground-based remote sensed NDVI measurements: validation and comparison with indirect techniques. *Canadian Journal of Remote Sensing*, 29(3), 381-387.
- Prskawetz, M. and Lexer, M.J., 2000. Evaluierung des LI-COR LAI-2000 zur Ermittlung des Blattflächenindex in Buchenjungbeständen. *Allgemeine Forst- u. Jagdzeitung*, 171, 185 – 191.
- Spice, T.A., Franklin, J.F., and Klopsch, M., 1990. Canopy gaps in Douglas-fir forests of the Cascade Mountains. *Canadian Journal of Forest Research*, 20, 649-658.
- Yamamoto, S.-I., 1995. Gap characteristics and gap regeneration in a subalpine old-growth coniferous forests, central Japan, *Ecological Research (Tokyo)*, 10, 31-39.

Height growth of regeneration in boreal forest canopy gaps – does the type of gap matter? An assessment with lidar time series

Udayalakshmi Vepakomma¹, Benoit St-Onge² & Daniel Kneeshaw³

¹Institut des sciences de l'environnement, Email: udayalakshmi_v@yahoo.co.uk

²Département de géographie, Email: st-onge.benoit@uqam.ca

³Département des sciences biologiques, Email: kneeshaw.daniel@uqam.ca
Université du Québec à Montréal, Centre-ville, Montréal, Canada, H3C3P8.

Abstract

Large canopy gaps in old-growth forests, formed as a result of tree fall events over time, could be composed of regeneration in various stages of growth different from that of single mortality events. Though important to understand forest dynamics such complex processes are rarely monitored due to limited techniques. Applying object-based techniques on a series of three lidar datasets acquired over nine years in boreal forests, we characterised gap events into old gaps, gap expansions and new random gaps. Combining broad species class from high resolution images, and individually locating gap saplings on the lidar surface, specieswise height growth across gradients of height was estimated. The results indicate distinct height growth patterns of both hardwood and softwood gap saplings in different gap events. The methods can potentially be extended to develop accurate juvenile growth patterns.

Keywords: height-growth, multi-temporal lidar, gap dynamics, advanced regeneration

1. Introduction

Canopy gaps created by the fall of one or more overstory trees are important for regeneration dynamics in old-growth forests (Pickett and White 1995). The availability of increased site resources enhances the height growth rates of all species within canopy gaps. Research in various forest systems showed that sapling height growth is a function of gap characteristics, such as gap size (Kneeshaw and Bergeron 1998). Due to the vulnerability of gap edge trees to mortality, some larger canopy gaps could be a result of tree fall events over successive periods of time (Runkle and Yetter 1987, Foster and Reiners 1986). As a consequence, such large gaps in an old-growth forest could be composed of regeneration in different stages of growth whereas gaps formed from a single mortality event should have a single regeneration cohort. Hence it is important to characterise the type of gap events to forecast growth patterns of the regeneration. However, gap formation (expansion vs a single event) is rarely investigated due to the difficulty in collecting data and the limited techniques available for monitoring canopy gaps over time. Moreover, measurement of a canopy gap, gap dynamic characteristics like gap expansions and closure and reliable measurement of height-growth in the field is complex. Conventional remote sensing based methods have been criticized for inadequately identifying gaps (Koukoulas and Blackburn 2004) while assessment of vegetation height is prone to error in closed canopies (St-Onge *et al.* 2004).

In recent decades lidar has emerged as a powerful tool in remote sensing to accurately measure canopy height and vertical structure (Lefsky *et al.* 2002). Owing to its high density and accuracy, the potential to detect tree fall and growth estimation using multi-temporal discrete small-foot print lidar data sets was also shown in a few recent studies (Hopkinson *et al.* 2008, Yu *et al.* 2006, Naesset and Gobakken 2005, St-Onge and Vepakomma 2004). Using tree matching

techniques on high density lidar, Yu *et al.* (2006) showed a good correspondence with field measurements. Lidar was effective in observing significant growth at plot and stand levels (Naesset and Gobakken 2005) and in detecting annual conifer growth (Hopkinson *et al.* 2008). St-Onge and Vepakomma (2004) compared and confirmed acceptable results of dissimilar density lidar data for expected forest height growth. Vepakomma *et al.* (2008a) validated the feasibility of using medium density small-foot print lidar to map several gap dynamic characteristics like canopy gap opening and closure of sizes ranging from 5 m² to 9.8 ha. Nonetheless, no studies have yet been conducted to characterise height growth patterns of vegetation in canopy gaps using lidar.

Assuming lidar accuracy and potential to estimate changes in forest growth with similar and dissimilar densities from earlier studies, we characterise the height growth patterns of gap saplings growing following different gap events by analysing a time series of lidar data. Using a validated method to locate individual trees/ sapling tops and identify their species class (hardwood or softwood), we quantified the height growth rates of saplings over four years in canopy gaps. By delineating the canopy gaps and identifying the nature of gap events as old existing gaps, new gap expansions and new random gaps, we investigated whether the height growth patterns vary between them.

2. Methods

2.1 Study area

The study site is within the conservation zone of the Teaching and Research Forest of Lake Duparquet (TRFLD, 79°22'W, 48°30'N), in the Province of Quebec, Canada. This area is characterized by small hills that vary in elevation between 227 m and 335 m. The mixed vegetation of this part of forest is composed of common boreal species, dominated by balsam fir (*Abies balsamea* L. [Mill.]), paper birch (*Betula papyrifera* [Marsh.]), and trembling aspen (*Populus tremuloides* [Michx]). The stand level age structure found at this site results from a fire driven disturbance regime (1760-1919), and a recent infestation of a defoliating insect (1970-1987) called the spruce budworm (*Choristoneura fumiferana* [Clem]). Most stands are mature or over mature reaching heights of up to 25 m. The climate is cold temperate with an average annual temperature of 0.8° C with annual precipitation of 857 mm. The frost free period lasts for nearly 64 days, while the length of the growing season is on average 160 days (Environment Canada 1993).

2.2 Lidar data

A time series of lidar data in three time steps was collected on June 28th 1998, August 14 to 16 2003, and July 15th, 2007. The 1998 survey was carried out using an Optech ALTM1020 flown at 700 m above ground level (AGL) operating at a pulse frequency of 5 kHz. with two passes for the first returns and one pass for the last returns, resulting in 0.3 and 0.03 hits/m² respectively. The 2003 survey was done with Optech's ALTM2050 lidar flown at 1,000 m AGL, with 50 kHz and 50% overlap between adjacent swaths resulting in 3 and 0.19 hits/ m². The 2007 survey was conducted using ALTM 3100 flown at 700 m AGL with 67 kHz and over 50% overlap between adjacent swaths resulting in 10 hits/ m² for the first returns. All returns were classified by the provider as ground and non ground and were assumed correct for the study.

Accuracy assessment of lidar derived canopy heights for 1998 and 2003 was carried out in two different studies with 36 (1998) and 77 (2003) field measured trees ranging in height from 5.6 m – 33.1 m that yielded an r^2 of 0.88 and 0.86 with an RMSE of 1.8 m and 1.85 m respectively (Véga and St-Onge 2008, Coops *et al.* 2004). It is to be noted that at the time of this study, the accuracy assessment of the 2008 data using field measurements was not performed. However,

visual and statistical comparisons of the 2007 CHM with high resolution images from the 2007 and 2003 lidar data sets showed a good match.

2.3 Lidar surface and gap characterisation

The three datasets were co-registered for temporal comparisons using the methods suggested by Vepakomma et al. (2008a). The Digital terrain model (DTM) was generated by combining the last returns in 1998 and 2003. The time series of canopy height distributions or canopy height models (CHMs) were generated using an optimised grid resolution (0.25 m) and an interpolation algorithm (a combination of local maxima and an inverse distance method) for accurate and reliable delineation of gap geometry. Defining a gap as an opening in the canopy caused by the fall of a single or a group of trees of a certain height (greater than 5 m, determined in the field), a highly accurate ground validated algorithm on the lidar CHMs was used to explicitly map canopy gaps for each of the years. Mapped gaps are individual objects of contiguous binary grid cells determined by a gap indicator function (Eq. 1). The comparison of 29 gaps measured in the field along 980 m of transect length with lidar delineated gaps showed a good matching of 96.5% overall accuracy.

$$G_i(x, y) = \begin{cases} 1 & \text{if } CHM_i(x, y) < a \\ 0 & \text{otherwise} \end{cases} \quad (1)$$

where $a = 5$ m in this study, $CHM_i(x, y)$ is the lidar height of the canopy surface in the i th year, (x, y) is a cell that does not belong to any open-ended system.

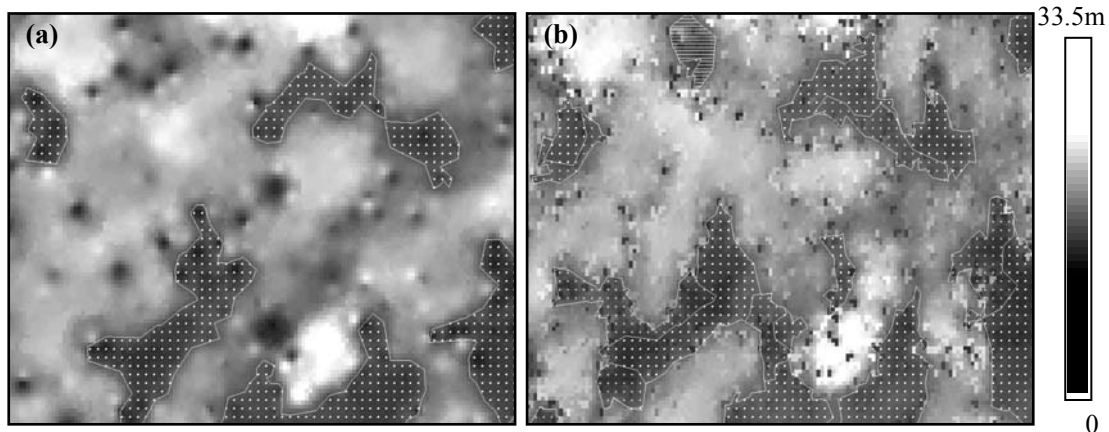


Figure 1: An example of automatically delineated canopy gaps. (a) Gaps in 1998 (dotted objects) overlaid on CHM_{1998} (b) Old gaps (dots), new gap expansions (crosses) and new random gaps (lines) that appeared between 1998 – 2003 overlaid on CHM_{2003} .

Gap objects were delineated on 1998 and 2003 lidar surfaces. We define old gaps as those gaps that are open in 1998 and 2003 while gaps that opened between 1998 and 2003 are new gaps. New gaps that share the edge of an existing gap in 1998 are gap expansions, otherwise they are considered new random gaps. Areas where the difference in vegetation height between 1998 and 2007 within a gap is greater than 5 m, i.e. the smallest difference that is considered to be too high for vertical growth, and contiguous with the gap edge, are classified as lateral growth of adjacent vegetation. Separating laterally growing gaps from regenerating areas reduces ambiguity in height growth patterns of regeneration. We performed various combinatorics on the delineated gap objects of 1998 and 2003 to define the nature of the gap events, namely, old gaps, new gap expansions and new random gaps. An example of automatically delineated canopy gap events is shown in Fig. 1.

2.4 Species class delineation

Orthorectified high resolution multi-spectral Vexcel UltraCamD image data acquired five weeks prior to the 2007 lidar data was used to classify the vegetation of the study area into broad species classes, namely, hardwood (HW) and softwood (SW). Canopy height derived from the lidar data was integrated with the spectral signatures of the image data to automatically extract individual image objects using eCognition v. 3.0. The overall accuracy of the image classification based on a comparison matrix with 25 hardwood and softwood field identified trees, and 15 open grown, non-forest locations is 91.5%.

2.5. Identifying Maximum Tree Height Locations and Extraction of Growth Statistics

Height growth statistics for individual saplings were estimated based on raw lidar returns from 2003 and 2007 extracted after identification of sapling tops on the CHM_{2007} . A local maxima filter with a circular non-overlapping (moving) window was applied to the CHM_{2007} to derive a layer of sapling apices, $LMAX(x,y)$. Local maxima filtering is a common technique first adopted to identify trees in high resolution optical imagery and successfully extended to lidar surfaces (Popescu and Wynne, 2004). We selected a search radius of 5 pixels (1.25 m) equal to the average crown radius of 30 visually interpreted sapling crowns of varying maximum heights (3-5 m). A local maximum within a search window that matches the height on the CHM i.e. $LMAX(x,y) = CHM_{2007}(x,y)$, is assumed to be the maximum height ($TMAX(x,y)$, hereafter $TMAX$) of the sapling crown. This method applied on CHM_{2003} was previously validated with 940 trees and saplings identified using manual photogrammetric methods on Ultra Cam D images of 2007 elsewhere in the study area (Vepakomma *et al.*, 2008b). An example of identified sapling tops is seen in Fig. 2.

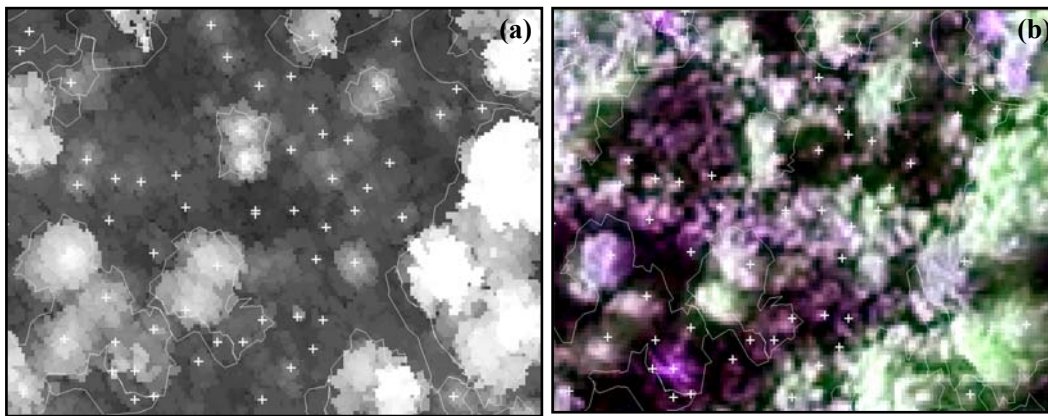


Figure 2: Identification of sapling tops (crosses) along with gap edges (solid line) shown on (a) the CHM_{2007} (b) UltraCam D Image of 2007. CHM brightness is proportional to the canopy height

Lidar raw point clouds of the vegetation (first returns) of 2003 and 2007 were extracted within a buffer zone of 0.5 m radius around each sapling top of $TMAX$. In order to make the lidar datasets of varying densities comparable, the lidar sampling point densities within these buffers were matched by randomly selecting n_i sample points for both years such that

$$n_i = \min(n_i^{2003}, n_i^{2007}) \quad (2)$$

where n_i^{2003} and n_i^{2007} are the number of first returns within the i^{th} buffer zone in 2003 and 2007 respectively. All buffer zones were further constrained to have a minimum point density of 3 hits /m² and a lidar determined height not less than 2 m of the zonal maxima to minimise

possible errors due to insufficient representation of canopy apices and lidar penetration into the foliage.

Sapling height growth was calculated as the differences in height of the sample maximum (MAXGTH) and sample average (AVGGTH) of the 2003 and 2007 first returns. Reference average (AVG03) and maximum (MAX03) sapling height for each buffer zone are the sample average and sample maximum of the difference in the height of the 2003 lidar first returns and their respective ground elevation extracted from the DEM. Growth rates in terms of average growth per unit height (AGTH), i.e. (AVGGTH / AVG03), and maximum growth per unit height (MGTH), i.e. (MAXGTH / MAX03) were used to assess growth. It is to be noted that MGTH and AGTH computed here are the rates of growth over the four growing seasons and being proportional growth they are unit free measures. Thus a MGTH value of 0.2 signifies a 20% maximum growth increase from its 2003 maximum reference height.

2.6. Height growth patterns of regeneration in canopy gaps

To understand if height growth patterns differ based on the nature of the gap events, we considered three windows with varying gap fraction (percentage of gap area) that constituted a total size of 26 ha. Since hardwood and softwood trees have different architecture and respond differently to available resources, we assessed AGTH and MGTH based on species class across gradients of sapling height and also between the gap events using:

- (1) exploratory statistics
- (2) scatterplots and
- (3) non-parametric regression estimation of MGTH given the initial height of the sapling.

To investigate whether distinction of the type of gap events is important for understanding growth patterns of regenerating saplings in gaps, we compare the statistics and models generated separately by pooling the sapling data.

3. Results

3.1. Canopy gap characteristics and sapling height

Delineation of canopy gap events indicates that about 16.8% of the study area is in canopy gaps during 1998 – 2003 of which 13.1% is composed of old gaps that opened before 1998 (Table-1).

Table 1: Gap characteristics in the study area

| <i>Statistic</i> | <i>Old gaps</i> | <i>Expansion*</i> | <i>Random*</i> | <i>Pooled</i> |
|---------------------------------|-----------------|-------------------|----------------|---------------|
| <i># Gaps</i> | 420 | 617 | 80 | 483 |
| <i>Total area in gaps (m2)</i> | 34028.7 | 8667.5 | 861.38 | 43557.58 |
| <i>% area in gaps</i> | 13.1 | 3.3 | 0.3 | 16.8 |
| <i>Minimum gap size (m2)</i> | 5.01 | 5.02 | 5.26 | 5.01 |
| <i>Maximum gap size (m2)</i> | 2988.7 | 288.9 | 87.3 | 6024.5 |
| <i>Mean gap size (m2)</i> | 80.9 | 149.8 | 28.7 | 104.9 |
| <i># of saplings identified</i> | 388 | 52 | 12 | 452 |
| <i>Avg. sapling height (m)</i> | 3.28 | 3.06 | 2.1 | 3.23 |
| <i>Mean MGTH (AGTH)</i> | 0.4 (0.7) | 1.23 (0.76) | 1.14 (0.6) | 0.76 (0.6) |

* Both expansions and random are new gaps that opened between 1998-2003

During the period 1998 - 2003, gaps are seen to be expanding at a higher rate and more frequently than the formation of random gaps. Average gap size of gap expansion is almost twice the average size of old gaps and seven times the average size of new random gaps. However, average gap size of pooled data is the largest at 6024.5 m².

In all, 452 gap saplings with a height ranging between 0.5 – 5.0 m were automatically identified in the 26 ha study area, of which 85% belong to the old gaps (Table-1). On average, the saplings in new gap expansions are fast growing compared to those in new random and old gaps. In all cases, the correlation between average and maximum sapling height generated by the two lidar datasets (2003, 2007) is very high at over 0.97 suggesting that growth between the two periods can be measured using multi-temporal lidar data.

3.3. Height growth patterns in canopy gaps

The average and maximum height of saplings in old gaps are higher than in new gaps (Table 2). The range of sapling height in old gaps is greater than that of saplings in new gaps. Except for saplings in old gaps, the maximum growth rates are higher than average growth rates. However, the height growth of HW and SW saplings within old and new gaps and between gap events is highly significant (Kruskal-Wallis ANOVA by ranks and Median tests, $p \approx 0$). SW saplings are taller than HWs in all the gap events (Table -2). The results indicate that HW saplings in old gaps and gap expansions are growing at a faster rate than SWs, but the contrary is noted in new random gaps. Though maximum MGTH is noted for HW saplings in old gaps, HWs are growing only slightly faster than SWs. On the other hand, HWs are growing at twice the rate of SWs in new gap expansions. Scatter plots and predictive models (Figs. 3 and 4) indicate that the height growth of saplings in all gap events is considerably different.

Table 2: Summary of growth statistics during 2003 – 2007 in various gap types

| <i>A. Hardwood sapling (s# Saplings in Old gaps : 138; new gap expansions: 23; new random gaps : 6)</i> | | | | | | | | | | | | |
|---|-----------------|------------|-------------|---------------------------|------------|-------------|------------------------|------------|-------------|---------------|------------|-------------|
| <i>Variable</i> | <i>Old gaps</i> | | | <i>New gap expansions</i> | | | <i>New random gaps</i> | | | <i>Pooled</i> | | |
| | <i>Min</i> | <i>Max</i> | <i>Mean</i> | <i>Min</i> | <i>Max</i> | <i>Mean</i> | <i>Min</i> | <i>Max</i> | <i>Mean</i> | <i>Min</i> | <i>Max</i> | <i>Mean</i> |
| <i>AVG03</i> | 0.42 | 6.53 | 3.25 | 0.30 | 4.34 | 2.34 | 0.82 | 2.94 | 1.43 | 0.30 | 6.53 | 3.06 |
| <i>MAX03</i> | 0.42 | 6.65 | 3.39 | 0.30 | 4.85 | 2.42 | 0.82 | 2.94 | 1.43 | 0.30 | 6.65 | 3.19 |
| <i>AVGGTH</i> | 0.10 | 4.8 | 0.90 | 0.01 | 5.45 | 1.26 | 0.01 | 2.02 | 0.50 | 0.12 | 19.60 | 1.25 |
| <i>MAXGTH</i> | 0.02 | 4.7 | 1.31 | 0.09 | 4.76 | 1.67 | 0.60 | 3.53 | 0.97 | 0.10 | 19.60 | 1.83 |
| <i>AGTH</i> | 0.10 | 4.8 | 0.40 | 0.02 | 2.72 | 1.15 | 0.50 | 2.13 | 0.62 | 0.01 | 5.45 | 0.61 |
| <i>MGTH</i> | 0.00 | 4.7 | 0.52 | 0.02 | 3.78 | 1.23 | 0.20 | 3.73 | 1.01 | 0.02 | 4.79 | 0.79 |

| <i>B. Softwood saplings: (# Saplings in Old gaps : 250; new gap expansions: 29; new random gaps : 6)</i> | | | | | | | | | | | | |
|--|-----------------|------------|-------------|---------------------------|------------|-------------|------------------------|------------|-------------|---------------|------------|-------------|
| <i>Variable</i> | <i>Old gaps</i> | | | <i>New gap expansions</i> | | | <i>New random gaps</i> | | | <i>Pooled</i> | | |
| | <i>Min</i> | <i>Max</i> | <i>Mean</i> | <i>Min</i> | <i>Max</i> | <i>Mean</i> | <i>Min</i> | <i>Max</i> | <i>Mean</i> | <i>Min</i> | <i>Max</i> | <i>Mean</i> |
| <i>AVG03</i> | 0.41 | 6.31 | 3.49 | 0.98 | 6.06 | 2.71 | 0.76 | 5.09 | 2.68 | 0.06 | 6.31 | 3.39 |
| <i>MAX03</i> | 0.41 | 7.19 | 3.71 | 0.98 | 6.99 | 2.84 | 0.76 | 5.78 | 2.79 | 0.06 | 7.19 | 3.60 |
| <i>AVGGTH</i> | 0.01 | 4.86 | 0.66 | 0.10 | 2.78 | 0.83 | 0.19 | 2.42 | 1.14 | 0.10 | 4.86 | 0.69 |
| <i>MAXGTH</i> | 0.00 | 4.74 | 1.08 | 0.08 | 4.63 | 1.33 | 0.67 | 4.49 | 2.46 | 0.00 | 5.00 | 1.12 |
| <i>AGTH</i> | 0.10 | 3.10 | 0.25 | 0.01 | 1.74 | 0.46 | 0.04 | 1.27 | 0.58 | 0.01 | 7.06 | 0.31 |
| <i>MGTH</i> | 0.00 | 3.78 | 0.36 | 0.02 | 2.01 | 0.61 | 0.14 | 4.47 | 1.26 | 0.00 | 3.78 | 0.58 |

4. Discussion

The ability of lidar to reliably estimate gap disturbance regimes is well known (St-Onge and Vepakomma, 2004, Koukoulas and Blackburn 2004, Vepakomma *et al.*, 2008a). Estimated gap sizes and gap fraction in this study falls within the reported range of characteristics of boreal forests found in earlier studies (McCarthy, 2001, Vepakomma *et al.*, 2008a). Gap expansion is a prominent feature in a number of forest ecosystems (Runkle, 1998, Worall *et al.*, 2005). Though less frequent in hardwood forests, similar to our observations here trees bordering an old gap are more vulnerable to mortality compared to interior canopy trees in wind fall prone *Picea-Abies* forests of New Hampshire (Worall *et al.*, 2005).

The Identification of saplings in old gaps was more successful than in new gaps. Owing to the longer period of opening, the range of sapling height in old gaps is wider than that in new gaps. A higher average height of 3.3.9 m in older gaps also enabled its easy identification on the lidar surface (Table-1). Identification of saplings within new random gaps was difficult due to their small sizes and to the lateral growth of adjacent vegetation.

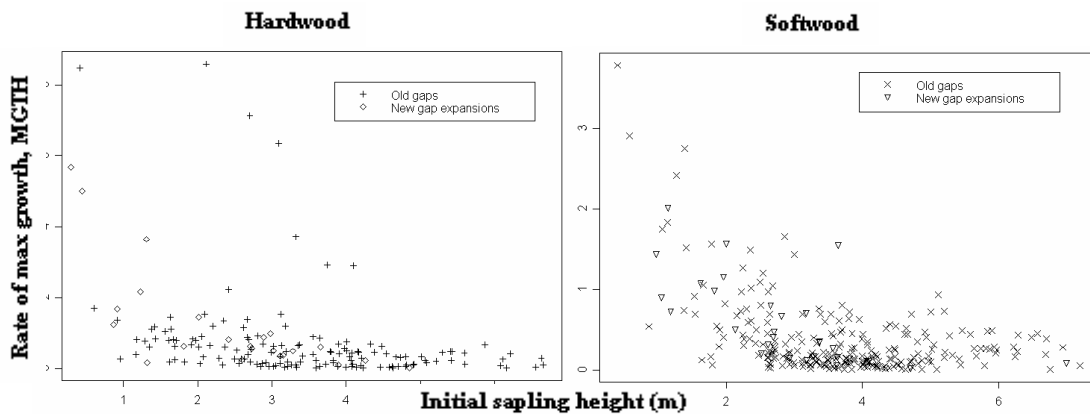


Figure 3: Scatterplot of the rate of maximum growth per unit height during 2003 – 2007 in old gaps and gap expansions.

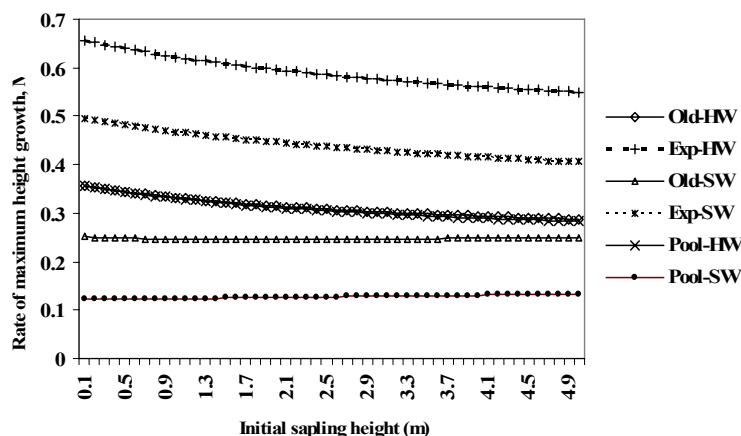


Figure 4: Estimated non-parametric regressions of the rate of maximum growth per unit during 2003 – 2007 height in old gaps and gap expansions (*Old stands for old gaps; Exp for new gap expansions, Pool for pooled dataset*)

Previous research in boreal forests has suggested that large gaps favour intolerant hardwoods while shade tolerant softwoods successfully regenerate in small gaps (Kneeshaw & Bergeron, 1998). The HWs in this forest are all shade intolerant and SWs are all shade-tolerant. The present analyses support this evidence as HWs grow faster in old gaps whose average gap size is larger than new gaps (Tables -1 and 2). SWs are growing faster in new random gaps that are smaller in size. The resources within gaps, especially light, increases with gap expansion, which primarily benefits the HW saplings growing in old gaps adjacent to the new gap openings. The HWs growing in the study area are shade intolerant (Kneeshaw *et al* 2006) and require high light levels to successfully recruit. The dominant conifers on the other hand are shade tolerant and they have been found to be successful in smaller gaps and in the shadier southern portions of gaps due to their requirement for higher moisture (McLaren and Janke, 1996).

The present results clearly indicate distinct growth patterns of saplings in different gap events. This suggests the need to characterise the type of gap events to forecast growth patterns of the regeneration. The use of time series of lidar data for documenting the height- growth differences of advanced regeneration in the canopy gaps spanning full range of height gradients is particularly relevant given the complexity of field based methods. This establishes multi-temporal lidar as an excellent tool to characterise gap dynamics, and thus provides insight into boreal forest dynamics. With rigorous field verification for height of regeneration, these methods can be extended to develop accurate height growth models for juvenile vegetation in a non-destructive way.

Acknowledgements

The authors gratefully thank National Scientific and Engineering Research Council of Canada and the Lake Duparquet Research and Teaching Forest, Quebec, for the financial support extended to accomplish this research.

References

- Coops, N. C., Wulder, M. A. Culvenor, D. S., and St-Onge, B. 2004. Comparison of forest attributes extracted from fine spatial resolution multispectral and lidar data. *Canadian Journal of Remote Sensing* 30(6): 855–866.
- Hopkinson, C., Chasmer, L., and Hill, R. J. 2008. The uncertainty in conifer plantation growth prediction from multi-temporal lidar datasets *Remote Sensing of Environment* 112(3): 1168-1180
- Kneeshaw, D. D., and Bergeron, Y. 1998. Canopy characteristics and tree replacement in the southern boreal forest. *Ecology* 79: 783–794.
- Kneeshaw, D., Kobe, R. K., Coates, K. D., and Messier, C. 2006. Sapling size influences shade tolerance ranking among southern boreal tree species. *Journal of Ecology* 94 : 471 -480.
- Koukoulas, S., and Blackburn, G. A. 2004. Quantifying the spatial properties of forest canopy gaps using Lidar imagery and GIS. *International J.of Remote Sensing* 25(15): 3049–3071.
- Lefsky, M. A., Cohen, W. B., Parker, G. G. and Harding, D.J. 2002. LIDAR remote sensing for ecosystem studies. *Bioscience*, 52 :9–30
- McCarthy, J. 2001. Gap dynamics of forest trees: With particular attention to boreal forests. *Environmental Reviews* 9: 1–59.
- McLaren, B.E., and Janke, R.A. 1996. Seedbed and canopy cover effects on balsam fir seedling establishment in Isle Royale National Park. *Canadian Journal of Forest Research* 26: 782–793.
- Næsset, E., and Gobakken, T. 2005. Estimating forest growth using canopy metrics derived from airborne laser scanner data. *Remote Sensing of Environment* 96: 453–465.
- Pickett, S.T.A., and White, P. S. 1985. The ecology of natural disturbance and patch dynamics.

Academic Press.

- Runkle, J.R. 1998. Changes in southern Appalachian canopy tree gaps sampled thrice. *Ecology*, 79: 1768–1780.
- St-Onge, B., and Vepakomma, U. 2004. Assessing forest gap dynamics and growth using multi-temporal laser-scanner data. In *Proceedings of the Laser- Scanners for Forest and Landscape Assessment — Instruments, Processing Methods and Applications International Conference*, Frieburg im Breisgau, 3–6 Octobre 2004 (pp. 173–178).
- Véga, C., and St-Onge, B. 2008. Height growth reconstruction of a boreal forest canopy over a period of 58 years using a combination of photogrammetric and lidar models. *Remote Sensing of Environment* 112 : 1784 – 1794.
- Vepakomma, U., St-Onge, B., and Kneeshaw, D. 2008a. Spatially explicit characterization of boreal forest gap dynamics using multi-temporal lidar data, *Remote Sensing of Environment* 112: 2326-2340.
- Vepakomma, U., St-Onge, B., and Kneeshaw, D. (2008b). Boreal forest height growth response to canopy gap openings – an assessment with multi-temporal lidar data. (manuscript)
- Worrall, J. J., Lee, T. D., and Harrington, T. C. 2005. Forest dynamics and agents that initiate and expand canopy gaps in Picea-Abies forests of Crawford Notch, New Hampshire, USA., *Journal of Ecology* 93:178-190
- Yu, X., Hyypae, J., Maltamom, M., and Kaartinen, H. 2006, Change detection techniques for canopy height growth measurements using airborne laser scanner data, *Photogrammetric Engineering & Remote Sensing* 72(12): 1339-1348.

Lidar remote sensing of bird canopy habitat use in the Northeastern United States

Scott J. Goetz¹, Daniel Steinberg², Matthew Betts³, Richard T. Holmes⁴, Patrick Doran⁵,
Ralph Dubayah⁶ & Michelle Hofton⁶

¹The Woods Hole Research Center, sgoetz@whrc.org

²Yale School of Forestry & Environmental Science

³Oregon State University, matthew.betts@oregonstate.edu

⁴Dartmouth College, richard.t.holmes@dartmouth.edu

⁵The Nature Conservancy, pdoran@tnc.org

⁶University of Maryland, mhofton@umd.edu

Abstract

A current challenge in biodiversity research is understanding the effect of vegetation structure on the potential of an ecosystem to support species richness and habitat use. We take advantage of the utility of satellite remote sensing, specifically lidar, for improving characterization of habitat structure and apply those advances to an exploration of bird habitat use in New England USA. In this study, we find that lidar metrics of canopy vertical structure and complexity provide unique and significant information for models of habitat use of a neotropical migrant bird species, the black-throated blue warbler, in the Hubbard Brook Experimental Forest, NH. Lidar metrics describing the vertical distribution of canopy elements and the complexity of canopy elements are thus both useful and important for biodiversity research, although we find that other aspects of habitat are equally important, including the type and seasonality of vegetation. Together these variables provide complementary information that advance biodiversity research and emphasize the relevance of remote sensing observations.

Keywords: bird diversity, canopy structure, habitat heterogeneity, habitat use, lidar

1. Introduction

Ecologists have long sought to explain patterns of biodiversity based on latitude, area, evolutionary rates, and other factors. Prior to the availability of satellite data, field-based studies at local spatial scales revealed the strong role of vegetation structure in driving biodiversity. Vegetation structure refers generally to the horizontal and vertical distribution of vegetation. MacArthur and MacArthur (1961) refined the broad concept of vegetation structure by defining foliage height diversity (FHD) as a measure of canopy layering, and suggesting its use as an indicator of biodiversity. Variations on the FHD concept have led to the development of several indices of forest structural complexity incorporating vertical and horizontal variation in tree size, canopy cover, shrub size, shrub cover, coarse woody debris and snags (McElhinny et al. 2005). Vertical and horizontal structural complexity drives biodiversity by creating a greater variety of microclimates and microhabitats, which in turn produce more diverse food and cover for a more diverse range of species (MacArthur and MacArthur 1961, Hunter 1999, Hill et al. 2004). Across landscapes, the distribution of seral stages, patch sizes, and connectivity of patches also influences habitat suitability (Turner et al. 2001). Thus biodiversity managers focus on maintaining variation in tree size, multiple canopy layers, presence of coarse woody debris, and other elements of forest structural complexity within forest stands and creation of a variety of landscape scale seral stages (Hunter 1999, Rapp 2004).

While satellite data have greatly enhanced understanding of the effects of ecosystem energy on biodiversity, no continental-scale quantification of vegetation structure has been available. One goal of our work is to test the utility of current airborne and space-borne data on vegetation structure for studies of biodiversity, and to develop guidelines for the next generation of satellite sensors for quantifying vegetation structure for understanding and managing biodiversity. Towards this end, the field-based understanding of vegetation structure and biodiversity has been greatly advanced by application of airborne lidar. Heterogeneity can be calculated directly from lidar-derived forest structure, using metrics such as vertical distribution ratio (Drake et al. 2002, Goetz et al. 2007, Vierling et al. 2008) and integrated measures of the complexity of the waveform that takes into account the roughness, slope, number of gaussian peaks, and amplitude of peaks in the waveform data (Dubayah et al. 2000, Hofton et al. 2004). Using these and related metrics, including canopy height, Goetz et al. (2007) were able to predict species richness of different bird guilds in the forests of the Patuxent National Wildlife Refuge (Maryland). This was true even in a relatively homogenous forest environment with little variability in traditional optical vegetation indices (e.g. NDVI). Use of lidar data provided an ability to detect variability in vegetation structure and density, which were critical variables describing the habitat use of bird species. Here we explore the habitat suitability (preferences) of a single bird species with specific habitat preferences, the Black-Throated Blue Warbler, *Dendroica caerulescens*, a well studied neotropical migrant breeding in northern hardwoods forests.

2. Methodology

In the Northeast United States, black-throated blue warblers tend to occupy mature deciduous forests with a well-developed and high-density understory (Holmes 1994, Doran and Holmes 2005). Our working hypothesis was that deciduous cover and understory structure and density are both vegetative characteristics that can be identified using optical and lidar remote sensing.

2.1 Study area

We analyzed a long-term data set of bird observations collected at the Hubbard Brook Experimental Forest (HBEF), located in the southern region of the White Mountain National Forest in central New Hampshire. HBEF was established in 1955 as a long-term research site used for the study of forest and watershed dynamics. The HBEF encompasses approximately 3037 hectares of hilly terrain, ranging in elevation from 222m at the lowest point of the brook to 1015m atop Mount Kineo on the southwest rim of the watershed. The region is dominated by northern hardwoods (Sugar Maple, Beech, Yellow Birch, and White Ash) at low to middle elevations, and is dominated by spruce and fir species at higher elevations and along the ridgelines (Schwartz et al. 2001). The forests within and surrounding the HBEF were logged selectively for spruce in the late nineteenth century and were logged intensively for both conifer and hardwood species in the early part of the twentieth century before being established as an experimental preserve in the 1960s.

2.1 Bird data sets

Data on the distribution and abundance of the Black-Throated Blue Warbler were collected in the summers of 1999, 2001, 2002, and 2006. A survey grid consisting of 371 points along 15 north-south transects was established throughout the HBEF (Figure 1) (Schwartz et al, 2001). Points spaced at 100 meter intervals along each transect were visited 3 times during the peak breeding seasons (late May through June) of 1999, 2002, and 2006 and twice in 2001. During each visit the abundance of Black-throated Blue Warblers was surveyed for 10 minutes using

fixed radius (50-m radius) point counts (Ralph et al. 1995, Doran and Holmes 2005). Surveys were performed between 0530-1000 by multiple trained observers in order to limit error in observer accuracy.

Using the abundance data collected over the 4 years, annual presence/absence was determined at each of the 371 survey sites. The black-throated blue warbler was considered present at a site if an individual was observed within 50 meters of the survey location, i.e. abundance was greater than 1. Similarly to Doran and Holmes 2005, presence/absence data were used to classify each survey site based on the number of years that the species was present (0, 1, 2, 3, or 4) over the duration of the study. It has been previously shown that high quality sites are consistently occupied year after year, regardless of interannual variability in abundance of a species, whereas low quality sites are only occupied during periods of high population density (Doran and Holmes 2005, Newton 1998, Sergio and Newton 2003). We used this index of multi-year presence as a surrogate for habitat quality or suitability. The greater the number of years occupied by the species, the better the quality of the habitat. The habitat quality index was constructed using all 4 years of data, as well as a separate index using only 3 years of observations (1999, 2001, & 2002), reserving 2006 data for testing.

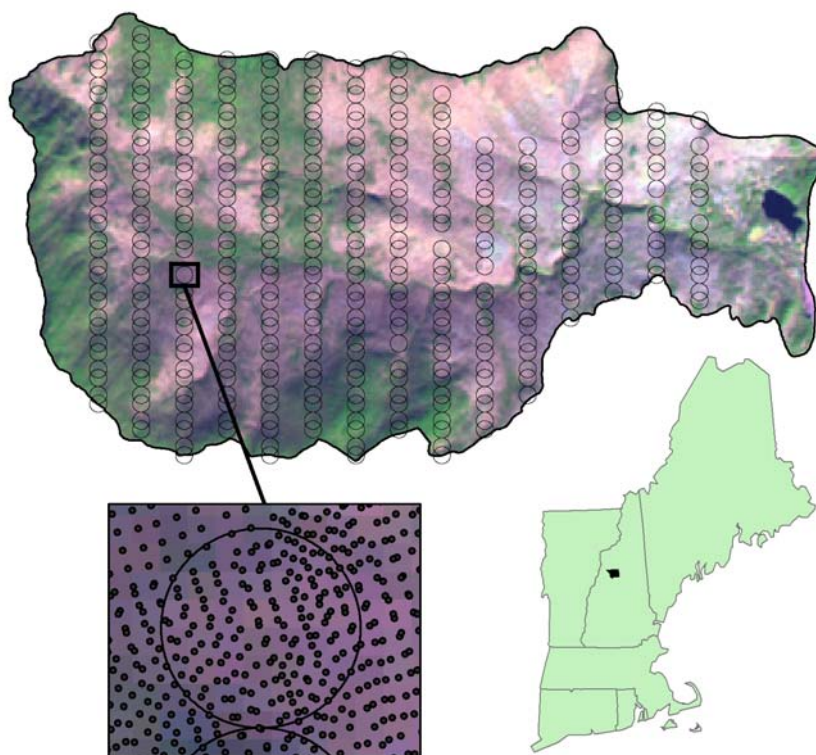


Figure 1. Hubbard Brook study area in central New Hampshire, showing a Landsat NDVI image and gridded bird observation areas. The lower left image shows the density of lidar shots within a given location.

2.2 Lidar data sets

Full waveform lidar data were acquired over the Hubbard Brook Experimental Forest with the Laser Vegetation Imaging Sensor (LVIS) in July of 2003. LVIS is a fully imaging, medium altitude, scanning laser altimeter. It has a 7° field of view within which footprint sizes can be varied from 1 to 80m depending on, among other factors, the altitude at which the instrument is

flown (Blair et al. 1999). LVIS digitizes the return signal and converts the waveforms to units of distance by accounting for the time elapsed between the initial laser pulse and the return.

Three products were derived directly from the LVIS waveform data including, ground elevation, canopy height (CH), and the height of median return (HOME). Each of these products is calculated in reference to the ground return; therefore accurate determination of the ground surface is an essential step in producing these metrics. The ground return is identified using an automated algorithm which initially applies a smoothing function to reduce noise in the waveform, and subsequently locates the first increase above a mean noise level, designated as the initial canopy return, and the center of the last Gaussian pulse, designated as the ground return. CH was calculated as the difference in height between the initial canopy return and the ground return. HOME was derived as the difference in height between the median of the entire waveform, including ground and canopy energies, and the ground return.

In addition to canopy height, ground elevation, and median height, we derived two higher-level products which provide information on the vertical distribution of vegetation biomass as well as the structural complexity of the canopy. The Vertical Distribution Ratio, or VDR, is an index of the vertical distribution of intercepted canopy elements (biomass) and ranges between 0 and 1 (Goetz et al. 2007). The VDR is a ratio of the distance between the canopy return and the height of median return to the total canopy height; $VDR = [CH - HOME] / CH$. In general, forested regions characterized by a dense canopy and sparse understory will exhibit lower VDR values due to the relatively short distance between CH and HOME. Areas characterized by a more even distribution of biomass throughout the vertical profile will exhibit larger VDRs (closer to 1).

Canopy complexity (COMP), by comparison to VDR, is an integrated measurement of the complexity of the waveform and takes into account the roughness, slope, number of gaussian peaks, and amplitude of peaks in a waveform and, like VDR, ranges from 0 to 1. Although we refer to it as canopy complexity, it is not a biophysical measurement as such, but rather a measure of the vertical complexity of the waveform. In forested regions, however, the vertical complexity of a waveform (COMP) is determined by the complexity of vegetation structure.

2.3 Landsat data sets

In addition to the lidar metrics, we examined metrics derived from optical imagery in relation to the bird richness data. Two Landsat ETM scenes (path/row 013/029), acquired in late October of 2000 and August of 1999, were converted to top-of-atmosphere reflectances using in-band spectral irradiances and a solar geometry model to correct for Earth-Sun distances and solar zenith angle variations (Goetz 1997). The images were subsequently georeferenced. The Normalized Difference Vegetation Index was calculated for both the leaf-on (August) and the leaf-off (October) scenes and the two scenes were differenced resulting in an image of seasonal NDVI change. This allowed us to evaluate and consider seasonality in vegetation cover and density.

Vegetation type for the study region was also examined. Using a vegetation type map of the HBEF which delineated regions of deciduous, coniferous, mixed predominantly deciduous, and mixed predominantly coniferous, we produced a continuous grid of percent deciduousness. This was analyzed in addition to the optical and lidar products.

2.4 Spatial and statistical analyses

Using a geographical information system (GIS), bird survey polygons were intersected with the lidar (LVIS) and optical (Landsat ETM) data products (Figure 1). The minimum, maximum, mean, and standard deviation of ground elevation, canopy height, median height, VDR, COMP,

leaf-on NDVI, and NDVI difference were computed for all lidar shots or Landsat cells falling within the boundaries of each 50m radius survey cell. These summaries were subsequently examined in relation to the habitat quality index derived from the BTBW occupancy data using an advanced regression tree technique known as “Random Forest.”

A “Random Forest” (RF) model builds upon the standard methods of constructing classification and regression trees as a technique for partitioning data based on a series of hierarchical binary splits of the predictor variables, resulting in a tree structure that terminates in nodes associated with discrete ranges in the response variable (Breiman 2001). With RF many trees are iteratively aggregated with cross calibration, reducing error in the overall model via boosting and bagging techniques. In addition to constructing each tree using a different bootstrapped sample of the data, the random forest algorithm incorporates a unique approach to splitting. Typically, each node is split using the optimal split among all predictor variables; in the RF algorithm, each node is split using the best predictor among a subset of predictors chosen at random at that node. This additional layer of randomness significantly increases the accuracy of the model and makes RF robust to overfitting.

Using the RF package in the R programming environment, habitat quality was modeled based on the suite of lidar and optical predictor variables described above. The model was run using both 3 and 4 years of bird population and distribution data. Because the random forest algorithm builds trees based on a bootstrap sample of data (reserving approximately 1/3 of the data for testing), it is not necessary to withhold data for testing after model creation. In spite of this, and in addition to running the model using all 4 years of data, we ran the model based on the first 3 years of data and examined the relationship between predicted habitat quality and occupancy in the fourth year.

3. Results

Lidar and optical data products varied throughout the study region; however, some patterns reflected spatial variation in elevation. General trends between lidar and optical predictor variables and habitat quality are shown in Figure 2. Good quality habitat, i.e. that with greater frequency of occupancy, was associated with a dominance of deciduous vegetation, a relatively high canopy height, increased vertical complexity, low VDR, and high seasonal change in NDVI (NDVI difference). Although clear trends exist between habitat quality and the selection of variables displayed, there was a large amount of variability in habitat metrics (both lidar and optical) within a single habitat quality class.

The random forest model based on 4 years of occupancy data explained 47% of the variation in habitat quality. Seasonal difference in NDVI, canopy height, elevation, and canopy complexity were selected as the most important predictors of BTBW habitat quality. This model was subsequently applied to the lidar and optical data summarized for each survey site and we examined the frequency of agreement and disagreement between the predicted and observed habitat quality (Table 1). Although the model produced habitat quality values in the range of 0 to 4, we grouped the range of predicted values into 3 habitat quality groups: best (quality of 3 or 4), average (1 or 2), and poor (0). Of the 251 sites predicted to have the best quality habitat, 199 or 79% of them were occupied for 3 or 4 years over the study period, while 17% were occupied for 1 or 2 years and only 4% were not occupied at all. About 58% of the sites identified as average quality habitat were occupied for 1 or 2 years, while 21% of these sites were occupied for 3 or 4 years, and the remaining 21% were not occupied at all. Of the 75 sites predicted as poor habitat, 73% were not occupied over the 4 years of study.

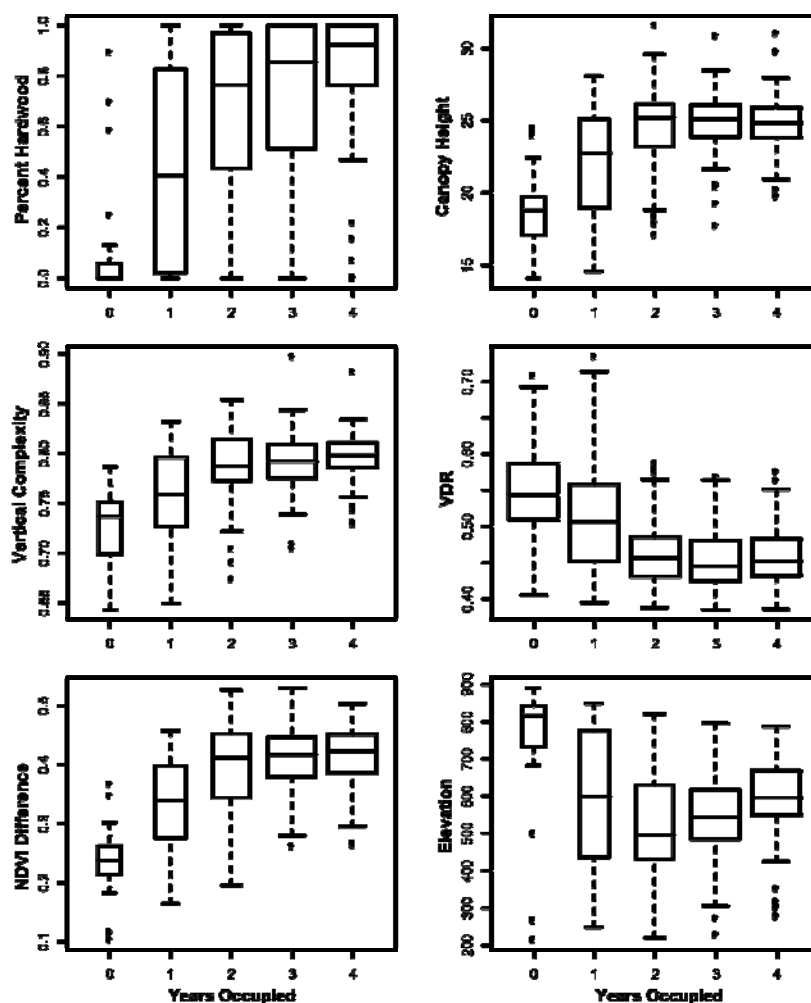


Figure 2. BTBW habitat occupancy relative to the predictor variables used in model development.

As with the model run based on 4 years of data, the random forest model of habitat quality derived from 3 years of occupancy data selected seasonal NDVI difference, elevation, canopy height, and vertical complexity as the strongest predictors of habitat quality. The 3-year model displayed an ability to predict presence/absence in the 4th year of the study period, with 73 sites identified as best quality (quality of 3), 198 as average quality (2) and 100 as poor quality (1 or 0). Thus about 90% of sites identified as best quality data were occupied in the 4th year of the study, while 81% of the average quality sites and only 46% of the poor quality sites were occupied (Table 2).

Table 1: Comparison of predicted occupancy among habitat quality groups.

| | | Predicted | | |
|--|---------|----------------------------------|-------------------------------------|----------------------|
| | | Best (3 or 4 years) 251 sites | Average (1 or 2 years) 105 sites | Poor (0) 75 sites |
| | Best | 199 (79%) | 22 (21%) | 9 (12%) |
| | Average | 42 (17%) | 61 (58%) | 11 (15%) |
| | Poor | 10 (4%) | 22 (21%) | 55 (73%) |

Table 2: Predicted presence or absence among habitat quality groups in year 4 based on model developed using year 1-3 observations.

| | | Predicted | | |
|----------|---------|----------------------|-----------------------|----------------------------|
| | | Best (3) 73 sites | Good (2) 198 sites | Poor (1 or 0) 100 sites |
| Observed | Present | 66 (90%) | 162 (81%) | 46 (46%) |
| | Absent | 7 (10%) | 36 (19%) | 54 (54%) |

4. Discussion

General trends between remotely sensed metrics of habitat and habitat suitability derived from occupancy data were as expected (Figure 2). Black-throated blue warblers are known to prefer mature forests with a dominance of deciduous vegetation (Doran and Holmes 2005) and we observed a strong positive trend between both habitat quality and percent deciduousness, as well as between habitat quality and canopy height (Figure 2a & b). Clear trends also existed with canopy complexity and the vertical distribution ratio (Figure 2c & d). Habitat quality increased with increasing vertical complexity, demonstrating that a more complex vegetation structure improves habitat for this species. Similarly, lower VDR values were associated with higher quality habitat. Low values of VDR indicate a more uniform distribution of vegetation biomass throughout the canopy profile. Both of these trends may be related to the preference by the black-throated blue warbler for locations with a well-developed understory (Holmes and Doran 2005, Holmes et al. 1996, Steele 1992), particularly the density of hobblebush (*Viburnum alnifolium*) shrubs, i.e., increased occupancy of sites with higher densities of hobblebush. A well-developed understory would have the effect of both lowering VDR, by effectively shifting the median height (HOME) down, and increasing COMP (a similar forest with no understory would have a lower COMP, due to the lack of the understory return in the waveform).

Seasonal change in NDVI was also positively correlated with habitat quality (Figure 2e). This trend is most likely associated with the relationship between vegetation type and seasonal NDVI difference, although it may also indicate a relationship between primary productivity and habitat quality. Deciduous vegetation shows greater phenological changes throughout the growing season than coniferous species, and this trend most likely reflects the preference of the black-throated blue warbler for deciduous forest. Greater seasonal changes in NDVI, however, also indicate greater rates of photosynthesis and primary productivity, which could sustain larger populations of *Lepidoptera*, the black-throated blue warbler's primary food source. The boxplot

of elevation as a function of habitat quality (Figure 2f) demonstrates the preference of black-throated blue warblers for low to mid-elevation (400-700m) regions. Areas of higher elevation are typically dominated by coniferous species or sparse vegetation along the rocky ridgelines. Again, the trend between habitat quality and elevation is not directly causal, but is more likely a result of vegetation cover as influenced by elevation.

The random forest model of habitat quality based on lidar and optical predictors and 4 years of occupancy data was skilled in terms of variance explained (Figure 2). When observed and predicted values of habitat quality were grouped into best, average, and poor quality categories, comparison of the observed and predicted values demonstrated strong overall agreement (Table 1). The random forest model based on 3 years of occupancy data was comparably good. Although the percent of variance explained based on the reserved data was relatively low (39%), when the model was applied to the lidar and optical data, and examined in relation to occupancy data from 2006 (year 4), it demonstrated strong predictive power (Table 2). Over 90% of the sites identified as best quality habitat were occupied in 2006. This is particularly interesting because it discounts the effect of individuals showing site fidelity because the 4-year gap between 2002 and 2006 makes it unlikely that the same individuals are returning to the same locations.

Results from sites identified as average or poor habitat were not as compelling. Just over 80% of habitats identified as average were occupied and 46% of the sites identified as poor habitat were occupied in the year 2006. This result, however, could be influenced by the relatively high abundance of black-throated blue warblers in that particular year. Total abundance of the BTBW over all sites in 2006 was higher than in previous years, thus good quality habitat was more limited and greater abundance and occupancy at average and poor habitat sites would be expected.

These results indicate that remotely sensed data can be used to predict habitat quality or suitability of the BTBW, even throughout a relatively homogenous environment. Utilization of lidar data in addition to optical data, provides the ability to sense changes in vegetation structure and density, which adds an integral layer of information to the characterization of habitat, particularly across a region which is relatively homogeneous in terms of spectral reflectance in optical imagery.

Our future work with these data will incorporate additional years of bird observations, focus on a range of different modelling variations, including different methods of sampling the bird observations (e.g. selecting every other grid location and using the remainder for testing), quantifying the influence of spatial autocorrelation, and exploring the utility of an information theoretic modelling approach for assessing habitat quality.

Acknowledgements

We acknowledge support from the NASA Applied Sciences Program, Ecological Forecasting theme, managed by Woody Turner and the NASA Interdisciplinary Science program managed by Diane Wickland. The field data were collected with the logistic support of the Northern Research Station, U.S. Forest Service, Newtown Square, PA with financial support from the National Science Foundation.

References

Blair, J. B., D. L. Rabine and M. Hofton, 1999, The Laser Vegetation Imaging Sensor (LVIS): a medium altitude, digitization-only, airborne laser altimeter for mapping vegetation and

- topography. *ISPRS Journal of Photogrammetry and Remote Sensing* 54: 115-122.
- Breiman, L. 2001. *Machine Learning* 45, 5–32.
- Doran, P. J. and R. T. Holmes, 2005, Habitat occupancy patterns of a forest dwelling songbird: causes and consequences. *Canadian Journal Of Zoology* 83(10): 1297-1305.
- Drake, J. B., R. Dubayah, D. B. Clark, R. G. Knox, J. B. Blair, M. A. Hofton, R. L. Chazdon, R. L. Weishampel, and S. Prince. 2002. Estimation of tropical forest structural characteristics using large-footprint lidar, *Remote Sensing of Environment*, 79: 305-319.
- Dubayah , R.O. and J.B. Drake. 2000. Lidar remote sensing for forestry applications. *Journal of Forestry* 98:44-46.
- Goetz, S. J., D. Steinberg, R. Dubayah, and B. Blair. 2007. Laser remote sensing of canopy habitat heterogeneity as a predictor of bird species richness in an eastern temperate forest, USA. *Remote Sensing of Environment* 108:254-263.
- Goetz, S. J. 1997. Multi-sensor analysis of NDVI, surface temperature, and biophysical variables at a mixed grassland site. *International Journal of Remote Sensing*, 18:71-94.
- Hill, R.A., Hinsley, S.A., Gaveau, D.L.A., & Bellamy, P.E., 2004. Predicting habitat quality for great tits. *International Journal of Remote Sensing*, 25, 4851-4855
- Hofton, M. A., L. E. Rocchio, J. B. Blair, and R. Dubayah. 2002. Validation of Vegetation Canopy Lidar sub-canopy topography measurements for a dense tropical forest. *Journal of Geodynamics* 34:491-502.
- Holmes, R.T., 1994, Black-throated Blue Warbler (*Dendroica caerulescens*). In *The birds of North America*. No 87. Edited by A. Poole and F. Gill. The Academy of Natural Sciences, Philadelphia, and The American Ornithologists' Union, Washington, D.C.
- Holmes, R. T., P. P. Marra and T. W. Sherry, 1996, Habitat-specific demography of breeding black-throated blue warblers (*Dendroica caerulescens*): Implications for population dynamics. *Journal Of Animal Ecology* 65(2): 183-195.
- Holmes R.T., T.W. Sherry, P.P. Marra, K.E. Petit, 1992, Multiple brooding and productivity of a neotropical migrant, the black-throated blue warbler (*Dendroica caerulescens*), in an unfragmented temperate forest. *The Auk* 109:321-333.
- Hunter, M. L. Jr. 1999. *Maintaining Biodiversity in Forest Ecosystems*. Cambridge University Press, Cambridge, UK.
- MacArthur, R. H. and J. W. MacArthur. 1961. On bird species diversity. *Ecology* 42:594-598.
- McElhinny, C., P. Gibbons, and C. Brack. 2005. Forest and woodland stand structural complexity: Its definition and measurement. *Forest Ecology and Management* 218:1-24.
- Newton, I, 1998, *Population limitation in birds*. Academic Press, San Diego.
- Rapp, V. 2004. *Ecosystems and people: managing forests for mutual gains*. Science Update 8. U.S. Department of Agriculture, Forest Service, Pacific Northwest Research Station Portland, OR.
- Ralph, C. J., J. R. Sauer, and S. Droege. 1995. *Monitoring Bird Populations by Point Counts*. General Technical Report PSW-GTR-149, USDA Forest Service, Albany, CA.
- Schwartz, P. M., T. J. Fahey, C. W. Martin, T. G. Siccama, and A. Bailey. 2001. Structure and composition of three northern hardwood-conifer forests with differing disturbance histories. *Forest Ecology and Management* 144:201-212.
- Sergio, F. and I. Newton, 2003, Occupancy as a measure of territory quality. *Journal Of Animal Ecology* 72(5): 857-865.
- Steele, B. B., 1992, Habitat selection by breeding Black-throated Blue Warblers at two spatial scales. *Ornis Scandinavica* 23(1): 33-42.
- Turner, M.G., R.H. Gardner, R.V. O'Neill. 2001. *Landscape Ecology in Theory and Practice: Pattern and Process*. Springer Verlag, New York.
- Vierling, K.T., Vierling, L.A., Gould, W.A., Martinuzzi, S., & Clawges, R.M., 2001. Lidar: shedding new light on habitat characterization and modeling. *Frontiers in Ecology and the Environment*, 6, 90-9.

Keynote Presentation 3

The use of large footprint waveform lidar for landscape characterization: past experience and future prospects

Ralph Dubayah

1149 Lefrak Hall, University of Maryland, College Park, MD 20737, USA.

dubayah@umd.edu

Abstract

The exploding use of small-footprint lidar over the last 10 years has to some degree obscured the development and application of large footprint waveform recording lidar. Such systems have included the airborne Laser Vegetation Imaging Sensor (LVIS) of NASA, the developed but unlaunched Vegetation Canopy Lidar (VCL) space mission, as well as the currently orbiting ICESAT satellite. A new space mission, the DESDynI (Deformation, Ecosystems, and Dynamics of ICE) mission, is currently under development by NASA as well which will provide global observations of land surface vertical structure using radar/lidar fusion. There is thus considerable interest in understanding both the potential and limits of large footprint waveform lidar for large area assessments. In this talk I present our experience using waveform lidar for a variety of environmental and forest-related applications. I begin by providing a brief overview of waveform lidar and show its equivalence to small-footprint discrete return systems. I next present a series of examples using the LVIS system for a variety of environmental applications. These include estimation of tropical forest biomass, carbon flux and dynamics, habitat mapping for endangered species (the ivory-billed woodpecker and California spotted owl), and derivation and mapping of forest fire fuel structure for montane coniferous forests. In addition, I outline our efforts to marry an ecosystem model with lidar-derived forest structure for improved carbon stocks and flux estimation. I then explore the use of space-based waveform observations from the ICESAT satellite. Lastly, I provide a preview of the next generation space-based lidar systems, including the planned DESDynI mission, which hopes to provide spatially continuous estimates of forest structure for the Earth.

Session 4: Waveform LiDAR

Representation of vegetation and topography within satellite LiDAR waveforms for a mixed temperate forest

Jacqueline Rosette¹, Peter North², Juan Suárez³ & Sietse Los⁴

¹Climate and Land-Surface Systems Interaction Centre, Geography Department, Swansea University, Swansea, SA2 8PP, UK. ggrosette@swansea.ac.uk

²Climate and Land-Surface Systems Interaction Centre, Geography Department, Swansea University, Swansea, SA2 8PP, UK. p.r.j.north@swansea.ac.uk

³Forest Research Agency of the Forestry Commission, Northern Research Station, Roslin, Midlothian, EH25 9SY, UK. juan.suarez@forestry.gsi.gov.uk

⁴Climate and Land-Surface Systems Interaction Centre, Geography Department, Swansea University, Swansea, SA2 8PP, UK. s.o.los@swansea.ac.uk

Abstract

Identifying the signal returned from vegetation within large footprint LiDAR waveforms relies upon estimating a representative ground surface beneath the canopy. Two methods of identifying the vegetation return within Geoscience Laser Altimeter System (GLAS) waveforms are presented. The first uses maximum elevation difference within a coincident digital terrain model (DTM) to estimate the ground position, whilst the second uses Gaussian decomposition to distinguish ground and vegetation components.

Estimated ground elevations within the waveforms are compared with coincident mean ground surface elevations from airborne LiDAR data and the Ordnance Survey 10 metre resolution DTM. Smallest differences are found between the Gaussian decomposition method and the two validation dataset elevations with mean offsets of -0.14m and -0.02 metres respectively. However, ground slope was found to account for 39% of variation in error using Gaussian decomposition whilst use of a terrain index from the coincident DTM removed this error source. The two methods respectively explained 68% (RMSE 4.4m) and 63% (RMSE 4.7m) of variance in comparison with airborne LiDAR estimates of vegetation height.

The radiative transfer model, FLIGHT, is used to model the sensitivity of the GLAS waveform to canopy properties and topography. Close correspondence is found between returned and simulated waveforms.

Keywords: ICESat/GLAS, Airborne LiDAR, FLIGHT, Topography, Vegetation

1. Introduction

Small footprint airborne LiDAR data provide a unique means of modelling complex topography beneath forest canopies (Figure 1), allowing the identification of hydrological systems, archaeological remains, potential access routes for forest management and the assessment of slope stability. This ability to represent a dynamic surface allows overlying vegetation to be related to topography to accurately demonstrate vegetation distribution for inventory or management purposes or to provide model inputs.

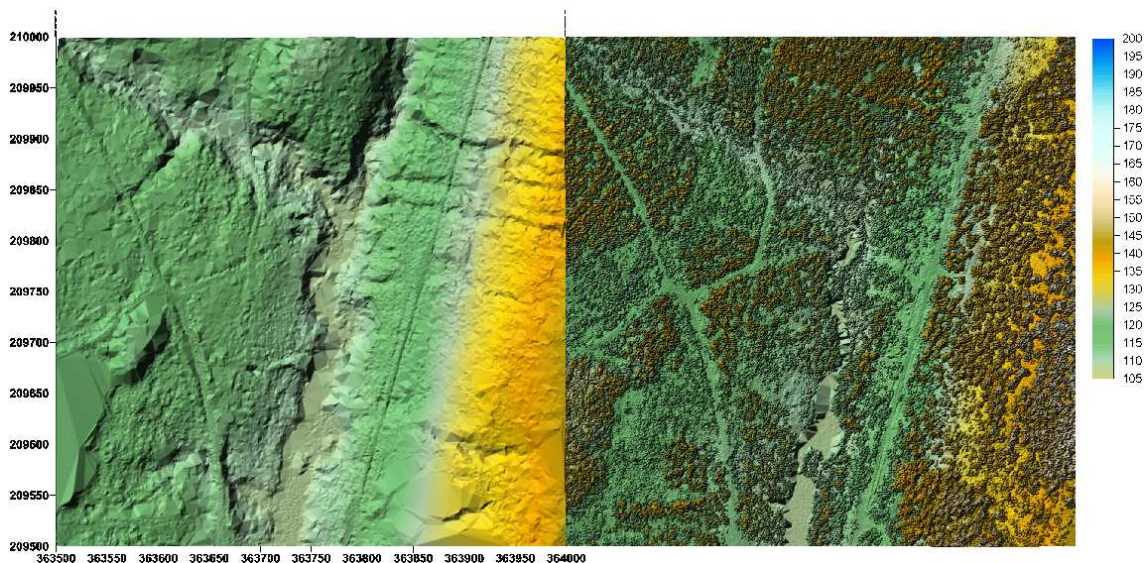


Figure 1. (left) Digital terrain model (DTM) of a 0.5km x 0.5km area of the Forest of Dean. (right) Coincident digital surface model (DSM) from airborne LiDAR data. Both models are 0.5m resolution and were produced with Golden Software Surfer 8 using linear interpolation with Delaunay triangulation.

Large footprint satellite LiDAR has great potential for monitoring vegetation presence and change on unprecedented scales (Hese *et al.*, 2005) and studies have successfully demonstrated the capabilities of LiDAR profiling in this respect (Harding and Carabajal, 2005; Helmer and Lefsky, 2006; Lefsky *et al.*, 2005; Lefsky *et al.*, 2007; Nelson *et al.*, 2008; Nelson *et al.*, 2004). However the broad footprint diameter poses the challenge of signals from the ground surface and vegetation being combined for footprints with complex terrain and vegetation distribution (Figure 2). This raises the question of whether a representative ground surface can be identified within waveforms, a factor which may be important in the estimation of vegetation height.

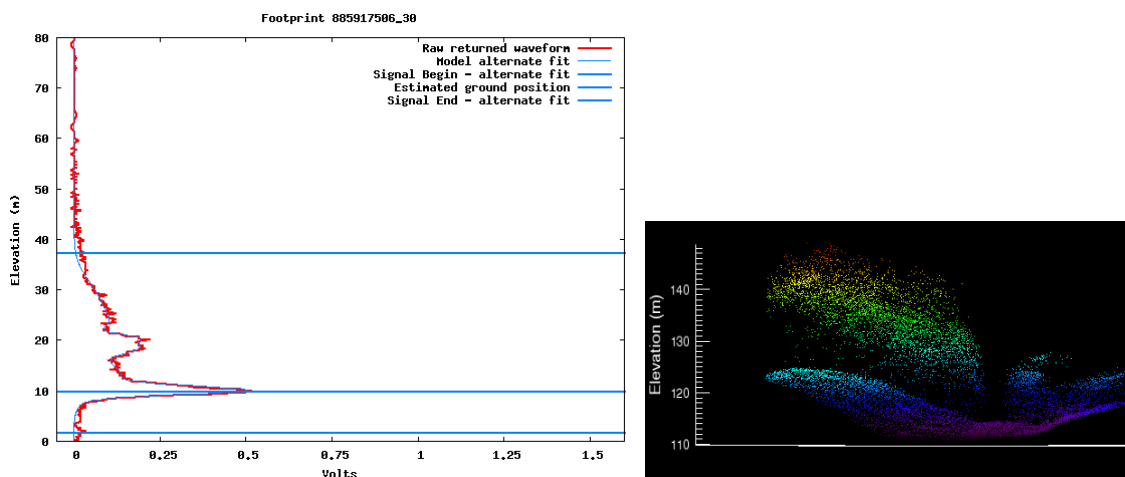


Figure 2: ICESat/GLAS waveform and coincident airborne LiDAR point cloud for a vegetated footprint with complex topography in the Forest of Dean.

This study therefore aims to assess the degree to which a representative ground elevation beneath vegetation can be estimated using large footprint full waveform LiDAR and the influence of slope on this estimate. From this, a comparison of estimates of maximum canopy height from satellite and airborne LiDAR are presented. The radiative transfer model, FLIGHT (North, 1996), is also used to model the effect of slope and vegetation properties on waveform shape.

2. Method

2.1 Study area

The Forest of Dean, Gloucestershire, UK, is a highly mixed forest in England which borders south Wales and covers an area of approximately 11,000 hectares. The forest falls under the responsibility of the Forestry Commission, a division of which, Forest Enterprise, maintains a database of site conditions, species composition and management criteria at a sub-compartment level. The forest is unusual in terms of the UK, containing approximately 50% conifers and broadleaves comprising pockets of ancient woodland as well as managed stands. Surface relief is also varied within the forest, ranging from near-flat terrain to elevation differences of up to 20 metres (m) within 70x70m sample areas used in this study. Both species heterogeneity and topography create a challenging study area for the application of satellite LiDAR.

2.2 Satellite LiDAR

The data source used within this project is the Geoscience Laser Altimeter System (GLAS), a full waveform LiDAR profiler, aboard the Ice, Cloud and land Elevation Satellite (ICESat). GLAS emits 1064nm pulses at a rate of 40 shots per second from an altitude of 600km. This produces footprints which are distanced at 172m intervals on the ground surface and, for the laser 3D operation used in this study, footprints have approximately 52m diameter and were acquired in October 2005. The laser is operated for an approximately month-long period, two-three times annually, aiming to repeat the same ground tracks and therefore providing the potential for changes over time to be monitored. Further information regarding the mission and system are provided by other authors (Abshire *et al.*, 2005; Brenner *et al.*, 2003; NSIDC, 2003; Schutz *et al.*, 2005; Zwally *et al.*, 2002).

2.2.1 Waveform processing

Two methods of estimating vegetation returns within GLAS waveforms (Rosette *et al.*, 2008) were used in this study. The first of these uses a multiple regression with waveform extent (the elevation difference between the beginning and end of the waveform signal) and a terrain index using the Ordnance Survey (OS) Land-Form PROFILE 10m digital terrain model (Lefsky *et al.*, 2005). Product GLA14 (NSIDC, 2003) provides a model fit to the raw waveform decomposed as the sum of six Gaussian peaks. The second method estimates the ground elevation as the centroid of either Gaussian Peak 1 or 2 whichever has greatest amplitude. Maximum vegetation height is estimated as the distance between this position within the waveform and the beginning of the waveform signal. These methods are hereafter referred to as R_{WT} and GP_{amp} respectively.

Elevations of the estimated ground positions within waveforms were calculated in order to assess the ability of each ICESat/ GLAS method to estimate ground elevation with respect to airborne LiDAR and OS DTM mean elevations. Waveform ground surface elevations were calculated as follows:

$$d_{elev} + d_{ld_RngOff} - d_{SigBegOff} - GLAS_{ht} - d_{gdHt} \quad (1)$$

whereby d_{elev} is the reference elevation of the ellipsoid; the land range offset, d_{ld_RngOff} , indicates the offset position within the waveform of d_{elev} ; $d_{SigBegOff}$ provides the offset of the beginning of the waveform signal; $GLAS_{ht}$ represents maximum vegetation heights estimated using GLAS data (methods described above); d_{gdHt} is the height of the geoid above that of the ICESat ellipsoid. All waveform parameters used are from product GLA14 as original units converted to metres. Offset positions are provided as a negative number with reference to the final data bin, furthest from the spacecraft, recorded in each 150m waveform ‘window’ and

indicate the distance from this position in metres.

2.2 Airborne LiDAR system

Airborne LiDAR data were captured using the Optech Airborne Laser Terrain Mapper (ALTM-3033) during August 2006. The Natural Environment Research Council Airborne Research and Surveying Facility offers this service through the Unit for Landscape Modelling, University of Cambridge. The flight was undertaken for the Forestry Commission of Great Britain Forest Research Agency. This first and last return laser scanner emits 1064nm pulses and produced approximately 20cm diameter footprints with 45cm average point spacing.

2.2.1 Data processing

Subsets of airborne Lidar data were created using a radius of 35m about each geo-located ICESat footprint position. This aims to compensate for some uncertainty in footprint position and eccentricity.

Using the airborne LiDAR ground class, mean slope within footprints was calculated with the aim of assessing the extent to which any differences observed between estimates from the two systems or field measurements may be a function of slope.

Since points were regularly distributed with little variation in point density across the study area, ground class surface models for each footprint area were created using linear interpolation with Delaunay triangulation. Maximum canopy height within each airborne LiDAR subset was calculated to allow a comparison to be made with satellite LiDAR estimates.

Projected plant cover was then calculated for each footprint using return point counts above the interpolated ground surface. A 0.5m height threshold was used to exclude the effects of low cover by ferns, brambles or grass to prevent artificial estimates of cover but to include energy distribution throughout the canopy in order to be comparable as far as possible with the waveform energy profile. 0.15m height bins were used for consistency with waveform resolution. Using these criteria, canopy cover was estimated as the number of all canopy points expressed as a fraction of total returns to provide input data for the radiative transfer model FLIGHT.

2.3 FLIGHT

To analyse theoretical sensitivity of the GLAS waveform to topography and canopy structure, we have developed a model of the interaction of waveform LiDAR with a three-dimensional canopy representation. The model is developed from the FLIGHT radiative transfer model (North, 1996), based on Monte Carlo simulation of photon transport. Foliage is represented by structural properties of leaf area, leaf angle distribution, crown dimensions and fractional cover, and the optical properties of leaves, branch, shoot and ground components. Important characteristics of the model are that it can represent multiple scattering of light within the canopy and with the ground surface, simulate the return signal efficiently at multiple wavebands, and model the effects of topography. Spatial and temporal sampling characteristics of the LiDAR instrument are explicitly modelled.

2.3.1 Model Inputs

Estimates of canopy cover from airborne LiDAR data were used as a model input to FLIGHT. The use of this dataset as an approximation of ground truth was supported by hemispherical photogrammetry calculations which produced R^2 of 0.77 and RMSE of 2% despite the small data

range available (Rosette *et al.*, submitted). Inputs of crown dimensions were based on field observations for a selection of ICESat footprint areas. Airborne LiDAR ground class data were used for the input of mean footprint slope. Species vegetation height and crown shape were determined from field observations or using the Forest Enterprise sub-compartment database and corresponding yield model estimates.

3. Results

Figure 3 shows estimations of within-footprint mean ground elevations from Ordnance Survey DTM and airborne LiDAR plus ICESat/GLAS estimated ground surface using both GP_{amp} and R_{WT} methods. The Gaussian decomposition method underestimated the airborne LiDAR (AL) and Ordnance Survey 10m resolution Land-Form PROFILE DTM (OS) mean ground elevations by 0.14m and 0.02 m respectively for the Forest of Dean pass. A summary of results is found in Table 4.

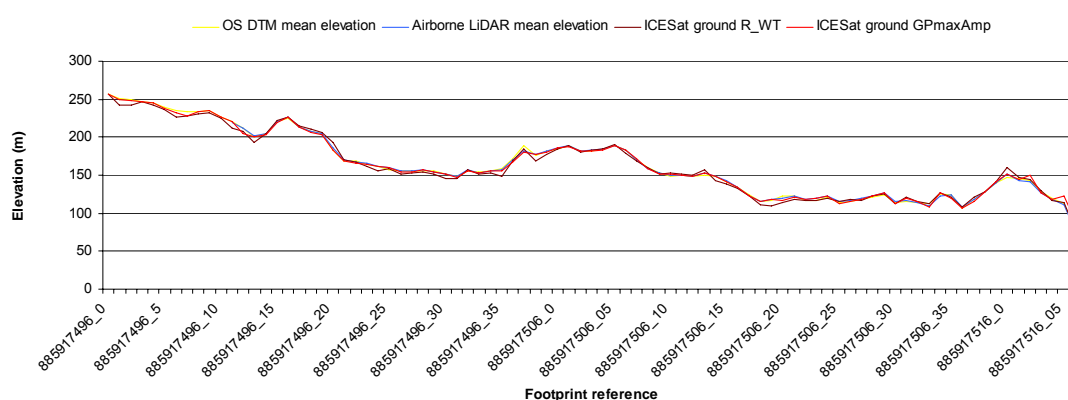


Figure 3. Identification of ground elevation using airborne and satellite LiDAR.

When compared with airborne LiDAR ground surface, mean slope calculated from the airborne LiDAR ground class explained 39% and 0.5% of the error using GP_{amp} and R_{WT} estimates of the ground surface respectively.

Table 4. Comparison of estimated ground surfaces using Ordnance Survey and LiDAR data.

| Comparison (m) | R _{WT} -AL | GP _{AMP} -AL | AL-OS | R _{WT} -OS | GP _{AMP} -OS |
|-----------------|---------------------|-----------------------|-------|---------------------|-----------------------|
| Mean offset | -0.97 | -0.14 | 0.12 | -0.84 | -0.02 |
| Max. difference | 9.02 | 12.73 | 3.05 | 12.07 | 13.11 |
| Min. difference | -9.64 | -7.36 | -8.56 | -10.43 | -8.63 |

The method of identifying the vegetation return using Gaussian decomposition from product GLA14 corresponded slightly closer than use of signal limits with a terrain index in comparison with vegetation height estimates from airborne LiDAR. Regression analysis for the two methods produced R² of 0.68, RMSE 4.4m and R² of 0.63, RMSE 4.7m respectively. The correlation using Gaussian decomposition is shown in Figure 4 and a further comparison between satellite and airborne LiDAR vegetation estimates are discussed in detail within (Rosette *et al.*, submitted).

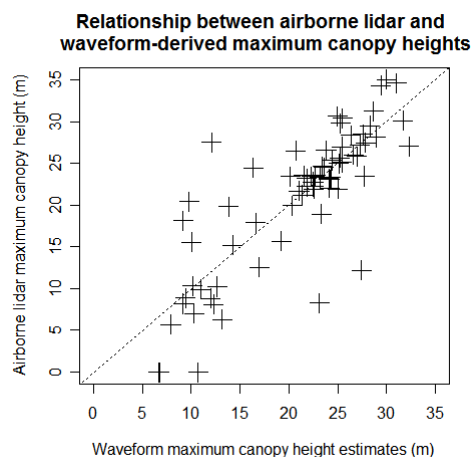


Figure 4. Relationship between airborne and satellite LiDAR maximum canopy height estimates using Gaussian decomposition (product GLA14).

The following figures show examples of ICESat/GLAS waveforms plus corresponding simulated returns from FLIGHT using inputs of footprint surface and overlying vegetation properties. A summary of estimated and measured vegetation heights is found in Table 5. For these examples in fact, better estimates of maximum canopy height were produced using multiple regression analysis with Waveform Extent and a Terrain Index.

Table 5. Examples of estimated vegetation heights from satellite and airborne LiDAR and coincident field measurements.

| Vegetation height estimation: | GP _{AMP} | R _{WT} | AL | Field |
|-------------------------------|-------------------|-----------------|-------|--------|
| Footprint 885917506_14 | 24.2m | 30.8m | 30.6m | 31 |
| Footprint 885917506_29 | 21.2m | 21.9m | 23.4m | - |
| Footprint 885917516_05 | 17.4m | 26.4m | 24.2m | 24.75m |

Figure shows a vegetated slope of 17.8° with species coverage of 60% Douglas Fir towards the top of the slope and the remaining area comprising oak beneath. Calculated top heights from records within the sub-compartment database and corresponding yield models for the two species are respectively 23.9m and 17.6m. The maximum observed field measurement from within the estimated footprint boundaries was 24.75m.

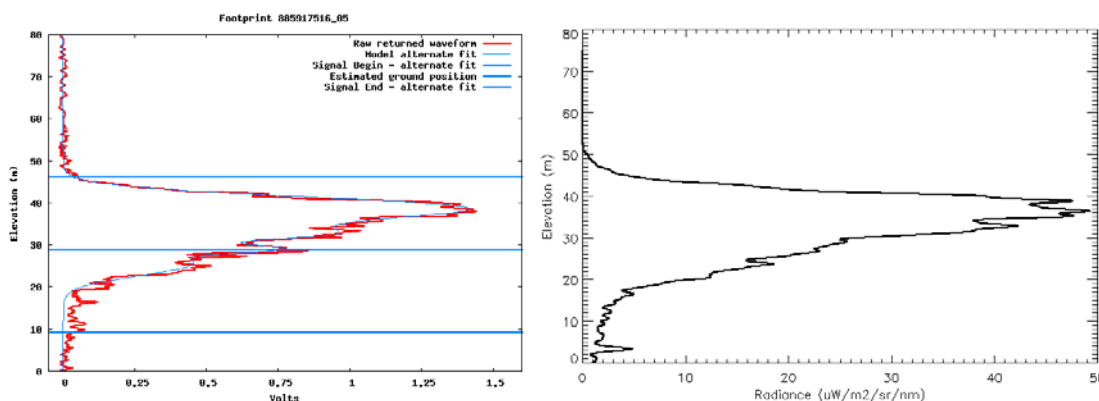


Figure 5: GLAS and simulated waveforms for a steep and continuously vegetated slope.

The footprint shown in Figure6 covers a pure stand containing 100% oak with top height estimated as 21.3m. Field measurements are not available for this site. Slope from airborne LiDAR data was calculated as 1.7°.

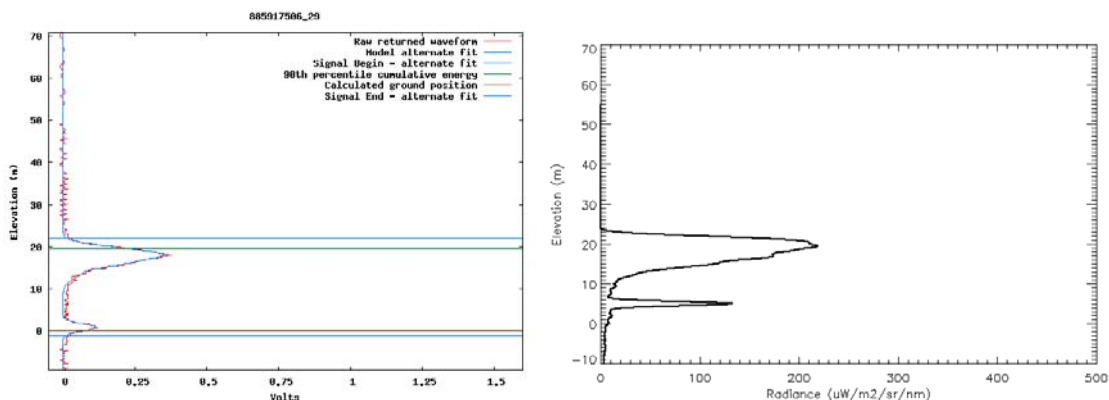


Figure 6: Returned waveform and simulation for a single layer canopy on level terrain.

Figure 7 shows an example of a footprint on a gentle slope (4.9°) which samples a stand of predominantly Douglas Fir of two ages: 29% of the area has estimated top height of 28.6m whilst 6% had calculated top height of 22.8m. The stand also contains 21% Oak (21.5m top height) with the remainder of the area being unplanted. Maximum tree height from field measurements was 31m.

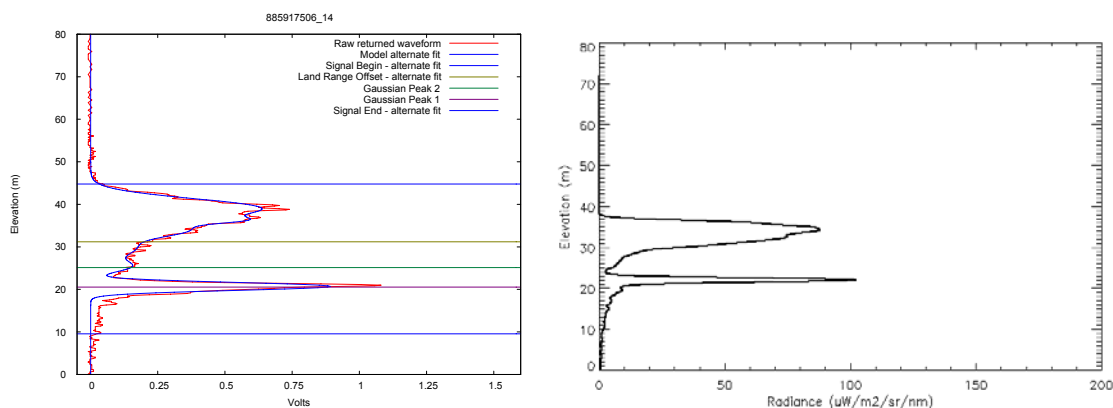


Figure 7: GLAS waveform and FLIGHT simulation for a multi-layered canopy on a gentle slope.

4. Discussion

This study has shown the ability to identify the vegetation signal from satellite LiDAR waveforms. For the Forest of Dean, the method using Gaussian decomposition to estimate ground elevation within the waveform ground peak produced the smallest mean error in comparison with both airborne LiDAR and Ordnance Survey Land-Form PROFILE DTM mean ground elevations. However, ground elevation for the ICESat/GLAS pass crossing the Forest of Dean was estimated with a mean error of less than 1m using both methods.

Slope was identified as a contributory factor for the minor negative offset using Gaussian decomposition whereas this had been successfully addressed using the Waveform Extent/Terrain Index method. A further explanation may be offered by the fact that the model fit is produced by the sum of Gaussian peaks and therefore the centroid of the Gaussian Peak with greatest amplitude may not always represent the most common ground elevation. Use of the largest amplitude inflexion point within the ground return may address this small error. For both methods a negative bias is seen in the estimation of the ground surface. For the R_{WT} method, this may be a result of the waveform ‘tail’ extending below the true lowest ground surface.

The results suggest that, for situations such as the Forest of Dean in which dense canopy cover or extreme slope do not prevent a representative ground surface from being detected, Gaussian

decomposition may offer an appropriate means of estimating ground elevation. Furthermore, GLAS estimations of ground elevation have shown considerable consistency across different laser operations (Sun *et al.*, 2008).

Estimates of maximum canopy height using R_{WT} and GP_{amp} methods compared well against airborne LiDAR estimates of the same. Regression analysis produced R^2 of 0.68, RMSE 4.4m and R^2 of 0.63, RMSE 4.7m for the two methods respectively.

Inputs of generalised crown shape and crown dimensions, vegetation height, canopy cover and slope were used for LiDAR waveform modelling within the radiative transfer model FLIGHT. Returned and simulated waveforms show similar properties.

The returned and modelled waveforms in Figure show the effect of combined returned signals from a sloped ground surface with relatively dense vegetation throughout the slope. Energy is therefore returned from ground and vegetation surfaces at similar elevations. This is one of the few sites at the Forest of Dean for which a ground peak cannot be distinguished within the waveform.

The GLAS waveform seen in Figure (left) shows the effect of a single layer oak canopy with most energy interception towards the uppermost canopy. However the simulated waveform anticipates that energy will also be returned from within the canopy. The low amplitude and laser penetration seen in the GLAS waveform may be a result of signal dampening due to variations in atmospheric transmittance. This remains to be determined.

The modelled and returned waveforms in Figure show signals from a multi-layered canopy on a gentle slope. Energy is returned throughout the canopy and the effect of multiple scattering between intercepted surfaces is seen in the ‘tail’ visible beneath the ground peak in both simulated and GLAS waveforms.

5. Conclusions

This study has shown the possibility of extracting representative ground surfaces from large footprint full waveforms which are comparable with airborne LiDAR and Ordnance Survey mean ground elevations. Slope was found to be a contributory factor in the small error found where Gaussian decomposition was used to estimate ground elevation. Estimates of maximum canopy height from satellite LIDAR waveforms corresponded closely with those using coincident airborne LiDAR. The effects of topography and canopy properties on waveform composition were successfully modelled using the radiative transfer model FLIGHT which aims to assist future waveform interpretation.

Acknowledgements

Many thanks are due to John Armston, Queensland Remote Sensing Centre, Indooroopilly, Australia, for kindly allowing use of the in-house LiDAR processing software. The Forestry Commission Forest Research Agency is also acknowledged for use of a subset of airborne LiDAR data for the Forest of Dean. This research is funded by the UK Natural Environment Research Council (NERC), forming part of the objectives of the Climate and Land-Surface Systems Interaction Centre (CLASSIC).

References

Abshire, J., Sun, X., Riris, H., Sirota, J., McGarry, J., Palm, S., Yi, D. and Liiva, P., 2005.

- Geoscience Laser Altimeter System (GLAS) on the ICESat Mission: On-orbit measurement performance. *Geophysical Research Letters*, 32(L21S02)
- Brenner, A., Zwally, H., Bentley, C., Csatho', B., Harding, D., Hofton, M., Minster, J-B., Roberts, L., Saba, J., Thomas, R. and Yi, D., 2003. Derivation of Range and Range Distributions from Laser Pulse Waveform Analysis for Surface Elevations, Roughness, Slope and Vegetation Heights, NASA Goddard Space Flight Center plus various others
- Brenner, A., Zwally, H., Bentley, C., Csatho', B., Harding, D., Hofton, M., Minster, J-B., Roberts, L., Saba, J., Thomas, R. and Yi, D., 2003. Derivation of Range and Range Distributions from Laser Pulse Waveform Analysis for Surface Elevations, Roughness, Slope and Vegetation Heights, NASA Goddard Space Flight Center plus various others
- Harding, D. and Carabajal, C., 2005. ICESat waveform measurements of within-footprint topographic relief and vegetation vertical structure. *Geophysical Research Letters*, 32 (L21S10)
- Helmer, E.H. and Lefsky, M.A., 2006. Forest Canopy Heights in Amazon River Basin Forests as Estimated with the Geoscience Laser Altimeter System (GLAS). USDA Forest Service Proceedings, RMRS-P-42CD
- Hese, S., Lucht, W., Schmullius, C., Barnsley, M., Dubayah, R., Knorr, D., Neumann, K., Riedel, T. and Schroter, K., 2005. Global biomass mapping for an improved understanding of the CO₂ balance - the Earth observation mission Carbon-3D. *Remote Sensing of Environment*, 94: 94-104.
- Lefsky, M., Harding, D., Keller, M., Cohen, W., Carabajal, C., Del Bom Espirito-Santo, F., Hunter, M., de Oliveira Jr., R. and de Camargo, P., 2005. Estimates of forest canopy height and aboveground biomass using ICESat. *Geophysical Research Letters*, 32 (L22S02)
- Lefsky, M.A., Keller, M., Pang, Y., de Camargo, P. and Hunter, M.O., 2007. Revised method for forest canopy height estimation from the Geoscience Laser Altimeter System waveforms. *Journal of Applied Remote Sensing*, 1: 1-18.
- Nelson, R., Næsset, E., Gobakken, T., Ståhl, G. and Gregoire, T., 2008. Regional Forest Inventory using an Airborne Profiling LiDAR. *Journal of Forest Planning*, 13(Special Issue 'Silvilaser'): 287-294.
- Nelson, R., Short, A. and Valenti, M., 2004. Measuring Biomass and Carbon in Delaware Using an Airborne Profiling Lidar. *Scandinavian Journal of Forest Research*, 19: 500-511.
- North, P., 1996. Three-Dimensional Forest Light Interaction Model Using a Monte Carlo Method. *IEEE Transactions on Geoscience and Remote Sensing*, 34(4 July): 946-956.
- NSIDC, 2003. ICESat/ GLAS Data at NSIDC. National Snow and Ice Data Center, [online] available from <http://nsidc.org/daac/icesat/>.
- Rosette, J.A., North, P.R.J. and Suárez, J.C., 2008. Vegetation Height Estimates for a Mixed Temperate Forest using Satellite Laser Altimetry. *International Journal of Remote Sensing*, 29(5): 1475-1493.
- Rosette, J.A., North, P.R.J., Suárez, J.C. and Armston, J.D., submitted. A Comparison of Biophysical Parameter Retrieval for Forestry using Airborne and Satellite LiDAR. *International Journal of Remote Sensing*, Special Issue ForestSat 2007
- Schutz, B., Zwally, H., Shuman, C., Hancock, D. and DiMarzio, J., 2005. Overview of the ICESat Mission. *Geophysical Research Letters*, 32(L21S01)
- Sun, G., Ranson, K.J., Masek, J., Guo, Z., Pang, Y., Fu, A. and Wang, D., 2008. Estimation of Tree Height and Forest Biomass from GLAS Data. *Journal of Forest Planning*, 13(Special Issue 'Silvilaser'): 157-164.
- Zwally, H., Schutz, B., Abdalati, W., Abshire, J., Bentley, C., Brenner, A., Bufton, J., Dezio, J., Hancock, D., Harding, D., Herring, T., Minster, B., Quinn, K., Palm, S., Spinhirne, J. and Thomas, R., 2002. ICESat's Laser Measurements of Polar Ice, Atmosphere, Ocean and Land. *Journal of Geodynamics*, 34: 405-445.

A Monte Carlo radiative transfer model of satellite waveform lidar

Peter North¹, Jacqueline Rosette², Juan Suarez³ and Sietse Los⁴

¹ Climate and Land-Surface Systems Interaction Centre, Swansea University, SA2 8PP, U.K. p.r.j.north@swansea.ac.uk

² Climate and Land-Surface Systems Interaction Centre, Swansea University, SA2 8PP, UK. ggrosette@swansea.ac.uk

³ Research Agency of the Forestry Commission, Northern Research Station, Roslin, Midlothian, EH25 9SY, UK. juan.suarez@forestry.gsi.gov.uk

⁴ Climate and Land-Surface Systems Interaction Centre, Swansea University, SA2 8PP, U.K. s.o.los@swansea.ac.uk

Abstract

We present a method and initial results for a model of the interaction of waveform lidar with a three-dimensional canopy representation. The model is developed from the FLIGHT radiative transfer model (North, 1996), based on Monte Carlo simulation of photon transport. Foliage is represented by structural properties of leaf area, leaf angle distribution (LAD), crown dimensions and fractional cover, and the optical properties of leaves, branch, shoot and ground components. Important characteristics of the model are that it can represent multiple scattering of light within the canopy and with the ground surface, simulate the return signal efficiently at multiple wavebands, and model the effects of topography. Spatial and temporal sampling characteristics of the lidar instrument are explicitly modelled. A sensitivity analysis gives expected effects of canopy parameters on the waveform, and indicates potential for retrieval of the canopy properties of fractional cover and leaf area, in addition to height.

Keywords: Waveform lidar, ICESat GLAS, radiative transfer model

1. Introduction

Global datasets of land surface biophysical variables are required from remote sensing to drive land surface parameterisations coupled to atmospheric general circulation models, and to calculate the exchange of carbon, water, energy and momentum fluxes between the land and atmosphere (Sellers et al., 1996; North, 2002; Alton et al., 2007). By recording temporal return, light detection and ranging (lidar) offers a unique measurement directly related to vegetation canopy height. While hitherto mostly applied using airborne platforms at local scale, the Geoscience Laser Altimeter System (GLAS) aboard the Ice, Cloud and land Elevation Satellite (ICESat) provides an opportunity to contribute to forest quantification and monitoring at regional and global scales (Schutz et al., 2005). Previous work supports the use of this data source for the estimation of canopy height and sub-canopy terrain, and, by correlation, further properties such as biomass (Lefsky et al., 2005; Harding and Carabajal, 2005; Rosette et al., 2008a). There is also ongoing research in estimation of further parameters such as vegetation cover, stemwood volume and plant area index (PAI), and their vertical profile (Koetz et al., 2006; Rosette et al., 2008b).



Figure 1: Example FLIGHT model output showing scene reflectance under solar illumination.

Increasingly, physically-based radiative transfer models of vegetation canopies have been used to constrain retrieval of land surface biophysical parameters, either by direct inversion or use in algorithm development. For lidar, radiative transfer models have been developed originally for atmospheric simulation (Platt, 1981), and recently several models have been developed for vegetation canopies which treat the light interaction at various degrees of complexity (Govaerts and Verstraete, 1998; Ni-Meister et al., 2001; Kotchenova *et al.*, 2003; Disney et al., 2006).

In this work we aim to extend the three-dimensional radiative transfer model FLIGHT (North, 1996) to model waveform lidar interaction at scales suitable for ICESat interpretation. The model is based on Monte Carlo solution of radiative transfer, and offers a consistent link from lidar-derived structure to full canopy optical response and vegetation photosynthesis (Barton and North, 2001; Alton et al., 2005). A further aim is to explore the theoretical potential of biophysical parameter retrieval from satellite waveform lidar.

2. Method

The Method is based on Monte Carlo evaluation of photon transport. Monte Carlo simulation is a versatile technique, which allows highly accurate estimation of light interception and bidirectional reflectance (Disney, et al., 2000). The technique requires sampling of the photon free-path within a canopy representation, and simulation of the scattering event at each interaction. By iteration we obtain accurate treatment of light interception and multiple scattering between foliage elements and the soil boundary. Overlapping crowns, and multiple scattering within and between different crowns and the ground surface are thus modelled. The particular challenge of modelling lidar interaction is the additional inclusion of time dependency of the response, governed by varying path length over multiple interactions forming the return, and the temporal spread of the incoming pulse.

Table 1: FLIGHT canopy input parameters

| Name | Units | Meaning | Value |
|-------------------------------------|--------------------------------|---------------------------------|-----------|
| PAI | m ² /m ² | Plant area index (one sided) | 3.0 |
| LAD | - | Leaf angle distribution | Spherical |
| F _c | - | Crown fractional coverage | 0.7 |
| F _g | - | Fraction of green foliage | 0.8 |
| F _b | - | Fraction of bark | 0.2 |
| E _{xy} | m | Ellipsoid horizontal radius | 8.0 |
| E _z | m | Ellipsoid vertical eccentricity | 8.0 |
| D _l | m | Leaf size diameter | 0.05 |
| DBH | m | Trunk diameter at breast height | 0.1 |
| S _r | 0-1 | Soil roughness | 0 |
| S _y | Deg | Terrain slope (yz plane) | 0 |
| H _{min} , H _{max} | m | Min/max height to crown start | 15,20 |
| ρ _L | - | Leaf reflectance | 0.4 |
| τ _L | - | Leaf transmittance | 0.4 |
| ρ _s | - | Soil reflectance | 0.15 |

2.1 Canopy representation

Foliage is approximated by structural parameters of area density, angular distribution, and size, and optical properties of reflectance and transmittance. The foliage is constrained to lie within geometric envelopes, defined by ellipsoidal or conical primitives. The locations of the crowns are normally generated statistically, parameterized by crown fractional cover, and canopy height range; however it is possible to define precise crown locations. Scene elements may also be explicitly represented by facets. Spectral reflectance and transmittance properties of the scene elements are also specified, normally approximated as bi-Lambertian. A list of parameters and typical values is given in Table 1. Figure 1 illustrates a typical canopy representation, output from the model under solar illumination conditions.

2.2 Sensor model

A generic description of a waveform lidar instrument is defined by parameters giving sensor location, beam energy, beam angular divergence and temporal spread. Both angular divergence and temporal spread are modelled as Gaussian. The set of parameters defining the lidar instrument are given in Table 2, with example values for GLAS used in the current study (Brenner et al., 2000).

2.3 Evaluation of lidar waveform

The original model (North, 1996) traced photon trajectories forwards from the source until absorption in the canopy or leaving the canopy boundary, when energy was accumulated in bins defined for each solid angle of exit. Subsequently the model was developed to sample paths from a given view direction to intercepted surfaces, and to accumulate the radiance contribution from these surfaces (Disney et al., 2000; Barton and North, 2002). The latter method is more

Table 2: Lidar sensor model

| Name | Units | Meaning | Value |
|-------------------|----------------|---|--------------------------|
| (P_x, P_y, P_z) | m | Sensor position relative to scene centre | (0,0,600000) |
| θ_0 | deg | Sensor zenith angle | 0 |
| ϕ_0 | deg | Sensor azimuth angle | 0 |
| sl | ns | Emitted RMS pulse width, assuming Gaussian (1sd) | 5 |
| q_T | rad | Half-width angle of beam divergence, Gaussian (1sd) | 0.00011 |
| $IFOV$ | rad | Detector IFOV | 0.0004 |
| A_T | m ² | Detector telescope area | 0.709 |
| T_{RTsm} | - | Roundtrip atmospheric trans. | 0.8 (532nm) 0.9 (1024nm) |
| E_{trans} | mJ | Total pulse energy | 32 (532nm); 72 (1064nm) |
| Δ_t | ns | Recording bin width | 1 |

appropriate for lidar calculation, as it is possible to efficiently estimate return for infinitesimal angles; this is necessary for lidar as viewing is made at the retro-reflection direction or ‘hot-spot’, where the reflectance changes very significantly with small changes in view angle.

The method proceeds by sampling n rays over the instrument IFOV. For each ray:

- (i) Find the intersection with the first surface facet (leaf/bark/soil)
- (ii) The facet illumination is calculated as the sum of direct and diffuse incoming light. The diffuse light term is calculated by recursive sampling of higher scattering orders. The radiance contribution is defined according to the standard rendering equation, depending on facet orientation with respect to illumination, and optical properties.
- (iii) For each facet and scattering order, both the radiance contribution and the total return path length to the sensor are calculated. The path length is equivalent to time of signal. For efficiency, ground-leaving radiance for unit incoming signal is initially recorded.
- (iv) The radiance is binned into m bins according to path length, whose width is defined by the sensor model temporal sampling.

The final step accounts for detector characteristics and pulse width:

- (v) The radiance values are converted into absolute power (mW) recorded in each temporal bin, dependent on the sensor aperture A_T , distance to sensor P_z and atmospheric round-trip transmission T_{RTsm} . The effect of pulse width is modelled by Gaussian convolution of the resultant output array, with amplitude dependent on emitted pulse energy E_{trans} .

The estimation error decreases as $n^{0.5}$. For results here we use a sampling of $n=10^4$, and obtain convergence after scattering order 8.

3. Results

3.1 Comparison with FLIGHT reflectance

The waveform was integrated over time and normalised by downwelling radiance to allow comparison with equivalent bidirectional reflectance factor (BRF) for the scenes generated by the original FLIGHT model. While some of the code is common between the original FLIGHT code and the lidar waveform model, the check is useful as the FLIGHT model BRF has been previously checked by intercomparison with other three-dimensional codes as part of the Radiation Model Intercomparison (RAMI) project (Widlowski et al., 2007). The recent analysis within RAMI of six selected three-dimensional models showed dispersion within 1% over a large range of canopy descriptions.

The surface reflectance is estimate from the lidar return as:

$$\rho_{surf} = \frac{\pi E_{rec} R^2}{E_{trans} A_t T_{RTatm}} \quad (1)$$

where E_{rec} (pJ) is calculated as

$$E_{rec} = \sum_{i=1}^m L_i \Delta_t \quad (2)$$

where energy is accumulated in m sample bins, where each sample bin i has accumulated power L_i (mW), and the bins correspond to temporal increment Δ_t ns .

Seventeen scenes were generated through independent variation of model parameters described in Table 3, with random spatial positioning of 200 crowns at 70% fractional cover. Figures 2 and 3 show comparison at 532nm and 1064nm respectively. Error bars denote scene spatial variation at the scale of the lidar footprint. The results show unbiased estimate of reflectance by the waveform integration, though with scatter about the line. This is expected as the lidar spatial sampling is much smaller than the whole scene simulated by FLIGHT.

3.2 Sensitivity analysis

Figures 3-4 show example model runs and sensitivity to variation in plant area index (PAI) and ground slope (S). Table 3 shows full results of a sensitivity analysis of modelled output to variation in canopy parameters. Each parameter is varied individually from a 'base case', specified by the central value in each set in the table; the remaining parameters are specified in Tables 1-2. The lidar waveform return power is recorded, integrated over time and partitioned into total return (TR), canopy return (CR) and ground return (GR). Partition is estimated on the basis of position in the waveform. Variation is shown as a percentage deviation from the base case waveform returns.

- Sensitivity to PAI is small in total return, with less than 2% variation for PAI from 2-5, from a base case PAI of 3, and a 17% reduction for PAI of 1. However the partitioned returns show much greater variation, with CR decreasing by over 50%, and a corresponding increase in GR over the same range.
- Variation in leaf angle distribution (LAD) shows impact on total return (-11% to +20%), with a greater impact on CR. Leaf angle will affect both total interception by the canopy by varying projected leaf area, and also the orientation of surfaces with respect to the incoming beam.
- Crown shape has a small impact on total return, with higher vertical and horizontal eccentricities decreasing the CR component relative to spherical crown return.

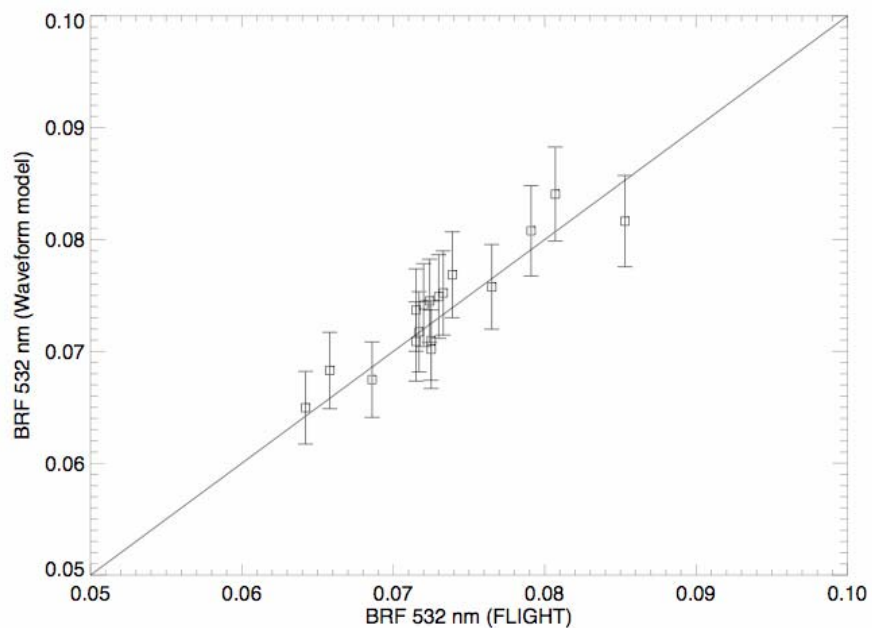


Figure 2: Bidirectional Reflectance Factor (BRF) simulated by FLIGHT vs BRF from time integration of modelled lidar waveform return at 532nm.

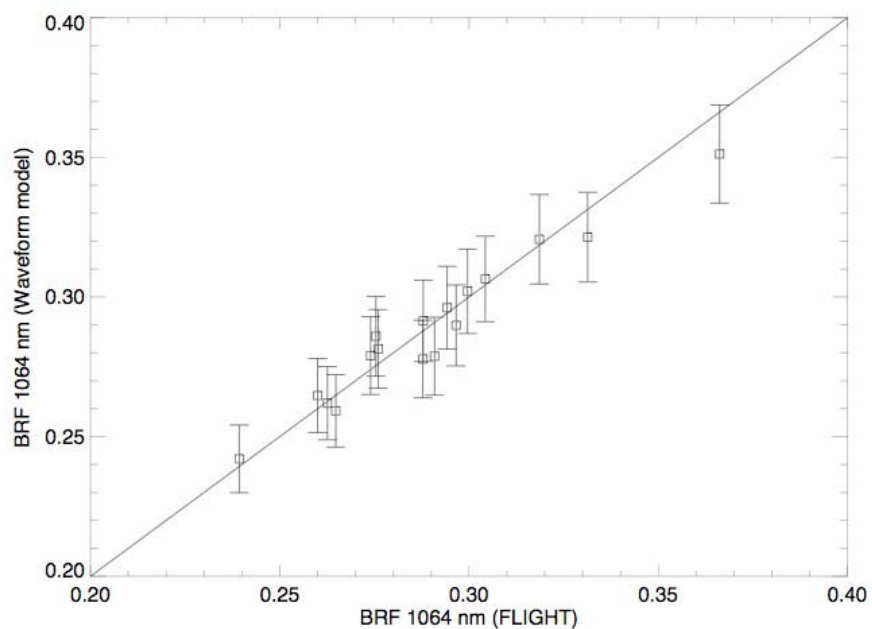


Figure 3: BRF simulated by FLIGHT vs BRF from time integration of modelled lidar waveform return at 1064nm.

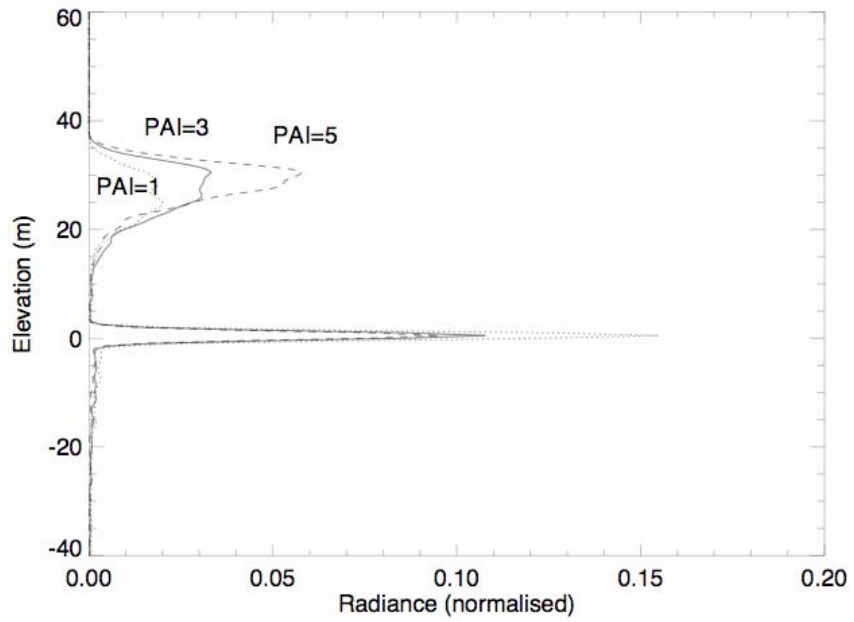


Figure 4: Example model output showing sensitivity of waveform return to plant area index (PAI) variation from 1 to 5.

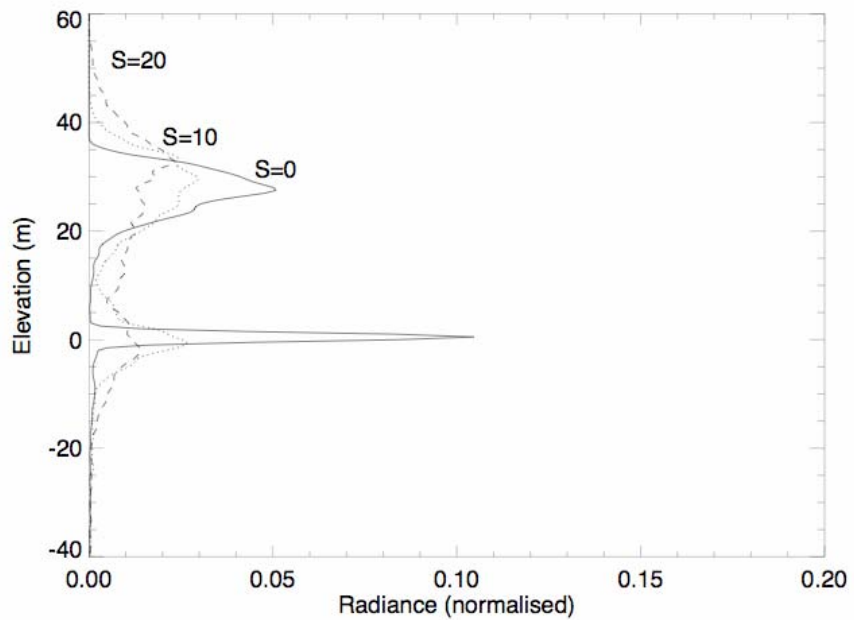


Figure 5: Example model output showing waveform sensitivity to variation in terrain slope, from 0 to 20 degrees.

Table 3: Sensitivity of waveform lidar return at 1064nm to variation in canopy parameters. Return is partitioned into total energy return (TR), canopy return (CR) and ground return (GR). Variation is shown as percentage deviation from the base case return.

| Parameter | Value | TR (%) | CR (%) | GR (%) |
|--------------|-------------|--------|--------|--------|
| PAI | 1 | -17 | -51 | +54 |
| | 2 | -1.8 | -14 | +25 |
| | 3 | - | - | - |
| | 4 | +1.6 | +5.1 | -6.0 |
| | 5 | 0 | +5.2 | -13 |
| LAD | planophile | +20 | +33 | -5.4 |
| | spherical | - | - | - |
| | erectophile | -11 | -19 | +4.5 |
| E_z/E_{xy} | .5 | -4.3 | -6.2 | 0 |
| | 1 | - | - | - |
| | 2 | -4.7 | -7.8 | +1.8 |
| ρ_L | .45 | +10 | +13 | +2.7 |
| | .4 | - | - | - |
| | .35 | -9.2 | -13 | -2.0 |
| τ_L | .45 | +5.1 | +5.8 | +3.7 |
| | .4 | - | - | - |
| | .35 | -4.3 | -4.9 | -3.0 |
| ρ_s | .2 | +10 | 0 | +32 |
| | .15 | - | - | - |
| | .1 | -10 | 0 | -31 |

Analysis of the leaf optical properties shows sensitivity to canopy reflectance (RL),

- with a slightly greater relative change in CR (13%) compared to input parameter (12%). Sensitivity to multiple scattering is illustrated by the effect of increasing leaf transmittance, and by the increase in GR.
- Variation in soil boundary reflectance (RS) shows direct sensitivity of GR, with impact on total return corresponding to area fraction in scene.

3.3 Evaluation of indices for canopy parameter retrieval

While total absolute lidar return is relatively insensitive to vegetation cover, relative to the various perturbing parameters, the differential response of vegetation and ground components suggests use of metrics based on these. However, while reliable separation of a canopy and ground component is frequently problematic, for example in steeply sloping terrain or very

dense canopies, there are some instances where separate canopy and ground waveforms can be identified. For example Rosette et al. (*submitted*) explored use of ratio of canopy to total waveform area in correlation with canopy cover in a mixed temperate forest, where separation of ground from canopy was based on Gaussian decomposition of the return pulse. Figure shows an example of a normalised index regressed against the vertically projected plant area index (VPAI). The waveform index (WI) is defined as

$$WI = (CR-GR)/(CR+GR) \quad (3)$$

The figure shows the index is sensitive to VPAI ($R^2=0.87$) while relatively insensitive to perturbing factors such as variation in leaf and soil optical properties. Such a normalised index would also be insensitive to absolute calibration of the return radiance.

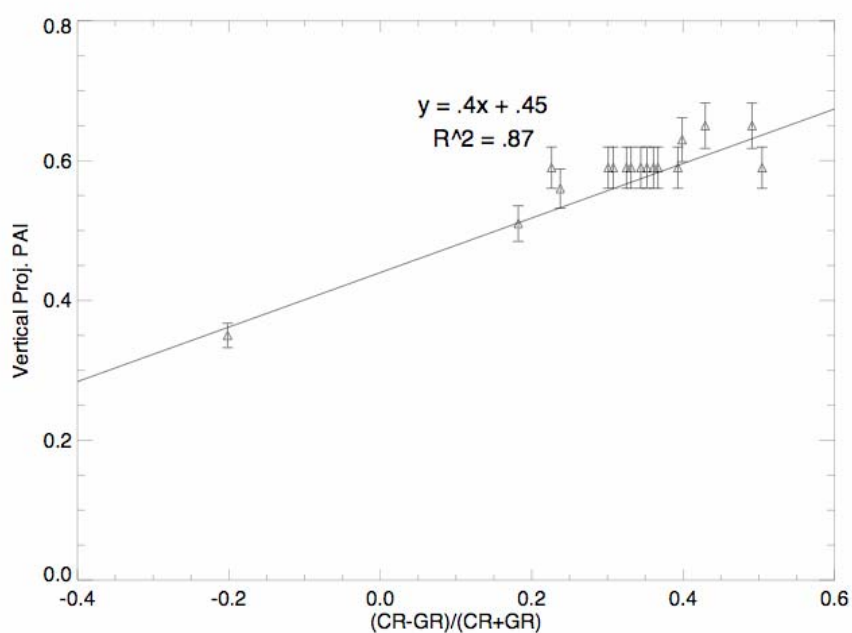


Figure 6: Vertically projected plant area index (PAI) vs index derived from waveform lidar, separated into canopy return (CR) and ground return (GR).

4. Discussion

We have presented a Monte Carlo radiative transfer model of waveform lidar for three-dimensional vegetation canopies, within the framework of the FLIGHT model (North 1996). Good agreement is found between the integrated waveform energy and directly derived BRFs from FLIGHT. A sensitivity analysis shows information content in the waveform signal related to canopy cover variation and perturbing factors such as plant area index (PAI) and optical properties. Further research is recommended to accurately model atmospheric scattering and absorption, and to test the model against a wider range of canopies.

Acknowledgements

This work is supported by the NERC Climate and Land-Surface Systems Interaction Centre, (CLASSIC). We acknowledge scientific input from Dr Malcolm Watson, BAe Systems.

References

- Alton, P., Mercado, L. and North, P., 2007. A sensitivity analysis of the land-surface scheme JULES conducted for three forest biomes: Biophysical parameters, model processes, and meteorological driving data. *GBC* 20, GB1008, doi:10.1029/2005GB002653.
- Alton, P.B., North, P., Kaduk, J. and Los, S.O., 2005. Radiative transfer modelling of direct and diffuse sunlight in a Siberian pine forest. *J. Geophys. Res.*, 110(D23): D23209.
- Barton, C.V.M. and North, P.R.J., 2001. Remote sensing of canopy light use efficiency using the photochemical reflectance index: model and sensitivity analysis. *Remote Sensing of Environment*, 78, 164-273.
- Brenner, A.C., Zwally, H.J., Bentley, C.R. et al. 2000. GLAS Algorithm Theoretical Basis Document 3.0, NASA GSFC.
- Disney, M. I., Lewis, P. and Saich, P., 2006. 3D modelling of forest canopy structure for remote sensing simulations in the optical and microwave domains, *Remote Sensing of Environment* 100(1), 114-132.
- Disney, M.I., Lewis, P. and North, P.R.J., 2000. Monte Carlo ray tracing in optical canopy reflectance modelling. *Remote Sensing Reviews*, 18(2-4), 197-226.
- Govaerts, Y.M. and Verstraete, M.M., 1998. Raytran: A Monte Carlo ray-tracing model to compute light scattering in three-dimensional heterogeneous media. *IEEE Transactions on Geoscience and Remote Sensing*, 36(2), 493-505.
- Harding, D. J., and Carabajal, C. C., 2005. ICESat waveform measurements of within-footprint topographic relief and vegetation vertical structure. *Geophysical Research Letters*, 32, L21S10, doi:10.1029/2005GL023471.
- Koetz, B., Morsdorf, F., Sun, G. et al., 2006. Inversion of a Lidar Waveform Model for Forest Biophysical Parameter Estimation. *IEEE Geoscience and Rem. Sens. Letters*, 3(1).
- Kotchenova, S.Y., Shabanov, N.V., Knyazikhin, Y., et al., 2003. Modeling lidar waveforms with time-dependent stochastic radiative transfer theory for remote estimations of forest structure. *Journal of Geophysical Research*, 108(D15), 4484, doi:10.1029/2002JD003288.
- Lefsky, M., Harding, D., Keller, M., et al., 2005. Estimates of forest canopy height and aboveground biomass using ICESat. *Geophysical Research Letters*, 32 (L22S02).
- Ni-Meister, W., Jupp, D.L.B., and Dubayah, R., 2001. Modeling lidar waveforms in heterogeneous and discrete canopies. *IEEE TGARS* 39(9), 1943-1958.
- North, P.R.J., 1996. Three-dimensional forest light interaction model using a Monte Carlo method. *IEEE Transactions on Geoscience and Remote Sensing* 34(5): 946-956.
- North, P.R.J., 2002. Estimation of fAPAR, LAI and vegetation fractional cover from ATSR-2 imagery. *Remote Sensing of Environment*, 80, 114-121.
- Platt, C.M.R., 1981. Remote Sounding of High Clouds. III: Monte Carlo Calculations of Multiple-Scattered Lidar Returns. *Journal of the Atmospheric Sciences*, 38(1): 156-167.
- Rosette, J.A., North, P.R.J. and Suárez, J.C., 2008a. Vegetation Height Estimates for a Mixed Temperate Forest using Satellite Laser Altimetry. *Int. J. of Rem. Sens.*, 29(5): 1475-1493.
- Rosette, J.A., North, P.R.J. and Suárez, J.C., 2008b. Satellite lidar estimation of stemwood volume: a method using waveform decomposition. *Photogramm. J. Finland*, 21(1): 76-85.
- Rosette, J.A., et al., *submitted*. A Comparison of Biophysical Parameter Retrieval for Forestry using Airborne and Satellite LiDAR. *Int. J. of Remote Sens.*,
- Sellers, P. J., Los S. O., Tucker C. J., et al., 1996. A revised land surface parameterization (SiB-2) for atmospheric GCMs. Part 2: The generation of global fields of terrestrial biophysical parameters from satellite data. *Journal of Climate*, 9(4), 706-737.
- Schutz B., Zwally, H., Shuman, C., Hancock, D. and DiMarzio, J., 2005. Overview of the ICESat Mission. *Geophysical Research Letters* 32: L21S01
- Sun, G., Ranson, K.J., Masek, J., et al., 2008. Estimation of Tree Height and Forest Biomass from GLAS Data. *Journal of Forest Planning*, 13: 157-164.
- Widlowski, J-L., Taberner, M., Pinty, B. et al., 2007. The third RADIATION transfer Model Intercomparison (RAMI) exercise: Documenting progress in canopy reflectance models. *Journal of Geophysical Research*, 112, D09111, doi:10.1029/2006JD007821.

Assessing the accuracy of forest height estimation with long pulse waveform lidar through Monte-Carlo ray tracing

Steven Hancock^{1,2}, Philip Lewis¹, Mathias Disney¹, Mike Foster³, Jan-Peter Muller²

1, Department of Geography, University College London, Gower street, London, WC1E 6BT. United Kingdom and NERC Centre for Terrestrial Carbon Dynamics.

shancock@geog.ucl.ac.uk

2, Mullard Space Science Laboratory, University College London

3, Lidar technologies ltd, Hovemere, United kingdom.

Abstract

The practicality of using an atmospheric differential absorption lidar (DIAL) such as ESA's A-scope for measuring vegetation is explored. Monte-Carlo ray tracing is used to simulate full waveform lidar responses over explicitly represented 3D forest models with both short and long temporal pulses. Deconvolution and Gaussian decomposition are used to estimate tree top and ground positions over a range of forest ages and stand densities. The errors of the height estimates are precisely quantified by comparison with the 3D model height. It is shown that (at least with a 12.5cm range resolution) an instrument optimised for atmospheric CO₂ measurement can successfully measure forest height over reasonably flat ground.

Keywords: Forestry, lidar, vegetation, simulation, 3D modelling.

1. Background

Carbon flux models are essential for understanding the complex processes involved in the Earth's climate (Woodward et al, 2004). These models need variables, such as biomass and leaf area index (LAI) at a range of scales and locations (Williams et al, 2005). Many areas are inaccessible and it would be prohibitively expensive to cover the world with airborne sensors. Space-borne remote sensing may be the solution.

One of ESA's six proposed Earth explorer missions, due for launch in 2012, is a space-borne full waveform lidar; the A-scope satellite (ESA, 2007). It will be optimised for measuring atmospheric CO₂ by differential absorption lidar (DIAL) with two laser wavelengths, one which causes resonance in the CO₂ molecule, one that does not. These will be close to either 1.65µm or 2.06µm. This paper investigates the ability of such an instrument to measure forest parameters.

2. Simulation system

Studies on estimating forest parameters from waveform lidar are promising; however positional uncertainty of remote measurements and the difficulty of field measurements make validation of real data difficult (Hyde et al, 2005). Computer simulations allow validation as the true parameters of the virtual forest are known. A Monte-Carlo ray tracer based upon the RAT library developed from "frat" (Lewis, 1999) was used to simulate a waveform lidar.

Explicit geometric forest models, in which every needle is described were used for the

simulations. Their creation is described in Disney et al. (2006). In a change to the method of Disney et al. (2006) needles were allowed to transmit light; trusting in the accuracy of the Prospect model (Jacquemond and Baret, 1990) in the absence of reliable transmittance data.

Using explicit 3D models is computationally expensive but avoids the assumption that canopies behave as turbid media; an assumption that ignores the heterogeneity of real trees. It is not clear how such an assumption would affect derived results, especially when derivation uses the same assumptions used to create the forest models (Widlowski et al, 2005).

Simulations were run with a range resolution of 12.5cm, a wavelength of 2.06 μ m, a 30m ground footprint and with and without a temporal laser pulse (100ns is proposed for A-scope). The laser pulse shape is applied to each return before binning so that quantisation noise is not ignored.

3. Realistic noise

A real direct detection instrument will suffer from noise from photon statistics, background light and detector noise. Photon statistic noise, n_s is modelled as Gaussian with a sigma of the square root of the number of photons measured in that bin. Background power, P_b , is given by the following equation (values used in this investigation are shown in brackets);

$$P_b = \rho \times E_\lambda \times \frac{TFOV^2}{4} \times A_r \times \cos(\vartheta_s) \times T_{atm} \times \Delta b \quad (1)$$

Where ρ is surface albedo (calculated from waveform), E_λ is solar energy in $Wm^{-2}sr^{-1}nm^{-1}$ (0.67), TFOV is the field of view in radians (0.0002rads), A_r is the receiver telescope area in m^2 (0.79 m^2), ϑ_s is the solar incidence angle (30 $^\circ$), T_{atm} is the atmospheric transmission (0.8) and Δb is the bandwidth in nm (10nm). This is combined with detector noise and converted to detected photon count to get background and detector noise $n_{b,d}$ with the following;

$$n_{b,d} = QE \times P_b \times \left(\frac{\lambda}{h \times c} \right) + \frac{1}{2 \times F} \times \left(\frac{QE \times \lambda}{h \times c} \right)^2 \times NEP^2 \times t \quad (2)$$

Where QE is detector quantum efficiency (0.5), λ is wavelength in m (2.06 μ m), h is Planck's constant in m^2kgs^{-1} , c is the speed of light in ms^{-1} , F is the excess noise factor of the detector (2) and NEP is the noise equivalent power on the detector after amplification in $W Hz^{-0.5}$ (assumed negligible). This is then multiplied by a random number between 0 and 1 and combined with the photon statistics, n_s to get total noise by;

$$noise = \sqrt{(n_{stats} + n_{b,d}) \times F} \quad (3)$$

Different levels of noise were simulated by assuming that the signal (noiseless waveform) included a certain number of photons. Noise effects were added and the resultant waveform scaled from photon count to reflectance for analysis. Different random number seeds were used to fully investigate the effect of noise on inversions. As the noise is added based upon signal photons the wavelength is irrelevant. 2.06 μ m will need a more powerful laser to get the same photon count from a forest than at 1.064 μ m. Figures 1 to 5 used 1.064 μ m (they are for an optimised canopy lidar), though 2.06 μ m should behave in a similar fashion for the same signal level.

4. Derivation of parameters

Two of the most important biophysical parameters for ecological models are biomass and leaf area index (LAI). These cannot be directly measured by lidar or any current remote instrument but can be related to tree height and canopy coverage through empirical relationships. More complex metrics combining height and canopy coverage with height (foliage profile) can be used to improve the accuracy of estimates (Lefsky et al, 1999). With any method tree height and canopy are the measurables needed to derive any parameters.

For tree height to be measured the position of the tree top and ground must be distinguishable from the waveform. If the topography is negligible over the laser footprint tree height can be found directly. Topography complicates the matter. It may be possible to use multi-spectral lidar to extract ground position from topographically blurred waveforms.

The tree top is the signal start above background noise in the absence of a pulse length. Taking it as the point at which the signal rises above the noise threshold will always lead to an underestimate. This contributes to the “well known underestimate of tree height by lidar” (Morsdorf et al. 2008). Data assimilation schemes such as the Kalman filter rely on unbiased observations (Williams et al, 2005). Tracking back through the waveform from the noise threshold to the mean noise level should provide an unbiased estimate. Figure 1 shows a histogram of the signal start position error with and without tracking back from the noise threshold. A negative error means a premature signal trigger; this was common in both methods.

Figure 2 shows the mean and modal signal start position errors against signal photon count. The means are biased by some premature triggerings caused by noise. It is hoped that these can be removed by looking at their distance from the ground and rejecting unrealistic tree heights. No attempt was made to calculate the ground position in this experiment due to the calculation’s computational expense. The modal error does not display this bias and shows that both methods giving similar outputs for large photon numbers (small noise) and the tracking method’s superiority at low signal levels (high noise).

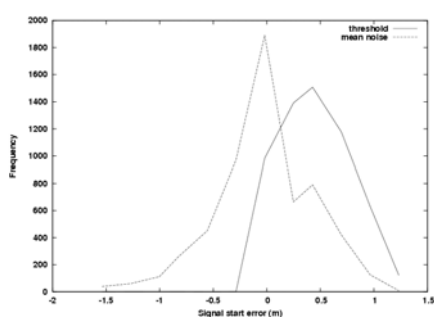


Figure 1. Signal start error histogram for 7,000 signal photons. The negative tail has been clipped for clarity.

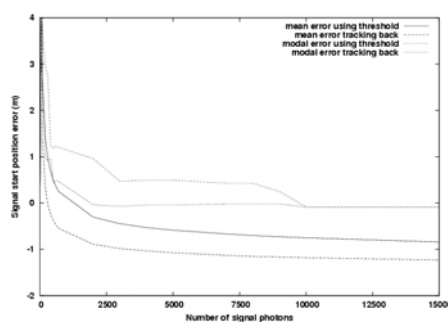


Figure 2. Mean and modal tree top error against number of signal photons for the two methods.

The ground position is much harder to extract. The traditional method is to decompose the waveform into a set of Gaussians by non-linear regression (Hofton et al, 2000). It must then be decided which Gaussian corresponds to the ground. An appropriate threshold (either amplitude or energy contained in the Gaussian) must be chosen to avoid any Gaussians caused by multiple scattering, noise or the canopy. This threshold is dependent upon canopy cover and wavelength. In denser canopies the ground return will be weaker, requiring a lower threshold. In sparser canopies more subterranean multiple scattering may be recorded requiring a higher threshold.

An implementation of the Levenberg-Marquardt method was used to minimise the root mean square difference between the fitted Gaussians and original signal (Press et al, 1994). This method is unstable, the error being affected by waveform shape, canopy cover and noise. Figure 3 shows one of the more successful attempts.

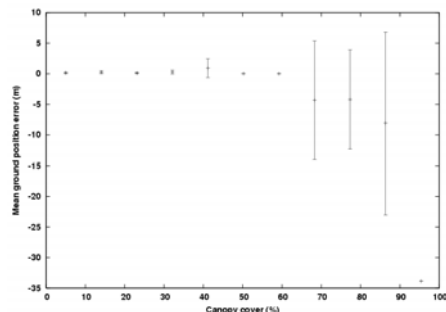


Figure 3. Mean ground position error for 4,000 photons against canopy cover. Bars show standard deviation

These methods perform reasonably well when the ground return contains significant energy and is distinguishable from the canopy return. In very dense canopies (>85% coverage) little signal reaches the ground and a proportion of the inversions will fail. The expected failure rate should be quantified to assess the method's global use as this canopy cover is not uncommon for evergreen broadleaf forests (Hofton et al, 2002). An iterative method to choose an appropriate threshold based upon an estimation of canopy coverage may be necessary.

Figure 4 shows the average energy contained in the nearest Gaussian to the ground, an indicator of how the threshold depends upon canopy cover. A failure is classed as a waveform without a Gaussian centred within (an arbitrary) 3m of the ground. The need for an iterative threshold selection is apparent.

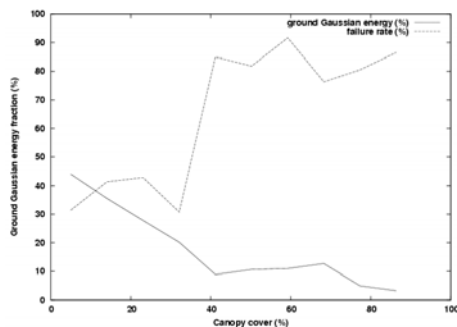


Figure 4. Fraction of waveform energy contained in nearest Gaussian to the ground.

These errors combine to give the tree height error. The signal start error is insensitive to canopy cover, possibly due to the shape of conifers (there is no more foliage at the tree top for dense than for sparse canopies). Figure 5 shows mean tree height error against canopy cover. An overestimate is suggested due to too low a threshold being used to select the ground Gaussian (0.75% of total energy).

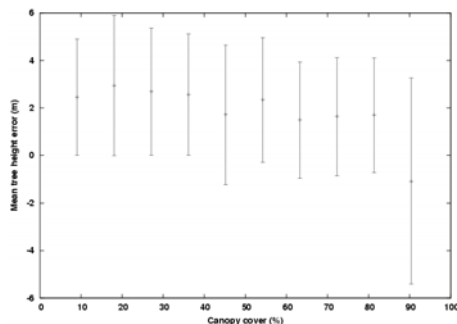


Figure 5. Mean tree height error against canopy cover. Bars show standard deviation.

5. Pulse length

All real lasers have a finite pulse length. This can range from short 6ns pulses such as ICESat’s GLAS up to 100ns for ESA’s proposed A-scope (for smaller linewidth). Any pulse length will blur the waveform, extending the signal start and merging ground and canopy returns. A Gaussian is a good approximation of the pulse shape. For 100ns pulses, corresponding to a Gaussian with a full width half maximum of 25m, this blurring is severe, obliterating any features (as shown in figure 6). If such an instrument is to be used for measuring vegetation some form of deconvolution is needed.

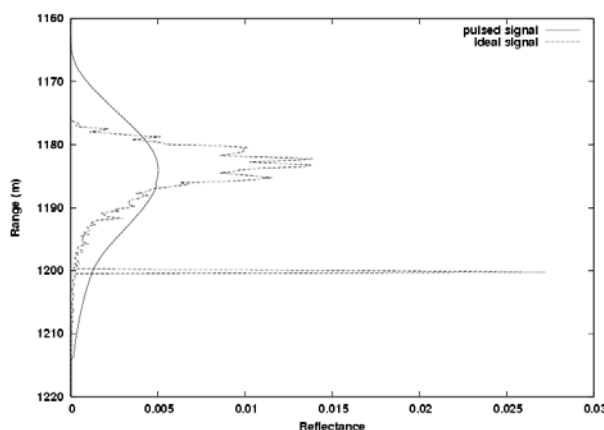


Figure 6. Simulations of an ideal and 100ns pulsed waveform over a Sitka spruce forest.

This can be done either by fitting functions with the known pulse width and shape to the waveform or a Fourier space deconvolution. As figure 6 shows, for long pulses there is little detail left to fit the function to. Any algorithm is more likely to fit a single larger amplitude Gaussian than the two Gaussians needed to de-blur.

Gold’s iterative re-blurring deconvolution method (Jansson, 1997) was selected for its relative robustness to noise. This method is given by the equation;

$$\hat{o}^{(k+1)} = \hat{o}^{(k)} \frac{i}{s \otimes \hat{o}^{(k)}} \quad (4)$$

Where i is the original waveform, s is the deconvolution function (normally the laser pulse) and $\hat{o}^{(k)}$ is the k^{th} estimate of the de-blurred waveform (initially taken as i).

Again simulations offer the advantage over reality of precise error analysis. Simulations were run with and without a pulse length. Deconvolved waveforms were compared to the ideal, pulseless waveforms.

6. Noise

Noise complicates the issue leading to wildly inaccurate products. We can be certain that there should not be any components of the waveform with a higher frequency than is contained in the laser pulse (Gurdev et al, 1993) and any such components can be taken as noise (which is high frequency). These can be removed by convolution with the laser pulse before deconvolution.

The following method was found to give the best results when deconvolving noised waveforms;

Noise statistics were calculated from a known empty portion (all signal more than 70m above the maximum intensity return).

Background noise was removed by subtracting a constant threshold, either the mean noise level plus three standard deviations or the maximum recorded noise level, whichever was greater.

The waveform was smoothed with the laser pulse.

The waveform was deconvolved with 6,000 iterations of Gold's method using the laser pulse convolved with the smoothing function as the deconvolution function.

Figure 7 shows that this gave an acceptable recreation of the ideal waveform for high noise levels (3,000 signal photons); an encouraging result. A waveform with clearly defined canopy and ground returns (without pulse length) was used for the initial investigation; it had a canopy coverage of 81% and a maximum tree height of 12.5m. This avoids the complications of trying to find low canopy or ground returns in the blurred waveforms.

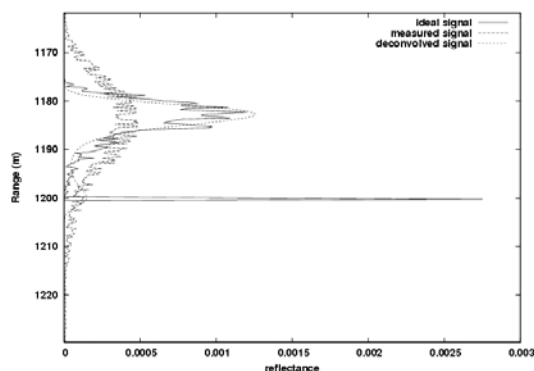


Figure 7, 3,000 signal photons, an acceptable recreation by deconvolution.

The above deconvolution method was applied to simulated A-scope waveforms for different noise levels. Figure 8 shows the mean accuracy of the inversion of height against signal photon count for a three different sets of noise added to a single waveform. The instability of the ground position estimate is apparent. A clear improvement of tree top position estimate with increasing signal to noise ratio is shown. More checks may highlight failures, improving certainty in the results. Care must be taken to separate the effects of noise, canopy cover and tree height.

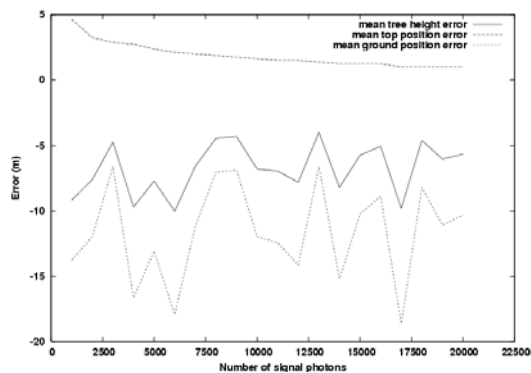


Figure 8. Tree height, tree top position and ground errors against signal photon count for a single waveform.

7. Conclusions

Tree height, top and ground position errors have been precisely quantified with simulated waveforms. A method for reducing tree top position bias has been tested and shown to perform well if at least 2,000 signal photons are measured (an easily achievable number). Some refining is needed to cope with the effect of varying canopy cover on ground position and premature triggering on tree top estimate. Above 3,000 photons errors are dominated by the algorithms. More robust algorithms may benefit from more signal photons (10,000 gives near perfect recreation of the ideal). This area needs more work before it can be considered operational.

This method relies on a clear separation between ground and canopy (after deconvolution). If the variation in ground height across the footprint is greater than the ground to foliage separation that will not be the case. This limits the areas such an instrument could be used. Smaller footprints aggregated together to ensure a tree top is recorded may be a solution; a high pulse repetition rate to allow a continuous track would be preferable. A second waveband with spectral contrast between ground and canopy will allow distinction in topographically mixed signals. Both of these would require extra equipment to be included which is unlikely in A-scope for such a secondary capability.

A-scope has a proposed laser wavelength of either 2.06 μm or 1.65 μm , neither of which has a strong reflectance from vegetation (the two wavelengths used in DIAL are too close to be of any advantage for vegetation). In this investigation noise levels were calculated by assuming a certain number of signal photons therefore wavelength had little impact upon this investigation. The choice of laser wavelength is likely to limit the maximum number of measurable photons.

The possibility of using long pulse lidar for measuring forest parameters has been demonstrated, given sufficient range resolution. The effect of range resolution on inversion accuracy must be quantified as A-scope is unlikely to have such a fine resolution (12.5cm in this investigation). Few waveforms and inversions were available for this investigation due to the computational expense of Monte-Carlo ray tracing and deconvolution by Gold's method. More samples are needed to fully test the methods under a range of conditions. The finer the range resolution the more information the deconvolution has and the more accurate the result is likely to be. This effect needs exploring.

Acknowledgments

This work was funded by the NCEOI (Natural environment research council Centre for Earth Observation and Instrumentation) for project SA-014-DJ-2007 (Hyperspectral Imaging LiDAR) and the Hollow waveguide technology for CO₂ and canopy measurements (A-scope) project

through the Centre for Terrestrial Carbon Dynamics (CTCD) and the EPSRC studentship no. GR/9054658.

References

- Disney, M., Lewis, P., Saich, P., 2006. 3-D modelling of forest canopy structure for remote sensing simulations in the optical and microwave domains. *Remote Sensing of Environment*, 100, pp. 114-132.
- ESA, 2007, 17th October. http://www.esa.int/esaCP/SEMhQH9ATME_index_0.html
- Guirdev LL, Dreischuh TN, Stoyanov DV, 1993. Deconvolution techniques for improving the resolution of long-pulse lidars. *Journal of the optical society of America*, 10, p2296-2306.
- Hofton MA, Minster JB, Blair JB. 2000. Decomposition of laser altimeter waveforms. *IEEE transactions on geoscience and remote sensing*, 38, pp. 1989-1996.
- Hofton MA, Rocchio LE, Blair JB, Dubayah R, 2002. Validation of vegetation canopy lidar sub-canopy topography measurements for a dense tropical forest. *Journal of geodynamics*, 34 pp. 491-502.
- Hyde P, Dubayah R, Peterson B, Blair JB, Hofton M, Hunsacker C, Knox R, Walker W. 2005. Mapping forest structure for wildlife habitat analysis using waveform lidar; validation of montane ecosystems. *Remote sensing of environment*, 96, pp. 427-437.
- Jacquemond and Baret, 1990. Prospect: A model of leaf optical properties spectra. *Remote sensing of environment*, 34, pp. 75-91.
- Jansson PA, 1997. Deconvolution of images and spectra, second edition, Academic press, p 115.
- Lefsky MA, Cohen WB, Acker SA, Parker GC, Spies TA, Harding D. 1999. Lidar remote sensing of the canopy structure and biophysical properties of Douglas-fir and western hemlock forests. *Remote Sensing of Environment*, 10, p339-361.
- Lewis, P. 1999. Three-dimensional plant modelling for remote sensing simulation studies using the Botanical Plant Modelling System. *Agronomie*, 19(3-4), pp. 185-210.
- Lovell, J.L., Jupp, D.L.B., Culvenor, D.S., Coops, N.C., 2003. "Using airborne and ground-based ranging lidar to measure canopy structure in Australian forests." *Canadian Journal of Remote Sensing* 29(5), pp. 607-622.
- Morsdorf F, Frey O, Meier E, Itten I, Allgöwer B, 2008. Assessment of the influence of flying altitude and scan angle on biophysical vegetation products derived from airborne laser scanning. *International journal of remote sensing*, 29, p 1387-1406.
- Press W.H., Teukolsky S.A., Vetterling W.T. Flanery B.P. 1994. *Numerical Recipes in C*. Cambridge University Press, second edition (with reprints).
- Reitberger J, Krzystek P, Stilla U. 2008. Analysis of full waveform LIDAR data for the classification of deciduous and coniferous trees. *International journal of remote sensing*, 29, pp. 1407-1431.
- Rosette JAB, North PRJ, Suarez JC. 2008. Vegetation height estimates for a mixed temperate forest using satellite laser altimetry. *International journal of remote sensing*, 29, pp. 1475-1493.
- Widlowski J-L, Pinty B, Lavergne T, Verstraete MM, Gobron N. 2005. Using 1-D models to interpret the reflectance anisotropy of 3-D canopy targets: Issues and caveats. *IEEE transactions on geoscience and remote sensing*, 4(9), pp. 2008-2017.
- Williams M, Schwarz PA, Law BE, Irvine J, Kurpuis MR. 2005. An improved analysis of forest carbon dynamics using data assimilation. *Global change biology*, 11, pp. 89-105.
- Woodward FI, Lomas MR, 2004. Vegetation dynamics – simulating responses to climate change. *Biological reviews*, 79, pp. 643-670.

Model Effects on GLAS-based regional estimates of forest biomass and carbon

Ross Nelson

Code 614.4, Biospheric Sciences Branch, NASA–Goddard Space Flight Center,
Greenbelt, Maryland 20771 USA, email: rfn104@gmail.com

Abstract

ICESat/GLAS waveform data are used to estimate biomass and carbon on a 1.27 million km² study area, the Province of Québec, Canada, below treeline. The same input data sets and sampling design are used in conjunction with four different predictive models to estimate total aboveground dry forest biomass and forest carbon. The four models include nonstratified and stratified versions of a multiple linear model where either biomass or $\sqrt{\text{biomass}}$ serves as the dependent variable. The use of different models in Québec introduces differences in Provincial biomass estimates of up to 0.35 Gt (range 4.94±0.28 Gt to 5.29±0.36 Gt). The results suggest that if different predictive models are used to estimate regional carbon stocks in different epochs, e.g., y2005, y2015, one might mistakenly infer an apparent aboveground carbon "change" of, in this case, 0.18 Gt, or approximately 7% of the aboveground carbon in Québec, due solely to the use of different predictive models. These findings argue for model consistency in future, LiDAR-based carbon monitoring programs. Regional biomass estimates from the four GLAS models are compared to ground estimates derived from an extensive network of 16,814 ground plots located in southern Québec. Stratified models proved to be more accurate and precise than either of the two nonstratified models tested.

1. Introduction

The forestry LiDAR community, having demonstrated and continuing to improve the utility of airborne LiDAR systems for forest measurement and monitoring, now must consider doing so from space. One civilian space LiDAR, the ICESat satellite (Ice, Cloud, and land Elevation Satellite) carrying the GLAS (Geosciences Laser Altimeter System) LiDAR, is currently in orbit. The U.S. may launch three additional space LiDAR systems over the next decade. This report briefly describes these proposed space LiDARs, the configurations of which are all under discussion and subject to change. We also introduce two concerns associated with space and airborne LiDAR instruments that must be addressed by our community if we hope to effectively monitor global forest resources with lasers. In order to monitor forest change at the regional, national, continental, or global scale, our estimates at time 1 (t1) and time 2 (t2) must be consistent. Spurious changes may be noted or actual changes may be missed if our t1, t2 estimates are not comparable. Assuming the use of the same sampling design, inconsistencies may be introduced by the use of different predictive models at t1, t2, and/or they may be introduced by sensor changes over time which might result in systematic measurement differences. The objective of this paper is to address the former, i.e., model consistency, providing one example of the degree to which the use of different predictive models impacts regional estimates of biomass and carbon.

1.1. U.S. Space LiDARs – Current Thoughts

The U.S. National Research Council (NRC), in a document known as the Decadal Survey (NRC 2007), has identified seventeen space missions of paramount importance to the U.S. scientific community for monitoring the status and function of the biosphere. The NRC suggests that

these seventeen missions be launched in the 2010 – 2020 timeframe. Three of these Earth remote sensing missions incorporate space LiDARs capable of measuring forest structure. These missions include (1) ICESat II, a follow-on to the current ICESat satellite (Abshire et al. 2005), designed to monitor ice sheet elevation changes; (2) DESDynI (Deformation, Ecosystem Structure, and Dynamics of Ice), primarily a solid Earth mission which couples an L-band RaDAR and LiDAR to map surface deformation; and (3) LIST (Laser Imaging for Surface Topography), a swath mapping LiDAR for global topography and hydrology. All will be in near-polar orbits.

The specific design of ICESat II and DESDynI is currently a topic of much discussion, so the descriptions below may not resemble the configurations that may ultimately reach orbit. In addition, the launch of these three satellites is by no means assured given the prerequisite that the U.S. Congress must find the funds needed to build and operate this hardware. However the Decadal Survey carries much weight at NASA, and the current expectation is that ICESat II will be launched somewhere in the 2015 timeframe in a flight configuration similar to the first ICESat, e.g., a single beam, waveform profiler with 50 m – 70 m footprints and an along-track post spacing of 140 m. The 2015 launch date is notable in that the ICESat I/GLAS LiDAR, currently collecting data during ~33 day, spring and fall campaigns, is expected to last an additional 1½ to 3 years, with the 3rd and final laser due to fail sometime between the spring of 2010 and the autumn of 2012. This leaves an ICESat I – ICESat II observational hole of 3-5 years if ICESat II launches in 2015.

The DESDynI and LIST missions will fly later. Expectations are that DESDynI will most likely be some sort of multi-beam LiDAR with ~25 m footprints and 25 m – 30 m post spacing, i.e., near-contiguous profiles along-track. Across-track, parallel profiles will be kilometers apart, perhaps on the order of 2 – 5 km separating each of the 3 – 5 beams on the satellite. DESDynI is currently configured as a joint L-band RaDAR and multibeam LiDAR satellite, but many aspects of this mission are under consideration and are actively being investigated, including the need to physically tie the RaDAR to the LiDAR on the same platform, orbital repeat times, baseline issues regarding the RaDAR acquisitions, the RaDAR acquisition capabilities, e.g., SAR vs. InSAR, LiDAR beam spacing, number of beams, off-nadir pointing capabilities, and pulse width. LIST is currently configured as a swath mapper, collecting global wall-to-wall coverage over its 5 year design life. The footprint of the contiguous pulses will be on the order of 5 m. Given LIST's late launch, most effort is going into research to address the ICESat II and DESDynI flight configurations.

1.2. Using ICESat/GLAS to Measure Forests

In the context of the current ICESat profiler and the possibility of an ICESat II follow-on, the forestry LiDAR community has entered a period where space-based LiDAR measurements are routinely collected globally and systematically, albeit with extended periods without space LiDAR measurements. With this capability comes questions concerning how we might best use these satellite ranging observations to measure, and more importantly, monitor forest biomass and carbon resources at regional, national, continental, and global scales.

Although the ICESat/GLAS LiDAR is not optimally configured for or operated as a vegetation assessment tool, these data have proved useful for biomass and carbon assessments across areas spanning hundreds of thousands of square kilometers. Kimes et al (2008) and Boudreau et al. (2008) report results of studies that employ the ICESat/GLAS LiDAR to estimate forest volume, biomass, and carbon in south central Siberia (just north of Mongolia) and in Québec, Canada, respectively. Kimes et al. (2008) uses 101,831 GLAS waveforms acquired along 55 orbits over a 10° x 12°, 811,414, km² area just northwest of Lake Baikal to attribute 16 forest cover type – canopy density classes derived from MODIS (Moderate Resolution Imaging

Spectrometer) data. Using field observations acquired on 51 GLAS pulses, they developed a sparse neural network relating GLAS waveform metrics to ground estimates of merchantable volume (Ranson et al. 2007). If they constrain their data and use only those pulses acquired on slopes of 10° or less as characterized using SRTM topographic information, their regional estimate of merchantable volume, $73.85 \times 10^6 \pm 5.33 \times 10^6 \text{ m}^3$ (one standard error), is within 1.1% of comparable ground estimates, $74.63 \times 10^6 \text{ m}^3$ (Shepashenko et al. 1998 per hectare estimate in conjunction with a percent forest cover estimate for the study area of 63% from an 1990 Russian forest map, V.I. Kharuk, pers. comm.). If GLAS pulses on all slopes are considered, the regional GLAS-based per hectare estimate of volume increases from $163.4 \pm 11.8 \text{ m}^3/\text{ha}$ to $171.9 \pm 12.4 \text{ m}^3/\text{ha}$, a 5.2% increase. This apparent increase in area-based volume estimates suggests that steeper slopes broaden the waveform response, increasing apparent canopy height and inflating the volume estimates. Slopes, as noted by Lefsky et al. (2005, 2007) and Rosette et al. (2008), negatively affect the height accuracy of the large-footprint GLAS waveform data, convolving forest canopy architecture with topography and increasing the vertical extent of the waveform.

Boudreau et al. (2008) uses a multiphase sampling approach to relate GLAS waveform and SRTM topographic measurements to field estimates of total aboveground dry biomass in Québec, Canada. They flew an airborne profiling LiDAR over existing ground plots and along GLAS orbital transects and developed two sets of equations. The first set relates field biomass estimates to airborne LiDAR metrics; the second set relates airborne LiDAR estimates of biomass to GLAS waveform metrics. They estimate that, on average, the forested areas of Québec south of treeline support $39.0 \pm 2.2 \text{ t/ha}$ of dry biomass. Botkin and Simpson (1990) report an average value of $41.8 \pm 10.1 \text{ t/ha}$ for all of the North American boreal forest based on stratified ground measurements.

These studies report the accuracy and precision of statistical approaches that may be used to conduct regional inventories using a space LiDAR. Of interest in this paper, however is an assessment of the need for consistency in model selection when estimating regional biomass repeatedly over time. The objective of this study is to quantify the degree to which model differences may affect regional estimates of biomass and carbon. Four different models are used to estimate standing dry biomass and carbon for all of Québec below treeline, a area encompassing 1.27 million square kilometers. In addition, results from the four models are compared to ground reference data to determine which of the models most closely estimates biomass in the southern half of the Province

2. Methods

The data sets and analysis procedures employed in this study are the same as those described in detail in Boudreau et al. (2008). This study incorporates the following data sets:

(1) ICESat/GLAS LiDAR waveform data: 104,044 GLAS waveforms acquired along 97 orbits across all of Québec, acquisition L2a, autumn 2003. Spacing between adjacent near-N-S orbits are very variable but average 15.6 km.

(2) Digital vegetation zone map of Québec: tessellates Québec into seven vegetation zones; from south to north: (2.1) Northern Temperate forest, (2.2) Mixedwood forest, (2.3) southern Boreal forest (commercial forest), (2.4) northern Boreal forest (noncommercial forest), (2.5) Taiga, (2.6) Treed Tundra, (2.7) Southern Arctic. The Southern Arctic, that vegetation zone whose southern border is identified as the Provincial tree line, was assumed to contain no forest biomass.

(3) Landsat ETM+ land cover map: up to 24 land cover classes identified in each vegetation zone. Forests are identified as being conifer, hardwood, or mixedwood; 3 canopy density classes in each forest cover type. Data resampled to a 25 m grid.

(4) SRTM digital elevation data: available up to 60° N latitude (the Provincial treeline tracks

around 58° - 59°N). 90 m pixels. 3x3 window around each GLAS pulse used to characterize local topography.

(5) Ministry of Natural Resources Québec (MNRQ) ground plots: 16,814 fixed area, 11.3 m radius, 400 m², temporary sample plots located in the southern 3 vegetation zones south of the commercial forest line that bisects the Boreal vegetation zone. Total aboveground dry biomass calculated on each plot.

(6) Profiling airborne LiDAR data (Nelson et al. 2003): flown over 295 MNRQ ground plots and over ~5000 km of GLAS orbits, summer 2005. The NIR profiler acquired sequential first/last returns on 0.40 m footprints at 0.12 m post spacing across ground plots and GLAS pulses. The profiling data are used to tie ground plot information to GLAS measurements.

These six data sets are utilized within a multiphase sampling framework. The airborne profiler was flown over 295 ground plots. Ground estimates of biomass were regressed against the airborne profiler measurements in order to develop predictive regressions based on the airborne measurements. One nonstratified equation ($R^2 = 0.65$) and a set of seven stratified ground-air equations (R^2 range from 0.51 – 0.73, Boudreau et al. 2008) are developed based on the Landsat land cover strata. The ground-air equation(s) is(are) then used to calculate airborne laser-based estimates of biomass on 1325 GLAS pulses measured by the airborne profiler.

Four different models are constructed (n=1325) to predict dry biomass as a function of GLAS waveform and SRTM topographic measurements. The four models follow:

· linear, nonstratified:

$$b_{air,ns} = -4.52 + 3.85 * w_{GLAS} - 6.59 * f_{GLAS} - 0.75 * r_{SRTM} \quad (1)$$

$$R^2 = 0.60, RMSE = 32.0 \text{ t/ha};$$

· linear, stratified:

$$b_{air,st} = 2.37 + 3.63 * w_{GLAS} - 5.92 * f_{GLAS} - 0.73 * r_{SRTM} \quad (2)$$

$$R^2 = 0.58, RMSE = 31.7 \text{ t/ha};$$

· square root, nonstratified:

$$\sqrt{b_{air,ns}} = 2.67 + 0.27 * w_{GLAS} - 0.83 * f_{GLAS} - 0.06 * r_{SRTM} \quad (3)$$

$$R^2 = 0.59, RMSE = 2.40 \sqrt{t/ha};$$

· square root, stratified:

$$\sqrt{b_{air,ns}} = 2.98 + 0.26 * w_{GLAS} - 0.65 * f_{GLAS} - 0.06 * r_{SRTM} \quad (4)$$

$$R^2 = 0.53, RMSE = 2.55 \sqrt{t/ha};$$

where $b_{air,ns}$ = an airborne profiling estimate of biomass calculated using the nonstratified ground-air equation,
 $b_{air,st}$ = an airborne profiling estimate of biomass calculated using the stratified ground-air equations,
 w_{GLAS} = vertical extent of the GLAS waveform, signal start to signal end,
 f_{GLAS} = the slope of the leading edge of the GLAS waveform; and
 r_{SRTM} = the range, in meters of the topographic difference found in a 3x3 pixel SRTM window centered on an GLAS pulse.

The variance inflation factors for all 4 models are less than 1.61; multicollinearity is not an issue (Myers 1989). The square-root transform is used in an attempt to control marked heteroskedasticity; the transform only marginally improved residual patterns. The square-root biomass values are back-transformed using the unbiased backtransformation technique reported by Gregoire et al. (2008).

In the context of this report, stratification refers to the development of equations, by cover type and vegetation zone, in the ground – air phase, not in the air – satellite phase. In other words, the b_{air} dependent variables in equations 2 and 4 above were calculated using stratified ground-air equations; the b_{air} in equations 1 and 3 were calculated using a generic or nonstratified ground-air equation (Boudreau et al. 2008, his Table 2). Attempts were made to develop stratified GLAS equations for the linear and square root models, but R^2 decreased and RMSEs increased as the latitude of the vegetation zones increased and as the average height of the trees decreased. Stratified GLAS equations in the Taiga and the Treed Tundra had R^2 values in the 0.1 – 0.2 range and were deemed unusable. This finding is not unexpected given the ground height – GLAS height comparisons reported in the literature. Sun et al. (2008) compares various GLAS height metrics to comparable airborne LiDAR estimates and reports RMSEs of 3 m – 5.5 m (his Table 2) in the temperate forests of the eastern U.S. Rosette et al. (2008) report ground-GLAS height RMSEs of 2.86 m after correcting for topography. Lefsky et al. (2005) report RMSEs associated with ground-GLAS maximum canopy height comparisons of ~4.5 m, and Lefsky et al. (2007), after correcting for local topography using trailing edge measures, illustrates an RMSE of 5m across diverse study sites in his Figure 3. Given this height scatter and the open, sparse, stunted coniferous nature of Québec's northern forests near treeline, one might conclude that GLAS does not have the measurement sensitivity to accurately measure high-latitude forests. As a result, stratified GLAS equations were not employed in this study due to the lack of predictive power of some of the northern equations. This lack of sensitivity in short-stature forests also calls into question the accuracy of the GLAS-based biomass and carbon estimates near treeline.

The stratified models, i.e., equations 2 and 4 above, were processed differently from the nonstratified models 1 and 3. Every GLAS shot was assigned to one of the Landsat land cover classes based on the plurality of the land cover types in a 3 x 3 Landsat ETM window that surrounded a given GLAS pulse. The nonstratified models were applied to all 104,044 GLAS shots collected over Québec regardless of the land cover identity of that GLAS pulse. So GLAS pulses judged (by the Landsat classification) to have illuminated barren areas, rock, moss, herb, etc, could still contribute to Provincial biomass if nonzero heights were measured by GLAS. In effect, in the nonstratified models, GLAS measurements trumped Landsat land cover identities, and a GLAS pulse could contribute to the biomass estimate even if the Landsat classification suggested that no forest biomass should exist on that spot illuminated by the GLAS pulse. Just the opposite was true with respect to the stratified models. Models 2 and 4 were utilized only on those GLAS shots judged to be capable of supporting forest biomass. In the case of the stratified models, then, specific cover types could never contain forest biomass regardless of what the GLAS pulses intercepting that cover type may have measured. The net result of this processing rule is that the nonstratified models have higher biomass totals for the Province because they accumulate estimates across larger areas.

The Ministry of Natural Resources Québec made available 16,814 temporary sample plots measured between 1998 and 2004. The intensity and location of the MNRQ TSP multiyear measurement campaign is illustrated in Boudewyn et al. (2007), his Figure 1. All plots are located south of the commercial forest line. A small portion of these plots, ones more recently measured, are used to develop the models discussed above. All 16,814 are used to validate the models.

3. Results

Table 1 reports per hectare and total biomass estimates for the entire 1.27 million km² Province of Québec south of treeline. The models are ranked, largest to smallest in terms of total Provincial biomass, and, as one would expect due to processing rules, the nonstratified models report the largest Provincial biomass totals.

The exact same data are input into each model to calculate model coefficients. Based on model differences alone, Provincial biomass and carbon estimates vary approximately 7% even under the ideal circumstance that all of the data input into the various models are identical. No such ideal circumstance would exist if one were monitoring regional biomass over time since the input data would certainly change between t1 and t2. The 7% difference amounts to, in Québec, a model-induced difference of 0.35 Gt of biomass, or 0.18 Gt of carbon assuming a conversion factor of 0.5 t C/1 t biomass (Gower et al. 1997; Houghton et al. 2000). Given a current carbon credit price of ~15 euros per ton carbon, this scenario might result in an undeserved carbon penalty or an unearned carbon credit of up to 2.64 billion euros for Québec, depending on which model was used at t1 and which at t2.

The results in Table 1 indicate that LiDAR-based biomass and carbon monitoring will require model consistency between measurement epochs or, alternatively, a post-processing statistical methodology that would equate current estimates with ones previously made using a different model or LiDAR sensor.

Table 1. Provincial estimates of total above ground dry biomass on 1.27 million km² south of tree line in Québec. Model estimates are ranked largest to smallest, top to bottom. All standard errors calculated assuming simple random sampling, covariances are included, prediction error is not.

| model | dry biomass estimates | | | Prov. biomass totals | |
|-----------------------------------|-----------------------|----------------------|------------------|----------------------|--------------------|
| | mean (t/ha) | stan. err. (t/ha) | coef.var. (%) | total (Gt) | stan. err. (Gt) |
| nonstratified, square root (3) | 41.72 | 2.82 | 6.8 | 5.29 | 0.36 |
| nonstratified, linear (1) | 40.63 | 5.21 | 12.8 | 5.15 | 0.66 |
| stratified, linear (2) | 39.73 | 3.32 | 8.4 | 5.04 | 0.42 |
| stratified, square root (4) | 38.94 | 2.17 | 5.6 | 4.94 | 0.28 |

The accuracy and precision of the four models can be assessed, at least in the three southern vegetation zones, by comparing GLAS-based estimates to biomass estimates on the 16,814 ground plots, accumulated across Landsat vegetation classes (Table 2). All four models underestimated ground-based southern provincial estimates by amounts ranging from -7.3 to -12.4%. Models (2) and (4), the stratified linear and stratified square route models, were, respectively, the most accurate and most precise at the regional level. The ground reference information and the stratified GLAS model results are reported in Table 2, by forest cover type within vegetation zone, and for the entire southern portion of the Province.

Table 2. A comparison of ground reference estimates of biomass with the stratified linear and stratified square-root GLAS model results for the three southern vegetation zones (VZ), by Landsat forest cover type. Northern Temperate vegetation zone – 109,769 km², Mixedwood vegetation zone – 98,101 km², Southern Boreal vegetation zone – 374,665 km². All standard errors are calculated assuming simple random sampling, covariances are included, prediction error is not.

| | MNRQ Ground Reference | | | GLAS – stratified, linear | | | GLAS–stratified,square root | | |
|-------------------------|-----------------------|----------------------|--------------|---------------------------|----------------------|-------------------|-----------------------------|---------------------|-------------------|
| | biomass (t/ha) | stan. err. (t/ha) | no. plots | biomass (t/ha) | stan. err. (t/ha) | difference (%) | biomass (t/ha) | stan.err. (t/ha) | difference (%) |
| Northern Temperate V.Z. | | | | | | | | | |
| conifer | 76.60 | 5.82 | 49 | 65.47 | 2.02 | -14.5 | 62.76 | 2.55 | -18.1 |
| deciduous | 77.85 | 4.95 | 176 | 89.70 | 4.47 | +15.2 | 91.74 | 4.85 | +17.8 |
| mixedwood | 65.91 | 2.79 | 313 | 82.66 | 0.85 | +25.4 | 82.74 | 1.78 | +25.5 |
| | | | | | | | | | |
| Mixedwood V.Z. | | | | | | | | | |
| conifer | 85.90 | 1.57 | 583 | 72.68 | 3.02 | -15.4 | 70.55 | 2.27 | -17.9 |
| deciduous | 75.00 | 2.98 | 290 | 83.27 | 2.63 | +11.0 | 83.39 | 2.61 | +11.2 |
| mixedwood | 87.15 | 1.43 | 1177 | 80.82 | 2.51 | - 7.3 | 79.69 | 2.17 | - 8.6 |
| | | | | | | | | | |
| Southern Boreal V.Z | | | | | | | | | |
| conifer | 86.36 | 0.37 | 10007 | 63.85 | 5.13 | -26.1 | 61.75 | 4.07 | -28.5 |
| deciduous | 56.71 | 1.77 | 617 | 60.54 | 1.52 | + 6.8 | 59.22 | 1.26 | + 4.4 |
| mixedwood | 82.16 | 0.73 | 3602 | 69.13 | 1.44 | -15.9 | 67.44 | 1.24 | -17.9 |
| | | | | | | | | | |
| Prov. Commercial Forest | 81.90 | 0.50 | 16814 | 75.93 | 3.03 | - 7.3 | 75.04 | 2.25 | - 8.4 |

4. Discussion

Within the next decade, the forestry LiDAR community can expect to have access to extensive data sets that will enable us to conduct regional and national assessments from space. Researchers have already demonstrated that, even with GLAS optimized for ice rather than vegetation measurements, analysts can develop comprehensive, extensive, timely estimates of forest biomass and carbon on areas encompassing hundreds of thousands to well over a million square kilometers. The use of space-based laser altimetry, specifically GLAS waveform data, currently presents numerous challenges, e.g., large footprints that convolve forest canopy structure with topography in the presence of slope, an apparent insensitivity to small, sparse woodland heights, significant laser power changes over time, data collection epochs - late fall, early spring- tailored to ice studies but non-optimal from a vegetation measurement/monitoring standpoint, changing footprint shapes and orientations, and noncontiguous profiles. But space LiDARs currently under design will mitigate many of these problems, though the slope issue is still outstanding as are questions concerning height sensitivity in low biomass situations near treeline.

Monitoring changes to aboveground biomass and carbon stocks over time using air-borne or space LiDARs raises it's own set of issues, issues that will come to the forefront and call into question the validity of those laser-based estimates if we do not address them ahead of time. If LiDAR surveys at time1 and time 2 are to be compared to assess, for instance, compliance with carbon agreements or to provide the quantitative estimates needed to purchase or sell carbon credits, then those t1 and t2 surveys must be consistent. Consistency in this context involves the use of:

- the same ground-based allometry at t1 and t2 (if new plots are measured),
- the same statistical framework, e.g. design, sample size, number of phases,
- the same predictive models,
- the same sensor, or a different sensor with the same flight configuration with respect to laser power, repetition rate, footprint size, pulse width.

The good news is that many of these factors are in our control – the allometry, the statistical framework, model selection. And if an analyst wants to update the allometry or improve/change her/his predictive models, she/he can do so and reprocess the old t1 data with the improved versions to insure comparability. What is most likely not in our control is the sensor, i.e., the operational characteristics of the airborne or space LiDAR. Airborne LiDAR technology is changing so rapidly that data providers commonly swap out their one or two year old scanners for newer, faster, improved versions. And the satellite LiDARs discussed in this paper typically have design lives of ~5 years. We can be fairly certain that most regional surveys done every five to ten years will be done with different sensors.

The results presented in this paper provide one example of the effects of allowing one item on this consistency checklist to stray. Provincial estimates changed ~7% due only to changes in model form and due to changes to the rules used to process the GLAS data. The forestry LiDAR community should begin to address questions concerning consistency and calibration in order to develop procedural or statistical techniques to ensure comparability of LiDAR-based surveys done years apart. These results provide an impetus to develop statistical procedures that can effectively draw equivalence between multitemporal, regional LiDAR-based biomass or carbon estimates that might not be directly comparable due, perhaps, to the use of different predictive models, different allometry, or changing LiDAR sensors in different measurement periods.

References

- Abshire, J.B., Sun, X., Riris, H., Sirota, J., McGarry, J., Palm, S., Yi, D., and Liiva, P. 2005. Geoscience Laser Altimeter System (GLAS) on the ICESat Mission: On-orbit measurement performance. *Geophysical Research Letters*, 32, L21S02.
- Botkin, D.B., and Simpson, L.G. 1990. Biomass of the North America Boreal Forest: A Step toward accurate global measures. *Biogeochemistry*, 9, 161-174.
- Boudewyn, P., Song, X., Magnussen, S., and Gillis, M.D. 2007. Model-based, volume to biomass conversion for forested and vegetated land in Canada. Info. Report BC-X-411, Natural Resources Canada, Canadian Forest Service, Pacific Forestry Centre, Victoria BC. 124 pgs.
- Boudreau, J.B., Nelson, R., Margolis, H., Beaudoin, A., and Guindon, L. 2008. An analysis of regional aboveground forest biomass using Airborne and Spaceborne LiDAR in Québec. *Remote Sensing of Environment*, accepted for publication.
- Gower, S.T., Vogel, J.G., Norman, J.M., Kucharik, C.J., Steele, S.J., and Stow, T.K. 1997. Carbon distribution and aboveground net primary production in aspen, jack pine, and black spruce stands in Saskatchewan and Manitoba, Canada. *Journal of Geophysical Research*, 102(D24), 29029-29041.
- Gregoire, T.G., Lin, Q.F., Boudreau, J., and Nelson, R. 2008. Regression estimation following the square-root transformation of the response. Accepted for publication, *Forest Science*.
- Houghton, R. A., Skole, D.L., Nobre, C.A., Hackler, J.L., Lawrence, W.H., and Chomentowski, W.H. 2000. Annual fluxes of carbon from deforestation and regrowth in the Brazilian Amazon. *Nature*, 403(24), 301-304.
- Kimes, D., Ranson, K.J., Sun, G., Nelson, R., Kharuk, V., and Montesano, P. 2008. Siberian Timber Volume Maps Derived from MODIS and ICESat/GLAS Data. Submitted to *Remote Sensing of Environment*.
- Lefsky, M., Harding, D., Keller, M., Cohen, W.B., Carabajal, C.C., Espirito-Santo, F.D.B., Hunter, M.O., and deOliveira, R. 2005. Estimates of forest canopy height and aboveground biomass using ICESat. *Geophysical Research Letters*, 32, L22S02, doi: 10.1029/2005GL023971.
- Lefsky, M.A., Keller, M., Pang, Y., deCamargo, P.B., and Hunter, M.O. 2007. Revised method for forest canopy height estimation from the Geoscience Laser Altimeter System waveforms. *Journal of Applied Remote Sensing*, 1, 013537.
- Myers, R. 1989. Classical and Modern Regression with Applications (2nd Ed.). Boston MA: PWS-Kent Publishing Co. 488 pp.
- National Research Council. 2007. Earth Science and Applications from Space: National Imperatives for the Next Decade and Beyond, Executive Summary. National Academies Press. 43 pgs. [downloadable pdf at <http://www.nap.edu/catalog/11820.html>, la= July 29, 2008]
- Nelson, R. F., Parker, G., and Hom, M. 2003. A Portable Airborne Laser System for Forest Inventory, *Photogrammetric Engineering and Remote Sensing*, 69(3): 267-273.
- Ranson, K.J., Kimes, D., Sun, G., Nelson, R., Kharuk, V., and Montesano, P. 2007. Using MODIS and GLAS Data to Develop Timber Volume Estimates in Central Siberia. IEEE IGARSS July 23-26, 2007, Barcelona, Spain, pgs.2306-2309. DOI: 10.1109/IGARSS.2007.4423302.
- Rosette, J.A.B., North, P.R.J., and Suárez, J.C. 2008. Vegetation height estimates for a mixed temperate forest using satellite laser altimetry. *International Journal of Remote Sensing*, 29(5), 1475-1493.
- Shepashenko, D., Shvidenko, A., and Nilsson, S. 1998. Phytomass (Live Biomass) and Carbon of Siberian Forests. *Biomass and Bioenergy*, 14, 21-31.
- Sun, G., Ranson, K.J., Kimes, D.S., Blair, J.B., and Kovacs, K. 2008. Forest vertical structure from GLAS: An evaluation using LVIS and SRTM data. *Remote Sensing of Environment*, 112, 107-117.

3D segmentation and classification of single trees with full waveform LIDAR data

J. Reitberger¹, P. Krzystek¹ & U. Stilla²

¹Dept. of Geoinformatics, University of Applied Sciences Muenchen, 80333 Munich, Germany, josef.reitberger@hm.edu, krzystek@hm.edu

²Photogrammetry and Remote Sensing, Technische Universitaet Muenchen, 80290 Munich, Germany, stilla@tum.de

Abstract

The paper highlights a new 3D segmentation technique that detects single trees with an improved accuracy. The method uses the normalized cut segmentation and is combined with a special stem detection method. A subsequent classification identifies tree species using salient features that utilize the additional information the waveform decomposition extracts from the reflected laser signal. Experiments were conducted in the Bavarian Forest National Park with conventional first/last pulse data and full waveform LIDAR data. The first/last pulse data result from a flight with the Falcon II system from TopoSys in leaf-on situation at a point density of 10 points/m². Full waveform data were captured with the Riegl LMS Q-560 system at a point density of 25 points/m² (leaf-off and leaf-on) and at a point density of 10 points/m² (leaf-on). The study results prove that the new 3D segmentation approach is capable of detecting small trees in the lower forest layer. This was practically impossible so far if tree segmentation techniques based on the canopy height model (CHM) were applied to LIDAR data. Compared to the standard watershed segmentation the combination of the stem detection method and the normalized cut segmentation performs better by 12%. In the lower forest layers the improvement is even more than 16%. Moreover, the experiments show clearly that the usage of full waveform data is superior to first/last pulse data. The unsupervised classification of deciduous and coniferous trees is in the best case 93%. If a supervised classification is applied the accuracy is slightly increased with 95%.

Keywords: LIDAR, Analysis, Segmentation, Forestry, Vegetation

1. Introduction

Single tree detection has been a key issue in forest inventory research. So far, nearly all methods have tackled the problem to detect single trees from the CHM, which is a result of a surface interpolation. Approaches presented – for instances – by Hyyppä et al. (2001), Solberg et al. (2006) or Brandtberg (2007) stand for such kind of methods. Typically, the detection rate of single trees is limited due to unavoidable smoothing effects in the interpolated surface. The main drawback is that trees and young regeneration in the intermediate and lower forest layers are invisible from the CHM surface and hence cannot be detected at all. Tree species classification using solely LIDAR data and features derived from the coordinates of the laser returns has been investigated – for instance – by Holmgren et al. (2004) who showed that the coniferous tree species Norway spruce and Scots pine can be classified with an overall accuracy of 95% using highly dense LIDAR data. Heurich (2006) demonstrates that classification of Norway spruce and European beech is possible with an overall accuracy of 97% in leaf-off situation. However, the tree segments were derived from LIDAR data acquired in leaf-on situation. The study refers to LIDAR data with a mean point density of 10 points/m² and clearly shows that desirable forest features like young regeneration could not be detected.

Recent advances in LIDAR technology have generated new full waveform scanners that provide a higher spatial point density and additional information about the reflecting characteristics of trees. Important issues like the calibration and the decomposition of full waveform data with a series of Gaussians, as well as the detection and classification of vegetation have been investigated by Wagner et al. (2006), Jutzi and Stilla (2006), Kirchof et al. (2008) and Reitberger et al. (2008a). Recently, Reitberger et al. (2008c) successfully showed that the new full waveform technology can significantly improve the detection rate of single trees using a 3D segmentation technique based on the normalized cut segmentation.

In this paper we present results of a tree species classification with full waveform data based on this new encouraging 3D tree segmentation technique. The objective of this paper is (i) to shortly highlight the new segmentation method that extracts single trees using full waveform LIDAR data, (ii) to demonstrate the improved detection rate of single trees, (iii) to prove the benefit of full waveform data both in leaf-on and leaf-off situation at different point densities, and (iv) to present classification results of a) deciduous and coniferous trees and b) spruces and fir trees.

2. Method

2.1 Normalized cut segmentation

The motivation of the normalized cut segmentation is to overcome the disadvantages of a CHM based watershed segmentation (e.g. Reitberger et al., 2008a), which calculates the tree positions $(X_{stem\ i}^{CHM}, Y_{stem\ i}^{CHM}) (i=1, \dots, N_{seg})$ from the local maxima of the CHM. Thus, neighbouring trees are often not separated and form a tree group instead of single trees. Moreover, smaller trees in the intermediate and lower height level cannot be recognized since they are invisible in the CHM. A special stem detection method (Reitberger et al., 2007) separates neighbouring trees and provides the stem positions $(X_{stem\ i}^{StDet}, Y_{stem\ i}^{StDet}) (i=1, \dots, N_{StDet})$ if there are enough stem reflections, and if the stem area can be reliably separated from the crown points by the crown base height. It fails of course when young regeneration and small trees are located below tall trees. A further drawback is that the crown points belonging to the original segment are not separated with respect to the detected stems. In order to tackle these problems we have set up a true 3D segmentation of single trees using the normalized cut method known from image segmentation (Shi and Malik, 2000), which uses the positions (x_i, y_i, z_i) of the reflections and optionally the pulse width W_i and the intensity I_i of the waveform decomposition (Reitberger et al., 2008b).

This segmentation divides a graph G formed by voxels given in a region of interest (ROI) into disjoint segments A and B (Figure 1a) by maximizing the similarity of the segment members and minimizing the similarity between the segments A and B . The corresponding cost function is

$$NCut(A, B) = \frac{Cut(A, B)}{Assoc(A, V)} + \frac{Cut(A, B)}{Assoc(B, V)} \quad (1)$$

with $Cut(A, B) = \sum_{i \in A, j \in B} w_{ij}$ as the total sum of weights between the segments A and B and

$Assoc(A, V) = \sum_{i \in A, j \in V} w_{ij}$ representing the sum of the weights of all edges ending in the segment A . The

weights w_{ij} between two voxels are basically a function of the LIDAR point distribution and features calculated from W_i and I_i . They define the similarity between the voxels. The minimization of $NCut(A, B)$ is solved by a corresponding generalized eigenvalue problem (Reitberger et al., 2008b). The approach can use auxiliary data like, for instance, the information

about the local maxima of a CHM $(X_{stem_i}^{CHM}, Y_{stem_i}^{CHM})(i=1, \dots, N_{seg})$ in order to weight the similarity between the voxels below the CHM maxima. Also, the results of the stem detection $(X_{stem_i}^{StDet}, Y_{stem_i}^{StDet})(i=1, \dots, N_{StDet})$ can be introduced to provide special weights for the voxels similarity. The figure 1b shows complex situations where the normalized cut segmentation works excellent and where the watershed segmentation and the stem detection fail.

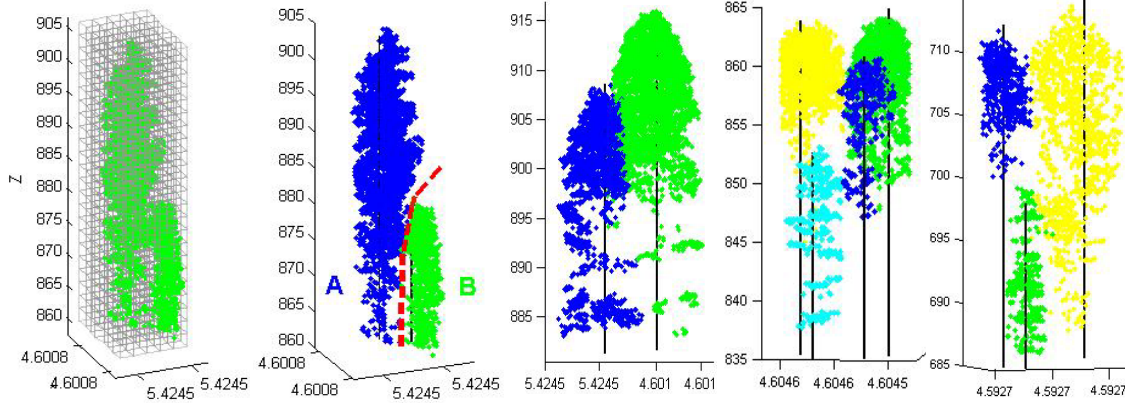


Figure 1a: Subdivision of ROI into a voxel structure and division of voxels into two tree segments A and B

Figure 1b: Examples of normalized cut segmentation with the reference trees as black vertical lines

2.2 Classification

We consider different types of salient features $S_t = \{S_g, S_i, S_l, S_w, S_n\}$ for the classification that are calculated using the N_t LIDAR points $X_i^T = (x_i, y_i, z_i, W_i, I_i)$ ($i=1, \dots, N_t$) in the segments. They are subdivided into five groups reflecting the outer tree geometry by S_g , the internal geometrical tree structure by S_i , the intensity-related features by S_l , the pulse width characteristics by S_w , and the number of reflections per waveform by S_n . Table 1 gives a short overview of the saliency definitions (see details Reitberger et al., 2008a).

Table 1: Definition of saliencies (“Sal.”) used in classification

| Sal. | Definition | Sal. | Definition |
|---------|---|---------|---|
| S_g^1 | Parameters $\{a_1, a_2\}$ of a parabolic surface | S_l^2 | Mean intensity in entire tree |
| S_g^2 | Mean distances of layer points to tree trunk | S_w | Mean pulse width of single and first reflections in the entire tree segment |
| S_i^h | Percentiles of the LIDAR points | S_n^1 | Average number of reflections between the first and last reflection in the waveform |
| S_i^d | Percentage of LIDAR points in a tree height layer | S_n^2 | Relation of the number of single reflections to the number of multiple reflections |
| S_l^1 | Mean intensities of height layers | | |

Tree species are classified both by an unsupervised and a supervised classification. Let S_t be the salient features of a tree t to be classified and let $C_k = \{\mu_k, \Sigma_k\}$ be the density probability model (mean, covariance matrix) of the k^{th} tree class. The clusters of different tree species are found by the Expectation-Maximization algorithm that approximates the distribution of a saliency subset $S \in S_t$ by fitting the parameters of the density model $p(S) = \sum_{k=1}^s \pi_k N(S | \mu_k, \Sigma_k)$ to

the data by a maximum-likelihood estimation with π_k as the mixing coefficients, $N(S | \mu_k, \Sigma_k)$ as the multivariate Gaussian distribution and s as the number of Gaussians (Heijden et al., 2004). The clusters of tree species statistically described by C_k are the results of the unsupervised classification. The supervised classification is a maximum likelihood classification by estimating the density probability models $C_k = \{\mu_k, \Sigma_k\}$ from a training subset S_{train} with $\hat{\mu}_k = \frac{1}{N_k} \sum_{n=1}^{N_k} S_n$ and $\hat{\Sigma}_k = \frac{1}{N_k - 1} \sum_{n=1}^{N_k} (S_n - \hat{\mu}_k)(S_n - \hat{\mu}_k)^T$ where N_k is the number of samples of the k^{th} class. The probability that a tree t with the saliencies S_t is a member of the k^{th} tree class is given by

$$p(S_t | C_k) = \frac{1}{(2\pi)^{\frac{d}{2}} \sqrt{|\hat{\Sigma}_k|}} \exp\left(-\frac{1}{2} (S_t - \hat{\mu}_k)^T \hat{\Sigma}_k^{-1} (S_t - \hat{\mu}_k)\right) \quad (2)$$

with d as the number of salient features.

3. Experiments

3.1 Material

Experiments were conducted in the Bavarian Forest National Park (49° 3' 19" N, 13° 12' 9" E) which is located in South-Eastern Germany along the border to the Czech Republic (Figure 2). There are four major test sites of size between 591 ha and 954 ha containing sub alpine spruce forest, mixed mountain forest and alluvial spruce forest as the three major forest types.

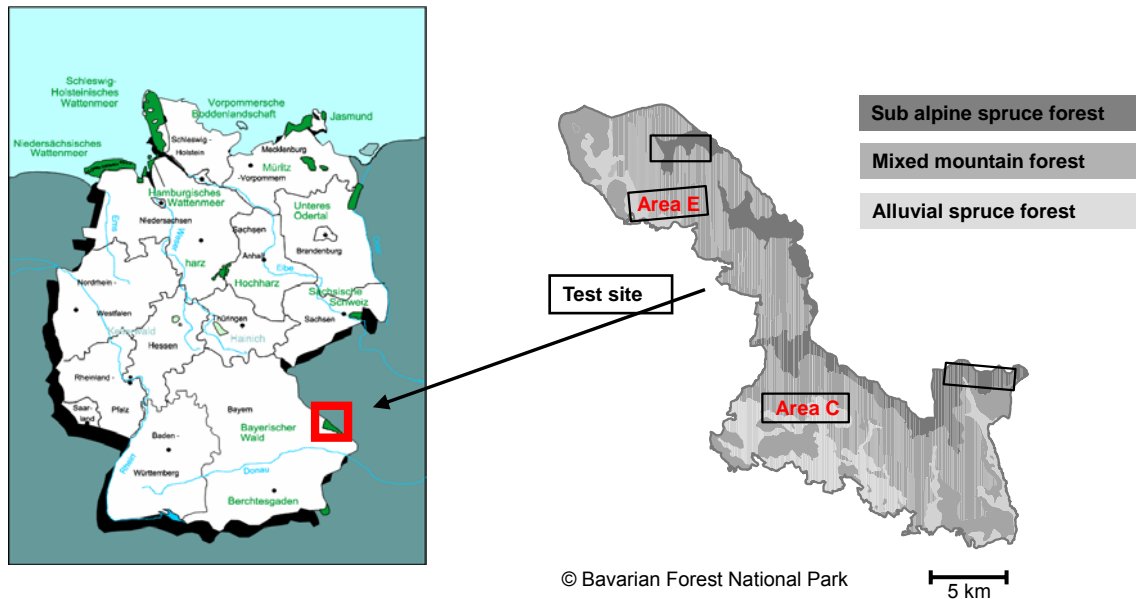


Figure 2: Location of the Bavarian Forest National Park in the map of Germany (left) and map of the park with its forest types and test sites (right).

18 sample plots with an area size between 1000 m² and 3600 m² were selected in the test sites E and C (Figure 3). Reference data for all trees with DBH larger than 10 cm have been collected for 688 Norway spruces (*Picea abies*), 812 European beeches (*Fagus sylvatica*), 70 fir trees (*Abies alba*), 71 Sycamore maples (*Acer pseudoplatanus*), 21 Norway maples (*Acer platanoides*) and 2 lime trees (*Tilia Europaea*). Tree parameters like the DBH, total tree height, stem position and tree

species were measured and determined by GPS, tacheometry and the 'Vertex III' system. Furthermore, the trees are subdivided into 3 layers with respect to the top height h_{top} of the plot, where h_{top} is defined as the average height of the 100 highest trees per ha (Heurich, 2006). The lower layer contains all trees below 50% of h_{top} , the intermediate layer refers to all trees between 50% and 80% of h_{top} , and finally, the upper layer contains the rest of the trees. Table 2 summarizes the characteristics of the individual sample plots.

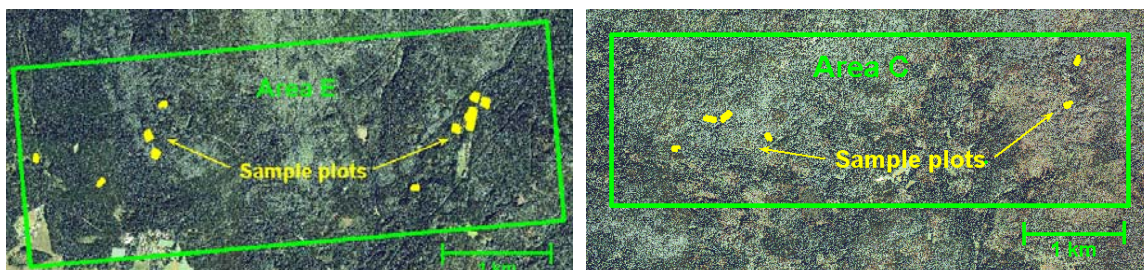


Figure 3: Orthophotos of the test sites E and C and the location of the sample plots

Table 2. Characteristics of sample plots

| Plot name | 21 | 22 | 55 | 56 | 57 | 58 | 59 | 60 | 64 | 65 | 74 | 81 | 91 | 92 | 93 | 94 | 95 | 96 |
|-----------------|------|------|------|------|------|------|------|------|------|------|------|------|------|------|------|------|------|------|
| Test site | C | C | E | E | E | E | C | C | C | C | E | E | E | E | E | E | E | E |
| Age [a] | 160 | 160 | 240 | 170 | 100 | 85 | 40 | 110 | 100 | 100 | 85 | 70 | 110 | 110 | 110 | 110 | 110 | 110 |
| Size [ha] | 0.20 | 0.20 | 0.15 | 0.23 | 0.10 | 0.10 | 0.10 | 0.10 | 0.12 | 0.12 | 0.30 | 0.30 | 0.36 | 0.25 | 0.28 | 0.29 | 0.25 | 0.30 |
| Height [m] | 860 | 885 | 610 | 640 | 765 | 710 | 810 | 890 | 835 | 875 | 720 | 690 | 764 | 767 | 766 | 768 | 750 | 781 |
| N/ha | 500 | 540 | 830 | 340 | 450 | 440 | 2150 | 380 | 430 | 810 | 700 | 610 | 260 | 170 | 240 | 250 | 240 | 200 |
| N lower layer | 37 | 19 | 77 | 31 | 0 | 10 | 76 | 8 | 13 | 53 | 11 | 29 | 31 | 13 | 7 | 15 | 6 | 30 |
| N interm. layer | 14 | 60 | 21 | 19 | 4 | 4 | 85 | 22 | 4 | 26 | 33 | 59 | 11 | 3 | 2 | 4 | 0 | 3 |
| N upper layer | 48 | 29 | 20 | 27 | 41 | 30 | 54 | 27 | 35 | 35 | 165 | 96 | 54 | 27 | 59 | 54 | 53 | 26 |
| Deciduous [%] | 66 | 79 | 5 | 10 | 0 | 14 | 1 | 100 | 87 | 96 | 29 | 100 | 75 | 100 | 66 | 97 | 10 | 86 |

LIDAR data of several ALS campaigns are available for the test sites. First/last pulse data have been recorded by TopoSys with the Falcon II system. Full waveform data have been collected by Milan Flug GmbH with the Riegl LMS-Q560 system. Table 3 contains details about the point density, leaf-on and leaf-off conditions during the flights and the footprint size. The term point density is referring to the nominal value influenced by the PRF, flying height, flying speed and strip overlap. These unique data sets allow the comparison of conventional and full waveform systems, which have been flown in the same area. However, the data set IV is only available for the 12 reference plots in test site E. This has to be considered when comparing results of other data sets with this data set. Naturally, the reference data have been updated for the individual flying dates. Reference trees are plotted in the figures 1a and 1b as black vertical lines.

Table 3: Different ALS campaigns

| Time of flight | Sept. '02 | May '06 | May '07 | May '07 |
|--------------------|-------------------|----------------|----------------|----------------|
| Data set | I | II | III | IV |
| Foliage | Leaf-on | Leaf-off | Leaf-on | Leaf-on |
| Scanner | TopoSys Falcon II | Riegl LMS-Q560 | Riegl LMS-Q560 | Riegl LMS-Q560 |
| Pts/m ² | 10 | 25 | 25 | 10 |
| HAAT [m] | 850 | 400 | 400 | 500 |
| Footprint [cm] | 85 | 20 | 20 | 25 |
| Ref. plots | all | all | all | Area E |

3.2 Segmentation results

The watershed segmentation ('W') and the new 3D segmentation technique ('NCut'), using both results from the watershed segmentation and from the stem detection, were applied to all the plots and data sets in a batch procedure without any manual interaction (Table 4). The accuracy and reliability of the presented methods are evaluated in the following way: The tree positions from the segmentation are compared with reference trees if (i) the distance to the reference tree is smaller than 60% of the mean tree distance of the plot and (ii) the height difference between h_{tree} and the height of the reference tree is smaller than 15% of h_{top} . If a reference tree is assigned to more than one tree position, the tree position with the minimum distance to the reference tree is selected. Reference trees that are linked to one tree position are so-called 'detected trees' and reference trees without any link to a tree position are treated as 'non-detected' trees. Finally, a tree position without a link to a reference tree results as a 'false positive' tree.

Table 4: Results of segmentation methods with data sets I, II, III and IV

| Data set | Method | Detected trees per height layer [%] | | | | False pos. [%] |
|------------------------------|--------|-------------------------------------|-----------|-----|-------|----------------|
| | | low. | intermed. | up. | total | |
| I (only area E) Leaf-on | W | 2 | 12 | 80 | 52 | 5 |
| | NCut | 15 | 27 | 77 | 55 | 13 |
| II Leaf-off | W | 5 | 21 | 77 | 48 | 4 |
| | NCut | 21 | 38 | 87 | 60 | 9 |
| III Leaf-on | W | 5 | 20 | 79 | 48 | 4 |
| | NCut | 17 | 32 | 86 | 58 | 10 |
| III (only area E) Leaf-on | W | 5 | 20 | 82 | 55 | 5 |
| | NCut | 24 | 35 | 88 | 66 | 11 |
| IV (only area E) Leaf-on | W | 6 | 21 | 84 | 57 | 6 |
| | NCut | 26 | 33 | 87 | 65 | 11 |

In the first instance, we want to highlight with data set II how the 3D normalized cut segmentation compares to the 2D watershed segmentation. The 2D segmentation leads to an overall detection rate of 48%, where the detection rate is rather poor in the lower forest layer. The 3D segmentation increases the detection rate considerably in the lower and intermediate layer with about 16%. This is remarkable and shows that the new segmentation technique can successfully detect smaller trees below the CHM. The improvement in the upper layer is 10% and the overall detection rate increases by 12%. The high spatial point density of the full waveform data, which practically contain all relevant reflections of the laser beam, turns out as the key factor to segment in 3D not only the dominant trees but also the dominated smaller trees in the lower and intermediate layers. However, this increased detection rate also deteriorates the reliability of the segmentation process by the factor 2 in terms of false positives. Figure 4 illustrates the improvement of the detection rate graphically.

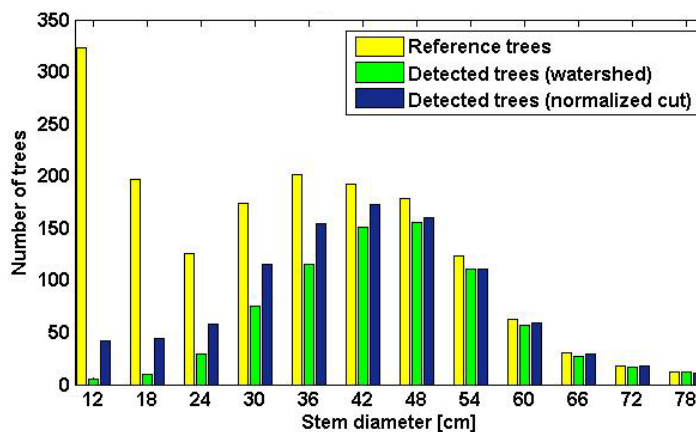


Figure 4: Comparison of single tree detection with data set II

The results given for leaf-off condition (data set II) can also be compared with full waveform data captured in the same area and with the same point density in leaf-on condition (data set III). As expected, the detection rate deteriorates in the case of the normalized cut segmentation in the lower and intermediate layer by roughly 5% due to the reduced penetration rate of the laser beam causing in turn a worse spatial distribution of the reflections. The number of false positives does not change significantly for the normalized cut segmentation.

If we restrict data set III to area E and compare it with data set IV the impact of the nominal point density on the segmentation methods can be analyzed. The comparison of both data sets shows that the detection rate and false positives are practically the same for both point densities. Obviously, although the number of penetrating laser beams is significantly reduced, the most relevant tree structures are still detected by reflections.

Finally, we compare the segmentation methods with respect to first/last pulse data (data set I) and full waveform data (data set IV) that have the same nominal point density. The total detection rate of the 2D watershed based segmentation is by 5% better for the full waveform data. The number of false positives is basically the same. The main reason for this is that the full waveform data represent the tree shape more precisely since the waveform decomposition even detects weak reflections and reflections resulting from adjacent targets. If we focus on the normalized cut segmentation, the benefit of full waveform becomes clearer with an increase of 10%. Most remarkably, the full waveform technique and the normalized cut segmentation outperform the conventional first/last pulse technique and the watershed segmentation by more than 20% in the lower and intermediate layer.

3.3 Classification results

First, we apply an unsupervised and a supervised classification between deciduous and coniferous trees to the 3D segments (Table 5). One fifth of the trees were randomly selected from the entire data set as a training data set for the supervised classification by keeping the proportion between the tree species. Also, both classification methods were applied 20 times in order to minimize the impact of the selection procedure and the initialization of the EM-algorithm of the unsupervised classification on the results. Thus, the numbers in table 5 refer to averaged classification values, whereby the best result of each data set and classification method is highlighted.

Table 5: Results of unsupervised („un.“) and supervised classification („su.“)

| Saliency | Overall accuracy (%) for data sets I - IV and for the 2D and 3D segments | | | | | | | | | |
|-------------------------------|--|-----|-----|-----|-----|-----|-------------------|-----|------------------|-----|
| | I (only area E) | | II | | III | | III (only area E) | | IV (only area E) | |
| | un. | su. | un. | su. | un. | su. | un. | su. | un. | su. |
| S_g^1 | 80 | 80 | 74 | 75 | 81 | 82 | 83 | 84 | 83 | 83 |
| S_g^2 | 80 | 78 | 75 | 78 | 80 | 82 | 83 | 82 | 81 | 81 |
| S_i^h | 62 | 66 | 73 | 72 | 64 | 67 | 66 | 66 | 65 | 70 |
| S_i^d | 66 | 67 | 68 | 76 | 68 | 74 | 69 | 73 | 65 | 70 |
| S_l^1 | | | 74 | 74 | 90 | 91 | 93 | 93 | 91 | 91 |
| S_l^2 | | | 81 | 81 | 93 | 94 | 97 | 96 | 95 | 97 |
| S_w | | | 75 | 79 | 52 | 51 | 54 | 56 | 60 | 64 |
| S_n^1 | | | 80 | 84 | 56 | 54 | 57 | 65 | 66 | 64 |
| S_n^2 | | | 89 | 93 | 62 | 63 | 61 | 65 | 57 | 57 |
| $S_g^2 + S_l^2$ | | | 81 | 86 | 90 | 94 | 93 | 97 | 91 | 97 |
| $S_g^2 + S_l^2 + S_w + S_n^2$ | | | 91 | 94 | 81 | 95 | 84 | 97 | 82 | 97 |

If we compare both classification methods with respect to the used saliencies and best results we recognize that in general the supervised classification is slightly better than the unsupervised classification. If we focus on the individual saliencies it is evident that the intensity related saliency S_l^2 turns out as the most important feature in the leaf-on case (data sets III and IV). Data set II proves that the saliency S_n^2 is the best single feature in the leaf-off case. Apparently, coniferous trees cause more single reflections than deciduous trees in leaf-off situation. The saliencies S_i^h and S_i^d describing the penetration of the laser beams in the segmented trees have very little impact on the classification results. The saliency S_w representing the pulse width of the reflections works in general better in the leaf-off case. Finally, the saliencies S_g representing the tree geometry have an almost constant impact on the classification in leaf-on and leaf-off situations. Even for data set I, which refers to first/last pulse data at a point density of 10 pts/m², the overall classification accuracy is almost the same as with full waveform data. Thus, this saliency seems to be significant even for the low point density.

The comparison between data set II and data set III indicates that both classification methods are almost the same for both foliage conditions. However, differing saliencies have been used. Furthermore, the results of data set III (only area E) and data set IV (only area E) show also clearly that the point density has practically no influence on the classification results. Thus, the lower point density of 10 pts/m² does not appear as disadvantageous. This is consistent with our experience that the segmentation results are also practically the same for both point densities. Finally, the comparison of data set I (only area E) and data set IV (only area E), which both refer to leaf-on situation and a nominal point density of 10 pts/m², indicates that the classification with first/last pulse data is significantly inferior by about 15% since only the coordinates of the reflections could be used and hence, the saliencies S_g and S_i could only be calculated for the classification.

The new 3D segmentation provides an interesting insight into the classification accuracy of single trees in different height layers. Table 6 shows how the supervised classification performs in leaf-off (date set II) and leaf-on (data set III) situations. As expected, there is almost no dependency on the height layer in the leaf-off case. Contrary, the classification accuracy deteriorates slightly for the lower and intermediate layers in the leaf-on case. Obviously, the differing classification results are influenced by the lower penetration rate in leaf-on situation.

Table 6: Classification accuracy in dependence on height layers

| Data set | Correctly classified trees per height layer [%] | | | |
|----------|---|--------------|-------|-------|
| | lower | intermediate | upper | total |
| II | 95 | 93 | 94 | 94 |
| III | 86 | 90 | 97 | 95 |

Lastly, we want to focus on the question how the tree species spruce and fir can be classified. Table 7 shows the confusion matrix for a supervised classification of 242 spruces and 42 firs, which are located in the sub area E.

Table 7: Confusion matrix of the best classification result for spruces and fir trees

| Classified tree species | Spruce | Fir | No. classified segments | User's accuracy |
|--|--------|-----|-------------------------|-----------------|
| Spruce | 230 | 8 | 238 | 97% |
| Fir | 12 | 34 | 46 | 74% |
| No. reference segments | 242 | 42 | 284 | |
| Producer's accuracy | 95% | 81% | | |
| Overall accuracy: 93% Kappa: 0.72 | | | | |

We used a combination of the saliencies S_g^2 , S_l^2 , S_w and S_n^2 . The firs, which are proportionally lower represented than spruces, could be classified with 81% accuracy. However, we noticed a standard deviation of 7.7% when we applied the classification procedure 20 times with randomly selected training data sets. We also tried to classify beeches and maples, but failed in any case. Thus, these tree species could not be identified with the data sets and the presented classification procedure.

4. Discussion

The watershed segmentation generates results comparable with results of Heurich (2006), who obtained a detection rate of 45% in almost the same reference areas using also the data set I. Moreover, the experiments prove that the usage of full waveform data is clearly superior to first/last pulse data. The comparison of the different foliage conditions demonstrates a higher detection rate for the leaf-off data set mainly in the lower and intermediate layer because of the higher penetration in unfoliated deciduous trees. Thus, the leaf-off situation seems to be the more appropriate flying time to segment trees in 3D, at least for mixed mountain forests that are scanned with a high point density. The experiment with the different point densities shows that a nominal point density higher than 10 pts/m² does not improve the detection rate considerably. However it remains to be seen whether a higher density is advantageous to estimate other parameters like for instance the timber volume. Summarizing, the significant improvement of the detection rate – apparent in the lower and intermediate layer – is influenced both by the full waveform data and the new normalized cut segmentation. The accuracy gain in the lower and intermediate layer is more than 20%.

The classification experiments demonstrate clearly that the overall accuracy is significantly increased by using full waveform data. In general, the accuracy is excellent even for the unsupervised classification. In case of the supervised classification we attained an overall accuracy of 95% for all reference data. Moreover, the results are practically independent on the point density and the foliage condition. Contrary, we have found a slight dependency of the overall accuracy on the height layer in leaf-on situation. However, the accuracy loss is compensated by a superior accuracy in the upper height layer in the leaf-on case. Spruces and firs could be successfully classified as different tree species. Since the number of fir trees was

low further experiments are needed. All in all, the increased detection rate of single trees leads to an increased number of correctly classified trees. For instance, a detection rate of 60% and a classification accuracy of 94% imply 56% correctly detected and classified trees. Finally, our classification results of 80% with first/last pulse data in leaf-on case compare excellent with the experiments of Heurich (2006). However, our results with the full waveform data in leaf-on situation are in any classification case better than the leaf-on results with first/last pulse data of this study.

Acknowledgements

We thank Dr. Marco Heurich and the Administration of the Bavarian Forest National Park for their productive contributions and for giving us the opportunity to use their remote sensing test sites.

References

- Brandtberg, T., 2007. Classifying individual tree species under leaf-off and leaf-on conditions using airborne lidar. *ISPRS Journal of Photogrammetry and Remote Sensing*, 61, pp. 325 – 340.
- Heijden, F. van der, Duin, R.P.W., Ridder, D. de and Tax, D.M.J., 2004, Classification, parameter estimation and state estimation – An engineering approach using MATLAB. John Wiley & Sons Ltd, The Atrium, southern Gate, Chichester, West Sussex PO19 8SQ, England
- Heurich, M., 2006. Evaluierung und Entwicklung von Methoden zur automatisierten Erfassung von Waldstrukturen aus Daten flugzeuggetragener Fernerkundungssensoren. Forstlicher Forschungsbericht München, Nr. 202, ISBN 3-933506-33-6. <http://meadiatum2/ub.tum.de/>. (Accessed February 18, 2007).
- Holmgren, J., Persson, Å., 2004, Identifying species of individual trees using airborne laser scanner. *Remote Sensing of Environment* 90 (2004) 415 – 423.
- Hyypä, J., Kelle, O., Lehtikoinen, M., Inkinen, M., 2001. A segmentation-based method to retrieve stem volume estimates from 3-D tree height models produced by laser scanners. *IEEE Transactions on Geoscience and Remote Sensing*, 39: 969 – 975.
- Jutzi, B., Stilla, U., 2006. Range determination with waveform recording laser systems using a Wiener Filter. *ISPRS Journal of Photogrammetry and Remote Sensing*, 61, pp. 95 – 107.
- Kirchhof, M., Jutzi, B., Stilla, U., 2008. Iterative processing of laserscanning data by full waveform analysis. *ISPRS Journal of Photogrammetry and Remote Sensing*, 63, pp. 99 – 114.
- Reitberger, J., Krzystek, P., Stilla, U., 2007. Combined tree segmentation and stem detection using full waveform LIDAR data. Proceedings of the ISPRS Workshop Laser Scanning 2007 and SilviLaser 2007, Volume XXXVI, PART 3/W52, 12 – 14th September 2007, Espoo, pp. 332 – 337.
- Reitberger, J., Krzystek, P., Stilla, U., 2008a. Analysis of full waveform LIDAR data for the classification of deciduous and coniferous trees. *International Journal of Remote Sensing*. Vol. 29, No. 5, March 2008 , pp. 1407 – 1431.
- Reitberger, J., Schnörr, Cl., Krzystek, P., Stilla, U., 2008b. 3D segmentation of full waveform LIDAR data for single tree detection using normalized cut. *IAPRS* Vol. XXXVII, Part B3a, 3 – 11th July 2008, Beijing, pp. 77 – 83.
- Reitberger, J., Schnörr, Cl., Heurich, M., Krzystek, P., Stilla, U., 2008c. Towards 3D mapping of forests: A comparative study with first/last pulse and full waveform LIDAR data. *IAPRS* Vol. XXXVII, Part B8, 3 – 11th July 2008, Beijing, pp. 1397 – 1403.
- Shi, J., Malik, J., 2000. Normalized cuts and image segmentation. *IEEE Transactions on Pattern Analysis and Machine Intelligence*, 22, pp. 888 – 905.
- Solberg, S., Naesset, E., Bollandsas, O. M., 2006. Single Tree Segmentation Using Airborne Laser Scanner Data in a Structurally Heterogeneous Spruce Forest. *Photogrammetric Engineering & Remote Sensing*, Vol. 72, No. 12, December 2006, pp. 1369 – 1378.

Wagner, W., Ullrich, A., Ducic, V., Melzer, T., Studnicka, N., 2006. Gaussian decomposition and calibration of a novel small-footprint full-waveform digitising airborne laser scanner. *ISPRS Journal of Photogrammetry and Remote Sensing*, 60, pp. 100 – 112.

Area-based parameterization of forest structure using full-waveform airborne laser scanning data

Bernhard Höfle^{1,2}, Markus Hollaus^{1,2}, Hubert Lehner¹,
Norbert Pfeifer¹ & Wolfgang Wagner^{1,2}

¹ Institute of Photogrammetry and Remote Sensing, Vienna University of Technology,
1040 Wien, Austria, ([bh](mailto:bh@ipf.tuwien.ac.at), [mh](mailto:mh@ipf.tuwien.ac.at), [hl](mailto:hl@ipf.tuwien.ac.at), [np](mailto:np@ipf.tuwien.ac.at), [ww](mailto:ww@ipf.tuwien.ac.at))@ipf.tuwien.ac.at

² Christian Doppler Laboratory “Spatial Data from Laser Scanning and Remote Sensing”

Abstract

Small-footprint airborne laser scanning (ALS) is increasingly used in vegetation and forest related applications. This paper explores the potential of full-waveform (FWF) ALS information (i.e. echo width and backscatter cross section) for tree species classification and forest structure parameterization. In order to obtain defined physical quantities, radiometric calibration of the recorded FWF data is performed by using a natural radiometric reference target (asphalt road). Based on a segmentation of the canopy surface, descriptive statistical values of laser echo attributes are derived and attached to the segment polygons, which represent large crown parts or even single trees. We found that average segment-based values of echo width and cross section are well suited to separate larch from deciduous trees (i.e. oak and beech). Additionally, the vertical distribution of the FWF information within a segment is specific for each tree species. On forest stand level a visual agreement of the segment-based FWF values with forest inventory reference data exists. We expect that with further investigation on the laser beam's interaction with vegetation calibrated FWF information can assist tree species classification and forest inventory.

Keywords: Airborne Laser Scanning, Waveform, Calibration, Segmentation, Vegetation

1. Introduction

Small-footprint Airborne Laser Scanning (ALS) has evolved to a state-of-the-art technique for topographic data retrieval with major utilization in Digital Terrain Model (DTM) generation, forestry and urban applications (e.g. building detection and modeling). The fields of applications steadily increase (e.g. glaciology, hydrology) but also developments in sensor design allow for improved data analysis in already established fields of applications, as for example full-waveform (FWF) recording systems have shown in the last few years. In forestry a large range of applications using ALS data have been presented in the last years (see proceedings of Natscan in Freiburg 2004, 3D Remote Sensing in Forestry in Vienna 2006, and previous Silvilaser conferences).

Two major methodological approaches for the extraction of forest information are predominant. The (1) distribution-based methods (e.g. Næsset 2004; Maltamo *et al.* 2004; Hollaus *et al.* 2007) use the canopy height or vertical distribution of laser echoes for estimating area-based forest inventory parameters (e.g. Lorey's mean height, stem number, basal area, and volume) by statistical means, which require an extensive set of field reference data. The (2) single-tree-based methods (e.g. Hyypä *et al.* 2001; Morsdorf *et al.* 2004) rely on the detection of individual trees and their geometrical reconstruction (e.g. tree height, crown shape), for which ALS data with high point densities are required. In contrast to these summarized methods, which use mainly the geometric information of discrete ALS data, the radiometric information

content of ALS data seems to be a promising data source for tree species classification. For example Moffiet *et al.* (2005) analyzed the so-called intensity of discrete echo digitization systems for classification. Also Brandtberg (2007) investigated the vertical distribution of intensities for different tree species under leaf-off and leaf-on conditions. Furthermore, Reitberger *et al.* (2008) and Litkey *et al.* (2007) analyzed full-waveform (FWF) ALS data for tree species identification.

However, if radiometric information of ALS data is used, an appropriate calibration of the data is required. For example Höfle and Pfeifer (2007) described data and model-driven approaches to correct the intensity values from discrete ALS systems. For the radiometric calibration of FWF ALS data Wagner *et al.* (2006) presents the theoretical basis for modeling the waveform as series of Gaussian pulses and proposed a calibration equation to estimate the backscatter cross section of each target. Briese *et al.* (2008) point out that natural reference targets (e.g. asphalt, gravel), whose reflectance is determined in situ by a reflectometer, can be used for radiometric calibration.

In this paper a new approach is introduced for area-based parameterization of forest structure with major focus on the additional information provided by FWF ALS systems (e.g. echo width, amplitude, and backscatter cross section). Through exploratory data analysis the distributions of the FWF point cloud attributes will be assessed, which is fundamental for understanding the backscattering characteristics of individual tree species. The proposed investigations are done for deciduous tree dominated forest stands in the West of Vienna.

2. Study area and datasets

The study area is located in the western part of Vienna, in the so-called Wienerwald (Vienna Woods), and covers about 80 hectares of forest. The used full-waveform ALS data are provided by the city of Vienna (MA41-Stadtvermessung) and were retrieved in the framework of the city-wide ALS project. The ALS data were acquired using a RIEGL LMS-Q560 full-waveform scanner during the winter and spring season 2006/2007 under leaf-off conditions. The LMS-Q560 uses near infrared (1500 nm) laser pulses with a pulse width of 4 ns while the scan angle range is $\pm 22.5^\circ$. Full-waveform decomposition has been performed by using the Riegl software Rianalyze². With full-waveform recording the number echoes that can be extracted is not limited beforehand as it is with discrete echo recording systems (e.g. mostly two echoes). Therefore, the number of echoes per shot is generally higher in full-waveform data, as for example the relatively high percentage of intermediate echoes shows (i.e. extracted echoes between first and last reflection). The average echo density is 16 laser echoes per m², with about 31.5% first echoes, 11% intermediate echoes (e.g. 2nd, 3rd echo), 31.5% last echoes and 26% single echoes (i.e. shots with only one reflection).

For the investigated forests, stand-level forest inventory (FI) data were provided by the ÖBf AG, which is the largest forest owner in Austria. The dominating tree species are red beech (*Fagus sylvatica*) with ~51%, oaks (*Quercus robur*, *Quercus petraea*) with ~23% and hornbeam (*Carpinus betulus*) with ~16%. The remaining areas are covered with ~6% larch (*Larix decidua*), 2% clearings and other deciduous and coniferous tree species. For the current analyses tree species (i.e. beech, oak, and larch) were classified for several single trees during a field trip.

3. Methods

The high point density (>16 echoes/m²) of the used full-waveform ALS dataset together with the

² http://www.riegl.com/airborne_scanners/lms_s560/rianalyze.htm

large areas that should be covered in operational forest inventory management require the application of methods, which are able to combine both, fast raster processing as well as detailed (“interpolation-free”) point cloud based information retrieval. Furthermore, the high point density allows generating high resolution raster datasets (e.g. 0.5m cell size), which guarantee sufficient spatial accuracy for area-wide forest analysis. Hence, an object-based raster analysis method combined with FWF point cloud information retrieval is introduced.

The workflow of the proposed analysis comprises the following steps:

1. Radiometric calibration and retrieval of FWF echo parameters using a defined calibration area;
2. Object-based raster analysis of the forest canopy using an edge-based segmentation procedure;
3. Building of an extensive segment feature (i.e. attribute) database;
4. Exploratory segment feature analysis using reference data on single tree and forest stand level.

3.1 Radiometric calibration

The physical observables after processing the full-waveform for each laser shot are the echo width and the amplitude for each echo. These observables are not only affected by the target properties (e.g. reflectance) but also by sensor (e.g. emitted pulse energy) and flight parameters (e.g. flying height). Therefore, it is advantageous for segmentation and classification purposes to switch to physical quantities, which take these dependencies into account, such as the backscatter cross section σ given in m^2 . If no calibration is performed, the investigation of the FWF information (e.g. echo amplitude) suffers from the drawback that the found quantities are not applicable for different sensors, flight parameters, flying dates, study areas, and flight strips (Wagner *et al.* 2008). The basic relation for the received power P_r , which is proportional to the product of the amplitude and echo width, is given in the radar equation (Eq. 1):

$$P_r = \frac{P_t D_r^2}{4\pi R^4 \beta^2} \cdot \eta_{\text{sys}} \eta_{\text{atm}} \cdot \sigma \quad \text{with} \quad \sigma = \frac{4\pi}{\Omega} \rho A \quad (1)$$

where P_t represents the transmitted power, D_r the receiving aperture diameter, R the path length, β the beam divergence, η_{sys} a system and η_{atm} an atmospheric transmission factor and σ the backscatter cross section, which combines all target parameters like illuminated area A , reflectivity ρ and directionality of the scattering of the surface Ω (Wagner *et al.* 2006; Briese *et al.* 2008). Some parameters can be assumed to be constant during one flight mission and therefore be combined in the calibration constant C_{cal} . Estimating the cross section of a reference surface allows determining C_{cal} (Eq. 2) by using path length, amplitude and echo width of echoes, which hit the reference surface. Then the backscatter cross section can be calculated for every single echo as following:

$$\sigma = C_{\text{cal}} R^4 P_r \quad \text{with} \quad C_{\text{cal}} = \frac{4\pi\beta^2}{P_t D_r^2 \eta_{\text{sys}} \eta_{\text{atm}}} \quad (2)$$

The calibration was carried out based on an asphalt road as reference target. The reflectance of the target was estimated by in situ measurements using a reflectometer (cf. Briese *et al.* 2008). Assuming Lambertian scattering of the reference target allows deriving the cross section of the reference target. Due to the lack of simultaneous meteorological data, the atmospheric attenuation effects are included in the calibration constant (Eq. 2). For echoes within the target, C_{cal} can be computed and an average value of the resulting calibration constants can be used for the calculation of σ for the whole data set.

3.2 Segmentation of the forest canopy

In order to enable an area-based investigation and parameterization of the forest structure larger spatial units have to be built. Firstly, this step should separate forested/vegetation areas from terrain as well as from other raised objects (e.g. buildings). Secondly, the object boundaries indicated in the normalized Digital Surface Model (nDSM) and lying within areas marked as vegetation should be preserved because they may represent the border between different tree species and forest types respectively, showing different signatures in the FWF data. Especially in dense deciduous forests with a mixture of small and large trees (in the sense of height and diameter) the detection of single trees can hardly succeed. Therefore, our approach aims at delineating convex objects elevated in the nDSM (i.e. canopy layer) using an over-segmentation, so that one tree can be represented by one, or more segments if a tree forms a crown with multiple tops. An edge-based segmentation procedure was implemented in the open source software GRASS GIS. The basic ideas behind the segmentation are that 1) convex objects of the canopy (i.e. nDSM) are separated by concave areas (i.e. valleys), 2) the normalized height of the vegetation exceeds a certain threshold (e.g. >2.0m above DTM), and 3) within vegetation multiple reflections occur. Since the segmentation is performed on the nDSM it is a 2.5D approach, which cannot delineate occluded objects in lower vegetation layers. Two raster layers are used as input for the segmentation (Figure 1a) – the nDSM and an echo ratio raster (Eq. 3):

$$\text{echo ratio [\%] per cell} = (n_{\text{first}} + n_{\text{intermediate}}) / (n_{\text{last}} + n_{\text{single}}) \cdot 100.0 \quad (3)$$

with echo ratio set to zero if no echo is within the cell and set to 100.0 if $(n_{\text{last}} + n_{\text{single}})$ is zero.

The edge detector is based on calculating the curvatures of the nDSM (minimum curvature in direction perpendicular to the direction of maximum curvature), threshold it (i.e. curvature < 0.0) and further skeletonize the potential edge areas to finally get the edge map. The chosen window size and the threshold on curvature determine the degree of canopy structure detail that is regarded, i.e. controls over- and under-segmentation. These derived edges are the potentially most exterior boundaries of a segment. Then the edge map is intersected with the areas fulfilling the height and echo ratio threshold. As a last step the final segments are derived by connected components labeling and vectorization of the region outline (Figure 1c).

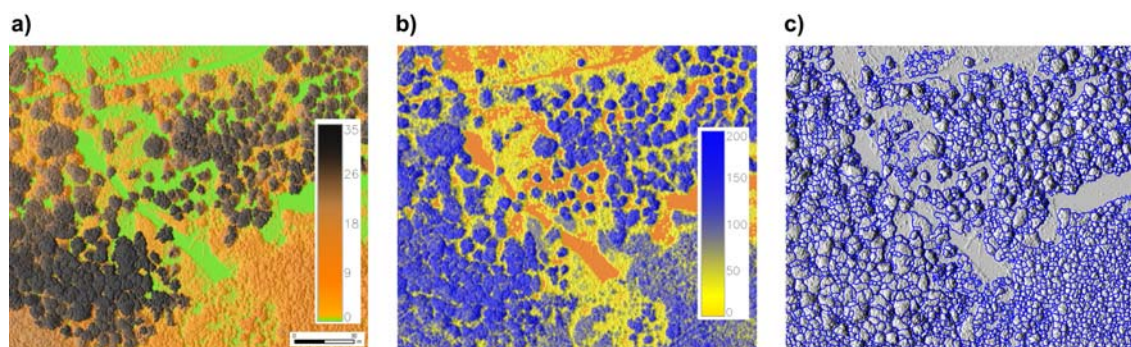


Figure 1: a) nDSM color-coded by normalized height, b) echo ratio raster, c) resulting segmentation of the canopy layer using the nDSM and the echo ratio raster (cf. Eq. 3).

3.3 Feature calculation

In order to extract the highest degree of information, feature extraction goes back to the 3D point cloud. For each segment the corresponding laser echoes are selected using a point-in-polygon test. Descriptive statistical values (min., max., mean, and std. deviation) are derived individually per segment for normalized point height, echo width, and backscatter cross

section. As the point cloud selection is performed in 2D the points of the highest vegetation layer have to be separated from the lower layers and the understory otherwise the segment features may not represent the tree species forming the canopy but a mixture of all trees in the vertical vegetation column of a segment. For this task a global minimum height threshold (e.g. > 3.0m) is defined, which should remove the understory. A dynamic minimum height threshold on normalized echo height – defined as percentage of the nDSM height (e.g. 50%) at the echo location – should further separate the top layer.

4. Results and discussion

4.1 Calibrated full-waveform information

Figure 2a shows an image of the study area with averaged echo cross sections where the brightest areas represent terrain (e.g. forest road and open grass) and dark areas mainly high vegetation. The grayscale variations within the forest coincide with different forest characteristics (e.g. tree species, age, canopy height and closure). Figure 2b shows averaged cross sections for echoes in the upper layer of the vegetation where major tree branches and stems become evident by their higher average cross section (light green color).

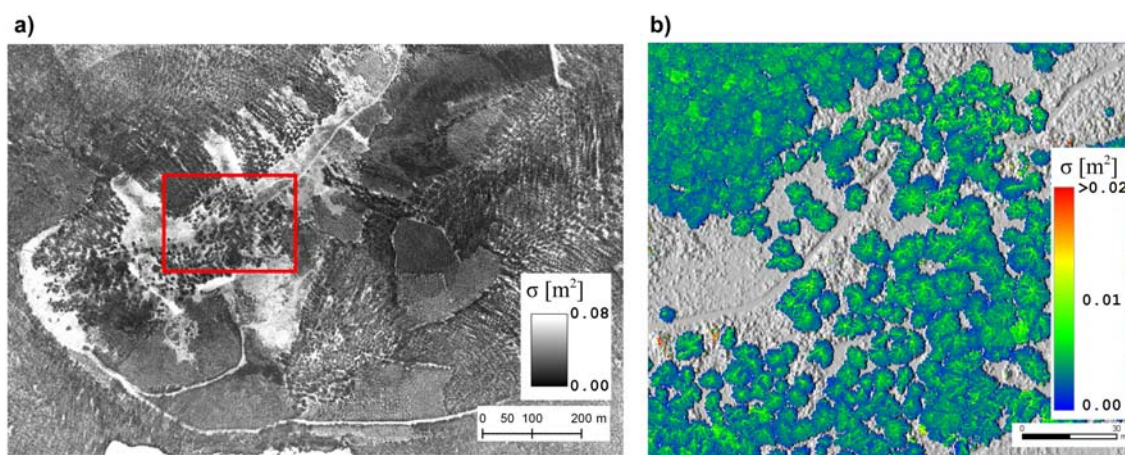


Figure 2: a) Average backscatter cross section per 0.5 x 0.5m cell using all laser echoes (red square shows extent of right subfigure) and b) average cross sections of echoes in the uppermost vegetation layer.

Extracting the target reflectance for vegetation echoes will be problematic because we do not know the illuminated area, the bidirectional reflectance distribution function (BRDF) of the target, as well as estimating the local incidence angles (e.g. on leaves) using the point cloud leads to great uncertainty. Hence, the backscatter cross section (BSC) and the echo width (EW) derived for each reflection are the parameters most suitable for further investigation in the field of vegetation analysis and forestry.

4.2 Canopy segmentation

The echo ratio is an appropriate parameter for separating solid objects (e.g. terrain, buildings) from vegetation indicated by high values. Visually evaluated this classification worked out very well (cf. Figure 1c) because the data acquisition was carried out under leaf-off conditions and deciduous trees are dominant within the area investigated. Dense canopies (e.g. coniferous trees or dense leaf canopy) where the laser beam is fully intercepted in the crown will cause low echo ratio values, and hence are not considered as vegetation. To overcome this problem other raster layers could be additionally included in the segmentation – such as surface roughness, echo width or backscatter cross section of points vertically close to the DSM. The applied

segmentation delineates objects that are clearly represented in the canopy layer. These objects may correspond with single trees if they are detached and build a single distinct crown, respectively. Large deciduous trees tend to build multiple convex crown parts, which results in one segment for each part. In the analyzed data no grouping of different canopies into one segment (under-segmentation) could be observed. If aiming at single tree or stem detection in a forest comparable to our study area, it becomes necessary to consider the third dimension (i.e. point cloud) and FWF information already in the detection process (e.g. Reitberger *et al.* 2007).

4.3 Exploratory segment feature analysis

On single tree and segment level, respectively, the echo width and backscatter cross section of three different tree species are investigated. The segments of 11 red beeches (spread over two stands; >30 m avg. height), 10 oaks (4 stands; >27 m avg. height) and 4 larches (same stand; >18 m height) were identified in the field. The derived statistics are based on echoes in the upper vegetation layer (as defined in Section 3.3) in order to avoid a mixture with echoes from smaller neighboring trees and the understory. Looking at the average segment values for echo width and cross section clearly shows that larch (avg. EW=5.35 ns, avg. BSC=0.0096 m²) is clearly separated from the deciduous species, whereas beech (avg. EW=4.44 ns, avg. BSC=0.0059 m²) and oak (avg. EW=4.41 ns, avg. BSC=0.0055 m²) show similar average values (cf. Figure 3a).

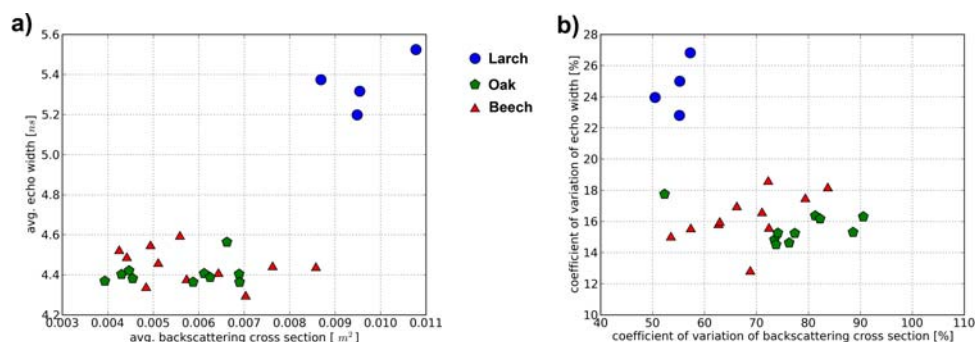


Figure 3: Tree species scatter plots of a) segment-based average of echo width vs. cross section and b) segment-based coefficient of variation (CV) of echo width vs. CV of cross section.

Concerning the variation of the FWF features oak shows a higher coefficient of variation (CV) in BSC and lower CV in EW than beech. In Figure 3b one oak tree with lower variation sticks out (CV of BSC=52%). In contrast to the other oaks (>27m height), the ‘outlier’ is a smaller tree with about 18 m height. This confirms that growth and age are an important factor, as important as tree species, for the backscattering properties parameterized by the FWF information.

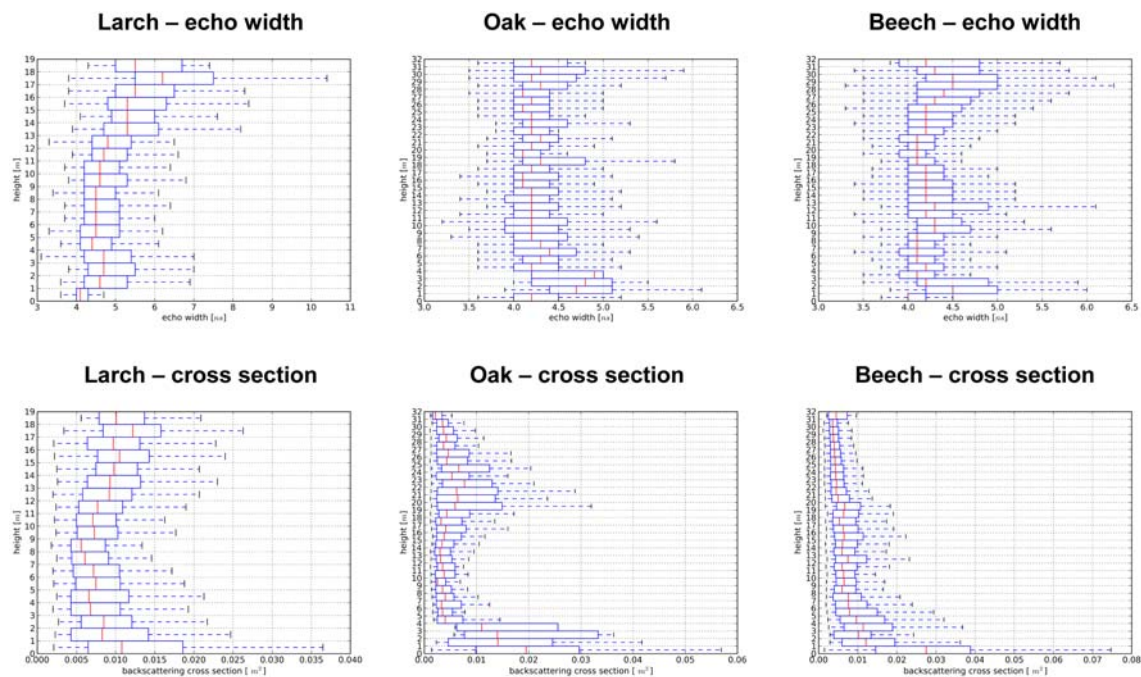


Figure 4: Boxplots in vertical profiles (1 m intervals) of echo width and cross section for the tree species larch, oak and beech. All echoes per tree segment are used.

For better understanding of the average segment values the vertical distribution of the FWF information for representative segments is shown in Figure 4. It can be seen that larch has the highest values of BSC in the uppermost part, which is strongly correlated with the echo width. Oak and beech show relatively constant average echo widths over the vertical profile but the BSC increases, which may be due to the increase of collision area (more and broader branches). Figure 5 gives a good impression how the segment FWF features could be used to find structurally homogeneous forest areas or could be used to determine the structural heterogeneity of defined units. It can be seen that the reference forest stand outlines generally coincide with a specific BSC and EW class, respectively, whereas some stands are characterized by a strong heterogeneity due to different tree species and age classes.

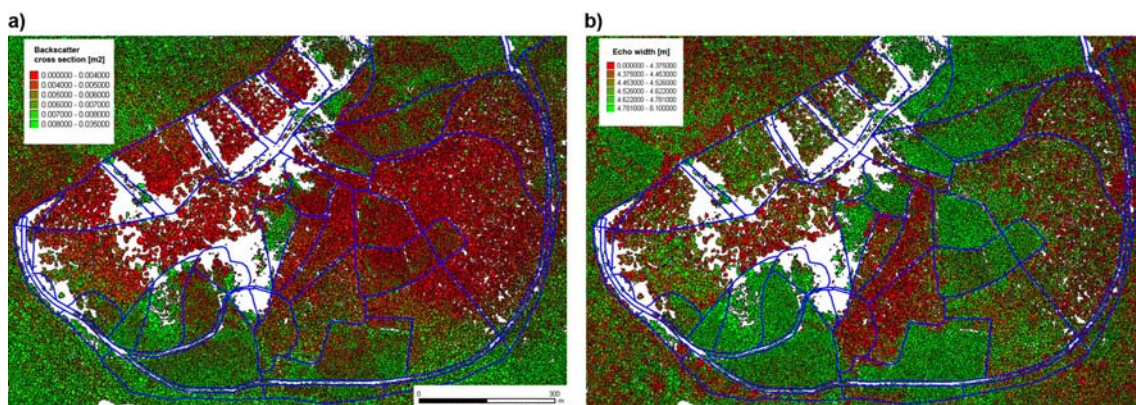


Figure 5: a) Segments colored by mean backscatter cross section of echoes in the upper vegetation layer. b) Segments colored by mean echo width. Blue boundaries are the forest stand outlines from the forest inventory reference data.

5. Conclusions

Up to now most studies utilize the geometric information of airborne laser scanning data to characterize forests at various scales (from single trees to forest stands). Recent studies have shown that the intensity data of discrete echo recording system is a supplementary source of information (e.g. Moffiet *et al.* 2005). The present paper shows that information provided by full-waveform laser scanning (e.g. echo width) and physical quantities derived by radiometric calibration of the recorded signal (e.g. backscatter cross section) have a great potential for tree species identification and large scale forest characterization, even under leaf-off conditions. Within the small selection of trees analyzed in detail a good separability between larch and deciduous trees (oak and beech) is found regarding average segment values of echo width and backscatter cross section. Additionally the vertical distribution of the FWF information yields specific characteristics for each tree species. In order to consolidate the findings more and extensive reference data has to be included. Furthermore, effects of different data acquisition settings (e.g. flight geometry) on echo width, amplitude, and cross section have to be quantified and separated from effects originating from the tree configuration (e.g. species, age).

Acknowledgements

We would like to thank the MA41-Stadtvermessung, City of Vienna, for providing the laser scanning data and the Österreichische Bundesforste AG for providing the reference data. Parts of this study were funded by the Austrian Federal Ministry of Agriculture, Forestry, Environment and Water Management (BMLFUW) in the framework of the project ÖWI-Regio and by the Austrian Research Promotion Agency (FFG) in the framework of the project SAR-X Environ.

References

- Brandtberg, T., 2007. Classifying individual tree species under leaf-off and leaf-on conditions using airborne lidar. *ISPRS Journal of Photogrammetry & Remote Sensing*, 61, 325-340.
- Briese, C., Höfle, B., Lehner, H., Wagner, W., Pfennigbauer, M. and Ullrich, A., 2008. Calibration of full-waveform airborne laser scanning data for object classification. In: *SPIE Laser Radar Technology and Applications XIII*, Orlando, Vol. 6950: pp. 8.
- Höfle, B. and Pfeifer, N., 2007. Correction of laser scanning intensity data: Data and model-driven approaches. *ISPRS Journal of Photogrammetry & Remote Sensing*, 62 (6), 415-433.
- Hollaus, M., Wagner, W., Maier, B. and Schadauer, K., 2007. Airborne Laser Scanning of Forest Stem Volume in a Mountainous Environment. *Sensors*, 7 (8), 1559-1577.
- Hyypä, J., et al., 2001, HIGH-SCAN: The first European-wide attempt to derive single-tree information from laserscanner data. *The Photogrammetric Journal of Finland*, 17, 58-68.
- Litkey, P., Rönnholm, P., Lumme, J. and Liang, X., 2007. Waveform features for tree identification. In: *Proceedings of the ISPRS Workshop "Laser Scanning 2007 and SilviLaser 2007"*. Espoo, Finland, 258-263.
- Maltamo, M., Eerikäinen, K., Pitkäinen, J., Hyypä, J. and Vehmas, M., 2004. Estimation of timber volume and stem density based on scanning laser altimetry and expected tree size distribution functions. *Remote Sensing of Environment*, 90, 319-330.
- Moffiet, T., Mengersen, K., Witte, C., King, R. and Denham, R., 2005. Airborne laser scanning: exploratory data analysis indicates potential variables for classification of individual trees or forest stands according to species. *ISPRS Journal of Photogrammetry & Remote Sensing*, 59 (5), 289-309.

- Morsdorf, F., Meier, E., Kötz, B., Itten, K., Dobbertin, M. and Allgöwer, B., 2004. LIDAR-based geometric reconstruction of boreal type forest stands at single tree level for forest and wildland fire management. *Remote Sensing of Environment*, 92(2), 353-362.
- Næsset, E., 2004. Practical Large-scale Forest Stand Inventory Using a Smallfootprint Airborne Scanning Laser. *Scandinavian Journal of Forest Research*, 19 (2), 164-179.
- Reitberger, J., Krzystek, P. and Stilla, U., 2007. Combined tree segmentation and stem detection using full waveform lidar data. In: *Proceedings of the ISPRS Workshop "Laser Scanning 2007 and SilviLaser 2007"*. Espoo, Finland, 332-337.
- Reitberger, J., Krzystek, P. and Stilla, U., 2008. Analysis of full waveform LIDAR data for the classification of deciduous and coniferous trees. *International Journal of Remote Sensing*, 29 (5), 1407-1431.
- Wagner, W., Ullrich, A., Ducic, V., Melzer, T. and Studnicka, N., 2006. Gaussian decomposition and calibration of a novel small-footprint full-waveform digitising airborne laser scanner. *ISPRS Journal of Photogrammetry & Remote Sensing*, 60 (2), 100-112.
- Wagner, W., Hollaus, M., Briese, C. and Ducic, V., 2008. 3D vegetation mapping using small-footprint full-waveform airborne laser scanners. *International Journal of Remote Sensing*, 29 (5), 1433-1452.

Session 5: Algorithm & techniques development

Estimation of effective plant area index using LiDAR data in forest of South Korea

Doo-Ahn Kwak¹, Woo-Kyun Lee¹ & Hyun-Kook Cho²

¹ Division of Environmental Science and Ecological Engineering, Korea University, Seoul 136-701, South Korea, leewk@korea.ac.kr

² Department of Forest Resource Information, Korea Forest Research Institute, Seoul 136-012, South Korea, hcho@forest.go.kr

Abstract

The Effective Plant Area Indices (PAI_e) of *Pinus koraiensis*, *Larix leptolepis* and *Quercus* spp. were estimated by calculating the laser-intercepted rate through the forest canopy using LiDAR data. Initially, the Laser Interception Index (LII), which is related to the canopy gap fraction, was generated by extracting the LiDAR data reflected through the canopy using *k*-means statistics. The LiDAR-derived PAI_e was then estimated by applying LII to the Beer-Lambert law. From a comparison of the LiDAR-derived to the field-derived PAI_e, the coefficients of the determination by the tree species was 0.82, 0.71 and 0.54 for *Pinus koraiensis*, *Larix leptolepis* and *Quercus* spp., respectively. The change in accuracy according to the tree species was attributed to the density of leaves and understory, the interference by stems, the amount of leaves and the vertical number of branches in the forest stands. From field estimations at the time of the study, *Pinus koraiensis* had dense leaves and *Larix leptolepis* had dense branches, while *Quercus* spp. had no leaves or a few big branches. This can be explained by the estimation of the field-derived PAI_e being influenced by the stem shadow and direct sunlight due to the few leaves and poor branches in the *Quercus* spp. stand surveyed, even though the estimation of the LiDAR-derived PAI_e was hardly affected by them.

Keywords: Leaf Area Index, Plant Area Index, LiDAR, Laser Interception Index, *k*-means clustering

1. Introduction

According to Jonckheere *et al.* (2004), there are several definitions for the LAI used in the field, which can be defined as the total one-sided area of leaf tissue per unit ground surface area (Watson, 1947). Schulze *et al.* (2005) suggested that the LAI could be determined by the sum of the projected leaf surface per soil area. On the other hand, Myneni *et al.* (1997) defined the LAI as the maximum projected leaf area per unit ground surface area. Such variously defined LAI can be derived from both the within and below canopy microclimate, control canopy water interception and radiation extinction, as well as water and carbon gas exchange (Bréda, 2003). Moreover, they provide information for biosphere modelling (Bonan, 1993) because they contain information on a number of relevant ecological process (Morsdorf *et al.*, 2006). Therefore, the LAI can play a key role within biogeochemical cycles in an ecosystem. The various methods for obtaining the LAI can be classified into two categories; direct and indirect measurements (Bréda, 2003). Direct methods are destructive and exhaustive due to harvesting vegetation. Moreover, such methods are time-consuming and labour-intensive when the LAI is obtained from field measurements. Thereby, the direct methods are suitable for vegetation with small structures, but are difficult to apply to large areas or trees (Bréda, 2003). On the other hand, the LAI by indirect and non-destructive methods can be easily estimated using the radiative characteristics of sunlight, which is dispersed or penetrates through the vegetation area. With such methods, remote sensing techniques, using satellite imagery and aerial photography,

have been applied to derive this measurement. Many such approaches are based on passive optical sensor systems and regression models (Cohen *et al.*, 2003) or radiative transfer modelling (Koetz *et al.*, 2004). However, one serious problem with remote sensing using passive sensor systems is that they are unable to describe the canopy shape and structure, and the vertical distribution of leaves because they do not contain the elevation information by itself. Light Detection and Ranging (LiDAR), especially using an active sensor system, has recently been used to extract surface information, and can acquire highly accurate object shape characteristics using geo-registered 3D-points (Kwak *et al.*, 2007). The LiDAR system can measure both vertical and horizontal forest structures, such as the tree heights, sub-canopy topographies and distributions in forested areas with high precision (Holmgren *et al.*, 2003). Such characteristics can be used to extract forest information. Morsdorf *et al.*, (2006) derived the LAI using fCover (fractional cover) and Riñano *et al.* (2004) obtained the LAI using the gap fraction distribution. Koetz *et al.* (2006) applied the LiDAR waveform model to generate the fCover and LAI from large footprint LiDAR data. However, it is difficult for large footprint LiDAR to extract forest information in small areas. The use of ground based laser scanners is limited by the topographical conditions of the study area as well as to small forest areas not broad forest areas. Barilotti *et al.* (2006) suggested an estimation of the LAI using the Laser Penetration Index (LPI) generated by the point density of LiDAR data, according to the penetration of a laser beam through the canopy of forested areas. However, the threshold value between the transmission and reflectance through the canopy cannot be applied to another forest stand, including fluctuant height understory, because the value was fixed to a height 1 m above the ground.

For such an indirect LAI estimation, a common method in the field is to use an optical sensor to acquire photosynthetically active radiation (PAR) using an AccuPAR-80 Linear PAR/LAI Ceptometer of Decagon Devices, LAI-2000 or hemispherical photography below the canopy (Pocewicz *et al.*, 2004). However, the values recorded with such instruments are not pure LAIs because clumping of the canopy components and the influence of individual tree stems and woody canopy components are not adjusted for (Pocewicz *et al.*, 2004). The value recorded without the consideration of clumping of the canopy components is defined as the effective LAI (LAI_e). Measurements that do not consider light interception by woody components are called the plant area index (PAI), and, if no adjustments are made for the clumping of canopy elements, the values measured by the instruments are referred to as the effective PAI (PAI_e). Therefore, the values measured with optical sensors in forest areas is almost the PAI_e (Pocewicz *et al.*, 2004).

Chen and Cihlar (1996) reported that the PAI_e estimation was more effective in representing the vegetation indices than the LAI estimation because the PAI_e could represent the sunlight interception well by the woody canopy elements and individual tree stems. Therefore, in this study, to approximate the LAI, the PAI_e of *Pinus koraiensis*, *Larix leptolepis* and *Quercus* spp. were estimated by calculating the rate of laser-intercepted LiDAR points through the canopy using LiDAR data. In particular, for the approximate LAI, an attempt was made to estimate only the PAI_e of the canopy part as classifying the LiDAR pulses reflected in forest stands into in- and below-canopy returns using the *k*-means clustering method.

2. Study area

The study areas were located in the Gwangneung Experimental Forest of the Korea Forest Research Institute (the upper left 127°7'30.72523"E, 37°48'0.42761"N and lower right 127°11'59.17548"E, 37°41'59.31795"N), and Mt. Yumyeong (the upper left 127°28'45.76074"E, 37°35'59.75109"N and lower right 127°30'6.98627"E, 37°35'6.27425"N), central South Korea. Situated from 160 to 573m above sea level, the study area is dominated by steep hills, with the main tree species being *Pinus koraiensis* (Korean Pine), *Larix leptolepis* (Japanese Larch) and *Quercus* spp. (Oaks), with approximately 1,017.36 ha selected for this study. In the study area,

the PAI_e was measured from 39 plots (13 plots per tree species), and 36 plots (12 plots per tree species) were measured to assess the accuracy. These plots were selected in such a way that the composition of the tree species was homogeneous.



Figure 1. Location of the study areas

3. Acquisition of LiDAR data and ground data

An Optech ALTM 3070 (a small footprint LiDAR system) was used to acquire the LiDAR data. The flight was performed on the 3rd April 2007. The study area was measured at an altitude of 1,400m, with a sampling density of 5~10 points per square meter, with a radiometric resolution, scan frequency and scan width of 12bits, 70Hz and $\pm 20^\circ$, respectively. The field survey was performed from the 1st to 4th April, 2008. The number of sample and test plots was 75 (25 plots per tree species). Each plot was 20m x 20m (400m²) in size, and the PAI_e of the plots was measured indirectly using the gap fraction method with an LAI-2000 instrument. The PAI_e was estimated using two LAI-2000 instruments, for the diffuse intensity above and below the canopy. One LAI-2000 used for above the canopy was set up with a 180° view cap on the top of the flux tower. The other LAI-2000 was installed for below-the canopy of the plots. The estimation below the canopy was carried out on the middle spots of each of four edge lines and in four directions from the centre of a square plot with a 180° view cap. The positions of the plots were acquired at breast height in the centre of each plot, using a GPS Pathfinder Pro XR manufactured by the Trimble Corporation.

Table 1. Descriptive statistics of the field measurements

| Species | Number of plots | Stand height(m) | | Canopy base height (m) | | Stand DBH(cm) | |
|-------------------------|-----------------|-----------------|------|------------------------|------|---------------|------|
| | | Mean | Std. | Mean | Std. | Mean | Std. |
| <i>Pinus koraiensis</i> | 25 | 15.6 | 2.3 | 6.8 | 2.3 | 32.7 | 5.5 |
| <i>Larix leptolepis</i> | 25 | 16.4 | 2.7 | 6.5 | 2.0 | 28.7 | 4.6 |
| <i>Quercus</i> spp. | 25 | 14.2 | 2.5 | 5.5 | 1.9 | 28.3 | 8.9 |

4. Method

4.1 Potential of using LiDAR for PAI_e estimation

The LiDAR system has the potential for obtaining geo-registered 3D-points; whereas, it is difficult to extract the 3 dimensional information of forested area using independent satellite imagery and aerial photography (Kwak *et al.*, 2007). The Laser pulses emitted from the LiDAR system are similar to that of sunlight with respect to the reflectance or transmission through the

canopy. In addition, they are suitable for representing the PAI_e because of the reflectance on the leaves and branches. Therefore, if stands have dense leaves and branches, the LiDAR points are mostly reflected in the canopy. On the other hand, LiDAR points are almost always transmitted to ground due to sparse leaves and branches.

The Beer-Lambert Law has been used to estimate the PAI_e in previous several studies (Pocewicz *et al.*, 2004). The PAI_e can be calculated using the Beer-Lambert Law, as shown in equation 1.

$$PAI_e = -\ln(I/I_0)/k_{sun} \quad (1)$$

where I and I_0 are the incident and below-canopy radiation respectively, and k_{sun} is the extinction coefficient for solar radiation. The PAI_e can be estimated using I/I_0 , which is known as the gap fraction (G_{sun}), and is defined as the probability of a light beam passing through the canopy without collision (Gower *et al.*, 1999). The gap fraction by solar radiation can be alternated with the ratio of the number of LiDAR returns transmitted through the canopy, to the total number emitted from the aircraft (G_{LiDAR}). In equation 1, k_{sun} can be calculated using equation 2 (Campbell, 1986).

$$k_{sun} = \frac{(x^2 + \tan^2 \theta)^{\frac{1}{2}}}{x + 1.744(x + 1.182)^{-0.733}} \quad (2)$$

where θ is the zenith angle of the sun and x the leaf angle distribution parameter, which is the ratio of the length of the horizontal to the vertical axes of the spheroid, and can be measured as the ratio of the projected area of an average canopy element onto a horizontal plane to its projection onto a vertical plane (Campbell, 1986). Campbell (1986) suggested that an assumption of an ellipsoidal angle distribution for the canopy elements was most useful. Using such an investigation, x was determined to be 1 when the PAI_e (Campbell labelled this LAI) was estimated in the study area and the angle distribution was assumed to be ellipsoidal. k_{sun} can be simplified to equation 3.

$$k_{sun} = \frac{2}{\cos \theta} \quad (3)$$

In equation 3, k_{sun} could be calculated using the solar zenith angle (θ) in the study area. However, for the PAI_e using LiDAR data, the k_{sun} value must be changed to the zenith angle of the emitted laser pulses from the aircraft (k_{LiDAR}) rather than the solar zenith angle. In this study, the k_{LiDAR} value was estimated using the laser zenith angle (θ) $\pm 10^\circ$, which is the median value of the scan angle of every point data reflected in a stand. Therefore, the PAI_e can be estimated from the ratio of the number of transmitted LiDAR returns and the laser zenith angle.

4.2 Classification of LiDAR data using k -means statistics

In order to calculate the gap fraction using LiDAR data (G_{LiDAR}), the transmitted laser pulses need to be detected and classified. In particular, the LiDAR returns only intercepted by the canopy must be clustered to estimate the canopy PAI_e only, which is far from the influence of stems among the woody elements, and approximates the LAI despite not including the woody elements of the canopy. Rianõ *et al.* (2004) attempted to test various clustering methods to classify the LiDAR data, such as a 3m fixed limit, minimum Euclidean distance clustering, k -means clustering and Expectation Maximization clustering. In this study, k -means statistics were used to classify LiDAR data and calculate the gap fraction. The k -means statistics is an algorithm used to classify or group attributes or features into k number of groups, and uses an iterative algorithm that

minimizes the sum of the distances (SOD) from each object to its cluster centroid, over all clusters (Equation 4).

$$SOD_{i...j} = \sum_i^j |Centroid_{i...j} - Object[n]| \quad (4)$$

This algorithm moves objects between clusters until the sum can be decreased no further. This results in a set of clusters that are as compact and well-separated as possible (MATLAB, 2006). In this study, the number of clusters (k) was determined to be two as to classify LiDAR returns into in-canopy and below-canopy LiDAR returns with the z (height) value of points. The initial points of each cluster can be selected by the user when carrying out k -means clustering. However, in this study, a random selection of k observations from LiDAR point data was used, with 100 iterations calculated. Moreover, the cluster was treated as an error if it was too small, e.g., the percentage of laser pulses of a group had less than $1/(\text{total number of clusters})^2$ (Rianõ *et al.*, 2004). Thereby, the laser interception indices (LII) according to the tree species was generated using the LiDAR returns reflected through the canopy.

4.3 Generation of Laser Interception Index

Barilotti *et al.* (2006) suggested the use of the laser penetration index (LPI), with the point density of the ground returns and vegetation returns in the sample plots. All LiDAR points were divided into two classes; high (height $\geq 1\text{m}$ above ground), and low (height $< 1\text{m}$ above ground) vegetation returns. However, in the case of various heights of the understory, the LPI was not flexible because the value used to distinguish the ground and high vegetation returns was fixed at a height 1m above the ground regardless of the characteristic of the forest stand. Therefore, the LII was calculated in order to apply flexible heights considering the characteristics of various forest stands, as shown in equation 5.

$$LII = \frac{N_{in\ canopy\ returns}}{N_{total\ returns}} = 1 - \frac{N_{below\ canopy\ returns}}{N_{total\ returns}} \quad (5)$$

where $N_{in\ canopy\ returns}$ is the number of LiDAR returns intercepted by the canopy, $N_{below\ canopy\ returns}$ is the number of LiDAR returns transmitted through the canopy and $N_{total\ returns}$ is the total number of LiDAR returns emitted from the aircraft. According to equation 5, the vegetation is dense if the value of LII is close to 1, but the vegetation is sparse if the value is close to 0. Incidentally, the LII is an opposite concept, which is related to the ground covered by the canopy, even when the LiDAR gap fraction (G_{LiDAR}), which is the ratio of transmitted LiDAR returns to the total LiDAR returns, is need to calculate PAI_e . Therefore, equation 5 must be changed into equation 6 in order to apply LII to the PAI_e .

$$G_{LiDAR} = \frac{N_{below\ canopy}}{N_{total\ returns}} = 1 - LII \quad (6)$$

Finally, the PAI_e can be estimated artificially by the tree species by substituting G_{sun} and k_{sun} for G_{LiDAR} and k_{LiDAR} , respectively as shown in equation 7.

$$PAI_e = -2 \cos \theta_{LiDAR} \cdot \ln(1 - LII) \quad (7)$$

5. Result and discussion

5.1 Classification of LiDAR data

As a result of the classification of the LiDAR returns using k -means clustering, the LiDAR returns by the tree species were classified into two clusters as shown in figure 3, because the LiDAR returns for both *Pinus koraiensis* and *Larix leptolepis* were almost reflected in the canopy and ground due to the dense leaves and branches with rare understories. *Quercus* spp. could also be divided into two clusters due to the larger number of ground returns than above ground returns. Figure 3 shows the typical distribution of the LiDAR returns according to the species of tree.

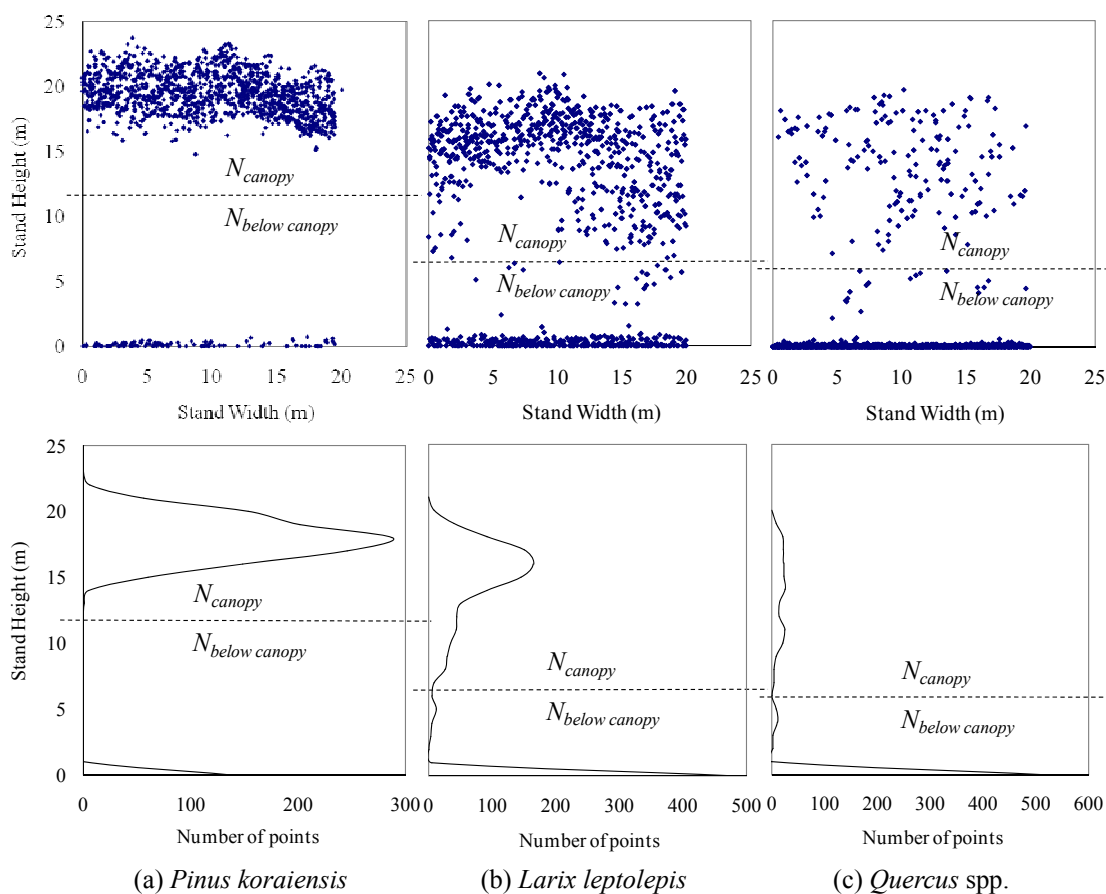


Figure 3. Distribution of the LiDAR returns and classification into two clusters by the tree species

The LiDAR data was partitioned into two groups, and then G_{LiDAR} was generated using N_{canopy} , $N_{below canopy}$ and N_{all} . Because few understories existed and abundant canopy in the plots for *Pinus koraiensis*, the LiDAR returns could be clearly clustered into two groups, without a middle point layer. However, some of the LiDAR pulses in the plots for *Larix leptolepis* and *Quercus* spp. were reflected in a middle point layer because there were some understories and no leaves when the field survey was carried out. Nevertheless, the results of k -means statistics with two centroids were acceptable because the threshold heights for classifying the in-canopy and below-canopy points were similar to the field-derived crown base heights, which were 6.5 and 5.5m for *Larix leptolepis* and *Quercus* spp., respectively. In particular, the LiDAR returns in the plots for *Quercus* spp. were clustered well into two parts, even with abundant LiDAR returns on the ground and a few on the branches as a result of the species having few leaves. These classification results were used to estimate the LiDAR-derived LAI using G_{LiDAR} .

5.2 Estimation of effective plant area index using LiDAR gap fraction

Using the G_{LiDAR} values, the LiDAR-derived PAI_e s, which mean the only canopy PAI_e s, were estimated by tree species. The PAI_e s of *Pinus koraiensis* were higher than those of *Larix leptolepis* and *Quercus* spp., because it is an evergreen needle tree with dense leaves. On the other hand, the PAI_e s of *Larix leptolepis* and *Quercus* spp. were relatively low because they had a few leaves and branches when the field survey was carried out, i.e. from 1st to 4th April. However, The PAI_e s of *Larix leptolepis* were much higher than those of *Quercus* spp.. This was attributed to the emitted LiDAR pulses being reflected on the many dense branches of *Larix leptolepis*, as shown in Figure 4.

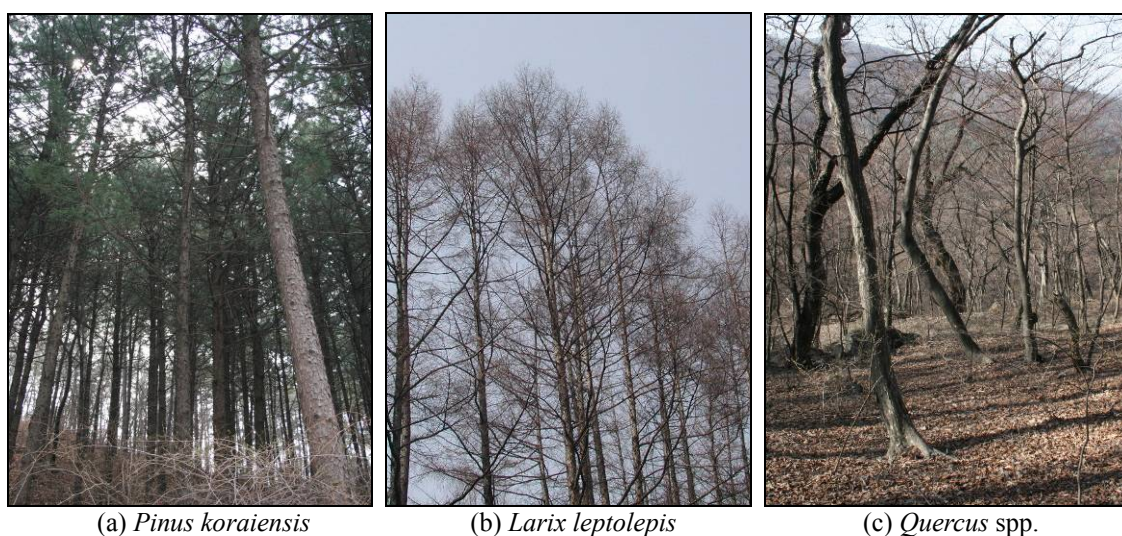


Figure 4. Structure of the stands surveyed by tree species

Linear regression analysis was carried out to determine the relationship between the LiDAR-derived and field-derived PAI_e . The coefficient of determination (R^2) and root mean square error (RMSE) were calculated to determine the accuracy of the estimated regression analysis (Table 2).

Table 2. Accuracy of the regression function generated by LPI and LII

| Tree species | Statistics | Results |
|-------------------------|------------|---|
| <i>Pinus koraiensis</i> | Function | $PAI_e = -0.629 \cdot \frac{\ln(G_{LiDAR})}{k} + 1.490$ |
| | R^2 | 0.75 |
| | RMSE | 0.40 |
| <i>Larix leptolepis</i> | Function | $PAI_e = -0.404 \cdot \frac{\ln(G_{LiDAR})}{k} + 1.694$ |
| | R^2 | 0.89 |
| | RMSE | 0.42 |
| <i>Quercus</i> spp. | Function | $PAI_e = -0.595 \cdot \frac{\ln(G_{LiDAR})}{k} + 0.983$ |
| | R^2 | 0.65 |
| | RMSE | 0.52 |

As a result, the accuracy for *Pinus koraiensis* was the highest of the three tree species, because

the LiDAR returns were mostly reflected through the canopy and rarely onto the ground without a middle point layer, which is similar to the transmission of solar radiation, because the stands of *Pinus koraiensis* have dense leaves. A greater number of LiDAR returns reflected in the canopy can provide a better description of the canopy. On the other hand, *Quercus* spp. showed only a slight relationship between the estimates and ground truth data, which was attributed to *Quercus* spp. having no leaves and a few branches on the tree stems compared with *Larix leptolepis*. No leaves on branches caused some estimation errors due to direct sunlight being sensed into the LAI-2000 or the other instruments when the PAI_e is measured. Therefore, *Quercus* spp. with no leaves and a few branches had fluctuating PAI_s . The PAI_e of *Larix leptolepis* was more stable because the abundant branches play the role of leaves.

5.3 Accuracy assessment

The PAI_e s estimated by regression analysis were evaluated using the field-derived PAI_s in 36 plots (12 plots by tree species) selected for verification. The accuracies for *Pinus koraiensis*, *Larix leptolepis* and *Quercus* spp. were 0.82, 0.71 and 0.54, respectively (Figure 5).

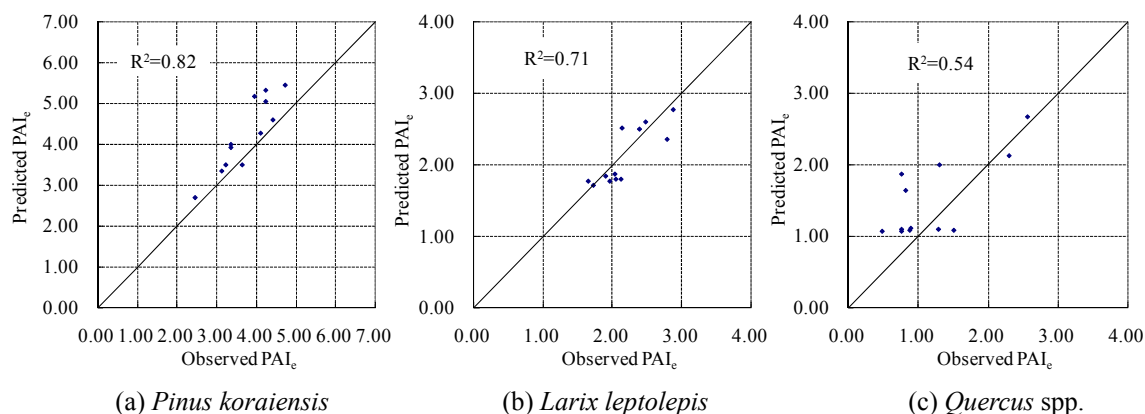


Figure 5. Evaluation of the estimated LAI analysis by the tree species

The estimated PAI_e s of *Pinus koraiensis* had the highest R^2 of the three tree species. This is due to the right measurement without the direct sunlight because *Pinus koraiensis* had abundant leaves on the branches. Moreover, the predicted PAI_e were mostly higher than the observed PAI_s in the test plots. This was attributed to the different amounts of understory between the sample and test areas. Namely, the understory of the test plots might have been less than that in the sample area. The estimated PAI_s for *Larix leptolepis* were relatively accurate due to the abundant branches, even though there were few leaves on the trees. The plenty branches decrease the estimation errors with LAI-2000 because they diffuse direct sunlight. Therefore, the accuracy for *Quercus* spp. was the lowest of the three tree species due mainly to the estimation errors with LAI-2000. The lack of leaves and the poor vertical distribution of the branches might have caused the poor results. When the PAI_s were measured in the *Quercus* spp. stands, the direct sunlight penetrating through the canopy influenced the actual PAI_s because LAI-2000 the recorded mixed value of the diffused radiation and direct sunlight in forested areas. Therefore, LAI-2000 has a weak point in that PAI_s need to be measured around sunrise or sunset. During Summer or early Autumn, the accuracy of the regression function and its evaluation should increase due to the larger number of laser pulses reflected on the leaves as well as the diffusion of direct sunlight by the leaves through the canopy for *Larix leptolepis* and *Quercus* spp.. The PAI_s estimation of trees without leaves, i.e. deciduous trees in late Autumn and early Spring, may be invalid from the point of view of evaluating the PAI_s for trees with the best leaves. However, such research may be valuable because the change in the amount of leaves can be monitored according to season.

The k_{LiDAR} derived using the LiDAR zenith angle and leaf angle distribution also plays an important role in assessing the accuracy. Indeed, each zenith angle of the LiDAR returns reflected in a forest stand has independent values because each LiDAR pulse is emitted from the respective angles due to the rotation of the sensor mounted in the LiDAR system. Therefore, the zenith angles of all the LiDAR returns of a target forest stand need to be detected and calculated for more accurate results when estimating the PAI_e from LiDAR data. In addition, the leaf angle distribution should be also applied with respect to the tree species, even though the leaf angle distribution in this study was assumed to have a value of 1, which suggests an ellipsoidal angle distribution. In future studies, three variables, the LII, laser zenith angle and leaf angle distribution must be considered for more reasonable and precise estimates of the PAI_e using LiDAR data.

6. Conclusion

The LAI was estimated using the laser interception index for three tree species, *Pinus koraiensis*, *Larix leptolepis* and *Quercus* spp.. In the PAI_e s equation by the Beer-Lambert Law, the gap fraction (I/I_0) for the sun was replaced by G_{LiDAR} , which is the ratio of the number of below-canopy points to that of all returns in the sample plots. The G_{LiDAR} was calculated by classifying the in-canopy and below-canopy points using k -means statistics. In the Beer-Lambert Law, the k_{sun} extinction coefficient was calculated using the solar zenith angle and leaf angle distribution. However, instead of k_{sun} , k_{LiDAR} could be generated using the laser zenith angle ($\pm 10^\circ$, median value of every point in sample plots) and leaf angle distribution ($x=1$, meaning of ellipsoidal leaf angle distribution). As a result, the coefficient of determination between the observed and predicted PAI_e for *Pinus koraiensis*, *Larix leptolepis* and *Quercus* spp. were 0.82, 0.71 and 0.54, respectively. When the PAI_e s are acquired in forest stands with few leaves and poor branches, such as deciduous trees in spring or winter, direct sunlight affects the estimation because the optical sensors, e.g. LAI-2000 and AccuPAR-80, measure the diffused radiation transmitted through the canopy. Therefore, the reason for the different PAI_e with regard to tree species was that *Larix leptolepis* and *Quercus* spp. had no leaves, and *Pinus koraiensis* had abundant leaves. The accuracy for *Larix leptolepis* was higher than that of *Quercus* spp. which is because *Larix leptolepis* has more abundant branches that play a role of diffusing the direct sunlight, while *Quercus* spp. had a poor branch distribution vertically. Therefore, with *Larix leptolepis* and *Quercus* spp., more accurate results than those found in this study are expected if the study is performed in late spring when their shoots and leaves begin to appear. The k_{LiDAR} derived using the LiDAR zenith angle and leaf angle distribution also plays a role in estimating the PAI_e using LiDAR data. Even when fixed values for the laser zenith angle and leaf angle distribution are used, future investigations should consider the actual laser zenith angles of each point in the target forest stands and the leaf angle distribution according to the tree species.

Acknowledgements

The authors wish to thank Kang-Won Lee, Managing Director of Hanjin Information System and Telecommunication Corporation, South Korea, for providing the LiDAR data.

References

- Barilotti, A., Turco, S. and Alberti, G., 2006. LAI determination in forestry ecosystem by lidar data analysis. *Proceedings of Workshop on 3D Remote Sensing in Forestry*, Vienna, Austria: 248-252.
- Bonan, G. B., 1993. Importance of leaf area index and forest type when estimating photosynthesis in boreal forests. *Remote Sensing of Environment*, 43, 303-314.

- Bréda, N. J. J., 2003. Ground-based measurements of leaf area index: a review of methods, instruments and current controversies. *Journal of Experimental Botany*, 54, 2403-2417.
- Campbell, G. S., 1986. Extinction coefficients for radiation in plant canopies calculated using an ellipsoidal inclination angle distribution. *Agricultural and Forest Meteorology*, 36, 317-321.
- Chen, J. M. and Cihlar, J., 1996. Retrieving leaf area index of boreal conifer forests using Landsat TM images. *Remote Sensing of Environment*, 55, 153-162.
- Cohen, W. B., Maieringer, T. K., Gower, S. T. and Turner, D. P., 2003. An improved strategy for regression of biophysical variables and landsat etm+ data. *Remote Sensing of Environment*, 84, 561-571.
- Gower, S. T., Kucharik, C. J. and Norman, J. M., 1999. Direct and indirect estimation of leaf area index, fAPAR, and net primary production of terrestrial ecosystems, *Remote Sensing Environ*, 70, 29-51.
- Holmgren, J., Nilsson, M. and Olsson, H., 2003. Estimation of tree height and stem volume on plots using airborne laser scanning. *Forest Science*, 49, 419-428.
- Jonckheere, I., Fleck, S., Nackaerts, K., Muys, B., Coppin, P., Weiss, M. and Baret, F., 2004. Review of methods for in situ leaf area index determination: Part i. theories, sensors and hemispherical photography. *Agricultural and Forest Meteorology*, 121, 19-35.
- Koetz, B., Schaepman, M., Morsdorf, F., Itten, K. and Allgöwer, B., 2004. Radiative transfer modeling within a heterogeneous canopy for estimation of forest fire fuel properties. *Remote Sensing of Environment*, 92, 332-344.
- Koetz, B., Morsdorf, F., Sun, G., Ranson, K. J., Itten, K. and Allgöwer, B., 2006. Inversion of a lidar waveform model for forest biophysical parameter estimation. *IEEE Geoscience and Remote Sensing*, 3, 49-53.
- Kwak, D. A., Lee, W. K., Lee, J. H., Biging, G. S. and Gong, P., 2007. Detection of individual trees and estimation of tree height using LiDAR data, *Journal of Forest Research*, 12, 425-434.
- MATLAB, 2006, Help document in program. Mathwork, United States of America.
- Morsdorf, F., Kötz, B., Meier, E., Itten, K. I. and Allgöwer, B., 2006. Estimation LAI and fractional cover from small footprint airborne laser scanning data based on gap fraction. *Remote Sensing of Environment*, 104, 50-61.
- Myneni, R., Nemani, R. and Running, S., 1997. Estimation of global leaf area index and absorbed par using radiative transfer models. *IEEE Transactions on Geoscience and Remote Sensing*, 35, 1380-1393.
- Pocewicz, A. L., Gessler, P. and Robinson A. P., 2004, The relationship between effective palnt area index and Landsat spectral response across elevation, solar insolation, and spatial scales in a northern Idaho forest. *Canadian Journal of Forest Research*, 34, 465-480.
- Riaño, D., Valladares, F., Condés, S. and Chuvieco, E., 2004, Estimation of leaf area index and covered ground from airborne laser scanner (Lidar) in two contrasting forests. *Agricultural and Forest Meteorology*, 124, 269-257.
- Schulze, E. D., Beck, E., Müller-Hohenstein, K., Lawlor, D., 2005. Plant ecology, Springer (eds), Berlin.
- Watson, D. J., 1947. Comparative physiological studies in the growth of field crops. I. Variation in net assimilation rate and leaf area between species and varieties, and within and between years. *Annals of botany*, 11, 41-76.

Comparing discrete echoes counts and intensity sums from ALS for estimating forest LAI and gap fraction

Svein Solberg

Norwegian Forest and Landscape Institute, 1431 Ås, Norway
svein.solberg@skogoglandskap.no

Abstract

Effective leaf area index (*LAI*) of a forest is mathematically related to gap fraction, and may be estimated from the penetration rate of airborne laser scanning (ALS). The aim of this study was to compare the usefulness of four alternative ALS penetration rates for this purpose, and in particular to determine if any of them could produce un-biased estimates of gap fraction. This would be valuable in forests having a large fraction of small gaps. A 21 km² pine forest was covered with ALS, and ground measurements of gap fraction and *LAI* were done with LICOR's LAI-2000 at 20 plots within the area. The alternative penetration rate methods utilizes intensity data and multiple echoes. All alternatives were strongly related to gap fraction and *LAI*. However, none of the alternatives provided un-biased gap fraction estimates. The simple method of first echo counting, after being categorized as canopy and gap echoes, turned out to have the smallest deviation from gap fraction, with a slight underestimation. The methods of summing up intensities and counting of multiple echoes overestimated gap fraction, however, they were still strongly related to gap fraction and *LAI*, and may serve as supplementary methods in dense canopies with many small gaps, due to their higher sensitivity to small gaps.

Keywords: laser scanning, ALS, LIDAR, gap fraction, LAI

1. Introduction

ALS is intuitively, with its high number of evenly distributed pulses, a perfect tool for sampling based estimation of an area property such as gap fraction or canopy cover, where the return of each pulse is classified as either canopy or gap. Canopy cover may further be converted into *LAI* by inverting the gap fraction and log-transformation based on Beer-Lambert law (Chen et al. 1997). It has been demonstrated that such log-transformed, inverted gap fraction data from ALS are very strongly and linearly related to *LAI* from ground based measurements with R² values around 0.90 and higher (Solberg et al. 2005, Solberg et al. 2006). We may, however, cast a critical view on this apparently promising method: *LAI* in those studies were derived from the gap fraction as sampled from the first echoes of the laser beams, and it is a general concern that these first echoes underestimate gap fraction because the footprint size of the beam is too large to penetrate down small gaps (Lovett et al. 2003; Morsdorf et al. 2006). Hence, the method will apparently only work in forests where gaps smaller than the footprint size are infrequent, or eventually that they make up some constant fraction of the total gap fraction.

The ALS data have, however, another and less used attribute that may be useful here: the intensity. Lovett et al. (2003) have presented the idea of estimating gap fraction by summing up intensity data. The intensity of an echo depends on the size of the hit object and its reflectivity. If the reflectivity were fairly constant and similar for canopy and ground, then the intensity will represent mainly the size of the hit object. A large object would produce a compact return pulse and a high intensity value, and vice versa. Thus, we might derive unbiased estimates of canopy cover and gap fraction by replacing the simple counting of echo categories by summing up their intensities. Small canopy objects will be given less weight compared to large objects, and in this way correspond to the fraction of cover within the footprint. Hence, although it may be

correct that an entire laser beam can not penetrate down small gaps, the gap fraction might still be correctly recorded as a reduced intensity of an echo. Another option is also available: It seems likely that one would get higher penetration rates, eventually producing un-biased gap fraction estimates, by including the intermediate and last echoes of the pulses. These echoes represent the deeper penetration of the laser beam into the canopy.

The aim of this study was to compare the usefulness of four alternative ALS methods for mapping of gap fraction and LAI, and in particular to test a hypothesis that we can derive unbiased estimates of gap fraction from ALS data by using intensity data and eventually all echo categories.

2. Method

2.1 Study area and data sets

The data for this study is taken from a laser scanning campaign in 2005, which is a large and homogeneous data set, with three replicated sets of measurements and ALS acquisitions during the summer. The study area, data set and results are described in full detail by Solberg et al. (2006), and is briefly outlined here. The aim of that campaign was to map the defoliation caused by insect attack on the trees. ALS data together with ground based measurements of *LAI* were gathered. The study area was a 21 km² large area along a river and a relatively flat, sandy valley area along it. The area was dominated by Scots pine.

ALS data were gathered on May 10th, August 1st, and September 1st, with two pulses per m², and a maximum scan angle after pre-processing of $\pm 12^\circ$. The technical properties of the scans were as follows:

- Aircraft: Piper PA31-310
- Mean flight altitude: 650 m above ground
- Laser scanner: Optech ALTM 3100C
- Wavelength: 1064 nm
- Pulse repetition frequency: 100 kHz
- Pulse width: 16 ns
- Pulse energy: 66 μ J
- Peak power: 4.1 kW
- Mean footprint diameter at the ground: 17 cm

The discrete return pulses were categorized as ‘only’; ‘first of many’; ‘intermediate’; and ‘last of many’, and in the further data handling here the two former categories were grouped together and termed ‘first’ echoes. Each echo had the variables x , y , z , dz , *intensity* and *echo category*, where dz represents the height above ground and all these variables were provided by the ALS acquisition company.

Twenty field plots were laid out over the area as a stratified, systematic sampling with four age classes (ranging from newly regenerated to old stands) and five replicates of each. At each of the three points of time *LAI* was measured at each plot using LICOR’s LAI-2000 plant canopy analyzer at five points of each plot (centre and 3m away towards the cardinal directions), and these measurements were tripled making a total of 15 measurements at each plot and each point of time. The measurements were done 1m above ground. Reference measurements at nearby open fields were done simultaneously and every 15 second, and every plot measurement was joined with the reference station measurement being closest in time. The *LAI* value obtained from LAI-2000 represents the hemi-surface area of the foliage objects, which is half their total surface area.

2.2 Calculus and statistics

ALS penetration rates were calculated for four alternative approaches, which was combinations of either using first echoes or using all echoes; and secondly, either doing echo counting or intensity summing. First, the echoes were classified into *canopy* echoes if they had dz values above 1m above ground, and *ground* echoes if less than 1m. For the echo counting approach the following model was used:

$$P = N_g / (N_g + N_c) \quad , \quad (1)$$

where P is the penetration rate, N_g is the number of ground echoes, and N_c is the number of canopy echoes. This was done on ALS data for five circles of various size (5; 10; 15; 20; and 25m) around each plot. In the case of using intensities the following model was used:

$$P = \sum I_g / (\sum I_g + \sum I_c) \quad , \quad (2)$$

where I_g and I_c are the intensity of a ground echo and a canopy echo, respectively. The influence of reflectivity was not included in this equation, because data on reflectivity was not available. This implies that if this approach should turn out to be successful, it would mean that reflectivity was equal for all hit objects. It can also be noted that this ratio is not affected by the variation in the distance from the laser scanner within the scanned area.

The data from the LAI-2000 were first calculated into effective leaf area index, LAI using the following model provided by the producer:

$$LAI = 2 \sum w_i \ln(GF_i^{-1}) / d_i \quad , \quad (3)$$

where i is the ring number, GF_i is gap fraction seen in the zenith angle direction of ring i ; The terms w_i and d_i are ring specific factors provided by the hardware producer, representing the observed canopy volume, and the view path length, respectively, for that ring. A median LAI value was then calculated based on the replicate measurements done at each plot and each point of time. The median was used in order to exclude the influence from outlier results, which may be frequent in such data due to the sub-optimal weather conditions during measurements, such as direct sun light and partly clouded sky. LAI was calculated with two alternatives: using rings 1-4 only, and using all rings 1-5.

The data from the LAI-2000 were secondly calculated into foliage orientation, - in two alternative ways, - first by assuming a spherical foliage angle distribution corresponding to a mean tilt angle of 60° , and second by calculating the mean tilt angle (MTA) based on the LAI-2000 data. The projected fraction of the foliage area, $G(\theta)$ is equal to $\cos(MTA)$, and this is half the hemi-surface area for a spherical foliage angle distribution. MTA was calculated with the default method using the Fv2000 software which is shipped with the LAI-2000 hardware. As for LAI , MTA was calculated both for rings 1-4 and for all rings 1-5. It turned out that this produced a number of cases having the inappropriate MTA values 0 and 90° . In order to counteract these problems, each plot was provided with its median MTA value, being calculated across replicates and across repeated measurements during the season, however, where all values of 0 and 90° degrees were discarded from the median calculation.

Vertical gap fractions might be derived directly from the innermost ring, with its near-vertical view of $\pm 12^\circ$. This gap fraction, however, suffers from large random errors as a very tiny bit of

the canopy is seen with this ring, depending strongly on where the instrument is put, which could be under a tree or in a between-tree gap. The alternative and robust method applied here was to utilize the data from the other rings of LAI-2000. The random error is then considerably reduced as a much larger canopy volume is measured. Each ring has a gap fraction in its view direction, and these gap fractions were recalculated into one common, vertical gap fraction based on LAI and on foliage orientation:

$$LAI = \frac{1}{G(\theta)} \ln(GF^{-1}), \text{ and hence } GF = e^{-G(\theta) \cdot LAI} \quad (4)$$

After this preparation of ALS and LAI-2000 data, they were combined for modelling. A gap fraction corrective, c , was introduced for handling of systematic under- (or over-) estimation of gap fraction when using ALS penetration rate:

$$GF = P^c, \quad \ln GF = c \cdot \ln P \quad (5)$$

This model has two intuitively suitable properties. First, it is a relationship that meets the requirement that the ALS penetration rate and the gap fraction have to be equal in two cases; - when gap fraction is zero (a completely opaque canopy layer) and when it is one (a clear cut), while in-between here the relationship can be either linear or non-linear. Second, it works as a scaling factor in a model used for estimating LAI based on ALS penetration, and hence, allowing LAI to be strictly linearly related to $\ln(P^{-1})$ even if the gap fraction estimate is biased:

$$LAI = \frac{1}{G(\theta)} \ln(GF^{-1}) = \frac{c}{G(\theta)} \ln(P^{-1}), \quad (6)$$

where the ALS penetration rate is an unbiased estimate of gap fraction if $c=1$; it underestimates gap fraction if $c<1$; and vice versa.

In this study no-intercept regression models are widely used, and such models don't have a trivial definition for the coefficient of determination (R^2), and I used the following formula in accordance with recommendations from Kvålseth (1985).

$$R^2 = 1 - \frac{n}{n-p} \frac{\sum (y - \hat{y})^2}{\sum (y - \bar{y})^2}, \quad (7)$$

where n is the number of observations, p is the number of model parameters, \hat{y} is the model prediction for a given observation y , and \bar{y} is the mean of all observations y .

3. Result

For analyzing the relationships between ALS penetration rates and LAI-2000 gap fractions it turned out that the optimal selection of data (the strongest relationships) were obtained by using ALS data from within a 15m radius around the plot centre, and by excluding the outermost ring of LAI-2000. This is reasonable as the forest stands are fairly small and stand edges are likely to be seen by the outermost ring in many cases. Hence, the outermost ring does not contribute with valuable data, but rather produce noise only, and is hence excluded from estimation of both LAI and MTA .

All the alternative ALS penetration rates were strongly correlated to gap fraction, having R^2 values ranging from 0.71-0.94. However, none of the four methods produced unbiased estimates of gap fraction. Compared to the simple method of counting first echoes, all the three other methods produced higher penetration rates, as expected. Not only had these gap fraction estimates higher values, but they were biased the opposite way, - overestimating gap fractions. The results were fairly similar for the two alternatives for foliage orientation. Assuming a spherical foliage angle distribution was apparently quite right: The more detailed estimation of *MTA* indicated slightly more horizontally oriented foliage, however, the difference was minor, and also it introduced new random errors causing lower R^2 values.

The two alternative counting methods, i.e. using either first or all echoes, were equally good in terms of strength of relationship, and also they were equally much biased, although they were biased in opposite ways. As seen in Fig. 1 the penetration rates calculated this way were generally close to the gap fractions (circle symbols and solid fit lines, Fig. 1).

In addition to being weaker related to gap fraction, the intensity based approaches suffered in general from a poorer fit than the counting methods. Inspection of residual plots revealed a tendency of non-linearity. The intensity based penetration rates represented an overestimation of gap fraction, particularly at higher values (triangles, Fig. 1). In particular, summing up intensities for all echoes produced much higher values than the gap fractions.

Table 1: Results of no-intercept log-log models for LAI-2000 gap fractions against ALS penetration rates (Eq. 5). The estimated slope is an estimate of the gap fraction corrective, *c*. Results of the various alternatives for data selection and handling are presented (echo categories used; counts versus intensity sums; and foliage orientation assumed to follow a spherical foliage angle distribution or estimated mean tilt angle *MTA*)

| Echoes used | Method | Foliage orientation | <i>c</i> | R^2 | Residual check |
|-------------|----------------|---------------------|----------|-------|----------------|
| First | Echo counts | Spherical | .77 | .94 | Ok |
| --“-- | Intensity sums | --“-- | 1.17 | .86 | Curved |
| All | Echo counts | --“-- | 1.12 | .94 | Ok |
| --“-- | Intensity sums | --“-- | 1.45 | .87 | Curved |
| First | Echo counts | MTA | .81 | .83 | Ok |
| --“-- | Intensity sums | --“-- | 1.22 | .72 | Ok |
| All | Echo counts | --“-- | 1.18 | .81 | Ok |
| --“-- | Intensity sums | --“-- | 1.51 | .71 | Ok |

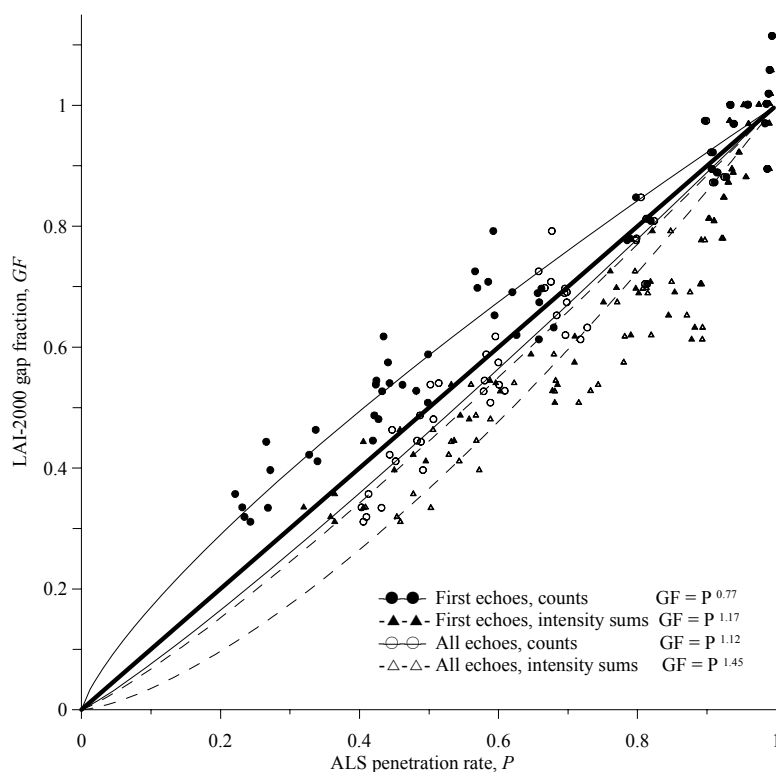


Figure 1: Gap fraction, GF , plotted against ALS penetration rates calculated in four alternative ways, based on rings 1-4 of LAI-2000 and assuming a spherical foliage angle distribution. The lines represent the fit functions (Table 1). A few GF values are above 1.0 which result from higher light intensities measured in a plot compared to the reference measurement in an open field nearby.

Two models of LAI as a function of ALS penetration rates (Eq. 6) are shown in Fig. 2, and is a reformulation of the results shown in table 1. The tendency of a non-linear relationship for the intensity-based method is shown in Fig. 2, right. At low LAI values, this method tend to underestimate LAI . In comparison, the echo counting method is straight linear.

LAI , as well as its changes from before to after insect defoliation, were now estimated based on each of the four alternative ALS penetration rates for the entire area with a 10x10m grid, producing a large data set of 139720 grid cells having four alternative LAI and LAI change values. The parameter estimates for the slopes in these LAI models were equal to $c/G(\theta)$. This corresponds to two times the c parameter estimate (Table 1), being 1.54; 2.34; 2.24; and 2.90, respectively for the four methods (counting first echoes, summing intensity of first echoes, counting all echoes, and summing intensities of all echoes). This is implicitly based on the assumption that foliage orientation is the same all over, which seems to be quite correct based on the results presented above (Table 1). All alternatives LAI variables were strongly correlated. However, again, the intensity based methods had a tendency of non-linearity, which tended to underestimate LAI at low LAI values and vice versa (Fig. 3, left), as shown above (Fig. 2, right). The two echo counting methods, however, were linearly related over the entire LAI range. All the LAI change variables were highly correlated, and despite its tendency of non-linearity, the intensity based method was the one being most strongly correlated to the LAI change based on echo counting ($R^2=0.93$, Fig. 3, right).

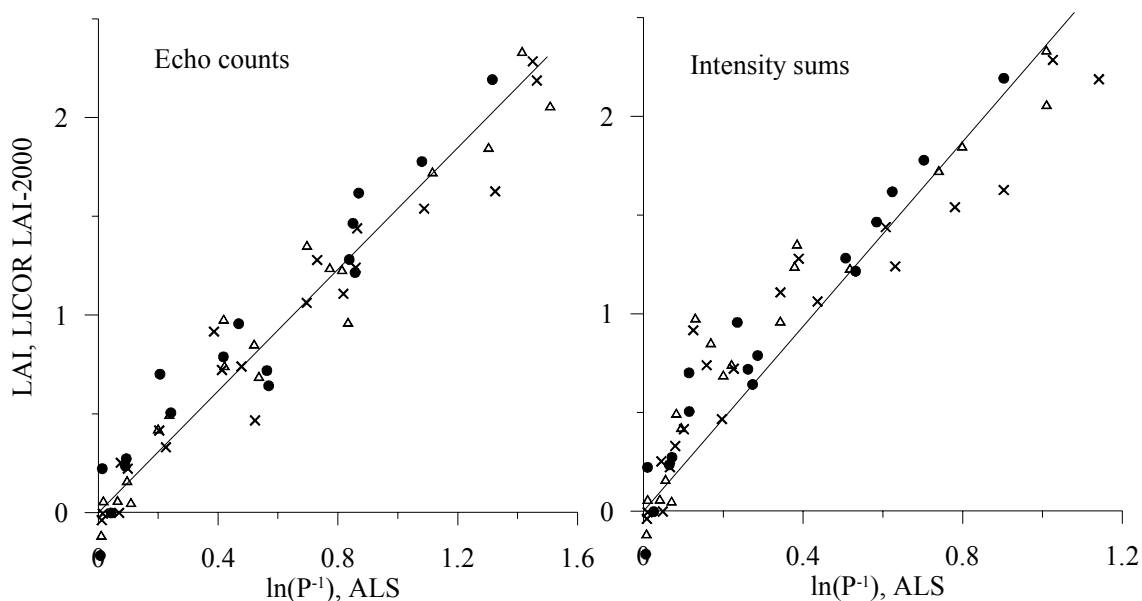


Figure 2: LAI from ground based measurements with LAI-2000 based on rings 1-4 plotted against log-transformed ALS penetration rate data (P^{-1}) from ALS data. The two alternative penetration rates are derived from using first echo counts (left) and first echo intensity sums (right). Data are from three repetitions in time: ● May; x August; and Δ September.

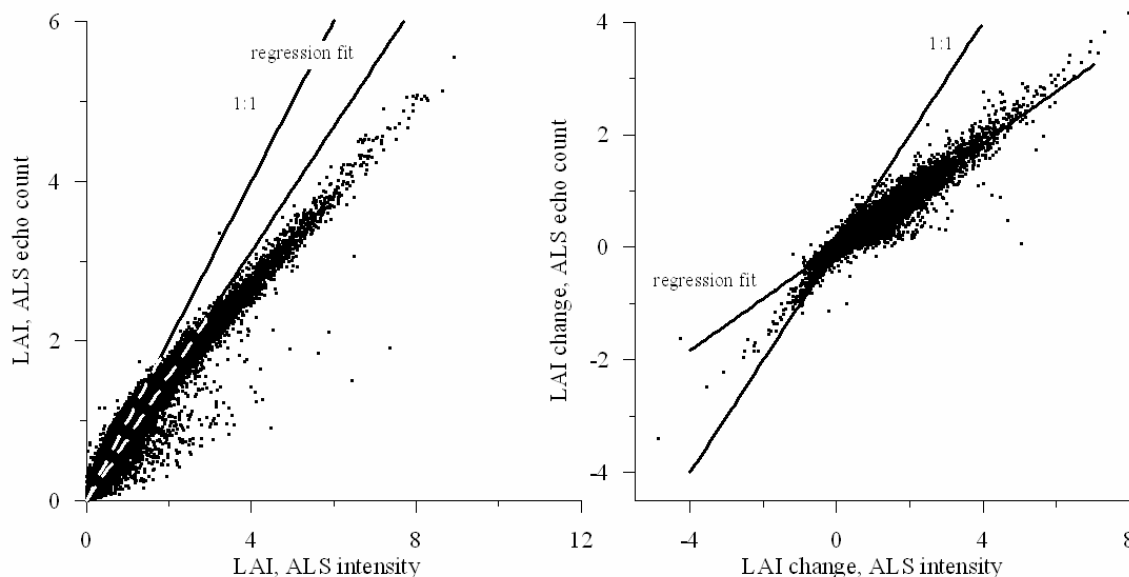


Figure 3: LAI, and its change during the summer, calculated for a 10x10m grid using the two ALS alternative methods echo counting and intensity summing. N=139720.

First echoes from the canopy had generally lower intensity than those from the ground, with mean values being 70 and 130, respectively. Defoliation caused both a higher fraction of echoes to penetrate the canopy layer and a reduced intensity of canopy echoes. The intensity of ground echoes was not affected.

4. Discussion

Using the standard method of counting first echoes was the most appropriate method in this data set. Compared to LAI-2000 measurements it underestimates gap fraction corresponding to a 20-30% underestimation of *LAI*. However; it is experienced in other studies that LAI-2000 normally underestimates *LAI* with some 15% because of light scattering in the canopy (Chen et al. 1997). It is likely that such a systematic error is present in this data set, since the LAI-2000 measurements often were carried out in sub-optimal weather conditions such as mid-day sunshine and partly cloudy. If we in the present data set adjust up the *LAI* data from LAI-2000 with 15%, then the method of counting first echoes would produce almost un-biased estimates of gap fraction. The parameter estimates of the gap fraction corrective, c , in Table 1 would then increase to 0.89 for a spherical foliage angle distribution, and to 0.93 if using the calculated mean tilt angles. For comparison, the other alternative penetration rates would then strongly overestimate gap fraction, with parameter estimates, c , ranging from 1.29 and upwards.

The results discussed above are not likely to depend much on footprint size and other acquisition settings. It is often claimed though, that the penetration of ALS downwards into the forest canopy depends on footprint size and pulse energy, and related factors such as flight altitude. However, a physical explanation for this is not evident and straight-forward: On one hand large footprints are intuitively less able to penetrate down small gaps as compared to small footprints. On the other hand, when large footprints hit the canopy they may be fragmented into a high number of non-detectable echoes, having their first detectable echo located deep down in the canopy, causing an apparent deeper canopy penetration. A careful review of a number of studies addressing the influence of footprint size and other ALS acquisition factors (Nilsson 1996; Lovell et al. 2003; Næsset 2004) suggests that when using first echoes (echo categories 'only' and 'first of many') the acquisition factors have generally minor influence on canopy penetration.

As expected, it is possible to estimate gap fraction and *LAI* from summing up echo intensities. The relationships with ground based measurements were strong, having R^2 values of 0.86-0.87. However, compared to the simpler method of counting echoes, it was a less appropriate method, having lower R^2 values; showing a non-linearity in the relationships; and having systematic overestimation of the gap fraction. This overestimation becomes particularly large if we assume that LAI-2000 overestimates *LAI*. This overestimation may have two causes: The intensity is likely corresponding to the size of the hit object, i.e. the uppermost canopy objects the laser beam hits. The fraction of the footprint that is continuing downwards through the canopy is then handled as if it continued all the way down to the ground, representing gaps. However, the photons may well hit canopy objects further down. The interpretation is visualized in Fig. 4. If using the echo counting method, an echo is weighed as if the laser beam hit an opaque object covering the entire footprint, which obviously represents an underestimation of the gap fraction within that footprint. And if using the intensity summing method, the echo is given a weight corresponding to the size of the uppermost hit branch, which represents an overestimation of the gap fraction. A second problem with the intensity based method is that the reflectivity may indeed be variable, and hence, the results obtained here may only be valid for this type of forest, - pine trees growing on soils covered mostly by reindeer lichens. Pine trees are found to have a particularly low canopy reflectance as compared to many other foliage objects because of multiple scattering within the shoots (Smolander and Stenberg, 2003). Laboratory experiments have demonstrated that the backscatter from the reindeer lichens *Cladina* and *Cladonia* with the NIR wavelength used in ALS is very high, eventually being exceptionally intense when the lichens have complex branching structures (Kaasalainen and Rautiainen, 2005).

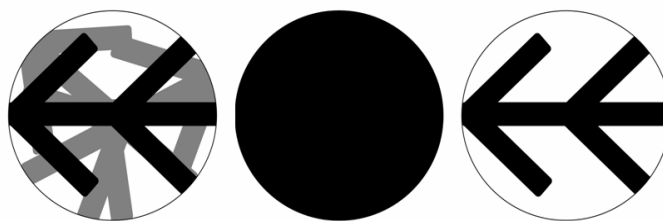


Figure 4: An imagined case where a circular laser beam footprint hits a canopy (black = uppermost canopy object, grey=canopy objects lower down and white=gap (left); discrete echo counted as a full reflection (black circle) causing underestimation of gap size (centre); and echo intensity corresponding to the size of the uppermost canopy object (black) causing overestimation of gap size as objects deeper down are taken as gap.

Using echo counting and including all echo categories (i.e. including intermediate and last echoes) produced close to un-biased estimates of gap fraction, and had as strong relationships to ground based measurements as using first echoes only. As an estimate of gap fraction it was biased, i.e. overestimating gap fraction. However, even if it could not produce un-biased estimates of gap fraction, it represents a valuable method alternative to be used in very dense canopies. *LAI* estimation based on first echoes may easily get saturated in ALS scans having few pulses per square meter and if one wants to map *LAI* with a high spatial resolution. The saturation problem here refers to cases when there are no ground echoes, and then *LAI* can not be estimated. By including the intermediate and last echoes the saturation problem will be much reduced. However, the usefulness of this approach may be limited by the minimum time distance needed to separate two echoes: If the canopy layer has a low surface height, there might not be enough time to separate multiple echoes. And there may be hardware-specific differences in this minimum time distance, which would cause inconsistencies in multi-temporal ALS data sets from different producers.

Finally, the methods based on intensity sums and counting of all echoes may be useful for forest health monitoring in forests having small gaps, due to their higher sensitivity to small gaps, and as they were strongly correlated to the other *LAI* change variables.

4. Conclusion

The aim of this study was to compare four alternative ALS penetration rates for estimation of gap fraction and *LAI*. None of the alternatives produced unbiased estimates of gap fraction. The best result was obtained by estimating gap fraction as the fraction of the first echoes that were classified as ground echoes. This produced slightly underestimated gap fraction values, however, they were strongly correlated to the ground measured gap fractions. The methods of summing up intensities and counting of multiple echoes overestimated gap fraction, however, they were still strongly related to gap fraction and *LAI*, and may serve as supplementary methods in dense canopies with many small gaps, due to their higher sensitivity to small gaps.

Acknowledgements

The Norwegian research council, together with the fund Skogtiltaksfondet and the Ministry of Agriculture and Food, are acknowledged for funding the REMFOR project, in which this study is carried out.

References

- Chen, J. M., Rich, P.M., Gower, S.T., Norman, J.M. and Plummer, S., 1997. Leaf area index of boreal forests: Theory, techniques, and measurements. *Journal of Geophysical Research*, 102(D24), 29429–29444.
- Kaasalainen, S. and Rautiainen, M., 2005. Hot spot reflectance signatures of common boreal lichens. *Journal of Geophysical Research-Atmospheres*, 110 (D20), D20102.
- Kvålseth, T.O., 1985. Cautionary note about R^2 . *The American Statistician*, 39/4: 279-285.
- Lovell, J.L., Jupp, D.L.B., Culvenor, D.S. and Coops, N.C., 2003. Using airborne and ground-based ranging LiDAR to measure forest canopy structure in Australian forests. *Canadian Journal of Remote Sensing*, 29: 607-622.
- Morsdorf, F., Kotz, B., Meier, E., Itten, K.I. and Allgower, B., 2006. Estimation of LAI and fractional cover from small footprint airborne laser scanning data based on gap fraction. *Remote Sensing of Environment*, 104(1):50-61.
- Næsset, E., 2004. Effects of different flying altitudes on biophysical stand properties estimated from canopy height and density measured with a small-footprint airborne scanning laser. *Remote Sensing of Environment*. 91, 243-255.
- Nilsson, M., 1996. Estimation of tree heights and stand volume using an airborne lidar system. *Remote Sensing of Environment* 56, 1–7.
- Smolander S. and Stenberg, P., 2003. A method to account for shoot scale clumping in coniferous canopy reflectance models. *Remote Sensing of Environment*, 88(4), 363-373.
- Solberg, S., Næsset, E., Aurdal, L., Lange, H., Bollandsås, O.M. and Solberg, R., 2005. Remote sensing of foliar mass and chlorophyll as indicators of forest health: preliminary results from a project in Norway. *Proceedings of ForestSat 2005* (H. Olsson, editor), 31 May – 3 June 2005, Borås, Sweden (Report 8a of the National Board of Forestry, Sweden), pp. 105-109.
- Solberg, S., Næsset, E., Hanssen, K.H. and Christiansen, E., 2006. Mapping defoliation during a severe insect attack on Scots pine using airborne laser scanning. *Remote Sensing of Environment*, 102, 364-376.

Modelling multi-spectral LIDAR vegetation backscatter – assessing structural and physiological information content

Felix Morsdorf¹, Caroline Nichol¹, Timothy J. Malthus¹, Genevieve Patenaude¹ & Iain H. Woodhouse¹

¹School of Geosciences, University of Edinburgh, Edinburgh EH8 9XP, Scotland, UK
felix.morsdorf@ed.ac.uk

Abstract

The concept for a new multi-spectral canopy LIDAR (MSCL) instrument was tested by simulating return waveforms using models providing tree structure (TREEGROW) and leaf reflectance (PROSPECT). The proposed instrument will take measurements at four different wavelengths, which were chosen according to physiological processes altering leaf reflectance. The modelling was used to assess both the structural and physiological information content such a device could provide, especially if the normally structure-dominated return waveform would pick up small changes in reflectance at the leaf level. Multi-spectral waveforms were simulated for models of single Scots pine trees of different ages and at different stages of the growing season. It was shown that the LIDAR waveforms would not only capture the tree height information, but as would also pick up the seasonal and vertical variation of NDVI computed from two of the four MSCL wavelengths inside the tree canopy. It could be demonstrated that a new multi-wavelength LIDAR predictor variable could significantly improve the retrieval accuracy of photosynthetically active biomass opposed to using a single wavelength LIDAR alone. It remains unclear, however, if these findings would persist for forest stands; thus such experiments simulating more complex scenarios will be the next task in this modelling framework.

Keywords: LIDAR, full-waveform, modelling, multi-spectral, NDVI

1. Introduction

Understanding the dynamics of the global carbon cycle is one of the most crucial scientific and societal problems of the 21st century. A key part of this understanding is being able to measure and monitor (a) the magnitude of terrestrial carbon sinks, by mapping their horizontal and vertical structure, (b) rapid as well as long term change resulting from natural and human-induced disturbances (e.g. deforestation, fire, desertification) and (c) the subsequent recovery processes. Laser remote sensing has been widely used to infer estimates of vegetation structure and biomass (Lim and Treitz, 2004, Hyyppä et al., 2001, Patenaude et al., 2004), at various scales ranging from single-tree level (Morsdorf et al., 2004) to landscape-level depending on the application and/or LIDAR system used. For example, the LIDAR waveforms obtained by the spaceborne GLAS instrument have been successfully exploited for estimations of above ground biomass (Rosette et al., 2008). On the other hand, passive multi- and/or hyperspectral earth observations (EO) systems have been used to provide estimates of the physiological state of vegetation, including the discrimination of healthy versus stressed canopies (Nichol et al., 2000 and 2002, Malthus and Karpouzli, 2003). The combination of both approaches into an active multi-spectral LIDAR should join the capabilities of LIDAR and passive multi-spectral EO, while remedying some of their shortcomings when used on their own (Koetz et al., 2007), such as the dependency on solar illumination when using passive instruments. The aim of this modelling study is to show some of the potential advantages of a multi-spectral LIDAR for both the estimation of vegetation structure and physiology state and to

feed back some insights into the constraints for the technical specifications of a prototype instrument. This will be achieved by combining a tree structural model, a leaf optical properties model and a model of the LIDAR measurement process together with auxiliary data about the typical physiological change occurring during a growing season. Our aim is to show that the MSCL would pick up both the structural and physiological change while adding explanatory value as opposed to using a single-wavelength LIDAR.

2. Methods

The modelling approach used to simulate LIDAR return waveforms in this study consists of three different models, one each for the leaf optical properties, the tree structure and the LIDAR measurement process. These different components and their inputs and outputs are described in the next three sections, followed by a description of the sensitivity experiment setup.

2.1 Leaf Optical Model

A widely used model of leaf optical properties (PROSPECT, Jacquemoud and Baret, 1990), was utilized to compute reflectance and transmission values of leaf tissue at the proposed MSCL wavelengths. PROSPECT was not explicitly designed to model needle reflectance, as it constructs the leaf from a number of parallel plates to resemble broadleaf structure. However, as was shown by Moorthy et al. (2008), inversion performance of leaf biochemical properties were just as good, if not better, using PROSPECT than the LIBERTY model (Dawson et al., 1998), which was specifically designed to model needles. PROSPECT has four main input parameters, which are leaf water and chlorophyll content, a leaf structure parameter (number of plates) and dry matter content. As we were interested in modelling the capability of detecting changes in NDVI during a growing season, we varied the chlorophyll concentrations for first and second year needles according to values measured by Moorthy et al. (2008), which are presented in Table 1. They measured the chlorophyll concentration in first and second year pine needles over four months. Chlorophyll concentration changes are quite large for first year needles and increase strictly monotonically. For second year needles, however, the increase over time is much smaller, with even a decrease from July to August. For each month, different chlorophyll values were used, leaving all other input parameters constant. Leaf water content would be expected to vary as well during a growing season, but would not affect the MSCL wavelengths, hence it was not considered here.

Table 1: Chlorophyll concentrations used for modelling pine needle reflectance as measured and published by Moorthy et al. (2008).

| Measured Chlorophyll $\mu\text{g}/\text{cm}^2$ | First year needles | Second year needles |
|---|--------------------|---------------------|
| June | 16.67 | 37.5 |
| July | 22.90 | 43.8 |
| August | 24.52 | 40.5 |
| September | 29.28 | 42.2 |

The gained reflectance and transmittance values (see Figure 1) were then assigned to cylinders in the TREGROW output representing shoots. For bark and twigs, the same measured spectra of pine trees were used, as in the study of Koetz et al. (2004).

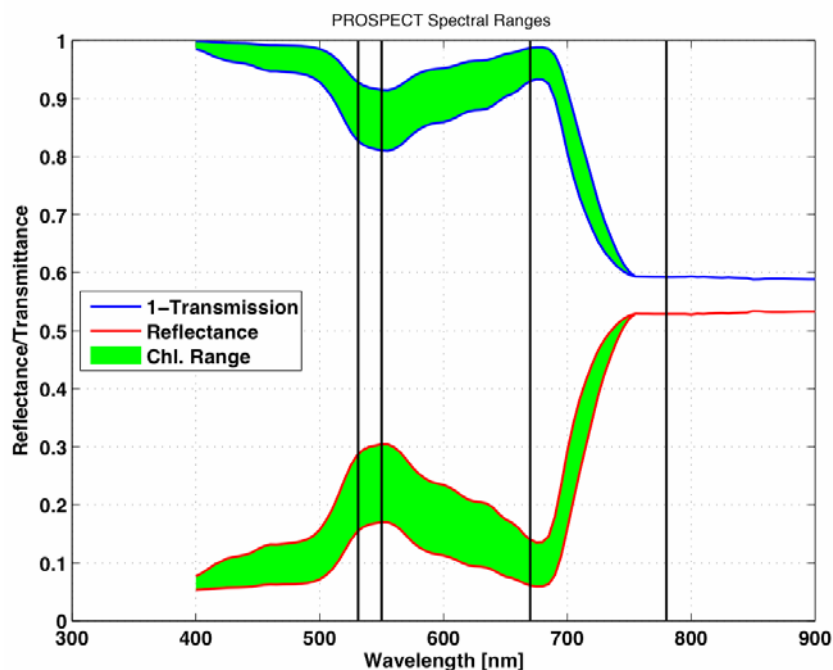


Figure1: Spectral response of leaf reflectance and transmittance as modelled by PROSPECT. The filled green areas denote the range of values spanned by the chlorophyll concentrations presented in Table 1. The vertical black lines represent the proposed MSCL wavelengths.

2.2 Tree Structural Model

We used the TREEGROW model (Leersnijder, 1992) to produce ecologically sound representations of Scots pine trees at different ages. The model has been parameterized to simulate both Scots pine and Norway spruce trees found on a test site in Sweden (see Woodhouse and Hoekmann (2000) for details). It was used previously by Woodhouse and Hoekman, (2000) and Disney et al., (2006) to model radar backscatter and passive hyperspectral signatures, respectively.

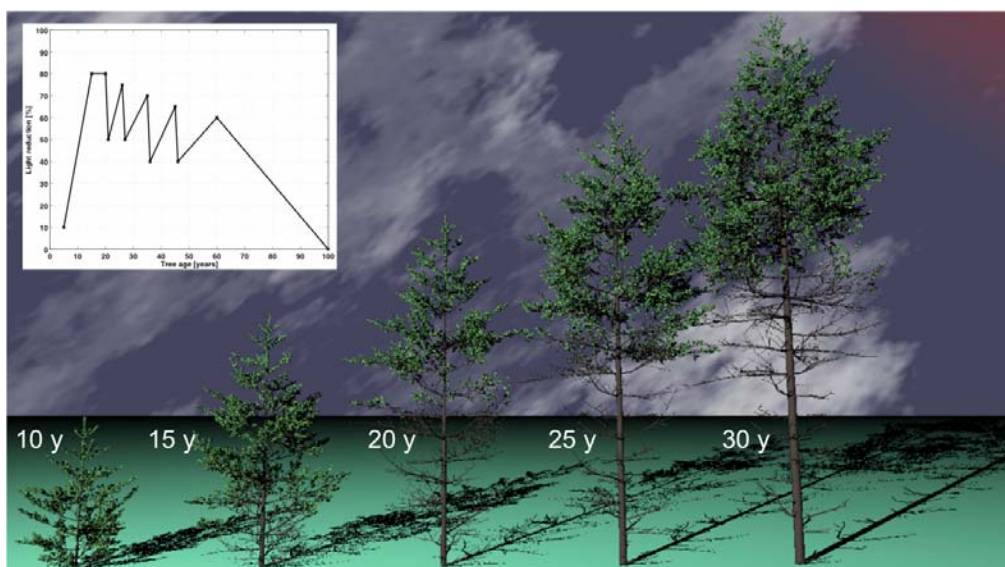


Figure 2: RGB composite rendering of the same modeled Scots pine at 5 different ages. The default TREEGROW light versus age curve (top left) was used to account for self-pruning and thinning.

The model output consists of cylinders of different sizes representing branches and shoots, with the age of each branch being stored by the model. These ages are later used to assess the development stage of each cylinder and assign reflectance values of either needles or bark to the cylinders. The cylinders representing the shoots are constructed using a semi-transparent texture in the POV-Ray scene files, in order to account for shoots not being opaque (see Figure 2). A more sophisticated implementation of shoot scattering (such as described by Disney et al. (2006) or Smolander and Stenberg, (2003)) is currently in development. The default light versus age curve was used to establish thinning and pruning in the model trees, as if they would have grown in a managed forest stand, since in a later modelling stage these trees would be used to construct stand-sized forest patches.

2.3 LIDAR Measurement Model

The approach to model LIDAR returns used in this study was previously developed and published by Morsdorf et al. (2007). It builds upon the open-source ray-tracing program POV-Ray, whose scene and light descriptions could be adapted to represent the LIDAR measurement process. It incorporates reflectance and transmission, and could potentially account for multiple scattering, however in the way that the model is implemented now, it only allows for single scattering. The POV-Ray scene description enables the user to construct scene with arbitrary complex geometry, as such it was quite straightforward to convert the TREEGROW output into POV-Ray readable files. Light distribution can be explicitly modelled across beam and thus can be set up to match those of existing LIDAR instruments. POV-Ray is being used to model both a depth and an intensity image from the perspective of the emitter/receiver optics; these two images are then combined to form an approximate cross-section profile assuming the single canopy elements act as Lambertian scatterers. Following that, this cross-section is convoluted with a laser pulse of specific length and shape, again according to the specification of the prototype instrument. An illustration of the modelling process can be found in Figure 3 and the model development and validation is described in more detail in Morsdorf et al. (2007).

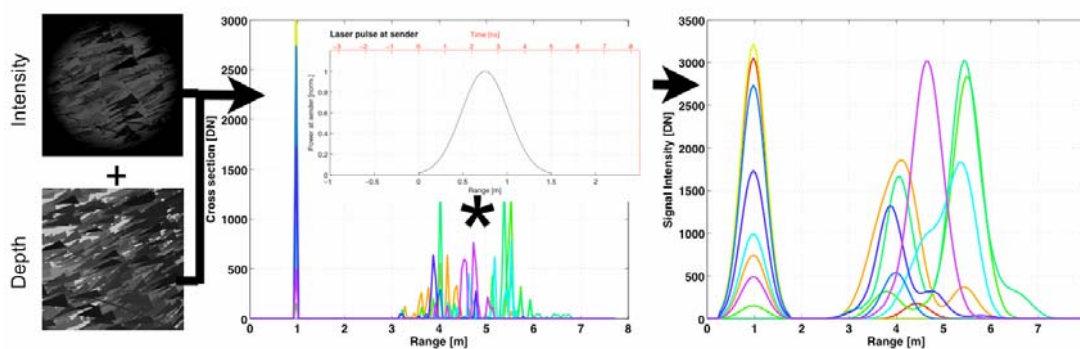


Figure 3: Illustration of waveform generation process based on intensity and depth image (left). The cross-sections (middle, at bottom) derived from these images is convoluted with a Gaussian shaped laser pulse of 5 ns length (middle, at top) to obtain the modeled LIDAR return waveforms (right).

2.4 Sensitivity study – structure and physiology

TREEGROW was used to grow the same Scots pine tree from year one to year 50, with the data being exported to a POV-Ray scene file every five years. Trees aged from 10 to 50 years were used, and tree heights obtained reached from 2.5 to just over 18 meters. For each of the tree ages, four different trees had shoot reflectance assigned with reflectances based on the chlorophyll

concentration for June, July, August and September. Note that first and second year needles would get different reflectance values based on their different chlorophyll concentrations. Thus, if the ratio of first to second year needles changes during maturing of the tree, it is expected to show in the modelled waveforms.

The LIDAR model was set up in a way that a single tree would be situated on a flat, horizontally levelled, spectrally homogenous plane with a spectral response of an Ericaceae understory (see Koetz et al., 2004 for details). The simulated LIDAR instrument illuminated the tree from directly above, being placed at a height of 500 m. To ensure that the total energy available to scene would not change, the beam size was fixed for all trees at different ages (and thus sizes) by making sure that the tallest tree was fitting the illuminated area. The LIDAR pulse shape was set to be of Gaussian shape and the pulse length was set to 4.75 ns (~ 1.43 m) full width at half maximum (FWHM), resembling the pulse length of the prototype instrument. For each of the four LIDAR wavelengths (531, 550, 670 and 780 nm) to be modelled, a separate (greyscale) POV-Ray scene file had to be produced, since POV-Ray only allows for one transmittance value in its RGB colour model.

3. Results and Discussion

In Figure 4, three return waveforms for 30, 40 and 50 year old trees are plotted side by side with a “real” canopy volume computed from the model tree. It was possible to differentiate between photosynthetically active canopy volume (shoots) and woody material volume (twigs, branches) in the tree model. Canopy volume was chosen as a proxy for biomass, as its computation from the model trees is straightforward and correlation with biomass should be strong and linear. The modelled waveforms exhibit the same vertical structure for all four wavelengths, but have different amplitudes. For this reason (and to save space) we present only the 780 nm waveform in Figure 4. From those waveforms, the most striking effect is the amount of smoothing due to the rather long laser pulse of 1.43 meters at FWHM; all vertical features in the canopy volume profile smaller than this distance are smoothed out. A deconvolution of the return waveform with the original laser pulse could help to reveal these features again, but for this step the original laser pulse shape needs to be known. A second feature of the return waveform is an apparent increase in tree height as well due to the convolution with the laser pulse, which makes the trees appear about 0.75-1 meter taller in the return waveform. A regression (not shown here) of LIDAR derived heights with the real heights of the model trees resulted in an R^2 of 0.99, with a mean overestimation of model tree height by LIDAR by about 0.7 m, which is an effect of the convolution with the laser pulse. As with the smoothing effect before, a remedy to this with a real LIDAR system would be to know the length and the shape of the transmitted pulse and do a deconvolution. This is the reason why this information is generally provided to the user in the two commercially available single wavelength, full-waveform systems from Optech and Riegl.

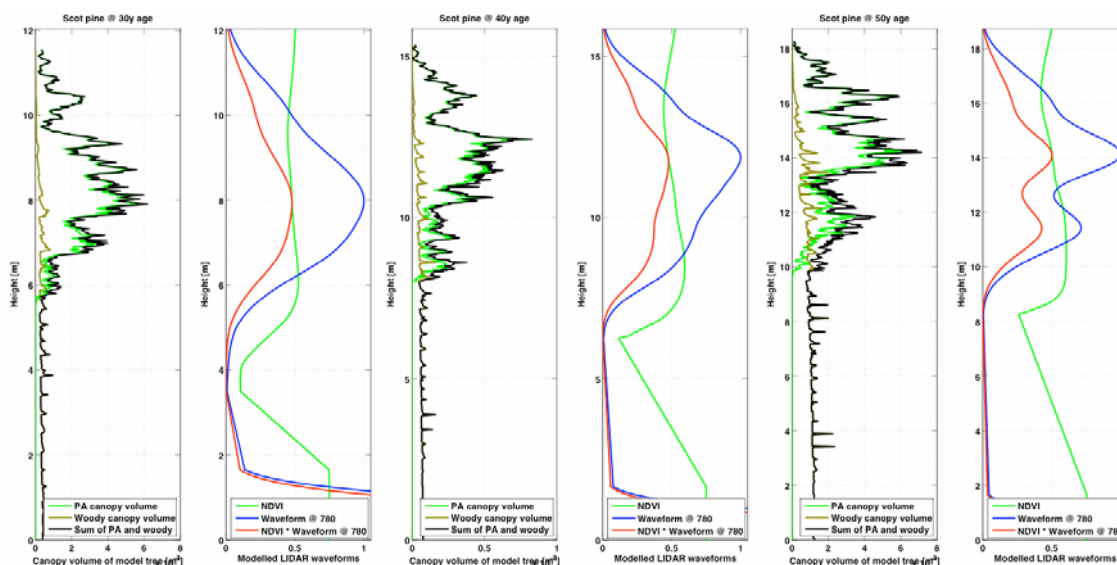


Figure 4: Canopy volume profiles and simulated LIDAR waveforms for trees of 30,40 and 50 years of age. Right panels show both photosynthetic active (PA) and woody volume components, while left panels show backscatter at 780 nm (blue), the NDVI (see Equation 1) profile (green) and a resulting waveform (red) from the multiplication of the two.

So the height information can be very well retrieved from the modelled waveforms, which is not surprising, since LIDAR remote sensing is a more or less direct measurement of canopy height. But we were also interested in assessing the physiological information content of a multiple wavelength LIDAR system. To do so, a representative measure has to be derived from the waveforms; just visually comparing the waveforms at different wavelengths would not reveal a vertical signal in the physiology. Since two of the modelled bands are enclosing the red edge (the sharp increase of reflectance/transmittance between 670 and 780 nm, see Figure 1), we are capable of computing a NDVI profile for the modelled trees according to the equation below:

$$NDVI = \frac{R_{780} - R_{670}}{R_{780} + R_{670}} \quad (1)$$

This spectral band ratio is depicted as a green line in the right panels of Figure 4.

We were interested in quantifying the seasonal variation in this NDVI profile, which should be induced by the gain in chlorophyll concentration. In Figure 5, the vertical profiles of NDVI are depicted for selected trees; the profiles are computed for the crown extension only. Vertical extent of the tree crown was inferred manually for each tree and height thresholds for distinguishing crown material/backscatter from non-crown parts were established. NDVI increases towards the end of growing season, reaching its maximum in September. A vertical variation of NDVI is visible as well and could be explained by either the light versus age curve used to alter the ratio of “green” and “brown” canopy elements or by the ratio of first to second year needles varying vertically inside the canopy, or a combination of the two. The increase in NDVI during the growing season is largest towards the top of the tree, which is explained by the top having a larger fraction of first year needles showing a much larger variation of chlorophyll concentrations from June to September as opposed to second year needles (Table 1). However, the seasonal signal of NDVI was smaller than the vertical variation inside the tree crown.

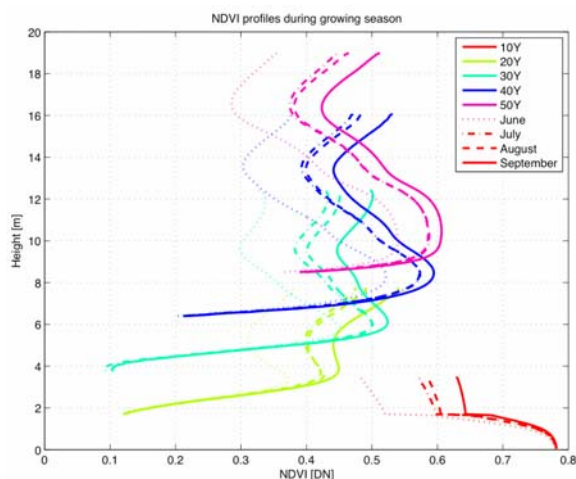


Figure 5: NDVI profiles during a growing season for model trees of different ages. Colours denote ages, line styles denote month. NDVI varies vertically and is largest towards the end of the growing season, when needles have their maximum chlorophyll concentration.

One of the main benefits for a multi-spectral LIDAR would be to more accurately provide estimates of the photosynthetic active (or “green”) biomass, and thus providing a better estimate of gross primary productivity (GPP). It is well known that LIDAR instruments can provide good estimates of the vertical canopy profile, but it has not been shown in previous studies that they are able to discriminate woody and leafy canopy material, even though backscatter at 1064 nm would be of different intensity for those two vegetation components, at least in terrestrial laser scanning. However, the cumbersome calibration of airborne intensity data in vegetation and the spectrally and structural inhomogeneous canopy as illuminated by the laser footprint has yet prevented the exploitation of this information.

We computed the total canopy volume for each tree crown and correlated those with the LIDAR backscatter from the tree crown. The LIDAR backscatter was processed in two different ways, first just by summing up the backscattered energy at 780 nm (not affected by changes in chlorophyll concentration) and then by multiplying the backscatter at this wavelength with the NDVI profile to possibly retrieve a backscatter value adopted to the ratio of “green” to “brown” canopy elements. In Figure 6, these two LIDAR backscatter indicators computed for each of the nine trees are plotted over photosynthetic active canopy volume.

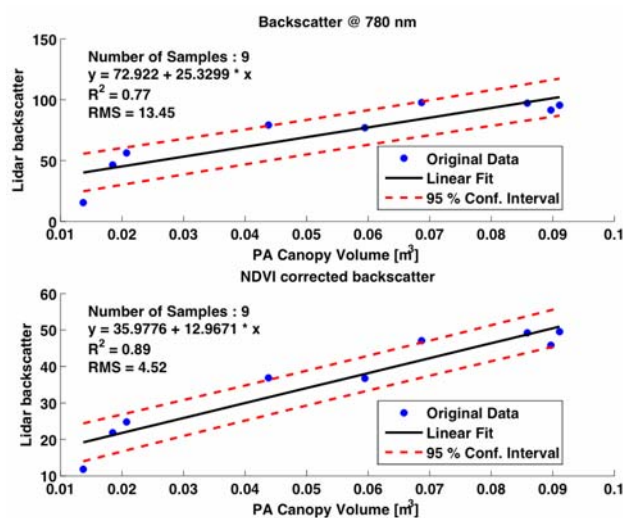


Figure 6: LIDAR backscattered energy of the tree crown versus photosynthetic active canopy volume. Using just a single, unmodified waveform (780 nm, top) will yield lower r-square than using a NDVI corrected waveform (bottom).

Using only the backscatter at 780 nm as a predictor variable, 77 % of the photosynthetic active canopy volume variation can be explained. Using the NDVI-corrected backscatter, this value increased to 89 % explained variance, revealing a potential benefit of using multiple wavelengths for estimation of photosynthetic active vegetation elements.

4. Conclusions and Outlook

The scope of this work was to illustrate the potential advantage(s) and data products of a multi-spectral canopy LIDAR (MSCL) in a modelling study. Using a tree structural model and a model of leaf optical properties, we were able to simulate multi-spectral return waveforms for Scots pine trees of different ages (thus heights) and different physiological states during a growing season. It was possible to pick up both the signal of tree growth (height evolution) and the change in chlorophyll content over a growing season by computing NDVI profiles of the trees. NDVI would vary vertically inside the tree crown to a larger extent than its seasonal cycle, with the largest seasonal variations being in the top part of the tree. The first year needles, that are abundant at the top of the tree, can explain this, since they show a much stronger seasonal variation of chlorophyll content. A new multi-spectral LIDAR predictor variable for photosynthetic active canopy elements was defined by multiplying the NDVI profile and the backscatter profile at the reference wavelength of 780 nm. This predictor variable explained a larger percentage of photosynthetic active canopy volume variation than a single wavelength alone was able to. However, it remains unclear whether this finding will persist as well in modelled forest stands, as opposed to modelled measurements of single isolated trees as done in this study. The modelling work presented in this paper is just the first of a whole set of modelling experiments undermining the concept of a multi-spectral LIDAR instrument. Further tests are going to be carried out with simulated stands constructed of TREEGROW trees of different ages, including a spectrally different understory layer and topographic undulations. Ultimately, these experiments will help explaining variations in waveforms as captured by a prototype instrument and lead to undermining the potential of future spaceborne missions with multi-spectral canopy LIDAR instruments.

References

- Dawson, T. P., Curran, P. J. and Plummer, S. E., 1998. LIBERTY--Modeling the Effects of Leaf Biochemical Concentration on Reflectance Spectra. *Remote Sensing of Environment*, 65, 50-60.
- Disney, M., Lewis, P. & Saich, P., 2006. 3D modelling of forest canopy structure for remote sensing simulations in the optical and microwave domains *Remote Sensing of Environment*, 100, 114-132.
- Hyypä, J., Kelle, O., Lehtikoinen, M. and Inkinen, M., 2001. A segmentation-based method to retrieve stem volume estimates from 3-d tree height models produced by laser scanners. *IEEE Transactions on Geoscience and Remote Sensing*, 39, 969-975.
- Jacquemoud, S. and Baret, F., 1990. PROSPECT: A model of leaf optical properties spectra *Remote Sensing of Environment*, 34, 75-91.
- Koetz, B., Schaepman, M., Morsdorf, F., Itten, K. and Allgöwer, B., 2004. Radiative Transfer Modeling within a Heterogeneous Canopy for Estimation of Forest Fire Fuel Properties *Remote Sensing of Environment*, 2004, 92, 332-344.
- Koetz, B., Sun, G., Morsdorf, F., Ranson, K., Kneubuhler, M., Itten, K. and Allgöwer, B., 2007. Fusion of imaging spectrometer and LIDAR data over combined radiative transfer models for forest canopy characterization. *Remote Sensing of Environment*, 106, 449-459.
- Leersnijder, R.P., 1992. PINOGRAM: a pine growth area model. Wageningen Agricultural University, The Netherlands.
- Lim, K. and Treitz, P., 2004. Estimation of aboveground forest biomass using airborne scanning discrete return LIDAR in Douglas-fir. In: M. Theis, B. Koch, H. Spiecker, H. Weinacker (Eds.). *Proceedings of ISPRS working group VIII/2 "Laser-Scanners for Forest and Landscape Assessment"*. Freiburg, University of Freiburg: 149-152.
- Malthus, T.J. and Karpouzli, E. (2003). Integrating field and high spatial resolution satellite based methods for monitoring shallow submersed aquatic habitats in the Sound of Eriskay, Scotland, UK. *Int. Jour. of Remote Sensing*, 24(13):2585-2593.
- Moorthy, I., Miller, J. R. and Noland, T. L., 2008. Estimating chlorophyll concentration in conifer needles with hyperspectral data: An assessment at the needle and canopy level *Remote Sensing of Environment*, , In Press, Corrected Proof.
- Morsdorf, F., Meier, E., Kötz, B., Itten, K. I., Dobbertin, M. and Allgöwer, B., 2004. LIDAR-based geometric reconstruction of boreal type forest stands at single tree level for forest and wildland fire management *Remote Sensing of Environment*, 3, 353-362.
- Morsdorf, F., Frey, O., Koetz, B. and Meier, E., 2007. Ray Tracing for Modeling of Small Footprint Airborne Laser Scanning Returns, *International Archives of Photogrammetry and Remote Sensing Volume XXXVI*, Part 3 / W52, 294-299.
- Nichol, C. J., Grace J. et al. (2000). Remote sensing of photosynthetic light use efficiency of boreal forest. *Agricultural and Forest Meteorology* 101 : 131-142.
- Nichol C. J., Grace J. et al. (2002). Remote sensing of photosynthetic light use efficiency of a Siberian boreal forest. *Tellus* 54B: 677-687.
- Patenaude, G., Milne, R. H. R., Gaveau, D., Briggs, B. & Dawson, T., 2004. Quantifying forest above ground carbon content using LiDAR remote sensing. *Remote Sensing of Environment*, 93, 368-380.
- Rosette, J., North, P. and Suarez, J., 2008. Vegetation height estimates for a mixed temperate forest using satellite laser altimetry. *International Journal of Remote Sensing*, 29, 1475-1494.
- Smolander, S. and Stenberg, P., 2003. A method to account for shoot scale clumping in coniferous canopy reflectance models. *Remote Sensing of Environment*, 88, 363-373.
- Woodhouse, I.H. and Hoekman, D.H., 2000. Radar modelling of coniferous forest using a tree growth model. *International Journal of Remote Sensing*, 21,8,1725-1737.

Diameter distribution modelling using ALS

Johannes Breidenbach¹, Christian Gläser² & Matthias Schmidt³

¹Forstliche Versuchs- und Forschungsanstalt Baden-Württemberg, Abteilung Biometrie und Informatik, Johannes.Breidenbach@forst.bwl.de

²Georg-August-Universität Göttingen, Institut für Statistik und Ökonometrie, Christian_Glaeser@gmx.de

³Nordwestdeutsche Forstliche Versuchsanstalt, Abteilung Waldwachstum, Matthias.Schmidt@nw-fva.de

Abstract

The Weibull distribution is one of the most frequently used functions in forestry to fit diameter or height distributions. However, estimating the location parameter of the Weibull distribution frequently causes numerical problems because it is highly correlated with the scale and shape parameters. The location parameter is therefore usually fixed to a certain value. We propose to use the reversed generalized extreme value distribution (RGE) to overcome this limitation. The RGE is a reparametrization of the Weibull distribution that allows estimation of the location parameter. We apply the RGE in the context of a generalized linear model (GLM). In the GLM, the tree diameter is assumed to be the RGE distributed response. It is estimated using area-based methods (vegetation height metrics). While visual comparison reveals a good conformity of the RGE with observed diameter distributions, the smallest diameter (location parameter) is in tendency underestimated by the RGE. For the distribution means, the RMSE is 2.12 cm with a bias of 0.29 cm.

Keywords: reversed generalized extreme value distribution, Weibull distribution, GAMLSS, lidar

1. Introduction

Several studies proved that small footprint airborne laser scanner data (ALS) can be used for estimating forest parameters either using single tree detection algorithms (e.g., Persson et al. 2002, Peuhkurinen et al. 2007) or area-based (also referred to as *plot-wise*) approaches (e.g., Nilsson 1996, Magnussen & Boudewyn 1998, Næsset 2002). Due to their robustness, the latter are used in Scandinavia on operational scales since several years (Næsset 2004). Area based approaches usually provide plot level estimates such as total volume, basal area or mean height. However, for predicting timber assortments, the diameter distribution of a forest stand is needed as an important parameter.

Generally, non-parametric (e.g., Maltamo & Kangas 1998) and parametric (e.g., Hafley & Schreuder 1977) methods can be used to model diameter distributions. Aim of parametric methods is to estimate the parameters of a distribution function. Due to the possibility of using biological interpretable parameters, parametric methods enjoy a high popularity. The Weibull distribution is an often-used function to model diameter distributions (e.g., Bailey & Dell 1973, Nagel & Biging 1995, Cao 2004). Several authors also used ALS to estimate the parameters of Weibull distributions (e.g., Gobakken & Næsset 2004, Mehtätalo et al. 2007).

In managed forests, it frequently occurs that the smallest diameter on sample plots with large trees is larger than zero or the smallest measured tree (calliper limit). However, while the

Weibull distribution has a location parameter, its estimation causes numerical instability since the scale and the shape parameter are highly correlated with it. The location parameter is therefore usually fixed to a certain value (e.g., Breidenbach et al. 2008, Gobakken & Næsset 2004, Cao 2004). The probability of the occurrence (density) of small trees will then be overestimated.

In this paper we describe the use of the generalized extreme value distribution (Johnson et al. 1995), which is provided by (Rigby & Stasinopoulos 2005) as the reversed generalized extreme value distribution (RGE). It is a reparametrization of the three-parameter Weibull distribution and can be used to estimate also the location parameter. We applied a generalized linear model (GLM, Nelder & Wedderburn 1972) with the diameter as the RGE distributed response. The parameters of the RGE distribution are estimated using plot-wise vegetation height metrics derived from small footprint, low density ALS data. Due to the plot design, a combination of several truncated RGE distributions was used.

2. Material and Methods

2.1 Study area

The tree species composition of the 50 km² study site is a managed forest, dominated by Norway spruce (*Picea abies* L. Karst.) with a 70% proportion by area, beech (*Fagus sylvatica* L.) with 11% and silver fir (*Abies alba* Mill.) with 10%. More details on the forest structure are given in Table 1.

Table 1: Forest characteristics of the study site

| | Minimum | Median | Mean | Maximum |
|--|---------|--------|-------|---------|
| Stem number [ha ⁻¹] | 22.1 | 397.8 | 497.3 | 2829 |
| Stem volume [m ³ ha ⁻¹] | 7.2 | 412.7 | 413.2 | 1193 |
| Basal area [m ² ha ⁻¹] | 1.8 | 36.8 | 36.8 | 81.9 |
| Basal area mean diameter [cm] | 7.5 | 35 | 35.8 | 68.8 |
| Mean height [m] | 5.1 | 25 | 24.6 | 40.7 |

2.1.1 Plot establishment

In 2002, a permanent sample-plot inventory was carried out on a 100 m (easting) by 200 m (northing) grid. Trees with a diameter at breast height (dbh) of at least 7 cm were measured on concentric sample plots with a maximum diameter of 12 m. To increase the efficiency of the inventory, trees with a dbh <30 cm were sampled on plots with smaller radii. This results in four possible plot sizes of 2, 3, 6 and 12 m, where trees with a minimum dbh of 7, 10, 15 and 30 cm are measured.

2.1.2 Laser data

The laser scan data were collected with an Optech ALTM 1225 laser scanner in winter 2003/2004, i.e. about one year after the inventory took place. A flight altitude of approx. 900 m above ground yielded an average distance of 1 m between scan points on the ground. The first as well as the last pulse data were automatically classified by the data provider into vegetation- and ground points (reflection from terrain surface).

A digital terrain model (DTM) with one meter pixel spacing was computed from the ground returns using the average height of returns if several reflections were located within one pixel

and bilinear interpolation if no return was within the pixel. The value of the respective DTM pixel was subtracted from the first pulse vegetation raw data to obtain vegetation heights. Vegetation height metrics (e.g., percentiles and mean) were derived for every sample plot (Næsset 2002).

2.2 Parameter estimation

The reversed generalized extreme value distribution (RGE) is obtained from the generalized extreme value distribution (Johnson et al. 1995, p.76) by replacing y with $-y$ and ξ by $-\xi$ (Rigby & Stasinopoulos 2005). It has the density

$$f(y | \xi, \theta, \gamma) = \frac{1}{\theta} \left\{ 1 + \gamma \left(\frac{y - \xi}{\theta} \right) \right\}^{\frac{1}{\gamma-1}} \cdot S(y | \xi, \theta, \gamma) \quad (1)$$

defined for $\xi - \frac{\theta}{\gamma} < y < \infty$

where the equation $S(y | \xi, \theta, \gamma)$ is given by

$$\exp \left(- \left\{ 1 + \gamma \left(\frac{y - \xi}{\theta} \right) \right\}^{\frac{1}{\gamma}} \right)$$

which is defined for $-\infty < \xi < y + \frac{\theta}{\gamma}$, $\theta, \gamma > 0$.

If a is the location, b the scale and c the shape parameter, the density of the Weibull distribution is denoted

$$f(y | a, b, c) = \frac{c}{b} \left(\frac{y - a}{b} \right)^{c-1} \exp \left[- \left(\frac{y - a}{b} \right)^c \right] \quad (2)$$

for $b, c > 0$.

The RGE is a reparametrization of the Weibull distribution in that

$$a = \xi - \frac{\theta}{\gamma}, \quad b = \frac{\theta}{\gamma} \quad \text{and} \quad c = \frac{1}{\gamma}.$$

The parameters of the RGE distribution were estimated using plot-wise derived vegetation height metrics from ALS raw data. The equation $f(y | \xi, \theta, \gamma)$ was therefore extended to $f(y_i | \xi_i, \theta_i, \gamma_i)$.

Due to the concentric sample plot design, we constructed four censored RGE distributions for every possible plot radii by

$$g_R(y_i | \xi_i, \theta_i, \gamma_i) = \frac{f(y_i | \xi_i, \theta_i, \gamma_i)}{\int_L^U f(x | \xi_i, \theta_i, \gamma_i) dx} \quad (3)$$

where U and L are the upper and lower bounds of the diameters for the concentric sample plot

with radius R , respectively. This resulted in the functions g_2, g_3, g_6, g_{12} .

The likelihood function for the parameter estimation is therefore

$$L = \sum_{i=1}^n \ln (g_2(y_i | \xi_i, \theta_i, \gamma_i) 1_2(y_i) + g_3(y_i | \xi_i, \theta_i, \gamma_i) 1_3(y_i) + g_6(y_i | \xi_i, \theta_i, \gamma_i) 1_6(y_i) + g_{12}(y_i | \xi_i, \theta_i, \gamma_i) 1_{12}(y_i)) \quad (4)$$

with $1_U(y_i)$ as size-class dependent indicator functions. If $U \in \mathfrak{R}$ then

$$1_U(y_i) = \begin{cases} 1 & y_i \in U \\ 0 & y_i \notin U \end{cases} \quad (5)$$

The parameters are bound to the predictor variables with link functions h :

$$\xi_i = h_1^{-1}(x'_{(\xi),i} \beta_{(\xi)}) \quad \theta_i = h_1^{-1}(x'_{(\theta),i} \beta_{(\theta)}) \quad \gamma_i = h_1^{-1}(x'_{(\gamma),i} \beta_{(\gamma)}).$$

where x are the predictor variables, β are the coefficients. The identity is the link function for ξ and the natural logarithm is the link function for θ as well as γ .

The likelihood function was maximized using the Nelder-Mead algorithm implemented in the function *optim* (Venables & Ripley 2002), within an *R* environment (R Development Core Team 2007)

On average, 12 trees were measured on a sample plot. The predicted distribution can therefore not be compared with observations from one sample plot. Therefore, the observations from plots similar with respect to the explanatory variables are aggregated to what we will call *vegetation height quartile classes* for the remainder of the text. Then, the predicted RGE distribution can be compared with the histogram of the observations.

3. Results

The first and third quartile (Qu1 and Qu3) of the vegetation height were selected as predictor variables for all parameters. Their interaction term (Qu1 * Qu3) was considered as predictor variable for the ξ and θ parameters.

The parameters of the RGE distribution can be predicted by

$$\begin{aligned} \xi_i &= 4.15 + -1.20 \text{ Qu1}_i + 1.93 \text{ Qu3}_i + 0.02 \text{ Qu1}_i \text{ Qu3}_i \\ \theta_i &= 0.97 + -0.03 \text{ Qu1}_i + 0.11 \text{ Qu3}_i + -0.001 \text{ Qu1}_i \text{ Qu3}_i \\ \gamma_i &= -0.31 + 0.03 \text{ Qu1}_i + -0.05 \text{ Qu3}_i \end{aligned} \quad (6)$$

Compared with a Weibull distribution (location parameter fixed at the calliper limit) directly fitted to the observations, the RGE distribution matches well to the observed diameter distributions (Figure). The smallest estimated diameter of the RGE distribution is usually above the calliper limit and especially for plots with large trees, larger than for the Weibull distribution. However, compared with the actual observations, the size of the smallest diameter is still underestimated (Figure).

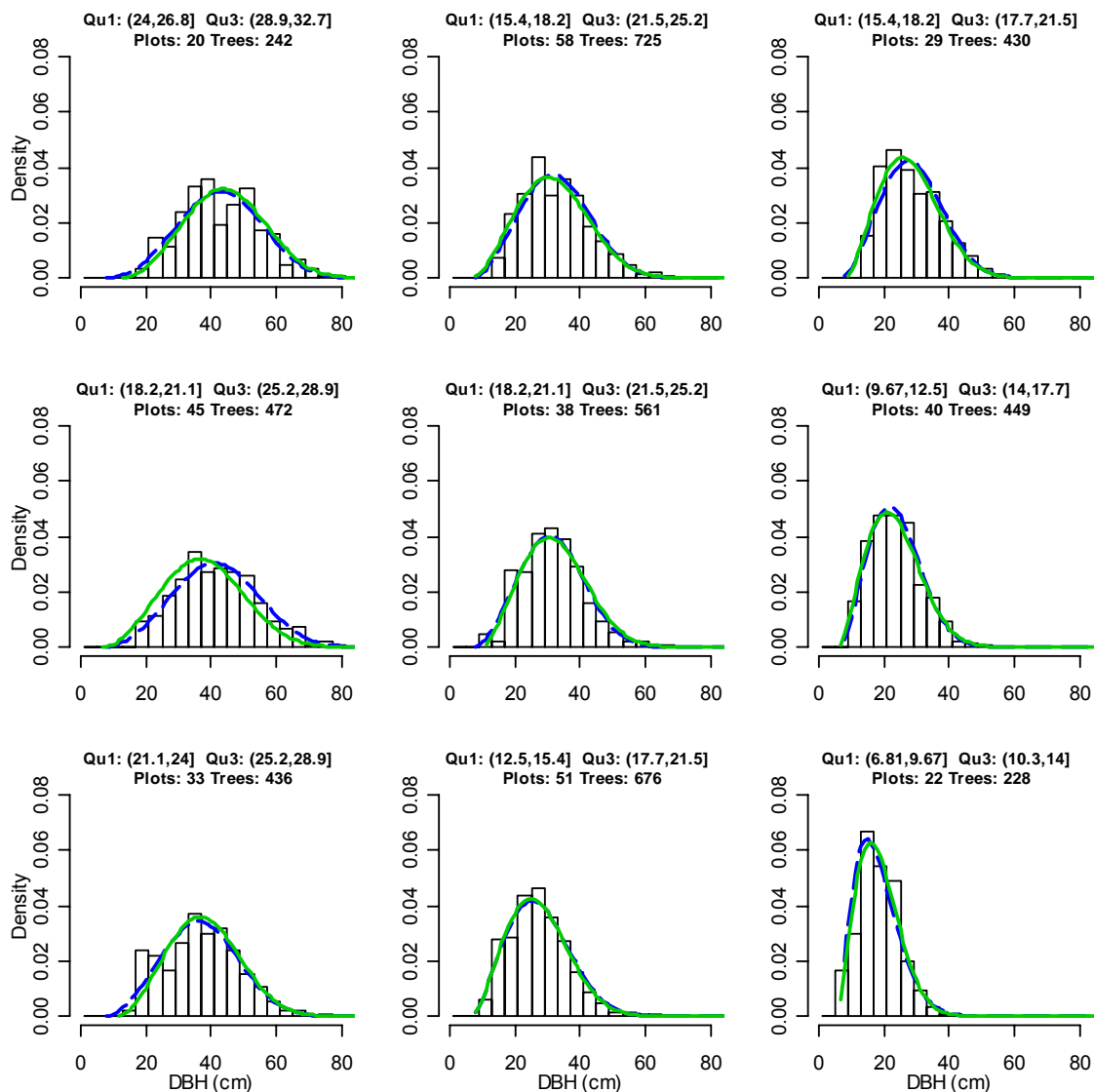


Figure 1: Probability density distribution of observed DBH (histogram) and predicted RGE distributions (solid graph) for the 9 most densely populated laser-derived vegetation height quartile classes. The dashed curve marks the Weibull distribution which has been directly fitted to the observations. Qu1 denotes the class width of the first quartile (m) and Qu3 the class width of the third quartile (m). Plots and trees represent the number of sample plots and trees in the corresponding plot strata.

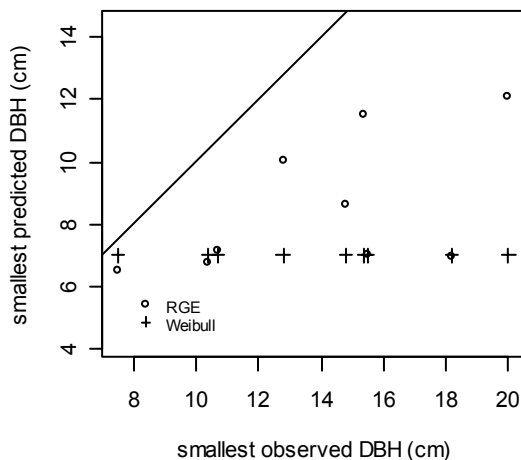


Figure 2: Smallest predicted DBH using the RGE and Weibull distribution and smallest observed DBH (solid line = 1:1 line).

The means of the RGE and the observed distribution was computed for the 20 most densely populated quartile classes (containing at least 3 Plots). As the good conformity of the predicted distribution with the observed distribution supposes, the difference between the mean of the RGE distribution and the mean of the observations is rather small (Figure 3). The RMSE is 2.12 cm with a bias of 0.29 cm.

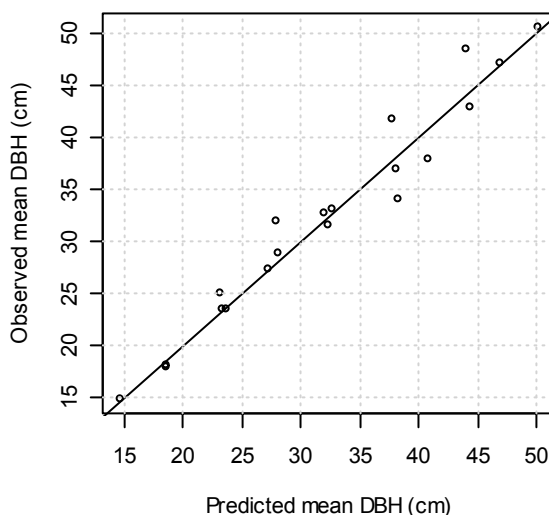


Figure 3: Observed versus predicted mean DBH for the 20 most densely populated quartile classes (circles) and 1:1 line (solid line).

4. Discussion

Numerical problems may occur while estimating the location parameter of the Weibull distribution (e.g., Gobakken & Næsset 2004) because the parameters are highly correlated. Therefore, the location parameter is usually fixed to zero or some other value (e.g., Cao 2004). The reversed generalized extreme value distribution (RGE), as described by Rigby &

Stasinopoulos (2005), is a reparametrization of the Weibull distribution. Since the location parameter of the Weibull distribution is obtained from a combination of the three parameters of the RGE distribution that are not strongly correlated, it can be estimated.

The proposed RGE distribution can be used to estimate diameter distributions. For the prediction of assortments, information about tree heights (for a solution see for example Mehtätalo et al. 2007) and tree species are also required. In this study, we assumed the observations to be independent of one another. Another topic of future research will be how spatial autocorrelation affects the statistical models. Standard errors of the coefficients will also need to be computed. To do so, derivations of the log-likelihood function can be used to compute the Fisher information matrix. The inversion of the Fisher information is the covariance matrix of the parameters.

The GLM used here is the state of the art method to fit conditional distributions. It allows the prediction of parameters, also if reference data stem from small sample plots. Consequently, potential multimodal distributions are not likely to occur since small patches of forest are relatively homogenous.

Acknowledgements

We like to thank Mikis Stasinopoulos and Bob Rigby, the developers of the generalized linear models for location, scale and shape (GAMLSS), for their help and the provision of the RGE distribution. We acknowledge the comments of two anonymous reviewers that helped to improve the quality of this paper.

References

- Bailey, R. and Dell, T., 1973. Quantifying diameter distributions with the Weibull function. *Forest Science*, 19, 97-104.
- Breidenbach, J., Gläser, C., Schmidt, M., 2008. Estimation of diameter distributions by means of airborne laser scanner data. *Canadian Journal of Forest Research*, 38(6), 1611-1620.
- Cao, Q., 2004. Predicting parameters of a Weibull function for modeling diameter distribution. *Forest Science*, 50, 682-685.
- Gobakken, T. and Næsset, E., 2004. Estimation of diameter and basal area distributions in coniferous forest by means of airborne laser scanner data. *Scandinavian Journal of Forest Research*, 19, 529-542.
- Hafley, W. and Schreuder, H., 1977. Statistical distributions for fitting diameter and height data in even-aged stands. *Canadian Journal of Forest Research, NRC Research Press*, 7, 481-487.
- Johnson, N., Kotz, S. and Balakrishnan, N., 1995. *Distributions in Statistics: Continuous Univariate Distributions*, Vol. 2. Wiley, New York.
- Magnussen, S. and Boudewyn, P., 1998. Derivations of stand heights from airborne laser scanner data with canopy-based quantile estimators. *Canadian Journal of Forest Research*, 28, 1016-1031.
- Maltamo, M. and Kangas, A., 1998. Methods based on k-nearest neighbor regression in the prediction of basal area diameter distribution. *Canadian Journal of Forest Research*, 28, 1107-1115.
- Mehtätalo, L., Maltamo, M. and Packalén, P., 2007. Recovering plot-specific diameter distribution and height-diameter curve using ALS based stand characteristics. In: P. Rönholm, P.; Hyypä, H. & Hyypä, J. (Eds.). *ISPRS Workshop on Laser Scanning 2007 and SilviLaser 2007*.
- Næsset, E., 2002. Data acquisition for forest planning using airborne scanning laser. *Forestsat Symposium 2002*.

- Næsset, E., 2004. Practical large-scale forest stand inventory using a small-footprint airborne scanning laser. *Scandinavian Journal of Forest Research*, 19, 164–179.
- Nagel, J. and Biging, G., 1995. Schätzung der Parameter der Weibullfunktion zur Genierung von Durchmesservertellungen. *Allgemeine Forst- und Jagdzeitung*, 166, 185-189.
- Nelder, J. and Wedderburn, R., 1972. Generalized Linear Models. *Journal of the Royal Statistical Society. Series A (General)*, JSTOR, 135, 370-384.
- Nilsson, M., 1996. Estimation of tree heights and stand volume using an airborne lidar system. *Remote Sensing of Environment*, 56, 1- 7.
- Persson, A., Holmgren, J. and Söderman, U., 2002. Detecting and measuring individual trees using an airborne laser scanner. *Photogrammetric Engineering and Remote Sensing*, 68, 925-932.
- Peuhkurinen, J., Maltamo, M., Malinen, J., Pitkänen, J. and Packalén, P., 2007. Preharvest Measurement of Marked Stands Using Airborne Laser Scanning. *Forest Science, Society of American Foresters*, 53, 653-661.
- Rigby, R. and Stasinopoulos, D., 2005. Generalized Additive Models for Location Scale and Shape. *Journal of the Royal Statistical Society: Series C (Applied Statistics)*, 54, 507-554.
- R Development Core Team. R., 2007. A Language and Environment for Statistical Computing. *R Foundation for Statistical Computing*.
- Venables, W. & Ripley, B., 2002. *Modern Applied Statistics with S*. Springer, New York.

A new automated approach for co-registration of national forest inventory and airborne laser scanning data

Wouter Dorigo¹, Markus Hollaus^{1,2}, Klemens Schadauer³ & Wolfgang Wagner^{1,2}

¹Institute of Photogrammetry and Remote Sensing, Vienna University of Technology, Gusshausstrasse 27-29, 1040 Vienna, Austria; email: wd@ipf.tuwien.ac.at

²Christian Doppler Laboratory for “Spatial Data from Laser Scanning and Remote Sensing” at the Institute of Photogrammetry and Remote Sensing, Vienna University of Technology, Gusshausstrasse 27-29, 1040 Vienna, Austria; email: mh@ipf.tuwien.ac.at; ww@ipf.tuwien.ac.at

³Department of Forest Inventory at the Federal Research and Training Centre for Forests, Natural Hazards and Landscape, Seckendorff-Gudent-Weg, 1130 Vienna, Austria; email: klemens.schadauer@bfw.gv.at

Abstract

Airborne laser scanning (ALS) data are often used for downscaling point based forest inventory (FI) measurements in order to obtain spatially distributed estimates of forest parameters. Such downscaling algorithms usually consist in a direct coupling between selected FI parameters and ALS data collected at the field sampling locations. Thus, adequate co-registration between FI and ALS data is an essential pre-processing step in order to get accurate predictive relationships. The current paper presents a new, automated co-registration approach which iteratively searches for the best match between an ALS based canopy height model and the tree positions and heights measured during the FI. While the basic principle of the algorithm applies to various types of FI sampling configurations, the co-registration approach has been specifically developed to take into account the tree selection criteria posed by angle count sampling. Several criteria are employed to detect possible ambiguous solutions and to reduce post-processing efforts by an image operator. Model validation was based on National Forest Inventory (NFI) and ALS data of the Austrian Vorarlberg province.

Results show that 67% of the sample plots could be accurately automatically co-registered (i.e. distance to reference data set < 4 m). All solutions with deviations from the reference data set > 4 m were correctly marked by the algorithm as being ambiguous. Applying the automatically co-registered sample plots in a growing stock model provided estimates that were clearly superior to those obtained with the original plot positions and even slightly outperformed those based on manual co-registration. As the developed algorithm will be part of an operational processing chain for Austrian NFI data, it has a high practical relevance.

Keywords: LiDAR, relative orientation, relascope, Austria, mountainous environment

1. Introduction

Forest inventories (FIs) are usually based on field measurements performed at selected sampling units. This way of sampling provides statistically derived measures of forest conditions which, depending on the sampling density, are representative for large to medium size administrative units such as countries or provinces. If information is required for smaller administrative units, like municipalities or forest stands, the available forest information has to be downscaled using additional, spatially distributed information sources such as multi-spectral satellite imagery (Koukal, 2004) or aerial photographs (Holmström *et al.*, 2001). In recent years, airborne laser

scanning (ALS) has proven a very promising alternative data basis for spatializing point based forest inventories (Maltamo et al., 2007). Its capability of accurately describing the horizontal and vertical distribution of canopy elements makes ALS well suited for the quantitative assessment of structural forest parameters such as tree density, tree height, and stem volume.

The downscaling procedure generally consists of two consecutive steps: i) establishment of a consistent relationship between selected forest inventory parameters and laser scanning data of the field measurement locations (e.g., by k-nearest neighbours or multiple regression), and ii) deploying the relationship thus obtained to the entire laser scanning data set in order to obtain the spatially distributed forest inventory. Establishing a predictive relationship between FI data and ALS relies on a direct coupling between canopy height information contained in the ALS data and the forest and tree attributes of the FI. Therefore, accurate spatial agreement is of vital importance for accurate calibration of the established relationships (Farid et al., 2006; Hollaus et al., 2007). Nevertheless, the coordinates of sampling locations and tree positions are often still measured with non-differential GPS units, leading to positioning errors up to several meters. This is particularly true in mountainous terrain where due to topography the number of visible satellites is significantly reduced compared to flat terrain. In contrast, ALS data typically have planimetric errors of less than 50 cm, making it very suitable as a geographic reference for the FI data. If tree positions and heights of the trees within the sampling units are known, a data analyst can adapt the positions of the FI data to the ALS data set by visual interpretation. This might, however, be a time-consuming and tedious task, especially if several thousands of sampling units have to be co-registered, such as in the case of national forest inventories.

To overcome this problem, the current paper presents a new, automated approach for the co-registration of FI and ALS data. While the basic principle of the approach applies to various types of FI sampling configurations the study will concentrate on data of the Austrian National Forest Inventory (NFI) which is based on angle count sampling (Bitterlich, 1948). Section 2 describes more in detail the characteristics of the NFI, even as the specifications of the used ALS data. The co-registration procedure is presented in Section 3, while its results are presented and discussed in Section 4. Conclusions and outlook are given Section 5.

2. Study site and data

2.1 Study area

The novel co-registration procedure was developed based on ALS and NFI data of the Vorarlberg province in Austria (Figure 1a). Elevation in the Vorarlberg province ranges from 396 m to 3,312 m asl. The landscape is mainly characterized by high alpine areas, coniferous and mixed forests, shrubs, meadows, and sparsely settled areas in the valley floors. The average timberline ranges between 1,700 and 2,000 m. According to the NFI 2000/2002³ Vorarlberg is covered with about 97,000 ha of forest, representing a forest cover fraction of 37.3%. The main tree species in Vorarlberg are spruce (*Picea abies*; 53.9% of the total area covered by forests), fir (*Abies alba*; 11.6%) and beech (*Fagus sylvatica*; 9.6%). 66.9% of the forested area can be classified as coniferous forest, 23.8% as deciduous forest, while the rest consists of open spaces, shrubs, and bare surfaces⁴.

2.2 Airborne laser scanning data

The ALS data were acquired within the framework of a commercial terrain mapping project covering the entire district of Vorarlberg. Since terrain mapping campaigns require snow-free

³ http://web.bfw.ac.at/i7/Oewi.oewi0002?geo=8&isopen=0&display_page=0

⁴ http://web.bfw.ac.at/i7/Oewi.oewi0002?geo=0&isopen=3&display_page=22

and leaf-off conditions, a prerequisite that is usually not simultaneously met for valley floors and high altitudes, the data were acquired during several flight-campaigns in the years 2002 to 2004. The data were acquired by the company TopScan GmbH, Germany deploying Airborne Laser Terrain Mapper systems (ALTM 1225, ALTM 2050) and the company Terra Digital GmbH, Germany which employed a Leica-Scanner ALS50. The flying heights of the ALS campaigns vary between ~500 and ~2,000 m above ground and minimum point density is 1 point/m². For this study, georeferenced 3D-point clouds and digital terrain (DTM) and surface models (DSM) with a resolution of 1 m were provided by the Land Survey Administration Feldkirch. Canopy height models (CHM) were calculated by subtracting the DTM from the DSM.

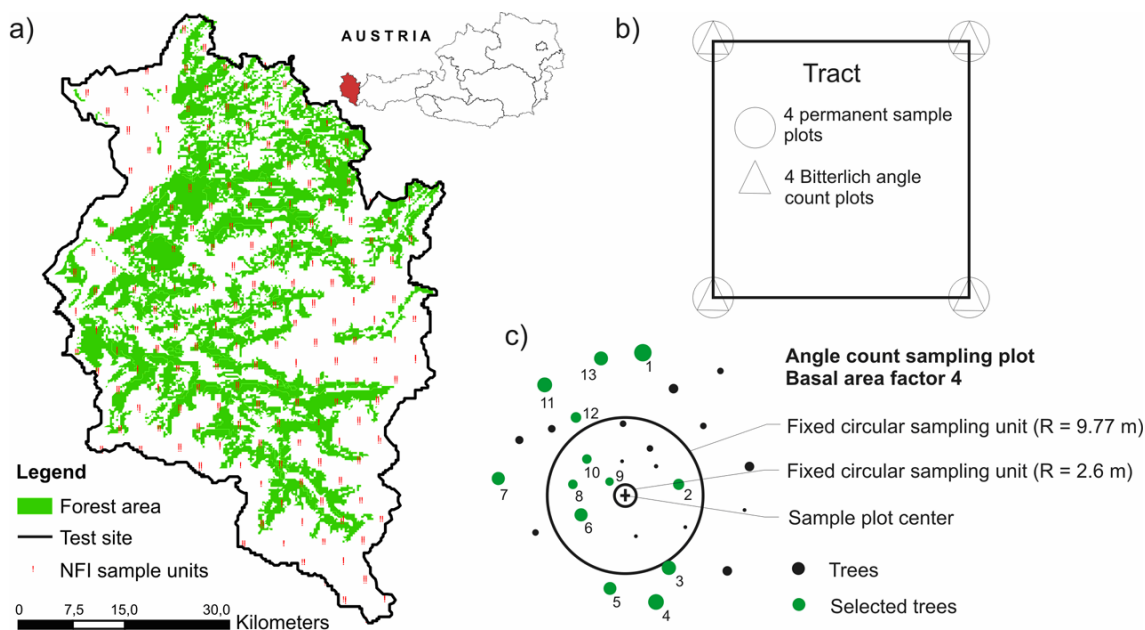


Figure 1: a) Location of Vorarlberg study site. Shown is the forested area overlain with the NFI sample units. b) Configuration of sampling units within a tract as employed at the Austrian NFI. c) Configuration of a sampling unit.

2.3 Forest inventory data

The development of the co-registration procedure was based on Austrian NFI data from the assessment period 2000/2002. The NFI is carried out in regular time intervals of six to eight years and comprises more than 170 attributes that provide information on quantity, quality and trends of the Austrian forests. The attributes relevant for this study are given in Table 1. The sampling design of the NFI is a permanent sampling grid pattern where tracts are regularly distributed (3.89 km grid size) over Austria. Each tract is made up of four sampling units spaced in a square at a distance of 200 m (Figure 1b). The single sampling units comprise a fixed large circular sampling area of 300 m² (R=9.77 m), a fixed small sampling area of 21 m² (R=2.60 m), and an angle count sampling plot (also called Bitterlich plot). While the fixed large circular plot is used to capture site specific properties, within the small sampling circle every tree with a diameter at breast height (DBH) between 50 and 105 mm is characterized. Within the angle count sampling the selection of trees is based on a relascope measurement of DBH and consequently the plot has a variable size. A basal area factor of 4 was employed. For a subset of the sample trees heights were measured with a VERTEX III⁵, while data models were used to estimate heights of the remaining sample trees (Gschwantner and Schadauer, 2004).

⁵ <http://www.haglofsweden.com/products/VertexIII/>

Within the forested area of Vorarlberg 132 sampling units are available (Figure 1). Since no reliable dGPS measurements were available to test the accuracy of the automated co-registration results, reference centre coordinates of each sample plot were determined by manually seeking the optimum fit between tree positions and heights measured by the NFI and the CHM. To do this, the absolute positions of the trees within each plot were calculated from the geographical coordinates of the sample plot centres and the polar coordinates of the individual trees. These coordinates were then converted into ArcGIS shapefiles which, in combination with the NFI heights of each tree, facilitated a visual comparison with the CHM and finally a manual adaptation (Figure 2). 98 of the 132 sampling units could be unambiguously co-registered in this way. The errors of the measured NFI centre coordinates thus established ranged between 0.00 and 54.00 m with an average of 8.50 m.

Table 1: Attributes of the Austrian NFI that are relevant for the presented co-registration procedure.

| Variable | Unit | Measurement principle |
|--|---|---|
| Center coordinates (X,Y) of individual sample plots | m (GK Austria meridian 28 coord. system) | Non-differential GPS. In case of bad receiving computed from GPS measurement in a nearby open space and eccentric compass |
| Polar Azimuth from plot centre | gon | ultrasonic range instrument |
| Distance from plot centre | cm | Calliper, Measuring tape |
| Diameter at breast height (DBH) | mm | Ultrasonic measurement with VERTEX III |
| Tree height | dm | Using key proposed by (Schieler and Hauk, 2001) |
| Tree type and tree class (indicating vitality, growth stage, and relationship with neighbouring trees) | - | |

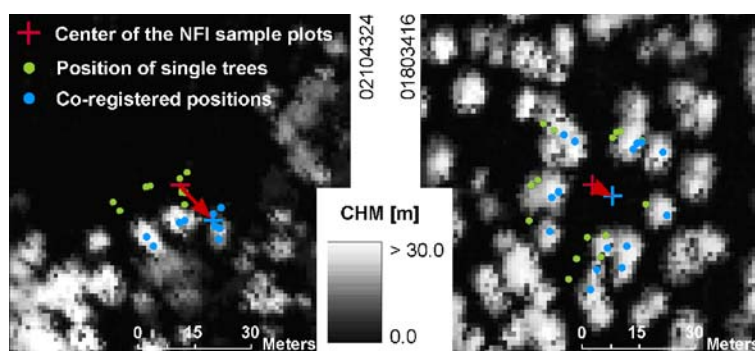


Figure 2: Relative orientation between tree positions, sample plot centre coordinates and the CHM for sample plots 02104324 and 01803416. The red vector indicates the manual shift applied to co-register NFI data to the CHM

3. Automated co-registration

3.1 Model description

An automated co-registration procedure was developed in order to overcome the manual adjustment step between NFI data and CHM described in the previous paragraph. The approach searches iteratively within a specified search window for the best fit between the tree heights measured during the NFI and the heights contained in the CHM (Figure 3-a). Thus, the height difference (D) for a given sample plot centre coordinate x,y within the search window can be given by:

$$D_{x,y} = \sum_{t=1}^N c_t \cdot |H_{NFI,t} - H_{CHM,t}| \quad (1)$$

where N is the number of trees measured in one NFI sample plot, $H_{NFI,t}$ is the height assessed

during the NFI for tree t , and $H_{CHM,t}$ is the value of the canopy model at the location of tree t . Tree class parameter c is introduced in the cost function to account for the vigorousness of a tree and its social status with respect to the surrounding trees (Schieler and Hauk, 2001). It is thus an indicator for its “visibility” in the CHM. The tree class parameter can take a value of 1 (e.g. tree crown is part of bottom canopy layer), 2 (e.g. tree crown belongs to middle canopy layer), or 4 (e.g. predominant or solitary tree). The c factor is normalized for the total number of trees in the sample plot.

It is assumed that within an angle count plot the measured tree positions have an accuracy of ± 1.0 m relative to the sample unit centre. To allow both for these small measurement errors and for the uncertainties resulting from rasterizing the ALS data the NFI tree height is compared with the highest CHM value in a 3×3 pixels (i.e. 3×3 m²) window around the tree location.

Calculating the height difference in the proposed way only considers tree height differences but does not account for the configuration of the angle count sampling. In fact, the angle count sampling only includes those trees that at a certain distance from the sample plot centre have a minimum DBH, defined by the basal area factor. To avoid solutions that conflict with this sampling principle, the minimum tree height required to fall within the sampling was introduced. This is done as follows: For every distance from the centre coordinate the minimum required DBH is calculated. Through an empirical relationship between DBH and height (Table 2), and correcting for the uncertainty in this function, the minimum required tree height for each distance from the sample plot centre is calculated (Figure 3-c). By subtracting the minimum required tree height from the CHM subset (which is defined by the position of the sample plot centre in the search window and by the distance of the outermost tree to the sample plot centre) one obtains the parts of the tree crowns that should be included in the angle count sampling (Figure 3-b). The hypothetical tree crowns that are actually included in the angle count sampling are derived from the NFI parameters by relating crown shape and extension to BHD according to the allometric functions proposed by (Hemery et al., 2005) (Figure 3-d). Subtracting the minimum required tree height (Figure 3-c) from the simulated tree crown model provides the image that is directly comparable with Figure 3-b (Figure 3-e) and in the ideal case would look identical.

As can be seen in Figure 3-d and e the simulated crown shapes are only a rough approximation of the actual crown shapes. For this reason we decided not to compare the complete simulated and measured “visible” tree crowns but, instead, only compare the apexes of the trees while the rest of the simulated tree crown pixels were excluded in the cost function (Figure 3-f). Tree and non-tree pixels are equally weighted in the cost function, i.e. the sum of the weights attributed to the tree apexes (while still accounting for social stand differences) equals the sum of all non-tree pixels (Figure 3-f). Hence, equation (1) can now be written as:

$$D_{x,y} = \sum_{p=1}^N c_p \cdot |H_{NFI,p} - H_{CHM,p}| \quad (2)$$

where $H_{NFI,p}$ is pixel p in the adapted tree crown model (Figure 3-e), $H_{CHM,p}$ the equivalent pixel in the adapted CHM subset (Figure 3-b) and c the weight of the pixel according to Figure 3-f. The D -values of one sample plot is scaled between 0-1 and the coordinate x,y within the search window providing the smallest D value is eventually assumed the new, co-registered sample plot centre coordinate.

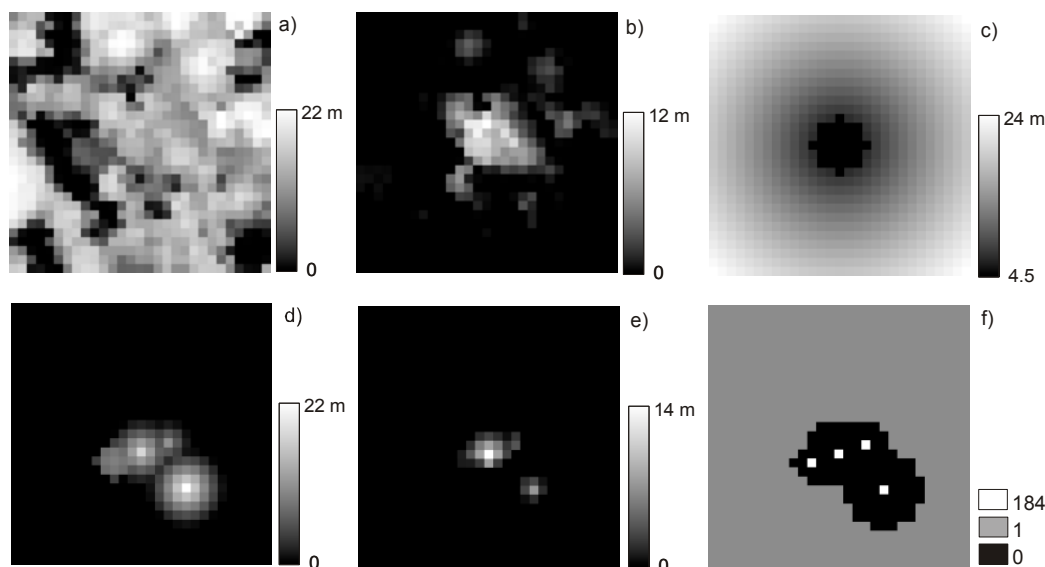


Figure 3: Example of data sets used for co-registration of sample plot 00504100: a) subset extracted from the input CHM around position x,y within search window; b) Difference between CHM subset and minimum tree height required to be sampled in Bitterlich plot (shown in c); d) simulated tree crown model; e) difference between simulated tree crown model and minimum required tree height (shown in c); f) weight attributed to every pixel in cost function.

Table 2: Empirical regression functions between BHD and tree height based on Austrian NFI 2000/2002.

| Type | Regression function | # observations | R ² |
|------------|--|----------------|----------------|
| Coniferous | Tree height = $7.3677 * \text{BHD}^{0.5957}$ | 25201 | 0.73 |
| Deciduous | Tree height = $14.455 * \text{BHD}^{0.4695}$ | 7459 | 0.66 |
| Mixed | Tree height = $8.9211 * \text{BHD}^{0.5604}$ | 32660 | 0.70 |

3.2 Quality flagging

Even if the proposed iterative procedure leads to a global minimum, it is possible that due to errors in the CHM, NFI measurements, and model approximations the obtained minimum does not correspond to the actual optimum position. Identifying those sample plots that potentially have an ambiguous solution is a key element in the workflow since these samples may require manual post-processing by an image processor. Following criteria were considered when marking a solution as ambiguous. In this respect all sample plots that require manual post-processing should be included whereas as few as possible accurately co-registered samples should be included in order to reduce unnecessary quality controls by the image processor:

1. When among the smallest residuals more than one spatial cluster exists (Figure 4 – middle).
2. When residuals are sorted and plotted, a steep slope stands for an unambiguous solution while a flat slope suggests several plausible solutions. (Figure 4 – right)
3. When sample plot has a predominance of deciduous trees, since these have less pronounced tree apexes than conifers and were acquired under leaf-off conditions
4. When distance between original centre coordinate and co-registration result is larger than 20 m.

4. Results

The accuracy of the automated co-registration procedure was investigated by computing the distances between the automatically co-registered sample plot centre coordinates and the centre coordinates that could be unambiguously manually allocated by the image processor. For visual interpretation the distances were sorted in ascending order (Figure 5a). The figure shows that 67 of the 98 sample plots (i.e. 68%) were correctly co-registered, with a distance to the manually obtained results ranging between 0.08 and 3.64 m. The causes of several sample plots not being correctly co-registered (defined as those with a distance included the issues already pointed out in paragraph 3.2, i.e. the presence of multiple solutions and the predominance of deciduous trees (Figure 5c). In addition, two of the incorrectly co-registered sample plots had a manual solution outside the iteration search window ($60 \times 60 \text{ m}^2$) and also CHMs with a point density of less than 1 point/m^2 appeared problematic (Figure 5b).

Figure 5 additionally shows the results of the quality flagging. It can be seen that all of the points with a deviation $> 4 \text{ m}$ were marked “ambiguous”, leading to an omission error of 0%. Similarly, all plots with a deviation $< 4 \text{ m}$ were marked “unambiguous”. Hence, the overall accuracy of quality flagging amounts 74%. In contrast, 26 plots showing only small deviations from manual co-registration results were incorrectly tagged as “unambiguous”, leading to a commission error of 45%. As a consequence, these 26 samples will be superfluously controlled during post-processing.

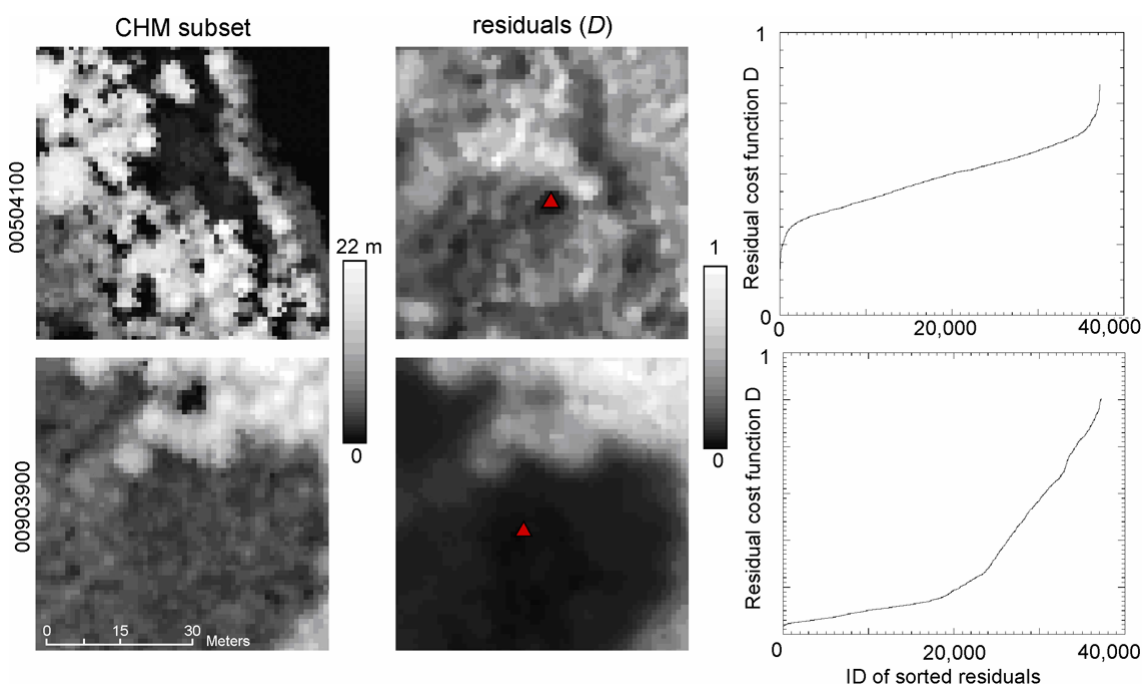


Figure4: Quality measures considered during co-registration, demonstrated for sample plot 00504100 (top) and 00903900 (bottom): the spatial distribution of residuals elucidates if more than one or very large clusters of minimum residuals exist (middle), the red triangle indicates the absolute minimum; the slope of the sorted residuals at the smallest absolute D-value indicates if the found absolute minimum is likely to be the global minimum or if several local minima exist (right).

5. Discussion and conclusion

With a correct co-registration of 67% of the sample plots the automated algorithm has the potential of significantly reducing pre-processing efforts in order to obtain more accurate ALS based predictive models. This is best illustrated with a practical example. For this purpose we calibrated and cross validated the growing stock model of (Hollaus et al., 2008) for 3 different co-registration states of the NFI, using i) the original, ii) the automatically co-registered, and iii) the manually co-registered sample plot centre coordinates. The selection of centre coordinates was based on the 41 sample plots that during automated co-registration were marked “unambiguous”. Calibration and cross validation was based on in situ growing stock measurements collected at each sample plot within the framework of the Austrian NFI (Gabler and Schadauer, 2006). Four sample plots were excluded from growing stock measurements and model calibration due to the absence of trees with sufficiently large DBH.

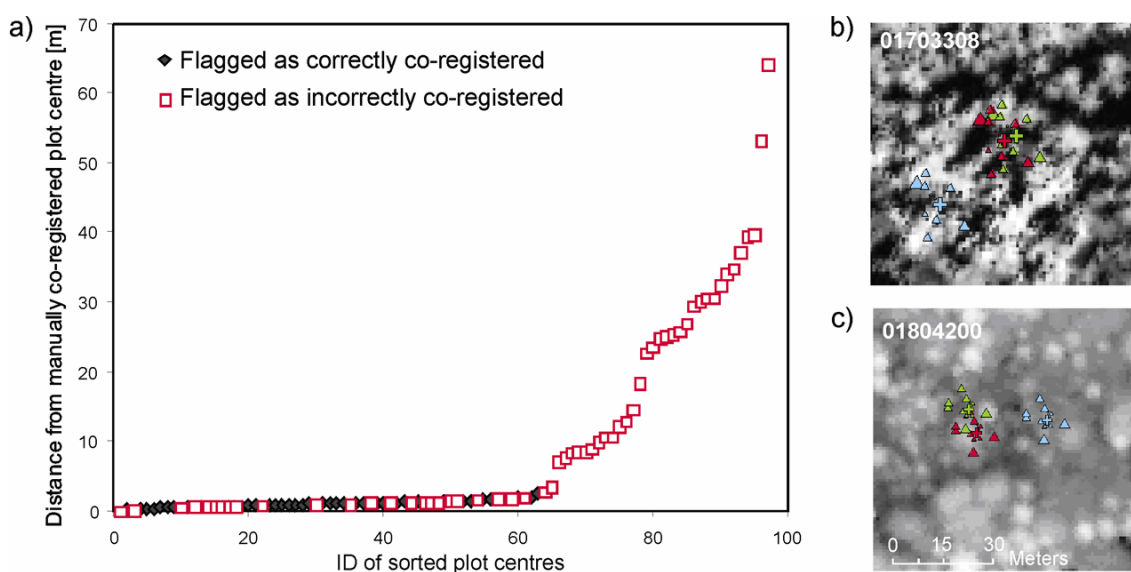


Figure 5: a) Distance between automatically and manually co-registered sample plot centre coordinates, sorted in ascending order. Black diamonds indicate the points that during co-registration were flagged “unambiguous” while red squares were marked “ambiguous”. b, c) Examples of incorrectly co-registered sample plots. b) shows a plot dominated by deciduous trees, c) is characterized by an insufficient ALS point density. Red triangles (crosses) show the original tree (centre point) locations, blue the results of the automated, and green the results of the manual co-registration.

Figure 6 shows that using the automatically co-registered data yields significant improvement (both R^2 and relative standard deviations (SD) obtained by cross validation) compared to the original sample plot centre coordinates and even slightly outperforms the accuracy obtained when using the manually co-registered sample plot centre coordinates.

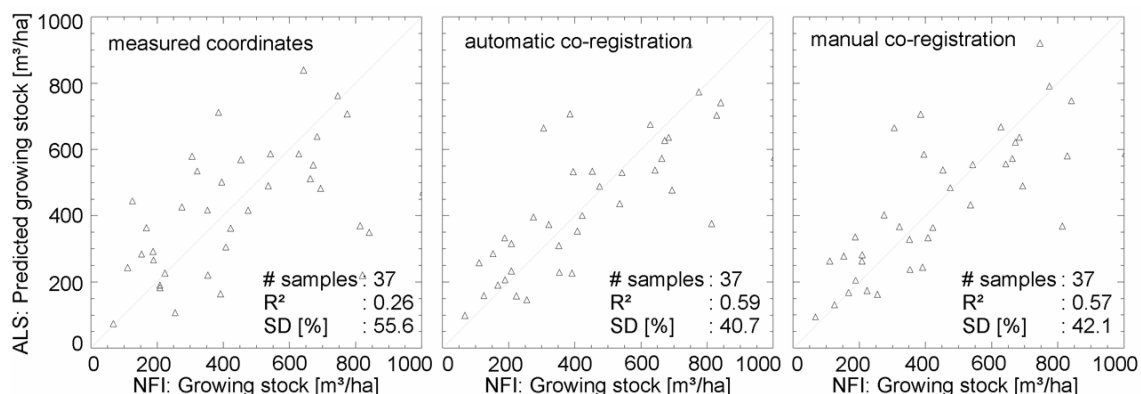


Figure 6: Effect of co-registration on calibration of ALS based growing stock model of (Hollaus et al., 2008). Left plot shows the results when original sample center coordinates measured by GPS are used, the middle (right) plot when automatically (manually) co-registered coordinates are used.

The above example illustrates the practical relevance of adequate co-registration between FI and ALS data in general and the potential of the automated algorithm in performing this task in particular. Moreover, the quality flagging allows the user to identify those results that should be treated with precaution or require manual post-processing. Future efforts will concentrate on testing the developed algorithm on other data sets. In this context, a higher overall accuracy is expected when ALS data with a higher point density is used. Since the developed algorithm will be part of an operational processing chain for Austrian NFI data, it has a high practical relevance.

Acknowledgements

We would like to thank the Landesvermessungsamt Feldkirch for granting the use of the ALS data. Parts of this study were funded by the Austrian Federal Ministry of Agriculture, Forestry, Environment and Water Management (BMLFUW) in the framework of the project ÖWI-Regio.

References

- Bitterlich, W., 1948. Die Winkelzählprobe. *Allgemeine Forst-und Holzwirtschaftliche Zeitung*, 59 4-5.
- Farid, A., Goodrich, D.C. and Sorooshian, S., 2006. Using airborne lidar to discern age classes of cottonwood trees in a riparian area. *Western Journal of Applied Forestry*, 21(3), 149-158.
- Gabler, K. and Schadauer, K., 2006. Methoden der Österreichischen Waldinventur 2000/02 - Grundlagen, Entwicklung, Design, Daten, Modelle, Auswertung und Fehlerrechnung, *BFW-Berichte*, 135, 132 pp.
- Gschwantner, T. and Schadauer, K., 2004. Datenmodelle der Österreichischen Waldinventur 2000/2002. BFW Dokumentation, 4, 76 pp.
- Hemery, G.E., Savill, P.S. and Pryor, S.N., 2005. Applications of the crown diameter-stem diameter relationship for different species of broadleaved trees. *Forest Ecology and Management*, 215(1-3), 285-294.
- Hollaus, M., Dorigo, W., Wagner, W., Schadauer, K., Höfle, B. and Maier, B., 2008. Large-area growing stock estimation based on airborne laser scanning and national forest inventory data. *International Journal of Remote Sensing*, Submitted.
- Hollaus, M., Wagner, W., Maier, B. and Schadauer, K., 2007. Airborne laser scanning of forest stem volume in a mountainous environment. *Sensors*, 7(8), 1559-1577.

- Holmström, H., Nilsson, M. and Ståhl, G., 2001. Simultaneous Estimations of Forest Parameters using Aerial Photograph Interpreted Data and the k Nearest Neighbour Method. *Scandinavian Journal of Forest Research*, 16, 67-78.
- Koukal, T., 2004. Nonparametric Assessment of Forest Attributes by Combination of Field Data of the Austrian Forest Inventory and Remote Sensing Data, PhD thesis, Universität für Bodenkultur, Vienna, 115 pp.
- Maltamo, M., Packalén, P., Peuhkurinen, J., Suvanto, A., Pesonen, A. and Hyypä, J., 2007. Experiences and possibilities of ALS based forest inventory in Finland, *ISPRS Workshop on Laser Scanning 2007 and SilviLaser 2007*, Espoo, Finland.
- Schieler, K. and Hauk, E., 2001. Instruktion für die Feldarbeit - Österreichische Waldinventur 2000/2002, Dienstanweisung, FBVA, Wien, 199.

Probability models for individually segmented tree crown images in a sampling context

James W. Flewelling

Seattle Biometrics & Analysis, LLC., 9320 40th Ave. NE, Seattle, WA 98115 USA
flewelling@seattlebiometrics.com

Abstract

Individually segmented tree crowns are an increasingly common intermediate product for forest inventories using ALS and/or high resolution digital photography. Empirical models are often used to predict the species and sizes of the individual trees associated with each individually delineated tree crown (ITC). Data for such models can come from purposive sampling or from design-based probability sampling. In either case, the empirical predictions will have errors, both with respect to tree size and species. Furthermore, the data used for modeling will often have incorrect matches between ITCs and sample trees. Probability models are well suited to deal with the problem of incorrect matches, false positives and omissions. Examples of such models are shown for a forest in the southern U.S., consisting of pine plantations and naturally regenerated pine stands, with various amounts of natural fill-in of both pine and hardwood. The probability models, coupled with design-based probability sampling, can be unbiased for selected measures of yield by species at the stratum level.

Keywords: remote sensing, sampling, tree crowns, matching.

1. Introduction

Forest inventories involving extensive remotely sensed data such as that from LiDAR, coupled with ground sampling, are in increasingly common use. The analysis of the remotely sensed data can be on an area basis (Næsset, 2004), or may be based on segmentation of individual tree crowns (ITCs). The latter approach may have the greater intuitive appeal. Næsset et al. (2004) and Maltamo et al. (2007) give overviews of recent experiences with the various methods. Gougeon and Leckie (2003) summarize research in individual crown segmentation going back over twenty years. Many different sources of remotely sensed data, singularly or combined, can be used to delineate individual tree crowns (ITCs). Reports of crown delineation based on LiDAR include Hyypä et al. (2001a), and Persson et al. (2002).

Aside from the need for calibration, there are several basic problems which hinder the accuracy of predictions based on ITC. These include incorrect segmentation, undetected dominant trees, hidden trees (Mehtatalo, 2006), incorrect species predictions, and the likelihood that allometric relationships used to predict diameter as a function of height and crown area will vary with stand history and other factors. Though species identification is improving over the 50% error rate reported by Hyypä et al. (2001b), correct species identification of all or most ITCs has been an elusive goal. Progress in species identification has been reported by Gougeon and Leckie (2003) and Holmgren and Persson (2004),

The data used to fit ITC to tree prediction relationships are often selected without benefit of a rigorous sampling methodology. The ITCs are the entities upon which the predictions are based; however they are seldom used to construct a sample frame. Furthermore, the linkages between the sample ITCs and the trees they correspond to are often very subjective or incomplete. The inventory study that is the subject of this paper utilizes the full set of ITCs to form a rigorous

sample frame. The linkage between sample ITCs and sample trees uses methodology which is almost free of subjectivity. The theory is reported in Flewelling (2006) and Flewelling (2008). Section 2 of the present paper has a brief description of the study material, and all the processing steps prior to the development of the probability models.

2. Study Material and Preliminary Processing

The forest being inventoried consisted of two blocks in the coastal plain of Texas, USA. The majority of the stands were either plantations of slash pine or loblolly pine. Others were naturally regenerated pine. Significant amounts of hardwood were in the natural stands, and in the planted stands in one of the two blocks. An inventory was available showing past management practices including age of establishment and thinning history. Stand boundaries were in a geographic information system (GIS). The inventory described here excludes stands of age 12 and younger, and excludes stands which had been classified as hardwoods; those stands were inventoried using different methods. The inventory presented here is comprised of 1573 stands with a total area of 14,800 ha.

2.1 Remotely Sensed Data and Processing

Two types of remotely sensed data were available: LiDAR and color-infrared (CIR) digital photography (red, green and near infrared channels). The LiDAR data were acquired using an Optech Altm 3100 sensor. Specifications were for a minimum of five postings per square meter. Only the first and last returns from each LiDAR pulse were retained. The LiDAR data were used to create a digital elevation map; the first returns were converted to values of height above ground, and further converted to 0.5 by 0.5 m pixels. Pixel heights were set to the highest return in each pixel; pixels without returns had heights imputed from neighbouring pixels. The CIR data were fused with the pixelized LiDAR data.

Individually delineated tree crowns (ITCs) were identified over the entire forest by applying a semi-automatic valley-following technique (Kelle et al., 2007) with similarities to that of Hyypä et al. (2001a). Each ITC is represented by a contiguous set of whole pixels. ITC height was determined as the greatest of the pixel heights; ITC area was determined as the sum of the areas of the pixels; ITC location was determined as the geometric mean of the pixel locations. ITC color was determined as the average of the color values of the pixels.

All ITCs were assigned a species group (SPG). The two species groups were pine and hardwood. The assignments were made through an operator-guided training process, which was calibrated separately by stand type and block. The assignment methodology used a neural network approach, based mainly on the color data. This approach allows a species-group probability to be assigned to each ITC. Subsequently each ITC was assigned a putative species group: the species group with the higher probability. Every stand had species cover assessed ocularly. The putative species group assignments for the ITCs within each stand were adjusted to match the overall assessment for the stand.

2.2 Sampling

Stands were grouped into twenty-two sampling strata based upon block, species planted, thinning history, origin, and age. Within each stratum several stands were selected without replacement for sampling; the probability of selection was proportional to stand area; most strata had six stands selected; one strata had four stands selected. Within the GIS representation of each selected sample stand, two points were randomly selected to become plot centers.

A field crew was given the coordinates of each preselected plot center. They used survey-grade GPS equipment to travel to the preselected locations in the forest, and monumented plot centers at those locations. Fixed-area circular field plots, of size 0.04858 ha, were established at each location. Field measurements included the species, location, and diameter (DBH) of each tree whose diameter exceeded a threshold (D_{\min}) of 7.493 cm. Location data (horizontal distance and azimuth) were sufficient to allow for the calculation of the breast-height location of each tree relative to the plot center. A sample of heights was recorded for each species on each field plot. The height data were used to fit height-diameter curves by species for each plot; unmeasured tree heights were imputed from the curves. Sample weights, which are required for unbiased estimation, were computed for each ITC. Further details are as described in Flewelling (2008).

2.2 Plot Registration

The field plots are not assumed to have been located perfectly. The determination of the location of the field plot on the crown map is accomplished with a computer-assisted system that overlays the field-determined stem map on a representation of the remotely sensed data. After the registration is completed, the location of the field plot's center on the ITC map becomes the accepted location for the sample.

2.3 ITC and Tree Matching

A statistically valid procedure was required to identify the tree or trees to be associated with each ITC. Such a procedure is described by Flewelling (2008); that procedure was applied here to all the ITCs whose centers were within crown analysis plots of size 0.03644 ha, centered about each of the corrected plot centers. The procedure used was similar to that described by Persson et al. (2002). Each ITC was expanded by up to 1 m in each direction to form Veroni tessellations. Field sample trees whose coordinates were within a particular ITC's expanded area were tentatively matched to that ITC. Infrequently, trees not falling within any of the ITC tessellations were matched to the nearest ITC if the match appeared to be physically correct. The trees which are matched to particular ITCs can be referred to as directly associated trees.

3. Methods

Probability models were developed to predict the number and species of trees associated with each ITC. For trees predicted by these probability models, conditional regression equations were required to predict tree diameter. The resultant regression predictions of DBH were further modified using a common "tripling" technique which increases the dispersion of predicted diameters and heights, but which does not alter the predicted yield. Heights are predicted as a function of DBH and the LiDAR-based height of the ITC. A separate simpler model accounts for trees not associated with ITCs.

3.1 Species and Count Predictions

For each stand there are two components of the overall prediction: trees inferred directly from ITCs and an unseen component. The unseen stand component contains relatively few trees, which are usually smaller than the other trees. The unseen component is addressed in section 3.5. This section deals only with the directly associated trees.

There are many possible combinations of matched trees for a single ITC. A notation system was devised to track the possible outcomes for an ITC match. The notation allows for a count (C) of the trees to be associated with a particular ITC, allows for identifying the species group of the associated trees, and tracks the trees by comparative DBH. The largest tree associated with an ITC is referred to as a primary tree; any smaller trees associated with an ITC could be referred

to as secondary trees. Secondary trees which are not the second-largest are also referred to as tertiary trees.

The independent data for the ITCs includes stratum, and:

| | |
|--------------------|--|
| SPG _{ITC} | Assigned species group: P=pine, H=hardwood |
| A | Crown area (m ²). |
| H _{ITC} | Height of the ITC (m) |

All the ITC heights are 4 m or greater. The variables being predicted are:

| | |
|---------------------|---|
| SPG _{TREE} | Species group for a tree: P for pine, H for hardwood. |
| DBH | Diameter at breast height. (cm.), |
| HT | Total tree height (m) |
| EC | Expected tree count; also expressed as E(C). |
| TRS | Tree-record sequence, a code used to track predicted trees. |

The first of the probability equations for ITCs classified as pine is:

$$\Pr\{C \geq 1\} = \text{logit}^{-1}(L) = \exp(L) / [1 + \exp(L)] \quad (1)$$

where L is a linear function of A, H_{ITC}, and their cross product. Other equations for the pine ITCs have the same form, but different coefficients. There are two more “count equations” ; these predict $\Pr\{C \geq 2 | C \geq 1\}$ and $\Pr\{C \geq 3 | C \geq 2\}$. The unconditional probabilities for counts 0, 1, 2, and ≥ 3 can be computed by combining the foregoing empirical equations according to standard rules for probability expressions.

The above equations deal with tree count. Tree species are predicted separately by the size order of the directly associated trees. Subscripts 1, 2 and 3 refer to the largest-DBH tree associated with an ITC, the second largest, and all others. Species probabilities are predicted for the pine ITCs as:

$$\Pr\{\text{SPG}_1 = P | C = 1\} = \text{logit}^{-1}(c_0 + c_1 \times A + c_2 \times H_{ITC} + c_3 \times A \times H_{ITC}) \quad (2)$$

where the inverse logit function is as defined in Eqn. 1. Coefficients c₀ through c₃ for a representative stratum are (-2.43, -0.455, 0.1667, -0.01553). Other equations of the same form predict $\Pr\{(\text{SPG}_1 = P) | C \geq 2\}$, $\Pr\{(\text{SPG}_2 = P) | C \geq 2, \text{SPG}_1 = P\}$, $\Pr\{(\text{SPG}_2 = P) | C \geq 2, \text{SPG}_1 = H\}$, $\Pr\{(\text{SPG}_2 = H) | C \geq 2, \text{SPG}_1 = P\}$, $\Pr\{(\text{SPG}_2 = H) | C \geq 2, \text{SPG}_1 = H\}$. The latter equations are sufficient to calculate probabilities that the species of the largest and second largest trees are (P, P), (P, H), (H, P) or (H, H). The conditional expected count of tertiary trees for the pine ITCs, E{C of tertiary Conifers | C ≥ 3 } and E{C of tertiary Hardwoods | C ≥ 3 } are estimated as constants.

This completes all of the empirical computations for E(C) on possible realizations of the probability models for pine ITC’s. Table 1 shows all the realizations, and their expected counts. The tree-record sequences (TRS) are arbitrary labels. Each ITC that had been classified as a pine produces twelve tree records with the expected counts shown in Table 1. The ITCs classified as hardwoods have a similar, but simpler set of prediction equations; these are not shown.

3.2 DBH Predictions

DBH is predicted as a function of crown area and ITC height, using the following model for all primary trees and second-position trees associated with pine ITCs:

$$DBH = a_0 + a_1 \times \{ 1 - \exp[a_3 \times (A)^{a_4} \times (H_{ITC})^{a_5}] \}^{a_2} \quad (3)$$

Most coefficients are constant across all strata, but do vary with TRS. An all-strata weighted regression is used to estimate the coefficients. Coefficient a_3 is subsequently revised by stratum such that the weighted sum of predicted basal areas associated with the sample ITCs is exactly equal to the weighted sum of the basal area of the ground sample trees for that TRS and stratum.

The tertiary trees associated with pine ITCs use a different equation for DBH. The predicted values are always between D_{min} and the predicted diameter of the second-largest associated tree. As with the previous equation, the fit is constrained so as to have unbiased predictions for basal area by stratum.

3.3 Tripling

Tripling is a commonly used mechanism to increase variance of model predictions. Each original predicted tree record is split into three, each representing one-third the original E(C). The DBHs for the three new records ($i = 1, 3$) are:

$$DBH_i = \text{SQRT} \{ (D_{min})^2 + (1 + f_i \times k) [DBH^2 - (D_{min})^2] \} \quad (4)$$

where $(f_1, f_2, f_3) = (-1, 0, 1)$, and k is set so that the variance of the predicted DBHs are similar to the variance of the observed DBHs.

3.4 Tree Height Predictions

There are two sources of height predictions: one based on a commonly used height-DBH relationship, and the other based on the LiDAR derived height of the ITC. The first of these is referred to as the allometric height prediction:

$$HT_A = BH + a_1 \times \exp(a_2 / DBH) \quad (5)$$

where BH is breast height, 1.37 m. Coefficients are fit separately by stratum and the species group of the tree.

The above prediction of height is used as an independent variable in the final regression, which incorporates both sources of information:

$$HT = BH + a_1 \times (HT_A - BH) + a_2 \times (HT_{ITC} - BH) \quad (6)$$

Fitting is done separately for the planted strata and the natural strata. Coefficients vary with tree species group, and with match position. The coefficients are constrained such that the weighted sum of the product of basal areas and heights is unbiased.

3.5 Unseen Trees

Some trees are not detected at all in the ITC generation process, or fail to be linked to an ITC. For each sampling stratum, all such trees are put into a per-hectare listing of trees, showing species group, DBH and the count per ha. represented by each entry.

4. Results

False positives, ITCs with no matching trees, were 9.9% of the total; for such ITCs which had been identified as pine or hardwood respectively, the false-positive rates were 9.1% and 16.4%. The crown area of these false ITC's was 4.0% of the total area of all ITC's. Unseen trees were 2.5% of the total, representing 1.4% of the basal area. Results for all the matched ITCs and trees are in Table 2. Each such ITC is matched, on average, to 2.06 trees. The primary trees represent 48% of the total number of matched trees and 74% of the total matched basal area.

The forest-wide average stand tables for pine and hardwood are shown in Figure 1. The observed and predicted stand tables are in good accord. The two most notable errors are that the hardwood trees in the lowest DBH class (8 cm) are underestimated, and the peak prediction for pine at DBH class 12 cm does not exactly match the field data.

Table 1: Predicted species and counts for trees associated with ITCs classified as pine.

| TRS | Description | SPG _{TREE} | E(C) |
|-----|------------------|---------------------|---|
| 1 | Single Tree | P | $\Pr\{C = 1\} \times \Pr\{\text{SPG}_1 = P \mid C=1\}$ |
| 2 | Single Tree | H | $\Pr\{C = 1\} \times [1 - \Pr\{\text{SPG}_1 = P \mid C=1\}]$ |
| 3 | Larger of (P,P) | P | $\Pr\{C \geq 2\} \times \Pr\{\text{species}=(P,P) \mid C \geq 2\}$ |
| 4 | Smaller of (P,P) | P | $\Pr\{C \geq 2\} \times \Pr\{\text{species}=(P,P) \mid C \geq 2\}$ |
| 5 | Larger of (P,H) | P | $\Pr\{C \geq 2\} \times \Pr\{\text{species}=(P,H) \mid C \geq 2\}$ |
| 6 | Smaller of (P,H) | H | $\Pr\{C \geq 2\} \times \Pr\{\text{species}=(P,H) \mid C \geq 2\}$ |
| 7 | Larger of (H,P) | H | $\Pr\{C \geq 2\} \times \Pr\{\text{species}=(H,P) \mid C \geq 2\}$ |
| 8 | Smaller of (H,P) | P | $\Pr\{C \geq 2\} \times \Pr\{\text{species}=(H,P) \mid C \geq 2\}$ |
| 9 | Larger of (H,H) | H | $\Pr\{C \geq 2\} \times \Pr\{\text{species}=(H,H) \mid C \geq 2\}$ |
| 10 | Smaller of H,H) | H | $\Pr\{C \geq 2\} \times \Pr\{\text{species}=(H,H) \mid C \geq 2\}$ |
| 11 | Tertiary pine | P | $\Pr\{C \geq 3\} \times E\{C \text{ of tertiary Conifers} \mid C \geq 3\}$ |
| 12 | Tertiary Hdwd | H | $\Pr\{C \geq 3\} \times E\{C \text{ of tertiary Hardwoods} \mid C \geq 3\}$ |

Table 2: Summary of matched ITCs and trees. Forest-wide estimates from 0.0364 ha analysis plots.

| Match | Tree Species | Trees per ha | | | Basal area (m ² /ha) | | | Basal Area (%) |
|-----------|--------------|--------------|------|-----|---------------------------------|------|------|----------------|
| | | ITC species | | | ITC Species | | | |
| | | Pine | Hdwd | All | Pine | Hdwd | All | |
| Primary | Pine | 308 | 13 | 321 | 13.1 | 0.4 | 13.5 | 68 |
| | Hdwd | 35 | 25 | 60 | 0.7 | 0.6 | 1.3 | 6 |
| | All | 343 | 38 | 381 | 13.7 | 1.0 | 14.8 | 74 |
| Secondary | Pine | 216 | 6 | 222 | 3.4 | 0.1 | 3.4 | 17 |
| | Hdwd | 151 | 32 | 183 | 1.3 | 0.3 | 1.7 | 9 |
| | All | 368 | 38 | 405 | 4.7 | 0.4 | 5.1 | 26 |
| All | Pine | 524 | 19 | 543 | 16.5 | 0.5 | 17.0 | 85 |
| | Hdwd | 186 | 57 | 243 | 2.0 | 0.9 | 2.9 | 15 |
| | All | 711 | 76 | 787 | 18.5 | 1.4 | 19.9 | 100 |

5. Discussion

The modeling and sampling approach presented here produces unbiased results at the stratum level. Most other methods of using remote sensing in forest inventory estimation either are unbiased, or could be made unbiased through a strategy of adjustments based upon randomly located sample plots. For example, consider a system based on individual crown delineation coupled with empirical relationships to predict DBH and height as functions of crown characteristics. The regressions could be based on non-representative data and, as a consequence, could not be directly used for unbiased estimation. However, if the regression results were subsequently adjusted, perhaps with a ratio estimator, the adjusted results would be unbiased by stratum.

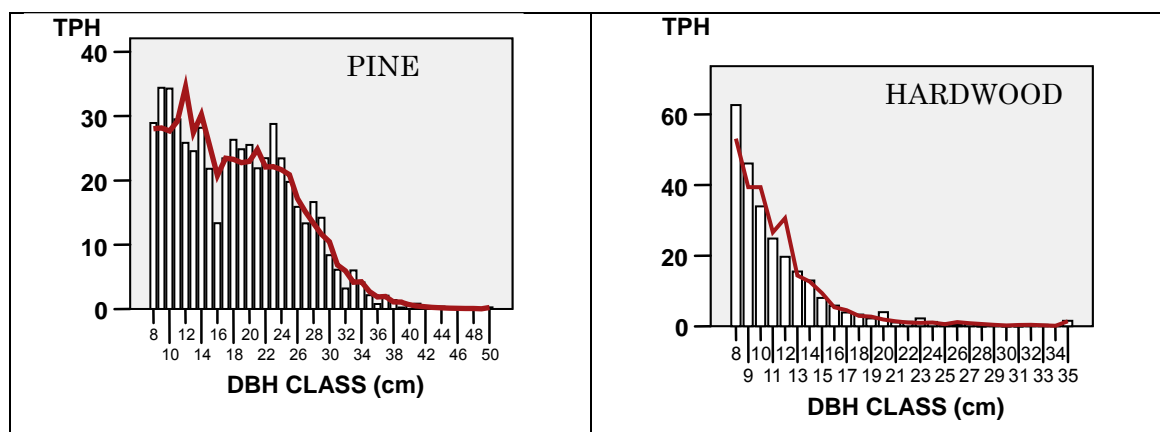


Figure 1. Trees per hectare by 1 cm diameter classes for pine (left) and hardwood (right). Histograms represent observed ground plot data; the overlaid line are the predictions.

The approach presented here has an added advantage of statistical efficiency due to an almost-exact matching between the remotely sensed sample and the ground sampling. Plot registration error is minimized, and correlations between the remotely sensed data and the corresponding ground data are maximized. Consider that a perfectly registered plot may have several crowns whose centers are near the plot boundary. Without crown and tree matching, it is just a matter of chance whether the trees actually associated with these ITCs will be inside the ground plot or outside the ground plot. With good matching, that uncertainty is removed, making each plot more valuable for the purpose of ratio adjustment. The benefit of highly correlated tree and crown data also accrues to the present method, even though there is no explicit ratio adjustment based on yields of sample plots.

A goal that is hinted at in various papers and presentations is that data obtained from crown segmentation, together with good allometric relationships, may lessen or eliminate the need for on-the-ground sampling. That goal is unlikely to be realized while the non-primary trees associated with the ITC's constitute over a quarter of the total basal area (Table 2). Mehtatalo (2006) reviewed the literature on unseen trees; such trees would often include what I have referred to as secondary trees. He concluded that the problem of unseen trees won't be eliminated through direct analysis of remotely sensed data. He proposed using distributional models to correct for censoring. However, it should not be assumed that tree size distributions will always be regular. The probability models presented here have the potential to account for unseen or secondary trees in most situations where the desired one-to-one correspondence between ITCs and trees is lacking. And the predicted DBH distributions appear to be reasonable.

Apart from the modeling, there remains a lot of uncertainty about how best to associate sample ITCs and sample trees. The method described here is a type of cluster sampling. To be valid, the matches must be invariant to the random positioning of the plots. Though not a statistical requirement, the best methods will have matches which closely correspond to the apparent physical reality. Tree-top matching as shown by Korpela et al (2007) is probably better than matching based on ground projections. Another promising method could model the entire crown in three dimensions as proposed by Andersen et al. (2002), and then search for intersections of boles and crowns at some intermediate height.

Reliable estimates of mean square error (MSE) for the estimators of basal area and volume by stand could not be obtained due to the small number of sample stands in each stratum. Flewelling (2008) reported on a different study with similar methodology but with fewer strata and more samples per stratum than in the present study. The reported root mean square error for stand basal area in that inventory was 9.7%. The less-than-trustworthy pooled-variance result for the present study corresponds to a root mean square error for merchantable basal area of 21.3%; the corresponding figure for merchantable volume is 24.3%. Merchantable trees are those with DBH \geq 11.4 cm; outside-bark cubic volumes are from stump height (15.2 cm) to a 7.6 cm small-end outside-bark top diameter. As should be expected in a studies utilizing LiDAR to predict diameter distributions and heights, the stand-level errors in volume are only slightly greater than the stand level errors in basal error, for errors measured as percentages. If there had been more samples per stratum, the estimated variances would be expected to be lower, and the estimates of the variances would be expected to be much more reliable.

One of the shortcomings in the present analysis is the forced binary decision on species group for each ITC. Estimates of species probabilities are potentially more useful than discrete estimates. The proprietary neural network approach to species classification did provide a means to estimate species probabilities for ITCs. Those probabilities were not used because of concerns as to whether the computations were correct. Without regard to that particular concern, most methods of assigning species should be able to also assign probability estimates for the species. For example, a discriminant analysis based on the three color channels and the separate mean profiles for pine and hardwood would produce species probability estimates for each ITC. The mean profiles for the two species groups could be from subjectively selected ITCs or they could be a random subset of the sample data. A different approach used in agriculture (Foody et al., 2006) focuses on the species of most interest, which would be pine in this case. The color values from the training set for pine could be used to describe a multivariate distribution. Relative probabilities of being pine would be assigned to the ITCs based upon probability density values computed from that multivariate distribution. There is no need for a similar multivariate distribution for hardwoods. The methods used in the present study, and the suggested alternatives, all share a common feature of keeping the computations on the CIR data separate from the other probability computations. Hence the analyses are simplified, at a cost being unable to fully explore interactions of the CIR data and the LiDAR derived characteristics of the ITCs.

If probability estimates of species for the ITCs had been directly used, there would have been no need to make up separate sets of equations for pine-classified ITCs and hardwood-classified ITCs. Instead, a single set of probability equations could have been fit, using as one of the independent variables a logit transformation of the initially predicted pine probability. Such an approach would have retained more information on the species inference than was possible with the binary approach to species estimation. If ocular estimates of crown cover percentages were available for each stand, these could easily be brought into this estimation process by adding a stand-dependent constant to each logit-transformed probability such that the resultant ITC-area-weighted mean pine probability for a stand matched the ocular estimate.

Regardless of whether the models presented here or some other models are used, the statistical characteristics of errors for predictions based on ITCs will be substantially different from those seen in traditional stand-level inventories. Traditional inventories can be unbiased by stand for all major attributes, including the diameter distributions. Models based upon remotely sensed data, without ground sample data in every stand, are not unbiased by stand. At best, unbiasedness holds at the stratum level, usually for a small set of attributes. For the models presented here, unbiasedness at the stratum level holds for numbers of trees, basal area, and the basal area- height product, overall and by species.

Acknowledgements

The Harvard Endowment Fund supported this study and has given permission to publish the details. The overall project was coordinated by Adam Rousselle of Falcon Informatics, and completed in 2005. As part of that effort, the present author developed and fully described in an unpublished report the complete set of prediction equations which are summarized here. Significant portions of the preliminary processing described in Section 2 were performed or designed by Bob Pliszka, Olavi Kelle and Vesa Leppanen. The comments of two anonymous reviewers are appreciated.

References

- Andersen, H., Reutebuch, S., and Schreuder, G. 2002. Bayesian Object Recognition for the Analysis of Complex Forest Scenes in Airborne Laser Scanner Data. In *ISPRS Commission III, Symposium 2002 September 9 - 13, 2002, Graz, Austria*, pages A-035 ff (7 pages).
- Flewelling, J., 2006. Forest Inventory based on individual tree crowns. Presentation at: Western Mensuration Meeting, June 18-20, 2006, Fortuna, California. Available at: <http://www.growthmodel.org/wmens/m2006/flewelling.ppt> (viewed July 31, 2008).
- Flewelling, J., 2008. Forest inventory predictions from individual tree crowns: regression modeling within a sample framework. In: *Proceedings of the 8th Annual Forest Inventory and Analysis Symposium*. Oct. 16-19, 2006. Monterey Bay, California, In press.
- Foody, G.M., Mathur, A., Sanchez-Hernandez, C., and Boyd, D. 2006. Training set size requirements for classification of a specific class. *Remote Sensing Environ.* 104:1-14.
- Gougeon, F.A, and Leckie, D.G. 2003. Forest information extraction from high spatial resolution images using an individual tree crown approach. *Information Report BC-X-396*. Victoria, BC: Canadian Forest Service, Pacific Forestry Center. 29 p.
- Holmgren, J., and Persson, Å. 2004. Identifying species of individual trees using airborne laser scanning. *Remote Sensing Environ.* 90:415-423.
- Hyypä, J., Kelle, O., Lehikoinen, M. and Inkinen, M., 2001a. A segmentation-based method to retrieve stem volume estimates from 3-d tree height models produced by laser scanners. *IEEE Transactions on Geoscience and Remote Sensing*, 39, 969-975.
- Hyypä, J., Schardt, M., Haggrén, H., Koch, B., Lohr, U., Scherrer, H.U., Paananen, R., Luukkonen, H., Ziegler, M., Hyypä, H., Pyysalo, U., Friedländer, H., Uuttera, J., Wagner, S., Inkinen, M., Wimmer, A., Kukko, A., Ahokas, A. and Karjalainen, M., 2001b. HIGH-SCAN: The first European-wide attempt to derive single-tree information from laserscanner data. *The Photogrammetric Journal of Finland* 18, pp. 43-53.
- Kelle, O., Macom, E., Pliszka, R., and Mathawan, N. 2007. Method of feature identification and analysis. *U.S. Provisional Patent Application* 60/814,715. Filed June 19, 2006.

- Korpela, I., Dahlin, B., Schäfer, H., Bruun, E., Haapaniemi, F., Honkasalo, J., Ilvesniemi, S., Kuutti, V., Linkosalmi, M., Mustonen, J., Salo, M., Suomi, O., and H. Virtanen, H. 2007. Single-tree forest inventory using LiDAR and aerial images for 3D treetop positioning, species recognition, height, and crown width estimation. 2007. In: P. Ronnholm, H. Hyypä, and J. Hyypä (Eds.). *Proceedings of ISPRS workshop "Laser Scanning 2007 and Silvilaser 2007."* Espoo, Finland, p. 227-233.
- Maltamo, M., Packalén, P., Peuhkurinen, J., Suvanto, A., Pesonen, A., and Hyypä, J. 2007. Experiences and possibilities of ALS based forest inventory in Finland. 2007. In: P. Ronnholm, H. Hyypä, and J. Hyypä (Eds.). *Proceedings of ISPRS workshop "Laser Scanning 2007 and Silvilaser 2007."* Espoo, Finland, p. 270-279.
- Mehtatalo, L. 2006. Eliminating the effect of overlapping crowns from aerial inventory estimates. *Canadian Journal of Forestry Research*, 36: 1649-1660.
- Næsset, E., 2004. Accuracy of forest inventory using airborne laser scanning: evaluating the first Nordic full-scale operational project. *Scandinavian Journal of Forest Research*, 19: 554-557.
- Næsset, E., Gobakken, T., Holmgren, J., Hyypä, J., Hyypä, H., Maltamo, M., Nilsson, M., Olsson, H., Persson, Å. and Söderman, U., 2004. Laser scanning of forest resources: the Nordic experience. *Scandinavian Journal of Forest Research*, 19: 482-499.
- Persson, Å.; Holmgren, J.; Söderman, U. 2002. Detecting and measuring individual trees using an airborne laser scanner. *Photogrammetric Engineering and Remote Sensing*, 68: 925-932.

Session 6: Terrestrial laser scanning & laser cameras

Single-scan TLS methods for forest parameter retrieval

P. Litkey¹, X. Liang¹, H. Kaartinen¹, J. Hyypä¹, A. Kukko¹ & M. Holopainen²

¹Finnish Geodetic Institute, Department of Remote Sensing and Photogrammetry,
Masala, Finland

[@fgi.fi">\(\[@fgi.fi">paula.litkey, xinlian.liang, juha.hyypa, harri.kaartinen, antero.kukko\]\(mailto:paula.litkey, xinlian.liang, juha.hyypa, harri.kaartinen, antero.kukko\)\)@fgi.fi](mailto:paula.litkey, xinlian.liang, juha.hyypa, harri.kaartinen, antero.kukko)

²University of Helsinki, Department of Forest Resource Management, Finland
markus.holopainen@helsinki.fi

Abstract

Using a terrestrial laser scanner (TLS) in single-scan mode for achieving plot level reference data in forests is proposed in this paper. In single-scan operation the amount of data is small compared to multi-scan and the registration of different scans is not needed, thus both the measurement and the processing are faster and fully automatic. The scan geometry was utilized in the development of the processing method. The forest scene complexity and that some trees are totally shadowed by the others are the main limiting factors to the use of single-scan TLS. We expect our methods to operate well at least on single layer, pine dominated economically exploited boreal forests. The main result of the TLS based forest parameter method is the location and stem curve for each tree that was detected. In traditional forest ground truth reference measurements, each tree is manually measured in the reference plot and the tree location is not recorded. The possibility to record the location of major trees by TLS makes the plot information usage more practical: corrections can be done, they can be used as permanent plots, they serve as a basis of future individual tree based forest inventory. In our test area, 85% of the 52 trees that were manually found from the TLS data slice inside 60m range could be found automatically.

Keywords: TLS, single-scan, one-storey-forest, stem curve

1. Introduction

Terrestrial laser scanning has been used for detailed modelling of individual trees and canopies in (Pfeifer et al 2004; Pfeifer and Winterhalder 2004; Gorte and Pfeifer 2004; Hosoi and Omasa 2006; Fleck et al 2007; Danson et al 2007; Xu et al 2007 and Chasmer et al 2006). More automatic methods for forest parameter determination have been considered in (Bienert et al 2006a, 2006b, 2007; Aschoff and Spiecker 2004 and Király & Brolly, 2007). Using TLS for plot level inventory offers a fast and efficient means of automatically determining basic tree parameters such as the number and position of trees, diameter at breast height (DBH) and tree height. In Aschoff and Spiecker (2004) semi-automatic tree detection method is presented. The method is based on first filtering the data and, thus, generating the Digital Terrain Model (DTM) and then processing the scanner data in horizontal slices and using the Hough transform to detect circular point distributions. The layer data are then rasterized and saved in image format with different horizontal layers in channel information; the trees are detected from the image data. In Bienert et al (2006a) and Király and Brolly (2007) the tree detection is also based on horizontal layers; starting from breast height, DTM is generated for ground point reduction in order to provide breast height measures for each tree. In Bienert et al (2006a) and Király and Brolly (2007) the points are clustered, in Bienert et al (2007) the clusters are rasterized and the shape of the clusters is studied in order to detect trees. In Bienert et al (2006a and 2007) a method for detection and modelling that works on both single- and multiple scan data was presented.

Most of the previously reported tree trunk modelling methods require total coverage of the trunk and are thus only usable in multiple scan mode (MSM) terrestrial scanner data. These methods operate on single-tree point clouds and the detection of trees is manual. The emphasis is on accurate modelling of the tree trunk and branches. In (Pfeifer et al 2004; Gorte and Pfeifer 2004) an accurate cylinder based model of the trunk is described. A free form curve based model for trunks is presented in Pfeifer and Winterhalder (2004). In most of the models, cylinder or circle fitting is used in the horizontal layers to model the trunk. Least squares circle fitting algorithms are considered in Chernov and Lesort (2005). In Thomas and Mili (2007) a generalized M-estimator is used for robust fitting of circles to laser scanner data in defect detection. The noise level in the forest TLS data is large and the need for either more effective noise reduction or more robust circle fitting is evident in order to have reliably operating automatic forest parameter estimation.

In this paper, we first present the geometric and technical background for processing the data using vertical sweep lines and then give details on the detection, filtering and modelling phases in chapter 2. In chapter 3 results of a pilot study in boreal pine forest are presented, the automatic result is compared with results manually measured from the same TLS data. The results and the applicability of the methods are discussed in chapter 4.

2. Method

The method presented in this paper consists of first detecting possible trunks in a range image clustering and then processing the point clouds corresponding to each cluster separately. The point clouds are first filtered to eliminate non-tree objects; second, the trunk point clouds are filtered to remove branches. For each trunk point cloud, the ground level is estimated using histogram of the points that are situated closer than 1 m from the trunk point cloud centre. Finally, a circle is fitted to each 20 cm horizontal slice of the trunk point cloud and a model is composed using the circles and their centres.

As the scan progresses, vertical sweep lines of measured points are saved for each horizontal angle. In Figure 1 in the left image, the pink disc represents the fast vertical sweep pattern and the black arch slower horizontal rotation. In the right image the consecutive sweeps are coloured to visualize the sweeps on a trunk.

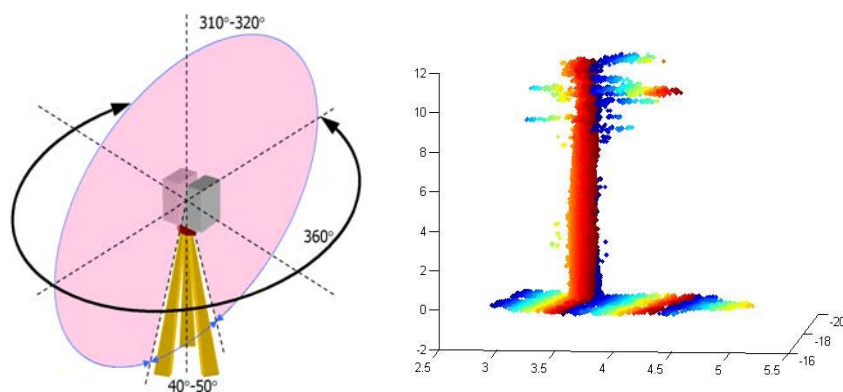


Figure 1: Left: The operating principle of a typical terrestrial laser scanner. Right: A typical single tree trunk point cloud with prism colouring to visualize the vertical scan lines on the tree.

Instead of starting with horizontal layers, the detection is done in range images. In single scan mode data objects that are occluded by others are not seen and thus for each pair of angles, only

one measured distance is possible. Only the points that are visible to the scanner are used in trunk detection. Horizontal layers are applied for each trunk separately after the detection and filtering. The branches that cause difficulties in stem modelling are filtered out before modelling phase.

2.1 Data

TLS-data was collected using a Faro 880HE80 terrestrial laser scanner, which is a high-speed scanner with a data acquisition rate of 120000 points per second. The scanner uses continuous laser to measure the distances based on phase-shift measurement. The scanning was carried out in November 2007 at the test site located near Kajaani in eastern Finland. The measurement resolution that was used in the scanning produced a point spacing of 0.6 mrad (6 mm at the distance of 10 metres) within the single-scan point cloud.

2.2 Trunk detection

The trunk detection algorithm is based on processing the range data as a row-column raster, where rows and columns represent relatively constant scanner angle values. Points close to each other with similar distances from the scanner are assigned to the same cluster. The distance from the scanner is corrected distance in cylindrical coordinates, not the original one in spherical coordinates, so that the distance of points forming a vertical line will be equal. The found clusters are further processed to select the ones with vertical shape and to unite trunks that have been cut into pieces because of occlusions by branches. The detection method used is described in Liang et al (2008). Figure 2 shows the found trunks in a slice of the homogenous Kajaani test site and on a more complex mixed forest site in Nuuksio.

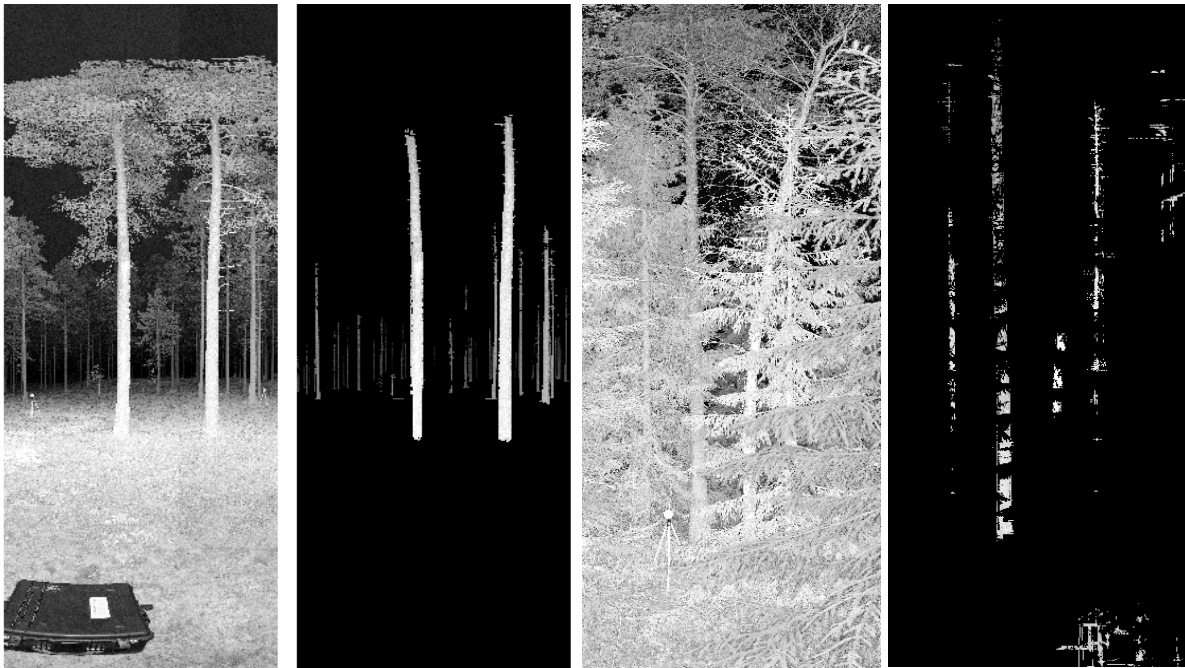


Figure 2: Two pairs of images: original intensity image left and the corresponding found trunk clusters right (dark image). Left pair: a pine forest slice. Right pair: a more complex forest scene.

From Figure 2 it can be seen that the method is working well on a single layer forest, but with more details and tilted trees, the performance is not as good. Due to the tree branching and occlusion from the canopy in the upper part of the trunk, there remain some points in the

clustered trunk that have to be filtered out in order to have an optimal trunk point cloud. It is probable that different forest types require different parameters in the clustering.

2.3 Trunk filtering and local ground level determination

The trunk point cloud obtained from the detection contained some branch and ground points that had to be filtered out before modelling. The sweep that contained mostly trunk points consists of points whose plane distance from the scanner is close to constant. In Figure 3, three trunk point clouds located at different distances from the scanner are shown. Although the vertical and the horizontal spacing between the consecutive points and sweep lines is a function of the distance, long vertical lines of scan points mark the trunk. The points that fall on the branches in the two sides of the tree result in shorter and more shattered lines. Lines where the minimum vertical difference between consecutive points exceeded some limit were removed and only lines whose length exceeded a suitable threshold were accepted in order to remove the branch points on the sides. Ideally the limits could be derived from the scanner geometry so that the limits would be distance dependent.

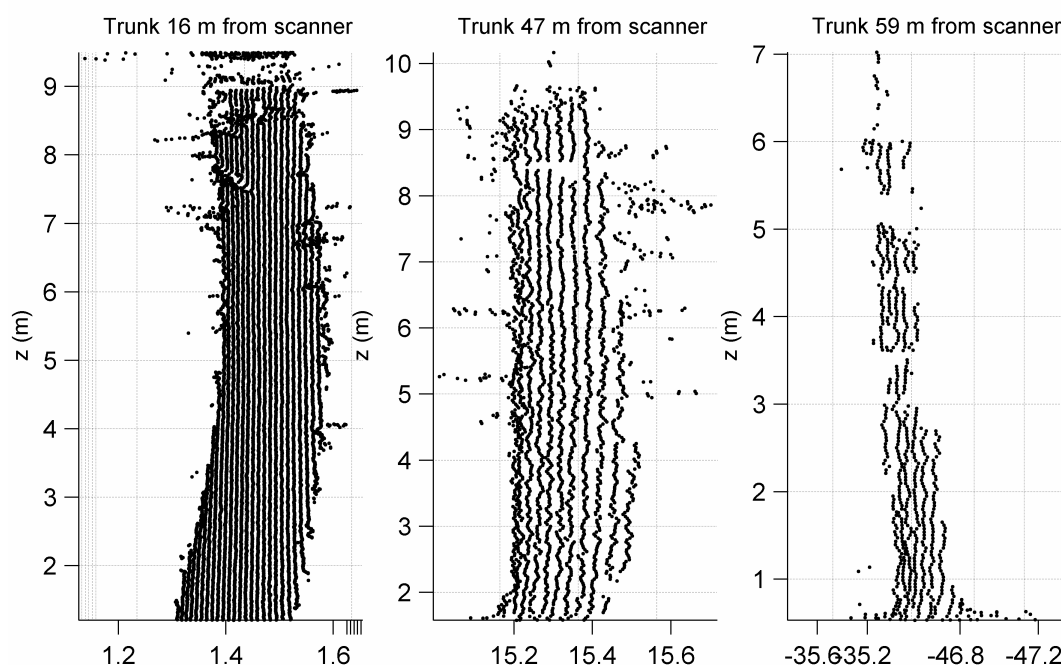


Figure 3: Left and middle: two trunks of approximately the same diameter that are located in different distances from the scanner. Right: a trunk 59 metres away, the point cloud could not be modelled.

A line was fitted to the sweep line points and points that deviated from the linear trend were filtered out to remove the branch points that were in the direction towards the scanner. Before line fitting, points further away from the line median distance than twice the standard deviation were discarded. In Figure 4, the line filter result and the principle are demonstrated. In the left plot, a very noisy set of trunk points is plotted in black and the stem points after line filtering in colours. A single sweep line filtering is shown in the right plot. The original points are plotted in black and the points that are selected as trunk points are plotted in cyan with the fitted line in blue.

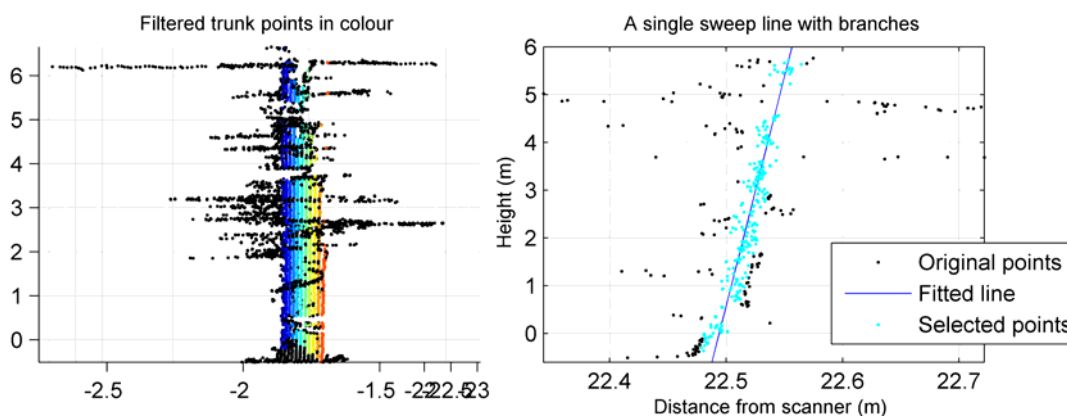


Figure 4: Left: a very noisy point cloud in black dots with the line filtered trunk points in colour. Right: line filter operation in a noisy line: cyan points are selected as true trunk points

To compare the modelling result with DBH reference measurement, the ground level was robustly determined using the histogram of the points inside 1 m radius from the detected trunk point cloud centre.

2.4 Trunk modelling

The trunk was modelled in a two-stage procedure, where first circles were fitted to the trunk point cloud in 20 cm high horizontal slices. The circle-fitting algorithm was least squares where the objective function is the Euclidean distance from points to the circle. The optimization method used was Nelder-Mead. Second the statistics of the distribution of the centre points and radii of the fitted circles were studied and the slices whose circle had a too large or small radius or whose centre was too largely offset from the others were discarded. The model is a collection of circles at different heights along the trunk. For this study we have used one circle per height meter. For each meter, the circle with the least deviation from the fitted radius value was selected. The centre points of the circles represent the stem curve of the tree. The trunk parameters can be estimated at any height between the maximum and minimum height of the model by linear interpolation from the closest circles. The different stages of the filtering and modelling process are shown in figure 5.

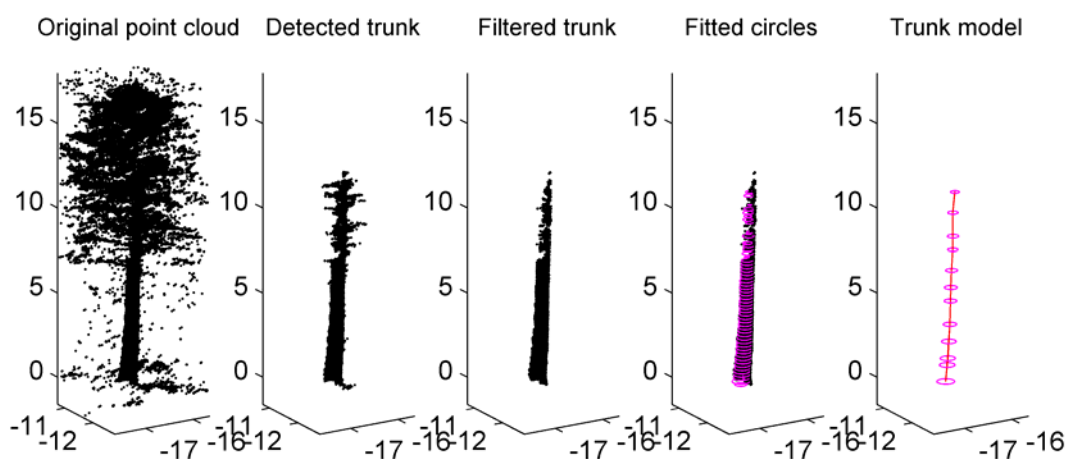


Figure 5: From left: the original point cloud, the detected trunk cluster, filtered trunk point cloud, circles fitted to the point cloud and rightmost the circles selected to form the trunk model.

3. Results

Manual trunk detection was performed on a slice of the pine forest data seen in Figure 2. Faro Scene software was used for the manual measurements. The location of the tree trunk was visually determined and measured from the intensity image of the scanned point cloud; also a 3D-view of the measured points was used to verify the correctness of the measurement. The result for the manual detection is plotted in Figure 6 in red circles. The automatically found and modelled trunks are plotted on the same plot with black crosses (+). In addition to the modelled trunks, there were also trunks that were detected but could not be modelled. These are marked with 'x'. (An example of a trunk point cloud that could not be modelled can be seen in Figure 3, far right.) The small trees marked with green circles in Figure 6 are so narrow that there were not enough scan sweep lines that hit the trunk for successful detection.

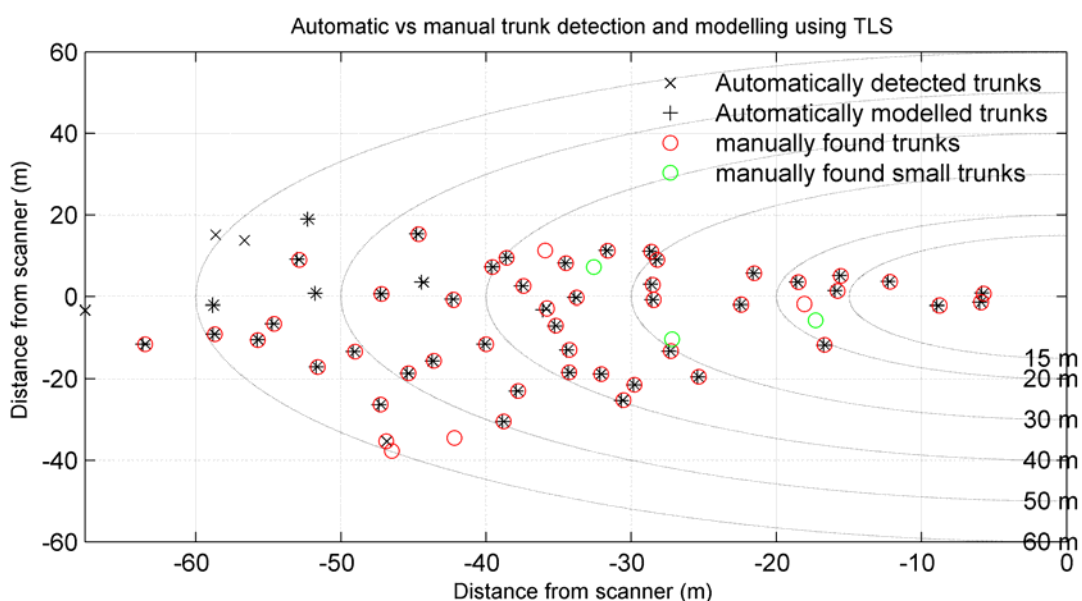


Figure 6: Results for tree trunk modelling in one layer forest. The scanner is in the origo. Black asteriks inside a red circle denotes a succesful detection and modelling. Red circle alone is a trunk that the automate missed. Black asteriks alone is a trunk that was not found manually and black x an automatically found trunk that could not be modelled.

The results for different distance slots from the scanner are presented in Table 1. In the columns “manual”, “automatic” and “automatic/manual%”, the manual result is considered to be true and the success in finding the same trees automatically is reported in the two following columns. There were also four trunks that were found by the automatic system but not by the manual detection, these were located at the distance 40 – 60 m from the scanner. The trunk detection location accuracy could not be evaluated, because the manual location is in the side of the tree and the automatic result is the centre of the trunk. The DBH was not measured manually because the accuracy of the result would be inconstant due to increasing point cloud deviation as the distance from the scanner increases. For trees within 15 m radius from the scanner, on site reference measurement was available. The reference material consists of DBH measures taken clockwise on the plot with no location data. The error from the reference was computed for 10 trees that were inside the 15-meter reference plot, six trees from another data slice (in Figure 7.) that were not in the manual reference were included in addition to the four that can be seen in Figure 6. The Root Mean Squared (RMS) error from the calliper-measured reference was 0.03 m.

Table 1: Detection and modelling results at different distances from the scanner for the slice in Figure 6.

| Distance (m) | Manual | Automatic | Automatic /manual% | Distance (m) | Cumulative detection % |
|--------------|--------|-----------|--------------------|--------------|------------------------|
| 0 – 15 | 4 | 4 | 100 % | | |
| 15 – 20 | 5 | 3 | 60 % | 0 – 20 | 78 % |
| 20 – 30 | 7 | 6 | 86 % | 0 – 30 | 81 % |
| 30 – 40 | 17 | 15 | 88 % | 0 – 40 | 85 % |
| 40 – 50 | 9 | 9 | 100 % | 0 – 50 | 88 % |
| 50 – 60 | 10 | 7 | 70 % | 0 - 60 | 85 % |
| Total | 52 | 44 | 85 % | | |

The cumulative detection percentage is represented two rightmost columns of Table 1. It can be seen that the detection result seems to be high through the distances. In reality, it is likely that small trees exist further away from the scanner also, but they have not been detected in the manual process.

The detection and modelling result for another slice of data is shown in Figure 7. It can be seen that the result is similar to Figure 6. There was no manual reference data for this slice, but visual inspection of the point clouds proved that most of the detected point clouds were trees or of cylindrical shape. Results for both of the slices indicate that the visibility to the scanner is the main factor in detection and modelling success. As the distance to the scanner increases, the point cloud gets sparser. In circle fitting, however, the coverage of the trunk cross section is more relevant to the success of the modelling than the point cloud density.

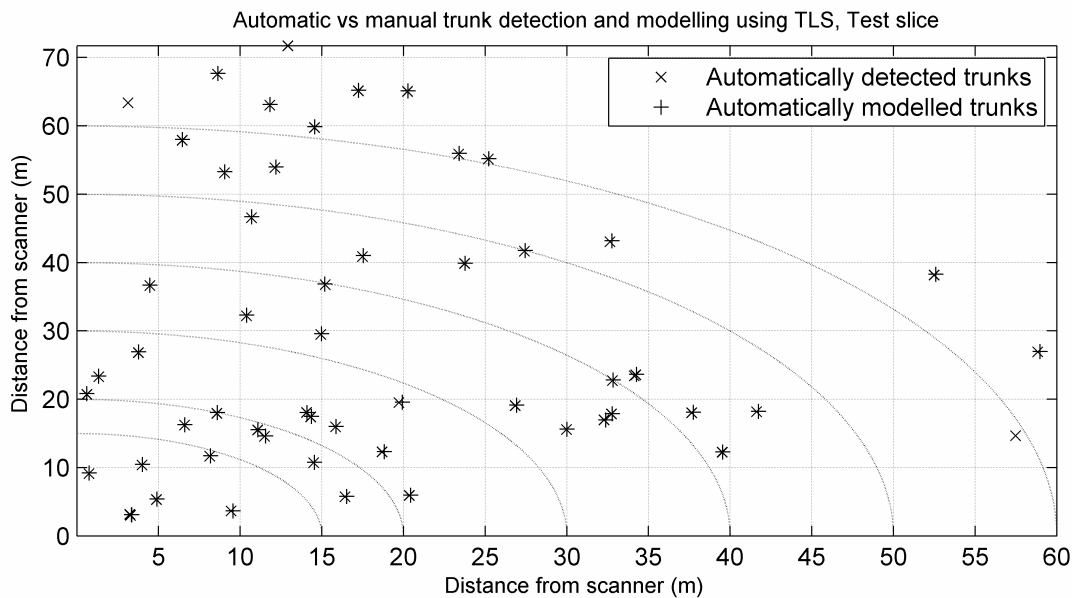


Figure 7: Trunk detection and modelling results for a test slice. The scanner is in the origo. Black x are the centers of trunk point clouds and black + are the centers of trunk models.

In Figures 6 and 7, a modelled trunk is a trunk for which reasonable circles could be fitted and thus DBH, location and volume could be estimated. The trunk models could only be evaluated for DBH measures of the ten trees that were in 15 m distance from the scanner. For full model performance evaluation, field data from several heights is needed. In visual inspection, most of the model circles were well aligned with the trunk point cloud. The estimation of model performance using model deviation from trunk point cloud was not used, because this deviation

does not tell if the model describes the trunk, it only tells if the model fits the points. In close ranges the model deviation from point cloud is mainly indicative of the point cloud deviation (surface noise), further away the number of points is reduced and thus the deviation due to the large number of points is lessened. In high parts of the trunk, occasional branch points can lead to fitting a too large circle with small deviation from point cloud, which visual inspection can prove wrong although the model error is acceptable. This kind of errors cannot be handled if manual reference measurement is not available.

4. Conclusion and discussion

We anticipate that during 2010s, major forest areas in Scandinavia will be assessed using airborne laser scanning. Since the point density of laser scanning is also increasing, it is possible to start using individual tree based forest inventory techniques, which require reference plots having the following capabilities:

- Small amount of dominant tree heights used to calibrate tree height underestimation of ALS
- Location of trees to allow the calibration of tree finding capability of individual tree based inventory
- Tree species classification for the detected trees
- Correct basal area and stem volume of the plot to calibrate applied volume retrieval algorithm

The height underestimation of ALS can be calibrated using e.g. couple of dozen correct height measurements obtained from several plots. High density TLS have previously shown to be superior to hypsometric measurements. The location information can be improved using several single scan TLS measurements without registration, since correct stem number and location of stem is expected to be more important to individual tree based ALS inventory than the knowledge of diameters of each tree. Accurate basal area and stem volume can be obtained even though the accuracy of individual stem diameter estimation would be in the order of several cm. We have a method for retrieving two of the four above listed capabilities, location and volume, and we expect in future studies to be able to model also tree species and dominant tree heights.

The result of this study shows that in one-storey forest it is possible to automatically detect and model trees that are visible to the scanner and within some predetermined distance from the scanner, i.e. fixed plot size. The overall tree detection result of 85 % in 60 m range from the scanner is acceptable, though optimistic when more general plots are considered. Bienert et al (2006a) reported 87 % to 100 % results in single scan mode for 15 m circular plots and 100% for 12 m plot in multiple scan mode. In Bienert et al (2007) 97 % overall detection rate was reported for several 15 m plots and 94 % for a similar size plot with heavy branching. The result presented in Table 1 shows that instead of a distance limit, a visibility limit could be used in single scan TLS tree detection. According to our results, the achievable plot size for a single scan TLS measurement could be larger than the plot sizes used in manual measurements. New reference measurements from larger plots will be needed to validate this assumption.

The modelling part of the work was left with less attention than the detection and filtering parts for two reasons 1: we did not have reference data from many heights and distances 2: we found that a clean trunk point cloud allowed for many different modelling schemes including cylinder- and circle fitting, and the model should be selected only after considering what is the purpose of the data collecting. Inside 15 m the RMS error to reference was 3 cm. Bienert et al (2006a) reported standard deviations from calliper-measured reference between 1.23 and 2.47 cm for different types of plots. In Bienert et al (2007) standard deviation from harvester data was 2.48 cm. In Pfeifer and Winterhalder (2004) a single tree was modelled in multiple-scan mode with

stem point cloud deviation from the model 1.75 cm using cylinders and 1.54 cm using B-splines.

We expect that the by the combined use of higher density ALS and TLS, a universal solution to forest inventory can be developed and the need to use forest inventory models will decrease. In such a concept the problems of plot boundary effects will decrease. We also expect that superior stem volume estimation can be obtained using individual tree based forest inventory compared to the distribution based inventory, since presently the individual tree based forest models (deriving stem volume from DBH and height) produce a significant systematic and random error source. When tree bark structure and the fact that the trunks do not have circular cross sections are considered, the use of DBH measures whose accuracy is very high is questionable. Our study indicates that single scan mode data are of considerable interest in single layer, pine dominated economically exploited boreal forests because the accuracy of the results compared with the multiple scan mode accuracy is eligible especially when processing time is considered.

Acknowledgements

Academy of Finland (Improving forest supply chain by means of advanced laser measurements) and Tekes (Development of automatic, detailed 3D model algorithms for forests and built environment) are acknowledged for financial support.

References

- Aschoff, T. and Spiecker, H., 2004. Algorithms for the automatic detection of trees in laser scanner data. In: Thies, M., Koch, B. Specker, H. and Weinacker, H. (Eds.). IAPRS working group VIII/2 "Laser-Scanners for Forest and Landscape Assessment". Freiburg, University of Freiburg: 66-70.
- Bienert, A., Scheller, S., Kesane, E., Mullooly, G. and Mohan, F., 2006a. Application of terrestrial laser scanners for the determination of forest inventory parameters. In: International Archives of Photogrammetry, Remote Sensing, and Spatial Information Sciences, Vol. 36-5.
- Bienert, A., Maas, H. and Scheller, S., 2006b. Analysis of the information content of terrestrial laserscanner point clouds for the automatic determination of forest inventory parameters. ISPRS WG VIII/11 & EARSeL joint Conference '3D Remote Sensing in Forestry', Vienna, 14-15 February.
- Bienert, A., Scheller, S., Keane, E., Mohan, F. and Nugent, C., 2007. Tree detection and diameter estimation by analysis of forest terrestrial laserscanner point clouds. In: P. Rönholm, H. Hyypä, J. Hyypä (Eds.). Proceedings of the ISPRS Workshop 'Laser Scanning 2007 and SilviLaser 2007'. Espoo.50-55.
- Chasmer, L., Hopkinson, C. and Treitz, P., 2006. Investigating laser pulse penetration through a conifer canopy by integrating airborne and terrestrial lidar. *Canadian Journal of Remote Sensing* 32, 2, 116-125.
- Chernov, N. and Lesort. C., 2005. Least squares fitting of circles. *Journal of Mathematical Imaging and Vision*. 23, 239-251.
- Danson, F.M., Hetherington, D., Morsdorf, F., Koetz, B., and Allgöwer, B., 2007. Forest canopy gap fraction from terrestrial laser scanning. *IEEE Geoscience and Remote Sensing Letters* 4,1,157-160.
- Fleck, S., Obertreiber, N., Schmidt, I., Brauns, M., Jungkunst, H.F. and Leuschner, C., 2007. Terrestrial lidar measurements for analysing canopy structure in an old-growth forest. In: P. Rönholm, H. Hyypä, J. Hyypä (Eds.). Proceedings of the ISPRS Workshop 'Laser Scanning 2007 and SilviLaser 2007'. Espoo.125-129.
- Gorte, B., Winterhalder, D., 2004. Reconstruction of Laser-Scanned Trees using Filter Operations in the 3D-Raster Domain. International Archives of Photogrammetry, Remote Sensing and Spatial Information Sciences Vol. XXXVI, Part 8/ W2: 39-44.

- Gorte, B., Pfeifer N., 2004, Structuring laser-scanned trees using 3D mathematical morphology. *International Archives of Photogrammetry and Remote Sensing*, Vol. XXXV, B5, pp. 929-933.
- Hosoi, F. and Omasa, K., 2006. Voxel-based 3-D modeling of individual trees for estimating leaf area density using high-resolution portable scanning lidar. *IEEE Transactions on Geoscience and Remote Sensing*, 44, 12, 3610-3618.
- Király, G. and Broly, G., 2007 Tree height estimation methods for terrestrial laser scanning in a forest reserve. In: P. Rönholm, H. Hyypä, J. Hyypä (Eds.). *Proceedings of the ISPRS Workshop 'Laser Scanning 2007 and SilviLaser 2007'*. Espoo. 211-215.
- Liang, X, Litkey, P., Hyypä, J., Kukko, A., Kaartinen, H. and Holopainen, M. 2008. Plot level trunk detection and reconstruction using one-scan-mode terrestrial laser scanning data. *IEEE Proceedings of 2008 international workshop on earth observation and remote sensing in Beijing, China Jun 30 - Jul 2*.
- Pfeifer, N., Gorte, B., Winterhalder D., 2004. Automatic reconstruction of single trees from terrestrial laser scanner data. *International Archives of Photogrammetry and Remote Sensing*, Vol. XXXV, B5, 114-119.
- Pfeifer, N. and Winterhalder D., 2004. Modelling of Tree Cross Sections from Terrestrial Laser-Scanning Data with Free-Form Curves. *International Archives of Photogrammetry, remote sensing and spatial information sciences*, Vol XXXVI, part 8/W2, 76-81.
- Thomas, L. and Mili, L., 2007. A robust GM-estimator for the automated detection of external defects on barked hardwood logs and stems. *IEEE Transactions on Signal Processing*, 55, 7, 3568-3576
- Xu, H., Gosset, N. and Chen, B., 2007. Knowledge and heuristic-based modeling of laser scanned trees. *ACM Transactions on Graphics*, Vol 26, No 4, Article 19.

Impact of the sampling design on the quality of ground-based LiDAR datasets

Dimitry Van der Zande¹, Inge Jonckheere¹, Jan Stuckens¹, Willem Verstraeten¹ & Pol Coppin¹

¹Katholieke Universiteit Leuven, Biosystems Departement, M3-BIORES, Celestijnenlaan 200, BE-3001, Leuven, Belgium dimitry.vanderzande@biw.kuleuven.be

Abstract

This research was undertaken to study the influence of the sampling design and laser beam density of ground-based LiDAR measurements on the quality of laser datasets in terms of shadowing. The generation of virtual forest stands by means of stochastic L-systems as tree descriptors were opted for based on the study frame. The dynamic plant modeler and plant nursery natFX (Bionatics, CIRAD, Montpellier, France) was used to simulate full grown forest stands of two tree species (i.e. *Fagus sylvatic* and *Platanus acerifolia*). Next, hemispherical laser measurements with different laser beam densities were simulated according to three different sampling patterns (i.e. single, diamond, and corners) inside these virtual forest stands through the use of ray-tracing technology. An adjusted sampling design has proven its effectiveness since an average decrease of 27.27% in shadowing in comparison with a single measurement was obtained. This contrasts with an average decrease of 13.64% by increase of the laser beams density by a factor 25. Afterwards, contact frequency values, calculated from the virtual laser data sets, were utilized to successfully model the shadowed parts of the canopy demonstrating the potential of ground-based laser scans to capture the 3D leaf distribution inside a full grown forest stand.

Keywords: ground-based LiDAR, virtual forest stands, sampling design, shadow effect

1. Introduction

One of the challenges of Light Detection And Ranging (LiDAR) research in forestry is the quantification of the 3D structure of forest canopies and their components (individual tree crowns) in an accurate and comprehensive manner. The forest canopy is a unique part of the forest ecosystem which fulfills the important role of cycling material and energy through photosynthesis and transpiration, maintaining forest microclimates, and providing habitats for various species (e.g. Erdelen, 1984; Fitzjarrald and Moore, 1995). The description of the structure of this interface between vegetation and atmosphere plays a key role in the understanding of biophysical processes at different levels.

Ground-based LiDAR systems offer unique opportunities in terms of viewing angles and point densities needed to model canopy structure in high detail. The static setup of a ground-based laser scan, in comparison with a moving airborne platform, allows comprehensive beam coverage of the area of interest. Several studies on ground-based LiDAR systems have used one or a combination of single range imagery to make individual tree measurements or plot level summaries (e.g. Radtke and Bolstad, 2001; Parker *et al.*, 2004; Watt and Donoghue, 2005). Hitherto, applications exploring the use of scans acquired from multiple viewpoints to assess the spatial distribution of canopy structure are rare (Henning and Radtke, 2006, Takeda *et al.*, 2007, Hosoi and Omasa, 2006). The biomass profile, being the vertical distribution of phyto-elements (leaf, stem, twig, etc.) density above the ground, is the most commonly used parameter to describe

the biomass distribution in the measured forest stands. This vertical structure is often represented by the leaf area density (LAD) per height bin, where LAD is defined as the total one-sided leaf area per unit layer volume (Weiss *et al.* 2004) for a vertical stratified canopy. The LAI/LAD calculation from multi angular laser data can be based on the inclined point quadrat method by Warren-Wilson (1960, 1963) or on gap fraction inversion, a methodology also used to determine LAI of a forest stand using hemispherical photographs. Hosoi and Omasa (2006) described a methodology for voxel based 3D modeling of the LAD by calculating the contact frequency of the laser beams in an arbitrary volume.

The level of detail in which the LAD distribution can generally be determined strongly depends on the laser beam distribution inside the forest canopy. This varies with the distance to the laser device and the leaf density of the measured space which causes shadowing (Van der Zande *et al.*, 2006). In case of a first return laser device, the laser measurement variability along angular viewing differences, or shadowing, is caused by the physical laser pulse/object interactions and is an intrinsic characteristic of the laser device. This is due to reflection of an emitted laser pulse by the first object it encounters. Spatial information of the vegetative elements located behind the target/object is therefore not available due to the shadow effect. Consequently, these background objects have to be measured from different angles to obtain comprehensive laser coverage. When quantifying the distribution of the vegetative elements inside a canopy, this shadowing needs to be minimized, firstly to secure a certain accuracy of the contact frequency measurements per volume of choice and secondly to minimize the ‘blind spots’ or areas of which no information could be gathered.

To enable an accurate study of the interaction of laser beams with a complex organized object like a canopy, a detailed description of the 3D organization of the vegetative elements in the canopy is required. The lack of detailed, consistent, and precise reference information of forest structure hinders this approach. A solution is offered by simulation techniques which enable the reconstruction of forest stands in a virtual environment. Structural aspects such as leaf surface distribution are calculated directly during the simulation process, resulting in the generation of accurate reference data of the virtual forest stand. LiDAR range images can subsequently be acquired using ray tracing algorithms. Ray tracing algorithms are based on tracing the path of a ray of light through a scene as it interacts with objects in an environment and therefore strongly resembles the LiDAR principles. This technique allows detailed studies of light beam/canopy interactions and their effect on the quality of the LiDAR measurements which is only limited by the degree of complexity of the reconstructed forest stand. From remote sensing modeling point of view, it is important to obtain realistic descriptions of the forest stand, which complies with three main criteria: (1) a description based on architectural growth processes capable of simulating various tree species over various conditions (age, density, environment, etc.); (2) a description based on experimental data; and (3) a description capable of providing realistic 3D trees. The AMAP model (Atelier de Modelisation et d’Architecture des Plantes), developed by CIRAD (Montpellier, France), meets these criteria making it a valuable tool for simulating forest stands for quality testing of LiDAR measurement protocols. The AMAP model is a growth simulation software that respects the plant’s genetic coding and reconstitutes the tree morphology and natural esthetics in synthetic 3D images. These canopy models have gained acceptance as a research tool in forestry and have led to increasingly convincing visualizations due to recent developments in information technology, more specifically in the field of simulation technologies (Jonckheere *et al.*, 2006).

This research studies the influence of the sampling design and laser beam density of ground-based LiDAR measurements on the quality of the collected laser datasets in terms of shadowing. A total of three virtual forest stands were generated, varying in tree species (i.e. *Fagus sylvatica*, *Platanus acerifolia*) and thus structural built-up. Next, ray-tracing technology allowed for the simulation of hemispherical laser measurements, with varying laser beam densities, inside these virtual forest

stands. These individual laser measurements were simulated in three different sampling patterns (i.e. single, diamond, and corners) to determine the optimal sampling design guarantying a minimal shadow effect.

2. Materials and Method

2.1. 3-D canopy simulation

Two homogeneous forest plots with fully grown broadleaf trees (*Fagus sylvatica*, *Platanus acerifolia*) were simulated in a virtual environment using the dynamic plant modeler and plant nursery natFX (Bionatics, CIRAD, Montpellier, France) that interfaces with an architectural plant model called AMAP (CIRAD, Montpellier, France). A forest plot consisted of four individual trees of the same specie placed in a regular pattern in a 3D volume with a ground surface of 15 m side and a height of 30 m. The total LAI of the forest plots was calculated during the simulation process and was 4.50 for the *Fagus* stand and 5.15 for the *Platanus* stand. The architectural differences between the species (Fig. 1) resulted in structural diversity between the forest plots enabling a robust analysis of the factors influencing shadowing and thus the quality of the LiDAR datasets.

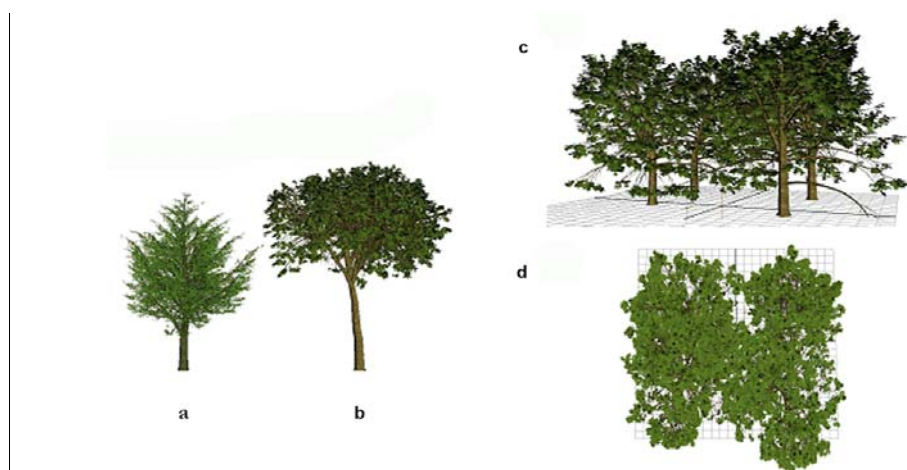


Fig. 1. Fully grown broadleaf trees of three species were simulated in a virtual environment using the Bionatics plant nursery, natFX: (a) *Fagus sylvatica*, (b) *Platanus acerifolia*. A forest plot consisted of four individual trees of the same specie placed in a regular pattern (c,d).

2.2. Laser measurement simulation

Tracking of the virtual laser beams through the canopy was done using the physically based rendering theory (pbrt, Pharr & Humphreys, 2004) as ray-tracer algorithm. Viewing rays can be shot into the scene to see whether they interact with any of the objects in the scene (Pharr and Humphreys, 2004), which strongly resemble the LiDAR principles. Specifications of the commercially available Laser Measurement System 200 (LMS200, Sick AG, Germany) were used as a standard template to characterize simulated laser beams (i.e. wavelength and beam divergence) and hemispherical measurement pattern (GMP). The LMS200 is a non-contact optical active sensor which scans its direct surroundings in a 2D pattern. By mounting it on a dynamic measurement platform like a rotating table, a 3D hemispherical measurement pattern is enabled. The full description of the characteristics of the laser device and measurement platform can be found in Van der Zande et al. (2006). To reproduce the hemispherical GMP for the virtual laser beams, the environmental camera of the pbrt-package was selected. This camera traces rays in all directions around a specific point in the scene (i.e. laser measurement location). Each beam

was described by its polar coordinates (φ, α), where the zenith angle (α) ranged from 0 to $\pi/2$ and the azimuth angle (φ) from 0 to 2π . The zenith resolution was fixed at 0.25° while the azimuth resolution was set at 0.1° and exceptionally at 0.02° for the central standard measurements. Different laser beam densities were acquired by adjusting the azimuth resolution of a laser scan by considering portions of the emitted laser beams. Each laser beam was traced up to the first vegetative element (represented as a collection of triangles) it interacted with. As the LMS200 was used as a template, at least 10% of the emitted light energy had to be reflected in order for the virtual laser system to register a distance measurement (Sick, AG).

2.3. Sampling design

By measuring a canopy scene from different directions the probability that a certain vegetative element (e.g. leaf) is reached by at least one laser beam increases since a more comprehensive laser beam coverage of the measured object is obtained. In this study, three different sampling strategies were investigated: (1) single, (2) diamond and (3) corners (Fig.2).

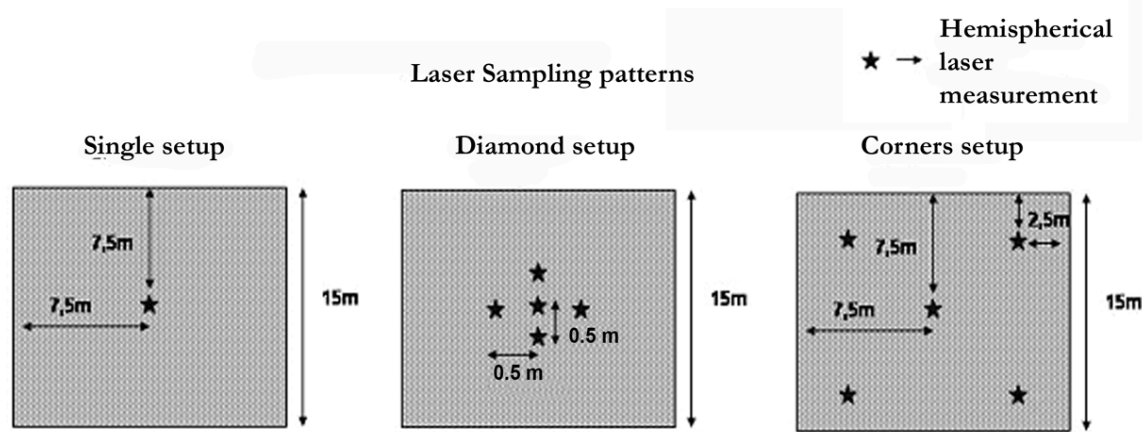


Fig. 2. Illustration of the three different sampling designs tested in this study: single, diamond and corners. The last two setups consisted of five individual hemispherical laser measurements positioned in a specific geometric format while the central setup function as a reference measurement.

The last two sampling designs consisted of five individual hemispherical laser measurements positioned in a specific geometric format (Fig.2) in an effort to minimize the shadow effect. By altering the azimuth resolution of the individual hemispherical measurement, different laser beams densities were available per measurement setup (Table 1). For comparison purposes, the azimuth resolution of the central single measurement was chosen so that the total amount of emitted laser beams matched that of the combination of the five separate laser scans of the diamond and corners setups.

Table 1. Alternation of the azimuth resolution of the hemispherical laser scans resulted in different laser beams densities per measurement

| # laser beams (millions) | Single (azimuth angle) | Diamond & Corners (azimuth angle) |
|--------------------------|------------------------|-----------------------------------|
| 6.48 | 0.02° | 0.10° |
| 3.24 | 0.04° | 0.20° |
| 1.30 | 0.10° | 0.50° |
| 0.65 | 0.20° | 1.00° |
| 0.26 | 0.50° | 2.50° |

2.4. Laser data processing

A single hemispherical laser measurement consisted of 259,200 up to 6,480,000 separate distance measurements depending on the resolution set up (Table 1). Each laser beam was characterized by a zenith angle, an azimuth angle and a beam divergence. The voxel-based contact frequency (Hosoi and Omasa, 2007) was generated in three steps from the virtual LiDAR datasets:

1) *Registration*: The five datasets of the diamond and corners setup, with their own coordinate system, were registered into a single comprehensive laser data set or 3D point cloud using a standard translation and rotation algorithm based on their known relative positions;

2) *Voxelization*: The 3D space considered was arbitrarily subdivided into ‘small’ cubic voxels of 10 cm in side. This resulted in voxel arrays of 150 x 150 x 250 voxels. Following the methodology of Hosoi and Omasa (2006), the ‘small’ voxels were characterized depending on beam/voxel interaction. For voxels with at least one intercepted laser beam attribute 1 was assigned. Attribute 2 was assigned to voxels that were intersected by laser beams without interception. Attribute 3 was granted to voxels that were not touched by any laser beam.

3) *Contact frequency calculations based on LiDAR measurements*: The ‘small’ voxels were grouped into ‘large’ voxels of 100 cm in side consisting of 1000 ‘small’ voxels each. The contact frequency (CF) for each ‘large’ voxel was calculated as follows:

$$CF(\theta) = n_1 / (n_1 + n_p) \quad (1)$$

With n_1 the number of ‘small’ voxels with attribute 1 and n_p the number of voxels with attribute 2. The contact frequency was calculated for each ‘large’ voxel and could then be extrapolated to the small voxels which could not be reached by any beam (i.e. voxels with attribute 3). Only the laser beams exiting a voxel in the opposite side as from which they entered were considered as passing beams. This ensured a minimal traveling path of 10 cm through the voxel for an accurate contact frequency calculation.

3. Results

3.1. Relative shadow effect

The extent of the shadow effect was investigated by determining the number of effectively ‘filled’ voxels that were hit by at least one laser beam that interacted with the leaf material (i.e. voxels with attribute 1). The relative shadow effect (RS) was calculated as the proportion of ‘filled’ voxels which were not seen by the laser system, these filled voxels were incorrectly given the attribute 2 or 3 instead of attribute 1. Fig. 3 shows the RS-values for each of the different sampling patterns in the two forest stands and this for five resolution settings.

The average shadow effect for a single laser scan ranged from 68.74% to 82.38% depending on the beam density. This means that an increase of the number of laser beams with a factor of six reduced the shadow effect by 13.64%. The logarithmic character of the decrease of RS with increasing number of laser beams demonstrated that tackling the shadowing problem by sheer hardware improvement would not be cost-efficient. These results support the need for adjusted sampling designs of multiple laser scans from different locations to improve the probability that voxels would be reached by at least one laser beam. In the case of the diamond set-up the average RS-values ranged from 46.67% to 74.4%. This decrease of 27.75% due to increasing resolution settings differed significantly from the decrease of 13.64% in the case of a single measurement. These results also show that the use of five low resolution scans instead of one high resolution scan, with a similar amount of total laser beams, significantly reduced the

shadow effect with 27.75%. Considering the RS-values, the corners sampling design showed results similar to the diamond set-up. Fig. 4.b illustrates the direct comparison of the vertical distribution of the filled voxels (attribute 1) derived from the LiDAR datasets with the reference profile and this for the different sampling designs. The shadow effect becomes visible as the measured profiles show an underestimation compared to the reference profile. This underestimation is considerably higher in case of the single LiDAR measurement compared to the diamond and corners setups which is consistent with previous results (Fig. 4). The general shape of the reference profile is observable in the three measured profiles showing the potential of laser systems, like the LMS200, to capture essential structure information which could be used to model the actual leaf distribution.

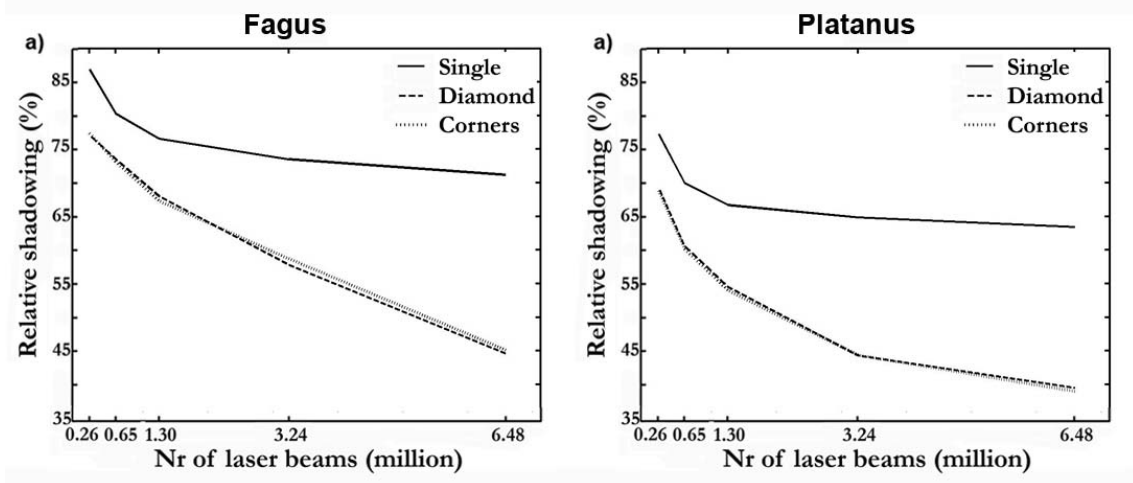


Fig. 3. The relative shadowing (RS) decreased significantly as a function of the different sampling setups for the two virtual forest stands ((a) Fagus and (b) Platanus). The diamond and corners setup were compared to the single design.

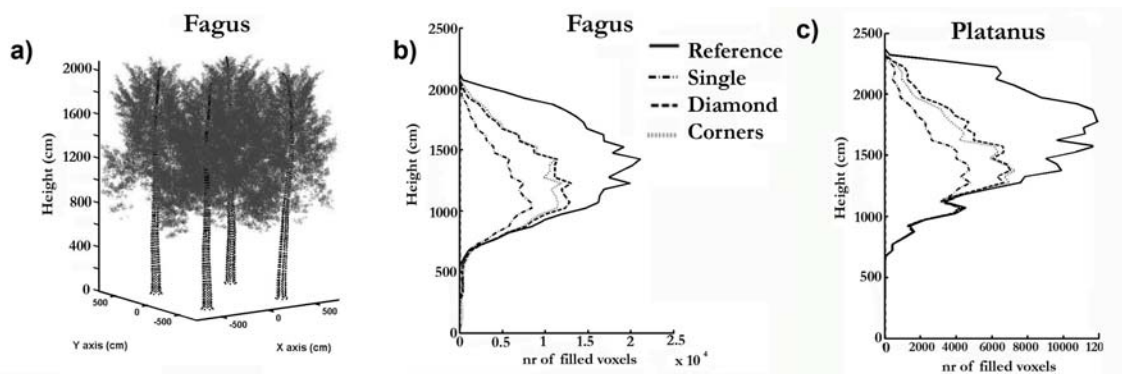


Fig. 4. Direct comparison of the vertical distribution of the filled voxels (attribute 1) derived from the LiDAR datasets with the reference profile for the different sampling designs (Fagus (a,b), and Platanus (c)).

3.2. 3D distribution of the shadow effect

The 3D distribution of the measured filled voxels, and thus also the 3D shadowing, were visualized as a collection of horizontal slices for the different sampling patterns in the Fagus stand (Fig. 5). The availability of this detailed 3D description of the shadow effect enables a more thorough analysis of the actual laser beam/canopy interaction. Where the study of the

relative shadowing did not reveal a significant difference between the diamond and corners setup, this 3D study exposed that the central area suffered mostly from shadowing and that this is more profoundly present in the corners measurements. The peripheral areas on the other hand, are less affected by the shadowing using this last set-up.

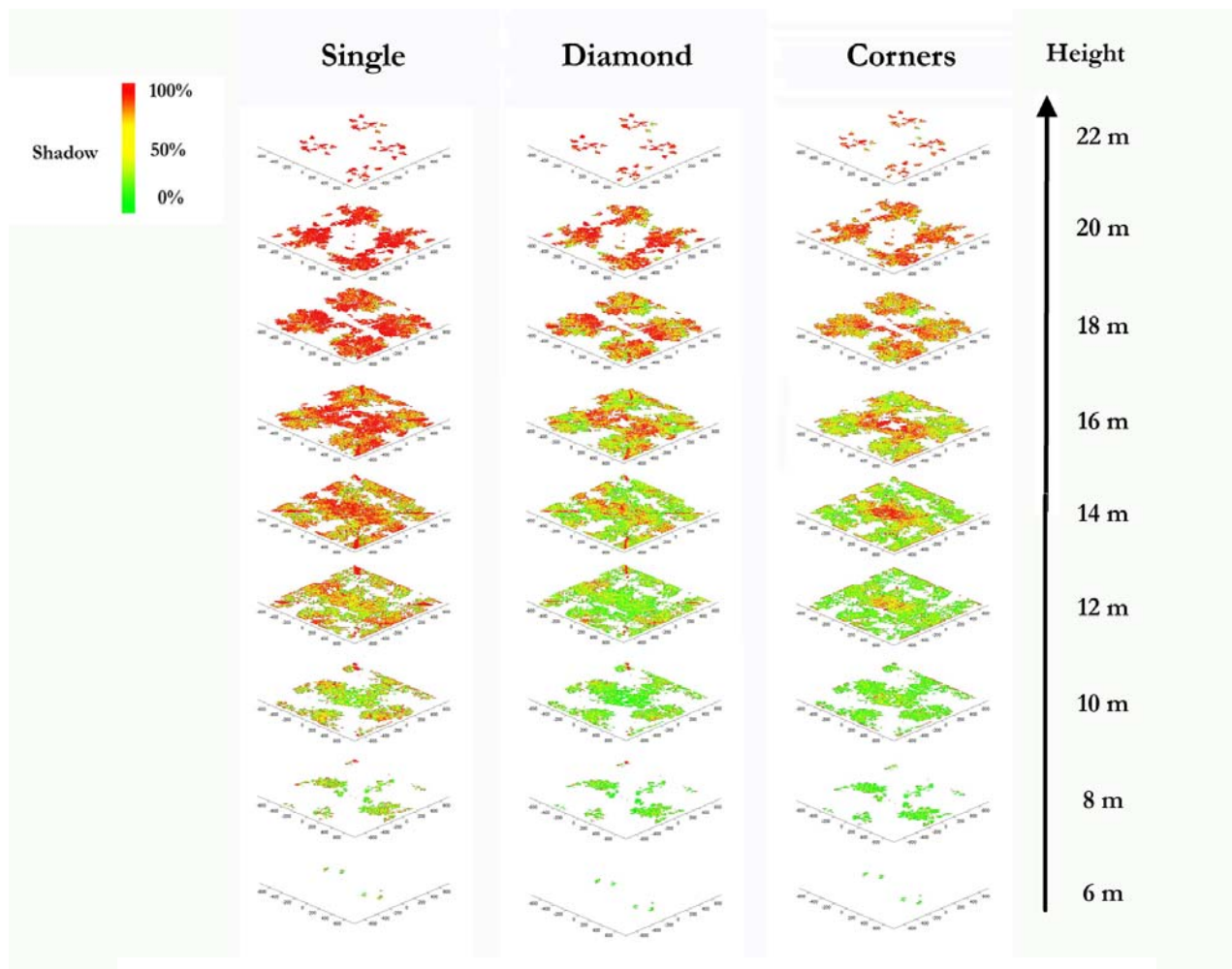


Fig. 5. The 3D distribution of the measured filled voxels. The 3D shadowing is visualized as a collection of horizontal slices for the different sampling patterns in the Fagus stand.

3.3. Contact frequency calculations for modelling purposes

Whereas an adjusted sampling design shows great potential in minimizing this effect, values of up to 55% are still detected. This means that for an accurate structural description of the actual leaf distribution, at least 55% of the canopy needs to be modeled using the information extracted from the measured parts of the canopy. Up to this point only the voxels with attribute 1 were used for the analysis enabling the shadow effect mapping. In order to correct for the shadow effect, more information needs to be extracted from the LiDAR datasets. This is done by including the empty voxels (voxels with attribute 2) in the further analysis. The method presented by Hosoi and Omasa (2006) introduced the calculation of contact frequencies per unit of volume from the ratio calculated using Eq. 1. This ratio is then extrapolated to the voxels in that unit of volume for which no information is available (i.e. voxels with attribute 3). This methodology was used to study the potential capacity of a LiDAR scanner to estimate the real leaf distribution in forest canopies. The large voxels that had a coverage of 100% were analyzed as an accuracy assessment for the estimation of the leaf density inside those large voxels. For

the diamond setup in the Fagus stand, a total of 1807 voxels (37% of total) were available for analysis. A linear regression between the calculated contact frequency and the actual leaf density resulted in a R^2 -value of 0.97. The linear regression model showed an underestimation of 22% which could only be caused by leaf/laser beam interactions since every small voxel in the considered large voxels had been scanned and no direct shadow effect was present. The large voxels were grouped according to their laser coverage and on each of these groups this accuracy assessment described above was repeated. Table 2 presents the linear relations between the contact frequencies, calculated from the diamond and corners LiDAR datasets, and reference datasets. The decreasing laser coverage results in decreasing slopes of the linear regressions. This indicates that the degree of underestimation of the leaf densities from contact frequencies increased with shadowing. While these underestimations reach values up to 89.00%, the R^2 values indicated that even with low laser coverage an accurate estimation of the leaf density is possible.

Table 2. The slope and R^2 -values of the linear relations between the contact frequencies, calculated from the diamond and corners LiDAR datasets, and reference datasets are presented.

| Laser Coverage | Fagus | | | | Platanus | | | |
|----------------|---------------|----------------|---------------|----------------|---------------|----------------|---------------|----------------|
| | Diamond slope | R ² | Corners slope | R ² | Diamond slope | R ² | Corners slope | R ² |
| Full | 0.78 | 0.97 | 0.80 | 0.98 | 0.90 | 0.94 | 1.00 | 0.99 |
| 80%-100% | 0.45 | 0.86 | 0.52 | 0.89 | 0.59 | 0.82 | 0.85 | 0.81 |
| 60%-80% | 0.21 | 0.85 | 0.29 | 0.90 | 0.39 | 0.78 | 0.74 | 0.84 |
| 40%-60% | 0.15 | 0.86 | 0.21 | 0.85 | 0.39 | 0.78 | 0.71 | 0.83 |
| 20%-40% | 0.09 | 0.74 | 0.12 | 0.71 | 0.37 | 0.69 | 0.90 | 0.60 |
| 0%-20% | *** | *** | *** | *** | *** | *** | 1.38 | 0.39 |

Using these findings, two sets of correction factors per laser coverage class were extracted enabling the correction of the leaf density estimation based on measured contact frequencies. Fig. 6 demonstrates the corrected profiles in comparison with the reference profile. This proved the potential of the ground-based LiDAR technology to measure complex structure of objects such as forest canopies. Even when shadowing and leaf/laser beam interactions are responsible for the fact that almost 55% of the leaves could not be measured, the LiDAR datasets still contain enough information to accurately describe the distribution of vegetative elements in a 3D space.

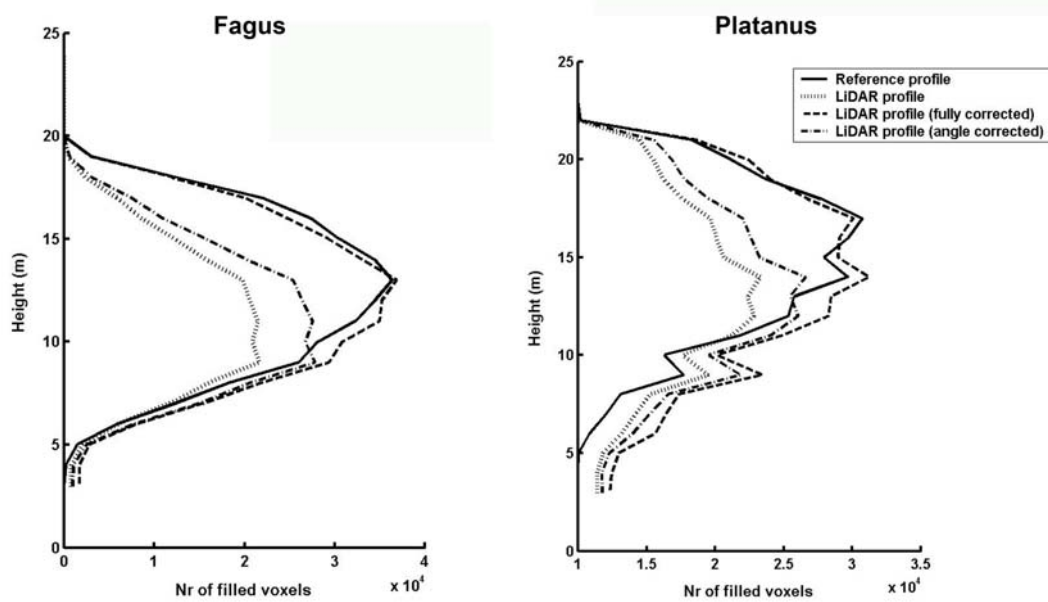


Fig. 6. Comparison of the corrected (angle corrections and full corrections) with the reference profile.

4. Discussion

This paper explored the potential of simulation and ray tracing techniques for structural algorithm development for LiDAR datasets. The results showed substantial improvements in the quality of the datasets when measuring a forest stand from different locations in comparison with a single measurement. This allowed laser beams to enter the canopy under a variety of angles and directions and that increased the probability of a laser beam to penetrate the canopy deeper than it would be possible when measuring from a single location. This caused a decrease of the shadow effect, as it also enabled more accurate density estimates of the shadowed parts of the canopy. In order to maximize the quality of the LiDAR datasets, these results suggest a combination of the diamond and corners sampling setups. However, an increase in the number of separate laser scans would in reality imply more labor and time consuming field campaigns, a factor of unimportance in virtual LiDAR studies. The registration of the separate laser scans to one comprehensive scan was errorless in this controlled environment while under real circumstances the combined registration error could negatively affect the results. Hence, a delicate balance should be pursued between the number of measurement positions and the shadow effect.

Acknowledgements

We would like to acknowledge the useful technical information about the LMS200 by Sick, A.G. (Germany), and their willingness to contribute to this project. Funding support for this project has been provided by FWO Flanders (Project no. G.0407.05). Finally, credit is due to Cas Van der Zande for creating the right atmosphere for the writing of this paper.

References

Erdelen, M., 1984. Bird communities and vegetation structure. I. Correlations and comparisons of simple and diversity indices. *Oecologia*, 61, 277–284.

- Fitzjarrald, D.R., and Moore, K.E., 1995. Physical mechanisms of heat and mass exchange between forest and the atmosphere. In: M. Lowman, and N. Nadkarni (Eds.). *Forest Canopies*. Academic Press, California, USA, 45–72.
- Henning, J.G., and Radtke P.J., 2006. Ground-based laser imaging for assessing three-dimensional forest canopy structure. *Photogrammetric Engineering and Remote Sensing*, 72 (12), 1349-1358.
- Hosoi, F., and Omasa, K., 2006. Voxel-Based 3-D Modeling of Individual Trees for Estimating Leaf Area Density Using High-Resolution Portable Scanning Lidar. *IEEE Transactions on Geoscience and Remote Sensing*, 44 (12), 3610-3618.
- Jonckheere, I., Nackaerts, K., Muys, B., Van Aardt, J., and Coppin, P., 2006. A fractal dimension based modelling approach for studying the effect of leaf distribution on LAI retrieval in forest canopies. *Ecological Modelling*, 197 (1-2), 179-195.
- Parker, G.G., 1995, Structure and microclimate of forest canopies. In: M. Lowman, and N. Nadkarni (Eds.). *Forest Canopies*. Academic Press, California, USA, 73–106.
- Parker, G.G., Harding, J.H., and Berger, M.L., 2004. A portable LIDAR system for rapid determination of forest canopy structure. *Journal of Applied Ecology*, 41, 755–767.
- Phar, M. and Humphreys, G. (Eds.), 2004. *Physically Based Rendering: from Theory to Implementation*. Morgan Kaufmann Publishers, San Fransisco, USA.
- Radtke, P.J. and Bolstad, P.V., 2001. Laser quadrat sampling for estimating foliage-height profiles in broad-leaved forests. *Canadian Journal of Forest Research*, 31, 410–418.
- Takeda, T., Oguma, H., Sano, T., Yone, Y., and Fujinuma, Y., 2007. Estimating the plant area density of a Japanese larch (*Larix kaempferi* Sarg.) plantation using a ground-based laser scanner. *Agricultural and Forest Meteorology*. In press.
- Van der Zande, D., Hoet, W., Jonckheere, I., van Aardt J., and Coppin, P., 2006. Influence of measurement set-up of ground-based LiDAR for derivation of tree structure. *Agricultural and Forest Meteorology*, 141 (2), 147-160.
- Warren-Wilson J., 1960. Inclined point quadrats. *New Phytologist*, 59, 1-8.
- Warren-Wilson J., 1963. Estimation of foliage denseness and foliage angle by inclined point quadrats. *Australian Journal of Botany*, 11, 95-105.
- Watt, P. and Donoghue, D., 2005. Measuring forest structure with terrestrial laser scanning. *International Journal of Remote Sensing*, 26 (7), 1437–1446.
- Weiss, M., Baret, F., Smith, G.J., Jonckheere, I., and Coppin, P., 2004. Review of methods for in situ leaf area index (LAI) determination. Part II. Estimation of LAI, errors and sampling. *Agricultural and Forest Meteorology*, 121 (1-2), 37-53.

Accuracy and efficiency of the Laser-camera

Timo Melkas¹, Mikko Vastaranta² & Markus Holopainen²

¹Metsäteho Ltd, Finland, timo.melkas@metsateho.fi

²University of Helsinki, Department of Forest Resource Management, Finland,
mikko.vastaranta@helsinki.fi, markus.holopainen@helsinki.fi

Abstract

A new measuring device – the Laser-camera - was tested under typical forest conditions. With the device, constructed of a Canon EOS 400D digital reflex camera with an integrated Mitsubishi ML101J27 laser line generator, diameters of trees can be measured from the centre of a sample plot without having to visit the trees. The Laser-camera's principle is based on the reflection of a laser line and a point on a tree stem and the processing of digital images. The study material was gathered during the period in 2007-2008 from 13 circular sample plots and included a total of 728 diameter measurements from 265 trees. The standard error of the diameter observations, using semiautomatic interpretation, was 6 mm (5.3%). The accuracy of the diameter observations (standard error) was maximum for spruce (5.0 mm, 4.4%, followed by birch (6.4 mm, 3.3%) and pine (7.6 mm, 7.6 %). The most common errors were caused by the laser point not hitting the tree stem, branches in front of the stem hampering visibility or incorrect definition of the direction and height of the measurement. Overall tree diameter measurements can be obtained with a Laser-camera rapidly (10 s/tree) and with good reliability and efficiency. The future goal will be to integrate laser technique with an altimeter, data collection unit and GPS receiver inside a weatherproof Laser-camera device. This will enable ready checking of the measurement results in the field from the screen of the digital camera and the measuring of the diameters at any height of a tree, the heights, locations, as well as quality variables of trees.

Keywords: forest mensuration, stem diameter, laser, image processing, digital camera

1. Introduction

Tree diameter is one of the most important stand variables used in forest resource inventory, forest planning and timber measuring. Diameter-at-breast height ($d_{1.3}$) is in most cases the independent variable in single-tree and stand-level models describing the growing stock. Decisions concerning forest management procedures (silvicultural treatments, thinnings and final cuttings) are often made either directly or indirectly from tree diameter measurements. Tree diameter has traditionally been measured using a various callipers or a tallmeter. The use of such devices has always required the observer to visit the tree.

The future of forest resource inventory and forest planning will be based to an increasing extent on remote-sensing, airborne laser scanning (ALS) and methods based on digital photogrammetry. Remote-sensing methods give results at least as accurate in measuring standwise total volume (e.g. Naesset 2004; Naesset *et al.* 2004; Holmgren 2003) and single-tree information (e.g. Hyypä and Inkinen 1999; Korpela 2004; Korpela *et al.* 2007; Hyypä *et al.* 2004-2007; Maltamo *et al.* 2004) as traditional field measurement methods that are used in operative forest planning.

Field measurements that are based on traditional methods are expensive, hence the need to develop more accurate, efficient and simple ways to measure growing stock variables. The objective is to develop a method that does not require actual visits to the tree, i.e. remote-sensing methods that are used from within the forest.

Terrestrial laser scanning (TLS) methods have brought new opportunities to the measurement of growing stock attributes, particularly those that measure tree quality (Jutilla *et al.* 2007, Henning ja Radtke 2006, Watt ja Donoghue 2005, Hopkinson *et al.* 2004). Currently, however, postprocessing of TLS data is laborious and time-consuming due to the lack of available algorithms and software programs with which one can generate attributes that depict the desired sample plot growing stand attributes from 3D data clouds collected by the TLS (Watt and Donoghue 2005). TLS research in the field of forest applications has so far focused mainly on the estimation of single sample plots and individual tree attributes, not on the development of inventory methods applicable to large forest areas.

TLS has been used on the stand level in projects aiming at developing ways to combine two-dimensional laser observations with harvester measuring (Miettinen *et al.* 2007). The aim of these studies was to develop an automatic method for the mapping of tree locations (Forsman and Halme 2005) and to define the diameter distributions of a stand (Jutilla *et al.* 2007). Based on the spatial information gathered and the diameter distribution, it is then possible to formulate a plan for the removal of trees.

Laser-based devices for the measurement of tree diameter have been developed and tested, e.g. in the United States (Carr 1992, 1996; Williams *et al.* 1999), but the devices have not been easy enough to use efficiently and their prices have not been competitive against traditional forest-planning measurement devices (Skovgaard *et al.* 1998; Parker and Matney 1999). Devices that are based on multisensor systems or laser technologies have likewise not been reliable enough in terms of diameter measurements; the measurement accuracy was in one case 19.6 - 24.6 mm (Clark *et al.* 2001).

Kalliovirta *et al.* (2005) developed a device - the Laser-relascope - that enables measurement of tree variables without having to visit the tree. The device includes a laser rangefinder, a variable-width slot with a fixed-length arm, an electronic altimeter, a data collection/processing unit, and a Global Positioning System (GPS) receiver and makes it possible to measure the diameter distribution of a sample plot and the heights and locations of the trees from the centre point of the sample plot. It uses distance and angle information to determine the diameter of a tree and functionally is a combination of a relascope and dendrometer. The standard error of the diameter measurements was 8.2 mm at best (Kalliovirta *et al.* 2005). The accuracy was dependent on the distance, measuring time of a tree, $d_{1,3}$, the observer and the individual's familiarity with the laser-relascope (Kalliovirta *et al.* 2005, Laasasenaho *et al.* 2002). The standard error varied from 6.8 mm to 15.8 mm depending on the observer (Laasasenaho *et al.* 2002). Measuring precision of the height (S.D. 4.9 cm) and the location (32 cm) measurements were favourable and unbiased (Kalliovirta *et al.* 2005).

The goal of Ojanen (2005) was to develop a method to measure tree diameters with a ± 5 mm level of uncertainty and to eliminate error caused by the observer. The method tested in laboratory conditions is based on laser technology, digital camera technique and digital image processing. The optimal measurement distance varied between 1 - 15 meters. The Laser-camera is the first prototype in which the method was tested under forest conditions.

Varjo *et al.* (2006) studied the accuracy of diameter measurements at different heights of the stem using a simple digital camera (Canon PowerShot). A method was developed in which a tapering model (Lappi 1986) was used in supervising the image interpretation (Juujärvi *et al.* 1998). The distance to the tree was defined by using laser distance-measuring device. The geometry of the image plane of the camera in relation to the tree measured was solved automatically using a reference marker stick in front of each tree and trigonometry.

The aim of this study was to determine the efficiency and accuracy as well as technical feasibility and adaptability of a laser- and digital photography-based device under forest conditions. The Laser-camera was developed at the Centre for Metrology and Accreditation with the objective to develop a device for the measurement of growing stock variables (diameter distribution, tree heights, locations and quality attributes) from the centre of a sample plot, without having to visit the trees. The focus of the study was on the improvement in diameter measurement accuracy elimination of error caused by the observer and integration of laser technology with a digital camera.

2. Method

2.1 Study material

The study material was gathered during the year-end period in 2007 - 2008 from two different locations in Espoo, Finland: Nuuksio (n = 10, r = 7.98 m) and Espoonlahti (n = 3, r = 10.0 m), from a total of 13 circular sample plots. The sample plots were located so that the variation in their growth stock, development stage (advanced growth forest to mature forest) and site type (rich site to very poor site) was as wide as possible.

For testing of the device, the trees of the sample plot were numbered by attaching a number label on the side of each tree with the label's lower edge at breast height. The diameter measurement was taken below the number label. Tree species and $d_{1.3}$ (vertically against the centre of the sample plot) were determined for the trees with a steel caliper. The study material included a total of 728 diameter measurements from 265 trees (Table 1). The distribution of diameter observations by tree species is illustrated in Figure 1.

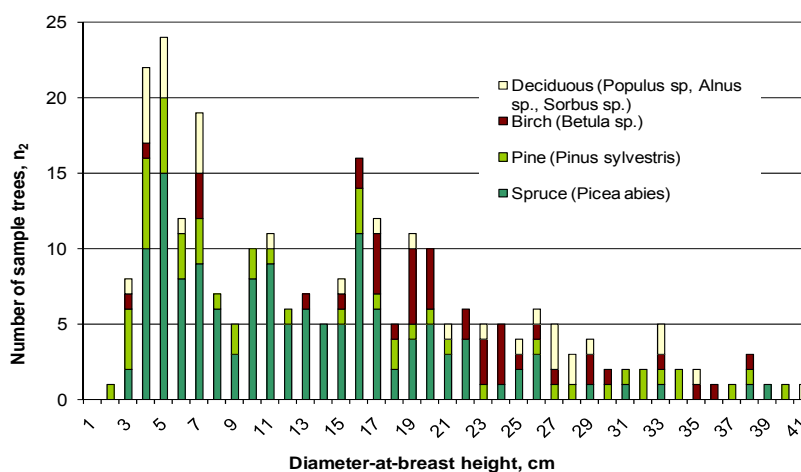


Figure 1. Diameter distributions of spruce, pine, birch and other deciduous sample trees.

Table 1. Description of the study material. Number of tree diameter measurements (n_1), number of sample trees (n_2) and the minimum/maximum values, average and standard deviation (S.D.) of the tree diameter measurements by tree species. The reference diameters were measured using a steel caliper.

| | n_1 | n_2 | minimum | maximum | average | S.D. |
|---|------------|------------|------------|-------------|-------------|------------|
| Pine (<i>Pinus sylvestris</i>) | 153 | 53 | 4.4 | 46.5 | 15.7 | 11.7 |
| Spruce (<i>Picea abies</i>) | 386 | 137 | 5.2 | 40.9 | 14.8 | 7.8 |
| Birch (<i>Betula</i> sp.) | 108 | 42 | 5.0 | 40.4 | 22.8 | 7.7 |
| Deciduous ¹ | 81 | 33 | 4.7 | 47.8 | 20.9 | 11.7 |
| All observations | 728 | 265 | 4.4 | 47.8 | 16.9 | 9.7 |

1) aspen ($n_1 = 51$), rowan ($n_1 = 17$), alder ($n_1 = 13$)

The trees were photographed with a Laser-camera in the field from the centre of the sample plot. Afterwards the tree diameter measurements were interpreted from the photographs. If the tree was not visible from the centre of the plot, the observer moved several steps in order to enhance visibility. The majority of photos taken with the Laser-camera were interpreted afterwards with the help of an interpretation software program developed for this specific purpose. Repetition measurements were conducted, starting from the fourth sample plot in such a way that from the three following sample plots two diameter measurements were measured per tree and from the last sample plots (7) four measurements were done. The number of measurements was increased when new information concerning functioning of the devices was obtained.

The time spent conducting the sample plot measurements was defined to an accuracy of 1 min based on time stamps recorded on the image files. The sample plot measurements were conducted by measuring tree diameters with a Laser-camera. Two photographs were taken from each tree during each measurement occasion. The number of observations gathered from each tree varied from one to four observations.

2.2 Laser-camera

The Laser-camera under study consists of a Canon EOS 400D digital reflex camera with an integrated Mitsubishi ML101J27 laser line generator. The Laser-camera used Canon's EF 70 - 300 mm f/4.5 – 5.6 DO IS USM objective. The resolution of the camera is 10 megapixels. A software program for the visual interpretation of photographs and validation of measurement results was developed with a Canon Software Development Kit. With the program, one can check the measurement result by visual means as well as by adjusting the camera settings, if desired. If the border markers are incorrectly placed, they can be manually adjusted to their correct locations and thus help determine the true diameter. Interpretation of images was performed using the image-processing software either under real-time field conditions or afterwards.

The laser line generator is turned on automatically as the camera focuses. An electronic altimeter can be added to the device (Masser Ltd.), to enable the gathering of diameter observations from different stem heights. The weight of the Laser-camera is approximately 1.5 kg; the camera (0.51 kg) and the objective (0.72 kg) make up most of the weight. The price of the laser camera prototype is 2600 - 3000 €, while the field computer costs around 1000 € (Kivilähde 2008).

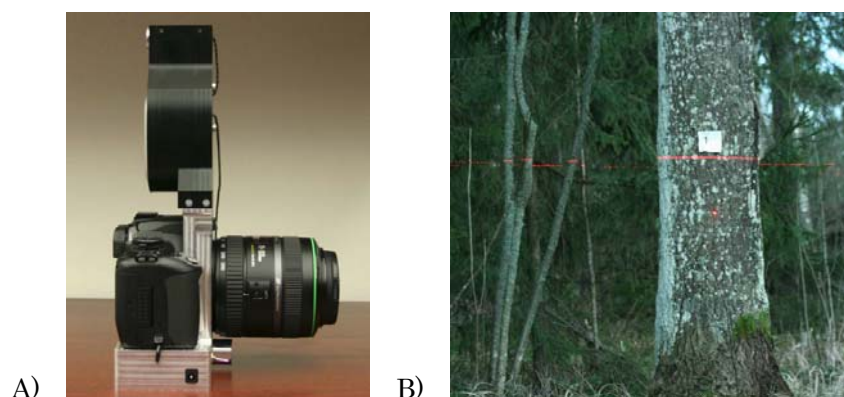


Figure 2. A) The Laser-camera consists of a Canon EOS 400D digital reflex camera with an integrated Mitsubishi ML101J27 laser line generator. An inclinometer can also be added to the device. B) Principle of breast height diameter measuring. (Photographs© Jani Kivilähde & Mikko Vastaranta)

2.3 Principle of diameter measuring

The principle of measuring tree diameters with the new Laser-camera prototype is based on the reflection of a laser line and point on a tree stem (Figure 2). The laser line reflection breaks at the border lines of the tree stem so that the stem diameter can be measured, based on the length of the reflected laser line. The length of the laser line can be obtained from the photograph as the number of pixels and local image scale. The scale of the photograph can be derived from the invariable distance between the laser line and point. The interpretation software focuses on the stem and automatically recognizes the laser beam and laser point reflected on the tree stem calculating the tree diameter based on these. The measurement is obtained from the centre of the photograph.

The program functions either fully automatically so that the user has only to open the picture from the file (.jpeg) and the diameter measurement is found directly from the screen or semiautomatically. If the user notices errors in the photograph resulting from the automatic photo interpretation method, the diameter measurement can be derived from the photo manually, either during the field measurements or afterwards.

2.4 Accuracy of diameter measurements

Tree diameter measurements measured with a Laser-camera were compared with measurements conducted with a traditional method (a steel caliper). Bias, S.D. and standard error were calculated for all the study material and separately for Norway spruce, Scots pine, birch and other deciduous trees (aspen, alder, rowan).

The diameter measurement error was defined as

$$e_{-d} = d_{1.3laser} - d_{1.3ref} \quad (1)$$

where $d_{1.3ref}$ represents the reference diameter and $d_{1.3laser}$ the diameter measured with a Laser-camera.

The reliability of the measurements was examined using estimation of mean-square errors (MSE). Since the true values of diameter were assumed to be known, MSE can be divided into the variance and square of the bias (Cochran 1977). The estimate of bias was given by

$$b[e_{-d}] = e_{-d} = \frac{1}{n} \sum_{i=1}^n e_{-d_i} \quad (2)$$

and the standard error was given by

$$s[e_{-d}] = \sqrt{\frac{1}{n-1} \sum_{i=1}^n [e_{-d_i} - e_{-d}]^2}, \quad (3)$$

where n is the number of observations and d is the diameter.

When calculating standard errors for different methods and the measurement errors are independent, the standard error of reference method can be taken into account as follows:

$$s[e_d]_{method} = \sqrt{s[e_d]^2 - s[e_d]_{ref}^2}, \quad (4)$$

where $s[e_d]_{ref}$ is the standard error for steel calipers.

Clear outliers were excluded from the material. The main reason for excluding the outliers was either that the laser point reflected by the Laser-camera did not hit the tree stem (the laser point was either reflected on the branches in front of the tree, or they did not hit the tree stem at all) or the measurement height of the diameter observation or direction did not correspond with the reference measurement. The number of clear outliers was significant (176 in total) as the measurement results were not immediately visible to the measurer in the screen of the camera having most of them been measured without the use of a field computer. Another reason for the high number of outliers was that the measurement height was constant and did not reflect, for instance, visibility that impacts the precision of measurement results.

If it was observed during postprocessing that the automatism of the diameter observation did not function correctly, the border markers that depicted the tree stem (semiautomatic interpretation) were moved to match the true border lines of the tree in the image. The goal was to make the measurement depict the situation under field conditions. The measurement can be verified in the field enabling the observer to exclude outliers and make a new diameter observation immediately.

2.5 Efficiency of measuring the diameter

The efficiency of the measuring device was determined by measuring sample plots in different stand types and comparing the results with reference measurements. The time spent measuring the sample plots was documented to an accuracy of 1 min.

3. Results

3.1 Accuracy of breast height diameter measurements

The standard error of diameter observations using semiautomatic interpretation was 6 mm (5.3%). The proportion of bias was 2.5 mm, i.e. the results obtained with the Laser-camera were slightly overestimated. The relative standard error was approximately 4% for trees with widths of above 7 cm, and approximately 10% for trees with widths below this. (Figure 3).

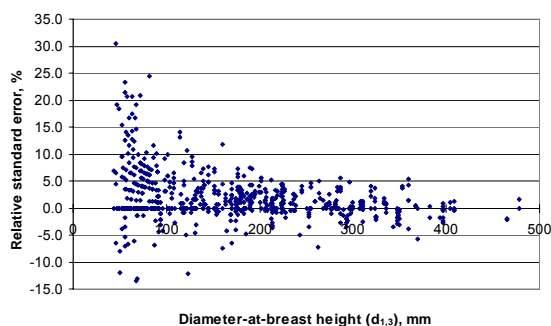


Figure 3. Relative differences in diameter observations obtained with a Laser-camera and reference diameter ($d_{1.3laser} - d_{1.3ref}$), as a function of diameter.

The accuracy of the diameter observations (standard error) was maximum for spruce 5.0 mm (4.4%), followed by birch 6.4 mm (3.3%) and pine 7.6 mm (7.6%). Other deciduous trees

(aspen, rowan, alder) resulted in a standard error of 6.1 mm (6.0%). Bias for all tree species, excluding other deciduous trees, was positive. Pine resulted in a bias almost twice the magnitude of that for spruce and birch (see Table 2). The results were calculated, assuming that the reference measurements were the true values.

Table 2. Precision of breast height diameter observations using semiautomatic image processing.

| | n | d _{1,3} | bias, mm | bias, % | S.D, mm | S.D., % | S.E., mm | S.E., % |
|---------------------------------------|-----|------------------|-------------|---------|------------|---------|------------|---------|
| Pine (<i>Pinus sylvestris</i>) | 124 | 17.2 | 4.6 | 4.8 | 6.0 | 5.8 | 7.6 | 7.6 |
| Spruce (<i>Picea abies</i>) | 272 | 16.9 | 2.2 | 1.8 | 4.5 | 4.0 | 5.0 | 4.4 |
| Birch (<i>Betula sp.</i>) | 88 | 22.8 | 2.5 | 1.0 | 5.9 | 3.1 | 6.4 | 3.3 |
| Deciduous¹ | 68 | 21.9 | -0.6 | 1.5 | 6.1 | 5.8 | 6.1 | 6.0 |
| All observations | 552 | 18.5 | 2.5 | 2.3 | 5.5 | 4.8 | 6.0 | 5.3 |

1) aspen (n₁ = 51), rowan (n₁ = 17), alder (n₁ = 13)

The success rate of the diameter observations, using semiautomatic image interpretation, was approximately 80% for all tree species except spruce, which had a success rate of 70%. The measurement of diameter was clearly more successful (by as much as 20%), when semiautomatic image interpretation was used instead of the fully automatic method. (Table 3.)

Table 3. Success rate of observations by tree species and for all study material.

| | Automatic method | Semiautomatic method |
|---|------------------|----------------------|
| Pine (<i>Pinus sylvestris</i>) | 51.6 | 81.0 |
| Spruce (<i>Picea abies</i>) | 58.0 | 70.5 |
| Birch (<i>Betula sp.</i>) | 80.6 | 81.5 |
| Deciduous¹ | 60.5 | 84.0 |
| All observations | 57.4 | 75.8 |

A diameter result was obtained for approximately 60% of all observations, with a standard error of 12.7 mm, when the automatic method was used. This method, thus, required manual checking of the diameter results, to ensure that they were reliable enough.

The measuring distance had no impact on measuring accuracy. The trees were located not more than 10 m from the sample plot centre point. For the purpose of the project goals, the optimal operational distance was defined as 2 - 15 m.

3.2 Efficiency of tree diameter measurements

It required approximately 7.5 min to measure a sample plot of about 22 trees and 10 sec to measure the diameter of one tree stem. The measurement time included observation of the tree stem at breast height, focusing of the camera objective and taking of the image. The results did not include checking of the measurement result under field conditions, since they were checked afterwards.

4. Discussion

The results obtained with the Laser-Camera were very promising compared with the measurements taken with traditional measuring devices. The accuracy of a Laser-camera is at least as good as that of a steel caliper. In earlier studies, the standard error of a steel caliper varied between 2.7 mm and 6.9 mm (Hyppönen and Roiko-Jokela 1978; Päivinen *et al.* 1992). The results obtained with the Laser-camera were clearly better than those obtained with other laser technology-based devices. The Barr & Stroud and Criterion laser dendrometers (Williams *et al.* 1999) showed standard errors of 8.8 mm and 14.3 mm for measuring upper diameters. According to a study by Varjo *et al.* (2006) the standard errors of diameters varied between 7.0

mm and 9.4 mm, depending on the measuring height (2.5-6.5 m) and the size of the tree. Compared with results obtained with the Laser-relascope, standard error was approximately 3 - 5 mm lower.

Traditionally, it has been assumed that diameter measurements obtained with a steel caliper, are true values. In reality, however, standard errors are also found in steel caliper measurements. If the standard error of reference measurements is taken into account, the accuracy of the Laser-camera (semi-automatic) is 7.1 mm for pine, 5.8 mm for birch and 4.2 mm for spruce. For all the study material, the standard error was 5.4 mm. It was assumed that the standard error of a steel caliper is 2.7 mm (Hyppönen and Roiko-Jokela 1978).

Tree diameter measurements can be obtained with a Laser-camera rapidly (10 s /tree), with good reliability and efficiency. Another advantage of the device is that the procedure for each measurement can be documented and be returned to if exceptions or errors are found within the results. Future diameter measurements will be obtained from various tree stem heights enabling, for instance, the usage of more than one tree diameter measurement result when calculating tree volume. This will enable the use of more accurate volume models (Laasasenaho 1982; Varjo *et al.* 2006).

The future goal will be to integrate the laser technique with an altimeter, data collection unit and GPS receiver inside a weatherproof Laser-camera device. This will enable ready checking of the measurement results in the field from the screen of the digital camera, measuring of the diameters at any height of the tree and measuring the heights, locations, quality variables of the trees. To integrate this type of quality into the Laser-camera, more cooperation will be required with camera manufacturers.

Acknowledgements

The Laser-camera prototype was developed in cooperation between the Centre for Metrology and Accreditation, Helsinki University of Technology (Metrology Research Institute), Masser Ltd and the University of Helsinki (Department of Forest Resource Management). The project was also funded by Metsäteho Ltd. and the Forestry Development Centre TAPIO. The field tests were conducted with funding by the Academy of Finland and Metsämiesten säätiö – foundation. We thank Prof. Erkki Ikonen, Ph.D. Mikko Merimaa ja M. Sc. Jani Kivilähde for building the device and its technical implementation, Prof. Annika Kangas for invaluable comments, and especially Emeritus Professor Jouko Laasasenaho, who first introduced the concept of the Laser-camera.

References

- Carr, B., 1992. Using laser technology for forestry and engineering applications. Compiler 10: 5-16
- 1996. Using Criterion 400 and Impulse 200 laser instruments to accurately measure trees. Compiler 14, 6-12
- Clark, N., Zarnoch, S., Clark III, A. and Reams, G. 2001. Comparison of standing volume estimates using optical dendrometers. Julkaisussa: Reams, G., MacRoberts, R. and Van Deusen, P. (Ed.); Proceedings of the second annual Forest inventory and Analysis symposium (FIA). 17-18.10.2000; Salt Lake City, UT. Gen. Tech. Rep. SRS-47. Asheville, NC: U.S. Department of Agriculture, Forest Service, Southern Research Station. pp. 123-128.
- Cochran, W.G., 1977. Sampling techniques (third ed.). Wiley (1996).

- Forsman, P. and Halme A. 3-D. 2005. Mapping of natural environments with trees by means of mobile perception. *IEEE Transactions on Robotics* 20 (3): 482-490.
- Henning, J. G. and Radtke, P. J., 2006. Detailed stem measurements of standing trees from ground-based scanning lidar. *Forest Science* 52(1): 67-80.
- Holmgren, J. 2003. Estimation of forest variables using airborne laser scanning. Doctoral dissertation. *Acta Universitatis Agriculturae Sueciae. Silvestria* 278. SLU, Umeå, Sweden. 43 p.
- Hopkinson C., Chasmer, L., Young-Pow, C., and Treitz, P. 2004. Assessing forest metrics with a ground-based scanning lidar. *Can. J. For. Res.* 34: 573-583.
- Hyppönen, M. and Roiko-Jokela, P. 1978. Koepuiden mittauksen tarkkuus ja tehokkuus. Summary On the accuracy and effectivity of measuring sample trees. *Folia Forestalia* 356 25 p.
- Hyypä, J., Hyypä, H., Leckie, D., Gougeon, F., Yu, X., and Maltamo, M., 2007, Review of methods of small-footprint airborne laser scanning for extracting forest inventory data in boreal forests. *International Journal of Remote Sensing*, in press.
- , Hyypä, H., Litkey, P., Yu, X., Hagggrén, H., Rönnholm, P., Pyysalo, U. Pitkänen, J. and Maltamo, M., 2004, Algorithms and methods of airborne laser scanning for forest measurements. *Proceedings of the NatScan conference, October 3 - 6, 2004, Freiburg, Germany.*
- , and Inkinen, M. 1999. Detecting and estimating attributes for single trees using laser scanner. *The Photogrammetric Journal of Finland* 16 : 27-42.
- , Mielonen, T., Hyypä, H., Maltamo, M., Yu, X., Honkavaara, E., and Kaartinen, H., 2005, Using individual tree crown approach for forest volume extraction with aerial images and laser point clouds. In *Proceedings of ISPRS Workshop Laser Scanning 2005, September 12-14, 2005, Enschede, Netherlands, (Netherlands: GITC bv), XXXVI, Part 3/W19, pp. 144-149.*
- , Yu, X., Hyypä, H. and Maltamo, M., 2006, Methods of airborne laser scanning for forest information extraction. *EARSel SIG Forestry. In International Workshop 3D Remote Sensing in Forestry Proceedings, Vienna, 14-15 Feb. 2006, pp. 63-78.*
- Jutila, J., Kannas, K. and Visala, A. 2007 "Tree Measurement in Forest by 2D Laser Scanning," in *International Symposium on Computational Intelligence in Robotics and Automation, CIRA, Jacksonville, FL: 2007: 491-496.*
- Juujärvi, J., Heikkonen, J., Brant, S. and Lampinen, J. 1998. Digital Image Based Tree Measurement for Forest Inventory. *Proc. of SPIE – The international society for optical engineering: Intelligent robots and computer vision XVII: Algorithms, techniques and active vision, Boston USA, November 2 - 4, volume 3522, pp. 114-123.*
- Kalliovirta, J., Laasasenaho, J. and Kangas, A., 2005. Evaluation of the Laser-relascope. *Forest Ecology and Management* 204: 181-194
- Kivilähde, J. 2008. Kehitysympäristö puustotunnusten mittaukseen kuvankäsittelytekniikoilla. Abstract: Mobile Development Environment for Image-Based Measurements of Tree Attributes. Master's Thesis. Helsinki University of Technology, 89 p. (in Finnish)
- Korpela I. 2004. Individual tree measurements by means of digital aerial photogrammetry. *Silva Fennica monographs* 3. 93 p.
- , Dahlin, B., Schäfer, H., Bruun E., Haapaniemi, F., Honkasalo, J., Ilvesniemi, S., Kuutti, S., Linkosalmi, M., Mustonen, J., Salo, M., Suomi, O. and Virtanen, H.. 2007. Single-tree forest inventory using LiDAR and aerial images for 3D treetop positioning, species recognition, height and crown width estimation. *IAPRS Volume XXXVI, Part 3 / W52, 2007. pp. 227-233*
- Laasasenaho, J. 1982. Taper curve and volume functions for pine, spruce and birch. *Seloste: Männyn, kuusen ja koivun runkokäyrä- ja tilavuusyhtälöt. Communicationes Instituti Forestalis Fenniae* 108. 74 p.
- , Koivuniemi, J., Melkas, T. and Rätty, M. 2002. Puuston mittaaminen etäisyyden- ja kulmanmittauslaitteella. Measuring growing stock with a device including a rangefinder and an inclinometer. *Metsätieteen aikakauskirja* 3/2002: 493-497 (in Finnish).

- Lappi, J. 1986. Mixed linear models for analyzing and predicting stem form variation of Scots pine. *Communicationes Instituti Forestalis Fenniae* 134: 1-69
- Maltamo, M., Eerikäinen, K., Pitkänen J., Hyypä, J. and Vehmas, M. 2004. Estimation of timber volume and stem density based on scanning laser altimetry and expected tree size distribution functions. *Remote Sensing of Environment* 90: 319-330.
- Miettinen, M., Öhman, M., Visala, A. and Forsman, P. 2007. "Simultaneous localization and mapping for forest harvesters," in *IEEE International Conference on Robotics and Automation, IEEE, Rome, Italy, 10-14 April 2007*, pp. 517-522.
- Naesset, E. 2004. Practical large-scale forest stand inventory using a small-footprint airborne scanning laser. *Scandinavian Journal of Forest Research* 19: 164-179.
- , Gobakken, T., Holmgren, J., Hyypä, H., Hyypä, J., Maltamo, M., Nilsson, M., Olsson, H., Persson, Å. and Söderman, U. 2004. *Laser Scanning of Forest Resources: The Nordic Experience. Scand. J. For. Res.* 19: 482-499.
- Ojanen, M. 2005. Puun halkaisijan mittaaminen kuvankäsittely tekniikoin. Abstract: Measurement of a tree diameter using image processing. Master's Thesis. Helsinki University of Technology, 76 p. (in Finnish)
- Parker, P. C. and Matney, T. G., 1999. Comparison of optical dendrometers for prediction of standing tree volume. *Southern J. Appl. Forestry* 23 (2): 100-107
- Päivinen, R., M. Nousiainen, M. and Korhonen K.T., 1992. Puutunnusten mittaamisen luotettavuus. Accuracy of certain tree measurements, *Folia Forestalia* 787, 18 p. (in Finnish with English summary).
- Skovgaard, J. P., Johannsen, V. K. and Vanclay, J. K., 1998. Accuracy and precision of twodendrometers. *Forestry* 71 (2) : 131-139.
- Varjo, J., Henttonen, H., Lappi, J., Heikkinen, J. and Juujärvi, J. 2006. Digital horizontal tree measurements for forest inventory. Working Papers of the Finnish Forest Research Institute 40. 23 p. <http://www.metla.fi/julkaisut/workingpapers/2006/mwp040.htm>.
- Watt, P. J. and Donoghue, D. N. M. 2005. Measuring forest structure with terrestrial laser scanning. *International Journal of Remote Sensing* 26 (7): 1437-1446.
- Williams, M., Cormier, K., Briggs, R. and Martinez, D., 1999. Evaluation of the Barr & Stroud FP15 and Criterion 400 laser dendrometers for measuring upper diameters and heights. *Forest Science* 45 (1): 53-61.

Spatial quantification of vegetation density from terrestrial laser scanner data for characterization of 3D forest structure at plot level

Durrieu¹ S., Allouis¹ T., Fournier² R., Véga¹ C., Albrech¹ L.

¹UMR TETIS Cemagref/Cirad/ENGREF-AgroParisTech, Maison de la Télédétection, 34093 Montpellier Cedex 5, France,

sylvie.durrieu@teledetection.fr, tristan.allouis@teledetection.fr,
cedric.vega@teledetection.fr, laurent.albrech@teledetection.fr

²Centre d'Applications et de Recherche en Télédétection, Université de Sherbrooke, Sherbrooke (Québec) Canada, Richard.Fournier@USherbrooke.ca

Abstract

Precise description of forest 3D structure at plot level is required for sustainable ecosystem management. However, a detailed structure description from traditional field measurements is tedious. We propose an innovative method to quantify in 3D the spatial distribution of forest structure from terrestrial lidar data. The method rests on the hypothesis that the normalized number of laser returns within a given volume element is proportional to the density of vegetation material inside this volume. The developed model is based on analysis made inside Svoxels (spherical voxels) to compute a spatialized vegetation density index. The model was tested on two different scans of the same plot. The resulting vegetation density index well represents the vegetation structure as observed within the lidar point cloud. Quantitative analyses confirmed a global consistency of the results within and between scans. However, we observed a slight bias in the computed density indexes. It might be mainly explained by occlusions, which cause 1) a slight decrease of the density index with distance and 2) local differences in density index between scans. Future work will focus on improving our algorithm and correcting biases. These results are promising for the development of quantitative measures of the 3D forest structure.

Keywords: Terrestrial lidar, forest canopy, 3D model, architecture, stand structure

1. Introduction

Precise description of 3D structure of forests is useful for timber resource monitoring, ecosystem management and preservation, or improved understanding on ecosystem functioning. However the spatial complexity of forests makes structure measurement very difficult, particularly since structure is not a satisfyingly defined feature (Fleck *et al.* 2007). A complete 3D plot description is not conceivable using traditional field inventory methods. The recent development of terrestrial lidars allows to acquire very detailed 3D data on forest structure. It opens up new opportunities to derive metrics closely linked to forest structure and to reduce time and costly field measurements (Hopkinson *et al.* 2004).

Terrestrial lidars were originally developed for civil engineering (see Lichti *et al.* (2002) for examples of systems and applications). Recent studies expanded their use on tree or stand structure measurements. Most of them focused on estimating traditional field-based forest parameters. Hopkinson *et al.* (2004) first demonstrated that it is possible to locate and identify individual trees with high precision and to measure total tree height and diameter at breast height (dbh). Tree heights were however underestimated of about 1.5 m when compared with field validation data. This was mostly due to low sampling density at the upper canopy level

caused by occlusion effects of the signal and a suboptimal survey protocol. Results for mean dbh differed by only 1 cm from tape measurements. Similar results were obtained by other authors for both height and dbh measurements using semi-automatic data extraction methods (Watt and Donoghue 2005; Fleck *et al.* 2007; Wezyk *et al.* 2007). Other forest parameters such as stem density, total basal area, gross and merchantable timber volume were also estimated from terrestrial lidar data with a good agreement when compared with traditional field measurements (*e.g.* volume estimations within 7% of the traditional field estimations (Hopkinson *et al.* 2004)). Other efforts dealt with automatic tree location and height, dbh, stand basal area or timber volume estimations (Aschoff *et al.* 2004; Bienert *et al.* 2007; Király and Brolly 2007; Wezyk *et al.* 2007).

The very high sampling rate of terrestrial laser systems allows to generate detailed 3D canopy models therefore opening up the possibility to analyze fine scale stand structure, foliage distribution, canopy light transfer or leaf area indices that are important to understand and model forest function and dynamic. However few studies have demonstrated the interest of such systems for ascertaining parameters beyond those from the traditional inventories. As an exception, Fleck *et al.* (2007) proposed a method to quantify canopy projection far much precise than the 8-point canopy projection from a ground operator used in traditional inventories. As other non-traditional measures, Danson *et al.* (2007) proposed a method to estimate canopy directional gap fraction and Van der Zande *et al.* (2006) an approach for vegetation profile reconstruction. Studies using terrestrial lidar show much opportunity for developing new methods for forest canopy metrics that will take full advantage of terrestrial lidar datasets. One of the main issues will be to solve the problem of the distance-dependent varying point density from the lidar returns.

This paper introduces an innovative approach to analyze the vegetation structure from 3D point clouds acquired with terrestrial lidar. The method quantifies the 3D spatial distribution of forest canopy material in volume elements (~dm level). It makes available operational calculations linking the 3D point cloud recorded by a terrestrial lidar with the spatial distribution of the vegetation. This study was also performed considering the link between airborne lidar and field data with the aim of improving information extraction from airborne lidar data on forested areas. Indeed airborne lidars proved capable to estimate the spatial distribution of forest parameters such as height, crown area, timber volume or biomass at both tree or stand level (Lim *et al.* 2003). However these airborne estimates require local calibration through acquisition of field data.

2. Method

2.1 Study area and field data

The main study site is part of a National Environmental Observatory (ORE Draix) located in the southern part of the French Alps. It is part of the Haute-Bléone state forest, mainly composed of black pine (*Pinus nigra*) planted in the 1880's to protect against soil erosion. Most of the stands are even-aged and mature. Elevations range from 802 to 1263 m. Traditional field inventory was conducted during December 2007 within circular plots of 15 m and 9 m radius. Within the plot the following characteristics were measured for all the trees with dbh > 7 cm: dbh, total and timber heights, crown base height, crown diameter and tree position. For the purpose of that study, we focused on a 15 m circular plot having a tree density of 66 stems/ha and located on a flat area.

2.2 Data acquisition with the terrestrial lidar

Terrestrial lidar surveys were made on March 2008 using an ILRIS-3D system (Optech Inc,

Toronto, Canada). The system measures the laser returns within a window 40° wide in both horizontal and vertical directions. The laser emits and measures light at 1,500 nm. Point density of each scan is controlled by the operator. The system can register the intensity and distance for either the first or the last backscattered signal. In our study, we selected primarily the last returns considering that they would provide a better statistical representation of the vegetation distribution compared with first returns. However, first and last returns were recorded at some particular system base stations (*i.e.* system location) for comparison and quality assessment. The ILRIS-3D base stations were selected outside the plot at varying distance from the plot centre and separated by an angle of about 120° relating to the plot center. Artificial targets (polystyrene spheres with 8 cm diameter) were distributed within the plot and measured using differential GPS and total station to improve the alignment (co-registration) and the georegistration of the scans acquired from different base stations.

2.3. Method developed for quantifying the spatial distribution of vegetative elements

The objective of this study was to develop an algorithm to calculate vegetation density from lidar returns visible in the form of point clouds. The point density needs to be locally transformed into density of vegetation components. We used a statistical approach hypothesizing that the interception rate is related to the vegetation density. Such an approach was preferred to a formal physical-based model (e.g. Beer-Lambert law) because of the heterogeneity of distribution of canopy components and also because of the relatively small footprint of the laser beam compared to vegetation elements size. Estimation of density index throughout a scene involved first dividing the plot-space into constant volume elements (voxels). For each voxel, we calculated (1) the number of lidar points within the voxel and (2) the number of laser beams entering the voxel. The density index of each voxel is given by the ratio (1) / (2). Our method has two spatial characteristics: a regularly spaced grid of voxel centers and the use of spherical voxels.

2.3.1. Regular 3D grid and spherical voxels

Voxel centers were arranged on a 3D grid regularly distributed along x, y and z axes. The grid was georeferenced in the Lambert III conformal conic coordinate system and was used to process each scan of a same plot. Computations from all scans of the plot could therefore be compared and integrated. Before processing each scan, the Lambert III grid is changed into the Cartesian system of the scan. The transformation model is computed using (1) The Lambert III coordinates of target centers, measured on the field (total station + DGPS), and (2) the Cartesian coordinates of the targets, measured on each scan by fitting a spherical shape on its corresponding point clouds. The 3D Reshaper [®] software was used for that purpose. A minimum of 4 spheres was required for computing the transformation model.

Data acquisition with the terrestrial lidar follows a spherical geometry. We therefore adopted a spherical geometry to simplify computations on the resulting point cloud from lidar measurements. Lidar position was taken as the origin of the spherical system. The space illuminated by the lidar was already divided into voxels. Therefore each voxel center was associated with a spherical coordinate (r, θ, φ) and bounded with the following conditions:

1. 4 angles: $\theta_{\min} = \theta - d\theta$, $\theta_{\max} = \theta + d\theta$, $\varphi_{\min} = \varphi - d\varphi$ and $\varphi_{\max} = \varphi + d\varphi$,
2. 2 distances: $r_{\min} = r - dr$, $r_{\max} = r + dr$,

with dr set to half the grid resolution. This new volume is referred to as the spherical voxel or Svoxel (Figure 1). We set $d\theta$ and $d\varphi$ to ensure a constant volume of Svoxels ($V = R^3$, with R the 3d resolution of the grid). The resulting Svoxels have the following properties:

1. Distortion of a Svoxel compared to the reference voxel is proportional to r (cf. figure 1),
2. Distortion of a Svoxel increases when angles θ and φ increase,
3. Svoxels are not strictly contiguous. Small overlaps or gaps can occur which are more

- important for larger values of θ and φ ,
4. For a given center point, the Svoxels generated from different base station locations will not strictly overlap due to slight changes in shape and orientation. The highest differences will occur when comparing Svoxels from scan with a 45° (modulo 90°) difference between viewing angles.

Even with these properties, differences between voxels and Svoxels remain small and it is thus assumed that they are not detrimental to precise density index computation.

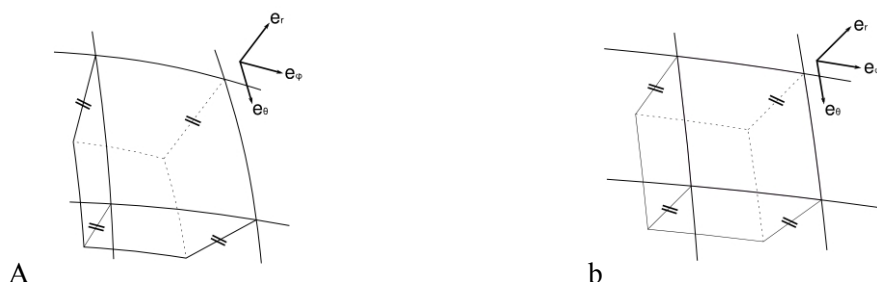


Figure 1: Shape of a Svoxel at 1 m (a) and at 3 m (b) for 50 cm grid resolution.

2.3.2 Algorithm to calculate density index of the grid points

The following algorithm was implemented to calculate the density index of each Svoxel in the lidar scanning field of view:

1. Generation of a 3D regularly spaced grid in Lambert III at a resolution R ,
2. Projection of the grid in the sensor Cartesian system,
3. Switch scan point cloud and grid into spherical system,
4. For each point of the grid :
 1. Computation of the theoretical number of laser beams ($N_{\text{theoretical}}$) entering the Svoxel based on the point density selected for the scan. This number decreases with distance to the sensor due to the scanning geometry.
 2. Evaluation of the number of laser beams intercepted before the targeted Svoxel (N_{before} : points satisfying the 4 angles equation with a distance lower than r_{min}). The difference between $N_{\text{theoretical}}$ and N_{before} represents the number of beams reaching the Svoxel.
 3. Identification of the number of returns inside the targeted Svoxel (N_{inside} : points satisfying the 4 angles and 2 distances equations).
 4. Computation of the vegetation density index D , such as:

$$D = N_{\text{inside}} / (N_{\text{theoretical}} - N_{\text{before}}) * 100 \quad (1)$$

If $N_{\text{theoretical}} - N_{\text{before}} = 0$, a no-data value is assigned. If $N_{\text{theoretical}} - N_{\text{before}}$ is lower than a given threshold T_s , results are considered as non-significant because too few beams are available to assess Svoxel density. Output of results in Lambert III.

5. Steps 2 to 5 can be reapplied to other scans of a same plot acquired from other base stations.

2.4 Data analysis and validation

For this preliminary study the algorithm was applied on 2 out of the 8 scans available for the plot. Scan density was set to 6.24 mm (resp. 7.02 mm) at 15 m for scan 1 (resp. scan 2) and the last returns were recorded. Three Svoxel resolutions were selected: 0.25, 0.5 and 1 m. Results

were first evaluated from a preliminary visual assessment where Svoxels with a positive and significant density index were visualized on the lidar 3D point clouds of selected trees. Preliminary tests allowed us to adopt a value of 50 for the threshold defined for non-significant values (T_s).

Then two sets of procedures were realized:

1. In order to evaluate the result consistency inside a given scan, several stand crowns located at various distances from the base station 1 were extracted and the distribution of positive and significant density indices were analyzed. Results on four black pines and one Spanish fir (*Abies pinsapo*) were compared (cf. Fig 2).
2. Density index values obtained from two different base stations were also compared to evaluate the consistency of the results between different scans. This preliminary analysis defined if results from multiple scans can be compared and merged.

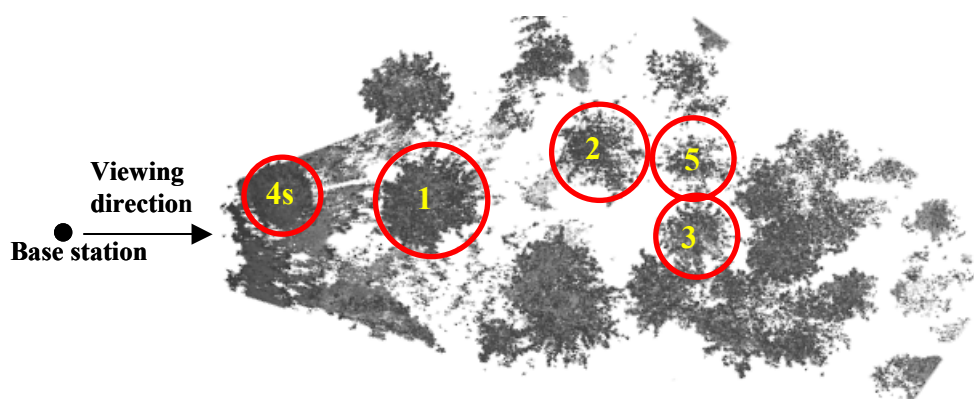


Figure 2: The tree crowns selected for analysis are shown on the 3D point cloud obtained from the system position 1 and viewed from the top. Crowns represent black pine (1, 2, 3 and 5) and Spanish fir (4).

3. Results and discussion

3.1 Visual analysis

The method gave visually consistent results. Figure 3 compares the point cloud from the original scan and the values of the density index for Svoxels on a vertical slice of a black pine crown. The tree shape is well described by Svoxels with density index values apparently reasonable: highest density values are logically located along the trunk and close to large branches regardless of the Svoxel size. Tree outline description quality is getting coarser when Svoxel size increases. However decreasing the Svoxels size increases the rate of non-described areas (no-data Svoxels) of the crown due to occlusions (i.e. mutual shading) particularly at the back part of the tree. Therefore researches have to be conducted to define the Svoxel size providing the optimal description of the vegetation structure. The optimal Svoxel size is expected to vary with the stand structure (density, tree dimensions and tree arrangement). Furthermore the number of beams generated by the lidar should be high enough to allow enough intercepted beams by the tree structures of the scene. While the point density at each Svoxel varies greatly according to the scanning parameters and the occlusion effects between canopy elements, the computed density indexes are relatively homogeneous within the crowns. The link between spatial distribution of canopy components and density index of Svoxels follows the general density patterns expected for these conifers. However, a slight dissymmetry remains between density index of Svoxels of the crown facing the scanner system and those on the back part of the tree. This may be explained by a heterogeneous spatial distribution of vegetation

elements. The occlusion of some vegetation elements may bias the density index values (Fig. 4). At tree level, underestimation and overestimation effects do not offset each other inducing a slight underestimation towards the back of the crown (Fig. 3).

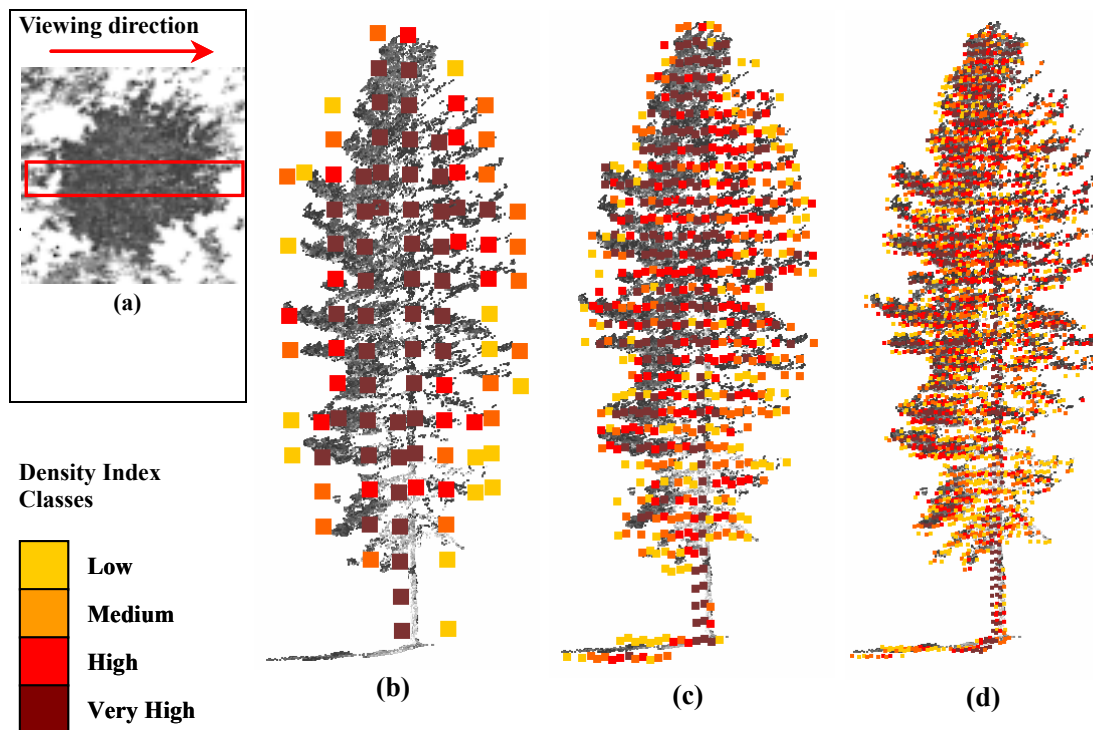


Figure 3: Density index were computed for the three grid dimension (0.25, 0.5, 1m). Density index are superimposed on their corresponding Svoxel centre on the lidar 3D point cloud. Results are given for a slice cut through a tree in the scan direction (a). Density index were separated into 4 classes using quartiles.

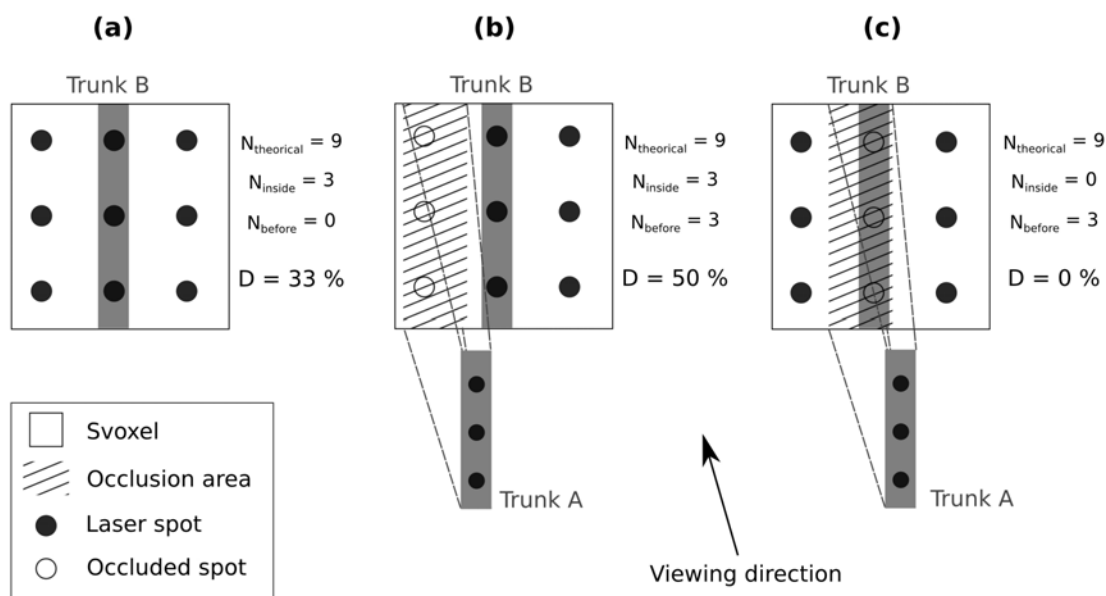


Figure 4: Effect of occlusion on the density index: (a) When Trunk B in the Svoxel is hit by 3 beams out of 9 it leads to a density index of 33 %. (b) When Trunk A external to the Svoxel is hit by 3 incoming beams but does not mask another canopy element in the Svoxel, the density index becomes 50 %. (c) When Trunk A masks trunk B and no other vegetation components is hit in the Svoxel, the density index is 0 %.

3.2 Comparative analysis of different tree crowns in a same scan

Results for the five selected trees are summarized in table 1. The number of Svoxels with a positive and significant density index gives an indication of the number of Svoxels used for computing each mean tree density index. It varies significantly from one tree to another and cannot be simply related to distance from the lidar system. This number depends on Svoxel size, tree size, distance from the sensor and occlusion patterns. As for the mean density values, we expected similar values for a same species. Although values were relatively similar for the 4 black pine trees (table 1), their mean density index varied respectively from 10 to 13.4 %, 9.8 to 12.8 % and 8.3 to 14.6 % for the 25 cm, 50 cm and 1 m Svoxel resolutions respectively. Since only few trees were analyzed this could be due to natural tree heterogeneity. However, further tests on more trees are required to validate if a bias could originate from occlusion effects, similarly as what was observed for the density index in front and towards the back of individual crowns. In such case density index would decrease with the amount of obstacles in the path of the light beams. This trend can be observed from our dataset for all Svoxel resolutions but not very clearly (table 1). For instance when comparing results for black pine 3 and 5, tree mean index is clearly affected by the vegetation present between the lidar system and the observed tree: black pine 3, is less affected by occlusions (see figure 2) than black pine 5 and has a higher density index (table 1). We hypothesize that occlusions of the incident beams might be the main contributor to this bias. The anomalies related to the distance probably result from (1) a decrease of the sampling density with distance to the lidar system and (2) a change in the spatial distribution of the laser beams entering the Svoxels. Occlusions transform the regular sampling pattern into an irregular. In heterogeneous middles, this transformation may biased the density index computation. Additional analyses are necessary to evaluate the incidence of this bias on the quality of vegetation characterization. Combining scans acquired from various base stations will allow to quantify and partly correct this bias.

Table 1: For each tree crown density index mean and standard deviation were computed for 3 grid resolutions: 25, 50 and 100 cm. The theoretical entering beam number gives an indication of the crown distance from the lidar system.

| Svoxel resolution | | Spanish fir 4s | Black Pine 1 | Black Pine 2 | Black Pine 3 | Black Pine 5 |
|-------------------|---|-----------------------|-----------------------|-----------------------|-----------------------|-----------------------|
| Distance | | 15 m | 21 m | 33 m | 39 m | 39m |
| 25 cm | Number of Svoxel with significant positive value inside the crown | 3455 | 7328 | 1172 | 1558 | 457 |
| | Mean $N_{\text{theoretical}}$ | 1821 | 585 | 285 | 212 | 214 |
| | Mean density index (standard deviation) | 14.2 (15.1) | 12.9 (14.0) | 13.4 (14.8) | 11.4 (13.1) | 10.0 (13.2) |
| 50 cm | Number of Svoxel with significant positive value inside the crown | 705 | 1859 | 777 | 566 | 349 |
| | Mean $N_{\text{theoretical}}$ | 7199 | 2317 | 1103 | 840 | 829 |
| | Mean density index (standard deviation) | 15.9 (15.7) | 12.8 (12.8) | 11.3 (12.1) | 10.5 (11.5) | 9.8 (12.8) |
| 1 m | Number of Svoxel with significant positive value inside the crown | 136 | 396 | 244 | 136 | 116 |
| | Mean $N_{\text{theoretical}}$ | 28405 | 9271 | 4380 | 3354 | 3288 |
| | Mean density index (standard deviation) | 17.8 (18.4) | 14.6 (14.0) | 11.0 (11.3) | 10.8 (11.7) | 8.3 (9.6) |

Histograms of the density index values allow to compare the distribution for the 5 selected crowns for the three grid resolutions. Figure 5 presents the histogram for a Svoxel grid resolution of 50 cm. The histograms are comparable for all the pines. For the Spanish fir a slight difference can be noticed on figure 5 and was observed at all the 3 resolutions: density index frequencies are higher than those from the pines for densities ranging from 20 to 50. Consequently standard deviations were similar for all the black pine crowns and were higher for the Spanish fir (table 1). A higher foliage density for this species could explain this result, even if the density index computation bias is likely to contribute to this difference. This open up the possibility to classify species using density index distribution.

3.3 Comparison of density index for two scans

Table 2 recaps the results of the comparison of the 2 studied scans for two grid resolutions (0.5 and 1 m). The total number of Svoxels was calculated for a grid including the circular plot. After merging two scans from different base stations we noticed that the no-data values represented only about 12 % of the total number of Svoxels in the plot for all grid resolutions. The Svoxel centers, for which a significant density index value was computed from both scans, are only about 55 % of the total number of Svoxels of the grid. This low value is explained by the fact that only the bottom part of the plot was scanned in the second scan. The significant differences in the magnitude for the “Mean density index difference” and the “Mean difference for positive and significant density index values” are explained by a high number of Svoxels located in vegetation gaps. These Svoxels, with a null index value, are consistent between scans. Large differences in density index values are observed inside the vegetation elements. For the 50 cm grid resolution about 15 % of the density index values differ from less than 1 % and 45 % from less than 5 % but 20 % of the Svoxels have index values with a difference higher than 20 %. Part of these differences can be explained by (1) the difference between the Svoxel shapes observed from two points of view and (2) by the type of vegetation material hit by the laser beams. For example trunks or large branches can be sources of differences since they are not seen at the same place according to the base station location (back part of them, relative to view point, is occluded). Some differences may also be related to the potential bias we previously

mentioned. All these hypotheses will have to be verified. Merging results from various scans is expected to improve the reliability of the density index. Lastly, we observed from the results that mean differences decrease with resolution while standard deviation increase. This tends to confirm the influence of large wooded elements present in the Svoxel on density index value differences. Actually, when grid resolution is getting coarser the proportion of large wooded elements inside the Svoxel decreases thus reducing the mean difference.



Figure 5: Histograms of density index values (positive and significant) for 5 tree crowns and for a Svoxel resolution of 50 cm.

Table 2: Results of comparison between density index values computed for two scans.

| Svoxel resolution | Total number of Svoxel in the grid | Mean difference of density indices (SD) [Number of Svoxels] | | | Mean difference for positive and significant density index values (SD) [Number of Svoxels] | | |
|-------------------|------------------------------------|---|-------|----------|--|--------|--------|
| 1 m | 58499 | -1.4 | (6.4) | [432175] | -4.1 | (11.5) | [698] |
| 50 cm | 467999 | -0.7 | (5.4) | [208531] | -3.1 | (16.1) | [2266] |

4. Conclusion

We proposed an innovative method to quantify spatial distribution in 3D of forest structure from terrestrial laser scanner data. The method rests on the hypothesis that the amount of laser beam returns inside a Svoxel (volume element defined in the lidar spherical coordinate system) is proportional to the density of vegetation material included inside this Svoxel. First results appeared very promising despite a persisting bias resulting from occlusions. While the density indexes globally confirm our hypotheses, some adjustments are required to improve further the interrelationship between the lidar returns and the amount of forest components in the Svoxels. Future work will focus on improving our algorithm, refining calculations, and correcting biases. In-depth analysis of scans acquired in both first and last pulse modes and multi-scan comparisons and combinations at different grid resolutions also need to be tested out. Our analysis was an essential prerequisite for developing a method aiming at merging the different scans acquired on a same plot. This study was realized considering the prospect of establishing a link between airborne lidar data and field data with the aim of improving information extraction from airborne lidar data on forested areas. These results are very promising for the development of quantitative measures of the 3D forest structure that will meet the actual information needs in the fields related to forest ecology and management.

Acknowledgements:

This research was made possible though funding provided by the Centre National d'Etudes Spatiales (CNES). We are also thankful to the GIS Draix for its logistical support during the fieldwork.

References

- Aschoff, T., Thies, M. and Spiecker, H., 2004. Describing forest stands using terrestrial laser-scanning. In, XXth ISPRS Congress. *International Archives of the Photogrammetry, Remote Sensing and Spatial Information Sciences*, Istanbul, July 12-23, pp. 5.
- Bienert, A., Scheller, S., Keane, E., Mohan, F. and Nugent, C., 2007. Tree detection and diameter estimations by analysis of forest terrestrial laser scanner point clouds. In: H.H. P. Rönholm, J. Hyypä (Editor). *Proceedings of the ISPRS Workshop 'Laser Scanning 2007 and SilviLaser 2007'*. Espoo, September 12-14, 2007, Finland: 50-55.
- Danson, F.M., Hetherington, D., Morsdorf, F., Koetz, B. and Allgöwer, B., 2007. Forest canopy gap fraction from terrestrial laser scanning. *IEEE Geoscience and Remote Sensing Letters*, 4(1), 157-160.
- Fleck, S., Obertreiber, N., Schmidt, I., Brauns, M., Jungkunst, H.F., and Leuschner, C., 2007. Terrestrial lidar measurements for analysing canopy structure in an old-growth forest. In: H.H. P. Rönholm, J. Hyypä (Editor). *Proceedings of the ISPRS Workshop 'Laser Scanning 2007 and SilviLaser 2007'*. Espoo, September 12-14, Finland: 125-129.
- Hopkinson, C., Chasmer, L., Young-Pow, C. and Treitz, P., 2004. Assessing forest metrics with a ground-based scanning lidar. *Canadian Journal of Forest Research*, 34(3), 573-583.
- Király, G. and Brolly, G., 2007. Tree height estimation methods for terrestrial laser scanning in a forest reserve. In: H.H. P. Rönholm, J. Hyypä (Editor). *Proceedings of the ISPRS Workshop 'Laser Scanning 2007 and SilviLaser 2007'*. Espoo, September 12-14, Finland: 211-215.
- Lichti, D.D., Gordon, S.J. and Stewart, M.P., 2002. Ground-based laser scanners: operation, systems and applications. *Geomatica*, 56(1), 21-33.
- Lim, K., Treitz, P., Wulder, M., St-Onge, B., and Flood, M., 2003. Lidar remote sensing of forest structure. *Progress in Physical Geography*, 27, 88-106.
- Van der Zande, D., Hoet, W., Jonckheere, I., Van Aardt, J., and Coppin, P., 2006. Influence of measurement set-up of ground-based LiDAR for derivation of tree structure. *Agricultural and forest meteorology*, 141, 147-160.
- Watt, P.J., and Donoghue, D.N.M., 2005. Measuring forest structure with terrestrial laser scanning. *International Journal of Remote Sensing*, 26(7), 1437-1446.
- Wezyk, P., Koziol, K., Glista, M. and Pierzchalski, M., 2007. Terrestrial laser scanning versus traditional forest inventory. First results from the Polish forests. In: H.H. P. Rönholm, J. Hyypä (Editor). *Proceedings of the ISPRS Workshop 'Laser Scanning 2007 and SilviLaser 2007'*. Espoo, September 12-14, Finland: 424-429.

Terrestrial laser scanners to measure forest canopy gap fraction

F.M. Danson¹, R.P. Armitage¹, V. Bandugula¹, F.A. Ramirez¹, N.J. Tate², K. J. Tansey²
& T. Tegzes³

¹Centre for Environmental Systems Research, School of Environment and
Life Sciences, University of Salford, Manchester M5 4WT, UK
f.m.danson@salford.ac.uk

²Department of Geography, University of Leicester, Leicester, LE1 7RH, UK

³Infoterra Ltd, Atlas House, 41 Wembley Road, Leicester LE3 1UT, UK

Abstract

The directional gap fraction in forest and woodland canopies is the primary information that is used for the non-destructive estimation of canopy leaf area index (LAI). In this study the directional gap fraction of a mixed species forest stand was measured using three different terrestrial laser scanners providing measurements with two different beam divergences at two different wavelengths. Gap fractions estimated from the laser scanners were compared to the gap fraction derived from hemispherical photographs recorded near simultaneously. The results showed that differences in wavelength gave rise to contrasting intensity images which contained complementary information on canopy composition. Wider beam divergence gave rise to lower estimates of gap fraction, and the terrestrial laser scanners underestimated gap fraction when compared to data derived from the hemispherical photographs. Beam divergence, laser wavelength and range-related variation in intensity all affect gap detection. These issues are discussed and future data processing techniques to provide consistent estimates of canopy gap fraction from terrestrial laser scanners are discussed.

Keywords: terrestrial laser scanner, gap fraction, forest canopy

1. Introduction

There has been an explosion of research examining the interaction of airborne laser scanner (ALS) data with forest and woodland canopies (see Omasa *et al.*, 2007 for a recent review), and some significant advances in measuring and modelling these interactions have been made over the last decade (Nilsson 1996; Hyyppä *et al.* 2001; Næsset 2004). ALS provide both spatial and spectral (intensity) data on vegetation properties and the laser scanner data may be related to canopy cover or leaf area index, or may be used to estimate canopy height and crown shape (Koetz *et al.* 2006; Morsdorf *et al.* 2004; Hopkinson and Chasmer, 2007). In contrast to ALS, terrestrial laser scanners (TLS) have the advantage of higher point density, rapid and cheap deployment and multi-angular sampling capability. These features make TLS suitable for point or plot-based surveys of forest structure, and potentially an information source for validating ALS data collected for the same sites.

There are relatively few studies that have used TLS to measure vegetation structure despite the advantages indicated above. Most of the studies published to date using TLS have focussed on the measurement of forest stand variables, including tree height, stem taper, diameter at breast height and planting density (e.g., Hopkinson *et al.* 2004; Thies *et al.* 2004; Watt and Donoghue 2005; Henning and Radtke 2006a). A small number of studies have attempted to use TLS for characterizing canopy variables like leaf area index, canopy cover and the vertical distribution of foliage, and a notable early contribution was the work of Tanaka *et al.* (1998) who coupled a laser source and a digital CCD camera to measure foliage profile in vegetation canopies. The

system was developed to use two different laser wavelengths to map the woody and green material in the canopy (Tanaka *et al.* 2004). Radtke and Bolstad (2001) used a laser range finder to conduct a point quadrat survey in order to determine vertical foliage profile in a broad-leaved forest. LAI estimates from the laser survey were not significantly correlated with LAI derived from litter fall surveys however, and problems with such hand-held systems were highlighted. Lovell *et al.* (2003) used a tripod-mounted laser scanner to determine directional gap fraction in woodland stands of different species and found close correlation with data from hemispherical photography. They also successfully estimated LAI of the stands by using gap fraction data. Henning and Radtke (2006b) tested the application of a TLS to measure a wide range of variables in mixed species broad-leaved woodland and published the first comparisons of single site multi-temporal TLS data for vegetation canopies. Estimation of plant area index and LAI was based on the computation of laser hits within voxels of 0.5m. More recently, a TLS voxel-based approach to the calculation of leaf angle distribution to derive LAI was adopted by Hosoi and Omasa (2007).

Most ALS studies to estimate LAI and canopy cover have been based on the assumption that the ratio of ground returns to total returns is equivalent to the gap fraction in the zenith direction. TLS have the advantage of sampling canopy gap fraction in multiple directions and in this case a Poisson model may be used to derive LAI. With TLS it is the ratio of total laser shots in a given direction to laser shots with a return signal above the noise threshold in the same direction that yields gap fraction estimates; this is likely to provide more accurate estimates of LAI than the vertical sampling of an ALS.

Wagner *et al.* (2006) developed a special form of the radar equation to compute the return power of a laser pulse for a given geometric setting, in which they introduce the cross-section of the scatterer:

| | |
|---|-----|
| $P_r = \frac{P_t D_r^2}{4\pi R^4 \beta_t^2} \sigma$ | (1) |
|---|-----|

Where P_r is the power at the receiver, P_t the laser pulse energy at the transmitter, D_r is the aperture diameter of the receiver optics, R the distance between the laser and the target, β_t is the beam divergence and σ is the backscatter cross-section, defined as:

| | |
|---|-----|
| $\sigma = \frac{4\pi}{\Omega} \rho_s A_e$ | (2) |
|---|-----|

Where Ω is the angle defining a backscattering cone due to surface roughness, ρ_s is the reflectivity of the scatterer and A_e is the illuminated area of the scattering element. From Equation 1 we can see that, for a given TLS, the beam divergence, pulse energy and receiver optics are fixed, and so return power depends on range, target reflectivity and the area of the target within the beam. The return power required to record a laser ‘hit’ also depends on the way in which the instrument analyses the return waveform. Target detection uses a threshold signal above the instrument noise and this threshold may be fixed or depend on a function related to the peak amplitude of the return intensity. A further issue is that target detection will also depend on the wavelength of the laser, since the return signal depends on target reflectivity. Hence, a target with low reflectance may not be detected at the same range as one with a higher reflectance. The objective of this research was to explore these relationships by comparing the directional gap fraction measured at a single forest plot using three different TLS with two different beam divergences, and two different wavelengths.

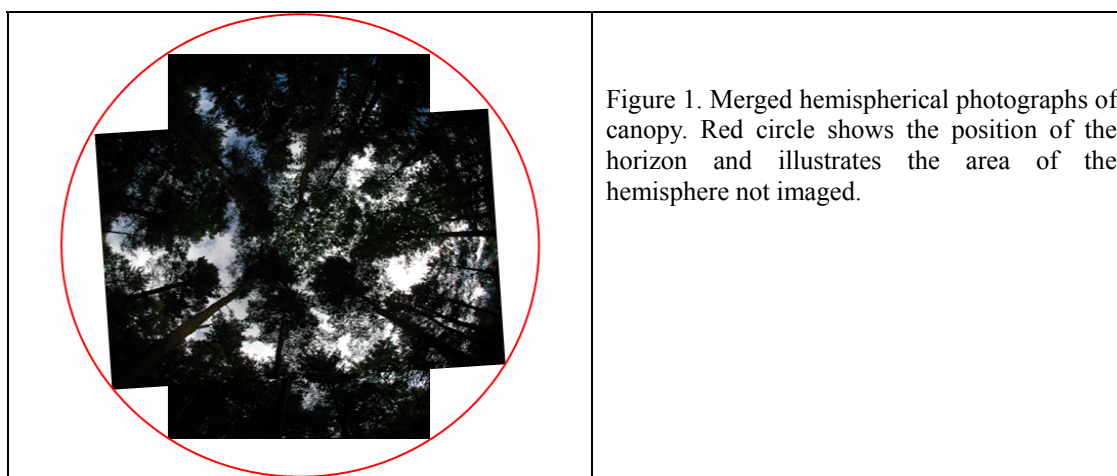
2. Methods

The study area was Martinshaw Wood, located 10km NW of Leicester, UK at British National Grid reference SK510072. The woodland consists of 102ha of mixed species stands owned and managed by the Woodland Trust. The stand used for the measurements consisted of an overstorey dominated by Corsican Pine with Scots Pine and Oak, and an understorey of Hazel, Sycamore, Birch, Hawthorn and Goat willow. Three different Riegl™ TLS (Table 1) were used to collect data following the methodology of Danson *et al.* (2007a), where the laser scanners were mounted on a tripod at a height of 1.5m and oriented to scan in hemispherical mode over a zenith angle range of -90° to $+90^{\circ}$, using the full 80° field of view of the instruments. Two orthogonal scans were recorded so that most of the hemisphere was imaged by the two scans; gap fractions from the two orthogonal scans were later averaged. The angular sampling resolution was set to 0.108° with all instruments recording the ‘last return’ only. A single scan consisted of approximately 1.2 million points and each point was recorded as a set of x, y, z and intensity values. The complete set of measurements (3 TLS \times 2 scans) was completed within approximately 50 minutes. A Nikon digital SLR fitted with a hemispherical lens was mounted on the tripod and levelled, and two orthogonal photographs taken. This lens provides a 180° field of view across the image diagonal and the two orthogonal images were later merged to form a single image of approximately 9 megapixels covering most of the hemisphere (Figure 1).

Table 1: Technical comparison of terrestrial laser scanners used

| Riegl model | Beam divergence | Wavelength | Angular step sampling | Maximum range $\rho > 80\%$ |
|-------------|-----------------|------------|-----------------------|--------------------------------|
| LMS-Z210i | 2.7 mrad | 900nm | 0.108° | 650m |
| LMS-Z390i | 0.3 mrad | 1550nm | 0.108° | 400m |
| LMS-Z420i | 0.27 mrad | 1550nm | 0.108° | 1000m |

To compute the directional gap fraction for the laser scanner data the number of ‘hits’ (laser shots with measured echo) in 5 degree zenith bands (0-4.9, 5-9.9, etc.) was computed by comparing the measured data with the expected number of ‘shots’ in the same zenith bands, derived from a model which takes into account the scan geometry and angular step sampling of the scanners (Danson *et al.* 2007a). The ratio of hits to shots was used to derive the average canopy gap fraction in a given zenith band. The hemispherical photographs were analysed using the Gap Light Analyzer software (Frazer *et al.* 2000) with different thresholds to differentiate the canopy from the sky.



3. Results

Simple visualisation of the laser scanner data showed the striking difference in intensity values caused by differences in laser scanner wavelength (Figure 2). The Z210i data show low intensity for the tree stems and branches and higher intensity for dense areas of foliage. In contrast the Z390i and Z420i scans show high intensity for the tree stems and relatively lower intensity for the foliage. There is also evidence in Figure 2 that the Z210i ‘sees’ fewer gaps in the canopy than the other two TLS. It should be noted that cross comparison of the intensity values between the intensity images from the three scanners is not advisable since the intensity data are not cross-calibrated between the scanners.

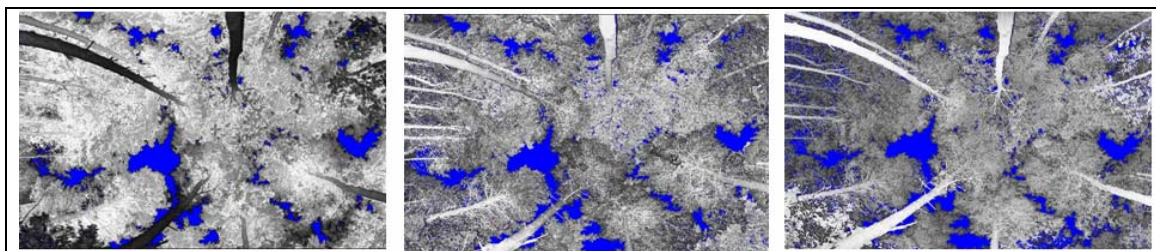


Figure 2. Intensity images of forest canopy in cylindrical projection from Z210i (left), Z390i (middle) and Z420i (right). Sky gaps are blue.

The canopy directional gap fraction computed from the three laser scans showed a similar pattern with a very low gap fraction at zenith angles between 0° to 20°, maximum gap fractions of approximately 13% at zenith angles between 25° to 30° and lower gap fractions at higher zenith angles. The Z210i data showed a 2-3% lower gap fraction across all zenith angles; the Z390i and Z420i showed very similar gap fractions up to 35° and thereafter the Z420i showed a 3-4% larger gap fraction (Figure 3).

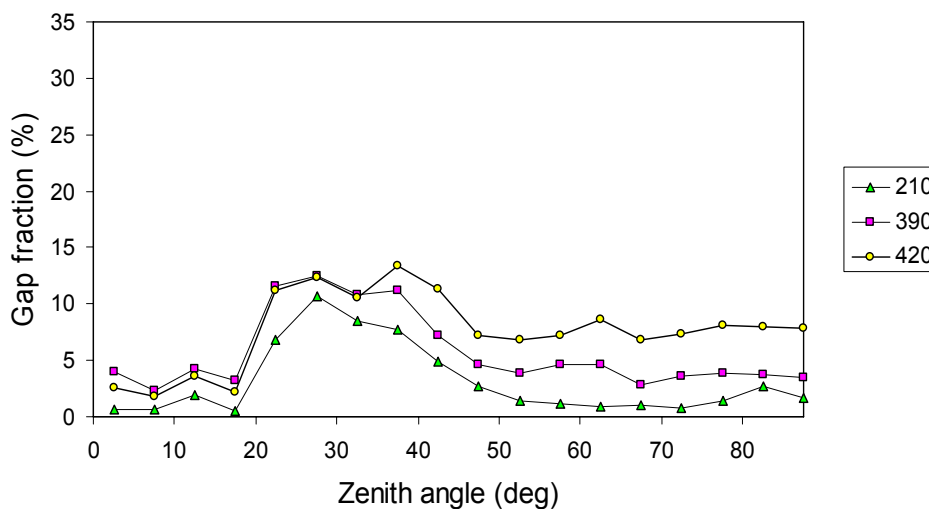


Figure 3. Directional gap fractions computed from three different laser scanners.

Comparison of the gap fraction computed from the laser scanners and the hemispherical photographs showed large differences in the magnitude and shape of the gap fraction distributions (Figure 4). Gap Light Analyzer allows different threshold to be applied to separate sky and non-sky elements. Using an automatic threshold of 128 (T128) produced a maximum gap fraction of 26% compared to 13% for the Z390i. Using a higher threshold (T200) which

reduced the sky fraction in the photographs resulted in a lower gap fraction, closer in magnitude to that of the laser scanner data, but again different in shape (Figure 4).

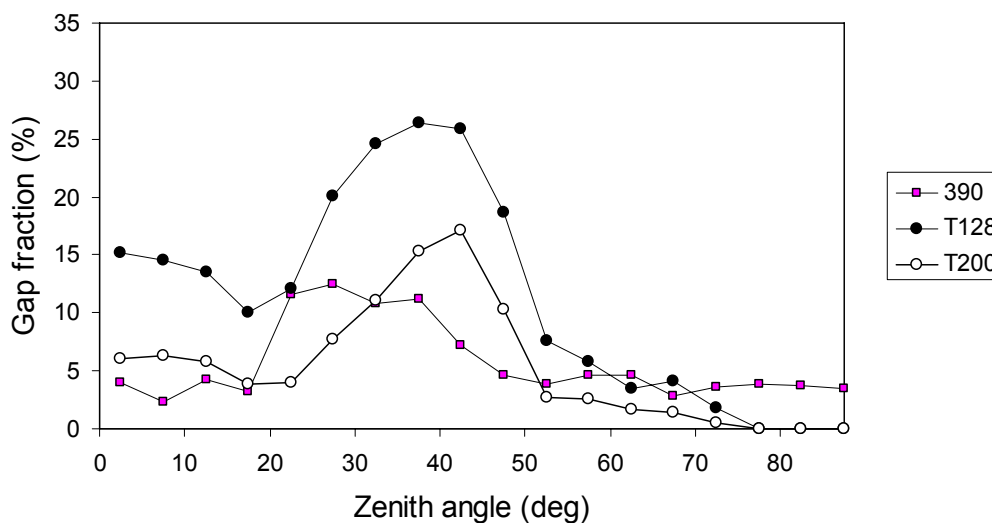


Figure 4. Comparison of gap fraction derived from Z390i laser scanner, and hemispherical photographs with two different thresholds (T128 and T200)

4. Discussion

The variations in intensity in the laser scanner data (Figure 1) are related to differences in the reflectance properties of the scattering elements. At a laser wavelength of 900nm (Z210i) the reflectance of vegetation is greater than the reflectance of the tree stems, since this is the wavelength region of greatest scattering and lowest absorption for green vegetation. In contrast, 1550nm (Z390i and Z420i) is a region of water absorption for vegetation and it is likely that the green vegetation has a lower reflectance than the tree stems. These spectral contrasts provide an opportunity for classification of laser data, according to intensity, in order to separate woody and green material using multiple wavelengths. Two factors add complexity here however, first, where the scattering elements do not fully occupy the laser beam, a lower intensity may be recorded and this may be interpreted as comprising objects with lower reflectance, second, we have identified a range-dependent variation in intensity which is related to the scanner optical system rather than to the physics of the radar equation (Danson et al., 2007b). It will be necessary to characterize and correct this variation before the intensity data can be properly interpreted. It will also be necessary to examine the directional reflectance properties of forest canopy targets since the return intensity is also affected by variation in target bidirectional reflectance distribution function.

The differences in measured canopy directional gap fraction between the three laser scanners are primarily related to differences in beam divergence. The Z210i produces a beam that is 30mm wide at 10m range whereas the Z390i and Z420i produce beams which are 3mm and 2.7mm wide at 10m range respectively. The Z210i therefore does not ‘see’ the smaller gaps in the canopy because the probability of a scattering element appearing within the wider beam is greater. The directional gap fraction measured by the Z390i and Z420i, with similar beam divergence, is very similar up to the 35-40° zenith band, but the higher gap fraction for the Z420i at larger zenith angles is difficult to explain. The Z420i has a much longer range and slightly narrower beam than the Z390i and these may affect the echo detection characteristics; further investigation and experimentation of this point is clearly required. It may also be the

case that the Z420i was measuring a slightly different part of the canopy since no attempt was made to accurately co-locate the scans from the three instruments.

The difference in directional gap fraction estimates from the laser scanner data and the hemispherical photography is striking and we hypothesise that it is related to the way in which pulses are detected by the laser scanners. Small objects, occupying a small proportion of the area of the beam, appear to be detected by the laser scanners. If gaps occupying less than 50% of the laser beam are detected by the laser scanner then this will lead to an underestimation of the gap fraction. We have experimented with filtering the laser scanner data to remove points with low intensity hypothesised to correspond to larger gaps. Removal of these points increases the gap fraction estimates but the range-related intensity variation mentioned earlier must be addressed before this approach can be properly tested.

5. Conclusions

Terrestrial laser scanners have the potential to revolutionise the measurement of vegetation canopy structure. However, commercially available instruments are primarily designed to measure ‘hard’ objects like buildings and terrain. The application of this technology to measure soft targets like vegetation canopies presents some real challenges of data collection, data interpretation and modelling. Comparisons with hemispherical photographs are useful since such data have been used to measure forest canopy gap fraction for many years. It is clear however that further data processing will be required before the measurements converge. Further research is required to explore the use of intensity data in the calculation of gap fraction, to address some of the issues identified above. It is clear that intensity calibration will be vital if we are to use this information to improve gap fraction calculations. A better understanding of the interactions of TLS with vegetation canopies should yield new methods for characterising forest and woodland canopies and provide a practical way of validating studies undertaken with ALS data.

Acknowledgements

The Woodland Trust is acknowledged for allowing access to Martinshaw Wood. Two anonymous referees provided useful comments which have been used to enhance the paper.

References

- Danson, F.M., Hetherington, D., Morsdorf, F., Koetz, B. & Allgower, B., 2007a. Forest canopy gap fraction from terrestrial laser scanning. *IEEE Geoscience and Remote Sensing Letters* 4, 157-160.
- Danson, F.M., Giacosa, C. & Armitage, R.P., 2007b. Two-dimensional forest canopy architecture from terrestrial laser scanning. In *International Archives of Photogrammetry, Remote Sensing and Spatial Information Sciences*, Vol. XXXVI, Part 7/C50, Schaepman M, Liang S, Groot N, Kneubuhler M (eds). March 12-14, Davos, Switzerland: International Society for Photogrammetry and Remote Sensing.
- Frazer, G. W., Canham, C. D. & Lertzman, K. P., 2000. Gap light analyzer (GLA), Version 2.0: Image-processing software to analyze true-color, hemispherical canopy photographs. *Bulletin of the Ecological Society of America* 81, 191-197.
- Henning, J.G., & Radtke, P.J., 2006a. Detailed stem measurements of standing trees from ground-based scanning lidar. *Forest Science* 52, 67-80.
- Henning, J.G., & Radtke, P.J., 2006b. Ground-based laser imaging for assessing three-dimensional forest canopy structure. *Photogrammetric Engineering and Remote Sensing* 72, 1349-1358.

- Hopkinson, C., Chasmer, L., 2007. Modelling canopy gap fraction from lidar intensity. ISPRS Workshop on Laser Scanning 2007 and SilviLaser 2007, Espoo, September 12-14, 2007, Finland. *IAPRS Volume XXXVI, Part 3 / W52*, 190-194.
- Hopkinson, C., Chasmer, L., Young-Pow, C. & Treitz, P., 2004. Assessing forest metrics with a ground-based scanning lidar. *Canadian Journal of Forest Research* 34 (3), 573–583.
- Hosoi, F and Omasa, K., 2007. Factors contributing to accuracy in the estimation of the woody canopy leaf area density profile using 3D portable lidar imaging. *Journal of Experimental Botany* 58(12), 3463–3473,
- Hyypä, J., Kelle, O., Lehikoinen, M., & Inkinen, M., 2001. A segmentation-based method to retrieve stem volume estimates from 3-d tree height models produced by laser scanners. *IEEE Transactions on Geoscience and Remote Sensing* 39, 969–975.
- Koetz, B., Morsdorf, F., Sun, G., Ranson, K. J., Itten, K., & Allgower, B., 2006. Inversion of a lidar waveform model for forest biophysical parameter estimation. *IEEE Geoscience and Remote Sensing Letters* 3, 49–53.
- Lovell, J. L., Jupp, D. L. B., Culvenor, D. S., & Coops, N. C., 2003. Using airborne and ground-based ranging lidar to measure canopy structure in Australian forests, *Canadian Journal of Remote Sensing* 29 (5), 607–622.
- Morsdorf, F., Meier, E., Kötz, B., Itten, K. I., Dobbertin, M., & Allgöwer, B., 2004. Lidar- based geometric reconstruction of boreal type forest stands at single tree level for forest and wildland fire management. *Remote Sensing of Environment* 3 (92), 353– 362.
- Næsset, E., 2004. Effects of different flying altitudes on biophysical stand properties estimated from canopy height and density measured with a small-footprint airborne scanning laser. *Remote Sensing of Environment* 91(2), 243–255.
- Nilsson, M., 1996. Estimation of tree heights and stand volume using an airborne lidar system. *Remote Sensing of Environment* 56, 1–7.
- Omasa, K., Hosoi, F., & Konishi, A., 2007. 3D lidar imaging for detecting and understanding plant responses and canopy structure. *Journal of Experimental Botany* 58(4): 881–898,
- Radtke, P.J., & Bolstad, P.V. 2001. Laser point-quadrat sampling for estimating foliage-height profiles in broad-leaved forests. *Canadian Journal of Forest Research* 31, 410-418.
- Tanaka, T., Yamaguchi, J., & Takeda, Y., 1998. Measurement of forest canopy structure with a laser plane range-finding method - development of a measurement system and applications to real forests. *Agricultural and Forest Meteorology* 91, 149-160.
- Tanaka, T., Park H. & Hattori, S., 2004, Measurement of forest canopy structure by a laser plane range-finding method improvement of radiative resolution and examples of its application, *Agricultural and Forest Meteorology* 125 (1-2), 129-142.
- Thies, M., Pfeifer, N., Winterhalder, D., & Gorte, B. G. H., 2004. Three dimensional reconstruction of stems for assessment of taper, sweep and lean based on laser scanning of standing trees, *Scandinavian Journal of Forest Research* 19 (6), 571–581.
- Wagner, W., Ullrich, A., Ducic, V., Melzer, T. & Studnicka, N., 2006. Gaussian decomposition and calibration of a novel small-footprint full-waveform digitising airborne laser scanner. *ISPRS Journal of Photogrammetry and Remote Sensing* 60, 100 – 112.
- Watt, P. J. & Donoghue, D. N. M., 2005. Measuring forest structure with terrestrial laser scanning. *International Journal of Remote Sensing* 26, 1437–1446.

Poster Presentations

Extraction of vegetation for topographic mapping from full-waveform airborne laser scanning data

Cici Alexander¹, Kevin Tansey¹, Nicholas J. Tate¹, Sarah Smith-Voysey² & Jörg Kaduk¹

¹ Department of Geography, University of Leicester, United Kingdom
ca90@le.ac.uk, kjt7@le.ac.uk, njt9@le.ac.uk, jk61@le.ac.uk

² Ordnance Survey Research Fellow, Newcastle University, United Kingdom
sarah.smith-voysey@newcastle.ac.uk

Abstract

Most of the research using lidar on vegetation has focussed on deriving forest and single tree characteristics. Very few studies have looked at mapping vegetation, including low vegetation, for topographical mapping. The aim of this study was to evaluate the classification and extraction of vegetation characteristics for topographic mapping using full-waveform airborne laser scanning data. The laser data were captured at a height of approximately 950m above ground level providing a point density ranging from 0.5-0.8 points per m². A subset of points representing the various surfaces – vegetation, roads and buildings – was extracted and analysed to identify surface attributes to be used for further analysis and classification. Vegetation was classified into three categories based on height from the ground. The training dataset comprised approximately 16000 points selected from one million data points. A Triangulated Irregular Network (TIN) was created from the elevation of the points. Classification was undertaken on the point cloud based on the local statistical variation of attributes of TIN triangles as well as attributes of the individual points. We show that a decision-tree classifier performs significantly better than k-means clustering based on the train-all-test-all accuracy. Future work will establish the accuracy of the classification of vegetation objects on untrained data.

Keywords: Full-waveform Lidar, Vegetation, Mapping, Classification

1. Introduction

The measurement of distances using laser scanning (Lidar), is fast becoming a standard tool in the fields of remote sensing, surveying and mapping. Laser scanning can provide accurate and fast digital models of the topography, and vertical structures of target surfaces at much lower field-operation costs point-for-point, with reduced post-processing time and effort compared to traditional survey methods. There are two distinct techniques used in lidar systems based on how the return signal is recorded. The more commonly used discrete return lidar systems record single or multiple return signals for every emitted pulse. The other emerging technique is waveform-digitizing lidar which samples and records the full waveform of the return signal to capture a complete elevation profile within the target footprint, or the area illuminated by the laser beam (Flood, 2001).

Most of the research on vegetation studies using lidar has been in forestry and can be divided into stand-based and individual tree-based studies. Stand-based studies have focussed on extracting characteristics like canopy height, canopy openness and tree-species composition and derived information like average stem diameter, forest biomass, Leaf Area Index and canopy volume (Harding et al., 2001; Hollaus et al., 2006). Individual tree-based studies mainly look at location, crown delineation, height and species identification (Holmgren and Persson, 2004; St-Onge, 1999; Suárez et al., 2005). These studies were based on lidar data alone, or lidar with optical imagery

(Bork and Su, 2007; Hill et al., 2002; Hill and Thomson, 2005; Hyde et al., 2005). There are only a few studies, which have looked at mapping vegetation, including low vegetation, for topographical mapping from lidar data.

The classification of vegetation points from lidar point clouds is considered to be a challenge, especially in the case of low vegetation, and is a focus of current research. The analysis of discrete return data relies on the spatial relationship of the points. However, the full-waveform data give additional information about the objects in the path of the laser pulse (Wagner et al., 2006). This could lead to the development of classification methods based on the information from each point with less reliance on spatial relationships, which would simplify the processing significantly. Many analytical waveform solutions are based on Gaussian decomposition (Hofton et al., 2000; Wagner et al., 2006). The assumption is that the scattering properties of a cluster of targets can be described by a Gaussian function. An extended target could be described by a series of Gaussian functions, where each pulse represents a cluster of targets too close to be differentiated. This method gives estimates of the location and scattering properties of the targets. These include pulse width, amplitude, range and cross-section of each detected echo, and the number of returns and total cross-section of each laser pulse (Wagner et al., 2008).

Some of these attributes, which are direct properties of the return signal, have been used for distinguishing vegetation and non-vegetation points from full-waveform data (Ducic et al., 2006; Wagner et al., 2008). Their values, however, could be dependent on the method of waveform decomposition used.

Classification mainly employs parametric classification, decision-tree approaches and k-means clustering. Ducic et al. (2006) used a decision tree, but could classify the returns only into vegetation and non-vegetation due to the difficulty in separating trees and shrubs (vegetation) from grass, roof and road (non-vegetation). This could be because their aim was to classify points without using elevation or relationship to adjacent points.

Charaniya et al. (2004) have been able to classify discrete return lidar data into trees, grass, roads and building roofs with a classification accuracy of 66% - 84%. In their study, the lidar data were interpolated to a regular grid, and classification was based on normalised height, height variation, multiple returns, luminance and intensity. The luminance values were obtained from an additional grey scale aerial image.

Increasingly further attributes of the surface derived from the lidar, e.g. roughness and mean slope etc., are used for classification. Miliareisis and Kokkas (2007) employed parametric classification and k-mean clustering for the extraction of building and vegetation classes from lidar DEMs based on elevation, roughness, mean slope and standard deviation of the slope of grid cells.

This study classifies points based on parameters extracted from full-waveform data into vegetation, roads and building roofs. The classified points are converted to polygons by dissolving Thiessen polygons based on the estimated class. The points within the vegetation polygons will be analysed in future work to classify vegetation itself into different sub-classes to be represented within a three-dimensional topographical map.

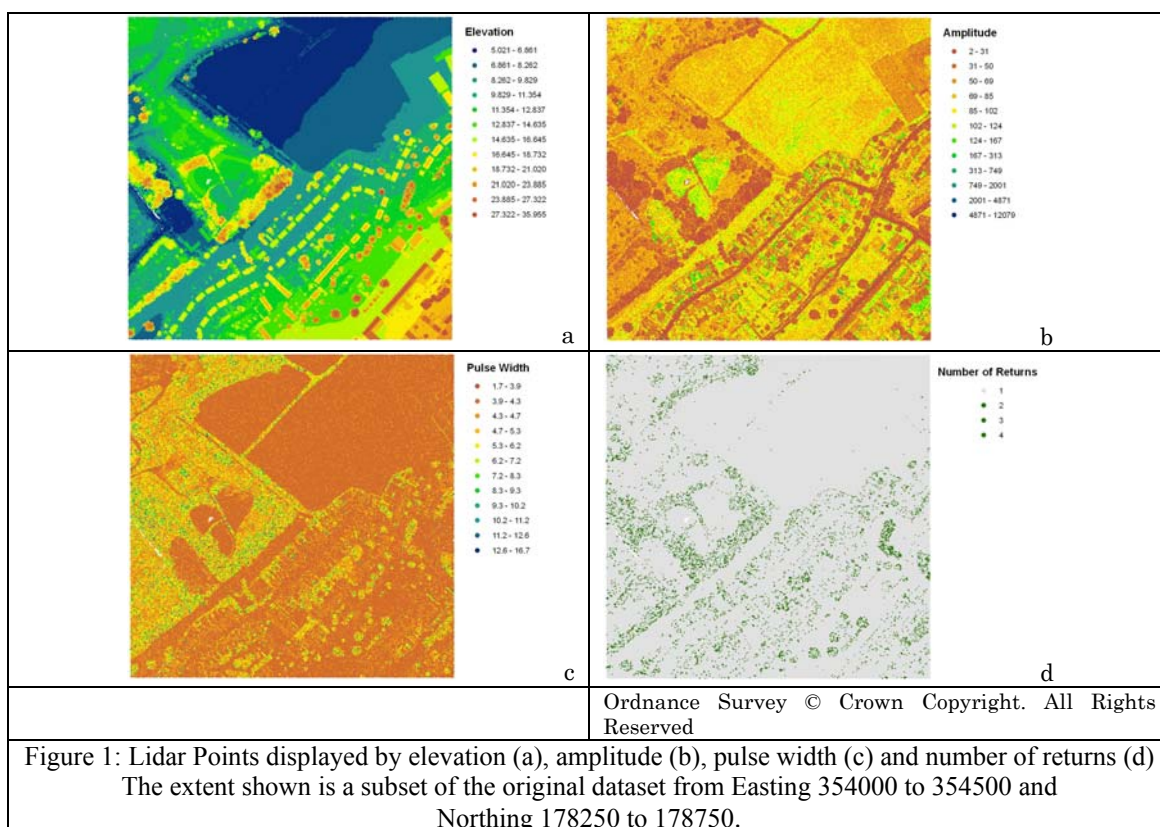
2. Study Area and Dataset

A full-waveform lidar dataset was obtained, over the Avonmouth area of Bristol, using LiteMapper5600 Airborne Lidar Terrain Mapping System in August, 2006. The study area is 1 km², from Easting 354000 to 355000, and Northing 178000 to 179000 (OS British National Grid coordinates), which includes a range of land use and landcover types. In addition to stands of

trees, there are trees along the road, shrubs in gardens in the residential areas as well as grassland. The land use includes residential, commercial and institutional areas and agricultural land.

The LiteMapper system makes use of RIEGL LMS-Q560 laser scanner, and data were captured at a height of approximately 950m above ground level. The point density ranged from 0.5-0.8 points per m² per flightline. Four flightlines, with overlaps, covered the whole study area. The raw waveforms were decomposed using the standard method, Gaussian Pulse Fitting, available in the commercial package RiAnalyze™ 560. RiWorld™ 560 was used to transform the data into WGS Cartesian coordinates. This was converted to British National Grid before further analysis.

The extracted points were displayed in ArcMap™ using the various attributes. All the returns were made use of for the analysis, which along with the overlapping swath widths of the flight lines generated above 1000000 points giving an average point density of approximately 1 point per m². The topographic features could be distinguished to a certain extent by displaying points by elevation, amplitude, pulse width and the number of returns (Fig. 1). Elevation from mean sea level is calculated from the location and orientation of the sensor, and the distance or range to the target. The amplitude is a measure of the strength of the return pulse. The pulse width refers to the standard deviation of the pulse in the Gaussian decomposition. The number of returns denotes whether the point is one of a single, two, three or more hits of a single emitted pulse.



3. Methodology

Attributes of individual points as well as attributes based on the spatial relationship of points to neighbouring points were used in the classification process. Amplitude, pulse width and the number of returns of each point were used as attributes of the individual points. A Triangulated Irregular Network (TIN) was created from all the extracted points. Local height variation of a

point was taken as the difference between the maximum and the minimum elevation values of the nodes of TIN triangles attached to each point. Variation of slopes and aspects of attached TIN triangles were used to analyse whether the different surfaces could be separated. The parameters considered were average and standard deviation of slopes and aspects.

An approximate terrain model was created from the lidar points making use of the lowest point in a 10m grid. A TIN was created from these points. There were a few outliers, which were removed manually. They could be identified as nodes of the triangles with steeper slopes or with higher elevation than the surrounding points. These were removed in two steps by creating a TIN after each selection. The final TIN, generated from the selected points, was converted to a 2m grid. The terrain elevation was subtracted from the elevation of each point to get the elevation of the point above the ground, or the normalised elevation.

The topographic features can broadly be classified into natural and man-made features. The natural features consist mainly of vegetation and were divided, based on the elevation, into low (<0.5m), medium (0.5 – 2.5m) and high (>2.5m). The intervals were chosen based on the approximation of terrain elevation and the assumption that building roofs are higher than 2.5m. The man-made features were divided into roads and buildings. The buildings were sub-divided into those with flat and pitched roofs. Training polygons were created for the above six landcover classes using lidar points and an ortho-rectified aerial image. The training polygons contained 16378 points in all, out of which 9835 were vegetation points, 2367 road points and 4176 building points.

The lidar points were classified using five methods. First we used a k-means clustering requiring 12 clusters. In the second method, the means of the attribute values for the various classes in the training dataset were given as the seed points for clustering. The first four principal components of the data were seen to represent 79% of the total variance of the original data, and were used for unsupervised classification in the third method. Next, the means of the canonical variables grouped by the landcover type were used as initial cluster centres for classification. Elevation was grouped into three – less than 0.5m, 0.5 to 2.5m and greater than 2.5m – and a classification was done using this instead of the actual elevation from the terrain for each of the above methods. The last method involved generating a decision tree using the training dataset for classifying the lidar points into the six classes (Figure 2). The significance of the attributes was analysed by taking out one attribute at a time and testing the accuracy of the classification, maintaining similar number of nodes for the decision tree.

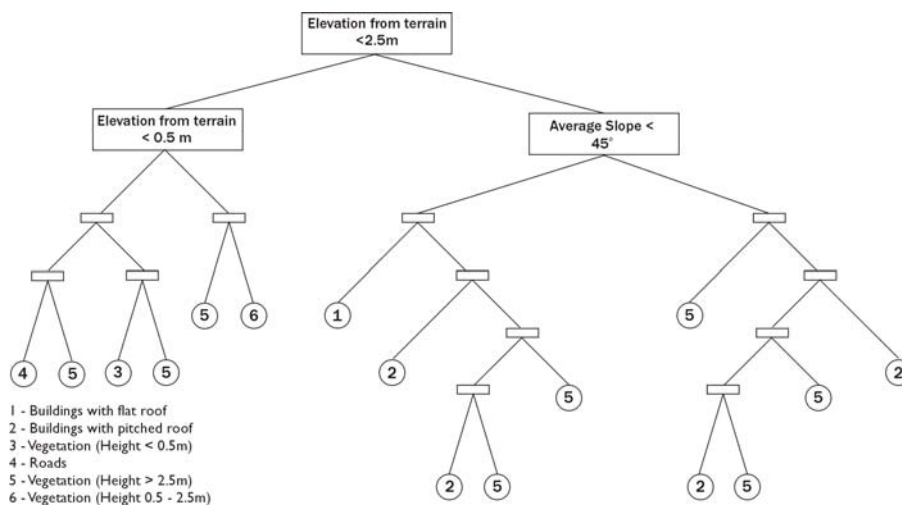


Figure 2: The pruned decision tree for classification

4. Results

Landcover maps were generated using the various classification methods (Fig. 3a-e). Some of the misclassifications become evident on visual analysis, and some by comparing with OS MasterMap™ polygons and an aerial photograph (Fig. 3f-g).

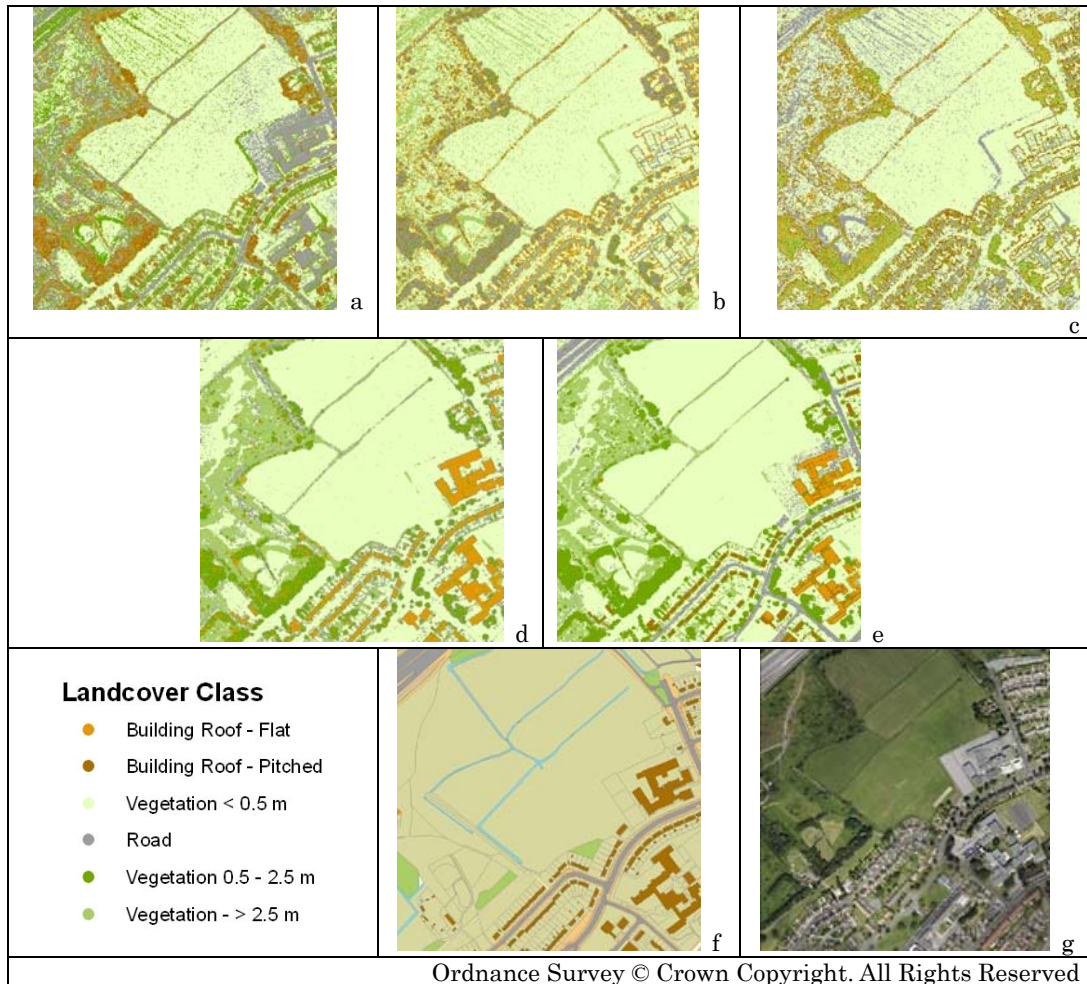


Figure 3: Landcover maps generated using the classes from a) unsupervised k-means classification, b) unsupervised classification with attribute means from the training dataset as seed points, classification using c) variables from principal components analysis, d) canonical variables, e) decision tree classifier and f) OS MasterMap™, g) Aerial Photograph

Table 1 shows the number of correctly classified points from each category, and the overall accuracy for each method. The accuracy assessment makes use of only the training data. Only 36% of the points were correctly classified by the first method. All the flat roofed buildings were misclassified, and the accuracy was very low for trees (3%). The accuracy was the highest for grass and road (88% and 84% respectively). The overall accuracy of the classification increased to 58% in the second method though the accuracy was still low for flat roofed buildings. The misclassification between pitched roofs and trees decreased with this method. The overall accuracy using principal components was higher than that of the first classification, but lower than that of the second. There was an increase in the classification accuracy for pitched roofed buildings and trees. The overall accuracy from canonical variables was almost double of that using the principal components. The accuracy of classification of flat-roofed buildings increased from 0 to 93%. The significant misclassification was that of shrubs as grass.

Table 1: Overall accuracy for k-means Classifications

| | Veg < 0.5m | Veg 0.5 – 2.5m | Veg > 2.5m | Roads | Flat Roof | Pitched Roof | Overall Accuracy |
|------------------|------------|----------------|------------|-------|-----------|--------------|------------------|
| Method 1 | 2189 | 412 | 166 | 1989 | 0 | 1139 | 35.99 % |
| Method 2 | 2078 | 754 | 2100 | 2188 | 1 | 2440 | 58.38 % |
| Method 3 | 2009 | 59 | 817 | 2095 | 0 | 2286 | 44.36 % |
| Method 4 | 2420 | 930 | 4979 | 2207 | 628 | 3202 | 87.72 % |
| Number of points | 2496 | 1927 | 5412 | 2367 | 674 | 3502 | 16,378 |

Grouping the elevation attribute into three, increased the classification accuracy from 36% to 54% for the first, from 58% to 60% for the second and from 88% to 94% for the fourth method. However, for the third method based on principal components, the accuracy reduced from 44% to 40%.

The overall accuracy of the classification using the decision tree on the training dataset was 98% (Table 2). The pruned decision tree does not make use of the two attributes, standard deviation of aspects and the number of returns. It was seen that the classified elevation and amplitude contributed the most to the accuracy of the classification. Excluding elevation from the decision tree reduced the overall accuracy to 80% and excluding amplitude reduced the accuracy to 88%. Excluding pulse width reduced the accuracy only slightly from 98.1% to 97.65%.

Table 2: Error Matrix for Classification using the pruned Decision Tree
The accuracies are for the data used in the training dataset on a train-all-test-all basis.

| | Veg < 0.5m | Veg 0.5 – 2.5m | Veg > 2.5m | Road | Flat-roof | Pitched-roof | User's Accuracy |
|---------------------|------------|----------------|------------|-------|-----------|--------------|-----------------|
| Veg < 0.5m | 2492 | 3 | 0 | 1 | 0 | 0 | 99.84 |
| Veg 0.5 – 2.5m | 1 | 1922 | 4 | 0 | 0 | 0 | 99.74 |
| Veg > 2.5m | 0 | 1 | 5268 | 0 | 1 | 142 | 97.34 |
| Road | 36 | 7 | 28 | 2296 | 0 | 0 | 97.00 |
| Flat-roof | 0 | 0 | 0 | 0 | 670 | 4 | 99.41 |
| Pitched-roof | 0 | 0 | 152 | 0 | 13 | 3337 | 95.29 |
| Producer's Accuracy | 98.54 | 99.43 | 96.63 | 99.96 | 97.95 | 95.81 | 98.10 |

5. Discussion

The height variation is a measure of the roughness of the surface and is expected to be high for vegetation. This was seen to be more useful than standard deviation and absolute deviation from the mean of elevations within a window in the case of rasterised data (Charaniya et al., 2004). Local statistical variation of attributes of grid cells has been used for separating buildings from other surfaces (Alharthy and Bethel, 2002; Miliarisis and Kokkas, 2007). This was adapted for point data by making use of the variation of attributes of TIN triangles attached to a point. Out of these, the average aspect was found to be of not much use since even flat surfaces could have minor differences in their aspects.

Box-and-whisker plots were used to analyse the various attributes grouped into categories. The amplitude values of roads and trees seem to be lower than that of grass, shrubs and buildings. Though the values overlap, amplitude seems to be a useful attribute in separating roads from low vegetation. The pulse widths are higher and of a wider range for vegetation than for grass, roads or buildings as seen from earlier studies (Ducic et al., 2006). The number of returns is more than one for vegetation and building edges. There are some multiple returns from roads, which could be from overhanging vegetation or vehicles.

The normalised elevation, or elevation from the estimated terrain, is useful in separating buildings from the other classes, especially road and grass. The lower outliers in vegetation are probably from, or close to the ground. The mean slope of the TIN triangles, which has the point as the common node, seems useful in identifying trees, which have larger height variations and hence, higher average slopes. The higher values of the outliers in the roads could be from vehicles, or branches of trees. The standard deviation of slopes of TIN triangles attached to a point is lower and less variable for road, grass and buildings with flat roof. This additional attribute is expected to aid in the correct classification of surfaces if the terrain itself is sloping. The standard deviation of aspects of attached TIN triangles was found to be lower for buildings with pitched roofs than those with flat roofs. This could be because even for a relatively flat horizontal surface, there are minor variations in the aspects. This is less pronounced in sloping roofs. However, this is only of limited use since this is not applicable in the case of ridges and features on the pitched roof. Nevertheless, this attribute is included as the separation of vegetation and pitched roof seems to be the most difficult, and it could be useful in the classification process.

A matrix of scatter plots of the various attributes, grouped by the landcover classes, was generated to analyse the inter-relationships between the attributes. Amplitude and average slope seem to bring out the best separation between the classes. Some of the derivatives of elevation – height variation, average slope, standard deviation of slope and standard deviation of aspect – seem to have a high correlation (Table 3). The average slope has a high correlation with elevation as well as height variation, which is to be expected.

Table 3: Matrix of correlation coefficients of the attributes

| | Amplitud e | Widt h | Elevatio n | Av_slop e | Std_slop e | Std_aspec t | Ht_va r | Nu m |
|----------------|---------------|-----------|---------------|--------------|---------------|----------------|------------|---------|
| Amplitud e | 1 | | | | | | | |
| Width | -0.3 | 1 | | | | | | |
| Elevation | -0.28 | 0.34 | 1 | | | | | |
| Av_slope | -0.43 | 0.38 | 0.75 | 1 | | | | |
| Std_slope | -0.19 | 0.29 | 0.45 | 0.44 | 1 | | | |
| Std_aspec t | -0.13 | 0.05 | -0.09 | -0.03 | 0.02 | 1 | | |
| Ht_var | -0.38 | 0.29 | 0.54 | 0.77 | 0.26 | 0.04 | 1 | |
| Num | -0.4 | 0.07 | 0.28 | 0.57 | 0.12 | 0.07 | 0.42 | 1 |

5.1 Classification by clustering

Cluster analysis groups objects into clusters or groups based on the similarity of their attributes. The k-means method is considered to be suitable for clustering large amounts of data. It partitions the observations in the data into k mutually exclusive clusters in a c-dimensional space where c is the number of attributes used in the classification process (Mathworks, 2008a; Miliareisis and Kokkas, 2007). The required number of clusters, k, has to be provided by the user.

Subtractive clustering is an algorithm for estimating the number of clusters and the cluster centres in a dataset. The range of influence of the cluster centre has to be specified for each dimension, and 0.2 to 0.5 is considered to be the optimum range of values. A value of 0.5 would mean that the range of influence is half the width of the data space for the particular attribute (Mathworks, 2008b). Values from 0.2 to 0.5 were considered for the range of influence with an increment of 0.1. The number of estimated clusters were 12, 7, 4 and 3 respectively. Twelve clusters were considered for further work since it would be easy to re-classify this into the six landcover classes.

The attribute values were transformed using z-score to standardise the differing value ranges of the attributes. In z-score transformation, the mean of the attribute values is subtracted from the data value and the resulting value divided by the attribute standard deviation. The training dataset was partitioned into twelve clusters in the first method. The initial cluster centroid positions are chosen at random by the k-means classifier, and the classification would differ depending on the location of the seeds. To avoid this, the cluster centres generated by subtractive clustering were used as the seed points. The clusters were then re-classified into the six landcover classes based on their proximity to the mean of the attribute values for the different classes in the c-dimensional space. This was done by a k-means classification of the centroid locations, with six as the desired number of classes and the attribute value means as the seeds. In the second method, the attribute value means from the training dataset were chosen as the initial cluster centres.

As shown by the correlations between attributes (Table 3) there is some redundancy in the information content of the whole data set. Principal components analysis is a method to reduce this by generating a new set of variables. All the principal components are orthogonal to each other and each component is a linear combination of the original variables. As in the unsupervised classification, the number of clusters was determined by subtractive clustering. Six clusters were identified, and the k-means classification was done using the mean attribute values of the transformed dataset from subtractive clustering as seed points. The six clusters were reclassified into the six landcover classes as earlier based on their proximity.

The canonical variables are linear combinations of the original variables, chosen to maximize the separation between groups, or the six landcover classes. Among all possible linear combinations, the first canonical variable has the maximum separation between groups. The second canonical variable has the next maximum separation subject to it being orthogonal to the first, and so on. The first four canonical variables were used for the k-means classification with the means of the canonical variables as the seed points.

5.2 Classification Using Decision Tree

The first four methods are based on the assumption that the populations of each group are normally distributed. Decision trees offer a non-parametric alternative and do not require such assumptions or simplifications. The attributes – amplitude, pulse width, elevation class, average slope, standard deviation of slopes, standard deviation of aspects, height variation and the number of returns – were used as the input for creating a classification tree. Maximum deviance reduction was chosen as the splitting rule for generating the decision tree. This created a decision tree with a large number of nodes, which clearly over-fitted the training dataset. The dataset was partitioned into ten random subsamples. For each subsample, a tree was fitted to the remaining data, which was then used to predict the subsample. This was used to derive an optimum level of pruning for the decision tree (Mathworks, 2008b). The ‘best’ level appeared to change with each trial due to the random selection of the subsamples. So, the mode of the best pruning level out of hundred was selected. The original decision tree contained 491 nodes, which was pruned to 31 nodes with a pruning level of 23. This decision tree was used to classify the original dataset.

As seen from the decision-tree diagram, it is difficult to separate buildings with pitched roofs and vegetation higher than 2.5m. This was mainly for the building edges and features like chimneys on the roof. Medians on roads, marked in a lighter colour, have higher amplitudes and are classified as low vegetation. Similarly, some of the vehicles are classified as vegetation of medium height. Some points on trees, possibly with dense foliage, are classified as buildings. It can be seen from the MasterMap data that some of the buildings are not detected, and are classified as vegetation of medium height. This is mainly because some of the smaller buildings are less than 2.5m in height.

6. Conclusion and Future Work

We show that a decision-tree classifier performs significantly better (98% accurate) than k-means clustering (88%) based on the train-all-test-all accuracy. Though it was seen that the standard deviation of aspects and the number of returns were not as useful as expected, it could be due to the selected classes. Standard deviation of aspects could be useful in segmenting the pitched roofs for roof modelling and the number of returns could be useful in sub-classifying vegetation. The average slope and height variation are dependent on the point density, and the pulse width depends on the method of waveform decomposition. These will have to be modified for other datasets. Amplitude is dependent on various factors like the sensor, flying altitude, incidence angle and surface reflectance. Amplitude, corrected for these factors, would be a useful attribute if the classification method is to be applied on other datasets. The classification could be further improved based on the spatial relationships between the classified polygons (de Almeida et al., 2007). Further work is required to test the accuracy of the classification on untrained data.

Acknowledgements

This study was conducted with financial support and data from Ordnance Survey, Southampton. We would like to thank Dr. David Holland (OS) and the two anonymous reviewers for their comments and suggestions.

References

- Alharthy, A. and Bethel, J., 2002. Heuristic Filtering and 3D Feature Extraction from Lidar Data. *International Archives of Photogrammetry and Remote Sensing*, **34-3A**, A.29-A.35.
- Bork, E.W. and Su, J.G., 2007. Integrating LIDAR data and multispectral imagery for enhanced classification of rangeland vegetation: A meta analysis. *Remote Sensing of Environment*, **111**, 11-24.
- Charaniya, A., Manduchi, R. and Lodha, S., 2004. Supervised Parametric Classification of Aerial LiDAR data. *'Real-Time 3D Sensors and their use' Workshop, in conjunction with IEEE CVPR, Washington D.C., June 2004*.
- de Almeida, J.P., Morley, J.G. and Dowman, I.J., 2007. Graph theory in higher order topological analysis of urban scenes. *Computers, Environment and Urban Systems*, **31**, 426-440.
- Ducic, V., Hollaus, M., Ullrich, A., Wagner, W. and Melzer, T., 2006. 3D Vegetation Mapping and Classification Using Full-Waveform Laser Scanning. *Workshop on 3D Remote Sensing in Forestry*, 211-217. Vienna.
- Flood, M., 2001. Lidar activities and research priorities in the commercial sector. *ISPRS Workshop on Land Surface Mapping and Characterization using Laser Altimetry*. Annapolis, Maryland.
- Harding, D.J., Lefsky, M.A., Parker, G.G. and Blair, J.B., 2001. Laser altimeter canopy height profiles: methods and validation for closed-canopy, broadleaf forests. *Remote Sensing of Environment*, **76**, 283-297.
- Hill, R.A., Smith, G.M., Fuller, R.M. and Veitch, N., 2002. Landscape modelling using integrated airborne multi-spectral and elevation data. *International Journal of Remote Sensing* **23**, 2327-2334.
- Hill, R.A. and Thomson, A.G., 2005. Mapping woodland species composition and structure using airborne spectral and LiDAR data. *International Journal of Remote Sensing*, **26**, 3763-3779.
- Hofton, M.A., Minster, J.B. and Blair, J.B., 2000. Decomposition of Laser Altimeter Waveforms. *IEEE Transactions on Geoscience and Remote Sensing*, **38**, 1989-1996.
- Hollaus, M., Wagner, W., Eberhöfer, C. and Karel, W., 2006. Accuracy of large-scale canopy heights derived from LiDAR data under operational constraints in a complex alpine environment. *ISPRS Journal of Photogrammetry and Remote Sensing*, **60**, 323-338.
- Holmgren, J. and Persson, A., 2004. Identifying species of individual trees using airborne laser scanner. *Remote Sensing of Environment*, **90**, 415-423.
- Hyde, P., Dubayah, R., Peterson, B., Blair, J.B., Hofton, M.A., Hunsaker, C., Knox, R.G. and Walker, W., 2005. Mapping forest structure for wildlife habitat analysis using waveform lidar: Validation of montane ecosystems. *Remote Sensing of Environment*, **96**, 427-437.
- Mathworks, 2008a. Fuzzy Logic Toolbox™ User's Guide.
- , 2008b. Statistics Toolbox™ User's Guide.

- Miliaresis, G. and Kokkas, N., 2007. Segmentation and object-based classification for the extraction of the building class from LIDAR DEMs. *Computers & Geosciences*, **33**, 1076-1087.
- St-Onge, B.A., 1999. Estimating individual tree heights of the boreal forest using airborne laser altimetry and digital videography. *ISPRS Workshop on Mapping Surface Structure and Topography by Airborne and Spaceborne Lasers*. La Jolla, USA, November 1999.
- Suárez, J.C., Ontiveros, C., Smith, S. and Snape, S., 2005. Use of airborne LiDAR and aerial photography in the estimation of individual tree heights in forestry. *Computers & Geosciences*, **31**, 253-262.
- Wagner, W., Hollaus, M., Briese, C. and Ducic, V., 2008. 3D vegetation mapping using small-footprint full-waveform airborne laser scanners. *International Journal of Remote Sensing*, **29**, 1433-1452.
- Wagner, W., Ullrich, A., Ducic, V., Melzer, T. and Studnicka, N., 2006. Gaussian decomposition and calibration of a novel small-footprint full-waveform digitising airborne laser scanner. *ISPRS Journal of Photogrammetry and Remote Sensing*, **60**, 100-112.

Use of airborne LIDAR in the estimation of individual tree heights in natural forest

Marcos Vinicius Giongo Alves (mgiongo@gmail.com); Ugo Chiavetta (uchiavetta@unimol.it); Gherardo Chirici (gherardo.chirici@unimol.it); Marco Marchetti (marchettimarco@unimol.it)

Abstract

Natural resources management, for both economical and conservative purposes, needs detailed and precise spatially related information. Forest inventories based on field assessment are the basic source of information to support forest management at local level as at large area level for strategic forest planning. Forest information acquired in the field are extremely expensive, even if acquired on small areas on the basis of sampling techniques. Information available through Airborne Laser Scanning (ALS) based on LIDAR (Light Detection and Ranging) technology is potentially useful in estimating vertical and horizontal structure of forest, such information cannot be detected by traditional optical sensors.

The precision and accuracy of LIDAR based estimations are strongly influenced by site conditions and by the characteristics of the sensors.

The purpose of this work is to evaluate the accuracy of tree height estimations obtained with the use of LIDAR and compare it with field real data in a multilayered complex forest dominated by *Auracaria angustifolia* located in Curitiba, PR (Brazil). The first results cast a promising light on the possible use of LIDAR data in estimating forest structure even in such complex conditions.

Keywords: LIDAR, tree heights, VERTEX

LINHE Project: development of new protocols for the integration of digital cameras and LiDAR, NIR and Hyperspectral sensors

Antolín, R¹., Calzado-Martínez, C²., Gómez, A¹., Manzanera, J.A³, Meroño, J.E², Pedrazzani, D⁴., Pérez, H.H⁴., Roldán-Zamarrón, A⁵., Santos, I⁵. & Valbuena, R³.

¹Stereocarto S.L. Paseo de la Habana 200, Madrid, Spain.

rantolin.agomez@stereocarto.com

²E.T.S.I Agrónomos y Montes UCO, Cordoba, Spain. jma2camac@uco.es

³E.T.S.I. Montes, UPM, C.Universitaria, Madrid, Spain.

joseantonio.manzanera.r.valbuena@upm.es

⁴GMV S.A., Isaac Newton 11, Tres Cantos, Spain. hperez@gmv.es

⁵TRAGSA, Julián Camarillo 6B, Madrid, Spain. aroldan@tragsa.es

Abstract

The LINHE project aims to develop applications for forest management based on the combined use of LiDAR data, images from spaceborne (multi and hyperspectral) and airborne sensors (panchromatic, colour, near infrared), and NIR field data from a portable sensor. The integration of the different types of data should be performed in a rapid, intuitive, cost-effective and dynamic way. In order to achieve this objective, new algorithms were developed and existing ones were tested, for the correlation of data collected in the field and those gathered by the different sensors. Specific software (LINHE prototype viewer) was developed to support data gathering and consultations, and it was tested in three different forest ecosystems, so as to validate the tool for forest management purposes. The optimisation of the synergic capabilities derived from the combined use of the different sensors will allow the enhancement of their efficiency and provide accurate information for operational forestry.

Keywords: LiDAR, Digital photogrammetric Camera, hyperspectral spaceborne sensors, land NIR sensor, forest inventory

1. Introduction

The use of LiDAR (Light Detection and Ranging) technology in different forestry applications is a research line in which universities, technology centres and private companies are currently involved. Commonly, research in LiDAR topics is mainly focused on developing algorithms able to analyse the vast quantity of data gathered. These algorithms (or filters) aim to obtain different digital elevation models of the terrain and of objects attached to and detached from it. Most of these filters were tested and analysed in Sithole and Vosselman (2003). ALS (Airborne Laser Scanning) provides information about forested areas by a direct quantification of certain forest parameters such as tree height (Hyypä et al 2005; Pearsson et al 2002; Popescu et al 2002; Riaño et al 2002) or density related variables as the penetrability index (Morsdorf et al 2005; Riaño et al 2004), and biomass products (Lefsky et al 1999) as forest fuels, carbon sequestration or leaf area index (Roberts et al 2005). Measuring the backscattered intensities of the laser pulses at different heights allows studying the vertical stratification of the canopy cover at a stand level. However, works on LiDAR data applications for forest inventory, such as forest stand control and assessment (Næsset et al 2004; Parker et al 2004), are scarce.

The optimization of the synergic capabilities derived from the combined use of different types of sensors enhances their efficiency by providing accurate information which can be very useful for operational forestry. This approach allows, for instance, adjusting the relationship between

altimetric LiDAR information and individual trees of the forest stand. Even more, it allows relating accurate estimates of sub-stand parameters, i.e. crowning dimensions, height and diameter at breast height or *DBH* (Hyypä and Inkinen 1999), with stand density -by means of canopy detection algorithms-, and structure -by mapping the spatial distribution of dominance and canopy gaps. LiDAR may benefit from image support (Riaño et al 2007; StOnge et al 2001), supplied by video film or by a conventional photogrammetric camera, in order to establish structures. Although it has been hinted that the intensity of the return may provide information about structures, the necessary software has yet to be developed, and at this point this line of research is still at an academic level. Moreover, digital cameras offer RGB colour, panchromatic and infrared images as georeferenced digital products. Combining ALS and photogrammetric data, simultaneously obtained using the same aerial platform, might enhance the possibility of gathering information from ecosystems by adding biological and physical environmental features to the metric parameters obtained by laser.

Additional information captured by other sensors (mid-infrared sensors, near infra-red -NIR- and/or visible spectrum) aids the classification of LiDAR data and it is eventually used to expand the range of predictions across those areas where the use of LiDAR will be too expensive or unfit for the estimation of other valuable information (species distribution, tree health or phenological stage). The infrared spectrum has been traditionally used to evaluate vegetative stages of plants, assess fire damage, track the evolution of pests or pathologies, etc. Combining several sensors offers the advantage of obtaining different kinds of data during the same flight (the principle of capture once and use several times...), although it also poses multiple technical problems yet to be resolved. On the other hand, the possibility of obtaining thematic cartography in real time is opened. "Real time mapping" is currently receiving much attention as will drastically reduce the production cycle (in hours or days) and therefore the production costs.

Hyperspectral images are ideal tools for environmental applications. Fine spectral resolution is important for the discrimination of certain features such as vegetation health or distribution, which can be difficult to detect with medium resolution optical systems or commercial aerial photography configurations. Vegetation has a unique spectral signature which enables it to be distinguished readily from other types of land cover in an optical/near-infrared image. Hence, a characteristic spectral signature can be used for the identification of vegetation types or conditions. The level of resolution of those images offers a local improvement to the use of medium resolution optical from satellite platforms since it can provide a better definition of the relationships between stand structure (stand density or canopy cover) and reflectance. This provides more flexibility in terms of data acquisition, and improves the chances of getting cloud free images. Furthermore, they can provide the sampling material for extending predictions over large areas using cheaper data such as satellite images or thematic layers in a software GIS.

2. Project description and objectives

This paper intends to be a brief description of the LINHE project. The project aims to design and develop a framework (LINHE tool) able to integrate and analyse georeferenced data in order to set up viable and operational applications for forest management purposes. The LINHE tool for forest management consists on a set of procedures and utilities, including techniques for processing and analysing the different data types, the methodologies employed for data acquisition and a prototype viewer. LiDAR data, images from spaceborne (multi and hyperspectral) and airborne sensors (panchromatic, colour, near infrared), and NIR field data from a portable sensor were handled, as well as field measurements and estimations of different forest parameters. The LINHE tool is intended to allow the integration of data in a rapid, intuitive, cost-effective and dynamic way. In order to achieve this objective, it was proposed to implement new algorithms and to test existing ones dealing with data correlation.

The project proposes a methodological model to apply the mentioned technologies to the improvement and sustainability of forest management, dealing with and taking advantage of the different spectral, temporal and spatial resolution offered by the sensors. In order to design a system capable of monitoring both high and low frequency changes in forests, a cross spatial and temporal resolution system must be established, using data from multiple satellite and in-situ data sources. As a consequence, gaps and overlaps in earth observation data, ground systems, methods, and scientific knowledge were identified from the experience gained in developing and executing prototype projects.

Additionally, the following objectives were pursued: i) to increase operational use of earth-observation data for policy decision making at national, regional, and global levels; ii) to provide validated products which can be used to derive reliable information concerning the forest component of the carbon budget for research and policy use; iii) to promote common data processing standards and interpretation methods, which are necessary for inter-comparison of regional studies; iv) to stimulate advances on multiple sensors, large volume datasets and information management and dissemination; v) to use data from multiple sensors, in combination with in-situ data, to produce validated prototype products which satisfy the identified users requirements; vi) to enhance the use of earth-observation products for forest management and scientific research concerning forest biophysical processes; vii) to provide the necessary tools for enhancing the actual use of current Spanish National Forest Inventories in order to support decisions at an operational level; and viii) to optimize ALS missions intending to reckon flight parameters for the determination of optimal and minimal configurations for the parameters retrieval at stand and tree levels.

During the Project, and in order to accomplish these objectives, different tasks have been carried out such as: i) analysis and definition of the requirements for simultaneous management of heterogeneous data; ii) establishment of LIDAR and digital camera data acquisition methodology; iii) definition of hyperspectral sensors characteristics; iv) establishment of land mobile platform data acquisition methodology; v) definition of characteristic parameters and specifications of the study ecosystems; vi) hyperspectral, LIDAR, NIR and in situ data acquisition; vii) post-process software development; viii) and analysis of data correlations.

3. Study areas

Three different forest ecosystems were considered in the present project, with different species, forest structure and climatic conditions, as well as very different management needs. The three study areas are located in Spain, as shown in Figure 1. A brief description of them is presented here.

The Pedroches region is located in Cordoba, in Southern Spain, and is covered by sparse vegetation dominated by *Quercus ilex* (dehesa forest). The main interest of the study was to lay the groundwork for the integration of different sensors, with different spatial, spectral and temporal resolution, in order to optimize the methodology for complex ecosystems assessment and monitoring.

The second study area, the Rodenal Region, is located in Guadalajara, in the Peninsula North-Central part of Spain. In July 2005, a forest fire affected around 12000 ha of *Pinus pinaster* and *Quercus pyrenaica* forests. The main interest in this area was to employ remotely sensed data to estimate fire severity levels and vegetation recovery, which provide very valuable information for forest managers to plan restoration works.

The third study area is Valsaín, a Scots pine (*Pinus sylvestris* L.) forest located in the province of Segovia, in Central-Northern Spain. The main interest of the study in this area was to determine the main parameters that could be estimated by LiDAR in order to provide inventory data which could help decision making of forest managers, not only for wood production purposes, but also for conservation measures, as the Valsaín forest is home for protected species, such as imperial eagle (*Aquila adalberti*), black vulture (*Aegypius monachus*) or the *Graellsia isabellae* butterfly.

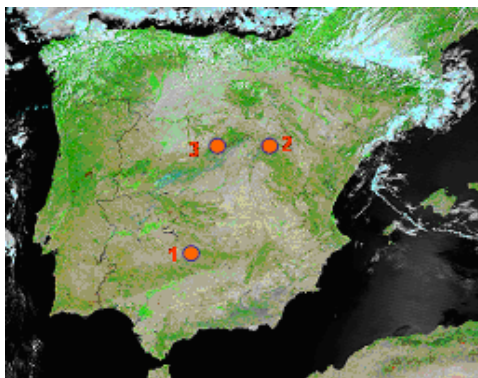


Figure 1: Study areas: (1) Pedroches, (2) Rodenal, (3) Valsaín (Terra-MODIS image acquired on 30/07/2005, downloaded from MODIS Rapid Response System)

4. Material and methods

For the three regions, flights were performed for the acquisition of combined LiDAR and photogrammetric data, using an ALS50_II Leyca SN073 LiDAR sensor and a DMC ZI SN020 digital camera simultaneously. The flying height was 1200 m above the ground, with a flight speed of 140 knots. Laser sensor parameters were set to a maximum scan frequency of 78 kHz and a laser field of view angle of 31°. For the photogrammetric survey, the following parameters were set: 12 cm ground sample distance, 60% forward overlap and 50% overlap between strips. In addition to the data obtained in the aforementioned flights, different kinds of field and satellite data were obtained and processed for the three study areas, as explained below.

The sensors involved were LiDAR, Landsat TM, Z/I DMC digital camera, a portable NIR spectrophotometer, and a GER 3700 spectroradiometer. To calibrate and validate the various sensors, six areas (of approximately 100 ha each) were selected, where on-field inventory data were collected: coverage of pasture, bushes and trees, existence of *Quercus ilex* regeneration, height, diameter at breast height, etc. The LiDAR and Z/I DMC camera survey was over 13000 ha wide.

In the Rodenal Region, a Landsat-TM satellite acquired 5 days after the fire (05/08/2005) was employed for the estimation of fire severity levels, while data from the LiDAR and photogrammetric flight were used for the monitoring of vegetation recovery. Field data consisting on a visual classification of fire severity levels were collected in July 2006. A second field survey was carried out in October 2007, which provided information about vegetation height and coverage, in order to estimate vegetation recovery in the area. The area surveyed by the LiDAR flight was about 4600 ha.

In Valsaín, a first survey allowed to complete some lacking information of forestry monitoring. Amongst other, different forestry parameters such as trunk and stem dimensions, tree heights, first branch heights, tree positioning, etc., were measured. The research has been carried out in a

high-relief, dense forest compartment with tall trees in even aged stands. Some of the stands may be two-storied due to the presence of regeneration. Other accompanying vegetation are oaks (*Quercus pyrenaica*), common juniper (*Juniperus communis*), legume bushes such as *Genista florida*, ferns (*Pteridium aquilinum*), etc. Other surveys were focused on GPS georeferencing to support the LiDAR flights. The area surveyed by LIDAR was about 850 ha.

5. Results

5.1 Pedroches region (Cordoba, Southern Spain)

Spectral reflectance was measured on field intended to compile a specific spectral library as reference for elements identification (trees, pasture, soil) in remote sensing images. Vegetation coverage (especially tree coverage) is a fundamental parameter in forest management. In this work, an approach to vegetation coverage estimation has been planned by the combination of the different sensor advantages, at diverse spectral, temporal and spatial resolutions.

For detailed scales, an airborne digital camera Z/I DMC was used. DMC images (15 cm pixel size) were classified into a two-step procedure: Firstly, an unsupervised classification for sun lit soil discrimination has been applied to band 1 (in the blue region), which showed a better separability for the targeted classes (vegetation and shadowed soil -with low DN values- vs. sun lit soil, with higher DN values). Two classes were discriminated and a mask was applied to the image in order to separate the tree-crowns and their shadows. Then, a supervised classification was applied to the previously selected area. Three classes were considered: sun lit vegetation, shadowed vegetation and shadowed soil; a maximum likelihood algorithm was used for pixel classification. Tree coverage was obtained as a sum of both sun lit and shadowed tree crowns fractions in seven control plots, showing values from 6,6 up to 35,5% of tree coverage.

Using spectrometry field measurements on known-reflectance tarps (grey plastic-made, black plastic-made and white reference tarps -Spectralon, 99% diffuse reflectance standard- and a rocky surface), linear calibration equations have been derived for each DMC band, showing r^2 higher than 0,99 in all cases. These equations relate values measured by the digital camera to reflectance values at wavelength intervals corresponding to the four DMC spectral bands.

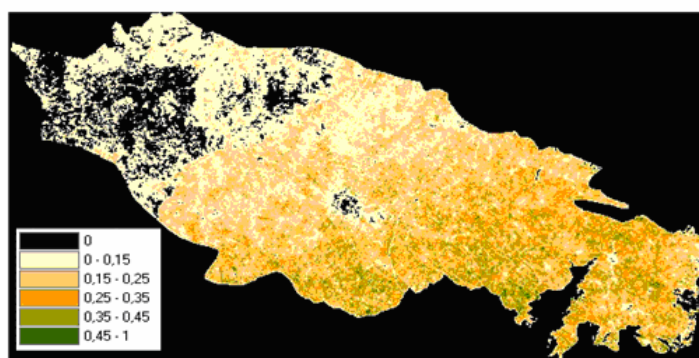


Figure 2: Tree coverage (values ranking from 0 to 1) per Landsat pixel in Pedroches area (Córdoba, Spain).

For a medium scale, Spectral mixture analysis was used to estimate subpixel vegetation coverage on a Landsat TM image (17th July, 2007). Given the forest coverage homogeneity in the study area, four components were considered: *Quercus ilex* trees (green vegetation in summer), dried pasture, soil and shadow. A linear mixture model was obtained using spectral

field data (spectral libraries mentioned above). The model was validated using the previous DMC-based forest coverage estimate in seven plots, showing a correlation of $r^2 = 0,89$; also a certain tree coverage infraestimation was detected comparing Landsat model to DMC results (MBE = 2,8). Figure 2 shows *Quercus ilex* coverage in Pedroches area.

However, as historic DMC images were not available, temporal changes have been analyzed using Landsat imagery, comparing two linear mixture models from 1995 and 2007 images of the same area. In this period, tree coverage in Pedroches has shown to be stable in a 66,84% of the study area. Coverage variation has been lesser than 30% in all the cases; a coverage increase has been found in a 17,49% of the area, and a decrease in the 15,66%. These results fit with field data (defoliation, tree losses and establishment of new trees) periodically collected from 2000 to 2007 in six dehesa exploitations. RMS errors for both models are compiled in Table 1.

Table 1: RMS errors in linear mixture models

| Model | RMS mean | RMS max | % of pixels with RMS max > 0,02 |
|--------------|----------|---------|---------------------------------|
| Landsat 1995 | 0,0036 | 0,0430 | 0,44 % |
| Landsat 2007 | 0,0064 | 0,2625 | 0,02 % |

Besides, LiDAR data were used to obtain a vertical characterization of the different layers present in this region. The main interest in dehesa ecosystems is to assess the existence of *Quercus ilex* regeneration around the tree trunks, as the lack of regeneration is one of the main problems in this region. For that purpose, some different LiDAR digital models, such as Digital surface models (DSM), digital terrain models (DTM) and normalized digital surface model ($nDSM = DSM - DTM$) were reckoned using LiDAR ENVI Tools. Vegetation models allowed high detailed height distribution maps, as stems are clearly recognizable in the sparse vegetation cover. Within this situation, it is easy to make a comparison between LiDAR results and field measurements as individual trees are easily recognized. However, low regeneration trees or seedlings (under 50 cm) were not detected by LiDAR.

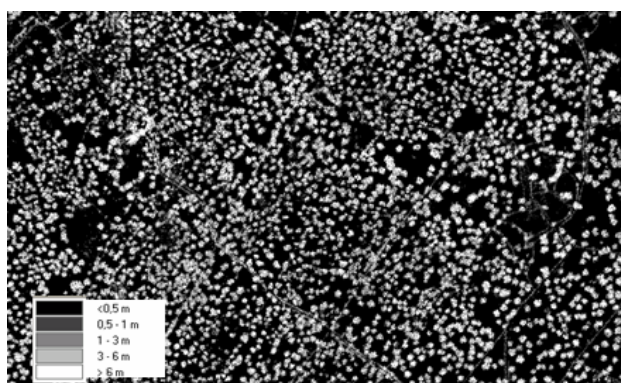


Figure 3: Distribution of maximum heights of vegetation in a dehesa area obtained from LiDAR data.

At a very high spatial resolution level, a portable NIR spectrophotometer was used on field for characterizing the spectral response from tree leaves, soil, shrubs and pasture. NIR sensors could be used either as a secondary measuring method, thus needing to be calibrated against a primary reference method, or it can be also used as a primary method using the spectral data alone to correlate with quality indicators (Williams, 2001; Shenk and Westerhaus 1995). The complexity of the spectroscopy signal and the great amount of generated data (most of it is redundant due to overlapping bands) are other factors affecting their use. However, the LINHE project dealt with the problem of generating both qualitative and quantitative chemometric

models. In a qualitative approach, PLS2 discriminant analysis of pre-treated spectra (Standard Normal Variate and De-trending methods were applied) showed that NIR spectroscopy was able to correctly classify leaves coming from trees of different defoliation levels in an 86,5% of samples; and sun lit pasture vs. shadowed pasture in a 99% of cases.

On the other hand, quantitative models for estimating K and water content in *Q. ilex* leaves were calculated (n=100 leaves). This models are still preliminary and need to be improved using a higher quantity of samples. At the time these models become robust, they may be used to calibrate other sensors included in this project, or to describe dehesa ecosystems at a detailed level. For example, quantitative estimates of parameters from NIR datasets, using a manageable data volume for a complex project with lots of sensors, technologies and data from different sources.

5.2 Rodenal Region (Guadalajara, North-Central Spain)

One of the aims of the project in this area was to obtain a fire severity map based on satellite data that can be useful for post-fire forest management. The map was obtained by processing and classifying one post-fire Landsat-TM image, according to the following phases: i) first of all, a geometric correction was performed; ii) the Normalized Burnt Ratio (*NBR*):

$$NBR = (NIR - SWIR) / (NIR + SWIR)$$

was obtained so as to evaluate fire severity levels, as it combines the two Landsat bands with a most significant response to fire effects, band 4 (*NIR*) and band 7 (*SWIR*) (Key and Benson 1999); iii) the perimeter of the affected area was obtained, and a mask was processed containing only the burned area; iv) finally, a 3-class unsupervised classification was performed, which produced a map containing three levels of fire severity (high, moderate and low). More detailed information on this process can be found in Roldán et al. (2006). Field data on fire severity levels were used as “ground truth” for validation purposes. A global precision of 72,73% and a kappa index of 0,57 were obtained for the fire severity map. These results are considered acceptable, specially taking into account that only one post-fire image was used and that field data were only used for validation purposes, and not for training.

The second goal in this study area was to monitor vegetation recovery after the fire: to know whether there is vegetation growing in the area, and what is its height. For this purpose, LiDAR digital models were obtained: DSMs, DTMs and nDSMs provide information about vegetation cover and height. The combination of nDSMs and DTMs allowed to identify the different situations that can be found in the field: bare soil, surviving *Pinus* stands and *Quercus* sprouts. Bare soil areas were easily detected by using the DTM, while the nDSM clearly showed the surviving *Pinus* stands. On the contrary, many patches of very dense and/or very low *Quercus* sprouts were misclassified or unclassified. On the one hand, very dense vegetation makes it impossible for the laser beam to reach the soil, and those vegetation patches are therefore classified as terrain, which also produces inaccuracies in the estimation of the average height. On the other hand, very low vegetation (under 30 cm) is not even detected. These problems did not allow a proper assessment of vegetation recovery by means of LIDAR data. Riaño et al. (2007) and Streutker and Glenn (2006) suggest to use spectral information from aerial digital images acquired simultaneously to the LiDAR survey to solve the former problems. Unfortunately, this information did not prove useful in the present case, as the flight took place in November, when *Quercus* sprouts showed very little activity, and the acquired spectral information was therefore not valuable. Some improvement in the classification of *Quercus* sprouts was obtained by reducing the grid size when obtaining the nDSMs, but further work is necessary on this topic, so as to improve the mapping of *Quercus*.

5.3 Valsaín (Segovia, central Spain)

The LINHE tool for forest management was provided with Landsat ETM+-derived imagery of the study area. The Landsat ETM+ scene was atmospheric, radiometric and relief corrected. A cover map of Valsaín forest was generated by supervised classification of surface reflectivity, obtaining 8 cover classes: urban or residential, herbaceous, bush, woody perennials, deciduous, bare soil and water covers. The overall accuracy of the classification was close to 70%. Also, the surface moisture index was generated with PCI Geomatica 10.0 KOS Manager using the short wave infra-red (SWIR) band 5 reflectivity. Finally, the Normalised Difference Vegetation Index (NDVI) map of Valsaín forest was obtained from the red and NIR bands (3 and 4, respectively). All these products were provided to the LINHE tool server.

LiDAR height distribution derived from LIDAR digital models within wooded zones was related to distributions of heights, diameters, basal areas and volumes from field data obtained in the Valsaín pine wood. Therefore, a comparison was made between some parameters reckoned from in field measurements and those reckoned from LiDAR digital models. For this comparison, the next parameters were measured in field: diameter, tree height, height of the first living branch, stem width, tree position, basal area, trunk volume, stem height, area and volume, and vegetation density. A nDSM height average map was computed from LiDAR data. Figure 4 shows the Valsaín pine forest orthophoto image, superimposed with the crown model obtained from LIDAR data.

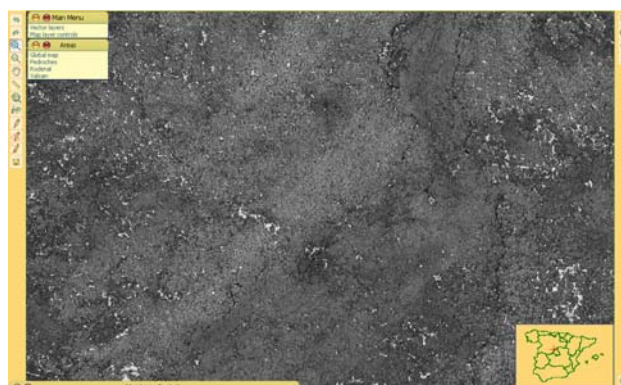


Figure 4: Orthophoto image of Valsaín pine forest, superimposed with vectorial LiDAR points

The first results of the comparison suggest coherence between LiDAR and field measurements, showing different average height in different testing zones. Height values of about 0 and 10 meters, which are expected in regeneration zones and zones with no homogeneous vegetation densities, have been observed. LiDAR height histograms have a great resemblance with distribution histogram variables from the forest inventory.

5.4 LINHE viewer

An important element of the LINHE tool is the LINHE prototype viewer, which allows a dynamic access to georeferenced data (raw and processed). The viewer is tailored with simultaneous access to the thematic results, querying properties, editing tools and printing of cartographic outputs.

The viewer is a very useful tool for data managing and cataloguing, meant to support data forest management, as it allows simultaneously visualizing a great amount of data (vector and raster layers) from the different sensors involved, with different spatial resolution and different

formats. It is also a suitable tool for homogenization and standardization purposes, as the Inspire Directive (2007) has been applied. It can be considered as a useful complement to the more complex analysis tools used in remote sensing (commercial GIS programs). The viewer offers the possibility of i) performing some data analysis procedures such as vector layer queries, ii) visualizing the metadata of the information layers using ISO 19115 standard, iii) adding new vector layers, iv) measuring distances and areas, and v) generating maps in .pdf format for printing. The viewer's architecture is Open Source based, on geographical servers and client elements, and it has been developed upon a *free* and *open source software*, hence licensing is not required. Usage is intuitive and no prior GIS knowledge is required. A web access is the sole software installation requirement prior to working with the LINHE viewer. The viewer can extract and show on screen all the information contained in each point.

6. Discussion and future work

The different data types, methodologies and processing techniques employed and developed within the LINHE Project, and the variety of ecosystems considered, provide a wide range of relevant information for the analysis and management of forest ecosystems.

The LINHE tool fulfils the principal aim of the project, which is the generation and integration of different geospatial information layers for forest planning. LINHE Project was developed during two years, and unfortunately a large amount of time was employed in data acquisition. Although interesting results for data integration and forest management have been obtained, further analyses and deeper correlation studies are necessary in order to obtain more conclusive results. So far, ALS data have been used to reckon height digital models intended to estimate forest parameters such as mean height or position, but it is considered necessary to deepen into how LiDAR data can help to estimate other useful parameters for forest management and inventory. The analysis of LIDAR intensity responses is an interesting field which was not considered in the present project. Besides, further surveys with Terrestrial Laser Scanning (TLS) are planned as future work, from which very interesting results are expected.

In addition, new implementations for upcoming versions of the LINHE viewer are already planned, which are expected to include: i) raw data and thematic data downloading capabilities; ii) .shp file format export capabilities of new data records; iii) restricted user's access and iv) PDA data handling capabilities.

Acknowledgements

Authors want to thank the Spanish *Ministerio de Industria, Turismo y Comercio* (MITYC) for providing funding for the present study, within the research project "LINHE: Desarrollo de nuevos protocolos de integración de sensores LiDAR, cámara digital, IR cercano e hiperespectral" (project: FIT-330221-2006-10). The following Spanish organizations participated in this project: Stereocarto S.L., TRAGSA, GMV, Universidad de Córdoba and Universidad Politécnica de Madrid.

References

- European Parliament and The Council of The European Union, 2007. Establishing an Infrastructure for Spatial Information in the European Community (INSPIRE). *Official Journal of the European Union*, L108. http://www.ec-gis.org/inspire/directive/L_10820070425en00010014.pdf (Last accessed: July-2008).
- Hyypä, J., Hyypä, H., Litkey, P., Yu, X., Haggrén, H., Rönholm, P., Pyysal, U., Pitkänen, J., Maltamo, M., 2005. Algorithms and methods of airborne laser scanning for forest

- measurements. *International Archives of Photogrammetry, Remote Sensing and Spatial Information Sciences*, VolXXXVi-8/W2.
- Key, C.H., and Benson, N.C., 1999. The Normalized Burn Ratio (NBR): a Landsat TM Radiometric Measure of Burn severity, *United States Geological Survey* (USGS).
- Kraus, K., and Pfeifer, N., 1998. Determination of terrain models in wooded areas with airborne laser scanner data. *ISPRS Journal of Photogrammetry and Remote Sensing*, 53, 193–203.
- Lefsky, M. A., Cohen, W. B., Parker, G. G., and Harding, D. J., 2002. Lidar remote sensing for ecosystem studies. *Bioscience*, 52, 19 – 30.
- Lefsky, M. A., Harding, D., Cohen, W. B., Parker, G. G., and Shugart, H. H., 1999. Surface Lidar remote sensing on basal area and biomass in deciduous forests of eastern Maryland, USA. *Remote Sensing of Environment*, 67, 83 – 98.
- Næsset, E., Gobakken, T., Holmgren, J., Hyypä, H., Hyypä, J., Maltamo, M., Nilsson, M., Olsson, H., Persson, A., and Söderman, U., 2004. Laser scanning of forest resources: the Nordic experience. *Scandinavian Journal of Forest Research*, Volume 19, Number 6 / December 2004, pp 482 – 499.
- Parker R., and Evans D., 2004. An Application of LiDAR in a Double-Sample Forest Inventory. *Western Journal of Applied Forestry*, Volume 19, Number 2, April 2004, 95–101.
- Riaño, D. Chuvieco, E., Condés, S., González-Matesanz, J., Ustin, S.L., 2004. Generation of crown bulk density for *Pinus Sylvestris* from Lidar. *Remote Sensing of Environment*, 92, 345 – 352.
- Riaño, D. Chuvieco, E., Ustin, S.L., Salas, J., Rodríguez-Pérez, J.R., Ribeiro, L.M., Viegas, D.X., Moreno, J.M. and Fernández, 2007. Estimation of shrub height for fuel-type mapping combining airborne LiDAR and simultaneous color infrared ortho imaging. *International Journal of Wildland Fire* 16, 341 – 348.
- Riano, D., Meier, E., Allgower, B. and Chuvieco, E., 2002. Gereneration of vegetation height, vegetation cover and crown bulk density from airborne laser scanning data. In: Viegas (Ed.). *Forest Fire Research & Wildland Fire Safety*. Millpress, Rotterdam, ISBN: 90-77017-72-0.
- Riano, D., Meier, E., Allgower, B., Chuvieco, E., and Ustin, S. L., 2003. Modeling airborne laser scanning data for the spatial generation of critical forest parameters in fire behavior modeling. *Remote Sensing of Environment*, 86(2), 177 – 186.
- Roldán-Zamarrón, A., Merino-de-Miguel, S., González-Alonso, F., García-Gigorro, S. and Cuevas, J.M., 2006. Minas de Riotinto (south Spain) forest fire: Burned area assessment and fire severity mapping using Landsat 5-TM, Envisat-MERIS, and Terra-MODIS postfire images, *Journal of Geophys. Res.*, 111, G04S11, doi: 10.1029/2005JG000136.
- Roberts, S.D., Dean, T.J., Evans, D.L., McCombs, J.W., Harrington, R.L. and Glass, P.A., 2005. Estimating individual tree leaf area in loblolly pine plantations using LiDAR-derived measurements of height and crown dimensions. *Forestry Ecology and Management*, 213, 54 – 70.
- Shenk, J. and Westerhaus, M.O., 1995. Analysis of agriculture and food products by Near Infrared Reflectance Spectroscopy. *Monograph NIR Systems*. p. 124.
- Sithole, G. and Vosselman, G., 2004. Experimental comparison of filter algorithms for bare-Earth extraction from airborne laser scanning point clouds. *ISPRS Journal of Photogrammetry and Remote Sensing*, 59 (1-2): 85 – 101.
- StOnde, B.A. and Achaichia, N., 2001. Measuring forest canopy height using a combination of lidar and aerial photography data. *International Archives of Photogrammetry and Remote Sensing*, Volume XXXIV-3, W4 Annapolis, MD, October 22-24.
- Streutker, D.R. and Glenn, N.F., 2006. LiDAR measurement of sagebrush steppe vegetation heights. *Remote Sensing of Environment* 102: 135 – 145.
- Williams, P.C. and Norris, K., 2001. Near-Infrared technology in the agricultural and food industries, 2nd edition. *American Association of Cereal Chemists*, Inc. St. Paul, Minnesota, USA.

A proposed approach incorporating lidar and aerial imagery for large area estimates of lodgepole pine (*Pinus contorta*) volume killed by mountain pine beetle (*Dendroctonus ponderosae*)

Christopher W. Bater¹, Nicholas C. Coops¹, Michael A. Wulder², & Joanne C. White²

¹Department of Forest Resources Management, University of British Columbia,
cbater@interchange.ubc.ca, nicholas.coops@ubc.ca

²Canadian Forest Service, Natural Resources Canada, mwulder@pfc.cfs.nrcan.gc.ca
jowhite@pfc.cfs.nrcan.gc.ca

Abstract

The volume of pine killed by mountain pine beetle is a critical indicator of an infestation's impact on timber supply. Operationally, mountain pine beetle damage is typically mapped by broad-scale aerial surveys, and recorded damage is combined with existing forest inventory data to generate coarse estimates of volume losses. In this communication, we propose an alternative approach to improve the precision of volume estimates and to this end, present a sampling methodology that combines high spatial resolution digital aerial imagery and small footprint discrete return lidar data collected over 0.25 ha photo plots selected from representative sampling transects. Species composition, diameter, and mountain pine beetle attack stage are manually interpreted from the imagery, while lidar provides accurate measures of dominant stand height. Species-specific equations are then used to estimate the volume of pine mortality, which may then be extrapolated across a larger area of interest using forest inventory data.

Keywords: forest inventory, timber supply, lidar, digital aerial imagery, volume, mountain pine beetle

Estimation of bivariate diameter and height distributions using ALS

Johannes Breidenbach¹, Christian Gläser² & Matthias Schmidt³

¹Forstliche Versuchs- und Forschungsanstalt Baden-Württemberg, Abteilung Biometrie und Informatik, Johannes.Breidenbach@forst.bwl.de

²Georg-August-Universität Göttingen, Institut für Statistik und Ökonometrie, Christian_Glaeser@gmx.de

³Nordwestdeutsche Forstliche Versuchsanstalt, Abteilung Waldwachstum, Matthias.Schmidt@nw-fva.de

Abstract

In this paper, we present a method for estimating a bivariate height and diameter distribution based on airborne laser scanner data (ALS). ALS are analyzed with the area-based method. To construct a bivariate likelihood function, we assume that the diameters are Weibull distributed and the heights are normal distributed where the expectation value is modelled with the Näslund function. Comparison of predicted and observed mean diameter distributions result in an RMSE of 2.78 cm and a bias of 0.48 cm. Comparisons of observed and predicted height distributions are still to come.

Keywords Weibull distribution, Näslund function, lidar, GLM

1. Introduction

High density (i.e., >1 return m^{-1} , Magnusson et al. 2007) Airborne laser scanning data (ALS) can be used to estimate attributes of single trees (e.g., Persson et al. 2002, Popescu et al. 2003). Low density ALS data are usually analyzed using area-based methods (Næsset 2002) that result in plot-level estimates of, for example, timber volume or basal area. The lower flying height required to produce higher density ALS data causes longer flight times per area. Therefore, costs obviously increase with the density of the raw data. This may be one reason for why area-based methods are already used in operational forest inventories (Næsset 2004). Additionally, some studies show, that the density of the laser data may be reduced in a wide range without a significant lost of information (Magnusson et al. 2007, Gobakken and Næsset 2007). Consequently, further cost reductions may be possible with future generation of laser scanners that allow larger flying heights.

While plot level estimates of, for example volume, is an important piece of information, for the actually wanted prediction of assortments, at least diameter, but also height distributions are needed. Magnussen & Boudewyn (1998) estimated height distributions using ALS. Methods for estimating diameter distributions were shown, for example by Gobakken & Næsset (2004). However, height and diameter distributions cannot be combined if they are estimated independently. While Schreuder & Hafley (1977) and Zucchini et al. (2001) proposed functions to fit bivariate distributions, only Mehtätalo et al. (2007) used a regression model to fit a bivariate height and diameter distribution conditional on ALS data. They first used the method of moments to fit regression models for the height distribution as a function of the diameter and the diameter distribution as a function of ALS data. They then applied the method of parameter recovery to obtain the parameters of the bivariate distribution.

In this study, we use the log-likelihood method to estimate the bivariate distribution of height and diameter. The diameters are assumed to follow the Weibull distribution given metrics from ALS data. Opposed to Mehtätalo et al. (2007), we need to deal with several tree species. Therefore, tree height is modelled using the Näslund function given diameter and metrics from ALS data. However, different tree species are not addressed separately.

2. Material and Methods

2.1 Study area

The tree species composition of the 50 km² managed forest that served as study site is dominated by Norway spruce (*Picea abies* L. Karst.) with a 70% proportion by area, beech (*Fagus sylvatica* L.) with 11% and silver fir (*Abies alba* Mill.) with 10%. More details on the forest structure are given in Table 1.

Table 1: Forest characteristics of the study site

| | Minimum | Median | Mean | Maximum |
|--|---------|--------|-------|---------|
| Stem number [ha ⁻¹] | 22.1 | 397.8 | 497.3 | 2829 |
| Stem volume [m ³ ha ⁻¹] | 7.2 | 412.7 | 413.2 | 1193 |
| Basal area [m ² ha ⁻¹] | 1.8 | 36.8 | 36.8 | 81.9 |
| Basal area mean diameter [cm] | 7.5 | 35 | 35.8 | 68.8 |
| Mean height [m] | 5.1 | 25 | 24.6 | 40.7 |

2.1.1 Plot establishment

In 2002, a permanent sample-plot inventory was carried out on a 100 m (easting) by 200 m (northing) grid. Trees with a diameter at breast height (dbh) of at least 7 cm were measured on concentric sample plots with a maximum diameter of 12 m. To increase the efficiency of the inventory, trees with a dbh <30 cm were sampled on plots with smaller radii. This results in four possible plot sizes of 2, 3, 6 and 12 m, where trees with a minimum dbh of 7, 10, 15 and 30 cm are measured. On each sample plot the height of the two largest trees per species were measured using angle measurement instruments. The height of the other trees was estimated based on local diameter-height curves calibrated with the measured trees.

2.1.2 Laser data

The laser scan data were collected with an Optech ALTM 1225 laser scanner in winter 2003/2004, i.e. about one year after the inventory took place. A flight altitude of approx. 900 m above ground yielded an average distance of 1 m between scan points on the ground. The first as well as the last pulse data were automatically classified by the data provider into vegetation- and ground points (reflection from terrain surface).

A digital terrain model (DTM) with one meter pixel spacing was computed from the ground returns using the average height of returns if several reflections were located within one pixel and bilinear interpolation if no return was within the pixel. The value of the respective DTM pixel was subtracted from the first pulse vegetation raw data to obtain vegetation heights. Vegetation height metrics (e.g., percentiles and mean) were derived for every sample plot (Næsset 2002).

2.2 Parameter estimation

If a is the location, b the scale and c the shape parameter, the density of the Weibull distribution is denoted by

$$f(y|a,b,c) = \frac{c}{b} \left(\frac{y-a}{b} \right)^{c-1} \exp \left[- \left(\frac{y-a}{b} \right)^c \right] \quad (1)$$

for $b, c > 0$.

To estimate the diameter distribution, equation 1 was extended to $f(d_i | a, b_i, c_i)$ where d is a diameter, to conditional the scale and shape parameters on predictor variables. The location parameter (a) was set to the calliper limit (7 cm) because estimation of this parameter frequently causes numerical problems (Gobakken and Næsset 2004).

Due to the concentric sample plot design, we constructed four censored Weibull distributions for every possible plot radii by

$$g_R(d_i | a, b_i, c_i) = \frac{f(d_i | a, b_i, c_i)}{\int_L^U f(x | a, b_i, c_i) dx} \quad (2)$$

where U and L are the upper and lower bounds of the diameters for the concentric sample plot with radius R , respectively. This resulted in the functions g_2, g_3, g_6, g_{12} .

The parameters are bound to the predictor variables (laser metrics) with link functions

$$h_{(P)}^{-1}(x'_{(P),i} \beta_{(P)}),$$

where $x_{(P)}$ are the predictor variables, β are the coefficients and P is either b or c . The link function for both parameters is the natural logarithm.

The height distribution given DBH and ALS data is assumed to follow a normal distribution:

$$f(h_i | \mu_i(P_\mu), \sigma) = \frac{1}{\sqrt{2\pi} \sigma} \exp \left(- \frac{1}{2} \left(\frac{h_i - \mu_i(P_\mu)}{\sigma} \right)^2 \right) \quad (3)$$

where the expectation value μ is an extended Näslund function that includes metrics from ALS and P_μ are its parameters:

$$\mu_i(d_i, x_i, \beta_{0(Näs)}, \beta_{1(Näs)}, \beta_{2(Näs)}) = 1.3 + \left(\frac{d_i}{\beta_{0(Näs)} + \beta_{1(Näs)} x_i + \beta_{2(Näs)} d_i} \right)^3 \quad (4)$$

where $\beta_{0(Näs)}, \beta_{1(Näs)}$ and $\beta_{2(Näs)}$ are coefficients of the Näslund function and x_i is a predictor variable derived from ALS data.

The bivariate height- and diameter distribution is given by

$$g_R(d_i | a, b_i, c_i) * f(h_i | \mu_i(d_i, x_i, \beta_{0(Näs)}, \beta_{1(Näs)}, \beta_{2(Näs)}), \sigma) = f(d_i, h_i | x_i, \beta) \quad (5)$$

The bivariate likelihood function can then be denoted as

$$LLK = \sum_{i=1}^n \ln \left(\begin{matrix} g_2(d_i | a, b_i, c_i) 1_2(y_i) + g_3(d_i | a, b_i, c_i) 1_3(y_i) + \\ g_6(d_i | a, b_i, c_i) 1_6(y_i) + g_{12}(d_i | a, b_i, c_i) 1_{12}(y_i) \end{matrix} \right) + \sum_{i=1}^n \ln(f(h_i | \mu_i(P_\mu), \sigma)). \quad (6)$$

where $1_U(y_i)$ are size-class dependent indicator functions. If $U \in \mathfrak{R}$ then

$$1_U(y_i) = \begin{cases} 1 & y_i \in U \\ 0 & y_i \notin U \end{cases}.$$

The likelihood function was maximized using the Nelder-Mead algorithm implemented in the function *optim* (Venables & Ripley 2002), within an R environment (R Development Core Team 2007)

On average, 12 trees were measured on a sample plot. The predicted distribution can therefore not be compared with observations from one sample plot. Therefore, the observations from plots similar with respect to the explanatory variables are aggregated to what we will call *vegetation height quartile classes* for the remainder of the text. Then, the predicted distributions can be compared with the histogram of the observations.

3. Results

The first and third quartile (Qu1 and Qu3) of the vegetation height and their interaction term (Qu1 * Qu3) were considered as predictor variables for the Weibull scale and shape parameters. The Qu3 was used as additional predictor variable for the height distributions besides the DBH.

The parameters of the Weibull distribution can be predicted by

$$\begin{aligned} b_i &= 1.05 + 0.04 \text{ Qu1}_i + 0.11 \text{ Qu3}_i - 0.002 \text{ Qu1}_i \text{ Qu3}_i \\ c_i &= -0.19 + 0.09 \text{ Qu1}_i + 0.02 \text{ Qu3}_i - 0.002 \text{ Qu1}_i \text{ Qu3}_i \end{aligned} \quad (7)$$

Tree height can be predicted by

$$\mu_i = d_i / (4.03 - 0.10 \text{ Qu3}_i + 0.30 d_i) \text{ with standard deviation } 2.23.$$

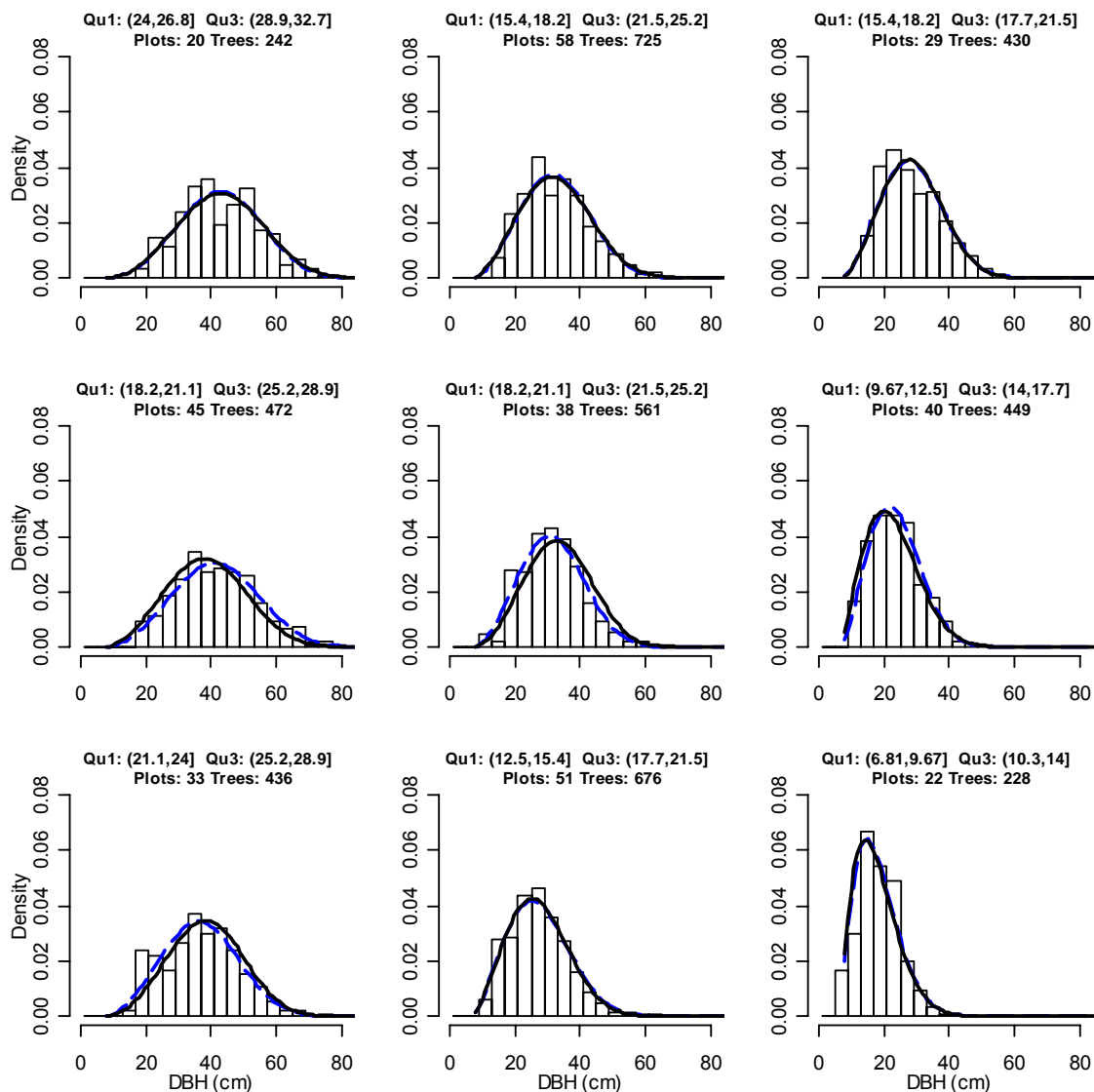


Figure 1: Probability density distribution of observed DBH (histogram) and predicted Weibull distributions (solid graph) for the 9 most densely populated laser-derived vegetation height quartile classes. The dashed curve marks the Weibull distribution which has been directly fitted to the observations. Qu1 denotes the class width of the first quartile (m) and Qu3 the class width of the third quartile (m). Plots and trees represent the number of sample plots and trees in the corresponding plot strata.

The predicted diameter distribution fits well to the observed diameter distributions (Figure). Results for height distributions are not yet available, however the comparison of the expectation value with observed heights is promising (Figure 2). For this graphic, Qu3 was estimated given DBH. (However, the regression model is weak with $R^2=0.3$.)

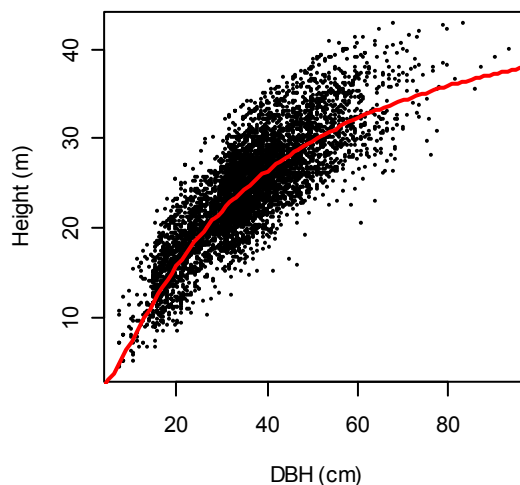


Figure 2: Predicted and observed height given DBH.

The means of the Weibull and the observed distribution was computed for the 20 most densely populated quartile classes (containing at least 3 Plots). As the good conformity of the predicted distribution with the observed distribution supposes, the difference between the mean of the Weibull distribution and the mean of the observations is rather small (Figure 3). The RMSE is 2.78 cm with a bias of 0.48 cm.

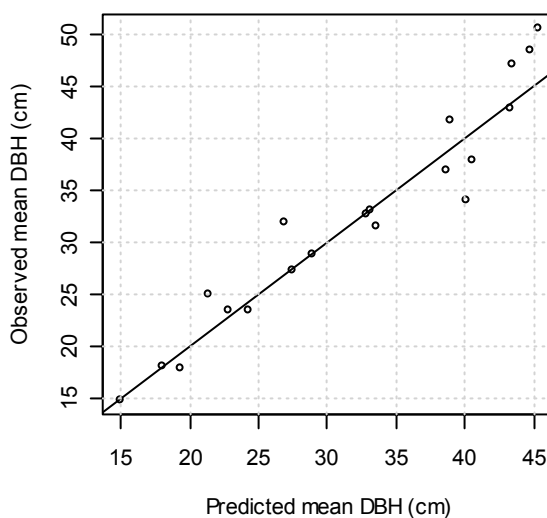


Figure 3: Observed versus predicted mean DBH for the 20 most densely populated quartile classes (circles) and 1:1 line (solid line).

4. Discussion

The proposed bivariate distribution can be used to estimate diameter and height distributions. Since we did not use the parameter recovery method (Mehtätalo et al. 2007), we obtain density distributions. They need to be combined with an estimation of stem number or basal area to get

stem numbers per diameter class. For the prediction of assortments, information about tree species are also required. In this study, we assumed the observations to be independent of one another. One major drawback of the used data material is that not all tree heights were measured. This reduces the variance to be modelled.

Acknowledgements

We acknowledge the useful comments of two anonymous reviewers.

References

- Gobakken, T. and Næsset, E., 2004. Estimation of diameter and basal area distributions in coniferous forest by means of airborne laser scanner data. *Scandinavian Journal of Forest Research*, 19, 529-542.
- Gobakken, T. and Næsset, E., 2007. Assessing effects of laser point density on biophysical stand properties derived from airborne laser scanner data in mature forest In E. Rönnholm, P.; Hyypä, H. & Hyypä, J. (ed.), *ISPRS Workshop on Laser Scanning 2007 and SilviLaser 2007*, 200.
- Hafley, W. and Schreuder, H., 1977. Statistical distributions for fitting diameter and height data in even-aged stands. *Canadian Journal of Forest Research, NRC Research Press*, 7, 481-487.
- Magnussen, S. and Boudewyn, P., 1998. Derivations of stand heights from airborne laser scanner data with canopy-based quantile estimators. *Canadian Journal of Forest Research*, 28, 1016-1031.
- Magnusson, M.; Fransson, J. and Holmgren, J., 2007. Effects on Estimation Accuracy of Forest Variables Using Different Pulse Density of Laser Data. *Forest Science*, 53, 619-626.
- Mehtätalo, L., Maltamo, M. and Packalén, P., 2007. Recovering plot-specific diameter distribution and height-diameter curve using ALS based stand characteristics. In: P. Rönnholm, P.; Hyypä, H. & Hyypä, J. (Eds.). *ISPRS Workshop on Laser Scanning 2007 and SilviLaser 2007*.
- Næsset, E., 2002. Data acquisition for forest planning using airborne scanning laser. *Forestsat Symposium 2002*.
- Næsset, E., 2004. Practical large-scale forest stand inventory using a small-footprint airborne scanning laser. *Scandinavian Journal of Forest Research*, 19, 164–179.
- Nilsson, M., 1996. Estimation of tree heights and stand volume using an airborne lidar system. *Remote Sensing of Environment*, 56, 1- 7.
- Persson, A., Holmgren, J. and Söderman, U., 2002. Detecting and measuring individual trees using an airborne laser scanner. *Photogrammetric Engineering and Remote Sensing*, 68, 925-932.
- Popescu, S. C.; Wynne, R. H. and Nelson, R. F. Measuring individual tree crown diameter with lidar and assessing its influence on estimating forest volume and biomass. *Canadian Journal of Remote Sensing*, 2003, 29, 564–577
- R Development Core Team. R., 2007. A Language and Environment for Statistical Computing. *R Foundation for Statistical Computing*.
- Venables, W. & Ripley, B., 2002. *Modern Applied Statistics with S*. Springer, New York.
- Zucchini, W.; Schmidt, M. and Gadow, K. v., 2001. A model for the diameter-height distribution in an uneven-aged beech forest and a method to assess the fit of such models *Silva Fennica*, 35, 169 -183

Monitoring capercaillie habitat using ALS

Johannes Breidenbach¹, Veronika Braunisch²

¹Forstliche Versuchs- und Forschungsanstalt Baden-Württemberg, Abteilung Biometrie und Informatik, Johannes.Breidenbach@forst.bwl.de, Veronika.Braunisch@forst.bwl.de

Abstract

Two areas of which one was populated by capercaillie were compared with respect to canopy cover. The canopy cover was computed for hexagons with an area of 452 m² as the proportion of canopy pixels in a digital surface model. The populated area reveals 3-8 times more open canopy structures. Since the capercaillie relies on the availability of open forest, this observation is accordant with the needs of the capercaillie. These first results indicate that ALS can be used to map potential and monitor existing habitat areas. It may support the planning and evaluation of measures implemented to stop the further degradation of the habitat quality, which is likely to be the cause for the decreasing population in the last decades.

Keywords: habitat monitoring, endangered species, capercaillie, lidar

1. Introduction

Endangered species have an indicator function in evaluating the endeavour of integrating the needs of forest management, nature conservation, tourism and game hunting in a multifunctional forestry. The capercaillie (*Tetrao urogallus*) is such an indicator species for parts of the Black Forest, Germany. Capercaillie forests are characterized by a low canopy cover and a high degree of structural diversity. In addition, habitat suitability is mainly defined by the availability of blueberry (*Vaccinium myrtillus*) as its main summer-food and conifer, preferably pine (*Pinus sylvestris*) needles as the main source of food in winter.

To ensure the continuance of the remaining sub-populations in the Black Forest, the forest management in the capercaillie habitat is being adapted to provide the forest structures that the capercaillie relies on. Suchant and Braunisch (2004) found that a suitable habitat consists of at least 10% unstocked area or open canopy and that at least 20% of the area should have an intermediate canopy cover between 50-70%. In addition, less than 30% of the area should be covered with dense forest (e.g., regeneration or thickets).

In the recent years, many studies proofed that airborne laser scanning (ALS) can be used to estimate various forest parameters (e.g., Nilssen 1996, Næsset, 1997, Magnussen and Boudewyn 1998). In Scandinavia, it has become an operational tool in forest inventories (Naeset 2004). Due to its ability of describing the vertical distribution of the vegetation canopy in three dimensions, it is obvious that ALS could also be used for mapping habitat structures. The number of studies with this background are, however, still limited. Hinsley et al. (2002) found that the ALS-derived canopy height can be used as a surrogate for tree density index. They used this statistical relation for assessing the habitat quality of Great Tits (*Parus major*) and Blue Tits (*Parus caeruleus*). Dees et al. (2006) presented methods for describing general habitat structures in forests as they are defined in the Flora-Fauna-Habitat directive (FFH) based on ALS and other remote sensing data. In a shrubland environment, Leyva et al. (2002) used ALS-derived surface models to identify different shapes of shrub-formations that can be related

to potential habitat of black-capped vireo (*Vireo atricapillus*). Using large footprint ALS and other remote sensing techniques Hyde et al. (2005) estimated canopy heights and biomass. The estimations were then used to evaluate the quality of the forest structure for wildlife habitat.

In this paper, a concept for monitoring the habitat structure of capercaillie based on ALS is presented. Two adjacent forest areas are compared with respect to the proportion of crown cover classes. Both areas are suitable habitat regarding climatic and topographic attributes and human land use (Braunisch & Suchant 2007). However, just one area is inhabited by capercaillie. Aim is to describe differences of forest structures that may be the cause for why capercaillie is found in just one of the areas. First results for canopy cover are presented.

2. Material and Methods

2.1 Study areas

Both study areas are located in the northern part of the distribution range of capercaillie in the Black Forest, Germany. The distribution range of capercaillie in Germany was determined by geographically explicit observations made by experts such as foresters and local hunters over several years (Braunisch and Suchant 2006). The distribution range was last updated in the year 2003. The area where capercaillie was observed, named CO in the remainder of the text, is approximately 64 km² in size. The area where capercaillie was absent, named NC in the remainder of the text, is about 36 km² in size. The two areas are separated from each other by the valley of the *Große Enz* river. The smallest distance between the areas is about 2 km.

Since the study areas contain both, public and private forests with many different land owners, no consistent inventory information is available. However, data from the second national forest inventory (2002) can be used to characterize the forest in the county in which the study areas are located (Kändler et al. 2006). The county level forest is dominated by Norway spruce (*Picea abies* L. Karst.) with a 39% proportion by area, silver fir (*Abies alba* Mill.) with 30%, pine (*Pinus sylvestris*) with 19% and beech (*Fagus sylvatica* L.) with 12%. The mean volume is 360.6 m³ ha⁻¹. It should be noted however, that these parameters may be different in the two study areas.

2.1.2 Laser data

The laser scan data were collected with an Optech ALTM 1225 laser scanner in winter 2003/2004. A flight altitude of approx. 900 m above ground yielded an average distance of 1 m between returns on the ground. The first as well as the last pulse data were automatically classified by the data provider into vegetation- and ground points (reflection from terrain surface).

The commercial software TreesVis (Weinacker et al. 2004) was used to derive two elevation models: A digital terrain model (DTM) with one meter pixel spacing was computed from the ground returns. A digital surface model (DSM) with the same pixel spacing as the DTM was derived from all first pulse data. With a threshold of 1 m, the normalized digital surface model (nDSM, DSM minus DTM) was classified into canopy and ground pixels.

The study areas were tessellated into hexagons with an area of 452 m² each. The relative canopy cover was computed as the proportion of canopy pixels to all pixels. The hexagonal tiles were classified as light, intermediate and closed canopy cover. The intervals for the classification are given in Table 1.

Table 1: Intervals for canopy cover classes.

| Canopy cover class | Canopy cover class # | Interval of relative canopy cover (%) |
|--------------------|----------------------|---------------------------------------|
| open | 1 | 0 – 50% |
| intermediate | 2 | 50 – 70% |
| dense | 3 | 70 – 100% |

3. Results

The two study areas can be well differentiated based on their canopy structure: In the CO area, more than 23% and 10% of the hexagon tiles possess open or intermediate canopy cover classes. This is 8 and 3 times more than in the NC area. It is also apparent, that the proportion of intermediate canopy density (50%-70% canopy cover) is below the minimum level of 20% even for the CO area. This however, seems to be levelled out to some extent by the 23% proportion of light canopy cover, which is 13% more than the minimum level for this class.

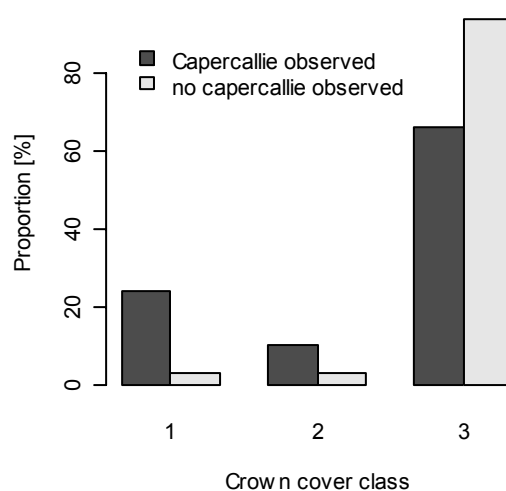


Figure 1: Distribution of the canopy cover classes in the CO and the NC areas.

4. Discussion

Information on stand density, derived from stand height was used by Hinsley et al. (2002) for quantifying the habitat quality of songbirds. We used the canopy cover, which is in fact the inverse of the gap fraction, to characterize the habitat quality of an area populated with capercallie and a non-populated area. The proportion of open canopy structures was between 3 and 8 times higher in the populated area. This is in accordance with the ecological needs of the capercallie: i) Light on the forest ground due to canopy gaps results in a high abundance of blueberries which comprise the main source of food in summer time, ii) low canopy cover is frequently associated with a higher diversity of horizontal stand structure and iii) open areas may facilitate to take refuge from predators.

These first results indicate, that ALS data can be used for monitoring structural aspects of habitat quality for capercallie over large spatial scales. However, further research is needed to

in order to quantify other forest structure parameters relevant to the species. A monitoring concept is needed to guarantee that the habitat quality does not further degrade. Since ALS data are still quite expensive, it might make sense to also analyse other remote sensing data sets for this purpose. Nuske et al. (2007) describe a method to model the gap fraction with orthophotographs. However, the inconsistent quality of the available images and shading effects would make the analysis of orthophotographs cumbersome in our case.

Acknowledgements

We would like to acknowledge valuable comments of Prof. Barbara Koch and two anonymous reviewers.

References

- Braunisch, V., Suchant, R., 2006. Das Raufußhühner - Monitoring der FVA. In: Berichte Freiburger Forstliche Forschung 64, 47-65. (In German)
- Braunisch, V., Suchant, R., 2007. A model for evaluating the 'habitat potential' of a landscape for capercaillie Tetrao urogallus: a tool for conservation planning. *Wildlife Biology* 13/1, 21-33.
- Dees, M., Straub, C., Langar, P. and Koch, B., 2006. Remote sensing based concepts utilising SPOT 5 and LIDAR for forest habitat mapping and monitoring under the EU Habitat Directive. In: Lamb, A., Hill, R., Wilson, D., Bock, M., Ivits, E., Dees, M., Hemphil, S. and Koch, B. (Eds.): ONP 10 Test & Benchmarks Report. pp. 53-78.
- Hinsley, S.; Hill, R.; Gaveau, D. and Bellamy, P., 2002. Quantifying woodland structure and habitat quality for birds using airborne laser scanning. *Functional Ecology*, 16, 851- 857
- Hyde, P.; Dubayah, R.; Peterson, B.; Blair, J.; Hofton, M.; Hunsaker, C.; Knox, R. and Walker, W., 2005. Mapping forest structure for wildlife habitat analysis using waveform lidar: Validation of montane ecosystems. *Remote Sensing of Environment*, 96, 427-437.
- Kändler, G.; Schmidt, M.; Bösch, B. and Breidenbach, J., 2006. Bundeswaldinventur 2 (BWI2): Regionale Ergebnisse für Baden-Württemberg Forstliche Versuchs- und Forschungsanstalt Baden-Württemberg, Abteilung Biometrie und Informatik – CD ROM.
- Leyva, R. I., Henry, R. J., Graham, L. A. and Hill, J. M., 2002. Use of LIDAR to determine vegetation vertical distribution in areas of potential black-capped vireo habitat at Fort Hood, Texas. In *Endangered species monitoring and management at Fort Hood, Texas: 2002 annual report*. The Nature Conservancy, Fort Hood Project, Fort Hood, Texas, USA.
- Magnussen, S. and Boudewyn, P., 1998. Derivations of stand heights from airborne laser scanner data with canopy-based quantile estimators. *Canadian Journal of Forest Research*, 28, 1016-1031.
- Næsset, E., 1997. Estimating Timber Volume of Forest Stands Using Airborne Laser Scanner Data. *Remote Sensing of Environment*, 61, 246-253
- Næsset, E., 2004. Practical large-scale forest stand inventory using a small-footprint airborne scanning laser. *Scandinavian Journal of Forest Research*, 19, 164 –179.
- Nilsson, M., 1996. Estimation of tree heights and stand volume using an airborne lidar system. *Remote Sensing of Environment*, 56, 1- 7.
- Nuske, R., Ronneberger, O., Burkhardt, H. and J. Saborowski, 2007. Self-Learning Canopy Gap Mapping for Aerial Images using Photogrammetric Height, Color, and Texture Information. *Forestsat Symposium 2007*.
- Suchant, R., Braunisch, V., 2004. Multidimensional habitat modelling in practical management – a case study on capercaillie in the Black Forest, Germany. *Ecological Bulletins* 51, 455 – 469.
- Weinacker, H.; Koch, B.; Heyder, U. & Weinacker, R., 2004. Development of filtering, segmentation and modelling modules for Lidar and multispectral data as a fundament of an automatic forest inventory system. In Thies, M.; Koch, B.; Spiecker, H. & Weinacker, H. (ed.). *ISPRS Working Group VIII/2 'Laser-scanners for forest and landscape assessment'*, University of Freiburg, 2004

Characterization of forest stands using full waveform laser scanner and airborne hyperspectral data

Henning Buddenbaum¹ & Stephan Seeling¹

¹University of Trier, Remote Sensing Department, Behringstr., 54286 Trier, Germany, buddenbaum@uni-trier.de, seelings@uni-trier.de

Abstract

Full waveform airborne laser scanning was assembled into voxels and combined with airborne hyperspectral data. This combined data set offers a detailed insight into the structure and the reflective properties of tree stands. A comparison of stand photographs and aggregated full waveforms shows the close relation between the stand structure and the waveforms so that the potential of the waveforms to act as a key variable for remote sensing characterization of stand structure is evident.

Keywords: Full waveforms, hyperspectral data, hemispherical photos

1. Introduction

Full waveform airborne laser scanning (ALS) offers a maximum of information about the three-dimensional structure of forest stands. As the canopy elements of forest stands (leaves, needles, twigs, branches) are usually smaller than the diameter even of small-footprint laser scanners, the laser beam often is reflected several times inside a canopy so that a complex echo waveform results. In dense canopies this waveform contains information only about the tree crowns, in looser canopies there are also echoes from the ground.

The maximum of spectral information, apart from laboratory spectroscopy, can be obtained by airborne hyperspectral imagery (Vane & Goetz 1988). Both, full waveform airborne laser scanner data and airborne hyperspectral data are available for the study area, the Idarwald forest in south-western Germany. In this study, these two very rich data sets are combined to get a very detailed insight into the stand structure. These structural analyses are validated using fish-eye lens photography of many of the stands.

2. Material and Methods

2.1 Study area

The area of study (49°40'N, 7°10'E) is the Idarwald forest in south-western Germany on the north-western slope of the Hunsrück mountain ridge. The dominant tree species are Norway spruce (*Picea abies*), beech (*Fagus sylvatica*), oak (*Quercus petraea*) and Douglas fir (*Pseudotsuga menziesii*). Active forestry practices in this area include selective cutting, plantation establishment and thinning.

2.2 Data used

In July 2003 a Hymap image of the study area was acquired. The original data set contains 128 reflective channels in the spectral range of 440 to 2480 nm with spectral resolutions between 10 and 20 nm (Cocks et al. 1998). Due to noise six of the channels were eliminated. Data preparation steps included a cross-track illumination correction, a parametric atmospheric

correction and a parametric geocorrection to the local Gauss-Krüger system (Schlerf et al. 2004, Buddenbaum et al. 2005).

In September 2005 laser scanner data was acquired using a Riegl LMS-Q560 (Hug et al. 2004) which records full waves. The data set is available as first echo, last echo and only echo single point files and as waveform data. The data provider filtered a ground point data set from the last and only echo files. Figure 1 shows all waves within a radius of 1 m around a point on the ground. A flight pattern with ten overlapping flight lines was chosen so that nearly all of the study area was seen from at least two angles. This is a commonplace flight pattern chosen in order to increase the probability of seeing ground pixels through dense crowns and to account for the asymmetry in canopy level data collected at varying scan angles (Hopkinson et al. 2008, Holmgren et al. 2003). Additionally, full coverage of the area could be guaranteed.

In addition to the remote sensing data, field work was conducted in September 2005. 28 stands of Norway spruce and beech were sampled in plots of 30 m × 30 m size. Parameters measured included tree height, crown height, crown radius in four directions, stem diameter at breast height, LAI (measured by a Li-Cor LAI 2000 Plant Canopy Analyzer), number of trees and canopy closure. Nine hemispherical digital photos using a fish-eye lens have been taken of each stand in order to document the stand structure.

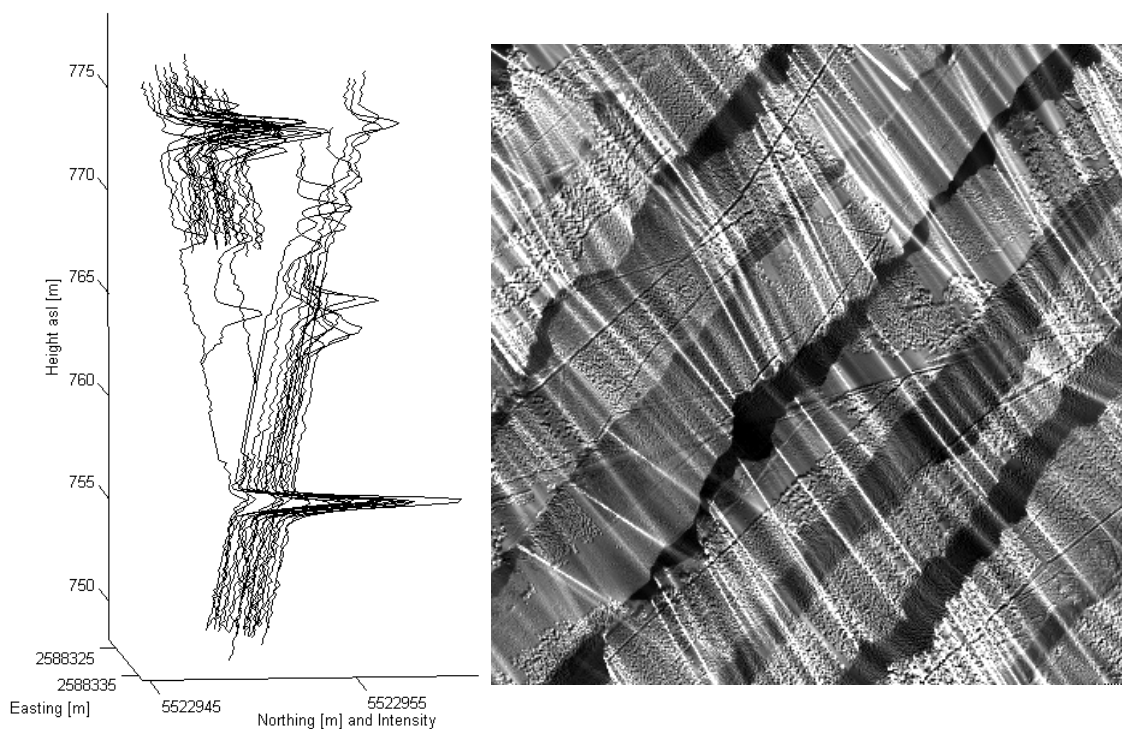


Figure 1: Left: Full waveforms from two flight lines converging on a small ground area. The ground level is at about 756 m asl where the lowest peaks occur. Right: Frequency of laser hits in an area of 400 x 400 Pixels; flight line overlapping and aircraft motions can be seen.

2.3 Methods

To reduce the amount of data and to align the full waveform ALS data to the hyperspectral data all waves within a ground area of 5 m x 5 m – the geometric resolution of the hyperspectral data – were combined. The data were to be expressed as voxels (volume elements, Figure) of 5 m x 5

m x 0.5 m volume. Each voxel contains the mean intensity with which laser pulses were reflected in the according volume element. As a basis for this combination a 5 m x 5 m DEM was created from the ground point data set. For every waveform the ground position was calculated. The intensity curve was interpolated to 0.5 m steps starting at the ground height taken from the corresponding ground pixel. All values within a voxel were added while a counter in another array was increased. At the end the accumulated intensities were divided by the number of hits per pixel, resulting in an average waveform for each pixel. The result was saved as a multiband file similar to the hyperspectral data set. This procedure took a processing time of about 5 days. As the maximum tree height in the study area is about 38 m, 76 bands were created. Only the highest stands contain data in the last bands; in clearings there are data only in the first band. All intensity echoes were assigned to the position of their ground pixel; in the creation of the voxel data set we did not consider the slanted view direction but treated all waves as if they had been recorded from nadir direction. This approach of creating a voxel data set is different from that of e.g. Popescu & Zhao (2008) as the voxels were filled with fullwave intensity data, not with single points.

The multiband ALS image and the hyperspectral image were stacked. The layerstack of hyperspectral and laser data contains 198 bands.

Figure 3 shows examples of Hymap-ALS "spectra". The left part of each graph is the reflection spectrum, the right part is the height profile of the pixel (or voxel). It is very difficult to recognize the age of a tree stand from the reflection spectrum alone; in combination with the ALS spectrum this becomes much easier. For example, the reflectance spectra in the upper right part and the lower left part of the figure are hardly distinguishable. In a classification they would very likely be put in the same class. Only the additional information offered by the ALS data shows the differences in stand structure clearly.

Figure shows more examples of the good accordance of ALS height profiles and the tree stands. The photos were produced using fish-eye hemispherical images. The images were "unrolled" so that the central pixel in the original image corresponds to the top line of the result, the circumference of the original image corresponds to the bottom line of the result (upper part of the figure). The upper parts of these photos look distorted but the unrolled images give a better visual impression of the stand than the original circular images.

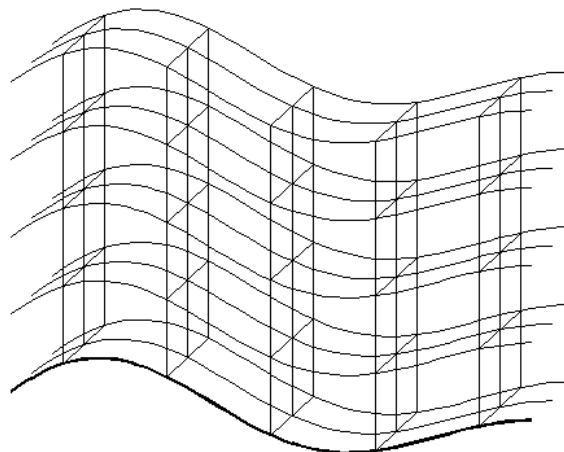


Figure 2: Voxels above ground

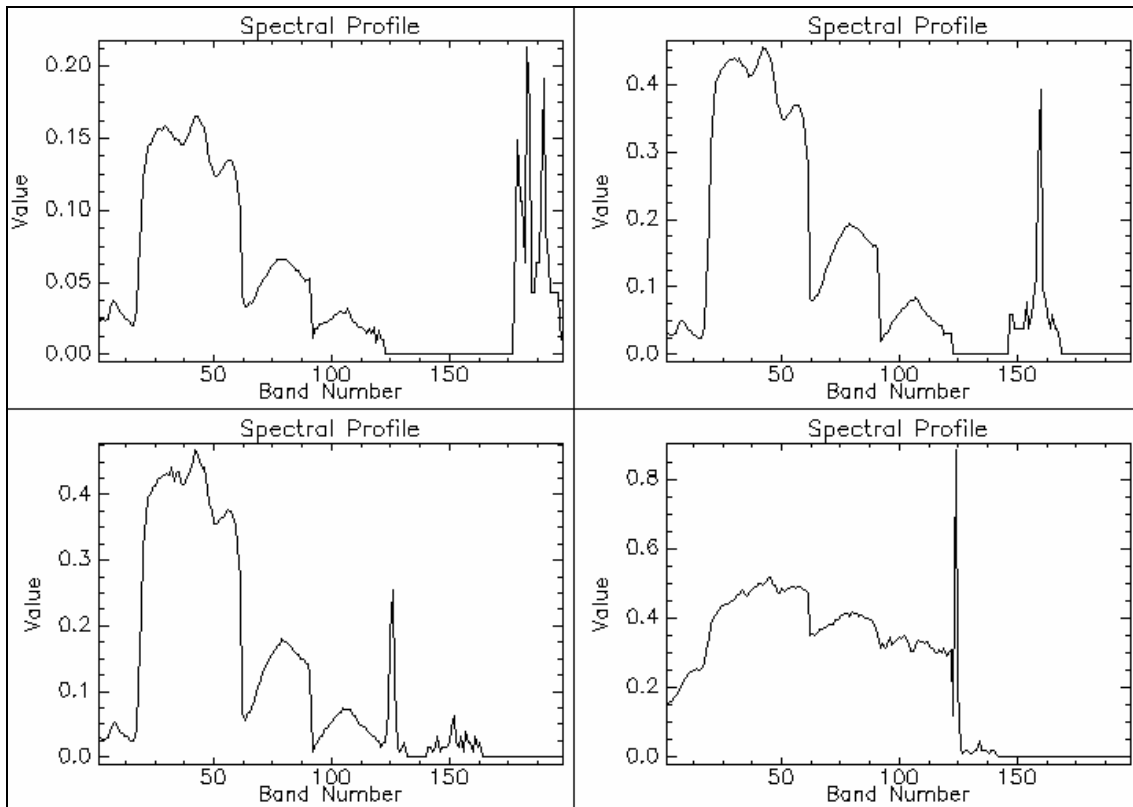


Figure 3: Combined hyperspectral and laserscanner data. Bands 1–122 contain the reflection from 440 to 2480 nm wavelengths. Bands 123–198 contain the mean laser intensity in a pixel. The upper left graph shows an old coniferous stand with high trees and no laser echo from the ground. The upper right graph shows a younger stand that is also too dense to allow a ground echo. The lower left graph a much less dense stand with a very clear ground echo. The lower right graph shows a forest track where nearly all of the laser echo comes from the ground.

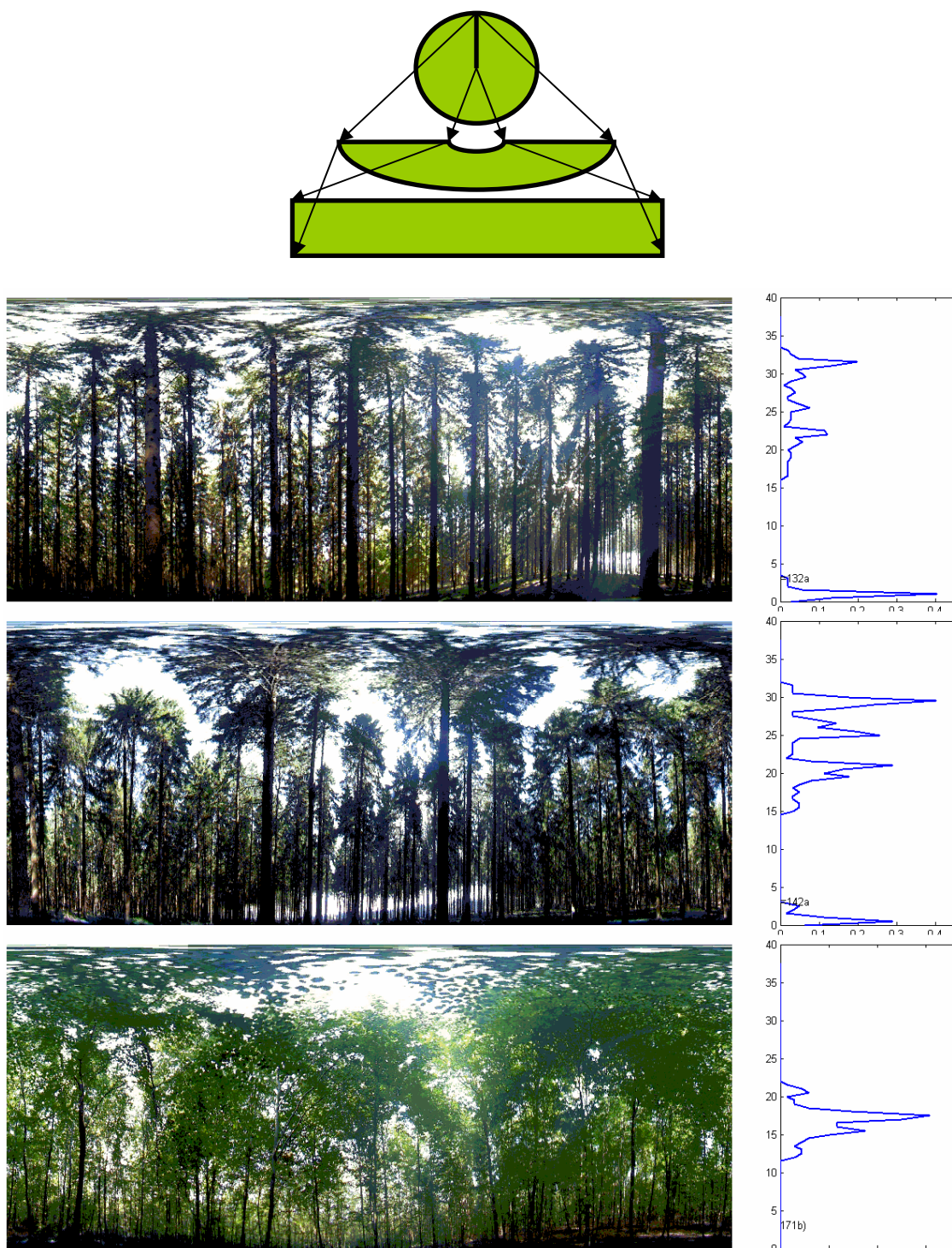


Figure 4: Unrolled hemispherical photos and corresponding ALS height profiles

3. Results and discussion

The results of this study are still preliminary. The combination of hyperspectral reflection data and airborne laser scanner full wave data is promising. The potential of characterizing the

optical and structural features of forest stands by remote sensing is large and not yet fully exploited. While the discrimination of deciduous and coniferous trees works best using the reflection spectra, the discrimination between younger and older stands as well as the discrimination between dense and thinned stands can be better accomplished with ALS data. This can clearly be seen by an analysis of the hemispherical photos and their waveform spectra which serves as a visual validation.

Point clouds and tree height layers from first pulse or difference of first pulse and ground ALS data are a more compact means of characterizing stand age, but only the full wave data show the crown structure in a detailed way, especially if there are several layers of trees. Besides the stand age, which is mostly expressed in the tree heights, the ALS data shows the density of crowns. This might be used as a validation data set for a spectral mixture analysis of the hyperspectral data if vegetation and soil are unmixed.

A classification of the combined data set was tried but did not succeed due to numerical instability caused by the many zeros in the data set. When a SAM classification was carried out on a subset of the data, the overall accuracy was significantly raised when adding the ALS voxel data to the Hymap data. Instead of using the full dataset, a single channel containing the tree heights was combined with an MNF rotated version of the Hymap data (Green et al. 1988). With these data Norway spruce and Douglas fir stands were classified into four and two age classes, respectively, similar to the approach in Buddenbaum et al. (2004). The accuracy of a maximum likelihood classification was raised from 71.6 % using the Hymap data alone to 77.3 % (Kappa coefficient rose from 0.639 to 0.713). These promising results show further potential of the combination of classic remote sensing data with ALS data.

References

- Buddenbaum, H., Schlerf, M. and Hill, J., 2005: Classification of coniferous tree species and age classes using hyperspectral data and geostatistical methods. *International Journal of Remote Sensing*, 26: 5453–5465.
- Cocks, T., Jenssen, R., Stewart, A., Wilson, I., and Shields, T., 1998: The HyMap Airborne Hyperspectral Sensor: The System, Calibration and Performance. *1st EARSEL Workshop on Imaging Spectroscopy*, Zurich, October 1998.
- Green, A.A., Berman, M., Switzer, P. and Craig, M. D., 1988: A Transformation for Ordering Multispectral Data in Terms of Image Quality with Implications for Noise Removal. *IEEE Transactions on Geoscience and Remote Sensing* 26 (1), 65–74.
- Hopkinson, C., Chasmer, L. and Hall, R.J., 2008: The uncertainty in conifer plantation growth prediction from multi-temporal lidar datasets. *Remote Sensing of Environment*, 112: 1168–1180.
- Holmgren, J., Nilsson, M. and Olsson, H., 2003: Simulating the effects of lidar scanning angle for estimation of mean tree height and canopy closure. *Canadian Journal of Remote Sensing*, 29 (5): 623–632.
- Hug, C., Ullrich, A., and Grimm, A., 2004: Litemapper-5600 – A Waveform-digitizing Lidar terrain and vegetation mapping system. In: Thies, M., Koch, B., Spiecker, H. & Weinacker, H. (Hrsg.): *Proc. ISPRS Workshop 'Laser-Scanning for Forest and Landscape Assessment'*, Freiburg, Germany, 3-6 Oct 2004. ISPRS Archives Vol. XXXVI, Part 8/W2, 24–29.
- Popescu, S.C., and Zhao, K., 2008: A voxel-based lidar method for estimating crown base height for deciduous and pine trees. *Remote Sensing of Environment*, 112: 767–781.
- Schlerf, M., Atzberger, C., and Hill, J., 2005: Remote sensing of forest biophysical variables using HyMap imaging spectrometer data. *Remote Sensing of Environment*, 95: 177–194

Vane, G, and Goetz, A.F.H., 1988: Terrestrial Imaging Spectroscopy. *Remote Sensing of Environment* 24: 1-29.

Ticking all the boxes: the added value of heritage surveys of woodland by LiDAR

P. Crow¹, B.J. Devereux⁶, G.S. Amable²

¹ Environmental and Human Sciences Division, Forest Research, Alice Holt Lodge, Farnham, Surrey GU10 4LH. peter.crow@forestry.gsi.gov.uk

² Unit for Landscape Modelling, University of Cambridge, Sir William Hardy Building, Tennis Court Road, Cambridge CB2 1QB

Abstract

Mapping archaeological features is a key activity for understanding and maintaining national heritage records by government and for historic landscape reconstruction by scientists and academia. Such mapping has hitherto relied on collection and interpretation of aerial photography. Archaeological features reveal themselves in photography as crop marks or field patterns caused by shadowing and highlighting of small variations in terrain morphology. However, this approach to mapping has some clear limitations, as features beneath forest canopies cannot be detected at all. In the UK forestry covers some twelve percent of the landscape and thus represents a significant area in which the archaeological record is incomplete or entirely missing. Areas affected by this problem in other parts of the world may be significantly higher. For organisations charged with recording and managing heritage this is a serious problem because the only viable approach – ground survey – is both difficult and expensive.

The emergence of small footprint, airborne LiDAR is now rapidly opening up new approaches to mapping heritage features. Previous work by the present authors has demonstrated that with appropriate visualisation techniques, hillshading of LiDAR DEM's can offer a much more effective approach to feature detection than photography. Furthermore, they have also demonstrated that the ability of LiDAR to penetrate forest canopies opens up the potential for airborne mapping of sub-canopy archaeological features.

The application of this technology to some British forests has already led to the discovery of many, previously unknown sites of potential archaeological significance. As such, the dissemination of the findings is receiving considerable interest within the heritage sector, media and wider public. There are limitations to the survey method and caveats with the data and informing project partners and stakeholders of the pros and cons of a LiDAR survey over a wooded landscape is essential. However, this very process of knowledge transfer has highlighted the many other potential benefits of the survey and this paper will examine some of them. Examples include opportunities to engage with volunteers in the on-site identification of features identified in hillshaded images.

The very 3-dimensional nature of these heritage surveys allows interactive visualisation of historic landscapes, cross-sectional analysis of individual monuments and provides a powerful mechanism for dissemination and engagement. The data is also of use to other non-heritage professionals such as forest and landscape managers and planners, providing information about the forest structure and a landscape both with and without woodland cover. In the longer-term, findings from these surveys can be used to create heritage trails within forests, thereby increasing their cultural value through increased education and recreation.

Experience from these heritage surveys has already shown the significant diversity of applications of the surveys and data. This in turn can be used to build partnerships in advance of undertaking new surveys.

Small footprint, full waveform LiDAR modelling of canopy 3d structure in complex, semi-natural woodland communities

B.J. Devereux⁷, G.S. Amable¹, J. Liadsky², P. Crow³

¹Unit for Landscape Modelling, University of Cambridge, Sir William Hardy Building, Tennis Court Road, Cambridge CB2 1QB. bjd1@cam.ac.uk

²Optech Incorporated, 100 Wildcat Road, Toronto, Ontario, Canada M3J 2Z9

³ Environmental and Human Sciences Division, Forest Research, Alice Holt Lodge, Farnham, Surrey GU10 4LH

Abstract

The last decade has seen the rapid emergence of LiDAR technology as a tool for terrain and vegetation analysis. Large footprint LiDAR systems developed by NASA have been used to examine the three dimensional structure of forest stands with a view to measurement of key forest parameters including biomass, LAI, above ground carbon content and carbon flux. They have also provided a basis for satellite deployment of LiDAR technology (e.g. ICESAT) which will enable global monitoring of these variables. In parallel, there has been a dramatic growth in small footprint, discrete return systems that have found extensive application in terrain modelling, measurement of tree heights and statistical estimation of other key forest variables.

To date, it is undoubtedly the case that small footprint systems have been limited to measurement of discrete returns – first, last and sometimes one or two intermediate pulses – by data volume and bandwidth issues which have prevented the capture and storage of small footprint, full waveform returns. A consequence of this is that their potential for measuring the full vertical structure of forest canopies has been restricted.

This paper will describe the design, construction and implementation of a small footprint, full waveform LiDAR tailored for forestry applications. The system measures and records the full waveform return for sub-meter footprints at a frequency of up to 70 Khz. It has a vertical height resolution of 15cm over a maximum height range of approximately 65 m. The system is a fully integrated extension to an Optech ALTM 3033 device with Applanix GPS and IMU positioning.

The performance of the system will be evaluated by presenting results from full waveform LiDAR surveys of Woodwalton Fen Site SSSI in Eastern England and the Alice Holt research forest in Hampshire. Waveform properties for both deciduous and coniferous forest types will be described and their potential for measuring canopy height, openness, density, vertical structure and gaps will be evaluated. A methodology for assessing the accuracy of the results will be presented based on gap fraction analysis from hemispherical photography and ground-based laser scanning techniques.

The results will highlight biases which occur when discrete return observations are used to model 3d structure. They will also demonstrate that such bias can be overcome with full waveform data and effective calibration/integration and modelling techniques. The results carry important implications for measurement of above ground biomass, carbon content and LAI.

Estimating forest biomass in mixed broad-leaved forests of the Italian pre-Alps

Sara Fusco¹, Dirk Pflugmacher², Alan Kirschbaum², Warren Cohen³, Donato Chiatante¹
& Antonio Montagnoli¹

¹ University of Insubria, Department of Environmental Sciences, Via Valleggio, 11
22100 Como, Italy

² Oregon State University, Department of Forest Science, 321 Richardson Hall,
Corvallis, OR 97331, United States

³ USDA Forest Service, Pacific Northwest Research Station, Forestry Sciences
Laboratory, 3200 SW Jefferson Way, Corvallis, OR 97331, United States

Abstract

Estimation of forest biomass for inventorying carbon stocks has gained importance as a result of the Climate Convention and the Kyoto Protocol. Estimation of forest biomass on the regional and global scale is therefore of great importance. Many studies have demonstrated that lidar is an accurate tool for estimating forest biomass. However, results vary with forest types, terrain conditions and the quality of the lidar data. In Italy many regional governments are acquiring low density lidar data for topographic and bathymetric mapping. We examine whether this type of data are useful for measuring forest attributes, such as biomass.

In this study, we investigated the utility of low density lidar data (< 2 points m²) for estimating forest biomass in the mountainous forests of northern Italy.

As a first study site we selected a 2x2 km area in the Valsassina mountains in Lombardia. The region is characterized by mixed and broad-leaved forests with variable stand densities and tree species compositions. The site is representative for the entire Pre-Alps region in terms of type of forest and geomorphology. The main forest types are coppice management with plantations of chestnut (*Castanea sativa*), beech (*Fagus sylvatica*), birch (*Betula pendula*), linden (*Tilia cordata*), ash (*Fraxinus excelsior*), poplar (*Populus tremula*) and natural stands of oak (*Quercus spp*).

We collected field data for 27 randomly located circular plots (radius=10m) in May 2008. In each plot we measured and determined tree height, DBH and tree species for trees with a DBH greater than 5cm. We used allometric equations to calculate total aboveground tree biomass and subsequently plot-level biomass (Mg ha⁻¹). Lidar data was collected in June 2004. The objectives of this work were: (i) to develop models of forest biomass from plot-level lidar height metrics and (ii) to understand if low density lidar is accurate enough in high slopes to produce a map of forest biomass for the region.

Our results indicate that low density lidar can be used to estimate forest biomass in our study region with acceptable accuracies. The best height results show a R² from final model 0.87 and the RMSE 1.02 m (8,3% of the mean). The best biomass model explained 59% (R²) of the variance in the field biomass. Leave-one-out cross validation yielded an RMSE of 30,6 Mg ha⁻¹ (20,9% of the mean).

A comparison of Gradient Nearest Neighbor and Most Similar Neighbor imputation methods to map forest cover types of Western Oregon

D. Gagliasso¹, H. Temesgen², S. Hummel³

¹Contact: donald.gagliasso@oregonstate.edu, Tel.: 408-655-8789; M.S. Student, OSU
Dept. of Forest Resources

²Assistant Professor, Forest Biometric and Measurements, Oregon State University

³Research Forester, Pacific Northwest Research Station, United States Forest Service

Abstract

Various imputation methods are used to generate forest biomass estimates in the United States. The Gradient Nearest Neighbor (GNN) and Most Similar Neighbor (MSN) are two such imputation methods that combine satellite imagery, ground data, and environmental data to generate biomass estimates at a regional scale. However, there is little confidence on how accurate these estimates are at a local scale. This case study will estimate the amount of agreement between the GNN and MSN imputation methods in a forested landscape. Light Detection and Ranging (LiDAR) data will be used to increase the confidence of these imputation methods to estimate forest biomass at the local scale, in forests of Western Oregon.

Remote mining: from clustering to DTM

J. García-Gutiérrez¹, F. Martínez-Álvarez², D. Laguna-Ruiz¹ and J. C. Riquelme¹

¹Department of Computer Science, University of Seville, Spain.

[jgarcia, dlaguna, riquelme}@lsi.us.es](mailto:{jgarcia, dlaguna, riquelme}@lsi.us.es)

²Area of Computer Science, Pablo Olavide University, Spain.

fmaralv@upo.es

Abstract

LIDAR data acquisition is becoming an indispensable task for terrain characterization in large surfaces. In Mediterranean woods this job results hard due to the great variety of heights and forms, as well as sparse vegetation that they present. A new data mining-based approach is proposed with the aim of classifying LIDAR data clouds as a first step in DTM generation. The developed methodology consists in a multi-step iterative process that splits the data into different classes (ground and low/med/high vegetation) by means of a clustering algorithm. This method has been tested on three different areas of the southern Spain with successful results, verging on 80% hits.

Keywords: LIDAR, DTM, clustering.

1. Introduction

The Regional Ministry for the Environment of Andalusia, the regional government in the South of Spain, owns two LIDAR sensors. Recently, this public entity has decided to develop a software system to improve the cartographic and environmental services using this technological advance because of the LIDAR's well-known capacity to create 3D models with high quality. In this context it is necessary to be able to obtain a DTM from LIDAR data point clouds and to distinguish ground and non-ground (vegetation) impact. Nowadays, most of the software used to perform this kind of work is based on proprietary systems like Terrascan (*Terrasolid Limited 2002*). Our goal has been to develop free software in the near future to classify LIDAR data. As an initial step our study has been centered on applying data mining techniques (k-means clustering) to a LIDAR point cloud in order to obtain a digital elevation model (DEM).

Others authors have worked in how to build DTM from LIDAR data previously. A method for filtering laser data (Vosselman 2000) is proposed closely related to the erosion operator used for mathematical grey scale morphology. This method is based on height differences in a representative training dataset, then filter functions are derived that either preserve important terrain characteristics or minimize the number of classification errors. The work (Haugeraud and Harding 2001) propose a method for deforestation to identify ground and non-ground points based on the geometry of surface in the neighborhood of each return. Zhang (Zhang *et al.* 2003) uses a progressive method to erase non-ground points based on a threshold to study height differences among points.

In more recent times, the paper (Sithole and Vosselman 2005) makes classifications, by using a segmentation process in the LIDAR data point cloud. Then, every segment is classified on the basis of the geometric relations to the rest of segments. Bartels (Bartels *et al* 2006) presents a new filter based on statistical moments from data cloud to distinguish ground and non-ground

points in an efficient way. In addition, in (Evans and Hudak 2007), an iterative multiscale algorithm for classifying LIDAR returns that exceed positive surface curvature thresholds have been developed. The authors maintain that the results show very few commission errors and high quality models.

Most of the approaches to develop DTM are based on grid techniques or on some kind of preliminary process like rasterization. This kind of techniques usually introduces distortion in the system that is studied and it can be an error source. In this situation, data mining techniques can be applied for optimal results because:

- It does not need any preprocess that could produce errors in the results.
- It can be easily applied to big datasets as, for example, the LIDAR data clouds.

Data mining is defined by Piatetski-Shapiro (Piatetski-Shapiro *et al.* 1991) as: “*the set of techniques that are concerned with finding patterns in data which are interesting (according to some user-defined measure of interestingness, e.g., with coverage above the requested threshold) and valid (according to some user defined measure of validity, e.g., classification accuracy)*”. These kinds of techniques can be applied to any data source in general and it can particularly be applied on LIDAR data without loss of precision.

Clustering is one a widely used data mining techniques. There are lots of clustering strategies, but perhaps the most extended method is k-means. It has been applied on bioinformatics, pattern recognition and even in remote sensing and LIDAR data, too. In this way, we can find approaches like Filin’s (Filin 2004) which makes DSM by studying the angles among neighbors. k-means classical algorithm is used by Filin’s approach applied to the attribute set obtained from a data cloud. In this way, every point has a set of angles with its neighbors as a result of Delaunay’s triangularization. From this data and the position of every point, the author builds clusters to identify each surface. Other approaches use k-means as help to segment data and get the individual trees. Thus, Morsdorf (Morsdorf *et al.* 2004) chooses local maxima inside the cloud as the initial point of every cluster. Then the algorithm builds clusters surrounding each maximum and with this, it gets the vegetation structure, an important parameter in fire risk assessment and fire behaviour modelling. Others techniques from data mining like neural networks are used with a similar purpose. Thus, Fernandes (Fernandes *et al.* 2005) developed a one-layer perceptron to classify signals from terrestrial LIDAR automatically in order to discover forest fire in early phases. The authors maintain their approach has detection efficiency of 93% and a false alarm percentage of 0.041%.

This paper is concerned with the separation of ground and vegetation points in Mediterranean woods from LIDAR data. The main novelty of this approach is the applying of clustering techniques to the build of DTM and concretely the build of a digital elevation model (DEM) from a previous deep classification.

The paper is organised as follows: In Section 2, the zone under study is presented and our approach is detailed. Section 3 presents results on high, medium and low resolution LIDAR data. The paper discusses results, proposes future avenues and concludes in Section 4.

2. Method

Our method is based on a multi-step k-means clustering applied to a LIDAR data cloud. Each step divides the original data cloud in two sets. Each set identifies the points for a possible classification: ground, low vegetation, med vegetation and high vegetation. We lean on the silhouette function to decide if it is possible to keep on dividing data. In the next paragraphs we describe the k-means algorithm, the silhouette function and a deeper description of our approach

is shown.

The k -means algorithm was originally presented by MacQueen (1968). For each cluster, its centroid is used as the most representative point, where the centroid μ_j of a group of elements x_j is defined as the centre of gravity of all the elements comprising the cluster.

The aim is to minimize intra-cluster variance, or the squared error function:

$$V = \sum_{i=1}^k \sum_{x_j \in C_i} |x_j - \mu_i|^2 \quad (1)$$

k -means is the most popular method to perform clustering. It is an efficient and scalable method especially useful to deal with large datasets. It presents a computational complexity $O(nkt)$, where n is the number of objects, k the number of clusters and t , the number of iterations. A local optimum is reached when $k \ll n$ and $t \ll n$, which is a very common situation.

The selection of an optimum number of clusters is still an open task. Recently, several approaches have been developed in order to determine this number (Hamerly and Elkan, 2003; Yan and Ye, 2007) but its application has been demonstrated to be useful only in individual areas. In this sense, the silhouette function (Kaufmann and Rouseeuw, 1990) provides a measure of the cluster's separation and can be used as a general-purpose method.

Let's consider an item i (already clustered) that belongs to the cluster A . We evaluate the average dissimilarity of i to all the other objects of A is evaluated and denoted by $a(i)$. Analogously, the average dissimilarity of i to all the objects of B is called $dis(i, B)$. The next step consists of computing $dis(i, B)$ for every $B \neq A$ and, subsequently, the smallest dissimilarity is chosen and noted by $b(i) = \min\{dis(i, B)\}$, $B \neq A$. Thus, $b(i)$ represents the dissimilarity of i to its neighbour cluster. Finally, to determine how well a point is clustered, the silhouette function, shown in equation (3), is applied:

$$silh(i) = \frac{b(i) - a(i)}{\max\{a(i), b(i)\}} \quad (2)$$

Its value varies between -1 and $+1$, where $+1$ denotes clear cluster separation and -1 marks points with questionable cluster assignment. If cluster A is a set containing a single member, then $silh(i)$ is not defined and the most neutral choice is to set $silh(i) = 0$. The objective function is the average of $silh(i)$ over the N objects to be classified, and the best clustering is reached when the above mentioned function is maximized.

2. 1. Algorithm

The classification method is based on three iterations to classify all data. The first iteration classifies high vegetation. If the resulted clustering has a good silhouette value, it continues with medium vegetation and finally low vegetation. The unclassified data at last iteration is the ground data. In Figure 1, the process description can be seen for i -th iteration. Thus, iteration is divided into four steps. The first step takes the raw LIDAR data as input and builds a matrix as output with the minimum height of the terrain in every cell. To obtain good results it is necessary to set the cell size as a parameter for the algorithm. This parameter will determinate the size of the terrain contained in a cell of the matrix. This will be very important in the next step.

Once the matrix has been built, we go into step 2. For each point from the raw LIDAR cloud, a

new measure is added, the biggest height difference that is calculated between the point height and the neighbour cells in the matrix, where the cell that could contain the point is included as a neighbour too. This new measure needs to know which cells are neighbours. A new parameter ϵ has to be given. This parameter can be defined as the biggest distance between the cell that includes the point and a possible neighbour cell. This parameter is related closely to the resolution of the data cloud and it will define the portion of terrain that is processed, together with the parameter in the paragraph before, to calculate the maximum height difference among points. It is important to realize parameter ϵ will be bigger for LIDAR data with low resolution and vice versa.

The next step is the application of the k-means algorithm to the cloud trying to divide it into two clusters. It leans on the data with the added measure to build the classification. At the end of the execution, a new classification is obtained as output. The cluster with a higher mean height is the new group of classified points. Iteration provides a new class from high vegetation to low vegetation. At last, the algorithm tries to validate the results in the last step.

In step 4, the algorithm takes the results of k-means and uses Silhouette function to decide if it is a good clustering or not. Silhouette provides a measure for every point weighting the inter-clustering distance. The measure may be between -1 and 1 where value 1 is the best and -1 is the worst. In this step, a mean for all the points is calculated and if the clusters have a silhouette mean over 0.6 the clustering is considered good. Otherwise, it is considered a bad clustering and the algorithm rollbacks, changes the points classification to ground points and ends.

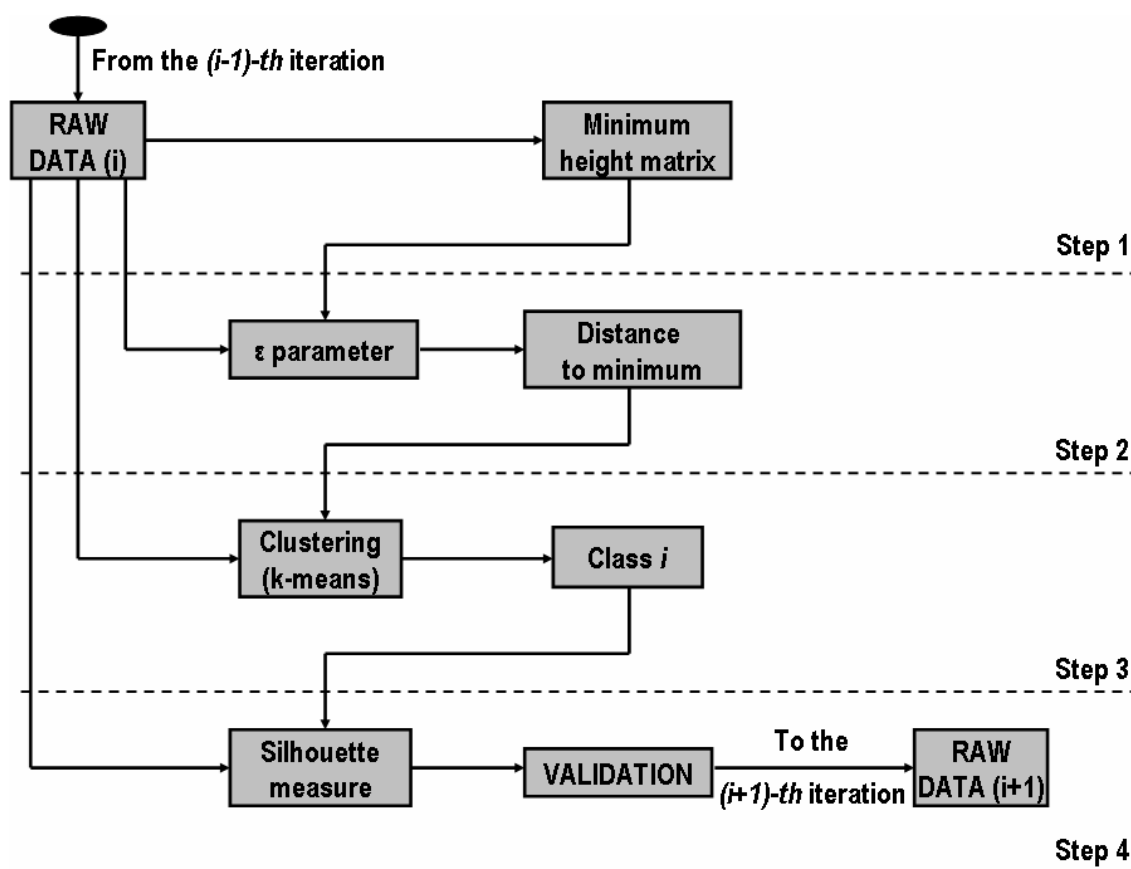


Figure 1: i -th iteration of the extracting information process.

2.2 Study area

We have chosen three study areas with different morphological (topographical) signature, with the aim of obtaining a comprehensive assessment of our algorithm, covering a forest burned and not burned area mountain range in Cerro Muriano (Córdoba) and two marshland areas, one within a Natural Setting in Isla Cristina (Huelva) and the other in Marismas del Odiel (Huelva). The task of classification is especially arduous since the terrains under study are not regular enough.

The following information was available for the study area: (i) sets of aerial photographs taken in the period from 2005 to 2007 at 1-meter resolution; (ii) medium scale lithological and land use maps in digital format; and (iii) a high-resolution (HR) digital elevation model (DEM) obtained by spatial correlation of images, including breaklines and manual edition in troubled areas. The HR DEM was used to obtain digital representations of the topographic surface of the study area, including elevation, shaded relief, and slope maps. The digital maps were exploited for visual testing, based on their morphological (topographical) appearance.

3. Results

Mediterranean woods are some of the most variable environments we can find in Europe. They usually have very little vegetation and it has a great variety of heights, forms... So the samples we have used are deemed to be difficult to filter. We have centred on vegetation because it is the most important feature for the Regional Ministry. Further studies are planning to extend the results to zones with buildings, bridges...

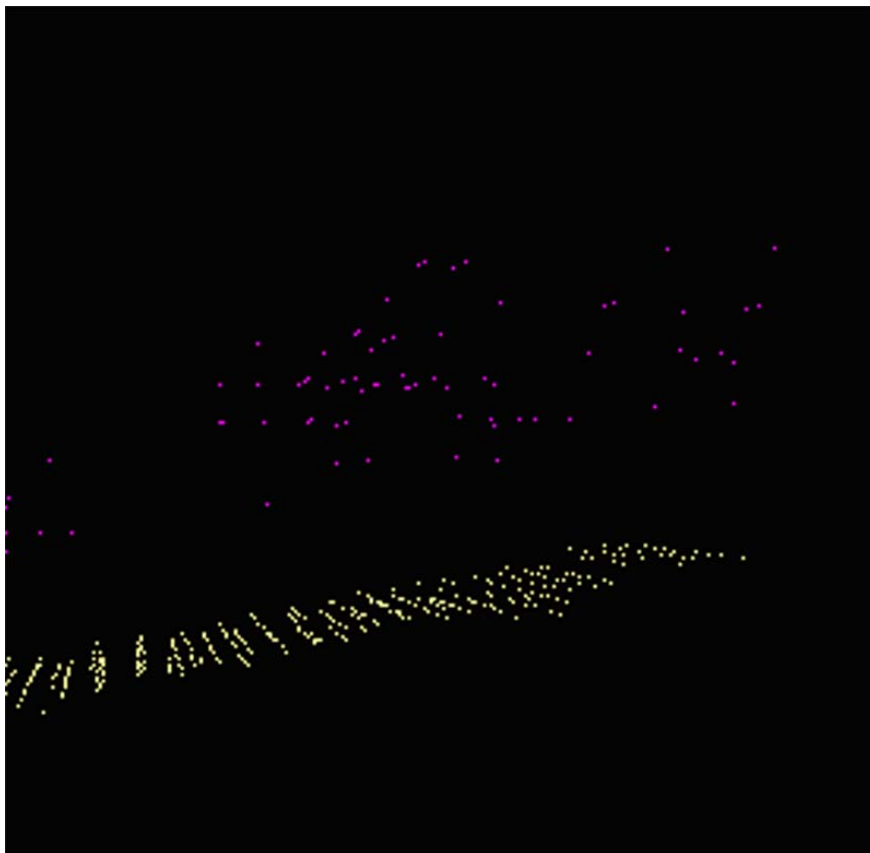


Figure 2: Part of the classification for Cerro Muriano in an early step.

The data has been processed for three zones representing the variability of the vegetation in the South of Spain. After numerous tests and estimating the ϵ value as a function of the inverse of the resolution of each dataset, we determined the optimum value of ϵ is 2 for Cerro Muriano dataset and 1 for the other two ones. The results have been compared against manually classified points. Table 1 presents the total error in every zone. The total error presents the number of misclassified points as a percentage of all studied points in the sample.

Table 2: Total error.

| Zone | Number of points | Number of hits | Extractive rate (%) | Error (%) |
|-------------------------|------------------|----------------|---------------------|-----------|
| Cerro Muriano (Córdoba) | 140 | 112 | 80 | 20 |
| Odiel (Huelva) | 140 | 121 | 86.4 | 14.6 |
| Isla Cristina (Huelva) | 140 | 100 | 71.4 | 18.6 |
| Total | 420 | 333 | 79.28 | 20.72 |

The great error in the Cerro Muriano zone appears because it has a very low resolution. This flight was orthographic and a LIDAR sensor was mounted to make testing on the area. The low resolution affects the results even if parameter ϵ is got increased. In addition, the zone of Isla Cristina is an extremely difficult zone because it's a marshland. The mean height is very low and the differences between the short vegetation and the ground are hard to find. A solution to this problem is still being investigated.

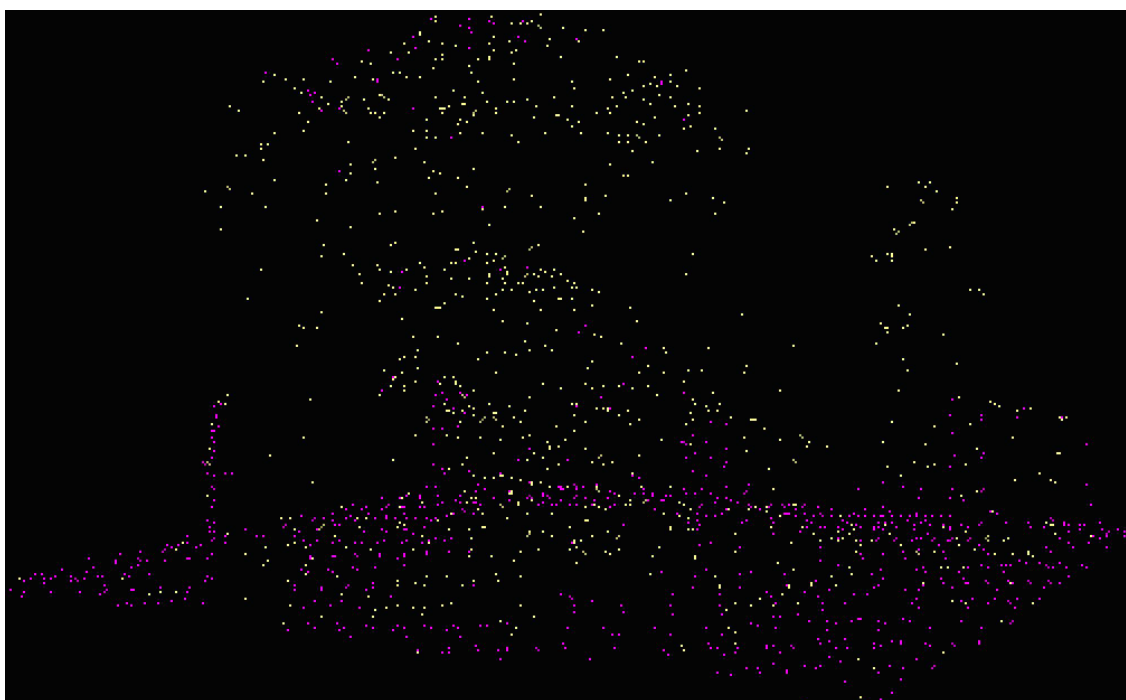


Figure 3: Example of area misclassified in Isla Cristina.



Figure 4: Part of the classification for marshland of Huelva.

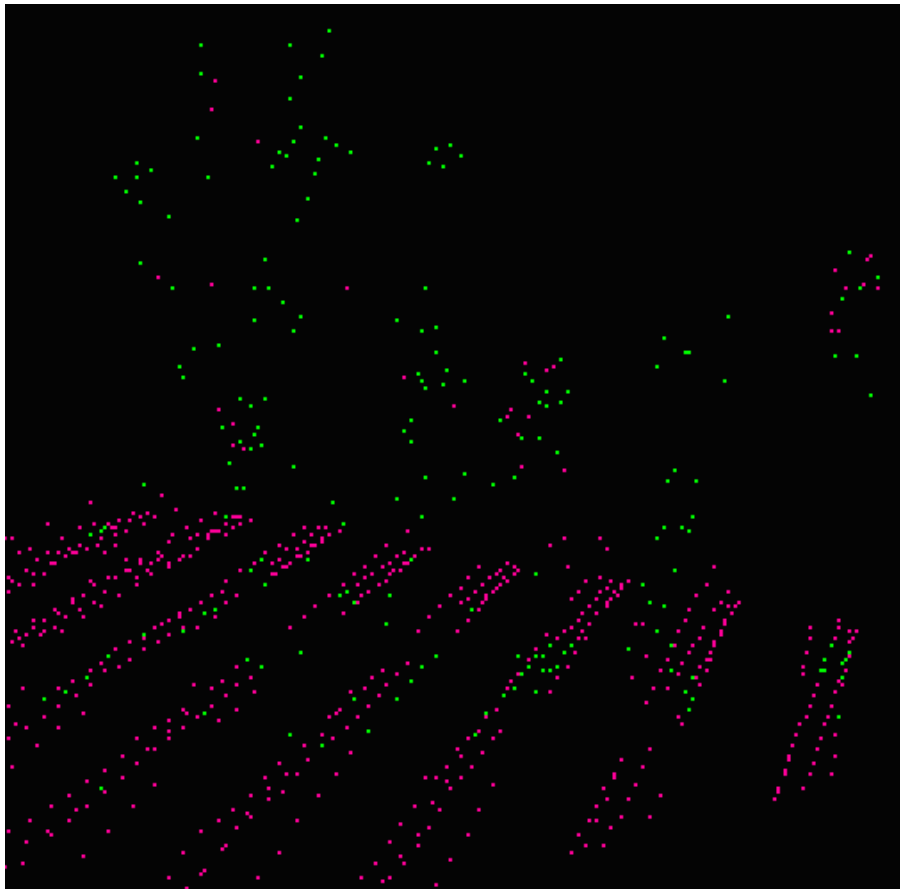


Figure 5: Example of area classified in Odjel.

One of the outstanding conclusions that can be deduced from the experiments is that our approach performs in very similar way in all landscapes. Very few algorithms are been tested on Mediterranean lands and a deep comparative study among the set of algorithms that can be found nowadays is needed to determinate if our approach can compete with them when software based on our approach is available.

3.1. Outliers

Laser scanner data sometimes contain isolated points that have large systematic error. In the developed algorithm clusters with a very small size (typically one or two points) are classified as outliers and can be deleted. If this situation appears, iteration is done again without the removed points.

4. Discussion

LIDAR data from Mediterranean woods has been analyzed in this work. To be precise, a new clustering-based approach has been proposed in order to distinguish vegetation from ground. Thus, it has been demonstrated that different kinds of profiles can be differentiated by applying a well-known data mining technique, such as k-means, integrated in a multi-step cascade process of feature extraction. A parameter is calculated in every step and subsequently used as an input of the following step. The accuracy shown is certainly promising since no extra computation, apart from the k-means, is added to the approach, achieving a low computational cost.

Concerning to future work, it can be stated that this initial division into two main classes could be very useful in order to classify miscellaneous grounds or vegetation. Moreover, this data split allows the classes to be considered and further analyzed in a different way since ground and vegetation do not show the same behaviour to laser pulses.

Acknowledgements

The authors want to acknowledge the financial support from the Spanish Ministry of Science and Technology, project TIN2007-68084. They also want to acknowledge the support provided by the Regional Ministry for the Environment of Andalusia.

References

- Bartels, M., Wei, H. and Mason, D.C., 2006. DTM generation from lidar data using skewness balancing. *In ICPR06*.
- Evans, Jeffrey S. and Hudak, Andrew T., 2007. A multiscale curvature algorithm for classifying discrete return lidar in forested environments. *IEEE Transactions On Geoscience And Remote Sensing*.
- Fernandes, Armando M., Utkin, Andrei B., Lavrov, Alexander V. and Vilar, Rui M, 2005. Design of committee machines for classification of single-wavelength lidar signals applied to early forest fire detection. *Pattern Recognition Letters*, 26:625-632.
- Filin, S., 2004. Surface classification from airborne laser scanning data. *Computers and Geosciences*.
- Hamerly, G. and Elkan, C., 2003. Learning the k in k-means. *Proc. of the NIPS*.
- Haugerud, R. A. and Harding, D. J., 2001. Some algorithms for virtual deforestation (vdf) of lidar topographic survey data. *International Archives Of Photogrammetry Remote Sensing And Spatial Information Sciences*, 34(3):211-218.

- Morsdorf, F., Meier, E., Kötz, B. and Itten, K.I, 2004. Lidar based geometric reconstruction of boreal type forest stands at single tree level for forest and wildland fire management. *Remote Sensing of Environment*, (92):353-362.
- Piatetski-Shapiro, G., Frawley, W. J. and Matheus, C. J., 1991. Knowledge discovery in databases: an overview. *AAAI-MIT Press*.
- TerraSolid Limited, 2000. TerraScan for microStation, user's guide.
- Sithole, G. and Vosselman, G., 2005. Filtering of airborne laser scanner data based on segmented point clouds. *ISPRS 2005*.
- Vosselman, George, 2000. Slope based filtering of laser altimetry data. *IAPRS, XXXIII*.
- Yan, M., and Ye, K., 2007. Determining the number of clusters using the weighted gap statistic. *Biometrics*, 63, 1031–1037.
- Zhang, K., Chen, S., Whitman, D., Shyu, M., Jianhua, Y. and Zhang, C., 2003. A progressive morphological filter for removing nonground measurements from airborne lidar data. *IEEE Transactions on Geoscience and Remote Sensing*, 41(4):872-882.
- Link to the Regional Ministry from Environment of Andalusia web:
<http://www.juntadeandalucia.es/medioambiente/site/web/>

Planimetric offset adjustment of multitemporal laser scanner data

Mariano García¹, Elena Prado², David Riaño^{3,4}, Emilio Chuvieco¹ and Mark Danson⁵

¹ Department of Geography, University of Alcalá. Alcalá de Henares, 28801. Madrid (Spain).

mariano.garcia@uah.es ; emilio.chuvieco@uah.es

² Remote Sensing Area, National Institute of Aerospace Technology (INTA), Crta. de Ajalvir Km 4, 28850 Torrejón de Ardoz, Madrid pradooe@inta.es

³ Institute of Economics and Geography, Spanish National Research Council (CSIC), Albasanz 26-28 28037 Madrid (Spain). driano@ieg.csic.es

⁴ Center for Spatial Technologies and Remote Sensing (CSTARS), University of California, 250-N, The Barn, One Shields Avenue, Davis. CA 95616-8617, USA

⁵ Centre for Environmental Systems Research, School of Environment and Life Sciences, University of Salford, Manchester M5 4WT, UK.

Abstract

LiDAR (Light Detection and Ranging) data have shown a great potential for 3D modelling applications. This potential lies on the ability of LiDAR systems to generate highly dense 3D point clouds for describing the terrain surface. Several error sources affect the position accuracy of the 3D points, which are represented as offsets between the overlapping areas. Several methods have been developed to correct these displacements using height or intensity data. This paper proposes a three steps procedure to correct the offset observed between a multitemporal dataset. Firstly intensity images were generated. Secondly, an area based image correlation technique was applied to extract evenly distributed control points. Finally the control points were used to determine the parameters of a global transformation by least squares. The technique showed good performance for the study area reducing significantly the planimetric discrepancies observed.

Keywords: LiDAR, planimetric adjustment, image matching, least squares

1. Introduction

LiDAR (Light Detection and Ranging) data have shown a great potential for several applications such as generation of Digital Terrain and Surface Models (DTM and DSM), generation of 3D object models, forest inventory, etcetera (Maas and Vosselman, 1999; Næsset *et al.*, 2004). This potential lies on the ability of LiDAR systems to generate highly dense 3D point clouds which describe the terrain surface. Therefore, 3D modelling will be influenced by the accuracy with which the coordinates (X, Y, Z) of the point cloud are determined.

In the case of digital terrain model applications the height accuracy is the most important factor to take into account; however, in other 3D modelling applications discrepancies in the Z coordinate as well as in X and Y coordinates have to be determined (Maas, 2001). A wide variety of error sources affect the position accuracy of the 3D points, which in general terms can be grouped into: alignment errors, precision of range determination, errors of the scanning mirror, and GPS/INS system (Huising and Gomes Pereira, 1998; Maas, 2001). The latter commonly accounts for the largest errors, with errors up to 10 to 20 centimetres in the height and 50 centimetres in planimetry (Maas, 2001). These errors are represented as offsets or discrepancies between the overlapping areas of adjacent or crossing strips in relative terms or as offset at ground control points in absolute terms. Special attention has been paid to the relative adjustment of overlapping strips. As a result, several procedures have been suggested to overcome those displacements (Crombaghs *et al.* 2000; Maas, 2001; Vosselman, 2002a; Pfeifer

et al., 2005).

Pfeifer *et al.* (2005) grouped the methods into those that only consider the observed discrepancies between the points from two adjacent strips, and those methods that are based on a model of the sensor system relating each point to its original observation. Sensor-based models have the main advantage that allow to assessing the true problem and not merely cope with the phenomena (Kager, 2004). Kager (2004) proposed a method for simultaneous 3-D fitting of laser data applying correction polynomials to the registered orientation elements as a function of time. Tie-features were used for the block adjustment. The main limitation for the application of sensor-based methods is that require data that are not usually available to end-users. Thus, several methods which consider the discrepancies between points from adjacent strips have been proposed. Pfeifer *et al.* (2005) proposed a method that used tie surfaces through segmentation of the LiDAR data into planar patches. Subsequently the segments were judged according to quality and distance criteria. Finally, Comparison of the height of one segment to a plane formed by the points in the adjacent strip(s) allowed determination of height offset.

Other researchers propose to use linear features, which simplify the processing and increase the accuracy, such as gable roofs or ditches to measure the strip shifts (Vosselman, 2002a; Lee *et al.* 2007). Lee *et al.* (2007) proposed a 5-steps algorithm where planimetric offset are determined first and subsequently the height is corrected. The algorithm implies generation of a data structure (Triangular Irregular Network, TIN), segmentation of points into planar patches (e.g. roofs), determination of the intersection line between planar patches, distance measurement between lines, and application of a global transformation to correct the data.

Maas (2000) presented a procedure to precisely determine strip discrepancies in all three coordinate directions, based on least squares matching applied to LiDAR data in a TIN structure. In this method, several patches were selected. The height of a given point in one of the strips was compared to the height of points of the other strip interpolated in the TIN mesh at the same location. This difference gave an observation equation that was used to determine the shift parameters. The TIN structure has the advantage that non-interpolated raw data are used, avoiding the bias introduced by grid interpolation in occlusion areas. However, despite the advantages of a TIN structure over an interpolated grid, the method required patches containing significant height contrast in orthogonal coordinate directions. In regions where this requirement is impossible or difficult to fulfil, intensity images can be used for planimetric shift determination using matching techniques (Maas, 2001; Maas 2002; Vosselman, 2002b). Image matching is commonly applied in photogrammetry and airborne remote sensing for the establishment of correspondence between images. The methods used in image matching can be grouped into: Intensity or area based methods, feature based methods and relational methods (Lerma, 2002).

Though the methods afore mentioned have been applied to the adjustment between adjacent and crossing strips, they could be applied to a multitemporal LiDAR dataset of a given area in the same manner. Also, the methods have been developed for areas where linear or surface elements such as gable roofs, roads or ditches are easier to extract. This paper shows the utility of area-based matching applied to intensity images to estimate and correct the planimetric offset between two dataset acquired over a complex forested area in Spain, where the application of feature-based techniques is difficult. A three steps procedure was applied to extract evenly distributed control points by an area based image correlation technique, which are then used to determine the parameters of a global transformation by least squares.

2. Methods

2.1. Study area and data set

This study was carried out over a forested area located in the Natural Park of “Alto Tajo” in Guadalajara, Central Spain (UL: 40° 56' 49" N; 2° 14' 49" W; LR: 40° 48' 25" N; 2° 13' 21" W). The area is characterized by a high diversity of species, mainly pines (*Pinus sylvestris* L., *Pinus nigra* Arn., *Pinus pinaster* Ait.) and oaks (*Quercus faginea* Lam., *Quercus ilex* L and *Quercus pyrenaica* Willd.). The mean height of the study area is 1200 m, with a maximum height of 1403 m and a minimum height of 895 m.

The study area was flown twice at the end of the spring of 2006, in May 16th and June 3rd. with an Optech 3033 LiDAR system. The flying height was 2050 m above mean sea level with a maximum scan angle of $\pm 12^\circ$, a point density of approximately 2.3 points/m². The dataset consists of 3 strips flown in north-south direction with no overlap, and a crossing strip for calibration purposes, covering an area of approximately 382 Km². The data available included X, Y and Z coordinates in UTM-zone 30 (WGS84), both first and last returns, and the intensity of each return.

Inspection of the relative adjustment between the two LiDAR flights showed a good relative fitting in the Z direction but revealed a systematic offset in the XY direction. Therefore, in order to determine the magnitude of this displacement and to correct it, an image matching technique was applied to the intensity images generated from the laser data and subsequently a global transformation was used.

2.2. Planimetric offset determination

In the previous section several methods proposed to correct the offset between LiDAR datasets have been described. Most of the methods were developed for urban areas, using linear features or surface elements to determine shift in the three coordinates. Our study area, with very few gable roofs (only in one strip out of three) or linear elements, hampered the application of feature-based methods. In addition the main objective of this study was to correct the planimetric offset of the datasets. Thus, an area based correlation technique was applied to the intensity images. The method presented in this paper was carried out in three steps. Firstly, intensity images were created from the point cloud data. Second, an area-based method was applied over each strip to extract sufficient number of control points. Subsequently, the extracted control points were used to derive the parameters of a global transformation by least squares.

2.2.1. Generation of intensity images

Application of an area based matching requires the generation of a raster from the irregularly distributed point cloud, so the grey-level or digital number (DN) distribution of the two images can be compared. Therefore, the original point data were interpolated into a grid with a spatial resolution of 0.5m, using a normal core interpolation method. This method uses the intensity values for a given number of points within a defined radius that defines the interpolation area. A 2 m radius was used for the interpolation area. The interpolated values are calculated based on a distance weighted average. The weighting function decreases as an exponential function of the distance (Wyseman, PCI Geomatics, personal communication). Since intensity images presented a clear speckle noise, a median filter was applied to reduce its effect over the matching process (figure 1).



Figure 1: Intensity image generated using normal core interpolation (left) and intensity image filtered using a median filter (right)

2.2.2. Planimetric offset determination

The basic assumption of area based methods for image matching is that homologous pixels have similar radiometric (or intensity in LiDAR data) values. Area based control points extraction methods search to optimize a predefined objective function, defined by a similarity measure such as correlation coefficient, normalized cross correlation, or mutual information, based on template matching (Liu *et al.* 2006). The template can be the whole of the image or a subset.

Determination of the planimetric offset was carried out using a routine developed by Prado (2007). This routine computes the correlation coefficient between two $M \times N$ matrices. One of these matrices is established as the reference window (master), while the other matrix (slave) is moved vertically and horizontally over the master. The size of these windows was set to 100x100 pixels. Thus, the images were divided in subsets of 100x100 pixels. For each subset the slave window was moved over the master (up to ± 3 pixels) and the correlation coefficient (r) was computed. As a result the routine provides an image where the DN value represents the maximum correlation coefficient (r) found, and two images where each pixel represents the shift in X and Y that made maximum the correlation coefficient. These images allow detecting the existence of a given pattern in the distribution of the X and Y offsets. Also, since the images are divided in subsets of 100x100 pixels, the error can be evaluated locally, mapping the offset along the whole of the strips.

Usually, since it is very difficult to obtain a maximum value in the correlation process ($r=1$) a minimum threshold is established to accept a point, for example $r=0.5$ (Lerma, 2002). In this study, a threshold of $r=0.8$ was applied to the correlation values obtained, in order to extract the definite control points to be later used in the determination of the parameters of the global

model by least squares. Also a regular grid was created and overlaid to the correlation images. Thus, only those points of the grid that laid over pixels with a correlation value equal or greater than 0.8 were used as ground control points. This made it possible to extract evenly distributed control points over the overlapping area along the strips.

2.2.3. Transformation model determination

The control points previously extracted were used to calculate the coefficients of the global function to be applied. Approximately 85% of the extracted points were used as control points; the remaining 15% was used as validation points. Since the displacements observed over the overlapping area did not show local deformations (figure 2), a 2D affine transformation was applied to correct the planimetric offset between the intensity images. This geometric transformation, was applied to the LiDAR June 3rd data to match with May 16th data.

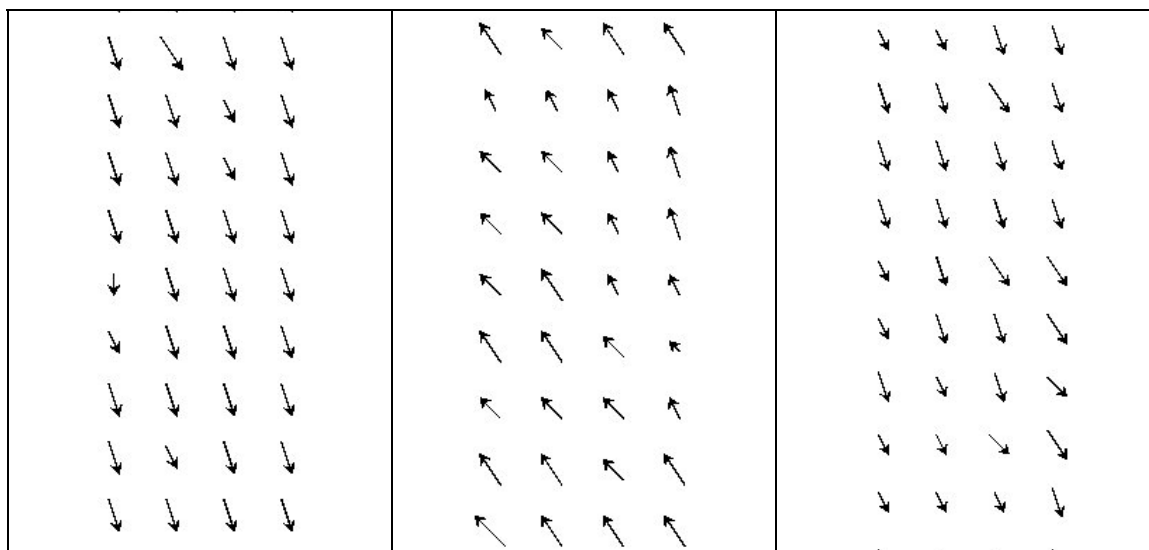


Figure 2: Subsets of the vector plots that show the pattern of the planimetric offset observed for the three strips. From left to right 1f-1s; 2f-2s; 3f-3s (1f, 2f, 3f: refers to the first day flight; 1s, 2s, 3s: refers to the second day flight)

The mathematical model of the affine transformation can be represented as:

$$\begin{pmatrix} X' \\ Y' \end{pmatrix} = \begin{pmatrix} a & b & c \\ d & e & f \end{pmatrix} \begin{pmatrix} X \\ Y \\ 1 \end{pmatrix} \quad (1)$$

Where a, b, c, d, e, and f represent the geometric parameters of the transformation, (X', Y') are the transformed coordinates and (X Y) are the observed coordinates, both in the UTM 30-WGS84 system.

3. Results

The routine applied to determine the planimetric offset, produced three new images, namely the correlation coefficient, the X-shift ($\square X$) and the Y-shift ($\square Y$) where the correlation found

reached a maximum. Table 1 presents the mean correlation coefficients computed for each strip (the mean value was computed for all pixels of the correlation images, not only for those having a correlation value higher than the threshold applied). It also presents the maximum displacements (ΔX_{max} , ΔY_{max}) found at the control and validation points, and the number of control points and validation points used in each case. As can be seen from this table, the offset was higher for the Y coordinate than the X coordinate. Also, the sign of the error changed according to the direction of the flight, i.e. the first and the third strip were flown in the same direction N-S while the second was flown in an S-N direction. A slightly lower correlation coefficient was found for the first strip, since the characteristics of the area covered by this strip made more difficult to perform the matching. The number of control points found in the first strip was nearly half of the number of points extracted in the other two strips.

Table 1: Correlation coefficients and control points extraction (*1f, 2f, 3f: refers to the first day flight; 1s, 2s, 3s: refers to the second day flight)

| Strip * | Mean Correlation Coefficient | Control Points | Check Points | $\Delta X_{max}(m)$ | $\Delta Y_{max}(m)$ |
|---------|------------------------------|----------------|--------------|---------------------|---------------------|
| 1f-1s | 0.48 | 40 | 7 | -1 | 1.5 |
| 2f-2s | 0.55 | 82 | 12 | 1 | -1.5 |
| 3f-3s | 0.54 | 94 | 14 | -1 | 1.5 |

Table 2 shows the geometric parameters of the 2D affine transformation obtained from least squares, which were subsequently applied to the original data sets.

Table 2: Geometric parameters of the 2D affine transformation

| Strip * | a | b | c | d | e | f |
|---------|----------|------------------|---------|------------|-----------|---------|
| 1f-1s | 0.999404 | $6.603 e^{-6}$ | 0.0054 | -0.0001175 | 0.999986 | -0.0223 |
| 2f-2s | 0.999930 | $-8.749 e^{-6}$ | -0.0028 | -0.001187 | 1.0000107 | 0.0146 |
| 3f-3s | 0.998103 | $-2.1434 e^{-5}$ | 0.0003 | 0.0002042 | 0.9999997 | -0.0166 |

When applying these parameters to the check points the offsets were reduced considerably. Thus for the first strip the root mean square error (rmse) in X and Y before correcting the shifts were 0.46 m and 1.41 m respectively, whereas after applying the 2D affine transformation the rmse were 0.24 m in X and 0.33 m in Y. For the second strip similar results were obtained, with an rmse for the X coordinate of 0.56 m and 1.45 m for the Y coordinate before the correction, and after the affine transformation the rmse in X was 0.24 m and 0.27 m in Y. Finally for the third strip the results were, $rmse-X=0.55$ m and $rmse-Y=1.29$ m before correction, and after applying the transformation model the $rmse-X$ and the $rmse-Y$ were reduced to 0.23 m and 0.30 m respectively.

Figure 3 shows a subset of one of the strips before and after correcting the planimetric offset observed. It can be seen that the datasets show a systematic shift in the horizontal plane, and that this displacement is corrected after applying the 2D affine transformation.

After correcting the X,Y offset, it was verified the relative fitting of the data in the Z direction. Thus, a flat area with sparse vegetation was selected from each strip, and a DTM was generated for those areas. Subsequently, the DTMs generated for the second flight (before and after the correction) were compared to the DTMs generated for the first flight. Table 3 shows the mean and the standard deviation of the absolute differences between the DTMs generated.

Table 3: Verification of the Z adjustment before and after the planimetric correction

| Strip * | □□Z Before | | □□Z After | |
|---------|-------------|--------------------|------------|--------------------|
| | Mean | Standard deviation | Mean | Standard deviation |
| 1f-1s | 0.058 | 0.043 | 0.073 | 0.044 |
| 2f-2s | 0.056 | 0.050 | 0.066 | 0.050 |
| 3f-3s | 0.140 | 0.100 | 0.070 | 0.060 |

Similar values were obtained for the first and second strips. The highest difference was observed for the third strip, where the mean difference after the affine transformation was reduced from 14 cm to 7 cm. This could be explained because the area used in this strip presented a certain feature and, therefore the planimetric offset influenced the vertical component.

4. Conclusions

Throughout this paper it was demonstrated that application of image matching techniques to intensity images interpolated from the 3D point cloud, can be useful to determine the planimetric offset observed between two LiDAR flights carried out over a forested area, especially when feature-based techniques are difficult to implement due to the lack of linear features. Correction of this displacement it is important when performing a multitemporal study or even to increase the point density by merging the data from the two flights when they are carried out close in time. Point density has shown to be more important than other variables as the footprintsize, in determining certain forest variables as crown area and volume area (Goodwin et al., 2006)

Though in the case of a global deformation, as it was the one observed for our data, an optimal matching leads to the final transformation model without explicitly generating the control points (Liu *et al.* 2006), the two step approach used here (extraction of control points and determination of transformation parameters by least squares) would allow to detect more complex local deformations. In such a case, local transformation as for example piecewise linear models or local weighted mean model could be applied. These methods usually need a large number of evenly distributed control points since the parameters of the transformation vary across different regions over the image.

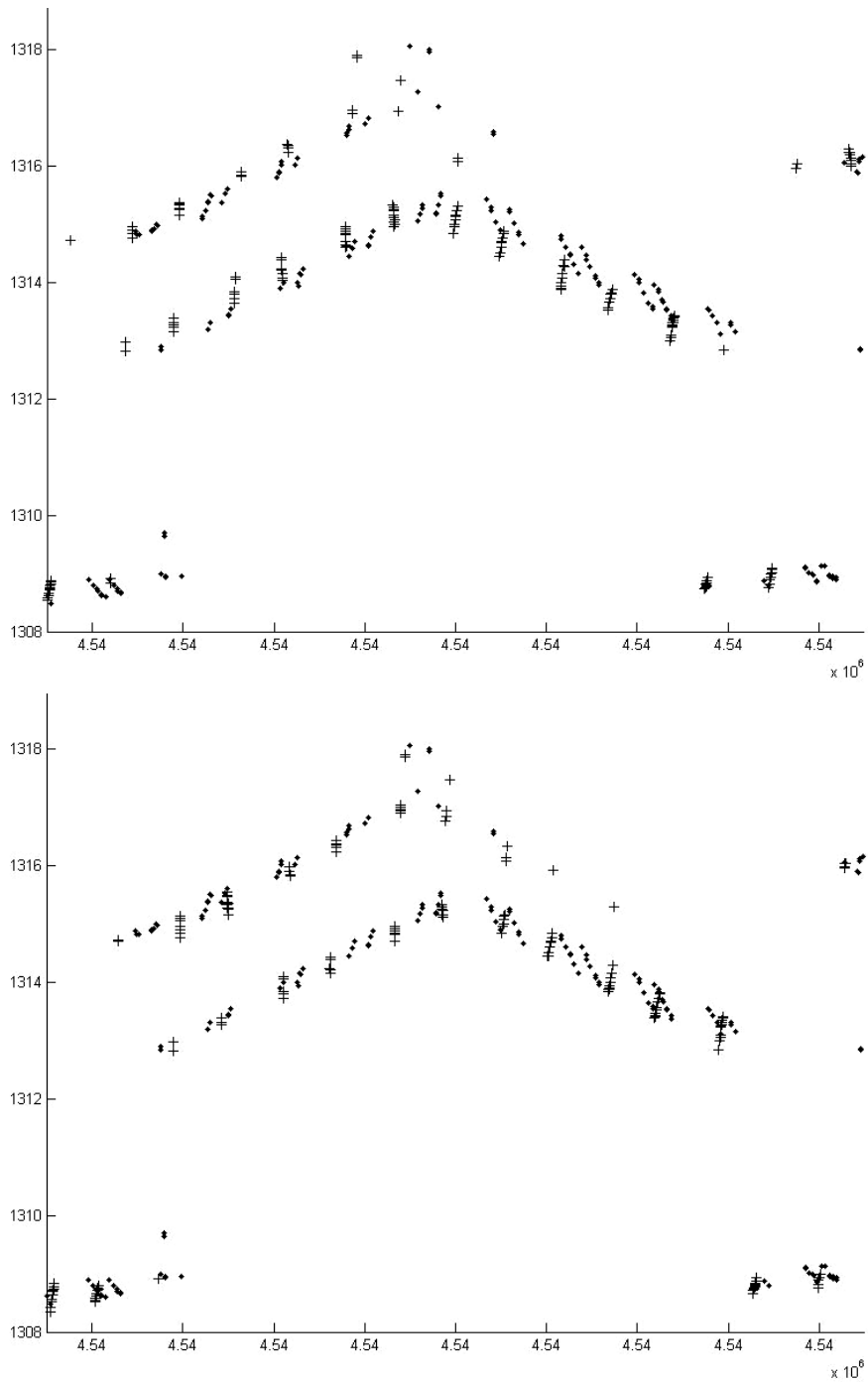


Figure3: Adjustment of the strips before (top) and after (bottom) application of the affine transformation. Dots represent data from the first flight. Crosses represent data from the second flight

Acknowledgements

The UK Natural Environment Research Council are acknowledged for the provision of the image data as part of the Airborne Remote Sensing Facility 2006 Mediterranean Campaign, grant WM06-04.

J.A. Malpica, from the Department of Mathematics of the University of Alcalá, provided valuable suggestions. Comments from the anonymous reviewers are also acknowledged.

References

- Crombaghs, M.J.E., Brügelmann, R. and de Min, E.J., 2000. On the adjustment of overlapping strips of laser altimeter height data. In: *International Archives of Photogrammetry and Remote Sensing*, vol. 33, part B3/1, pp. 224-231.
- Goodwin, N.R., Coops, N.C. and Culvenor, D.S. 2006. Assessment of forest structure with airborne LiDAR and the effects of platform altitude. *Remote Sensing of Environment*, 103, 140-152.
- Huising, E.J. and Gomes Pereira, L.M., 1998. Errors and accuracy estimates of laser data acquired by various laser scanning systems for topographic applications. *ISPRS Journal of Photogrammetry and Remote Sensing*, 53 (5), 241-261.
- Kager, H., 2004. Discrepancies between overlapping laser scanning strips – simultaneous fitting of aerial laser scanner strips. In *International Archives of Photogrammetry and Remote Sensing*, Vol. XXXV, B/1, pp. 555-560, Istanbul, Turkey.
- Lee, J., Yu, K., Kim, Y. and Habib, A.F., 2007. Adjustment of discrepancies between LiDAR data strips using linear features. *IEEE Geoscience and remote sensing letters*, 4 (3), 475-479.
- Lerma, J.L., 2002. Fotogrametría moderna: analítica y digital. Editorial U.P.V., pp. 427-477.
- Liu, D., Gong, P., Kelly, M. and Guo Q., 2006. Automatic registration of airborne images with complex local distortion. *Photogrammetric Engineering and Remote Sensing*, 72 (9), 1049-1059.
- Maas, H.-G. and Vosselman, 1999. Two algorithms for extracting buildings models from raw laser altimetry data. *ISPRS journal of Photogrammetry and Remote Sensing*, 54, 153-163
- Maas, H.-G., 2000. Least-squares matching with airborne laserscanning data in a TIN structure. In: *International Archives of Photogrammetry and Remote Sensing*, vol. 33, part B3/1, pp. 548-555.
- Maas, H.-G., 2001. On the use of reflectance data for laserscanner strip adjustment. In: *International Archives of Photogrammetry, Remote Sensing and Spatial Information Sciences*, vol. 34, part 3/w4, pp. 53-56.
- Maas, H.-G., 2002. Methods for measuring height and planimetry discrepancies in airborne laserscanner data. *Photogrammetric Engineering and Remote Sensing*, 68 (9), 933-940.
- Næsset, E., Gobakken, T., Holmgren, J., Hyyppä, H., Hyyppä, J., Maltamo, M., Nilsson, M., Olsson, H., Persson, A. and Söderman, U. (2004). Laser scanning of forest resources: The Nordic experience. *Scandinavian Journal of Forest Research*, 19, 482-499
- Pfeifer, N., Oude Elberink, S. and Filin, S., 2005. Automatic tie elements detection for laser scanner strip adjustment. In: *International Archives of Photogrammetry and Remote Sensing. Proceedings of Laserscanning*, vol. 36, part 3/w3, pp. 174-179.
- Prado, E. 2007. Mejoras en la evaluación y corrección de errores de registro en imágenes hiperespectrales AHS para estudios multitemporales. MSc Thesis. Departamento de Geografía. Universidad de Alcalá.
- Vosselman, G., 2002a. Strip offset estimation using linear features. In: *3rd international workshop on mapping geo-surficial processes using laser altimetry*, pp. 1-9.
- Vosselman, G., 2002b. On the estimation of planimetric offsets in laser altimetry data. In: *International Archives of Photogrammetry, Remote Sensing*, vol. 34, part 3A, pp. 375-380.

LiDAR mapping of canopy gaps in continuous cover forests; a comparison of canopy height model and point cloud based techniques

Rachel Gaulton & Tim J. Malthus

The School of GeoSciences, The University of Edinburgh, Drummond Street,
Edinburgh, EH8 9XP, R.Gaulton@sms.ed.ac.uk, tjm@geo.ed.ac.uk.

Abstract

In continuous cover forest systems, canopy gaps are created by management activities with an aim of encouraging natural regeneration and of increasing structural heterogeneity. Canopy gaps are difficult to map from the ground and LiDAR may provide a means to accurately assess gap distribution, allowing more effective monitoring. This paper presents a new approach to gap delineation, based on identifying gaps directly from the point cloud and avoiding the need for interpolation of returns to a canopy height model (with associated errors). Areas of canopy are identified through local maxima identification, filtering and clustering of the point cloud, and gaps are then identified and delineated in a GIS environment.

When compared to field mapped gap outlines, the algorithm has an overall accuracy of 88% for data with a high LiDAR point density and accuracy up to 77% for lower density data. The method provides an increase in producer's accuracy, of on average 8%, over a method based on the use of a canopy height model. Results indicate that LiDAR data can be used to accurately delineate gaps in managed forests, potentially allowing more accurate and spatially explicit modelling of understorey light conditions.

Keywords: spatial structure, airborne laser scanning, gap delineation, clustering, forestry.

1. Introduction

The distribution, shape and extent of gaps in forest canopies can influence a range of ecological factors including the understorey light regime and vegetation, microclimate and soil moisture (Page and Cameron 2006) as well as influencing other considerations such as the aesthetic appeal of the stand. Continuous cover forestry (CCF) is a management approach that maintains a forest cover over time, by the selective felling of single or small patches of trees, and aims to produce a more diverse forest structure (Mason and Kerr 2004). Canopy gaps within CCF forests result from both management activities and natural disturbances such as windthrow and allow the occurrence of natural regeneration in the understorey, reducing the need for re-planting. Monitoring such stands presents new challenges, as detailed and spatially explicit information is needed on a more frequent time-scale than for traditional clear-cut systems.

Airborne laser scanning provides high resolution information on vertical and horizontal aspects of forest structure and may allow the study and monitoring of fine-scale spatial structural heterogeneity of stands in the process of conversion to CCF, through the identification and delineation of canopy gaps. By examining the spatial distribution and characteristics of canopy gaps, indices of spatial structure can be developed with direct relevance to important ecological parameters, whilst the gap distribution itself is useful in predicting understorey conditions.

This paper examines the use of discrete return, small footprint LiDAR data for the delineation of canopy gaps (mainly resulting from management) in Sitka spruce (*Picea sitchensis*) plantations. A new approach, delineating gaps directly from the LiDAR point cloud, is developed and

compared to previous approaches based on the use of a canopy height model (CHM). The accuracy of delineations is assessed against independent field measurements.

2. Background

A canopy gap can be viewed as a lowering of the surrounding forest canopy below a certain height threshold. Information on the height of the canopy surface can therefore aid the identification of gaps. A number of studies have examined the potential of surface models derived from digital photogrammetric techniques for identifying canopy openings (Nuske *et al.* 2007; Betts *et al.* 2005; Nakashizuka *et al.* 1995). Small-footprint discrete return LiDAR sensors have been widely used to derive locations, heights and crown sizes of individual trees (Falkowski *et al.* 2006; Koukoulas and Blackburn 2005; Suárez *et al.* 2005). However, very little explicit consideration has been given to delineation of canopy gaps from LiDAR data.

The assumption that mapping canopy gaps using LiDAR is straightforward (Nuske *et al.* 2007) has not been tested. Koukoulas and Blackburn (2004) mapped canopy gaps from LiDAR data of deciduous woodland, with the aim of describing gap spatial structure and within-gap vegetation types. A CHM was generated from the raw data and a fixed height threshold (four metres) was used to define a gap. Morphological shrinking functions were then applied to isolate individual gaps. However, by applying a 'hard' height threshold to delineate gaps, the algorithms used do not lend themselves to applications in uneven-aged stands likely to result from CCF. A recent study by Zhang (2007) examined the use of LiDAR for delineating gaps in mangrove forests. The fixed height threshold method of Koukoulas and Blackburn (2004) was compared to a mathematical morphology based method, using opening and closing operations, in which the threshold height was determined as a ratio of whole gap height. However, neither study undertook a formal accuracy assessment of the gap delineations or any comparison to field data. In Koukoulas and Blackburn (2004) field measurements were not felt to be comparable and delineations from aerial photographs too inaccurate. Zhang (2007) compared LiDAR delineations to a slope grid generated from the canopy model but not to field data. Further work is therefore needed to assess the potential of LiDAR data for accurate gap delineation, including comparison to appropriate field data.

Acquisition parameters such as scanning angle and point density could have considerable impact on the accuracy of gap delineations. A number of studies have considered the influence of flight altitude (Morsdorf *et al.* 2008; Goodwin *et al.* 2006; Næsset 2004) and scan angle (Morsdorf *et al.* 2008; Ahokas *et al.* 2005) on the retrieval of biophysical properties, including individual tree height and crown width. Maximum scan angle (from nadir) is likely to influence the range of angles at which LiDAR pulses interact with the canopy and ground, the spacing of pulses (across track) and the distance that laser pulses travel through the forest canopy. As large scan angles can result in areas of shadow where the pulses do not penetrate adjacent tree crowns, this seems likely to have a significant influence on the delineation of canopy gaps. Point density is also likely to influence accuracy, as at low point density the canopy drip-line of trees (defined below) may be frequently missed. Although the influence of point density and scanning angle on the accuracy of gap delineations is not explicitly investigated in this paper, at lower densities or in areas of shadow, the averaging involved in interpolation of point data to CHMs is likely to compound these problems and reduce the precision of delineations. The process of producing a CHM also leads to the loss of data from different levels in the canopy, preserving just lidar returns from the surface, leading to a further reduction in the information available for gap delineation. This paper therefore develops an alternative approach, avoiding the use of a CHM and instead delineating gaps directly from the point cloud.

3. Data collection and pre-processing

3.1 Study sites

The three study sites are located in Sitka spruce (*Picea sitchensis*) plantations in the UK. Aberfoyle, Scotland is the site of a CCF trial area. Two one hectare plots were used for field measurements, one in a stand in the early stages of transformation (AbP1) and the other in a traditionally managed plantation that had been lightly thinned (AbP2). Clocaenog Forest in North Wales is also a CCF trial area, managed by the University of Wales, Bangor. One plot (CLG1) is a thinned control plot, whilst the other (CLG4) has been managed as a uniform shelterwood since 2004. The final study site is Glasfynydd Forest in South Wales. This is the site of a Forest Research thinning experiment. Plots were established in 50 year old stands and thinned (in 2002 and 2005) to 69% (plot GLT) and 60% (plot GHT) of their original basal area. The plots exhibit a range of canopy gap sizes and distributions due to their management history.

3.2 LiDAR and field data

Airborne campaigns were carried out over all three sites in summer 2006. Discrete return LiDAR data (first and last returns) for Glasfynydd and Clocaenog were collected by the NERC Airborne Research and Survey Facility at an average point density of 1.2 returns per m² with a maximum scan half-angle of 20 degrees. Data for Aberfoyle was acquired by the Environment Agency at a much higher point density (11.4 returns per m²) and a maximum scan half-angle of 10 degrees.

A gap can be viewed as a ‘hole’ in the forest canopy caused by the loss or removal of one or multiple trees, thereby excluding small gaps within tree crowns or between neighbouring trees. To allow the comparison of field and LiDAR data, a more complete definition is needed. For the purposes of this study, a gap boundary is defined by a line at ground level (the drip-line) located vertically beneath the inner most point reached by the foliage of a tree crown at any level, at that point on the gap perimeter, as suggested by Brokaw (1982). A gap must have a minimum area of 5m² and must extend down to at least ten metres from ground level (closure occurs when regeneration reaches an average height of ten metres).

A detailed ground survey of all plots was carried out in September 2005 for Aberfoyle and summer 2006 for the Welsh sites. Full data sets including tree positions and dimensions were available for Clocaenog and Glasfynydd and these were up-dated by re-measuring a subset of trees. A 50m by 50m subplot was established in each plot and the boundaries of all canopy gaps (fitting the study definition) were surveyed. As it was not possible to survey every point along the canopy drip-line of gap boundaries, the resulting field-mapped boundaries were to some degree generalised. A Total Station survey, from a GPS baseline, was used to record points located directly below the drip-line wherever significant changes in the orientation of the gap boundary occurred. Several points were recorded per tree crown. Gap boundaries were mapped for all plots except CLG1.

3.3 LiDAR pre-processing

Pre-processing of LiDAR data was carried out using FUSION (McGaughey 2007). A digital terrain model was generated from the last return data by filtering to leave bare earth points, using an iterative process adapted from Kraus and Pfeifer (1998). A gridded DTM was generated from these points with a cell size of 2m. The accuracy of the DTM was assessed against height measurements obtained during the GPS and total station survey, resulting in an average RMSE of 1.1m. This error falls within the vertical accuracy levels of the GPS positions so the absolute accuracy of the DTM could not be assessed further. To determine the degree to which the DTM represented variation in the ground surface (a factor perhaps more important to this study than absolute height), the relationships between total station surveyed points and the

heights extracted for the same locations from the DTMs were examined, giving a strong linear relationship (R^2 of 0.93-0.99, $P < 0.001$) and suggesting that the DTM accurately represented variation in the ground surface within the plots. The corresponding value of the DTM was then subtracted from the first return point data to convert from elevation to height above ground.

A canopy height model (cell size of one metre for the Welsh sites and 0.5 metres for Aberfoyle) was generated from the first returns, also within FUSION. The highest first return (from the point cloud, converted to height above ground) was assigned to each grid cell, with missing values interpolated by averaging of neighbouring values. The use of a TIN to generate the CHM was also investigated but produced poorer results in this study. Heights derived from the final CHM were compared against field measured tree heights (from 2007) for plot CLG1, resulting in a correlation co-efficient of 0.95 ($P < 0.001$) and a mean error of -1.55m.

4. Methodology

Two methods were used to delineate gaps from the first return LiDAR data. In the first, a relative height threshold of 66% of local tree height was applied to the CHM. This threshold was found to correspond to the canopy drip-line through manual measurements of the point clouds of 45 individual trees located in open areas or on gap edges. A surface representing the top of the canopy was first generated by applying a moving window (with a radius of 5.5 metres) and taking the maximum value in the window to represent the maximum local tree height for the centre pixel. This filter size was selected as large enough not to cause the resulting canopy top raster to fall into small gaps between trees whilst preserving the spatial variation in tree heights within the stand. Pixels in the original CHM were then classified as gaps if they had heights lower than 66% of the local height of the canopy top raster. All pixels in the CHM with a height of less than 10 m were also included in the gap class to account for those in the centre of large gaps.

The alternative method delineates gaps directly from the LiDAR point cloud without interpolation to a CHM. As many gaps contain large areas of shadow with few LiDAR returns, the algorithm focuses on the identification and delineation of areas of canopy, with gaps being found subsequently by default. The algorithm is composed of a number of stages including the identification of local maxima (as points higher than their neighbours), filtering to remove returns from below the canopy drip-line (less than 66% of local tree height), clustering of lower canopy returns into separate clusters around each identified maxima (limited by a radius corresponding to the maximum tree crown size) and merger and delineation of clustered points to retrieve gap delineations. The initial stages (identifying local maxima and clustering of returns) are similar to the approach taken by Tiede *et al.* (2005) to assign point data to individual tree crowns, but the clustering method differs by first filtering the point cloud to leave only returns from above the canopy drip-line. Figure 1 shows the full point-based processing scheme.

Following filtering and clustering, the locations and cluster memberships of the points are processed in a GIS environment to produce vector gap outlines. Any points that have not been assigned to a cluster are removed at this stage. First, a buffer (of fixed radius) is applied to the points, and those points with the corresponding cluster memberships (associated with the same maxima) are merged into a single polygon. Any 'holes' fully enclosed within a cluster polygon are removed leaving polygons representing tree crowns. The areas of test plots representing gaps (i.e. all areas not included in the canopy polygons) are then retrieved. The gap polygons are then dilated to reconstruct full gap extent. The point density of the data determines the optimum distances for buffers to merge points, with the radius of buffers approximately equal to the distance between adjacent scan lines in the along-track direction (the direction in which the largest point spacing was present). A small buffer remains surrounding the clustered canopy

points (i.e. the gaps are not dilated by the full buffer distance), as such points are unlikely to be located precisely on the canopy edge. All specified parameters for each plot are presented in Table 1 and vary according to the LiDAR point density. The clustering radius (R) can be estimated as approximately double the average along-track spacing of LiDAR returns. The search radius, S, used for maxima location can be estimated from field data (or in the absence of such data, from optical or lidar intensity images) so as to be slightly larger than the average crown diameter.

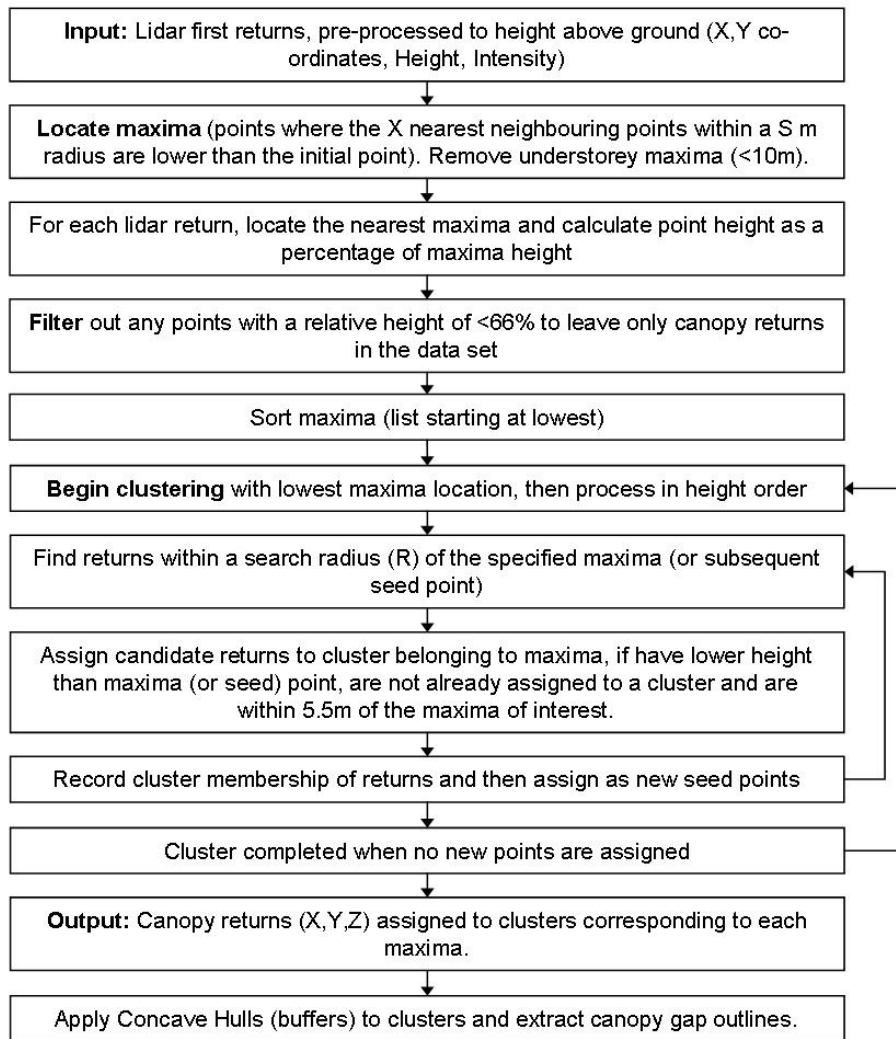


Figure 1: Point-based processing scheme for delineation of gaps from LiDAR data.

Table 1: Final parameters selected for point-based processing of each plot.

| Plot | Number of neighbours (X) | Search radius (S) | Cluster radius (R) | Buffer distance | Distance gaps dilated |
|------|--------------------------|-------------------|--------------------|-----------------|-----------------------|
| AbP1 | 100 | 3 m | 1 m | 0.5 m | 0.25 m |
| AbP2 | 100 | 3 m | 1 m | 0.5 m | 0.25 m |
| GLT | 20 | 3 m | 2 m | 1 m | 0.5 m |
| GHT | 20 | 3 m | 2 m | 1 m | 0.5 m |
| CLG1 | 20 | 3 m | 2 m | 1 m | 0.5 m |
| CLG4 | 20 | 3 m | 3 m | 1.5 m | 1 m |

Before assessing accuracy against field data, any gaps identified as having an area of less than 5 m² were removed. In the case of the CHM-based method of gap delineation, accuracy was assessed by a pixel based comparison (confusion matrix) of the classified raster with a raster of the field mapped gap distributions for sub-plots of AberP1, CLG4, GHT and GLT. AberP2 was excluded from the assessment due to difficulties in accurately co-registering the field and LiDAR data. For the point based method, a confusion matrix was calculated directly from the vector delineations. The total area of canopy gap identified in each sub-plot using both methods was also compared with the overall area delineated in the field. A separate assessment of the accuracy of the maxima identification stage for the point-based method was also carried out for plots where tree positions were available (either field mapped or obtained visually from the CHM). A maxima was considered to correspond to a field mapped tree if it lay within a 2m radius of the field position (the average crown radius for the stands).

5. Results

Table 2 shows the correspondence between identified maxima (from the point-based method) and field mapped tree positions. Good levels of accuracy were achieved for all plots, with the majority of trees identified. Some commission errors occurred, but this is unlikely to have a significant effect on the performance of the algorithm as a whole.

Table 2: Accuracy of maxima identified from LiDAR first return point data compared to field measured tree positions (except for AbP1, where ‘field’ positions were manually identified from the CHM).

| Plot | Producer’s accuracy (%) | User’s accuracy (%) |
|------|-------------------------|---------------------|
| CLG1 | 85.7 | 75.2 |
| CLG4 | 88.0 | 79.0 |
| GLT | 73.2 | 68.0 |
| GHT | 86.2 | 69.7 |
| AbP1 | 94.8 | 83.8 |
| Mean | 85.6 | 75.1 |

Figure 2 shows an example of the results of the clustering stage of the algorithm for two plots, one with a high point density (AbP1) and the other with much lower point density (CLG4). In general the points form compact clusters around field mapped tree positions, although there are some instances in which clusters also include parts of neighbouring crowns.

The final gap delineations using this method for the same two plots are shown in Figure 3. The majority of gap areas are correctly identified in both cases but greater errors can be seen for the plot with lower density LiDAR data. This was confirmed by the results of the formal accuracy assessment, as presented in Table 3. The corresponding results for the CHM-based method are also included. Overall accuracy was slightly higher for all plots using the point-based method (an increase of 3.7% on average), whilst the producer’s accuracy of the gap class was considerably improved in most cases (average increase of 8.3%). Table 4 compares the total derived gap area in each sub-plot to that mapped in the field. It can be seen that both the CHM and point-based methods generally under-estimate gap area. The point-based approach usually retrieves a greater gap area than the CHM-based method and the results are also more consistent between plots.

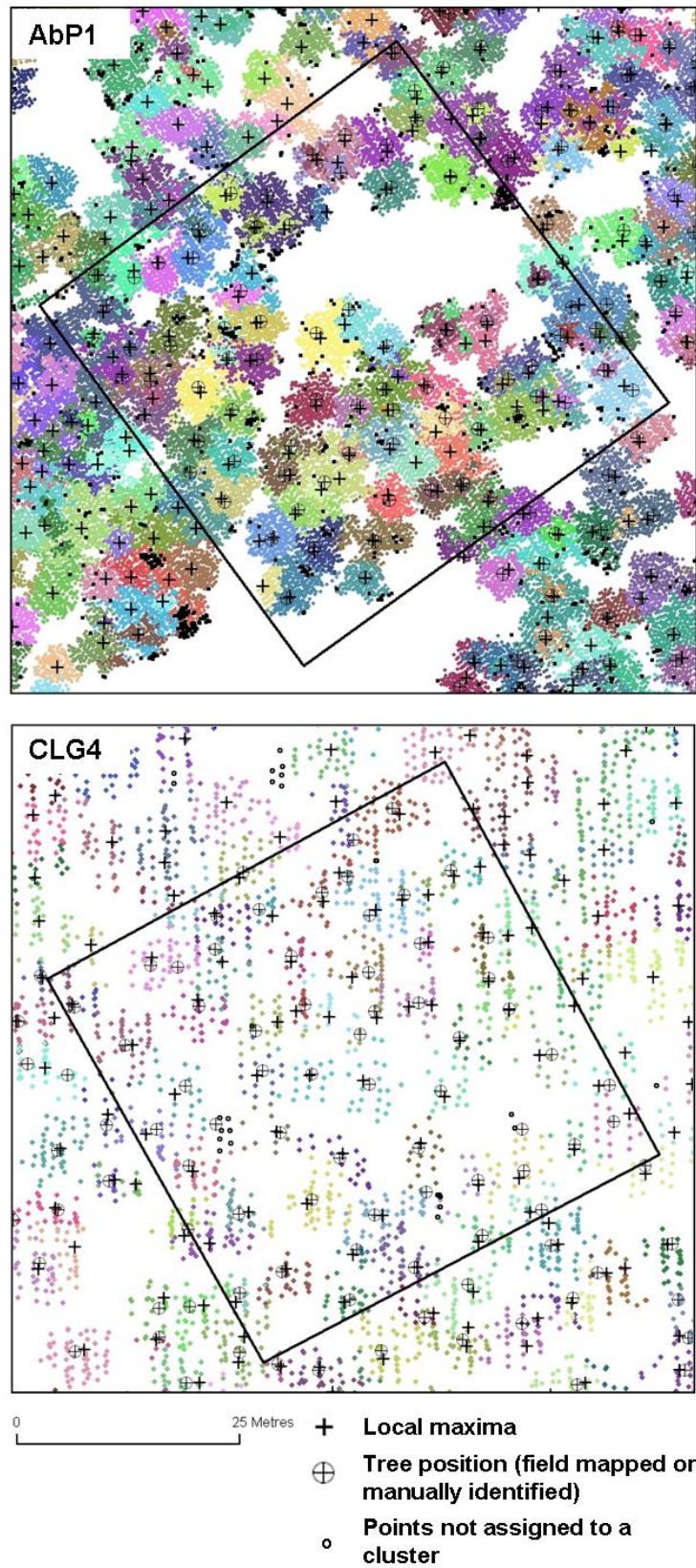


Figure 2: Examples of the results of the clustering stage of the point-based algorithm for plots CLG4 and AbP1. Locations of local maxima used as seeds and the locations of trees (field mapped for CLG4, visually identified for AbP1) are also shown. Colours are randomly assigned to clusters.

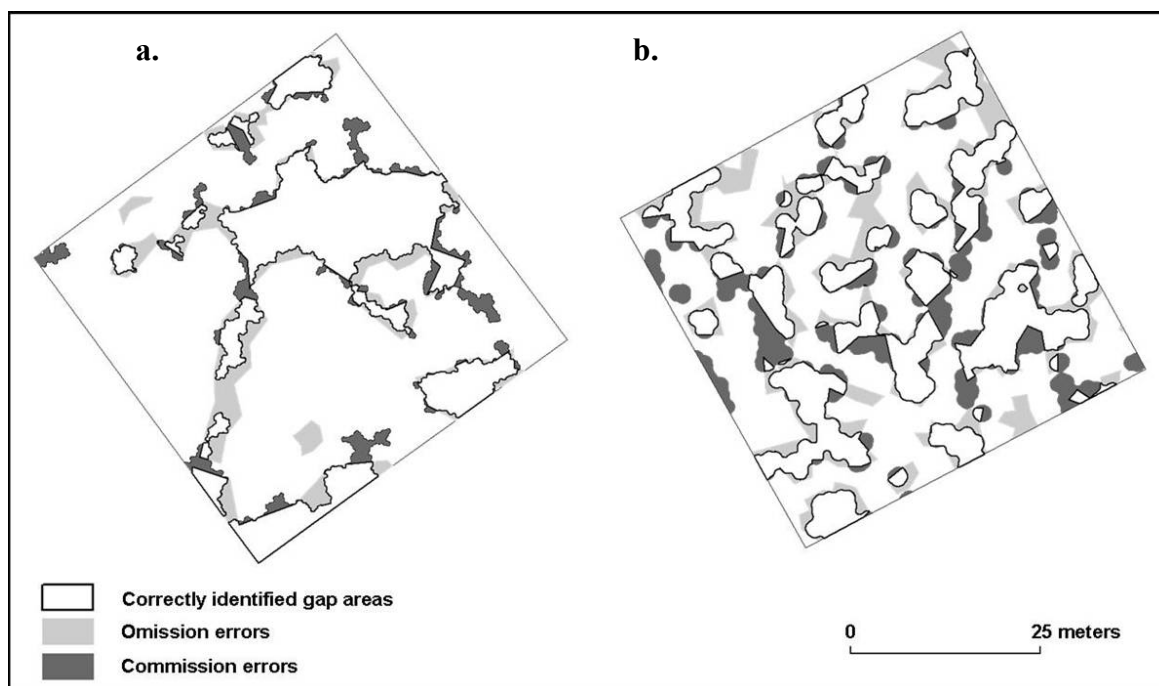


Figure 3: Results of the point-based gap delineation algorithm for plots AbP1 (a.) and CLG4 (b.).

Table 3: Confusion matrix results for a comparison of field mapped canopy gaps to point and CHM –based LiDAR delineations. The producer’s and user’s accuracies are those of the ‘gap’ class.

| Plot | Method | Overall accuracy (%) | Producer’s accuracy (%) | User’s accuracy (%) | Kappa co-efficient |
|------|-------------|----------------------|-------------------------|---------------------|--------------------|
| AbP1 | Point-based | 87.8 | 74.9 | 82.7 | 0.70 |
| | CHM-based | 85.2 | 79.7 | 73.1 | 0.66 |
| CLG4 | Point-based | 77.2 | 69.3 | 72.5 | 0.52 |
| | CHM-based | 70.7 | 62.6 | 62.8 | 0.39 |
| GHT | Point-based | 72.8 | 61.4 | 70.9 | 0.43 |
| | CHM-based | 71.6 | 47.6 | 76.8 | 0.39 |
| GLT | Point-based | 74.8 | 46.7 | 81.0 | 0.43 |
| | CHM-based | 70.6 | 29.3 | 89.2 | 0.31 |
| Mean | Point-based | 78.2 | 63.1 | 76.8 | 0.52 |
| | CHM-based | 74.5 | 54.8 | 75.5 | 0.44 |

Table 4: Comparison of the total gap area identified within sub-plots by field mapping and LiDAR delineation using the point and CHM –based methods.

| Plot | Method | Field mapped gap area (m ²) | LiDAR derived gap area (m ²) | Error (%) |
|-------------|-------------|---|--|-----------|
| AbP1 | Point-based | 750 | 679 | -9.5 |
| | CHM-based | | 817 | 9.0 |
| CLG4 | Point-based | 1016 | 972 | -4.3 |
| | CHM-based | | 997 | -1.9 |
| GHT | Point-based | 1080 | 935 | -13.5 |
| | CHM-based | | 671 | -37.9 |
| GLT | Point-based | 957 | 552 | -42.3 |
| | CHM-based | | 316 | -66.9 |
| RMSE | Point-based | | | 22.8 |
| | CHM-based | | | 38.7 |

6. Discussion and Conclusions

Both methods provide accurate gap delineations when applied to LiDAR data collected with a high point density. However, when lower point density data is used, the method based on an interpolated CHM can result in significant errors, probably due to the low number of returns located in canopy gaps and resulting interpolation errors. In these circumstances, the accuracy of gap retrieval can be improved by the use of methods based on the LiDAR point cloud, although the point-based method does require the careful selection of appropriate parameters for each data set. These can be estimated from basic field data (or the examination of optical imagery) and from the along-track point spacing of the LiDAR data, as described in the methodology.

It is not possible to compare the accuracy of the developed algorithm to those used in other studies of LiDAR gap delineation (Zhang 2007; Koukoulas and Blackburn 2004) as these studies did not attempt to assess the accuracy of resulting delineations. However, the results compare reasonably with those of Nuske *et al.* (2007) who used colour, texture and height information from aerial photographs to delineate gaps in Beech stands with a recall of 57-79% and a precision of 68-77% when compared to manual delineations. Whilst field and LiDAR delineations were felt to be generally comparable in this study, allowing the assessment of accuracy, the approach did have limitations. Errors in the GPS baselines used for the field survey led to error in registration of the field and LiDAR data for some plots. As only a limited number of points on the gap boundaries could be surveyed, the field boundaries are unavoidably generalised and some smaller gaps may have been missed altogether. These factors could account for a significant proportion of the remaining error in the delineations, suggesting 'true' accuracy may be higher than that reported.

LiDAR data can allow the accurate delineation of canopy gaps in stands in the process of transformation to CCF systems, although the influence of scan angle on results is yet to be determined. The resulting gap distributions may be used to develop indices of spatial structure that allow the monitoring of such stands but further work is needed to assess the usefulness of such indices and to integrate the spatially explicit gap information into models of understorey light levels.

Acknowledgements

This work was funded by a NERC CASE studentship with the Forestry Commission (NER/S/A/2004/12732). We would like to thank the NERC ARSF and the Forestry Commission for supplying LiDAR data and the NERC FSF and GEF for providing ground instrumentation. We are very grateful to Sophie Hale (Forest Research) and the Tyfiant Coed Project at the University of Wales, Bangor for access to field data and to all those who assisted during the fieldwork, especially V. Barron and P. Wieland. Particular thanks are due to J.C. Suárez and I.H. Woodhouse for advice and support.

References

- Ahokas, E., Yu, X., Oksanen, J., Hyypä, J., Kaartinen, H. and Hyypä, H., 2005. Optimization of the scanning angle for countrywide laser scanning. In *Proceedings of the International Archives of Photogrammetry, Remote Sensing and Spatial Information Sciences*, G. Vosselman and C. Brenner (Eds). XXXVI, Part 3/W19, 115-119.
- Betts, H.D., Brown, L.J. and Stewart, G.H., 2005. Forest canopy gap detection and characterisation by the use of high resolution Digital Elevation Models. *New Zealand Journal of Ecology*, 29, 95-103.
- Brokaw, N.V.L., 1982. The definition of a treefall gap and its effect on measures of forest

- dynamics. *Biotropica*, 14, 158-160.
- Falkowski, M.J., Smith, A.M.S., Hudak, A.T., Gessler, P.E., Vierling, L.A. and Crookston, N.L., 2006. Automated estimation of individual conifer tree height and crown diameter via two-dimensional spatial wavelet analysis of lidar data. *Canadian Journal of Remote Sensing*, 32, 153-161.
- Goodwin, N.R., Coops, N.C. and Culvenor, D.S., 2006. Assessment of forest structure with airborne LiDAR and the effects of platform altitude. *Remote Sensing of Environment*, 103, 140-152.
- Koukoulas, S. and Blackburn, G.A., 2004. Quantifying the spatial properties of forest canopy gaps using LiDAR imagery and GIS. *International Journal of Remote Sensing*, 25, 3049-3071.
- Koukoulas, S. and Blackburn, G.A., 2005. Mapping individual tree location, height and species in broadleaved deciduous forest using airborne LiDAR and multi-spectral remotely sensed data. *International Journal of Remote Sensing*, 26, 431-455.
- Kraus, K. and Pfeifer, N. 1998. Determination of terrain models in wooded areas with airborne laser scanning data. *ISPRS Journal of Photogrammetry and Remote Sensing*, 53, 193-203.
- Mason, B. and Kerr, G., 2004. Transforming even-aged conifer stands to continuous cover management. *Forestry Commission Information Note 40*. Forestry Commission, Edinburgh.
- McGaughey, R., 2007. *FUSION / LDV: Software for LiDAR Data Analysis and Visualisation*. USDA Forest Service, Pacific Northwest Research Station.
- Morsdorf, F., Frey, O., Meier, E., Itten, K. and Allgöwer, B., 2008. Assessment of the influence of flying height and scan angle on biophysical vegetation products derived from airborne laser scanning. *International Journal of Remote Sensing*, 29, 1387-1406.
- Næsset, E., 2004. Effects of different flying altitudes on biophysical stand properties estimated from canopy height and density measured with a small-footprint airborne scanning laser. *Remote Sensing of Environment*, 91, 243-255.
- Nakashizuka, T., Katsuki, T. and Tanaka, H., 1995. Forest canopy structure analyzed using aerial photographs. *Ecological Research*, 10, 13-18.
- Nuske, R., Ronneberger, O., Burkhardt, H. and Saborowski, J., 2007. Self-learning canopy gap mapping for aerial images using photogrammetric height, colour, and texture information. In: *Proceedings of ForestSat 2007*. Montpellier, France.
- Page, L.M. and Cameron, A.D., 2006. Regeneration dynamics of Sitka spruce in artificially created forest gaps. *Forest Ecology and Management*, 221, 260-266.
- Suárez, J., Ontiveros, C., Smith, S. and Snape, S., 2005. Use of airborne LiDAR and aerial photography in the estimation of individual tree heights in forestry. *Computers and Geosciences*, 31, 253-262.
- Tiede, D., Hochleitner, G. and Blaschke, T., 2005. A full GIS-based workflow for tree identification and tree crown delineation using laser scanning. In: U. Stilla, F. Rottensteiner and S. Hinz (Eds.). *The Proceedings of the ISPRS Workshop CMRT 2005*. Vienna, Austria: 9-14.
- Zhang, K., 2007. Identification of gaps in mangrove forests with airborne LIDAR. *Remote Sensing of Environment*, doi:10.1016/j.rse.2007.10.003.

Integration of intensity information and echo distribution in the filtering process of LIDAR data in vegetated areas

J. Goepfert, U. Soergel, A. Brzank

Institute of Photogrammetry and GeoInformation, Leibniz Universität Hannover,
Germany

goepfert@ipi.uni-hannover.de, soergel@ipi.uni-hannover.de, brzank@ipi.uni-hannover.de

Abstract

Accurate digital terrain models (DTM) are crucial for many applications in coastal management, such as simulation of flood risk scenarios. Airborne LIDAR sensors generate dense height information of large areas for the derivation of suitable DTM in an efficient manner. However, the accuracy and reliability of the LIDAR DTM points suffer if the laser beam interacts with vegetation. Several filter algorithms were developed, which usually apply geometric criteria to eliminate the vegetation points. However, in areas of very dense vegetation and rough terrain, where only few laser pulses are able to penetrate the canopy, such processing often fails resulting in an upward height shift of the derived DTM. In this paper additional features are proposed, which correspond to the reflectance characteristics of the backscattering objects, to support the filtering process. The introduced new algorithm uses intensity information and the distribution of multiple echoes for adaptive weight update in an iterative surface fitting procedure. The benefit of the integration of these new features in the filtering method is shown for several areas covered by different types of coastal shrubberies.

Key words: LIDAR, vegetation, intensity, multiple echoes, filtering

1. Introduction

1.1 Motivation

In the last few years airborne LIDAR arises to one of the most important techniques for the derivation of area-wide digital terrain models. The advantages of this contact free measurement method are especially noticeable in the coastal region of the German North Sea, where access for terrestrial surveying is limited due to dense vegetation on the islands and frequently flooded terrain in the Wadden Sea. The LIDAR DTM quality depends basically on the sensor and flight parameters (e.g., scanner device and flying altitude), the applied post-processing methods (e.g., strip adjustment and georeferencing), and the scene topography. In case of moderate surface roughness in non-vegetated areas LIDAR DTM usually provide a standard deviation in height of less than 15cm. However, if the laser beam interacts with vegetation, the accuracy and reliability of the LIDAR DTM points suffer depending on the type of plants and season. Especially, the plant height and density influence the penetration rate of the laser pulses. Low vegetation often can not be separated from the ground beneath, resulting in reflection composed of mixed signals, whose center of gravity is located above the terrain surface. Consequently, the measured time of flight and the resulting distance to the sensor are too short, leading to a bias (**height shift**). Tall vegetation may cause multiple echoes at various height levels, which can be resolved if the provided range resolution of the scanner system is high enough. Many filtering techniques developed for DTM generation rely on the assumption that the last echo represents the ground. However, even these echoes are frequently caused entirely by backscatter from low vegetation layers resulting again in a shorter distance measurement. Several filter algorithms were developed, which use geometric criteria to eliminate the vegetation points from the data set (see section 1.2 for more details). The most important requirement of these filters is the existence of a suitable number of ground points. However, the study area located at the coast of the German part of the North Sea is covered by various dense

vegetation types, which prevent the penetration of the laser pulses in large areas. Another problem arises from the aspect that the vegetation often occurs in small valleys. Therefore, vegetation points are sometimes lower than the surrounding ground on the ridges. These facts lead to unsatisfactory results of common filter algorithms. In this paper a new method is introduced, which integrates the reflectance characteristics of the backscattering objects, in order to support the filtering process.

1.2 State of Research

Various filter algorithms for eliminating non-ground points in LIDAR data sets were developed considering different landscape types. Sithole (2005) provides a comprehensive overview about the existing methods, their classification depending on diverse criteria, a description of the ISPRS filter test (see also Sithole and Vosselman (2004)), and an approach of a new filter technique. Sithole distinguished the filter algorithms regarding data structure, neighbourhood, measure of discontinuity, single step vs. iterative, basic filter concepts, and external information. Four main groups were defined according to the following basic filter concepts:

- Slope based (e.g., Vosselmann, 2000)
- Block minimum (e.g., Wack and Wimmer, 2002)
- Surface based (e.g., Kraus and Pfeifer, 1998)
- Clustering/Segmentation (e.g., Brovelli, 2002)

The use of multiple echoes and reflectance information was another criterion. However, among all contributors of the ISPRS test only the algorithm of Brovelli (2002) considered the difference between the first and last echoes in the labelling process. The stored intensity values given for every LIDAR point were not yet integrated in any of the analysed filtering methods. However, several approaches for classification of objects from the LIDAR point clouds exploited this feature. For example, Moffiet et al. (2005) investigated the capabilities of the different returns (ground and vegetation, first, last, and single pulse) as well as the related intensity to classify diverse tree types. Tóvári and Vögtle (2004) used the intensity values among other features, in order to discriminate buildings, vegetation, and terrain.

A sound physical model of the complex interaction between the laser beam and distributed scatterers located inside the beam cone is a prerequisite for interpretation and analysis of full-waveform LIDAR data provided by some advanced sensor devices. Based on the radar equation Jelalian (1992) described the fundamental relations between the emitter, the reflecting object and the receiver applied to the lidar technique. Sensor and target dependent parameters are separated and an object dependent cross section is defined. Additionally, Wagner et al. (2006) pointed out the dependencies between the spatial variations of the cross section and the amplitude as well as the width of the reflected echoes. In the next step these theoretical considerations should result in practical applications of the intensity and echo width in classification and filtering algorithms.

The approach described in this paper is mainly based on robust filtering proposed by Kraus and Pfeifer (1998). This iterative algorithm uses linear prediction as interpolation method for the initial surface modelling. The residuals of the LIDAR points with respect to the surface of the previous iteration determine the weights for the next adjustment iteration using a special transfer function (Equation 1). Low weights are assigned to points lying above the fitted surface (probably vegetation), while points located beneath the surface (probably ground) are given a high weight. The algorithm stops, if the changes of the unknowns are below a predefined threshold or the maximum number of iterations is reached. Finally, a threshold with regard to the residuals is defined, in order to classify the LIDAR points.

$$p(r_i) = \begin{cases} 1 & \text{for } g < r_i \\ \frac{1}{1+(a \cdot (g-r_i)^b)} & \text{for } g \geq r_i \end{cases} \quad (1)$$

where $p(r_i)$ = weight of point i r_i = residual of point i
 a, b = definition of steepness g = shift in the direction of r_i

2. The new filtering algorithm

2.1 Initial Considerations

This part of our research project was focused on the analysis of the influence of different coastal vegetation types on the accuracy and reliability of airborne LIDAR data. Initially, the height shift caused by the vegetation was investigated based on several control areas. Additionally, the relationship between different object as well as data driven features (vegetation height and density or standard deviation in height) and the accuracy of the LIDAR data in vegetated areas was analysed (Göpfert and Heipke, 2006). Subsequently, the most meaningful features (e.g., intensity values) were used, in order to perform a supervised classification of the LIDAR data into predefined accuracy intervals. However, the features have the drawback that the accuracy intervals do not correspond to distinct and easily separable clusters in feature space, which is required for classification methods that partition the feature space into crisp regions assigned to the different classes. Considering a single vegetation type the height shift exhibits a rather continuous characteristic. Thus, in a new approach (Goepfert and Soergel, 2007) this issue was tackled by modelling the height shift with respect to the features using continuous functions. This function fitting process is realised in areas, where control measurements are available. Subsequently, the adjusted functions of the different features were used to estimate the height shift for LIDAR points within other regions of similar vegetation. Figure 1 visualises two examples of the modelled dependencies between the intensity values and the height shift for training areas of different size in the leaf-off period.

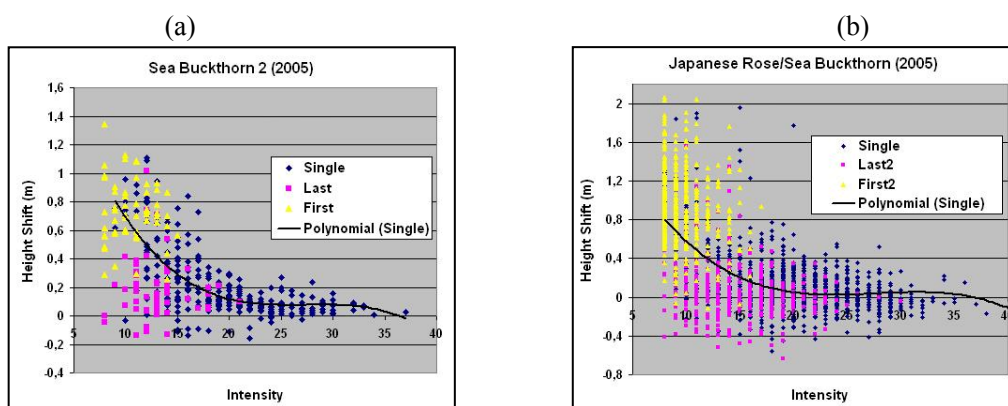


Figure 1: Dependency between intensity values and height shifts for multiple and single echoes of two areas with different size in leaf-off period: a) 297 single echoes, b) 1183 single echoes (Riegl-Scanner LMS-Q560)

However, the second method still has several drawbacks. On the one side multiple extensive control measurements are required as training areas in order to fit robust functions and guarantee the transferability to other regions. On the other side the larger (and thus more inhomogeneous) the training areas, the larger are the residuals of function fitting (see Figure 1). Due to the rise in the inhomogeneity of the vegetation height and density distribution, the significance of the intensity values suffers. Figure 2 illustrates this relationship: if the vegetation heights differ significantly in the area of interest, similar cross sections (and thus intensity values) can result for echoes in various heights above the ground. Therefore, the applicability of the intensity values depends on the size of the considered neighbourhood. Thus, the training areas of the second approach have to be small enough with respect to the homogeneity of the vegetation and large enough regarding robust function fitting. Furthermore, the fact that higher vegetation often occurs in valleys and therefore similar cross sections, which are related to different height shifts, are located in the same absolute

height makes the situation even more complicated in larger training areas of considerable ground and vegetation variations (Figure 2).

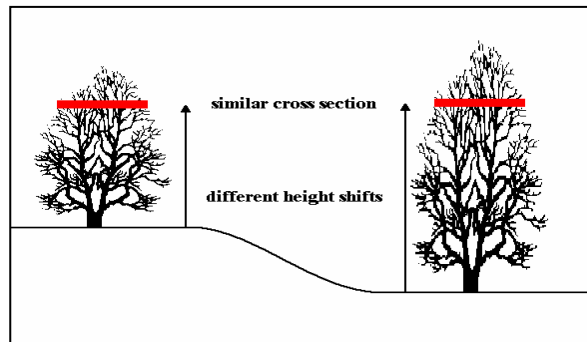


Figure 2: The correlation between the intensity values (corresponding to the reflecting cross section) and height shifts strongly depends on the homogeneity of the vegetation height and density distribution in the area of interest.

Additionally, other **statements** about the intensity distribution can be made by analysing Figure 1, which are important in designing a new filtering algorithm:

1. The higher the single echo is located in the vegetation, the smaller is its intensity value.
2. Single echoes exist with intensity values as well as height shifts similar to first reflections.
3. Due to a loss of energy caused by preceding reflections, which are above the detection threshold, the mean intensity of true last echoes is smaller than the same value of single undisturbed ground echoes.
4. The intensity of last echoes varies strongly depending on the object cross sections and the amount of pulse energy of the previous echoes. Because these influencing variables are difficult to separate, the intensity values of last echoes are less useful.

Besides the results of the data analysis theoretical considerations support the use of intensity in the filtering process. The intensity values given with the data might be derived from the measurements in different manners by the providers. However, in any case they represent a function of the signal amplitude, which depends on the spatial variation of the cross section (see Wagner et al., 2006). Reflectivity, directionality of the scattering, and the effective area of the reflecting surface of an object are combined in the concept of the cross section. This cross section is defined to model properties of individual point targets. In order to address distributed targets, a so-called differential cross section is more appropriate. Therefore, the amplitude of the echoes as well as the intensity values of the LIDAR points are related to the characteristics of parts of a complex object, such as plant structure, and consequently to the vegetation density. In the basic case of normal incidence with uniform intensity, flat bare ground yields a homogeneous cross section (coinciding with the circular footprint) as well as a narrow pulse width and high amplitude, whereas for a signal consisting of terrain and low vegetation contributions the pulse width is expanded and the amplitude is attenuated. Considering coastal shrubberies in the leaf-off period, the higher the echo in the vegetation, the thinner are the branches, which contribute to the cross section. Therefore, the amplitude as well as the intensity values also decrease theoretically for elevated LIDAR points.

2.2 The New Approach

While in the previous methods the intensity directly participates in the calculation of the height shift as one of the features, in the new algorithm it is used for the determination of the weights during an iterative robust surface fitting^{§§}. Several considerations support this indirect integration of the intensity in the process. For instance, if the estimation of the height shift is dominated by the feature intensity in the second approach, the resulting surface can strongly diverge from the related LIDAR heights. In order to avoid this effect, the LIDAR heights are the only direct feature (observations) in

^{§§} The basic concept of robust filtering can be found in Kraus and Pfeifer (1998).

$$p_i = p(r_i) \cdot p(I_i) \quad (3)$$

where p_i = total weight of point i
 $p(r_i)$ = weight component of point i based on the residual
 $p(I_i)$ = weight component of point i based on the intensity or echo distribution

In order to calculate the overall weights of the LIDAR echoes, the values defined directly by the residuals and the weights resulting from the analysis of the intensity and echo distribution are multiplied (Equation 3). The weights are updated according to the mentioned rules and the process stops after a predefined maximum number of iterations. Finally, the residual of the central LIDAR point is stored and the mask continues to the next last or single echo in the file. After processing all LIDAR points in the file the filtering is performed by comparing the residuals with a defined threshold.

Due to the dependence of the intensity values on features of the laser scanning devices, such as temporal pulse stability and the applied intensity measurement method, their applicability is checked for every iteration and window position according to the statement 1 in chapter 2.1. If the single echoes below the fitted surface have smaller intensity values than the points above, this constraint of the model is met and the intensity is used in the filtering process. Otherwise, only the first part of the weight, which is directly derived from the residuals, is used. The information “Intensity used” in the experiments (see below) refers to this test.

3. Results

The experiments are based on three flight missions and several training areas, which were surveyed by using tachymetry and GPS techniques. The data for the first mission were collected in March 2004 during a measurement campaign of the company TopScan with an ALTM 2050 scanner from Optech covering the East Frisian island Juist. The flying altitude was 1000m and the system provided an average point density of 2 points/m². Most of the investigations were carried out using data collected by the company Milan-Flug GmbH covering the region of the East Frisian Island “Langeoog” in leaf-off periods (April 2005 and 2006). During these campaigns a LMS-Q560 sensor (Riegl company) was used. From 600 m altitude the system provided an average point density of 2.9 points/m². The training areas consist of several populations of coastal shrubberies, such as Japanese rose, common sea buckthorn, and creeping willow. A detailed description of the reference data can be found in Göpfert and Heipke (2006).

The experiments in this section focus on the verification of the benefit, which is obtained by integrating intensity and multiple echo information in the filtering process. Two initial tests quantify the influence of the neighbourhood size (Table 1) and the number of iterations (Table 2) on the surface modelling accuracy with respect to the control measurements based on the training area “Willow 2” in strip 1 of the flight mission “Langeoog 2005”. Additionally, they determine suitable values of these two parameters for the subsequent investigations. The parameters a and b of the function for robust filtering (Equation 1) are set to 1.5 and 2, while 0 is assigned to g for all the following tests.

In the first experiment the surface fitting is performed in 3 iterations (according to the findings in Table 2) using a plane concerning neighbourhoods of different area (Table 1). If the size of the moving window is enlarged, the mean value and the standard deviation of the differences between the true (control measurements) and the fitted surface increase. With larger windows the adjusted plane is not able to model the variations of the real surface with adequate accuracy. The radius is limited to 2.5m in the further analysis as a suitable compromise based on the following considerations. On one side the relatively large value is chosen, in order to preserve a minimum number of points for surface fitting as well as for the discrimination of vegetation and ground echoes

based on the residuals. This successful distinction is required for robust filtering as well as for the determination of the intensity transfer function. With respect to this separability of the echoes a suitable radius depends on the penetration rate of the laser beam in the current vegetation. Enough points, which conform to statement 1 in section 2.1 (test for the use of intensity), should exist in the mask for the applicability of intensity in the algorithm. The higher percentage of the “used intensity” in larger neighbourhoods (last column of Table 1) supports these considerations. On the other side a larger radius decreases the accuracy of the fitted surface and the quality of the intensity transfer function in areas with inhomogeneous vegetation (see also Figure 1 and 2).

Table 1: Influence of the size of the defined neighbourhood on the mean and standard deviation of the differences between the true (control measurements) and the fitted surface, number of considered points, and the percentage of window positions with used intensity (control area “Willow 2” in strip1 of flight “Langeoog 2005”)

| Radius (m) | Mean (cm) | Std. Dev. (cm) | Number of Points | Intensity used (%) |
|------------|-----------|----------------|------------------|--------------------|
| 1,5 | 5,12 | 7,70 | 24 | 73,7 |
| 2,0 | 5,33 | 7,98 | 42 | 77,7 |
| 2,5 | 5,41 | 9,08 | 63 | 81,2 |
| 3,0 | 5,68 | 10,85 | 92 | 84,5 |
| 5,0 | 7,83 | 19,20 | 250 | 95,1 |

Table 2 illustrates the influence of the number of iterations on the accuracy of the method. Obviously, the mean and the standard deviation of the differences between the true and the estimated residuals decrease continuously and a stable solution is achieved after a few iterations, which is an indicator for the applicability of the method. In the further analysis three iterations are used.

Table 2: Influence of the number of iterations on the mean and standard deviation of the difference between the true (control measurements) and the estimated surface, (control area “Willow 2” in strip1 of flight “Langeoog 2005”)

| | Iterations | | | | |
|-----------------------|------------|-------|-------|-------|-------|
| | 1 | 2 | 3 | 5 | 10 |
| Mean (cm) | 7,021 | 5,479 | 5,413 | 5,408 | 5,408 |
| Std. Dev. (cm) | 10,375 | 9,146 | 9,078 | 9,073 | 9,073 |

The percentage of the LIDAR points, in whose vicinity the intensity values correspond to the residuals (see statement 1 in section 2.1), is above 90 % for most of the training areas, located in populations of different coastal shrubberies (Table 3). A lower percentage is observed for most of the areas of smaller point density. This result confirms the initial experiments related to moving windows of different size (Table 1). A potential explanation of this phenomenon takes the location of the training areas into account. The two test regions “Willow 2” and “Rose 2” are situated at the border of strip 2 of the campaign 2005. Due to the larger inclination of the laser beam compared to the nadir view the penetration rate and the variations of the cross sections are smaller. Therefore, the significance of the intensity may decrease at the border of the flight strip. The increasing standard deviations for the two test sites support this assumption.

The applicability of the reflectance information is also limited to coastal shrubberies (Figure 4). While the points with the used intensity are sparsely and randomly distributed in the meadow and heath, this information is almost always integrated during the surface fitting procedure of points in the test side “Sea Buckthorn 2” (green dots in Figure 4a) and the region of shrubbery on the left border of the image (see the biotope mapping in Figure 4b). Due to the low vegetation heights and different backscattering cross sections of meadow and heath the significance of the intensity feature is poor. However, this underlines the usefulness of intensity values as one feature among others for classification purposes.

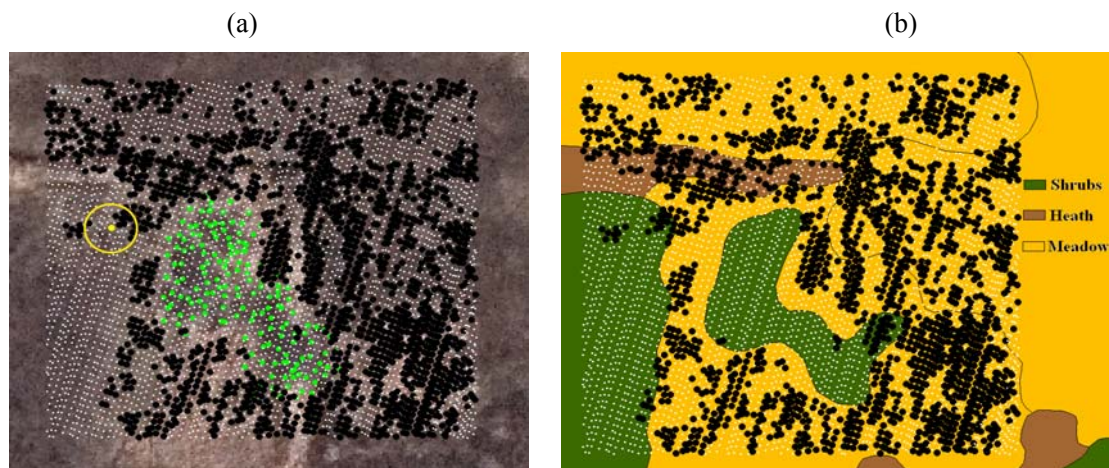


Figure 4: If the distribution of intensity values and the related residuals correspond to the theory in the area of interest (yellow circle in (a) – diameter: 5m), intensity is used for filtering (small white points), otherwise not (black points). The green points in (a) belong to control measurements for an entire population of Sea Buckthorn. Background: (a) orthophoto, (b) biotope mapping.

Table 3 summarises the mean and the standard deviations of the differences between the true (control measurements) and the fitted surface for all test sites and flight campaigns using different methods. In comparison to the initial fitting, the robust filtering forces the surface to the lower LIDAR echoes with respect to the control measurements in every test region. The integration of the reflectance information always enhances this effect. Additionally, the standard deviation decreases for 67% of the test sites by using the intensity based weights.

The discrepancies of the mean differences between the various test sites seem to a large extent to depend on their location in the flight strip. Due to suboptimal post processing by third parties the strips are somewhat tilted. This results in systematic offsets depending on the location within the flight strip. However, because of the small size of the test sites (average: 20m x 20m) this issue does not significantly influence the comparison of the methods discussed here. If the variation of the ground increases, the use of the second order surface slightly improves the results. However, the trend is similar to the application of the plane.

Table 3: Information of the different control areas: overall number of LIDAR points, percentage of window positions with used intensity, number of points in the neighbourhood ($r=2.5m$), mean and standard deviation of the difference between the true (control measurements) and the fitted surface for the initial fitting, robust filtering, and robust filtering with intensity information

| Test Side | Number of LIDAR Points | Intensity used (%) | Number of Points in Vicinity ($r=2.5m$) | Plane (cm) | | | | | |
|---|------------------------|--------------------|---|-------------|------|-------------|------|---------------|------|
| | | | | Initial | | Robust | | Robust + Int. | |
| | | | | Mean | Dev. | Mean | Dev. | Mean | Dev. |
| Juist 2004 (Scanner: ALTM 2050; Altitude: 1000m) | | | | | | | | | |
| Rose/Willow | 4046 | 89,7 | 48 | 53,9 | 58,2 | 50,8 | 56,6 | 43,7 | 52,4 |
| Langeoog 2005 (LMS-Q560; 600m) | | | | | | | | | |
| Rose/Sea Buckthorn (Strip1) | 3015 | 99,8 | 63 | 15,0 | 17,4 | 12,7 | 16,6 | 11,0 | 16,4 |
| Rose/Willow (Strip1) | 497 | 99,4 | 57 | 20,6 | 7,4 | 19,6 | 7,2 | 18,1 | 7,1 |
| Sea Buckthorn 1 (Strip1) | 820 | 99,1 | 67 | 15,0 | 12,5 | 14,3 | 12,3 | 12,7 | 11,9 |
| Sea Buckthorn 2 (Strip1) | 574 | 91,6 | 60 | 16,5 | 11,1 | 15,7 | 10,5 | 13,9 | 9,3 |
| Rose 1 (Strip1) | 736 | 96,5 | 57 | 7,8 | 8,3 | 7,3 | 8,2 | 6,4 | 8,2 |
| Rose 2 (Strip1) | 450 | 91,8 | 62 | 6,5 | 4,2 | 6,3 | 4,1 | 5,5 | 4,2 |
| Rose 2 (Strip2) | 265 | 89,8 | 37 | -2,4 | 5,4 | -2,5 | 5,4 | -3,7 | 5,6 |
| Willow 1 (Strip1) | 419 | 93,1 | 68 | 12,6 | 6,0 | 12,3 | 6,0 | 10,8 | 5,9 |
| Willow 2 (Strip1) | 453 | 81,2 | 63 | 7,0 | 10,4 | 6,4 | 9,8 | 5,4 | 9,1 |
| Willow 2 (Strip2) | 260 | 77,3 | 37 | 4,8 | 12,2 | 4,1 | 11,9 | 3,2 | 12,6 |
| Beach Grass (Strip1) | 705 | 87,2 | 59 | 13,8 | 20,6 | 13,7 | 20,6 | 12,8 | 20,7 |
| Langeoog 2006 (LMS-Q560; 600m) | | | | | | | | | |
| Sea Buckthorn 1 (Strip11) | 522 | 94,8 | 42 | 2,1 | 11,1 | 0,9 | 11,0 | -1,3 | 10,7 |
| Sea Buckthorn 2 (Strip11) | 302 | 74,2 | 31 | -1,9 | 10,5 | -2,9 | 9,7 | -5,5 | 8,0 |
| Sea Buckthorn 2 (Strip12) | 199 | 80,9 | 21 | -1,4 | 10,2 | -2,3 | 9,5 | -4,8 | 9,0 |

4. Conclusions

A new filtering algorithm was introduced, which transfers the intensity and echo distribution of LIDAR points into weights for a locally adaptive iterative surface fitting approach. The method was investigated using different test sites covered by coastal shrubberies during leaf-off periods. The results show that the integration of the reflectance information slightly forces the fitted surface to the lowest LIDAR echoes regarding the control measurements in every test region. Furthermore, the new algorithm decreases the standard deviation of the differences between the true and estimated residuals with respect to robust filtering in many test areas.

However, the points for the intensity transfer function are determined only empirically. In future research the separability of the intensity values of the lowest and the highest echoes with regard to the previous fitted surface should be analysed using statistical tests. The significance of this feature can be further used, in order to decide about the integration of the reflectance information and subsequently to define the transfer function.

In future work additional features provided by modern full waveform sensors, shall be exploited. For instance, the pulse width can be a quality criterion by itself. It describes the uncertainty of the target surface and the range measurement for the related echo and can therefore be easily integrated in the determination of the weights of the filtering process.

The promising findings in this paper encourage us to investigate the transferability of the method to other vegetation types. For instance, the assumption that the higher the LIDAR echoes in the vegetation the smaller the cross sections and the intensity values, could also be true for deciduous trees during the leaf-off period, because, among others, the cross section is also influenced by the diameter of the reflecting branches.

Acknowledgements

This research has been financed by the Federal Ministry of Education and Research under project no. 03KIS050. We acknowledge the support of our project partners: Department of Rural Area Husum, Federal Waterways Directorate, and the Lower Saxony Water Management, Coastal Defence and Nature Conservation Agency Division Norden-Norderney.

References

- Brovelli, M., Cannata, M. and Longoni, U., 2002. Managing and processing lidar data within GRASS. *Proc. of the Open Source GIS-GRASS users conference*, Trento, Italy, 29 pages.
- Göpfert, J. and Heipke, C., 2006. Assessment of Lidar DTM Accuracy in Coastal Vegetated Areas: In *IntArchPhRS*, Vol. XXXVI/3, Bonn, Germany, pp. 79-85.
- Goepfert, J. and Soergel, U., 2007. Estimation of the lidar height offset in coastal vegetated areas. In *IntArchPhRS*, Vol. XXXVI/3, Espoo, Finland, pp. 156-161.
- Jelalian, A.V. 1992. *Laser Radar Systems*. Artech House, Boston and London.
- Kraus, K. and Pfeifer, N., 1998. Determination of terrain models in wooded areas with airborne laser scanner data. In *ISPRS Journal of Photogrammetry & Remote Sensing*, Vol. 53 (4), pp. 193-203.
- Moffiet, T., Mengerson, K., Witte, C., King, R. and Denham, R. 2005. Airborne laser scanning: Exploratory data analysis indicates variables for classification of individual trees or forest stands according to species. In *ISPRS Journal of Photogrammetry & Remote Sensing*, Vol. 59 (5), pp. 289-309.
- Sithole, G., 2005. Segmentation and Classification of Airborne Laser Scanner Data, *Dissertation*, TU Delft, Netherlands, 146p.
- Sithole, G., Vosselman, G., 2004. Experimental comparison of filter algorithms for bare-earth extraction from airborne laser scanning point clouds. *ISPRS Journal of Photogrammetry & Remote Sensing*, Vol. 59 (1-2), pp. 85-101.
- Tóvári, D. and Vögtle, T., 2004. Object Classification in Laser-Scanning Data. *IntArchPhRS*, Vol. XXXVI, Part 8/W2, pp. 45-49.
- Vosselman, G., 2000. Slope based filtering of laser altimetry data. In *International Archives of Photogrammetry and Remote Sensing*, Vol. XXXIII, Part 3B, pp. 935-942.
- Wack, R. and Wimmer, A., 2002. Digital terrain models from airborne laser scanner data - a grid based approach. In *IntArchPhRS*, Vol. XXXIV, Part 3B, pp. 293-296.
- Wagner, W., Ullrich, A., Ducic, V., Melzer, T. and Studnicka, N., 2006. Gaussian decomposition and calibration of a novel small-footprint full-waveform digitising airborne laser scanner. In *ISPRS Journal of Photogrammetry & Remote Sensing*, Vol. 60 (2), pp. 100-112.

Land cover classification of rural areas using LiDAR data: a comparative study in the context of fire risk

G. Gonçalves^{1,2}, L. Seco³, F. Reyes³ & D. Miranda³

¹ Institute for Systems and Computers Engineering at Coimbra, Portugal

² Department of Mathematics, University of Coimbra, Apartado 3008, 3001-454
Coimbra, Portugal gil@mat.uc.pt

³ University of Santiago de Compostela - Superior Polytechnical School of Lugo -
Campus Universitario s/n, 27002 Lugo {lgseco,freyes,dmiranda}@usc.es

Abstract

In fire risk, correct description of topographic and fuel properties is critical to improve fire danger assessment and fire behaviour modelling. Many rural areas are now scanned using LiDAR sensors. In some of these areas the information registered by the sensor includes not only the geometric characteristics of the Earth's surface, given by the coordinates (x,y,z) of the LiDAR point cloud, but also the reflectance of the objects located on this surface, which is given by the backscattered intensity of echo reflection. The main objectives of this paper are to assess the performance of three land cover supervised classification methods of LiDAR data: Maximum Likelihood (ML), simple pixel hierarchical and object-oriented classification. In this way, three "bands" were computed from LiDAR data: the normalized height (nH), the height difference between the first and last echo (Hdiff) and the LiDAR intensity (I), which is the only spectral band of the feature space. Using data from training sites and the transformed divergence index, the separability of roads, buildings, high vegetation and low vegetation classes was evaluated. The comparison among these three classification methods was done using orthoimagery as reference data. The obtained results indicate that an evident superiority doesn't exist among the three methods.

Keywords: LiDAR, Intensity, Fire risk, Land cover, Supervised classification, Rural areas

1. Introduction

1.1 Motivation

Forest fires are one of the major challenges for natural resources management in many places in the world. Spain and Galicia are not an exception, being this autonomous community one of the most punished regions in Europe. Forest risk variables could be grouped into tree levels: topographic variables, fuel variables and variables related to human activity. Correct description of topographic and fuel properties is critical to improve fire danger assessment and fire behaviour modelling, since they guide both fire ignition and fire propagation, and fuel is the only vertex of "fire triangle" (fuel, oxygen and heat) that human action can modify directly. Moreover, in the proximity of buildings and infrastructures, there are more chances that fire was caused by higher human presence. The fact that most fires are caused by humans suggests that increased accessibility to forests will increase the possibilities of fire. Implicitly, actions around elements of special concern for humans are given priority, mainly because fire in the proximity of those places represents a risk to life. Because the safety of people and houses is a priority during fire extinction, prevention models should also consider this factor as a priority.

In this sense, correct classification of roads, buildings, high vegetation and low vegetation is very important in the later extraction of those variables. Airborne Laser Scanning (ALS), also

known as LiDAR (Light Detection And Ranging) has shown a great potential in fast and accurate geographic data acquisition below canopy closure. This active remote sensing technique records not only the geometric characteristics of the Earth's surface, but also the reflectance of the objects located on this surface. The backscattered intensity of reflection (also referred as intensity) is basically a function of the laser wavelength, which is typically in the near infrared (NIR) spectra region (0.7 - 1.5 μm for topographic applications), the range from sensor to the object and the composition and orientation of the object or surface. Because different materials have different reflectances, the intensity can be used for classifying land cover.

Nowadays, because many rural areas are scanned using Lidar sensors is indispensable to know if it is possible to use this data alone to extract the forest risk variables. Thus, the main objectives of this paper are to assess the performance of three supervised classification methods of LiDAR intensity data: maximum likelihood classification, simple hierarchical pixel classification and object-oriented classification. In this context, three bands were computed from LiDAR data: the normalized height (nH) which contain the information about the height of the objects; the height difference between the first and last echo (Hdiff); and the LiDAR intensity which is a spectral band in the NIR region. Then, using data from training sites and the transformed divergence index, the separability of the input feature space was evaluated. Finally, the object identification was made using the three classification methods. The comparison among these three classification methods was done using orthoimagery as reference data.

1.2 Related work

In spite of the great majority of the LiDAR systems have the capacity to record the received signal intensity, the great part of the published work has been done in the filtering, classification and segmentation of the 3D point cloud (x,y,z) – the primary result of LiDAR system – based on the geometric characteristics of this cloud. What is of our knowledge, a few works have been using the variable intensity in the processing of the point cloud.

Song *et al.* (2002) evaluated the possibility of using LiDAR intensity data for land-cover classification. The LiDAR point intensity has converted to a grid by using three different interpolation techniques. Using a transformed divergence method the separability of intensity data for four classes (asphalt roads, grass, house roofs and trees) has assessed. They conclude that LiDAR intensity can be used for land-cover classification and state if more features, such as DSM, and more processing, such as intensity normalization, are added better results could be reached and more classes identified.

In Matikainen *et al.* (2003) the feasibility of using LiDAR data (intensity and geometry of LiDAR point cloud) for automatic building detection in the context of map updating is investigated. Using an object-oriented classification method the feature space formed by an nDSM and by an intensity image is classified in two classes: buildings and not-buildings. A similar approach has conducted by Brennan *et al.* (2006), but considering a larger number of information classes and segmentation levels.

Charaniya *et al.* (2004) used a supervised parametric classification technique to classify roads, roofs, trees and grass. The feature space was formed by using LiDAR derived data (nDSM, intensity, height variation, difference of first and last echo) and the luminance of a grey scale aerial photo. Data fusion was made by using a classification algorithm based on the Gaussian mixture model and Expectation Maximisation. The obtained results allowed them to conclude that: i) the normalized height and height variation are important geometric features for the classification procedure; ii) the intensity and luminance (i.e. non-geometric features) are useful for separating the grass (low vegetation) from roads; iii) using the intensity as the only

non-geometric feature the overall classification was slightly worse, but the tree classification was improved. A similar work was conducted by Bartels *et al.* (2006) but adding also an 8-bit NIR aerial photo to the feature space and incorporating additional knowledge and considering contextual relationships among classes.

Finally, in Höfle *et al.* (2007) the return amplitude of each eco (that is the intensity) is corrected in order to obtain a value that is proportional or equal to the surface reflectance. The intensity variations and systematic errors due to spherical loss, topographic and atmospheric effects are corrected by two independent methods: data and model-driven approaches. They conclude that both methods can achieve a significant reduction of local intensity variation within a regular neighbour to a 1/3.5 of the original variation and offsets between flight strips to 1/10. They pointed out that the need for normalized intensity values area justified for large data sets containing strong elevation differences. As the height variations in this study are very small we used the original uncorrected intensity values.

2. Methodology

2.1 Data and study area

The study area (Figure 1) is located in the north of Galiza (Spain) and it is composed basically by a small residential zone and a forest zone, whose dominant species is *Eucalyptus Globulus*. In geomorphologic terms, in spite of the altitudes varying between 230 and 370m, the relief of the zone is quite accentuated.

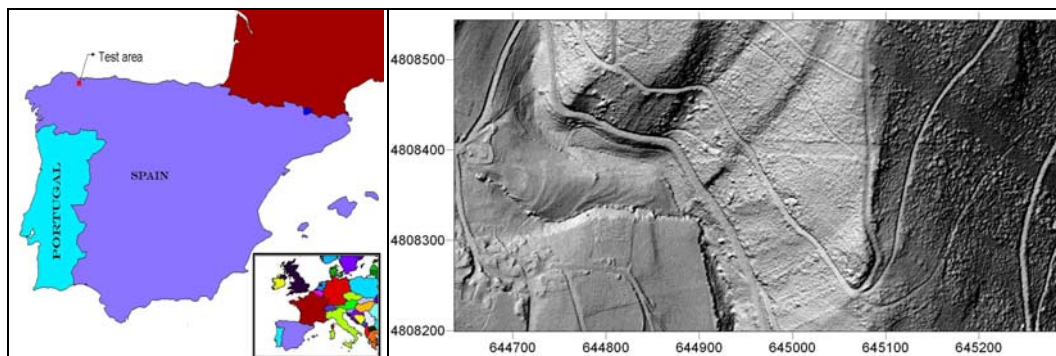


Figure 1: The location and shaded relief of the test area

The LiDAR data were acquired in November 2004 with Optech's ALTM 2033 (www.optech.ca) from a flight altitude of 1500m (ASL). The LiDAR sensor works with a laser wavelength of 1064 nm and the beam divergence was set to 0.3 mrad. The pulsing frequency was 33 kHz, the scan frequency 50 Hz, and the scan angle ± 10 degrees. The first and last return pulses were registered. The complete study area was flown in 18 strips and each strip was flown three times, which gave an average measuring density of about 4 points per square meter.

2.2 Features, classes and separability

In order to run image classification methods in the LiDAR data, these (intensity and the original and the filtered point cloud) have to be converted to a grid format. Take into account the pulse density (4pts/m²) the cell size chosen was 0.5m. In this way each one of the features used in the classification procedure was derived from the original and filtered LiDAR data by using the kriging interpolation method with linear variogram. The parameters chosen for the interpolation of each grid are given in table 1. However as it was indicated in (Gonçalves, 2006) for these

sampling densities and for this cell size the influence of the interpolation method is not important for the subsequent classification procedure. The kriging interpolator was chosen by the fact that it can produce a smooth topographic surface and in the case of intensity values it can remove some of its noise more effectively.

2.2.1 Features

For image classification purposes we identify three features to be used (see figure 2):

- Normalized height (nH). This feature is obtained by subtracting the morphological filtered DTM from the original DSM. The DSM was interpolated from the first LiDAR return. The morphological adaptive filter used to obtain bare earth points from the LiDAR point cloud is described in (Gonçalves-Seco *et al.* 2007). The DTM was interpolated from these bare earth points corresponding to the last return LIDAR. This feature is created to exclude the influence of topography from the classification process and is useful to differentiate the high objects (high vegetation and buildings) from the low objects (low vegetation and roads).
- Height difference between the first and last return (Hdiff). Depending on the laser and object characteristics the LIDAR shot can penetrate through the objects and backscattered to the sensor at different height levels of the objects. In the case of first and last pulse acquisition, some of the shot energy can be returned to the sensor from the top of the penetrable objects while another part of its energy continues her path until reaching the terrain where is backscattered to the sensor. In this study this feature is used to identify the high vegetation areas, and it acts as a measure of height texture.
- Intensity (I): Since the laser unit of the LiDAR system uses light from the near infrared portion of the spectrum we use this feature to introduce spectral knowledge in the classification procedure. This is the only non-geometric information provided by the sensor and the intensity image is interpolated from the first LiDAR return.

Table 1: Kriging interpolation parameters:

| Interpolated Grid | Error variance | Scale, Length, Anisotropy ratio, Anisotropy angle |
|---------------------------|----------------|---|
| DSM (first and last echo) | 8.76 | 2,1,2,125.7 |
| DIM | 1.5 | 1,0,2,125.7 |
| DTM | 8.76 | 2,1,2,125.7 |

2.2.2 Classes

In the context of fires in rural areas we can devise four information classes that they play a central role in the fire risk management: roads, buildings, high vegetation and low vegetation. In fact, beyond topographic variables estimated from DTM (for example the slope, the altitude and aspect which affects, respectively, the fire spread, the occurrence and fire behaviour and regulates temperature levels and relative humidity), in the proximity of roads and buildings, there are more chances that fire was caused by higher human presence. The fact that most fires are caused by humans suggests that increased accessibility to forests will increase the possibilities of fire. Implicitly, actions around elements of special concern for humans are given priority, mainly because fire in the proximity of those places represents a risk to life. Because the safety of people and houses is a priority during fire extinction, prevention models should also consider this factor as a priority (Gonçalves-Seco *et al.*, 2007b). High and low vegetation can help to represent fuel properties at surface and crown level, such as dead and live fuel load, canopy cover and height, vertical and horizontal structure of the canopy, the quantity of biomass and fuel moisture content (Pyne *et al.*, 1996).

2.2.3 Separability assessment

In order to assess the signature separability in the feature space the transformed divergence method (TDI) was used. The TDI index between two classes i and j is derived from the likelihood ratio of any pair of classes and varies within in the interval $[0,2]$ (Richards *et al.*, 2006):

$$\text{TDI}_{ij} = 2 \times (1 - e^{-d_{ij}/8}) \quad (1)$$

where

- $d_{ij} = \frac{1}{2} \text{Tr} \{(\mathbf{C}_i - \mathbf{C}_j)(\mathbf{C}_j^{-1} - \mathbf{C}_i^{-1})\} + \frac{1}{2} \text{Tr} \{(\mathbf{C}_i^{-1} + \mathbf{C}_j^{-1})(\mathbf{m}_i - \mathbf{m}_j)(\mathbf{m}_i - \mathbf{m}_j)^t\}$
- \mathbf{C}_i , \mathbf{C}_j , \mathbf{m}_i , and \mathbf{m}_j are the covariances and means for the classes i and j , respectively,
- Tr is the trace function.

The greater the value of TDI the greater is the signature separability based on this feature space and training data. In general a TDI value of 2.0 is considered to be indicator of perfect separability while a value of 0 indicates complete overlap between the signatures of the two classes. Values greater than 1.9 are considered good separability and values less than 1.7 are considered poor separability.

2.3 Classification methods

In general, image classification procedures can be categorized into supervised and unsupervised, depending on the presence of previous knowledge about the land cover types, and into parametric and nonparametric depending on the assumptions made about the multivariate normal distribution of the N -dimensional feature space. In the case of high resolution (HR) imagery data some authors (Brennan *et al.*, 2006; Li *et al.*, 2007) argue that is not practical to classify the image using traditional pixel-based classification methods, such as supervised parametric (e.g. maximum likelihood), because they have considerable difficulties to deal with the rich information content present in the HR 2-D data and they produce a characteristic and inconsistent salt-and-pepper classification. They purpose more advanced approaches such as object-oriented segmentation and classification techniques to overcome these problems.

In the context of land cover classification of small footprint LiDAR data (i.e high resolution 2½-D data) the maximum likelihood and object oriented methods are the more used. Because of this high spatial resolution of LiDAR data set we are interested to study also the performance of simple hierarchical classification when compared to the maximum likelihood and the more advanced object-oriented classifier.

2.3.1 Maximum Likelihood

The Maximum Likelihood Classifier (ML) is perhaps the most commonly used supervised parametric classifier because of its robustness and its easy availability in almost any image classification software package (Lu *et al.*, 2007). Under the assumption of multivariate normal distribution of the classes examined a pixel \mathbf{x} is classified by this method to belonging to the class w_i if it minimizes the discriminate function $g_i(\mathbf{x})$ (that is, it has the maximum likelihood of correct assignment)

$$g_i(\mathbf{x}) = (\mathbf{x} - \mathbf{m}_i)^T \mathbf{C}_i^{-1} (\mathbf{x} - \mathbf{m}_i) + \ln \mathbf{C}_i \quad (2)$$

where \mathbf{m}_i and \mathbf{C}_i are the mean vector and covariance matrix of the class under examination (w_i) computed from the training data.

2.3.2 Simple hierarchical classification

In this classification method we used binaries queries (or decisions) to place pixels into classes. Each query divides the pixels in a set of images into two classes based in an expression. Each new class can be divided into two more classes based on another expression. The algorithm used to build this classifier is given in figure 2 and has been implemented using *MatLab*TM language. Only three (par3,par4,par5) of the six classification parameters are computed from the intensity values of the training areas. The other three parameters are height thresholds and can be computed from the characteristic of LiDAR flight: par1 defines the minimum height of the high objects (buildings and trees); par2 defines the minimum height of penetrable objects; par6 depends on LiDAR system and defines minimum height echo separation.

Algorithm 1: Hierarchical classification

```

Input : I[m, n] ; /* Intensity image */
         nH[m, n] ; /* Normalized Height image */
         Hdifff[m, n] ; /* Height difference image */
         Roads, Buildings, Hveg, Lveg ; /* Attribute classes */
         par1, par2 par3, par4, par5, par6 ; /* Classification parameters */
Output: ImClas[m, n]; /* Classified image */

begin
  Imclas[m, n] ← 0
  foreach pixel[i, j] ∈ ImClass do
    if nH[i, j] ≥ par1 ; /* Separate high from low objects */
    then
      if Hdifff[i, j] ≥ par2 ; /* Separate penetrated objects */
      then
        | pixel[i, j] ∈ Hveg
      else
        | pixel[i, j] ∈ Buildings
      end
    else
      if I[i, j] ≥ par3; /* Maximum intensity value for roads */
      then
        | pixel[i, j] ∈ Lveg
      else
        if I[i, j] ≥ par4 and I[i, j] ≤ par5; /* Intensity values for roads */
        then
          | pixel[i, j] ∈ Roads
        else
          if Hdifff[i, j] ≤ par6; /* Separate roads from low vegetation */
          then
            | pixel[i, j] ∈ Roads
          else
            | pixel[i, j] ∈ Lveg
          end
        end
      end
    end
  end
end
end

```

Figure 2: Simple hierarchical classification algorithm.

2.3.3 Object-oriented classification

In object-oriented classification approaches image analysis is done in object space rather than pixel space and objects are used as the information carriers for further classification. Image segmentation is the main step that is used to convert an image into multiple objects. In *eCognition*TM software object-oriented image analysis is performed into three steps: multiresolution segmentation, creation of general classes and classification rules. In the first step,

images segments are defined and calculated using a bottom-up region-merging segmentation. In his patented algorithm (version 4.02) the parameters that control image segmentation are: scale, color, smoothness and compactness. The scale parameter (S_c) is an abstract value to determine the maximum possible change of heterogeneity caused by fusing several objects. Color (C) is the most important criteria for creating meaningful objects and defines the contribution of spectral values to define homogeneity of each object. Smoothness describes the similarity between the image object borders and a perfect square. Compactness (Cl) describes the "closeness" of pixels clustered in an object by comparing it to a circle (Baatz et al, 2004). These image segments have to be calculated on several hierarchical levels in a "trial and error" process to result in final image segments to represent single objects of interest (Navulur, K., 2006). In the second step Class Hierarchy are build by creating and defining classes. In our case, we have used only one level for the multiresolution segmentation and the parameters used for this segmentation are given in table 2. The rules used for the class definition are the same that we have used for the decision tree of the simple hierarchical pixel classification method.

Table 2: Image segmentation parameters.

| | |
|---------------------------------|-------------------------------|
| Layer weights | nH = 10; I = 1; Hdiff = 1 |
| Scale and homogeneity criterion | Sc=10; C=0.1; Cl=0.3; S = 0.7 |

2.4 Classification accuracy assessment

In order to assess the accuracy of the results obtained by the three classification methods a random sample of 770 points are generated and manually classified using an orthoimage of the test area. This sample is used to generate an error matrix for each classification method. From these error matrixes several measures are computed to describe the accuracy of land cover classification. As global measures we will use the overall accuracy (P_c) which gives the overall percentage of area correctly classified and the overall kappa statistic (k) which takes into account the whole confusion matrix including its off-diagonal elements. As local measures (i.e class accuracy) we will use the producer's accuracy (PA) which gives the percentage of correctly classified pixels from the collected class samples, and the user's accuracy (UA) which gives the percentage of pixels which were correctly assigned to one particular class.

3. Results

3.1 Separability of class signatures

Table 3 shows the results obtained for the separability analysis of class signatures. The average separability is 1.96 which means that the four classes forming the feature space can, in principle, be correctly separated using the signatures computed from the training data. The minimum separability is between buildings and high vegetation. This means that the feature space is not enough to achieve a good separability between these two classes.

Table 3: Separability measures using TDI. Class-1 = roads; Class-2 = buildings; Class-3 = high vegetation; Class-4 = low vegetation

| Name | Class-1 | Class-2 | Class-3 |
|---------|---------|---------|---------|
| Class-2 | 2.000 | | |
| Class-3 | 2.000 | 1.764 | |
| Class-4 | 2.000 | 2.000 | 2.000 |

3.2 Classification methods

Figure 4 shows the training areas and the results of the three classification methods. Figure 4a (left) shows the training areas (in red) superimposed over the orthoimage that was used to classify manually the random sample. Note that the date of this orthoimage is previous to the date of LiDAR flight. Figure 4b, 4c and 4d shows, respectively the results obtained for the ML, simple hierarchical and object-oriented classifiers. For the simple hierarchical classifier the following values were used for the six parameters: 1.5,0.5,34,0,20,0. Although the three classifiers they produce correct and similar qualitative results, the object-oriented classifier gives visually better results in the labelling of the building and roads classes.

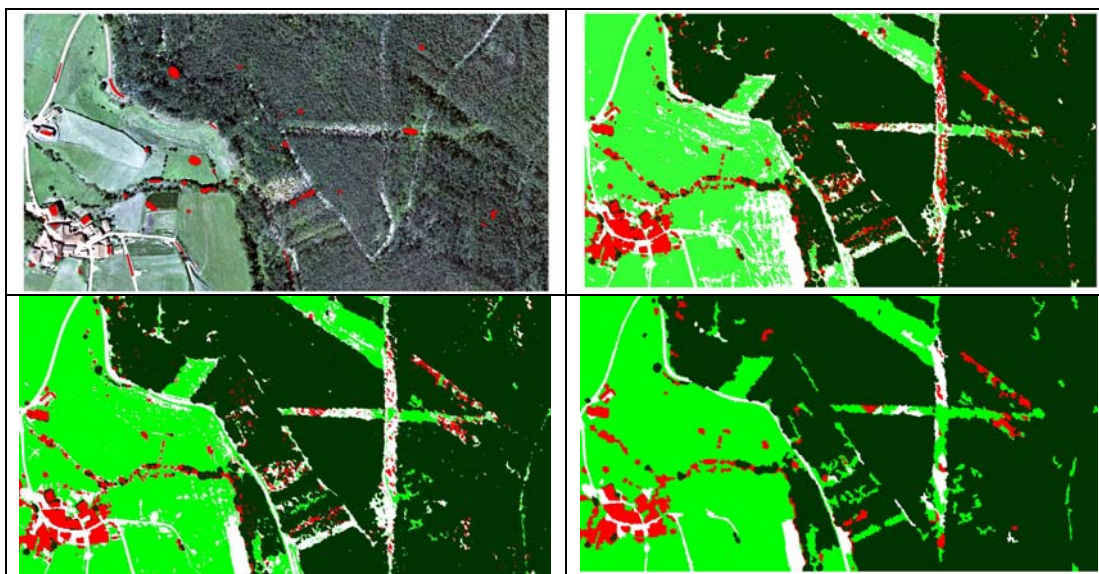


Figure 4: Training areas and results of the classification methods. First row: training data (left) and results of ML classifier (right). Second row: results of the simple hierarchical (left) and object-oriented classifiers (right)

3.3 Accuracy assessment

The error matrix and some accuracy measures for the two classification methods are given in table 4. In this table the PA and UA accuracies also given for each class. The global measures such as Pc and k are also given. The global measures indicate that the object-oriented classifier is slightly better than the ML and simple hierarchical classifiers (better Pc and K values). However the PA for the building class is higher in ML classifier than in simple hierarchical and object-oriented classifiers. In any way, for the three classifiers, the user accuracy of the roads and building classes are not good as the user accuracy of high vegetation and low vegetation.

Table 4. Error matrix and accuracy measures for the three classification methods. Legend: UA - user accuracy (%); PA - producer accuracy (%); Pc - overall accuracy; k – overall kappa statistic.

| | Maximum likelihood | | | | | Simple hierarchical | | | | | Object-oriented | | | | |
|----|---------------------|----|-----|-----|----|---------------------|----|-----|-----|----|---------------------|----|-----|-----|----|
| | 1 | 2 | 3 | 4 | UA | 1 | 2 | 3 | 4 | UA | 1 | 2 | 3 | 4 | UA |
| 1 | 20 | 1 | 00 | 55 | 26 | 22 | 6 | 5 | 50 | 27 | 18 | 2 | 0 | 15 | 51 |
| 2 | 1 | 31 | 22 | 10 | 48 | 0 | 28 | 13 | 4 | 62 | 0 | 28 | 11 | 5 | 64 |
| 3 | 0 | 0 | 414 | 9 | 98 | 0 | 0 | 421 | 10 | 98 | 0 | 0 | 424 | 11 | 97 |
| 4 | 4 | 2 | 7 | 194 | 94 | 3 | 0 | 4 | 204 | 97 | 7 | 4 | 8 | 237 | 93 |
| PA | 80 | 91 | 93 | 72 | | 88 | 82 | 95 | 76 | | 72 | 82 | 96 | 88 | |
| | Pc = 85.6; K = 0.75 | | | | | Pc = 87.7; K = 0.79 | | | | | Pc = 91.8; K = 0.85 | | | | |

4. Conclusions and future work

The obtained results indicate that it is possible to add to the traditional LiDAR point cloud classification (terrain and off-terrain points) a larger number of typical classes of these areas. The normalized height allowed the separation of the high objects from low. The LiDAR intensity allowed to unbundled the roads from the low object class and the height difference between the first and last echo allowed to isolate the objects that can be penetrated by the LiDAR shots (vegetation).

The error matrix obtained for the classification methods shows that, in the context of the forest risk of rural areas, an evident superiority doesn't exist between the three methods. In these conditions, the method of simple hierarchical pixel classification can be used in bulky LiDAR point clouds for the extraction of the four classes pertinent for the subsequent generation of the fire risk variables. However some difficulties subsist in the separation of the high vegetation and building classes. The low user accuracy verified for the roads can be due to the fact that we have put in the same class the asphalted roads and non-asphalted roads. We could think that the consideration of one more class (non-asphalted roads or forest roads) will improve the results. However, the consideration of this class would also bring the additional problem of the separation between non-asphalted roads and low-vegetation class.

The limitations of the three classifiers relates to misclassification of high vegetation and buildings, which are consistent with those of Brennan *et al.* (2006). Some others limitations/difficulties were found in the classification accuracy assessment. In fact, due to the high resolution of LiDAR data it is important that the resolution of the reference data will be much better than the LiDAR computed “images”. In case we use ortoimages as the reference data these images have to be true ortoimages, what are very difficult to achieve in forested environments. However, the use of stereoscopic images can be a solution to achieve a correct manual 3D-classification of the reference data.

Finally, as future work, we can incorporate contextual knowledge into the classifiers to distinguish between buildings and high vegetation. In fact, we intended to use the shape and area parameters to identify isolated trees in a post classification step of the simple hierarchical pixel classifier.

Acknowledgements

Many thanks to R. Crecente and R. A. Díaz Varela from the Land Laboratory of University of Santiago de Compostela for their valuables comments and suggestions. The data used in this work was funded by by the Galician Government (Xunta de Galicia) and Land Laboratory (University of Santiago de Compostela).

References

- Alharthy, A., Bethel, J., 2002. “Heuristic filtering and 3D Feature extraction from LIDAR data”. *ISPRS Commission III Symposium*, Graz, Austria. September 9.
- Axelsson, P., 1999. “Processing of laser scanner data – algorithms and applications”. *ISPRS Journal of Photogrammetry and Remote Sensing*. Vol 54, No. 2-3, Págs. 138-147.
- Bartels, M., Wei, H., and Ferryman, J., 2006. Analysis of LIDAR Data Fused with Co-Registered Bands. In CD: *Proceedings of the IEEE international Conference on Video and Signal Based Surveillance* (November 22 - 24). AVSS. IEEE Computer Society, Washington, DC, 60.

- Baatz, M., Benz, U., Dehghani, S., Heynen, M., Höltje, A., Hofmann, P., Lingenfelder, I., Mimler, M., Sohlbach, M., Weber, M., Willhauck, G., 2004. eCognition User Guide 4
- Charaniya, A., Manduchi, R., Lodha, S., 2004. "Supervised parametric classification of aerial LIDAR data". *IEEE Conference on Computer Vision and Pattern Recognition Workshop*, Págs. 30-38.
- Coren, F., Visintini, D., Prearo, G., Sterzai, P., 2005. "Integrating LiDAR intensity measures and hyperspectral data for extracting of cultural heritage". *Workshop Italy-Canada for 3D Digital Imaging and Modelling: applications of heritage, industry, medicine and land*.
- Gonçalves, G., 2006. Analysis of interpolation errors in urban digital surface models created from LIDAR data. *Proceedings of 7th International Symposium on Spatial Accuracy Assessment in Natural Resources and Environmental Sciences*. pp 160-168. Lisbon, Portugal.
- Gonçalves-Seco, L., Miranda, D., Crecente, R., Farto J., 2006. "Digital Terrain Model generation using airborne LIDAR in forested area of Galicia, Spain". *Proceedings of 7th International Symposium on Spatial Accuracy Assessment in Natural Resources and Environmental Sciences*. Págs. 169-180. Lisbon, Portugal
- Gonçalves-Seco L., Fraga-Bugallo, B., Crecente Maseda, R., Miranda Barrós, D., 2007b. "Automatic extraction of forest and terrain fuel variables with airborne lidar to determine structural fire risk". *Proceedings of ForestSat'07*, 9 pp. Montpellier (France).
- Höfle, B., Pfeifer, N., 2007. Correction of laser scanning intensity data: data and model-driven approaches. *ISPRS Journal of Photogrammetry and Remote Sensing*, 62 415-433.
- Li, H., Gu, H., Han, Y. and Yang, J., 2007. Fusion of High-Resolution Aerial Imagery and LIDAR Data for Object-oriented Urban Land-cover Classification Based on SVM. *ISPRS Workshop on Updating Geo-spatial Databases with Imagery & The 5th ISPRS Workshop on DMGISs*, Urumchi, China. <http://www.commission4.isprs.org/urumchi/> (accessed 7 March 2008)
- Lu, D. and Weng, Q., 2007. A survey of image classification methods and techniques for improving classification performance. *International Journal of Remote Sensing*, 28:5, 823 - 870
- Maas, H.-G., 1999. "The potential of height texture measures for the segmentation of airborne laserscanner data". *Fourth International Airborne Remote Sensing Conference and Exhibition / 21st Canadian Symposium on Remote Sensing*, Ottawa, Ontario, Canada, 21-24 June.
- Matikainen, L., Hyypä, J., Hyypä, H., 2003. Automatic detection of buildings from laser scanner data for map updating. *International Archives of Photogrammetry, Remote Sensing and Spatial Information Sciences* 34 (Part 3/W13), 218–224.
- Navulur, K., 2006. Multi-spectral image analysis using the object oriented paradigm. CRC Press, Inc.
- Pyne, S. J., Andrews, P. L., & Laven, P. D., 1996. Introduction to wildland fire. New York: Wiley & Sons Press: 22–45.
- Richards, J. A. and Jia, X., 2006. Remote Sensing Digital Image Analysis: an Introduction. 4rd. Springer-Verlag New York, Inc.
- Sithole, G., 2005. "Segmentation and classification of Airborne Laser Scanner Data". *Publications on Geodesy* 59. Nederlandse Commissie voor Geodesie, Delft, The Netherlands, 184 pgs.
- Song, J.H., Han, S.H., Yu, K.Y., Kim, Y.I., 2002: "Assessing the possibility of land-cover classification using LIDAR intensity data". *ISPRS Commission III Symposium*, Graz, Austria. September 9.

Using LiDAR technology in forestry harvest planning.

David González¹, Julio Becker^{1,2}, Eduardo Torres², José Albistur², Manuel Escudero³,
Rodrigo Fuentes¹, Helio Hinostroza² and Felipe Donoso⁴.

¹Universidad de Concepción. College of Forestry Sciences, dgonzale@udec.cl

²Forestal MININCO S.A.

³Consulting Forest Company.

⁴ Universidad de Concepción. College of Engineering.

Abstract

Managing forest resources can be highly time and resource demanding and requires significant amount of data collection in the field plus the indispensable filtering necessary to provide the information. High performance LiDAR remote sensing technology has become an effective tool for use in applications on forest harvest planning. In the field of forestry, the LiDAR measurements of the forested areas can provide high quality data on three dimensional characterizations of digital terrain model (DTM). This study presents the accuracy evaluation of the LiDAR DTM data over forest planted field in order to use in forest harvest machinery assignment procedure, to finally delineate harvest units for spatial forest planning.

1. Introduction

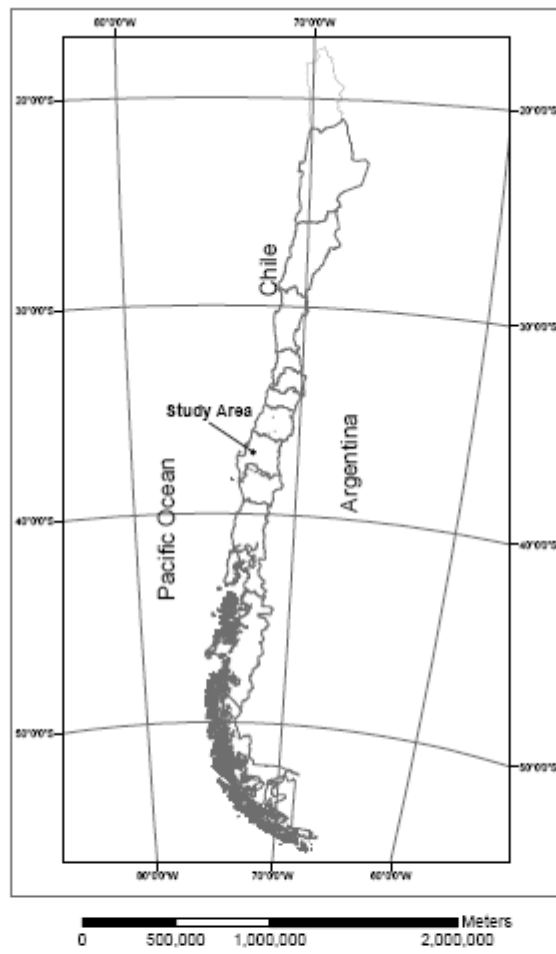
Airborne light detection and ranging is emerging as a prominent tool to provide accurate digital terrain models (DTMs) of forest areas, since it can penetrate beneath the forest canopy. This technology is providing a new conception in the forest harvest planning for forest companies transform it in a robust source for the extraction of DTMs.

High resolution of topographic data has the potential to differentiate one of the main morphological features of the landscape its elevation properties. For this study, 1 m spatial resolution of DTM was derived from the last pulse LiDAR data obtained by filtering the vegetation points (Leaves, branches, stems, bark), (Slatton et al, 2007). The study was conducted in a property of a forest company located in the center valley in the BioBio region, Chile. The results suggest a suitable capability of LIDAR in the recognition and description of the surface ground elevation, giving the potential to generate digital terrain models.

In previous studies, LiDAR data was used to evaluate the surface roughness as a useful approach to detect landslide areas (McKean and Roering, 2004), and to characterize and differentiate the landslide morphology and activity (Glenn et al, 2006), being a useful technology to be apply on the ground morphology description (James et al, 2006; Storesund and Minear, 2006). The present study analyses the capability of airborne LiDAR-derived data in the recognition of ground morphology to assign with accuracy the forest harvest machinery and allow delineate harvest units for spatial forest planning.

2. Study area

The study area is located in the Eastern of the coast mountain of BioBio region, Chile. This region concentrates most of the forest plantation in the country (52 %) (Figure 1, 2 and 3).



UTM Projection
Huso 18 South

Datum WGS 84



Figure 1: Location of study area.

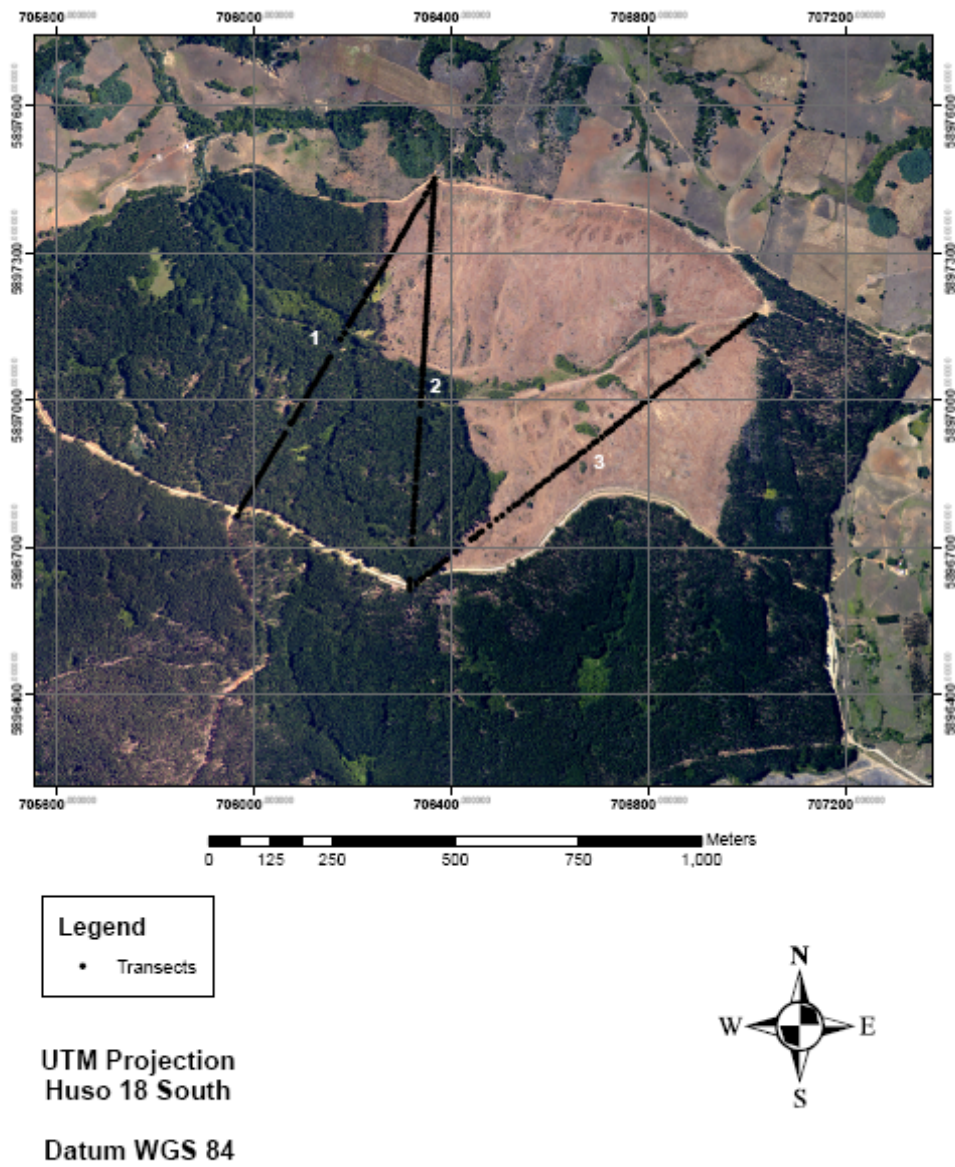


Figure 2: Aerial photo and the three transect location.

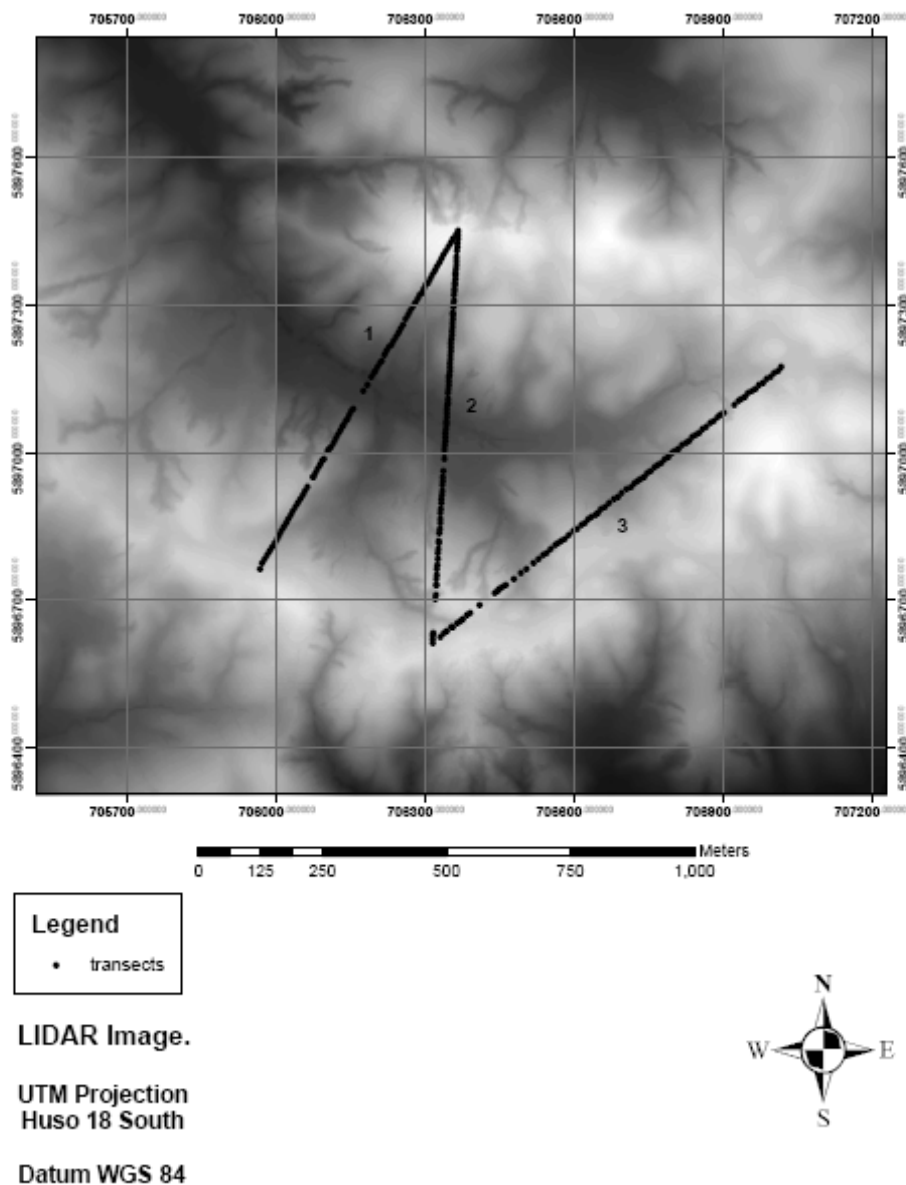


Figure 3: LiDAR imagery and the three transect location.

The LiDAR data was processed by using ArcGis v9.1 software package.

LiDAR data specifications: The LiDAR and photographic data were acquired from a airplane using an ALTM 3100 OPTECH, and Digital camera, flying above ground level during dense forest adult plantations conditions in Summer 2005.

GPS data specifications: The Geodesic GPS double frequency, code P, 18 channels, brand TRIMBLE, model 4000SSi, Everest technology, was utilized to generate the four vertices of the three elevation transects (See Fig. 2, Fig. 3 and table 1) to generate the three elevation profiles showed in following figures 5, 6 and 7. The topographic station that was used to take z variable (elevation axis) within each transect corresponds to LEICA model TC-303.

Morphology data acquisition: The elevation profile for each transect was generated by a topographic station along each of the three transects line, assembly them with GPS in the extreme transects points to link local data from topographic station, and world wide coordinate system (UTM). Thus, were generated a data sets that describe the elevation profile of each one of the three transect under analysis. The criteria used to take z variable using topographic station along the transect was every two meters, at least that the point has bad access, always measuring the forward movement distance along the line.

3. Methods

The three elevation profiles were generated by the use of topographic station along each transects line, assemble with GPS located in the extreme of the transect points. Thus, were generated a data sets that describe in suitable accuracy, the elevation profile of each one of the three transect under the study area using Geodesic cartographic base.

The LiDAR onboard instrument over flu the study area before the forest was clear up. The LiDAR corresponding elevation profile from those three transects were generated assisted by ArgGis software using LiDAR image file using Geodesic cartographic base.

The GPS - topographic station combination work to collect data after the forest was harvested (to reduce the ground measurements error) generate the reference ground data from the three transects. This elevation profile built from the three transects were taken from the field touching the mineral soil, scratching the trash and the branches when it was necessary (Fig. 2, Fig. 3 and Fig. 4).

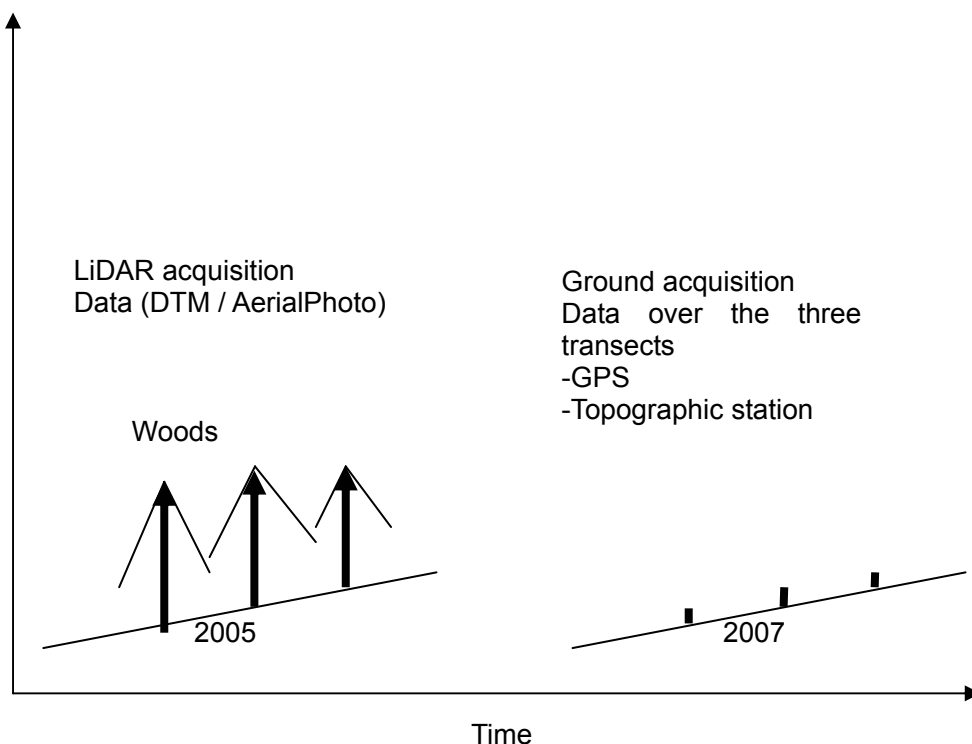


Figure 4: Scheme of data acquisition period from the study site.

4. Results

The Figures 5, 6 and 7 show the elevation profiles of the three transects, from two sources, the reference one that come from geodesic GPS, and other come from LiDAR source. We appreciate the small difference between both sources which is quantified in tables 2, 3 and 4 where it is showed the error distribution in the elevation z exe of the 3D system, where the maximum error distribution of z exe over the three transects is mostly concentrate between 0 to 1 meter. The resume table 5 shows that the 92 % of the data for all distance of the three transects (Table 4) shows an error concentrate between 0 and 1 meter. The 6 % of error is concentrate between 1 and 2 meters and 2 % between 2 and 3 meters.

The source of the error comes mostly from the upper and lowest topographic position, but we do not know the exactly reason of this error distribution.

Were taking 280 sampling points from whole three transect, which are distributed as shows following table 1.

Table 1: Sampling point distribution by transect.

| Transect number | Sampling points |
|-----------------|-----------------|
| 1 | 80 |
| 2 | 120 |
| 3 | 80 |

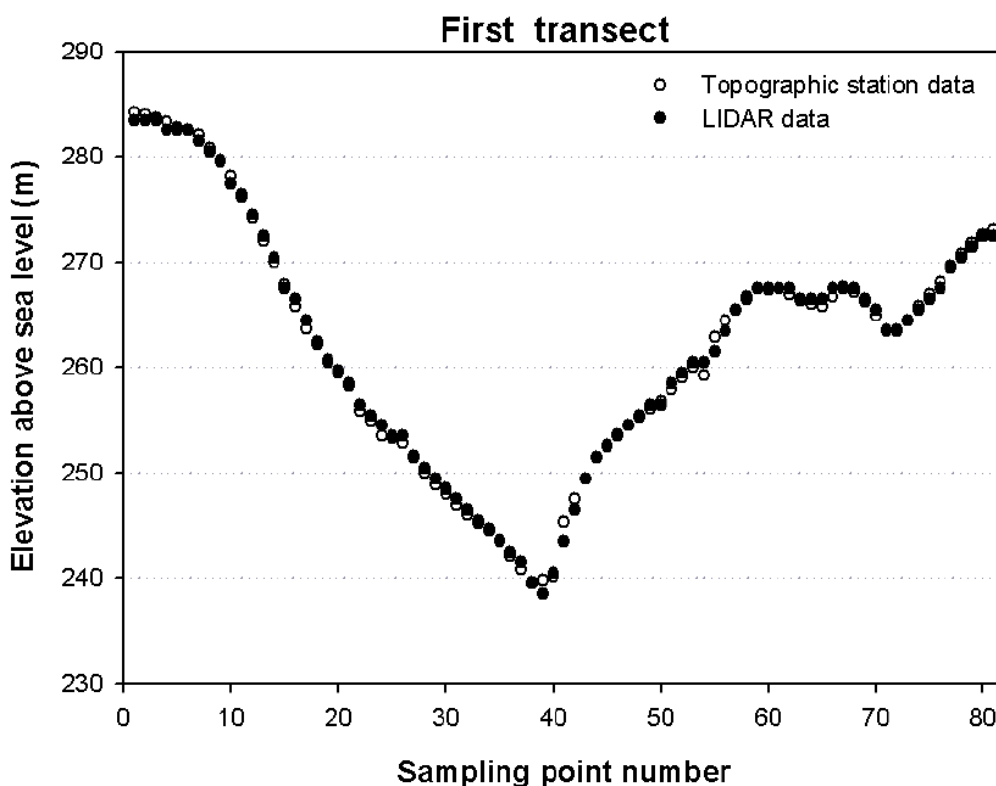


Figure 5: Elevation profile for the transect 1.

Table 2: Error distribution for transect 1.

| Error range (m) | Error distribution (%) |
|-----------------|------------------------|
| 0-1 | 93 |
| 1-2 | 7 |
| 2-3 | 0 |

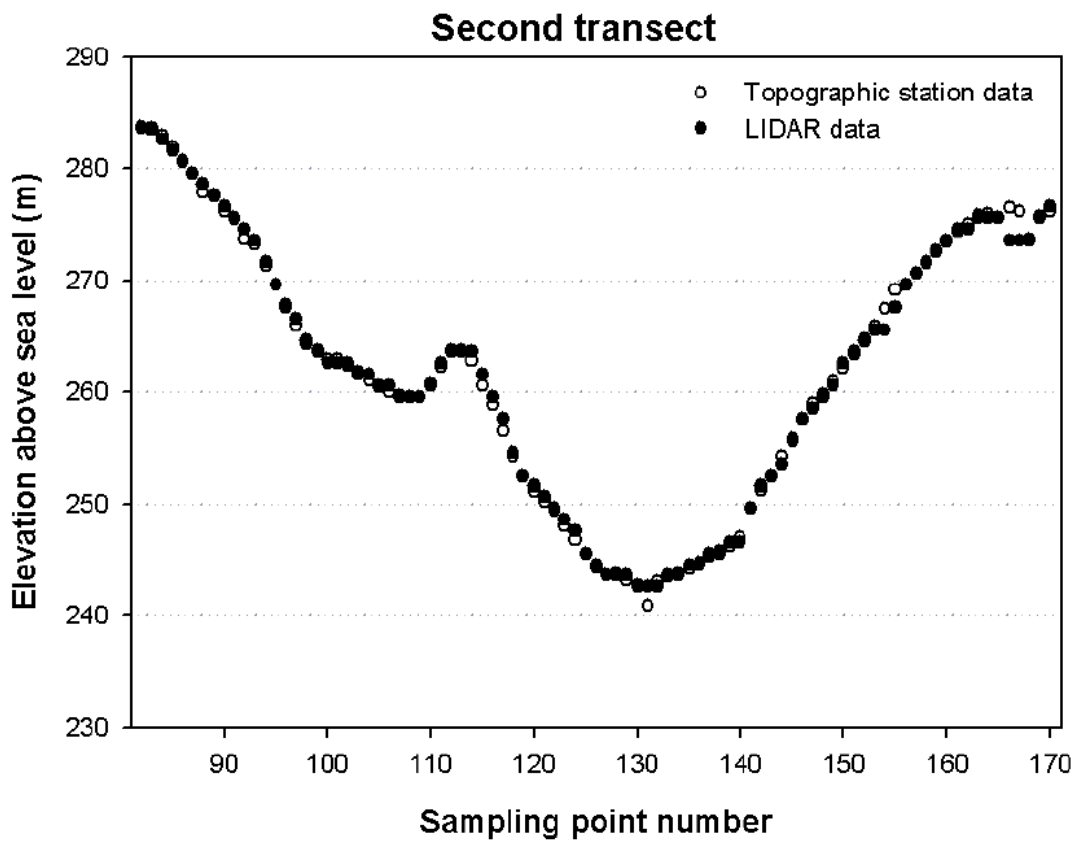


Figure 6: Elevation profile for the transect 2.

Table 3: Error distribution for transect 2.

| Error range (m) | Error distribution (%) |
|-----------------|------------------------|
| 0-1 | 93 |
| 1-2 | 5 |
| 2-3 | 2 |

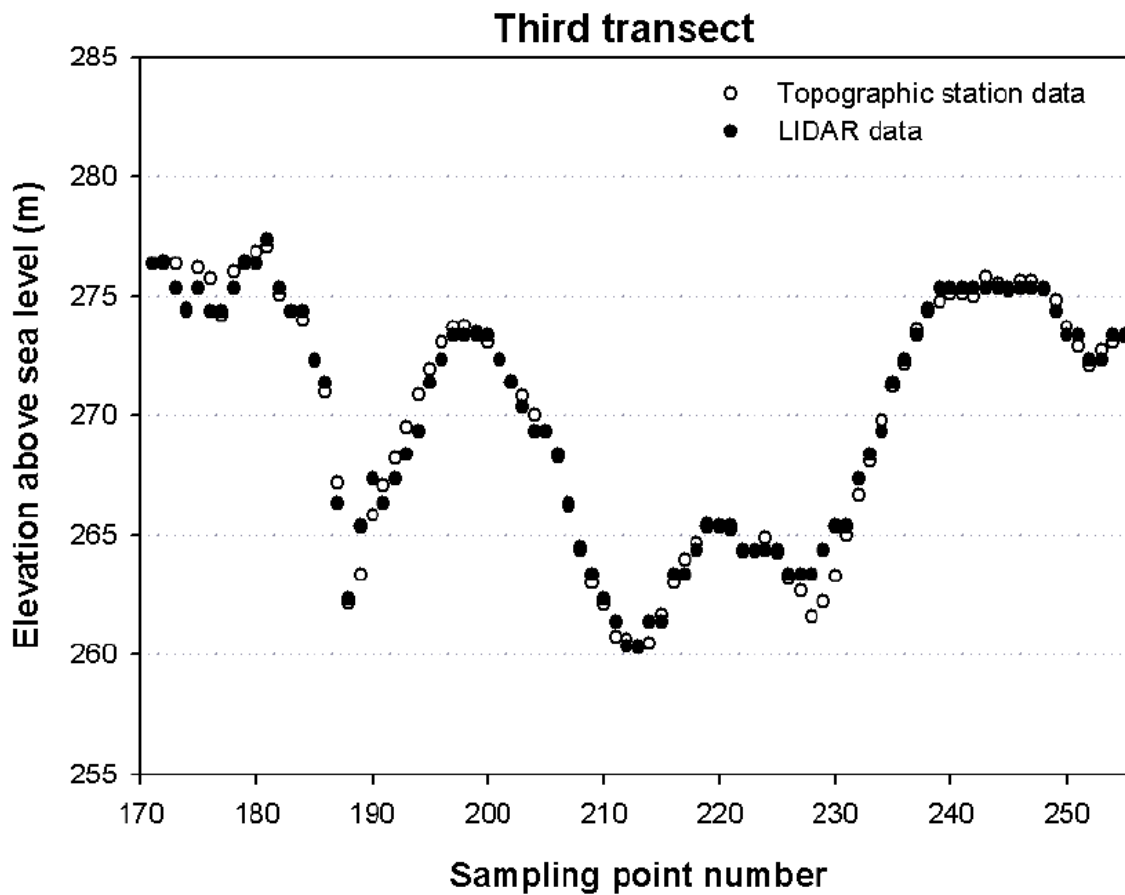


Figure 7: Elevation profile for the transect 3.

Table 4: Error distribution for transect 3.

| Error range (m) | Error distribution (%) |
|-----------------|------------------------|
| 0-1 | 91 |
| 1-2 | 6 |
| 2-3 | 3 |

Table 5: Total error distribution for the three transects.

| Error range (m) | Error distribution (%) |
|-----------------|------------------------|
| 0-1 | 92 |
| 1-2 | 6 |
| 2-3 | 2 |

5. Discussion

The results of simple statistical analyses indicate that the results were consistent and well taking. The GPS and topographic data sources are improved its quality because no forest was there at the ground measurement time. In this way we reduce the source of the errors from the ground measurements.

Others researchers work find that the effect of vegetation canopy covers which has different structure and several forest canopy levels are presented in the forest. In this case of our research, there was just one forest canopy cover planted at the same season, which has similar management and same plantation density without under canopy cover vegetation presented in there.

6. Conclusions

DTM LiDAR-derived data allow the recognition of ground morphology to assign with accuracy the forest harvest machinery allowing delineate harvest units for spatial forest planning.

References

- Cavalli Marco, Tarolli Paolo Marchi , Lorenzo and Dalla Giancarlo Fontana. 2008. The effectiveness of airborne LiDAR data in the recognition of channel-bed morphology. *Catena* 73(3).
- Glenn, N.F., Streutker, D.R., Chadwick, D.J., Thackray, G.D., Dorsch, S.J., 2006. Analysis of LiDAR-derived topographic information for characterizing and differentiating landslide morphology and activity. *Geomorphology* 73, 131-148.
- James L.A., Watson D.G. and Hansen W.F.. 2006. Using LiDAR data to map gullies and headwater streams under forest canopy: South Carolina, USA, *Catena* 71(1).
- MaKean, J., Roering, J., 2004. Objective landslide detection and surface morphology mapping using high-resolution airborne laser altimetry. *Geomorphology* 57, 331-351.
- Slatton, K.C., Carter, W.E., Shrestha, R.L., Dietrich, W.E., 2007. Airborne laser swath mapping: Achieving the resolution and accuracy required for geosurficial research. *Geophysical Research Letters* 34, L23S10 doi:10.1029/2007GL031939.
- Storesund R.and Minear J.. 2006. Evaluation of ground-based LiDAR for use in fluvial geomorphology and river restoration, *Eos Trans.* 87 (52).

Using LIDAR and Normalized Difference Vegetation Index to remotely determine LAI and percent canopy cover

Alicia M. R. Griffin¹, Sorin C. Popescu², Kanguang Zhao³

¹School of Earth and Space Exploration, Arizona State University, alicia.griffin@asu.edu

²Spatial Sciences Laboratory, Department of Ecosystem Science and Management, Texas A&M University, s-popescu@tamu.edu

³Spatial Sciences Laboratory, Department of Ecosystem Science and Management, Texas A&M University, zhaokg@tamu.edu

Abstract

The goal of this study was to use airborne LIDAR (Light Detection and Ranging) to evaluate percent canopy cover (PCC) and leaf area index (LAI) in loblolly pine forests of the southeastern United States, in order to address forest management and ecological concerns. More specific objectives were to: (1) Develop scanning LIDAR methods to estimate PCC and LAI over primarily coniferous forests; and (2) investigate whether a LIDAR and normalized difference vegetation index (NDVI) data fusion through linear regression improve estimates of these forest canopy characteristics. Scanning LIDAR data was used to derive local scale PCC estimates through use of the height bin method; then TreeVaW, a LIDAR software application, was used to locate individual trees to derive an estimate of plot-level PCC. A canopy height model (CHM) was used to determine tree heights per plot. QuickBird multispectral imagery was used to calculate NDVI. LIDAR- and NDVI-derived estimates of plot-level PCC and LAI were compared to field observations for 43 plots over 47 km². Linear regression analysis resulted in LIDAR-only models explaining 84% and 78% of the variability associated with PCC and LAI, respectively; it is concluded that LIDAR alone can be used to estimate these canopy parameters.

Keywords: LIDAR, leaf area index, percent canopy cover, forest inventory

1. Introduction

Leaf area index (LAI) and percent canopy cover (PCC) are important biophysical and ecophysical factors in addressing forest management issues such as fuel models and forest inventory, and ecological concerns including carbon sequestration and climate change. LAI is defined as one-sided leaf area per unit ground surface area (Chapin *et al.* 2002), while PCC is defined as the percent of a forest area occupied by the vertical projections of tree leaves (Avery and Burkhart 1994). LAI is especially important to ecological processes such as photosynthesis and net primary production (Coops *et al.* 2004), while PCC, also called canopy cover, is important in assessing canopy structure. PCC has grown in importance as a result of the needs to quantify the global woody biomass, quantify global carbon stocks and globally assess the condition of ecosystems (Hansen *et al.* 2002). Determining this information through remote sensing methods is an efficient and effective way to model such processes.

Field, or *in situ*, measurements of LAI and canopy cover are necessary to validate remotely sensed values. Direct methods of estimating LAI include destructive sampling of the forest canopy, leaf litterfall collection and vertical point-quadrant sampling (Duranton *et al.* 2001). Indirect methods, less time-consuming than direct methods, range from employing a spherical densiometer, which is dependent on human intuition and level of experience (Englund *et al.* 2000), to plant canopy analyzers such as the Li-COR LAI-2000, to hemispherical photography (Riaño *et al.* 2004). This study employs hemispherical photography analysis because it is a precise and less time-consuming data collection process; however, it has been shown to

underestimate field values of LAI (Mussche *et al.* 2001; Merilo *et al.* 2004; Jonckheere *et al.* 2005).

Previous studies have related multispectral imagery to forest canopy characteristics. Landsat ETM+ satellite data can be used to accurately predict LAI for coniferous forests by direct plot-level correlation and geostatistical analysis (Berterretche *et al.* 2005). Another study (Schlerf and Atzberger 2006) examined the use of hyperspectral remote sensing data to predict LAI, with an R^2 value of 0.73 relative to ground measurements. The normalized difference vegetation index (NDVI) calculated from Landsat TM data has been used, either singly or in combination with other indices, to estimate LAI (Curran *et al.* 1992; Pocewicz *et al.* 2004) as can other vegetation indices (Baret and Guyot 1991).

LIDAR remote sensing has become more widely used and accepted in ecological and forest inventory studies in recent years (Nelson *et al.* 1984; Means *et al.* 2000; Lefsky *et al.* 2002; Reutebuch *et al.* 2005). Small-footprint laser scanners have been successfully used to predict mean tree height, with one regression explaining 83% of the variability in ground-truth mean tree height (Naesset and Bjerknæs 2001; Naesset 2004). Waveform LIDAR has been shown to predict 75% of the variability in LAI in Douglas-fir and western hemlock forests (Lefsky *et al.* 1999). Airborne scanning LIDAR has also been shown to be accurate in estimating biophysical parameters of forest stands (Popescu *et al.* 2004), and to be an excellent predictor of hemispherical photography-estimated LAI and PCC (Riaño *et al.* 2004). Scanning LIDAR was also found to have a strong correlation with hemispherical photo-estimated LAI (Lovell *et al.* 2003). Most recently, Morsdorf *et al.* (2006) used small-footprint airborne laser scanning data to predict fractional canopy cover and LAI, with R^2 values of 0.73 and 0.69, respectively.

Percent canopy cover can be found at the plot or stand level by examining tree locations and crown dimensions. Crown radius models have been used to accurately estimate non-overlapping canopy cover. Gill *et al.* (2000) used ordinary least-squares linear regression equations to calibrate canopy cover values derived from forest inventory data; their model had an R^2 value of 0.67. Roberts *et al.* (2005) estimated individual tree leaf area through linear regression between ground data and LIDAR-derived estimates of tree height and crown dimensions, finding that leaf area was consistently underestimated. A LIDAR-derived canopy height model (CHM) can be processed to accurately identify individual trees and their heights in forest or rangeland, as shown in studies, some using the local maximum focal filtering software program TreeVaW (Popescu *et al.* 2002; Popescu and Wynne 2004; Koch *et al.* 2006).

This study attempts to relate scanning LIDAR data to *in situ* LAI and PCC values through simple linear regression with NDVI. LIDAR height bins, the products of a LIDAR processing technique that breaks the vertical forest structure into viewable “slices,” are utilized as an innovative method of calculating PCC and LAI (Popescu and Zhao 2008). Theoretically, the combination of LIDAR-estimated canopy characteristics such as height and PCC with vegetation indices will result in an accurate predictor of LAI and PCC.

The goal of this study was to develop a use of LIDAR in evaluating percent canopy cover and leaf area index of primarily pine and mixed pine-hardwood forests typical of the southeastern United States. Specific objectives were to:

- (1) Develop scanning LIDAR methods to estimate PCC and LAI over primarily pine forests in East Texas; and
- (2) use multiple linear regressions to predict PCC and LAI using LIDAR and NDVI.

2. Study Site and Data Collection

2.1 Study Area

The study area is located in the southern United States (30°42'N, 95°23'W), in East Texas. It includes a portion of the Sam Houston National Forest, characterized by deciduous and pine stands with an urban interface and an area of 47.45km². The study area is composed of 28.08km² (59.17%) of pine forest (primarily loblolly pine, *Pinus taeda*), 10.84km² (22.84%) of deciduous forest, and 8.54km² (17.99%) of non-forested areas including urban areas, agricultural fields, etc. The average diameter at breast height (DBH) is 31cm, average tree height is 20m, average crown diameter is 5.9m and the average height to crown base is 11.8m. A mean elevation of 85m, with a minimum of 62m and a maximum of 105m, and gentle slopes characterize the topography of the study area.

The ground reference data were collected between May 2004 to July 2004 by photographing canopy characteristics on 53 evenly distributed circular plots of which 35 covered 404.7m² (0.1 acre) and 18 covered 40.5m² (0.01 acre). The 18 smaller plots were in areas of young pine plantations, with little variation of tree height or crown width. A hemispherical photograph of the forest canopy was taken from the center of each plot and each plot was mapped by recording GPS coordinates for the plot center.

2.2 Hemispherical Photographs for Ground Reference Data

A hemispherical photograph of the forest canopy was taken from the center of each plot at 1.5m above ground level (resolution of 3264×2448 pixels) using a horizontally-leveled Nikon CoolPix 8700 digital camera and a FC-E9 fisheye lens. Ten plot photographs contained sun glare and other non-uniformities due to various light conditions at the photograph cell and proximity of clearings to the plots, and were removed from the analysis. Of the remaining 43 plots, 35 plots were in loblolly pine forest, 5 plots were in hardwood stands, and 4 plots were in mixed forest. Thus the results of this study will be most applicable to loblolly pine forest. The photographs were analyzed for plot-level PCC and LAI using HemiView Canopy Analysis Software (©Delta-T Devices Ltd., UK).

LAI was estimated by HemiView algorithms to be half of the total leaf area per unit ground surface area, based on the ellipsoidal leaf angle distribution. The HemiView calculation of LAI (LAI_{obs}) is based on Beer's Law:

$$G(\theta) = e^{(-K(\theta) \times LAI_{obs})} \quad (1)$$

where G is gap fraction and $K(\theta)$ is the extinction coefficient at zenith angle θ (range computed for the canopy during processing). HemiView measures gap fraction values directly from the hemispherical photo, then finds the values for the extinction coefficient and LAI that best fit for an ellipsoidally distributed theoretical canopy, then applies those values in subsequent calculations. HemiView-calculated LAI is termed "effective LAI" as it does not account for non-random distribution of foliage, possibly underestimating actual LAI.

In HemiView, PCC is defined as the vertically projected canopy area per unit ground area. It is calculated as follows assuming the canopy has an ellipsoidal leaf angle distribution:

$$PCC_{obs} = \left[1 - e^{(-K(x,0) \times LAI_{obs})} \right] \times 100 \quad (2)$$

where $K(x,0)$ is the extinction coefficient for a zenith angle of zero and x is the ellipsoidal leaf angle distribution parameter, defined as the ratio between the semihorizontal and semivertical

axes of an ideal ellipsoid.

2.3 LIDAR Data

LIDAR data for the study area was collected in March 2004, during the leaf-off season, from an average of 1000m above ground level by M7 Visual Intelligence of Houston, Texas. The LIDAR system (Leica ALS40 Airborne Laser Scanner, Atlanta, GA, USA) records first and last returns per laser pulse and has horizontal and vertical accuracies of 20-30cm and 15cm, respectively. The LIDAR system provided a 10° swath from nadir for a total scan angle of 20°, resulting in a point density of 2.6 points/m² (distance between laser points is thus 0.62m). The average swath width was 350m, with 19 north-south flight lines and 28 east-west flight lines. LIDAR point elevations were interpolated to form a digital surface model with a spatial resolution of 0.5m, with only the highest laser hits per 0.5m x 0.5m cells being used in the interpolation to better characterize the top canopy surface using techniques described by Popescu and Wynne (2004). The CHM, a three-dimensional model of vegetation height with a resolution of 0.5m, was created by subtracting ground elevation from the digital surface model. The CHM was interpolated to a cell size of 2.5m prior to any calculations.

Though the LIDAR data was collected during the leaf-off season, this was not expected to adversely impact the PCC and LAI estimates. The majority of the study area plots (34) were pine stands, thus retaining foliage during the leaf-off season. However, scanning LIDAR pulses would still be returned from large and small branches on hardwood and mixed stands during the leaf-off season; the pulses “lost” due to the lack of leaves would be negligible (Nelson 2006).

2.4 NDVI Values from a QuickBird Image

Multispectral, orthorectified QuickBird imagery (leaf-off, 2004; DigitalGlobe, Longmont, CO, USA) was available for the study area as well with a resolution of 2.5m. These data were used to calculate NDVI as defined by Baret and Guyot (1991):

$$NDVI = \frac{(NIR - R)}{(NIR + R)} \quad (3)$$

where *NIR* is the near-infrared reflectance value and *R* the red reflectance value for a given pixel.

3. Methods

3.1 Percent Canopy Cover Estimates from LIDAR Data

Three distinct methods were employed to derive PCC from LIDAR data: two involving the use of height bins and one that determines tree locations from the CHM. Height bins are the products of an original LIDAR processing technique that breaks the vertical forest structure into viewable “slices;” this technique is an emerging method of using LIDAR data in forest inventory (Popescu and Zhao 2008). Height bins are created by subdividing normalized laser point returns into intervals defined by a range of heights. Laser points in each height interval are normalized to percentages by the total number of points above the projected ground area of each pixel. Percentages of laser canopy hits are considered to be especially appropriate for LIDAR estimation of canopy properties (Riaño *et al.* 2004). For this study, eleven height bins were generated through software developments described by Popescu and Zhao (2008), with height ranges of 0-0.5m, 0.5-1.0m, 1.0-1.5m, 1.5-2.0m, 2.0-5.0m, 5.0-10m, 10-15m, 15-20m, 20-25m, 25-30m, and >30m. These height bins were generated as a multiband image of the predefined

height intervals and $2.5\text{m} \times 2.5\text{m}$ pixel dimensions.

Two estimates of PCC were derived from the bins. The first method assumes that the crowns of interest belong to trees with a height of over 2.0m; a sum of the seven uppermost height bins (HB_5 through HB_{11}) is used to model PCC:

$$PCC_{lidar,5-11} = \sum_5^{11} HB_n \quad (4)$$

where HB_n is a height bin image band of number n .

The second method assumes that any laser point that is returned from on or near the ground, i.e. HB_1 , was from a pulse that did not encounter a canopy obstruction. Therefore, the equation used to derive PCC is as follows:

$$PCC_{lidar,1} = 1.0 - HB_1 \quad (5)$$

where notation is the same as in Equation 4.

The third method of deriving PCC from LIDAR data was performed at the plot level only. Individual trees were located and their crowns measured on the LIDAR-derived CHM through automated processing with TreeVaW software. TreeVaW is an IDL-executable program (Interactive Data Language, ©2006, ITT Industries Inc., USA) that uses a continuously varying filter window to detect tree locations, tree heights and crown radii, with algorithms described in Popescu and Wynne (2004) and Popescu *et al.* (2004). In summary, TreeVaW software identifies single trees using an adaptive technique for local maximum focal filtering, operating on the assumption that laser values of high elevation in a spatial neighborhood represent the highest part of a tree crown.

TreeVaW was used to identify individual tree locations and crown size for each field plot. The total projected crown area for each plot is (A_{crown}) calculated; TreeVaW-derived PCC is:

$$PCC_{trvw} = \frac{A_{crown}}{A_{plot}} \quad (6)$$

where A_{plot} is the total plot area.

3.2 Statistical Analysis of Predictions

SAS software (SAS Institute, Inc., Cary, NC, USA) was used to relate various LIDAR-derived variables and NDVI variables to plot-level observed values of PCC and LAI. Least-squares estimates of PCC and LAI were fitted to linear regression models for eight different datasets, including varying combinations of the independent variables. Stepwise selection was employed in each regression to determine the variables remaining in each model. Variables retained in each regression were significant at the 0.05 level.

Finally, two simple linear regressions were performed to directly compare observed PCC and LAI (PCC_{obs} and LAI_{obs}) with LIDAR-derived PCC using Height Bins 5-11 ($x_{PCC_{lidar,5-11}}$). These regressions were performed using Microsoft Excel software (Microsoft Corporation, Redmond, WA, USA), in order to determine how well a single LIDAR-derived parameter could predict both PCC and LAI.

4. Results and Discussion

4.1 Results

LIDAR-estimated PCC variables using Height Bins 5-11 are present in the models with the greater coefficients of determination, while the models incorporating TreeVaW-derived PCC values have the lowest coefficients of determination. The model with the highest R^2 value for PCC used LIDAR-estimated PCC (Height Bins 5-11), NDVI variables and CHM variables; this model had an R^2 value of 0.86 as well as a low RMSE value (9%). However, a PCC model using only LIDAR-derived variables had an R^2 value of 0.84 and an identical RMSE value. It can be concluded that the NDVI variables are relatively unimportant in predicting PCC when compared to LIDAR-derived variables. The model selected to predict PCC is thus:

$$PCC_{pred} = 0.01 + 0.93x_{PCClidar,5-11} + 0.01X_{chm} - 0.01x_{chm} . \quad (7)$$

Where PCC_{pred} is the predicted value of PCC, $x_{PCClidar,5-11}$ is the mean of LIDAR-derived PCC using Height Bins 5-11, X_{chm} is the maximum value of the CHM and x_{chm} is the mean value of the CHM.

The strongest LAI model was found using the first regression method with LIDAR-derived (Height Bins 5-11) variables only; this model has an R^2 value of 0.78 and a comparatively low RMSE value. The prediction models incorporating both LIDAR and NDVI variables in general have higher coefficients of determination than those using only LIDAR-derived values, but by such a small range as to be negligible. Thus, LIDAR variables can be used without NDVI information to predict PCC and LAI. The model selected to predict LAI is:

$$LAI_{pred} = 0.05 + 3.47x_{PCClidar,5-11} \quad (8)$$

Where LAI_{pred} is the predicted value of LAI and $x_{PCClidar,5-11}$ is the mean of LIDAR-derived PCC using Height Bins 5-11.

When plotting LAI_{pred} against observed values of LAI (LAI_{obs}), a square root transformation was applied to LAI_{obs} to compensate for a slightly curvilinear relationship (Figure 1a); the transformation found a linear relationship with a high coefficient of determination ($R^2 = 0.85$). The coefficient of determination for the untransformed variable (LAI_{obs}) was calculated as well and found to be 0.75. The regression results for PCC_{pred} and LAI_{pred} compare well to other studies. Riaño *et al.* (2004) attained coefficients of determination of approximately 0.75 for PCC and approximately 0.90 for LAI and concluded that LIDAR was an excellent measure of both. Scanning LIDAR was found to have a strong correlation with hemispherical photo-estimated LAI in the study of Lovell *et al.* (2003), returning R^2 values between 0.77 and 0.98.

When comparing observed field values to the selected model-predicted values (Figure 1a), it is seen that LIDAR-derived estimates slightly overestimate both PCC and LAI. This is consistent with the aforementioned studies and is possibly influenced by the small number of plots with low LAI values. Another possible source of error is that LIDAR data was collected during the leaf-off season while ground-reference data was collected during the leaf-on season. The majority of ground plots, 34 plots out of the total 43, were in pine plantations or pine stands and thus the majority of trees would have retained their needles for both the LIDAR and field data collections.

The simple linear regression results between observed PCC and LAI (PCC_{obs} and LAI_{obs}) and

LIDAR-derived PCC using Height Bins 5-11 ($x_{PCC_{lidar,5-11}}$) are promising, with r^2 values of 0.80 and 0.85 and RMSE values of 9.29% and 7.86% for PCC_{obs} and $SQRT(LAI_{obs})$, respectively. A square root transformation was again used to correct a curvilinear LAI_{obs} relationship to a linear relationship with LIDAR-derived PCC values (Figure 1b). The equations describing these LIDAR-predicted canopy characteristics (PCC_{pred_lidar} and LAI_{pred_lidar}) are:

$$PCC_{pred_lidar} = 0.95x_{PCC_{lidar,5-11}} + 1.42 \quad (9)$$

$$LAI_{pred_lidar} = [0.02x_{PCC_{lidar,5-11}} + 0.45]^2 \quad (10)$$

4.2 Discussion

LIDAR-predicted PCC and LAI are comparable in accuracy to the selected regression models. These models are even preferable in the long term because of their simplicity. It is interesting to note that the TreeVaW-derived PCC was removed through stepwise selection and thus not present in the final regression model, though TreeVaW software has performed well in related studies (Popescu and Wynne 2004; Popescu and Zhao 2008). One possible explanation for TreeVaW's lack of performance in the current study is that its continuously varying filter window identifies only dominant and co-dominant trees, while hemispherical photography captures understory vegetation in addition to the taller tree crowns. TreeVaW processing of a LIDAR-derived CHM, while an effective way to locate individual trees and determine tree crown dimensions, was not an accurate method of determining plot-level PCC.

Estimation of forest structural attributes is one of the more thoroughly pursued applications of LIDAR remote sensing (Lefsky et al. 2002; Riaño et al., 2004). One goal of this study was to develop a linear regression relating LIDAR data and multispectral imagery to ground-reference values of PCC and LAI for hardwood and pine forests. Linear regression analysis of LIDAR variables explains 84% of the variance associated with plot-level PCC and 78% of the variance for plot-level LAI. A second objective was to evaluate whether LIDAR and NDVI data fusion would improve estimates of PCC and LAI. While data fusion did improve PCC model coefficients of determination by 2%, this was not a great enough improvement to justify retaining NDVI variables in the final PCC prediction model. LAI regression models were unaffected by the inclusion of NDVI variables; LIDAR-derived parameters alone were a good predictor of plot-level LAI. In the process of investigating linear regression analysis, it was found that LIDAR-derived PCC had an excellent relationship to field values of PCC and LAI. Simple linear regressions related LIDAR-derived PCC to field values of PCC and LAI, an exciting development for future ecological studies in primarily loblolly pine forests. Using LIDAR to directly determine these canopy properties would make the process accurate and efficient. Finally, the overall objective of this study was to develop a use of LIDAR in evaluating forest canopy parameters such as PCC and LAI. Results clearly show that scanning LIDAR data can be used to accurately estimate PCC and LAI.

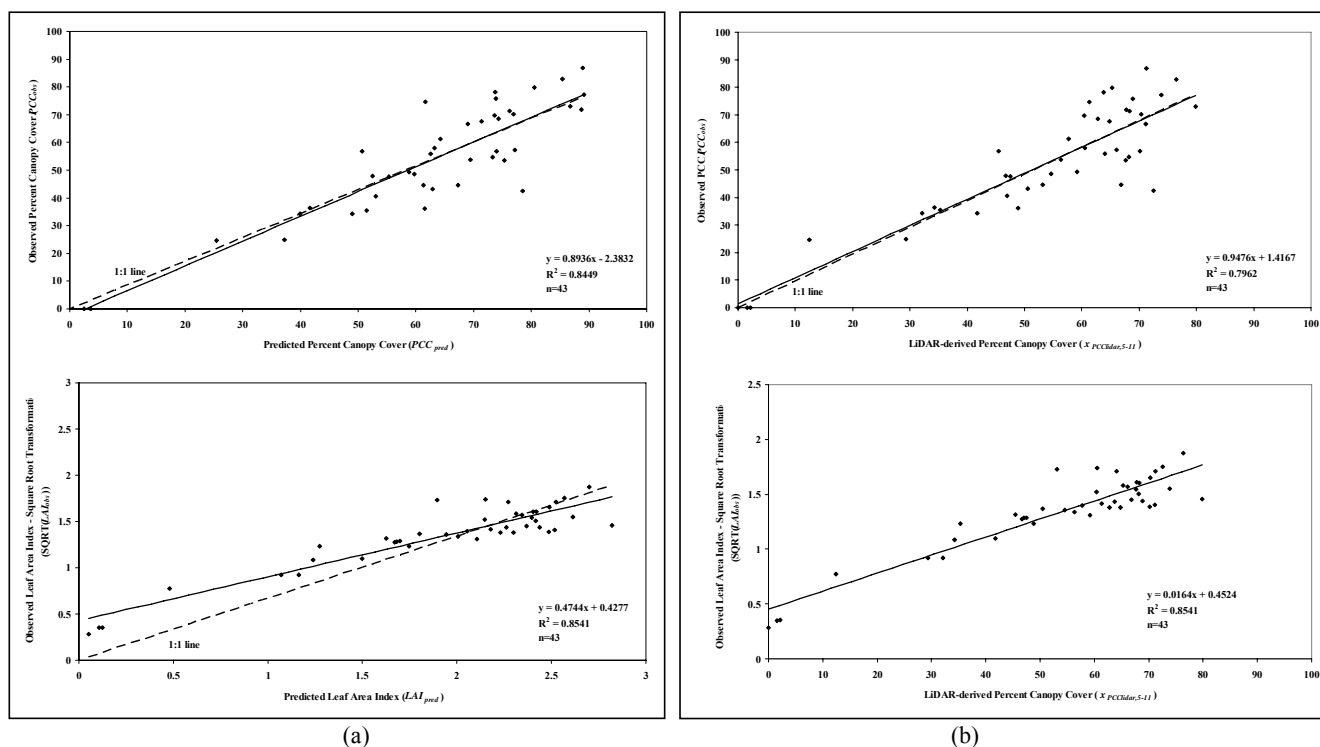


Figure 1: (a) Observed percent canopy cover (PCC) and leaf area index (LAI) compared to predicted PCC and LAI.
 (b) Observed percent canopy cover (PCC) and leaf area index (LAI) compared to LIDAR-derived PCC.

LIDAR data processing by the height bin method, as used in this study, has the potential to become a standardized method of large-scale LIDAR forestry data processing. This approach was shown to be effective and accurate in predicting PCC and LAI in this study and has also been used in a study concerning mapping surface forest fuels (Mutlu *et al.* 2008). The height bin method has also been used in conjunction with TreeVaW processing to estimate biophysical parameters of individual trees, such as total tree height, crown width, and height to crown base (Popescu and Zhao 2008).

Determining ground reference values of LAI using hemispherical photography immediately introduced the possibility of underestimating these values (Merilo *et al.* 2004), although other indirect methods of measuring LAI tend to underestimate it as well (Mussche *et al.* 2001; Bréda 2003). In the future it may be helpful to determine a scale for LAI values, to calibrate them with direct measurements and compensate for clumping factors (Bréda 2003; Coops *et al.* 2004). Doing so may increase the agreement between the estimated LAI and ground reference values.

5 Conclusions

Our approach is unique in that it combines LIDAR estimates of PCC derived from height bins with a LIDAR-based CHM to estimate forest canopy characteristics through regression analysis. This method proved to be an accurate estimate of plot-level PCC and LAI, allowing us to predict these values at a local scale. PCC and LAI are important biophysical parameters in carbon sequestration and climate studies. Since LIDAR data can be acquired fairly quickly compared to ground-level forest inventory, our method could allow for fast, accurate, more effective ecological research as well as forest management.

References

- Avery, T.E. and Burkart, H. E., 1994. *Forest Measurements, 4th Ed.* New York: McGraw-Hill, Inc.
- Baret, F. and Guyot, G., 1991. Potentials and limits of vegetation indices for LAI and APAR assessment. *Remote Sensing of Environment*, 35, 161-173.
- Berterretche, M., Hudak A.T., Cohen W.B., Maier-sperger, T.K., Gower, S.T. and Dungan, J., 2005. Comparison of regression and geostatistical methods for mapping Leaf Area Index (LAI) with Landsat ETM+ data over a boreal forest. *Remote Sensing of Environment*, 96, 49-61.
- Bréda, N.J.J., 2003. Ground-based measurements of leaf area index: a review of methods, instruments and current controversies. *Journal of Experimental Botany*, 54 (392), 2403-2417.
- Chapin, F.S., Matson, P.A. and Mooney, H.A., 2002. *Principles of Terrestrial Ecosystem Ecology.* (p.108) New York: Springer Science and Business Media, Inc.
- Coops, N.C., Smith, M.L., Jacobson, K.L., Martin, M. and Ollinger, S., 2004. Estimation of plant and LAI using 3 techniques in a mature native eucalypt canopy. *Austral Ecology*, 29, 332-341.
- Curran, P.J., Dungan, J.L. and Gholz, H.L., 1992. Seasonal LAI in slash pine estimated with Landsat TM. *Remote Sensing of Environment*, 39, 3-13.
- Duranton, H., Soudani, K., Trautmann, J. and Walter, J., 2001. Comparison of optical methods for estimating canopy openness and leaf area index in broad-leaved forests. *Comptes Rendus de l'Académie des Sciences*, 324(4), 381-392.
- Englund, S.R., O'Brien, J.J. and Clark, D.B., 2000. Evaluation of digital and film hemispherical photography and spherical densiometry for measuring forest light environments. *Canadian Journal of Remote Sensing*, 30, 1999-2005.
- Gill, S.J., Biging, G.S., and Murphy, E.C., 2000. Modeling conifer tree crown radius and estimating canopy cover. *Forest Ecology and Management*, 126, 405-416.
- Hansen, M.C., DeFries, R.S., Townshend, J.R.G., Sohlberg, R., Dimiceli, C., and Carroll, M., 2002. Towards an operational MODIS continuous field of percent tree cover algorithm: Examples using AVHRR and MODIS data. *Remote Sensing of Environment*, 83, 303-319.
- Jonckheere, I., Muys, B., and Coppin, P., 2005. Allometry and evaluation of in situ optical LAI determination in Scots pine: A case study in Belgium. *Tree Physiology*, 25, 723-732.
- Koch, B., Heyder, U. and Weinacker, H., 2006. Detection of individual tree crowns in airborne LIDAR data. *Photogrammetric Engineering and Remote Sensing*, 72(4), 357-363.
- Lefsky, M.A., Cohen, W.B., Acker, S.A., Spies, T.A., Parker, G.G., and Harding, D., 1999. Lidar remote sensing of biophysical properties and canopy structure of forest of Douglas-fir and western hemlock. *Remote Sensing of Environment*, 70, 339-361.
- Lefsky, M.A., Cohen, W.B., Parker G.G., and Harding, D.J., 2002. LIDAR remote sensing for ecosystem studies. *BioScience*, 52(1), 19-30.
- Lovell, J.L., Jupp, D.L.B., Culvenor, D.S. and Coops, N.C., 2003. Using airborne and ground-based ranging LIDAR to measure canopy structure in Australian forests. *Canadian Journal of Remote Sensing*, 29, 607-622.
- Means, J.E., Acker, S.A., Fitt, B.J., Renslow, M., Emerson, L. and Hendrix, C., 2000. Predicting forest stand characteristics with airborne scanning LIDAR. *Photogrammetric Engineering and Remote Sensing*, 66(11), 1367-1371.
- Merilo, E., Heinsoo, K. and Koppel, A., 2004. Estimation of leaf area index in a willow plantation. *Proceedings of the Estonian Academy of Sciences, Biology, Ecology*, 53(1), 3-13.
- Morsdorf, F., Kötz, B., Meier, E., Itten, K.I., and Allgöwer, B., 2006. Estimation of LAI and fractional cover from small footprint airborne laser scanning data based on gap fraction. *Remote Sensing of Environment*, 104, 50-61.
- Mussche, S., Samson, R., Nachtergale, L., De Schrijver, A., Lemeur, R. and Lust, N., 2001. A

- comparison of optical and direct methods for monitoring the seasonal dynamics of leaf area index in deciduous forests. *Silva Fennica* 35(4), 373-385.
- Mutlu, M., Popescu, S.C., Stripling, C. and Spencer, T., 2008. Mapping surface fuel models using LIDAR and multispectral data fusion for fire behavior. *Remote Sensing of Environment*, 112 (1): 274-285.
- Naesset, E. and Bjercknes, K., 2001. Estimating tree heights and number of stems in young forest stands using airborne laser scanner data. *Remote Sensing of Environment*, 78, 328-340.
- Naesset, E., 2004. Practical large-scale forest stand inventory using a small-footprinting airborne scanning laser. *Scandinavian Journal of Forest Research*, 19, 164-179.
- Nelson, R., Krabill, W. and MacLean, G., 1984. Determining forest canopy characteristics using airborne laser data. *Remote Sensing of Environment*, 15, 201-212.
- Nelson, R., 2006. Personal communication, properties of scanning LIDAR. Sept. 29, 2006.
- Pocewicz, A.L., Gessler, P. and Robinson, A.P., 2004. The relationship between effective plant area index and Landsat spectral response across elevation, solar insolation, and spatial scales in a northern Idaho forest. *Canadian Journal of Remote Sensing*, 34, 465-480.
- Popescu, S.C. and Wynne, R.H., 2004. Seeing the trees in the forest: using LIDAR and multispectral data fusion with local filtering and variable window size for estimating tree height. *Photogrammetric Engineering and Remote Sensing*, 70(5), 589-604.
- Popescu, S.C., Wynne, R.H. and Scrivani, J.A., 2004. Fusion of small-footprint LIDAR and multispectral data to estimate plot-level volume and biomass in deciduous and pine forests in Virginia, USA. *Forest Science*, 50, 551-565.
- Popescu, S.C., Wynne, R.H., and Nelson, R.H., 2002. Estimating plot-level tree heights with LIDAR: local filtering with a canopy-height based variable window size. *Computers and Electronics in Agriculture*, 37(1-3), 71-95.
- Popescu, S.C. and Zhao, K., 2008. A voxel-based LIDAR method for estimating crown base height for deciduous and pine trees. *Remote Sensing of Environment* 112(3):767-781.
- Reutebuch, S.E., Anderson, H. and McGaughey, R.J., 2005. Light Detection and Ranging (LIDAR): An emerging tool for multiple resource inventory. *Forest Science*, 103(6), 286-292.
- Riaño, D., Valladares, F., Condés, S. and Chuvieco, E., 2004. Estimation of leaf area index and covered ground from airborne laser scanner (LIDAR) in two contrasting forests. *Agricultural and Forest Meteorology*, 124, 269-275.
- Roberts, S.D., Dean, T.J., Evans, D.L., McCombs, J.W., Harrington, R.L., and Glass, P.A., 2005. Estimating individual tree leaf area in loblolly pine plantations using LIDAR-derived measurements of height and crown dimensions. *Forest Ecology & Management*, 213, 54-70.
- Schlerf, M. and Atzberger, C., 2006. Inversion of a forest reflectance model to estimate structural canopy variables from hyperspectral remote sensing data. *Remote Sensing of Environment*, 100, 281-294.

Using airborne LiDAR and Landsat data to derive biomass at regional scale in the Canadian northern boreal forest

L. Guindon¹, A. Beaudoin¹, R. Nelson² and J. Boudreau³

¹Canadian Forest Service - Laurentian Forestry Centre, Québec, Canada
e-mail: lguindon@cfl.forestry.ca

²Biospheric Sciences Branch, NASA Goddard Space Flight Center, Greenbelt, Maryland, USA

³Département des Sciences du Bois et de la Forêt, Université Laval, Québec, Canada

Abstract

Aboveground biomass information of the northern boreal forests of Canada is required to report on the state of Canada's forests. This information need is being partly met through the recent completion of a satellite land cover map over the forested areas of Canada, an initiative of the Earth Observation for Sustainable Development of Forests (EOSD) project supported by the Canadian Space Agency. Within the EOSD framework, a biomass mapping strategy based on the integration of field and multi-sensor / multi-resolution satellite data has been developed. It includes a biomass mapping method that has been tested successfully for coniferous forests over three northern pilot regions. This method estimates biomass using optical high spatial resolution imagery (HSRI), such as QuickBird, providing surrogate sampling plots (SSP) to compensate for the lack of forest inventories. HSRI-derived SSP are subsequently scaled across a Landsat mosaic using the kNN algorithm for regional mapping purposes. However, HSRI shows significant spectral limitations to estimate biomass for all northern boreal cover types as well as sampling design issues for large-scale implementation.

In this paper, we consider profiling airborne lidar data as a newer and viable alternative to HSRI data due to the strong potential to estimate biomass operationally for a wide variety of cover types over long stretches of northern boreal forests. We describe a lidar-based biomass mapping method and present preliminary results obtained over a northern pilot region in Quebec. This region is covered by a normalized mosaic of 11 Landsat scenes and includes hundreds of ground sampling plots (GSP). We used the portion of the NASA PALS (Portable Airborne Lidar System) data set crossing the pilot region, made of four long transects containing over 4 million PALS lidar pulses acquired at a nominal post spacing of 0.25 m. The PALS data set was acquired in 2005 within the NASA Québec Carbon Lidar Project (QCLP).

First, biomass is derived from PALS transect data to provide SSP. Quadratic mean height (QMH) is extracted from PALS data within contiguous 30m cells along the PALS transects. Biomass is estimated across these cells using QMH as a predictor of biomass through regression equations developed using GSP within the QCLP project. Few hundreds of these 30m biomass cells are used in a sampling process to generate SSP. Second, lidar-derived SSP are scaled across the normalized mosaic of Landsat TM/ETM data using the kNN algorithm used operationally for inventory applications in Sweden and Finland. Finally error estimates (bias and RMSE) are obtained through cross-validation using SSP or directly from GSP.

We present preliminary results mainly for the dominating coniferous black spruce forests. At local level, good estimates of biomass were achieved using PALS data with R^2 up to 60 % and RMSE down to 14.2 t/ha depending on the QMH-biomass equation used. At regional level, R^2 better than 50% and RMSE around 25-30 t/ha were obtained using kNN algorithm driven by

lidar-derived SSP. Errors were slightly higher than using the HRSI-based method but were still satisfactory towards implementation. We also present the potential of the lidar-based method in deciduous and mixed stands. Finally we discuss the overall merits and drawbacks of the lidar-based vs the HRSI-based methods, as well as perspectives for large-scale implementation.

Utilization of tree species stratum data in forest planning simulations

Markus Holopainen¹, Antti Mäkinen¹, Mikko Vastaranta¹, Jussi Rasinmäki¹, Juha Hyyppä², Hannu Hyyppä³ and Petri Rönnholm³

¹University of Helsinki, Department of Forest Resource Management,
markus.holopainen@helsinki.fi, antti.makinen@helsinki.fi,
mikko.vastaranta@helsinki.fi, jussi.rasinmaki@helsinki.fi

²Finnish Geodetic Institute, juha.hyyppa@fgi.fi

³Helsinki University of Technology, hannu.hyyppa@tkk.fi, petri.ronnholm@tkk.fi

Abstract

The objective here was to investigate the theoretical benefit of using tree species stratum forest inventory data instead of stand-level mean data in forest-planning simulations. This comparison was based on timing differences in thinning and clear-cuttings during a 20-year simulation period. The development of stand characteristics (age, basalarea, volume, dominant height, mean height, mean diameter) in those stands not harvested during the simulation period was also scrutinized. The calculations were performed with SIMO simulation and optimization software. In all 245 tree-wise measured circular plots established in 2007 in the vicinity of the Evo Forest Station, Finland, were used as study material. The results show that the use of tree species stratum data in forest-planning simulations is highly relevant from the viewpoint of both the development of stand characteristics and the timing of logging operations. The relative standard errors stemming from the level of input data varied from 2.1% to 20.6% and from 58% to 84% in stand characteristics and timing of logging operations, respectively. The significance of the stratum-wise input data culminated in the functioning of the species-wise growth models at different stages of stand development. The results can be utilized in assessing the suitability of airborne laser scanning-based estimation methodologies in integrating detailed forest inventory with forest planning and operational logging planning.

Keywords: Airborne laser scanning (ALS), forest management planning, simulation, tree species detection, tree species stratum

1. Introduction

Laser scanning can be used in two spatial levels to estimate the volume of tree stock: (i) at the stand or plot level, using height and density distribution features derived from laser pulses (e.g. Holmgren 2003; Lim *et al.* 2003; Næsset 1997a, 1997b, 2002, 2004, Suvanto *et al.* 2005) or (ii) at the single-tree level, using tree height and crown width measurements (Hyyppä and Inkinen 1999, Persson *et al.* 2002, Popescu *et al.* 2003, Leckie *et al.* 2003, Maltamo *et al.* 2004). Stand-level laser scanning is more cost-efficient, due to its sparser pulse density (Holopainen & Talvitie 2006). On the other hand, single-tree interpretation makes it possible to understand on the stand's diameter/height joint distribution which facilitates forest-planning simulation and optimization, logging site planning, bucking control and wood procurement logistics.

However, the accuracy of estimating tree species stratum-level data has so far been rarely studied, although the significance of tree species in forest-planning simulation and optimization calculations is considerable. Packalén and Maltamo (2007) investigated the accuracy of estimating tree species stratum-level data with feature-based laser scanning, digital orthophotos and the nonparametric k-most similar neighbour (k-MSN) method in eastern Finland. The accuracy levels derived were considerably poorer than those of stand mean volume (V). On the

stand level, the relative root-mean-square-error (rmse) of the estimated stratumwise mean V varied from 28% (pine, *Pinus* L.) to 62% (deciduous), while the relative rmse of stand mean V was 10%. On the plot level, the respective stratumwise statistics varied from 51% to 102%, while the relative rmse of plot mean V was 20.5% (Packalén and Maltamo 2007).

Tree species stratum-level data are also error-prone in cases of traditional visual estimation and relascope plot-based estimation. Haara and Korhonen (2004) investigated the accuracy of visual estimation in eastern Finland. Their study showed that on the stand level the relative rmse of stratumwise mean V varied from 29.3% (pine) to 65% (deciduous), while the relative rmse of stand mean V was 24.8%. In other words, the estimation accuracy of the tree species stratum data presented in Packalén and Maltamo (2007) is similar to that of traditional visual estimation.

Another method for obtaining tree species stratum data is single-tree detection and interpretation. Airborne laser scanning (ALS) tree species detection was studied by Holmgren and Persson (2004), Korpela (2004), Korpela *et al.* (2007) and Kaartinen and Hyypä (2008). These studies showed that tree species can be determined to about 50-95% accuracy, depending on laser pulse density, availability of aerial photographs and automation state. The automation of tree species interpretation is one of the major challenges remaining in individual tree interpretation.

In Finland, a new feature-based k-MSN laser-scanning method for estimating stock characteristics is currently being adopted in private forest management planning. Currently, the focus is on how to integrate the inventory data in the respective simulation and optimization calculations. It is then crucial to be aware of how inventory data of varying accuracy and scale affects the simulation results, e.g. the timing of loggings, which is of the significant economic importance to the forest owner.

The effect of inventory data accuracy on forest-planning simulation results was investigated e.g. with the cost-plus-loss method and by analysing the timing of loggings and respective net yield (Barth and Ståhl 2007, Eid 2000, Eid *et al.* 2004, Duvemo and Lämås 2006, Duvemo *et al.* 2007, Holopainen and Talvitie 2006, Holopainen *et al.* 2008). However, the effect of the scale of the inventory data, e.g. stratum data versus mean data, has not previously been investigated in this context.

1.1 The objective

The objective here was to clarify the significance of tree species stratum data in forest-planning simulations and was accomplished by comparing the simulation results of mean data with those of stratum data.

The comparisons were performed by stand characteristics (age (a), basal area (BA), V , dominant height (H_{dom}), mean height (H_{gm}), mean diameter-at-breast height (D_{gm})) 20-year future simulation for stands not affected by loggings and by the timing of the first logging operation (thinning or clear-cutting) encountered during the simulation period for stands affected by loggings. Stratumwise characteristics calculated on the basis of the single-tree measurements were used as reference data.

2. Material and Methods

2.1 Study area

The research material comprised 245 treewise fixed-radius (9.77 m) field plots measured in summer 2007 in an app. 2000-ha managed forested area located in the vicinity of Evo Forest

Station, Finland (61.19°N, 25.11°E). The sampling of the field plots was based on prestratification of existing stand inventory data. The plots were located with Trimble's GeoXM 2005 Global Positioning System (GPS) device (Trimble Navigation Ltd., Sunnyvale, CA. USA), and the locations were postprocessed with local base station data, resulting in an error of 0.6 m. The following variables were measured in trees having a breast height diameter (DBH) of over 5 cm: location, tree species, crown class, DBH, height (h), lower limit of living crown and crown width.

2.2 Stand classes

The three (four) currently dominant tree species in forests in Finland are Scots pine *Pinus sylvestris* L., Norway spruce *Picea Abies* H. Karst., and silver birch *Betula pendula* Roth and downy birch *Betula pubescens* Ehrh. hereafter collectively referred to as birch. The most common alternatives with respect to a tree species mix are therefore 1) a single-species stand, 2) a two-species stand and 3) a three-species stand. The significance of tree species stratum data was analysed by these three stand classes. Appropriate sample plots for each class were selected by the criteria presented in Table 1.

Table 1. Stand classes used in the study.

| Stand class | Description | Criteria |
|-------------|----------------------|---|
| 1 | Single-species stand | Basal Area (BA) of the main tree species is greater than 90% of the total BA |
| 2 | Two-species stand | Combined BA of the two main tree species is greater than 90% of the total BA. Neither BA is greater than 70% of the total BA. |
| 3 | Three-species stand | BA of each of the three main tree species is greater than 20% of the total BA. |

The stock statistics concerning the initial state of the field sample plots are presented in Table 2.

Table 2. Initial stock statistics.

| Stand class | | Age, a | BA, m ² | V, m ³ | DgM, cm | (H _{gM}), m |
|-------------|-----|--------|--------------------|-------------------|---------|-----------------------|
| 1 | avg | 73 | 18.8 | 184.1 | 23.8 | 19.1 |
| | min | 26 | 0.4 | 1.2 | 5.5 | 3.8 |
| | max | 124 | 68.6 | 764.0 | 51.3 | 33.8 |
| 2 | avg | 71 | 19.9 | 177.6 | 21.6 | 17.2 |
| | min | 42 | 1.5 | 7.6 | 9.4 | 6.7 |
| | max | 193 | 42.1 | 487.5 | 48.9 | 29.8 |
| 3 | avg | 59 | 22.5 | 180.6 | 19.4 | 16.5 |
| | min | 37 | 7.0 | 27.4 | 9.0 | 7.2 |
| | max | 73 | 38.1 | 347.2 | 39.8 | 27.0 |
| Total | avg | 70 | 19.7 | 181.3 | 22.4 | 18.0 |
| | min | 26 | 0.4 | 1.2 | 5.5 | 3.8 |
| | max | 193 | 68.6 | 764.0 | 51.3 | 33.8 |

The sample plot sites varied from grove to dry heath and the development classes from advanced seedling stands to regeneration stands. Most of the sample plots were situated in advanced thinning stands (47%), regeneration stands (25%) or young thinning stands (24%). The remaining plots were situated in advanced seedling stands (2), shelter tree stands (1), seed tree stands (2) and seedling tree stands with an upper storey (1).

In the single-species stand class, 60% (41) of the sample plots were located in pine stands, 31% (21) in spruce stands and 9% (6) in birch stands. In the two-species stand class, 23 (46%) of the sample plots were situated in spruce-dominant stands, 14 (28%) in pine-dominant stands and 13 (26%) in birch-dominant stands. In the three-species stand class, the dominant tree species was spruce in 13 (65%) cases, birch in 4 (20%) cases and pine in 3 (15%) cases.

2.3 Simulations

The calculations were carried out using SIMO simulation and optimization software (SIMO simulation framework, Tokola *et al.* 2006, Mäkinen *et al.* 2008), which enables performance of both tree- and stand-level simulations; here, the tree-level simulator was utilized. The nonspatial tree-level growth models found in SIMO are, for the most part, similar to those found in the MELA2002 and MOTTI simulators (Hynynen *et al.* 2002, Salminen *et al.* 2005). They include growth models for all sites and tree species in Finland, including separate models for peat lands. The tree-level simulator can be used to simulate the growth of either sample trees measured in the field or descriptive trees generated on the basis of a theoretical diameter/height distribution.

In our study, the simulation was performed at the single-tree level. The statistics for the strata and compartments were derived as sums and means of the simulated tree properties. The procedure was based on the following two simulations carried out with SIMO software: i) the single stratum simulation and ii) the reference simulation.

In the single-stratum simulation a single tree species stratum was formed from the treewise plot data. The species having the greatest number of stems of plot trees with aDBH greater than 5 cm was selected as the stratum's main tree species.

In the reference simulation, multiple strata were formed from the treewise plot data representing the true initial and simulated final states. The result of the reference simulation was assumed to depict the final state of the stock. Reference simulation results regarding the timing of operations and development of stand characteristics were used as reference data with which the results of the single-stratum simulation were compared. The length of the simulation period was set at 20 years. Two types of simulation were then performed: those in which operations were not allowed, making it possible to compare stand characteristics at the end of the simulation period and those in which operations were allowed, making it possible to compare the timing of the next logging operation. Thinnings and clear-cuttings were studied separately; natural drainage was not allowed in either case. The comparisons were based on standard errors and biases.

3. Results

3.1 Final-state stand characteristics

Deviations of model outputs in final-state stand characteristics (a, BA, V, Dgm, Hgm, Hdom) were investigated by comparing the reference simulation results to single-stratum simulation results by stand classes presented in Table 1.

Table 3. Deviations of model outputs in final-state stand characteristics. Reference simulation versus single-stratum simulation. Relative deviation values calculated by reference stand values given in brackets.

| Stand Class | Obs. | | Age, a | | BA, m ² | | V, m ³ | | Dgm, cm | | Hgm, m | | H _{dom} , m | |
|-------------|------|------|--------|--------|--------------------|--------|-------------------|--------|---------|--------|--------|--------|----------------------|--------|
| 1 | 68 | bias | 0.7 | (0.8) | 0.6 | (1.7) | 1.7 | (0.5) | -0.1 | (-0.3) | -0.2 | (-1.1) | 0.3 | (1.2) |
| | | se | 1.5 | (1.6) | 1.8 | (5.1) | 11.4 | (3.2) | 0.6 | (2.1) | 0.5 | (2.2) | 0.5 | (2.3) |
| 2 | 50 | bias | -0.4 | (-0.5) | 1.8 | (4.7) | 12.2 | (3.4) | 0.3 | (0.9) | -0.3 | (-1.5) | -0.6 | (-2.8) |
| | | se | 17.1 | (19.7) | 5.6 | (14.5) | 75.9 | (20.9) | 1.9 | (6.9) | 1.3 | (6.4) | 2.6 | (12.0) |
| 3 | 20 | bias | -2.2 | (-2.9) | 2.8 | (6.0) | 19.6 | (4.7) | 0.3 | (1.1) | 0.0 | (0.2) | -0.2 | (-1.1) |
| | | se | 8.5 | (10.9) | 8.4 | (18.0) | 85.9 | (20.6) | 1.7 | (6.6) | 0.9 | (4.7) | 2.0 | (9.4) |
| Total | 138 | bias | -0.1 | (-0.1) | 1.4 | (3.6) | 8.1 | (2.2) | 0.1 | (0.3) | -0.2 | (-1.0) | -0.1 | (-0.5) |
| | | se | 10.8 | (12.4) | 4.7 | (12.5) | 56.1 | (15.2) | 1.4 | (4.9) | 0.9 | (4.4) | 1.8 | (7.9) |

The error statistics (model outputs) derived for the final-state stand characteristics presented in Table 3 indicate that the use of stratumwise stock data is significant in each of the three stand classes studied. The greatest influence can be seen in the two-species and three-species stand classes. In the one-species stands, where the proportion of other species is less than 10%, the single-stratum simulation results approach the reference simulation results and the respective deviations are clearly smaller than those in the other two stand classes. The differences between the error statistics of the two-species and three-species stand classes were not very large.

The most significant standard errors were related to stand V (3.2-20.6%) and BA (5.2-18.0%). On the other hand, the mean characteristics such as H_{gm} (2.2-6.4%) and D_{gm} (2.1-6.9%) were not as sensitive to the use of single-stratum simulation. A minor bias (3.4- 6.1%) can be observed in the simulation results of stand V and BA. However, single-stratum simulation of H_{gm} and D_{gm} did not result in significant bias.

The standard errors increased rapidly as the simulation period lengthened in both multispecies stand classes (Figure 1). In stand class 1, secondary tree species (max. 10%) did not cause significant deviations. An especially strong increase in standard errors was found in stand V. When single-stratum simulation was used, the simulation period length did not have large affect the simulation error of the mean stand characteristics. In these cases the final state standard errors were only about 5%.

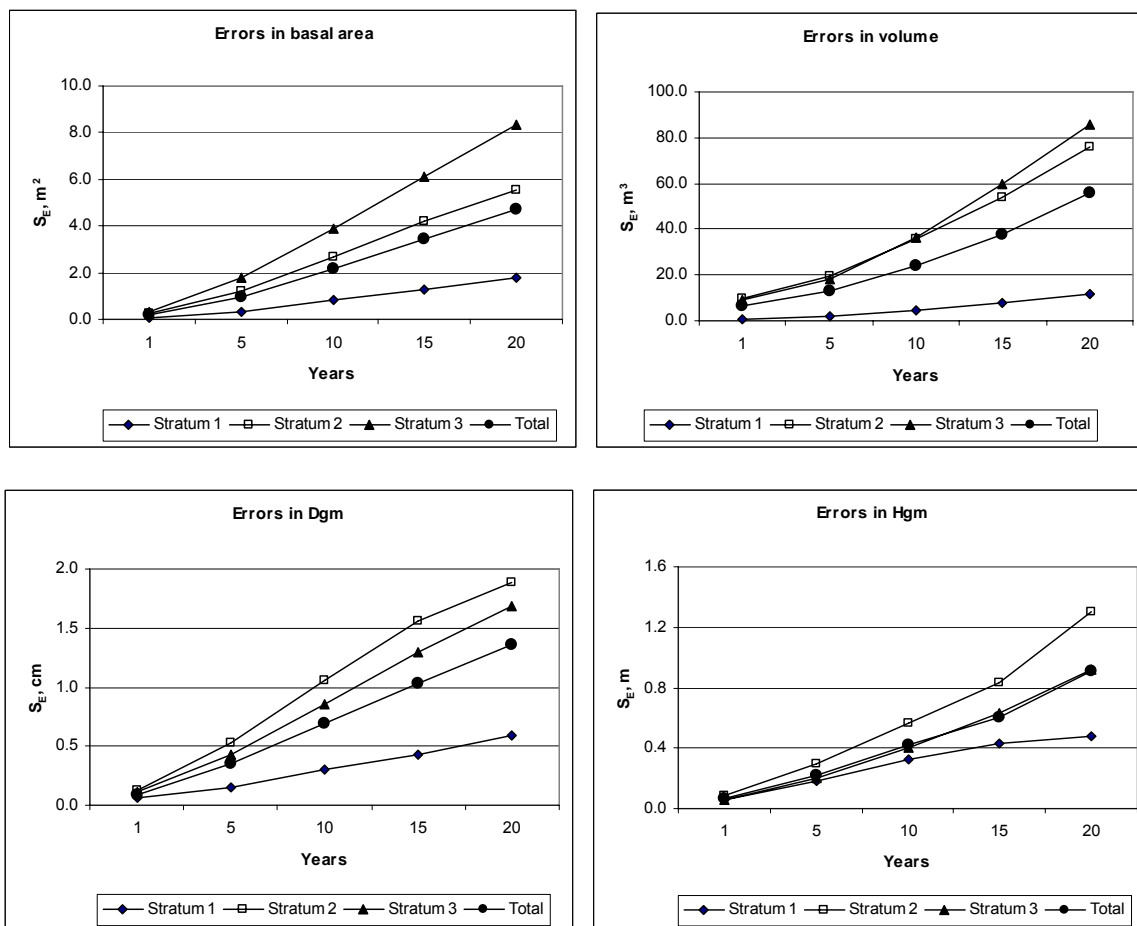


Figure 1. Error standard errors by simulation year (1-20) and stand class.

3.2 Timing of operations

Differences in the timing of simulated thinnings and clear-cuttings were then investigated (Table 4).

Table 4. Error in timing of the next logging operation. Reference simulation versus single-stratum simulation. The proportion of correctly defined operations (logging type identical) is given in brackets.

| Stand class | Operation | Obs. | Bias | s_e |
|-------------|----------------------|------|------|-------|
| 1 | | 47 | -0.3 | 1.0 |
| | Thinning (100) | 21 | -0.7 | 1.5 |
| | Clear-cutting (100) | 26 | 0.0 | 0.5 |
| 2 | | 38 | 0.9 | 4.3 |
| | Thinning (66.7) | 21 | 1.6 | 4.5 |
| | Clear-cutting (73.7) | 17 | 0.2 | 4.0 |
| 3 | | 19 | 0.8 | 3.3 |
| | Thinning (73.3) | 14 | 0.5 | 3.1 |
| | Clear-cutting (80.0) | 5 | 1.8 | 4.3 |
| Total | | 104 | 0.4 | 3.0 |
| | Thinning (80.7) | 56 | 0.4 | 3.3 |
| | Clear-cutting (36.0) | 48 | 0.3 | 2.7 |

The standard errors in timing varied from 0.5 to 1.5 years and from 3.1 to 4.5 years in single-species and multispecies stands, respectively; i.e. stratumwise simulation also had significantly influences the level of these errors. The errors found in multispecies stands are especially significant in this respect, since the average time to the next logging operation was only 5.3 years, resulting in 58-84% relative standard errors. No significant differences were found in the timing errors of thinnings and clear-cuttings. A slight timing bias (0.2-1.8 years) was also registered.

The definition of the next operation was fully correct only in the single-species stand class. Furthermore, the operation was defined correctly on an average of 66.7-73.7% and 73.3-80% of the cases in the two-species and three-species stand classes, respectively.

4. Discussion

The objective here was to investigate the significance of tree species stratum data in forest-planning simulations by comparing the simulation results obtained using mean stand characteristics with those obtained by stratumwise data. The simulations were carried out using actual treewise measured field material and the SIMO simulation software. Comparisons were performed on the development of stand characteristics during the simulation period (20 years) and the timing of the first logging operation occurring during the simulation period.

The simulation period commonly used in forest planning in Finland is 20 years, the same as the period length used in this study. In addition, a simulation period of this length ensures that the number of simulated operations is sufficient and that the functioning of the growth models is revealed. Since the development of stand characteristics without logging operations was also investigated, it was not deemed necessary to further extend the simulation period.

In light of the present results, the use of tree species stratum data in forest-planning simulations is highly relevant from the viewpoint of both the development of stand characteristics and the timing of logging operations. The relative standard errors stemming from the level of input data varied from 2.1% to 20.6% and from 58% to 84% in stand characteristics and timing of logging operations, respectively. The largest standard error in the stand characteristics was found for stand V (3.2-20.6%) and BA (5.2-18.0%), probably because the V increment simulation was based on the increment functions of D_{gm} and H_{gm} , which naturally vary by tree species. The stratumwise data were not as relevant for simulating mean characteristic development (H_{gm} and D_{gm}) as it was for simulating BA and V development, probably because the mean characteristics are BA-weighted and the dominant species thus always has the greatest influence in the calculations.

A slight bias was registered in the simulation results of stand V and BA (3.4-6.1%). However, no bias was found in the simulation results of the mean characteristics. If the intraspecies variation in a stand was not addressed, the simulations could have slightly underestimated the development of BA and V due to differences in the specieswise growth models. Simulation of the mean characteristics is not as sensitive to this type of variation. In general, the significance of the stratumwise input data culminates in the functioning of the specieswise and sitewise growth models at different stages of stand development. Future investigations should further address these factors.

Our study highlights the importance of tree species stratum data in forest-planning simulations. It is therefore essential to acquire stratumwise data for forest-planning input data. The results of our study could be utilized for assessing the suitability of ALS methods for feature-based or single-tree estimation when detailed forest inventory data are integrated with forest planning and operational logging planning.

Acknowledgements

This study was made possible by financial aid from the Finnish Academy.

References

- Barth, A. and Ståhl, G., 2007. Determining sampling size in a national forest inventory by cost-plus-loss analysis. In: Barth, A. Spatially Comprehensive Data for Forestry Scenario Analysis – Consequences of Errors and methods to Enhance Usability. *Doctoral thesis No 2007:101*. SLU, Faculty of Forest sciences.
- Duvemo, K. and Lämås, T., 2006. The influence of forest data quality on planning processes in forestry. *Scandinavian Journal of Forest Research*, 21, 327-339.
- Duvemo, K., Barth, A. and Wallerman, J., 2007. Evaluating sample point imputation techniques as input in forest management planning. To appear in *Can.J.For.Res.*
- Eid, T., 2000. Use of uncertain inventory data in forestry scenario models and consequential incorrect harvest decisions. *Silva Fennica*, 34, 89-100.
- Eid, T., Gobakken, T. and Næsset, E., 2004. Comparing stand inventories for large areas based on photo-interpretation and laser scanning by means of cost-plus-loss analyses. *Scandinavian Journal of Forest Research*, 19, 512-523.
- Haara, A. and Korhonen, K., 2004. Kuvioittaisen arvioinnin luotettavuus. *Metsätieteen aikakauskirja*, 4/2004, 489-508. (in Finnish).
- Holmgren, J., 2003. Estimation of forest variables using airborne laser scanning. PhD Thesis. *Acta Universitatis Agriculturae Sueciae, Silvestria 278*, Swedish University of Agricultural Sciences, Umeå, Sweden.
- Holmgren, J. and Persson, Å., 2004. Identifying species of individual trees using airborne laser scanning. *Remote Sensing of Environment*, 90, 415-423.
- Holopainen, M. and Talvitie, T., 2006. Effects of data acquisition accuracy on timing of stand harvests and expected net present value. *Silva Fennica*, 40, 531-543.
- Holopainen, M., Mäkinen, A., Rasinmäki, J., Hyyppä, J., Hyyppä, H., Kaartinen, H., Viitala R., Vastaranta, M. and Kangas, A., 2008. Effect of tree level airborne laser scanning accuracy on the timing and expected value of harvest decisions. *Submitted to European Journal of Forest Research*.
- Hynynen, J., Ojansuu, R., Hökkä, H., Siipilehto, J., Salminen, H. and Haapala, P., 2002. *Models for predicting stand development in MELA system*. Finn. For. Res. Inst. Res. Pap. 835.
- Hyyppä, J. and Inkinen, M., 1999. Detecting and estimating attributes for single trees using laser scanner. *The Photogrammetric Journal of Finland*, 16, 27-42.
- Kaartinen, H. and Hyyppä, J., 2008. EuroSDR-Project Commission 2 "Tree Extraction", *Final Report*, In: *EuroSDR - European Spatial Data Research, Official Publication*, in press.
- Korpela, I., 2004. Individual tree measurements by means of digital aerial photogrammetry. PhD thesis. *Silva Fennica. Monographs 3*. 93 p.
- Korpela, I., Bruun, E., Haapaniemi, J., Honkasalo, J., Ilvesniemi, S., Kuutti, V., Linkosalmi, M., Mustonen, J., Salo, M., Schäfer, H., Suomi, O. and Virtanen, H., 2007. Single tree forest inventory using Lidar and aerial images for 3D treetop positioning, tree species recognition, height and crown width estimation. In Rönholm, P., Hyyppä, H. and Hyyppä, J. (editors). *Proceeding of the ISPRS Workshop "Laser Scanning 2007 and SilviLaser 2007"*. Espoo, September 12-14, 2007, Finland.

- Leckie, D., Gougeon, F., Hill, D., Quinn, R., Armstrong, L. and Shreenan, R., 2003. Combined high-density lidar and multispectral imagery for individual tree crown analysis. *Canadian Journal of Remote Sensing*, 29, 633–649.
- Lim, K., Treitz, P., Wulder, M., St. Onge, B. and Flood, M., 2003. *LIDAR remote sensing of forest structure*. *Progress in Physical Geography*, 27, 88-106.
- Maltamo, M., Eerikäinen, K., Pitkänen, J., Hyypä, J. and Vehmas, M., 2004. Estimation of timber volume and stem density based on scanning laser altimetry and expected tree size distribution functions. *Remote Sensing of Environment*, 90, 319–330.
- Mäkinen, A., Kangas, A., Kalliovirta, J., Rasinmäki, J. and Välimäki, E., 2008. Comparison of tree-wise and stand-wise forest simulators by means of quantile regression. *Forest Ecology and Management*, 255, 2709-2717.
- Næsset, E., 1997a. Determination of mean tree height of forest stands using airborne laser scanner data. *ISPRS Journal of Photogrammetry and Remote Sensing*, 52, 49-56.
- Næsset, E., 1997b. Estimating timber volume of forest stands using airborne laser scanner data. *Remote Sensing of Environment*, 61, 246-253.
- Næsset, E., 2002. Predicting forest stand characteristics with airborne scanning laser using a practical two-stage procedure and field data. *Remote Sensing of Environment*, 80, 88-99.
- Næsset, E., 2004. Practical large-scale forest stand inventory using a small footprint airborne scanning laser. *Scandinavian Journal of Forest Research*, 19, 164-179.
- Packalén, P. and Maltamo, M., 2007. The k-MSN method in the prediction of species specific stand attributes using airborne laser scanning and aerial photographs. *Remote Sensing of Environment*, 109, 328-341.
- Persson, Å., Holmgren, J. and Söderman, U., 2002. Detecting and measuring individual trees using an airborne laser scanner. *Photogrammetric Engineering & Remote Sensing*, 68, 925-932.
- Popescu, S., Wynne, R. and Nelson, R., 2003. Measuring individual tree crown diameter with lidar and assessing its influence on estimating forest volume and biomass. *Canadian Journal of Remote Sensing*, 29, 564–577.
- Salminen, H., Lehtonen, M. and Hynynen, J. 2005. Reusing legacy FORTRAN in the MOTTI growth and yield simulator. *Computers and Electronics in Agriculture*, 2005, 103-113.
- Tokola, T., Kangas, A., Kalliovirta, J., Mäkinen, A. and Rasinmäki, J., 2006. SIMO—SIMulointi ja Optimointi uuteen metsäsuunnitteluun. *Metsätieteen aikakauskirja*, 1, 60–65 (in Finnish).

Accuracy of automatic tree extraction using airborne laser scanner data

Harri Kaartinen¹, Juha Hyyppä¹, Xinlian Liang¹, Paula Litkey¹, Antero Kukko¹, Xiaowei Yu¹, Hannu Hyyppä² & Markus Holopainen³

¹Finnish Geodetic Institute, <firstname>.<lastname>@fgi.fi

²Helsinki University of Technology, hannu.hyyppa@tkk.fi

³University of Helsinki, markus.holopainen@helsinki.fi

Abstract

The objective of the EuroSDR/ISPRS Tree Extraction project was to evaluate the quality, accuracy, and feasibility of automatic or semi-automatic tree extraction methods mainly based on high-density laser scanner data. This paper summarizes the major general finding based on laser scanning approaches. Results showed that the tree extraction method is the main factor on the achieved accuracy. When the laser point density increases from two points to eight points per m², the improvement in crown delineation accuracy was marginal, but in the case of feasible methods the accuracy of the tree location and especially the tree height determination improves, but also deterioration of the accuracy was reported. Individual tree based inventory requires also individual tree based reference collected in the field; this calibration is needed to reduce underestimation of tree height, calibration of the basal area and stem volume and possibly to verify experimentally the quality of the product.

Keywords: tree extraction, airborne laser scanning, automation, EuroSDR, ISPRS

1. Introduction

The first application of airborne laser scanning (ALS) for forestry was the determination of terrain elevations (e.g. Kraus and Pfeifer 1998; Vosselman 2000), followed by standwise mean height and volume estimation (e.g. Næsset 1997a,b), individual tree based height determination and volume estimation (e.g. Hyyppä and Inkinen 1999; Brandberg 1999; Ziegler et al. 2000; Hyyppä et al. 2001), tree species classification (e.g. Brandtberg et al. 2003; Holmgren and Persson 2004) and measurement of forest growth and detection of harvested trees (e.g. Yu et al. 2004). Extraction of the forest variables has been recently divided into two categories: inventories done at stand or plot level and inventories based on individual trees or groups of trees. These categories relate to the need of the forestry information. At the same time laser scanning is increasingly becoming a core data set for mapping authorities and the pulse density of the laser scanning is increasing constantly. In addition to forest inventory, tree information is used e.g. in flight obstacle mapping, power line mapping, real estate visualization and mapping, and telecommunication planning. The results obtained for individual tree extraction has varied significantly from study to study (percentage of correctly delineated trees has ranged from 40 to 93 %) (see e.g. Hyyppä and Inkinen 1999; Persson et al. 2002; Brandtberg et al. 2003; Leckie et al. 2003; Straub 2003; Popescu et al. 2003; Andersen et al. 2002; Morsdorf et al. 2003; Wack et al. 2003). It is not known how much of this variation is caused by the methods and how much by the forest conditions. Concerning the methods there is a trend towards using more efficiently the point cloud data, rather than segmenting pure laser-derived DSMs. In EuroSDR/ISPRS Tree Extraction project twelve participants around the world extracted the trees in given forest test sites. The first objective of this study was to study the accuracy and feasibility of various methods using the same test data. The second objective of the study was to find out how the pulse density affect on individual tree extraction. More detailed comparison of the methods and

their differences and similarities is a subject of another paper.

2. Material

2.1 Study area

Two forest test sites were close to each other in southern Finland, about 18 km west of Helsinki. Test sites were very diverse; partly flat and partly steep terrain, areas of mixed and more homogenous tree species at various growth stages. Main tree species were Scots pine, Norway spruce and silver and downy birches. The area of test site A was 2.6 ha and test site B 5.8 ha.

2.2 Delivered data for tree extraction

For test sites ALS data (Table 1) with three different pulse densities (2, 4 and 8 points per m²) was delivered to the participants. A DTM with 0.5 m grid spacing was calculated using Terrascan (based on Axelsson 1999, 2000, 2001) and visually checked before delivery as ASCII-grid. Delivered training data included species, location, DBH and crown delineation (3-5 points) of 75 trees. Training data was measured in the field using a tacheometer, and it was meant for the participants to calibrate their methods into Scandinavian forest conditions.

Table 1. ALS data of the study area

| | |
|---------------------|---|
| Acquisition | 29 th of June 2004 |
| Instrument | Optech ALTM 2033 |
| Flight altitude | 600 m |
| Pulse frequency | 33 000 Hz |
| Field of View | ± 9 degrees |
| Measurement density | 2 per m ² per echo per strip |
| Swath width | 185 m |
| Mode | First and last pulse |

2.3 Reference data for quality verification

Reference data for quality verification was collected with ground surveys and terrestrial laser scanner. RTK-GPS (Leica SR530) and tacheometer (Trimble 5602S DR200+) equipment were used to create a ground control point (GCP) network over the study area. Location of spherical reference targets for terrestrial laser scanner (Faro LS880HE) was determined with tacheometer measurements on the basis of the GCPs. For RTK-GPS –measurements the same GPS reference station was used as for airborne laser scanning. Terrestrial laser scanning (TLS) was carried out in 48 locations to obtain laser point coverage of all reference trees on five test plots, two plots on test site A and three plots on test site B. Together the five plots covered an area of 0.48 ha (5.7 % of test site area). Reference data included the location and species of 352 trees and the height of 254 trees.

Point clouds of individual terrestrial laser scanings were georeferenced using spherical reference targets and Faro Scene software. Same software was used to transform the point clouds to a 3D-mesh, which was then exported in VRML2 format to Geomagic Studio software for editing and exporting to DXF format. 3D DXF vectors of individual scanings were combined using Bentley MicroStation for additional editing and measurement of tree parameters. Measured tree parameters included tree trunk location, tree top location, tree height and crown delineation. Intensity images of original scanings in Faro Scene software were used to determine tree species and crown base height.

2.4 Produced tree extraction results

Participants were requested to extract trees using the given material. They were allowed to use any method and data combination. Participants were asked to provide from each tree that they could extract tree location and height, crown delineation, and height of crown base or the volume of the crown, if possible. Of twelve participants, eleven used ALS data for tree extraction and nine used solely ALS data.

3. Methods

3.1 Methods used by participants

The methods have been reported in detail in Kaartinen and Hyypä (2008, forthcoming). Here a more anonymous, brief description of the key elements in the methods is given.

Method A was implemented in eCognition Expert. The method can be divided into four main tasks: 1) creation of a forest mask, 2) initial split of the forest mask, 3) splitting the forest mask into tree crowns and 4) correction of over split crowns. A low pass filter was applied to remove small gaps and too many local minima and maxima. The creation of the forest mask was made by thresholding the CHM images at a height of 2 m. The method uses the highest point/pixel in the object as the seed and expands the seed to the crown boundaries, identified by a positive difference between the current and proposed pixel. This was repeated until all areas within the current object had been included into new objects. The difference required to form a boundary was defined with a threshold. The threshold was initially high and a boundary was formed only where a large difference occurs, in this case 1 m. The key to this method is the classification of objects into two groups, crowns and crown-clusters. Those objects identified as crowns were removed from further splitting iterations and only considered later, while crown-clusters were processed further in the hope of separating the crowns contained within.

Method B was fully automatic using raw laser points and it had the following steps: (1) a DSM was created, (2) a DTM was created, (3) a CHM/nDSM was created, (4) the CHM was filtered with different Gaussian filters resulting in different images, (5) the different images are segmented separately and the segment chosen for a specific area is selected through fitting a parabolic surface to the laser data, (6) the height and crown diameter were estimated for the identified trees.

Method C was based on a tree model with three geometric parameters (size, circularity and convexity of the tree crown). The processing strategy comprises four steps. First, a wide range of scale levels of the DSM was created. The second step was a segmentation, which is achieved by applying a watershed transformation. In the third step the best hypothesis for a crown from the overlapping segments of all levels based on the tree model was selected. The selection of the best hypotheses was achieved with the help of fuzzy functions for the tree model parameters.

In **method D**, a DSM pixel was considered to be a low, differing pixel, if at least seven (surface models from point density of 8 pulses/m²), or six (other point densities) of the eight-neighbourhood were more than five metres higher than the pixel itself. These pixels were replaced with the median of the more than five metres larger neighbour pixel values. The DTM was then subtracted from the final DSM to get a CHM for tree crown segmentation. Before segmentation, the CHM was smoothed with height based filtering. Five Gaussian filters were used so that the filter size increased along the height of pixel being smoothed. Smallest and largest σ values were selected by visually ensuring that the number of local maxima was reasonable at both ends of the tree height range. A negative image of the height filtered image

was then created for watershed segmentation that was used to separate tree crowns from each other. Watershed regions associated with the local minima in the negative image were identified using a drainage direction following algorithm. To get the boundaries between crowns and background, pixels lower than two metres in the height filtered image were masked out from the crown segments. Finally small segments (at most three pixels in size) were combined with one of the neighbour segments, being it a tree crown or background, based on the smallest average gradient on the common segment boundary. Tree locations and heights were then obtained from the location and value of the pixel having the highest value within each segment.

In **method E**, the process comprises several steps, i.e. retain uppermost echoes, interpolate them into a DSM-grid, find local maxima in the DSM, run a region-growing algorithm with some restrictions in order to derive objects belonging to the class of objects often named star objects. The DSM was now divided into segments that represented tree crowns, while parts of the area were not covered by trees and had no DSM value. The DSM was adjusted (lifted) using the residuals between the DSM and the first echoes. The 90 percentile of the residuals was calculated, and this frequently turned out to be around 70 cm, and this was added to all z values in the DSM. The tree heights were derived as the z value of the local maxima after this adjustment.

In **method F**, tree locations and tree height were computed from the CHM. The CHM was computed by selecting the highest canopy height in each grid cell. Furthermore, each trunk of the training trees was located with a window size of 3x3 (i.e., 3 metres), and a height histogram with one-metre interval was used to build up a laser classification tree model for species determination. The highest laser elevation value among laser hits on a specific area (i.e. 3x3 metres), is assumed to be the potential trunk location of the tree. Two approaches were used to estimate the potential tree locations. The first approach was whereby running a local maximum filter in the CHM with a window size of 3x3 (i.e., three-metre squares), all potential tree locations were selected. The second method was that the 3x3 local maximum filter processes only heights less than 15 metres in the CHM. The first approach was applied to test site B, and the second approach was used on test site A. The crown widths were derived based on the training tree data and the CHM. The empirical relationship between the height of the trees and their searching crown size was defined.

Method G employed an automatic algorithm of local maxima (LM) filter with circular moving window of varying sizes. Local Maximum Filter is often used to locate tree position based on the assumption that the highest elevation corresponds to the tree apex. When applying the LM filter, the window size has great influences on tree identification. On the other hand, the taller the tree is, the larger the crown width. Thus the determination of filter size was based on the relationship between the crown size and tree height. Prior information was utilized to derive such a relationship; to predict the crown size, regression models were fitted with tree height as the independent variable. For the test data, about ninety trees for each test site were visually identified from the CHMs and the corresponding heights and crown width were manually recorded by on-screen measurement. The crown diameter was the average of two values measured along two perpendicular directions from the location of the tree top.

In **method H**, an algorithm, which removes the points (ground and not ground) derived from the echoes penetrated inside the crown from the dataset, was implemented. At first, the algorithm provides a triangulation of all the points; the following step is the removal of all the vertexes that present a difference greater than a fixed threshold. The procedure therefore allows a correct DSM to be obtained. The method applied for tree counting was based on a morphological analysis of the laser point distribution. For this purpose the Top Hat algorithm was implemented. This is a mathematical function of image elaboration, which allows the top elements at the scale of the represented values to be found. The mathematical formulation of the Top Hat is related to

the theory of image processing formulated by Serra (1982, 1988). In some cases, because of the presence of small height variations among adjoining points belonging to the same crown, more than one apex can be counted for each tree. In order to minimize this kind of error a control algorithm was introduced. It detects and corrects the apexes, which are erroneously classified (these are often localized at the edge of the crown). In order to delineate single crowns an algorithm of region growing was implemented.

Method I is based on local maxima detection in the CHM and a following cluster analysis of the raw data with found local maxima as starting points. The DSM generation includes the choice of four parameters, which are destination grid resolution, search radius, and size and shape of a Gaussian smoothing function. The outcome of the cluster analysis is the raw data being flagged with a distinct number of all returns presumably belonging to a tree. This cluster is then treated by a routine, which takes the relevant measures from the point cloud. These are the following:

- Position (x, y) is derived as the centre of gravity of the echo positions belonging to the cluster.
- Tree height is computed as the maximum height of the cluster's echos.
- Crown diameter is estimated using the convex hull of the cluster by transferring the circumference of the convex hull to a radius assuming circular shape.

3.2 Methods used for evaluation

Tree location accuracy was evaluated by measuring distances from every reference tree to the nearest tree found on the delivered model. For tree location the coordinates of the reference treetop were used. Only distances within 5 metres from the reference tree were included in the analysis. If several reference trees have hits on the same tree in the analyzed model, only the best match according to distance and height was accepted to analysis, other observations were disregarded. Location accuracy was analyzed for two cases: all trees and trees over 15 m tall. The trees approved for location accuracy evaluation were also used for tree height evaluation, and again two cases were used: all trees and trees over 15 m tall.

The crown delineation accuracy was evaluated by comparing the total delineated area of reference trees on test plots to delivered model delineation. If a participant did not deliver crown delineation as vector data, the crown covered area was determined as a circle around the trunk location by using the radius or area delivered by the participant, and final delineated area was obtained as a union of these circles.

Trees in the reference test plots were extracted also manually by an FGI employee to get an idea of what accuracy can be achieved this way. Extraction was executed using laser scanner data (8 points per m²) and GIS software. Also aerial images were used for interpretation purposes. Trees were delineated visually by using laser points which were colour coded based on the elevation, and the location and height were measured by finding the highest laser points within the delineated trees. Ground height was interpreted visually in a 3D-view. The results of this manual extraction are marked as "Manual" in the figures in section 4. Results and discussion.

If the observed value differed from the reference value more than $\text{mean} \pm 3 \cdot \text{STD}$, it was considered as gross error, or outlier, and was removed. In tree height analysis first all values deviating more than 10 metres from the ground truth were removed.

4. Results and discussion

In following figures the laser point densities are marked after the method ID, for example, B_2

for two points, B_4 for four points and B_8 for eight points per m².

4.1 The amount of extracted trees

The amount of extracted trees on the reference test plots is shown in Figure 1. The amount of extracted trees reveals how many percent of the true trees have been extracted. In order to provide non-biased estimates e.g. for volume, the correct percentage rate should be as high as possible. The percentage of detected trees varied between 25 to 90% implying different capabilities in detecting suppressed trees. Best models were significantly better in separating tree groups into individual trees compared to the manual method. Surprisingly, there was no improvement in the detection rate when the pulse density was increased from 2 to 8 points per m². It is still expected that there should be more focus on finding smaller trees under the dominating storey. In principle, the higher pulse density should result in better tree finding capability, but that is subject to the forest type. It seemed that the test site was relatively suitable for individual tree detection even with a pulse density as low as 2 points per m². We expect that in younger stands density of 8 points per m² would have been beneficial.

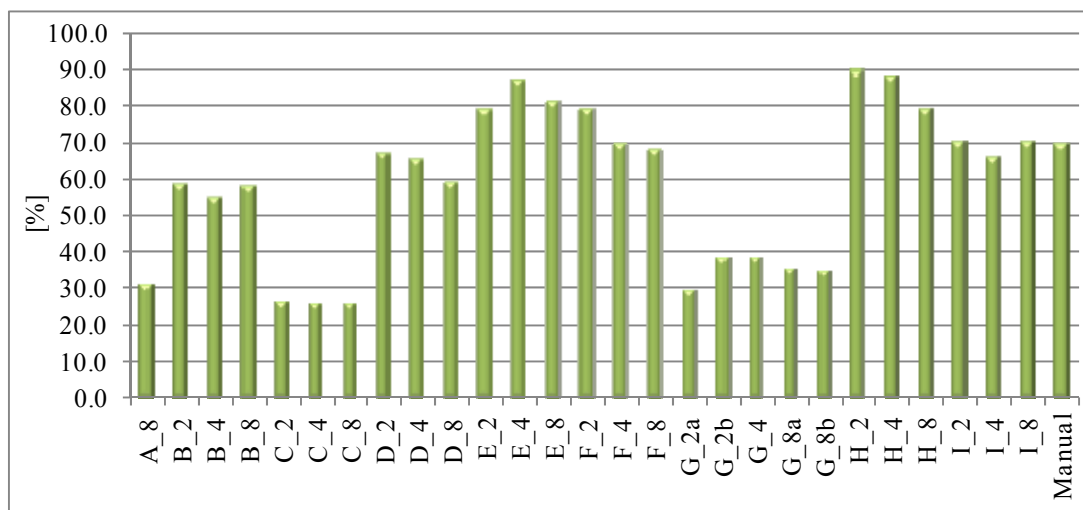


Figure 1. Amount of extracted trees.

4.2 Tree location accuracy

The results clearly showed that the variability of tree location is small as a function of point density and it mainly changes as a function of the model provider (Figure 2). Obviously, the calibration of the models with the given training data has not been successful and several models assumed the trees to be significantly larger in width (e.g. A, C, I). With the best models for all the trees, the mean location error was less than 1 m and the difference with 2, 4 and 8 points per m² was negligible. With trees over 15 m, standard deviation of 0.5 m was obtained. The automatic models were as good as manual processing of the point cloud in determining the tree locations. In tree finding, there were in general few outliers.

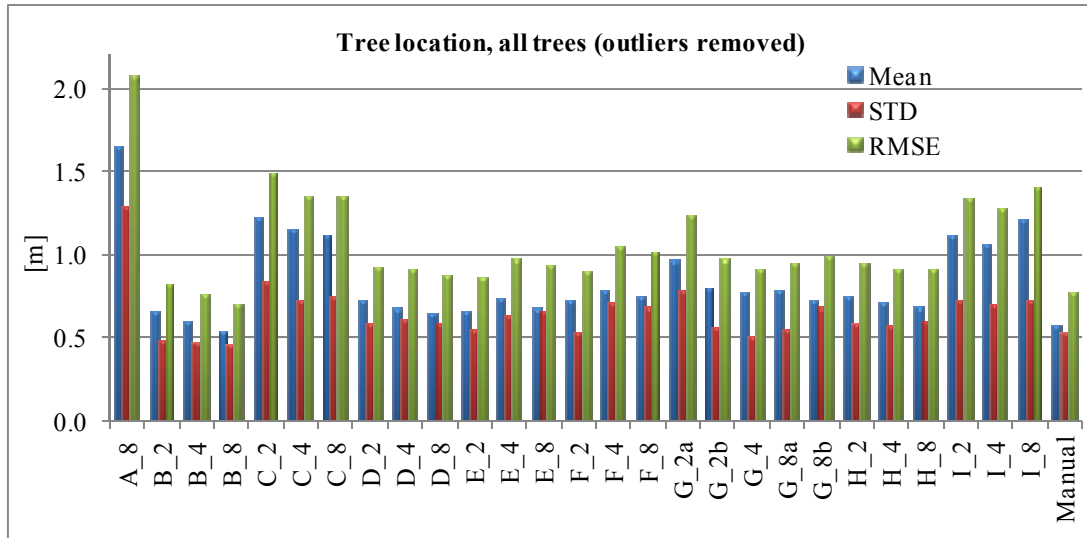


Figure 2. Tree location accuracy.

4.3 Tree height accuracy

Tree height quality analysis showed again that the variability of the point density was negligible compared to method variability (Figure 3). With the best models RMSE of 60 to 80 cm was obtained for tree height. High quality tree heights were obtained by models of B, D and G. The results with the best automatic models were significantly better than those with the manual process. In general, both the underestimation of tree height and standard deviation were decreased as the point density increases. The overestimation of the model E to tree height was due to the correction applied to the tree height in the preprocessing phase. The main reason for the difference of the laser-based methods was that some of the methods used significantly stronger filtering in the preprocessing phase. It can also be concluded that when comparing the results from literature, the forest conditions play a major role. With the model D, a low detection rate for tree finding has been published, but in the comparison, it showed to be one of the best algorithms.

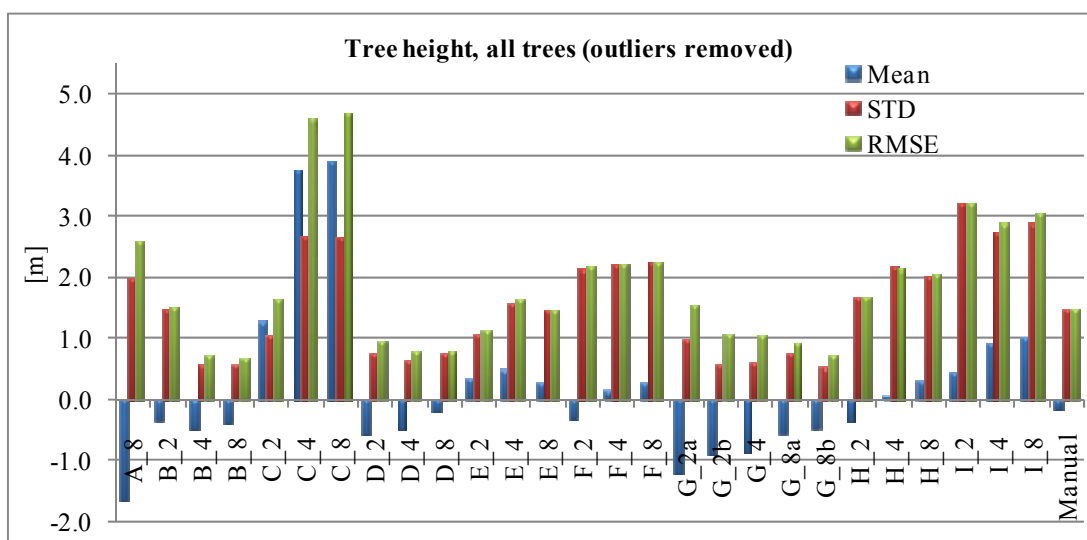


Figure 3. Tree height accuracy.

4.4 Crown delineation accuracy

Total crown area seems to vary significantly between the models (Figure 4). The errors leading to false total crown area are: inadequate tree finding capability (small trees missed), inadequate filtering of the raw point cloud data or DSM (leading to too large crowns but too few of them) and inadequate calibration of the method with the given reference data. The models, which have been tested more with practical forestry, have already more experience in this calibration, such as the B and E methods.

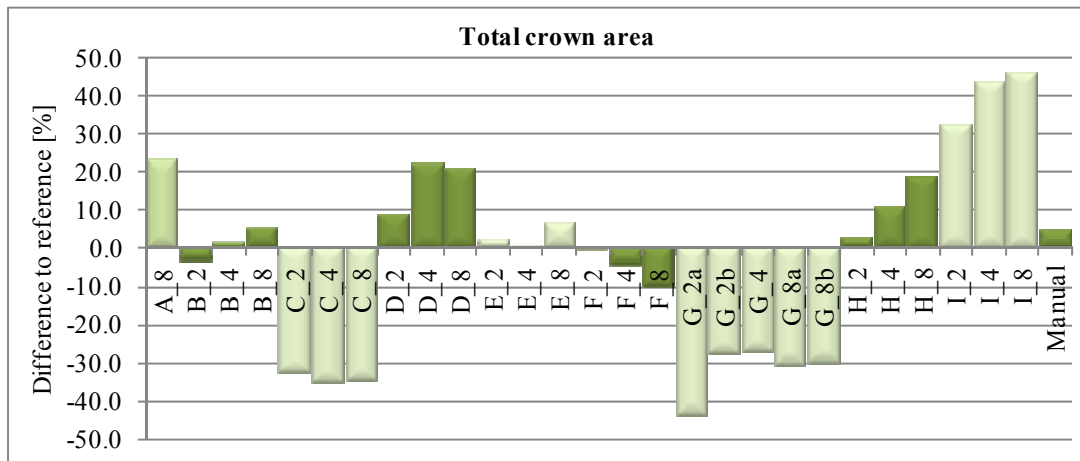


Figure 4. Total crown area accuracy.

5. Conclusion

The following conclusions were drawn:

- Results showed that the extraction method is the main factor on the achieved accuracy and surprisingly high variability of the results were provided by various methods.
- Before using the methods into operational forests inventory, the methods should be carefully verified.
- The quality of the method versus other methods cannot be verified without testing the methods in the same forest conditions since the effect of the variability of the forest conditions is assumed to have a high impact on achieved accuracy (by comparing the results achieved those with previous literature). Thus, more comparison of the methods should be done in the future.
- More detailed analysis of reasons why certain method failed and succeeded in this test should be reported in near future. Differences and similarities of the methods should be reported.
- When the laser point density increases, the accuracy of the tree location, detection rate of smaller and more trees and especially the tree height determination can be improved, but in practise, the improvement depends on the method. Surprisingly, deteriorating of the accuracy by the applied methods was also reported.
- Individual tree based inventory required individual tree based reference collected in the field. Visual interpretation of the airborne laser point cloud is not a feasible way to do the calibration of the extraction method, since this calibration is needed to reduce especially the underestimation of tree height, and for the calibration of the basal area and stem volume.
- Individual tree based solutions may be applied even with lower point densities (e.g. using 2 points per m²), but the optimal point density is most probably dependent on tree

size and density of the forest. This proposes further possibilities of using individual tree based methods.

Acknowledgements

All participants, i.e. Iris Lingenfelder (Definiens AG), Åsa Persson (FOI), François Gougeon (Pacific Forestry Centre), Aiko Sukdolak, Bernd-Michael Wolf and Christian Heipke (University of Hannover), Manuela Hirschmugl (Joanneum Research), Juho Pitkänen (Finnish Forest Research Institute), Svein Solberg (Norwegian Forest Research Institute), Erik Næsset (University of Life Sciences), Jee-cheng Wu (National Ilian University), Sorin Popescu (Texas A&M University), Felix Morsdorf (University of Zürich), Roeland de Kok and Piotr Wezyk (Progea Consulting) and Andrea Barilotti and Francesco Sepic (University of Udine), are gratefully acknowledged for cooperation in the project. François contributed remarkably to the planning of the project. Support of FM-Kartta Oy (currently Blom-Kartta Oy) in providing data for the project is gratefully acknowledged.

References

- Andersen, H-E, Reutebuch, S. and Schreuder, G., 2002. Bayesian Object Recognition for the Analysis of Complex Forest Scenes in Airborne Laser Scanner Data. In *International Archives of the Photogrammetry, Remote Sensing and Spatial Information Sciences*, 34, part 3A, pp. 35-41.
- Axelsson, P., 1999. Processing of laser scanner data - algorithms and applications. *ISPRS Journal of Photogrammetry and Remote Sensing*, 54, pp. 138-147.
- Axelsson P., 2000. DEM Generation from Laser Scanner Data Using Adaptive TIN Models. In *International Archives of Photogrammetry and Remote Sensing*, 33, Part B4, pp. 110-117.
- Axelsson, P., 2001. Ground estimation of laser data using adaptive TIN models. In *Proceedings of OEEPE workshop on airborne laserscanning and interferometric SAR for detailed digital elevation models*, Royal Institute of Technology, Stockholm, Sweden. Publication No. 40. CD-ROM. pp. 185-208.
- Brandtberg, T., 1999. Automatic individual tree-based analysis of high spatial resolution remotely sensed data. PhD thesis, *Acta Universitatis Agriculturae Sueciae, Silvestria* 118, Swedish University of Agricultural Sciences, Uppsala, Sweden. 47 p.
- Brandtberg, T., Warner, T., Landenberger, R. and McGraw, J., 2003. Detection and analysis of individual leaf-off tree crowns in small footprint, high sampling density lidar data from the eastern deciduous forest in North America. *Remote Sensing of Environment*, 85, pp. 290-303.
- Holmgren, J. and Persson, Å., 2004. Identifying species of individual trees using airborne laser scanning. *Remote Sensing of Environment*, 90, pp. 415-423.
- Hyypä, J. and Inkinen, M., 1999. Detecting and estimating attributes for single trees using laser scanner. *The Photogrammetric Journal of Finland*, 16, pp. 27-42.
- Hyypä, J., Schardt, M., Haggrén, H., Koch, B., Lohr, U., Scherrer, H.U., Paananen, R., Luukkonen, H., Ziegler, M., Hyypä, H., Pyysalo, U., Friedländer, H., Uuttera, J., Wagner, S., Inkinen, M., Wimmer, A., Kukko, A., Ahokas, E. and Karjalainen, M., 2001. HIGH-SCAN: The first European-wide attempt to derive single-tree information from laserscanner data. *The Photogrammetric Journal of Finland*, 17, pp. 58-68.
- Kaartinen, H. and Hyypä, J., 2008. EuroSDR/ISPRS Project, Commission II "Tree Extraction", Final Report. *EuroSDR – European Spatial Data Research, Official Publication*, in press.
- Kraus, K. and Pfeifer, N., 1998, Determination of terrain models in wooded areas with airborne laser scanner data. *ISPRS Journal of Photogrammetry and RemoteSensing*, 53, pp.193-203.
- Leckie, D., Gougeon, F., Hill, D.,Quinn, R., Armstrong, L. and Shreenan, R., 2003. Combined

- high-density lidar and multispectral imagery for individual tree crown analysis. *Canadian Journal of Remote Sensing*, 29(5), pp. 633–649.
- Morsdorf, F., Meier, E., Allgöwer, B. and Nüesch, D., 2003. Clustering in airborne laser scanning raw data for segmentation of single trees. In *International Archives of the Photogrammetry, Remote Sensing and Spatial Information Sciences*, 34, (part 3/W13), pp. 27-33.
- Næsset, E., 1997a. Determination of mean tree height of forest stands using airborne laser scanner data. *ISPRS Journal of Photogrammetry and Remote Sensing*, 52, pp. 49-56.
- Næsset, E., 1997b. Estimating timber volume of forest stands using airborne laser scanner data. *Remote Sensing of Environment*, 61, pp. 246-253.
- Persson, Å., Holmgren, J. and Söderman, U., 2002. Detecting and measuring individual trees using an airborne laser scanner. *Photogrammetric Engineering & Remote Sensing*, 68(9), pp. 925-932.
- Popescu, S., Wynne, R. and Nelson, R., 2003. Measuring individual tree crown diameter with lidar and assessing its influence on estimating forest volume and biomass. *Canadian Journal of Remote Sensing*, 29(5), pp. 564–577.
- Serra, J., 1982. *Image analysis and mathematical morphology*, Vol. 1. Academic Press.
- Serra, J., 1988. *Image analysis and mathematical morphology: theoretical advances*. Academic Press.
- Straub, B., 2003. A top-down operator for the automatic extraction of trees - concept and performance evaluation. In *Proceedings of the ISPRS working group III/3 workshop '3-D reconstruction from airborne laserscanner and InSAR data'*, 8-10 October 2003, Dresden, Germany, pp. 34-39.
- Vosselman, G., 2000. Slope based filtering of laser altimetry data. *International Archives of Photogrammetry and Remote Sensing*, 33, No. B3/2, pp. 935-942.
- Wack, R., Schardt, M., Lohr, U., Barrucho, L. and Oliveira, T., 2003. Forest inventory for Eucalyptus plantations based on airborne laser scanner data. In *International Archives of the Photogrammetry, Remote Sensing and Spatial Information Sciences*, 34, Part 3/W13, pp. 40-46.
- Yu, X., Hyypä, J., Kaartinen, H. and Maltamo, M., 2004. Automatic detection of harvested trees and determination of forest growth using airborne laser scanning. *Remote Sensing of Environment*, 90, pp. 451-462.
- Ziegler, M., Konrad, H., Hofrichter, J., Wimmer, A., Ruppert, G., Schardt, M. and Hyypä, J., 2000. Assessment of forest attributes and single-tree segmentation by means of laser scanning. *Laser Radar Technology and Applications V*, 4035, pp. 73-84.

Distinguishing between live and dead tree biomass on North Rim of the Grand Canyon with lidar data

Yunsuk Kim^a, Zhiqiang Yang^a, Warren B Cohen^a, Chris Lauer^b

^aDepartment of Forest Science, Oregon State University, Corvallis, OR 97331, USA

^bSouthern Colorado Plateau Network, NPS. Northern Arizona University, Flagstaff, AZ 86011, USA

Abstract

Accurate estimates of both live and dead biomass in forested ecosystem are important for carbon dynamics studies and forest management. Lidar remote sensing has been used successfully to estimate live biomass, but few studies estimated dead biomass. In this study, our primary goal was to distinguish between live and dead biomass in a mixed coniferous forest on North Rim of the Grand Canyon using small footprint discrete lidar. The study is a part of a project to develop forest structure monitoring protocols for the National Park. The park's goal is to understand present and future ecosystem states and dynamics, biodiversity, habitat, movements of organisms, and flow rates of energy and materials. We examined lidar intensity values for differentiating live vs dead trees using field measurement on 58 plots measured in 2007. We found that lidar intensity values hold great promise for separating dead from live trees. Applying regression techniques we modeled both live and dead biomass.

North Rim forests consist of mixed conifer, dominated by Spruce fir (*Picea spp.*) and Subalpine fir (*Abies lasiocarpa*) on the higher elevation, mixed conifer with various combinations of ponderosa pine (*Pinus ponderosa*), Douglas-fir (*Pseudotsuga menziesii*), Engelmann spruce (*Picea engelmannii*), blue spruce (*Picea pungens*), white fir (*Abies concolor*), and quaking aspen (*Populus tremuloides*) in the mid elevation, and pure ponderosa pine forest on the lower elevations. The park has been preserved by the federal government since late 19th century, at which time grazing and wildfire have been suppressed. This has resulted in development of structures associated with older forest, including a significant amount of standing dead trees.

In this study, lidar intensity was used to separate the first return pulses into live and dead trees. We hypothesized that dead trees have lower intensity values relative to live trees. Regression analysis, and associated cross validation demonstrated that live and dead tree biomass were separable. Total biomass estimation averaged 251.1 Mg ha⁻¹ (R² = 0.83, RMSE = 61.5 Mg ha⁻¹, bias: 0.35 Mg ha⁻¹), dead averaged 54.7 Mg ha⁻¹ (R²: 0.52, RMSE: 41.9 Mg ha⁻¹, bias: -1.28 Mg ha⁻¹). Live biomass was estimated as the difference of total and dead, averaging 195.4 Mg ha⁻¹ (R²: 0.69, RMSE: 55 Mg ha⁻¹, bias: 0.45 Mg ha⁻¹).

Keywords: small footprint, lidar, forest, biomass, dead trees, North Rim USA

Detection of weak and overlapping pulses from waveform airborne laser scanning data

Yu-Ching Lin¹, Jon Mills² & Sarah Smith-Voysey³

¹ Geomatic Engineering, Newcastle University, UK; yu-ching.lin@ncl.ac.uk

² Geomatic Engineering, Newcastle University, UK; j.p.mills@ncl.ac.uk

³ Research, Ordnance Survey, UK; Sarah.Smith-Voysey@ordnancesurvey.co.uk

Abstract

Airborne laser scanning has become a popular technique to estimate canopy height and forest structure. However, current discrete laser scanning systems still suffer the limitation of 3m multi-target resolution and the loss of information about range estimation. In order to improve range resolution and accuracy, new generation small-footprint waveform laser scanning data were investigated. A new approach was developed to detect targets from complex overlapping and weak pulses, which are likely to occur in vegetated areas. The algorithm is based on the popular Gaussian decomposition method and contains two main processing procedures. The shapes of overlapping pulses are analysed to find visible peaks and overlapping peaks, and then reasonable constraints and checks are applied to the fitting process. The test results showed the developed detection algorithm resolved overlapping pulses very well as long as the pulse shapes illustrated asymmetric behaviour or a non-Gaussian distribution. Weak pulses exhibiting a Gaussian shape were also successfully detected.

Keywords: laser scanning, waveform, detection

1. Introduction

Airborne laser scanning has developed rapidly to become the technique of choice for high resolution terrain model generation and detailed vertical distribution of canopy structure in vegetated areas. Current pulsed laser scanning systems are based on time-of-flight techniques to estimate range distances between scanners and targets. Pulse detection methods are applied to detect targets and determine range in order to measure the elapsed time. However, different methods can result in different range resolution (i.e. the ability to differentiate two neighbouring targets from one another) and different range accuracy (i.e. the ability to seek the corresponding positions from transmitted and received pulses) (Baltasvias, 1999; Wagner et al., 2004b; Jutzi and Stilla, 2005). Inaccurate range determination obviously reduces the accuracy of the three-dimensional laser points (Baltasvias, 1999), thereby indirectly affecting the estimate of forest characteristics (e.g. canopy height). In order to meet the demand for high accuracy applications, studies into range estimation are therefore necessary.

In general, typical pulse detection methods applied in discrete laser scanning systems are normally threshold-based (e.g. peak detection, leading edge detection, constant fraction detection) - (Lemmens, 2007). Return pulses with strong, nearly perfect peaks are primarily detected. The common difficulty, however, is to detect weak pulses and complex overlapping pulses, which are likely to occur in vegetated areas. Weak pulses below the threshold go undetected and information about targets which present low reflectance or have been observed at a distance is discarded (e.g. ground information under canopy). On the other hand, when the distance between successive targets diminishes, overlapping pulses are present (Baltasvias, 1999; Wiechert, 2004). The shapes of overlapping pulses are variable and can differ significantly to standard returns, making it virtually impossible for typical pulse detection methods to resolve targets correctly. Therefore, multi-target resolution is seriously limited

(Baltsavias, 1999; Katzenbeisser, 2003) and range distance can be inaccurately estimated (Jutzi and Stilla, 2006). For example, when overlapping pulses occur in areas of low vegetation, ground height could be overestimated. Wiechert (2004) has emphasised that the capability of target separation has a great impact on the quality of elevation models derived from laser scanning data.

Established discrete laser scanning systems only provide three-dimensional coordinates of points and their associated intensity values. Users are unable to determine the errors caused due to the limitations of the pulse detection methods used because the information about range estimation is missing. Moreover, most systems only capture first and (or) last return, or up to four returns, the information in between have been discarded. Commercial small-footprint waveform airborne laser scanning systems have recently become available that store the entire waveform of each received pulse, thereby offering users the opportunity to apply their own pulse detection methods in order to detect targets and define ranges. This creates significant opportunities to overcome the shortcomings of typical pulse detection methods. New potential for improving the classification of laser points is also expected using waveform data (Flood, 2001; Pfeifer et al., 2004; Wagner et al., 2004a) since the characteristics of targets are believed to be present in the waveform (Brenner et al., 2003).

Since 2004, new generation commercial small-footprint waveform laser scanning systems have emerged on the market (Hug et al., 2004; Lemmens, 2007) and there has been an increasing interest in maximising the potential of waveform data. Wagner et al. (2007) investigated the emerging benefits of using this new waveform data. In general, studies have focussed on overcoming the limitation of discrete laser scanning systems. For example, various detectors have been developed to extract more laser points than discrete systems (Persson et al., 2005; Nordin, 2006; Reitberger et al., 2006). However, little attention has been paid to detecting targets from complex pulses and validating results. On the other hand, parameters related to target characteristics have been extracted from waveform data in order to improve the classification of laser points, which has been a popular and challenging research issue for discrete data (Doneus and Briese, 2006; Wagner et al., 2006; Mandlbürger et al., 2007). Thus far, the relationship between target characteristics and derived parameters has not been studied in detail and not widely examined over different land cover types (Doneus and Briese, 2006; Mandlbürger et al., 2007; Pfeifer and Briese, 2007). More research effort is required into the issue of whether this so-called additional information can offer more reliable analysis for different applications and how to integrate it with other datasets (Jutzi and Stilla, 2005; Mandlbürger et al., 2007; Pfeifer and Briese, 2007).

This paper presents a method to detect targets from weak and overlapping pulses in order to achieve high range resolution and accuracy. The method also provides an important foundation for extracting the correct surface features of individual targets. The overview of waveform data derived from a Riegl LMS-Q560 is introduced in Section Two. Section Three presents the details of the developed method. Section Four contains a qualitative validation and comparison with commercial software. Finally, the main findings of the study are summarised in Section Five.

2. Full-waveform data

Waveform data from a Riegl LMS-Q560 full-waveform laser scanner were used in this study. The specifications of this laser scanner are presented in Ullrich et al. (2008). For each timestamp the transmitted waveform, received waveform and scan angle are stored. The sampling rate for digitising the waveform is 1GHz. The waveform is constructed as an amplitude-against-time dataset. The shape of transmitted waveforms is a Gaussian-like distribution (Wagner et al., 2006) as shown in Figure 1 (a). The received waveform is the record

of the returned energy from each laser pulse and can vary with the height distribution of the illuminated surface (Harding et al., 1994). The simplest cases of received waveforms are composed of nearly perfect peaks. For example, Figure 1 (b) shows the received waveform with two returns which are both similar to the shape of the transmitted pulse. More difficult cases are waveforms with complex shapes which are not like the transmitted pulse (see Figure 2). Moreover, waveforms with weak pulses also exist (see Figure 1(c)).

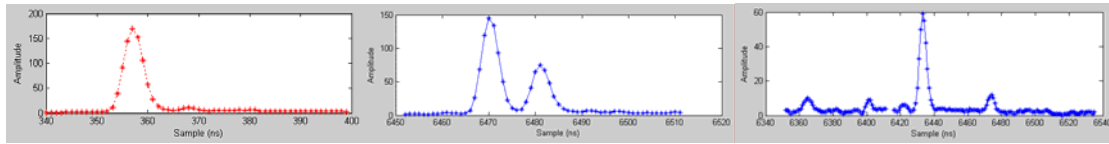


Figure 1: (a) Example of transmitted waveform (b) Received waveform with nearly perfect peaks (c) Received waveform with weak pulses (note Y-axis scale change for illustrative purposes)

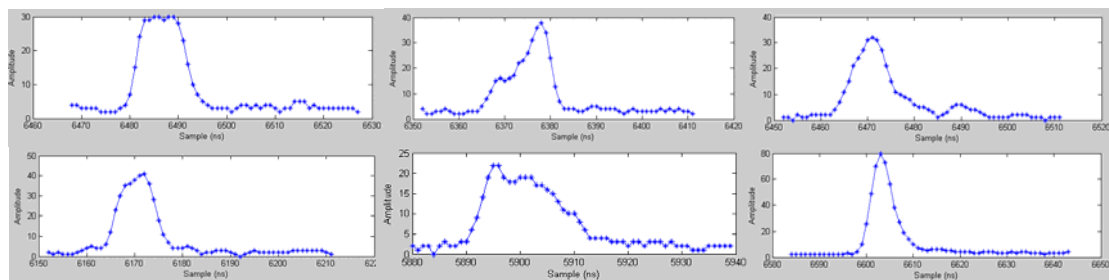


Figure 2: Received waveforms with complex shapes (note Y-axis scale change for illustrative purposes)

After examining different examples of typical received waveforms, a number of questions stand out:

- How many individual targets are hidden within a complex waveform?
- Where is the relative point for range estimation?
- Are weak pulses targets or noise?

A method was developed to seek the answers for the above questions and is described in Section Three.

3. Methodology

Because pulses are transmitted with a Gaussian-like distribution, the Gaussian decomposition method can be used for range estimation. This assumes that each return is Gaussian in nature and that the received signal is a sum of individual Gaussian distributions (Hofton et al., 2000). Fitting Gaussian functions to waveform data provides each return with a parametric description which can be used to store pulse shape information and decreases the effect of noise. Hofton et al. (2000) and Jutzi and Stilla (2005) concluded that the Gaussian decomposition method can improve the accuracy of range measurement compared with algorithms using only single values (e.g. peak algorithm, leading edge algorithm). The algorithm developed herein is therefore based on the Gaussian decomposition method. Waveform data from each laser pulse can be modelled using equation (1). The width parameter is $\sqrt{2}$ times the standard deviation of the Gaussian peak.

$$y = N_{level} + \sum_{i=1}^n A_i \exp \left[- \left(\frac{t - t_i}{width_i} \right)^2 \right] \quad (1)$$

Where A = the amplitude of i th Gaussian t_i = the i th Gaussian peak

N_{level} = noise level of the waveform n = the number of Gaussians
 $width_i$ = pulse width of i th Gaussian

In order to get good fits and reasonable estimates, two main processing procedures are applied.

3.1 Initial Parameter Estimates

Reasonable initial estimates of the number of targets to be detected and the coefficients of Gaussian functions are needed for good fits to be achieved. The main task of this procedure is finding potential peak positions from weak and overlapping pulses. Firstly, visible peaks need to be found for the presence of standard returns. Figure 3 shows the workflow adopted for finding visible peaks. Local maxima are selected as the candidates for visible peaks. A_T is a threshold to separate signal from background noise. A more stringent check is further applied on weak visible peaks (A_S is the threshold for selecting weak peaks) and neighbouring samples since only weak returns with pulse-like shapes should be identified as illuminated targets. In addition, the separation between two visible peaks must be greater than half the pulse length. Any peaks found within this distance are treated as noise. This is based on the assumption that when the separation between two Gaussian components diminishes to less than one pulse length, there is only one main peak existing, and at separations of less than half a pulse length, pulses become entirely like one standard Gaussian distribution. This assumption is demonstrated using simulated data and illustrated in Figure 4.

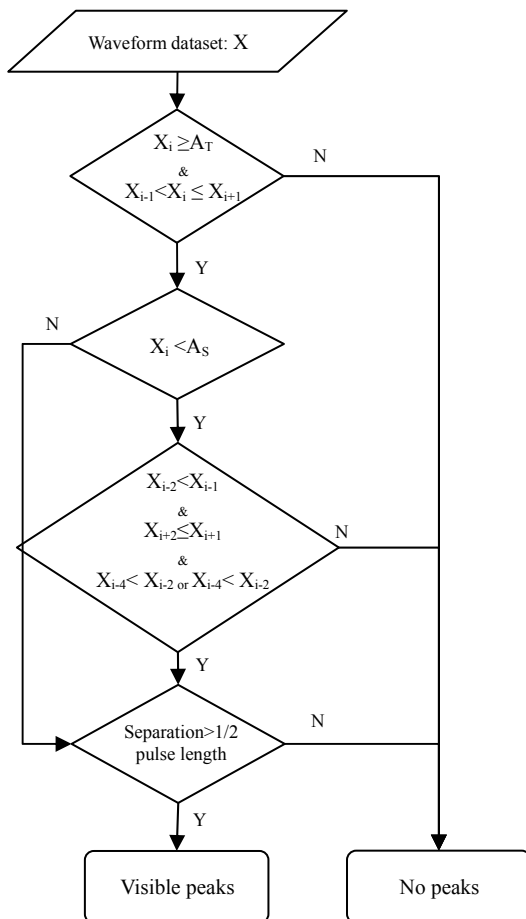


Figure 3: Flowchart for finding visible peaks

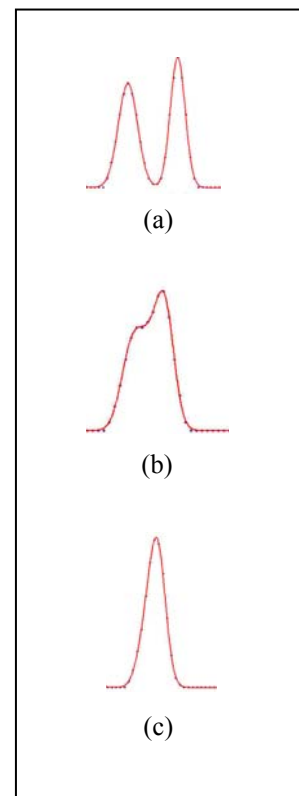


Figure 4: Simulation of received waveform from two returns with different separation (a): 3 pulse length (b): 1 pulse length (c): 1/2 pulse length

Based on the above assumptions, in order to resolve overlapping pulses, the shapes of pulses are analysed to find overlapping peaks. The flowchart for this stage is presented in Figure 5. Essentially, the algorithm looks for asymmetric pulses. It is implemented to find inflexion points on both sides of primary visible peaks. In addition, in order to decrease the sensitivity of finding inflexion points caused by noise effects, step (a) in Figure is applied. Step (b) limits the place where overlapping peaks can be identified to avoid detecting spurious peaks from background noise. Finally, if the number of samples on the edge of a primary peak is much greater than those on the edge of the transmitted pulse, one overlapping peak is forced to exist. Figure 6 shows the examples of detecting visible and overlapping peaks. Once visible and overlapping peaks are detected, initial values for the corresponding amplitude and timing point will also be selected. An initial width value for each Gaussian component is chosen to be the same value as the width of the transmitted pulse.

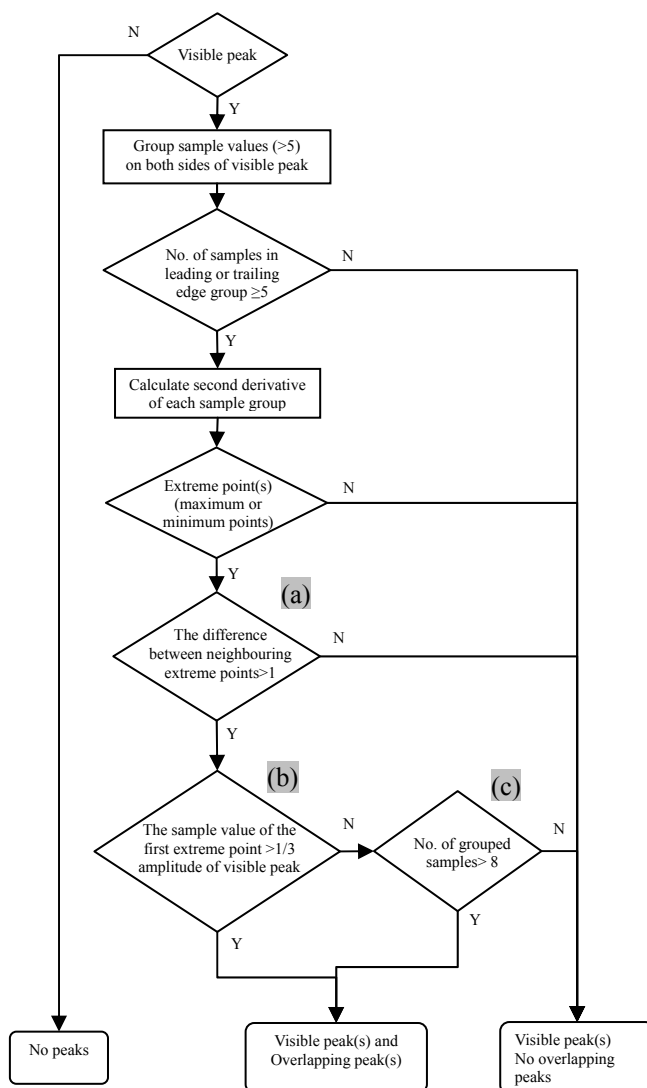


Figure5: Flowchart for finding overlapping peaks

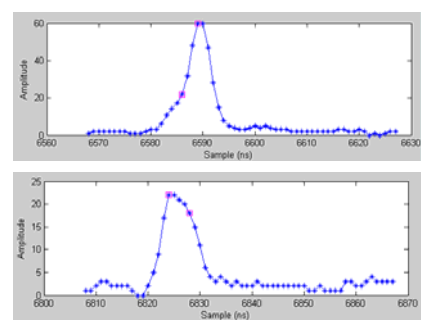


Figure 6: Examples of detecting visible and overlapping peaks

3.2 Parameter Optimization

In order to identify any peaks missed during the first procedure, remove noise, and determine the best estimation of peak positions, Gaussian fitting with reasonable constraints and checks are applied. The flowchart for this stage is presented in Figure 7. In the fitting process, a non-linear optimization technique – the Trust Region algorithm (Branch et al., 1999) – is used to apply constraints on parameter estimates. The lower boundary for Gaussian amplitude is specified as 2, which is the DC offset value, to avoid erroneous estimation. At first, initial parameter estimates from the first procedure (refer to Section 3.1) are used in Gaussian-fitting. Residual maximums from the Gaussian fit are checked to find the peaks missed during the first procedure. Since the ringing effect generates spurious small peaks immediately after pulses with high amplitudes, in order to avoid finding the peaks resulting from ringing, the corresponding amplitude of the sample with high residual value is further checked. Step (a) in Figure 7 selects ambiguous peaks which could result in overlapping and weak pulses to perform further checks, otherwise individual Gaussian parameters are taken as the best estimation. Step (b) contains final checks for reasonable parameter estimates. If any unreasonable parameter is found, the peak will be removed. The constraints are applied on special cases. Sep < 2ns is to limit the minimum separation between two peaks to 2ns, which is 1/2 pulse length of the Riegl LMS-Q560 system, based on the assumption described in Section 3.1. In order to avoid erroneous estimates, thresholds for estimated amplitude and width are applied (e.g. $A < A_{min}$, $Width > \sigma_{max}$, $Width < \sigma_{min}$). Moreover, $A < (Max(x))/10$ & $D_{is} < S_r$ & $Max(x) > P_m$ is set to remove peaks generated by the ringing effect. To prevent detecting background noise, $A < A_w$ & ($Width > \sigma_{wi}$ or $< \sigma_{wm}$) is set to limit the width boundary of extreme weak pulses and $A < A_d$ & $Width > \sigma_d$ is the constraint for potential weak pulses. Finally, $Sep < S_o$ & $DW < D_o$ is applied to check the width difference between two extremely-overlapping pulses whose separation is close to half the pulse length. It is assumed that the width difference between two overlapping peaks must be big enough to allow the presence of a non-Gaussian shape.

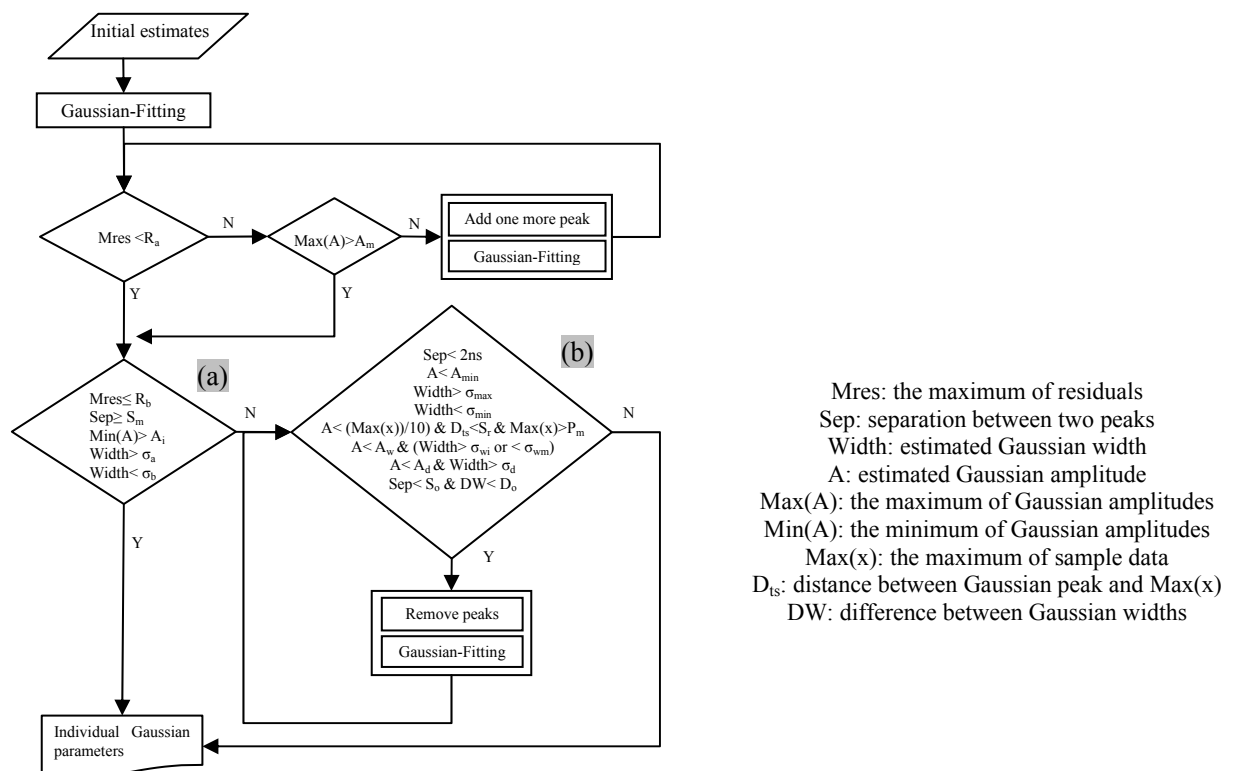


Figure 7: Flowchart for the best estimation of the number of targets and peak positions

4. Results

Waveform data from a Riegl LMS-Q560 full-waveform laser scanner were collected over different land cover classes in Bristol, United Kingdom in August 2006 and used to test the developed approach. Qualitative validation for the detection of overlapping pulses and weak pulses was performed by examining 3D points and orthoimages acquired from the same platform. The performance was compared with commercial software which also processes waveform data.

4.1 Qualitative Validation for Overlapping Pulses

In Great Britain the height of most safety barriers along motorways is 0.61 ± 0.03 m from the ground to the centre of the barrier beams (Wignall et al., 1999). This height can result in overlapping pulses if lasers hit both the barrier and the ground within the footprint. In order to validate the result of resolving overlapping pulses, waveforms that interacted with vehicle safety fences were investigated. Figure 8 shows a sample of examined motorway and red points represent laser points known to interact with safety barriers. Figure 9 (a) and (b) shows sections of laser points as derived from commercial software and the developed algorithm respectively. Figure 9(c) illustrates the corresponding waveforms. It is apparent that the developed algorithm resolved overlapping pulses very well, and the hidden peaks were successfully found. It is evident that more points were extracted using the developed algorithm than with the commercial software.



Figure 8: Examined motorway in Bristol

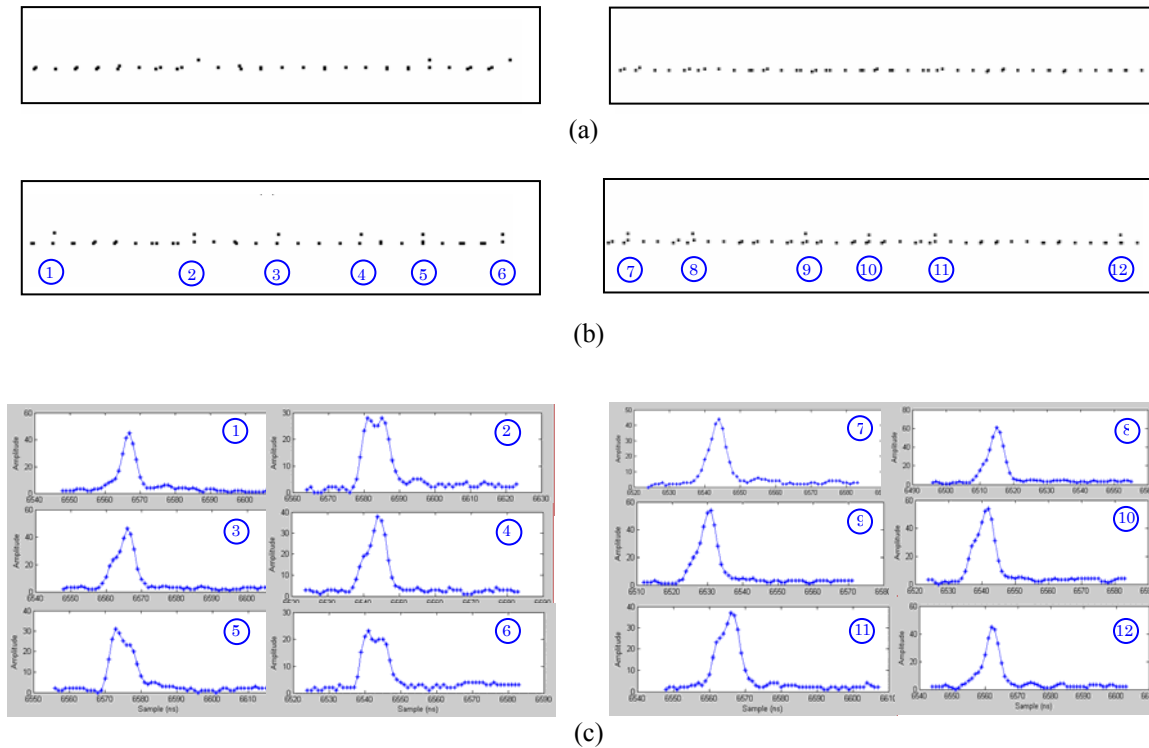


Figure 9: (a) Points from commercial software (b) points from the developed algorithm (c) corresponding waveforms

4.2 Qualitative Validation for Weak Pulses

Figure 10 shows an example of detecting weak pulses in a vegetated area. Red points represent 3D points with low amplitude. Compared with the commercial software, weak pulses are more likely to be detected using the developed algorithm. Interestingly, numerous weak pulses occurred at positions of potential ground points beneath forest canopies. This implies that these laser pulses penetrated the vegetation to the ground level, but the energy of the last returns was very weak to the point of being undetectable by the commercial algorithm.

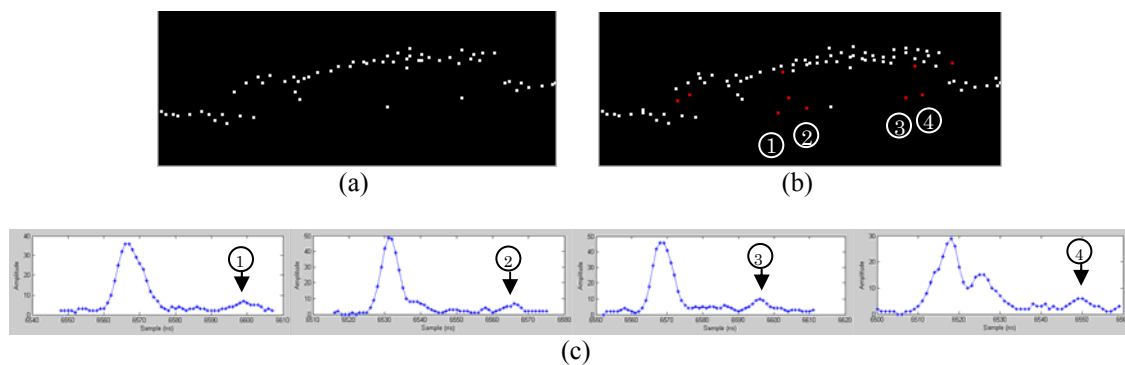


Figure 10: (a) Points from commercial software (b) points from developed algorithm (c) corresponding waveforms

5. Conclusion

This paper has presented a new approach to resolve overlapping pulses and detect weak pulses from small-footprint waveform laser scanning data. The results show the shapes of overlapping pulses were found to be variable and depend on the amplitude, widths and separation distance of overlaid individual pulses. Due to the success of finding overlapping peaks, multi-target resolution has been improved. Moreover, the range accuracy will be improved as peak positions from individual returns are successfully identified. This benefit can potentially reduce the risk of overestimating ground height in vegetated areas. On the other hand, successfully detecting weak pulses can offer the opportunity to acquire more accurate digital terrain models in vegetated areas. Further research is being performed to provide a quantitative validation of these findings, as well as exploring the benefits of waveform parameters (amplitude, width and range) which are extracted after successfully identifying individual targets. It is expected that these waveform parameters offer additional information to further discriminate between on- and off-terrain points, thereby further enhancing outputs from airborne laser scanning.

References

- Baltsavias, E.P., 1999. Airborne laser scanning: basic relations and formulas. *ISPRS Journal of Photogrammetry & Remote Sensing*, 54: 199-214.
- Branch, M.A., Coleman, T.F. and Li, Y., 1999. A Subspace, Interior, and Conjugate Gradient Method for Large-Scale Bound-Constrained Minimization Problems. *SIAM Journal on Scientific Computing*, 21(1): 1-23.
- Brenner, A.C., Zwally, H.J., Bentley, C.R., Csatho, B.M., Harding, D.J., Hofton, M.A., Minster, J.-B., Roberts, L., Saba, J.L., Thomas, R.H. and Yi, D., 2003. Geoscience Laser Altimeter System (GLAS) - Derivation of Range and Range Distributions From Laser Pulse Waveform Analysis for Surface Elevations, Roughness, Slope, and Vegetation Heights. <http://www.csr.utexas.edu/glas/atbd.html> [Accessed: December 2006].
- Doneus, M. and Briese, C., 2006. Digital terrain modelling for archaeological interpretation within forested areas using full-waveform laserscanning. *The 7th International Symposium on Virtual Reality, Archaeology and Cultural Heritage VAST*, Athens, Greece. 155-162.
- Flood, M., 2001. Lidar activities and research priorities in the commercial sector. *International Archives of Photogrammetry and Remote Sensing*, 34(3/W4): 3-7.
- Harding, D.J., Blair, J.B., Garvin, J.B. and Lawrence, W.T., 1994. Laser altimetry waveform measurement of vegetation canopy structure. *Geoscience and Remote Sensing Symposium, 1994. IGARSS '94. Surface and Atmospheric Remote Sensing: Technologies, Data Analysis and Interpretation., International*. 1251-1253
- Hofton, M.A., Minster, J.B. and Blair, J.B., 2000. Decomposition of Laser Altimeter Waveforms. *IEEE Transactions on Geoscience and Remote Sensing*, 38(4): 1989-1996.
- Hug, C., Ullrich, A. and Grimm, A., 2004. Litemapper-5600 – A waveform-digitizing LIDAR terrain and vegetation mapping system. *International Archives of Photogrammetry, Remote Sensing and Spatial Information Sciences*, 36(8/W2): 24-29.
- Jutzi, B. and Stilla, U., 2005. Measuring and processing the waveform of laser pulses. *Optical 3-D Measurement Techniques VII*, 1: 194-203.
- Jutzi, B. and Stilla, U., 2006. Range determination with waveform recording laser systems using a Wiener Filter. *ISPRS Journal of Photogrammetry & Remote Sensing*, 61(2): 95-107.
- Katzenbeisser, R., 2003. *Technical note on: Echo detection*, TopoSys GmbH, Germany.
- Lemmens, M., 2007. *Product Survey on Airborne Lidar Sensors*, GIM International, 21 (2)
- Mandlbürger, G., Briese, C. and Pfeifer, N., 2007. Progress in LiDAR sensor technology - chance and challenge for DTM generation and data administration. *Photogrammetric Week 2007*. 159-169.

- Nordin, L., 2006. *Analysis of waveform data from airborne laser scanner systems*. Master Thesis, Lulea University of Technology.
- Persson, Å., Söderman, U., Töpel, J. and Ahlberg, S., 2005. Visualization and analysis of full-waveform airborne laser scanner data. *International Archives of Photogrammetry, Remote Sensing and Spatial Information Sciences*, 36(3/W19): 103-108.
- Pfeifer, N. and Briese, C., 2007. Geometrical aspects of airborne laser scanning and terrestrial laser scanning. *International Archives of Photogrammetry and Remote Sensing*, 36(3/W52): 311-319.
- Pfeifer, N., Gorte, B. and Elberink, S.O., 2004. Influences of vegetation on laser altimetry - analysis and correction approaches. *International Archives of Photogrammetry, Remote Sensing and Spatial Information Sciences*, 36(8/W2): 283-287.
- Reitberger, J., Krzystek, P. and Heurich, M., 2006. Full-waveform analysis of small footprint airborne laser scanning data in the Bavarian forest national park for tree species classification. *Workshop on 3D Remote Sensing in Forestry*: 218-227.
- Ullrich, A., Studnicka, N., Hollaus, M., Briese, C., Wagner, W., Doneus, M. and Mücke, M., 2008. Improvements in DTM generation by using full-waveform airborne laser scanning data.
http://www.riegl.com/airborne_scanners/airborne_photo_gallery/downloads/Ullrich_et_al_2007_Moskau_engl.pdf [Accessed: 28 Feb, 2008].
- Wagner, W., Eberhöfer, C., Hollaus, M. and Summer, G., 2004a. Robust filtering of airborne laser scanner data for vegetation analysis. *International Archives of Photogrammetry, Remote Sensing and Spatial Information Sciences*, Freiburg, Germany. 56-61.
- Wagner, W., Roncat, A., Melzer, T. and Ullrich, A., 2007. Waveform analysis techniques in airborne laser scanning. *international Archives of Photogrammetry and Remote Sensing*, 36(3/W52): 413-418.
- Wagner, W., Ullrich, A., Ducic, V., Melzer, T. and Studnicka, N., 2006. Gaussian decomposition and calibration of a novel small-footprint full-waveform digitising airborne laser scanner. *ISPRS Journal of Photogrammetry & Remote Sensing*, 60: 100-112.
- Wagner, W., Ullrich, A., Melzer, T., Briese, C. and Kraus, K., 2004b. From single-pulse to full-waveform airborne laser scanners: potential and practical challenge. *International Archives of Photogrammetry, Remote Sensing and Spatial Information Sciences*, 35(B3): 201-206.
- Wiechert, A., 2004. *Linking laser scanning to surveying and visualization*, Geo Informatics, 7, pp. 48-51.
- Wignall, A., Kendrick, P.S., Ancill, R. and Copson, M., 1999. *Roadwork: theory and practice*, 4 Butterworth Heinemann, Zoxford; Boston

Estimation of tree lists from airborne laser scanning data using a combination of analysis on single tree and raster cell level

Eva Lindberg¹, Johan Holmgren¹, Kenneth Olofsson¹,
Håkan Olsson¹ and Jörgen Wallerman¹

¹ Swedish University of Agricultural Sciences, Department of Forest Resource Management, SE-901 83 Umeå, Sweden, (Eva.Lindberg@srh.slu.se)

Abstract

Airborne laser scanning produces high resolution data which opens up for estimation methods on individual tree level. However, the detection rate depends on the forest structure, and typically suppressed trees below a dominant tree layer are not detected. This paper presents a method to produce tree lists consistent with unbiased estimates on raster cell level. First, automatic delineation of tree crown segments was performed. The number and attributes of trees were estimated within segments. Second, forest variables were estimated on a field plot level using both laser canopy height distribution and results from tree detection. Percentiles of the stem diameter and tree height distributions were estimated using regression models. Third, the estimated percentiles were used as input for imputation of field trees from similar field plots in order to create a target distribution matrix. The number of trees in this matrix was estimated by scaling with the estimated total volume for each field plot. Finally, the initial tree list obtained from the tree crown segmentation was adjusted by using the estimated target distribution matrix. Random errors and bias for stem volume and stem number estimates could be reduced by combining analysis on tree and raster cell level.

Keywords: Lidar, single tree, area based, tree list, diameter distribution

1. Introduction

High resolution airborne laser scanning, ALS, data (≥ 10 measurements m^{-2}) can be used for analysis on a tree level (e.g. Hyypä *et al.* 2001; Persson *et al.* 2002; Solberg *et al.* 2006). A digital height model is created from laser data and image analysis techniques, most often Individual Tree Crown delineation, ITC, are used to detect individual trees and measure position, height, and canopy shape. This method is now being marketed as operational. However, the detection rate depends on the forest structure (Persson *et al.* 2002). Thus, estimates that are based only on analysis of individual trees might be biased (Maltamo *et al.* 2004).

ALS is used operationally in Scandinavia for estimation of forest variables on raster cell level, the so called area based method, usually with regression models built on the Laser Canopy Height, LCH. The area based method generally produces forest variable estimates with high accuracy (Næsset *et al.* 2004) and low bias (Maltamo *et al.* 2006). Single tree methods usually have lower accuracy and underestimate the amount of trees (Næsset *et al.* 2004). Maltamo *et al.* (2004) have suggested a combination of methods to use the high accuracy from area based methods and the information for the dominant tree layer from single tree methods

The aim of this study is to develop methods to supply an information system with a list of trees, each tree with estimated attributes, e.g. stem diameter and tree height. A method is presented to estimate tree lists with a combination of individual tree and raster cell level estimates. The

objective is to develop and validate a method that produces tree lists consistent with unbiased estimates on a raster cell level.

2. Material and Methods

2.1 Study area

The study area is 1989 hectare large and located in the north of Sweden (lat. 64° 25' N, long. 14° 50' E). The dominating tree species are Norway spruce (*Picea Abies*), birch (*Betula spp*) and Scots pine (*Pinus Silvestris*). The elevation ranges from 325 to 658 m a.s.l., which means that the site is located close to the limit for productive forest.

2.2 ALS data

The laser data acquisition was performed on August 7 and 8 2007 using a Leica ALS50-II airborne laser scanning system carried by a helicopter. The flying altitude was 600 m and the scan angle ± 16 degrees, resulting in a scan width of 375 m and a scan density of about 10 points m^{-2} . Laser returns were classified as ground or non ground using a progressive Triangular Irregular Network (TIN) densification method (Axelsson 1999, 2000) in the TerraScan software (Soininen 2004), and the ground returns were used to derive a Digital Terrain Model (DTM).

2.3 Field data

The area was divided into five strata using an existing stand register and a total of 179 field plots were allocated (Table 1). The field plot radius was 6 m in stratum 1-3 and 8 m in stratum 4-5. The position of the field plots were measured using a Global Navigation Satellite System (GNSS). The trees on the field plots were measured using the Forest Management Planning Package (Jonsson *et al.* 1993). Within the plots, all trees with a stem diameter larger than the minimum stem diameter, 40 mm in stratum 1-3 and 60 mm in stratum 4-5, were callipered and tree species was recorded. The positions of the trees were registered relative to the centre of each plot by measuring azimuth and distance with a compass and ultrasonic device, respectively. The position of a tree was not measured if the tree had a large inclination.

Table 1: Summary of field plot data

| Stratum | Selection criterion | Number of field plots | Species composition, percentage pine/spruce/other | Stem volume, average and 5/95 percentiles ($m^3 ha^{-1}$) | Stem density, average and 5/95 percentiles (ha^{-1}) |
|---------|---|-----------------------|---|---|--|
| 1 | Age 25-74 years, pine dominated ($\geq 60\%$) | 23 | 61/25/14 | 40, 28/59 | 1484, 539/2847 |
| 2 | Age 25-74 years, spruce dominated | 29 | 0/65/35 | 49, 13/122 | 1524, 654/2493 |
| 3 | Age 25-74 years, mixed forest | 33 | 31/40/29 | 43, 6/132 | 1299, 601/2440 |
| 4 | Age >75 years, spruce dominated | 60 | 9/74/17 | 119, 41/218 | 895, 540/1450 |
| 5 | Age >75 years, pine dominated or mixed forest | 34 | 36/56/8 | 140, 51/261 | 895, 413/1577 |

2.4 Individual tree crown delineation, ITC

The first task was to automatically delineate tree crowns based on geometric tree crown models. A correlation image was produced by using geometric tree models and a Digital Canopy Model (DCM) derived from ALS height data. The correlation image was then smoothed and used for segmentation: a seed was placed at each pixel, with a DCM value greater than the height threshold and with a positive correlation value, and was allowed to climb to the neighbour pixel with the highest correlation value. The pixels with seeds climbing to the same local maximum defined a tree crown segment (Holmgren et al. 2006). The result was crown segments; each included an individual tree or a group of trees. The tree position was estimated by taking the x, y-position of the maximum canopy height value within the segment, and a measure of tree height (H) was achieved from the value of the maximum. The crown area of an individual tree could be derived by counting the number of pixels of a segment. A width (W) of a segment was derived assuming that a tree crown was circular.

2.5 Field plot matching

The three dimensional spatial pattern of the laser detected trees were matched with the spatial pattern of field measured positions of individual trees on a plot. The trees detected in ALS data were automatically linked to field measured trees (Olofsson *et. al* 2008).

2.6 Estimation on tree segment level

Each segment should ideally correspond to one tree on the ground but in reality, one segment may enclose several trees or one tree may be divided into several segments (Figure 1). Single tree properties have been estimated in two different ways: With regression models for variables of one tree in each segment, ITC, and with regression models for variables of the largest tree plus variables of the other trees in the segment, ITC with classification.



Figure 1: Example of polygons from segmentation of ALS data and field measured trees shown as point symbols and circles with radius proportional to diameter.

2.6.1 Classification of segments to determine number of trees

Features were extracted from ALS data within the segments in order to model the number of field trees within a segment. Only segments where the centre was located inside a field plot and at least 2 m from the boundary were used in the analysis to reduce the number of segments covering ground outside field plots, referred to as reference segments. The variables 1-2 (Table 2) were calculated from laser data, the rest were derived from field data.

Table 2: Variables used for analysis on tree crown segment level

| | Variable | Description |
|----|--------------------|--|
| 1 | W | \sqrt{A} , A is the area of the segment |
| 2 | W/mean(W) | Mean(W) is the mean of segment widths within same plot |
| 3 | N | Number of field measured trees within segment |
| 4 | D _{max} | Maximum field measured stem diameter found within segment |
| 5 | D _{other} | Sum of field measured stem diameter for other trees within segment |
| 6 | H _{max} | Maximum field measured tree height found within segment |
| 7 | H _{other} | Mean of field measured tree height for other trees within segment |
| 8 | B _{max} | Maximum field measured basal area found within segment |
| 9 | B _{other} | Sum of field measured basal area for other trees within segment |
| 10 | V _{max} | Maximum field measured stem volume found within segment |
| 11 | V _{other} | Sum of field measured stem volume for other trees within segment |

The strongest correlation for number of field measured trees inside segment was obtained for W and W/mean(W). W and W/mean(W) were divided into eight intervals and each reference segment was placed in an interval in order to estimate the probability for a reference segment to enclose a certain number of trees. The number of segments enclosing 1, 2, 3 and 4 or more field measured trees respectively was calculated for each interval and divided by the total number of segments in the interval.

$$P(N = i) = \frac{n_i}{\sum_{i=1}^{N_{max}} n_i} \quad (1)$$

where n_i = number of segments enclosing i field measured trees in the interval and $N_{max} = 4$. $P(N = i)$ is an estimate of the probability for a segment to enclose i field measured trees. The reference segments were used to build regression functions for 4-11 (Table 2). The regression was done separately for segments enclosing different number of field measured trees.

An unknown segment was first placed in an interval determined by W and W/mean(W). The number of trees inside the segment was estimated as the sum of the probability to have a certain number of trees inside the segment times the number of trees.

$$N_{estimated} = \sum_{i=1}^{N_{max}} P(N = i) \times i \quad (2)$$

2.6.2 Estimation of tree variables from segments

The variables 4-11 (Table 2) were estimated in each segment as

$$A_{estimated} = \sum_{i=1}^{N_{max}} P(N = i) \times A_i \quad (3)$$

where A_i is the value of the variable calculated from a regression model for segments enclosing i field measured trees.

The result for each segment was an estimate of variables for the largest tree in the segment, i.e. 4, 6, 8 and 10 (Table 2). ITC with classification also resulted in an estimate of variables for the rest of the trees in the segment, i.e. 5, 7, 9 and 11 (Table 2). The later estimate was divided by

the estimated number of trees minus one to get an estimate for each tree.

$$A^t_{estimated} = A_{estimated} / (N_{estimated} - 1) \quad (4)$$

If the result for the tree diameter was below the minimum value for the field measured tree diameter, $N_{estimated}$ was iteratively reduced with one until the resulting tree diameter was above the minimum value. If the tree diameter was too small even when divided by one, the estimate was discarded. The estimates for the largest tree and the rest of the trees were put in a list of tree candidates.

2.7 Estimation on raster cell level

2.7.1. Estimation based on laser canopy height distribution, LCH

Several features, height percentiles, average height of laser reflections, standard deviation of laser reflections and vegetation ratio, were derived based on the Laser Canopy Height (LCH) distribution by using vegetation returns. In order to exclude returns from below the canopy, e.g. shrubs and stones, vegetation returns were defined as returns with a vertical distance to the DTM greater than one meter and 10% of the maximum height within the plot/raster cell. These features were used to build regression models for the field measured percentiles for stem diameter and height distributions at 25%, 50%, 75% and 100%, as well as average stem volume per hectare and number of stems per hectare. Stepwise regression was used to find the most significant variables and Seemingly Unrelated Regression (SUR) was finally used to model the percentiles (Table 3).

Table 3: Seemingly unrelated regression (SUR) for tree height and stem diameter distribution using laser canopy height distribution

| SUR model for stem diameter percentiles | SUR model for tree height percentiles |
|--|--|
| $D_{25} \sim p_{10} + p_{70} + z_{avg} + z_{stdh} + \text{vegratio}$ | $H_{25} \sim p_{10} + p_{70} + z_{avg} + z_{stdh} + \text{vegratio}$ |
| $D_{50} \sim p_{70} + z_{avg} + z_{stdh} + \text{vegratio}$ | $H_{50} \sim p_{70} + z_{avg} + z_{stdh} + \text{vegratio}$ |
| $D_{75} \sim p_{70} + z_{avg} + z_{stdh} + \text{vegratio}$ | $H_{75} \sim p_{95} + z_{avg} + z_{stdh} + \text{vegratio}$ |
| $D_{100} \sim p_{95} + z_{avg} + z_{stdh} + \text{vegratio}$ | $H_{100} \sim p_{95} + z_{avg} + z_{stdh} + \text{vegratio}$ |

The regression model used to estimate stem volume per hectare was (Eq. 5) and the regression model used to estimate number of stems per hectare was (Eq. 6). The result was corrected for logarithmic bias (Holm, 1977).

$$\log(\text{Vol}) \sim \log(p_{90}) + \log(\text{vegratio}) + \log(z_{avg}) \quad (5)$$

$$\text{Dens} \sim p_{90} + z_{stdh} + \text{vegratio} \quad (6)$$

where D_{25} , D_{50} , D_{75} and D_{100} = 25, 50, 75 and 100 percentile from field measured tree diameter, H_{25} , H_{50} , H_{75} and H_{100} = 25, 50, 75 and 100 percentile from field measured tree height, Vol = stem volume per hectare, Dens = number of stems per hectare, p_{10} , p_{20} , ... = 10, 20, ... percentile from laser reflection heights on plot, z_{avg} = average height of laser reflections on plot and z_{stdh} = standard deviation of laser reflections on plot and vegratio = vegetation ratio, the number of laser reflections from vegetation divided by the total number of laser reflections on plot.

2.7.2. Estimation based on laser canopy height distribution, LCH, and distribution of detected trees, ITC

The laser reflection variables were combined with variables from individual tree detection aggregated on plots and used to build regression models for the field measured variables. Stepwise regression was used to find the most significant variables and SUR was used to model the percentiles (Table 4).

Table 4: Seemingly unrelated regression (SUR) for tree height and stem diameter distribution using distribution of detected trees

| SUR model for stem diameter percentiles | SUR model for tree height percentiles |
|--|--|
| $D_{25} \sim p_{10} + Z_{avg} + \text{vegratio} + D_{60}(\text{ST}) + H_{50}(\text{ST})$ | $H_{25} \sim p_{10} + Z_{avg} + \text{vegratio} + D_{60}(\text{ST}) + H_{50}(\text{ST})$ |
| $D_{50} \sim p_{30} + Z_{avg} + \text{vegratio} + D_{60}(\text{ST}) + H_{75}(\text{ST})$ | $H_{50} \sim p_{30} + Z_{avg} + \text{vegratio} + D_{60}(\text{ST}) + H_{75}(\text{ST})$ |
| $D_{75} \sim p_{70} + Z_{avg} + \text{vegratio} + D_{75}(\text{ST}) + H_{80}(\text{ST})$ | $H_{75} \sim p_{70} + Z_{avg} + \text{vegratio} + D_{75}(\text{ST}) + H_{80}(\text{ST})$ |
| $D_{100} \sim p_{95} + Z_{avg} + \text{vegratio} + D_{75}(\text{ST}) + H_{100}(\text{ST})$ | $H_{100} \sim p_{95} + Z_{avg} + \text{vegratio} + D_{75}(\text{ST}) + H_{100}(\text{ST})$ |

The regression model used to estimate stem volume per hectare was (Eq.7) and the regression model used to estimate number of stems per hectare was (Eq. 8).

$$\text{Vol} \sim \text{vegratio} + \text{Vol}(\text{ST}) \tag{7}$$

$$\text{Dens} \sim p_{90} + \text{vegratio} + \text{Dens}(\text{ST}) + H_{100}(\text{ST}) \tag{8}$$

where $D_{10}(\text{ST}), D_{20}(\text{ST}), \dots = 10, 20, \dots$ percentile from diameters from individual tree detection, $H_{10}(\text{ST}), H_{20}(\text{ST}), \dots = 10, 20, \dots$ percentile from heights from individual tree detection, $\text{Vol}(\text{ST}) =$ stem volume per hectare from individual tree detection and $\text{Dens}(\text{ST}) =$ number of stems per hectare from individual tree detection.

2.8 Adjusting tree candidate list from estimates on raster cell level

The estimates of tree diameter and height percentile, stem volume and stems per hectare were used to identify plots with similar distributions. This was done by finding the plots with the smallest sums of squared differences between the values, i.e. the nearest neighbours. Plots were included in the list one by one until the number of trees was at least 800 or the number of included plots was 10.

The field measured trees on plots with similar distributions were put into a field distribution matrix where each row corresponded to a tree height percentile and each column to a tree diameter percentile (Table 5). The percentiles were calculated from the list of trees on similar plots.

Table 5: The distribution matrixes used for the analysis

| Field distribution | Target distribution | Stem distribution |
|---|---|--|
| $N_{f11} \ N_{f12} \ N_{f13} \ N_{f14} \ N_{f15}$ | $N_{t11} \ N_{t12} \ N_{t13} \ N_{t14} \ N_{t15}$ | $N_{st11} \ N_{st12} \ N_{st13} \ N_{st14} \ N_{st15}$ |
| $N_{f21} \ N_{f22} \ N_{f23} \ N_{f24} \ N_{f25}$ | $N_{t21} \ N_{t22} \ N_{t23} \ N_{t24} \ N_{t25}$ | $N_{st21} \ N_{st22} \ N_{st23} \ N_{st24} \ N_{st25}$ |
| $N_{f31} \ N_{f32} \ N_{f33} \ N_{f34} \ N_{f35}$ | $N_{t31} \ N_{t32} \ N_{t33} \ N_{t34} \ N_{t35}$ | $N_{st31} \ N_{st32} \ N_{st33} \ N_{st34} \ N_{st35}$ |
| $N_{f41} \ N_{f42} \ N_{f43} \ N_{f44} \ N_{f45}$ | $N_{t41} \ N_{t42} \ N_{t43} \ N_{t44} \ N_{t45}$ | $N_{st41} \ N_{st42} \ N_{st43} \ N_{st44} \ N_{st45}$ |
| $N_{f51} \ N_{f52} \ N_{f53} \ N_{f54} \ N_{f55}$ | $N_{t51} \ N_{t52} \ N_{t53} \ N_{t54} \ N_{t55}$ | $N_{st51} \ N_{st52} \ N_{st53} \ N_{st54} \ N_{st55}$ |

The number of trees N_{fij} in each interval was multiplied by a scaling factor.

$$S_{\text{Vol}} = \frac{\text{Volume on plot from area estimates}}{\text{Total volume on similar plots}} \quad (9)$$

The result was an estimated target distribution matrix where each element corresponded to a tree diameter and height percentile and the value $n_{ct,j}$ corresponded to the number of trees on the plot in each percentile. The distribution of tree candidates was calculated by summing the number of tree candidates $n_{stt,j}$ in each percentile given by the target distribution. Tree candidates with a tree diameter or height larger than the 100 percentile were excluded from the list.

The difference between the target distribution and the candidate distribution was calculated for each interval. If the number of tree candidates was too big, that number of tree candidates was excluded from the list. If the number of tree candidates was too small, that number of trees with correct tree diameter and height was added to the list by selecting trees at random from the list of field measured trees. The result was a list of trees with distribution and stem volume on plots predicted by the estimates on plot level.

The result was aggregated on plot level and the procedure was repeated 50 times to study the average accuracy of the estimation.

2.9 Validation

RMSE and bias of stem volume per hectare and stem number per hectare was calculated for each method. Error index for tree heights, diameters and basal area on each plot was also calculated. The error index EI is defined as (Reynolds *et al.* 1988),

$$EI = \frac{1}{N_T} \sum_{j=1}^m |T_j - I_j| \quad (10)$$

where I_j is the number of estimated trees to histogram class j , T_j is the number of actual trees in class j , and N_T is the total number of actual trees. This index measures the proportion of mismatch between two histograms based on given class boundaries.

3. Results

For estimation of stem volume, marginally lower RMSE was obtained from the model based on individual tree crown delineation after accumulation to plot level (Table 6, A) compared to the area based method that used laser canopy height percentiles as explanatory variables in the regression model (Table 6, C). For estimation of number of stems, RMSE was lower for the method based on LCH distribution compared to the ITC based method. ITC resulted in a large negative bias which was reduced to zero by using LCH.

Both RMSE and bias was reduced for the ITC based method by classification of segments (Table 6, A and B). Further reduction of RMSE was possible if the estimates on segment level were summed to plot level and then used together with vegetation ratio as explanatory variables in a linear regression model (Table 4 and Eq. 7). By using this method (Table 6, D) for estimation of stem volume, the bias could be reduced to zero and the lowest RMSE was obtained. Adjusting the tree lists with the diameter-height distribution target matrix did not change the volume estimates much. For the stem number estimates, both RMSE and bias were reduced (Table 6, E and F).

Table 6: RMSE and bias for stem volume and stem number estimates on plot level using the methods: Individual Tree Crown delineation (ITC), ITC with classification, Laser Canopy Height (LCH) distribution, LCH and ITC distributions, ITC with adjustment, and ITC with classification and adjustment. Percentages of mean values within brackets

| Method | Stem volume (m ³ ha ⁻¹) | | Stem number (ha ⁻¹) | |
|--|--|------------|---------------------------------|-------------|
| | RMSE | Bias | RMSE | Bias |
| A ITC | 35 (36%) | -14 (-14%) | 595 (52%) | -403 (-35%) |
| B ITC with classification | 33 (34%) | -2 (-3%) | 515 (45%) | -208 (-18%) |
| C LCH distribution | 35 (37%) | -2 (-2%) | 358 (31%) | 0 (0%) |
| D LCH and ITC distribution | 31 (33%) | 0 (0%) | 339 (30%) | -2 (0%) |
| E ITC with adjustment | 34 (36%) | 4 (4%) | 402 (35%) | 44 (4%) |
| F ITC with classification and adjustment | 33 (34%) | 4 (4%) | 411 (36%) | 52 (5%) |

The error index, which measures the proportion of mismatch between two histograms, decreased after adjustment of tree lists with the diameter-height distribution target matrix. This was observed for tree height, stem diameter, and basal area distributions, although the difference was most obvious for tree height and stem diameter distributions (Table 7).

Table 7: Error index for distribution of tree height, stem diameter, and basal area, on plot level using the methods: Individual Tree Crown delineation (ITC), ITC with classification, ITC with adjustment, and ITC with classification and adjustment.

| Method | Error index | | |
|--|-------------|---------------|------------|
| | Tree height | Stem diameter | Basal area |
| A ITC | 98 | 97 | 90 |
| B ITC with classification | 109 | 99 | 92 |
| E ITC with adjustment | 95 | 92 | 89 |
| F ITC with classification and adjustment | 96 | 93 | 89 |

4. Discussion

This study examined combinations of area based estimations and single tree estimations from segmentation. Such a combination gives more accurate estimation of stem volume per hectare than area based estimations only. The result for stem volume from LCH area based estimation was slightly less accurate than the result from ITC but it is not possible to draw any conclusions from that since the difference was small. RMSE was higher for all methods compared to other studies (Maltamo et al. 2006, Næsset et al. 2004). One reason may be that the plot size was small. Trees standing close to a plot boundary may have a big part of their branches on the other side. It is likely that the overall accuracy would be higher if a larger plot size was used. The proportion of deciduous forest was high, approximately 30% in stratum 2 and 3, which may degrade the accuracy considerably (Næsset *et al.* 2004). The analyses are not done with stratified data. Stratification of data and use of separate regression models for different strata may improve the accuracy of the estimates. However, the aim of this study is to compare the different methods and their results relative to each other using the same dataset.

The study has also proposed a new method to create tree lists from estimation of forest variables on raster cell level. Those tree lists are more accurate estimates of stems per area unit than tree lists from individual tree detection. However, the RMSE of stem volume per area unit is almost the same. This may be due to the random selection from the list of field measured trees.

The error index was lower for the tree lists adjusted with results from the area based method. Individual tree detection works best for larger trees and the area based method probably adds

most information for smaller trees. It may be possible to improve this by deriving larger trees from individual tree detection and adjusting the distribution according to results from the area based method for smaller trees. This is in line with the method used by Maltamo *et al.* (2004).

Acknowledgements

This study was financed by Prevista A/S and Formas. . The National Property Board financed the ALS data and field data for this study.

References

- Axelsson, P. 1999. Processing of laser scanner data – algorithms and applications. *ISPRS Journal of Photogrammetry and Remote Sensing* 54:138-147.
- Axelsson, P. 2000. DEM generation from laser scanner data using adaptive TIN models. *International Archives of Photogrammetry and Remote Sensing* 33:110-117.
- Holmgren, J. and Wallerman, J., 2006. Estimation of tree size distribution by combining vertical and horizontal distribution of LIDAR measurements with extraction of individual trees. In: T. Koukal and W. Schneider (Eds.). In Proceedings from Workshop on 3D Remote Sensing in Forestry, Vienna, Austria, 14-15 February 2006, pp. 168-173. University of Natural Resources and Applied Life Science, Vienna, Austria.
- Holm, S. 1977. Transformationer av en eller flera beroende variabler i regressionsanalys. Swedish University of Agricultural Sciences, Stockholm, HUGIN rapport nr 7. 21 pp. (in Swedish).
- Hyypä, J., Kelle, O., Lehtikainen, M. and Inkinen, M., 2001. A segmentation-based method to retrieve stem volume estimates from 3-d tree height models produced by laser scanners. *IEEE Transactions on Geoscience and Remote Sensing*, 39, 969-975.
- Jonsson, B., Jacobsson, J. and Kallur, H., 1993. The forest management planning package. Theory and application. *Studia Forestalia Suecica* 189, Swedish Univ. of Agric. Sci., Umeå, Sweden. 56 p.
- Maltamo, M., Eerikäinen, K., Packalén, P. and Hyypä, J., 2006. Estimation of stem volume using laser scanning-based canopy height metrics. *Forestry*, 79:2, 217-229.
- Maltamo, M., Eerikäinen, K., Pitkänen, J., Hyypä, J. and Vehmas, M., 2004. Estimation of timber volume and stem density based on scanning laser altimetry and expected tree size distribution functions. *Remote Sensing of Environment*, 90, 319-330.
- Næsset, E., Gobakken, T., Holmgren, J., Hyypä, H., Hyypä, J., Maltamo, M., Nilsson, M., Olsson, H., Persson, A., and Söderman, U., 2004. Laser Scanning of Forest Resources: The Nordic Experience. *Scandinavian Journal of Forest Research*, 19, 482-499.
- Olofsson, K., Lindberg, E. And Holmgren, J. 2008. A method for linking field-surveyed and aerial-detected single trees using cross correlation of position images and the optimization of weighted tree list graphs. Submitted to Silvilaser 2008, 8th international conference on LiDAR applications in forest assessment and inventory. Edinburgh, Heriot-Watt University.
- Persson A., Holmgren J. and Soderman U. 2002. Detecting and measuring individual trees using an airborne laser scanner. *Photogrammetric engineering and remote sensing*, 68:9, 925-932.
- Reynolds, M. R., Burk, T. E. and Huang, W.C. 1988. Goodness-of-fit tests and model selection procedures for diameter distribution models. *Forest science*, 34 :2, 373-399.
- Soininen, A. 2004. TerraScan for MicroStation, User's Guide. Terrasolid Ltd., Jyväskylä, Finland. 132 p.
- Solberg, S., Naesset, E. and Bollandsas, O.M. 2006. Single tree segmentation using airborne laser scanner data in a structurally heterogeneous spruce forest. *Photogrammetric Engineering and Remote Sensing*. 72: 12, 1369-1378.

Observational evidence for links between increased drought severity and land-cover change

S. O. Los¹, J. A. Rosette¹ and P.R.J. North¹

¹Climate and Land-Surface Systems Interaction Centre (CLASSIC), Department of Geography, School of the Environment and Society, Swansea University, Singleton Park, Swansea SA2 8PP email: s.o.los@swansea.ac.uk

Abstract

During the past millennium man has significantly changed the land-surface vegetation. Land-cover change by man has occurred since prehistoric times, but has accelerated over the past decades. Model studies indicate that changes in land cover affect climate, e.g., models indicate in the Sahel a causal link between reduction of vegetation and increased drought severity in the Amazon triggered by extensive deforestation.

Here we present observational evidence for land-cover change at the global scale and a subsequent link with the intensification of drought. We analyse global climate data, data on historic land use and satellite data indicating vegetation height (ICESAT / GLAS) and amount of solar radiation absorbed for photosynthesis (AVHRR / SeaWiFS). Analysis of these data indicates that vegetation height and the amount of solar radiation absorbed for photosynthesis are reduced in regions of the world where vegetation is significantly altered by humans. These reductions in vegetation appear the most severe in some regions in the tropics and sub tropics. Moreover, we find that droughts are significantly more severe in areas where vegetation has changed, both in regions where vegetation growth is limited by precipitation as well as in regions where vegetation growth is limited by temperature.

Keywords: GLAS/ICESAT, land-cover change, land-atmosphere interactions

An analysis of the relationships between tree growth and crown information derived from airborne LiDAR data

Tohru Nakajima¹, Yasumasa Hirata², Takuya Hiroshima³,
Naoyuki Furuya⁴ and Satoshi Tatsuhara⁵

¹Graduate School of Agricultural and Life Sciences, the University of Tokyo,
nakajima@fr.a.u-tokyo.ac.jp

² Forestry and Forest Products Research Institute, hirat09@affrc.go.jp

³Graduate School of Agricultural and Life Sciences, the University of Tokyo,
hiroshim@uf.a.u-tokyo.ac.jp

⁴Forestry and Forest Products Research Institute, nfuruya@ffpri.affrc.go.jp

⁵Graduate School of Agricultural and Life Sciences, the University of Tokyo,
tatsu@fr.a.u-tokyo.ac.jp

Abstract

The objective of our study was to estimate the relationship between crown information and individual tree growth using airborne light detection and ranging (LiDAR) data. We established two study plots in the University of Tokyo Forest in Chiba for the analysis of canopy information. We conducted a linear regression analysis between the crown lengths and widths obtained from ground surveys and those obtained from airborne LiDAR data. The crown lengths and crown widths obtained from airborne LiDAR data were correlated with those obtained from ground surveys ($R^2=0.46$, $R^2=0.56$). Next, we compared the crown surface area derived from airborne LiDAR data to tree growth observed in the study plot. The crown surface areas obtained from airborne LiDAR data were highly correlated with tree growth obtained from ground surveys ($R^2=0.95$). Thus, airborne LiDAR accurately measured individual tree growth. We also compared tree growth to the proportion of crown surface area to stem surface area calculated from a stem curve based on a field survey. An exponential regression between tree growth and the proportion of crown surface area to stem surface area was carried out, resulting in a coefficient of determination of 0.74.

Keywords: airborne LiDAR, crown, even-aged stands, stem, tree growth

1. Introduction

A forest grows due to the photosynthesis of its trees (Arain and Restrepo-Coupe 2005). Forest growth decreases as the respiration of trees increases (Bosc *et al.* 2003). This suggests that one can predict forest growth based on the balance between the photosynthesis and respiration of trees.

The main parts of a tree involved in photosynthesis and respiration are the canopy and wood including the stems, branches, and roots, respectively. To estimate forest resources, one can collect direct, ground-based data on woodiness, such as the diameter at breast height (DBH) and the number of stems. Various growth models have been developed based on stem information, including the tree height and DBH (Castedo-Dorado *et al.* 2007; Qin *et al.* 2007). However, it is difficult to measure a crown structure that is high and complex. It is even more difficult to measure crown information over a wide area. Thus, no growth models that include crown information have been developed for Japanese mountainous areas at the regional scale.

Previous studies have suggested the utility of remotely sensed data for measuring forest resources such as stand age (Farid *et al.* 2006), tree height (Hirata 2005; Takahashi *et al.* 2005; Næsset and Bjercknes 2001), and forest biomass (Labrecque *et al.* 2006). In addition, airborne light detection and ranging (LiDAR) data enable us to obtain a wide range of canopy information, including leaf area (Roberts *et al.* 2005), canopy fuel (Andersen *et al.* 2005), and canopy structure (Coops *et al.* 2007).

As mentioned above, it is important to analyze the relationship between woody information and canopy information in developing a growth model that considers the balance of respiration and photosynthesis. However, few previous studies have analyzed the relationship of crown information estimated from LiDAR and woody information measured by a ground survey in Japan.

The objective of our study was to model tree growth as a function of the crown surface area derived from airborne LiDAR data. First, we examined the accuracy of crown information derived from airborne LiDAR for calculating the crown surface area. We then conducted a linear regression analysis of the crown lengths and widths obtained from ground surveys and those obtained from airborne LiDAR data. Next, we compared the tree growth observed in the study plot to the crown surface area derived from airborne LiDAR data and the proportion of crown surface area to stem surface area calculated from a stem curve based on a field survey. Finally, considering the balance of tree photosynthesis and respiration for the development of the growth model, we discuss the predicted tree growth using crown information derived from airborne LiDAR data.

2. Methods

2.1 Study area

The University of Tokyo Forest in Chiba is located in the cities of Kamogawa and Kimitsu, Chiba Prefecture, Japan, between 50 and 370 m above sea level. The terrain is undulating with steep slopes, and most soils are of the brown forest type. The forest is located in a warm-temperate zone, with an average annual temperature of 14°C. The average rainfall is 2182 mm year⁻¹. The total forest area is 2216 ha, 824 ha (37%) of which comprise sugi (*Cryptomeria japonica*) and hinoki (*Chamaecyparis obtusa*) stands, 949 ha (43%) are natural hardwood forest, and 387 ha (17%) are natural conifer forest. The remaining 57 ha (3%) are demonstration forest. Stand age varies from approximately 10 to 100 years. Many permanent plots in sugi and hinoki stands have been established within the study site. The tree height and DBH were recorded approximately every 5 years in these permanent plots.

2.2 Data correction

2.2.1 Ground survey data

We conducted a ground survey in a 27-year-old hinoki stand to check the accuracy of crown length measurements obtained from airborne LiDAR. For ground surveys, a circular sample plot 22.6 m in diameter (0.04 ha) were established in the hinoki stand. DBH, tree height, base of the crown, crown width, and tree position were measured for all standing trees in each plot. We defined the base of the crown as the branch from which the crown continues all the way to the top (i.e., slightly higher than lowermost and solitary branches). We also measured the crown width from uphill and contralateral aspects. The tree positions were measured by differential global positioning system (DGPS) receivers (Trimble Navigation), Impulse 200 LR (Laser Technology), and MapStar System Electronic Compass Module II (Laser Technology). In calculating the observed crown length, the heights to the base of the crown were subtracted from

the heights of the trees. The heights to the base of the crown and the total heights of the trees were measured using VERTEXIII (Haglöf).

The tree positions were also measured in permanent plots aged 102 years to link the stem growth data and crown information obtained from airborne LiDAR.

2.2.2 Airborne LiDAR data

The ALMAPS-G4 (Asahi Laser Mapping System), which consists of the ALTM 3100 laser scanning system produced by Optech, Canada, GPS airborne and ground receivers, and an inertia measurement unit (IMU) that measures the helicopter's roll, pitch, and heading were used to acquire airborne LiDAR data. The laser scanner system transmits laser pulses at 1064 nm (near-infrared) and receives the first and last echoes of each pulse. The elapsed time between transmittance and reception is measured to calculate the distance between the system and the measured object.

Airborne LiDAR data were acquired on 14 August 2005. The flight altitude of the helicopter above the ground was approximately 500 m, and the average flight speed was approximately 19.4 m s⁻¹. The pulse repetition frequency of airborne LiDAR was 70 kHz, and the scan frequency was 27 Hz. The maximum scan angle (off nadir) was 18°. The beam divergence was 1.2 mrad. Therefore, the footprint diameter was approximately 60 cm. The interval between footprints was about 25 cm. Both first pulse and last pulse were acquired to identify forest canopy and topography data in rugged terrain.

Data from a region of interest (ROI) 200 m wide and 1700 m long were selected for this study. A digital elevation model (DEM) and a digital surface model (DSM; Fig. 1a) for the study area were prepared from the airborne LiDAR data, with a 25 cm cell size. Data for the digital canopy model (DCM) which delineates canopy height from the ground, were calculated by subtracting the DEM from the DSM.

2.3 Data analysis

2.3.1 Estimating the crown length and width from LiDAR data

The crown cross-sectional surface of the individual trees was estimated from LiDAR data with TNTmips ver. 6.6 (MicroImages, 2001). Using the DEM and DSM data, we estimated the crown cross-sectional surface of individual trees in each plot. The crown length and crown width of each tree were estimated from airborne LiDAR data using the TNTmips ver. 6.6 (MicroImages, 2001), software of the GIS and image-processing system. First, each tree was identified using the DEM and DSM. Tree height was obtained from the DCM showing the canopy surface height from the ground height, and was calculated by subtracting the DEM, i.e., the height above sea level, from the DSM, showing the surface of the canopy. When the plot was magnified, airborne LiDAR data could identify the crown of each individual tree as a DCM (Fig. 1b). We defined each individual tree derived from airborne LiDAR data with a tree positioning map measured by a ground survey.

Second, we estimated the crown cross-sectional surface. The crown length of each tree was estimated by subtracting the height to the base of the crown from the total tree height. We measured the height to the base of the crown on the rebound point obtained from the DSM cross-sectional surface (Nakajima *et al.* 2008; in press), because we considered the opposite side of objective tree canopy from the rebound point to be the crown of the neighboring tree (Fig. 2). The direction of the DSM cross-sectional surface was estimated from the average slope aspect derived from the DEM, because there was often more space for branch and leaf expansion on the slope side of trees.

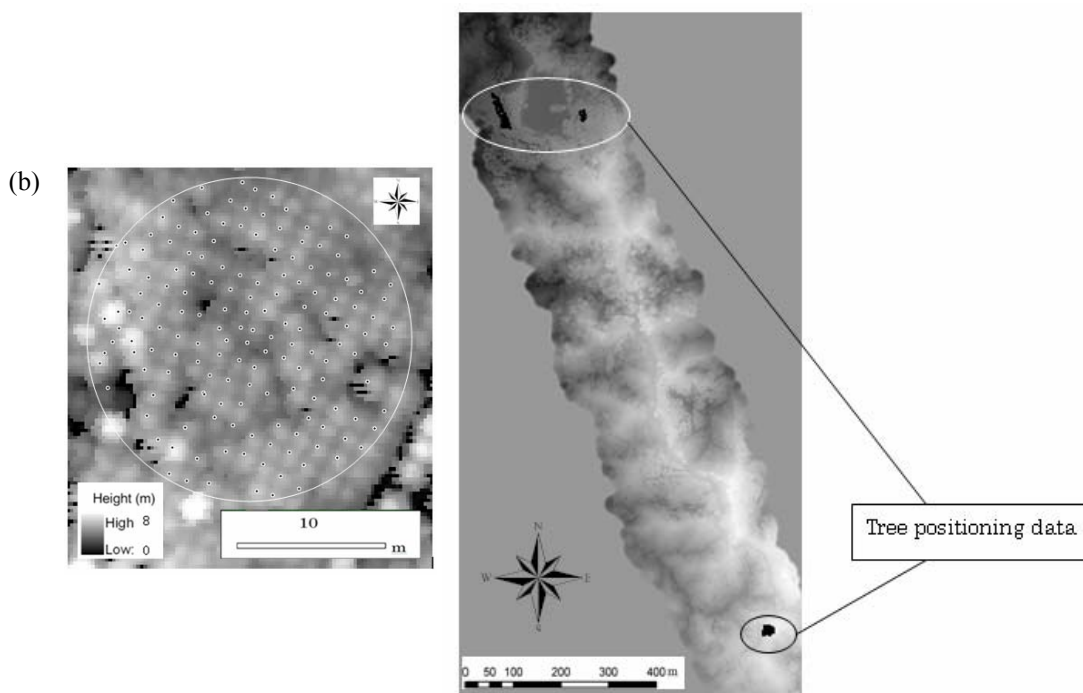


Figure 1: (a) Digital surface model and (b) digital crown model overlapped with tree positioning data

Figure 3 shows an example of a cross-sectional surface of a tree. We calculated the crown length, crown width, and width at approximately the middle point of the crown length for this figure. Third, the estimates of crown length and width from airborne LiDAR data were compared to the data measured manually on the plot. The crown lengths and widths obtained from ground surveys were regressed against the crown lengths obtained from airborne LiDAR. We then calculated the coefficient of determination. These crown information data were also used for estimating the crown surface area.

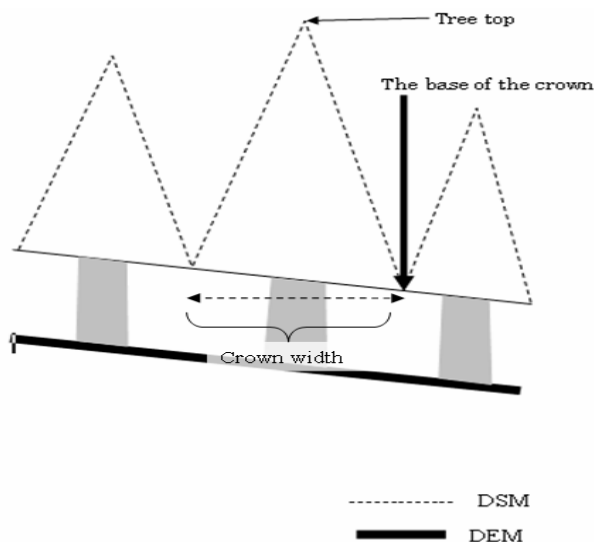


Figure 2: Position at which tree height was measured to determine the base of the crown. The base of the crown and crown width are indicated by a bold arrow and dotted arrow, respectively.

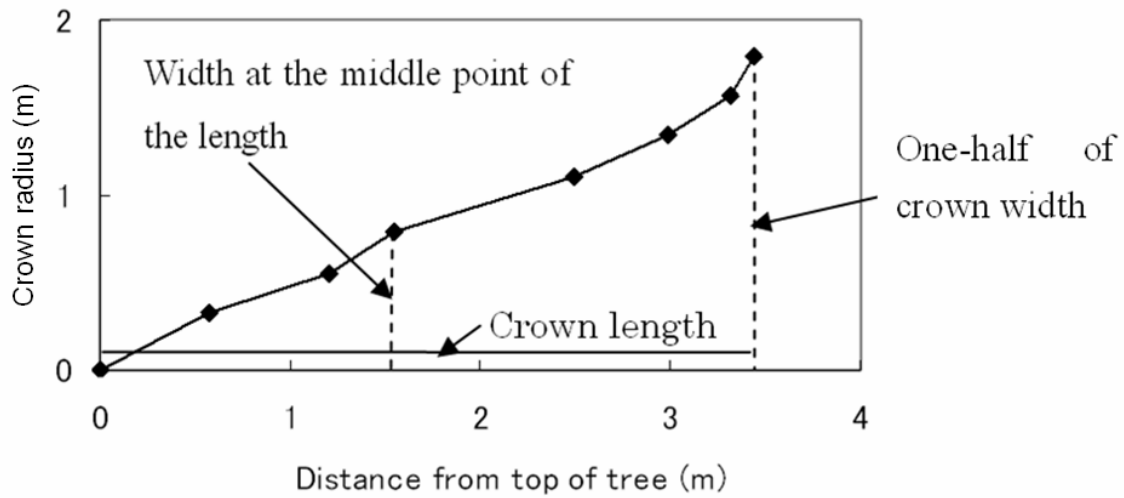


Figure 3: Example of the cross-sectional surface of a dominant tree

2.3.2 Estimation of tree growth using crown information derived from airborne LiDAR data

Finally, we obtained the relationship between the surface areas of the crown and stem using data derived from airborne LiDAR and the ground survey. In this study, we assumed that the stem surface and crown surface are the main parts of respiration and photosynthesis, respectively. This assumption is based on suggestions by previous studies that photosynthesis activity is very high on the crown surface (Kajihara 2000). Bosc *et al.* (2003) reported that the surface area of wood has a stronger relationship with respiration than with woody volume. With this assumption, we calculated the crown surface area and stem surface area and estimated the relationship of the individual tree growth and crown surface area or proportion of crown surface area to stem surface area.

2.3.2.1 Relationship between tree growth and crown surface area

In this procedure, we applied formula (1), the crown curve reported by previous studies (Kajihara 2000; Nakajima *et al.* in press), to the crown profile:

$$Y = \frac{DX}{aL + (2 - a)X} \quad (1)$$

where X : distance from the top of the tree (m)

Y : width at distance X (m)

D : crown width (m)

L : crown length (m)

a, b : parameters

The crown surface area is estimated with formula (2) showing the surface of the solid revolution of formula (1):

$$S_c = 2\pi \int_0^L Y \left\{ 1 + \left(\frac{dY}{dX} \right)^2 \right\}^{\frac{1}{2}} dX \quad (2)$$

where S_c : crown surface area (m²)

We calculated the crown surface area by integrating formula (2) with the Romberg quadrature and applied eight angles (45, 90, 135, 180, 225, 270, 315, and 360 degrees) of the crown around the tree top to these equations. We estimated the average value of the eight directions of crown surface area of the tree in the permanent plot. We compared the crown surface area to tree growth (m³ year⁻¹) over the past 20 years calculated from the Yamamoto-Schumacher formula (Forestry Agency 1970) applied to the plots measured twice. The crown surface was regressed against the stem growth. We then calculated the coefficient of determination.

2.3.2.2 Relationship between tree growth and the proportion of crown surface area to stem surface area

We calculated the stem surface area from tree height and DBH, observed during the ground survey, and the relative taper curve (Nakajima *et al.* in press). We applied the relative taper curve estimated in the University Forest in Chiba (Nagumo and Tanaka 1981). Formula (3) is the actual taper curve:

$$Y_s = \frac{D_s \left(\frac{\alpha X}{H} + \frac{\beta X^2}{H^2} + \frac{\gamma X^3}{H^3} \right)}{\alpha \left(1 - \frac{1.3}{H} \right) + \beta \left(1 - \frac{1.3}{H} \right)^2 + \gamma \left(1 - \frac{1.3}{H} \right)^3} \quad (3)$$

where Y_s : stem radius (m)

D_s : radius (m) at breast height (1.3 m)

H : tree height (m)

α, β, γ : parameters

The stem surface area is estimated with formula (4) showing the surface of the solid revolution of formula (3):

$$S_s = 2\pi \int_0^H Y_s \left\{ 1 + \left(\frac{dY_s}{dX} \right)^2 \right\}^{\frac{1}{2}} dX \quad (4)$$

where S_s : stem surface area (m²)

We calculated the stem surface area by integrating formula (4) with the Romberg quadrature. The crown surface divided by stem surface area was regressed against the stem growth (m³ year⁻¹) and was calculated as described above. We then calculated the coefficient of determination.

3. Results and discussion

3.1 Estimating the crown length and width from LiDAR data

The crown lengths and widths estimated by airborne LiDAR were plotted against those measured in the ground surveys (Fig. 4).

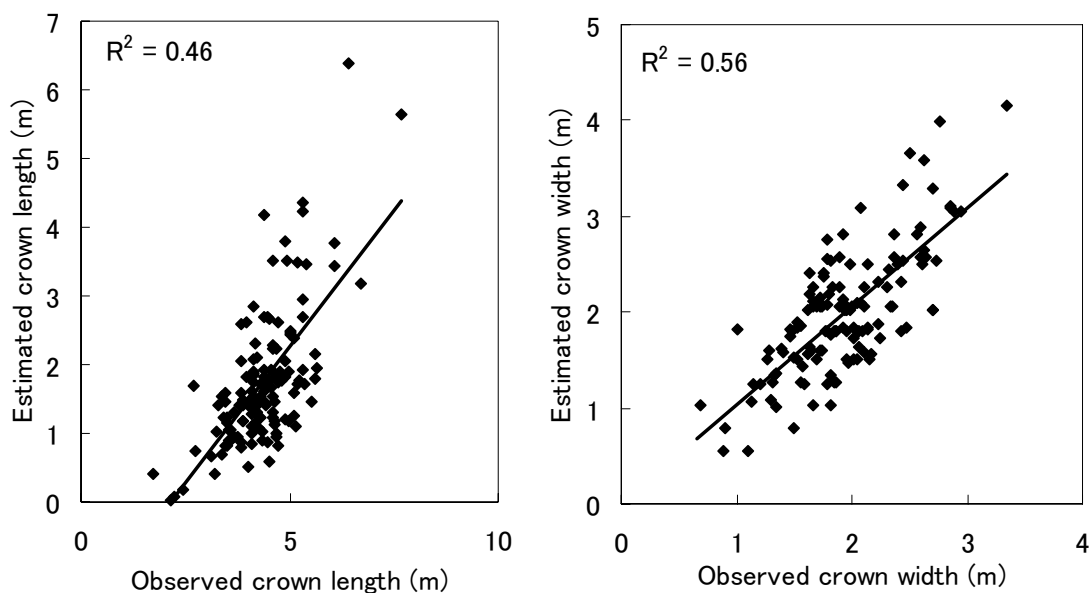


Figure 4: Crown lengths and widths estimated by airborne LiDAR

The coefficients of determination for crown length and width were 0.46 and 0.56, respectively. The first pulse of the airborne LiDAR captured the tendency of canopy size correctly because the distance between neighboring footprints was relatively narrow.

In particular, the constant and slope of the regression lines for crown length were -1.7202 and 0.7957, respectively. This result suggests the underestimation of crown length derived from airborne LiDAR data. A cause of the underestimation in this high-density sample plot (about 4000 stems ha^{-1}) could be that airborne LiDAR did not include the length of the shaded canopy. We verified the outcomes discussed above in the following way. In high-density stands, where branches shade other trees, we measured the sunlit canopy, as well as the shaded canopy, and included these data in the ground survey data because the shaded canopy was not completely dead. In other words, the length of the canopy in the survey was the sum of the sunlit and shaded canopies. However, the measurements included only the sunlit canopy, because the DSM measured by airborne LiDAR was obtained primarily from the first pulse, a laser that does not reach the shaded canopy. Therefore, differences between the crown lengths obtained from airborne LiDAR and ground surveys in high-density stands would be caused by an underestimation in airborne LiDAR, as airborne LiDAR did not include the length of the shaded canopy.

However, this difference would not be significant for predicting stand growth. Kajihara *et al.* (1989) compared the distribution of stem volume in sunlit and shaded canopies and found that a shaded canopy has no influence on the stem growth of sugi and hinoki. In other words, the surface area of the sunlit canopy per unit area has more impact on growth than that of the shaded canopy. Kajihara (1985) showed that the surface area of the sunlit canopy plays an essential role in the growth of sugi stands.

3.2 Estimation of tree growth using crown information derived from airborne LiDAR data

3.2.1 Relationship between tree growth and crown surface area

Figure 5 shows the relationship between tree growth and the crown surface area of the trees.

The coefficient of determination was 0.95. The P value and root mean square error (RMSE) were less than 0.01 and 0.008, respectively, suggesting a strong correlation between tree growth and crown surface area. This finding is also consistent with those of previous studies, which reported that in general, a larger crown surface area results in a greater annual increment (Kramer 1966).

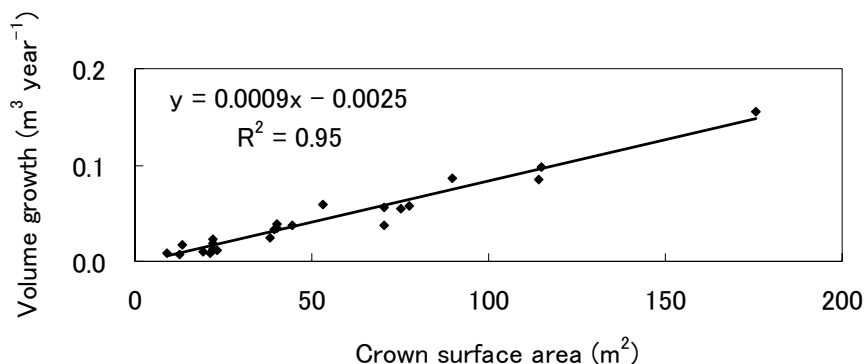


Figure 5: Relationship between individual tree volume growth and crown surface area

3.2.2 Relationship between tree growth and proportion of the crown surface area to stem surface area

Figure 6 shows the relationship between tree growth and the ratio of the crown surface area to the stem surface area of the trees. The coefficient of determination was 0.74. This result suggests a correlation between tree growth and the proportion of crown surface area to stem surface area. To predict tree growth considering both stem information and crown information, some previous studies (e.g., Cole and Lorimer 1994; Wyckoff and Clark 2005) reported that the best fit was a non-linear model. Thus, we expected that the relationship between individual tree volume and the ratio of the crown surface area to the stem surface area of the trees would be non-linear. The coefficient of determination was less than that between tree growth and crown surface area. However, this relationship (Fig. 6) might be more applicable to sugi, regardless of tree age, similar to the previous non-linear regression growth model (i.e., Cole and Lorimer 1994).

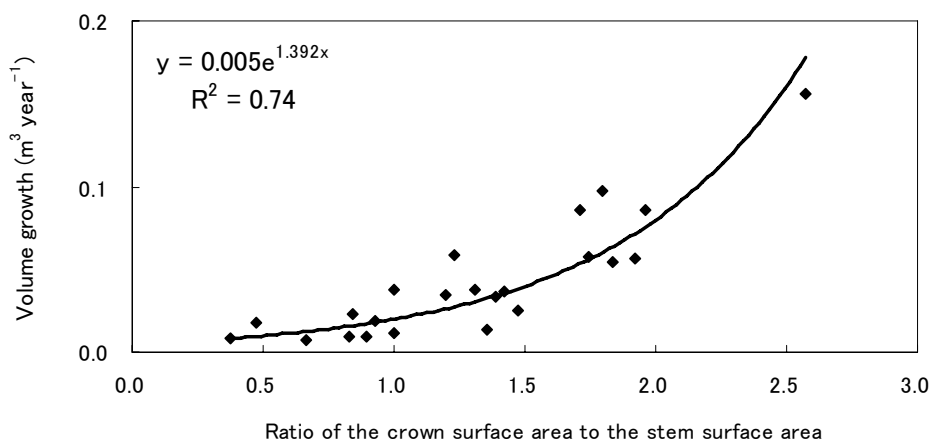


Figure 6: Relationship between individual tree volume and the ratio of stem surface area to crown surface area

As described above, we estimated the crown length by the DSM obtained from the first pulse. The first pulse reflected against the sunlit canopy does not include information on the shaded portion of the canopy, where sunlight is blocked by branches from other trees. In other words, Figures 5 and 6 suggest a strong relationship between the sunlit crown surface area and tree growth. This result is also consistent with previous reports that the shaded canopy does not contribute to tree growth (e.g., Kajihara 1985).

Note that we considered only the stem surface area as the main contributor to respiration. However, a tree respire not only on the surface of its stem but also on the surface of its branches and roots. Thus, to obtain an accurate estimation of the relationship between photosynthesis and respiration, we should compare the crown surface area to the sum of the surface area of stems, branches, and roots. Fukuda *et al.* (2003) showed the relationships between the total biomass and bole biomass of sugi depending on stand age. Given that stem biomass is highly correlated with the total biomass, it might be possible to estimate total tree growth based on stem growth models such as in Figures 6 or 7.

4. Conclusion

Airborne LiDAR was successful for acquiring precise measurements of crown lengths and widths in high-density stands. Based on these results, we estimated the relationship between tree growth and the crown surface area of individual trees. We found strong correlations between the crown surface area and tree growth. We also found that tree growth could be modeled as a function of the ratio of the crown surface area to the stem surface area.

Acknowledgments

We thank the staff of the University Forest in Chiba, University of Tokyo, for assistance with field measurements. We also thank the referees who reviewed early versions of the manuscript and provided helpful comments to improve our paper.

References

- Andersen, H.-E., McGaughey, R.J., Reutebuch, S.E., 2005. Estimating forest canopy fuel parameters using LIDAR data. *Remote Sensing of Environment*, 94, 441-449.
- Arain, M.A., Restrepo-Coupe, N., 2005. Net ecosystem production in a temperate pine plantation in southeastern Canada. *Agricultural and Forest Meteorology*, 128, 223-241.
- Bosc, A., De Grandcourt, A., Loustau, D., 2003. Variability of stem and branch maintenance respiration in a *Pinus pinaster* tree. *Tree Physiology*, 23, 227-236.
- Castedo-Dorado, F., Dieguez-Aranda, U., Alvarez-Gonzalez, J.G., 2007. A growth model for *Pinus radiata* D. Don stands in north-western Spain. *Annals of Forest Science*, 64, 453-465.
- Cole, W.G., Lorimer, C.G., 1994. Predicting tree growth from crown variables in managed northern hardwood stands. *Forest Ecology and Management*, 67, 159-175.
- Coops, N.C., Hilker, T., Wulder, M.A., St-Onge, B., Newnham, G., Siggins, A., Trofymow, J.A., 2007. Estimating canopy structure of Douglas-fir forest stands from discrete-return LiDAR. *Trees-Structure and Function*, 21, 295-310.
- Farid, A., Goodrich, D.C., Sorooshian, S., 2006. Using airborne lidar to discern age classes of cottonwood trees in a riparian area. *Western Journal of Applied Forestry*, 21, 149-158.
- Forestry Agency., 1970. "Volume table - eastern Japan -". Tokyo, Japan Forestry Investigation Committee. 333p (in Japanese)
- Fukuda, M., Iehara, T., Matsumoto, M., 2003. Carbon stock estimates for sugi and hinoki forests in Japan. *Forest Ecology and Management*, 184, 1-16.

- Hirata, Y., 2005. Relationship between tree height and topography in a *Chamaecyparis obtusa* stand derived from airborne laser scanner data. *Journal of Japanese Forestry Society*, 87, 497-503 (in Japanese with English summary).
- Kajihara, M., 1985. Estimation of stem-volume increment by using sunny crown-surface area and stem-surface area. *Journal of Japanese Forestry Society*, 67, 501-505 (in Japanese with English summary).
- Kajihara, M., 2000. "Stem growth and form estimated from canopy information". Tokyo, Japanese Society of Forest Planning Press. 139p (in Japanese).
- Kramer, H., 1966. Crown development in conifer stands in Scotland as influenced by initial spacing and subsequent thinning treatment. *Forestry*, 39, 40-58.
- Labrecque, S., Fournier, R.A., Luther, J.E., Piercey, D., 2006. A comparison of four methods to map biomass from Landsat-TM and inventory data in western Newfoundland. *Forest Ecology and Management*, 226, 129-144.
- MicroImages, Inc., 2001. TNTmips ver. 6.6. Lincoln, NE, USA.
- Næsset, E., Bjercknes, K.-O., 2001. Estimating tree heights and number of stems in young forest stands using airborne laser scanner data. *Remote Sensing of Environment*, 78, 328-340.
- Nagumo, H., Tanaka, M., 1981. Construction of a volume table with a relative stem-curve. *Journal of Japanese Forestry Society*, 63, 278-286 (in Japanese with English summary).
- Nakajima, T., Hirata, Y., Furuya, N., Takezoe, K., Suzuki, M., Tatsuhara, S., 2008. Estimating canopy information in *Cryptomeria japonica* and *Chamaecyparis obtusa* stands using airborne LiDAR data. *Journal of Forest Planning*, 41:313-318.
- Nakajima, T., Hirata, Y., Furuya, N., Takezoe, K., Suzuki, M., Tatsuhara, S., in press. The use of airborne LiDAR data to estimate the relationships between the crown surface area and stem surface area of *Chamaecyparis obtusa* stands. *Proceedings of the International Conference on Forest Growth and Timber Quality: Crown Models and Simulation Methods for Sustainable Forest Management*, United States Department of Agriculture Forest Service.
- Qin, J., Cao, Q.V., Blouin, D.C., 2007. Projection of a diameter distribution through time. *Canadian Journal of Forest Research-Revue Canadienne de Recherche Forestière*, 37, 188-194.
- Roberts, S.D., Dean, T.J., Evans, D.L., McCombs, J.W., Harrington, R.L., Glass, P.A., 2005. Estimating individual tree leaf area in loblolly pine plantations using LiDAR-derived measurements of height and crown dimensions. *Forest Ecology and Management*, 213,54-70.
- Takahashi, T., Yamamoto, K., Senda, Y., Tsuzuki, M., 2005. Estimating individual tree heights of sugi (*Cryptomeria japonica* D. Don) plantations in mountainous areas using small-footprint airborne LiDAR. *Journal of Forest Research*, 10,135-142.
- Wyckoff, P.H., Clark, J.S., 2005. Tree growth prediction using size and exposed crown area. *Canadian Journal of Forest Research*, 35:13-20.

An improved method of individual tree detection using airborne LiDAR

Katsumasa Oono¹, Yoichi Numata¹ & Atsushi Hirano²

¹ASIA AIR SURVEY CO.,LTD. E-mail:kat.oono@ajiko.co.jp

²TOKYO ELECTRIC POWER COMPANY E-mail: hirano.a@tepcoco.jp

Abstract

The aim of this research is to improve a method to identify individual trees using airborne LiDAR. In our research, “Crown Shape Index” was invented to detect individual tree tops. The index is calculated based on unevenness of grid digital height model (DHM). And the authors devised a new method that extracts crown area surrounding tree top by referring to statistics theory. The authors applied the index and method to a Japanese cedar forest. Crown Shape Index applied to low density forests resulted in 80 to 90% detection accuracy. With the increase in tree density, the accuracy dropped by 10 to 20%. Further, in order to understand the accuracy of Crown Shape Index, the identification result was compared with that of aerial photo interpretation by human eyes. As the result of this comparison, it was found that the Crown Shape Index method could detect 80 – 100% of the detection numbers by aerial photos. From this result, individual tree identification by Crown Shape Index is considered to have the same level of accuracy with manual aerial photos interpretation method.

Keywords: individual trees detection, LiDAR, Crown Shape Index

1. Preface

Forests fix CO₂ and contribute to restrain the global warming. Forests can maintain water resources and conserve soil and also provide space and environment for outdoor recreation. Recently, these functions of forests are highly evaluated.

In order to preserve precious forests, they should be managed properly and for that purpose, it is required to know exact conditions of forests.

One of the most basic information on forest is the number of trees growing in forests. Traditionally, on-the-spot investigations have been the most popular method for counting number of trees. However, with the development of LiDAR technologies, application of LiDAR data for forest survey has been studied and now the technology has great potential in individual stand detection.

Most researches on individual stand identification by LiDAR data have used DHM (Digital Height Model), which is the difference between DSM and DEM, as a criterion for the detection and watershed algorithm or local maximum filter as a method.^[1,2,3,4] Also, there was a research to identify individual stands based on crown shape model using raw laser pulse data.^[5]

Shape of crown, however, is very complex and particularly in dense forests DHM cannot give clear height difference between tree tops and edge of crowns. Thus, reliable detection of individual tree is difficult in dense forests.

In our research, we have invented a new index by processing DHM data of crown area to improve the individual trees detection result.

2. Study Area and Data Used

Study area is an artificial forest of *Cryptomeria japonica* (Japanese cedar) in Kosugi Village, Yamanashi Prefecture in central Japan. In the study area, square shaped plots whose size is almost equal to average tree height (20m) in the area were established and number of stands, DBH, tree height, slope angle, slope direction and coordinates of corner points of the plots were surveyed. GPS receiver was used to acquire the coordinates. Characteristics of the four plots are given on Table 1.

Table1: The forest state of investigation site

| Plot_No | average tree height (m) | average DBH (cm) | stand tree density (trees/ha) |
|---------|----------------------------|---------------------|----------------------------------|
| P1 | 20.8 | 27.0 | 860 |
| P2 | 21.2 | 28.2 | 1176 |
| P3 | 20.3 | 23.3 | 1964 |
| P4 | 18.7 | 21.1 | 2435 |

LiDAR data used in the research was acquired on December 1, 2006. Specifications for the data acquisition are summarized as Table 2.

Table2: Specifications for data acquisition

| | |
|-----------------------|---------------------|
| sensor | leica ALS50- II |
| laser pulse rate | 100KHz |
| scan rate | 62Hz |
| scan angle | ±9° |
| average point density | 4pts/m ² |
| Flying Height AGL | 1890m |
| position accuracy | X,Y < 0.20m |
| elevation accuracy | Z < 0.11m |
| Laser classification | Class 4 |

From this dataset, two sets of data were made. First, abnormal data were removed. Then, the data were filtered. From the two sets of data TIN was made and 0.5 meter grid data, DSM (Digital Surface Model) and DEM (Digital Elevation Model) were generated. Further, DEM was subtracted from DSM to make DHM (Digital Height Model) .

3. Individual Tree Identification Method

3.1 Development of Crown Shape Index

In DHM height difference between tree tops and edges of crown is not large. Therefore, it is difficult to identify individual trees with DHM. To deal with this problem, the authors have developed an index named Ridge/Valley Index.^[6] Its principle is as follows.

- 1) Prepare 0.5 meter grid DHM of canopy surface.
- 2) At First, “upper open degree” phi1 is calculated. This is an angle between a vertical line and a line which starts from each grid point of DHM and tangent to the crown surface, which is represented by DHM, within each search area.
- 3) Similarly, “lower open degree” phi2 is calculated.
- 4) Angle phi3 is calculated by the following formula:

$$\text{Phi3} = (\text{phi1} - \text{phi2})/2$$

5) Total 8 phis are calculated for 8 directions for each DHM grid point and their average is computed. This average is named as the Crown Shape Index.

Ridge/Valley Index expresses the condition of canopy at each grid point. The authors could emphasize the shape of canopy surface by using this index.

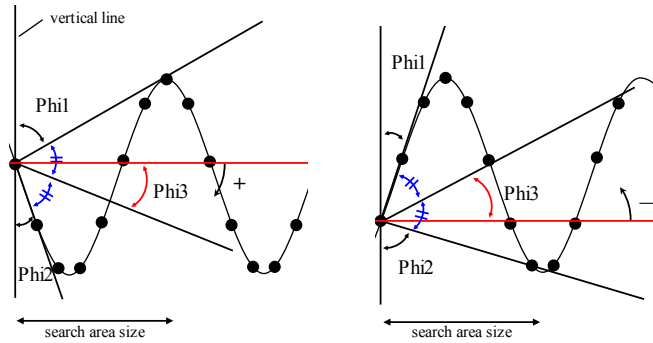


Figure1: Concept of Ridge/Valley Index (Cross section)

Difference in Ridge/Valley Index value of tree top and that of crown edge is larger than the difference given by DHM and also the index is almost the same for any tree top regardless of tree height. Since the index can represent outline of crown shape the authors assumed that it could be used for individual stand identification by using a uniform threshold value.

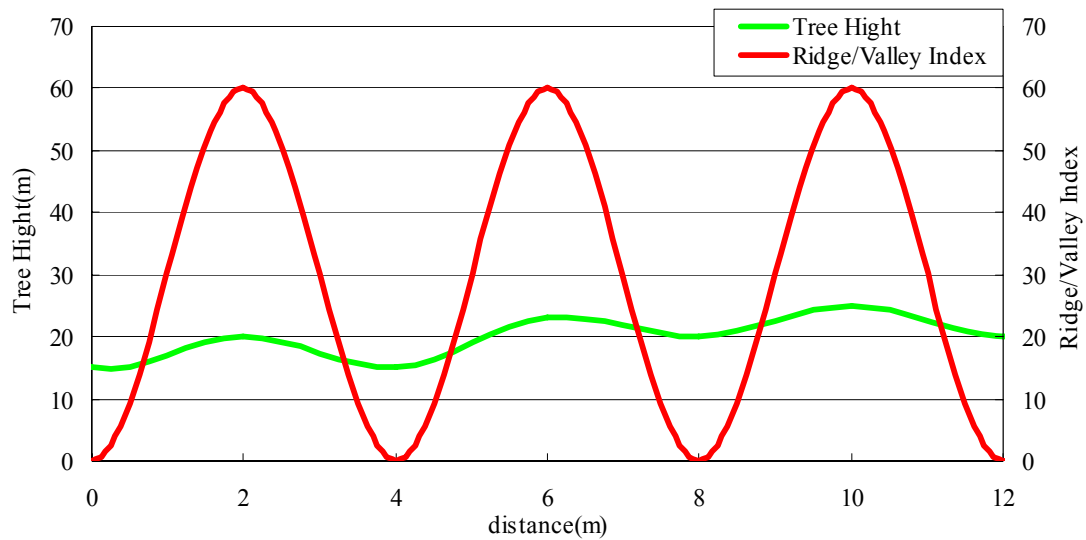


Figure2: Relation between Ridge/Valley Index and cross section of crown surface

It was found, however, that approximately only 70% of trees were identified by the index in low density forests (1000 stands/ha). This means there was much miss identification. Analysis of the results revealed that there were three issues which need to be dealt with.

1) Clarification of the shape of small crowns where height difference between tree tops and crown edge is small. (Although Ridge/Valley index can represent relatively flat crown area

- better than DHM, small crowns were not represented well.)
- 2) Prevention of the index value becomes extremely large at crown edges.
 - 3) Clarification of positions of tree tops

In order to solve these problems and to improve the accuracy of individual stand identification, the authors improved the Ridge/Valley Index.

Ridge/Valley Index can represent approximate shape of tree crowns by degrees. This index cannot work well in forests where crown surface is relatively flat.

To solve this problem a tree crown model was made based on the shape of ridge and valley formed by Upper Open Degree (ϕ_1) and Lower Open Degree (ϕ_2), and this model was defined as the Crown Shape Index. The principle of the Crown Shape Index is shown in Figure 3.

In Figure 3, relatively flat line represents the crown surface. Upper Open Degree and Lower Open Degree were switched to emphasize the undulation of crown surface. The lower undulated line is the result of this switching process.

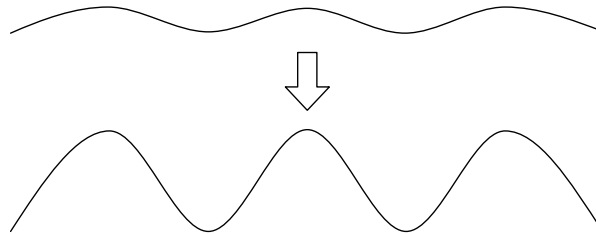


Figure3: Principle of Crown Shape Index

The Crown Shape Index is calculated as follows:

- 1) Upper and lower open degrees are replaced with pre-fixed values according to the following 5 criteria.
 1. $150 \leq \phi_1 \Rightarrow \phi_1 = 150$ 、
 $\phi_2 \leq 30 \Rightarrow \phi_2 = 30$
 (To prevent extreme values at crown edges)
 2. $90 \leq \phi_1 < 150 \Rightarrow \phi_1 = 150$ 、
 $30 < \phi_2 \leq 90 \Rightarrow \phi_2 = 30$
 (To emphasize convex part of crown shape)
 3. $30 \leq \phi_1 < 90 \Rightarrow \phi_1 = 30$ 、
 $90 < \phi_2 \leq 150 \Rightarrow \phi_2 = 150$
 (To emphasize convex part of crown shape)
 4. $\phi_1 < 30 \Rightarrow \phi_1 = \phi_1$ 、
 $150 < \phi_2 \Rightarrow \phi_2 = \phi_2$
 5. If DHM values of the surrounding 8 directions are higher than the DHM value of a grid point then 179.9 is assigned to ϕ_1 while 0.1 is assigned to ϕ_2 .
 (To emphasize the position of crown tops)
- 2) By using the Upper and Lower open degree value assigned according to the above 5 criteria, ϕ_3 is calculated by the same method with Ridge/Valley Index.

3) Average of ϕ_3 for 8 directions is computed. And this average is Crown Shape Index for that particular grid point.

Larger Crown Shape Index value represents convex area while smaller index represent concave areas.

3.2 Development of a method of individual stand identification

In individual stand identification using Ridge/Valley index, a uniform threshold value was used to extract crown area of each tree. However, since a uniform threshold value was used, if the index value is lower than the threshold value, the area cannot be identified as crown area even if the area is actually crown area.

To solve this problem, the authors tried to set a threshold value for each crown individually. For this purpose it is necessary to establish individual crown area for each tree. Individual crown area should be clearly separated from adjacent crown areas. If more than two crown areas are connected, they are regarded as belonging to one single tree and this result in smaller number of individual stand identified.

Therefore, the size of individual crown area for individual stand identification should be approximately half of the size of actual crown.

Relation with crown area and the smaller crown area surrounding tree top are shown in Figure 4.

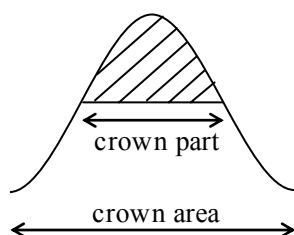


Figure 4: Crown area and area near tree top

Table 3 shows the ratio of crown part near tree top to the size of crown area for four cases of different pixel sizes. Average percentage of the crown top area against crown area is approximately 16% on Table 3.

Table3: Ratio of crown part

| | unit:pixel | | | |
|------------------|------------|-------|-------|-------|
| crown part | 1×1 | 2×2 | 3×3 | 4×4 |
| | 1 | 4 | 9 | 16 |
| crown area | 3×3 | 5×5 | 7×7 | 9×9 |
| | 9 | 25 | 49 | 81 |
| crown part ratio | 11.1% | 16.0% | 18.4% | 19.8% |
| average | 16.3% | | | |

The authors pondered if optional 9 pixels (3×3) are chosen, the 9 pixels will be regarded as normal distribution, because Crown Shape Index is regarded as normal distribution (in figure 5 left histogram). And we extracted the crown part by referring to statistics theory. When value is normal distribution, in statistics theory a range of $\pm 1 \sigma$ of the mean occupies 68% of total (figure 5). We exploited the theory and detected crown parts.

In order to detect the crown top area (crown part), we decide the threshold every local domain (crown area size). The threshold is the value that added standard deviation (σ) to the mean (μ) of Crown Shape Index of a domain. Centre value of the domain was compared with the threshold, and if centre value is bigger than the threshold, centre pixels form crown area surrounding tree top.

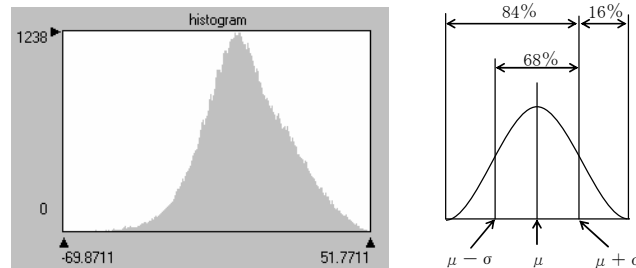


Figure 5: Histogram of Crown Shape Index and principle of determining threshold value

3.3 Flow of individual stand identification

Flow of individual stand identification where 0.5 meter grid DSM and DEM are used to compute Crown Shape Index is shown in Figure 6.

The points with the possibility to select the tree top are extracted by using a local maximum filter. A local maximum filter was applied to Crown Shape Index. In this case, the filtered domain was fixed to 3 pixels by 3 pixels. The filter replaces the value of the center point with the maximum value in the domain.

Crown Shape Index values before and after the process are compared. If the two values are equal, that point is identified as a possible tree top.

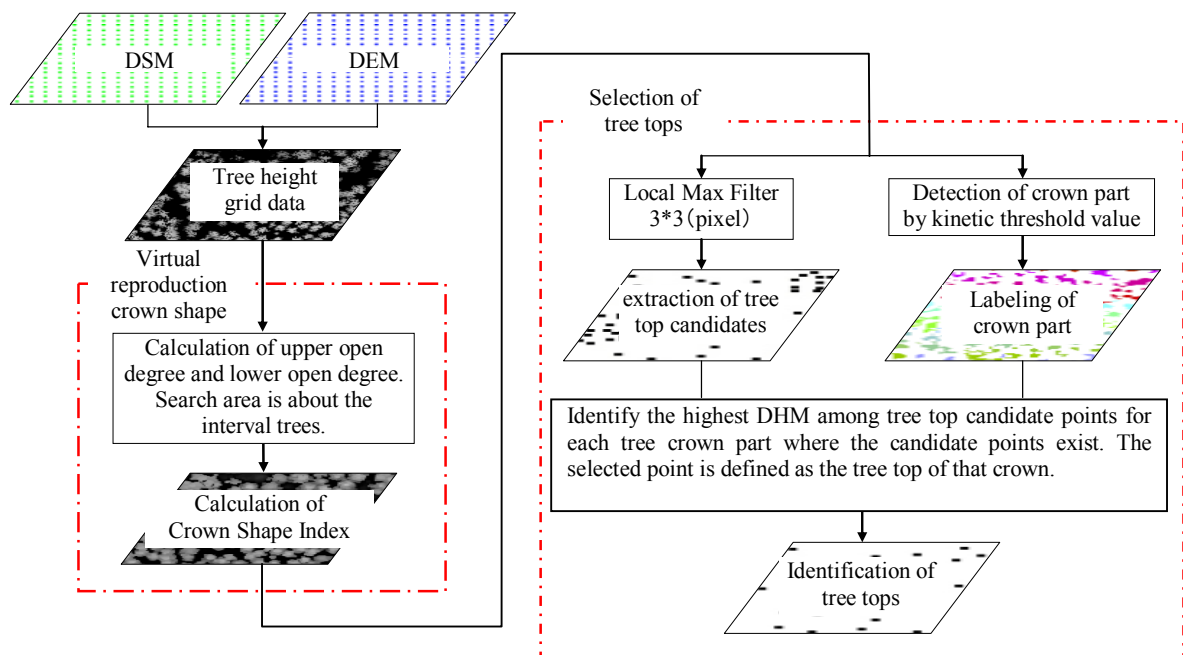


Figure 6: Flow of individual stand identifications using Crown Shape Index

4. Result

The result of the process described in Figure 6 is shown in Figure 7.

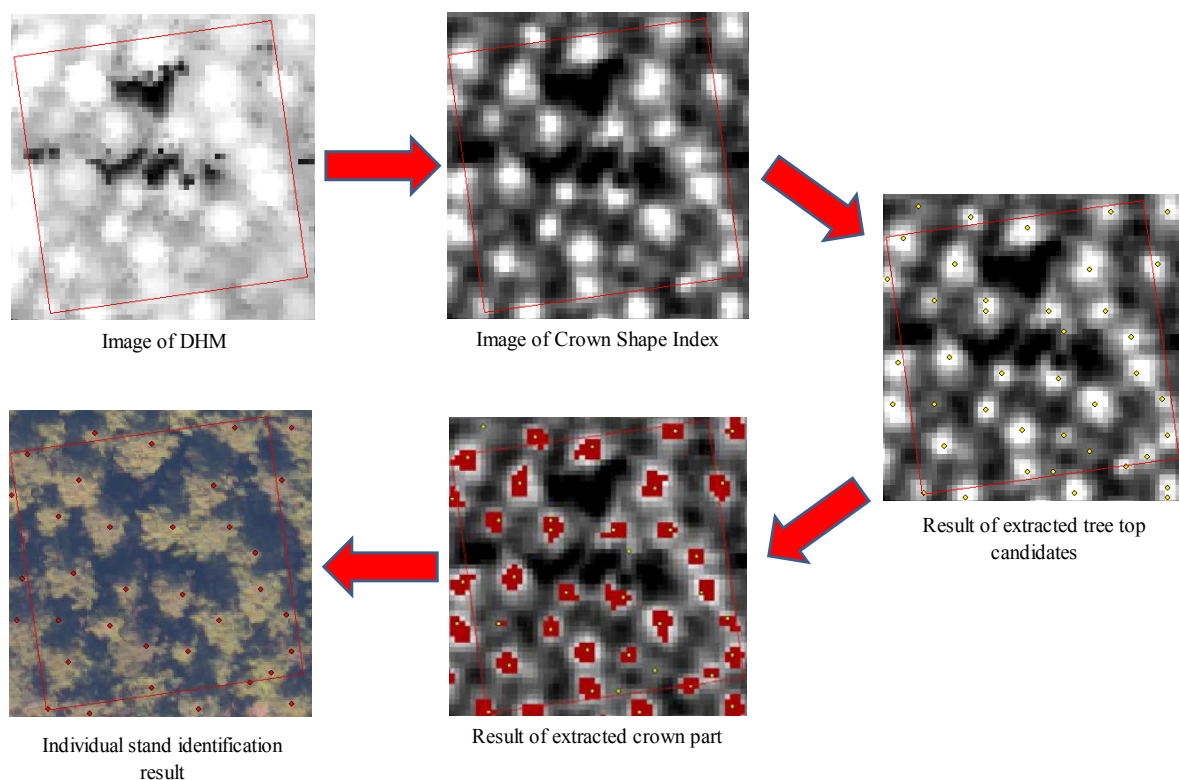


Figure 7: Individual stand identification result

Verification of the identification result was carried out by comparing with the result of field tree counting and tree counting by stereo view of aerial photos.

In order to increase the number of verification sites, more than one plot is established in P1, P2 and P4 stand and number of trees was counted in such plots. Verification result is summarized on Table 4.

Table 4: The rate of individual tree detection

| | | P1-1 | P1-2 | P2-1 | P2-2 | P-3 | P4-1 | P4-2 |
|--|----------------------------------|------|------|------|------|------|------|------|
| Stand tree density (tree/ha) | | 860 | | 1176 | | 1964 | 2435 | |
| The number of actual trees | | 30 | 28 | 67 | 76 | 64 | 69 | 63 |
| Aerial Photos | The number of detected tree tops | 28 | 27 | 55 | 70 | 53 | 47 | 54 |
| | The accuracy of detected trees | 93% | 96% | 82% | 92% | 83% | 68% | 86% |
| LiDAR data | The number of detected tree tops | 24 | 25 | 58 | 68 | 45 | 48 | 45 |
| | The accuracy of detected trees | 80% | 89% | 87% | 89% | 70% | 70% | 71% |
| The comparison of aerial photos and LiDAR data | | 86% | 93% | 105% | 97% | 85% | 102% | 83% |

In low density forests (P1 and P2) 90 to 100 % of trees were identified on stereo view of aerial photos. In dense forests, the accuracy drops by nearly 20%. In dense forests, number of suppressed tree increases and their small crowns are not easily identified by human eyes on aerial photos.

Crown Shape Index applied to low density forests resulted in 80 to 90% identification accuracy. With the increase in tree density, the accuracy dropped by 10 to 20%. This means that Crown Shape Index method showed similar accuracy dropping tendency with visual photo interpretation method with the increase in tree density. This may further indicate that LiDAR data could not detect small crowns of suppressed trees.

From the above results, the authors conclude that the accuracy of individual tree identification in low density forests increased from 70% of the Ridge/Valley Index method by using improved Crown Shape Index.

However, in dense forests, the accuracy is not high enough and further research is required.

Further, in order to understand the accuracy of Crown Shape Index, the identification result was compared with that of aerial photo interpretation by human eyes. The comparison result is summarized as the last row of Table 4. As the result of this comparison, it was found that the Crown Shape Index method identified 80 – 100% of the detection by aerial photos. From this result, individual tree identification by Crown Shape Index is considered to have the same level of accuracy with manual aerial photos interpretation method.

5. Conclusion

In this research, individual trees in forest were identified by using a newly developed Crown Shape Index which clearly represents tree crown shape.

It was confirmed that the Crown Shape Index had a great potential in individual stand identification at the same level of accuracy with aerial photo interpretation.

However, number of identified trees tends to be less than actual number of trees and further improvement of the index is required.

Further, the authors plan to apply the method to forest of other species in order to make the method applicable to various types of forests.

A system to calculate crown size and tree density from identified tree top and to select areas which require maintenance will also be developed to contribute to better forest management.

References

- Yone, Y., Oguma, H. and Yamagata, Y., 2002. Development of Measurement System for Carbon Sinks under the Kyoto Protocol – Measurement of Stem Volume and Carbon Weight of *Larix leptolepis* Stand by Airborne Lidar –. *Journal of Remote Sensing Society of Japan*, vol.22, No.5, 531-543.
- Imai, Y., Setojima, M., Funahashi, M., Matsue, M., Kagemoto, N., Yamagishi, Y. and Fujiwara, N., 2006. The individual tree information extraction of urban forests using airborne laser scanner and high resolution satellite image. *Proceedings of the 40th conference of The Remote Sensing Society of Japan*, 187-188.
- Matsue, K., Itoh, T. and Naito, K., 2006, Estimating forest resources using airborne LiDAR – Estimating stand parameters of Sugi (*Cryptomeria japonica* D. Don) and Hinoki (*Chamaecyparis obtuse* Endl.) stands with differing densities. *Journal of the Japan Society of Photogrammetry and Remote Sensing*, vol.45, No.1, 4-13.
- Hyypä, J., Kelle, O., Lehtikoinen, M. and Inkinen, M., 2001. A segmentation-based method to retrieve stem volume estimates from 3-d tree height models produced by laser scanners.

- IEEE Transactions on Geoscience and Remote Sensing*, 39, 969-975.
- Taguchi, H., Endo, T., Setojima, M. and Yasuoka, Y., 2006. A New Method for Individual Tree Detection Using Airborne LiDAR Pulse Data. *Proc. ACRS 2006 - 27th Asian Conference on Remote Sensing*
- Oono, K., Numata, Y., Mochizuki, H. and Hirano, A., 2006. Detection of individual trees and estimation of LAI using airborne LiDAR. *Silvilaser2006*, 16-20.

Mean height and variability of height derived from lidar data and Landsat images relationship

Cristina Pascual¹, Warren Cohen², Antonio García-Abril¹, Lara A. Arroyo³, Rubén Valbuena¹, Susana Martí-Fernández¹ and José Antonio Manzanera¹

¹Technical University of Madrid (UPM), E.T.S.I Montes,
Ciudad Universitaria s.n., 28040 Madrid, Spain. c.pascual@upm.es

²Forestry Sciences Laboratory, Pacific Northwest Research Station, USDA Forest Service, 3200 SW Jefferson Way, Corvallis, OR 97311, USA

³Centre for Remote Sensing and Spatial Information Science, School of Geography, Planning and Architecture, University of Queensland, Brisbane, QLD 4072, Australia.

Abstract

The mean and standard deviation of lidar-derived height data have shown to be important variables with which to summarize forest structure. However, lidar data has a limited spatial extent and a very high economic cost. Landsat data provides useful structural information in the horizontal plane and is easily accessible. The integration of both data sources offers an interesting opportunity to aid sustainable forest management. Different spectral indices (NDVI and Tasseled Cap) were obtained from three Landsat scenes (March 2000, June 2001 and September 2001), and the mean and standard deviation of lidar height measurements were calculated in 30 m square blocks. Correlation and forward stepwise regression analysis was applied to these data sets. Mean lidar height versus NDVI and wetness Tasseled Cap showed the best correlation coefficients (ranging between 0.65 and -0.73). The best regression models included NDVI and wetness for June and September as dependent variables (adjusted r^2 : 0.55 – 0.62). These results showed that lidar data can be used to train Landsat to map forest structure, and it should be interesting to further optimize this approach.

Keywords: lidar, Landsat, mean height, forest structure

1. Introduction

Canopy structure can be defined as the organization in space and time, including the position, extent, quantity, type and connectivity, of the aboveground components of vegetation (Parker, 1995; Lefsky *et al.*, 1999). Structure includes vertical (e.g. number of tree layers, understory vegetation) and horizontal features (e.g. spatial pattern of trees, gaps) as well as species richness (Maltamo *et al.*, 2005).

The mean and standard deviation of lidar-derived height data have shown to be variables that synthesise forest structure of the canopy. Zimble *et al.* (2003) used lidar-derived tree height variances to distinguish between single-story and multi-story forest classes. Lefsky *et al.* (2005a) pointed out that mean height and height variability figures derived from lidar data are strongly related to canopy indices and thus related to stand structure. These authors consider these variables to represent the same kind of enhancement of lidar data that the Tasseled Cap indices represent for optical remote sensing. Pascual *et al.* (2008) found that mean, median and standard deviation of height derived from lidar could be used to distinguish horizontally heterogeneous forest structure types.

Small footprint airborne laser scanners provide detailed information on the vertical distribution of forest canopy structure (Hyypä *et al.*, 2008), but over a limited spatial extent and with a high economic cost. Landsat data provides useful structural information in the horizontal plane and is much more accessible (Cohen & Spies, 1992). Therefore the integration of optical remote sensing imagery and lidar data provides improved opportunities to fully characterize forest canopy attributes and dynamics (Wulder *et al.*, 2007).

Hudak *et al.* (2002) developed spatial extrapolation of lidar data over Landsat images. Methods for the combination of lidar-derived metrics and optical images has been also devised (Chen *et al.*, 2004; Lefsky *et al.*, 2005b). In addition, two coincident lidar transects, representing 1997 and 2002 forest conditions in the boreal forest of Canada, were compared using image segments generated from Landsat ETM+ imagery (Wulder *et al.*, 2007).

Given the relationship between mean and standard deviation of height derived from lidar and forest structure, the objective of the present work is to evaluate the relationship between summaries derived from lidar and spectral information from the Landsat satellite. The final aim of this work is to establish whether Landsat data can be used to predict lidar forest canopy height (mean and standard deviation).

2. Methods

2.1 Study area

A 127.10 ha (1293 x 983 m) area, located on the western slopes of the Fuenfría Valley (40° 45' N, 4° 5' W) in central Spain, was selected as the study area. The Fuenfría Valley is located in the northwest portion of the Madrid region (Figure 1). The predominant forest is Scots pine (*Pinus sylvestris*, L.) with abundant shrubs (*Cytisus scoparius* (L.) Link., *C. oromediterraneus* Rivas Mart. *et al.*, *Genistaflorida* (L.)) in some areas.

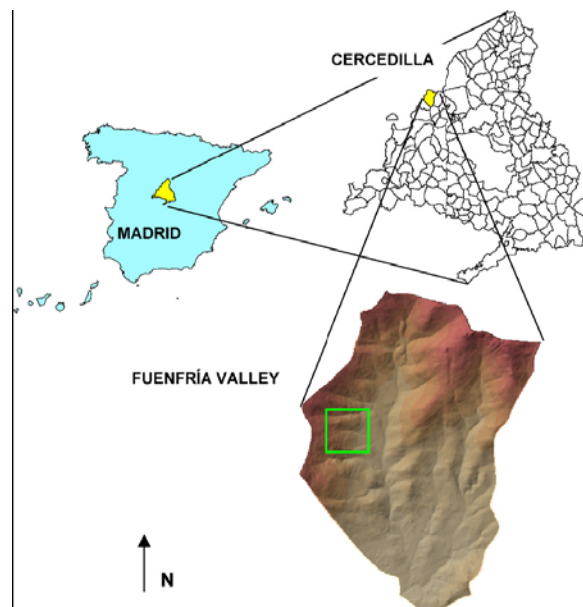


Figure 1: Study site. Fuenfría Valley, in the village of Cercedilla, northwest of Madrid (Spain).

There are small pastures on the lowest part of the hillside. In the northern sector of the study site there is an extensive rocky area. The site has a mean annual temperature of 9.4°C and precipitation averages 1180 mm per year. Elevations range between 1310 m and 1790 m above sea level, with slopes between 20% and 45%. The general aspect of the study site is east.

2.2. Lidar data

A small footprint lidar dataset was acquired by TopoSys GmbH over the study area in August, 2002. The TopoSys II lidar system recorded first and last returns with a footprint diameter of 0.95 m. Average point density was 5 points m⁻². The raw data (x, y, z-coordinates) was processed into two digital elevation models by TopoSys using the company's proprietary software. The digital surface model (DSM) was processed using the first pulse backscatters and the digital terrain model (DTM) was constructed from the last returns. Filtering algorithms were used to identify canopy and ground surface returns for an output pixel resolution of 1 m horizontally and 0.1 m vertically. According to TopoSys calculations the DSM and DTM positional accuracy was 0.5 m horizontally and 0.15 m vertically.

To obtain a digital canopy height model (DCHM), the DTM was subtracted from the DSM. Both the DTM and DCHM were validated before use by land surveying with a total station and ground-based tree height measurements. The vertical accuracies, calculated as Root Mean Square Error (RMSE) obtained for the DTM in open areas and the DCHM under forest canopy were 0.30 m and 1.3 m, respectively (Pascual, 2006). These accuracies were acceptable for this study, and were in agreement with previous studies. For example, Clark *et al.* (2004) reported RMSEs for DTMs ranging from 0.06 to 0.61 m and for DCHMs ranging from 0.23 m to 2.41 m in tropical landscapes.

2.2. Image data and preprocessing

In this study we used three Landsat ETM+ images from scene path/row (201/32) corresponding to three different dates (March 15th, 2000, June 6th, 2001 and September 10th, 2001). The Landsat images were georeferenced and radiometrically calibrated.

June and September's Landsat images were co-registered, at the Alcalá University's Geography Department, using digital highway maps of the Madrid region (E 1:50.000). RMSE was less than 30 m (1 pixel); the projection system was UTM (Datum Europeo 1950) with a pixel resolution of 30 m. We validated the image co-registration in the study area using a set of easily recognisable points.

From the March Landsat image, a subset area of 30 x 30 km was orthorectified. Control points were selected, taking as reference September's georeferenced image. The source of altitudinal information was a 20 m pixel DTM of the Madrid region. We used 38 control points, homogeneously spread out over the subset image. RMSE was 11.49 m (0.4 pixels). The COST absolute radiometric correction model of Chavez (1996) was applied to each image to convert digital counts to reflectance.

2.3. Lidar DCHM summaries (mean and standard deviation) and spectral indices

The DCHM lidar (1 m pixel) was degraded to 30 m cell blocks, providing a 30 m grid of 32 rows and 41 columns. The mean and standard deviation of the 900 lidar height values contained in each 30 x 30 m block were calculated. Two new 30 m pixel images of the mean and standard deviation of lidar height values were thus obtained.

NDVI and Tasseled Cap (TCAP) were calculated for the March, June and September Landsat images. TCAP transformation was obtained using coefficients for brightness, greenness and wetness derived by Crist (1985). According to Cohen *et al.* (2003), no published transformation exists to convert atmospherically-corrected ETM+ spectral data into Tasseled Cap indices. However, the authors have verified that Landsat TM and ETM+ are similar enough to assume

that any differences in Tasseled Cap indices derived from data from the two different sensors are minor.

2.4. Sample design and statistical analysis

First, we created a mask to exclude bare soil, rocks, pasture and shrubs from subsequent analysis (Figure 2) performing unsupervised classification of the September Landsat image. In addition, systematic sampling was used to reduce the spatial autocorrelation inherent in remote sensing imagery. The sampling procedure was designed based on semivariograms of the lidar DCHM mean height and wetness Tasseled component. Semivariograms were calculated using the free distribution software Variowin 2.2. (Pannatier, 1996). Mean lidar height was selected based on previous work (Pascual, 2006) and wetness TCAP component because is often related to forest structure (Cohen & Spies, 1992). The semivariance tends to stability at 130-150 m. Therefore, two samples were obtained, each using one out of every four or five pixels, one for statistical model building and the other to independently validate the model.

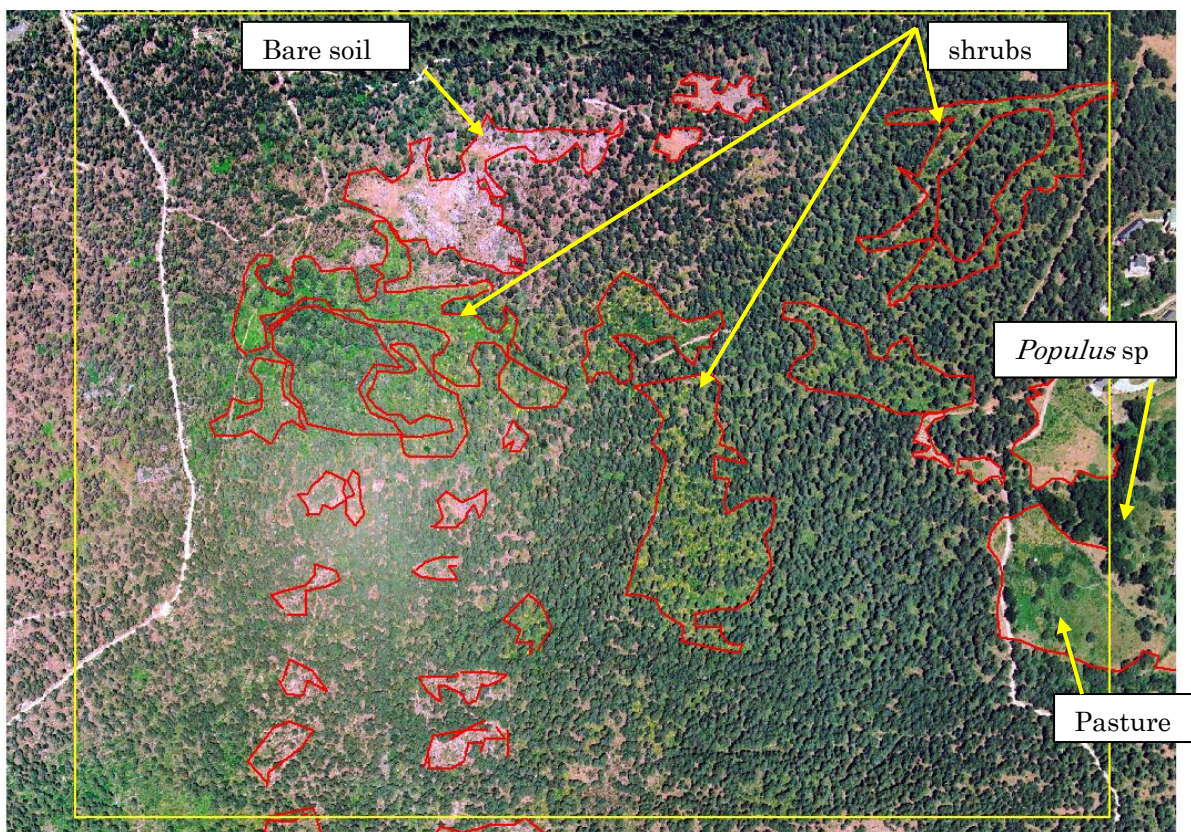


Figure 2: 0.5 m pixel digital orthophoto of the study area (yellow frame). Different covertures (pasture, bare soil, shrubs and *Populus* sp) were digitalised and labelled.

Pearson's correlation among Landsat spectral indices and lidar statistical descriptors was performed. Furthermore, forward step regression analysis ($p_{\text{enter}} = 0.05$; $p_{\text{remove}} = 0.05$) was carried out between both variable sets. All statistical analysis was conducted using STATISTICA 6.1 software. Before proceeding with regression analysis, the normality of the dependent and independent variables was verified and transformed when needed.

3. Results and Discussion

Mean lidar height and standard deviation of lidar height provided two images (Figure 3) with a gradient from black to white representing spatial variation in canopy height.

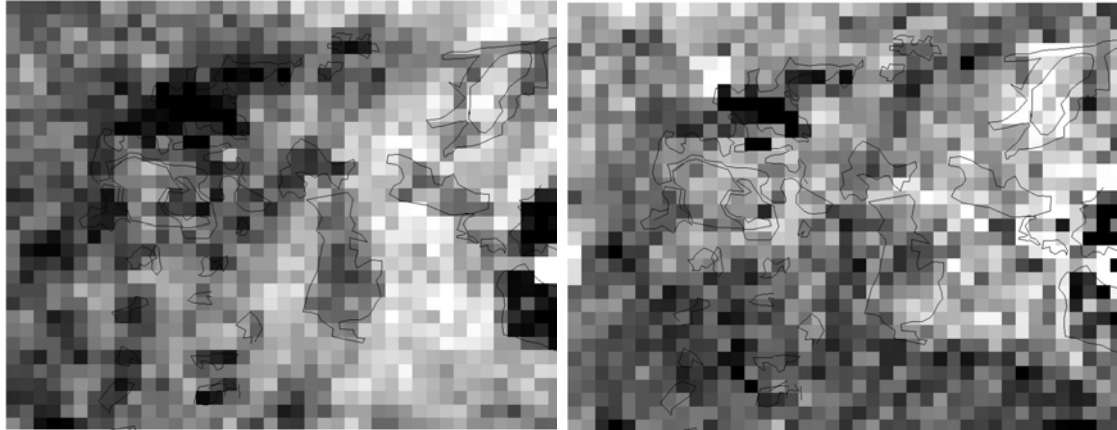


Figure 3: Mean lidar height image (30m pixel) (left) and Standard deviation of lidar height (right). Black to white gradient represent growing height values. Vectorial digitized covertures are included.

Correlations among NDVI indexes (Figure 4) and the square root of mean lidar height (\sqrt{hmean}) indicated a moderately strong relationship among these variables ($r = 0.65$, $r = 0.70$ y $r = 68$; $p = 0.05$; $n = 47$ for March, June and September respectively). Standard deviation of lidar height (sd_{30}) demonstrated an insignificant relationship with all NDVI indices for the three dates (Table 1).

Table 1: Pearson's correlation between lidar-derived metrics and spectral indices ($n = 47$).

| March 15th | | | | |
|----------------|-------|--------|-------|----------|
| | NDVI | Br | Gr | We |
| \sqrt{hmean} | 0.65* | -0.50* | 0.46* | 0.64* |
| sd_{30} | 0.20 | -0.16 | 0.18 | 0.20 |
| June 6th | | | | |
| | NDVI | 1/Br | Gr | Log(-We) |
| \sqrt{hmean} | 0.70* | 0.65* | 0.50* | -0.72* |
| sd_{30} | 0.30* | 0.13 | 0.26 | -0.11 |
| September 10th | | | | |
| | NDVI | 1/Br | Gr | Log(-We) |
| \sqrt{hmean} | 0.68* | 0.59* | 0.34* | -0.73* |
| sd_{30} | 0.29* | 0.15 | 0.17 | -0.04 |

*significant correlations $p < 0.05$; Br, Gr and We are brightness, greenness and wetness Tasseled components derived from ETM+.

Lu *et al.* (2004) found strong correlations between NDVI and forest attributes derived from field measurements. Nevertheless, Hall *et al.* (1995) and Franklin *et al.* (1997) do not consider this spectral index especially appropriate for the study of forest attributes because of the weak correlation that has been shown with certain parameters of vegetation. Regarding this, Lu *et al.* (2004) indicate that conclusions as to its application vary depending on the biophysical parameters and the characteristics of the study area.

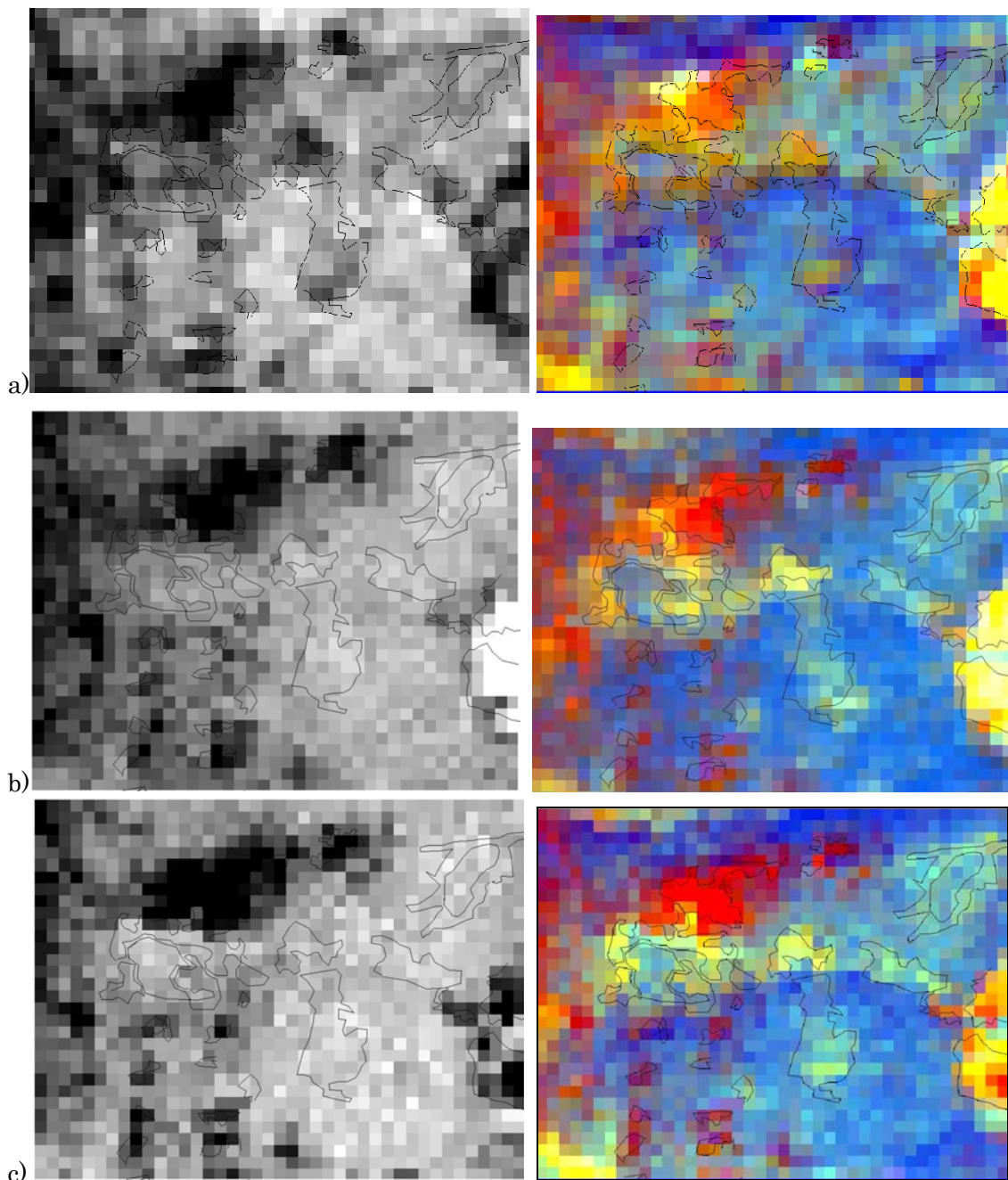


Figure 4: NDVI (left) and colour composition of the TCAP components (right): brightness in red channel; greenness in green channel and wetness in blue channel. a) March 15th; b) June 6th; and c) September 10th with the feature digitalized covertures (bare soil, pasture, shrubs).

Regarding TCAP transformation, the brightness and wetness of June and September (Figure 4) presented moderately strong correlations with the square root of mean lidar height ($r = 0.65$, $r = -0.72$ y $r = 0.59$ $r = -0.73$; $p = 0.05$; $n = 47$ respectively) (Table 1). When considering the Tasseled Cap components of each date separately, wetness presented higher correlations with the square root of mean height. Other authors have also reported strong correlations between the wetness component and multiple forest attributes measured in the field such as the *dbh* (diameter at breast height), crown diameter, mean height and basal area (Cohen & Spies 1992; Cohen *et al.* 1995). Wetness is considered the most interesting spectral index to estimate forest structure of dense formations (Cohen & Spies 1992; Cohen *et al.* 1995; 2001). In addition, this

component has been revealed as most significant when studying the temporal evolution of forests, such as mortality (Collins & Woodcok, 1994), harvesting and silvicultural activities (Wilson & Sader, 2002; Healey *et al.*, 2005) or in the evaluation of damage by plagues (Skakun, *et al.*, 2003). Standard deviation of lidar height (sd_30) and Tasseled components revealed weak and not significant correlations (Table 1).

Regarding regression analysis (Table 2), the three models presented coefficients of determination ranging from 0.55 to 0.63. Standard deviation of height derived from lidar (SD_30) was excluded from regression analysis due to low Pearson’s correlation (Table 1).

None of the three models presented colinearity problems (i.e. linear relationship among the independent variables problems). The variance inflation factor (VIF), as indicator of multicollinearity, did not present any variable values close to 5 or 10. According to Montgomery, *et al.* (2002) those are the thresholds that question regression coefficients estimated by minimum squares.

Table 2: Forward stepwise regression models

| Name | Models (forward stepwise regression) | r ² adjusted | RMSE |
|------------|---|-------------------------|------|
| Mod. NDVI | $\sqrt{hmean} = 1.137 - 0.0043 \cdot NDVI_mar + 0.0085 \cdot NDVI_jun$ | 0.55 | 4.07 |
| Mod. TCAP | $\sqrt{hmean} = 3.970 + 0.133 \cdot Gr_mar - 0.907 \cdot Log(-We_sep)$ | 0.62 | 4.58 |
| Mod. Mixed | $\sqrt{hmean} = 2.832 - 0.666 \cdot Log(-We_sep) + 0.140 \cdot \sqrt{NDVI_jun}$ | 0.59 | 4.32 |

A validation of regression analysis was performed using an independent sample of 54 pixels. Observed versus predicted values were represented in scatterplot graphs (Figure 5). All models showed a moderately strong adjustment ($r = 0.73$, $p = 0.000$; $r = 0.72$, $p = 0.000$ y $r = 0.79$, $p = 0.000$, $n = 54$ for Mod. NDVI, TCAP and MIXED respectively). Based on validation results, the best regression models were Mod. NDVI and Mod. MIXED.

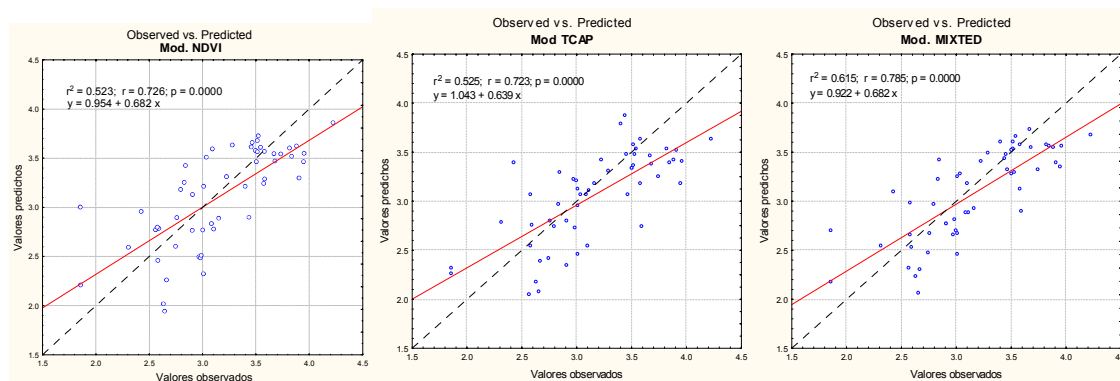


Figure 5. Scatterplots of independent (n=54) validation regression models (observed vs. predicted). Left (Mod. NDVI); middle (Mod. TCAP) and right (Mod. MIXED).

Conclusions

Mean lidar height derived from lidar for a Scot pine forest in Cercedilla was estimated through a combination of spectral indices derived from Landsat images. Wetness TCAP component showed higher correlations with square root of mean height derived from lidar. A wetness

relationship with forest structure has been reported by different authors. Regression models were explicative, because of the relationships among variables. Nevertheless regression models presented high variability (r^2 : 0.55 – 0.62) that diminished their predictive capacity. These results show that lidar data can be useful for training Landsat to map mean height. Given the relationship between mean lidar height derived from lidar and the forest structure, Landsat data can help to characterize forest structure. This approach should be analyzed in future research.

References

- Chavez, P., 1996. Image-based atmospheric corrections—Revisited and improved. *Photogrammetric Engineering and Remote Sensing*, 62, 1025–1036.
- Chen, X., Vierlinga, L., Rowell, E. and DeFelice, T., 2004. Using lidar and effective LAI data to evaluate IKONOS and Landsat 7 ETM+ vegetation cover estimates in a ponderosa pine forest. *Remote Sensing of Environment*, 91, 14–26.
- Clark, M.L., Clark, D.B. and Roberts, D.A., 2004. Small-footprint lidar estimation of sub-canopy elevation and tree height in a tropical rain forest landscape. *Remote Sensing of Environment*, 91, 68 - 89.
- Cohen, W. B. and Spies, T. A., 1992. Estimating structural attributes of Douglas-Fir western Hemlock forest stands from Landsat and SPOT imagery. *Remote Sensing of Environment*, 41, 1-17.
- Cohen, W. B., Spies, T. A. and Fiorella, M., 1995. Estimating the age and structure of forests in a multi-ownership landscape of western Oregon, U.S.A. *International Journal of Remote Sensing*, 16, 721–746.
- Cohen, W. B., Maiersperger, T. K., Spies, T. A. and Oetter, D. R., 2001. Modeling forest cover attributes as continuous variables in a regional context with Thematic Mapper data. *International Journal of Remote Sensing*, 22, 2279–2310.
- Collins, J. B. and Woodcock, C. E., 1994. Change detection using the Gramm–Schmidt transformation applied to mapping forest mortality. *Remote Sensing of Environment*, 50, 267–279.
- Crist, E. P., 1985. A TM tasseled cap equivalent transformation for reflectance factor data. *Remote Sensing of Environment*, 17, 301– 306.
- Franklin, S. E., Lavigne, M. B., Deuling, M. J., Wulder, M. A. and Hunt Jr., E. R., 1997. Estimation of forest leaf area index using remote-sensing and GIS data for modeling net primary production. *International Journal of Remote Sensing*, 18, 3459–3471.
- Hall, F. G., Shimabukuro, Y. E. and Huemmrich, K. F., 1995. Remote sensing of biophysical structure using mixture decomposition and geometric reflectance models. *Ecology Applications*, 5, 993-1013.
- Healey, S. P., Cohen, W. B., Zhiqiang, Y. and Krankina, O. N., 2005. Comparison of Tasseled Cap-based Landsat data structures for use in forest disturbance detection. *Remote Sensing of Environment*, 97, 301-310.
- Hudak, A. T., Lefsky, M. A., Cohen, W. B. and Berterretche, M., 2002. Integration of LiDAR and Landsat ETM+ data for estimating and mapping forest canopy height. *Remote Sensing of Environment*, 82, 397–416.
- Hyypä, J., Hyypä, H., Leckie, D., Gougeon, F., Yu, S. and Maltamo, M., 2008. Review of methods of small-footprint airborne laser scanning for extracting forest inventory data in boreal forests. *International Journal of Remote Sensing*, 29, 1339-1366.
- Lefsky, M. A., Cohen, W. B., Acker, S. A., Parker, G. G., Spies T. A. and Harding, D., 1999. Lidar remote sensing of the canopy structure and biophysical properties of Douglas-Fir

- Western Hemlock forests. *Remote Sensing of Environment*, 70, 339-361
- Lefsky, M. A., Hudak, A. T., Cohen, W. B. and Acker, S. A., 2005a. Patterns of covariance between forest stand and canopy structure in the Pacific Northwest. *Remote Sensing of Environment*, 95, 517–531.
- Lefsky, M. A., Turner, D. P., Guzy, M. and Cohen, W. B. ,2005b. Combining lidar estimates of aboveground biomass and Landsat estimates of stand age for spatially extensive validation of modelled forest productivity. *Remote Sensing of Environment*, 95, 549-558.
- Lu, D., Mausel, P., Brondízio, E. and Moran, E., 2004. Relationship between forest stand parameters and Landsat TM spectral responses in the Brazilian Amazon Basin. *Forest Ecology and Management*, 198: 149-167.
- Maltamo, M., Packalen, P., Yu, X., Eerikainen, K., Hyyppä, J., Pitkanen, J., 2005. Identifying and quantifying structural characteristics of heterogeneous boreal forests using laser scanner data. *Forest Ecology and Management*, 216, 41–50.
- Montgomery, D., Peck, E. and Vining, G., 2002. Introducción al Análisis de Regresión Lineal. Compañía Editorial Continental. México.
- Pannatier, Y. (1996). Variowin: Software for Spatial Data Analysis in 2D. Springer-Verlag. New York.
- Parker, G. G.,1995. Structure and microclimate of forest canopies. In Forest Canopies—A Review of Research on a Biological Frontier (M. Lowman & N. Nadkarni, Eds.), Academic, San Diego, pp. 73–106.
- Pascual, C., 2006. Análisis de la estructura forestal mediante teledetección: LiDAR (Light Detection And Ranging) e imágenes de satélite, Ph.D. thesis. Technical University of Madrid (UPM), Madrid.
- Pascual, C., García-Abril, A., García-Montero, L.G, Martín-Fernández, S., Cohen, W.B.,2008. Object-based semi-automatic approach for forest structure characterization using lidar data in heterogeneous *Pinus sylvestris* stands. *Forest Ecology and Management*, 255, 3677-3685.
- Skakun, R. S., Wulder, M. A. and Franklin, S. E., 2003. Sensitivity of the thematic mapper enhanced wetness difference index to detect mountain pine beetle red-attack damage. *Remote Sensing of Environment*, 86, 433-443.
- Wilson, E. H. and Sader, S. A, 2002. Detection of forest harvest type using multiple dates of Landsat TM imagery. *Remote Sensing of Environment*, 80, 385– 396.
- Wulder, M.A., Hana, T., White, J.C., Sweda, T. and Tsuzuki, H., 2007. Integrating profiling LIDAR with Landsat data for regional boreal forest canopy attribute estimation and change characterization. *Remote Sensing of Environment*, 110, 123-137
- Zimble, D.A., Evans, D.L., Carlson, G.C., Parker, R.C., Grado, S.C. and Gerard, P.D., 2003. Characterizing vertical forest structure using small-footprint airborne LiDAR. *Remote Sensing of Environment*, 87, 171 - 182.

The comparison of airborne laser scanning-based probability layers as auxiliary information for assessing coarse woody debris

Pesonen Annukka¹, Maltamo Matti¹, Petteri Packalén¹, Leino Olli²

¹Faculty of Forest Sciences, University of Joensuu, P.O. Box 111, FI-80101 Joensuu, Finland,

annukka.pesonen@joensuu.fi

matti.maltamo@joensuu.fi

petteri.packalen@joensuu.fi

²Department of Forest Resource Management, University of Helsinki, P.O. Box 27, FI-00014 Helsinki, Finland,

olli.pt.leino@helsinki.fi

Abstract

During the last 15 years the assessment of biodiversity has become more important in forestry. Coarse woody debris (CWD) has been recognized as one of the strongest indicators of forest biodiversity and the assessment of it has been emphasized in the development of new inventory methods for sparse populations. In this study, the use of airborne laser scanning (ALS)-based probability layers in guiding the sampling-based field inventory of CWD was tested on a field area of 286 hectares. The auxiliary information was used by implementing point proportional to size (PPS) sampling in the selection of the first stage sample units in simple random sampling (SRS) and adaptive cluster sampling (ACS). The sampling methods were compared by means of the accuracy of the mean volume (m^3ha^{-1}) estimates for CWD with fixed input effort specified as field working hours. The accuracy of CWD volume estimates with PPS and PPS+ACS, where ALS-derived probability layers were utilized, was higher than the accuracy of SRS and ACS. Thus, this paper introduces new possibilities for making the inventory of CWD more efficient.

Keywords: Airborne laser scanning, Coarse woody debris, Probability layers

1. Introduction

In large-scale forest inventories, information about the forest characteristics is often acquired using sampling, since an inventory of the total population is often expensive or even impossible. During recent decades, increasing attention has been paid to forest biodiversity on all its levels, from the variety of ecosystems to richness in species and genes. Coarse woody debris (CWD) has been recognized to be one of the most important indicators of forest biodiversity, since a high proportion of rare and specialised species is dependent on it (e.g. Siitonen 2001; Karjalainen and Kuuluvainen 2002). Traditional methods of measuring and modelling these attributes have been expensive and of low accuracy, because dead trees are rare and their existence is clustered (Kangas et al. 2004). Since forest biodiversity has been emphasized in forest policies and on the operational forest management level, a broad selection of inventory methods for CWD have been introduced and tested.

In general, objects which are more interesting than others may be included in the sample with a higher probability; this may be because better results are desired. Thus, different units in the population may be included in a sample with different probabilities (Thompson 2002). The use

of auxiliary information in combination with a field inventory has been studied widely (e.g. Ringvall et al. 2007). The multi-source National Forest Inventory of Finland, for example, utilizes satellite images in producing large area information about forest characteristics (Tomppo 1991). Due to the development of remote sensing, more accurate and lower-cost information is available to be used as auxiliary information. One of the most promising remote-sensing technologies for increasing the accuracy and efficiency of large-scale forest inventories is airborne laser scanning (ALS) (Næsset 2002; Maltamo et al. 2006), which produces a three-dimensional illustration of the forest area. ALS-derived variables can be used in producing probability layers, which represent, for example, the likelihood of CWD existing in each grid cell of the layer. ALS can be utilized in guiding the field inventory to the more interesting areas, and thus the efficiency of field sampling methods may be improved.

In this study, the possibility of utilizing ALS as auxiliary information by implementing point proportional to size (PPS) sampling in the location of sample units in simple random sampling (SRS) and adaptive cluster sampling (ACS) was studied with the forests in commercial use in Central Finland. The efficiency of PPS and PPS+ACS was compared with SRS and ACS, where auxiliary data is not utilized. The aim of this article is to present an extensive comparison of different ALS-derived probability layers in guiding the inventory of CWD in one large area from the perspective of efficiency.

2. Material

2.1 Study area and data collection

The field work for this study was carried out in the summer of 2007. The study area is located in Sonkajärvi district in Central Finland and the forest area assessed is in active commercial forest management use. The age structure of the stands in the area is slightly biased towards younger age classes, but all classes are present in the area. As typical in Central Finland, the area consists of a mosaic of mineral soils, water bodies and both drained and undrained peat lands.

The field data was collected by measuring randomly located 100-meter-wide strips in a north-south direction. All dead trees with a base diameter greater than 10 centimeters were measured. The characteristics recorded for the standing dead trees were the diameter at breast height (dbh) and total height. For snapped trees, the measured variables were the dbh, the lengths of the standing and downed parts and the direction of the downed part. For downed dead trees, the falling direction, the total length and the dbh were measured. If the snags were shorter than 1.3 metres or the breast height could not be assessed, the diameter in the middle was measured instead of the dbh. All the observations were located with GPS (Global Positioning System) devices and the differential corrected using a base station located in the same municipality.

For the simulation study, all the strips measured were artificially gathered to make a uniform area. The compilation was formed by replacing the strips measured in spatially true order into a new coordinate system so that the directions of the strips remained in a north-south direction. The total compilation area was 286 hectares, the dimensions of the rectangle being 1.1km*2.60km. The mean CWD volume in the study area was 2.69m³ha⁻¹, and the volumes ranged between 0m³ha⁻¹ and 69.2m³ha⁻¹.

2.2 Laser data and data processing

The Georeferenced ALS point cloud data from Sonkajärvi were collected on 27th and 28th July

2006 using an Optech ALTM 3100 scanner operating at a mean altitude of 2500 m a.g.l (above ground level), which resulted in a nominal sampling density of about 0.5 measurements per m² when the pulse frequency of 50 kHz was used. The data were captured using a half-angle of 15°, resulting in a swath width of 1350 m.

Both the first and last pulse data were recorded and the last pulse data were employed to generate a digital terrain model (DTM) using the method explained in Axelsson (2000). Above ground heights, i.e. canopy heights, for the laser points were obtained by subtracting the DTM at the corresponding location. The height distribution of the first and last pulse canopy height hits was used to calculate grid-wise percentiles for 0, 1, 5, 10, 20, ..., 90, 95, 99 and 100% heights (h_0, h_1, \dots, h_{100}) (see Næsset 2004), and cumulative proportional crown densities (p_0, p_1, \dots, p_{100}) were calculated for the respective quantiles. All metrics were calculated separately for both the first pulse data and the last pulse data. ALS-based variables were calculated with a vegetation limit of 0.5 meters.

3. Methods

3.1 Producing the probability layers

CWD measurements and ALS data were available from an independent study area in Juuka in Eastern Finland (Kotamaa 2007). The laser scanning equipment and measurements from this area were similar to those from the Sonkajärvi study area. Thus, the correlations between the ALS-derived height-, density- and intensity metrics and the CWD volumes were studied in the data available from Juuka. Using this data, we searched for the ALS-derived height metric which had the best correlation with the observed CWD volume. Respectively, we also searched for the density-, intensity- and deviation metrics which best correlated with the CWD volume.

Furthermore, two logistic CWD volume models were used in producing the probability layers. Two different independent modelling data were available from Juuka and Sonkajärvi region and were used in constructing the models. The logistic regression model can be expressed as follows (e.g., Hosmer and Lemeshow 1989; Dobson 1990):

$$\text{logit}(\pi_j) = \beta_0 + \beta_1 x_{1j} + \dots + \beta_i x_{ij} \quad (1)$$

$$\Leftrightarrow \pi_j = \frac{\exp(\beta_0 + \beta_1 x_{1j} + \dots + \beta_i x_{ij} + \varepsilon)}{1 + \exp(\beta_0 + \beta_1 x_{1j} + \dots + \beta_i x_{ij} + \varepsilon)}, \quad (2)$$

where π_j is the probability for observation y_j , β_0 the constant of the model and β_i the parameter to be estimated for independent variable x_i . x_{ij} is the i th independent variable connecting to the observation y_j and ε the error term of the model, $j = 1, 2, \dots, N$. Equation 2 is intrinsically bounded within the interval [0, 1].

Since the unknown model parameters are non-linearly related to π_j , Maximum likelihood (ML) method is used to estimate the model parameters in logistic regression (Alenius et al. 2003). The models were fitted using glm-function with the R software (R Development... 2006). The method searches the parameter estimates which maximize the log-likelihood function l (Eqn. 3) i.e. it finds the most probable values of distribution parameters for a set of data.

$$l = \sum_{j=1}^N [y_j \log \pi_j + (1 - y_j) \log(1 - \pi_j)] \quad (3)$$

In constructing logistic regression models, the existence of CWD (volume limit $0 \text{ m}^3\text{ha}^{-1}$) was given a binary outcome, and it was predicted with the continuous explanatory variables derived from ALS data. The model parameters and independent variables in the models were investigated in order to find the best fitting model in the modelling data. The models predict the probability of CWD existing in each grid cell. In the logistic model from Juuka, the parameter estimates for the model constant and independent variable $l_{h_{90}}$ were -3.2607 and 0.3434 , respectively; while the parameter estimates for the model constant and $l_{h_{30}}$ in the local model from Sonkajärvi were -0.9907 and 0.1443 , respectively. In the logistic models, $l_{h_{90}}$ and $l_{h_{30}}$ denote the height at which the accumulation of last return laser hit heights in the vegetation is 90% and 30%, respectively. However, it is worth noting that if locally fitted logistic models are used in practice in producing probability layers, the collection of field data for CWD modelling requires a field inventory, and that data as such could be used for estimating the sampling statistics of CWD volume in the area.

In this study, the total study area of $1.1\text{km} \times 2.60\text{km}$ was divided into grid cells of $20\text{m} \times 20\text{m}$. In total six different probability layers were constructed, four of which were produced by calculating the ALS-based variables for each grid cell, and two of which were produced using logistic models to predict the probability of CWD existing in each grid cell. Thus, either the value of ALS-derived variables as such or the value predicted with the logistic regression models determined the probability of each grid cell in the probability layer.

3.2 Sampling methods

The simulated sampling methods were simple random sampling (SRS) and adaptive cluster sampling (ACS). In these sampling methods, the simulated plots were squares – equalling the size and the location of the grid cells in the produced probability layers. The sample plots were placed in the study area by drawing grids randomly and with replacement. In SRS the estimator for the mean CWD volume (m^3ha^{-1}) was calculated as the mean of the inventoried plots

$$\hat{y} = \frac{1}{n} \sum_{i=1}^n y_i, \quad (4)$$

where y_i is the CWD volume (m^3ha^{-1}) on plot i and n is the number of plots. The variance estimate was obtained from the variation between the sample plots (see e.g. Gregoire and Valentine 2008) as

$$\text{vâr}(\hat{y}) = \frac{1}{n(n-1)} \sum_{i=1}^n (y_i - \bar{y})^2. \quad (5)$$

An estimator for the standard deviation of mean CWD volume is obtained by taking the square root of its variance.

In ACS a population is divided into N units and an initial sample of size n_1 is selected of these units. In ACS, simple random sampling without replacement was used to select an initial sample of the population, and whenever the amount of dead wood in a sampling unit exceeded the initially set limit, four neighbouring units of that unit were added to the sample (Thompson 1990). The volume limit of $30 \text{ m}^3\text{ha}^{-1}$ was used in this study, since it has been noticed to be effective in Finnish commercial forests (Pesonen et al. 2008a). The estimates for the population mean and variance were calculated using Horvitz-Thompson (HT)-estimator (Thompson 1990). If the network containing unit j is A_j , and m_j denotes the number of units in A_j , the probability that the initial sample intersects A_j is

$$\alpha_j = 1 - \frac{\binom{N - m_j}{n_1}}{\binom{N}{n_1}}. \quad (6)$$

An unbiased HT estimator for the mean is

$$\hat{\mu}_{HT} = \frac{1}{N} \sum_{k=1}^{\kappa} \frac{y_k^*}{\alpha_k}, \quad (7)$$

where κ is the number of distinct networks intersected by the initial sample and y_k^* is the sum of the y values for the k th network. The inclusion probability α_k is the same for all units in network k . The joint inclusion probability of networks j and k i.e the probability that one unit belongs to networks j and k is given by

$$\alpha_{jk} = \begin{cases} 1 - \frac{\binom{N - m_j}{n_1} + \binom{N - m_k}{n_1} - \binom{N - m_j - m_k}{n_1}}{\binom{N}{n_1}} & \text{for } j \neq k, \text{ and} \\ \alpha_j & \text{otherwise.} \end{cases} \quad (8)$$

The unbiased estimator for the variance of $\hat{\mu}_{HT}$ is

$$\hat{\text{var}}(\hat{\mu}_{HT}) = \frac{1}{N^2} \left[\sum_{j=1}^{\kappa} \sum_{k=1}^{\kappa} \frac{y_j^* y_k^*}{\alpha_{jk}} \left(\frac{\alpha_{jk}}{\alpha_j \alpha_k} - 1 \right) \right]. \quad (9)$$

In the selection of sampling units, it is possible to select the units by utilizing some previously available information and taking into account that each unit in the study area may not have the same inclusion probability. In this study, the plots were placed in the study area by utilizing ALS data as auxiliary information. The probabilities of CWD existing were derived from the produced probability layers, and the sample plots were placed in the grid cells with a probability proportional to the predicted probabilities.

In unequal probability sampling with replacement, PPS, an unbiased estimator for the population total is obtained as (see e.g. Thompson 2002)

$$\hat{\tau}_p = \frac{1}{n} \sum_{i=1}^n \frac{y_i}{p_i}, \quad (10)$$

where p_i is the probability of selecting the i th unit of the population, for $i = 1, 2, \dots, N$. In this study, the total CWD volume estimated from plot i was calculated by summing the observed volumes in a grid cell i and dividing the sum with the ALS-based estimate for the probability of a grid cell i to be included in the sample. The estimate for the mean volume per hectare was calculated by dividing the estimated total volume with the study area in hectares.

Similarly, in ACS it is possible to select initial sampling units with unequal probabilities. Roesch (1993) and Smith et al. (1995) have used PPS sampling in ACS in inventorying rare and clustered characteristics of trees and the number of wintering waterfowls, respectively. Smith et al. (1995) have presented the calculation of the estimates with unequal probabilities in ACS (PPS+ACS). In PPS+ACS the Equations 7 and 9 were used in calculating the estimators for the mean and variance. However, the intersection probabilities were then calculated as

$$\alpha_j = 1 - \left(1 - \frac{a_j}{A^*}\right)^{n_1} \quad \text{and} \quad (11)$$

$$\alpha_{jk} = \begin{cases} \alpha_j + \alpha_k - \left[1 - \left(1 - \frac{a_j + a_k}{A^*}\right)^{n_1}\right] & \text{for } j \neq k, \text{ and} \\ \alpha_j & \text{otherwise.} \end{cases} \quad (12)$$

In Equations 11 and 12 a_j denotes the probability of CWD existing in the j th network and A^* is the sum of predicted probabilities in the study region.

3.3 The simulation and comparison of different sampling methods

The alternative sampling methods with different probability layers were simulated in the study area where every downed and standing dead wood log was precisely located. The simulations were made for the combined CWD volume including both CWD materials.

Once the sample units were placed in the study area, the accuracy statistics for the simulated sampling methods were calculated based on the field measured CWD data. The estimates for the population mean, absolute and proportional standard error of mean were calculated. Different sampling methods were simulated with the study area 500 times. The mean and variance estimators in each simulation were calculated with equations specific to each sampling method, and the average of these was the mean and variance obtained for the specific sampling method.

Since the costs of field inventory methods vary depending on the measurement time and the travelling time between the plots, the time consumption of each sampling simulation was taken into consideration. For each sampling approach, the achieved accuracies with a fixed inventory time were calculated in order to make the different sampling strategies comparable.

4. Results

Different ALS-based probability layers were utilized in the placement of the sample units in PPS and PPS+ACS and the accuracy of the layers were compared in terms of the precision of the estimated mean CWD volume in the area by additionally taking into account the required inventory time of each sampling approach. The precision of the estimates varied notably between different probability layers.

The probability layers were formed using the variables which were observed to have the highest correlation with CWD volume. Thus, correlations were only analyzed in order to find the variables which have the highest correlation with CWD volume and the correlations were not utilized as such in producing the probability layers, but the layers were formed by calculating the value of the ALS-based variables for each grid cell of the layer. The ALS-derived height-, density-, deviation-, and intensity metrics which had the highest correlation with CWD volume in the Juuka data and the respective strengths of the correlations and their directions in the Sonkajärvi data are shown in Table 1. The correlations were similar in both regions. The ALS-derived heights at the upper percentiles captured by the first pulse and the standard deviation of heights had the strongest correlation with CWD volume. If the standard deviation of laser pulse heights increased, greater CWD volumes were observed in both areas, for example.

Table 1: The strengths and the directions of the correlations between CWD volume (m^3ha^{-1}) and ALS-based variables.

| ALS-based variable ^a | Juuka | Sonkajärvi |
|---------------------------------|--------|------------|
| f_h_{60} | 0.366 | 0.320 |
| f_h_{std} | 0.327 | 0.301 |
| l_i_{10} | -0.183 | -0.151 |
| f_p_{90} | -0.141 | -0.103 |

^a The prefix f or l denotes the laser pulse type, first or last pulse, h_{60} denotes the height at which the accumulation of laser hit heights in the vegetation is 60%, h_{std} is the standard deviation of the height distribution pulses. The p_{90} denotes the proportion of laser hits accumulating at the 90% height and i_{10} is the value of intensities accumulated in the 10th percentile.

The higher the correlation between CWD volume and the ALS-based variable was, the more improvement in the accuracy of volume estimates was usually achieved while utilizing probability layers in guiding the placement of sample plots. With a given inventory time in SRS, utilizing probability layers produced from ALS metrics of f_p_{90} , l_i_{10} , f_h_{60} and f_h_{std} produced 4%, 6%, 13% and 15% smaller standard errors of the mean for the CWD volume estimate, respectively (Figure 1); the respective improvements in the accuracy of ACS were 3%, 5%, 9% and 11% (Figure 2). The utilization of probability layers produced using logistic models applied in the Juuka and Sonkajärvi regions improved the accuracy of SRS with 8% and 10%, respectively, while the accuracy of ACS improved with 6% and 7%. Thus, the locally fitted logistic model was more accurate, but the ALS-derived height- and deviation metrics improved the accuracy of the estimates even more.

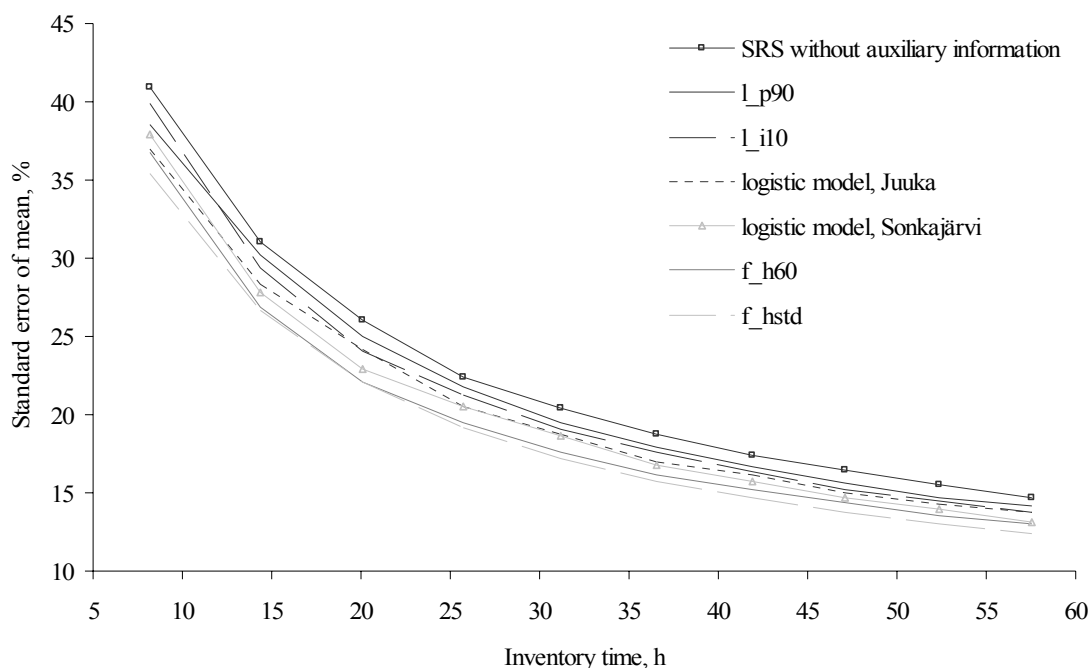


Figure 1: The standard error of mean for the CWD volume estimates in SRS without auxiliary information and utilizing different ALS-based probability layers.

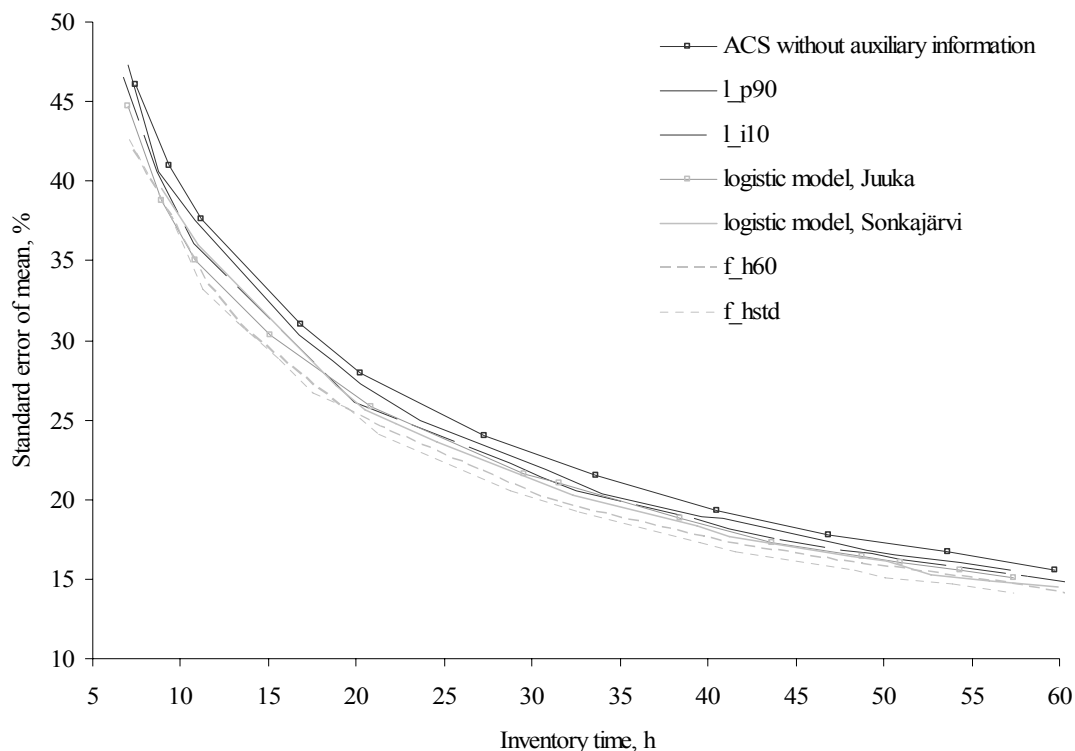


Figure 2: The standard error of mean for the CWD volume estimates in ACS without auxiliary information and utilizing different ALS-based probability layers.

5. Discussion

Since CWD is recognized to be a key factor for biodiversity in boreal forests, recently inventory techniques for assessing CWD have been developed (e.g. Thompson 1990; Buckland et al. 1993; Ståhl 1997). However, field surveys can still be expensive. This study focused on the possibilities for improving the efficiency of field inventories with SRS or ACS by utilizing different ALS-based probability layers as auxiliary information.

The utilization of probability layers in the guidance of field inventories improved the accuracy of CWD volume estimates. The efficiency of SRS and ACS could be improved notably when utilizing probability layers produced from ALS-derived height metric and standard deviation of heights, but only slight improvements were achieved when the probability layer was constructed from ALS-derived density- or intensity metrics, since there was only minor correlation between CWD volume and these variables. The efficiency of probability layers derived from both a locally fitted logistic CWD model and a logistic model from a separate area was weaker than direct ALS-derived height metrics, since the correlations between CWD volume and the predictions of logistic models were weaker. It could also be possible to combine different ALS variables in probability layers. Coefficients for these variables could be searched for by means of optimization or by modelling. However, in the case of modelling the drawback would be statistically non-significant independent variables in the constructed models.

Even the utilization of a locally fitted logistic CWD model could not improve the accuracy of SRS and ACS as much as direct ALS-derived variables. The same result was obtained when utilizing two linear regression models which were constructed using data available from Juuka and Sonkajärvi. Furthermore, there were considerable difficulties in the construction of linear regression models for predicting CWD volumes. The observed high accuracy of ALS-based

probability layers compared to model-based layers improves the usability of direct ALS metrics since then any previously fitted model and expensive modelling data for predicting the probabilities in grid cells are not required. Therefore, the usability of ALS-derived probability layers in guiding the field inventory is relevant and prior information about the correlations between the existence of CWD and ALS-based variables can be used in constructing the probability layers. This information can be obtained from nearby areas which have older modelling data, such as from Juuka in our case. Like Pesonen et al. (2008a, 2008b), this study found that CWD volume is strongly correlated with ALS-derived heights and the standard deviation of height pulses. Hence, these variables can be used in constructing the probability layers and used in making the field inventory more efficient; or, respectively, for achieving a given accuracy level less inventory load is needed.

This study focused on estimating the combined CWD volume including both downed and standing dead trees. The probability layers can also be produced separately for different CWD materials if the combined CWD volume is not in focus. It was observed in this study that the standard deviation of heights captured by the first pulse ALS data and the heights at upper percentiles correlated strongly with both downed and standing dead wood volumes. The utilization of probability layers which were constructed separately for both CWD materials, improved the accuracy of volume estimates in a manner similar to the case of combined CWD volume.

The direct estimation of CWD volumes in commercial forests have proved to be challenging with sparse pulse ALS data and only the accuracy of logistic regression with a volume limit of $0\text{m}^3\text{ha}^{-1}$ has proved to be appropriate (Kotamaa 2007); however, ALS data is suitable as auxiliary information in making the field inventory more efficient. The utilization of probability layers in guiding the field inventory of CWD is a new approach and while the costs of ALS data are decreasing quickly, data from increasingly large areas is being acquired. In this study, the costs of ALS data were assumed to be zero, which naturally is not true. Nowadays, while the inventory of living trees could be done accurately enough by utilizing ALS (e.g., Næsset 2007), the same ALS data, which is originally gathered for other purposes, could be utilized in CWD inventories as well. Further studies are focusing on how auxiliary information derived from ALS data could also be utilized in other field inventory methods than SRS and ACS.

Acknowledgements

The authors thank Ms Eveliina Kotamaa for her assistance in calculating the CWD volumes for the Juuka region and Dr Lauri Mehtätalo for his comments on the text. Many thanks are also due to the SilviLaser 2008 team for putting this format template together. This study is a part of the project “Mapping rare forest characteristics using remote sensing material and field data (decision No. 116313)”, funded by the Academy of Finland.

References

- Alenius, V., Hökkä, H., Salminen, H. and Jutras, S., 2003. Evaluating estimation methods for logistic regression in modelling individual-tree mortality. In: Amaro, A., Reed, D. and Soares, P. (eds.). Modelling forest systems. CABI, London, pp. 225–236.
- Axelsson, P., 2000. DEM generation from laser scanner data using adaptive TIN models. P. 110-117 in Proc. of XIXth ISPRS Conference, Vol. XXXIII, IAPRS, Amsterdam, The Netherlands.
- Buckland, S.T., Anderson, D.R., Burnham, K.P. and Laake, J.L., 1993. Distance sampling. Estimating abundance of biological populations. Chapman & Hall, London. 446 pp.

- Dobson, A.J., 1990. An introduction to generalized linear models. Chapman and Hall, London, 174 pp.
- Gregoire, T.G. and Valentine, H.T., 2008. Sampling strategies for natural resources and the environment. Chapman & Hall/CRC. 474 pp.
- Hosmer D.W., and Lemeshow, S., 1989. Applied Logistic Regression. John Wiley & Sons, 307 pp.
- Kangas, A., Aakala, T., Alanen, H., Haavisto, M., Heikkilä, J., Kaila, A., Kankaanpää, S., Kämäri, H., Leino, O., Mäkinen, A. and Nurmela, E., 2004. Lahopuuinventoinnin menetelmien vertailu Nuuksion ulkoilualueilla. [Metsätieteen aikakauskirja 1/2004](#): 43-51. (In Finnish.)
- Karjalainen, L. and Kuuluvainen, T., 2002. Amount and diversity of coarse woody debris within a boreal forest landscape dominated by *Pinus sylvestris* in Vienansalo wilderness, eastern Fennoscandia. *Silva Fennica* [36\(1\)](#): 147-167.
- Kotamaa, E., 2007. Lahopuun määrän ennustaminen laserkeilauksella talousmetsissä. University of Joensuu, Faculty of Forest Sciences, candidate's thesis in Forest Planning and Economics. (In Finnish).
- Maltamo, M., Malinen, J., Packalén, P., Suvanto, A. and Kangas, J., 2006. Nonparametric estimation of stem volume using airborne laser scanning, aerial photography, and stand-register data. [Canadian Journal of Forest Research](#) 36(2): 426-436.
- Næsset, E., 2002. Predicting forest stand characteristics with airborne scanning laser using a practical two-stage procedure and field data. *Remote Sensing of Environment* 80: 88-99.
- Næsset, E., 2004. Practical large-scale forest stand inventory using small-footprint airborne scanning laser. *Scandinavian Journal of Forest Research* 19: 164-179.
- Næsset, E., 2007. Airborne laser scanning as a method in operational forest inventory: Status of accuracy assessments accomplished in Scandinavia. *Scandinavian Journal of Forest Research* 22: 433-442.
- Pesonen, A., Leino, O., Maltamo, M. and Kangas, A. 2008a. Comparison of field sampling methods for assessing coarse woody debris and use of airborne laser scanning as auxiliary information. Manuscript.
- Pesonen, A., Maltamo, M., Eerikäinen, K. and Packalén, P., 2008b. Airborne laser scanning -based prediction of coarse woody debris volumes in a conservation area, *Forest Ecology and Management* 255: 3288-3296.
- Ringvall, A., Snäll, T., Ekström, M. and Ståhl, G., 2007. Unrestricted guided transect sampling for surveying sparse species. [Canadian Journal of Forest Research](#) 37: 2575-2586.
- R Development Core Team, 2006. R: A language and environment for statistical computing. R Foundation for Statistical Computing, Vienna, Austria. ISBN 3-900051-07-0, URL <http://www.R-project.org>
- Roesch, F.A., Jr., 1993. Adaptive cluster sampling for forest inventories. *Forest Science* 39: 655-669.
- Siitonen, J., 2001. Forest management, coarse woody debris and saproxylic organisms: Fennoscandian boreal forests as an example. *Ecological Bulletins* 49: 11-41
- Smith, D.R., Conroy, M.J. and Brakhage, D.H., 1995. Efficiency of adaptive cluster sampling for estimating density of wintering waterfowl. *Biometrics* 51: 777-788.
- Ståhl, G., 1997. Transect relascope sampling for assessing coarse woody debris: the case of a $\pi/2$ relascope angle. *Scandinavian Journal of Forest Resource* 12: 375-381.
- Thompson, S.K., 1990. Adaptive cluster sampling. *Journal of the American Statistical Association* 85: 1050-1059.
- Thompson, S.K., 2002. Sampling. Second edition. Wiley & Sons, New York.
- Tomppo, E., 1991. Satellite image-based national forest inventory of Finland. *International Archives of Photogrammetry and Remote Sensing* 28: 419-424. Proceedings of the Symposium on Global and Environmental Monitoring, Techniques and Impacts, 17-21 September 1990, Victoria, British Columbia, Canada.

Regional applicability of forest height and aboveground biomass models for the Geoscience Laser Altimeter System

Dirk Pflugmacher^{1*}, Warren B. Cohen², Robert E. Kennedy², Michael A. Lefsky³

¹Oregon State University, Department of Forest Science, 321 Richardson Hall, Corvallis, OR 97331, United States

²USDA Forest Service, Pacific Northwest Research Station, Forestry Sciences Laboratory, 3200 SW Jefferson Way, Corvallis, OR 97331, United States

³Center for Ecological Analysis of Lidar, Department of Natural Resources, Colorado State University, 131 Forestry Building, Fort Collins, CO 80523-1472, United States

Abstract

Accurate estimates of forest aboveground biomass are needed to reduce uncertainties in global and regional terrestrial carbon fluxes. The Geoscience Laser Altimeter System (GLAS) onboard the Ice, Cloud and land Elevation Satellite is the first spaceborne lidar sensor that will provide global estimates of forest height useful estimating forest biomass. In this study we investigated the utility of GLAS for large-scale biomass inventories. We compared accuracy and regional variability of GLAS height estimates in two eco-regions in the Eastern and Western United States using data from the U.S. Forest Service Inventory and Analysis (FIA) program and found that current GLAS algorithms provided generally accurate estimates of height. GLAS heights were at average 2-3 m lower than FIA estimates. To translate GLAS-estimated heights into forest biomass will require general allometric equations. Analyzes of the regional variability of forest height–biomass relationships using FIA field data indicated that general non-species specific equations are applicable without a significant loss of prediction accuracy. We developed height-biomass models from FIA data and applied them to the GLAS-estimated heights. Regional estimates of forest biomass from GLAS differed between 39.7 – 58.2 Mg ha⁻¹ when compared to FIA.

Neural network and quad-tree approach to extract tree position and height from LiDAR data

Francesco Pirotti¹, Alberto Guarnieri², Antonio Vettore²

¹ Department of Land and Agroforestry Systems, University of Padua, viale dell'Università 16, 35020 Legnaro Italy – francesco.pirotti@unipd.it

² CIRGEO, Research Center for Geomatics, University of Padua, viale dell'Università 16, 35020 Legnaro Italy – cirgeo@unipd.it

Abstract

This paper reports an analysis of results from processing return signals from canopy covers using an artificial neural network to find if there is an improvement on detecting tree height and position compared to a more classic local maximum filter approach. The hypothesis taken into consideration is that a neural network permits to insert several useful parameters in the decision process thus making it more “programmable” and apt to be used in different forest cover situations. Quad-tree is a method to organize the data to optimize the process done by the neural network.

We conclude that results from classic methods and the neural network both give significant results compared to ground-truth measured on the terrain. If the network is implemented with a certain number of trainers there is an improvement compared to the local maximum, but the difference is not statistically significant. Nevertheless further improvements can be foreseen in the future thanks to the intrinsic nature of neural networks to be able to include additional nodes to adapt itself to the final objective – tree recognition.

Keywords: neural network, local maximum filter, LiDAR

1. Introduction

New LiDAR technology has opened new frontiers in many fields which benefit from geomatic information. LiDAR surveys give three-dimensional spatial data with significant accuracy and also integrate other information such as intensity of return signal, metric and non-metric images as well as hyperspectral images to give end-users remotely sensed information which can be, to a certain degree, correlated to stand characteristics.

Forestry and related environmental sciences have been looking into LiDAR for accurate spatial modeling of trees and terrain. Land use mapping is of primary interest in land planning and LiDAR has proven a significant added value to classic remote sensing image classification methods (Lee and Shan, 2003).

In the field of forestry, future research is focused on LiDAR-processing methods which will permit to extract information at lower costs. Classic methods require forest characteristics to be assessed using ground-plots, field-data and statistical methods. Error sources and factors to consider in field methods are the reliability of the workers (human error), statistical method adopted (number of samples, variance, significance of the test) and costs.

LiDAR data and higher training of operators able to process remote sensing data correctly, will pay back in lower costs and higher accuracy for forest inventories. Of course remote sensing will never replace completely field work because ground truth and on-site experience are very important factors, but a lot of tedious and repeating forestry work can be substituted

with state of the art LiDAR data processing.

Tree species, mean diameter and height distribution in the stand are all information which are used in forest planning and inventories. This information can be correlated with LiDAR data with a certain amount of reliability. Tree top extraction from LiDAR data gives 80% accuracy in uneven stands, better than digital photogrammetry and comparable if not better than ground measurements (Koukoulas and Blackburn 2005; Stonge *et al.*, 2004; Magnussen *et al.*, 1999). Integration of LiDAR with remote sensing imagery (Bork *et al.* 2007) is also promising because of complementarity between the two types of data, one giving geometric information the other spectral information.

2. Methods

The process was applied to a small test site to check for accuracy of results by comparing with ground-measured truth.

2.1 Study area



Figure 1: Study area

The whole study area comprises of a watershed basin located in the Belluno province, in the Veneto Region in Italy. This area was chosen because it presents an interesting combination of orographic and vegetation characteristics. Steep slopes and flat ground are present, as well as bare soil/rock, grassland and four different tree-species. Height above sea level variation goes from a minimum of 1120 m to 2600 m. The stream-line follows an almost east → west direction as can be seen from figure 1 which is oriented north. Length of its major and minor axis are respectively 3125 and 2200 meters.

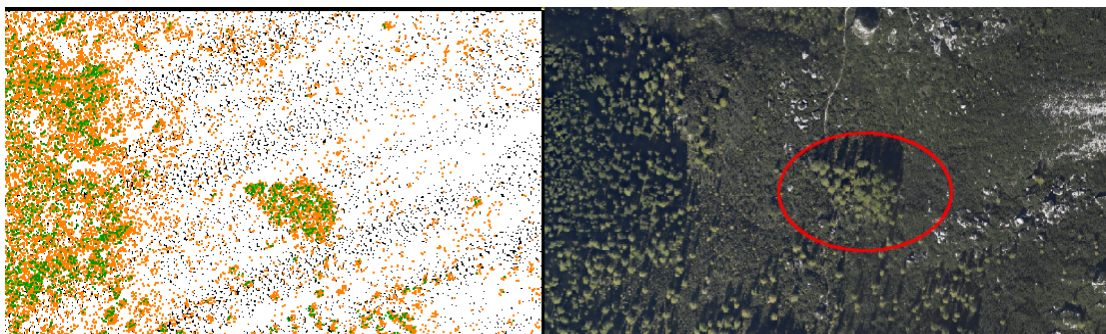


Figure 2: Sub-area used in analysis; left from laser points, right from RGB image

LiDAR and image data were recorded at the same time during a flight which took place the 13th of July around 14:00 Italian time. High resolution orthorectified images of the area at a mean spatial resolution of 15 cm were therefore available. Cloud of LiDAR points has a density of 6-11 pts / m² where a single signal return was detected. Density can get as high as 19 pts / m² where vegetation causes multiple returns.

Around 35% of the study area is covered by bare ground, and the rest is mostly covered by forest with a limited presence of grassland. Tree species present are: *Larix decidua*, *Picea abies*, *Pinus mugo* and *Fagus sylvatica*. Some salix is present at the lowest points of the basin, but not in significant numbers. There is a vast majority of *Larix decidua* and *Picea abies* which corresponds to Del Favero's classification of forest typologies (Del Favero 2004).

2.2 Dataset

For this particular analysis a sub-area was chosen with a total of 6000 m² and with 55750 points. The first step was to isolate the points belonging to the sub-area and to gather all information on ground truth. Tree breast height diameter (BHD) and tree height were recorded by a survey while geographic position was recorded using the high resolution image. Ground measures and the digital orthophoto were used to digitize canopy borders as well.

The first processing step was to correct absolute height values of points by subtracting the

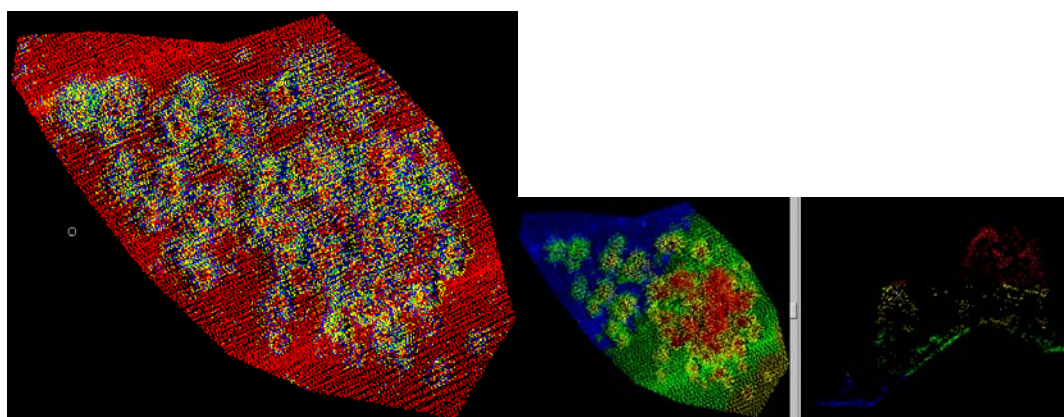


Figure 3: Sub-area for study: left – class by echo, middle – class by height, right right a section showing ground irregularity and canopy models.

ground model creating a new variable called dz which represents the height above ground of each point. The minimum threshold for points to consider was 0.5 m above the ground to filter

out most understory vegetation. After this process the dz variable had a maximum value of 29.32 m, which is reasonably close to that of the highest tree which is 29.81 m. LiDAR measure of tree height have an error which can be estimated from its components. First of all the error from the laser sensor: ± 0.3 m as reported by constructor. Then the highest point is not necessarily the actual tree top and since point density is about 6-11 pts / m² that would mean 0.2-0.3 m between points, therefore 0.1-0.15 m in the worst case scenario. The total is 0.45 m difference between points, which can be considered the same height-wise if canopy has a slope of one.

The LiDAR data in the sub-area was furthered filtered out in order to isolate a dataset with unique echo plus first-of-many echo (UFE). The points from the UFE set where included only if they did not belong to ground class (see equation 1).

This set gives us points which belong to vegetation, but without intermediate or last echoes, but only with unique echo and first-of-many echo. This is actually a subset of the previous dataset where intermediate and last echoes are removed thus giving us the position in space of the first surface which caused the return of the laser signal towards the sensor. The total number of points for this dataset was 20253.

$$\text{UFE} = \text{Unique U first-of-many} \cap \text{ground class} \quad (1)$$

This set gives us point population which represents the canopy model surface.

LiDAR data was processed with commercial software Terrascan from Terrasolid © , the neural network process was costum designed with a dynamic linked library developed in C language. The dataset was pre-processed with a low-pass filter correctly scaled to smooth out the noise due to leaf-scale variability.

2.3 Neural Network and quad-tree setup

The model for decision process is a back-propagation artificial neural network (ANN), while the organization in a quad-tree structure is integrated in the neural network. The structure of both the ANN and the quad-tree was setup using C code, compiled both as a library and as a stand-alone executable. The process reads the data, organizes points into quad-tree bins, sends data to the ANN, and receives feedback from the ANN for training.

2.3.1 Quad-tree organization

Data is fed to the first function as a table with these columns: x,y,dz,echo number and echo type. The spatial domain falls in the first three columns, whereas the others are added alphanumeric information. The spatial data will be processed contextually, furthermore topological relations such as nearest neighbour and focal statistics are important as they can give added criteria to the process. That is the reason why the data was organized into a quad-tree which assigns points to a certain address in the tree. In this case each “leaf” in the quad-tree is cannot have more than 9 points and less than 4 points. Spatially this means that each smallest square covers about half of a squared meter.

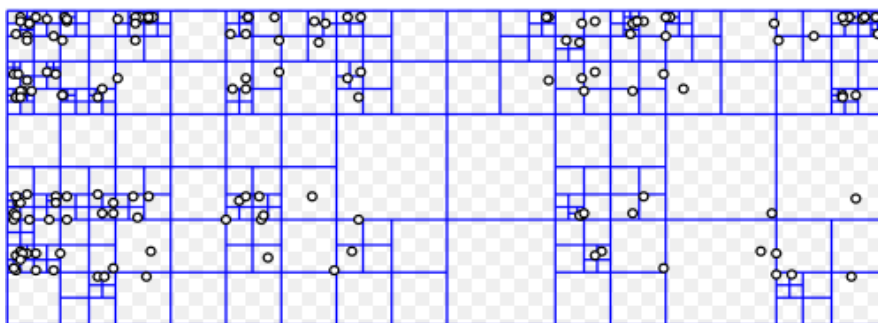


Figure 4: Example of quadtree organization

2.3.2 Neural network: nodes and neurons

The points are fed to the ANN, which evaluates criteria, assigns weights and defines if a point is part of tree-top or it is part of canopy and if it part of canopy borderline.

Criterion for assigning a point to the tree-top class and parameters which can be tuned in the ANN and therefore make up the hidden nodes:

1. Point is a local maximum considering a certain radius. Radius will actually be a multiple of the spatial resolution of the smallest “leaf” of quad-tree and is a parameters which can change to tune the ANN.
2. Point must have neighbors with a local density totaling at least the minimum point density divided by two around an area which is dependent on tree species and configuration. The area to consider is also a parameter which can vary.
3. To be considered actual top of the tree a point must coincide with topmost value of local kriging interpolation, if it does not then a new point is created with such coordinates.
- 4.

A variable number of points are used as trainers for the ANN, as backward propagation permits to calibrate parameters in the hidden nodes in order to improve accuracy at each iteration of the process.

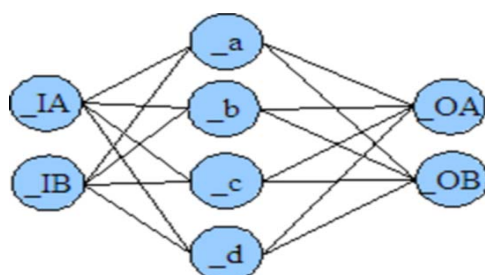


Figure 5: Neural Network: $_In$ = input nodes, $_n$ = hidden nodes, $_On$ = output nodes

The actual tree top is determined after using a kriging interpolator of the point itself and 18 nearest neighbors. The interpolation part was done by having a call to a separate module from GRASS open source software, as it would have been a hardous and time consuming task to implement a kriging interpolator directly in the C library.

3. Results

Encouraging results were found even if not significantly different from classic local maximum filters. The number of trainers previously set in the output layer is important, as will be discussed in the next section.

Table 1: Results from ANN using different number of training outputs

| Thinning operation | Number of trees correct | Number of trees incorrect* | Total trees found | RMSE of positioning (cm) |
|---------------------------------|-------------------------|----------------------------|-------------------|--------------------------|
| <i>Ground - truth</i> | 56 | <i>na</i> | 56 | <i>na</i> |
| Neural network with 2 trainers | 44 | 8 | 52 | 24 |
| Neural network with 4 trainers | 41 | 9 | 50 | 24 |
| Neural network with 8 trainers | 55 | 4 | 59 | 21 |
| Neural network with 14 trainers | 59 | 2 | 61 | 23 |
| Neural network with 20 trainers | 55 | 8 | 63 | 23 |
| Local maximum filter | 52 | 4 | 56 | 24 |

*Defined as not belonging to tree top but to canopy

4. Discussion and conclusions

The results seem promising even if not significantly different from the local maximum filter. If the network is implemented with a certain number of trainers there is an improvement compared to the local maximum, but the difference is not statistically significant. Nevertheless further improvements can be foreseen in the future thanks to the intrinsic nature of neural networks to be able to include additional nodes to adapt itself to the final objective – tree recognition.

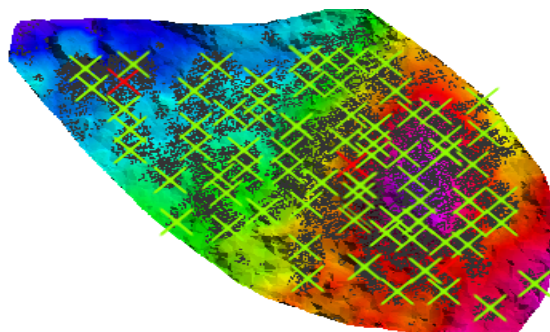


Figure 6: Point distribution on top of ground digital elevation model – green crosses represent trees found with 14 trainees while red crosses indicate misinterpretations.

Some drawbacks to this method are found in the complexity of its actual implementation by untrained professionals. Normalization of data, initial tuning of parameters and preprocessing of data should be done accurately, and it is often a source of error which heavily weights on final result.

There is a lot of testing and refinement to be done to this method. It will be an interesting phase in the future to measure other datasets in the Missiaga basin to find if forest types can be associated with weights and parameters which make up the trained ANN.

References

- Ananth U. Kini, Sorin C. Popescu, 2004. TreeVaw: a Versatile Tool for Analyzing Forest Canopy LiDAR Data – a Preview with an Eye towards the future. ASPRS Images to Decision: Remote Sensing Foundation for GIS Applications September 12-16, 2004
- Bork E. W., Su J. G. 2007. Integrating LIDAR data and multispectral imagery for enhanced classification of rangeland vegetation: A meta analysis Remote Sensing of Environment, 111, 11-24.
- Del Favero R. (2006), Carta regionale dei tipi forestali: documento base, Regione Veneto.
- Koukoulas, S., & Blackburn, G. A. 2005. Mapping individual tree location, height and species in broadleaved deciduous forest using airborne LIDAR and multi-spectral remotely sensed data. International Journal of Remote Sensing, 26, 431-455.
- Lee, D. S., & Shan, J. 2003. Combining LIDAR elevation data and IKONOS multispectral imagery for coastal classification mapping. Marine Geodesy, 26, 117-127.
- Magnussen, E., Eggermont, P., & LaRiccia, V. N. 1999. Recovering tree heights from airborne laser scanner data. Forest Science, 45, 407-422.
- Stonge, B., Jumelet, J., Cobello, M., & Véga, C. 2004. Measuring individual tree height using a combination of stereophotogrammetry and lidar. Canadian Journal of Forest Research, 34, 2122-2130.

Tree filtering for high density airborne LiDAR data

M.Z.A. Rahman, B. Gorte

Optical and Laser Remote Sensing, Department of Earth Observation and Satellite System (DEOS),
Faculty of Aerospace Engineering, Delft University of Technology, the Netherlands–

M.Z.AbdRahman@tudelft.nl, B.Gorte@tudelft.nl

Abstract

A high resolution Airborne LiDAR data creates better opportunity for an individual tree measurement and provides valuable results for more precise forest inventory. This paper presents tree filtering approach that able to separate dominant tree and undergrowth vegetation. The results can be used for a detailed individual tree measurement. This process is one of the main steps for a single tree extraction from the high resolution Airborne LiDAR data. The filtering technique lies on the fact that a dominant tree has distinct parts in the histogram that represent tree crown, tree trunk, and ground surface with or without undergrowth vegetation. The shape of the histogram was used to identify points that belong to the tree crown and the tree trunk. More points were assigned to the tree trunk based on an iterative analysis of the histogram at certain height above the ground surface. This step was coupled with the RG segmentation. It was found that the filtering routine failed to remove very close undergrowth vegetation. It was also observed that in order to get a good result, the tree filtering method needs at least small area of the tree trunk.

Keywords: High resolution Airborne LiDAR, RG segmentation, 1D Gaussian filter, Gaussian fitting

1. Introduction

Laser scanning is now becoming one of the important sources of information for forest applications. The laser beam with specific settings may be able to penetrate the forest structure, thus giving a better opportunity for accurate forest variable measurements. Hyyppä et al. (2004) has listed out numerous techniques and algorithms for tree variable extraction. The features and the predictors in the statistical method are being assessed from the laser derived surface models and point clouds. This information is then used to estimate forest parameters based on regression and discriminant analysis (Table 1). On the other hand, the image processing methods use the neighborhood information of point clouds and pixel of a Digital Surface Model (DSM). The physical features such as, tree crowns, individual trees, group of trees or the whole stands can be derived using this method. In this method, further step of forest parameters extraction are assessed using the existing models and statistical methods.

Table 1 : Tree variable extraction based on statistical method of LiDAR data (Hyypä, et al., 2004)

| Method | Description on method | Forest properties |
|---|--|--|
| Canopy profile area | The <i>canopy profile area</i> is directly related to the logarithm of the timber volume | Volume of timber |
| Height percentiles of the distribution of canopy heights | The <i>Height percentiles of the distribution of canopy heights</i> as predictors in regressions models to estimate mean tree height, basal area and volume | Predictors in regressions models to estimate mean tree height, basal area and volume |
| Canopy reflection sum, ground reflection sum and Canopy closure | <i>Canopy reflection sum</i> is the sum of the portion of the waveform return reflected from the canopy. <i>Ground reflection sum</i> is the sum of waveform return reflected from the ground multiplied by a factor correcting the canopy attenuation. <i>Canopy closure</i> is approximated by dividing the sum of the canopy and ground reflection sums | Predictors in regressions models to estimate tree height, basal area and volume |
| Canopy height and density metrics | <i>Canopy height metrics</i> included e.g. quantiles corresponding to the 0,10,...,90 percentiles of the first pulse laser canopy heights and corresponding statistics, where as <i>canopy density</i> corresponded to the proportions of both first and last pulse laser hits above the 0,10,...,90 quantiles to total number of pulses | Canopy height and density metrics |
| Tree cover and Surface cover | <i>Tree cover</i> is calculated from the proportion of laser hits from tree canopy divided by the total number of laser hits. <i>Surface cover</i> is defined as the proportion of laser hits from the surface and the total number of hits | Area of the tree and area of the ground surface |
| Relative standard deviation of tree heights, the proportion of single returns and the proportion of first return, proportion vegetation points, mean intensity, standard deviation of both single and surface returns | <i>The proportion vegetation point</i> is defined as a number of returns that are located above the crown base height divided by the total number of returns from the segment. This information is used for tree species classification | Tree species classification |
| Crown shape | <i>Crown shape</i> is defined by fitting a parabolic surface to the laser point cloud | Crown shape |

Litkey et al.(2007) pointed out that there are two main feature extraction methods that can be used to derive forest information from Airborne LiDAR data. The first method is based on a statistical canopy height distribution (e.g., Naesset (1997)) and the second approach is based on an individual tree detection (e.g., Hyypä and Inkinen (1999) and Persson, et al. (2002)). It was stated that the methods based on the statistical canopy height distribution typically use regression, non-parametric or discriminant analysis for forest parameter estimation. On the other hand, the individual-tree-based method uses the neighbourhood information of canopy height point clouds and the pixels of Canopy Height Model (CHM) to extract features such as crown size, individual tree height and tree location. The forest inventory data are then being estimated using existing models and statistical techniques.

Numerous studies stated that a discrete return laser scanner data can produce accurate information on a tree canopy since the quantiles of height distribution of laser scanner data area related to the vertical structure of the tree canopy (Maltamo, et al., 2004). Furthermore, since

some of the laser pulses penetrate the canopy of dominant trees, it is possible to analyze undergrowth vegetation. In their study, Maltamo et al. (2004) used a histogram plot to analyze multi-layered canopy structure. In this study it was concluded that the characteristics of the canopy height laser point data, especially the shape of the height distribution can be used to identify multi-layered stand structures. Reitberger et al. (2007) introduced a method to delineate tree crown and detection of stem position of single trees from dense Airborne LiDAR data. In this study, trees were delineated using a watershed algorithm on the CHM and the possible stem position was derived from the local maxima of the CHM. In this study, they have introduced a 3-step algorithm to search stem position in each tree segment. Firstly, all the points between the ground and the crown base height were separated and the points were clustered using hierarchical clustering based on their horizontal distances. Finally, the stem position was estimated using a robust RANSAC-based adjustment of the stem points.

The objective of this study is to develop a new tree filtering approach for high density airborne LiDAR data that is able to separate dominant trees and undergrowth vegetation. The filtering process is one of the main steps of individual tree variable measurement (refer Figure 1). In this paper, the filtering method was tested on different LiDAR datasets with different density of undergrowth vegetation. The results can be used for individual tree variable measurements of dominant trees and undergrowth vegetation. In this case, the tree measurement can be carried out directly on a single tree rather than based on the regression models.

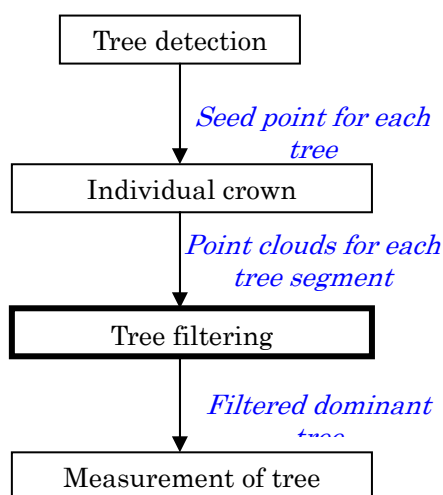


Figure 1: The overall flow for an individual tree measurement

2. Materials and method

2.1 Study site

This study was conducted at the Duursche Waarden floodplain, the Netherlands. The floodplain is along the IJssel River, which is the smallest tributary of the Rhine River in the Netherlands (Straatsma and Middelkoop, 2006). This area is partly covered by meadow and arable land and most of the areas have become nature. The vegetation in this area comprises of (1) softwood forest Willow (*Salix abla*, *Salix viminalis*), poplar (*Populus nigra*, *Populus x canadensis*), (2) hardwood forest oak (*Quercus robur*), ash (*Fraxinus excelsior*) and a small pine stand (*Pinus sylvestris*) on a river dune, together with (3) reed marshes (*Phragmites australis*), and (4) herbaceous vegetation with sedge (*Carex hirta*), sorrel (*Rumex obtusifolius*), nettle (*Urtica dioica*), thistle (*Cirsium arvense*) and clover (*Trifolium repens*).

2.2 LiDAR data

The LiDAR data used in this study was captured by the FLI-MAP 400 system. The FLI-MAP 400 is a helicopter mounted LiDAR system designed to capture highly detailed terrain features with high accuracy. It was claimed that the absolute accuracy of the FLI-MAP 400 data measured over hard and level surfaces is 2.5 to 3.0 cm. The system is capable of scanning in three directions (forward, down (nadir) and back) and this increases the chance of capturing a significant amount of reflected pulses from the ground even in a quite densely vegetated area. The FLI-MAP 400 data records maximum four laser reflections with an unmatched distance of 0.9 m, which enables optimal interpretation of a detailed terrain model even in vegetated areas. The data with an average density of 70 points per meter square were acquired during winter in 2007. The leaf-off data allow better penetration through a tree canopy and therefore the vertical structure of a tree can be easily revealed. In this study, 10 sample trees were selected with different tree species and undergrowth density. All samples were delineated manually and for further processing stage, each sample was attached with one seed point located on top of the tree.

2.3 Histogram-based tree filtering

In this study, the new tree filtering approach is called a histogram-based tree. This method relies on the fact that a dominant tree would have distinct parts in the histogram that represent tree crown, trunk, ground surface and undergrowth vegetation. Previous study by Straatsma and Middelkoop (2006) has shown that the shape of height distribution of a tree has a higher frequency of laser pulses from the crown and undergrowth vegetation. On the other hand, the reflected laser pulse from the trunk is at a lower frequency. The segmentation process starts from a seed point located on top of the tree crown, and the shape of histogram is used to identify points that belong to the tree crown and the tree trunk. The RG segmentation is then used to subdivide the points into the tree crown and the trunk. The search for the tree trunk continues by iteratively analyses the shape of the histogram at certain height above the ground. This process is coupled with the RG segmentation to assign additional points to the tree trunk. The process continues until it is no longer able to distinguish between tree trunk and the undergrowth vegetation. Furthermore, if the process stops before it reaches the ground surface, the tree trunk is extrapolated by fitting a three dimensional line (3D line) using the points which have been previously assigned as a tree trunk. The additional points for a tree trunk is then collected based on the distance between the line and the remaining point clouds.

2.5 One-dimensional (1D) Gaussian filtering

As explained earlier in section 2.3, the histogram of the point cloud distribution of a single tree was used as a reference to assign points into tree crown, tree trunk, undergrowth vegetation and ground surface. In this study, the boundary that marks each part of the tree on the histogram was defined automatically using a multi-modal Gaussian fitting routine. It was observed that, the original histogram contains noises that need to be removed in order to get better result in Gaussian fitting process. Thus, the first step was to smooth the histogram. A 1D Gaussian filter was used to smooth out the histogram surface. In this study, only one value of sigma (0.015) of Gaussian filter was used for all the datasets (refer Figure 2).

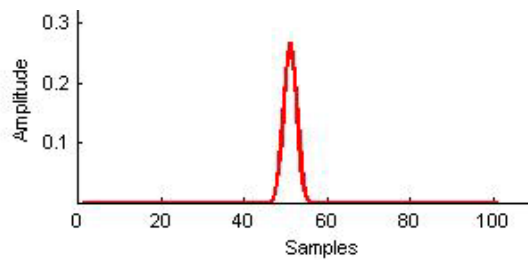
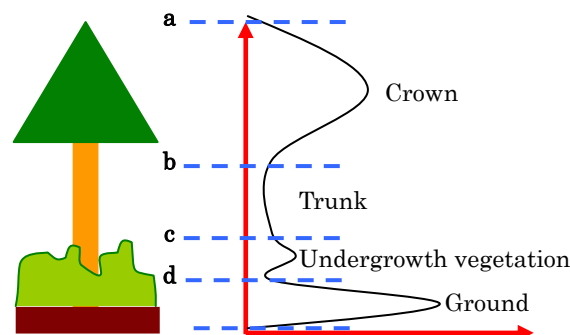


Figure 2: One-dimensional Gaussian filter

2.6 Gaussian fitting on histogram

A Gaussian fitting on the histogram was based on nonlinear curve-fitting problems in a least square sense which is available in Matlab (`lsqcurvefit`). This routine determines the possible number of Gaussian peaks based on the pre-defined values such as number of possible Gaussian shapes and Gaussian model parameters (sigma, position, frequency). In order to determine this information, the peaks in the histogram of a single tree can be assumed to have a composition of tree crown, undergrowth vegetation and ground surface (refer Figure 3). As depicted in Figure 3, the Gaussian fitting routine was then applied on the filtered histogram to define a specific boundary for these 3 parts. Each boundary was defined by 3σ value from the Gaussian each peak (μ).



- a - Starting level (elevation) for tree crown
- b - Starting level (elevation) for tree trunk
- c - Starting level (elevation) for undergrowth vegetation
- d - Starting level (elevation) for ground

Figure 3: Shape of histogram for a single tree

All tree samples were delineated manually by hand and a seed point was attached on top of each tree. A semi-automatic tree detection and crown segmentation will be explained later in another study. The histogram-based tree filtering process was carried out with the following steps:

1. Place a seed point on top of each tree.
2. Define growing distances for 3 parts, 1) tree crown, 2) tree trunk and 3) distance between a 3D line and point clouds to extract additional points for tree trunk
3. Calculate a histogram for a single tree and filter the histogram with 1D Gaussian filter
4. Fit a Gaussian function on the filtered histogram to extract 3 different parts of the tree, namely, 1) tree crown, 2) undergrowth vegetation and 3) ground surface
5. RG segmentation from the tree crown to the level that marks the beginning of the tree

trunk

6. RG segmentation for the tree trunk
7. Iteratively analyze the shape of the histogram to add more points to the tree trunk
8. Stop step (7) if the process is no longer able to distinguish between points that belong to the tree trunk, the undergrowth vegetation as well as the ground surface
9. Create a 3D line based on the points that have been classified as a tree trunk
10. Assign additional points to the tree trunk based on their distances to the 3D line.

Step (9) creates a 3D line, which intends to extrapolate tree the trunk until it reaches the ground surface. This will be the last step of collecting points for the tree trunk, since the filtering process as indicated in step (8) was no longer able to distinguish between the points that belong to the tree trunk, the undergrowth vegetation and the ground. This step assigned more points to the tree trunk by selecting points at certain distance from the extrapolated tree trunk (3D line). The tree filtering method basically needs three input parameters, namely growing distance for the tree crown, growing distance for the tree trunk, and distance between points to the interpolated 3D line. In general, large growing distance value was used for segmenting the tree crown, and small growing distance value was used for the tree trunk instead.

3. Results and discussions

The results showed that the histogram-based method performs quite well in separating the dominant trees and the undergrowth vegetation (refer Figure 5). Furthermore the 1D Gaussian filtering helps in reducing noises in the original histogram and enhanced the general shape of the histogram. This process subsequently eased the multi-modal Gaussian fitting on the smoothed histogram (refer Figure 4). However, it should be noted that, different setting of the Gaussian filter for example with different σ value would produce different result on a smoothed histogram. This could suppresses some useful information and reduce the effectiveness of the tree filtering method.

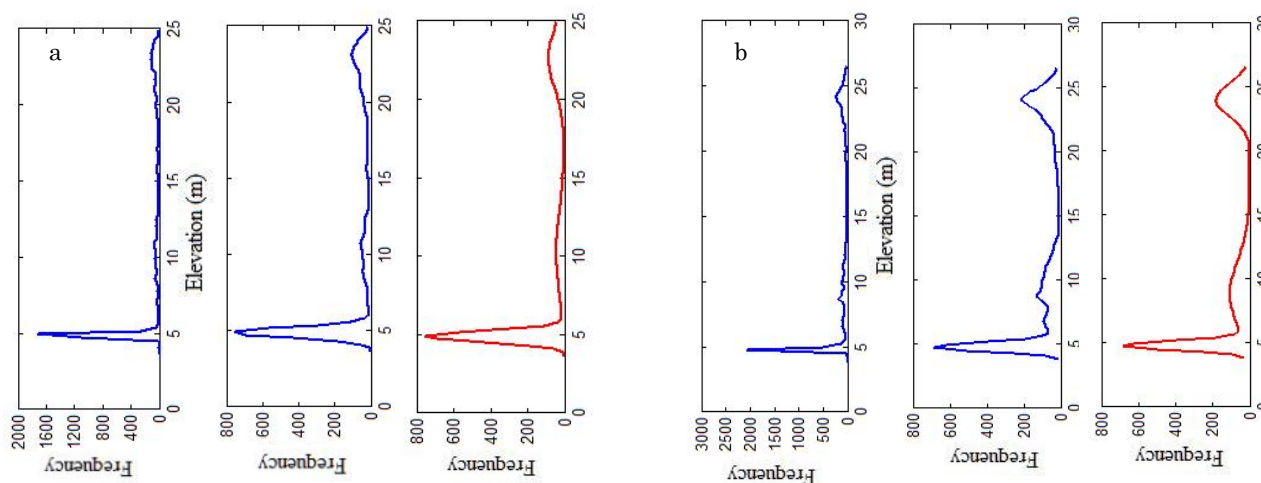


Figure 4: Examples of the original histogram, filtered histogram and fitted histogram for tree 1 (a) and tree 2 (b)

Figure 4 shows some examples of the original histogram, the smoothed histogram and the estimated Gaussian functions on the histogram.

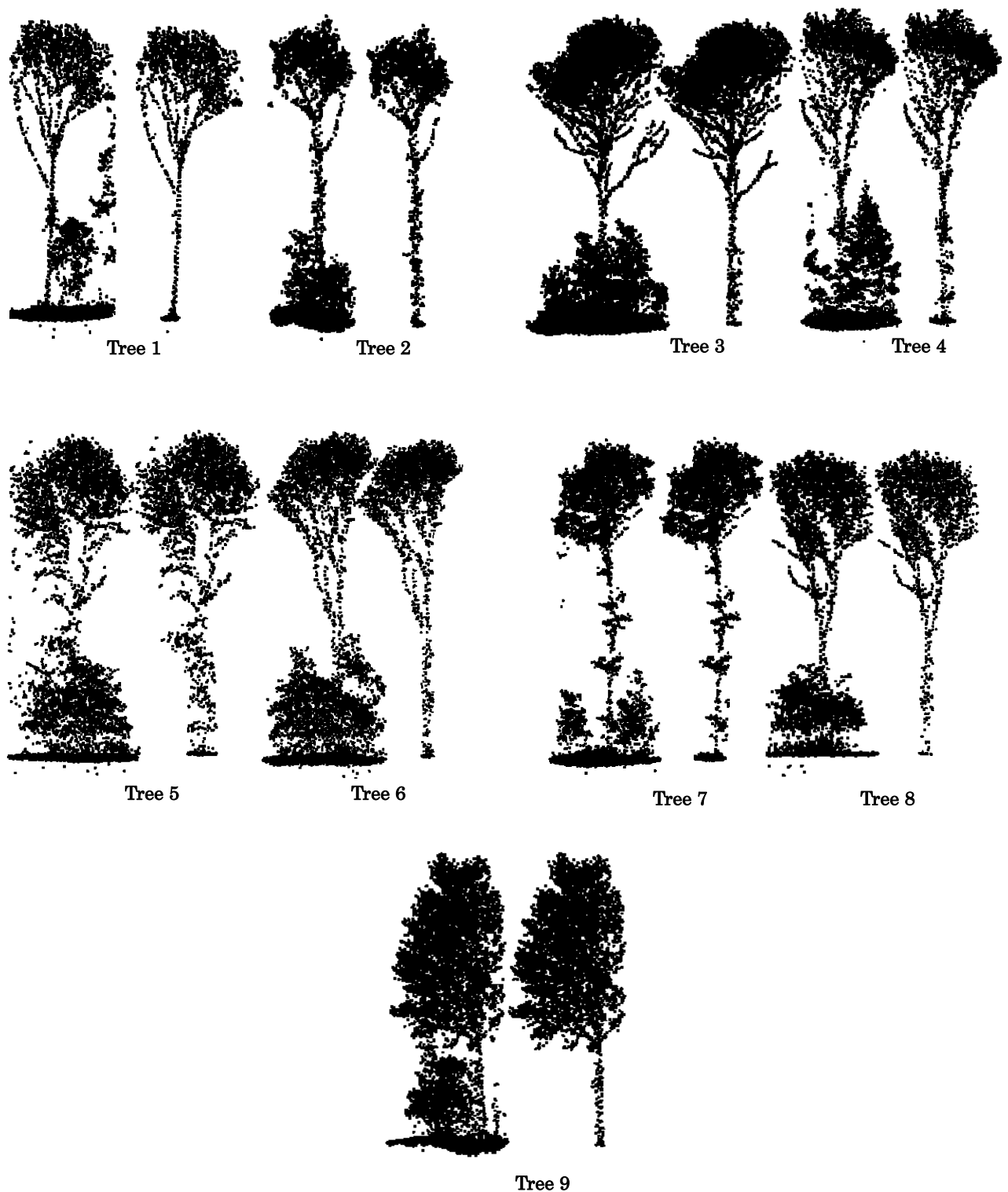


Figure 5: Original trees and filtered trees

In this study it was found that the histogram-based tree filtering method requires at least small area of a tree trunk and the reflected laser pulses from this area should be less than the tree crown. In this case it would be rather difficult for trees with dense branches along the tree trunk. Very small area of tree trunk caused overlapping boundary between the tree crown and the tree

trunk. Thus, 3σ value will not be appropriate to represent the boundary of each part. Figure 7 (a) shows an example for a tree condition where there is a very small area of tree trunk and the undergrowth vegetation is very close to the dominant tree. In this example, a special experiment was conducted to observe the size of the area for the tree trunk in the histogram. For this purpose, the σ value for 1D Gaussian filter was tuned from 0.0026 to 0.1 and the different between two levels (between b and c) was observed (refer figure 3). It was found that the Gaussian fitting routine failed to identify appropriate value for level b and c, in which the different between them (level b – level c) should have a positive value. Figure 7 (b) shows that the histogram-based approach failed to separate the dominant tree and the undergrowth vegetation.

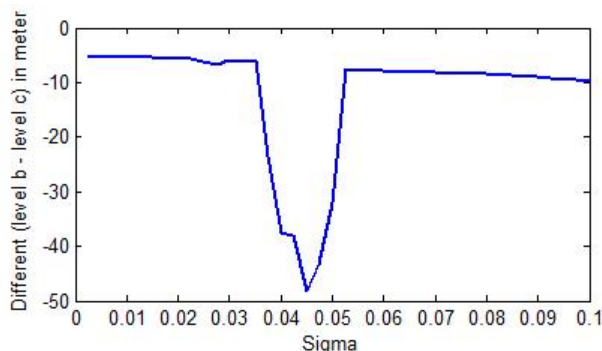


Figure 6: The different in meter for level b and level c

In this study, it was also observed that each tree requires different value of growing distance depends on the closeness of the undergrowth vegetation to the tree crown and the tree trunk (refer Table 2). Small growing distance should be used for very close undergrowth vegetation. Therefore, further study is required to optimize the tree filtering method, in which values for the growing distance should be defined based on the density of the undergrowth vegetation.

Table 2: Growing distance for each tree

| Dataset | Growing distance for tree crown (m) | Growing distance for tree trunk (m) | Growing distance for 3D line (m) |
|---------|-------------------------------------|-------------------------------------|----------------------------------|
| Tree 1 | 0.8 | 0.5 | 0.6 |
| Tree 2 | 0.8 | 0.6 | 0.5 |
| Tree 3 | 0.8 | 0.4 | 0.5 |
| Tree 4 | 0.8 | 0.6 | 1.0 |
| Tree 5 | 0.8 | 0.6 | 1.0 |
| Tree 6 | 0.5 | 0.4 | 0.5 |
| Tree 7 | 0.8 | 0.6 | 1.1 |
| Tree 8 | 0.5 | 0.4 | 0.5 |
| Tree 9 | 0.5 | 0.3 | 0.5 |

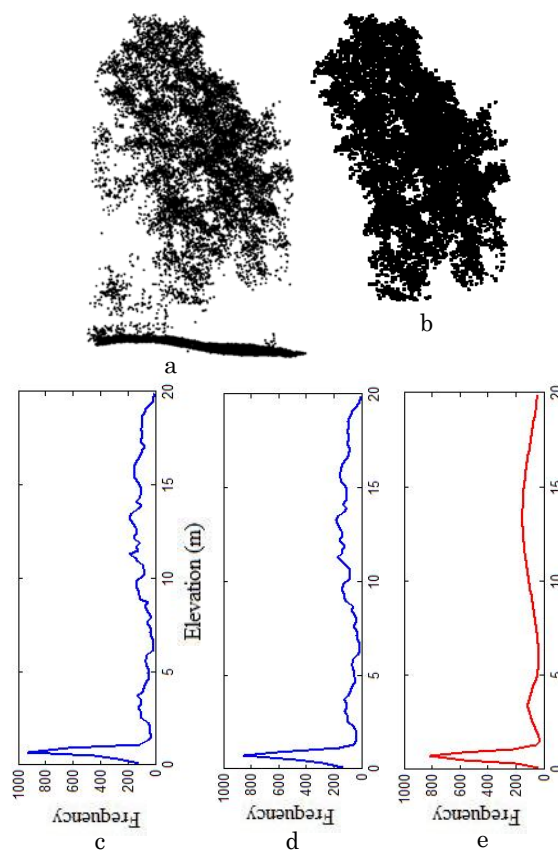


Figure 7: Original tree (a), filtered tree (b), original histogram (c), filtered histogram (d) and fitted histogram (e)

4. Conclusions

In general the histogram-based tree filtering method which aims at separating the dominant tree and undergrowth vegetation performed well on all datasets. The results can be used in further detailed tree variable measurement for instance, species identification, stem diameter, crown size, crown volume and etc. However, the filtering method failed to filter the dominant tree which is very close to the undergrowth vegetation. It was also shown that the filtering method still needs to be optimized by taking into account the density of the undergrowth vegetation. This information will be used as the basis to select proper growing distance values for tree crown, tree trunk and 3D line. Further study is also required to quantify the effect of different magnitude (σ) of the 1D Gaussian filter to the performance of the histogram-based tree filtering method. In future, this method will be applied together with the tree detection and crown delineation routines on a larger Airborne LiDAR dataset.

Acknowledgments

The authors would like to thank Rijkswaterstraat, The Netherlands for giving an opportunity to use the FLI-MAP 400 Airborne LiDAR data.

References

Hyyppä, J., et al. 2004. Algorithms and Methods of Airborne Laser-Scanning for Forest

- Measurements. In: M. Theis, B. Koch, H. Spiecker, H. Weinacker (Eds.). *Proceedings of ISPRS working group VIII/2 "Laser-Scanners for Forest and Landscape Assessment"*. Freiburg, University of Friburg: 82-89
- Hyypä, J., and M. Inkinen., 1999. Detecting and estimating attributes for single trees using laser scanner. *The Photogrammetric Journal of Finland*, 16, 27-42.
- Litkey, P., et al. 2007. Waveform features for tree identification. In: *Proceedings of ISPRS Workshop on Laser Scanning 2007 and SilviLaser*. Espoo, Finland: 258-263.
- Maltamo, M., et al., 2004. Estimation of timber volume and stem density based on scanning laser altimetry and expected tree size distribution functions. *Remote Sensing of Environment*, 90, 319-330.
- Naesset, E., 1997. Determination of mean tree height of forest stands using airborne laser scanner data. *ISPRS Journal of Photogrammetry and Remote Sensing*, 52, 49-56.
- Persson, A., J. Holmgren, and U. Soderman., 2002. Detecting and Measuring Individual Trees Using an Airborne Laser Scanner. *Photogrammetric Engineering Remote Sensing*, 68, 925 - 932.
- Reitberger, J., et al., 2007. Single tree detection in forest areas with high-density LiDAR data. *International Archives of Photogrammetry, Remote Sensing and Spatial Information Sciences*, 36, 139-144.
- Straatsma, M. W., and H. Middelkoop., 2006. Airborne Laser Scanning as a Tool for Lowland Floodplain Vegetation Monitoring. *Hydrobiologia*, 565, 87-103.

Individual tree recognition using LIDAR and aerial images: preliminary results

Ramon Riera^{1,3}, Mario Lamfri² & Cristina Vega-García³

¹Technical Office of Forest Fire Prevention, Barcelona Provincial Council, Barcelona, Spain rieratr@diba.cat

²Mario Gulich Institute, CONAE, Falda del Cañete, Córdoba, Argentina
lamfri@cett.conae.gov.ar

³Department of Agroforestry Engineering, University of Lleida, Lleida, Spain
cvega@eagrof.udl.cat

Abstract

A comparative study of three individual tree recognition methods is presented with a view to its application on forest inventory. It was tested on a mixed Mediterranean forest using aerial images from a DMC photogrametric camera, LIDAR airborne data (ALTM 3025E) with a density of 0.85 pulses/m² and a combination of both. DMC orthorectified images are composed of RGB channels having a spatial resolution of 10 cm. We performed a Minimum Noise Fraction rotation transform (MNF) on the RGB data in order to segregate the noise in the data. The LIDAR data product that we used was the Tree Canopy Model (TCM) image obtained by subtracting a Digital Terrain Model (DTM) from the Digital Surface Model (DSM). The DTM was generated from last echo points while the DSM was generated from first echo points. The field data was collected at tree level and geolocated with differential GPS techniques. An image segmentation method and an object-oriented classification were performed using eCognition Professional 4.0 software. This method allowed us to measure canopy cover and to identify individual trees, *via* trial-error processing by iterating weight, scale, colour and shape parameters at different levels.

The first tested results using DMC image interpretation and field data, present accuracies close to 70 % for tree density assessment with LIDAR data.

Keywords: LIDAR, aerial image, individual tree identification

Methods for improving the quality of a true orthomosaic of Vexcel UltraCam images created using a lidar digital surface model

Benoît St-Onge¹

¹University of Quebec at Montreal, Quebec, Canada st-onge.benoit@uqam.ca

Abstract

The combined analysis of lidar and image datasets for information extraction of forest structural attributes and composition requires that the image-to-lidar geometric correspondence be known accurately. We propose a series of methods for producing a 10 cm high quality true orthomosaic of Vexcel UltraCam images perfectly adjusted to the lidar digital surface model (DSM). First, we introduce a technique for filling the small cavities visible on lidar raster DSMs. We then assess the image-to-lidar registration using visualization and quantitative approaches. The small geometric discrepancy measured between the two datasets is then corrected. In the image overlap areas, the true orthomosaic is created by choosing the contributing image that has the smallest distance to the corresponding DSM pixel. Occluded pixels that can not be seen from any centre of perspective are then filled with synthetic values calculated according to their sunlit/shadowed state at the time the images were taken. The resulting true orthomosaic is perfectly registered to the lidar dataset, is complete (considering occluded pixels receive synthetic values), is not radiometrically altered, and shows no visible cut lines. The proposed process should greatly help the simultaneous analysis of lidar and image datasets.

Keywords: orthorectification, co-registration, mosaicking, UltraCam, filtering

1. Introduction

There is currently a clear trend towards the combined use of lidar and digital aerial images to produce fine scale forest maps useful in resource, biodiversity, and carbon inventories. Typically, structural attributes (height, density, etc.) are derived from the lidar canopy height model (CHM) while species composition and health are extracted from the images. A basic approach consists of processing both data types separately and integrating the results later in the process. This way of doing is however far from exploiting all the synergies between the lidar and image datasets. A more sophisticated approach would be to analyse all data simultaneously by associating image reflectance values to lidar height measurements. This requires that the images be “perfectly” registered to the lidar surface model and that true orthorectification (i.e. including visibility calculation, as per Mayr 2002) be used. Moreover, in the case of low altitude digital aerial photography, the image resolution is so high that the texture of individual crowns could be used as an additional criterion for species identification. This brings the requirement that the image texture should be modified as little as possible by the orthorectification and mosaicking processes. What is more, radiometric analysis of an orthomosaic must not be affected by such things as image-to-image histogram balancing and feathering along cut lines. All these requirements are currently not met by commercial orthorectification software. In addition, small misregistration problems cause the image to drape imperfectly over the 3D surface, which produces geometric warping in the resulting orthoimage, thus modifying crown texture and shape. Therefore, this study’s aim is to:

1. Achieve the best possible registration between high resolution aerial images and a lidar dataset so that each tree crown image is mapped exactly on the corresponding 3D lidar crown shape.

2. Create a seamless and complete true orthomosaic with the best possible preservation of radiometric and textural properties of the original aerial images.

This brings us to solve the following problems: the removal of small artefact cavities in the lidar digital surface model (DSM) in order to create a better reference 3D surface for the orthorectification, the detection and correction of subtle misregistrations between the lidar and the images caused by small direct georeferencing (GPS and IMU) errors, to find a way to take advantage of the high aerial image overlap in order to fill as much orthoimage pixels as possible with no radiometric modification, and to fill the orthoimage's empty pixels (resulting from occlusion) with plausible values.

2. Study region and materials

The study site falls within the Training and Research Forest of Lake Duparquet (TRFLD, 79°22'W, 48°30'N), in the Province of Quebec, Canada. It is characterized by small hills with elevations comprised between 227 m and 335 m. The mixed vegetation is composed of common boreal species, and dominated by balsam firs (*Abies balsamea* L. [Mill.]), paper birch (*Betula papyrifera* [Marsh.]), and trembling aspen (*Populus tremuloides* [Michx]). Most stands are mature or over-mature and reach heights of 25-30 m.

The lidar data was acquired on July 12th 2007 using an Optech ALTM3100 flown at approx. 650 m AGL. Strip overlap was sufficient to avoid data gaps. The density of the first returns was approx. 3.2 hits m⁻² (single density, i.e. outside strip overlaps). The lidar Z data was delivered as ellipsoidal heights. The GPS antenna/receiver was a Novatel and the IMU an Applanix AV510. The GPS and IMU were integrated in a tightly coupled solution using the POS AV 1.6 and POS Pac 4.3 software by Applanix. The vertical datum used was the GRS80 ellipsoid. The reference height of the base antenna was obtained from a geodetic point which Z data was expressed in CGVD28 orthometric height, which was converted to GRS80 using the CGG00E geoid undulation value.

The Vexcel UltraCam images were taken in full blue sky conditions on June 9th 2007 at approx. 1000 m AGL resulting in a 10 cm ground pixel size. Image overlap was approximately 80%. Only the panchromatic images were used in this study. The calibrated internal orientation parameter values were obtained from the aerial survey provider. Base data was logged using NovAtel DL GPS receivers with NovAtel Model 600-LB GPS antennas while the airborne platform used the Applanix POSAV 510 system. One base antenna was placed on a monument distinct from the one used for the lidar survey. Another one was set up as a spike and operated simultaneously. The two ground survey points were processed as a network with the geodetic point held fixed. Data was delivered as CGVD28 orthometric heights. We have converted those to GRS80 ellipsoidal heights using the GPS-H software from Natural Resources Canada and the CGG00E undulation table.

3. Methods and results

3.1 DSM creation

The design of the raster DSM creation process aims at producing a canopy surface grid that corresponds as closely as possible to reality in order to achieve a high quality of orthorectification. Because trees are not solid objects with a well defined surface but rather a hierarchical network of branches, twigs and leaves, the raster canopy surface is an abstraction of the true interface, along a vertical column, between the tree material and the medium in which the laser energy propagates. We here define the canopy surface, at the geoposition of a given

pixel, as the elevation at which all the tree material (within the spatial extension of the pixel) is found immediately below, and the open medium immediately above. The creation of the DSM involves gridding the first return elevations and then filling some of the surface cavities.

3.1.1 Gridding

The gridding procedure follows Vepakomma et al. (2008). First the pixels of an empty grid having a 10 cm resolution (equivalent to that of the images) are given the corresponding elevation values of the first returns. If more than one return falls into a given pixel, only the maximum value is retained. The remaining empty pixels are then filled by interpolated values obtained using the inverse distance weighed (IDW) method of ArcGIS 9.2 applied to the first return point data. A small portion of the resulting DSM is shown in figure 1a.

3.1.2 Cavity filling

Lidar DSMs of a tree canopy surface will normally show numerous small cavities (also reported in other studies, such as Leckie et al. 2003) of two types. “Drill holes” are caused by a near vertical laser shots penetrating in small openings of a crown and generating returns well below the generalized crown hull. They represent the true canopy surface elevation at a particular geoposition but cause a deep hole in the surface which may affect the orthoimage geometric quality. A more important problem is the presence of “overhang holes”, artefacts caused by oblique laser shots travelling close to the side of a crown and intercepting a first surface under the crown, close to ground level. The normal gridding process integrates these points to the canopy surface, generating deep cavities (easily visible in figure 1a) that must be removed. We propose a process that first detects cavities and then fills them with interpolated values.

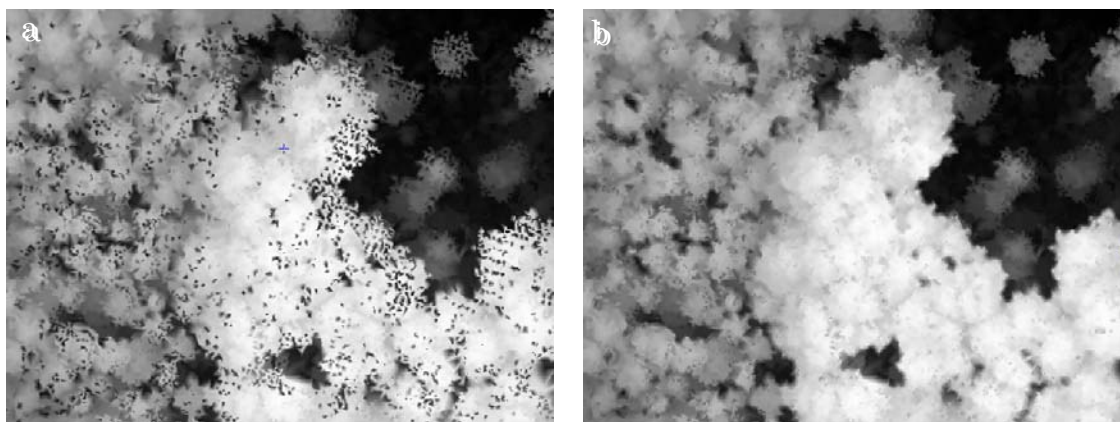


Figure 1 - a) Initial raster DSM showing cavities, and b) DSM after cavity filling. Image width is 64.4 m.

A circular Laplacian filter with negative values near the centre and positive values on the periphery is used to produce scores that reflect the likeliness that a cavity is present. These scores are then thresholded to produce a binary map showing the cavity locations. The filter radius determines the size of the detected cavity while the threshold value controls the depth of detected cavities relative to the surrounding pixels. We have empirically chosen these parameters' values such that the sharp elevation drop at the crowns' edges is not considered a cavity. Once the cavities are mapped, they are slightly dilated to ensure that the full extent of the cavity is captured. Cavity pixels are then given an interpolated value (IDW interpolation using the closest valid DSM pixels). In this study, we processed the DSM in two passes with the following parameter values for the Laplacian filter and dilatation radii respectively, pass 1: 3 and 2 pixels, pass 2: 1 and 0 pixel (no dilatation). The first pass removed most of the overhang

holes while the second pass removed many small drill holes. These algorithms were coded in C language (as all the other special purpose functions presented in this paper). The resulting DSM is presented in figure 1b. It can be seen that most cavities are filled, that the crown edges are not modified and that natural gaps between crowns are not filled. Note also that the rest of the canopy surface, including tree apex elevations, is not affected by the cavity filling process.

3.2 Misregistration assessment and correction

To ensure accurate orthorectification, the exact image to 3D scene correspondence must be established. Our goal is to first assess if systematic errors affect this correspondence, and then to apply the appropriate corrections. Various approaches have been proposed in the literature using area or feature based matching between the lidar surface and the images (e.g. Mitishita et al. 2008). Many of these rely on the presence of buildings or man-made structures. In this study, the landscape is almost entirely covered by vegetation and devoid of buildings. We therefore propose alternatives for working in these conditions, i.e. two visualization techniques and one quantitative method. Visualization is used to detect and understand the nature of the misregistration problems. Various system or manipulation errors in the independent direct georeferencing of the respective datasets can translate into a systematic misfit taking the form of an XY translation (e.g. caused by a horizontal datum error), a Z translation (e.g. caused by a vertical datum error), rotations (e.g. caused by errors in the boresight matrix or IMU drift). The first visualization technique consisted of draping the CHM image onto the cavity-filled DSM and to project it onto the UltraCam image plane according to the uncorrected camera orientation parameter values. If this synthetic rendering is well adjusted to the corresponding real image, we conclude that the initial uncorrected orientation is correct. Otherwise, we study the amount and directions of the discrepancy to comprehend the nature and origin of the misfit.

Figure 2 shows UltraCam image subsets and corresponding synthetic images in which brightness values are proportional to the CHM heights. The red contours correspond to the silhouettes of certain trees digitized according to the real aerial image. When transferred to the synthetic image, we see that for a subset located at the image centre (nadir view), the image contours (2a) correspond well to the projected CHM morphology (2c). However, for the subset taken near the corner of the image (2b), there is a clear displacement in the radial direction (2d). A similar misfit was visible at all image corners, for all inspected images. This strongly suggests that there is a scale problem, i.e., a Z offset between the image and lidar vertical datums. The other visualization technique consisted of orthorectifying a few overlapping images according to the uncorrected orientation and looking at the fit quality between the orthoimages over well defined and smooth surfaces (road segments). This analysis revealed that discrepancies existed (planimetric offsets in the corresponding patches of the orthoimages, not shown in this paper), corroborating the fact that a slight misregistration between the lidar and the images existed.

The quantitative analysis was based on computing the XYZ position of image conjugate points and comparing the Z value to the corresponding lidar elevation. Thirty points were measured on a set of four consecutive images. Precise features (inflections in the shadow silhouettes visible on road segments, e.g. figure 6) were used. Individual points fell on two to four images. Spatial intersection was computed for all intersecting rays for each possible pair of rays. For example, a conjugate point falling on all four test images yielded six different estimates of XYZ (1-2, 1-3, 1-4, 2-3, 2-4, 3-4). For each pair, the Y estimate was calculated based on Y_{01}, Z_{01} (Y and Z of the perspective centre for first image) and Y_{02}, Z_{02} according to Kraus and Waldhäusl (1994), giving two different Y estimates. Conjugate point coordinates leading to Y discrepancies of more than 20 cm were rejected, leaving only very accurate points. The average of the two Y values for each valid point was used as the Y estimate. The lidar elevation (Z_L) was read from the DSM at the ray intersection position XY for all valid combination of rays for all 30 points and subtracted from the photogrammetric Z_P , yielding 43 observations of elevation difference ($Z_P - Z_L$). The

average difference revealed a 1.41 m bias. The Z_0 value of the centre of projection of all images was corrected for that bias. After this correction, new synthetic images were produced (figure 3). No significant change is visible on the centre sub-image (3a), but the red contours on the corner subset now fit exactly with the visible CHM morphology (3b). Using the second visualization technique, we observed that the individual orthoimages now overlap almost perfectly. This signifies that the image to lidar correspondence is now solved with great accuracy.

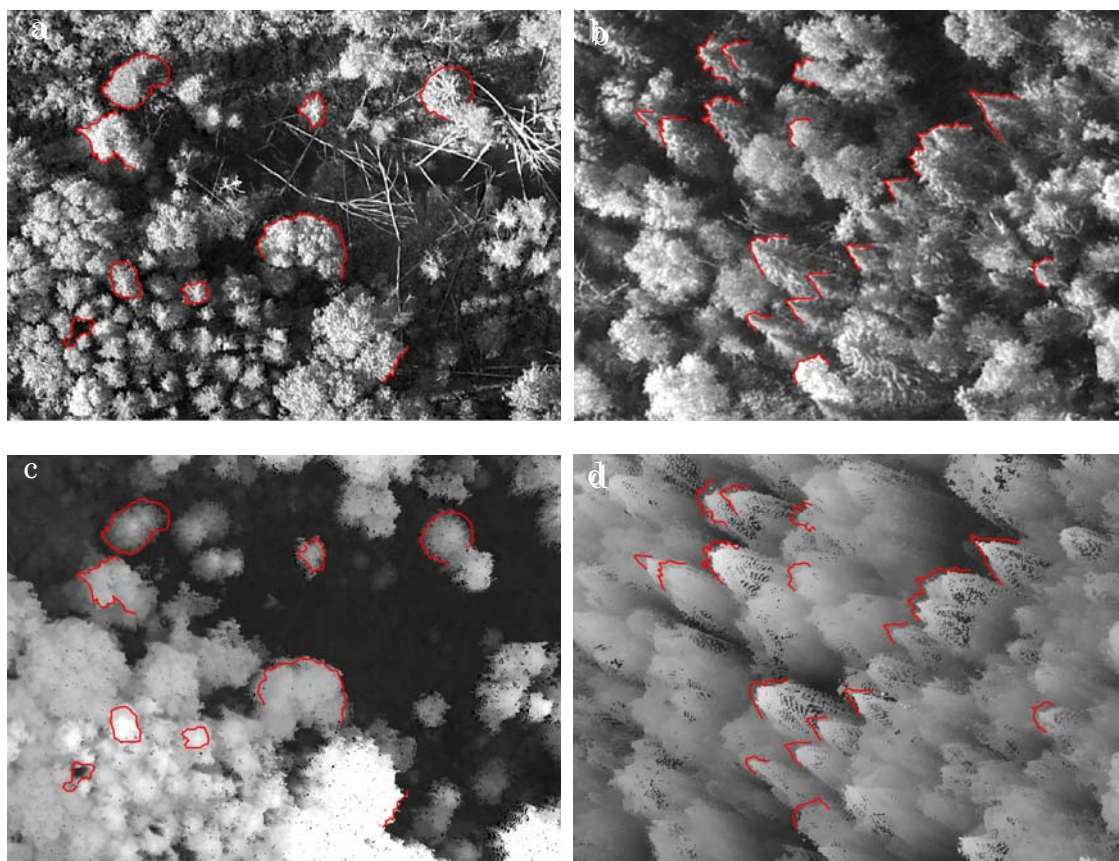


Figure 2 - a & b: two Vexcel UltraCam subimages, respectively extracted at the centre and near the top left corner of the sample image; c & d: CHM image draped over the DSM and projected into the Vexcel image plane according to the uncorrected orientation. The red contours were manually digitized on the real images and overlaid afterwards on the synthetic ones.

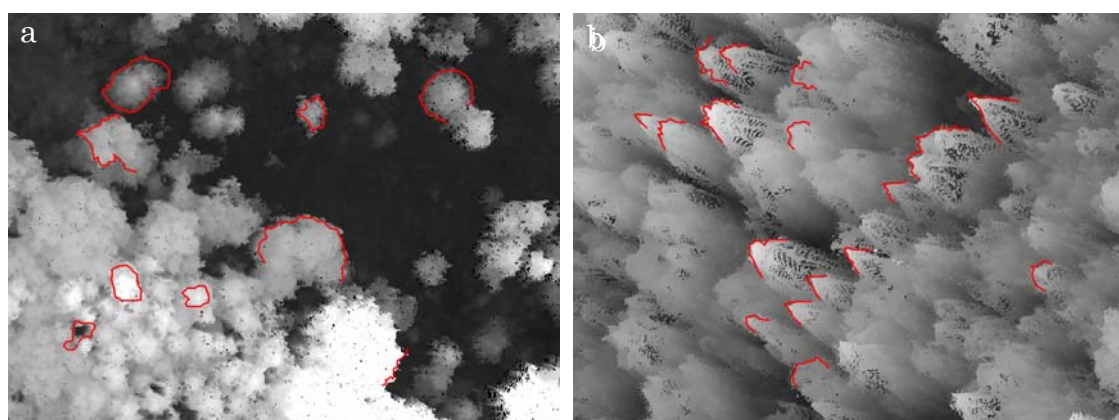


Figure 3 – Same as 2 c & d, after the absolute orientation was corrected.

3.3 True orthorectification and mosaicking

The goal of the orthorectification was to produce an orthomosaic with the best possible geometric and radiometric quality. True orthorectification calculates pixel visibility based on the 3D scene model (i.e. the lidar DSM) and leaves occluded pixels empty (Mayr 2002). In our proposed approach, a non-occluded ortho-pixel receives the value of the closest image. Proximity is established by retaining the image with the shortest distance between the DSM pixel and the centre of perspective, among all images encompassing this pixel. Visibility is computed using the classical z -buffer technique. This proximity approach has the following advantages: 1) the image with the most vertical view angle is always used (helping preserve the quality of the image texture and reducing BRDF effects), 2) a DSM pixel occluded in the closest image still receives a value if it can be seen from an other image, and 3) cut lines between images are optimal and automatically calculated. Moreover, we avoided inter-image histogram balancing as well as feathering along the cut lines (which are actually very complex due to the interspersed image contributions, e.g. figure 5b) between images to preserve the original radiometry.

Figure 4 presents an overview of the orthomosaic of four overlapping images (4a) with the map of the contributing image identity (4b). We see that at this scale the image appears seamless, that the contributing images each have their “principal domain” but contribute locally outside their domain. Note that black pixels indicate that the corresponding DSM pixel could not be seen from any of the images. Figure 5 shows an enlarged orthomosaic subset (5a) centred on a principal cut line between two images (visible in 5b and as a red dashed line in 5a). Even at this large scale the transition between the two images is invisible and the integrity of crown shapes and texture is preserved. Similar quality can be found along all cut lines.

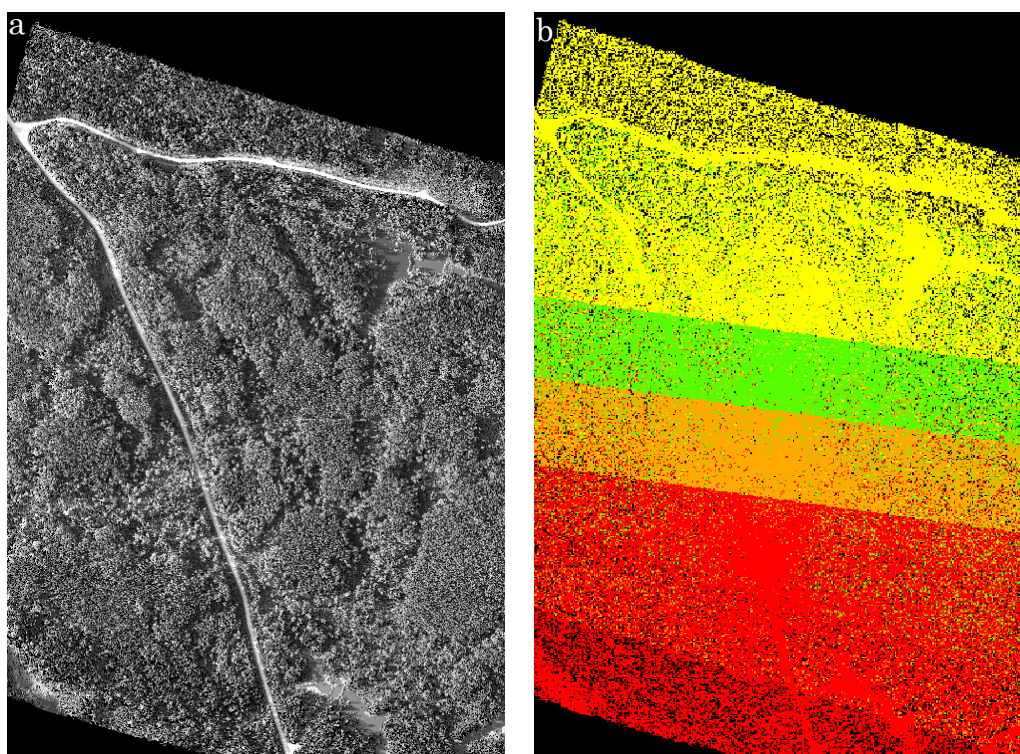


Figure 4 – a) Orthomosaic created from four Vexcel UltraCam images, b) Color-coded identification of the contributing image. No data pixels (in black) result from occlusion or absence of image data. Note that the nearest neighbour resampling used to reduce the scale of 4b for this figure degrades resolution.

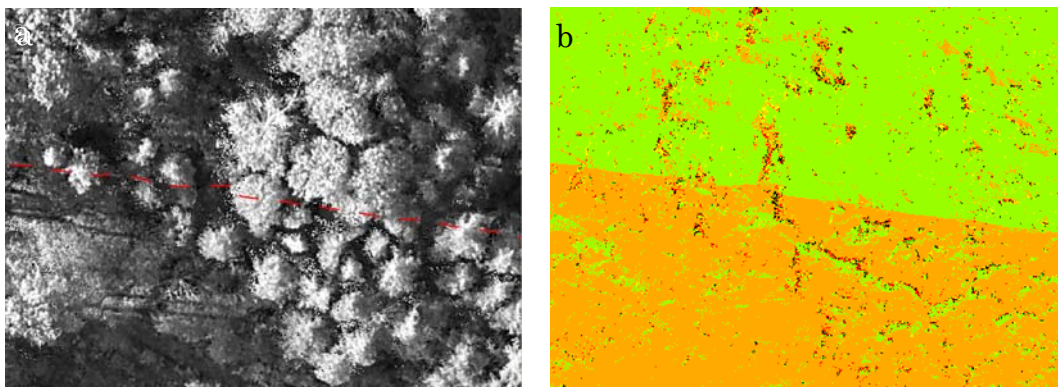


Figure 5 – Enlargement of a portion of 4 a & b. The principal cut line visible in 5b (transition between the green and orange zones) is drawn as a dashed red line in a.

3.4 Cosmetic filling

After the true orthorectification and mosaicking is complete, the DSM pixels occluded in all images have a no-data value. Although this represents the image acquisition reality, no-data pixels may be detrimental to the visual analysis of the orthomosaic, or cause problems for certain automated tree delineation algorithms. We have therefore produced a cosmetically filled version of the orthomosaic based on the following process. First, a map of projected shadows was calculated based on the lidar DSM. The average time at which the four test images were taken was extracted from the Vexcel images' GPS time stamps (images were taken at approx. 1.5 seconds intervals). The NOAA *Solar Position Calculator* was used to obtain the elevation and azimuth of the sun at the time of image capture. Shadows were computed based on the lidar DSM by modelling sun ray's as parallel lines. No-data orthomosaic pixels received a synthetic value which depended on the sunlit/shadowed state of the corresponding DSM pixel. Observations led us to conclude that, as a first approximation and pending further developments, a constant value for sunlit tree pixels would be acceptable. The overall average image value of visible sunlit trees was calculated and assigned to the sunlit no-data (occluded) pixels. A more complex solution was sought for the shadowed pixels. The high radiometric sensitivity of the Vexcel UltraCam makes individual trees discernable even in the shadowed areas. It appears that an important factor affecting the shadowed tree pixel values is the amount of diffuse sky irradiance received by each pixel. This quantity depends on height of the target pixel relative to that of its neighbours. Again as a first approximation, we have calculated the volume of tree material above the target pixel elevation in a 400 m² area centred on the target pixel. These volume values were regressed with all corresponding non-occluded shadow pixel image values, resulting in a model for predicting shadowed pixel brightness based on the 3D layout of its surroundings. This model was used to attribute a brightness value to occluded shadowed pixels.

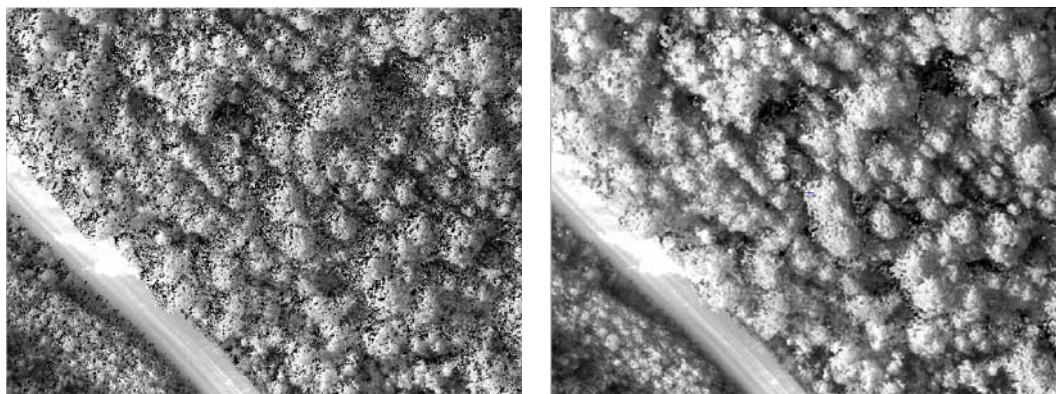


Figure 6 – a) raw orthomosaic (black pixel have no-data value), and b) orthomosaic after cosmetic filling.

As a final step, to remove small artefacts caused by the z -buffer technique used to calculate visibility, we have used a 3×3 Laplacian filter to detect anomalies (e.g. a single very bright pixel surrounded by dark values) and replaced their values by the 3×3 average calculated using the non-anomalous pixels. Only a very small portion of the orthomosaic is affected by this filtering. Figure 6 shows a subset of the “raw” orthomosaic (6a) and the corresponding cosmetically filled version. We observe that all pixels receive a value, and that for the most part, these values are sufficiently close to the plausible brightness levels as to improve visualization, and most probably, individual tree delineation.

4. Concluding remarks

The methods presented in this paper allow the creation of high quality complete and true orthomosaics with very few artefacts. As these orthoimages fit exactly with a lidar dataset, the simultaneous analysis of 3D and radiometric data at high resolution will likely be significantly improved. The cavity filling ensures that the image texture and crown shapes are not degraded during the rectification. The assessment of the misregistration between the datasets used in this study revealed a Z error of 1.41 m, despite all the care put in the positioning of the base GPS antennae, system mounting, direct georeferencing data collection and integration, and vertical datum transformations. Even such a small error affects the geometric quality of the orthoimages. Although the source of this error was not identified, the techniques presented here guarantee that the error itself can be detected and corrected. Moreover, note that using comparisons of Z_P and Z_L , other types of errors could be detected and empirically corrected. However, there is a limit to the registration between image and lidar data due to wind sway of the trees. In the presence of moderate or strong winds, the top of trees will sway by several decimetres such that the crown image and its 3D shape may not fit exactly even though the image and lidar datasets would be tightly registered. Improvements in the orthomosaic creation are still possible. We noted for example that the brightness values of a given crown viewed from two different consecutive images, although very similar, are significantly different. Radiometric calibration would therefore be a useful addition to the mosaicking process. What is more, rough radiometric approximations were made based on the sun and scene geometries to cosmetically fill occluded pixels. More sophisticated approaches involving rigorous radiometric modelling could be employed instead. Nevertheless, we have already achieved a level of image-lidar integration quality that should allow fruitful developments in the field of precise forest mapping.

Acknowledgements

We thank the National Science and Engineering Council of Canada for funding, and Chris Hopkinson for his much appreciated flexibility in scheduling the lidar survey.

References

- Kraus, K. and Waldhäusl, P., 1994. *Photogrammetry, Fundamentals and Standard*.
- Leckie, D., Gougeon, F., Hill, D., Quinn, R., Armstrong, L., Shreenan, R., 2003. Combined high-density lidar and multispectral imagery for individual tree crown analysis. *Canadian Journal for Remote Sensing* 29, 633-649.
- Mayr, W., 2002, True orthoimages. *GIM International*, 16, April, pp. 37–39.
- Mitishita, E., Habib, A., Centeno, J., Machado, A, Lay, J., and Wong, C, 2008. Photogrammetric and lidar data integration using the centroid of a rectangular roof as a control point. *The Photogrammetric Record*, 23, 19-35.
- Vepakomma, U., St-Onge, B. and Kneeshaw, D., 2008. Spatially explicit characterization of boreal forest gap dynamics using multi-temporal lidar data. *Remote Sensing of Environment*, 112, 2326-2340.

Quality assurance and quality control procedures of airborne scanning LiDAR for a nation-wide carbon inventory of planted forests

Peter R. Stephens¹, Robert J. McGaughey², Timothy Dougherty¹, Tim Farrier³, Bridget Geard⁴ & David Loubser¹

¹Ministry for the Environment, PO Box 10362, Wellington, New Zealand and
(Peter.Stephens, Tim.Dougherty, David.Loubser@mfe.govt.nz)

²USDA Forest Service, PO Box 352100, Seattle, USA and bmcgaughey@fs.fed.us

³New Zealand Aerial Mapping, PO Box 6, Hastings, New Zealand and Tim@nzam.com

⁴Ministry of Agriculture and Forestry, PO Box 2526, Wellington, New Zealand and
Bridget.Geard@maf.govt.nz

Abstract

To meet Kyoto Protocol obligations, New Zealand is required to estimate forest carbon stock change over the first commitment period (2008-2012). New Zealand has three categories of forest, namely: natural forest; forests planted prior to 1990; and forests planted in non-forest land after 31 December 1989. The forests planted after 31 December 1989 are called 'Kyoto forests'. The Kyoto forest carbon inventory system involves use of discrete return airborne LiDAR covering circular plots located on a 4 km grid. The plots are 0.06 ha in area. This paper describes the quality assurance and quality control procedures being used to ensure that the LiDAR data meet contract specifications. To be fit-for-purpose for forest carbon inventory the key LiDAR quality characteristics include: positional accuracy; first return density greater than three points per m²; no data decimation; correct file naming; and consistent classification of the ground returns within the point cloud.

Keywords: QA/QC, LiDAR, forest inventory, carbon, Kyoto Protocol

1. Introduction

New Zealand is a signatory to the Kyoto Protocol and the United Nations Framework Convention on Climate Change. A requirement under Article 3.3 of the Protocol is annual greenhouse gas reporting of carbon stock changes arising from land use, land-use change and forestry (LULUCF) activities. Reporting is required for the Protocol's first commitment period, from 2008 to 2012. Good Practice Guidance (IPCC 2003) for LULUCF activities requires carbon stock changes be estimated in an unbiased, transparent, and consistent manner. Further, a process and plan for implementing QA/QC (quality assurance and quality control) procedures is necessary to meet good practice.

To meet LULUCF reporting requirements, New Zealand is classifying forests into three categories: natural forest; forests planted prior to 1990; and forests planted after 31 December 1989 into non-forest land. The latter category is referred to as 'Kyoto forests'. Forests to be measured by New Zealand under the Protocol are defined by the following parameters: minimum area of 1 ha; at least 30 % canopy cover; at least 5 m in height (or the potential to reach this height under current management); and a width of at least 30 m. New Zealand planted forests are comprised predominantly (89 %) of radiata pine (*Pinus radiata*), with the remainder made up of other species, mostly (6 %) Douglas-fir (*Pseudotsuga menziesii*).

A plot-based forest inventory system has been developed for the New Zealand Kyoto forests.

Circular plots, 0.06 ha in area, are being located within these forests on a systematic 4 km grid. As field access to these mostly privately-owned forests is not guaranteed, LiDAR is being used to characterise all plots.

Airborne LiDAR provides a flexible data collection system. The laser signal can penetrate the forest canopy so that ground measurements can be made. Further, data collection is independent of sun angle and night collection is feasible. Over the past few years there have been considerable advances in LiDAR systems which have resulted in improved LiDAR positional accuracy and increased surface point density. This has resulted in cm-level ranging accuracies, significantly increased pulse rate frequencies (greater than 150 kHz) and provision for LiDAR intensity signals (as opposed to ranging observation only). The flexibility of airborne LiDAR, coupled with a high level of positional accuracy and point density, make LiDAR systems an attractive data acquisition tool for forest carbon inventory.

Although field-based carbon estimation is still an essential element of forest carbon inventory, the integration of LiDAR into such activities provides an opportunity to reduce total inventory cost and the need for extensive field-based sampling. Investigations into the potential of airborne LiDAR for forest carbon inventory have been undertaken (Drake *et al.* 2002, Nelson *et al.* 2003, Patenaude *et al.* 2004, and Stephens *et al.* 2007). In temperate deciduous woodland, LiDAR metrics explained 74% of the variation in above-ground carbon estimates, and 85% of the variation in above-ground estimates at the stand level (Patenaude *et al.* 2004). For planted forests in New Zealand, a study by Stephens *et al.* (2007) determined that total carbon per plot could be predicted by LiDAR metrics with a reasonable level of precision ($R^2=0.87$; RMS error=19 t (carbon) per ha (16%)).

For greenhouse gas inventory, quality control is defined as the routine technical activities used to measure and control the quality of the inventory as it is being developed. Quality assurance is defined as the system of review procedures conducted by personnel not directly involved in the inventory compilation/development process (IPCC 2003). These definitions differ with those used in the remote sensing industry (ILMB 2006; Stoker *et al.* 2007). The IPCC QA/QC definitions are used in the paper, where QC activities take place before the LiDAR acquisition mission, and the internal and external QA activities occur largely after the mission.

Emphasis on the development of QA/QC procedures for LiDAR data have been in support of topographic mapping. Csanyi *et al.* (2007) describe LiDAR ground targets designed for topographic mapping to support geodetic grade LiDAR surveys (digital surface mapping with very accurate elevations and horizontal positions).

This paper describes the QA/QC procedures used to ensure that discrete return LiDAR data acquired of forest carbon inventory plots met the aerial survey contract specifications.

2. Method

2.1 Study area

LiDAR data for this project was acquired across New Zealand, which is centered on 41° S and 174° E (Figure 1). A total of 758 inventory sites, located on a 4 km grid, were surveyed.

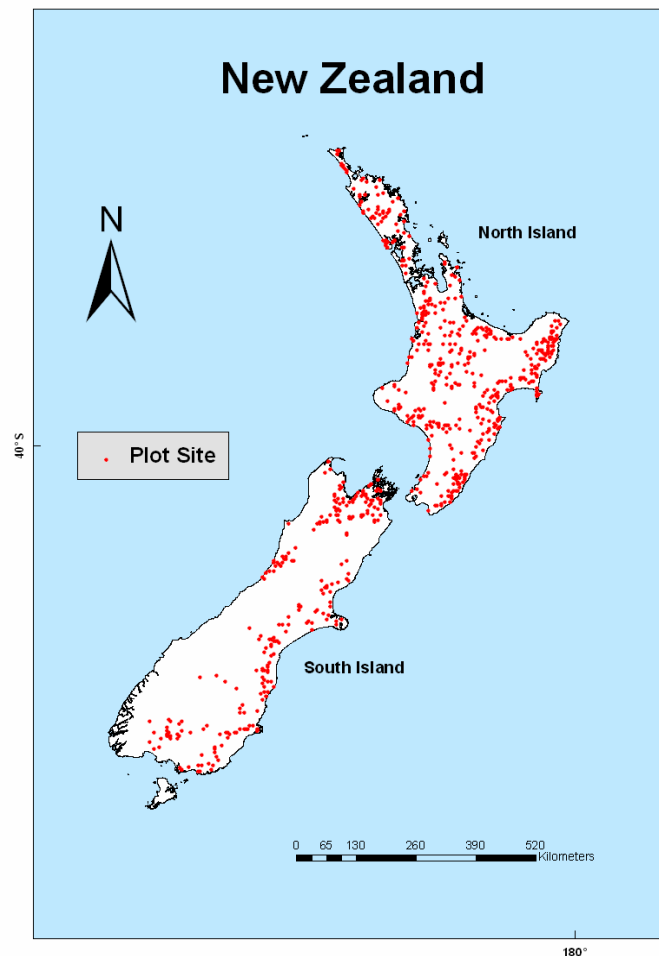


Figure 1: The location of the inventory plots across New Zealand.

2.2 Project specifications

The data acquisition specifications for this project included:

- A total of 758 sites to be flown, each site covering a circular area with a radius of 85 m, where the site centre is the middle of a 0.06 ha circular forest inventory plot.
- For each plot site the first return density for each site to be at least three points per m²
- Digital colour imagery is to be collected concurrently with the LiDAR data
- Data are to be acquired over a three month period (February to April 2008), with data supplied at regular intervals. QA to be undertaken within 10 days of receipt of data.
- Both sensors (LiDAR and digital colour photography) to acquire data along the full length of all flight lines
- Data to be in the NZ Transverse Mercator (NZTM) projection and NZGD2000 geodetic datum
- Project report and metadata documents to describe the capture method, sensor calibration procedures, data processing, contractor QA/QC approach and the outputs supplied to the client.
- No data decimation is to occur, except for atmospheric outliers.
- Data and information to be supplied in specified file formats, with the LiDAR data to be delivered in the LAS 1.0 format.

2.3 LiDAR system and data processing overview

The LiDAR survey was flown using a Cessna 207 aircraft. An Optech ALTM 3100EA LiDAR sensor was mounted in the aircraft, along with an integrated Rollei AIC digital camera. Table 1 summarises the LiDAR and flight parameters used to achieve a target point spacing of 0.5m. The digital camera was used in tandem with the LiDAR sensor. The resulting colour photography had a ground resolution of 0.2 m and a forward overlap of 30 per cent. The system also utilised an Applanix 510 Position and Orientation System (POS) that uses the GPS and IMU sensors, and a GPS-based computer controlled navigation system.

Table1: Summary of narrow beam, discrete return, LiDAR data and flight details

| System | Wavelength | Scan angle | Pulse frequency | Scan frequency | Swath width | Footprint diameter* | Ground speed | Flying height** |
|--------------------|------------|------------|-----------------|----------------|-------------|---------------------|--------------|-----------------|
| Optech ALTM 3100EA | 1064 nm | ± 6 deg | 70 kHz | 53Hz | 170 m | 0.27 m | 105 knots | 1200 m |

* beam divergence based on full width and half height of beam; ** height above ground level

The POS data were processed using Applanix POSpac software and the LiDAR 3D point cloud generation was completed using DASHMap™ software. LiDAR point cloud classification, product generation and orthophoto production was accomplished using the TerraSolid suite of LiDAR processing software.

2.4 QA/QC activities undertaken by contractor

Data acquisition and pre-processing began with the application of rigorous sensor calibration procedures to ensure relative accuracy of the point cloud with absolute positional accuracy being maintained through adopting “procedures that have been demonstrated to produce data with particular horizontal and vertical accuracy values” (FGDC 1998).

Sensor calibration was a key QC activity. LiDAR boresight alignment and scanner scale parameters were determined from LiDAR data collected over a calibration range located close to the aircraft operating base. The calibration range was flown at regular intervals during the aerial acquisition phase of the project. These data were used to confirm whether or not the boresight alignment and scanner scale parameters varied over time. The LiDAR point intensity data were also monitored by reviewing histograms of point intensity values within a subset of the calibration range, and checking for changes in their shape and statistical characteristics.

The absence of a suitable network of continuously operating GPS reference network base stations in New Zealand, and the geographic extent of the project, made it necessary to use advanced Precise Point Positioning (PPP) algorithms during the post-processing of the POS GPS data. To monitor the performance of the PPP output, base stations were operated from time to time throughout the project. When collected, the base station data were used to generate differential GPS (dGPS) based sensor trajectories and these were then used in the QA of the PPP based sensor trajectories.

Following the generation of the LiDAR point cloud with DASHMap™ software, QA of the collected data for swath width/site coverage and point cloud density was undertaken after loading the LiDAR data into TerraScan LiDAR processing software. The target outgoing pulse point density of four points per square metre (with a minimum of three points) in a single flight line required the aircraft pilot and sensor operator to be vigilant in maintaining correct ground speed, altitude and track over steeply undulating terrain.

Rigorous folder and file naming conventions built around unique site identifies and acquisition dates was used to track the data from its raw state after off-load from storage devices on the aircraft through to delivered products. The products were delivered in blocks created on the date of acquisition and were accompanied by ISO 19115 compliant metadata XML files containing both mandatory and optional field entries.

2.5 QA activities undertaken by client

QA activities undertaken by the client involved use of the FUSION LiDAR visualisation and analysis software (McGaughey *et al.* 2004) and ERDAS IMAGINE software. Batch processing of LiDAR data with the FUSION software was undertaken to assess data for all flight lines and all classified sites. The batch processing produced HTML QA reports, which contained numeric and image outputs.

For each LiDAR flight line and each site datasets, FUSION was used to determine first return (pulse) density, return density, and to produce an intensity image of the area covered by the datasets. A ground surface model was also created with FUSION from the flight line and site LiDAR datasets. The ground surface model is generated by filtering the LiDAR point cloud to identify ground returns. The filtering method used is an adaptation of the iterative method developed by Kraus and Pfeifer (1998). The FUSION filtering method is described in Andersen *et al.* 2006.

The FUSION LiDAR data viewer was used to visually assess the site point cloud LiDAR data classified by the contractor as ground surface. This was accomplished by comparing the classified data with the independently created (using FUSION) ground surface model, and by rotating the point cloud to establish if there were any points at an elevation less than those classified as ground surface. These assessments were undertaken for five per cent of the plot sites.

The ground surface model for the flight lines were exported from FUSION as a Surfer ASCII grid file. In ERDAS the elevations along the centreline of the flight line ground surface models were adjusted by applying an elevation offset obtained from reference to a 10 cm contour Geoid separation model. Then the adjusted elevations were compared with elevations for the same centreline sampling area in a national 15 m digital elevation model. This model has a vertical uncertainty of ± 10 m. Flight line elevation comparisons were to provide a 'reasonableness' check of LiDAR-derived elevations against a nation-wide digital elevation model.

File names and geographic position of all ploy data were checked using ARCInfo software. This was accomplished by comparing post-processing plot location shapefiles with shapefiles (with file names and spatial location) of plots to be surveyed.

3. Results

3.1 Sensor calibration

The LiDAR sensor calibration range was flown four times through the course of the acquisition. Height difference statistics between 600 ground surveyed points of the calibration range and the LiDAR point cloud were calculated following the checking of the boresight alignment and scanner scale parameters. Table 2 summaries these statistics and the range of return pulse intensity values for two of the calibration sorties. These are typical of the values obtained for each of the calibration flights.

Table 2: Summary of sensor calibration output for two calibration sorties

| Sortie | Flightline | Height difference mean (m) | Height difference Std Dev. (m) | Return pulse intensity range (min-max) |
|--------|------------|----------------------------|--------------------------------|--|
| 080127 | 1 | -0.002 | 0.06 | 1.4 to 6.8 |
| | 2 | -0.018 | 0.02 | 1.5 to 7.2 |
| 080213 | 1 | 0.002 | 0.03 | 0.7 to 6.7 |
| | 2 | -0.05 | 0.02 | 0.6 to 6.6 |

3.2 Precise Point Positioning

The expected accuracy of the precise point positioning method is 10 to 40 cm, subsequent to the convergence of the processing algorithms. This expectation was tested on six occasions through the course of the project where a GPS base station receiver was operated. Table 3 shows typical positional difference statistics between PPP and dGPS processed sensor trajectories. These results are in accord with expectations and confirm the validity of using PPP for this project.

Table 3: Summary of PPP v dGPS sensor trajectory for two sorties

| Sortie | Duration of sortie (hr:min) | Easting difference mean (m) | Northing difference mean (m) | Height difference mean (m) | Easting difference Std Dev (m) | Northing difference Std Dev (m) | Height difference Std Dev (m) |
|--------|-----------------------------|-----------------------------|------------------------------|----------------------------|--------------------------------|---------------------------------|-------------------------------|
| 080214 | 2:20 | 0.06 | -0.19 | -0.16 | 0.02 | 0.01 | 0.06 |
| 080314 | 3:10 | 0.22 | 0.12 | 0.10 | 0.10 | 0.12 | 0.09 |

All files were named in according to client specifications and the plot sites were found to be in the correct geographic position.

3.3 Assessment of LiDAR first return (pulse) density

A summary of the LiDAR return density results are provided in Table 4. In a few instances point densities were less than the minimum required. This occurred because of strong winds encountered by the aircraft, making it difficult to maintain the planned ground speed of 105 knots. Sites with a density less than three were re-flown.

Table 4: Summary of first return (pulse) LiDAR densities (returns per m²)

| Data delivery date | Number of sorties | Number of plots flown | Maximum return density | Minimum return density | Mean return density | Plots to re-fly |
|--------------------|-------------------|-----------------------|------------------------|------------------------|---------------------|-----------------|
| 14-03-08 | 2 | 24 | 6.67 | 2.62 | 3.55 | 3 |
| 31-03-08 | 2 | 69 | 7.55 | 3.00 | 3.66 | 0 |
| 11-04-08 | 12 | 228 | 4.47 | 2.98 | 3.91 | 1 |
| 17-04-08 | 8 | 178 | 6.41 | 3.06 | 4.09 | 0 |
| 30-04-08 | 2 | 29 | 5.39 | 3.04 | 3.96 | 0 |
| 14-05-08 | 4 | 87 | 5.87 | 3.12 | 3.99 | 0 |
| 28-05-08 | 4 | 107 | 6.04 | 3.23 | 4.16 | 0 |
| 11-06-08 | 3 | 36 | 5.23 | 3.68 | 4.22 | 0 |

Intensity images (created with a dynamic range of 0-100) and the orthophotographs were of high quality. An example of the data acquired, and generated in this project, is illustrated in

Figure 2.

3.4 Assessment of LiDAR-derived ground surface models

Visual comparison of the contractor ground-classified data for the sites with the client created ground surface model showed no discernable difference between the two. Elevation profile differences for a typical flight line in steeply undulating hill country are shown in Figure 3.

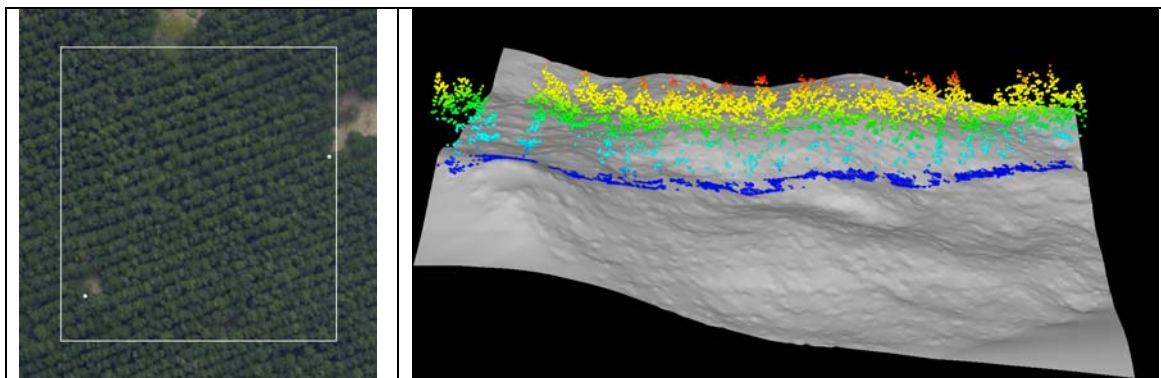


Figure 2: Left image shows an extract of a site orthophotograph. A circular plot site is located within the white rectangle. The two white points mark the ends of a transect through the site. The right image shows the client-produced ground surface model and a 5 m wide point cloud coloured using the height above ground along the transect. The first return density for the site is 3.46 points per m².

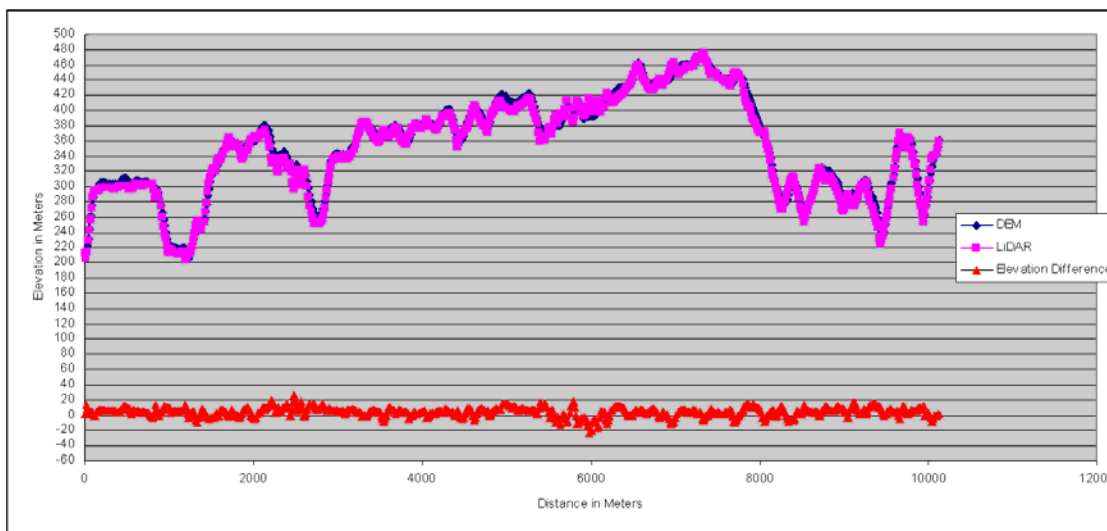


Figure 3: The top two lines show heights from Geoid-corrected LiDAR data and a corresponding profile from a national digital elevation model. The lower line shows the elevation differences between the two data sources. The large elevation difference is 25 m, 2.5 km into the flight line.

4. Discussion

Over the past decade many studies have demonstrated that airborne LiDAR can provide data appropriate for resource management, including forest inventory. Over this time LiDAR technology has been widely used for high-resolution terrain analysis and mapping. National QA/QC standards and guidelines for LiDAR data collection are well developed for terrain analysis and mapping (ILMB 2006; Stoker *et al.* 2007). However, standards and guidelines for

forestry applications are not as well advanced. McGaughey *et al.* (2006) described the requirements for LiDAR data for forestry measurements and highlighted the deliverables, specific to forestry applications that should be included in data acquisition contracts.

This operational LiDAR forest inventory project involved 758 small forest sites, on land ranging from sea level and 940 m elevation, and located over a large geographic area. The QA/QC activities undertaken by the contractor were designed specifically for the project, with quality being maintained through the application of flying skill, rigorous processes and advanced technology. Further, the QA processes undertaken by the client and conducted within 10 days of data delivery, were designed to provide rapid feedback to the contractor, and to ensure that the LiDAR data were appropriate for the intended purpose, namely forest carbon inventory. The QA/QC processes documented here provide a basis for establishing forestry standards and guidelines for airborne LiDAR data acquisition and processing.

References

- Andersen, H.-E., Reutebuch, S.E., and McGaughey, R.J., 2006. A rigorous assessment of tree height measurements obtained using airborne lidar and conventional methods. *Canadian Journal of Remote Sensing*, 32 (5), 355-366.
- Csanyi, N., Edwards, K., Grejner-Brzezinska, D., and Toth, C., 2007. Geodetic grade airborne LiDAR mapping. *In Proceedings of the Institute of Navigation, National Technical Meeting, January 22-24, 2007, San Diego, USA*, 1, 495-503.
- Drake, J.B., Dubayah, R.O., Clark, D.B., Knox, R.G., Blair, J.B., and Hoffman, M.A., 2002. Estimation of tropical forest structural characteristics using large-footprint LiDAR. *Remote Sensing of Environment*, 79, 305-319.
- Federal Geographic Data Committee, 1998. Geospatial Positioning Accuracy Standards Part 3: National Standard for Spatial Data Accuracy. FGDC-STD-007.3-1998.
- Kraus, K., and Pfeifer, N., 1998. Determination of terrain models in wooded areas with airborne laser scanner data. *ISPRS Journal of Photogrammetry and Remote Sensing*, 53, 193-203.
- ILMB, 2006. LiDAR specifications. Ministry of Agriculture and Lands, Integrated Land Management Bureau (ILMB), Base Mapping and Geomatic Services Branch, Victoria, British Columbia, Canada, Version 0.05, 35.
- McGaughey, R.J., Carson, W.W., Reutebuch, S.E., and Andersen, H.-E., 2004. Direct measurement of individual tree characteristics from LiDAR data. *In: Proceedings of the 2004 Annual ASPRS Conference, May 23-28 2004; Denver, Colorado: Bethesda, MD. American Society of Photogrammetry and Remote Sensing.* unpaginated CD-ROM.
- McGaughey, R.J., Andersen, H.-E., and Reutebuch, S.E., 2006. Considerations for planning, acquiring, and processing LiDAR data for forestry applications. *In Proceedings of the 11th Biennial USDA Forest Service Remote Sensing Applications Conference, April 24-28 2006, Salt Lake City, USA.*
- Nelson, R., Valenti, M.A., Short, A., and Keller, C., 2003. A multiple resource inventory of Delaware using airborne laser data. *Bioscience*, 53, 981-992.
- IPCC, 2003. Penman, J., Gytarsky, M., Hiraishi, T., Krug, T., Kruger, D., Pipatti, R., Buendia, L., Miwa, K., Ngara, T., Tanabe, K., and Wagner, F (Eds). *Good Practice Guidance for Land Use, Land-Use Change and Forestry*. IPCC National Greenhouse Gas Inventories Programme. Published for the IPCC by the Institute for Global Environmental Strategies: Tokyo, Japan.
- Patenaude, G., Hill, R.A., Milne, R., Gaveau, D.L.A., Briggs, B.B.J., and Dawson, T.P., 2004. Quantifying forest above ground carbon content using LiDAR remote sensing. *Remote Sensing of Environment*, 93, 368-380.
- Stephens, P.R., Watt, P. J., Loubser, D., Haywood, A., and Kimberley, M.O., 2007. Estimation of carbon stocks in New Zealand planted forests using airborne scanning LiDAR. *Proceedings ISPRS Workshop on Laser Scanning 2007 and SilviLaser 2007, September 12-14, Finland*, 389-394.

Stoker, J., Parrish, J., Gisclair, D., Harding, D., *et al.*, 2007. Report of the First National Lidar Initiative Meeting, hosted by the USGS Land Remote Sensing Program, Geography Discipline. Report Series OF 2007-1189, US Department of the Interior and US Geological Survey, 64.

Combining airborne laser scanning and GIS data to estimate timber volume of forest stands based on yield models

Christoph Straub¹, Matthias Dees¹, Holger Weinacker¹ & Barbara Koch¹

¹ University of Freiburg, Dept. of Remote Sensing and Landscape Information Systems, christoph.straub@felis.uni-freiburg.de, matthias.dees@felis.uni-freiburg.de, holger.weinacker@felis.uni-freiburg.de, barbara.koch@felis.uni-freiburg.de

Abstract

Timber Volume is one of the most important quantitative parameters to characterize a forest stand. This article evaluates a combination of Airborne Laser Scanning and GIS data to estimate timber volume of forest stands using standard forestry yield models. The input parameters into the models are the stand height and canopy density which are both derived from a normalized digital surface model. For the selection of suitable yield models, information about tree species composition from digital stand maps was used. The method was verified in a forest area in Southern Germany with 313 circular inventory plots each with a size of 452m². The relation between estimated timber volume and the volume calculated from the inventory data reached a correlation coefficient of $r = 0.74$ when regarding all sample plots. The plot values were averaged within forest stands of the same age class and a correlation of $r = 0.91$ was achieved. The relation for averaged values only for single-storied stands reached a correlation of $r = 0.98$.

Keywords: Airborne Laser Scanning, forestry, timber volume, yield models, inventory

1. Introduction

Airborne Laser Scanning (ALS) is an active remote sensing technique for the capturing of topographic data. Laser Mapping is based on a multi-sensor system whose main components are a laser scanner to measure the range/distance from the scanner in the aeroplane to the terrain surface, a Global Positioning System (GPS) and an Inertial Navigation System (INS). These components are usually mounted on a helicopter or an aeroplane. The survey area is scanned strip by strip and the range measurements are converted into a local coordinate system. The result is a point cloud, often referred to as “raw data”. Besides conventional ALS systems which record the first and last echo for each emitted laser beam, full wave scanners (which record the whole echo waveform) gain more importance (Wagner *et al.* 2008). In forests the laser pulses usually have multiple reflections from different vegetation layers and a certain amount of pulses will penetrate to the ground. Using a suitable filtering technique a digital terrain model - DTM (which represents the bare earth) and a digital surface model - DSM (which represents the height of objects on top of the bare earth like vegetation cover or buildings) can be derived from the point cloud. A large number of studies have shown the capability of ALS technology to accurately estimate important forest inventory parameters such as stand heights, basal area, and stand volume (Hyyppä *et al.* 2006, Koch *et al.* 2006, Hyyppä *et al.* 2004, Næsset 2002). A widely used approach is to relate laser-derived variables, representing canopy height and density, to ground-truth data from inventory plots for the calibration of regression models. The models are used in a second step to estimate forest inventory parameters e.g. timber volume for the entire study area (Hollaus *et al.* 2007, Næsset 2002, Means *et al.* 2000, Næsset 1997).

In the following paragraphs a method is described which combines ALS and additional information from GIS data to estimate timber volume of forest stands using standard forestry yield models. Yield models were developed in the past from extensive field measurements and

are summarized into yield tables which give information about structural forest parameters like timber volume attainable under certain conditions. First ideas of the method are described in (Dees *et al.* 2006).

2. Method

2.1 Study Area

The method, presented in the following paragraphs, was verified in a forest area with a size of 9.24 km² in Southern Germany located north of the city of Karlsruhe (coordinates of the upper left corner in Gauss Krüger: 3456300 (easting) / 5436100 (northing)). The tree species composition is shown in table 1.

Table 1: Tree species composition of the study site

| Tree Species | Percentage |
|--|------------|
| Scotch pine (<i>Pinus sylvestris</i>) | 51 % |
| Oak (<i>Quercus petraea</i>) | 14 % |
| Beech (<i>Fagus sylvatica</i>) | 10 % |
| Red oak (<i>Quercus rubra</i>) | 10 % |
| Douglas fir (<i>Pseudotsuga menziesii</i>) | 5 % |
| Hornbeam (<i>Carpinus betulus</i>) | 4 % |
| Other species such as birch (<i>Betula pendula</i>), spruce (<i>Picea abies</i>), larch (<i>Larix europaea</i>), lime tree (<i>Tilia cordata</i>), sycamore maple (<i>Acer pseudoplatanus</i>) | 6 % |

2.2 Remote Sensing Data

Full-wave laser scanner data and aerial images were acquired in August 2007 by TopoSys GmbH using the “Harrier 56” LIDAR system mounted on a helicopter. The scanner used in this system is the Riegl LMS-Q560. Important flight and system parameters are listed in table 2.

Table 2: Flight and system parameters of the flight campaign in summer 2007 with the “Harrier 56”

| Parameter | Value |
|---------------------|----------------------------|
| Range Capture | Full waveform digitization |
| Measurement rate | 100 kHz |
| Field of view | 45° |
| Swath width | 370m |
| Flying height | 450m AGL |
| Flying speed | 30m/s |
| Point density | 16 points / m ² |
| Vertical accuracy | < ±0.20 [m] |
| Horizontal accuracy | < ±0.5 [m] |

Both a terrain and a surface model with 1m resolution were derived from the point cloud. An “Active Surface Algorithm”, implemented in the software TreesVis, was used for filtering and interpolation. Details about the filtering technique can be found in (Weinacker *et al.* 2004). A normalized digital surface model (nDSM), in forests often referred to as canopy height model (CHM), was derived by subtracting the DTM from the DSM. True orthophotos (RGB and CIR) with 20 cm ground resolution were delivered by TopoSys GmbH.

2.3 Reference Data

Forest inventory data from summer 2006 was provided by the Department of Forestry of the Federal State of Baden-Württemberg. Permanent georeferenced sample plots were distributed over the study area on the intersections of a regular 100x200m raster. For each of the plots trees were measured in the field within concentric circles using the following different radii: 2m, 3m, 6m and 12m. Within each concentric circle trees with a diameter at breast height (DBH) greater than 7cm, 10cm, 15cm and 30cm were measured. Two top heights of the main crop and one top height of the dominated crop were measured using a Vertex® instrument. As an average top height for each plot the arithmetic mean of those height measurements was calculated. Stand height curves with the DBH as input parameter were used to estimate the heights of the remaining trees (Korn-Allan 2004). Based on these measurements the volume of single trees was computed and the timber volume in solid cubic meter per hectare (defined as the sum of all stems and branches with a diameter above 7cm) was derived for each plot. The position accuracy of the centre point of the sample plots was quantified in a current study with an average deviation of 3,77m compared to very accurate measurements using a theodolite (Breidenbach 2008).

2.4 Methodology

Yield models, developed and recommended for the Federal State of Baden-Württemberg, Southern Germany (MLR 1993) were used to estimate timber volume with metrics from ALS and GIS data as input parameters. The models describe the development of a forest stand throughout lifetime based on a specific forestry concept (treatment of a stand like moderate or strong thinning) and were set up for 16 different tree species. For each species several yield classes are defined which describe the influence of environmental conditions (climate, topography and soil). They are given in a tabular form and provide forestry parameters such as tree number per hectare, top height, basal area, mean diameter or volume as a function of the age. Due to the fact that ALS data provides very accurate height measurements the yield models were used to estimate timber volume as a function of top height. In general the following information is necessary for the application of yield models:

1. Tree species composition of a stand: Necessary for the selection of suitable models. Due to the fact that species classification from ALS data is still a challenge, except for the classification of coniferous and deciduous forest during leaf-off (winter) conditions (Straub 2006), tree species percentages of the forest management plan (formatted as GIS data) were integrated. For each species a separate function was derived from the yield tables. The species percentage was used as weighting factor.
2. Yield class: Describes the influence of environmental conditions and is necessary for the selection of a suitable model. As described in (Mette *et al.* 2002) information on the site condition is very important if stem biomass is estimated by the age of a stand. If stem biomass is estimated by the forest height the site condition has only a small effect. The statistical relation between (mid) height and (stem) volume of a stand is also known as the “law of Eichhorn” (Pretsch 2001). Thus the yield class was not further considered in this study.
3. “Degree of stocking”: The timber volume derived from a yield table is multiplied with the degree of stocking DS defined as the ratio of real basal area BA_{real} to the corresponding basal area from a yield table BA_{table} for moderate thinning (Kramer and Akça 1995):

$$DS = \frac{BA_{real}}{BA_{table}} \tag{1}$$

The result is an estimate of the actual volume of the stand. According to (Huss 1984) the degree of stocking can be estimated with remote sensing data using the tree crown cover also referred to as canopy density.

2.4.1 Top Height Estimation of Forest Stands using ALS Data

Top height is defined as the height of the hundred trees with largest diameter per hectare within a stand (Burschel and Huss 1997). Due to the fact that trees with the largest diameter are usually the highest trees, the top height represents the height of trees in the upper canopy level which can be modelled with ALS data. Several variables both derived from the point cloud/raw data (after subtracting the ground surface height) and the nDSM were verified in order to determine the best estimate for the top height. Similar to earlier findings (Næsset 2002, Means *et al.* 2000, Rieger *et al.* 1999) several height percentiles were calculated for each inventory plot from the raw data Raw_{60} , Raw_{70} , Raw_{80} , Raw_{90} , Raw_{max} (unlike previous studies no differentiation between first and last echo was made) and from the nDSM $nDSM_{60}$, $nDSM_{70}$, $nDSM_{80}$, $nDSM_{90}$, $nDSM_{max}$. The correlations of the laser metrics with the field data (as shown in table 3) were computed for 305 inventory plots (all plots with actual tree height measurements).

Table 3: Correlations of height percentiles from raw data and nDSM with height measurements from 305 inventory plots to estimate the top height of forest stands

| Height percentiles from nDSM | Correlation Coefficient (r) | Height percentiles from raw data | Correlation Coefficient (r) |
|------------------------------|-----------------------------|----------------------------------|-----------------------------|
| $nDSM_{max}$ | 0.84 | Raw_{max} | 0.84 |
| $nDSM_{90}$ | 0.87 | Raw_{90} | 0.84 |
| $nDSM_{80}$ | 0.84 | Raw_{80} | 0.78 |
| $nDSM_{70}$ | 0.80 | Raw_{70} | 0.62 |
| $nDSM_{60}$ | 0.74 | Raw_{60} | 0.44 |

The 90th percentile of the nDSM ($nDSM_{90}$) showed the highest correlation with the field data. The regression is shown in figure 1:

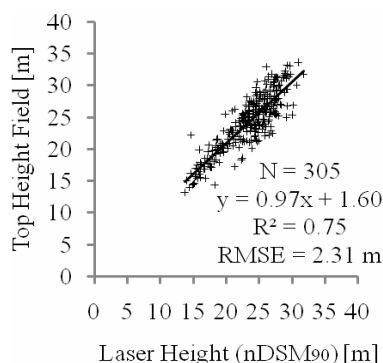


Figure 1: Estimation of the top height of forest stands from 90th percentile of the nDSM

2.4.2 Estimation of the Canopy Density from ALS data

Canopy density is defined as the ground covered by a vertical projection of tree crowns. For each sample plot the canopy density was estimated based on the nDSM which represents the canopy heights for each xy position. A threshold operation (selection of pixels with height values within a defined interval) was used to extract potential crown regions. The threshold operation is defined as

$$CR = \{(xy) \in R : \Delta h_{\min} \leq nDSM_{xy} \leq \Delta h_{\max}\} \quad (2)$$

where CR = Output region (crown regions)
 R = Region of Interest (ROI)
 $nDSM_{xy}$ = Height values of the nDSM for each xy position
 Δh_{\min} = Minimum height threshold
 Δh_{\max} = Maximum height threshold

Timber volume is defined by stems with a minimum diameter of 7cm. If a general relation of $height = diameter \cdot 100$ is assumed (for young trees), the minimum height of trees to be measured will be 7m which was defined for Δh_{\min} whereas Δh_{\max} was set to the maximum height value within the sample plots. The ratio of the size of extracted crown regions CR to the plot area was used as an estimate for canopy density.

2.4.3 Tree Species Information from GIS Data

A digital stand map was provided by the Department of Forestry. A total number of 101 stands are located in the study site. Tree species percentages of the forest management plan were assigned as attributes to the stands. The percentages are estimated in field based on the area covered by the crowns of each individual species in a stand and are given in units of 5 %. The accuracy of the estimation is not quantified but is assumed to be less than ± 5 %. Finally the tree species percentages were allocated to all sample plots located within each stand.

2.4.4 Estimation of the Timber Volume

A polynomial of second order was used to estimate timber volume as a function of top height:

$$V = a + bH + cH^2 \quad (3)$$

where V = Timber volume
 H = Top height
 a, b, c = Individual parameters for a tree species

Different parameters were derived from the yield tables for eight species using regression analysis (see table 4).

Table 4: Parameters derived from yield tables to estimate timber volume as a function of top height

| Tree species | Number of yield tables | a [m ³ /ha] | b [m ² /ha] | c [m/ha] | R^2 | Range | |
|--|------------------------|-----------------------------|-----------------------------|---------------|-------|-----------------|-----------------|
| | | | | | | Min. Height [m] | Max. Height [m] |
| Scotch pine (<i>Pinus sylvestris</i>) | 7 | - 90.2971 | 18.0819 | -0.0022 | 0.98 | 8.3 | 37.5 |
| Oak (<i>Quercus petraea</i>) | 7 | - 145.3082 | 16.4528 | 0.0684 | 0.99 | 7.8 | 40 |
| Beech (<i>Fagus sylvatica</i>) | 8 | - 160.3876 | 17.8205 | 0.0629 | 0.98 | 6.6 | 45.5 |
| Red oak (<i>Quercus rubra</i>) | 5 | - 88.6174 | 8.5654 | 0.2272 | 0.97 | 6 | 33.5 |
| Douglas fir (<i>Pseudotsuga menziesii</i>) | 12 | 33.0444 | 0.3091 | 0.4372 | 1 | 9.5 | 51.1 |
| Spruce (<i>Picea abies</i>) | 11 | - 154.5544 | 21.5093 | 0.1245 | 0.97 | 6.9 | 43.1 |
| Larch (<i>Larix Europaea</i>) | 5 | - 17.7444 | 7.1107 | 0.2381 | 0.99 | 11.1 | 43.2 |
| Lime tree (<i>Tilia cordata</i>) | 5 | 25.2515 | 8.2378 | 0.1333 | 1 | 13.2 | 32.6 |

For some deciduous species no yield models were available and the parameters for beech were used. For each sample plot the timber volume was estimated in solid cubic meter per hectare. The estimation of timber volume as a function of top height, tree species composition and degree of stocking can be written as:

$$V = DS \cdot \sum_{i=1}^n \left[(a_i + b_i H + c_i H^2) \cdot \frac{P_i}{100} \right] \quad (4)$$

where V = Estimated Timber volume in m³/ha
 a_i, b_i, c_i = Parameters for different tree species ($i = 1, \dots, n$)
 H = Top height in meter (estimated from ALS and calibrated with field data)
 P_i = Percentage of tree species (from digital stand map) ($i = 1, \dots, n$)
 DS = Degree of stocking (derived from the estimated canopy density)
 n = Number of different tree species within a stand

3. Result

Forest inventory plots (as described under 2.3) were used for verification. The comparison of estimated timber volume and inventory data was done for all sample plots as well as for averaged values which were derived from plots located within stands of the same age class. The age class was taken from the stand map. A correlation coefficient of $r = 0.74$ was reached when regarding all sample plots (a scatter plot with regression and RMSE is shown in figure 2). After averaging the estimated and the reference values for all stands with the same age class (both for single and multi-storied stands) a correlation of $r = 0.91$ was achieved (the scatter plot is shown in figure 3). The correlation with averaged values only for single-storied stands in the study site reached the highest correlation of $r = 0.98$ (the scatter plot is shown in figure 4). Information about the vertical stand structure was taken from the forest management plan.

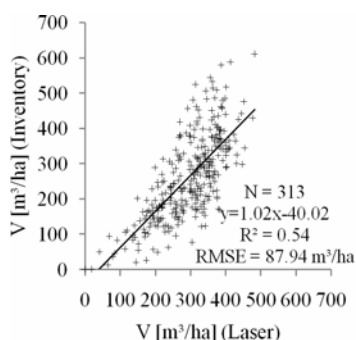


Figure 2: Timber volume estimation regarding all inventory plots

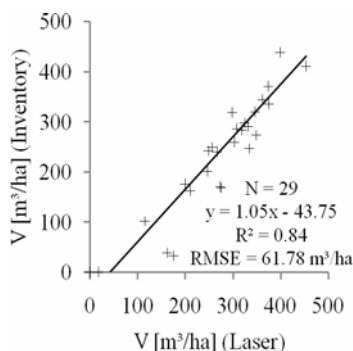


Figure 3: Timber volume estimation with averaged values for age classes (including both single and multi-storied stands)

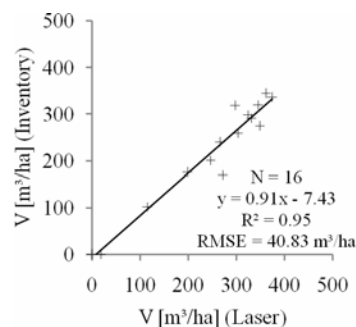


Figure 4: Timber volume estimation with averaged values for age classes (only single-storied stands)

4. Discussion

A method to estimate timber volume of forest stands based on ALS and GIS data using standard forestry yield models was presented. Inventory plots were used for verification. Top height of forest stands as one of the input parameter into the yield models was estimated from the 90th percentile of the nDSM. The relation of the height estimation on plot level reached a correlation coefficient of $r = 0.87$ and coefficient of determination of $R^2 = 0.75$. As second parameter the canopy density (tree crown cover) was estimated based on the nDSM by extracting all pixels with a height above 7m. The canopy density was used as an estimate for the degree of stocking to correct the timber volume derived from a yield model. For the selection of suitable yield models tree species information of the forest management plan (assigned as attributes to digital stand maps) were utilized. Parameter sets for eight tree species were derived from the yield tables as recommended for the Federal State of Baden-Württemberg, Germany.

A relation of $r = 0.74$ ($R^2 = 0.54$) was reached for timber volume estimation when regarding all sample plots. The high scatter on plot level can be explained by local variations of the forest structure which have a high influence if timber volume is estimated for small regions like the sample plots used in this study with a size of 452m². However the variation was compensated when plot values were averaged for larger units (here: stands of the same age class). The estimation for all stands located in the study area (both single-storied and multi-storied stands) reached a very satisfying accuracy of $r = 0.91$ ($R^2 = 0.84$). The variance can be further reduced if plot values are averaged only for single-storied stands of the study site with a very close relation of $r = 0.98$ ($R^2 = 0.95$). This may emphasize that yield models were originally developed for pure even-aged stands (homogeneous structure with small differences in age among individual trees).

Yield models attempt to quantify the development of a forest but nowadays higher growth rates are assumed than given by the models used in this study which were established between the years 1936 to 1992. Nevertheless the relation between height and volume will not change significantly (Mette *et al.* 2002).

To improve the volume estimation further studies will concentrate on the extraction of additional forest parameters from the full wave data e.g. the vertical stand structure. Automatic or semi-automatic classification of optical data will be tested to replace species information of the forest management plan by remote sensing data.

Acknowledgements

The authors would like to express their gratitude to the German environmental foundation - Deutsche Bundesstiftung Umwelt (DBU) which provided funding for the project.

References

- Burschel, P. and Huss, J., 1997. *Grundriß des Waldbaus*. Parey, Berlin, 67-68.
- Breidenbach, J., 2008. *Regionalisierung von Waldinventuren mittels aktiver Fernerkundungstechniken*. Doctoral Thesis (in press), 73.
- Dees, M., Straub, C., Wang, Y., Koch, B. and Weinacker, H., 2006. *Auswertung von zwei Laserscanner-Testdatensätzen: Waldkarten und Kenngrößen des Waldes*. Internal report of a demonstration project for E.ON-RuhrGas, Essen, Germany.
- Hollaus, M., Wagner, W., Maier, B. and Schadauer, K., 2007. Airborne Laser Scanning of Forest Stem Volume in a Mountaineous Environment. *Sensors*, 7, 1559-1577.
- Huss, J., 1984. *Luftbildmessung und Fernerkundung in der Forstwirtschaft*. Wichmann. Karlsruhe, 285.
- Hyypä, J., Hyypä, H., Litkey, P., Yu, X., Haggrén, H., Rönholm, P., Pyysalo, U., Pitkänen, J. and Maltamo, M., 2004. Algorithms and Methods of Airborne Laser Scanning for Forest Measurements. In: M. Thies, B. Koch, H. Spiecker, H. Weinacker (Eds.). *Proceedings of ISPRS working group VIII/2 "Laser-Scanners for Forest and Landscape Assessment"*. Freiburg, University of Freiburg: 82-89.
- Hyypä, J., Yu, X., Hyypä H. and Maltamo, M., 2006. Methods of Airborne Laser Scanning for forest information extraction. In: T. Koukal, W. Schneider (Eds.). *Proceedings of International workshop "3D Remote Sensing in Forestry"*, University of Natural Resources and Applied Life Sciences, Vienna: 63-78.
- Kramer, H. and Akça, A., 1995. *Leitfaden zur Waldmessenlehre*. J.D. Sauerländer's Verlag, Frankfurt am Main, 148.
- Koch, B., Heyder, U. and Weinacker, H., 2006. Detection of Individual Tree Crowns in Airborne Lidar Data. *Photogrammetric Engineering & Remote Sensing*, 72, 4, 357-363.
- Korn-Allan, E., v.d. Goltz, H., Blust, M. and Nothdurft, A., 2004. *Verfahrenshandbuch Betriebsinventur*. Version 1.1., Landesforstverwaltung Baden-Württemberg.
- Means, J. E., Acker, S.A., Fitt, B.J., Renslow, M., Emerson, L. and Hendrix, C. J., 2000. Predicting Forest Stand Characteristics with Airborne Laser Scanning LIDAR. *Photogrammetric Engineering & Remote Sensing*, 66, 11, 1367-1371.
- Mette, T., Papathanassiou, K.P., Hajnsek, I. and Zimmermann, R. 2002. Forest Biomass Estimation using Polarimetric SAR Interferometry. *Proceedings of IGARSS 2002*, Toronto, Canada, 2, 817-819.
- MLR, 1993. *Hilfstabellen für die Forsteinrichtung*. Ministerium für Ländlichen Raum, Ernährung, Landwirtschaft und Forsten Baden Württemberg, Stuttgart.
- Næsset, E., 1997. Estimating Timber Volume of Forest Stands Using Airborne Laser Scanner Data. *Remote Sensing of Environment*, 61, 246-253.
- Næsset, E., 2002. Predicting forest stand characteristics with airborne scanning laser using a practical two-stage procedure and field data. *Remote Sensing of Environment*, 80, 88-99.
- Pretzsch, H., 2001. *Modellierung des Waldwachstums*. Parey, Berlin.
- Rieger, W., Eckmüller O., Müllner, H. and Reiter, T., 1999. Laser-Scanning for the derivation of forest stand parameters. In: Beata M. Csatho (Ed.). *Proceedings of the ISPRS Workshop "Mapping Surface Structure and Topography by Airborne and Spaceborne Lasers"*. La Jolla, USA.
- Straub, C., 2006. Automatic Delineation and Classification of Forest Stands based on Airborne Laser Scanner Data. Master Thesis, Stuttgart.

- Wagner, W., Hyypä, J., Ullrich, A., Lehner, H., Briese, C. and Kaasalainen, S., 2008. Radiometric Calibration of Full-Waveform Small-Footprint Airborne Laser Scanners, In: Chen, J., Jiang, J., Baudoin, A. (Eds.). *Proceedings of the XXI ISPRS Congress*, Beijing, China: 163-168.
- Weinacker, H., Koch, B., Heyder, U. and Weinacker, R., 2004. Development of filtering, segmentation and modelling modules for LIDAR and multispectral data as a fundamental of an automatic forest inventory system. In: M. Thies, B. Koch, H. Spiecker, H. Weinacker (Eds.). *Proceedings of ISPRS working group VIII/2 "Laser-Scanners for Forest and Landscape Assessment"*. Freiburg, University of Freiburg: 90-95.

A practical application of airborne LiDAR for forestry management in Scotland

Juan Suárez¹, Jacqueline Rosette², Bruce Nicoll¹ and Barry Gardiner¹

¹Forest Research Agency of the Forestry Commission, Northern Research Station, Roslin, Midlothian, EH25 9SY, UK. juan.suarez@forestry.gsi.gov.uk

²Climate and Land-Surface Systems Interaction Centre, Geography Department, Swansea University, Swansea, SA2 8JP, UK. ggrosette@swansea.ac.uk

Abstract

This paper presents an assessment of the risk of windthrow for an area of ancient woodland of high environmental importance in Scotland, UK. ForestGALES (Geographical Analysis of the Losses and Effects of Storms in Forestry) is a process-based model, which identifies wind vulnerability. The collection of plot-level field data has previously permitted this model to be run for stand-level analysis. In this study, airborne LiDAR data were used to produce a normalised canopy height model (CHM). An algorithm was designed within Definiens Developer 7.0 object oriented analysis software in order to delineate individual tree crowns from the CHM. The results of this delineation were used to develop regression equations using individual tree height and crown width to estimate diameter at breast height. This aims to allow structural vegetation properties to be related to the spatial distribution of individuals. The spatial arrangement of individual tree heights and diameters at breast height were used to generate tree lists and use them as inputs to ForestGALES. This allowed the stability of individual trees to be mapped by modelling the critical wind speed at which they are predicted to be overturned. This offers a substantial improvement on previous model outputs and provides important data, which can inform forest management decisions.

Keywords: Airborne LiDAR; high point density; canopy delineation; windthrow

1. Introduction

Topographic exposure, the degree of exposure to Atlantic storms, shielding from adjacent vegetation together with individual tree dimensions are factors that need to be considered when modelling susceptibility to wind. Understanding these processes and site-specific risk will not only allow appropriate management of wind risk but also permit the optimum felling age of stands to be identified. Airborne LiDAR data enables the locations, heights and canopy dimensions of individual trees to be mapped and therefore addresses many of the data requirements for assessing vulnerability to wind (Suárez *et al* 2008).

Glen Affric consists of an area of lochs, moorland and mountains in the Scottish Highlands. It contains one of the largest ancient Caledonian pinewoods in Scotland, consisting of species such as Scots pine, junipers, birches, willows and aspen. This diverse landscape provides habitats for a wide range of plant, animal and bird species. As a result, it has been designated a Caledonian Forest Reserve, National Scenic Area and National Nature Reserve. Since the 1960s, the core area of Glen Affric has been under conservation management by the Forestry Commission of Great Britain in recognition of its high environmental value (Forestry Commission 2008a, 2008b).

2. Aims

Forest management plans contemplate a progressive transition from a traditional planting and clear-felling to a natural system characterised by a permanent presence of trees, selective cuttings and natural regeneration. The ultimate goal is the progressive substitution of non-native species for those ones that define a Caledonia forest.

However, this area is regularly subjected to storm events coming from the North Atlantic added to permanent waterlogged conditions, which makes it vulnerable to wind damage during those storm events. This study was conducted as part of the EU-funded Interreg project StormRISK. The aim was to test the capabilities of LiDAR analysis to provide more accurate information than that routinely gathered in the field by the forest district. In particular, this work looked at mapping structural differences within the forest stands such as the spatial distribution of individual trees, distance between neighbours, individual tree heights and stem diameters. All this information has been used to generate tree lists that were subsequently input into the ForestGALES model (Geographical Analysis of the Losses and Effects of Storms in Forestry) to make predictions of the Critical Wind Speed required to overturn each tree.

ForestGALES is a process-based model which enables risk of wind damage to be assessed for different management scenarios and with changing conditions due to stand growth (Gardiner *et al* 2004, Forestry Commission 2008b, Suárez *et al* 2008). Given local site characteristics, the model therefore identifies the wind speed at which windthrow will occur. Risk is expressed as the recurrence period of the critical wind speed calculated to overturn an average tree within a stand. These return times have been mapped for Britain using wind strength scores called DAMS (Detailed Aspect Method of Scoring).

3. Data

Airborne LiDAR data were acquired for an area of 58 km² on 9th, 11th and 13th June 2007 by The Environment Agency Science Enterprise Centre on behalf of Forest Research. The Optech ALTM 3100 LiDAR system was used recording up to four return echoes per laser shot at approximately 0.25m resolution. This resulted in an average pre-processed point density of approximately 12-16 points/ m² producing good energy penetration throughout the canopy (Figure 1).

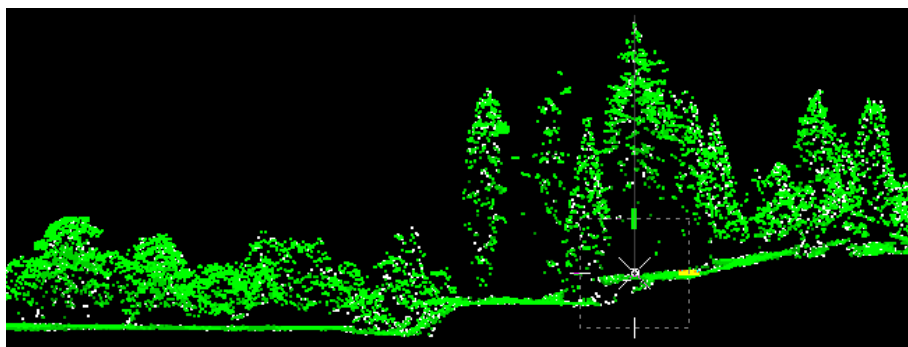


Figure 1. LiDAR point cloud cross section of Glen Affric, Scotland. Image produced with Terrascan.

4. Methods

A subset of airborne LiDAR data was used for a 1km x 2km area representing the range of surface and vegetative characteristics present within Glen Affric (Figure 2). This study area comprises stands of Scots Pine (*Pinus sylvestris*), Birch (*Betula spp.*), European Larch (*Larix decidua*), Douglas Fir (*Pseudotsuga menziesii*), mixed conifers, Sitka Spruce (*Picea sitchensis*), Norway Spruce (*Picea abies*) and Lodgepole Pine (*Pinus contorta*) in order of occurrence.

Scots Pine formed the oldest and youngest stands of 208 and 8 years old respectively. For the purposes of this study, field measurements and models for stands of Scots Pine (*Pinus sylvestris*) are to be used for validation. The LiDAR data were processed as outlined below.

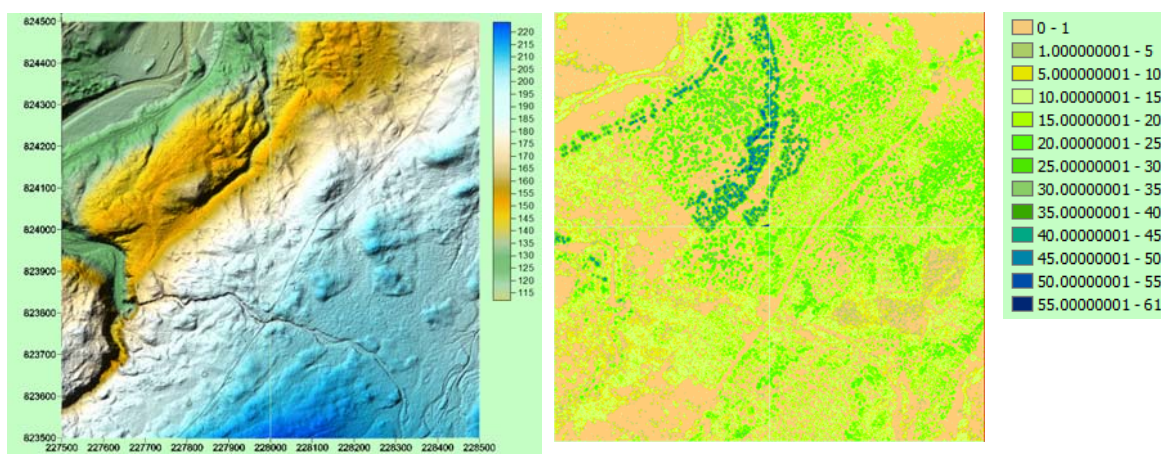


Figure 2. (left) 0.5m resolution digital terrain model of a 1km x 1km area produced with Golden Software Surfer 8. (right) Canopy height model of the same area using ArcGIS 9.1

A ground return class was determined from last return echoes using Terrascan 007.008 Software an extension application for Bentley Microstation V8 2004. This ground class and all first return data were subsequently exported and converted into regular 0.5m resolution raster geotiffs using Delaunay triangulation with linear interpolation. A canopy height model (CHM) was calculated as the difference between the digital terrain model (DTM) created from the ground class and the digital surface model (DSM) from the first return data using ArcGIS 9.1.

An algorithm was designed within Definiens Developer 7.0 to delineate individual tree canopies solely from the LiDAR-derived 0.5m resolution canopy height model. Firstly the CHM was smoothed with a kernel of 3x3 and local maxima were located and classified as tree tops. Areas of ground or understorey vegetation, plus canopy ‘edges’ were identified and used as boundaries to prevent further canopy growth. Tree tops were subsequently extended radially until either meeting an adjacent canopy or designated boundaries and a mask was applied to limit irregularly shaped polygons. Tree top locations were then saved as point shapefiles and polygons representing individual canopies were also exported with associated maximum canopy height, area, maximum and minimum radii, width and polygon centroid co-ordinates.

An allometric relationship between canopy width and height with diameter at breast height (DBH) was developed using the Forest Research Environmental Database (FRED) containing field measurements for more than 15,000 trees over the entire country. This model allowed the estimation of stem diameters for each individual tree.

Thus, stand information obtained from the FC sub-compartment database was used to generate mean wind conditions inside the forest canopy for each stand in ForestGALES. Tree lists

generated from LiDAR were used to calculate resistive factors at tree level. Finally, edge effects were estimated from the distance between each individual to its neighbours (Figures 3-5).

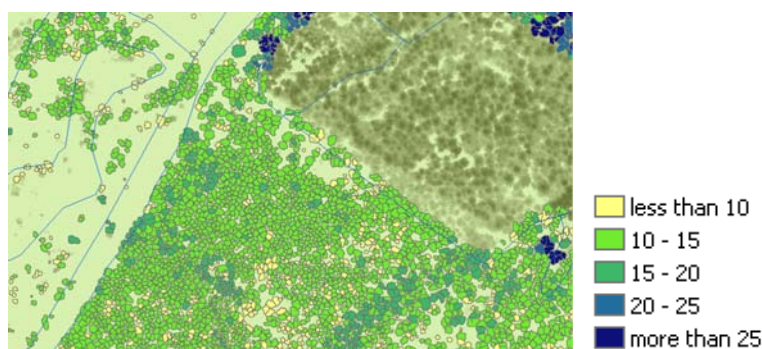


Figure 3. Estimation of individual tree heights (in m).

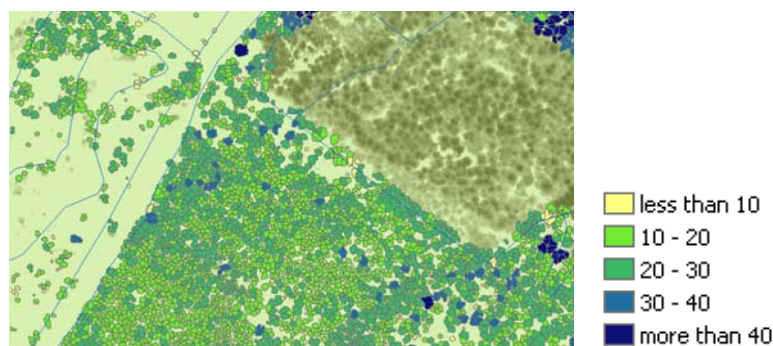


Figure 4. Estimation of individual DBH (in cm).

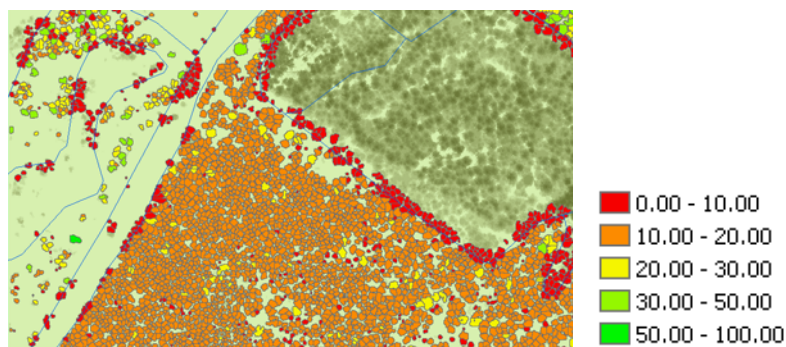


Figure 5. Critical wind speed for overturning each tree (in ms^{-1}). The most stable trees are depicted in green.

5. Results and Discussion

The canopy delineation method produced a better description of the influence of stand structure on the risk of wind damage. This is a substantial improvement compared to the normal way of operating ForestGALES, with just mean stand parameters, because it allows the most vulnerable parts of the stand to be located. This is true for those individuals that are not properly sheltered by neighbours or present lower taper values. In Figure 5, the most vulnerable trees, depicted in red, are around the edges of the stand or inside the forest canopy if their taper relationships are below 80. On the contrary larger canopy dimensions, high taper values and sheltered trees are more stable and require higher critical wind speed values for overturning. Most of those trees, depicted in orange, require wind speeds between 10 and 20 ms^{-1} .

The practical consequences for future management plans will contemplate the choice of thinning practices (normally ruling out thinning), the degree of exposure to certain parts of the stand when clearfelling neighbouring stands, the location of forest roads (normally avoiding the sudden exposure of vulnerable individuals), etc.

The limitations of the ForestGALES method come from the modelling of the adaptation of trees to changing exposure conditions. In this case, most of the trees around the edges of the stands or those trees growing in open stands or in total isolation are already very well adapted to wind conditions. In particular, those individuals that form part of the remnants of the ancient Caledonian pinewood have been growing in isolation for more than 100 years without being affected by windthrow (top left of Figure 5). Therefore, this method seems to be more useful for new plantations (like the one than occupies most of the image) than for isolated individuals. More research will be required in the future for parameterising this adaptation to wind.

Acknowledgements

Many thanks to the Fort Augustus Forest District under whose responsibility Glen Affric lies and to the Interreg North Sea region StormRISK for funding this research.

References

- Forestry Commission, 2008a, Glen Affric. Available online from:
<http://www.forestry.gov.uk/website/wildwoods.nsf/LUWebDocsByKey/ScotlandHighlandNoForestGlenAffric> date accessed: May 2008
- Forestry Commission, 2008b, Improving the ecological content of Forest Plans; A Case Study from Glen Affric, Forestry Commission Scotland, Forest Research, May 2008
- Gardiner, B.A., Suárez, J.C., Achim, A., Hale, S. and Nicholl, B. 2004, ForestGALES 2.0; A PC-based wind risk model for British Forests. Forestry Commission Publications. Edinburgh. ISBN 0855386320. 60pp
- Suárez, J., Garcia, R., Gardiner, B. and Patenaude, G., 2008, The Estimation of Wind Risk in Forests Stands using Airborne Laser Scanning (ALS). *Journal of Forest Planning*, 13, 165-185.

Red-cockaded Woodpecker (*Picoides borealis*) habitat analysis via remote sensing

Scott Tweddale¹, H. Alexis Londo², Joelle M. Carney³, David L. Evans⁴, Scott D. Roberts⁵, Robert C. Parker⁶ and Stephen C. Grado⁷

¹US Army Corps of Engineers, Construction Engineering Research Laboratory,
Scott.A.Tweddale@erdc.usace.army.mil

²Department of Forestry, Mississippi State University, alondo@cfr.msstate.edu

³Department of Forestry, Mississippi State University, jcarney@cfr.msstate.edu

⁴Department of Forestry, Mississippi State University, devans@cfr.msstate.edu

⁵Department of Forestry, Mississippi State University, sroberts@cfr.msstate.edu

⁶Department of Forestry, Mississippi State University, rparker@cfr.msstate.edu

⁷Department of Forestry, Mississippi State University, sgrado@cfr.msstate.edu

Abstract

Multi-spectral imagery and multiple-return light detection and ranging (LIDAR) data were used to assess forest composition and structure for determining habitat suitability for red-cockaded woodpecker (*Picoides borealis*; RCW). Object-oriented classification of the imagery yielded covertype and distinguished between loblolly (*Pinus taeda*) and longleaf (*Pinus palustris*) pine with an accuracy of 80.8% when combining both pine species into one class and 73.7% when classifying pine species separately. The average stem diameter for pine areas was estimated using LiDAR data to identify and estimate individual stem heights. Field-derived height-diameter relationships were used to estimate diameter distribution. LiDAR-estimated mean basal area (BA - square meter/hectare) for canopy trees (14.05 m²/ha) and canopy trees in the top quartile of height (7.03 m²/ha) was not significantly different from field measurements of basal area for all trees (15.6 m²/ha) and top quartile trees (8.05 m²/ha) for 69 plots distributed across three sample areas ($\alpha = 0.05$). The density of midstory/understory hardwoods derived from LIDAR in 4 height strata; 0.5 – 2.1 m, 2.1–4.6 m, 4.6 m to height to live crown (HLC), and canopy, were correlated with field measurements of total cover, resulting in an R² of 0.0, 0.26, 0.36 and 0.60 for each stratum, respectively.

1. Introduction

The endangered red-cockaded woodpecker (*Picoides borealis*; RCW) of the Southern United States is the only species of woodpecker to excavate nest cavities within the trunks of living pine trees (preferably mature longleaf pine (*Pinus palustris*)) old enough to have developed sufficient heartwood (Zwicker and Walters 1999). Midstory and understory vegetation height and composition are important in characterizing the quality of RCW habitat. Rudolph et al. (2002) found that RCWs prefer to forage on trees where there was low density midstory vegetation and that foraging occurred at greater heights above ground on sites with greater midstory heights and densities. Zwicker and Walters (1999) stated RCWs were found to have preferences for pines >23 cm diameter at breast height (dbh) and avoided pines <13 cm dbh.

The basic information required for describing forest type and structure is often expensive and time consuming to collect in the field and requires periodic updates to remain valid (Xiao and McPherson 2004). Detailed identification of individual tree species or species groups has been demonstrated in analysis of digital multi-spectral imagery (Knight et al. 2004; Casey 1999;

Batten and Evans 1997; Hughes et al. 1986). Fusing spectral with light detection and ranging (LiDAR) data can take advantage of the strengths of both sensors for the purpose of improving estimates of forest stand characteristics (Leckie et al. 2003; McCombs et al. 2003).

Modern LiDAR systems generate x,y,z coordinate data from aerial platforms by laser ranging, operating at pulse rates of up to 200 kHz as noted in recent technology specifications from data providers. The spatial resolution, measurement accuracy and spectral response of these systems to vegetation have lead to a significant body of research on the use of LiDAR data for forest assessments. There are a variety of different approaches taken towards tree recognition and height determination (Popescu and Wynne 2004; Brandtberg et al. 2003; Persson et al. 2002; Zimble 2002; Eggleston 2001). The approach used in this project is based on the one described by McCombs et al. (2003). Tree locations with heights derived from LiDAR have a number of possible uses in defining the structural character of a stand, and thus the habitat suitability for different wildlife species (Hinsley et al. 2002; Zimble et al. 2003; Hill et al. 2004).

The overarching goal of this research was to demonstrate the use of high resolution multi-spectral imagery and LiDAR remote sensing technologies to generate a landscape-scale habitat preference variable expressed as geospatial layers available for habitat suitability modeling for the RCW. Specifically, the objectives were to: 1) determine pine and hardwood canopy species composition within forest stands, 2) determine the average size (diameter distribution) of pine dominated stands, and 3) assess the spatial distribution and total cover of midstory/understory hardwoods and other ground cover.

2. Methods

A 30 km² study area was selected for analysis that encompasses three separate forest tracts located along a corridor between 2 populations of RCWs in Hoke County, North Carolina. The tracts include: a private forest land managed partly for pine straw production, a state owned conservation area, and the southwest corner of a federally managed military base. The area is located within the Coastal Plain which is characterized by flat land to gently rolling hills and valleys. The vegetation of this region includes: grassland and early-successional habitats, pine woodland, and river bottoms. Elevation ranges from sea level near the coast to about 183 m in the Sand Hills of the Southern Inner Coastal Plain (Outcalt and Sheffield 1996, North Carolina Geographical Survey 2005).

2.1 Data Acquisition

LiDAR data were acquired July 13, 2005 at a nominal posting density of 4.0 points per m² and recorded as first, only (only 1 return was recorded), second, and third returns in Universal Transverse Mercator (UTM; NAD83, GRS80) x, y, and z coordinates. The data were used to generate canopy and ground elevation raster models at a resolution of 0.5 m for each of the study tracts. These models were used to determine locations of trees and their associated heights for evaluation of stand structure.

Airborne multi-spectral (CIR) imagery was acquired July 26, 2005 at 0.25 m resolution in four spectral channels: blue (450 nm), green (550 nm), red (650 nm), and NIR (850 nm). The individual frames were ortho-rectified to a ground digital elevation model (DEM) and mosaiced for each of the three study area tracts.

Field data were collected in November/December 2006 for training and validation of classifications made with the multi-spectral data and analysis of measurements calculated from the LiDAR data. Coordinates for 69 plot centers were randomly generated and circular plots

were established at these points using a radius 11.3 m and nesting an inner plot of radius 8 m. These plots were distributed across all three study areas and their location recorded with real-time differential GPS. Within the larger plot, total number of stems and total tree height, dbh, location, height to live crown (HLC), crown diameter, and species of each overstory/midstory stem were recorded. Overstory/midstory trees were defined as those trees with dbh greater than 2.54 cm. In the inner nested plot, understory vegetation measurements of total height, location, crown diameter, whether they were single or multiple stems, and species were recorded. The plot data were used to assess the accuracy of individual stem identification with LIDAR and to develop height-diameter relationships for prediction of stem diameters on LiDAR-detected pine trees. The midstory/understory observations were assessed for area coverage and coupled with LiDAR point densities to predict total cover of the vegetation under the main canopy (see section 2.4).

2.2 Canopy Species Classification

Field site inspections indicated that much of the longleaf pine tended to occur as either open-grown individuals or in small groups that could be readily distinguished from other targets. Broadleaf hardwoods tended to occur in clumps either in gaps between pine crowns or in contiguous stands at lower slope positions and along drainages. Because each target of interest occurs as a group of pixels rather than an individual pixel, a segmenting (object-based) image classification rather than pixel-based image classification technique was applied using eCognition 4.0.

The segmentation process was interactively guided to utilize scale, color, and shape parameters to generate image objects that covered individual tree crowns or groups of trees visible in the imagery. Member functions to separate shadow objects from non-shadow objects were instituted first followed by member functions to distinguish between vegetation objects and non-vegetation objects in the non-shadow areas. Member functions to ascertain longleaf, loblolly, hardwood, and other vegetation were subsequently applied to the vegetation objects. All multispectral bands and a Normalized Difference Vegetation Index (NDVI) were input into the classifier.

Classification accuracy was assessed using 552 points, including 109 samples for each of the 3 tree species and 75 samples each for shadow, bare ground, and low vegetation. Classification accuracy was calculated from samples based on commonly reported methods of error matrix calculations (Congalton and Green 1999).

Due to the misregistration between LiDAR and the imagery, the final classification was generalized by calculating the majority class present in an aggregation window size of 6m-by-6m. This facilitated the ability to match vegetation types to LiDAR derived trees. This was an important step in determining the dominant stand type by size class in the RCW habitat evaluation process.

2.3 Pine Size Class Determination

Individual pine tree data from all field plots were analyzed to determine the relationship between tree height and stem diameter using regression procedures. This regression function was then applied to LiDAR-identified trees to estimate a diameter for each stem.

All probable canopy trees were identified and mapped within the three study tracts by use of the LiDAR elevation models and modified procedures adopted from those first described by McCombs et al. (2003). One difference between this procedure and that described in McCombs et al. (2003) was that spectral data were not incorporated into the identification

function due to spatial misregistration between the multispectral and LiDAR data. The second and most important difference is that the new procedure introduces stem density and crown size dependent functionality in tree identification and therefore is more adaptable to ranges of conditions over which the model is applied.

The procedure consisted of two spatial process models which identified and estimated heights of probable tree locations in the main canopy of forest stands using the canopy and bare ground LiDAR surfaces. A smoothing filter was used to eliminate pits where LiDAR points penetrated the main canopy. The model identified clumps of pixels in the canopy height surface that were higher than a set percentage of neighboring pixels. Identification of these clumps of pixels was determined by using a focal rank utility with a variable search filter size keyed to the size of small, medium and large target tree crowns based on relative stem density. The resulting clumps were subjected to a sieving operation based on the estimated smallest tree crown to eliminate small groups of pixels that were not likely trees. The output clumps from this model, as well as the canopy and bare ground surfaces, were passed to the second model, which extracted the location and height value of the highest pixel in each clump as a tree location. A distance function was used to delete trees adjacent to, but shorter than nearby neighbors (probable false tree identified) based on tree height. Short trees were allowed to be closer together than tall trees. These geospatial data were used to develop the size class analysis for all pine areas.

The classification developed from the multi-spectral data was used to label all LiDAR-identified trees as to tree type (pine or hardwood). The diameter at breast height (dbh) to height relationship developed from the field data was applied to all LiDAR-identified pine trees to attribute those tree locations with estimated dbh. The last step was to examine the relative size of LiDAR-identified pines on a unit area basis to generate a geospatial layer of tree sizes grouped by the three diameter size classes: < 24.5 cm, 24.5 to 35 cm, and > 35 cm and pine type (loblolly or longleaf). These three pine size classes, along with evaluations of hardwood competition and midstory/understory total vegetation cover form the basis for identification of either areas currently suitable for RCW habitat or areas that, through proper management, could be made suitable for use by RCWs.

2.4 Midstory/Understory Density Analysis

Density of LIDAR returns in the canopy, > 4.6 m and > HLC, and three understory/midstory strata, 0.5 m to 2.1 m, > 2.1 m to 4.6 m, > 4.6 m and < HLC, were used to estimate understory/midstory vegetation total cover. The ground elevation value was subtracted from each LiDAR return height to determine height above terrain for each LiDAR point. The number of LiDAR returns in each height stratum were summed on 1.0 m grid cells to assign cell values representing return density by stratum. Total LiDAR shot density (first and only returns) was utilized to normalize the point densities at each level for changes in total shot density due to flight line overlap and scan line expansion and compression due to variable flying conditions. The normalized LiDAR density values were compared to field measurements of understory/midstory vegetation cover for all field plots.

An analysis of the field data indicated the mean HLC occurred at 10.5 m for all dominant/co-dominant pine tree observations. However, HLC varies spatially, so a method was developed to characterize the spatial variation in HLC and adjust the threshold that separated understory/midstory and canopy returns accordingly.

The LiDAR detected trees with associated heights were first attributed for the height to base of live crown using a regression relationship derived from field measurements of total height to HLC. The HLC values at tree locations were then spatially “grown” in all horizontal

directions using a focal analysis kernel to create a continuous raster layer that characterized the canopy cutoff height based on the spatial variation of crown base height. This was then used to classify all points as either canopy or subcanopy points. Establishment of a raster surface that characterized spatial variation in HLC allowed the threshold height separating the midstory from canopy to be varied across the terrain rather than using a constant HLC to establish the threshold height. The comparisons of field measures of understory/midstory total cover and LiDAR return density was performed for the modified definition of height classes as described in the previous section.

3. Results and Discussion

3.1 Canopy Species Composition

The overall accuracy of the resulting classification after separating the pine cover type into loblolly and longleaf was 73.73%, with an overall kappa statistic of 0.682. The overall classification accuracy increased to 80.80% when loblolly and longleaf were combined into one pine cover type, and the overall kappa statistic increased to 0.737.

3.2 Pine Size Class Determination

The tree identification model identified most canopy trees and some smaller trees in canopy gaps and open areas. The comparison of dominant/co-dominant plot trees to LiDAR-identified trees revealed some inconsistencies in this procedure's ability to detect all trees. Due to imprecision in the ground based GPS measurements, tree matching of field measured trees was difficult. This was largely attributed to assumed errors in GPS fixes on plot locations and the field measurement errors in tree location establishment relative to these GPS positions.

LiDAR derived trees were matched to the overstory/midstory field measured observations where possible in order to assess the accuracy of the tree finding model. Some adjustment for plot location was necessary to match LiDAR derived trees with field observations. These procedures produced 476 matched trees (65 hardwood and 411 pine) from a possible 730 trees for a detection rate of 65.21%. The privately managed area (71.96% agreement) and state managed tract (65.66% agreement) performed better than the federally managed tract (58.96% agreement). Overall, this is theorized to be due to the variations in growing conditions and site qualities. As expected, LIDAR detection of pine trees (54.0% agreement) proved more successful than hardwood detection (13.0% agreement).

After assessing the performance of the tree finding model using all field measured trees as validation, a subset of the field measured trees was selected in an attempt to identify dominant and co-dominant stems in the canopy. For each plot, the limiting height for the upper quartile (top 25%) was determined and was used to subset the field data by only retaining stems with height in the upper quartile. This subset provided a total of 335 possible trees (70 hardwood and 278 pine) of which 28 hardwood and 195 pine were matched for an agreement of 66.57%. Again the privately managed tract (76.09% agreement) and state managed tract (68.52% agreement) performed better than the federally managed tract (58.52% agreement) (Table 1).

Table 1. Site and overall accuracy results of the pairing of LiDAR derived trees with field observations of trees in the upper quartile of total tree height by plot.

| Privately Owned | | | | | | |
|----------------------------------|-----------------|-------------|-----------------|----------------------|---------------------|--------------|
| Field Samples | | | | LiDAR Samples | | |
| | Hardwood | Pine | Loblolly | Longleaf | | Model |
| Matched | 7 | 63 | 4 | 59 | Matched | 70 |
| Omission | 23 | 21 | 3 | 18 | Commission | 22 |
| Total | 30 | 84 | 7 | 77 | Total | 92 |
| % | | | | | | |
| Matched | 23.33 | 75.00 | 57.14 | 76.62 | % Matched | 76.09 |
| % | | | | | | |
| Omission | 76.67 | 25.00 | 42.86 | 23.38 | % Commission | 23.91 |
| Federally Managed | | | | | | |
| Field Samples | | | | LiDAR Samples | | |
| | Hardwood | Pine | Loblolly | Longleaf | | Model |
| Matched | 16 | 63 | 4 | 59 | Matched | 79 |
| Omission | 15 | 54 | 8 | 44 | Commission | 56 |
| Total | 31 | 117 | 12 | 103 | Total | 135 |
| % | | | | | | |
| Matched | 51.61 | 53.85 | 33.33 | 57.28 | % Matched | 58.52 |
| % | | | | | | |
| Omission | 48.39 | 46.15 | 66.67 | 42.72 | % Commission | 41.48 |
| State Managed | | | | | | |
| Field Samples | | | | LiDAR Samples | | |
| | Hardwood | Pine | Loblolly | Longleaf | | Model |
| Matched | 5 | 69 | 31 | 38 | Matched | 74 |
| Omission | 4 | 8 | 4 | 4 | Commission | 34 |
| Total | 9 | 77 | 35 | 42 | Total | 108 |
| % | | | | | | |
| Matched | 55.56 | 89.61 | 88.57 | 90.48 | % Matched | 68.52 |
| % | | | | | | |
| Omission | 44.44 | 10.39 | 11.43 | 9.52 | % Commission | 31.48 |
| All Three Tracts Combined | | | | | | |
| Field Samples | | | | LiDAR Samples | | |
| | Hardwood | Pine | Loblolly | Longleaf | | Model |
| Matched | 28 | 195 | 39 | 156 | Matched | 223 |
| Omission | 42 | 83 | 15 | 66 | Commission | 112 |
| Total | 70 | 278 | 54 | 222 | Total | 335 |
| % | | | | | | |
| Matched | 40.0 | 70.1 | 72.2 | 70.3 | % Matched | 66.57 |
| % | | | | | | |
| Omission | 60.0 | 29.9 | 27.8 | 29.7 | % Commission | 33.43 |

The tree finding model assigned the LiDAR measured height for each tree location. Using the LiDAR height measurement, it was possible to attribute each tree with an estimate of its diameter using the diameter height relationship developed from all field measured pine:

$$\ln(\text{dbh}) = -0.640235 + 1.0165769 * \ln(\text{Total Height}) \quad (1)$$

with an R^2 of 0.73 and RMSE of 0.26. This equation was developed from 689 intact pine trees greater than 7.62 cm in dbh. After assigning a height and dbh attribute to each LIDAR identified pine stem, LIDAR derived estimates of basal area were determined.

Comparisons between LiDAR derived estimates of height, dbh, and basal area and field measurements of these variables showed height estimates derived from LIDAR to be highly correlated with field measurements ($R^2=0.91$). LIDAR derived estimates of dbh and basal area (BA– square meter per hectare) were not as highly correlated with field measures ($R^2=0.54$ and $R^2=0.46$ respectively). Diameter estimates were based on height-diameter relationships which partially explain variations in diameter as a function of height. Therefore, errors associated with diameter estimates derived from height were compounded when these diameter estimates were used to estimate basal area.

Errors in omission and commission with the tree finding model also contributed to the errors in stem density and BA estimation, although omission and commission errors tended to cancel each other thus resulting in a fairly accurate estimation of stem density. The effects of the omission and commission trees on basal areas estimates were examined by evaluating the average of field measured BA compared to the average of LiDAR estimated BA by site for all overstory/midstory pine trees. These were separated into relevant dbh classes as defined in the RCW recovery guidelines (USFWS 2003). Significant differences were seen between the LiDAR estimates and the field measurements for the privately managed tract and the federally managed tract but across all the sites, there were no significant differences found. The analysis was repeated using only trees in the top quartile of height for each plot. Although significant differences can be seen in some of the diameter classes, field measured mean pine BA was not significantly different from mean LiDAR derived estimates of pine BA for each site separately and for all sites combined (LiDAR estimate = 14.03m²/ha vs. field measurement = 15.59 m²/ha). The errors in BA calculations by diameter classes can be attributed to the effect of the bias in the LiDAR estimated height on the calculated dbh value as well as the inclusion of omitted and committed trees into each diameter class.

3.3 Midstory/Understory Density Analysis

All returns from the LiDAR data were used in the midstory/understory density analysis. For each return, a ground elevation value and a HLC value was determined. The ground elevation value was required to calculate height above ground for each LiDAR return. The ground value was determined by matching the coordinates of each LiDAR return with the ground elevation model. The HLC value for each LiDAR return was determined by matching the coordinates of each LiDAR return with a raster model that characterized the spatial variation in HLC. The raster model of HLC was created using a two step process. First, HLC values for individual stems identified with LIDAR in the raster stem map were estimated using the regression relationship derived from field measurements of total height to HLC:

$$\text{HLC} = 0.69415 * \text{Total Height} - 1.51926 \quad (2)$$

with an R^2 of 0.78 and RMSE of 2.50. Next all tree locations in the raster stem map with total heights 4.6 m or less were removed. Moving a 3.5 m X 3.5 m kernel across the raster stem map, the HLC values estimated for each stem location were extended from the stem location to pixels in close proximity to the stem (areas under canopy and between stems) by assigning the lowest HLC value for any stems in the kernel to all remaining pixels in the kernel. In order to accurately characterize the spatial extent of the canopy while not extending the spatially

variable HLC surface into open areas with no canopy, the algorithm was repeated three times. These values and the ground elevation values were added as attributes for each LiDAR data point.

All LiDAR points were categorized into the height class bins in which they occurred. The height classes used in this portion of the study to create each bin were 0.5 m to 2.1 m, > 2.1 m to 4.6 m, > 4.6 m and < HLC, and > 4.6 m and > HLC. For each height class, the number of returns per 1.0 m pixel were summed and assigned to the pixel value. LiDAR returns below 0.5 m were not included in the analysis to eliminate confusion between near ground and ground returns.

For each field plot and for each height class, the sum of total area coverage for each midstory/understory tree canopy was calculated using the zonal sum statistic. All pixels representing coverage were summed for each plot yielding the zonal sum of coverage by plot. The number of pixels for each field plot was converted to square meters to determine total vegetation cover in each midstory/understory height class. Additionally the sum of the number of LiDAR returns intercepted in the same height class strata was summed for each plot.

The relationship between the sum of area for midstory/understory canopy coverage for each plot and the number of LiDAR interceptions for each height class was positively correlated. The correlations were greatest in the HLC to top of canopy ($R^2=0.60$) and second highest in the > 4.6 m to HLC strata ($R^2=0.36$). On the privately owned sited and the state managed site the second highest stratum (> 4.6 m to HLC) ($R^2=0.82$ - private and $R^2=0.94$ - state) performed better than the higher stratum (HLC to top of canopy) ($R^2=0.68$ - private and $R^2=0.70$ - state) (Table 2).

Table 2. Results of midstory/understory analyses between percent area coverage observed (square meters) and LiDAR interception density for each midstory/understory height class.

| | Privately Owned | | Federally Managed | | State Managed | | All Combined | |
|---------------------------------|-----------------|-------|-------------------|-------|---------------|-------|--------------|-------|
| | R square | RMSE | R square | RMSE | R square | RMSE | R square | RMSE |
| 0.5 to 2.1 meters | 0.04 | 27.42 | 0.06 | 8.51 | 0.26 | 27.42 | 0.00 | 26.37 |
| 2.1 meters to 4.6 meters | 0.31 | 12.38 | 0.65 | 7.86 | 0.20 | 15.64 | 0.26 | 13.02 |
| 4.6 meters to HLC | 0.82 | 6.10 | 0.41 | 33.90 | 0.94 | 6.43 | 0.36 | 37.14 |
| HLC to Canopy Top | 0.68 | 17.10 | 0.47 | 32.24 | 0.70 | 21.05 | 0.60 | 23.94 |

3.4 Landscape-scale Habitat Model

The results from this study outline methods to utilize multi-spectral imagery and LiDAR data to evaluate a series of forest stand parameters associated with RCW habitat that can not be feasibly assessed across extensive landscapes with traditional inventories alone. Not

only do these methods provide detailed habitat information at landscape scales and at reduced costs, but they also provide the capability to assess and monitor RCW habitat suitability in areas that are inaccessible to field surveys, including impact area safety zones on military installations and adjoining private land. Synoptic assessment and monitoring of RCW habitat suitability across a variety of land uses and ownership provides vital information to wildlife management professionals and other stakeholders in efforts to manage and monitor habitat conditions at regional and landscape scales. Information is also valuable to military land managers as they strive to manage pine forest to sustain the primary training mission while also managing forest conditions to maintain or improve habitat suitability for the species.

References

- Batten, S. and D.L. Evans. 1998. Forest stand assessments with high-resolution multispectral frame camera data. In: *Proceedings of the First International Conference on Geospatial Information in Agriculture and Forestry*. Volume I, 1998 June 1-3, Lake Buena Vista, FL. ERIM International, Inc., Ann Arbor, Michigan. p. 95-101.
- Brandtberg, T., T.A. Warner, R.E. Landenberger, J.B. McGraw. 2003. Detection and analysis of individual leaf-off tree crowns in small-footprint, high sampling density LiDAR data from the eastern deciduous forest in North America. *Remote Sensing of Environment* 85(2003), pp. 290-303.
- Casey, W. A. (1999) Forest species group classification using digital frame camera imager, MS Thesis, Mississippi State University, Starkville, MS, 55 p.
- Congalton, R. G. and K. Green. 1999. Assessing the Accuracy of Remotely Sensed Data: Principles and Practices. Lewis, Boca Raton, FL, 137 p.
- Eggleston, N.T. 2001. Tree and Terrain Measurements using Small-footprint Multiple-return Airborne LiDAR Data from Mixed Douglas-fir Forest in the Pacific Northwest. M.S. Thesis. Mississippi State University. 135 p.
- Hill, R.A., S.A. Hinsley, D.L.A. Gaveau and P.E. Bellamy. 2004. Predicting habitat quality of Great Tits (*Parus major*) with airborne laser scanning. *International Journal of Remote Sensing* 25(22): 4851-4855.
- Hinsley, S.A., R.A. Hill, D.L.A. Gaveau, and P.E. Bellamy. 2002. Quantifying woodland structure and habitat quality for birds using airborne laser scanning. *Functional Ecology* 16: 851-857.
- Hughes, J. S., D.L. Evans, and P.Y. Burns. 1986. Identification of two southern pine species in high resolution aerial MSS data. *Photogrammetric Engineering and Remote Sensing* 52(8):1175-1180.
- Knight, T.C., A.W. Ezell, D.R. Shaw, J.D. Byrd, and D.L. Evans. 2004. Identifying loblolly pine and four common competing hardwood species using multispectral reflectance analysis. *Proceedings of the 12th Biennial Southern Silvicultural Conference*. p. 336-342.
- Leckie, D., F. Gougeon, D. Hill, R. Quinn, L. Armstrong, and R. Shreenan. 2003. Combined high-density lidar and multispectral imagery for individual tree crown analysis. *Canadian Journal of Remote Sensing* 29: 633-649.
- McCombs, J., S. D. Roberts, and D. L. Evans. 2003. Influence of fusing lidar and multispectral imagery on remotely sensed estimates of stand density and mean tree height in a managed loblolly pine plantation. *Forest Science* 49(3):457-466.
- North Carolina Geographical Survey 2005. Division of Land Resources. Raleigh, NC <http://www.geology.enr.state.nc.us/Mineral%20resources/mineralresources.html>.
- Outcalt, K., and R. Sheffield. 1996. The longleaf pine forest: trends and current conditions, Resour. Bull. SRS-9. Asheville, NC: U.S. Department of Agriculture Forest Service. Southern Research Station. 1-23.
- Persson, A., J. Holmgren, and U. Söderman. 2002. Detecting and measuring individual tree using an airborne laser scanner. *Photogrammetric Engineering and Remote Sensing*

- 68(9):925-932.
- Popescu, S. C. and R. H. Wynne (2004). "Seeing the trees in the forest: Using lidar and multispectral data fusion with local filtering and variable window size for estimating tree height." *Photogrammetric Engineering and Remote Sensing* 70(5): 589-604.
- Rudolph, D., R. Conner, and R. Schaefer. 2002. Red-cockaded Woodpecker foraging behavior in relation to midstory vegetation. *Wilson Bulletin* 114(2):235-242.
- U.S. Fish and Wildlife Service. 2003. Red-cockaded Woodpecker (*Picoides borealis*) Recovery Plan: *Second Revision*. U.S. Fish and Wildlife Service, Atlanta, Georgia, USA.
- Xiao, Q., and E. McPherson. 2004. Using AVIRIS data and multiple-masking techniques to map urban forest tree species. *International Journal of Remote Sensing* 25(24):5637-5654.
- Zimble, D. 2002. Characterizing vertical forest structure using small-footprint multi-return airborne LiDAR. M.S. Thesis, Mississippi State University, Department of Forestry. 39 p.
- Zimble, D., D.L. Evans, G. Carlson, R. Parker, S.C. Grado, and P. Gerard. 2003. Characterizing vertical forest structure using small-footprint airborne lidar. *Remote Sensing of the Environment* 87:171-182.
- Zwicker, S., and J. Walters. 1999. Selection of pines for foraging by Red-Cockaded Woodpeckers. *Journal of Wildlife Management* 63:843-852.

Lidar and true-orthorectification of infrared aerial imagery of high *Pinus sylvestris* forest in mountainous relief

Rubén Valbuena¹, Tomás Fernández de Sevilla², Francisco Mauro¹, Cristina Pascual¹, Antonio García-Abril¹, Susana Martín¹ & José Antonio Manzanera¹

¹ Technical University of Madrid (UPM). Research Group for Sustainable Management (Tecnatura). Forestry Faculty. Ciudad Universitaria s/n. 28040 Madrid. Spain.

r.valbuena@upm.es

² Stereocarto S.L. Paseo de la Habana 200. 28036 Madrid. Spain.

tfsevilla@stereocarto.com

Abstract

The combination of various data sources has been demonstrated to be more effective than using them separately. Information retrieval is significantly improved by synergies between laser scanner and optical imagery. Digital photography relies on traditional orthorectification methods in order to accomplish an accurate spatial correspondence with Lidar products. We investigated combinatorial techniques in a high pine forest situated in mountainous relief in the Guadarrama Range (Spain). Results have shown critical inaccuracies in the integration of these data, even when obtained simultaneously. We propose the use of Lidar-derived DSM in the process of orthorectification of aerial imagery. We hypothesised that the use of true-orthophoto techniques for improving the planimetric accuracy of VHR can be reliable for forestry applications. The methodology slightly improved the geometrical results obtained, though radiometric results might be useless. Consequently, other possible solutions are also discussed.

Keywords: LiDAR, color infrared, true-orthorectification, forest management.

1. Introduction

Very High Resolution (VHR) optical imagery and Lidar have synergic capabilities for providing reliable data in operational forestry. For this reason, the integration of these data allows a cost-effective combination of techniques. Methodologies can benefit from the possibilities of both sensors: the potential of VHR imagery for thematic classification and index calculation (St-Onge and Cavayas 1997), and the accuracy of tree height information retrieved from Lidar (Lefsky *et al.* 1999). Extraction of Digital Elevation Models (DEM) from simultaneous Lidar can improve the automation of VHR imagery orthorectification. Estimation of forest parameters from Lidar can also be assisted by VHR. For instance, individual trees can be recognized and segmented from VHR imagery and their height and crown shape properties calculated from the Lidar point cloud (Leckie *et al.* 2005; Suárez *et al.* 2005).

Lidar can be used for improving traditional photogrammetric methods. It has been demonstrated that tree height retrieved from Lidar is more reliable than photogrammetry, since shade often obscures bare soil on aerial images (Hyypä *et al.* 2008). Correlation of image pairs for mass point detection is time-consuming because it requires the quality control of a technician. Thus, correlation has been demonstrated inefficient in forest areas with high dense canopy, though other automated matching techniques are being developed (Zhang and Gruen 2004). For this reason, traditional photogrammetry has been demonstrated insufficient for large scale forest monitoring (St-Onge and Achaichia 2001). Waser *et al.* (2008) used Lidar data for normalizing a DEM retrieved from correlation of Colour Infra Red (CIR) aerial images.

In order to integrate the information derived from diverse sensors, a correct adjustment of the spatial features obtained should be achieved (Honkavaara *et al.* 2006). The precision offered by both VHR and Lidar has to be accompanied by a proper accuracy assessment in order to be reliable for forest applications (Hyypä *et al.* 2000). Otherwise, the integration of these data cannot be properly accomplished, and such synergies will not emphasize meaningful *indices*, classifications or forest stand parameters. Some authors have encountered difficulties when combining both sources since the accuracy of Lidar is highly superior compared to aerial imagery (Packalen and Maltamo 2007). While a Lidar point cloud is orthogonally projected, VHR imagery has to be orthorectified.

The process for orthorectifying imagery produces a metrical scale document in a homogeneous orthogonal projection. VHR aerial photographs acquired on-flight with a matricial sensor present a pronounced conical perspective depending on the flight height and the Field of View (FOV). In order to change from conical to orthogonal projection and formulate the topographic correction, internal and external image orientation and a DEM are required (Baltsavias and Käser 1998). Two types of corrections are applied during the orthorectification process of an aerial image: the displacement due to the conic perspective of the original photography and the topography correction. The first component depends on the focal length of the image, radial distance from the projection centre to the object and the height of the vertical element over a given *datum*. The topographic correction is carried out by using the DEM.

Displacement due to the different height of the elements is therefore affected by the DEM utilized. A complete and exact correction is achieved when a rigorous model is used; but the object shift is not accurately corrected if the model is non-rigorous. Most frequently, the bare earth is used as reference surface, by means of a Digital Terrain Model (DTM). As a result, elements situated above the ground surface are located in a wrong position. In the traditional process of orthorectification of aerial imagery of forest areas, tree presence is consequently not modelled in the DEM. For this reason, trees might show in the orthophoto leaning over canopy gaps and tree tops are moved from their true location (see Figure 1; note that $a' \neq a''$). In some areas, the usefulness of imagery can be severely affected. Overlaying Lidar and VHR products can be ineffective if, for example, a tree crown is located in the orthophoto where bare soil is shown in a Canopy Height Digital Model (CHDM). In this way, matching different sources of information can be in some cases impossible.

A theoretical orthoimage of ideally straight trees should locate tree tops in the same position where tree bases are; usually, trees appear to lean instead. Lean observed in aerial picture can be caused by many factors:

1. the height of the tree;
2. DEM slope in radial direction outwards from the centre of the projection;
3. natural lean of tree trunks.

Factors 1 and 2 are caused by the use of a non-rigorous DEM for orthorectifying. The latter does not depend on remote sensing procedures, but is the cause of a large amount of variability which should be distinguished from the previous.

Significant displacement of tree tops might be observed when the trees are very tall. This lean can be determined as a planimetric distance between where the tree top should be and where it actually appears, in meters outwards from the centre of projection. Lean due to tree height can be theoretically calculated as follows (*formulae* adapted from Molina 2008):

$$dp = h \cdot \operatorname{tg} \alpha \quad (1)$$

This illustrates how the planimetric displacement (dp) of a feature above the DEM used in the

orthorectification is a function of the height of the feature from the DEM (h), and the FOV (α). Lean is therefore depending on the height of the elements in the picture, but also on camera and flight parameters: focal length, height of flight and maximum Euclidean distance from the centre of projection.

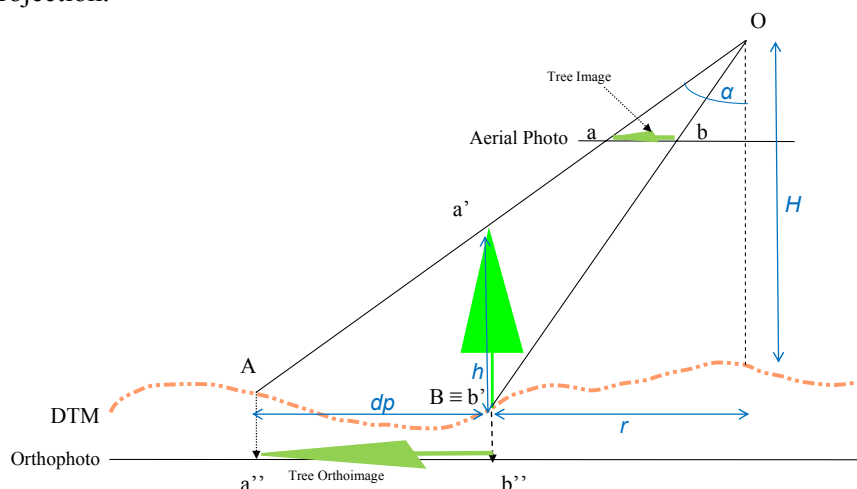


Figure 1: Lean caused by tree height when orthorectifying with a Digital Terrain Model (DTM).

Equation (1) assumes flat terrain, but object lean observed in the image also depends on the slope (s) of the DEM used for the correction. Objects upslope from the nadir point appear less leaned than calculated in (1), while those downslope appear more leaned (see Figure 2). This increase or decrease of the observed lean can be added to (1) as a slope component of lean (adapted from Molina 2008):

$$\Delta p = - dp \cdot k_s \quad (2)$$

$$k_s = \text{tg } s / (\text{tg } s + \text{tg } \alpha) \quad (3)$$

Hence, displacement is augmented or reduced (Δp) depending on the slope at the position of the tree. The Δp component will be positive for upslope positions, while negative for elements situated downslope. Its value is dependent on the slope correction factor (k_s) calculated in (3).

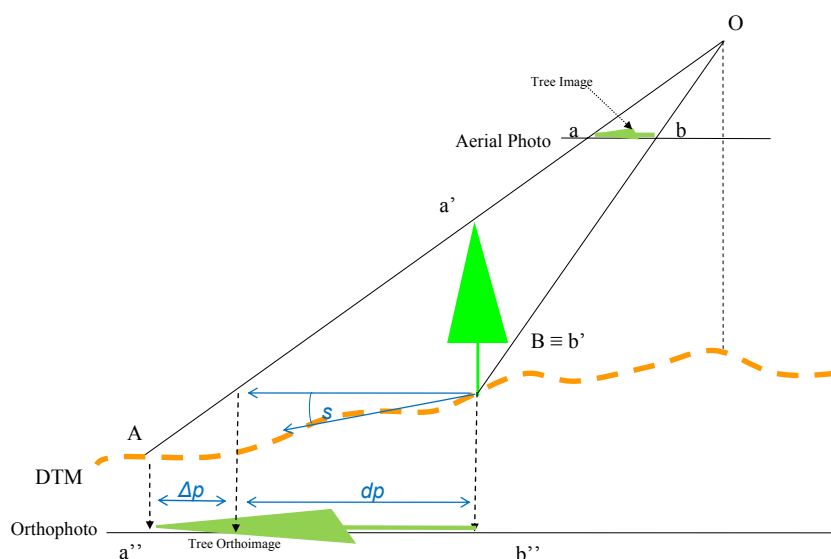


Figure 2: Lean increase due to a downwards slope of the Digital terrain Model (DTM).

Another source causing lean observed in pictures is the real natural lean of tree trunks. This can become significant in a high multi-structured forest. The topography of the study area can make tree trunks to be leaned systematically in a certain forest stand. The soil conditions and the relative position of trees themselves are factors affecting random trunk leaning. Random and systematic behaviour of variables describing image lean should therefore be analysed in forest environments.

Lean problems can be solved by generating a so-called true-orthophoto. Orthorectification of aerial photography over urban areas usually rely on these techniques, since they are highly necessary for avoiding occluded areas when features represented are significantly taller than wider, as buildings are (Schickler and Thorpe, 1998). However, studies using true-orthophoto in forested areas and natural landscapes are scarce (Küchler *et al.* 2004; Waser *et al.* 2008). We hypothesised that employing true-orthophoto when integrating Lidar and digital camera in forest stands with presence of tall trees will improve the results obtained with traditional orthophoto.

Generation of true-orthophoto is based on the use of a Digital Surface Model (DSM) instead of a DTM for correcting the planimetric position of each pixel. When the orthorectifying process is made using a DSM, every pixel of the resulting orthoimagery has the digital number captured from its real point of view from the sensor. Then, every element is located at its truly orthogonal position (Figure 3). By doing this, whenever a tree crown is repositioned properly, a blind spot occurs. The mosaicking procedure fills these hidden areas from another picture. An analysis of visibility defines the quality of each pixel from the slope relative to the viewing angle, the distance to the centre of projection and the distance to a blind spot. Flight parameters are therefore critical in improving the quality of this process, since better overlapping increases the quality of every pixel and reduces the possibilities of finding areas completely hidden in all pictures (Shiren *et al.* 1989).

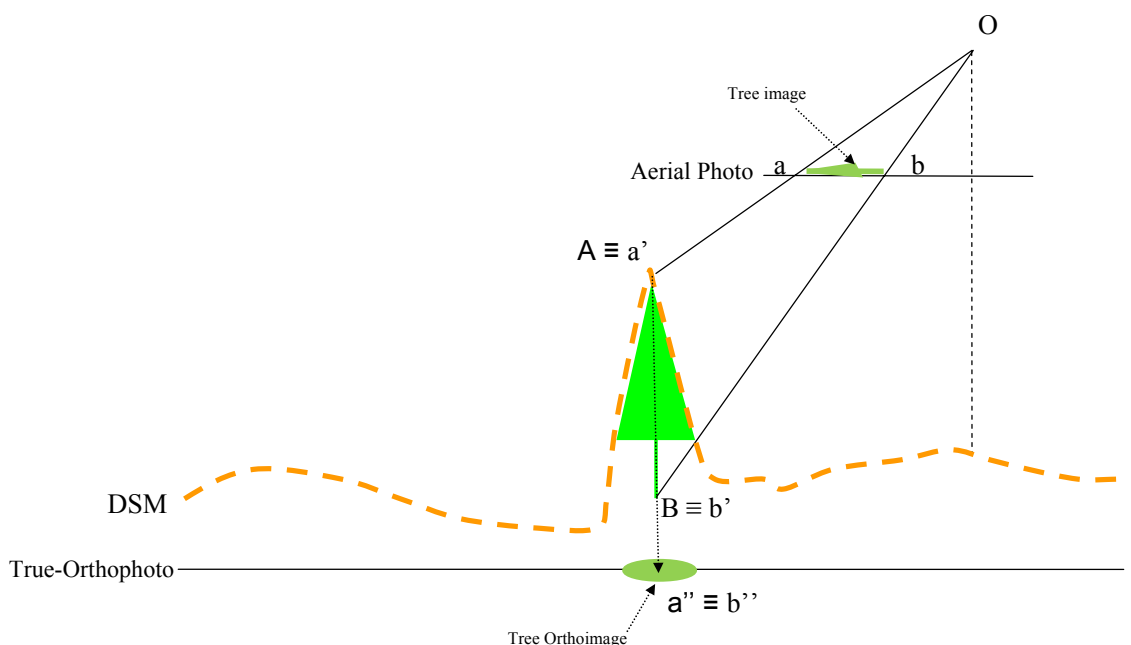


Figure 3: Lean correction by using a Digital Surface Model (DSM) in the orthorectification process.

A comparison of Figure 1 and Figure 3 illustrates how the tree top (a'') is located in the orthoimage in a wrong position when using the DTM, but it is spatially coincident with the tree base when using an unrealistically perfect DSM.

2. Material and Methods

2.1 Study area

The study area includes a portion (latitude, 40°53'31" - 41°15'22"N; longitude, 3°59'33" - 4°17'34"W) of the state-owned Scots pine (*Pinus sylvestris* L.) forest of Valsain, situated in the province of Segovia (Spain). The landscape of the site is characterized by steep slopes, ranging between 10-30%, since it is located in the Central Mountain Range, with elevations between 1265 and 2015 m above sea level in Alicante, Spain. The research has been carried out in a dense forest compartment with tall trees and pronounced relief, factors which are still challenging for assessing Lidar accuracy (Hyypä *et al.* 2008), and which complicate the orthorectification process as well.

2.2 Airborne sensors and dataset

Stereocarto S.L. captured Lidar and imagery simultaneously using the same airborne platform. Both sensors were carried by a CESSNA 404-Titan with double photogrammetric window. The flight was performed on September 10, 2006 over a surface area of approximately 800 ha. Flight height was 1500 m above ground level.

Lidar scan was made using an ALS50-II sensor from Leica Geosystems, Switzerland. Laser pulse rate was 55 kHz measuring an average of two points per m², with footprint diameters of 0.51 m at nadir. A FOV of 25° rendered a 665 m scan width with 40% side lap. Airplane ground speed was 140 knots. A value of intensity was captured for each one of a maximum of four discrete returns per pulse. Recording height accuracy was 0.15 m.

Panchromatic, RGB colour, and near infrared images were captured using a DMC camera from Zeiss-Intergraph, Germany. DCM camera has a focal length of 120 mm with a system of frame Charge-Coupled Device (CCD) array sensors. Forward overlap was 60%, while sidelap was 40%. The result was three strips with 55 VHR images of 15 cm ground sample distance and 12 bit of radiometric resolution.

The trajectory and altitude of each sensor was calculated independently using different Global Positioning and Inertial Navigation Systems (GPS/INS). The differential GPS solution was obtained using three reference stations: SGVA (designated by Technological Agricultural Institute of Castilla y León Region (ITACYL); latitude: 40° 56' 57,44"N; longitude: 4° 7' 13,21"W), YEBE (designated by Spanish National Geographic Institute (IGN) network; latitude: 40° 31' 29,63"N; longitude: 3° 5' 19,06"W), and MAD2 (designated by NASA worldwide network; latitude: 40° 25' 38,03"N; longitude: 4° 14' 57,08"W). The final positioning trajectory solution was combined from these three reference stations. The spatial reference system was the European Terrestrial Reference System 1989 (ETRS89). Planimetric coordinates were represented using the Universal Transverse Mercator (UTM) projection, zone 30 north. The altimetric *datum* was the mean sea level in Alicante, Spain. Elevations were described using orthometric altitudes. The Ibergo95 geoid model was used to transform from elevations over GRS80 ellipsoid to the geoid.

Lidar elevation differences between overlap strips were under sensor tolerance, so that the point cloud was georeferenced without additional adjustments. The external orientation parameters from the images were obtained using a combined method of direct georeference and aerotriangulation using seven control points. Finally, the consistency of both datasets was checked using stereoscopic methods, by viewing the point cloud superimposed over the photogrammetric models of image pairs.

2.3 Lidar products

Prior to obtaining state-of-the-art primary Lidar products such as DTM, DSM and CHDM, the raw cloud point was processed using Terrascan software from Terrasolid, Finland. The first classification step was to remove low and air points. Then, ground points were classified by using the geometric conditions of maximum terrain slope of 75°, iteration angle of 12° and iteration distance of two metres. A filter was applied in search for building points (Axelsson 1999), as some small houses were located in the study area. Finally, unclassified points were considered as vegetation class. Quality control of classification was made by an operator using the imagery as a reference data layer.

A one metre regular grid DTM was obtained using a triangulated model from the ground class Lidar points. Intermediate points and last of many returns within 1x1 m cell were removed from vegetation class as a previous step for DSM generation. DSM was then obtained using a triangulated model from ground class points and the remaining vegetation class points. CHDM was finally obtained subtracting DSM minus DTM models.

2.4 Very High Resolution orthoimagery

Traditional orthophoto was obtained from RGB and CIR images by using the Lidar DTM. Co-linearity method was applied for correcting the position. The digital number of each 15 cm pixel was assigned with a bilinear resampling method. The seam line of a final mosaicked product was optimized by selecting the most nadir area from each photograph.

True-orthofoto was obtained as well from RGB and CIR images by using the Lidar DSM. Besides the topography correction, visibility algorithm was also utilised for detecting occluded areas. Nearest neighbour was used for resampling. Mosaicking was performed for the most nadir areas and for occluded areas too. In the true-orthophoto, no digital number was assigned for pixels not showing information from any of the images, so that they remained as no-data gaps.

2.5 Reference data

A total of six rectangular inventory plots of 40x60 meters were placed in the study area, measuring every tree height with a laser vertex hypsometer. We placed 2-3 landmarks so that every trunk in the plot was able to be aimed at with a Total Station NIKON DTM-332 from Trimble, California. To avoid the obstruction of vegetation, phase differential GPS measurements were taken in October 10, 2007 at nearby positions in absence of canopy cover. Simultaneous GPS observations were also taken at a ground control station in Coberteros (designated by IGN; latitude: 40°42'5,08"N; longitude: 3°57'23,67"W) for differential correction. Static observations were taken with HiperPro receiver from Topcon Positioning Systems Inc., California, and their own software was used for post-processing. The position of tree trunks was finally deducted from a polygonal itinerary between the landmarks and the dGPS occupations. We applied the same transformations described for flight dataset, assuring a proper equivalence. The uncertainty of these measurements was demonstrated to be under a tolerance of ± 0.30 m in all cases.

3. Results

A comparison of the Lidar-derived products and the field reference information showed significant correspondences. A pair-wise analysis showed an average difference of 0 ± 0.15 m between the altimetry of the reference dataset and the elevations of the DTM product; the accuracy of georeferencing processes and the precision of the sensor were therefore confirmed.

When validating the inventory, CHDM tended to underestimate tree height, since the presence of outliers showed few planimetric mismatches in a discrete tree-by-tree comparison without any correlation algorithm for spatial matching. This is explained because the real orthogonal projection on the ground of some tree tops is not coincident with the tree base, due to the presence of naturally leaned trunks in the study area. This leads to a high presence of random noise in every planimetric tree-by-tree analysis. Nevertheless, no systematic lean tendencies were found in the study area.

Contrary to the other two information datasets, orthorectified aerial imagery showed important displacements of planimetric information. This led to significant mismatching of Lidar products with imagery products, *i.e.* indices, classifications and photo-interpreted features. This was of critical importance, since integration of sensors was therefore unsuccessful in many cases. In order to distinguish displacements caused by random tree trunk lean from picture lean, the spatial distribution of planimetric errors was compared to the theoretical lean of trees calculated from (1) and (2). According to the parameters shown in Figure 1, the Euclidean distance to the centre of the projection (r) and the flight (H) and tree (h) heights; equation (1) can be reformulated as:

$$dp = h \cdot r / (H - h) \tag{4}$$

The theoretical spatial distribution of lean errors was calculated (see Figure 4) for every position in the study area by using the calculated CHDM elevation as tree height in the equation (4), and the DTM for deducing the terrain slope at each pixel in radial direction outwards from the projection centre in (2) and (3). Real displacements were measured as the planimetric Euclidean distance between the tree base reference data and the tree top interpreted at the orthoimage. Observed lean showed a significant correlation with theoretical lean, presenting the same spatial distribution pattern. This demonstrated that the mismatching was provoked by the perspective itself, and not just by randomly distributed natural trunk lean.

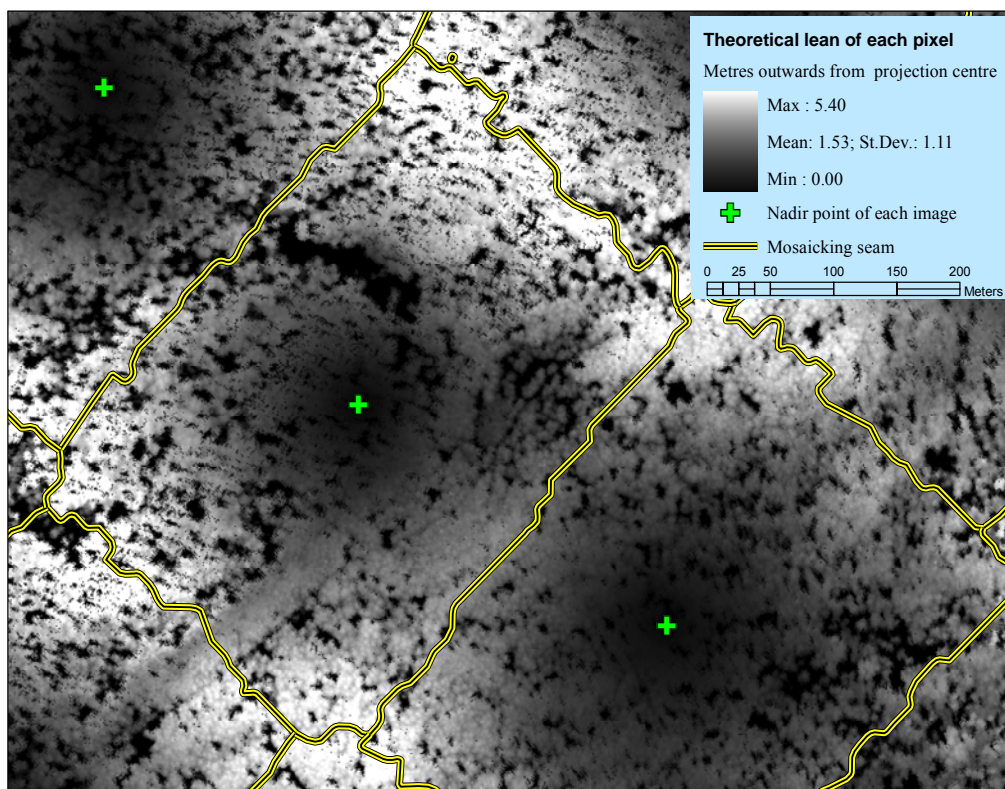


Figure 4: Raster model showing the spatial pattern distribution of lean suffered by each pixel.

Tree tops observed from true-orthophotography were also compared with the reference position of their corresponding base. Planimetric shift was significantly reduced compared to traditional orthophoto. True-orthoimagery was verified as a reliable methodology for improving geometrical accuracy of aerial information, as shown in Figure 5. Errors were distributed randomly and showed no spatial pattern, so that they can be assumed to be dependent on other factors than the Euclidean distance to the projection centre of the picture. However, individual tree shapes were found distorted in many cases, so that true-imagery is less practicable for photo-interpretation purposes than traditional DTM-derived orthophoto.

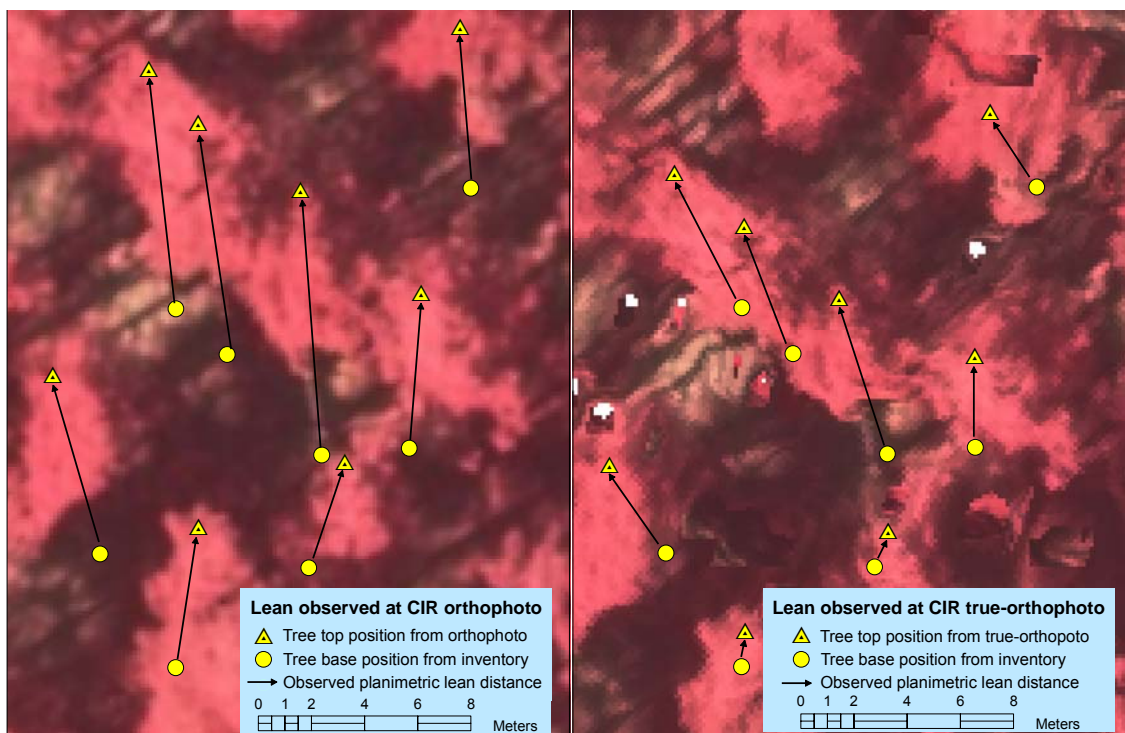


Figure 5: Comparison of mismatching between planimetric positions of tree base measured in the field and tree top position interpreted from false colour infrared orthophoto (left) and true-orthophoto (right).

4. Discussion

Simultaneous acquisition of Lidar in a photogrammetric flight notably increases the automation of the procedures and reduces processing time and costs for orthoimagery production. Lidar obtains mass points automatically, therefore reducing the need for quality control and minimising error occurrence. Thus, traditional photogrammetric correlation was still challenging in densely forested canopies, so Lidar introduced an exceptional advantage concerning DEM calculation from photogrammetric flight. VHR imagery needs to rely on precise data that only Lidar can nowadays offer.

In order to integrate information simultaneously obtained from different sensors, a proper geometric correspondence between them has to be accomplished. Terrain slope and tree height were deemed important factors regarding the difficulties in achieving the orthogonal location of features in aerial imagery. It was demonstrated that lean of tree tops in orthoimagery was caused by the presence of tall trees and steep terrain.

True-orthorectification of aerial imagery has significantly improved the planimetric adjustment

of tree tops. Nevertheless, radiometric properties have suffered numerous deficiencies. The consistency and usefulness of the radiometric information in true-orthophotos is yet to be tested. Thus, DSM-derived orthophoto contained numerous artefacts and no-data gaps, due to the visibility analysis' process. Photo-interpretation of features is more difficult than those in traditional orthophoto. Isolated tree crowns showed more deformities than stands presenting continuous canopies; these results are coherent with those obtained by other authors (Leckie *et al.* 2003). Distortion of tree crown may reduce the possibilities of any analysis of texture or crown shape.

Alternative possibilities for solving lean problems in future flights over high canopies in mountainous areas concern changes in:

1. the digital camera;
2. flight parameters;
3. alternatives for orthophoto calculation; as those discussed in this article.

The displacement of the vertical objects in the photographic images can be reduced by using larger focal length, or using linear array sensors with pushbroom technology instead of CCD array ones, where vertical displacement is bidirectional instead of radial. Linear array would accomplish lean errors to be distributed transversally to the flight line direction. Flight parameters should be modified by increasing the sidelap in order to optimise mosaicking procedures. Changes in flight height are not considered since spatial resolution would be reduced.

Acknowledgements

Authors want to thank the Spanish *Ministerio de Industria, Turismo y Comercio* (MITYC) who funded this study within the research project "LINHE: Desarrollo de nuevos protocolos de integración de sensores LiDAR, cámara digital, IR cercano e hiperespectral" (project: FIT-330221-2006-10). Partner institutions of LINHE project are: Stereocarto S.L.; GMV Aerospace and Defence S.A.; TRAGSA; University of Córdoba (UCO); and Technical University of Madrid (UPM).

References

- Axelsson, P. 1999. Processing of laser scanner data – algorithms and applications. *ISPRS Journal of Photogrammetry and Remote Sensing*, 54, 138-147.
- Baltsavias, E. and Käser, Ch. 1998. DTM and orthoimage generation — a thorough analysis and comparison of four digital photogrammetric systems. *Int. Arch. Photogramm. Remote Sens.* 32 (4), 42–51.
- Honkavaara, E., Ahokas, E., Hyypä, J., Jaakkola, J., Kaartinen, H., Kuitinen, R., Markelin, L. and Nurminen, K. 2006. Geometric test field calibration of digital photogrammetric sensors. *ISPRS Journal of Photogrammetry and Remote Sensing*, 60 (6), 387-399.
- Hyypä, J., Hyypä, H., Inkinen, M., Engdahl, M., Linko, S. and Yi-Hong, Z. 2000. Accuracy comparison of various remote sensing data sources in the retrieval of forest stand attributes. *Forest Ecology and Management*, 128, 109–120.
- Hyypä, J., Hyypä, H., Leckie, D., Gougeon, F., Yu, X. and Maltamo, M., 2008. Review of methods of small-footprint airborne laser scanning for extracting forest inventory data in boreal forests. *International Journal of Remote Sensing*, 29, 1339-1366.
- Küchler, M., Ecker, K., Feldmeyer-Christe, E., Graf, U., Küchler, H. and Waser, L.T. 2004. Combining remotely sensed spectral data and digital surface models for fine-scale modelling of mire ecosystems. *Community Ecology*, 5(1), 55–68.

- Leckie, D.G., Gougeon, F.A., Walsworth, N. and Paradine, D. 2003 Stand delineation and composition estimation using semi-automated individual tree crown analysis. *Remote Sensing of Environment*, 85 (3), 355-369.
- Leckie, D.G., Gougeon, F.A., Tinis, S., Nelson, T., Burnett, C.N. and Paradine, D. 2005 Automated tree recognition in old growth conifer stands with high resolution digital imagery. *Remote Sensing of Environment*, 94 (3), 311-326.
- Lefsky, M.A., Cohen, W.C., Acker, S.A., Parker, G.G., Spies T.A. and Harding, D. 1999. Lidar remote sensing of the canopy structure and biophysical properties of douglas-fir western hemlock forests. *Remote Sensing of Environment*. 70, 339–361.
- Molina, S. 2008. Departamento de fotogrametría de TRAGSATEC. Jornadas Técnicas del Plan Nacional de Ortofotografía.
- Packalen, P. and Maltamo, M. 2007. The k-MSN method for the prediction of species-specific stand attributes using airborne laser scanning and aerial photographs, *Remote Sensing of Environment*, 109 (3), 328-341.
- Schickler, W. and Thorpe, A 1998. Operational procedure for automatic true orthophoto generation. *Int. Arch. Photogramm. Remote Sens.* 32 (4), 527–532.
- Shiren, Y., Li, L. and Peng, G., 1989. Two-dimensional seam-point searching in digital image mosaicking. *Photogramm. Eng. Remote Sens.* 55 (1), 49–53.
- St-Onge, B.A. and Cavayas, F. 1997. Automated forest structure mapping from high resolution imagery based on directional semivariogram estimates. *Remote Sensing of Environment*, 61 (1), 82-95.
- St-Onge, A. and Achaichia, N. 2001. Measuring forest canopy height using a combination of LiDAR and aerial photography data. *International Archives of Photogrammetry and Remote Sensing*, XXXIV-3/W4, 131–137.
- Suárez, J., Ontiveros, C., Smith, S. and Snape S. 2005. Use of airborne LiDAR and aerial photography in the estimation of individual tree heights in forestry. *Computers & Geosciences*, 31, 253–262.
- Waser, L.T., Baltsavias, E., Eckera, K., Eisenbeiss, H., Feldmeyer-Christe, E.H., Ginzler, C., Küchler, M. and Zhang L. 2008. Assessing changes of forest area and shrub encroachment in a mire ecosystem using digital surface models and CIR aerial images. *Remote Sensing of Environment*, 112, 1956–1968.
- Zhang, L. and Gruen, A. 2004. Automatic DSM Generation from linear array imagery data. *International archives of photogrammetry, Remote Sensing and Spatial Information Sciences*, 35 (B3), 128–133.

Comparison of different Laser-based methods to measure stem diameter

Mikko Vastaranta¹, Timo Melkas⁴, Markus Holopainen¹, Harri Kaartinen², Juha Hyypä² & Hannu Hyypä³

¹University of Helsinki, Department of Forest Resource Management, Finland, mikko.vastaranta@helsinki.fi, markus.holopainen@helsinki.fi

²Finnish Geodetic Institute, harri.kaartinen@fgi.fi, juha.hyypa@fgi.fi

³Helsinki University of Technology, Research Institute of Modeling and Measuring for the Built Environment, Finland, hannu.hyypa@hut.fi

⁴Metsäteho Ltd, timo.melkas@metsateho.fi

Abstract

The Terrestrial Laser Scanner (TLS), the Laser-camera and the Laser-relascope were used to measure tree diameter at breast height (dbh) in boreal forest conditions. Reference diameters were measured with steel calipers, which are the most common measuring equipments for diameter. The data consisted of 122 trees from six forest sample plots in Nuuksio National Park and the Saunalahti area in southern Finland.

The results showed that the TLS and the Laser-camera are about as accurate as traditional means in diameter measurements, where as using Laser-relascope the same accuracy was not obtained. The standard errors for the TLS, Laser-camera and Laser-relascope were 8.3 mm (4.5%), 8.5 mm (4.9%) and 17.5 mm (10.1%), respectively. The bias in the TLS measurements was only 0.5 mm (0.3%) and in the Laser-camera measurements 0.6 mm (0.3%). The Laser-relascope's bias was overall 9.1 mm (5.2%).

The TLS and Laser-camera were determined to be accurate methods of measuring dbh. These methods also enable the measurement of other characteristics, such as diameters at multiple heights, which can improve volume or tree quality estimates. These possibilities need further research.

Keywords: Forest mensuration; stem diameter; accuracy; Terrestrial Laser Scanning; laser

1 Introduction

The most important variable in forest management planning at a single tree level is stem diameter at breast height (dbh). With dbh, tree height and tree species, all the important stand characteristics, such as growing stock and basal area, can be estimated. Forest management planning will increasingly utilize more remote sensing methods due to their improved cost-efficiency and the enhanced accuracy of some new remote sensing methods, such as airborne laser scanning (ALS). In Finland, the accuracy of the stand characteristics estimated by ALS is as accurate as the stand characteristics assessed by the traditional ocular field inventory (Suvanto et al. 2005). Still, a single tree's dbh cannot be measured directly by ALS data and is estimated based on laser-derived tree height and other laser information, such as crown size. Such estimates needs proper reference data to decrease the bias in it. Thus, there is also need to develop improved field techniques to measure stem diameters and stem volume cost-effectively and reliably.

Traditional means of field measurements are labour intensive and time consuming. Additional measurements, such as diameter measurements from multiple heights, would enhance the accuracy of volume estimation in preharvest measurements or of modelling growth in forest management planning, but such additional field measurements have in practise been limited due to a lack of efficient means. There are also many other exploitable stand or tree characteristics, where there exist no effective traditional means to measure. These characteristics include e.g. biomass, leaf area, crown characteristics or quality of stem. The development of field measuring devices has not been very intensive in recent years, although there have been some attempts to develop and test new efficient and easier to use devices for forest measurements (e.g. Carr 1992; Carr 1996; Williams et al. 1999; Kalliovirta et al. 2005; Varjo et al. 2006), but these new devices are not yet widely used. Developed new devices have been inaccurate, expensive or hard to use in the field. The reasons for the slow development of easy-to-use field measurements are e.g. variable forest environments, which are challenging for all measuring devices, and a limited market. Field measuring devices in the future must be precise, quick, user friendly and water- and shockproof. Furthermore, the device should enable the efficient measurement of all the basic tree characteristics from the centre of a sample plot, and the price of the device should be reasonable (Kalliovirta et al. 2005).

As stated earlier, there is an urgent need for development of new, terrestrial remote sensing-based techniques, which can produce diameter-type information not achievable by means of airborne remote sensing. Such new methods should be preferably more cost-efficient and accurate than traditional field measurements. New laser-based techniques have showed some promises for that kind of use (e.g. Danson et al. 2007; Hopkinson et al. 2004; Watt and Donoghue 2004; Kalliovirta et al. 2005). Terrestrial laser scanning is an efficient and objective option to collect accurate field data. It uses the same range-finding measurement technologies as ALS to derive the 3D position of objects within the scanner field of view by collecting 3D data clouds of several million data points in a few minutes. Applications of terrestrial laser scanning for forestry have not been widely studied, although its potential for forest related measurements have been more understood in recent years. Watt and Donoghue (2005) scanned two forest sample plots with a terrestrial laser scanner (TLS) and compared the results to field measurements. The results demonstrated that accurate measurements of tree diameters can be derived directly from the laser scan point cloud return in instances where the sensor's view of the tree is not obstructed. Hopkinson et al. (2004) also accurately measured stem location, tree height and density from the TLS data. Danson et al. (2007) studied with promising results how the forest canopy gap fraction could be determined with TLS. Canopy-related characteristics have been hard to measure by other means.

Kalliovirta et al. (2005) used a Laser-relascope, which was also used in this study, to measure tree diameter, height and location. They reported the Laser-relascope's standard error for tree diameter, height, and position of 8.2 mm, 49 cm and 32 cm. Although the Laser-relascope was accurate enough, the results were observer-dependent and the most time-consuming part of the measurements was the diameter measurement. Juujärvi et al. (1998) and Varjo et al. (2006) have studied digital cameras (Canon PowerShot) applicability for measurement of stem diameter from different heights. They developed a method where a laser-rangefinder, digital photograph and calibration stick were used to determine stem diameter for the desired height of the stem. Interpretation of the digital photograph was controlled with taper curve models (Lappi 1986). The accuracy of stem diameter determination varied from 7.0 to 9.4 mm (RMSE) with a bias of 0.6-2.8 mm. The height of the measurements varied from 2.5 to 6.5 meters.

This study concentrates on the accuracy of measuring stem diameters by different means, because of the importance of that variable in forest management planning and calibration of ALS-based estimates. Stem diameters were measured by four different methods: By 1) TLS, 2)

Laser-camera, 3) Laser-relascope and for reference by 4) traditional means with steel calipers. The aim of this study was to test the new measuring devices in typical forest conditions. The accuracy (i.e. bias and precision) of the diameter estimates were examined.

2. Methods and materials

2.1 Study area

The data for this study were collected from the Nuuksio and Saunalahti areas in Espoo in southern Finland. Six circular sample plots were measured for the study by different means. The plots included altogether 122 Scots pines (*P. sylvestris*), Norway spruces (*P. abies*), birches (*B. pendula* and *B. pubescens*) and other deciduous trees. The stand development classes were advanced thinning stands or mature stands and site conditions varied from grove-like moor to rocky cliff top. The radius of sample plot used in Nuuksio was 7.98 m and in Saunalahti 10.0 m. The sample plots in Nuuksio (3) are located in a national park and the plots in Saunalahti (3) are in an urban forest. The variation in tree level in one plot was obviously more diverse than in economically managed forests in Finland, because the stands were uneven-aged. The reference measurements in the study areas were carried out in fall 2007 and winter 2008. General information about the diameter measurements in the sample plots is presented in table 1.

Table 1. General information about the diameter measurements (mm). Measured with reference device, steel caliper.

| | N | min | max | mean | s.d. |
|-----------------|-----|-----|-----|------|------|
| Pine | 26 | 44 | 465 | 194 | 112 |
| Spruce | 52 | 54 | 265 | 137 | 58 |
| Birch | 25 | 50 | 404 | 225 | 91 |
| Other deciduous | 19 | 47 | 478 | 171 | 124 |
| Total | 122 | 44 | 478 | 173 | 96 |

2.2 Measurement methods and equipment

2.2.1 Reference measurements

The traditional measurements, which were used as reference, included all the plots general information, such as forest site conditions and the stand's development class. In the traditional measurements, tree species and diameter at breast height (dbh) was determined. Dbh was measured using a steel caliper, and the breast height was marked on the tree. The measurements were always carried out from the same direction of the trees to minimize unwanted error sources.

2.2.2 Terrestrial Laser Scanner

A Faro 880HE80 TLS was used to scan the sample plots. FARO LS 880 HE80 is based on phase measurements with maximum measurement speed of 120000 points/sec, laser wavelength of 785 nm, vertical field of view 320°, horizontal field of scan view 360°, beam divergence of 0.25 mrad (0.014°) and linearity error of 3 mm (at 25 m and 84 % reflectivity). Only one scan per sample plot was used for manual dbh measurements. The scanner was stationed in or near the centre of the plot. The same measurement resolution was used for all scannings, producing a point spacing of 6 mm at the distance a 10 metres.

In Nuuksio the scannings were carried out in November 2007. In Saunalahti, scannings were

performed two growing periods prior reference measurements, in November 2005. Stands in Saunalahti were mature, thus, diameter growth was expected to be slow. Still this may cause minor errors in results for trees located there.

Faro Scene software was used for all measurements. First the ground level at the tree stem was determined in the scanned data by using a 3D-view of the scanned laser points (Figure 1, left). From the ground level a height of 1.3 metres was measured and marked in the intensity image (Figure 1, right). At the marked height, the intensity image was used to measure the horizontal angles to the left and right side of the stem and the distance to the middle of the stem. These values were used to compute the radius of the tree, thus obtaining the dbh of the tree.

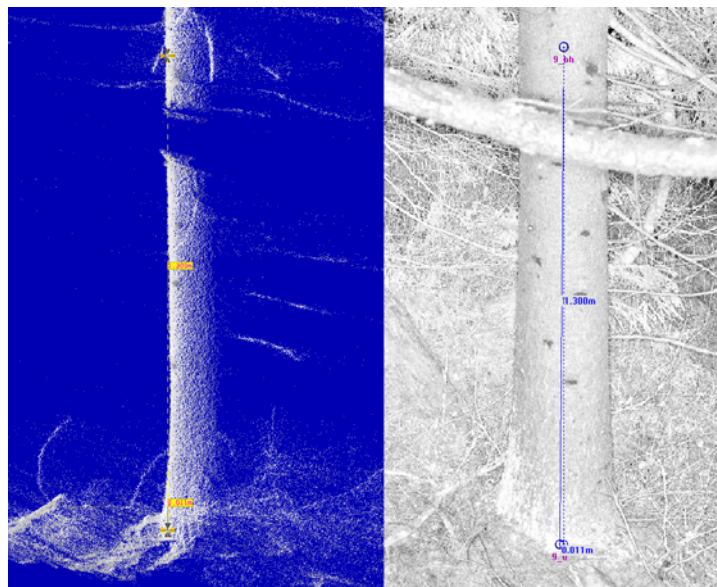


Figure 1. Scanned laser points of one tree stem, side view on the left, intensity image on the right. Ground level and 1.3 metre height are shown on both images.

2.2.3 Laser-camera

A Laser-camera consists of a Canon EOS 400D digital reflex camera with an integrated Mitsubishi ML101J27 laser line generator. The measurement of the tree diameter is performed by using the length and relative position of the laser line on the image. The method is developed by Ojanen (2005). The device enables the measurement of tree diameter from any desired height, in this study diameters were measured at dbh. Image interpretation was performed with specifically designed computer software in a data processing unit. The diameters could be measured automatically or semi-automatically. When using the semi-automatic method, digital images were checked in the field or afterwards. If errors are located in the digital photo, the markers that define the outline of a tree stem can be set manually. When images were checked immediately, the data processing unit was also used at the site. Afterwards, semi-automatic corrections were made when measurement errors were detectable from the digital photo. In future, the data processing unit is planned to be integrated into the camera. For a more detailed description of the Laser-camera, readers are referred to Kivilähde (2008) or Melkas et al. (2008).

2.2.4 Laser-relascope

The Laser-relascope is functionally a combination of a relascope and a dendrometer. It uses distance and angle information to determine the diameter of a tree. The distance between the device and a tree is measured with a laser instrument. In addition to a laser rangefinder, it also

includes an electronic compass for determining the position of the tree (bearing and distance from the centre of a sample plot), and an electronic inclinometer is included for height measurements. For a more detailed description of the Laser-relascope, readers are referred to Kalliovirta et al. (2005).

2.3 Calculating the accuracy of diameter measurements

Plot measurements taken by traditional means were used as a reference. The differences between the reference values and the values measured with different means were calculated to examine the accuracy, i.e. both the bias and precision of the measurements. The first assumption was that the values measured in reference measurements were the true values. However, all the reference measurements with steel calipers also include measurement errors. For purpose of comparison, those errors were taken into account by using information from previous studies (Hyppönen and Roiko-Jokela 1978; Päivinen et al. 1992). Previously reported standard errors were used as the standard errors for the reference methods when estimating the accuracy of different methods. If it is not mentioned separately that steel caliper errors have been taken into account, the reference measurements are assumed to be correct. Student's paired t-test was used to test were the diameters measured by different means were statistically different from one another.

The diameter measurement error for different measurements was defined as

$$e_d = d - d_0, \quad (1)$$

where d_0 represents the reference diameter and d the diameter measured with different means.

The reliability of the measurements was examined with the estimation of mean square error (MSE). Because the true values of the variables were assumed to be known, the MSE can be divided into the variance and the square of the bias (Cochran, 1977). The estimate of the bias (mean error) was given by

$$b[e_x] = e_{\bar{x}} = \frac{1}{n} \sum_{i=1}^n e_{x_i} \quad (2)$$

and the standard error was given by

$$s[e_x] = \sqrt{\frac{1}{n-1} \sum_{i=1}^n [e_{x_i} - e_{\bar{x}}]^2}, \quad (3)$$

where n is the number of observations and x is the diameter (measured by the reference and the method under observation).

When calculating standard errors for different methods and the measurement errors are independent, the standard error of reference method can be taken into account as follows:

$$s[e_x]_{method} = \sqrt{s[e_x]^2 - s[e_x]_{reference}^2} \quad (4)$$

where $s[e_x]_{reference}$ is the standard error for steel calipers.

3. Results

The precision and bias of diameter measurements were studied. The actual accuracy of the devices in measuring dbh was calculated from the data measured in the reference measurements with a steel caliper. The most accurate method of measuring dbh was the TLS (Table 2; Figure 2). The Laser-camera had nearly the same accuracy. Both methods had a bias of only 0.3%. The overall standard errors of TLS and the Laser-camera were 8.3 mm (4.5%) and 8.5 mm (4.9%), respectively. The accuracy (standard error) of steel calipers is reported to vary between 2.7 mm and 6.9 mm (Hyppönen and Roiko-Jokela 1978; Päivinen et al. 1992). The standard error calculations for TLS and the Laser-camera taking the standard errors of steel calipers into account enhances the accuracy of these two methods. In our calculations, the standard errors for TLS varied from 4.6 mm (2.5%) to 7.9 mm (4.2%) and for the Laser-camera from 5.0 mm (2.9%) to 8.1 mm (4.7%). Student's paired t-test was used to test were the diameters measured by different means were statistically different from one another. It revealed that there were no statistically significant differences between the reference method and the TLS ($t=0.56$) or the reference method and the Laser-camera ($t=0.75$). Differences in measurements between reference method and Laser-relascope were significant ($t=5.65$). On the basis of these results, we can state that in practice TLS and the Laser-camera are as accurate as the reference method.

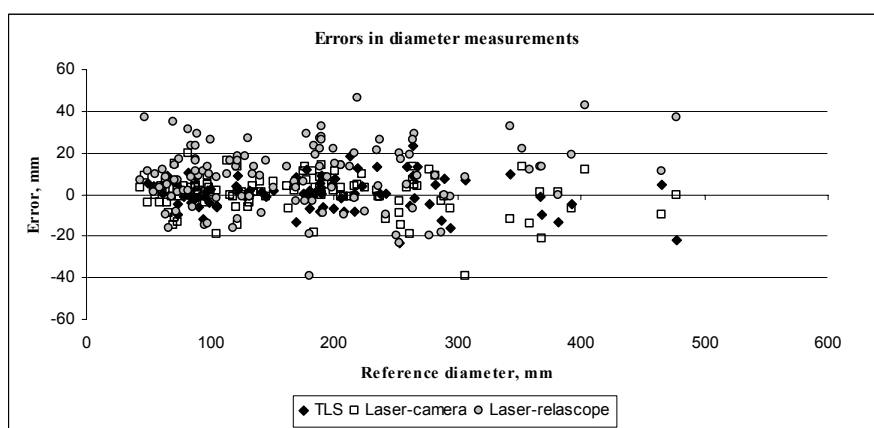


Figure 2. Errors in the diameter measurements with different means.

Table 2. Accuracies of diameter measurements (mm), bias and standard error proportioned to the mean diameter in parenthesis.

| Method | n | bias | S_E | S_E^* | S_E^{**} |
|-----------------|-----|-------------|---------------|--------------|--------------|
| TLS | 82 | 0.52 (0.28) | 8.31 (4.46) | 7.86 (4.21) | 4.64 (2.49) |
| Laser-camera | 120 | 0.58 (0.34) | 8.51 (4.94) | 8.09 (4.69) | 5.02 (2.91) |
| Laser-relascope | 119 | 9.06 (5.24) | 17.49 (10.11) | 17.28 (9.99) | 16.07 (9.29) |

* S_E without steel calipers S_E as reported in Hyppönen and Roiko-Jokela 1978 (2.7 mm).

** S_E without steel calipers S_E as reported in Päivinen et al. 1992 (6.9 mm).

The Laser-relascope's accuracy was relatively poor compared to these other two methods. The bias was 9.1 mm (5.2%) and the standard error was 17.5 mm (10.1%), varying by 16.1-17.3 mm (9.3-10.0%) if the standard error for steel calipers is taken into account. Kalliovirta et al. (2005) have reported a standard error of 8.2 mm for the Laser-relascope and variation with it among measurers (8.0-16.1 mm). Those results show that the accuracy of this method is really dependent on the measurer. The Laser-camera, which is actually an improved version of the Laser-relascope, is easy to use and does not need such an experienced measurer. Kalliovirta et al. (2005) also noticed that a diameter measurement with the Laser-relascope is not easy enough to use in actual field work and the measurements are subjective. Those were main reasons to start

the development of the Laser-camera.

The accuracy of measuring the three main tree species in Finland, pine, spruce and birch, vary slightly between the methods (Table 3). The variation in accuracy for the three main tree species was with TLS 6.1-9.8 mm, with the Laser-camera 8.2-10.5 mm and with Laser-relascope 16.4-20.6 mm. With TLS or the Laser-camera all the main tree species were measured accurately enough for practical use. What is most important is to obtain observations from every tree in a sample plot with these methods. For some reason deciduous trees (birches and other deciduous) were measured the most inaccurately in this study, although, with laser-based methods, it is easily assumed that trees with many under story branches, such as spruces, would be the most inaccurate to measure. One guideline for all of these laser-based methods is that visibility to the stem must be clear.

Table 3. The Accuracy of diameter measurements (mm) by tree species, bias and standard error proportioned to the mean diameter in parenthesis.

| Method | n | bias | S _E |
|-----------------|----|---------------|----------------|
| TLS | | | |
| Pine | 16 | 0.11 (0.05) | 6.14 (2.88) |
| Spruce | 35 | 3.07 (2.08) | 7.64 (5.18) |
| Birch | 21 | 0.20 (0.09) | 9.78 (4.53) |
| Other deciduous | 10 | -7.08 (-3.21) | 11.23 (5.09) |
| Laser-camera | | | |
| Pine | 26 | 0.96 (0.49) | 8.26 (4.25) |
| Spruce | 51 | 0.94 (0.68) | 8.16 (5.92) |
| Birch | 25 | -0.44 (-0.20) | 10.45 (4.64) |
| Other deciduous | 18 | 0.44 (0.27) | 7.72 (4.62) |
| Laser-relascope | | | |
| Pine | 26 | 10.81 (5.44) | 16.36 (8.24) |
| Spruce | 47 | 8.53 (6.47) | 16.37 (12.42) |
| Birch | 25 | 8.44 (3.75) | 20.56 (9.14) |
| Other deciduous | 21 | 8.81 (5.13) | 18.60 (10.83) |

4. Discussion

In this study new measuring devices were tested in forest conditions. The accuracy (i.e. bias and precision) of diameter measurements were examined. Based on this study, it seems that with new laser-based methods, TLS and the Laser-camera, stem diameter can be measured as accurate as it is measured in traditional field measurements with steel calipers. This study concentrated on stem diameter measuring accuracy, because of the importance of that variable in forest management planning and calibration of ALS-based estimates. The accuracy of the measurements of other variables need further studies.

TLS measurements in Saunalahti's three plots were completed in 2005 (two growth periods ago). This may cause bias in the TLS results for those plots, although the stands were mature, thus, the diameter growth is expected to be slow. All the other measurements were performed in 2007. It was impossible to get an observation from every tree in a plot with the TLS, because there was only one scan per plot. That problem should be fixed with more scanings per plot before accurate plot level estimates could be calculated. If several scanings are needed, it will add the amount of field work and post-processing notably.

Traditional methods are labour intensive and time consuming. Steel calipers can provide accurate diameter measurements and a useful reference data, but now it can be noted that there are other similarly accurate options with a wide range of other possibilities that traditional measurements do not offer, e.g. the measurement of diameters at multiple heights, which would improve volume estimates and give valuable information about tree quality. The Laser-camera's principle for diameter measurement has been significantly improved from its previous prototype, the Laser-relascope. Laser-relascope's functionalities besides measuring diameter - including measuring tree heights and producing tree maps - made the device promising itself, but Laser-camera's principle for diameter measurements is a major improvement and should be added on to it. The Laser-camera has given promising results and, thus, should be developed further together with the Laser-relascope. The price of the Laser-camera would be on a totally different scale than the price of an expensive TLS.

In earlier studies laser technology has been used to measure stem diameter in multiple ways. The accuracy of measuring diameters have varied from 8 mm to 16 mm with Laser-relascope (Kalliovirta et al. 2005) and from 8.8 mm to 14.3 mm with laser dendrometers (Skovgaard et al. 1998; Parker and Matney 1999). With a camera-based system Varjo et al. (2006) obtained an accuracy varying from 7.0 mm to 9.4 mm. Achieved accuracies in this study are within the same level, 8.3 mm with TLS, 8.5 mm with Laser-camera and 17.28 mm with Laser-relascope. Laser-camera was in first test under forest conditions in this study and in the study of Melkas et al. (2008). When Ojanen (2005) developed Laser-camera's measuring method, the aim was to create a method that is able to measure stem diameter with an accuracy of ± 5 mm. Results from this study are promising for Laser-camera, although such level of accuracy was not quite achieved.

Based on results in this and earlier studies, it can be noted that the achieved accuracies with laser-based methods are already in acceptable levels considering steel caliper's accuracy, which is reported to vary between 2.7 and 6.9 mm (Hyppönen and Roiko-Jokela 1978; Päivinen et al 1992). In this kind of comparison studies, results obtained by using steel caliper are often taken as an absolutely truth. With laser-based measuring methods, it is more important to concentrate on developing these new methods that can be used in daily field work and help to automatize measured data's possible post-processing.

TLS and the Laser-camera can both provide new and useful methods for producing accurate diameter measurements for reference data for research and forest inventories on different scales. The Laser-camera is easy to use, the price would be reasonable, and the diameter measurements are accurate. If the primary interest is classic stand characteristics, the Laser-camera would be an efficient and accurate option after other functionalities from the Laser-relascope have been added to it. On the other hand, TLS gives totally new possibilities for the measurement of forest stands. Although this study only compared the diameter measurements, TLS can provide a wide range of objective measurements of different stand characteristics (e.g. Hopkinson et al. 2004; Watt and Donoghue 2005; Henning and Radtke 2006; Danson et al. 2007). The TLS method does not depend on plot size, and larger plots or whole stands could also be measured at a reasonable cost, which has been almost impossible with traditional means. TLS applications in forestry need further studies.

In general, there is a need for devices that make forest field inventory easier. New laser-based methods are promising for this. Still, further studies are needed in order to develop these methods to be able to displace traditional methods in practical work.

Acknowledgements

This study was made possible by financial aid from the Finnish Academy project Improving forest supply chain by means of advanced laser measurements.

References

- Carr, B., 1992. Using laser technology for forestry and engineering applications. *Compiler* 10, 5–16.
- Carr, B., 1996. Using the Criterion 400 and Impulse 200 laser instruments to accurately measure trees. *Compiler* 14, 6–12.
- Cochran, W.G., 1977. *Sampling techniques* (third ed.). Wiley (1996).
- Danson, M., Hetherington, D., Morsdorf, F., Koetz, B. and Allgöwer, B., 2007. Forest Canopy Gap Fraction From Terrestrial Laser Scanning. *IEEE Geoscience and Remote Sensing Letters*, (4)1.
- Hopkinson, C., Chasmer, L., Young-Pow, C. and Treitz., P., 2004. Assessing forest metrics with a ground-based scanning lidar. *Canadian Journal of Forest Research*, 34, 573–583.
- Hyppönen, M. and Roiko-Jokela, P., 1978. Koepuiden mittauksen tarkkuus ja tehokkuus. On the accuracy and effectivity of measuring sample trees. *Folia Forestalia*, 356 (in Finnish with English summary).
- Juujärvi, J., Heikkonen, J., Brandt, S. and Lampinen, J., 1998. Digital image based tree measurement for forest inventory. *Proceedings of SPIE – The international society for optical engineering: Intelligent robots and computer vision XVII "Algorithms, techniques and active vision"*. Boston, USA: 3522, 114-123.
- Kalliovirta J., Laasasenaho J. and Kangas A., 2005. Evaluation of the Laser-relascope. *Forest Ecology and Management* 204, 2-3, 181-194.
- Kivilähde, J., 2008. *Mobile Development Environment for Image-based Measurement of Tree Attributes*. Master's Thesis. Helsinki University of Technology. 89 + 16 pages. (In Finnish, abstract in English)
- Lappi, J., 1986. Mixed linear models for analyzing and predicting stem form variation of Scots Pine. *Communications Institutii Forestalis Fenniae*, 134, 1-69.
- Melkas, T., Vastaranta, M. and Holopainen, M., 2008. The accuracy and efficiency of Laser-camera. Submitted to proceedings of Silvilaser 2008, Edinburgh, UK.
- Ojanen, M., 2005. *Measurement of a tree diameter using image processing*. Master's Thesis. Helsinki University of Technology, 76 pages. (In Finnish, abstract in English)
- Parker, P. C. & Matney, T. G., 1999. Comparison of optical dendrometers for prediction of standing tree volume. *Southern J. Appl. Forestry* 23 (2) :100-107
- Päivinen, R., M. Nousiainen, M. and Korhonen K.T., 1992. Puutunnusten mittaamisen luotettavuus. Accuracy of certain tree measurements, *Folia Forestalia*, p. 787 (in Finnish with English summary).
- Skovgaard, J. P., Johannse, V. K. & Vanclay, J. K., 1998. Accuracy and precision of two dendrometers. *Forestry* 71 (2) : 131-139.
- Suvanto A., Maltamo, M., Packalen, P. and Kangas, J., 2005. Kuviokohtaisten puustotunnusten ennustaminen laserkeilauksella. *Metsätieteen aikakauskirja* 4, 413– 428.
- Varjo, J., Henttonen, H., Lappi, J., Heikkonen, J. and Juujärvi, J., 2006. Digital horizontal tree measurements for forest inventory. *Working Papers of the Finnish Forest Research institute* 40.
- Watt, P.J. and Donoghue D. N. M., 2005. Measuring forest structure with terrestrial laser scanning. *International Journal of Remote Sensing*, 26, 7, 1437–1446.
- Williams, M., Cormier, K., Briggs R. and Martinez, D., 1999. Evaluation of the Barr Stroud

FP15 and Criterion 400 laser dendrometers for measuring upper stem diameters and heights. *Forest Science*. 45, 1, 53–61.

Estimating crown base height for Scots pine by means of the 3D geometry of airborne laser scanning data

Jari Vauhkonen

University of Joensuu, Faculty of Forest Sciences, P.O. Box 111, 80101 Joensuu, Finland – jari.vauhkonen@joensuu.fi

Abstract

Crown base height (CBH) is an important factor in relation to several characteristics of the tree stock. This paper introduces approaches for estimating tree-level CBH from airborne laser scanning (ALS) data that employ features of computational geometry. For that purpose, the concepts of Delaunay triangulations and alpha shapes were applied and compared with approaches based on analysing return frequencies and predicting CBH by linear regression. These approaches were evaluated using test data on a total of 133 sawlog-sized Scots pine trees detected and delineated from ALS data with a density of approx. 4 returns m⁻². The results suggest that variables based on cross-section area and the frequencies of crown returns within predefined height bins are the most accurate for estimating CBH. By combining the best CBH estimate with the estimated tree height in linear regression, an RMSE of 1.5 m (14%) was achieved. Although the accuracy of estimating CBH was lower using the 3D geometry approaches presented here, they were considered to have potential for further development.

Keywords: LIDAR; computational geometry; Delaunay triangulation; alpha shape

1. Introduction

Previous studies have shown that it is possible under Scandinavian conditions to detect 40-70% of all trees using the individual tree delineation approach with airborne laser scanning (ALS) data (Persson *et al.* 2002; Maltamo *et al.* 2004). Although the tree detection rate and segmentation accuracy are highly dependent on forest structure, the trees that are detected are highly representative of the dominant tree layer, which is the most significant part of the forest for many applications. The individual tree information could be used either as such or as a complement to area-based approaches in applications such as characterising the growing stock (Persson *et al.* 2002; Holmgren and Persson 2004), monitoring its development (Yu *et al.* 2004) and planning timber procurement (Peuhkurinen *et al.* 2007). The rapid developments currently taking place in ALS technology will enable the necessary point density to be achieved with lower data acquisition costs in the near future, whereupon more interest will obviously be shown in single-tree methods.

Besides tree height, the height of the tree crown is an important characteristic obtainable from tree-level ALS data, since the crown base height (CBH) is related to tree growth, forest health, timber quality, the need for silvicultural operations and their optimal timing, for example. Due to the laborious measurements involved, CBH is seldom measured in the field, however, and it is also difficult to model using more commonly recorded field observations (e.g. Hynynen 1995). Some approaches that employ ALS data for estimating CBH have been presented in the last few years. Maltamo *et al.* (2006), comparing variables based on both ALS and field measurements, concluded that the accuracy of predicting the CBH was in practice similar at both the tree and plot level regardless of the source of the predictors. Plot-level approaches have usually been based on analysing the height distribution of laser returns (Næsset and Økland 2002; Andersen *et al.* 2005; Maltamo *et al.* 2006), whereas at the tree level various properties of

the delineated 3D point clouds have been used to derive CBH (Pyysalo and Hyypä 2002; Holmgren and Persson 2004; Maltamo *et al.* 2006; Solberg *et al.* 2006; Holmgren *et al.* 2008; Popescu and Zhao 2008).

Pyysalo and Hyypä (2002) developed polygon models for extracting features from individual tree ALS data with a density of approx. 10 returns m^{-2} and claimed that the upper canopy could be described in detail but parameters extracted from the lower parts were less accurate. The CBH was overestimated by 3 m. Holmgren and Persson (2004) divided a dataset of approx. 5 returns m^{-2} into 0.5 m height layers and defined the CBH as the distance from the ground to the lowest point above the highest layer that contained less than 1% of the non-ground points. This gave a correlation of 0.84 between estimated and measured CBH and led to an overestimation of 0.75 m. In a later study, Holmgren *et al.* (2008) approximated the tree crown using the alpha shape technique, calculating the area of the shape in voxel height layers and determining the CBH as the smallest area, within certain limits, below the maximum shape area. They now achieved a higher correlation between the estimated and measured CBH values (0.91), but were not able to determine whether this was because of the more efficient algorithm or the considerably higher density of approx. 50 returns m^{-2} . In this case the CBH was underestimated by 0.61 m. Solberg *et al.* (2006), for one, examined the deciles calculated from the first return height distribution. CBH was set at the upper of two neighbouring deciles having the largest height difference in between. This approach resulted in an overestimation of 3 m (RMSE 3.5 m). Recently Popescu and Zhao (2008) used ALS data with a density of 2.6 returns m^{-2} to extract pulse frequency and intensity data with height bins defined in terms of 0.5 x 0.5 x 1.0 m voxels. They fitted the resulting vertical profile to a polynomial and defined the CBH as the height corresponding to an inflection point in the polynomial. Overestimations of 0.36 and 0.12 m in the frequency and intensity approaches, respectively, were removed in Popescu and Zhao (2008) by obtaining the final CBH estimate by means of linear regression. In that way the RMSE was approx. 2 m for the frequency approach and slightly more for the intensity-based approach.

Most of the previous approaches seem to require the operator to define the essential parameters, such as the division of the height bins. As an individual tree is quite a small sample unit, it is crucial for estimation accuracy that the predefined parameters should be in the correct relation to the density of the data, for example. An approach that was capable of adapting to the properties of the source data could also reduce the need for field reference material. Computational geometry is a branch of computer science that deals with the study of algorithms and data structures for solving problems stated in terms of basic geometrical objects, such as points, line segments and polygons. As major attention is paid to the computational efficiency of the algorithms, the use of these could be advantageous for dealing with high density ALS data. So far it is mainly the concept of Delaunay triangulation that has been used in preprocessing the data (e.g. Hyypä *et al.* 2001), while alpha shapes, for example, have recently been introduced for the later analysis (Holmgren *et al.* 2008; Vauhkonen *et al.* 2008). Here it is assumed that by employing suitable computational features it could be possible to estimate CBH independently of the properties of the ALS data.

The purpose of this study was to apply the concepts of Delaunay triangulations and alpha shapes to the prediction of the CBH for sawlog-sized Scots pine trees (*Pinus sylvestris* L.), bearing in mind the importance of this metric with respect to several attributes of this tree species in particular. The methods developed here were compared with alternative approaches adopted from earlier studies.

2. Material

Altogether 14 30 x 30 m square plots typically located in pure Scots pine stands on less fertile soils were established in the southern part of Koli National Park (lat. 63°1'19"N, long.

29°53'10"E) in North Karelia, eastern Finland, during the spring of 2006. All trees with a diameter at breast height of more than 5 cm were mapped and the attributes of each were recorded. Differentially corrected Global Positioning System measurements were used to determine the positions of the four corners of each of the plots. The accuracy of the positioning in the XY direction was approx. 1 m. Tree locations within a plot were measured using one corner as the origin and projecting the trees onto the same coordinate system as in the ALS data by affine transformation using the measured corner positions as reference points.

Georeferenced ALS point data were collected from an area of approx. 2500 ha in Koli on July 13, 2005, using an Optech ALTM 3100 scanner. Three Differential Global Positioning System receivers were employed to record the carrying platform position: one on the aircraft and two on the ground (the first as the base station and the second for back-up). ALS data was acquired using a mean altitude of 900 m above ground level, resulting in a nominal sampling density of about 4 returns m². Elevations within the test area varied from 95 m to 350 m (local zero sea level), resulting in a varying sampling density across the target. The divergence of the laser beam (1064 nm) was 0.26 mrad. The data were captured using a scanning angle of ±11 degrees, which resulted in a swath width of about 350 m. The last pulse data were employed to generate a digital terrain model (DTM) by the method explained in Axelsson (2000) using a grid of 1 m. Height values for the laser points were obtained by subtracting the corresponding DTM values. Points with a value over 0.5 m were classified as vegetation hits. The canopy height model (CHM) was interpolated to a grid of 0.5 m using canopy heights by taking the maximum value of the laser measurements within a radius of 0.5 m.

The individual trees were detected from the CHM using a method described by Pitkänen *et al.* (2004) in which the CHM was first low-pass filtered using Gaussian kernels with the size of the smoothing window and the intensity of the smoothing increasing as a stepwise function of the heights of the CHM. Local height maxima were searched for from the filtered CHM (Pitkänen *et al.* 2004), and all the pixels were classified in the binarization as belonging either to the tree canopy or to the background area. Finally, watershed segmentation was performed to create the crown segments. A crown segment was linked to a field-measured tree if 1) only one field tree was met inside the segment and 2) the difference between the maximum height value within the segment and the field height was less than 2 m. The study was further focused into sawlog-sized (diameter at breast height over 17 cm) Scots pine trees (N=133). The heights measured in the field for the study trees ranged from 12.1 to 27.2 m, with an average of 19.5 m, and the CBH values from 4.8 to 18.8 m, with an average of 11.1 m.

3. Methods

The main attention here was focused on extracting information from tree-level ALS data using Delaunay triangulation (Figure 1c), a widely known technique in the literature of computer science, while another computational geometry technique that was also applied was the concept of alpha shapes (Edelsbrunner and Mücke 1994). An alpha shape can be regarded as a weighted Delaunay triangulation from which all the simplices which have an empty circumsphere with a squared radius larger than the defined alpha value have been removed. Although illustrated in 2D (Figure 1c), the computations regarding both concepts were performed in 3D using the functionality of the Open Source library CGAL (<http://www.cgal.org>). The reference methods employed information on the vertical profiles of trees (Figure 1a and b). The methods based on return frequencies (Holmgren and Persson 2004; Solberg *et al.* 2006; Popescu and Zhao 2008), cross-section area (Holmgren *et al.* 2008) and linear regression (Maltamo *et al.* 2006; Popescu and Zhao 2008) were adapted slightly for the present purpose. Thus, the variables considered in the estimation were obtained by

1. constraining Delaunay triangulation by average triangle size (*avgtri*) and alpha value (*alphatri*);

2. extracting connected alpha shape components from the tree base (*comp*);
3. analysing layered (*A_bins*) and incremental (*A_incr*) accumulation of 2D area;
4. analysing vertical profile based on return frequencies (*freq*); and
5. linear regression based on tree height (*h*) and the previous variables.

The first approach was based on detecting discontinuities in the 3D triangulation in terms of large tetrahedra (see the 2D representation in Figure 1c). Two alternative methods were applied for classifying a tetrahedron as unacceptably large. In the average triangle (*avgtri*) method, the highest 50% returns were first triangulated and the volume of an average tetrahedron was used as this criterion. In addition to the volume, metrics such as circumradii and different edge lengths were considered for the same purpose with more or less the same result. In the *alphatri* approach, a predefined alpha value was used for the same purpose. Efforts were made to link an alpha value with the tree size by means of the estimated tree height, but as the same result could be obtained using different alpha values, this was found troublesome. Here $\alpha=4$ was chosen with respect to the reference data. In the actual algorithm, the neighbouring cells of the highest tetrahedron were traversed and if a cell was considered small by the given criterion, its neighbours were also traversed, this being repeated for as long as possible. The crown base height was then defined as the height of the lowest vertex in the obtained structure.

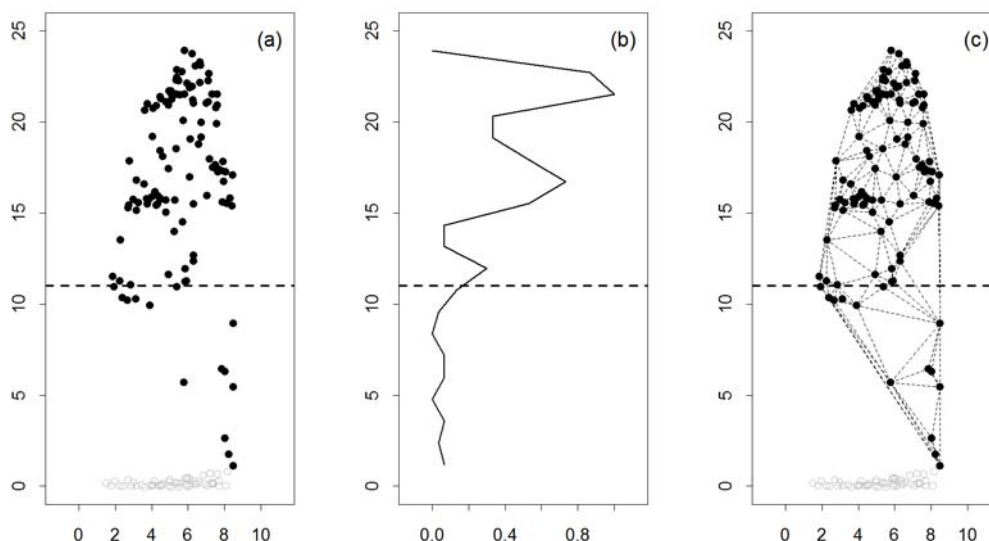


Figure 1: Possibilities for extracting information from ALS data. The ALS profile of an example tree (a), normalised return frequencies within 10% height bins (b), and Delaunay triangulation performed using the point data (c), illustrated in 2D for ease of visualization. The field-measured CBH is illustrated using a dashed line and ground hits using grey circles.

In the *comp* approach, connected components were removed from the lowest parts of an alpha shape generated with the full point data (Figure 2). An alpha value with one connected component was used as a starting point and the alpha values were traversed in descending order until a new component was split or the minimum height value of the highest component was changed. The first split component was allowed to intersect the previous, but otherwise the removal was accepted only if the component was located below the current main component. If not, the procedure was stopped and the CBH was defined as in the previous paragraph.

Third, the vertical profile of the point cloud (Figure 1b) was analysed. A 2D area approximated by the convex hull technique (*A_bins*) and return frequencies (*freq*), both extracted using overlapping 10% height bins with bin values of 5, 10, ..., 95% of the tree height, were

considered in the analysis. The value within a height bin was normalized using the largest bin value, resulting in values between 0 and 1. Values less than 0.1 were considered to be zeros. The CBH was defined as the lowest point within the first of 2 sequential zero bins below the maximum. The height bins had some overlap and 2 zero classes were considered in order to be sure not to detect a false CBH caused by the height bin division and the low pulse density. In a variation utilizing the 2D area (A_{incr}), the maximum area of the point cloud was first calculated and the point cloud was then traversed from the 20% tree height towards the top. While traversing, the area including the traversed point was calculated, and the crown base was defined at the point where the area calculated in this way exceeded a threshold of 20% of the maximum area.

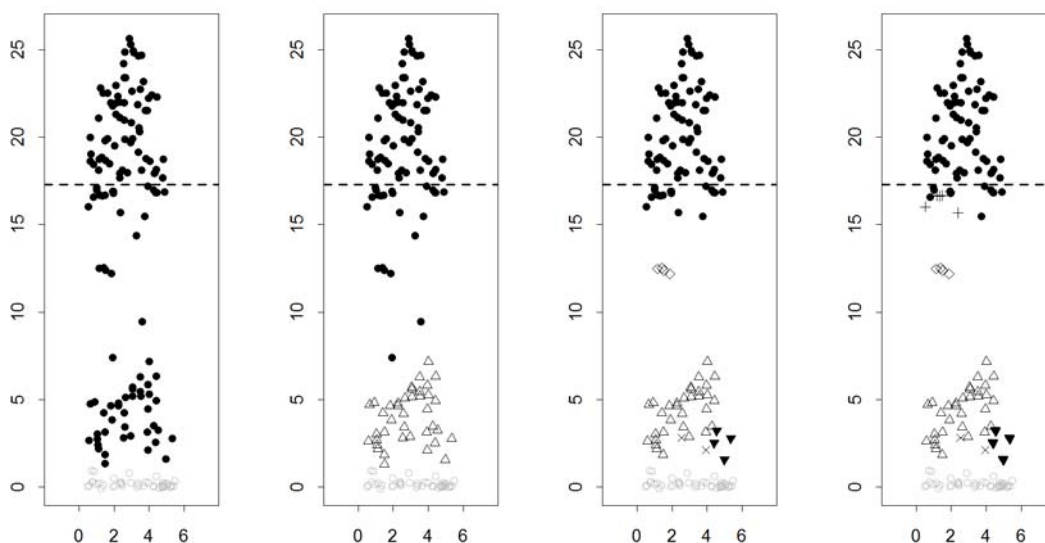


Figure 2: The first and last two steps of the *comp* algorithm in the case of an example tree. From left to right, 1, 2, 5 and 6 connected components illustrated using different symbols were separated from the point cloud during the traverse of alpha values. When the last split component (cross (+) symbols in the right-hand figure) overlapped the main component, the procedure was stopped and the previous main component was output as the result of the algorithm. The CBH measured in the field is illustrated using a dashed line. Note that the result was obtained in 3D and, thus, differs from 2D interpretation.

Finally, the CBH was predicted using linear regression. First the tree height alone was used as the independent variable, second all previous estimates were added to the model and any variables that were insignificant at the 95% confidence level according to the *t*-test scores were removed. The final CBH prediction was produced using leave-one-out cross validation, i.e. by fitting the regression model to all the observations except for the target tree itself.

The reliability of estimating the CBH was measured in terms of RMSE and bias:

$$RMSE = \sqrt{\frac{\sum_{i=1}^n (CBH_{field_i} - CBH_{pred_i})^2}{n}}, \text{ and} \tag{1}$$

$$bias = \frac{\sum_{i=1}^n (CBH_{field_i} - CBH_{pred_i})}{n}, \tag{2}$$

where n is the number of trees, CBH_{field_i} the reference and CBH_{pred_i} the predicted CBH for tree i . The relative RMSEs were calculated by dividing the absolute RMSE values by the mean reference CBH.

4. Results

The 3D geometry methods presented here were slightly poorer than the reference methods with respect to estimation accuracy (Table 1), with RMSE values ranging from 2.77 to 3.88 m as opposed to approx. 2 m for the other methods. The estimation accuracy with all methods seems to slightly decrease as tree size increases (Figure 4).

The differences in output between the methods are illustrated in Figure 3. The 3D methods actually produce a subset of the initial point cloud that is adjusted from the lower parts of the crown, whereas the other methods only output a vertical CBH boundary. Compared to other approaches, the 3D methods are slightly more vulnerable to gaps in the vertical profile above the field-measured CBH (e.g. Figure 3b). Thus, the lower accuracy of the 3D methods is mainly caused by several clear outliers (Figure 4), although the average results (Table 1) are, however, fairly close to each other.

Table 1: Estimation accuracies of the different methods.

| $CBH_{pred} =$ | RMSE, m | RMSE, % | bias, m |
|---|---------|---------|---------|
| <i>avgtri</i> | 3.88 | 34.9 | 0.522 |
| <i>alphatri</i> | 2.77 | 24.9 | 0.115 |
| <i>comp</i> | 2.83 | 25.4 | -0.945 |
| <i>A_bins</i> | 1.84 | 16.6 | 0.411 |
| <i>A_incr</i> | 2.17 | 19.5 | -0.738 |
| <i>freq</i> | 1.81 | 16.3 | 0.004 |
| $-0.68 + 0.62 \times h$ | 2.03 | 18.2 | -0.001 |
| $-0.51 + 0.29 \times h + 0.57 \times A_bins$ | 1.54 | 13.9 | -0.006 |

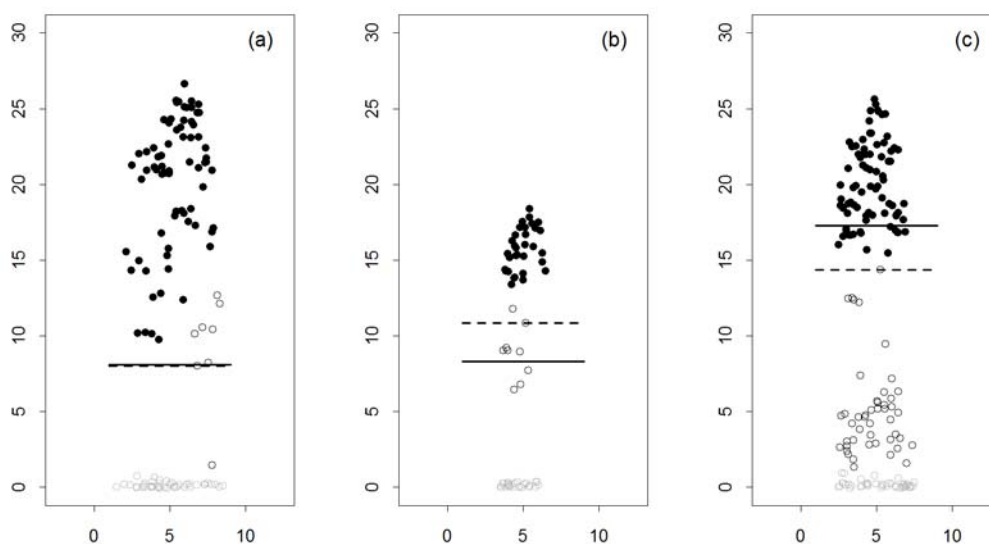


Figure 3: Differences in output between the methods – CBH as measured in the field (thick line), CBH estimate with the *freq* approach (dashed line), output of the *comp* method (black filled dots), and other laser returns (circle symbols).

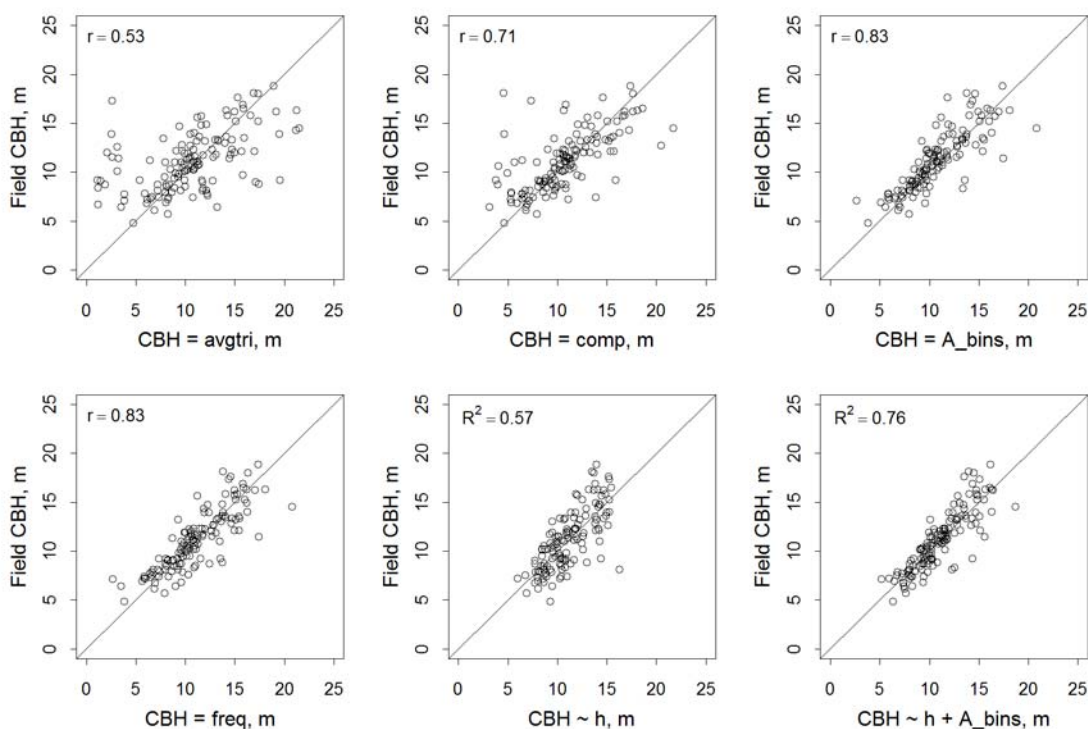


Figure 4: CBH estimates produced by different methods vs. CBH measured in the field.

5. Discussion

It was assumed here that by employing a 3D computational geometry approach new information could be obtained for estimating CBH. The results show that this estimation could be done more accurately using simpler methods. In previous studies, for example, Popescu and Zhao (2008) obtained RMSEs of around 2 m with a very similar sample arrangement. In fact, when predicting from tree height, their results practically equalled those obtained here, although the best result obtained here (RMSE 1.5 m) was slightly more accurate. The present results, in common with those of Popescu and Zhao (2008), show that it is possible to obtain accurate CBH estimates with modest pulse densities. Considering the pulse densities used in estimation, the accuracy of the developed 3D methods is also comparable with figures reported elsewhere (e.g. Pyysalo and Hyypä 2002, Holmgren and Persson 2004). It should be noted, however, that only Scots pine trees were considered here. In the study of Popescu and Zhao (2008), for example, the difference between pine and deciduous trees was of significance.

An objective for this study was to develop methods that could be adapted to the properties of ALS data. The methods introduced here make use of 3D triangulations of point clouds, which in principle do not need *a priori* knowledge. The main error source consisted of several outliers, so that it is likely that by using higher density data the true discontinuities in the point clouds could be detected more accurately and, thus, the number of potential outliers could possibly be reduced. On the other hand, *a priori* knowledge of the extremes in the data, e.g. not allowing the CBH to be closer than 15% to the tree height at both ends, could possibly reduce the inaccuracy with lower density data. Speaking of pulse-level analysis, a higher density would increase the computational burden, which on the other hand could be constrained by using the efficient structures of computational geometry. Computation was very straightforward with the density considered here, although the code had not yet been optimized at all.

It can also be noted that, interpreted visually, the CBH values measured in the field may differ considerably from the point profile (Figure 3b-c). One reason for this is that the field measurement is made to the base of the lowest branch, whereas the scanner records reflections mainly from the top of the branch. The level of correspondence between the ALS-based CBH estimate and the ground truth is thus dependent on the technical definition of the CBH (see also Solberg *et al.* 2006). In view of this, the 3D measurements may in fact also produce a fair approximation of the living crown, but as the linear models are fitted to the field reference data, they logically generate better results in terms of the RMSE and bias figures.

With respect to the accuracy of certain applications, such as species recognition based on the properties of the point cloud (Holmgren *et al.* 2008; Vauhkonen *et al.* 2008), it may be crucial that the tree crown returns are accurately separated from those representing other trees and the undergrowth. The tree detection rate may vary in mature forests (Persson *et al.* 2002; Maltamo *et al.* 2004), and where the canopy is closed, better results may in general be gained using area-based approaches (e.g. Næsset and Økland 2002). However, given suitable conditions for the single-tree approach, the new methods presented here could be further developed towards 3D segmentation, which would be of help in providing accurate input point data for the applications of the ALS technique.

Acknowledgements

The support by the Academy of Finland (project 12193: “High Resolution Remote Sensing Potential to Measure Single Trees and Site Quality”) is gratefully acknowledged. Additionally, the author would like to thank Mr. Jussi Peuhkurinen for having performed the preprocessing of the tree data, and him, Prof. Matti Maltamo, Prof. Timo Tokola, Mr. Malcolm Hicks and two anonymous reviewers for their help in preparing the manuscript.

References

- Andersen, H.E., McGaughey, R.J. and Reutebuch, S.E., 2005. Estimating forest canopy fuel parameters using lidar data. *Remote Sensing of Environment*, 94, 441-449.
- Axelsson, P., 2000. DEM generation from laser scanner data using adaptive TIN models. *International Archives of Photogrammetry and Remote Sensing*, 54, 138-147.
- Edelsbrunner, H. and Mücke, E.P., 1994. Three-dimensional alpha shapes. *ACM Transactions on Graphics*, 13, 43-72.
- Holmgren, J. and Persson, Å., 2004. Identifying species of individual trees using airborne laser scanner. *Remote Sensing of Environment*, 90, 415-423.
- Holmgren, J., Persson, Å. and Söderman, U., 2008. Species identification of individual trees by combining high resolution LiDAR data with multi-spectral images. *International Journal of Remote Sensing*, 29, 1537-1552.
- Hynynen, J., 1995. Predicting tree crown ratio for unthinned and thinned Scots pine stands. *Canadian Journal of Forest Research*, 25, 57-62.
- Hyypä, J., Kelle, O., Lehikoinen, M. and Inkinen, M., 2001. A segmentation-based method to retrieve stem volume estimates from 3-dimensional tree height models produced by laser scanner. *IEEE Transactions on Geoscience and Remote Sensing*, 39, 969-975.
- Maltamo, M., Eerikäinen, K., Pitkänen, J., Hyypä, J. and Vehmas, M., 2004. Estimation of timber volume and stem density based on scanning laser altimetry and expected tree size distribution functions. *Remote Sensing of Environment*, 90, 319-330.
- Maltamo, M., Hyypä, J. and Malinen, J., 2006. A comparative study of the use of laser scanner data and field measurements in the prediction of crown height in boreal forests. *Scandinavian Journal of Forest Research*, 21, 231-238.

- Næsset, E. and Økland, T., 2002. Estimating tree height and tree crown properties using airborne scanning laser in a boreal nature reserve. *Remote Sensing of Environment*, 79, 105-115.
- Persson, Å., Holmgren, J. and Söderman, U., 2002. Detecting and measuring individual trees using an airborne laser scanner. *Photogrammetric Engineering & Remote Sensing*, 68(9), 925-932.
- Peuhkurinen, J., Maltamo, M., Malinen, J., Pitkänen, J. and Packalén, P., 2007. Preharvest measurement of marked stands using airborne laser scanning. *Forest Science*, 53, 653-661.
- Pitkänen, J., Maltamo, M., Hyypä, J. and Yu, X., 2004. Adaptive methods for individual tree detection on airborne laser based canopy height model. In: M. Theis, B. Koch, H. Spiecker, H. Weinacker (Eds.). *Proceedings of ISPRS working group VIII/2 "Laser-Scanners for Forest and Landscape Assessment"*. Freiburg, University of Freiburg, 187-191.
- Popescu, S.C. and Zhao, K., 2008. A voxel-based lidar method for estimating crown base height for deciduous and pine trees. *Remote Sensing of Environment*, 112, 767-781.
- Pyysalo, U. and Hyypä, H., 2002. Reconstructing tree crowns from laser scanner data for feature extraction. *ISPRS Commission III Symposium*. The International Archives of Photogrammetry, Remote Sensing and Spatial Information Science, vol. XXXIV, 302-309.
- Solberg, S., Næsset, E. and Bollandsås, O. M., 2006. Single tree segmentation using airborne laser scanner data in a structurally heterogeneous spruce forest. *Photogrammetric Engineering & Remote Sensing*, 72(12), 1369-1378.
- Vauhkonen, J., Tokola, T., Packalén, P. and Maltamo, M., 2008. *Identification of Scandinavian commercial species of individual trees from airborne laser scanning data using alpha shape metrics*. Submitted manuscript.
- Yu, X., Hyypä, J., Kaartinen, H. and Maltamo, M., 2004. Automatic detection of harvested trees and determination of forest growth using airborne laser scanning. *Remote Sensing of Environment*, 90, 451-462.

Potential and limits of extraction of forest attributes by fusion of medium point density LiDAR data with ADS40 and RC30 images

Lars T. Waser¹, Christian Ginzler², Meinrad Kuechler³, Emanuel Baltsavias⁴

^{1,2,3} Swiss Federal Research Institute WSL, Land Resources Assessment, 8903 Birmensdorf, Switzerland, email: ([waser](mailto:waser@wsl.ch), [ginzler](mailto:ginzler@wsl.ch), [kuechler](mailto:kuechler@wsl.ch))@wsl.ch

⁴Institute of Geodesy and Photogrammetry, ETH Zurich, 8093 Zurich, Switzerland, email: manos@geod.baug.ethz.ch

Abstract

This study presents an approach for semi-automated derivation of forest attributes (area, composition, stands) by fusion of medium point density LiDAR data with ADS40 and RC30 images to support tasks of the National Forest Inventory (NFI). In a first step, two different canopy height models (CHMs) are generated using a LiDAR DTM with two DSMs derived from the LiDAR data and RC30 images. In a second step, forest area was obtained using a logistic regression approach and explanatory variables from both CHMs. Based on the forest area, tree composition and main tree species are modelled again using logistic regression models and explanatory variables derived from both the ADS40 and RC30 aerial images. In a third step, forest stands are extracted by combining homogenous parts of the CHM with tree species information. Generally, results based on LiDAR CHM produced less satisfactory results due to lower quality. High accuracy for the extraction of forest area, main tree species ($\kappa = 0.7$ to 0.9) is obtained. Further research is needed for the extraction of forest stands. The present study reveals the potential and limits to derive forest attributes and highlights possibilities of their usage for tasks of the Swiss National Forest Inventory.

Keywords: Canopy height model, DSM/DTM, Forestry, high-resolution, multisensor

1. Introduction

Extraction of forest attributes from airborne remote sensing data have grown over time and will continue to do so in the future since exact information on forest extend, structure and composition is needed for many environmental, monitoring or protection tasks. The present study focuses on the extraction of these attributes and was carried out in the framework of the Swiss National Forest Inventory (NFI) and the Swiss Mire Monitoring Program (Brassel and Lischke, 2001).

Recent progress in three-dimensional remote sensing mainly includes digital stereo-photogrammetry, radar interferometry and LiDAR (Watt and Donoghue 2005, Baltsavias *et al.* 2007). E.g. by subtracting a digital terrain model (DTM) from the corresponding digital surface model (DSM), canopy height models (CHMs) can be calculated that serve as basis for other forest attributes. Using digital photogrammetry, DSMs are generated via image matching, often using cross-correlation (Hyypä *et al.* 2000) or less frequently multi image-matching approaches (Zhang and Gruen 2004). Meanwhile several LiDAR systems are commercially available (Naesset and Gobakken 2005), enabling the derivation of DTMs from such data as well (Baltsavias 1999). Several studies have integrated LiDAR with optical remotely sensed data to estimate forest attributes such as stand composition, tree height, crown diameter, basal area, and stem volume (e.g. Straub 2003; St-Onge *et al.* 2004, Hollaus *et al.* 2006, Baltsavias *et*

al. 2008). Combining some of these attributes can be used to evaluate extent of forest area (Waser *et al.* 2008a), detect changes in forest stands (Waser *et al.* 2008b), and determine tree/shrub species (Holmgren and Persson 2004). According to Scott *et al.* (2002) modern regression approaches have proven particularly useful for modelling spatial distribution of tree species and communities. Thus, high-resolution remote sensing data in combination with regression analyses are promising for modeling forest composition and tree species (e.g. Lamonaca *et al.* 2008). The objective of this study is to develop a methodology for derivation of fractional forest cover, detection of main tree species and derivation of forest stands.

2. Method

2.1 Study area

Models have been developed and tested for four forest ecosystems in the northern Pre-alpine zone of Switzerland. In this paper we present a representative test site (approx. 47°18' N and 9°14' E) which has an extent of approx. 3 km² and is characterized by a varying terrain, mixed land cover and deciduous and coniferous forests with a core mire area (see Fig. 1).

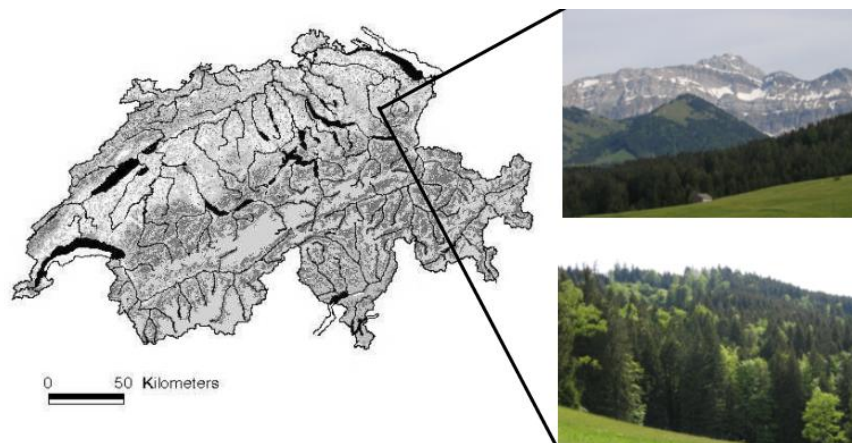


Figure 1: Test site with typical mixed forests

2.2 Remote sensing data

To ensure that this study is also of practical relevance for the NFI, only remote sensing data which are available for large areas or for entire Switzerland have been used.

2.2.1 ADS40 RGB images

Leica airborne digital sensor (ADS40 first generation) images Level 1 (un-rectified) of August 2005, RGB bands (16 bit), and ground sample distance 0.25m. An orthoimage was generated using the LiDAR DSM described below. Main advantage: The image data is available for the area of entire Switzerland every three years.

2.2.2 RC30 CIR images

Leica RC30 frame camera, 4 CIR (colour infrared) aerial images (1 strip) of July 2005, bands: red, green, near-infrared, scale 1:5,600 and an orthoimage that was generated with a spatial resolution of 0.25 m. Main disadvantage: The images are only available on request and do not cover entire Switzerland. Orientation of the CIR aerial images was performed in LPS (Leica

Photogrammetry Suite) and the following accuracies were obtained: the a posteriori sigma 0 was 0.32 pixel and the RMSE for the control points: X=0.06 m, Y=0.06 m, Z=0.17 m and RMSE for the check points are X=0.06 m, Y=0.06 m, Z=0.24 m. Main disadvantage: The image data is only acquired on request and not available for entire Switzerland.

2.2.3 RC30 DSM derived from CIR images

High-resolution DSM data is indispensable since accurate surface information of the forest area is very important for modelling forest composition, e.g. tree species. Thus, for the four RC30 CIR images a matching method was applied that can simultaneously use any number of images (> 2). It is implemented in the operational, quasi-complete photogrammetric processing package Sat-PP which supports satellite and aerial sensors with frame and linear array geometry (for further details see Zhang (2005) and Zhang and Gruen (2004)). In principle, the matching method consists of three mutually connected components: an image pre-processing, a multiple primitive multi-image matching (MPM) and a refined matching procedure. This automated DSM generation provides high accuracy and enables to produce very dense (grid spacing = 3-4 x GSD) and detailed DSMs that allow a good 3D modeling of trees and shrubs (see Fig. 2).

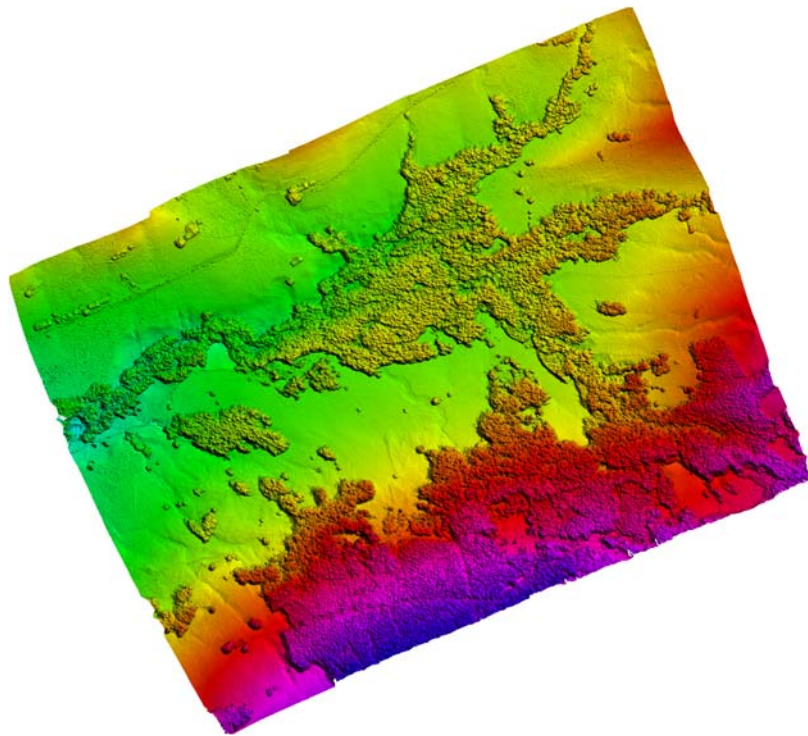


Figure 2: DSM derived from the RC30 CIR images generated by the SAT-PP matcher. The DSM is coded in color from light green (light in BW) to cyan (dark in BW) for lowest and highest elevations.

2.2.4 LiDAR DSM and DTM data

National LiDAR DSM and DTM data from 2003, leaves-on was used. The data was acquired by Swissphoto AG / TerraPoint using a TerraPoint ALTMS 2536 system with an average height above ground of 1200 m. From the LiDAR data (first and last pulse), both a DTM and DSM were generated by the Swiss Federal Office of Topography (SWISSTOPO). The average density of the DSM data was 1-2 points / m² and the height accuracy (1 sigma) 0.5 m for open areas and 1.5 m for vegetation. The DTM has an average point density of 0.8 points / m² and height

accuracy (1 sigma) of 0.5 m (Artuso *et al.* 2003). The raw LiDAR data provided by SWISSTOPO were converted using SCOP++ V5.3 (INPHO) to a raster with 1 m resolution.

2.3 Training and reference data-sets

A ground survey was carried out in summer 2006 and 2007. In total, for 480 trees we collected: i) tree positions using a sub-decimeter GPS with differential correction, ii) tree heights using a tachymeter and iii) determination of eight tree species. These are: *alder*, *maple*, *birch*, *beech*, *ash*, *sorbus* (all deciduous trees) and *white fir*, *spruce* (coniferous trees). This information was used for calibration and validation of the models.

2.4 Forest area

The forest / non-forest decision is based on several steps: In a first step, two canopy height models (CHM) were produced (CHM1 = RC30 DSM – LIDAR DTM; CHM2 = LiDAR DSM – LiDAR DTM). Then both CHMs were used to extract potential tree areas according to the > 3 m tree height and minimum tree area of 500 m² definitions by the NFI (Brassel and Lischke 2001). In a second step, non-tree objects (buildings, rocks etc.) of both CHMs were removed using normalized difference vegetation index (NDVI) information (low values) obtained from the CIR aerial images. In a third step, based on the two canopy covers two fractional shrub/tree covers were produced using a logistic regression approach (McCullagh and Nelder 1983) with a probability (0 to 1) for each pixel to belong to the class “forest”. The explanatory variables consist of six commonly used topographic parameters derived from the CHMs (aspect, curvature, slope and three local neighbouring functions) as described in detail in Waser *et al.* (2008a). The result is a fractional forest cover of the test site with a probability for each pixel to belong to the class “forest”. Various cover strata with different probability ranges for forest are computed (see Table 1).

2.5 Distinction of main tree species

Since distinction of tree species is based on the fractional forest cover – all pixels with a forest probability of less than 0.2 were skipped.

In a first step, individual tree or groups of tree have to be extracted before modelling tree species. For better segmentation the ADS40 images and CIR aerial images were smoothed using ArcGIS focal functions. In a second step segmentation of the RC30 and ADS40 images was applied using the Definiens developer 7.0 software (Baatz and Schaepe 2000). This segmentation provides groups of trees and single trees with similar shapes and spectral properties. For each pixel within a segmented tree group or tree object, probability belonging to one of the eight main tree species was calculated using logistic regression models. As explanatory variables we used 12 parameters derived from the ADS40 images and the RC30 images: original bands of RGB (3 variables) and CIR (3 variables), the ratio of each CIR and RGB band divided by the sum of the corresponding 3 bands (6 variables). These parameters have shown best performance based on empirical tests and step-wise methods. 240 tree individuals (half of the field data) were used as training data. The usage of parameters from the CHMs as explanatory variables didn't further improve the results.

2.6 Forest stands

According to the Swiss NFI a stand can be defined by the three parameters *composition*, *diameter at breast height* (dbh) and *structure* (multi-layers of tree cover). *Composition* can be determined using the distinction of coniferous / deciduous trees and classification of the eight tree species as performed in 2.5. Since it is not possible to obtain the diameter at breast height

from the input data-sets tree height information and minimum tree area (500 m²) was used instead. Tree height is indirectly linked with the diameter of a trunk. Four tree height classes according to the definition by the NFI were built using the CHMs: 3-8 m, 8-15 m, 15-25 m and > 25 m. Minimum tree area and the dominating tree heights per segment (tree group or tree object) were calculated using different moving window approaches.

3. Results

3.1 Forest area

The predicted forest area was validated using a pixel-to-pixel comparison on 240 randomly sampled reference field measurements. For this validation the corresponding pixel clusters (5x5 pixel window) of the measured 240 tree/shrub samples and 150 non-tree samples, respectively were used. Table 1 presents the correspondence between the pixels of randomly sampled shrubs/trees > 3 m and the five modelled individual shrub/tree cover strata. A tree/shrub cover stratum of e.g. 10–100% (0.1–1) means that all pixels with a probability higher than 10% are assigned to forest. The following statistical measures were used: correct classification rate (*CCR*), consumer's accuracy, producer's accuracy, kappa coefficient and correlation coefficient (r^2). The accuracies for five different tree/shrub cover strata are given for both CHMs in table 1. Higher accuracies are obtained by using the topographic parameters from the RC30 DSM as explanatory variables. Best correspondence between the models and field data is obtained for cover stratum 20-100% when using the RC30 DSM variables, and 30-100% when using the LiDAR DSM variables.

Table 1. Accuracies of both canopy covers for five different strata. 1st lines are based on the LiDAR DSM variables, whereas second lines were obtained from the RC30 DSM variables.

| Cover stratum | 10-100% | 20-100% | 30-100% | 40-100% | 50-100% |
|------------------|---------|---------|---------|---------|---------|
| <i>CCR</i> | 0.841 | 0.883 | 0.902 | 0.891 | 0.863 |
| | 0.923 | 0.971 | 0.958 | 0.935 | 0.921 |
| <i>Cons. Ac.</i> | 0.801 | 0.861 | 0.922 | 0.865 | 0.836 |
| | 0.817 | 0.965 | 0.954 | 0.956 | 0.938 |
| <i>Prod. Ac.</i> | 0.842 | 0.863 | 0.897 | 0.857 | 0.835 |
| | 0.924 | 0.934 | 0.912 | 0.881 | 0.834 |
| <i>Kappa</i> | 0.721 | 0.786 | 0.843 | 0.782 | 0.761 |
| | 0.802 | 0.915 | 0.903 | 0.883 | 0.856 |
| r^2 | 0.765 | 0.782 | 0.821 | 0.812 | 0.747 |
| | 0.832 | 0.924 | 0.908 | 0.891 | 0.864 |

Fig. 3 clearly shows the different extent of canopy covers with tree height classes when a) using the LiDAR CHM and b) using the RC30 CHM. For comparison purposes the DSMs were resampled to 1 m. The varying extent of forest area is due to quality differences of the LiDAR data and the RC30 DSM but also due to deforestation between 2003 and 2005.

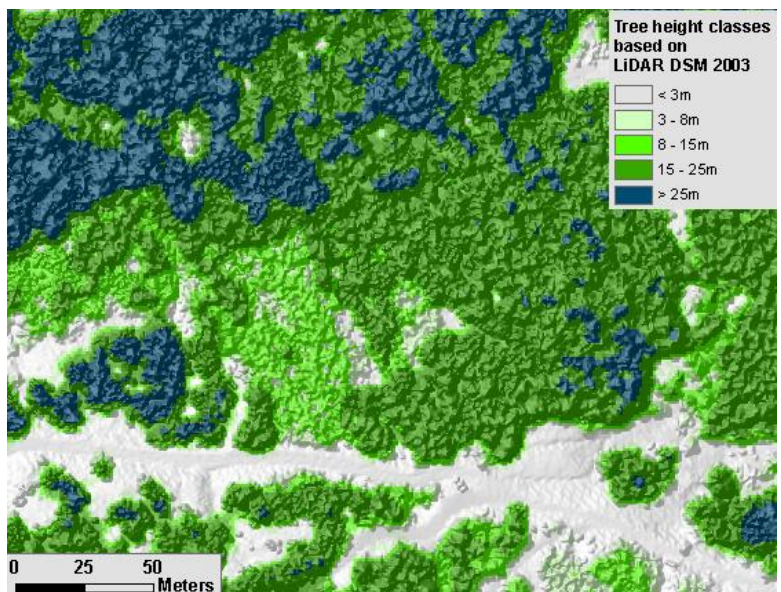


Figure 3a. Extracted forest area and tree height classes based on the LiDAR CHM of 2003.

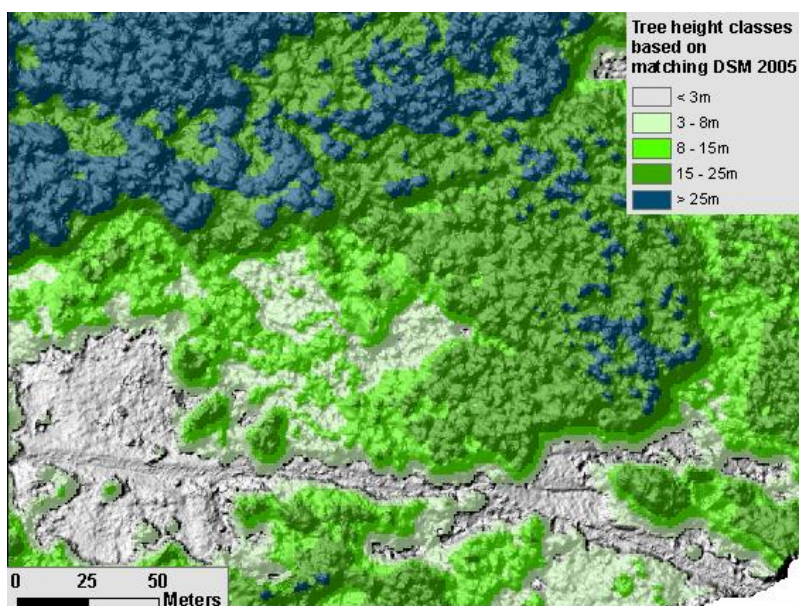


Figure 3b. Extracted forest area and tree height classes based on the CHM of the RC30 DSM of 2005. New deforestation is visible in the left part of the area.

3.2 Tree species

In general, best distinction is obtained when combining both ADS40 and CIR data as explanatory variables. Low *CCR* is obtained when considering all eight tree species. Therefore the focus was laid on five main tree species (spruce, white fir, ash, beech, birch). Table 2 reveals the accuracies using either CIR images, ADS40 images or a combination of both data-sets and shows that best results are obtained from the latter. Table 2 also reveals that this improvement is less pronounced for deciduous trees.

Table 2. Correct classification rate (*CCR*) values of the five main tree species as obtained by logistic regression. Kappa (*K*) values are the average for all five species.

| based on | <i>spruce</i> | <i>white fir</i> | <i>ash</i> | <i>beech</i> | <i>birch</i> | <i>K</i> |
|------------|---------------|----------------------|------------|--------------|--------------|----------|
| CIR | 0.75 | 0.64 | 0.81 | 0.80 | 0.76 | 0.68 |
| ADS40 | 0.86 | 0.85 | 0.84 | 0.82 | 0.78 | 0.75 |
| CIR+ ADS40 | 0.92 | 0.88 | 0.91 | 0.86 | 0.84 | 0.86 |

3.3 Forest stands

Fig. 4 shows that forest stand classes are obtained by a combination of tree heights and forest composition. Tree height classes were used as equivalence to diameter at breast height according to the Swiss NFI. However, since no forest stand maps exist from this region, the quality control of the different forest stands was performed visually using stereo-image interpretation. In general, the typical stand classes are well represented when accepting some discrepancies especially in stand classes with lower tree heights (3-8 m).

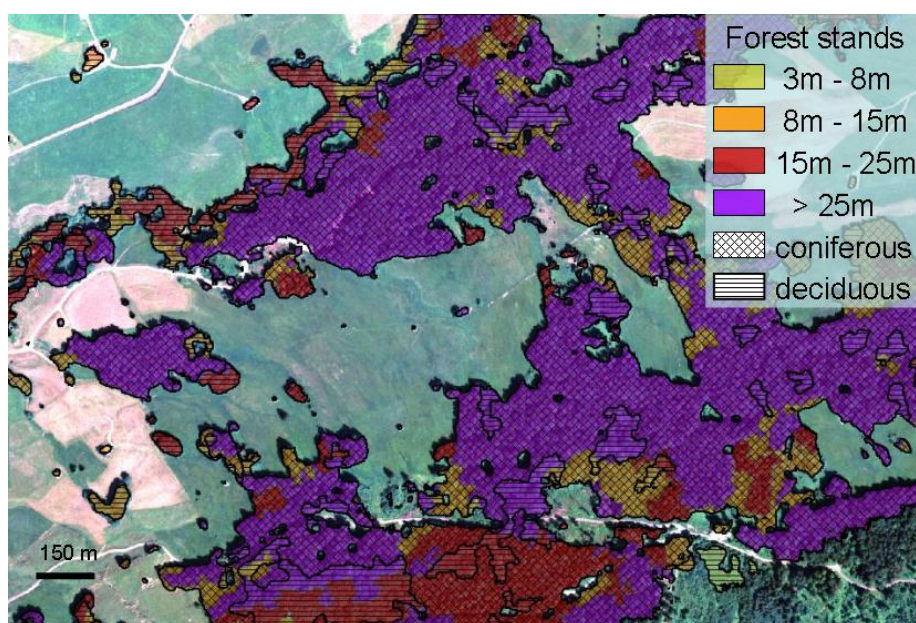


Figure 4. Forest stand classes as obtained by combining tree heights and dominant tree type according to the Swiss national forest inventory (NFI).

4. Discussion

This study highlights the potential of combining airborne remote sensing data with logistic regression models to obtain forest attributes such as area, tree species and stands on sub-pixel level. The **first objective**, the extraction of forest area, was achieved semi-automatically with high accuracy using either LiDAR or RC30 DSM data. Generally, the usage of explanatory variables from the RC30 DSM produced better accuracies. Highest correspondence between fractional canopy cover and field data was obtained for the fractional canopy cover strata of 20-100% using the RC30 DSM and 30-100% using the LiDAR DSM, respectively. However, this validation is based on trees > 3 m and it has to be kept in mind that accuracies may vary when considering also shrubs/trees < 3 m for validation. But detailed visual stereo-image interpretation confirmed that most small trees are then within the forest area when using the two canopy cover strata. Since this study clearly reveals that accuracy of fractional canopy covers

strongly depends on the accuracy of the DSM data, newly developed, high-quality matching methods are indispensable. The usage of a dense and accurate DSM is an absolute prerequisite in order to be able to derive accurate topographic parameters which in turn are used to derive the fractional canopy covers. Although the LiDAR DSM in this study has a lower point density than the RC30 DSM the obtained results for extraction of forest area are yet useful, and will be applied for larger forest areas on regional or national level. Moreover, in near future, we will be able to produce high-quality DSMs also from ADS40 data.

The **second objective**, the distinction of main tree species, was achieved semi-automatically and mediocre to high accuracies were obtained. First, simple distinction between deciduous trees and coniferous trees revealed higher accuracies than the distinction of several tree species. Second, better results were obtained when using ADS40 data, especially for coniferous tree species. Anyhow, distinction of tree species based on CIR aerial image information at least produced satisfactory results for *spruce*, *ash*, *beech* and *birch* and partly satisfactory for *white fir*. Best results were obtained when combining both sensors as input for the logistic regression models. However, both sensors failed to distinguish further deciduous trees with good quality. Possible reasons are that *alder*, *maple* and *sorbus* are often grouped have smaller crowns, are partly covered from each other or from other more dominant species and also have very similar spectral properties. Tests revealed that an implementation of variables derived from both LiDAR and RC30 DSM didn't improve the results. Therefore distinction of tree species only depends on the spectral information.

Two final remarks are given here: i) advantages of this approach are that only few training data is needed and this method can be applied semi-automatically – also for larger regions; ii) an important disadvantage is the availability of both image data, whereas the CIR aerial images are only available on request for selected areas within Switzerland. Unfortunately, with this first generation ADS40 sensor, the NIR line CCD is placed far away from the RGB CCDs and thus the NIR image looks very different and cannot be combined with the RGB images. Therefore, in near future the focus will be laid on single usage of the 2nd generation ADS40 sensor where all four spectral CCDs have the same position. This will improve the results, by using also the NIR information. Another advantage will be the availability of newest ADS40 imagery for entire Switzerland every three years. In this case, the dependence on image on request will cease to exist. To make this approach more valuable and applicable for e.g. entire Switzerland it is also planned to test other tree species of different geographical regions (e.g. Central and Southern Alps). Another approach will be the usage of tree texture properties and of the seasonal variability of tree species using multi-temporal data.

The **third objective**, the extraction of forest stands, produced visually satisfactory results but still suffers from some limitations. Structure, the third necessary parameter to define a stand, had to be ignored since it can only be derived from full-waveform LiDAR data. Another drawback is that we used tree height classes supposing a relation to the diameter at breast height. Nevertheless, with the fusion of national LiDAR data and spectral information we are able to extract semi-automatically stand classes that will help for a better understanding of the structure of forest.

To summarize, this study clearly shows the potential and the limits of the fusion of medium-footprint LiDAR data and ADS40 imagery (and also CIR aerial images) to extract the forest attributes: area, composition and stand. These forest attributes will help to support some tasks in the Swiss NFI (e.g. stereo-image interpretation, field surveys) and might be useful for updating existing forest masks, forest management and protection tasks on a regional level and in future also on a national level. The study also reveals that the use of nation wide available LiDAR data is obvious, but in case of Switzerland restricted due to operational constraints. In Switzerland the medium footprint LiDAR data does not meet the requirements for single tree detection and accurate derivations of forest parameters as performed in many case studies and in forest inventories. Additionally, the LiDAR data acquisition time is not focused on single specific

questions the data has to serve for different purposes. A future alternative would be to derive DSMs from ADS40 data for entire Switzerland with at least the accuracy of the LiDAR data.

Acknowledgements

The study was funded by the Swiss Agency for the Environment, Forest and Landscape (BAFU) and WSL. We acknowledge Patrick Thee for his support in the field surveys.

References

- Akca, D., 2005. Registration of point clouds using range and intensity information. In: E. Baltsavias, A. Gruen, L. Van Gool, M. Pateraki (Eds.). *The International Workshop on Recording, Modeling and Visualization of Cultural Heritage*, Ascona, Switzerland, May 22-27, Taylor & Francis/Balkema, Leiden: 115-126.
- Artuso, R., St. Bovet, St., and Streilein, A., 2003. Practical methods for the verification of country-wide terrain and surface models. *Proceedings of the ISPRS working group III/3 workshop XXXIV-3/W13. 3-D reconstruction from airborne laserscanner and InSAR data*, 8-10 March, 2003, Dresden, Germany.
- Baatz, M. and Schäpe, A., 2000, Multiresolution Segmentation – an optimization approach for high quality multi-scale image segmentation. In: J. Strobl, T. Blaschke and G. Griesebner (eds.). *Angewandte Geographische Informationsverarbeitung Vol. XII*, (Heidelberg, Germany, Wichmann Verlag), pp. 12-23.
- Baltsavias, E., 1999. Airborne laser scanning: existing systems and firms and other resources. *ISPRS Journal of Photogrammetry and Remote Sensing*, 54, 164-198.
- Baltsavias, E., Gruen, A., Eisenbeiss, H., Zhang, L. and Waser, L.T., 2008. High Quality Image Matching and Automated Generation of 3D Tree Models. *International Journal of Remote Sensing*, 29(5), 1243 - 1259.
- Brassel, P. and Lischke, H., 2001. *Swiss National Forest Inventory: methods and models of the second assessment*. Birmensdorf, Swiss Federal Research Institute WSL, 336 p.
- Gruen, A. and Akca, D., 2005. Least squares 3D surface and curve matching. *ISPRS Journal of Photogrammetry and Remote Sensing*, 59(3), 151-174.
- Hollaus, M., W. Wagner, W., Eberhöfer, C., and Karel, W., 2006. Accuracy of large-scale canopy heights derived from LiDAR data under operational constraints in a complex alpine environment. *ISPRS Journal of Photogrammetry and Remote Sensing*, 60(5), 323-338.
- Holmgren, J. and Persson, A., 2004. Identifying species of individual trees using airborne laser scanner. *Remote Sensing of Environment*, 90, 415-423.
- Hyypä, J., Hyypä, H., Inkinen, M., Engdahl, M., Linko, S., and Yi-Hong, Z., 2000, Accuracy comparison of various remote sensing data sources in the retrieval of forest stand attributes. *Forest Ecology and Management*, 128, 109-120.
- Küchler, M., Ecker, K., Feldmeyer-Christe, E., Graf, U., Küchler, H., and Waser, L.T. 2004. Combining remotely sensed spectral data and digital surface models for fine-scale modeling of mire ecosystems. *Community Ecology*, 5(1), 55-68.
- Lamonaca, A., Corona, P., Barbati, A. Exploring forest structural complexity by multi-scale segmentation of VHR imagery. *Remote Sensing of Environment* (2008), doi:10.1016/j.rse.2008.01.017.
- McCullagh, P. and Nelder, J.A., 1983. *Generalized linear models*. Chapman and Hall, London, 511 p.
- Naesset, E. and Gobakken, T., 2005. Estimating forest growth using canopy metrics derived from airborne laser scanner data. *Remote Sensing of Environment*, 96, 453-465.
- Scott, J.M., Heglund, P.J., Samson, F., Haufler, J., Morrison, M., and Wall, B., 2002. *Predicted species occurrences: issues of accuracy and scale*, Island Press, Covelo, California, 868 p.

- St-Onge, B., Jumelet, J., Cobello, M., and Vega, C. 2004. Measuring individual tree height using a combination of stereophotogrammetry and lidar. *Canadian Journal of Forest Research*, 34(10), 2122-2130.
- Straub, B., 2003. Automated Extraction of Trees from Aerial Images and Surface Models. *The International Archives of Photogrammetry and Remote Sensing*, XXXIV-3/W8, 157-164.
- Waser, L.T., Baltsavias, E., Ecker, K., Eisenbeiss, H., Ginzler, C., Küchler, M., Thee, P. and Zhang, L., 2008a. High-resolution digital surface models (DSM) for modelling fractional shrub/tree cover in a mire environment. *International Journal of Remote Sensing*, 29(5), 1261 - 1276.
- Waser, L.T., Baltsavias, E., Ecker, K., Eisenbeiss, H., Feldmeyer-Christe, E., Ginzler, C., Küchler, M., Thee, P. and Zhang, L., 2008b. Assessing changes of forest area and shrub encroachment in a mire ecosystem using digital surface models and CIR-aerial images. *Remote Sensing of Environment*, 112(5), 1956 - 1968.
- Watt, P.J. and Donoghue, D.N.M., 2005. Measuring forest structure with terrestrial laser scanning. *International Journal of Remote Sensing*, 26(10), 1437-1446.
- Zhang, L. and Gruen, A., 2004. Automatic DSM generation from linear array imagery data. *The International Archives of Photogrammetry, Remote Sensing and Spatial Information Sciences*, XXXV, Part B3, 2004: 128-133.
- Zhang, L., 2005. Automatic Digital Surface Model (DSM) Generation from Linear Array Images, PhD Thesis, Report No. 88, Institute of Geodesy and Photogrammetry, ETH Zurich, Switzerland.

Developing strategies for large scale forest inventories combining LiDAR data, satellite imagery and regional yield models

Markus Weidenbach, Roeland de Kok, Piotr Wezyk and Stanislaw Szombara

LandConsult.de, office@landconsult.eu

Geographic Information Management and Environmental Planning, Schenkenzell,
Germany

University of Agriculture, Krakow, Poland

ProGea Consulting, Krakow, Poland

Abstract

The work illustrates a practical and economical way to combine airborne laser scanning data (ALS) and spectral information from Quickbird satellite imagery or digital orthophotos with regional yield models in order to assess the stand volume and other relevant forest parameters. New methods to integrate Laser Scanning and Remote Sensing into the traditional stand wise forest taxation are shown on examples of (a) state owned and mainly even-aged forests in Saxonia and Poland and (b) privately owned all-aged plenter woods (Plenterwald) in the Black Forest in Baden-Wuerttemberg. The automatic detection of trees from Quickbird Satellite images and true-orthophotos by means of Object Based Image Analysis (OBIA) as well as the detection of trees purely based on laser point data is shown. Tree height, location, density, distribution and tree type of each of the more than 165000 automatically detected trees, all stored in a GIS database, are used as input information to apply different regional yield models. For even-aged forests, homogenous stands and/or tree groups have been defined to assess the volume of the growing stock considering tree species, age (if known), density and stand openings. For all-aged and nature-like plenter woods (Plenterwald), the assessment of the growing stock is based on single tree information, and on specific auxiliary yield tables for plenter woods. The LiDAR and spectral measurements and volume estimations have been compared with the actual field taxation. The results are discussed and critical issues such as the potential of satellite and ALS data to derive relevant forestry parameters, or the possible costs for such an analysis, are addressed and recommendations for an economic workflow and system integration are given.

Describing the selected canopy layer parameters of the Scots pine stands using ALS data

Wezyk P., Tompalski P., Szostak M., Glista M., Pierzchalski M.

Laboratory of GIS & Remote Sensing, Faculty of Forestry,
Agricultural University in Krakow, Poland
rlwezyk@cyf-kr.edu.pl

Abstract

The purpose of the study was to determine the usefulness and improve understanding of ALS technology in acquisition of selected parameters of canopy layers for individual trees and whole stands. This approach based on ALS data (TopoSys fiber scanner) was compared to reference data from forest inventory (432 Scots pines). The results of our study indicate the following: (1) height for single trees derived from ALS data leads to underestimation (mean difference -0.90 m or +0.12 m depending on CHM generation algorithm); (2) mean height for a stand was higher (+0.85 m) than the height from SILP database what can results in whole Milicz Forest district in underestimation of the wood volume; (3) mean height of a stand (understanding as 95th percentile of the FE point cloud) was +0.46 m higher than the height from SILP inventory database; (4) it was possible to estimate the base of crown with underestimation of 0.52 m; (5) length of crown measured during the forest inventory was +0.42 m higher if compared to ALS data (analysis of histogram); (6) crown surface area was slightly greater and crown volume was slightly smaller than the reference; (7) homogeneity of an even-aged-pine stand is questionable. In the very near future the new approach of forest inventory supported with ALS data is expected as a list of the new parameters and guidelines.

Keywords: tree height, base of crown, tree crown length, surface area and volume, homogeneity

1. Introduction

One of the most significant parameters used by foresters is the tree stand height. The definition of timber volume of a single tree or stand is based on formulas which use mainly the diameter at breast height (DBH) and tree height, thus the accuracy in the estimation of the timber stock is directly linked with the quality of these parameters. In management forests, particularly single-species and even-age tree stands, artificially renewed from homogenous genetic material, height should not vary too much, provided the forest site conditions are the same and human treatments (e.g. thinning) are identical. The traditional measurement of tree height with hypsometer is affected by the instrument error and subjectivity in pointing the tree top by the operator. In some situations, high density of the stand, windy weather or a small number of leaves may cause additional errors. Methods using the remote sensing technologies (e.g. photogrammetry) have been known for decades, but they have always been work intensive. Nowadays these methods become more and more competitive due to the technology of digital airborne cameras and the process of automatic stereo-matching (Baltsavias *et al.* 2008). Other technologies, such as radar or LiDAR offer a completely new approach in forest practice in the measurement of selected parameters. LiDAR is not limited to the circular inventory plot, on which foresters used to describe the whole stand, but validation studies are generally performed at the plot level or at the tree level (Means *et al.* 2000) because of the reference data. The measurements of the stand height with ALS have already been studied by many authors (Næsset 1997, 2004, Kwak *et al.* 2007). Given that the accuracies of the estimation of tree stand height

(h) are usually different, there is a general trend towards underestimation of this feature (Hyypä et al. 2004, Maltamo et al. 2004, Rönnholm et al. 2004, Yu et al. 2004). Only few studies (Næsset and Økland 2002, McGaughey *et al.* 2004) show a reverse trend of overestimation. ALS data is also used in the definition of other parameters, such as: base of crown (Næsset and Økland 2002, Hall *et al.* 2005, Popescu and Zhao 2008), crown depth/L (Næsset and Økland 2002, Maltamo *et al.* 2006), crown diameter (Popescu *et al.* 2003), density of stems in a stand (Riaño et al. 2003, Hall et al. 2005), biomass (Lim and Treitz 2004, Popescu 2007) or timber volume (Næsset 2004, Hollaus et al. 2007).

2. Method

2.1 Study area

For this study we chose forest stands located in a central-west part of Poland (51°27' N; 17°12' E) belonging to the Forest District of Milicz and owned by the Wroclaw Regional Directorate of the Polish State Forest National Holding. In this area different GI technologies (ALS, TLS, photogrammetry) are tested in terms of their usefulness in forest inventory (Wezyk *et al.* 2007). In this paper we present the results from our studies based on 21 inventory plots covered with Scots pine. Depending on the stand age, the plot size varies from 50m² (26 years) to 500m² (107 years).

2.2. Reference data

The reference data used in this project came from several sources. One of them, the most often quoted, is later on referred to as forest inventory. This measurement, based on the Polish State Forests inventory guidelines (IUL PGLP 2003), was carried out in August 2006 by the company Taxus SI Ltd. The inventory campaign delivered the selected tree taxation parameters like: tree species, position on the inventory plot (polar measurement), height of tree (h_t), base of crown, DBH, diameter at 5.0 m, centre of the crown position and shape of the crown. Height of tree and base of crown were measured using the hypsometer Vertex III (Haglöf, Sweden) with 0.1 m accuracy. Another set of reference data comes from the SILP database (the descriptive database of the Polish State Forest) and was updated in year 2005 (regular forest inventory). However, SILP database provides information for a whole stand as an average height, DBH, volume and other parameters. The centres of the plots were determined with dGPS survey (Trimble Pathfinder ProXRS). Data collected with Terrestrial Laser Scanning (TLS; FARO LS 880) was also used (Wezyk *et al.* 2007).

2.3. ALS data

The airborne campaign was carried out in July 2007 using the TopoSys glass fiber scanner Falcon II with a so called “swing mode”. The mean relative height of flight was about 550 meters above the ground. The mean point density was ca. 14 pts/m² (varied from 9 to 18 pts). Single scans were delivered in ASCII format (raw data) and raster format data as well (DSM and DTM).

2.4. Hardware and software

In this project Terrascan and Terramodeler (Terrasolid Ltd.) software was used in the processing and classification of the point cloud (ASCII XYZ) and DTM generating. In calculating of the canopy metrics, the FUSION (McGaughey 2007) was used. The LASEdit (Cloud Peak) software was used to control the correctness of the file structure *.LAS, the ArcViewGIS 9.1 (ESRI) in 3D GIS analyses (GRID) and Statistica 8.0 (StatSoft Inc.) for statistical purpose.

2.5. Canopy surface and height

Surfaces representing the forest canopy were generated using the FUSION software

(McGaughey 2007). Two different crown models (called: CHM1 and CHM2) were saved in *.dtm format. The CHM1 surface was generated without preserving the local maxima from point cloud but with two filters - median and smoothing filter. The CHM2 surface was generated with the additional option of “preserve the local maxima and minima”. The canopy surfaces were exported to the ASCII GRID (ESRI) and in this environment the 3D analyses, like calculating the volume and surface area of the canopy layer, were performed. The heights of single trees (h_i) were defined by GIS analysis overlaying the polygons representing the outline of the crown with layer CHM2 (GRID zonal statistic). For the needs of the vertical structure analysis (histogram generation) and the prediction of base-of-living-crown, ALS was used as point cloud XYZ. Similarly, the mean height for selected compartments was calculated as 95th percentile (FUSION software) of the ALS point cloud and not from the modelled CHM1 and CHM2 surfaces. In this case we accepted size of pixel representing the tree crown as 10 by 10 meters.

2.6. Estimation of the base-of-crown based on the ALS histograms

Based on the percentage distribution (above 1%) of the number of LiDAR impulses from the point cloud in height gradient (0.5m intervals) the histogram of the base of crown for individual tree and for the whole compartment was made. These results were compared to the visual interpretation made by 7 operators. The length of green crown may be defined as the vertical distance from the tree top to the lowest living branch. While the upper limit (tree height) can be objectively defined, the base of crown is often very subjective to ascertain.

2.7. Tree crown shape

The centre of the crown and the edges of 8 opposite sites of the crown were projected vertically to the ground by forest inventory in July 2006. Some trees between forest inventory (2006) and LiDAR flight (2007) were cut down (thinning) so authors decided to use the crown shapes collected from TLS (2006), which had more accurate outlines. Crown TLS outlines were used in defining e.g. density of points in individual crowns, maximal high point inside the crown polygon or the crown base, with the methods available in FUSION program and 3D GIS spatial analysis.

2.8. Tree crown surface area and volume

Crown surface area and volume can be approximated by assuming that the crown is a regular geometric solid like a cone or paraboloid. If we assume that a cone is a reasonable approximation for the Scots Pine crown, the surface area (Equation 1 after Avery and Burkhart 2002) and volume (Equation 3 after Avery and Burkhart 2002) can be computed. However, if a paraboloid is chosen, then crown surface and volume would be computed using different formulas Equation 2 after Laar & Akca (1997) and Equation 4 after Brack (2008) respectively. In each equation the same crown width value (CW) was used, determined on the TLS data.

$$CSA = \frac{\pi CW}{2} * \sqrt{L^2 + \left(\frac{CW}{2}\right)^2} \quad (1) \quad CV = \frac{\pi CW^2 CL}{12} \quad (3)$$

$$CSA = \frac{\pi CW}{12 CL^2} (4 CL^2 + \frac{1}{4} CW^2)^{3/2} \quad (2) \quad CV = \pi \frac{CW^2 CL}{8} \quad (4)$$

where: CSA – crown surface area [m²]; CV – crown volume [m³]; CW – crown width [m]; CL – crown length [m]

3. Results and discussion

3.1 Height

Firstly the results of height measurements obtained with different methods (SILP descriptive data base, forest inventory = F.INV, TLS, CHM1 and CHM2) were subduced to a statistic variance analysis. The significance of differences was tested with a non-parametric Friedman's (ANOVA) test for many variables and a Wilcoxon test for two variables. Analyzing all the 432 pines, high and highly significant differences were found in comparison of two groups of methods: traditional measurement with hypsometer (forest inventory 2006) with TLS and ALS methods (CHM1 and CHM2) as well as SILP (2005). The analysis in age groups up to 60 years and above 60 year old trees showed significant differences ($0.01 < p < 0.05$) in comparison with CHM2 and forest inventory/TLS/CHM1 (up to 60 years old), and additionally for older tree stands (above 60 years old) with the pairs of forest inventory methods and TLS/CHM1.

Generally, a typical trend was observed in the comparison of traditional field measurements (Vertex; Haglöf) and ALS technology. Graph (Fig. 1) and Tab1 clearly shows that ALS (CHM1 and CHM2) method of individual trees height measurement result in underestimation up to -0.90 m (SD=1.77 m) in case of CHM1 surface and -0.12m (SD=1.81 m) for CHM2, respectively. The difference of height read from two surfaces: CHM1 and CHM2 were on average 0.75 m (CHM2 was generated with option "preserve local maxima"). The additional analysis on the ALS point cloud were made of first echo (FE) points to defining the highest point within the crown. This analysis showed that the CHM2 canopy surface was closer to highest points (+0.20m) than CHM1 (-0.50m).

The mean height of the Scots pine read from the SILP (2005) data base was 1.14 m lower than gathered during the forest inventory (2006), which could indicate inaccuracies of the previous measurements (the localizations of the inventory plots of 2005 are unknown). Yearly mean height increment was only about $0.15 \div 0.20$ m in those pine stands. Mean difference between forest inventory (2006) and TLS showed -0.98 m value, which could indicate the underestimation of terrestrial laser scanner, however only assuming full correctness of reference data. This convinces the authors that the tree height reference, based on quite a subjective measurement, should not necessarily be taken as unquestionable, even when the state-of-the-art hypsometer was used. Considering the quality of height (h_t) from ALS, one should keep in mind that reference data are collected with a basically unknown error (estimated 5-10%). Therefore additional test was made in the field using the same hypsometer and 6 observers. The comparison was made on three conifer trees and its result confirms that height measurement is very subjective (st. dev. 0.56m, maximum difference from mean: +0.67m and -0.79m). The only reliable way to measure tree height, requires cutting down the tree or applying very accurate surveying with total station (Andersen *et al.* 2006).

A key factor in defining the tree height with ALS methods seems to be the selection of the algorithm to generate DTM. In case of the occurring understory or a small number of points (LE) on the ground due to a very dense forest canopy - the underestimation of tree height can take place (Pyysalo 1999). Another important step is generating the canopy surface model (CHM). The result of the comparison to the highest point within the crown indicates that CHM2 presents the reality rather accurately (-0.12m) then CHM1 surface, what results in a greater difference between CHM2 and the SILP database (+0.85 m; $R^2=0.95$; SD= 1.02 m; Tab.1). Concurrently, it has to be remembered that SILP data base (2005) values does not necessarily have to be reliable for a whole compartment.

The carried out regression analysis for all the pairs of measurement methods showed that the lowest value of the determination coefficient ($R^2=0.73$) was find for the group of variables:

SILP – forest inventory (Tab.1). Satisfactorily high indexes $R^2=0.95$ were obtained in the regression analysis for both variables CHM1 and CHM2 based on data obtained from ALS, in the relation to explanatory variable SILP.

There were not high differences between our results and other projects regarding the height determination of deciduous forest stands. In most papers, the mean error of the estimation of height took values below zero, indicating the underestimation of tree height based on ALS (Hyypä *et al.* 2004, Maltamo *et al.* 2004, Rönnholm *et al.* 2004, Yu *et al.* 2004, Andersen and Breidenbach 2007) or close to zero; i.e. equal to the reference (Næsset 2004). Only results were obtained only by Næsset and Økland (2002) and McGaughey *et al.* (2004), show relatively small “overestimation” to the reference (respectively +0.18m and +0.29m).

Tab. 1 - Statistics of tree height (h_i) measured by selected methods. (**) – very high significant differences, $p<0.01$; (*) – significant differences, $0.01<p<0.05$; (n) – not significant differences; all 432 trees

| | | F. INV | SILP | TLS | CHM1 | CHM2 |
|--------|---------------------|--------|------------|------------|------------|-----------|
| F. INV | mean difference [m] | | -1.14 (**) | -0.98 (**) | -0.90 (**) | -0.12 (n) |
| | R^2 | | 0.73 | 0.81 | 0.81 | 0.80 |
| | SD of difference | | 2.15 | 2.18 | 1.77 | 1.81 |
| SILP | mean difference [m] | | | 0.02 (n) | 0.13 (n) | 0.85 (*) |
| | R^2 | | | 0.96 | 0.96 | 0.95 |
| | SD of difference | | | 1.01 | 0.94 | 1.02 |
| TLS | mean difference [m] | | | | 0.08 (n) | 0.83 (**) |
| | R^2 | | | | 0.95 | 0.94 |
| | SD of difference | | | | 0.86 | 0.94 |
| CHM1 | mean difference [m] | | | | | 0.75 (**) |
| | R^2 | | | | | 0.98 |
| | SD of mean | | | | | 0.58 |

3.2 Base and the length of crown

Mean difference between the base of crown determination using the traditional forest inventory method and ALS data was +0.52 m, indicating the underestimation by LiDAR (SD=1.5 m). The analysis of histograms on 0.5m slices of the point cloud ALS, e.g. for 214c (19.89 ha) showed that 82,30 % points (of over 2.5 million) remained in the layer, and only 12.5% of all impulses reached the ground. Regression analysis ($R^2=0.65$) indicates relation between field and ALS measurements (Fig. 2). Further analyses of the point cloud ALS showed that in compartment 214c (plots no.: 25, 27, 28 and 29) mean base of crown read from histogram by 7 operators was 15.9 m and thus was lower (-1.59 m) from that calculated automatically (17.49 m) for individual trees. It was found that mean base of crown differed by +1.65 m from the value defined for the whole compartment. There can be many causes for the problem of correct definition of the base of crown. First of all, the compactness of foliage conditions as well as the occurrence of dead branches on stems (underestimation +1.4 m above reference (Chasmer *et al.* 2006). Næsset & Økland (2002), Hall *et al.* (2005) and recently by Popescu & Zhao (2008) obtained similar coefficients R^2 equalling: 0.53, 0.80 and 0.79, respectively.

Additional test done during the field campaign on three conifer trees by the same 6 operators, showed that the base of crown measurement can vary from +1.11m to -0.76m (st. dev. 0.69) from the mean value. This result confirms that also the base of living crown measurement is very man-dependent.

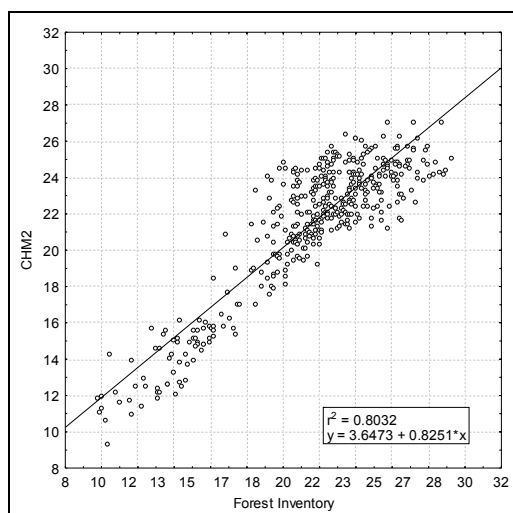


Fig. 1 - Regression analysis for the height (h_t) of the single tree for the CHM2 variable explained by the forest inventory ground truth data.

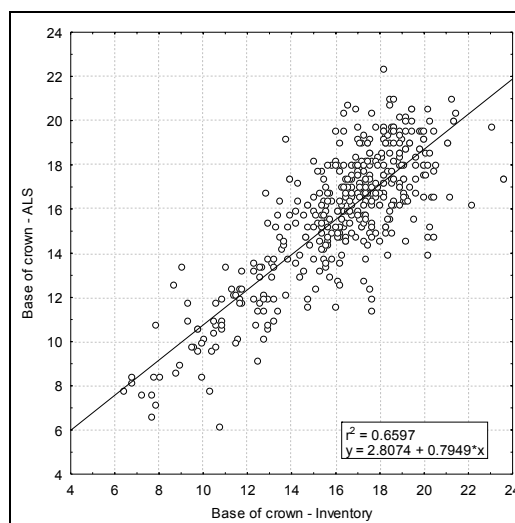


Fig. 2 - Linear regression for the base of living crown estimated from ALS (reference = Forest inventory)

The accuracy of the definition of crown length (L) was probably affected by the base of crown rather than the tree height estimation using ALS. Mean difference in the lengths (L) of crowns compared to reference data (forest inventory) was -0.42 m, which generally mean underestimation for the ALS method. For younger tree stands (<80 years) the difference in crown length (L) was only -0.22 m, while in older trees (>80 yr) as much as -0.56 m. Regression analysis showed relatively low value of coefficient $R^2=0.28$. The higher explaining value $R^2=0.51$ for crown lengths estimated from ALS was obtained by Næsset & Økland (2002) in their studies.

3.4 Crown area surface and volume of the tree and canopy layer

Carried out analysis of the crown surface area and crown volume were based on formulas (1, 3) for cone and (2, 4) for paraboloid.

Results for crown surface area indicate differences of about 15.1% and 36.6% (for cone and paraboloid method respectively) in the surface of the individual tree crowns. Crown surface area defined in GIS analyses for CHM (surface 3D + projection on a 2D surface) showed the differences reaching from 17.4% (cone) to 26.5% (paraboloid) compared to the sum of the crown areas of individual trees. Generating the canopy surface (CHM) makes the area of canopy layer differ by c.a. 11% to 28.6% compared to the sum of crown surface area calculated for individual crowns. Clear declining trend in crown surface area value with the age of the stand was also noticed.

The volume of the forest canopy defined from ALS surface is slightly smaller than the sum of individual crowns defined by the forest inventory (on average -9.0% for cone and -38.5% for paraboloid). The difference in volume between the solid generated from CHM (3D) with its base (2D) with the sum of individual crowns understood as paraboloid reached the average value of -38.7% (ALS) and -38.5% (forest inventory). Such differentiation resulted from the structure of the crown, difference in defining its length (L), and the CHM interpolation errors.

3.5 Homogeneity of the stand

Mean height of tree stands in analysed compartments, defined by authors as the 95th of the point cloud (FE only), varies from SILP data base (+0.47m; SD=0.60). It should be added that possibly the growth of tree stands from year 2005 to 2007 would partially equalize this difference. The authors did not know the localization of the sample plots used in defining the SILP height used in 2005. The differences in measured taxation features can be relatively high. This can result from the differentiation of a soil micro-site, cultivation procedures carried out during the forest stand lifetime, and random phenomena (breaking of the trees, pest invasion etc). Mean difference between height defined for the whole compartment and the mean height of the inventory plots was -0.37 m (SD=0.95). The spatial distribution of height (mean value H=20.96m) in a selected forest compartment 232b is presented in Fig. 3.

It is well known that the distribution of the DBH in the forest stand is close to normal, therefore there are also differences in the tree heights. However, in many cases, the spatial distribution of tree height in a single compartment indicates that the borders do not contain homogeneous stands (as it is shown in Fig. 3) because of diversity of the soil, humidity, solar radiation, wind etc.

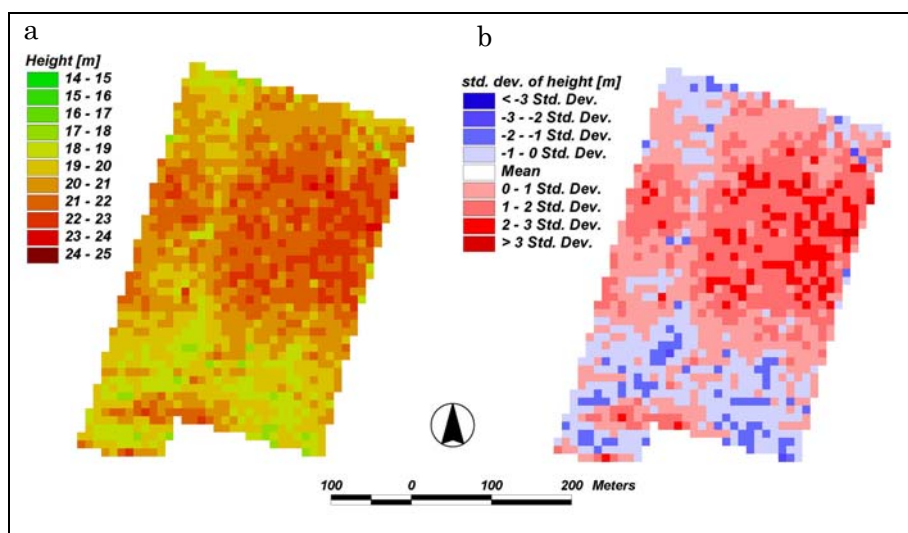


Fig. 3. Spatial distribution (a) and standard deviation (b) of height in compartment 232b.

4. Conclusions

Presented study addressed different questions related to the 3D spatial distribution of laser beams within a canopy of Scots pine stands using a different set of ground truth data, like forest inventory measurements, TLS, SILP databases, and ALS data. Seeking alternative methods of defining the base of crown height is encouraged by the fact that traditional methods are very time consuming and subjective. ALS technology for the first time gives the opportunities of describing the whole tree stand and not only its fragments represented by forest inventory plots. The results of our study indicate the following: (1) height for single trees derived from ALS data leads to small underestimation depending on CHM generation algorithm (e.g. 0.12 m for CHM2); (2) mean height for a stand was higher (+0.85 m) than the height from SILP database what can results in whole Milicz Forest district in underestimation of the wood volume; (3) mean height of a stand (understanding as 95th percentile of the FE point cloud) was +0.46 m higher than the height from SILP inventory database; (4) it was possible to estimate the base of crown with slight underestimation (-0.52 m) using the histogram of the ALS data; (5) length of crown measured from ALS was lower compared to reference data (0.42 m); (6) crown surface

area was slightly greater and crown volume was smaller than the reference; (7) spatial homogeneity of height in the even-aged pine stand is questionable and lead to the urgent revision of the compartment borders. In the very near future new approaches of forest inventory supported with ALS data is expected as a list of new parameters and guidelines. Paper shows a need of further studies on ALS integration with other data sources (like TLS, digital aerial imageries) as a potential cost-effective operational forest inventory method for estimation of whole stand biomass. Future studies based on the single-tree approach should lead to precise forestry and to the optimization of forest inventory, like the new methodology in forest sampling.

Acknowledgements

Many thanks to the General Directorate of the Polish State Forest National Holding for financing of the RTD project: “Elaborating the method of forest inventory, based on the integration of selected geomatic techniques” managed by Warsaw Agricultural University (SGGW).

References

- Andersen H.-E. & Breidenbach J., 2007. Statistical properties of mean stand biomass estimators in a lidar-based double sampling forest survey design. Rönholm P., Hyypä H. i Hyypä J. (eds.): *ISPRS Workshop on Laser Scanning 2007 and SilviLaser 2007*. Espoo, Finland. International Archives of Photogrammetry, Remote Sensing and Spatial Information Sciences. XXXVI, Part 3 / W52.
- Andersen H. E., Reutebuch S. E. & McGaughey R. J., 2006. A rigorous assessment of tree height measurements obtained using airborne lidar and conventional field methods. *Canadian Journal of Remote Sensing*, Vol: 32 (5), 355-366.
- Avery T. E. & Burkhart H. E., 2002. Forest measurements. McGraw-Hill.
- Baltsavias E., Gruen A., Eisenbeiss H., Zhang L. & Waser L. T., 2008. High-quality image matching and automated generation of 3D tree models. *International Journal of Remote Sensing*, Vol: 29 (5), 1243-1259.
- Brack C., 2008. Tree crown. <http://sres-associated.anu.edu.au/mensuration/crown.htm#area>
- Chasmer L., Hopkinson C. & Treitz P., 2006. Investigating laser pulse penetration through a conifer canopy by integrating airborne and terrestrial lidar. *Canadian Journal of Remote Sensing*, Vol: 32 (1-2), 116-125.
- Hall S. A., Burke I. C., Box D. O., Kaufmann M. R. & Stoker J. M., 2005. Estimating stand structure using discrete-return lidar: An example from low density, fire prone ponderosa pine forests. *Forest Ecology and Management*, Vol: 208 (1-3), 189-209.
- Hollaus M., Wagner W., Maier B. & Schadauer K., 2007. Airborne laser scanning of forest stem volume in a mountainous environment. *Sensors*, Vol: 7 (8), 1559-1577.
- Hyypä J., Hyypä H., Litkey P., Yu X., Haggren H., Rönholm P., Pyysalo U., Pitkanen J. & Maltamo M., 2004. Algorithms and methods of airborne laser-scanning for forest measurements. Thies M., Koch B., Spiecker H. i Weinacker H. (eds.): *Laser-Scanners for Forest and Landscape Assessment: Proceedings of the ISPRS Working Group VIII/2*. Freiburg, Germany. International Archives of Photogrammetry, Remote Sensing, and the Spatial Information Sciences. XXXVI-8/W2.
- IUL PGLP, 2003. *Część 1. Instrukcja sporządzania planu urządzania lasu dla nadleśnictwa. Załącznik do zarządzenia nr 43 dyrektora generalnego lasów państwowych z dnia 18*

kwietnia 2003 r. Państwowe Gospodarstwo Leśne Lasy Państwowe. Warszawa.

- Kwak D. A., Lee W. K., Lee J. H., Biging G. S. & Gong P., 2007. Detection of individual trees and estimation of tree height using LiDAR data. *Journal of Forest Research*, Vol: 12 (6), 425-434.
- Laar A. V. & Akca A., 1997. Forest mensuration. Cuvillier Verlag. Gottingen.
- Lim K. S. & Treitz P. M., 2004. Estimation of above ground forest biomass from airborne discrete return laser scanner data using canopy-based quantile estimators. *Scandinavian Journal of Forest Research*, Vol: 19 (6), 558-570.
- Maltamo M., Hyypä J. & Malinen J., 2006. A comparative study of the use of laser scanner data and field measurements in the prediction of crown height in boreal forests. *Scandinavian Journal of Forest Research*, Vol: 21 (3), 231-238.
- Maltamo M., Mustonen K., Hyypä J., Pitkänen J. & Yu X., 2004. The accuracy of estimating individual tree variables with airborne laser scanning in a boreal nature reserve. *Canadian Journal of Forest Research*, Vol: 34 (9), 1791-1801.
- McGaughey R. J., 2007. Fusion/ldv: Software for lidar data analysis and visualization. Software manual. USDA Forest Service. Pacific Northwest Research Station.
- McGaughey R. J., Carson W., Reutebuch S. & Andersen H.-E., 2004. Direct measurement of individual tree characteristics from lidar data. *Proceedings of the Annual ASPRS Conference*. Denver. American Society of Photogrammetry and Remote Sensing.
- Means J. E., Acker S. A., Fitt B. J., Renslow M., Emerson L. & Hendrix C. J., 2000. Predicting forest stand characteristics with airborne scanning lidar. *Photogrammetric Engineering and Remote Sensing*, Vol: 66 (11), 1367-1371.
- Næsset E., 1997. Determination of mean tree height of forest stands using airborne laser scanner data. *ISPRS Journal of Photogrammetry and Remote Sensing*, Vol: 52 (2), 49-56.
- Næsset E., 2004. Practical large-scale forest stand inventory using a small-footprint airborne scanning laser. *Scandinavian Journal of Forest Research*, Vol: 19 (2), 164-179.
- Næsset E. & Økland T., 2002. Estimating tree height and tree crown properties using airborne scanning laser in a boreal nature reserve. *Remote Sensing of Environment*, Vol: 79 (1), 105-115.
- Popescu S. C., 2007. Estimating biomass of individual pine trees using airborne lidar. *Biomass and Bioenergy*, Vol: 31 (9), 646-655.
- Popescu S. C., Wynne R. H. & Nelson R. F., 2003. Measuring individual tree crown diameter with lidar and assessing its influence on estimating forest volume and biomass. *Canadian Journal of Remote Sensing*, Vol: 29 (5), 564-577.
- Popescu S. C. & Zhao K., 2008. A voxel-based lidar method for estimating crown base height for deciduous and pine trees. *Remote Sensing of Environment*, Vol: 112 (3), 767-781.
- Pyysalo U., 1999. A method to create a three-dimensional forest model from laser scanner data. *The Photogrammetric Journal of Finland*, Vol: 17 (1), 34-42.
- Riaño D., Meier E., Allgöwer B., Chuvieco E. & Ustin S. L., 2003. Modeling airborne laser scanning data for the spatial generation of critical forest parameters in fire behavior modeling. *Remote Sensing of Environment*, Vol: 86 (2), 177-186.
- Rönholm P., Hyypä J., Hyypä H., Haggrén H., Yu X. & Kaartinen H., 2004. Calibration of laser-derived tree height estimates by means of photogrammetric techniques. *Scandinavian Journal of Forest Research*, Vol: 19 (6), 524-528.

- Wezyk P., Koziol K., Glista M. & Pierzchalski M., 2007. Terrestrial laser scanning versus traditional forest inventory. First results from the polish forests. Rönnholm P., Hyypä H. i Hyypä J. (eds.): *ISPRS Workshop on Laser Scanning 2007 and SilviLaser 2007*. Espoo, Finland. International Archives of Photogrammetry, Remote Sensing and Spatial Information Sciences. XXXVI, Part 3 / W52. 424-429.
- Yu X., Hyypä J., Kaartinen H. & Maltamo M., 2004. Automatic detection of harvested trees and determination of forest growth using airborne laser scanning. *Remote Sensing of Environment*, Vol: 90 (4), 451-462.

Author Index (first author only):

| | |
|---------------------|-----------------|
| Abd Latif Z. | p.151 |
| Alexander C. | p.343 |
| Alves M.V.G | p.354 |
| Antolín R. | p.355 |
| Arroyo L.A. | p.113 |
| Barilotti A. | p.134 |
| Bater C.W. | p.365 |
| Breidenbach J. | p.266, 366, 373 |
| Buddenbaum H. | p.377 |
| Crow P. | p.384 |
| Danson F.M. | p.335 |
| Desclée B. | p.67 |
| Devereux B.J. | p. 386 |
| Dorigo W. | p.274 |
| Dubayah R. | p.178 |
| Durrieu S. | p.325 |
| Flewelling J. | p.284 |
| Fusco S. | p.387 |
| Gagliasco D. | p.388 |
| García-Gutiérrez J. | p.389 |
| García M. | p.398 |
| Gaulton R. | p.407 |
| Gobakken T. | p.14 |
| Goepfert J. | p.417 |
| Goetz S.J. | p.168 |
| Gonçalves G. | p.427 |
| González D. | p.437 |
| Griffin A.M.R. | p.446 |
| Guindon L. | p.456 |
| Hancock S. | p.199 |
| Heinzel J.N. | p.76 |
| Hill R.A. | p.III |
| Hirata Y. | p.144 |
| Höfle B. | p.227 |
| Holmgren J. | p.50 |
| Holopainen M. | p.105, 458 |
| Kaartinen H. | p.467 |
| Kim Y. | p.477 |
| Kwak D-A | p.237 |
| Litkey P. | p.295 |
| Lin Y-C | p.478 |
| Lindberg E. | p.488 |

| | |
|------------------|-------|
| Los S.O. | p.497 |
| Lucas R.M. | p.2 |
| Melkas T. | p.315 |
| Miura N. | p.126 |
| Morsdorf F. | p.257 |
| Nakajima T. | p.498 |
| Nelson R. | p.207 |
| Newton W.E. | p.124 |
| North P. | p.189 |
| Olofsson K. | p.95 |
| Oono K. | p.508 |
| Packalén P. | p.22 |
| Parker R.C. | p.30 |
| Pascual C. | p.517 |
| Pesonen A. | p.526 |
| Pflugmacher D. | p.536 |
| Pirotti F. | p.537 |
| Rahman M.Z.A. | p.544 |
| Reitberger J. | p.217 |
| Riera R. | p.554 |
| Rombouts J. | p.39 |
| Rosette J. | p.180 |
| Solberg S. | p.247 |
| St-Onge B. | p.555 |
| Stephens P.R. | p.563 |
| Straub C. | p.572 |
| Suarez J. | p.581 |
| Takahashi T. | p.86 |
| Tewddale S. | p.586 |
| Valbuena R. | p.596 |
| Van der Zande D. | p.305 |
| Vastaranta J. | p.606 |
| Vaukonen J. | p.616 |
| Vehmas M. | p.58 |
| Vepakomma U. | p.159 |
| Waser L.T. | p.625 |
| Weidenbach M. | p.635 |
| Wezyk P. | p.636 |